FEB - FRESENIUS ENVIRONMENTAL BULLETIN
Founded jointly by F. Korte and F. Coulston
Production by PSP - Vimy Str. 1e, 85354 Freising, Germany in
cooperation with PRT-Parlar Research & Technology
Vimy Str 1e, 85354 Freising

Printed in Germany-ISSN 1018-4619

Fresenius Environmental Bulletin is abstracted/indexed in:
Biology & Environmental Sciences, BIOSIS, CAB International, Cambridge Scientific abstracts, Chemical Abstracts, Current Awareness, Current Contents/Agriculture, CSA Civil Engineering Abstracts, CSA Mechanical & Transportation Engineering, IBIDS database, Information Ventures, NISC, Research Alert, Science Citation Index (SCI), Scisearch, Selected Water Resources Abstracts

CONTENTS

ORIGINAL PAPERS

LONG-TERM HEAVY METALS POLLUTION AND HEALTH RISK ASSESSMENT IN THE HAIHE RIVER, CHINA 3837
Shitao Peng, Ting Lei, Ran Zhou, Jianfeng Zhang, Xiaoli Wang

THE IMPACT OF LAND-USE CHANGE ON MONTHLY VARIATION OF SOIL NITROGEN IN AN AGRICULTURAL REGION AT MID-HIGH LATITUDE 3847
Linna Wu, Shengtian Yang, Changsen Zhao, Fanghua Hao, Guotao Dong, Yongan Yang, Zhiwei Wang, Hezhen Lou

THE INFLUENCE OF SELECTED VARIABLES ON THE PHOSPHORUS CONTENT IN BOTTOM SEDIMENTS OF THE SOLINA-MYCZKOWCE COMPLEX OF DAM RESERVOIRS 3859
Lilianna Bartoszek, Janusz A Tomaszek

ENHANCED ELECTROKINETIC REMEDIATION OF ZINC-CONTAMINATED SOILS NEAR A MINE TAILING WITH APPROACHING ANODE TECHNIQUE 3867
Zongping Cai, Dongrui Chen, Mengqing Xu, Zhanqiang Fang,Weishan Li,Qiming Huang

AN INDOOR AIR QUALITY WIRELESS MONITORING NETWORK WITHA CARBON DIOXIDE PREDICTION MODEL 3875
Sy-Yuan Kang, Chao-Heng Tseng, Ai-Jie Wang, Yi-Hsuan Shih, Nhat-Thien Nguyen

CUMULATIVE TOTAL DUST EXPOSURE CAUSES ACCELERATED CUMULATIVE ABNORMAL RATE OF PULMONARY FUNCTION IN COAL MINERS IN A CHINESE HAN POPULATION 3886
Qing-Zeng Qian, Xiang-Ke Cao, Fu-Hai Shen, Qian Wang, Hai-Yan Liu, Jun-Wang Tong, Jie Zhou

THE FATE OF MERCURY DURING COAL COMBUSTION: OCCURRENCE MODE, TRANSFORMATION, EXISTENCE FORM AND EMISSION 3895
Debo Li, Lili Fu, Qisheng Xu, Jie Gao, Jianyi Lu

EFFICIENT IN VITRO BULBLET REGENERATION FROM IMMATURE ZYGOTIC EMBRYOS OF FRITILLARIA IMPERIALIS AND F. PERSICA 3907
Derya Çakmak, Cengiz Sancak, Cuma Karaoglu, Muhammad Aasim, Iskender Parmaksiz, Sebahattin Ozcan

EFFECTS OF NITROGEN ADDITIONS ON SOIL SEED BANK OF A FRESHWATER MARSH IN SANJIANG PLAIN, NORTHEASTERN CHINA: A SHORT-TERM STUDY 3915
Guodong Wang, , Ming Wang, Ming Jiang

LONG-TERM VARIABILITY OF TOTAL NITROGEN AND TOTAL PHOSPHORUS CONCENTRATION AND LOAD IN THE SOUTH PART OF THE BALTIC SEA BASIN 3923
Piotr Ilnicki, Krzysztof Gorecki, Piotr Lewandowski, Ryszard Farat

STUDY OF THE MATRIX EFFECTS ON THE DETERMINATION OF IRON IN OILFIELD BRINES IN ALBANIA, USING AAS TECHNIQUE 3941
Edlira Baraj, Valbona Celo, Alma Shehu, Rajmonda Totoni, Besnik Baraj

IDENTIFICATION OF PHARMACEUTICAL WASTEWATER CHARACTERISTICS BASED ON PARTICLE SIZE DISTRIBUTION, BIODEGRADABILITY AND ACUTE TOXICITY 3948
Shan Liu, Zhe Qin, Chunxia Zhao, Da Lu, Shu-xuan Liang, Jianbing Li

AN ASSOCIATION BETWEEN AMBIENT POLLUTANTS AND HOSPITAL ADMITTED RESPIRATORY CASES IN AHVAZ, IRAN 3955
Mehran Khaefi, Gholamreza Goudarzi, Ahmad Reza Yari, Sahar Geravandi, Sina Dobaradaran, Esmaeil Idani, Parviz Javanmardi, Farid Youesfi, Bayram Hashemzadeh, Arman Shahriari, Mohammad Javad Mohammadi

STRUCTURAL PROPERTIES OF TIO2/SB NANOPARTICLES WITH DIFFERENT MOLAR RATIOS AND INVESTIGATION THE PHOTOCATALYTIC DEGRADATION OF AZO DYES UNDER UV IRRADIATION IN DIFFERENT CONDITION 3962
Maryam Nozari, Shahram Moradi Dehaghi

HYBRIDIZATION OF MoO_3 WITH BN NANOSHEETS FOR IMPROVING SOLAR-LIGHT-DRIVEN PHOTOCATALYSIS 3971
Junjie Yuana, Liang Liub, Hui Xub, Huaming Li

EFFECTS OF BENSULFURON-METHYL ON CELL MORPHOLOGY OF A.AZOTICA 3981
Li Li Guo, Jin Zhi Liao, Jian Ying Shen, Qiu Guang Shen

A COMPARATIVE STUDY OF FENTON AND ELECTRO-FENTON TREATMENT FOR COD REMOVAL FROM COKING INDUSTRY WASTEWATER 3987
Ruichao Peng, Ping Yu, Yunbai Luo

MODIFICATION MECHANISM OF AMPHOTERIC MODIFIER BS–12 ON TWO DIFFERENT CLAYS 3993
Wenbin Li, Zhaofu Meng, Qiong Wu, Dan Bai, Shaoe Xu, Yu Lu

ESTIMATION OF THE LONGITUDINAL DISPERSION COEFFICIENT FOR RIVER NETWORKS USING A DIFFERENTIAL EVOLUTION ALGORITHM 4004
Xiaodong Liu, Shengcheng Mei, Li Gu, Qile Tu, Zulin Hua

BENTHIC DIATOMS AS INDICATORS OF WATER QUALITY IN THE ACARLAR FLOODPLAIN FOREST (NORTHERN TURKEY) 4013
Tugba Ongun Sevindik, Fatma Kucuk

COMPOSTING OF MUNICIPAL OPEN MARKET WASTES WITH DIFFERENT MATERIALS 4026
Kamil Ekinci, Barbaros Salih Kumbul, Davut Akbolat, İbrahim Erdal, Berk Bitrak

ANAEROBIC OXIDATION OF LANDFILL CH4 AND N2O EMISSIONS BY AGED REFUSE AND COVER SOIL: EFFECTS OF ENVIRONMENTAL FACTORS 4036
Chaoran Li, Houhu Zhang, Shaojun Jiao, Zhehua Zhao

MORPHOLOGICAL AND MERISTIC DIFFERENCES AMONG FRESHWATER FISH, CYPRINION KAIS (CYPRINIDAE) POPULATIONS IN TIGRIS RIVER OF SOUTHEAST TURKEY 4045
Serbest Bilici, Arif Baysal, Tarık Cicek, Ersin Uysal, Erhan Unlu

RESPONSES OF MULTIPLE BIOMARKERS IN THE FISH HOPLOSTERNUM LITTORALE AFTER EXPOSURE TO CHROMIUM AND LEAD 4052
Analía Ale, Carla Bacchetta, Jimena Cazenave

EVALUATION OF SULFANILIC ACID REMOVAL FROM AQUEOUS SOLUTIONS BY ACTIVATED CARBON AND POLYMERIC RESINS 4060
Yue Sun, Deqiang Yin, Junfen Luo, Yan Xu

COMBINED TOXIC EFFECTS OF FIVE ESTROGENS ASSESSED BY YEAST ESTROGEN SCREEN ASSAY 4067
Zhaohan Zhang, Peng Gao, Lin Nan, Binyu Lu, Yujie Feng, Wei Liu, Nanqi Ren

SYNTHESIS AND CHARACTERIZATION OF TIO2 AND TIO2/CEO2 MICRO-SPONGE HETERO STRUCTURE: PHOTOCATALYTIC APPLICATIONS UNDER UV LIGHT 4078
Ali Imran Vaizogullar, Mehmet Ugurlu, Ibrahim Kula

DEGRADATION AND ITS CAUSES OF INFLUENZA A VIRUS IN EUTROPHIC FRESHWATER 4088
Mingjun Liao, Wei Liu, Kai Cheng, Yijun Zhao

FRACTAL OF RANDOM PORE AND DIRECTIVITY OF SOIL SEEPAGE 4093
Sun, Jichao, Liao, Qian

THE GENETIC HETEROGENEITY OF FACULTATIVE ALKALIPHILIC BACILLUS SPECIES ISOLATED FROM SODA LAKE 4103
Cumhur Avsar, Zeynep Yegin, Seyhan Civek, Ismet Berber

STAGE-DISCHARGE RELATIONSHIP IN TIDAL RIVERS FOR TIDAL FLOOD CONDITION 4111
Mohammad Sadegh Sadeghian, Meysam Salarijazi, Iman Ahmadianfar, Mohammad Heydari

POTABLE WATER QUALITY ASSESSMENT IN AL-HASSA, EASTERN REGION OF SAUDI ARABIA 4118
El-Sayed A Badr, Ahmed A Al-Naeem

ENHANCING BIOGAS PRODUCTION FROM ORGANIC FRACTION OF MUNICIPAL SOLID WASTE BY CO-DIGESTION WITH THICKENED WASTE ACTIVATED SLUDGE AND RICE STRAW 4130
Zaidun Naji Abudi, Zhiquan Hu, Bo Xiao, Nagham Rajaa, Song Chen

A RESEARCH ON THE SENSITIVITY OF TROUTS (ONCORHYNCHUS MYKISS) TO SOME METALS (HGCL2, ZNSO4, PBCL2) 4141
Bulent Verep, Ertugrul Terzi, E Sibel Besli

PROMOTIONAL EFFECT OF CE DOPING ON V2O5/TIO2-SNO2 CATALYSTS FOR SELECTIVE CATALYTIC REDUCTION OF NO BY NH3 4148
Yaping Zhang, Kai Shen, Wei Xiang, Haitao Xu, Kai Shen, Changcheng Zhou, Linjun Yang

ASSESSMENT OF SOME HEAVY METALS IN CANNED FISHES FOR HUMAN HEALTH 4157
Metin Caglar, Ozgur Canpolat

ISOLATION, CHARACTERIZATION AND PATHOGENICITY OF BACTERIA FROM OLIGONYCHUS UNUNGUIS (JACOBI) (ACARI: TETRANYCHIDAE) 4163
Nurcan Albayrak Iskender, Yasar Aksu

FLOW BEHAVIOUR AND RHEOLOGICAL ASSESMENT OF KAOLINITE/PDMS PASTES VIA CAPILLARY RHEOMETER 4171
Zurriye Gunduz, Mahir Alkan, Mehmet Dogan

THE INFLUENCE OF THE EM-A PREPARATION ON THE PROPERTIES OF STRUCTURE IN ARABLE MINERAL SOILS 4184
Piotr Gajewski, Zbigniew Kaczmarek, Wojciech Owczarzak, Bartłomiej Glina, Agnieszka Mocek–Płociniak, Eliza Gaweł, Mieczysław Grzelak, Dariusz Swierk

DIFFERENTIAL RESPONSE OF GROWTH, PHOTOSYNTHETIC PIGMENTS AND ANTIOXIDANT ENZYMES TO UV-B RADIATION IN TOMATO (SOLANUM LYCOPERSICUM L.) SEEDLINGS 4192
Kadriye Uruc Parlak

NEAR-INFRARED SPECTROSCOPY ANALYSIS OF VFA IN ANAEROBIC BIOLOGICAL TREATMENT OF HIGH CARBON-NITROGEN WASTEWATER WITH INTERVAL PARTIAL LEAST SQUARES REGRESS 4197
Jian Huang, Jian-yu Zhou, Qing-ye Sun, Hua Zhang, Yong Zhang, Meng Wang, Ling Ling

NaCL PRIMING ALLEVIATES THE INHIBITING EFFECT OF SALINITY DURING SEEDLING GROWTH OF PEAS (PISUM SATIVUM L.) 4202
Bulent Senturk, H Ozkan Sivritepe

COMPARATIVE INFLUENCES OF ORGANIC AND CONVENTIONAL HAZELNUT ORCHARD ON THE SOIL WATER CONTENT, ELECTRICAL CONDUCTIVITY, AND TEMPERATURE IN WESTERN BLACK SEA REGION OF TURKEY 4209
Selcuk Ozmen

EVALUATION OF EFFECTIVENESS OF GROUND IMPROVEMENT BASED ON RANDOM FIELD THEORY 4217
Jun Lin, Guojun Cai, Songyu Liu, Anand J Puppala, Haifeng Zou

ACUTE LETHAL TOXICITY TO THE MARINE COPEPOD ACARTIA TONSA OF THE REFERENCE ITEM 3,5-DICHLOROPHENOLE (3,5-DCP) ACC. TO ISO 14669 : 1999 (E) 4224
Martina Noack, Monika Koenig, Thomas Nowakowski, Udo Noack

THE INFLUENCE OF TEMPERATURE ON THE ATMOSPHERE-EXPOSED BIOFILM SYSTEM PROCESSING CHARACTERISTICS AND THE MICROBIAL COMMUNITY 4227
Dong Nie, Ming-Ji Jin, Ming-Zhe Xu

FEASIBILITY AND ECONOMIC ANALYSIS FOR SUPERCRITICAL CO2 EXTRACTION OF DIESEL FROM OIL SANDS 4235
Wang Yuzhen, Pu Lei, Gao Fen, Yang Jianqiao, Fang Changqing, Zhao Gaoyang, Li Yanhui, Wang Shuzhong

ONE-POT METHOD FOR SYNTHESIS OF COSE2-ETHYLENEDIAMINE NANOFLOWERS 4242
Xian Zhang, Fengqiong Shi

DISAPPEARANCE OF SOME FUNGICIDES IN MATURE APPLES IMMEDIATELY BEFORE SUPPLYING FRUIT TO THE CONSUMER 4246
Bartosz Piechowicz, Stanisław Sadło, Ewa Szpyrka, Kinga Stawarczyk, Michał Stawarczyk, Przemysław Grodzicki

EVALUATION OF CHOLINESTERASE FROM THE MUSCLE AND BLOOD OF ANABAS TESTUDINEUS AS DETECTION OF METAL IONS 4253
Siti Aqlima Ahmad, Mohd Khalizan Sabullah, Ain Aqilah Basirun, Ariff Khalid, Nur Adeela Yasid, Izzuanuddin Muhammed Iqbal, Nor Aripin Shamaan, Mohd Arif Syed , Mohd Yunus Shukor

ASSESSMENT OF HIGHWAY-INDUCED POLLUTION THROUGH PLANT AND SOIL ANALYSES, IN CASE OF ORDU CITY SECTION OF BLACK SEA COASTAL HIGHWAY 4261
Omer Atabeyoglu, Pervin Yesil, Murat Yesil

INFLUENCE OF CAPREOLUS CAPREOLUS L. AND CERVUS ELAPHUS L. FEEDING SIMULATION ON DISEASE INCIDENCE RATE AND MAIZE YIELDING 4269
Korbas Marek, Węgorek Paweł, Zamojska Joanna, Danielewicz Jakub, Jajor Ewa, Dworzanska Daria, Bandyk Andrzej, Horoszkiewicz-Janka Joanna

HEAVY METALS POLLUTION AND HEALTH RISK ASSESSMENT OF ATMOSPHERIC DUST OF LESS THAN 100MM ALONG A TYPICAL INDUSTRIAL CORRIDOR, CENTRAL CHINA 4277
Yong Zhang, Jiaquan Zhang, Changlin Zhan, Ruizhen Yao, Ting Liu, Li Zhang, Wensheng Xiao, Yongkui Wang, Jingru Zheng, Hongxia Liu

OPTIMIZATION OF HYDROTHERMAL SYNTHESIS CONDITIONS OF N-DOPED TIO2 USING RESPONSE SURFACE METHODOLOGY FOR PHOTOCATALYTIC DEGRADATION OF METHYLENE BLUE 4287
Xiaodan Zhao, Donghui Chen, Yurong Zhang, Manhong Huang, Zhenbang Deng, Zhen Zhou

DETERMINING THE IMPACT OF EXCESSIVE BORON ON SOME GROWTH CHARACTERS AND SOME NUTRIENTS AT THE EARLY GROWTH STAGE OF SUNFLOWER (HELIANTHUS ANNUUS L.) 4294
Sibel Day

PHOTOCATALYTIC DEGRADATION OF DICLOFENAC AND IBUPROFEN FROM SIMULATED WASTEWATER USING SIO2-TIO2-(RU, N) BY ARTIFICIAL LIGHT 4299
Waed R. Alahmad, Mahmoud A. Alawi

DYNAMIC CHARACTERIZATION OF PARTICLE-BOUND AND DISSOLVED NUTRIENTS IN ROOF RUNOFF 4309
Fa-hui Nie, Qing Yu, Rong-rong Liu, Zhan-meng Liu, Biao Wang

POTENTIAL OF DIFFERENT EUROPEAN WHITE ELM (ULMUS LAEVIS PALL.) GENOTYPES FOR PHYTOEXTRACTION OF HEAVY METALS 4318
Jovana Devetakovic, Dragica Stankovic, Vladan Ivetic, Mirjana Sijacic-Nikolic, Zoran Maksimovic

THE EFFECTS OF COPPER (CUCL2) ON MITOTIC CELL DIVISION OF LEBANON CEDAR (CEDRUS LIBANI) 4324
Ayse Ak Can, Gulcin Isik, Ersin Yucel

COMPOSITE BENTONITE MODIFICATED BY 3-AMINOPROPYLTRIETHOXYSILANE AND SODIUM SILICATE AND ITS EFFECTIVENESS TO CADMIUM REMOVAL 4327
Xingjie Hao, Xiaping Zhu, Li Zhou, Lin Wu

SIMULTANEOUS PROCESSES OF MINOCYCLINE DEGRADATION AND ELECTRICITY GENERATION IN AN AIR-CATHODE SINGLE CHAMBER MICROBIAL FUEL CELL 4334
Xiang Hu, Lingjuan Luo, Zhirong Sun

DECREASING MULTIPLE FRUIT IN PEACH (PRUNUS PERSICAE L.) USING SHADE NET AND KAOLIN 4345
Burhanettin Imrak

INTEGRATED HEALTH RISK ASSESSMENT NEAR A SMELTER BASED ON SOIL CD(II) POLLUTION 4351
Wen-bin Li, Zhao-fu Meng, Hua-yun Chen, Ze Liu, Lu Yu, Shao-e Xu, Wei Liu1

HABITAT PREFERENCES OF AQUATIC OLIGOCHAETA (ANNELIDA) SPECIES IN THE LAKE DISTRICT (TURKEY) 4362
Seray Yildiz

EVALUATION OF THE EFFECTS ON SOIL CARBON MINERALIZATION OF DELTAMETHRIN AND LAMBDA-CYHALOTHRIN USED TO CONTROL OF SOME INSECTS
IN OLIVE ORCHARDS 4374
Husniye Aka Sagliker, Ilay Cevik

EFFECTS OF FERTILIZER INPUT ON HEAVY METAL IN DIFFERENT SOILS 4381
Yukui Rui, Shutong Liu, Shengliang Li, Liming Liu

HYDROCHEMISTRY OF GROUNDWATER FROM THE LOOSE LAYER AQUIFER: QUALITY AND CONTROLLING FACTOR ANALYSIS 4387
Xianghong Liu, Jingcun Yu, Linhua Sun, Herong Gui

PHENOTYPIC, SEROTYPIC AND GENETIC CHARACTERIZATION AND ANTIMICROBIAL SUSCEPTIBILITY DETERMINATION OF VIBRIO ANGUILLARUM, ISOLATED FROM CULTURED SEA BASS (DICENTRARCHUS LABRAX L., 1758) IN THE SOUTHEAST BLACK SEA, TURKEY 4393
Fikri Balta

RESPONSES OF CO2 AND N2O EMISSIONS TO CARBON AND PHOSPHORUS ADDITIONS IN TWO CONTRASTING ALPINE MEADOW SOILS ON THE QINGHAI-TIBETAN PLATEAU 4401
Dongxue Wang, Yongheng Gao, Ping Wang, Xiaoyang Zeng

RADON IN THE INDOOR ENVIRONMENT – A REVIEW - 4409
Sabah Ahmed Abdul-Wahab, Emmanuel Ikhile, Lena Ahmadi, Ali Elkamel, Kaan Yetilmezsoy

ISOLATION AND IDENTIFICATION OF GLOMUS INTRARADICES IN SALT-ALKALI GRASSLAND AND ITS EFFECTS ON SALT TOLERANCE OF TRIFOLIUM REPENS 4439
Chunxue Yang, Fei Chen, Lili Li, Cong Li, Dafu Yu, Jixiang Lin

© by PSP Volume 25 – No. 10/2016, pages 3837-3846 Fresenius Environmental Bulletin

LONG-TERM HEAVY METALS POLLUTION AND HEALTH RISK ASSESSMENT IN THE HAIHE RIVER, CHINA

Shitao Peng[1], Ting Lei[2], Ran Zhou[1], Jianfeng Zhang[3,*], Xiaoli Wang[2]

[1]Laboratory of Environmental Protection in Water Transport Engineering, Tianjin Research Institute for Water Transport Engineering, Tianjin 300456, China
[2]College of Environmental Science and Safety Engineering, Tianjin University of Technology, Tianjin 300384, China
[3]National Engineering Laboratory for Improving Quality of Arable Land, Institute of Agricultural Resources and Regional Planning, Chinese Academy of Agricultural Sciences, Beijing 100081, China

ABSTRACT

Water samples collected from the Haihe River in China between 2001 and 2010 were analyzed for heavy metals and their health risk. Five heavy metals (As, Cr, Cu, Hg, and Pb) were determined in the water. The temporal variations in five metals concentrations generally decreased from 2001 to 2010. The concentrations of Cr, As, and Pb were similar in different sampling sites, while Hg and Cu exhibited the high concentrations in the downstream river next to the estuary. Results of principal component analysis (PCA) showed that Cr and Pb were derived from rock-derived and industrial wastewater, while As, Hg, and Cu was atmospheric deposition and industrial sewage originated. The health risks caused by metals in water were assessed by model recommended by the US Environmental Protection Agency. The health risk showed both the non-carcinogenic and carcinogenic risks were decreased from 2000 to 2010 as a consequence of the concentrations of heavy metals decreased in Haihe River. However, the non-carcinogenic risk exceeded 1 and carcinogenic risk were more than 1×10^{-5} in each years, indicating that there were non-carcinogenic and carcinogenic risks in water from Haihe River. Arsenic was the most important contributor to both non-carcinogenic and carcinogenic risks in the present study. In particular, both Cr and As all exhibited a carcinogenic risk above the acceptable or tolerable risk level in each years, indicating that long term exposure to such water can lead to cancer. Therefore, it is very important to control coal combustion and industrial sewage discharge for removing Cr and As in the water to minimize risks.

KEYWORDS:
Heavy metals, Water Source, Health risk, Haihe River

INTRODUCTION

Rivers are the most important inland water resources for human consumption, agricultural needs, and industrial and recreational purposes [1]. However, the water quality of river is significantly influenced by the heavy metals. Once the heavy metals release into river system, they can accumulate in microorganisms, aquatic flora and fauna, and then may enter into the human food chain and pose a huge threat to human health [2, 3]. Many fatal diseases such as eyelid edema, renal tumour, nasal mucous membranes and pharynx congestion, increase blood pressure and cardiovascular diseases, osteoporosis, nephritis, anuria, cancer, extensive lesions in the kidneys, headache and malfunctions of different systems of the body were induced by heavy metals [4, 5]. Therefore, assessing the risk of heavy metals in river water is an important goal to supply water for human consume.

Haihe River is the one of most important river in China. It covers 263,600 km^2 and with 70 million inhabitants. Due to a large number of wastewater were discharged into the river, Haihe River has been one of most serious polluted rives in China. Such would have a significant impact on the health of Bohai Bay. Over the last few decades, a few studies have been carried out in heavy metals in Haihe River. For example, Yuan and coworkers studied the metals in the sediment in Haihe River [6]. Liu and coworkers surveyed the heavy metal contamination and their distribution in different size fractions of the surficial sediment of Haihe River [7]. It can be seen that these studies focus on the heavy metals in sediments. To our best knowledge, there is no information on the metals in water of Haihe River. In particular, most previous research has focused on the short-term variations of heavy metals, and these studies cannot show the long-term

variation of heavy metals in the Haihe River. Furthermore, there are no researches on health risk assessment.

In the present study, a survey on the heavy metals concentration of the Haihe River was conducted from 2001 to 2010. The main objectives of this study were (1) to survey the temporal and special variation of heavy metals in the Haihe River, (2) to identify sources of heavy metals by principal component analysis, and (3) to assess the health risks caused by metals in water according to an assessment model recommended by the U.S. Environmental Protection Agency (USEPA).

MATERIALS AND METHODS

Field sampling. Six sampling sites were sampled in Haihe River (Fig. 1). The site 1 is located in the urban areas of Tianjin, the third largest industrial and commercial city in China, having a population of more than 11 million. The site 5 is located in Tanggu District, Tianjin, which is near the industrial and technological development zone. The site 6 is located in estuary.

Water samples were collected during three water periods from 2001 to 2010, including the dry period in May, the flood period from July to September, and the level period from October and November. Water samples were collected from the surface using Ruttner water sampler and kept in high grade sterilized plastic bottles. All the samples were filtered immediately with 0.45 µm filters and then acidified to pH < 2 with suprapure HNO_3. These samples were transported to the laboratory and kept in a refrigerator until analysis.

Heavy metals measurements. Five heavy metals including arsenic (As), mercury (Hg), lead (Pb), copper (Cu) and chromium (Cr) were determined in the present study. This is due to two reasons. One is these all of -them are the most important toxicological index of the drinking water in China except of the Cu. The other is that these five heavy metals are the most prevalence heavy metals and the important pollutants in Bohai Bay [8-9]. For the heavy metals measure, water samples (200 mL) were digested with 5 mL of di-acid mixture (HNO_3:$HClO_4$=9:4, v/v) on a hot plate and filtered by Whatman filter paper and made up the volume to 50 mL by double distilled water. Arsenic, Hg, Pb, and Cu were determined with Agilent 7500a ICP-MS (Agilent, USA). Chromium was done using diphenylcarbazide spectrophotometric. The limits of detection were 0.005 µg L^{-1} for Hg and Pb; 0.01µg L^{-1} for As and Cu; and 0.10 µg L^{-1} for Cr. The recoveries of heavy metals ranged from 87% to116%.

Health risk assessment of heavy metal. Human exposure to heavy metals via three main pathways including direct ingestion, inhalation through mouth and nose, and dermal absorption through exposures skin, while ingestion and dermal absorption are common for drinking water [10]. Health risk characterization was quantified by non-carcinogenic and carcinogenic risk. The two risks were calculated with following equation:

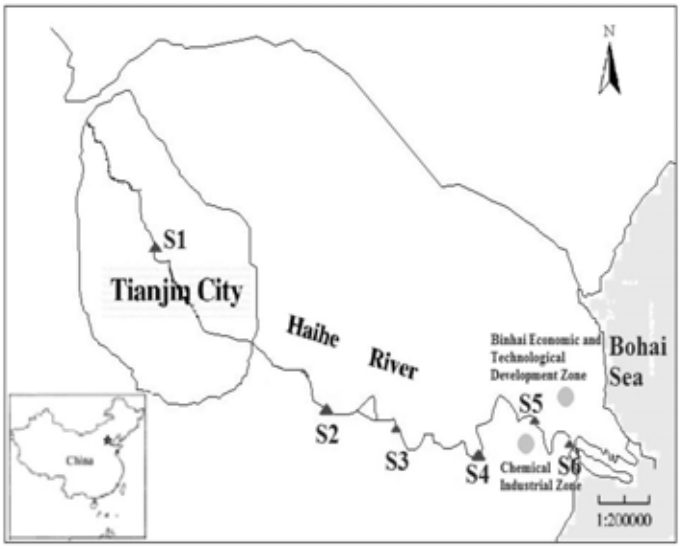

FIGURE 1
The sampling sites in Haihe River

$$HQ = \frac{CDI}{RfD} \quad (1)$$

$$R = SF \times CDI_{ca} \quad (2)$$

Where HQ (hazard quotient) is the non-carcinogenic risk. CDI and CDI_{ca} for the exposure dosage rate, including drinking and skin exposure; RfD was reference dosage. R is a cancer risk; SF is the cancer slope factor.

The total carcinogenic and non-carcinogenic risks were calculated with equations (3) and (4), respectively.

$$HI = HQ_{ing} + HQ_{der} \quad (3)$$

$$R_{total} = R_{ing} + R_{der} \quad (4)$$

Where HQ_{ing} and HQ_{der} indicates that the non-carcinogenic risk induce by ingestion and dermal absorption, respectively. R_{ing} and R_{der} indicates that the carcinogenic risk induce by ingestion and dermal absorption, respectively.

For the non-carcinogenic risks, if the HQ exceeds 1, there might be concern for non-carcinogenic effects. HI > 1 indicated a potential adverse effect on human health. For the carcinogenic risks, the acceptable or tolerable level of carcinogenic risks is lower than 1×10^{-5}.

Statistical analyses. The one-way ANOVA was performed to test the difference in the heavy metals concentration between different years and sampling stations. The principal component analysis (PCA) employed to identify sources of heavy metals. All the above analyses were used by SPSS 13.

RESULTS AND DISCUSSION

Concentration of heavy metals. In this study, five heavy metals including As, Cr, Cu, Hg, and Pb were determined in water. The heavy metals concentrations were significantly different in terms of both temporal and spatial variations (p<0.001). As shown in Fig. 2, the temporal variations in five metals concentrations generally decreased from 2001 to 2010. It was attributed to the efforts have been made to control the pollution loads by a series of environmental protection programs, such as the sewage treatment system establish and enforcement of the water pollution control regulations and in Tianjin in last decade [11].

It also can be seen that the high concentrations of Cr, Hg, Pb, and Cu were observed before 2004, and then decreased afterwards (Fig. 2). These trends may be explained by the fact that there was an increase in wastewater discharges, agricultural fertilizers and pesticides use before 2004 for the rapid population growth and economic development [12]. However, some environmental protection policies were establishment since 2004. For example, one of the most important policies, entitled *The Plan of Cleaning Bohai Sea*, was promulgated to control the discharge of contaminants into the Bohai Bay by the Central Government of China [13]. As one of most important tributaries into the Bohai Bay, the wastewater discharge into Haihe River was controlled and then may decrease the heavy metals in water when this policy was put into practice. In particular, the sediment dredging was carried out in Haiher River in 2003 [11]. It can significantly improve water quality. Furthermore, the public and scientific awareness related to the environmental restoration of Haihe River. As a result, the water quality of Haihe River gradually improved after 2004.

The spatial variations of heavy metals concentrations were showed in Fig. 3. In generally, the concentrations of Cr, As, and Pb were all similar in six sampling sites except of site 3 (Fig. 3). This is due to the site 3 were located in the Tangu District, Tianjin and surrounded by industry. It has been proved that serious pollution had been caused by industry [14]. As shown in the Fig 3, the high concentrations of Hg and Cu were found in the downstream river next to the estuary. Several factors might lead to the high concentrations of Hg and Cu in the downstream. First, the different locations were exposed to different pollution sources. In general, the downstream is usually thought to be more heavily polluted than upstream [15]. In particular, the estuary is usually a heavily polluted area [16]. For example, a relatively lower PAH concentration was reported in the Beitang Estuary sediments than in the upstream river sediments [17]. Second, there was a sewage drainage river, which discharged the wastewater into downstream of Haihe River. This may increase the heavy metals in water of downstream of Haihe River. These also indicate that there were different source for different heavy metals.

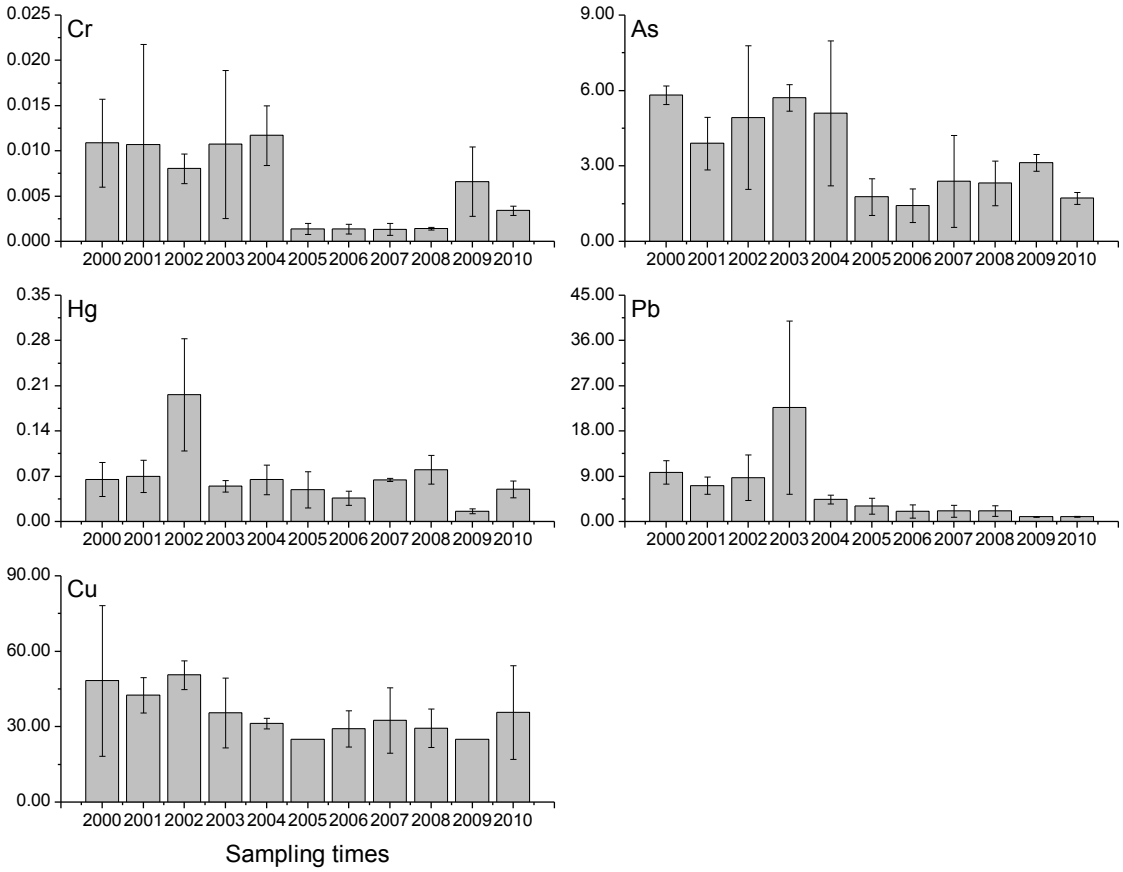

FIGURE 2
The temporal variation of heavy metals (μg/L)

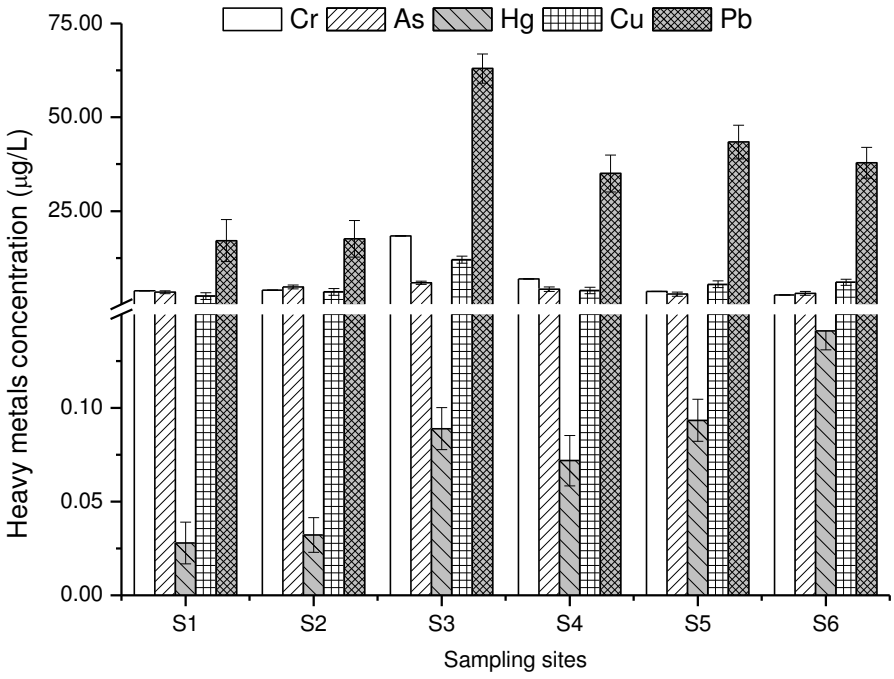

FIGURE 3
The spatial variation of heavy metals

TABLE 1
The average concentrations of metals (µg/L) in selected world rivers

Locations	Cr	As	Hg	Pb	Cu	Reference
Pearl River, South China	2.8	2.56	0.045	2.91	50	[18]
Yangtze River, East China	20.9	13.2	0.48	5.51	10.7	[19]
Yeongsan River, Korea	1.2	0.67	-	0.38	1.96	[2]
To Lich River, Vietnam	2.9	39.1	-	8.1	4.5	[20]
Thames, Great Britain	-	2.9	-	0.4	4.3	[21]
Seine River, France	53.6	-	-	36	19.4	[22]
River Nile, Egypt	<10	<8	-	6	25	[23]
Ghana stream rivers	2.65	30	-	1.4	-	[24]
Elqui River, Chile	26	1705	3	147	6082	[25]
Haihe River (average value)	6.19	3.65	0.07	5.70	34.76	This study

The mean concentrations of five heavy metals in water of Haihe Rivers in this study are higher than the values reported for Pearl River, South China except of Cu (Table 1). However, the concentrations of Cr, As, and Hg were lower than those reported in Yangtze River in China (Table 1). All the determined heavy metals in our study exhibited higher concentrations than the other reported rivers in Asia (not include China and As is an exception) and Europe (except for Cr in Seine River, France). In the present study, the heavy metals concentrations are similar to those in African, which are considered as pristine (Table 1). However, the five heavy metals in Haihe River were far below those in Elqui River, Chile (Table 1), which was polluted by mine wastewater [25]. Overall, the pollution levels of metals in Haihe River were relatively low in the present study.

The different criteria of drinking water quality were listed in Table 2. In the present study, all metals' average concentrations were below the maximum levels in drinking water recommended by WHO [26], USEPA [27], and China [28], except of the Cr. This indicates that the most of the collected heavy metals concentrations are within the range of safe drinking water in the present study. The concentration of Cr exceeded the highest level of the water quality criteria for drinking water, indicating that Cr maybe cause the negative effects to health of the local residents. It is well known that chromium is one of the most toxic heavy metals. It produces teratogenic, carcinogenic and mutagenic effects in biological systems [29]. For example, chromium has a major threat for the survival and growth, damage to tissue structures and alternations at biochemical and hematological parameters of fish [30, 31].

Sources of heavy metals. Natural forma1tion and anthropogenic activity are the pathways which the metals enter the environment. Natural pathways include weathering, biological activity, and volcanic activity, etc, while the anthropogenic activity including industrial processing of ores and metals, use of metals and metal components, use of fertilizer, discharge of human sewage, and combustion fossil fuels etc [3]. In the present study, principal component

TABLE 2
Water quality criteria for drinking water (µg/L)

	As	**Cr**	**Cu**	**Hg**	**Pb**	Referenc
WHO (2006)	10	50	2000	1	10	[26]
EPA (2012)						[27]
MCLG	0	5	1300	0	0	
MCL	10	5	1300	15	15	
MOH, China (2007)	10	5	1000	1	10	[28]
Haihe River (average value)	3.65	6.19	34.76	0.07	5.70	In this study

MCLG, maximum contaminant level goal; MCL, maximum contaminant level.

analysis (PCA) was used to identify the sources of heavy metals in water. There were two principal components (PCs) that could be extracted, they account for about 65.50% of the variance in original data (Table 3). The first PC accounts for 35.67% of the variance and has high loadings of Cr and Pb, indicating that the two heavy metals have the same source. Previous study showed that Cr is rock-derived source [32]. However, the concentration of Cr in the present study were higher the background value of the earth (1.0 μg/L, [33]), indicating that there are other source. This source may be industrial wastewater. It is due to there were many industries which are correlated to the Cr in the present study. For the Pb, it is often derived from traffic [34]. As the third largest industrial and commercial city in China, Tianjin has over 239 million passenger cars in 2012. Such cars may be one of the most important sources of Pb in the environment in Tianjin.

TABLE 3
Principal component analysis (PCA) of heavy metals

	PC I	PC II
Cr	0.55	0.35
As	-0.47	0.77
Hg	0.52	0.68
Pb	0.91	0.05
Cu	0.40	-0.56
Eigenvalue	1.78	1.49
Explained variance (%)	35.67	29.83
Total explained variance (%)	35.67	65.50

The second PC accounts for 29.83% of the total variance and was closely related to As, Hg and Cu (Table 3). This suggested some of As, Hg and Cu might come from the common sources. Many studies showed that atmospheric deposition was an important source of As, Hg, and Cu in water [3, 9, 35]. Arsenic is also arising from industrial sewage [32]. These indicate that heavy metals in As, Hg, and Cu in water of Haihe River was possibly atmospheric deposition and industrial sewage originated. For the atmospheric deposition, one is due to a coal-fired power plant located in south Tianjin and near to the downstream of Haihe River [11]. The other is due to most of heating is derived from coal combustion in the study area. Arsenic and Hg are easily volatilized from coal during combustion [36]. This is well demonstrated that the high concentration of As and Hg in the downstream of Haihe River as a consequence of the coal combustion. For the industrial sewage, it is due to the wastewater discharge into the Haihe River. In the present study, the downstream is located in the Binhai Economic and Technological Development Zone of Tianjin. There are a number of industries including biomedical, chemical, electronics, machinery manufacturing, iron and steel enterprises in this zone. These enterprises discharge some of their wastewater into rivers with little even no treatment and thus increased the concentrations of the metals in the water. In particular, e-waste processing is one of important origin of Cu [37]. Therefore, the industrial sewage is also one of most important source of the metals in the Haihe River.

Health risk. HQ of each heavy metal is summarized in Table 4 based on the ingestion ($HQ_{ingestion}$) and dermal absorption (HQ_{dermal}) of water. As shown in the Table 4, HQ of individual heavy metals were lower than 1 except of As in some years, suggesting that most of these heavy metals posed little hazard to local residents alone. However, HI exceeded 1 in each years (2007 and 2009 were two exceptions), indicating that long-term exposure to Haihe River water can cause the non-carcinogenic risk (Table 4). In the present study, the non-carcinogenic risk generally decreased from 2000 to 2010 in Haihe River. This is due to the concentration of heavy metals in the present study is decreased from 2000 to 2010 (Fig. 2).

Arsenic was the only metal which HQ was more than 1, and which contributed 0.02% to 78.18% with an average of 53.28% to the HI in Harhe River (Table 4). This suggests that As was the most important contributor which may cause the non-carcinogenic risk to the local residents.

In the present study, Cr and As were considered as the chemical compounds which have the potential carcinogenic risk. Both Cr and As carcinogenic risk were more than 1×10^{-5} (Table 4), demonstrating that the two heavy metals posed high carcinogenic risk to local residents. Similar to non-carcinogenic risk, the carcinogenic risk was also decreased from 2000 to 2010 as a consequence of the concentrations of Cr and As decreased in Haihe River. Arsenic was also the

TABLE 4
Non-carcinogenic and carcinogenic risk of heavy metals in Haihe River

	HQ						R		
	Cr	As	Hg	Pb	Cu	HI	Cr	As	R_{total}
2000	9.90E-02	2.72E+00	2.44E-01	1.02E-01	3.14E-01	3.48E+00	9.75E-05	2.11E-04	3.09E-04
2001	7.74E-02	1.63E+00	2.86E-01	4.14E-02	3.39E-01	2.37E+00	7.63E-05	1.27E-04	2.03E-04
2002	9.54E-02	1.59E+00	6.83E-01	3.82E-02	3.07E-01	2.71E+00	9.40E-05	1.24E-04	2.18E-04
2003	7.13E-02	1.73E+00	2.43E-01	1.14E-01	2.33E-01	2.39E+00	7.02E-05	1.35E-04	2.05E-04
2004	1.22E-01	1.59E+00	2.87E-01	3.95E-02	2.33E-01	2.27E+00	1.20E-04	1.24E-04	2.44E-04
2005	1.69E-02	9.26E-01	2.51E-01	2.46E-02	1.38E-01	1.36E+00	1.66E-05	7.21E-05	8.87E-05
2006	1.84E-02	6.91E-01	2.16E-01	1.14E-02	1.87E-01	1.12E+00	1.81E-05	5.33E-05	7.14E-05
2007	1.84E-02	1.32E-04	2.94E-01	2.59E-02	1.99E-01	5.37E-01	1.81E-05	1.03E-04	1.21E-04
2008	1.84E-02	8.15E-01	4.97E-01	1.68E-02	2.13E-01	1.56E+00	1.81E-05	6.55E-05	8.36E-05
2009	8.43E-02	1.08E-01	6.00E-01	7.16E-03	1.73E-01	9.72E-01	8.31E-05	8.39E-05	1.67E-04
2010	3.56E-02	5.41E-01	2.75E-01	7.16E-03	3.40E-01	1.20E+00	3.51E-05	4.21E-05	7.72E-05

main contributor (50.24%-85.05% with an average of 66.22%) of the total carcinogenic risk (Table 4).

Arsenic was the main was contributor to both non-carcinogenic and carcinogenic risk in Haihe River (Table 4). This indicates that As was the most important pollutant in the Haihe River. Arsenic can cause harm on human multiple system functions, including hypertension, cardiovascular diseases, neurological diseases, diabetes, Skin pigment metabolic abnormalities and keratinization of skin, influencing labor and viability of life, eventually leading to a variety of visceral cancer of the bladder, kidney, liver, etc. [38]. Thus, the concerted efforts are required to be taken to remove As in the water to minimize risks is very important. In the present study, the PCA results shown than As was derived from atmospheric deposition and industrial sewage (Table 3). Therefore, the control of the coal combustion and industrial sewage discharge is very important.

The concentration of Cr is low and has a low non-carcinogenic risk in this study. However, Cr is another metal which exhibited a carcinogenic risk above the acceptable or tolerable risk level in each year (Table 4). This indicates that long term exposure to low concentrations of Cr in drinking water can lead to cancer. Chromium is known to cause lung cancer in humans [39]. This indicates that the concerted efforts are also required to be taken to remove Cr in the water. Due to the source of Cr is industrial wastewater in this study. It is therefore to control industrial sewage discharge.

CONCLUSION

This study presents the long-term spatial and temporal trend analyses of the five heavy metals in water from Haihe River. The heavy metals concentrations were significantly different in terms of both temporal and spatial variations. In general, five heavy metals concentrations decreased from 2001 to 2010. There were three sources of the heavy metals including rock-derived, coal combustion, and industrial sewage. HQ of individual heavy metals were lower than 1 except of As in some years, while HI exceeded 1 in each years (2007 and 2009 were two exceptions), indicating that long term exposure to Haihe River water can cause the non-carcinogenic risk. Both Cr and As carcinogenic risk were more than 1×10^{-5}, indicating that the two heavy metals posed high carcinogenic risk to local residents. Arsenic was the most important contributor to both non-carcinogenic and carcinogenic risks in the present study. Chromium was also one of most important pollutants in water from Haihe River.

ACKNOWLEDGEMENTS

This work was supported by the International Science and Technology Cooperation Program of China（2015DFA20790）,the National Basic Research Program (973 Program) of China

(2013CB127406), and the National Natural Science Foundation of China (21307045, 21577172),.

REFERENCES

[1] Razmkhah, H., Abrishamchi, A., Torkian, A. (2010) Evaluation of spatial and temporal variation in water quality by pattern recognition techniques: A case study on Jajrood River (Tehran, Iran). Journal of Environmental Management 91, 852-860.

[2] Kang, J.H., Lee, Y.S., Ki, S.J., Lee, Y.G., Cha, S.M., Cho, K.H., Kim, J.H. (2009) Characteristics of wet and dry weather heavy metal discharges in the Yeongsan Watershed, Korea. Science of the Total Environment 407, 3482–3493.

[3] Ma L, Qin X, Sun N, Yang G. (2014) Human health risk of metals in drinking-water source areas from a forest zone after long-term excessive deforestation. Human and Ecological Risk Assessment 20, 1200-1212.

[4] Ikem, A., Egiebor, N.O. (2005) Assessment of trace elements in canned fishes (mackerel, tuna, salmon, sardines and herrings) marketed in Georgia and Alabama (United States of America). Journal of Food Composition and Analysis 18, 771-787

[5] Iwegbue, C., Nwajei, G.E., Arimoro, F.O. (2007). Assessment of contamination by heavy metals in sediments of Ase River, Niger Delta, Nigeria. Research Journal of Environmental Sciences 1, 220-228

[6] Yuan, C., Jiang, G., Liang, L., Jin, X., Shi, J. (2004) Sequential extraction of some metals in Haihe River sediments, People's Republic of China. Bulletin of Environmental Contamination and Toxicology 73, 59–66.

[7] Liu, L., Li F., Xiong, D., Song, C. (2006) Heavy metal contamination and their distribution in different size fractions of the surficial sediment of Haihe River, China. Environmental Geology 50, 431–438.

[8] Dai, M., Peng, S., Xu, J., Liu, C., Jin, X., Zhan, S. (2009) Decennary variations of dissolved heavy metals in seawater of Bohai Bay, North China. Bulletin of Environmental Contamination & Toxicology 83, 907–912.

[9] Zhan, S., Peng, S., Liu, C., Chang, Q., Xu, J. (2010). Spatial and temporal variations of heavy metals in surface sediments in bohai bay, north china. Bulletin of Environmental Contamination & Toxicology 84, 482–487.

[10] Kim, J. Y., Kim, K. W., Ahn, J. S., Ko, I., Lee, C. H. (2005). Investigation and risk assessment modeling of As and other heavy metals contamination around five abandoned metal mines in Korea. Environmental Geochemistry and Health 27, 193-203.

[11] Bai, J., Peng, S., Qin, X., Yang, X., Dai M. (2012) Evaluation of anthropogenic influences on rivers by dissolved metals: a case study in Tianjin, China. Fresen. Environ. Bull. 21, 1684-1688.

[12] Jun, X., Hao, H. (2006) Impacts of water pollution and shortage on economic development of the Haihe River Basin. Resources Science 28, 2-7.

[13] Zhou, R., Qin, X., Peng, S., Deng, S. (2014). Total petroleum hydrocarbons and heavy metals in the surface sediments of Bohai Bay, China: Long-term variations in pollution status and adverse biological risk. Marine Pollution Bulletin 83, 290-297.

[14] Peng, S, Wang, A., Wang, X., Zhou, R., Zhang, J. (2014) The long-term variations of water quality in the Haihe River, China. Fresen. Environ. Bull., 24, 883-880.

[15] Echols, K.R., Brumbaugh, W.G., Orazio, C.E., May, T.W., Poulton, B. C., Peterman, P.H. (2008). Distribution of pesticides, PAHs, PCBs, and bioavailable metals in depositional sediments of the lower Missouri River, USA. Archives of Environmental Contamination and Toxicology 55, 161-172.

[16] Pascual, M., Borja, A., Franco, J., Burdon, D., Atkins, J.P., Elliott, M. (2012) What are the costs and benefits of biodiversity recovery in a highly polluted estuary? Water Research 46, 205–217.

[17] Qin, X, Sun, H, Wang, C., Yu, Y., Sun, T. (2010) Impacts of crab bioturbation on the fate of polycyclic aromatic hydrocarbons in sediment from the Beitang estuary of Tianjin, China. Environmental Toxicology and Chemistry 29, 1248–1255.

[18] Cheung, K., Poon, B.H.T., Lan, C.Y., Wong, M.H. (2003) Assessment of metal and nutrient concentrations in river water and sediment collected from the cities in the Pearl River Delta, South China. Chemosphere 22, 1431-40.

[19] Wu, B., Zhao, D., Jia, H., Zhang, Y., Zhang, X., Cheng S. (2009) Preliminary risk assessment of trace metal pollution in surface water from Yangtze River in Nanjing Section, China.

Bulletin of Environmental Contamination and Toxicology 82, 405–409.

[20] Thuong, N.T., Yoneda, M., Ikegami, M., Takakura, M. (2013). Source discrimination of heavy metals in sediment and water of To Lich River in Hanoi City using multivariate statistical approaches. Environmental Monitoring and Assessment 185, 8065-8075.

[21] Neal, C., Jarvie H., Whitton, B., Gemmell, J. (2000) The water quality of the River Wear, north–east England. Science of the Total Environment 251/252, 153–72.

[22] Priadi, C., Bourgeault, A., Ayrault, S., Gourlay-Francé, C., Tusseau-Vuillemin, M. H., Bonté, P., Mouchel, J. M. (2011). Spatio-temporal variability of solid, total dissolved and labile metal: passive vs. discrete sampling evaluation in river metal monitoring. Journal of Environmental Monitoring 13, 1470-1479.

[23] Dahshan, H., Abd-Elall, A.M.M., Megahed, A.M. (2013). Trace metal levels in water, fish, and sediment from River Nile, Egypt: Potential health risks assessment. Journal of Toxicology and Environmental Health, Part A 76, 1183-1187.

[24] Asante, K.A., Agusa, T., Subramanian, A., Ansa-Asare, O.D., Biney, C.A., Tanabe S. (2007). Contamination status of arsenic and other trace elements in drinking water and residents from Tarkwa, a historic mining township in Ghana. Chemosphere 66, 1513-1522.

[25] Pizarro, J., Vergara, P.M., Rodríguez, J.A., Valenzuela, A.M. (2010) Metals in northern Chilean rivers: Spatial variation and temporal trends. Journal of Hazardous Materials 181, 747–754

[26] WHO. (2006). Guidelines for drinking-water quality, third ed., World Health Organization, Geneva.

[27] EPA (Environmental Protection Agency, US). (2012). Edition of the drinking water standards and health advisories.

[28] MOH (Ministry of Health, China). (2007). Standards for drinking water quality (GB5749-2006).

[29] Velma, V., Vutukuru, S.S., Tchounwou, P.B. (2009). Ecotoxicology of hexavalent chromium in freshwater fish: a critical review. Reviews on Environmental Health 24, 129-145.

[30] Kuykendall, J.R., Miller, K.L., Mellinger, K.N., Cain, A.V. (2006). Waterborne and dietary hexavalent chromium exposure causes DNA-protein crosslink (DPX) formation in erythrocytes of largemouth bass (*Micropterus salmoides*). Aquatic Toxicology 78, 27-31.

[31] Sadeghi, P., Savari, A., Movahedinia, A., Safahieh, A., Ajdari, D. (2014). An assessment of hematological and biochemical responses in the tropical fish *Epinephelus stoliczkae* of Chabahar Bay and Gulf of Oman under chromium exposure: ecological and experimental tests. Environmental Science and Pollution Research 21, 6076-6088.

[32] Bai, J., Cui, B., Chen, B., Zhang, K., Deng, W., Gao, H., Xiao, R. (2011) Spatial distribution and ecological risk assessment of heavy metals in surface sediments from a typical plateau lake wetland, China. Ecological Modelling 222, 301-306.

[33] Klavinš, M., Briede, A., Rodinov, V., Kokorite, I., Parele, E., Klavina, I. (2000). Heavy metals in rivers of Latvia. Science of the Total Environment 262, 175-183.

[34] Guéguen, F., Stille, P., Lahd Geagea, M., Perrone, T., Chabaux, F. (2012). Atmospheric pollution in an urban environment by tree bark biomonitoring–Part II: Sr, Nd and Pb isotopic tracing. Chemosphere 86 641-647.

[35] Wu, S., Xia, X., Lin, C., Chen, X., Zhou, C. (2010) Levels of arsenic and metals in the rural soils of Beijing and their changes over the last two decades (1985–2008). Journal of Hazardous Materials 179, 860–868.

[36] Chen, J., Liu, G., Kang, Y., Wu, B., Sun, R., Zhou, C., Wu, D. (2013). Atmospheric emissions of F, As, Se, Hg, and Sb from coal-fired power and heat generation in China. Chemosphere 90, 1925-1932.

[37] Luo, C., Liu C., Wang, Y., Liu, X., Li F., Zhang, G., Li, X. (2011) Heavy metal contamination in soils and vegetables near an e-waste processing site, south China. Journal of Hazardous Materials 186, 481–490.

[38] Smith E, Naidu R, Alston AM. Arsenic in the soil environment: A review. Advance in Agronomy, 1998, 64:149- 195

[39] Abreu, P. L., Ferreira, L. M. R., Alpoim, M. C., Urbano, A. M. (2014) Impact of hexavalent chromium on mammalian cell bioenergetics: phenotypic changes, molecular basis and potential relevance to chromate-induced lung cancer. BioMetals 27, 409-443.

Received: **10.12.2014**
Accepted: **12.04.2016**

CORRESPONDING AUTHOR

Jianfeng Zhang
National Engineering Laboratory for Improving Quality of Arable Land, Institute of Agricultural Resources and Regional Planning, Chinese Academy of Agricultural Sciences, Beijing 100081, China

E-mail: zhangjianfeng@caas.cn

© by PSP Volume 25 – No. 10/2016, pages 3847-3858 Fresenius Environmental Bulletin

THE IMPACT OF LAND-USE CHANGE ON MONTHLY VARIATION OF SOIL NITROGEN IN AN AGRICULTURAL REGION AT MID-HIGH LATITUDE

Linna Wu[1, 2], Shengtian Yang[1], Changsen Zhao[1*], Fanghua Hao[3], Guotao Dong[4], Yongan Yang[5], Zhiwei Wang[1], Hezhen Lou[1]

[1] State Key Laboratory of Remote Sensing Science, School of Geography, Beijing Normal University, Beijing Key Laboratory for Remote Sensing of Environment and Digital Cities, Beijing 100875, China
[2]College of Resource and Environment Engineering, Guizhou University, Guizhou, Guiyang, 550025, China
[3] State Key Joint Laboratory of Environmental Simulation and Pollution Control, School of Environment, Beijing 100875, China
[4]Yellow River Institute of Hydraulic Research, Zhengzhou 450003, China
[5]Agricultural Technology Promotion Center of Bawujiu Farm, Jiansanjiang Administration of the Agricultural Reclamation of Heilongjiang Province, Heilongjiang, Jiansanjiang, 156326, China

ABSTRACT

An understanding of the monthly variation of total soil nitrogen (TN) and ammonium nitrogen ($N\text{-}NH_4^+$) content under different types of land-use change is crucial to sustainable agricultural management, yet few studies have investigated this process at mid-high latitudes. In order to examine this, we compared the monthly variation of TN and $N\text{-}NH_4^+$ content for land that had undergone different land-use changes in a typical mid-high latitude agricultural region in Northeast China. The study was based on an ecohydrological model (EcoHAT). The model was forced by multi-source remote sensing data and validated using 106 soil samples collected from in-situ sites. The region was classified into seven land-use types, four of which were converted and three of which were unconverted. The converted types included dry land to paddy field (D2P), wetland to dry land (W2D), wetland to paddy field (W2P), and forest to dry land (F2D). The unconverted types included permanent dry land (D2D), permanent wet land (W2W), and permanent forest land (F2F). Results revealed the following: (1) the monthly increment rate of TN and $N\text{-}NH_4^+$ for converted land-use types was greater than for unconverted land-use types in a given month; (2) during the change period, the increment rate of TN for D2P from April to August was the highest of the all land-use types, and the increments and decrements of $N\text{-}NH_4^+$ in D2P were the highest for any land-use change from April to July and from July to October, respectively; and (3) the TN level decreased with the exception of W2D, while the $N\text{-}NH_4^+$ level increased after agricultural expansion. The rate of TN in D2P was clearly lower than 10.0% in April and was 8.5% in August compared to that of permanent dry land, while the increment rates of monthly $N\text{-}NH_4^+$ in F2D compared with F2F were 41.7% in April, 127.6% in July, and 97.6% in October, which was higher than for D2P (compared to D2D) and W2D and W2P (compared to W2W). These comparisons provided important new evidence of demonstrating the beneficial effects of sustainable agricultural development in mid-high latitude agricultural regions.

KEYWORDS:
Land use change; total soil nitrogen; soil ammonium nitrogen; mid-high latitude agricultural region

INTRODUCTION

With an increasing global population, food production is now a major concern of governments worldwide, and is especially so in China, which has the world's largest population [1]. To increase food production and meet the needs of a growing population, fertile natural land has been converted into farmland, while dry land has been converted into paddy fields, and these have become the dominant approaches in agricultural development worldwide. These methods have also brought about land-use changes that have caused significant spatial and temporal heterogeneity of soil nitrogen [2][3][4]. Variations in soil nitrogen and soil degradation arising from land-use changes may threaten future soil nutrients [5]; therefore, the character of land-use changes and soil nitrogen variations during agricultural cultivation have the potential to significantly impact food productivity

and sustainable development in agricultural regions [6]. It is thus necessary to understand the variations in soil nitrogen in the context of land-use change to ensure sustainable agricultural practices.

One important research concern has been the effect of temperature changes on the dynamics and variation of regional soil nitrogen in different climate zones [7] [8]. Koch [9] investigated the temperature sensitivity of nitrogen mineralization in three seasons (summer, autumn, and winter) and found that N mineralization showed temperature dependence above 0° in the Austrian alpine zone. Delgado-Baquerizo et al. evaluated the response of soil nitrogen dynamics to changes in temperatures under biological soil crusts in a semi-arid ecosystem [10], and Yun et al. [11] conducted a batch aerobic incubation with a sandy loam soil over 150 days at three different soil temperatures (10°C, 20°C, and 30°C) and indicated that net nitrification rate increased with increasing soil temperature in a middle latitude region. However, few researchers have investigated how the soil nitrogen cycle responds to temperature changes under different land uses. W.R. Cookson et al. clarified the mechanisms of short-term (2-weeks) nitrogen (N) cycling in forests, grassland, and arable soils in agricultural regions at high latitudes [12].A comparative study tested the long- and short-term temperature responses of soil nitrogen cycling in forest soils [13]. Furthermore, there is a large difference between the coldest month and the hottest month, and soil freeze-thaw processes often occur at middle and high latitudes, resulting in soil nitrogen transformation that is significantly different from low-latitude regions [14]. Since few researchers have considered the monthly variation of soil nitrogen at mid-high latitudes, it is important to investigate this in the context of land use change at middle and high latitudes.

Soil nitrogen limits photosynthesis and the primary production process of plants and thus impacts food production. Total soil nitrogen (TN) in surface soil is composed of inorganic nitrogen ($N\text{-}NH_4^+$ and $N\text{-}NO_3^-$) and organic nitrogen. In contrast to NH_4^+ ions, NO_3^- ions are generally not adsorbed into the negatively charged colloidal clay. Therefore, nitrate ions are mobile in the soil and are readily leachable into the water system [11], while $N\text{-}NH_4^+$ is readily absorbed into soil particle surfaces or fixed by soil mineral substances. For this reason, the level of total soil nitrogen and ammonium nitrogen ($N\text{-}NH_4^+$) is one of the most important indicators of soil fertility. Moreover, land-use changes cause temporal and spatial variations in fertilizer application, which lead to changes in the dynamics and variation of TN and $N\text{-}NH_4^+$. It is therefore important to look at the characteristics of TN and $N\text{-}NH_4^+$ in the context of land-use change, which can provide a basis for agriculture and land-use management and can improve the level of crop production in the case of land reclamation.

A number of studies have focused on the characteristics of TN and $N\text{-}NH_4^+$ in the context of land-use change. Some studies have found that the content of TN increases with changes in land use. The TN for tilled pasture has been found to be 51% higher than for natural pasture [15][16], and the content of total nitrogen (TN) was found to increase when land use went from irrigated farmland to vegetable land [4]. The amount of total nitrogen (TN) in wetland is significantly higher than in cultivated wetland [14][17]. In addition, the conversion of cropland to grassland has been found to contribute to TN sequestration [18], and the concentration of soil ammonium nitrogen ($N\text{-}NH_4^+$) in shrub land was higher than in farmland [19]. But other studies have confirmed that land reclamation reduces TN [20][21]. TN has suffered significant losses in reclaimed agricultural land compared to original forest in the semi-arid tropics [22], and Beheshti found that the stock of TN on 0-40 cm decreased 29% when forests were converted for rice cultivation [23]. The amount of TN and available nitrogen was found to decrease after transforming dry land to paddy field or forest to dry land [14]. Most current research, however, has focused on either comparing the TN and $N\text{-}NH_4^+$ content of different land-use types or on the average annual variation of TN and $N\text{-}NH_4^+$over a long period of land-use change, but few have studied the monthly variation of TN and $N\text{-}NH_4^+$ within a year of land-use change, and almost none have studied this in agricultural regions at mid-high latitudes.

In this paper, we compare the monthly TN and $N\text{-}NH_4^+$content for converted and unconverted land use, particularly in agricultural regions at mid-high latitudes. We use the comparison to: 1) identify the monthly variation for TN and $N\text{-}NH_4^+$; 2) clarify the variation for monthly TN and $N\text{-}NH_4^+$ during the crop growth season; and 3) examine the variation of TN and $N\text{-}NH_4^+$ after agricultural expansion in a given month in order to provide effective information of variation in monthly soil fertility for sustainable agricultural management.

METHODS AND MATERIALS

Study area. The Bawujiu Farm, located in the northeastern Sanjiang Plain in China, is a typical agricultural region at mid-high latitude (Fig.1). The farm has an area of 1350 km^2. It is in a region with a temperate monsoon climate, with a mean annual temperature of 2.9°C and an average frost-free period of 138 days [6][14]. Water and soil in the

wetlands freeze completely from late October to early April of the following year, and the highest temperatures are found in July [24]. Mean annual precipitation is 600 mm. Many of its wetlands and forests have been reclaimed as farmland, dry land has been converted to paddy fields, and the degree of land reclamation has rapidly intensified since 2000 with the increased use of fertilizer. In light of this, the effect of land-use change on the variation in TN and N-NH_4^+ has been the subject of intense study since 2000, with the goal of protecting food safety and providing a basis for future land-use management practices and agricultural management at mid-high latitudes.

Methodologies. EcoHAT-N model. A novel model for soil nitrogen simulation (named EcoHAT-N) was developed and integrated into the EcoHydrological Analysis Tool (EcoHAT) [25][26][27][28][29][30][31] for the present study. EcoHAT-N is a distributed model based on pixel calculation; we used it to calculate daily TN and N-NH_4^+ from 2000 to 2010. The EcoHAT-N framework is shown in Figure 2.

Soil Nitrogen Cycle in EcoHAT-N. Four soil N-cycle processes are considered in EcoHAT-N: nitrification, ammonia volatilization, denitrification, mineralization, and decomposition.

Nitrification was calculated as follows [32][33]:

$$N_{nit/vol,l} = NH_{4,l}^{+} \cdot \left(1 - \exp\left[-\eta_{nit,l} - \eta_{Vol,l}\right]\right) \quad (1)$$

$$N_{nit,l} = [1-\exp(-\eta_{nit,l})]/[1-\exp(-\eta_{nit,l})+1-\exp(-\eta_{Vol,l})] \times N_{nit/vol,l} \quad (2)$$

$$N_{vol,l} = [1-\exp(-\eta_{vol,l})]/[1-\exp(-\eta_{nit,l})+1-\exp(-\eta_{Vol,l})] \times N_{nit/vol,l} \quad (3)$$

where $N_{nit/vol,l}$, is the amount of ammonium converted via nitrification and volatilization in layer l, $\eta_{nit,l}$ is the nitrification regulator, $\eta_{vol,l}$ is the volatilization regulator, $N_{nit,l}$ is the amount of nitrogen removed from NH_4^+ to NO_3^- in layer l, $N_{vol,l}$ is the amount of nitrogen converted from NH_4^+ to NH_3 in layer l, and layer l is 0-20 cm of surface soil.

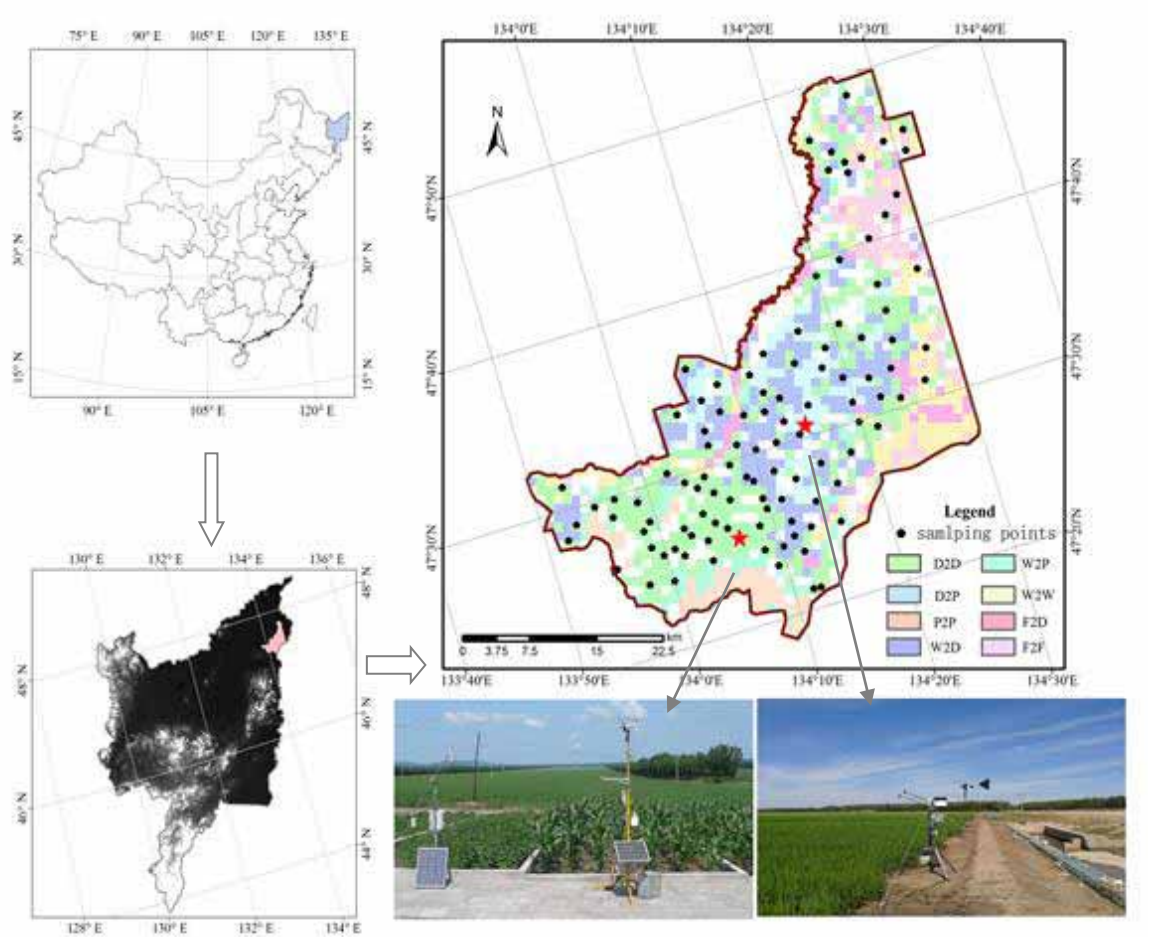

FIGURE 1
Location of study area and distribution of sampling points

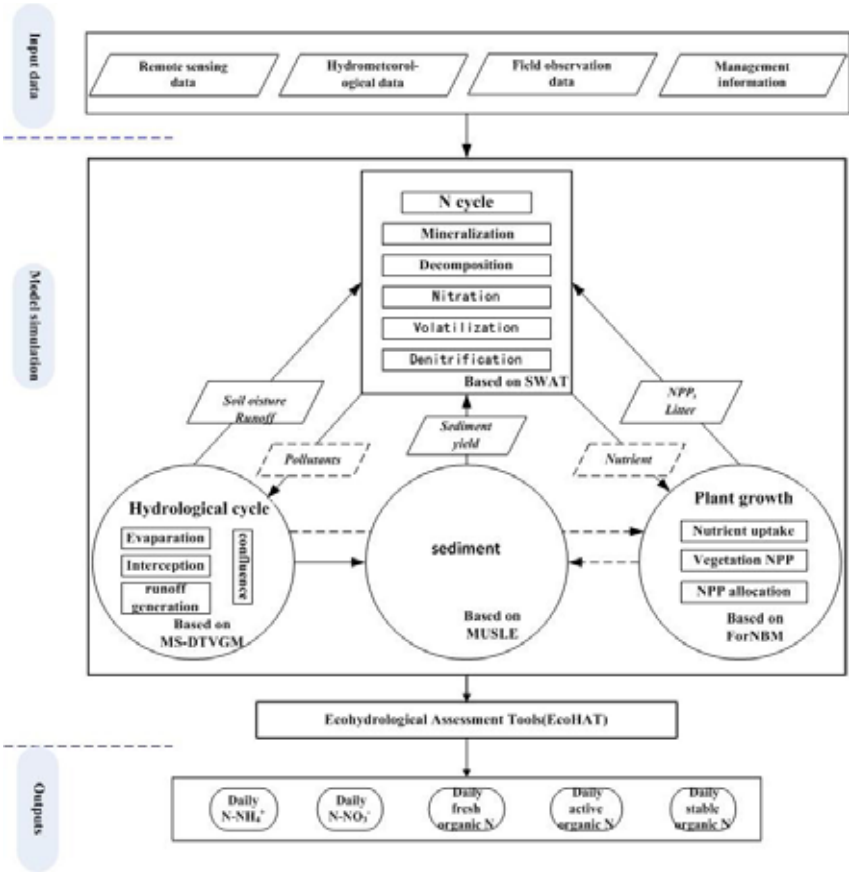

FIGURE 2
Modified from the framework of EcoHAT [31]

Denitrification was calculated as follows [34]:

$$N_{denit,\,l} = \begin{cases} NO3_l \cdot \left(1 - \exp\left\lfloor -\beta_{denit} \cdot \gamma_{tmp,\,l} \cdot orgC_l \right\rfloor\right), & \gamma_{sw,\,l} \geq \gamma_{sw,\,thr} \\ 0, & \gamma_{sw,\,l} < \gamma_{sw,\,thr} \end{cases} \quad (4)$$

where $N_{denit,l}$ is the amount of nitrogen lost to denitrification (kg N/ha), $NO3_l$ is the amount of nitrate in a layer l (kg N/ha), β_{denit} is the rate coefficient for denitrification (β_{denit}= 0.2 in this study), $\gamma_{tmp,l}$ is the nutrient cycling temperature factor for layer l, $\gamma_{sw,\,ly}$ is the nutrient cycling water factor for layer l ($\gamma_{sw,l}$=1.1 in this study), and $\gamma_{sw,thr}$ is the threshold value of the nutrient cycling water factor at which denitrification can occur.

Mineralization and decomposition were calculated as follows [35]:

$$N_{\min a} = \beta_{\min} \cdot orgN_{act} \cdot (\gamma_{tmp} \cdot \gamma_{sw})^{1/2} \quad (5)$$

$$N_{\min f} = 0.8 \cdot \delta_{ntr} \cdot orgN_{frsh} \quad (6)$$

$$N_{dec} = 0.2 \cdot \delta_{ntr} \cdot orgN_{frsh} \quad (7)$$

where $N_{mina,l}$ is the nitrogen mineralized from the humus active organic N pool(kg N/ha), β_{min} is the rate coefficient for mineralization of the humus active organic nutrients (β_{min}=0.003 in this study), $\gamma_{tmp,l}$ is the nutrient cycling temperature factor for layer l, $\gamma_{sw,l}$ is the nutrient cycling water factor for layer l ($\gamma_{sw,l}$=1.1 in this study), $org_{Nact,l}$ is the amount of nitrogen in the active organic pool (kg N/ha), $N_{minf,l}$ is the nitrogen mineralized from the fresh organic N pool (kg N/ha), $\delta_{ntr,l}$ is the residue decay constant rate, $orgN_{frsh,l}$ is the nitrogen in the fresh organic pool in layer l (kg N/ha), and $N_{dec,l}$ is the nitrogen decomposed from the fresh organic N pool (kg N/ha).

Hydrological, sediment, and plant-growth processes in EcoHAT-N. Nitrogen in soil moves and transforms along with water and sediment in the process of plant growth. In the EcoHAT-N, the hydrological process was simulated by MS-DTVGM and forced by remote sensing data [36], which calculated soil moisture, surface runoff, interflow, and leakage in soil for which the loss of nitrogen could be estimated. For sediment, the Modified Universal Soil Loss Equation (MUSLE) [37] was used to estimate the loss of nitrogen along with soil erosion. During the plant-growth process, three aspects of productivity (accumulation, productivity allocation, and nutrient uptake) were calculated following the research of Wang et al. [29] and were used to estimate the daily amount of nitrogen uptake.

TABLE 1
Area of land-use change and measured TN content

Land-Use Type	Description	Land Use （2000）	Current Land use （2010）	Pixels	Area(ha)	Samples	TN(t/ha)
Unconverted	D2D	Dry land	Dry land	350	35000	49	6.7±1.6
	W2W	Wetland	Wetland	90	9000	4	11.8±3.6
	F2F	Forest	Forest	61	6100	1	5.2
Converted	D2P	Dry land	Paddy field	234	23400	40	7.2±2.3
	W2P	Wetland	Paddy field	62	6200	2	9.5±2.0
	W2D	Wetland	Dry land	140	14000	9	9.3±4.0
	F2D	Forest	Dry land	61	6100	1	7.4

The TN column was the mean ±SE (standard error) of TN content

.

The experiment for validation of EcoHAT-N. To verify the result of the simulation with EcoHAT-N, 106 sampling points were located randomly with the spatial distribution of seven types of land-use change. In order to establish the spatial relationship between the simulation results and measured index of the soil nitrogen content, the distance between any two sampling points was 1000 m. The distribution of sampling points is shown in Figure 1. Soil samples were collected for seven types of land-use change from late April to early May. The eight land-use types were divided into two categories: (1) unconverted land use: 49 points in D2D, 4 points in W2W, and 1 point in F2F; (2) converted land use: 40 points in D2P, 2 points in W2P, 9 points in W2D, and 1 point in F2D (Tab.1).

During sampling it was apparent that the soils that clearly had been disturbed by human activities were abandoned, such as soils distributed on farmland ridges, beside roads, or near farmhouses. At each soil sampling point, five samples were collected and then mixed together to obtain one final sample, which was then placed into a sealed plastic bag. All soil samples were air-dried at 25.8°, cleaned of plant residue, ground so that they could pass through a 2 mm nylon sieve, and then stored in plastic bags. Soil TN was measured with a CHN Elemental Analyzer (EurovectorEA3000; EuroVectorSpA, Milan, Italy; dry combustion temperature, 900°). The statistical results of soil TN for different land-use changes are listed in Table 1.

The model simulation of soil TN content was compared to measured results of the same soil type. There were nine soil types in the study area: planosol, meadow Planosol, gley planosol, alluvial soil, dark brown soil, marsh soil, gley meadow soil, loamy meadow soil, and swamp soil. The simulation results and measured results were extracted with an overlaying soil map, and the simulated average value of soil TN and the measured average value in the same soil type were calculated. The R^2 of the simulated results and measured soil TN was 0.718 (Fig.3), confirming the credibility of EcoHAT-N.

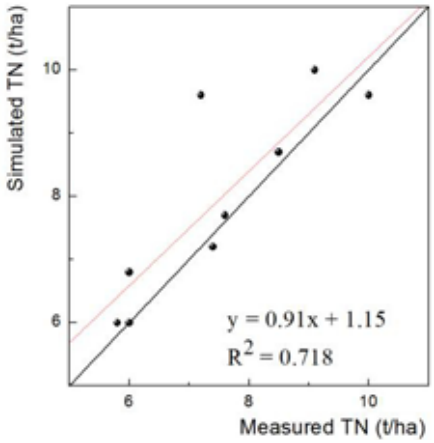

FIGURE 3
Correlation of simulated TN content and measured data for soil type

Note: the red line is fitting line and the black line is 1:1 line.

Observation method. The Bowen ratio flux measurement system and Zeno were set up to automatically measure (Fig.1), calculate, and store data, which included sensible heat flux, latent heat flux, water vapor flux and other surface and atmosphere exchange fluxes, precipitation, wind speed, soil moisture, and surface temperature. The observations were used for validation of the remote sensing dataset.

Datasets. Input datasets for EcoHAT-N included remote sensing data, hydrometeorological data, field observations, and management information. Remote sensing data were used

TABLE 2
The input datasets of EcoHAT-N

Input datasets	Data type	Revolution	Data resource	Processing method
Remote sensing data	Air temperature	1km	GLDAS	IDL
	Wind speed	1km	GLDAS	IDL
	Net radiation	1km	GLDAS	IDL
	Specific humidity	1km	GLDAS	IDL
	topography	90m	ASTER-GDEM	Image resample
	Land use	30m	Landsat-TM	Artificial visual interpretation and resample
	Vegetation cover	-	-	Remote sensing inversion[43]
	Root depth	-	-	Remote sensing inversion[44]
	LST	1km	MODIS	MRT tool
	Leaf area index	1km	MODIS	MRT tool
	Photosynthesis radiation absorption ratio	1km	MODIS	MRT tool
	Snow cover	1km	MODIS	MRT tool
Hydrometeorological data	precipitation	-	-	Spatial interpolation
Field observation data	soil moisture	-	Second National Soil Survey	IDL
	soil bulk density	-		IDL
	PH	-		IDL
	Leaf biomass per unit area	-		IDL
	The amount of N fertilizer	-		IDL
Management information	The application time of N fertilizer	-	Gathered in Bawujiu Farm	IDL
	The main crop type	-		IDL

primarily to retrieve daily land surface information, and were obtained from public free data platforms (http://www.usgs.gov/pubprod/).
Hydrometeorological data mainly included daily precipitation data obtained from the China meteorological science data sharing service (http://data.cma.cn/). Field observation data derived from the Second National Soil Survey, consisted of soil moisture, soil bulk density, pH, and leaf biomass per unit area. All the input data were processed into image format, the same spatial resolution (1km*1km), and a uniform projection and coordinate system.

Remote sensing data contained TM data, GLDAS, MODIS, and remote sensing inversion data. TM data were used to identify the main types of land-use transformations from 2000 to 2010. These were classified into one of two categories: converted or unconverted. The converted types included dry land to paddy field (D2P), wetland to dry land (W2D), wetland to paddy field (W2P), and forest to dry land (F2D). The unconverted types included permanent dry land (D2D), permanent wetland (W2W), and permanent forest (F2F). The areas of dry land converted to paddy field (D2P), wetland to dry land (W2D), and wetland to paddy field (W2P) were 234.0 km^2, 140.0 km^2, and 62.0 km^2, respectively, and were all located in areas with no terrain change, with the exception of forest converted to dry land (F2D) located in lower-slope hills (< 2°).

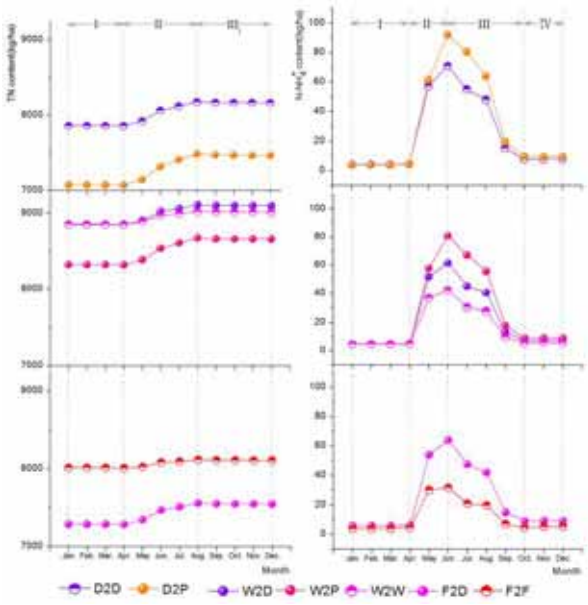

FIGURE 4
Variation of monthly TN and N-NH_4^+content for different types of land-use change

Management information was gathered by the agricultural technology promotion center of the Bawujiu Farm. The average amount of N fertilizer applied was 343.5 kg·ha^{-1}·y^{-1}on dry land and 585 kg·ha^{-1}·y^{-1}on paddy fields; the fertilizer was applied at the end of May and the end of June on dry land and at the end of May, June, and July on paddy fields. Soybean was the main crop on dry land and rice was the main crop on paddy fields. The growth season of the two crops was from April to October.

All input data and processing methods are listed in Table 2.

RESULTS AND DISCUSSION

Response of monthly TN under different types of land-use change. Greater rate of increase for the monthly TN content for converted land use. According to Fig.4 and Tab.3, from April to August, the monthly TN content for all land-use types ranged from 7.1 t/ha (D2P in April) to 9.1 t/ha (W2D in August) and increased each month. The monthly growth rates of TN for D2P, W2D, W2P, and F2D were higher than D2D, W2W, W2W, and F2F, respectively. The amount of monthly TN for D2P was 7.2 t/ha in May and 7.3 t/ha in June (Tab. 3), and the monthly growth rate of 2.39% was higher than for those in other land-use change types from May to June. From January to April, the monthly TN for different types of land-use changes was similar and stable,

TABLE 3
Simulated monthly TN and N-NH_4^+content for different types of land-use change

Land-use Change	TN(t/ha)					N-$NH4^+$(kg/ha)						
	Apr.	May	Jun.	Jul.	Aug.	Apr.	May	Jun.	Jul.	Aug.	Sep.	Oct.
D2D	7.9	7.9	8.1	8.1	8.2	4.4	57.3	70.9	55.1	48.1	15.0	7.7
D2P	7.1	7.2	7.3	7.4	7.5	4.2	61.6	92.1	80.6	64.0	19.4	9.7
W2D	8.8	8.9	9.0	9.0	9.1	4.9	51.7	61.5	44.9	40.5	13.3	7.2
W2P	8.3	8.4	8.5	8.6	8.7	4.8	57.8	80.7	67.1	55.6	17.6	9.0
W2W	8.9	8.9	9.0	9.0	9.0	4.9	36.9	42.2	30.4	27.8	9.6	5.5
F2D	7.3	7.3	7.5	7.5	7.6	6.3	54.0	64.0	47.6	42.0	14.8	8.9
F2F	8.0	8.0	8.1	8.1	8.1	4.4	30.2	31.7	20.9	19.7	7.0	4.5

Values in the table are the means of monthly TN and N-NH_4^+ content. D2D: permanent dry land, D2P: dry land to paddy field, W2D: wetland to dry land, W2P: wetland to paddy field, W2W: permanent wetland, F2D: forest to dry land, and F2F: permanent forest land from 2000 to 2010.

TABLE 4
Variation and rate of monthly TN and N-NH_4^+ for different types of land-use change

The Index Land-use Change	TN (from April to August)		N-NH_4^+ (from April to June)		(from June to October)	
	Increments (kg/ha)	Rate of Increase (%) ①	Increments (kg/ha)	Rate of Increase (times)②	Decrements (kg/ha)	Rate of Decrease (%)③
D2D	319.9	4.1	66.5	15.09	63.2	89.09
D2P	412.0	5.8	87.9	21.1	82.4	89.52
W2D	264.7	3.0	56.6	11.56	54.3	88.29
W2W	172.0	1.9	37.3	7.57	36.8	87.07
W2P	355.0	4.3	76.0	15.95	71.7	88.8
F2D	273.6	3.8	57.8	9.23	55.1	86.04
F2F	106.3	1.3	27.3	6.18	27.2	85.74

①was calculated by (TN on August – TN on April)/TN on April; ② was calculated by (N-NH_4^+on June –N-NH_4^+ on April)/N-NH_4^+ on April; ③was calculated by (N-NH_4^+on October –N-NH_4^+on June)/N-NH_4^+ on June.

but was also relatively higher and more stable from August to December. This was likely related to the lower air temperature in mid-high latitudes, which limited microbial activities and nitrogen accumulation [38].

The variation of monthly TN content during the increase period. According to Tab.4, the amount of increase in D2P was about 412.0 kg/ha, and the rate of increase from April to August was 5.8%, the highest of the all land-use types, followed by W2P, D2D, F2D, W2D, W2W, and then F2F, indicating that the rate of increase for converted land was higher compared to unconverted land. Furthermore, the rate of increase for D2P was higher than for W2P, while the rate of increase for F2D was higher than for W2D.

The lower level of monthly TN content for converted land-use types. According to Fig.5 and Tab.5, the monthly TN levels for converted land-use types (D2P, W2P, F2D) were much lower than those for the original land-use type (D2D, W2W, F2F) in a given month, with the exception of W2D. The decrement rates for D2P, W2P, and F2D in April were 10%, 6%, and 9%, respectively, which was higher than for other months; they then decreased in August to 8.5%, 3.9%, and 6.9%, respectively. There was almost no rate of change for W2D compared to W2W from April to August.

Response of N-$NH_4^+$to different types of land-use change. Increase in the monthly variation of N-NH_4^+content. From April to October, the monthly N-NH_4^+ content for all land-use types ranged from 4.2 kg/ha (D2P in April) to 92.1 kg/ha for D2P (in June). From April to June, the monthly N-NH_4^+ content for various land-use types increased each month, and decreased from July to October (Fig. 4). The amount of N-NH_4^+ content for D2P was 4.2 kg/ha in April and 61.6 kg/ha in May (Tab. 3). The monthly increment rate was 14 times faster than for those in other land-use types from April to May. While, the amount of N-NH_4^+ content for D2P was 64.0 kg/ha in August and was 19.4 kg/ha in September (Tab. 3).

TABLE 5
Change rate of monthly TN and N-NH_4^+ for converted land-use types

The Change rate of Monthly TN Content for Converted Land-use Types	TN (%)					N-NH_4^+ (%)					
	Apr.	May	Jun.	Jul.	Aug.	Apr.	May	Jun.	Jul.	Aug.	Sep.	Oct.
(D2P-D2D)/D2D	-10.0	-9.8	-9.3	-8.7	-8.5	-5.5	7.5	29.8	46.2	33.2	29.3	24.8
(W2D-W2W)/W2W	-0.1	0.1	0.6	0.8	1.0	-0.6	40.1	45.6	47.6	45.7	39.5	31.8
(W2P-W2W)/W2W	-6.0	-5.7	-4.9	-4.3	-3.9	-3.4	56.4	91.2	120.6	99.9	83.6	65.5
(F2D-F2F)/F2F	-9.0	-8.5	-7.6	-7.2	-6.9	41.7	78.9	101.8	127.6	112.6	112.5	97.5

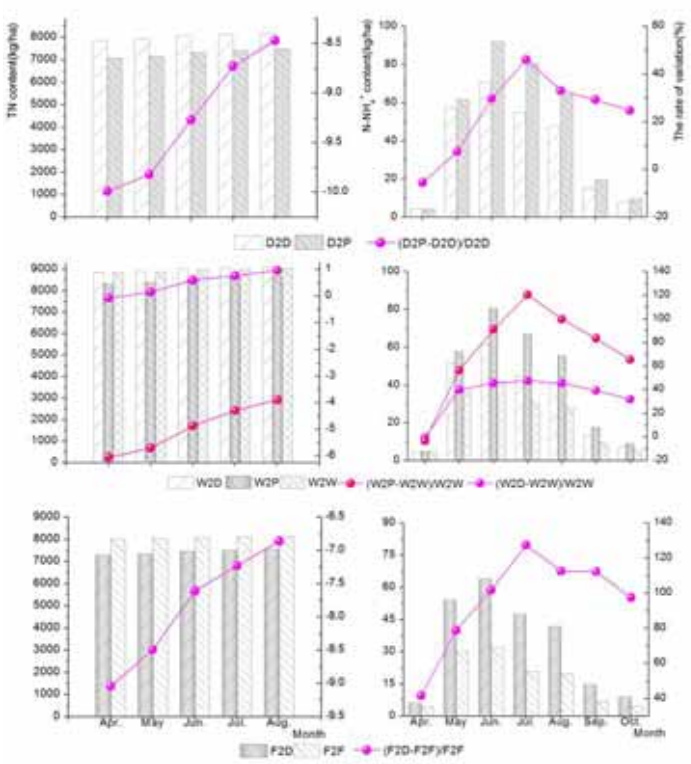

FIGURE 5
Comparison of the change rate of monthly TN and N-NH_4^+ between changed land uses and unchanged land uses

The monthly decrement rate of 69.63% was also higher than for other land-use type from August to September. Moreover, from January to March and from November to December, the monthly change in N-NH_4^+ for different types of land-use change was lower and more stable than from April to October.

The monthly variation of N-NH_4^+ content during the change period. According to Tab.4, from April to June, the rate of increase in converted land use was higher compared to unconverted land use, and the increment rate of 21.1% for converted dry land (D2P) was higher compared to converted wetland (W2D, W2P) and forest (F2D), permanent dry land (D2D), wetland (W2W), and forest (F2F) (Tab. 4). From July to October, the decrement rates for different land-use types were higher overall than the increment rates, but the order was similar to the increment rates among all land-use types. The increments and decrements in D2P were about 87.9 kg/ha and 82.4 kg/ha, respectively, and were the highest values for any land-use change during the increasing and decreasing periods (Tab. 4).

The higher level of monthly N-NH_4^+ content for converted land-use types. According to Fig.5, the monthly N-NH_4^+ values for D2P, W2D, W2P, and F2D were higher every month than those for D2D, W2W, W2W, and F2F, respectively, and the amount for W2P was greater each month than for W2D (Fig.5).The monthly N-NH_4^+ increment rates for D2P, W2D,W2P, and F2D compared with D2D, W2W, W2W, and F2F were respectively -5.5%, -0.6%, 3.4%, and 41.7% in April, 46.2%, 47.6%, 120.6%, and 127.6% in July, 24.8%, 31.8%, 65.5% and 97.5% in October. The monthly N-NH_4^+ increment rate in July for F2D compared with F2F was almost equal to that of W2P compared with W2W, which was significantly higher than for D2P compared with D2D, and for W2D and W2P compared with W2W (Tab.5).

Effect of N fertilizer on the variation of monthly TN for converted land-use types. In the study area, N fertilizer was applied on about 240 kg·ha^{-1} and 103.5 kg·ha^{-1} on dry land at the end of May and June, respectively, and about 240 kg·ha^{-1}, 172.5 kg·ha^{-1} and 172.5 kg·ha^{-1} on paddy fields at the end of May, June, and July, respectively. Consequently, the monthly TN for reclaimed land (W2D, W2P, and F2D) increased faster than for the original land use from April to August. Meanwhile, the amount of N fertilizer for dry land was less than that for paddy field, which led to an increase of monthly TN for dry land converted to paddy field

(D2P) from April to August. The most obvious simultaneous plant assimilation or significantly less in the same period, which led to the nitrogen accumulation in the surface soil under the current N fertilizer and planting pattern. However, a loss of TN was identified after the conversion of dry land to paddy field (D2P), wetland to paddy field (W2P), and forest to dry land (F2D) in a given month, and there was also a greater risk of soil nitrogen loss, which has been confirmed in other studies [6][39].

Response of the monthly N-NH_4^+ with temperature. In the study area, the air temperature and soil temperature significantly increased from April to July and then decreased from July to October [40]. The temporal variation of soil nitrogen is closely related to plant cycling [41] and nitrogen transformation [42], and higher temperatures could favor organic nitrogen mineralization [8]; hence, the monthly N-NH_4^+ content increased with N fertilizer application and organic nitrogen mineralization when crop-growth needs were lower from April to July, and the monthly N-NH_4^+ content decreased with temperature reduction and more crop-growth needs from July to October. The temperature did drop below 0℃ from January to March and from November to December [40] and constituted a frozen period with a dormant season. The lower air temperature in mid-high latitudes limited microbial activities and nitrogen accumulation [38]; therefore, there was little change in monthly N-NH_4^+ content.

CONCLUSIONS

Agricultural expansion resulted in changing land use in the study area from 2000 to 2010. The amount of monthly TN and N-NH_4^+ for converted land-use types increased faster in a given month than for unconverted land-use types, and the monthly increment rates of TN and N-NH_4^+ for D2P was 2.39% from May to June and 14 times higher in the period from April to May, respectively, which was higher than those in the other land-use change types. During the change period, the increment rate of TN for D2P from April to August was the highest of the all land-use types, and the increments and decrements of N-NH_4^+ in D2P was the highest amount for any land-use change from April to July and from July to October, respectively.

The monthly TN levels for converted land-use types (D2P, W2P, and F2D) were lower than the original land-use types in a given month with the exception of W2D, while the N-NH_4^+ level had increased after agricultural expansion. Compared to D2D, the rate of TN in D2P was clearly lower than 10.0% in April and 8.5% in August, while the reason for this is that there was either no increment rates of monthly N-NH_4^+ in F2D compared with F2F were 41.7% in April, 127.6% in July, and 97.6% in October; these values were significantly higher than for D2P compared with D2D, and for W2D and W2P compared with W2W.

Although agricultural expansion can increase grain production under the current fertilization system, the variation of monthly TN and N-NH_4^+ in reclaimed land presented unique characteristics compared to their original land-use types, posing a challenge for monthly agricultural management. This comparison of converted and unconverted land provides a basis for identifying the variation of soil fertility and adjusting monthly agricultural management in order to benefit the economy and environment and to encourage sustainable agricultural development in mid- high latitude.

ACKNOWLEDGEMENTS

This research was supported by the Key Program of the National Science Foundation of China (Grant Nos. 40930740), the General Program of National Natural Science Foundation of China (Grant Nos. 41271414, Grant Nos.41301496), and the Fundamental Research Funds for the Central Universities (HKY-JBYW-2013-22).

REFERENCES

[1] Dong G.T., Yang S.T., Bai J., Wang Z.W. and Zhang Y.C. (2013) Open innovation in the Sanjiang Plain: A new paradigm for developing agriculture in China. International Journal of Food, Agriculture and Environment, 11(3-4), 1108-1113.

[2] Dharmakeerthi R.S., Kay B.D. and Beauchamp E.G. (2005) Factors contributing to changes in plant available nitrogen across a variable landscape. Soil Science Society America Journal, 69(2), 453-462.

[3] Samaké O., Smaling E.M.A., Kropff M.J., Stomph, T.J. and Kodio A. (2005) Effects of cultivation practices on spatial variation of soil fertility and millet yields in the Sahel of Mali. Agriculture, Ecosystems and Environment, 109(3-4), 335-345.

[4] Kong X.B., Zhang F.R., Wei Q., Xu Y. and Hui J.G. (2006) Influence of land use change on soil nutrients in an intensive agricultural region of North China. Soil and Tillage Research, 88(1-2), 85-94.

[5] Bindraban P.S., Stoorvogel J.J., Jansen D.M., Vlaming J. and Groot J.J.R. (2000) Land quality indicators for sustainable land

management: Proposed method for yield gap and soil nutrient balance. Agriculture, Ecosystems & Environment, 81(2), 103-112.

[6] Ouyang W., Xu Y., Hao F.H., Wang X.L., Chen S.Y. and Lin C.Y. (2013a) Effect of long-term agricultural cultivation and land use conversion on soil nutrient contents in the Sanjiang Plain. Catena, 104, 243-250.

[7] Pathak H. and Rao D.L.N. (1998) Carbon and nitrogen mineralization from added organic matter in aline and alkali soils. Soil Biology and Biochemistry, 30(6), 695-702

[8] Bai J., Ouyang H., Deng W., Zhu Y., Zhang X. and Wang Q. (2005) Spatial distribution characteristics of organic matter and total nitrogen of marsh soils in river marginal wetlands. Geoderma, 124(1-2), 181-192.

[9] Koch, O., Tscherko, D. and Kandeler, E. (2007) Temperature sensitivity of microbial respiration, nitrogen mineralization, and potential soil enzyme activities in organic alpine soils. Global Biogeochemical Cycles, 21, GB4017, doi:10.1029/2007GB002983.

[10] Delgado-Baquerizo, M., Maestre, F.T. and Gallardo, A. (2013) Biological soil crusts increase the resistance of soil nitrogen dynamics to changes in temperatures in a semi-arid ecosystem. Plant Soil, 366, 35-47.

[11] Yun, S.I., Ro, H.M., Choi, W.J. and Han G.H. (2011) Interpreting the temperature-induced response of ammonia oxidizing microorganisms in soil using nitrogen isotope fractionation. Journal Soils Sediments, 11, 1253-1261.

[12] Cookson W.R., Osman M., Marschner P., Abaye D.A., Clark I., Murphy D.V., Stockdale E.A. and Watson C.A. (2007) Controls on soil nitrogen cycling and microbial community composition across land use and incubation temperature. Soil Biology and Biochemistry, 39, 744-756.

[13] Gilliam, F.S., Galloway, J.E. and Sarmiento, J.S. (2015) Variation with slope aspect in effects of temperature on nitrogen mineralization and nitrification in mineral soil of mixed hardwood forests. Candian Jouranl of Forest Research, 7(45), 958-962.

[14] Ouyang, W., Shan, Y.S., Hao, F.H., Chen, S.Y., Pu X. and Wang, M.K. (2013b) The effect on soil nutrients resulting from land use transformations in a freeze-thaw agricultural ecosystem. Soil and Tillage Research, 132, 30-38.

[15] Elljott, E.T. (1986) Aggregate structure and carbon nitrogen, and phosphorus in native and cultivated Soils. Soil Science Society of America journal, 50, 627-633.

[16] Sun, G., Wu, N. and Luo, P. (2005) Characteristics of soil nitrogen and carbon of pastures under different management in northwestern Sichuan. Acta Phytoecologica Sinica, 29(2), 304-310, in Chinese.

[17] Bai, J., Zhao, Q. and Lu, Q. (2014) Land-use effects on soil carbon and nitrogen in a typical plateau lakeshore wetland of China. Archives of Agronomy and Soil Science, 60(6), 817-825.

[18] Gelaw, A.M., Singh, B.R. and Lal, R. 2014. Soil organic carbon and total nitrogen stocks under different land uses in a semi-arid watershed in Tigray, Northern Ethiopia. Agriculture Ecosystem and Environment 188, 256-263.

[19] Xue, Z.J., Cheng, M. and An S.S. (2013) Soil nitrogen distributions for different land uses and landscape positions in a small watershed on Loess Plateau, China. Ecological Engineering, 60, 204-213.

[20] Davidson, E.A. Ackerman, I.L. (1993) Changes in soil carbon inventories following cultivation of previously untilled soils. Biogeochemistry, 20(3), 161-193.

[21] Kidron, G.J., Karnieli, A. and Benenson, I. (2010) Degradation of soil fertility following cycles of cotton–cereal cultivation in Mali, West Africa: A first approximation to the problem. Soil and Tillage Research 106(2), 254-262.

[22] Solomon, D., Lehmann, J. and Zech, W. (2000). Land use effects on soil organic matter properties 528 of chromic luvisols in semi-arid northern Tanzania: carbon, nitrogen, lignin and carbohydrates. Agriculture Ecosystem and Environment, 78(3), 203-213.

[23] Beheshti A., Raiesi F. and Golchin A. (2012) Soil properties, C fractions and their dynamics in land use conversion from native forests to croplands in northern Iran. Agriculture, Ecosystems and Environment, 148, 121-133.

[24] Yang, W.J., Cheng, H.G., Hao, F.H., Ouyang, W., Liu, S.Q. and Lin C.Y. (2012) The influence of land-use change on the forms of phosphorus in soil profiles from the Sanjiang Plain of China. Geoderma, 189-190, 207-214.

[25] Liu, C.M., Yang, S.T., Wen, Z.Q., Wang, X.L., Wang, Y.J., Li, Q. and Sheng, H.R. (2009) Development of ecohydrological assessment tool and its application. Science in China Series E: Technological Science, 52(7), 1947-1957.

[26] Wang, X.L., Yang, S.T., Mannaerts, C.M., Gao, Y.F. and Guo, J.X. (2009) Spatially explicit estimation of soil denitrification rates and land use effects in the riparian buffer zone of the large Guanting reservoir. Geoderma, 150(3-4), 240-252.

[27] Wang, X.L., Mannaerts, C.M., Yang, S.T., Gao,

Y.F. and Zheng, D.H. (2010a) Evaluation of soil nitrogen emissions from riparian zones coupling simple process-oriented models with remote sensing data. Science of the Total Environment, 408(16), 3310-3318.

[28] Wang, X.L., Yang, S.T., Mannaerts, C.M., Zeng, H.J. and Zheng, D.H. (2010b) Modeling riparian soil nitrogen removal based on a modified SWAT model coupled with remote sensing data. Sixth interactional symposium on digital earth: data processing and applications, 78411C:1-9.

[29] Wang, X.L., Wang, Q., Yang, S.T., Zheng, D.H., Wu, C.Q. and Mannaerts, C.M. (2011) Evaluating nitrogen removal by vegetation uptake using satellite image time series in riparian catchments. Science of the Total Environment, 409(13), 2567-2576.

[30] Yang, S.T., Dong, G.T., Zheng, D.H., Xiao, H.L., Gao, Y.F. and Lang, Y. (2011) Coupling Xinanjiang model and SWAT to simulate agricultural non-point source pollution in Songtao watershed of Hainan, China. Ecological Modelling, 222(20-22), 3701-3717.

[31] Lou, H., Yang, S., Zhao, C., Zhou, Q., and Bai, J., Hao, F. and Wu, L. (2015) Phosphorus risk in an intensive agricultural area in a mid-high latitude region of China. Catena, 127:46-55

[32] Reddy, K.R., Khaleel, R., Overcash, M.R. and Westerman, P.W. (1979) A nonpoint source model for land areas receiving animal wastes. I. Mineralization of organic nitrogen. American Society of Agricultural Engineers, 863-872.

[33] Godwin, D.C., Jones, C.A., Ritchie, J.T., Vlek, P.L.G. and Youngdahl, L.G. 1984. The water and nitrogen components of the CERES models. International Symposium on Minimum Data Sets for Agrotechnology Transfer. International Crops Research Institute for the Semi-Arid Tropics, 95-100.

[34] Neitsch, S.L. and Arnold, J.G., Kiniry, J.R. and Williams, J.R. (2005). Soil and water assessment tool theoretical documentation. Version 2005, Grassland, Soil and Water Research Laboratory, Agricultural Research Service, Temple, Texas, 193.

[35] Seligmand, N.G. and Van Keulen, V. (1981) PAPRAN: A simulation model of annual pasture production limited by rainfall and nitrogen. In M.J. Frissel and J.A. van Veeds. Simulation of nitrogen behaviour of soil-plant systems, Pudoc, Wageningen, 192-221.

[36] Cai, M.Y., Yang, S.T., Zeng, H.J., Zhao, C.S. and Wang, S.D. (2014) A distributed hydrological model driven by Multi-Source spatial data and its application in the Ili river basin of central Asia. Water Resources Management, 10(28), 2851-2866.

[37] Williams, J.R. and Berndt, H.D. (1977). Sediment yield prediction based on watershed hydrology. Transactions of the Asae, 20(6), 1100-1104.

[38] Bai, J., Wang, Q., Deng, W., Gao, H.F. and Tao, W.D. (2012) Spatial and seasonal distribution of nitrogen in marsh soils of a typical floodplain wetland in Northeast China. Environmental Monitoring and Assessment, 184(3), 1253-1263.

[39] Solomon, D., Lehmann, J., and Zech, W. (2000) Land use effects on soil organic matter properties of chromic luvisols in semi-arid northern Tanzania: carbon, nitrogen, lignin and carbohydrates. Agriculture Ecosystem and Environment, 78(3), 203-213.

[40] Ouyang, W., Huang, H.B., Hao, F.H. and Guo, B.B. (2013c) Synergistic impacts of land-use change and soil property variation on non-point source nitrogen pollution in a freeze–thaw area. Journal of Hydrology, 495, 126-134.

[41] Jobbágy, E.G. and Jackson, R.B. (2001) The distribution of soil nutrients with depth: Global patterns and the imprint of plants. Biogeochemistry, 53(1), 51-77.

[42] Bai, J.H., Deng, W., Zhu, Y.M. and Wang, Q.G. (2004) Spatial variability of nitrogen in soils from land/inland water ecotones. Communications in soil science and plant analysis, 35(5-6), 735-749.

[43] Nilson, T. (1971) A theoretical analysis of frequency of gaps in plant stands. Agricultural meteorology, 8(1): 25-38.

[44] Andersen, J., Dybkjaer, G., Jensen, K.H., Refsgaard, J.C. and Rasmussen, K. (2002) Use of remotely sensed precipitation and leaf area index in a distributed hydrological model. Journal of Hydrology, 264(1), 34-50.

Received: **10.11.2014**

Accepted: **15.08.2016**

CORRESPONDING AUTHOR

Changsen Zhao

State Key Laboratory of Remote Sensing Science, School of Geography, Beijing Normal University, Beijing Key Laboratory for Remote Sensing of Environment and Digital Cities, Beijing 100875,China

e-mail: zhaochangsen@bnu.edu.cn

© by PSP Volume 25 – No. 10/2016, pages 3859-3866 Fresenius Environmental Bulletin

THE INFLUENCE OF SELECTED VARIABLES ON THE PHOSPHORUS CONTENT IN BOTTOM SEDIMENTS OF THE SOLINA-MYCZKOWCE COMPLEX OF DAM RESERVOIRS

Lilianna Bartoszek*, Janusz A. Tomaszek

Rzeszów University of Technology, Department of Environmental Engineering and Chemistry, Rzeszów, Poland

ABSTRACT

The influence of selected variables on the content of phosphorus in the bottom sediments of Polish dam reservoirs was assessed with the aid of simple and multiple regression analyses. Multiple regression analysis, considering the simultaneous influence of selected variables on the phosphorus content in the bottom sediments, partially confirmed the results obtained using simple regression. The model obtained shows that increase in the phosphorus content of the Solina Reservoir sediments was associated with greater aluminium and manganese contents, as well as a lowering of sediment pH. In the Myczkowce Reservoir, the sediment content of phosphorus was higher where contents of iron and organic matter were greater, as well as pH values lower. The overall multiple regression model suggests that the content of phosphorus in bottom sediments of the Solina–Myczkowce dam reservoirs was related to a significant, and positive, degree to contents of aluminium, manganese and organic matter, as well as being inversely dependent on the sediment pH.

KEYWORDS:
phosphorus content, bottom sediments, dam reservoirs, multiple regression analysis, sediment components

INTRODUCTION

Phosphorus is subject to sedimentation in forms associated with organic matter, as well as in connection with ions of iron, manganese, aluminium and calcium, and with mineral suspensions. The precipitation of phosphorus from the water column proceeds ever more easily the higher is the content of ions of the aforementioned elements in water [1, 2]. According to Clement et al. [3], the abiotic processes such as the sedimentation of inorganic molecular phosphorus, as well as the adsorption of soluble inorganic forms of phosphorus onto the surface of suspended matter and sediments are responsible for retention in a reservoir. The sorption of phosphorus on oxides and hydroxides of iron (III) resembles that of oxides and hydroxides of manganese (IV), in that it is dependent on redox processes [4, 5, 6, 7]. The role of manganese in the cycling of phosphorus is regarded as less important than those of iron or aluminium, because this element is generally recorded in only small amounts in sediments [8]. Oxides of iron and compounds of aluminum have the capacity to form complexes with organic matter, especially humus compounds. A high content of Fe and Al in humus lakes may have a significant influence on the sedimentation of these metals, and in connection with that the sedimentation of phosphorus [9, 10, 11]. Organic matter may impact upon the sorption of phosphates in two directions: via the sorption of phosphates or the blocking of sorption sites [12]. Changes in the content of total P in the surface layers of the sediment are thus a reflection of the intensity of retention processes, or else releasing into the water column [13].

The aim of the work described here was to assess the influence of selected variables on contents of phosphorus in bottom sediments of the Solina–Myczkowce dam reservoirs, with the aid of simple and multiple regression analysis. The bottom sediments of the Solina–Myczkowce Reservoir complex are rich in iron, aluminium and manganese, as well as relatively poor in phosphorus, calcium and organic matter [14]. Nevertheless, the high content of iron in the sediments of studied reservoirs has little effect on phosphorus content in deposits.

MATERIALS AND METHODS

Study Sites. The Solina Reservoir is the largest (in terms of volume) and also the deepest dam reservoir in Poland. Along with the Myczkowce Reservoir, it falls within an enterprise known as the Zespół Elektrowni

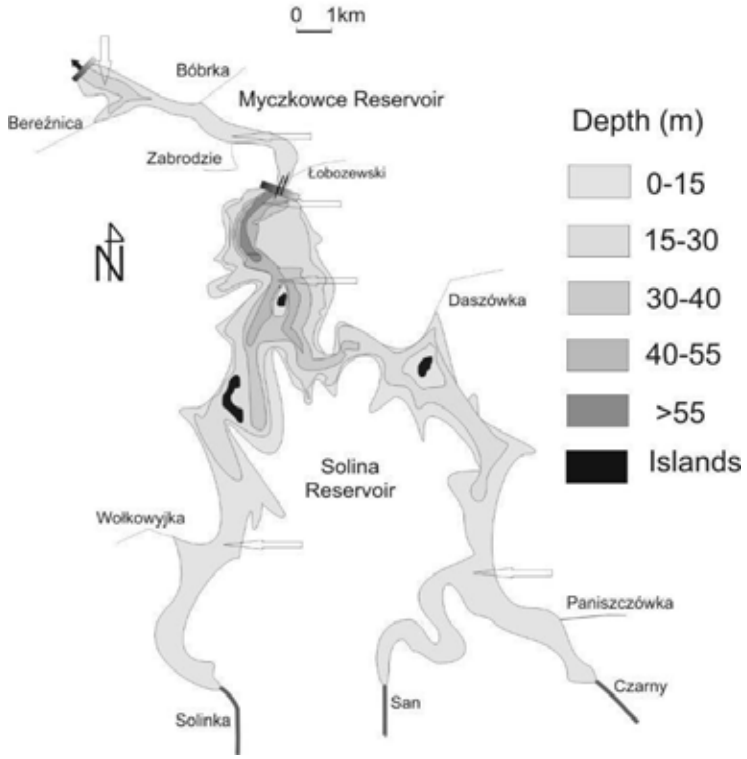

FIGURE 1
Distribution of measurement points in the Solina-Myczkowce Reservoirs

Wodnych Solina-Myczkowce S.A. The Myczkowce Reservoir in fact serves as the top-up reservoir for the operation of a pump storage power station. Solina and Myczkowce are thus two quite different bodies of water in terms of their morphometric parameters (Table 1). The main inflow into the Myczkowce Reservoir involves the waters of the River San (to the tune of more than 90%), originating from the hypolimnion of the Solina Reservoir [15]. The basin of the Solina-Myczkowce Reservoirs is mainly forest land with only limited settlement or agricultural use. Tourist and settlement infrastructure is mainly located in the near-confluence areas of tributaries and in the basin areas immediately around the bodies of water.

TABLE 1
Morphometric characteristics of the Solina-Myczkowce complex of dam reservoirs

Feature	Solina Reservoir	Myczkowce Reservoir
Area [km^2]	22	2
Maximum volume [M m^3]	502	10
Average (max.) depth [m]	22 (60)	5 (15)
Catchment area [km^2]	1174	1248
Water retention time [d]	214	4

Sediment Sampling and Analyses. Samples of bottom sediments were taken from four sites in the Solina Reservoir (depth from 14 to 55 m), as well as two sites in the Myczkowce Reservoir (3 and 11 m depth) (Fig. 1), once or twice a month in the May-November periods of two successive years 2005-2006 (16 series in all except two sites with 15 series). The 0-5 cm superficial layer was taken for analysis, averages being calculated for three sediment cores sampled with a gravity corer. Interstitial water was separated off by means of centrifugation (at 4000 revs/min). The sediment obtained in this way was air-dried at room temperature and then at 60°C, before being ground up precisely and sieved. The fraction with the < 0.9 mm grain size was retained for study in sealed PE bags in a dark place and at a temperature of 4°C. The bottom sediments were then mineralised in concentrated nitric acid HNO_3 (microwave digestion method at high pressure 2-4.5 MPa - UniClever II Plazmatronika).

The analyses of the studied variables in the mineralisates mainly made use of colorimetric methods, i.e. PN-EN 1189:2000 (for phosphorus), PN-ISO 6332:2001 (iron), DIN ISO 10566E30 (aluminium) and DIN 38406E2 (manganese). Colorimetric determinations were performed using an Aquamate spectrophotometer (from Thermo Spectronic, United Kingdom). The content of calcium in mineralisates was determined by means of AAS (Perkin Elmer, AAnalyst 300). Organic matter content in sediments was determined by roasting at a temperature of 550°C for 4 h. The pH of sediments (pH_{KCl}) was determined

potentiometrically in a colloidal suspension of 1 mol dm^{-3} KCl. The water content of sediments (W_o) was determined by drying at a temperature of 105°C to constant weight of sediment. Within a given sample there were three replicates for each determination, the mean value of three results not differing from the lowest result by more than 10% being noted.

The influence of selected variables on the phosphorus content in bottom sediments of the dam reservoirs was then assessed using simple and multiple regression analysis, with the significance level set at 0.05 [14, 16].

RESULTS AND DISCUSSION

Variability of the Total Phosphorus Concentrations – Simple Regression Analysis. The high contents of iron, aluminium and manganese in deposits are suggestive of a considerable influence of these elements on the processes of the sedimentation and deposition of phosphorus in the bottom sediments of the Solina–Myczkowce dam reservoirs (Table 2). There were no significant correlation between total phosphorus content in deposits and the measured parameters concentrations in the water of the studied reservoirs [14].

The studies have shown that superficial sediment nutrient concentrations are generally not significantly correlated with lake water quality across a range of lakes with a wide variety of trophic states [17].

Analysis of the statistically significant correlations between total P content and selected variables characterising deposits (Fig. 2a-d) revealed that the content of total P in the Solina Reservoir sediments could have been influenced (via a positive relationship) by the contents of aluminium, iron and manganese, as well as to a lesser extent by the content of organic matter (with a lower value for the correlation coefficient) (Table 3). In the sediments of the Myczkowce Reservoir it was possible to note a more significant (positive) influence on the

TABLE 2

Contents of total phosphorus ($P_{tot.}$), iron, aluminium, manganese and calcium [mg·g^{-1} of d.w.], and organic matter (OM) [%] in bottom sediments of the Solina – Myczkowce Reservoirs, as well as water content of deposits (W_0) [%] and sediment pH

		P_{tot}	Fe	Al	Mn	Ca	OM	W_0	pH_{KCl}
		[mg $g^{-1}$of d.w.]					[%]	[%]	[pH]
Solina n = 63	mean	0.846	43.3	38.8	2.40	9.93	8.59	65.9	6.80
	median	0.873	44.7	38.3	2.17	9.00	8.63	67.2	6.71
	minimum	0.650	26.2	31.0	1.01	3.79	6.98	52.6	5.89
	maximum	1.014	49.2	48.4	4.48	23.8	9.89	77.2	7.7
	SD	0.11	4.1	4.4	0.9	4.3	0.7	6.4	0.4
Myczkowce n = 31	mean	0.813	33.0	32.0	1.36	16.7	10.7	66.5	7.14
	median	0.797	34.1	32.0	1.34	12.4	10.4	67.0	7.14
	minimum	0.665	24.5	25.1	0.78	7.03	6.03	53.1	6.47
	maximum	0.996	45.6	44.6	2.05	32.9	15.2	77.5	7.92
	SD	0.09	4.3	4.4	0.3	7.8	2.4	6.5	0.3

TABLE 3

Relationships between contents of total phosphorus (Ptot.) [mg $g^{-1}$of d.w.] and selected parameters [mg g^{-1} of d.w.; or % in the case of OM and Wo] in the bottom sediments of the Solina and Myczkowce dam reservoirs (simple regression analysis)

Solina Reservoir					Myczkowce Reservoir				
y	f(x)	Correlation	n	Significance	y	f(x)	Correlation	n	Significance
$P_{tot.}$	Al	0.61	63	< 0.001	$P_{tot.}$	Al	0.41	31	< 0.05
	Fe	0.75		< 0.001		Fe	0.66		< 0.001
	Mn	0.62		< 0.001		Mn	0.38		< 0.05
	OM	0.44		< 0.001		OM	0.64		< 0.001
	pH_{KCl}	-0.75		< 0.001		pH_{KCl}	-0.66		< 0.001
	W_o	0.74		< 0.001		W_o	0.61		< 0.001

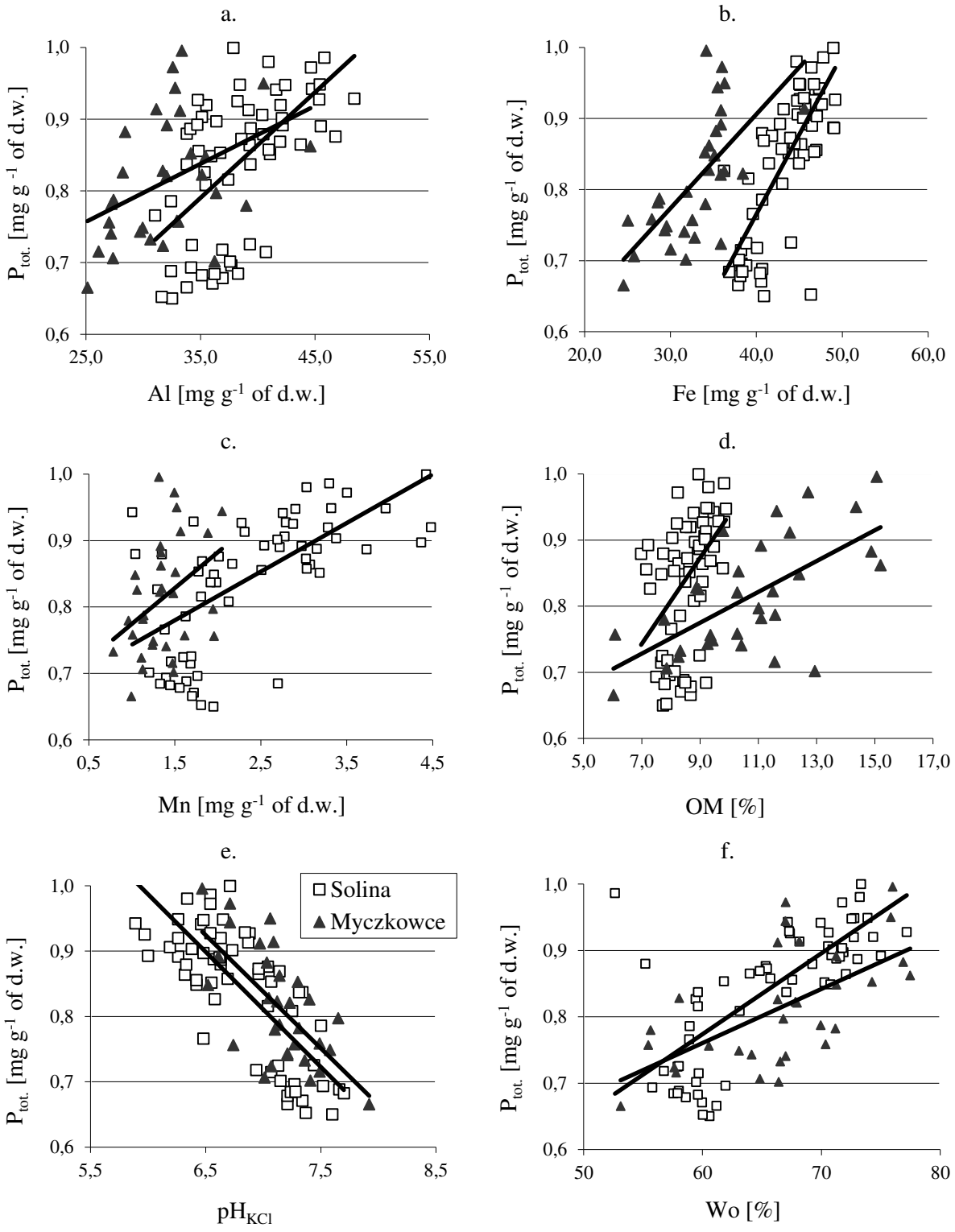

FIGURE 2
The influence of the contents of aluminium, iron, manganese [mg·g^{-1} of d.w.], organic matter (OM) [%] and sediment pH (pH_{KCl}), and the water content (W0) [%] on the total phosphorus content ($P_{tot.}$) [mg·g^{-1} of d.w.] in the bottom sediments of the Solina and Myczkowce dam reservoirs

content of total P in the case of the contents of iron and organic matter, as well as to a lesser extent aluminium and manganese (with lower correlation coefficients).

A further observation applying to the bottom sediments of each reservoir analysed concerned a significant inverse correlation between the content of total phosphorus and sediment pH (pH_{KCl}) (Fig. 2e). While such a negative relationship might attest to lower values for phosphorus content in association with higher values for pH (and *vice versa*), we do in fact know that the greatest solubility of phosphorus compounds (mainly as phosphates) applies at pH = 6-7. At a lower pH than that, P is mainly linked with iron and manganese, while at the higher one more and more with calcium [1]. According to Liu et al. [18], the lowest level of adsorption of phosphorus in bottom sediments occurs across the pH range 7–8. In fact, the highest pH values noted for deposits were 7.7 in the main reservoir and 7.9 in the top-up reservoir. The pH of the analysed deposits was in turn seen to depend greatly on the calcium content ($r = 0.85$; n = 63 Solina, and $r = 0.66$; n = 31 Myczkowce). In the case of small amounts of calcium in deposits, a lower pH favours the creation of links between phosphorus and the iron and manganese present in excess. A higher content of total phosphorus was reported in sediments of the lacustrine zones, in which there is a lower content of calcium and lower pH. More intensive sedimentation of autochthonous matter in this zone of the reservoirs influenced the higher contents of total P, while the lower content of calcium ensured that the formation of non-apatite linkages with phosphorus in deposits was very much favoured. Nevertheless, a sediment study by Bartoszek and Tomaszek [19] describing various fractions of phosphorus forms in the bottom sediments of the Solina – Myczkowce dam reservoir complex showed that non-apatite inorganic phosphorus fraction constituted the smallest part (c. 25%) of sediment total phosphorus in both reservoirs whereas organically associated phosphorus and calcium-bound phosphorus were the most abundant forms at levels 1.3–1.5 times greater than non-apatite inorganic-bound phosphorus.

In both reservoirs, it was possible to note a statistically-significant positive correlation between water content of sediments (W_o) and the content of total P in deposits (Fig. 2f). The content of water in sediments is known to increase with a greater organic matter content [20]. The water content of sediments presumably had a major influence on the diffusive transport of substances dissolved in near-bottom water into the interstitial water, as well as vice versa. The positive correlation between these parameters may suggest that prevalent diffusive transport of phosphorus compounds was between water and sediment, with deposition processes thus prevailing in the Solina and Myczkowce Reservoirs, over those whereby phosphorus was released from the sediments. Especially that water in the near-bottom zone of the Solina Reservoir throughout the period of study was characterized by a fairly good oxygenation (> 4 mg O_2 dm^{-3}) [14]. Nõges and Kisand [21] in fact reported an inverse correlation between water content in sediments and the content of phosphorus in combinations with iron and aluminium, as well as organic phosphorus.

Variability of the Total Phosphorus Concentrations – Multiple Regression Analysis. In summing up the work on the influence of selected variables on the content of total P ($P_{tot.}$) in the bottom sediments of the Solina–Myczkowce dam reservoirs, use was made of multiple regression analysis. The linear regression model was first founded, before statistical tests confirmed the linear co-dependence of the dependent variable ($P_{tot.}$) and each independent variable. The variables found to be most strongly correlated with others were iron (the subject of a strong correlation with manganese) and calcium (with sediment pH). Since the statistical Fisher–Snedecor

TABLE 4
Results of multiple regression analysis for the influence of selected variables on the content of total P [mg $g^{-1}$of d.w.] in bottom sediments of the Solina–Myczkowce dam reservoirs (F - Fisher–Snedecor test)

$r = 0.838$; $r^2 = 0.703$; F (4.89) = 52.638; $p < 0.001$; Estimation standard error: 0.056				
	Coefficient B	Standard error of B	Significance level(p)	Semi-partial correlation
Constant term	1.268	0.146	<0.001	
Aluminium [mg $g^{-1}$of d.w.]	0.003	0.001	0.008	0.157
Manganese [mg $g^{-1}$of d.w.]	0.028	0.008	<0.001	0.198
Organic matter (OM) [%]	0.019	0.003	<0.001	0.337
Sediment reaction (pH_{KCl})	-0.115	0.016	<0.001	-0.408

test (F) of this model showed that the influence of both iron and calcium on total P content turned out to be statistically insignificant ($p > 0.05$), these two variables were rejected from the model. Statistical assessment of the model (following the aforesaid rejection of calcium and iron) confirmed that all the remaining variables were significant for the total phosphorus content (Table 4). As the verification of the model through the analysis of residuals revealed no disturbances, the linear regression function obtained could be taken to sustain the view that the total P contents in the bottom sediments of the Solina-Myczkowce Reservoirs were most influenced by the content of manganese, of which a 1 mg g^{-1} of d.w. higher value was seen to be associated with a c. 0.028 mg g^{-1} of d.w. increase in phosphorus content, where remaining variables were kept constant.

$$\mathbf{P_{tot.}} = 1.268 + 0.003\ \mathbf{AL} + 0.028\ \mathbf{Mn} + 0.019\ \mathbf{OM} - 0.115\ \mathbf{pH_{KCl}} \pm 0.056 \quad (1)$$

A 1% rise in organic matter in bottom sediments would thus be associated with an increase in total P content equal to c. 0.019 mg g^{-1} of d.w. Among the studied factors, the content of aluminium was seen to have the most limited impact, a 1 mg g^{-1} of d.w. rise in it being associated with a total P content higher by just around 0.003 mg g^{-1} of d.w. In contrast, an acidification of sediment reaction by 1 unit of pH was associated with a raising of the content of total P by some 0.115 mg g^{-1} of d.w. Analysis of semi-partial correlation coefficients in turn suggests that the single variable organic matter content can of itself account for more than 11% ($0.337^2 \cdot 100\%$) of variability as regards the dependent variable $P_{tot.}$, once the influence of other variables had been excluded. Contents of aluminium and manganese, as well as sediment pH, respectively explain 2.5, 3.9 and 16.6% of variability in the dependent variable. The multiple regression model obtained is characterised by a high value for the multiple correlation coefficient ($r = 0.838$), as well as for the coefficient of determination ($r^2 = 0.703$). This denotes that 70% of the overall variability to the $P_{tot.}$ variable can be explained by the model.

In a similar way, the influence of selected parameters on the total phosphorus content in bottom sediments was analysed for each reservoir separately. The contents of total P in the Solina deposits were found to be higher where contents of aluminium and manganese were higher, and the pH of sediments lower, in line with the formula:

$$\mathbf{P_{tot.}} = 1.180 + 0.008\ \mathbf{AL} + 0.037\ \mathbf{Mn} - 0.109\ \mathbf{pH_{KCl}} \pm 0.054 \quad (2)$$

The obtained linear regression model explains c. 75% ($r^2 = 0.747$) of the variability in the content of total P in deposits of the main reservoir.

An increase in the total P content in the sediments of the top-up reservoir was associated with an increase in the content of iron and organic matter, as well as a lowering of sediment pH.

$$\mathbf{P_{tot.}} = 1.064 + 0.008\ \mathbf{Fe} + 0.013\ \mathbf{OM} - 0.093\ \mathbf{pH_{KCl}} \pm 0.047 \quad (3)$$

The obtained linear regression model explains c. 74% ($r^2 = 0.743$) of the overall variability to total P content in the bottom sediments of the top-up reservoir.

The sediments of Lake Dejguny were also the place of marked, significant, positive correlations between the content of total phosphorus and organic matter, aluminium and iron, this attesting to the important role played by these in the deposition of this biogenic element [22]. Multiple linear regression was used to examine relationships of sediment $P_{tot.}$ to other sediment constituents in Lake Taihu. This study revealed that the mineral/inorganic content of the sediments (represented by the Mn concentration) and the organic content (represented by the total carbon concentration - TC) are responsible for the majority (91%) of horizontal variability in $P_{tot.}$ concentrations in sediments of Lake Taihu (the obtained linear regression model: $P_{tot.} = 0.032\ TC + 0.49\ Mn$; $r^2 = 0.91$; n = 8) [23]. Kentzer [13] also found a very significant direct relationship between total P and organic matter in the deposits of the lakes studied. This attests to the fact that most phosphorus is deposited in sediments in the form of organic combinations, as would be confirmed by the positive correlation between phosphorus content and the water content of the deposits in the bodies of water analysed. Changes in iron and aluminum contents in the sediments occurred significantly more intense than manganese and total phosphorus, hence presumably less influence of iron on the sediment phosphorus concentrations. The rate of oxidation of dissolved manganese is much lower than the rate of release from sediments. Reduction of manganese begins at a dissolved-oxygen concentration of around 2-3 mg O_2 dm^{-3} [24], with the result that manganese may achieve maximal concentrations in the near-bottom water. In contrast, the reduction of iron mainly proceeds in anoxic conditions. The lack of a statistically significant influence of calcium on the phosphorus content in sediments (as noted with the aid of both simple and multiple regression analysis) reflects the formation of Ca-P linkages that are of limited mobility, as well as the relatively low content of the element in the deposits.

CONCLUSIONS

The multiple linear regression model obtained revealed that higher phosphorus contents in sediments of the Solina Reservoir were associated with increased contents of aluminium and manganese, as well as a lowering of sediment pH. The content of phosphorus in the bottom sediments of the top-up reservoir were in turn higher when contents of iron and organic matter were elevated, as well as with a decline in pH. The general model of multiple linear regression showed that the content of total P in bottom sediments of the Solina-Myczkowce complex of dam reservoirs was significantly (positively) dependent on contents of aluminium, manganese and organic matter, as well as inversely dependent on sediment pH (pH_{KCl}).

The role of manganese in the cycling of phosphorus is regarded as less important than those of iron or aluminium. The total P contents in the bottom sediments of the Solina-Myczkowce Reservoirs were most influenced by the content of manganese. The greater influence of manganese on the content of phosphorus in the Solina Reservoir sediments reflects the greater potential of manganese in redox reactions, as well as the slower kinetics of its oxidation, as opposed to that of iron. The iron present in large amounts in the Solina Reservoir sediments would appear to have a greater influence on the permanence of Fe-P linkages (through a high Fe/P ratio) than directly on the variability of concentrations of total P, including in the anoxic layers of bottom sediment. The pH of the sediments favoured the generation of non-apatite linkages with phosphorus.

There are various ways in which organic matter may exert an influence on the phosphorus content in bottom sediments. The direct way is via the major role played in the sedimentation of this element via organic linkages, while the indirect way is via the water content in deposits and hence the attendant processes by which phosphorus is exchanged between sediments and the water.

ACKNOWLEDGEMENTS

Research co-financed by the Ministry of Science and Higher Education, within the framework of research projects 2 PO4G 084 27 and N523 009 32/0288. We thank the members of the projects for their cooperation.

REFERENCES

[1] Kajak, Z. (1998) Hydrobiology-Limnology. Ecosystems of Inland Waters. PWN, Warsaw 1998 (in Polish).

[2] Sobczyński, T. (2009) Phosphorus release from lake bottom sediments affected by abiotic factors. Archives of Environmental Protection 35, 2, 67-73.

[3] Clement, A., Somlyody, L. and Koncsos, L. (1998) Modelling the phosphorus retention of the Kis-Balaton upper reservoir. Water Science and Technology 37, 3, 113-120.

[4] Ciglenečki, I., Pichler, S., Prohić, E. and Ćosović, B. (2006) Distribution of redox-sensitive elements in bottom waters, porewaters and sediments of Rogoznica lake (Croatia) in both oxic and anoxic conditions. Water, Air, and Soil Pollution 6, 537-545.

[5] Gonsiorczyk, T., Casper, P. and Koschel, R. (1998) Phosphorus-binding forms in the sediment of an oligotrophic and an eutrophic hardwater lake of the Baltic Lake District (Germany). Water Science and Technology 37, 3, 51-58.

[6] Sen, S., Haggard, B.E., Chaubey, I., Brye, K.R., Costello, T.A. and Matlock, M.D. (2007) Sediment phosphorus release at Beaver Reservoir, Northwest Arkansas, USA, 2002-2003: A preliminary investigation. Water, Air, and Soil Pollution 179, 67-77.

[7] Wang, Y., Shen, Z., Niu, J. and Liu, R. (2009) Adsorption of phosphorus on sediments from the Three-Gorges Reservoir (China) and the relation with sediment compositions. Journal of Hazardous Materials 162, 1, 92–98.

[8] Pardo, P., Lopez-Sanchez, J.F. and Rauret, G. (2003) Relationships between phosphorus fractionation and major components in sediments using the SMT harmonized extraction procedure. Analytical and Bioanalytical Chemistry 376, 248-254.

[9] Darke, A.K. and Walbridge, M.R. (2000) Al and Fe biogeochemistry in a floodplain forest: Implications for retention. Biogeochemistry 51, 1-32.

[10] Jonsson, A. (1997) Fe and Al sedimentation and their importance as carriers for P, N and C in a large humic lake in Northern Sweden. Water, Air, and Soil Pollution 99, 283-295.

[11] Petrovic, M. and Kastelan-Macan, M. (1996) The uptake of inorganic phosphorus by insoluble metal-humic complexes. Water Science and Technology 34, 7-8, 253-258.

[12] Kastelan-Macan, M. and Petrovic, M. (1996) The role of fulvic acids in phosphorus sorption and release from mineral particles. Water Science and Technology 34, 7-8, 259-265.

[13] Kentzer, A. (2001) Phosphorus and Its Bioavailable Fractions in Sediment of Lakes with Different Trophic Status. Publ. UMK, Toruń 2001 (in Polish).

[14] Bartoszek, L. (2008) The study of phosphorus compounds retention in the bottom sediments on the example of the Solina-Myczkowce

reservoirs. Unpublished doctoral dissertation, Faculty of Environmental Engineering of Lublin University of Technology, Rzeszów 2008 (in Polish).
[15] Koszelnik, P. (2009) Isotopic effects of suspended organic matter fluxes in the Solina reservoir (SE Poland). Environment Protection Engineering 35, 4, 13-19.
[16] Stanisz, A. (2000) Approachable Course of Statistics with Usage STATISTICA Program. Vol. 2. Linear and Nonlinear Models. StatSoft Poland, Krakow 2000 (in Polish).
[17] Trolle, D., Hamilton, D.P., Hendy, C. and Pilditch, C. (2008) Sediment and nutrient accumulation rates in sediments of twelve New Zealand lakes: influence of lake morphology, catchment characteristics and trophic state. Marine and Freshwater Research 59, 1067-1078.
[18] Liu, M., Hou, L., Xu, S., Ou, D., Yang, Y., Zhang, B. and Liu, Q. (2002) Adsorption of phosphate on tidal flat surface sediments from the Yangtze Estuary. Environmental Geology 42, 657-665.
[19] Bartoszek, L. and Tomaszek, J.A. (2011) Analysis of the spatial distribution of phosphorus fractions in the bottom sediments of the Solina – Myczkowce dam reservoir complex. Environment Protection Engineering 37, 3, 5-15.
[20] Håkanson, L. and Jansson, M. (2002) Principles of Lake Sedimentology (2nd ed.). The Blackburn Press, New Jersey 2002.
[21] Nõges, P. and Kisand, A. (1999) Horizontal distribution of sediment phosphorus in shallow eutrophic Lake Võrtsjärv (Estonia). Hydrobiologia 408/409, 167-174.
[22] Brzozowska, R., Dunalska, J. and Zdanowski, B. (2005) Preliminary characteristics of the chemical composition of the top-layer bottom deposits in Lake Dejguny (Mazurskie Lake District). Limnological Review 5, 11-16.
[23] Trolle, D., Zhu, G., Hamilton, D., Luo, L., McBride, C. and Zhang, L. (2009) The influence of water quality and sediment geochemistry on the horizontal and vertical distribution of phosphorus and nitrogen in sediments of a large, shallow lake. Hydrobiologia 627, 31-44.
[24] Pakhomova, S.V., Hall, O.J., Kononets, M.Y., Rozanov, A.G., Tengberg, A. and Vershinin, A.V. (2007) Fluxes of iron and manganese across the sediment-water interface under various redox conditions. Marine Chemistry 107, 319-331.

Received: **30.11.2014**
Accepted: **02.03.2016**

CORRESPONDING AUTHOR

Lilianna Bartoszek
Rzeszów University of Technology, Department of Environmental Engineering and Chemistry, al. Powstańców Warszawy 12, 35-959 Rzeszów, Poland

e-mail: bartom@prz.edu.pl

© by PSP Volume 25 – No. 10/2016, pages 3867-3874 Fresenius Environmental Bulletin

ENHANCED ELECTROKINETIC REMEDIATION OF ZINC-CONTAMINATED SOILS NEAR A MINE TAILING WITH APPROACHING ANODE TECHNIQUE

Zongping Cai[1,2], Dongrui Chen[2], Mengqing Xu[2], Zhanqiang Fang[2],Weishan Li[2,*],Qiming Huang[2].

[1]Guangdong Polytechnic of Environmental Protection Engineering, Guangdong Foshan 528216, China.
[2]School of Chemistry and Environment, Key Laboratory of Electrochemical Technology on Energy Storage and Power Generation of Guangdong Higher Education Institutes, Engineering Research Center of Materials and Technology for Electrochemical Energy Storage (Ministry of Education), South China Normal University, Guangzhou 510006,China

ABSTRACT

The soils contaminated by Zn near a mine tailing were remedied via an enhanced electrokinetical method utilizing approaching anodes (AAs). The variations of the removal efficiency and the soil pH as a function of the treatment time were determined. The maximum Zn removal efficiency was found to be as high as 63.4% under a voltage gradient of 1 V/cm for 48 hours; in contrast to 37.3% when the conventional electrokinetic remediation with one fixed anode (FA) was employed. Several anodes were inserted as AAs in the treated soils. They were switched from the anode towards the cathode allowing for high H^+ ions concentrations and high redox potentials to migrate fast towards the cathode. As a result, the soil remediation is accelerated. The mechanism of Zn electromigration behavior in soils during an enhanced EK method is described as the elution in an electrokinetically driven chromatogram.

KEYWORDS:
Electrokinetic remediation; approaching anodes (AAs); Zn contamination; soil remediation; mechanism.

INTRODUCTION

Soils contaminated by heavy metals becomes more and more serious in the recent years in many areas across the world [1-4]. A representative city is Shaoguan in Guangdong Province of China, a place that hosts many mine tailings and former industrial sites. Zn is a common contaminant in the soil near mine tailings, accumulated Zn in soil is harmful to plant, human health and the environment[5], resulting in the output of plant decreasing. It is reported that it is superfluous and poisoned when the concentration of Zn for the plant in soil reached 100.0 mg/kg and 400.0 mg/kg respectively[6].

Over the past few decades, electrokinetic (EK) remediation has been demonstrated to be one of the most effective methods for in situ or ex situ soil decontamination. Numerous EK remediation investigations have shown success in degrading soil contaminants and removing heavy metals [7-9].

In the EK remediation process, electrode reactions take place on the surface to generate protons (H^+) and hydroxyl (OH^-) at anode and cathode, respectively. The concentration of these ions near the electrodes creates an acid front that moves from anode to cathode and a basic front that moves the other way [10,11]. At the same time, the generation of OH^- ions at the cathode leads to the precipitation of the heavy metals called the "focusing effect" [12]. This is the main barrier to electrokinetic remediation of heavy metal contaminated soils [13].

Many studies have been performed with the aim to control the soil pH and enhance the capability of electrokinetic remediation for heavy metal removal. Measures include adding strong complexing agents, such as EDTA (Ethylene Diamine Tetraacetic Acid) into soil [14] and using ion exchange membranes (IEM) to control the pH and zeta potential [15]. These modified techniques are complicated and the use of additional chemicals or devices results in secondary contamination [16,17]. To enhance the electrokinetic remediation of heavy metals-contaminated soil, the distribution and mobility of H^+ ions and heavy metals in soils were investigated in this study. Usually, the EK process is operated with one fixed anode (FA). An enhanced EK method with approaching anodes (AAs) is believed to strengthen the remediation effect. Compared with other remediation methods, we speculate that if the area of the "focusing effect" can be migrated towards the cathode in a

step-by-step manner, more Zn would be precipitated in a narrow area and extracted from the contaminated soil. Therefore, to determine EK parameters suitable for the soil contaminated by Zn near a mine tailing in Shaoguan, local soils were picked up and examined with the approaching anode method.

MATERIALS AND METHODS

Soil preparation. Soil samples were collected near a mine tailing in Shaoguan, China. The measured concentration of Zn was 265.5 mg/kg for the collected soil samples and the moisture content was approximately 9.1%. The initial soil pH was 7.6. For each electrokinetic test, approximately 1000 g of dry soil sample was loaded into the electrokinetic cell. Distilled water was used as the electrolysis solution.

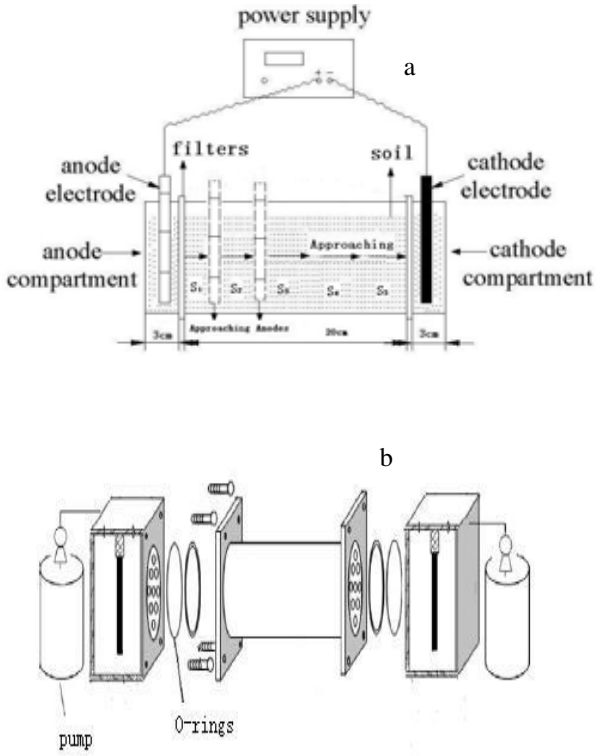

FIGURE 1

Schematic diagram of the electrokinetic laboratory apparatus with approaching anodes (AAs) technique ((a) experimental set-up and (b) detailed components of chambers and soil cell, unit: cm).

Electrokinetic cell. EK remediation experiments were carried out in a rectangular translucent plexiglas test cell with the following dimensions: length = 26.0 cm, width = 10.0cm, and height = 10.0 cm, as depicted in Fig. 1. The soil was filled into the cell up to a length of 20 cm. A constant voltage of 20 V (1 V cm^{-1}) was applied with a DC power source. The filter paper and an O-ring were used between the electrode chambers and the soil cell to avoid any possible leakage. Graphite was used for both anode and cathode and was inserted into each electrode chamber and connected with DC power. To provide an uniform electric current, the whole soil cross-section was covered with graphite electrode with a surface area of 54 cm^2 (3×9×2 cm). The thickness of the soil was 2 cm in anode compartment or cathode compartment. Electrode chambers were filled with distilled water, which was cycled by pumps to avoid concentration gradients within the compartments.

Methodology. The soil sample was divided into five sections within the cell, named S1–S5 moving from anode to cathode. EK remediation with AAs was operated in the same apparatus with the same intensity of electric field, except that five graphite electrodes were inserted as AAs in the treated soil. AAs were placed at distance of 3 cm, 6 cm, 9 cm,12 cm, and 15 cm from anode. They were sequentially switched on at 5 h,10 h, 15 h, 25 h and 36 h after the EK process started, and at the same time, the solution was refilled. Analysis was carried out in the same way with EK remediation based on FA. Soil pH was measured in the five different sections by a pH meter (soil/water = 1/2.5)，the pH and Cu concentration were measured after the remediation at different sections S1-S5 respectively.

For total Zn analysis, 0.2 g samples, in duplicate, were digested with HNO_3-HF-$HClO_4$ in 25 ml Teflon beakers for soil clearing up. An inductively coupled plasma-optical emission spectroscopy (ICP-OES, Agilent) was used to determine the concentration of total Zn. The pH and Zn concentration were measured for two samples from each section, and two standard soil samples (i.e., soil with a controlled concentration of heavy metals) were analyzed for quality control. The EK remediation experiments were repeated three times.

TABLE 1
Composition and properties of the experimental soil specimen.

Property	Value
Texture(%)	
Sand	19.3
Slit	62.4
Clay	18.3
Minerals (%)	
Chlorite	58.5
Mica	12.0
Smectite	4.4
Kaolinite	3.6
Pinguite	2.7
Feldspar	15.1
Picrite	3.7
Initial pH	7.6
Cation exchange capacity ($cmol \cdot kg^{-1}$)	15.3
Total organic carbon ($g \cdot kg^{-1}$)	10.9
Moisture content (m%)	9.1
conductivity ($us \cdot cm^{-1}$)	167.0
zero point charge(ZPC)	3.0-3.5
Zn (mg/Kg)	265.5
Pb (mg/Kg)	6.1
Cu (mg/Kg)	12.4

RESULTS AND DISCUSSION

Soil characteristics. Major physico-chemical characterizations of the experimented soil with respect to the soil pH, texture, organic carbon, cation exchange capacity, zero point charge(ZPC) and metallic contaminant content are tabulated in Table 1. The soil was composed of a number of minerals where $3MgO4SiO_2H_2O$ dominates and accounts for 58.5% in weight. The tested soil of the coastal plain showed a sandy texture, which can be attributed to the silt loam according to the USDA classification system. The soil was slightly alkaline, a typical feature in Southern China.

The charge characteristic of the clay minerals in the soil is that most of the experimented soils carry negative charges on the surface, and the negative charges increase with the pH value, indicating that the negative charge is variable. The positive charge was very low in the experimented soil [18]. Other metallic contaminant content in the sample has been provided in table 1, other than Zn, Pb 6.1 mg/Kg; Cu 12.4 mg/Kg. Other metallic contaminant is low than the limit of determination, which is 5 ug/L. The point of zero charge (ZPC) of the experimented soil, determined by potentiometric titration, is around 3.0-3.5. The ZPC of the soil can be a better indicator to evaluate the surface chemical property of the soil, which is the pH when the charge of grain surface is zero. It is necessary to keep the pH in soils to be low enough when most heavy metals are to be removed by EK remediation. With AAs method, the distance between anodes and the cathode is gradually shortened, migration distances of H^+ ions decrease. Therefore, ZPC indicates the efficiency of AAs remediation process. The low cation exchange capacity (about 15.3 $cmol.kg^{-1}$, due to low organic matter and clay contents) suggests that the Zn ions are not highly absorbed onto the soil particles, which is propitious to the migration of Zn ions in the soil [19].

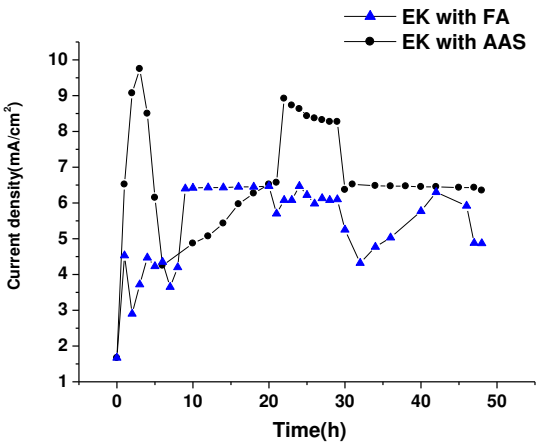

FIGURE 2
Variations of electric current intensity profile for the EK remediation with FA and with AAs.

Current changes during the experiments. The electric current is an indicator of the amount of ion electro-migration. The changes in the electric current during the treatments are shown in Fig. 2. During the EK remediation with AAs treatment, higher current density passed through the system than what was observed during the EK remediation with FA, and the current intensity fluctuated regularly. The current density of the EK remediation with AAs started from 1.67 mA/cm^2 and increased to the maximum value of 9.75 mA/cm^2. The maximum value for the EK remediation with FA treatment was 6.47 mA/cm^2, indicating the accelerated charge transport. Upon reaching the maximum value, the current density for the EK remediation with AAs began to decrease until it increased again to 8.92 mA/cm^2 after 22 hours because the precipitates re-dissolve and thus provide more ions for current transport. Finally, the current density decreased and reached a value of 6.35 mA/cm^2 for 48 hours. The decay in current intensity was due to the combination of the OH^- and H^+ ions yielding H_2O thereby removing ions that transport charges to the electrode chambers. In addition, the resistance in the interface between electrodes and electrolyte might increase due to the concentration polarization and water dissociation [20]. Ions with positive or negative charges move to both ends of the electric cell, as in electrodialysis, and result in the drop of ionic strength in soils and the current.

In the EK remediation with AAs, the electrolytic distance between working electrodes decreased gradually when relay anodes were switched on one by one in direction of the cathode. The electric current in EK remediation with AAs is higher than that with FA. The results obtained in this study suggested that the AAs method could maintain more mobile ions in the system. This phenomenon partially explained the possible mechanism of enhanced Zn and removal in the AAs tests.

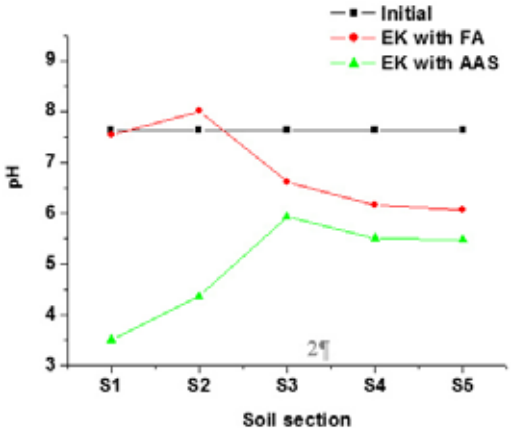

FIGURE 3
Soil pH profile for the EK remediation with FA and with AAs.

pH variation. Low pH in soil is necessary when most heavy metals are to be removed by means of EK remediation [21]. Fig. 3 shows the pH variations in the soil profiles during EK remediation with one FA and AAs. The soil pH was 7.6 before EK remediation. The pH of the soil close to the anode was 3.5 after EK remediation with AAs. This is significantly lower than that of other soil parts. It can be seen that the pH values in the soil bed drop evidently faster with AAs than with FA. During EK with AAs, when distance between electrodes is shortened step by step, migration distances of H^+ ions decrease. Therefore, H^+ ions can approach the cathode sooner.

Redox potential variation. Redox potential greatly influences chemical association of Zinc on soil particles. High redox potential near the anode indicates highly oxidizing conditions, while low redox potential near the cathode indicates reducing conditions. Redox potentials in the soil bed before and after EK remediation are depicted in Fig.4. Before EK remediation treatment, the redox potential of the soils is 18.5 V. After 48 hours of EK remediation with FA, redox potentials in treated soils decrease linearly from 19.0 V to 8.9 V along sites from the anode to the cathode. This is due to the electric potential of DC (Direct Current) and its

redox reactions at electrodes. In reductive environments, almost all particulate Zinc is complexed by insoluble organic matter or bonded to sulfide minerals. In contrast, Zn tends to be set off from soil particulates in oxidative environments because of the effect mechanisms of redox potential on heavy metals [22,23].After EK remediation with AAs, high redox potentials become offset to the cathode and are higher near the anode than after EK remediation with FA. Therefore, Zinc migration capability is enhanced in EK remediation with AAs.

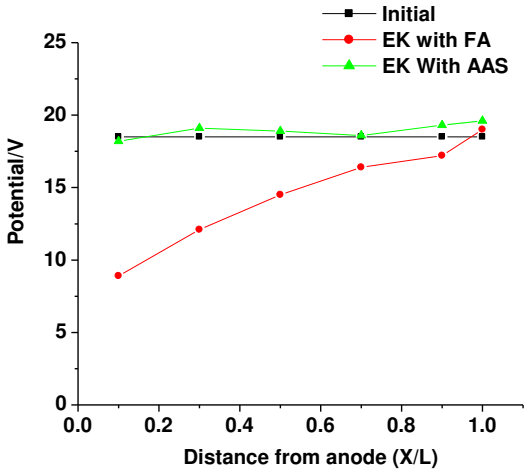

FIGURE 4
Variations of redox potential in the soil profiles before and after EK remediation with FA and with AAs.

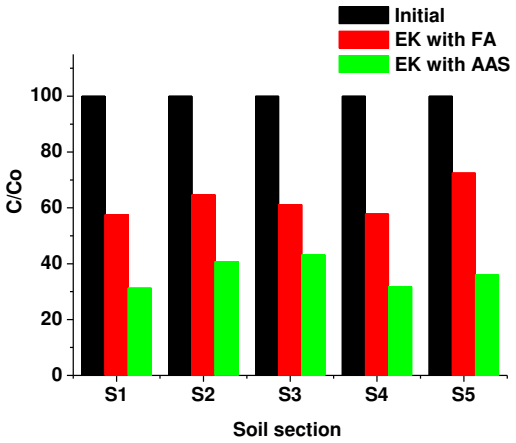

FIGURE 5
Zn^{2+} distribution in soil after EK remediation with FA and with AAs. (C/Co is represented for the proportion of Zn concentration after EK remediation and before EK remediation.)

Total Zn concentration variation. The changes of total Zn concentration in the soil bed during EK remediation are displayed in Fig.5, where C/C_o represents the ratio between Zn concentrations after and before EK remediation. Before the treatment the concentration of Zn was 265.5 mg/kg and Zn is removed from sections near the anode and accumulated near the cathode. After 48 hours, the average concentration of Zn for S_1 to S_5 region is 97.2 mg/kg using EK with AAs, compared to 166.6 mg/kg using EK with FA. Consequently, 63.4% of total Zn was removed using EK with AAs. This is in stark contrast with the 37.3% of total Zn removed via EK with FA. Therefore, the removal efficiency was enhanced and it shows great improvement of electro-migration velocity. The removal velocity of Zn concentration is the largest near the anode as shown by the increase in slope of the graph. During the EK process with AAs, soil turns to be in a more acidic condition, in which Zn exists in a free form. It can be presumed that the removal efficacy increased as more Zn ions desorbed from the soil particles as a consequence of pH decline.

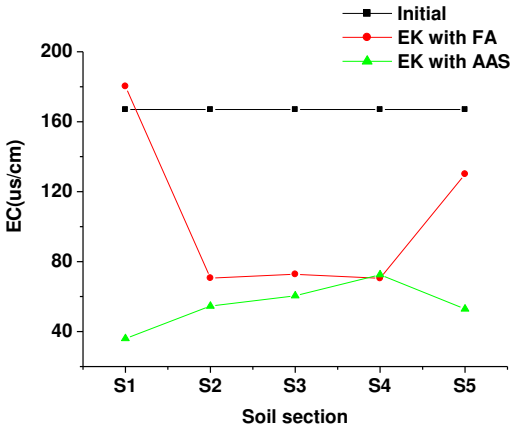

FIGURE 6
Comparsion of conductance of remnant Zn^{2+} for EK remediation with FA and with AAs.

Electrical conductivity. The results of the electrical conductivity (EC) characterization are presented in Fig. 6. The EC profile of the conventional electrokinetic remediation with FA after 48 h treatment was in the shape of a bowl. The EC was higher for S_1 and S_5 regions near the electrode chambers, and lower in S_2 to S_4 regions. This trend was observed because there were more H^+ species near the anode and more OH^- and Zn ions near the cathode [24]. The EC for EK remediation with AAs was similar. The EC was

higher for S_1 and S_5 regions, and higher for region S_3 because the precipitates re-dissolved due to higher concentration of Zn ions. Compared to the EC of electrokinetic remediation with FA, the EC of electrokinetic remediation with AAs was higher due to the increase of H^+ ion formation at the anodes as well as increased Zn ion desorption from the particles. Therefore, the EC for EK remediation with AAs coincided with the pH and Zn distribution profiles of Fig. 3 and 5.

Mechanism. The pH values and redox potentials in treated soils vary linearly after 48 h of EK remediation with AAs. Its mechanism lies in that OH^- ions are confined in the cathode compartment. Consequently, acidic fronts steadily move towards the cathode. Thereafter, H^+ ions have to react with negative groups in the soil solution and on soil particles when moving forward. The chemical reaction behavior of H^+ ions in soils during EK remediation with AAs process is similar to that in an electrokinetically driven chromatogram [25]. After EK remediation with AAs, the distance between the anodes and the cathode is gradually shortened. Thus the soil pH was lowered and Zn precipitated and re-dissolved before migrating towards the cathode. H^+ ions that were produced at the anode and continuously supplied into the treated soil are similar to a mobile phase. Soil particles react as a stationary phase. When the mobile phase pH decreases, heavy metals with positive charge will accelerate electro-migration towards cathode like elution. Many types of reactions occur during the remediation, including desorption, ion exchange, decomplexation, dissolution, destruction of the active sites on the soil surface, and diffusion from the inner sites of the crystal lattices. However, the most important aspect in electrochemical soil remediation is soil pH [14]. Often it is an acidic front, which is developing in the soil from the anode towards the cathode during EK remediation, used for mobilizing many heavy metals. When met with an acidic front, non-charged Zn fractions can be ion-exchanged by hydrogen ions according to the following equation.

$$PZn + 2H^+ = PH_2 + Zn^{2+} \quad \text{Eq. (1)}$$

The lower the soil pH becomes, the greater the positive charge Zn fractions. Zn with net positive charges will expedite to electro-migrate towards the cathode. Linear model pH may be the main mechanism that can account for the linear Zn removal velocity in EK remediation with AAs process. Low pH aids the release of heavy metals from the soil particles and reinforces the electroremediation effect [22], especially near the anode. This result illustrates why EK with AAs may be an effective treatment approach.

CONCLUSIONS

The application of conventional electrokinetic remediation with one fixed anode (FA) for 48 hours led to a Zn removal efficiency of about 37.3% from the soil near a mine tailing in Shaoguan city of Guangdong province in China. An enhanced EK method with approaching anodes (AAs) improved the efficiency to 63.4% under the same operation time. The improvement was attributed to an increased production of H^+ ions at the implemented anodes via water electrolysis and a greater desorption of Zn ions from the soil particles. Additionally, oxygen produced at the anodes changes the redox potential in the soil and results in Zn reorganization from oxidizable and stable forms to more dissoluble ones. More Zn can be thus removed from the soil than the conventional treatment does. Our method in decontaminating-polluted soils is associated with improved performances and low costs.

ACKNOWLEDGEMENTS

This work was financially supported from the joint project of National Natural Science Foundation of China (No. 21003054) and the scientific research project of Department of Education of Guangdong Province (Grant No. 2013CXZDA013).

REFERENCES

[1] Han,P., Li,C., Feng,X.Y., Ma,Z.H., Lu,A.X., Pan,L.G. and Wang,J.H. (2014) Impact of wastewater irrigation on the distribution of heavy metals in agricultural soils: A case study in Fangshan, Beijing. Fresen. Environ. Bull. 23(7A), 1662-1667.

[2] Li,Q., Wang,Y., Liu,J.S. and Wang,Q.C. (2014) Comparative assessment of heavy metals in suburban vegetable plots of Changchun, Dehui and Nongan, northeast

China. Fresen. Environ. Bull. 23(4), 1036-1044.

[3] Wang,T.C., Qu,G.Z.,Li,J., and Liang,D.L. (2014) Evaluation of the potential of soil remediation by direct multi-channel pulsed corona discharge in soil. J. Hazard. Mater. 264, 169-175.

[4] Chen,H.Y., Teng,Y.G., Lu,S.J., Wang,Y.Y., and Wang,J.S. (2015) Contamination features and health risk of soil heavy metals in China. Sci Total Environ. 512–513(15), 143-153.

[5] Pan,L.B., Ma.J., Wang,X.L., et al.(2016) Heavy metals in soils from a typical county in Shanxi Province, China: Levels, sources and spatial distribution. Chemosphere,148: 248-254.

[6] Yang,Z.H., Zhang,Z., Chai,L.Y., et al. (2016)Bioleaching remediation of heavy metal-contaminated soils using Burkholderia sp. Z-90. J.Hazard.Mater.,301(15): 145-152.

[7] Sun,T.R. and Ottosen,L.M. (2012) Effects of pulse current on energy consumption and removal of heavy metals during electrodialytic soil remediation. Electrochim. Acta 86, 28-35.

[8] Page,M.M. and Page,C.L. (2002) Electroremediation of contaminated soils. J. Environ. Eng. 128,208-219.

[9] Huang,J.Y., Liao,W.P., Lai,S.M., and Yang,R. (2013) Use of Hydraulic Pressure –Improved Electrokinetic Technique to Enhance the Efficiencies of the Remediation of PCP-Contaminated Soil. J. Environ. Eng. 139(9), 1213-1221.

[10] Méndez,E., Pérez,M., Romero,O, Beltrán,E.D., Castro,S., Corona, J.L., Corona,A., Cuevas,M.C., and Bustos,E. (2012) Effects of electrode material on the efficiency of hydrocarbon removal by an electrokinetic remediation process. Electrochim. Acta. 86, 148-156.

[11] Li,D., Xiong,Z., Li,S.C., Zhang,L.Y., and Wang,S.S. (2012) Near-anode focusing phenomenon caused by the high anolyte concentration in the electrokinetic remediation of chromium(VI) –contaminated soil. J.Hazard.Mater. 229, 282-291.

[12] Probstein,R.F. and Hicks,R.E. (1993) Removal of contaminants from soils by electric fields. Science. 260, 498-503.

[13] Lu,P., Feng,Q.Y., Meng,Q.J., and Yuan,T. (2012) Electrokinetic remediation of chromium and cadmium-contaminated soil from abandoned industrial site. Sep. Purif. Techno. l98, 216-220.

[14] Ottosen,L.M., Pedersen,A.J., Ribeiro,A.B., and Hansen,H.K. (2005) Case study on the strategy and application of enhancement solutions to improve remediation of soils contaminated with Cu, Pb and Zn by means of electrodialysis. Eng. Geol. 77, 317-329.

[15] Amrate,S., Akretche,D.E., Innocent,C., and Seta,P. (2006) Use of cation-exchange membranes for simultaneous recovery of lead and EDTA during electrokinetic extraction. Desalination. 193, 405-410.

[16] Rojo,A. and Cubillos,L. (2009) Electrodialytic remediation of copper mine tailings using bipolar electrodes. J.Hazard.Mater. 168, 1177-1183.

[17] Hansen,H.K., Rojo,A. and Ottosen,L.M. (2007) Electrokinetic remediation of copper mine tailings: Implementing bipolar electrodes. Electrochim.Acta.52, 3355-3359.

[18] Zhang,X.H., Zhang,G.L. and Yang,J.L. (2014) Dynamic Change of Point of Zero Charge Along a Typical Soil Chronosequence in Tropical Hainan Island and Its Implications for Pedogenesis. Soils. 46(2), 347-351.

[19] Rajić,L., Božo,D. and Dalmacija,M. (2012) Enhancing electrokinetic lead removal from sediment: Utilizing the moving anode technique and increasing the cathode compartment length.Electrochim. Acta. 86(30), 36-40.

[20] Shrestha,R., Fischer,R. and Rahner,D. (2003) Behavior of cadmium, lead and zinc at the sediment–water interface by electrochemi-cally initiated processes. Colloid. Surf .A. 222, 261-271.

[21] Zhou,D.M., Deng,C.F., Cang,L., and Alshawabkeh, A.N.(2005) Electrokinetic remediation of a Cu-Zn contaminated red soil by controlling the voltage and conditioning catholyte pH. Chemosphere. 61, 519-527.

[22] Cao,X.D., Chen,Y., Wang,X.R., and Deng,X.H. (2001) Effects of redox potential and pH value on the release of rare earth elements from soil. Chemosphere. 44, 655-659.

[23] Kamon,M., Zhang,H.Y. and Katsumi,T. (2002) Redox effects on heavy metal attenuation in landfill clay liner. Soi. Founda. 42, 115-118.

[24] Gunvor,M.K., Lisbeth,M.O. and Arne,V. (2009) Electrodialytic remediation of harbour sediment in suspension-Evaluation of effects induced by changes in stirring velocity and

current density on heavy metal removal and pH. J.Hazard. Mater. 169, 685-690.

[25] Xu,W.S. and Regnier,F.E. (1999) Electrokinetically-driven cation-exchange chromategraphy of proteins and its comparison with pressure-driven high-performance liquid chromatography. J.Chromatogr.A. 853, 243-256.

Received: **26.08.2015**
Accepted: **22.12.2015**

CORRESPONDING AUTHOR

Weishan Li
School of Chemistry and Environment, Key Laboratory of Electrochemical Technology on Energy Storage and Power Generation of Guangdong Higher Education Institutes, Engineering Research Center of Materials and Technology for Electrochemical Energy Storage (Ministry of Education), South China Normal University, Guangzhou 510006,China

E-mail: liwsh200@163.com

© by PSP Volume 25 – No.10/2016, pages 3875-3885 Fresenius Environmental Bulletin

AN INDOOR AIR QUALITY WIRELESS MONITORING NETWORK WITHA CARBON DIOXIDE PREDICTION MODEL

Sy-Yuan Kang, Chao-Heng Tseng*, Ai-Jie Wang, Yi-Hsuan Shih, Nhat-Thien Nguyen

Institute of Environmental Engineering and Management, National Taipei University of Technology, No.1,Sec. 3, Zhongxiao E. Rd., Taipei 10608, Taiwan.

ABSTRACT

In this study, a wireless air quality monitoring network was developed, and a field study was conducted at three sites at the National Taipei University of Technology. The network uses CO_2, temperature, and relative humidity sensors and ZigBee wireless monitoring software. System validation included laboratory calibration for measurement errors, comparisons of live and direct readings of the devices, and the establishment of a CO_2 concentration balance prediction model. This monitoring system can estimate the exchange values of indoor and outdoor spaces and verify the feasibility of prediction models. At the three sites, the average indoor in/out air exchange rate obtained using a ZG01 gas sensor were 17.21, 17.22, and 14.02 m^3/min, and those obtained using an AZ7722 gas sensor were 16.36, 18.88, and 11.66 m^3/min. According to the CO_2 concentration prediction model, the maximum number of people allowed at the three sites was 17, 18, and 12 in offices A, B, and C, respectively. When these numbers are exceeded, the CO_2 concentration is likely to be higher than the recommended concentration of 1000 ppm. Furthermore, the effect of increasing the number of in/out air exchange fans on the indoor CO_2 levels was assessed. According to the model predictions, installing one and two in/out air exchange fans reduces the indoor CO_2 concentration by 10.4% and 17.3%, respectively.

KEYWORDS:
Indoor Air quality, wireless monitoring network, CO_2, CO_2 monitor module.

INTRODUCTION

In December 2005, the Taiwan Environmental Protection Agency announced recommended levels for various components of indoor air to improve indoor air quality and protect public health and the environment. The Indoor Air Quality Management Act was passed in November 2011. In addition to establishing the powers and responsibilities of each agency and the essential regulatory norms for public spaces, the law mandated that automatic CO_2 monitoring equipment must be installed in public spaces. Furthermore, real-time monitoring data must be displayed at the entrances or in the major indoor areas of public spaces for providing real-time indoor air quality data to the administrators and the public.

However, currently, only a few public spaces have installed air quality sensors to monitor indoor air quality because of their high cost and installation difficulties. Furthermore, data transmission even to a computer for storage is difficult [1]. Wireless sensor networks (WSNs) have been increasingly applied to environmental monitoring in recent years, including in outdoor monitoring (water quality and agricultural monitoring), military monitoring, and indoor air quality monitoring [2]. Thus, developing various inexpensive and compact environmental monitoring sensors that can form a monitoring network is crucial. In addition, sensors must be able to transmit data under the constraints of low storage space and environmental costs [3]. The environment, sensors, and software must be considered when designing a WSN system because these factors affect system costs [4]. Some studies on indoor CO_2 prediction model is reported in the in/out air exchange system of the building, in the subway system and in the car such as Warren et al., Lawrence et al. and Griffiths et al. [5-7]. However, these studies did not use real-time CO_2 WSN system.

In 2013, Yu et al. Even through to compared the proposed algorithm with Trickle in terms of four metrics: dissemination time, energy consumption, number of packets and network lifetime. The experimental results showed that the transmission speed improved by 30%, and the transmission volume reduced to 42% of the original data volume. Used to network topology was set up the optimal parameter as 5*5 can be executed 1.79 times, and power consumption reduced to 30% of the original

consumption [8].

In a case study of an American elementary school gymnasium, Malcolm et al. compared the implementation of CO_2-based demand-controlled ventilation (CO_2-DCV) under the old and new ventilation standards in terms of the control strategies involved, the resulting energy savings, and the indoor air quality associated with each strategy. The results showed that cooling coil energy savings of 0.03% and 1.86% can be achieved using an occupancy detection control strategy under the new ASHRAE 62.1 and the old ASHRAE 62 conditions, respectively, when the in/out air exchange rate is 5% of the total supply airflow [9]. Hu et al. proposed a vehicular sensor network architecture to measure air quality for microclimate monitoring in city areas, where the CO_2 concentration in can differ by region and the number of mobile nodes can be high. Two message-efficient algorithms have been designed to address this concern [10].

Chaudhary et al. used WSNs for greenhouse parameter control in precision agriculture [11]. Khoshnevisan et al. used a nonparametric production function to assess the energy consumption efficiency of cucumber production in greenhouses and showed that energy use optimization influences the reduction of CO_2 emission [12]. Srbinovska et al. investigated the effects of energy consumption optimization on environmental benefits and reported that WSN architecture for vegetable greenhouse can achieve scientific cultivation and decrease the management costs of environmental monitoring. According to the analysis of the features of the greenhouse environment, a practical and low-cost greenhouse monitoring system was designed using WSN technology to monitor crucial environmental parameters, such as temperature, relative humidity and illumination [13].

In this study, a wireless transmission module was combined with a fixed sensor module to construct an air quality wireless monitoring network (AQWMN). The sensor measurements of indoor and outdoor air pollutant (CO_2) concentrations were transmitted through a wireless transmission module to a computer or a cloud for providing real-time air quality data to the users. In addition, a CO_2 balance measurement model was established. The CO_2 measurements were used to predict the site in/out air exchange rate and verify the prediction model. Moreover, on the basis of the predicted CO_2 levels, the model estimated the in/out air exchange rate and maximum number of people permitted at the site for ensuring the recommended indoor air quality.

METHODS

AQWMN structure and software. The AQWMN consists of two components. The first component is the wireless air quality monitoring system, which includes wireless intelligent sensor nodes, such as CO_2, temperature, and relative humidity sensor nodes, and an data gateway. The sensor nodes transmit gas level data to the gateway for data collection. The second component is the integrated wireless sensor graphical control interface system, which converts the indoor air quality data into the XML format for storage in a computer or a cloud, thus providing users and administrators the indoor air quality status of each node.

The upper half of the intelligent sensor nodes is responsible for data transmission, signal acquisition, calibration, and control. The lower half is the signal processing module, which converts each sensor parameter into the electronic form. In this study, depending on the sensor, different circuit components, such as voltage adders, amplifiers, multiplexers, and low-pass filters for signal acquisition and retrieval, were used (Fig. 1).

The design of the information integration gateway software and that of the intelligent sensor nodes are partly similar. The gateway collects data from the sensors and transmits it to a computer or cloud. The information integration gateway itself is not directly connected to the network. The collected pollutant data must be reformatted by the computer software before transmission. Installing Microsoft NET Framework 4 and TL2303 hardware drivers and setting sensor IDs and Comport are essential for data collection and storage.

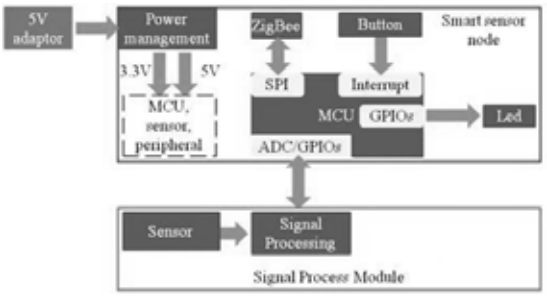

FIGURE 1
Structure of the Intelligent sensor node

Sensor Selection. The CO_2 sensor screening is based on sensor principles and the scope of its monitoring. In this study, three CO_2 sensors of different specifications were used: the TGS4161, a

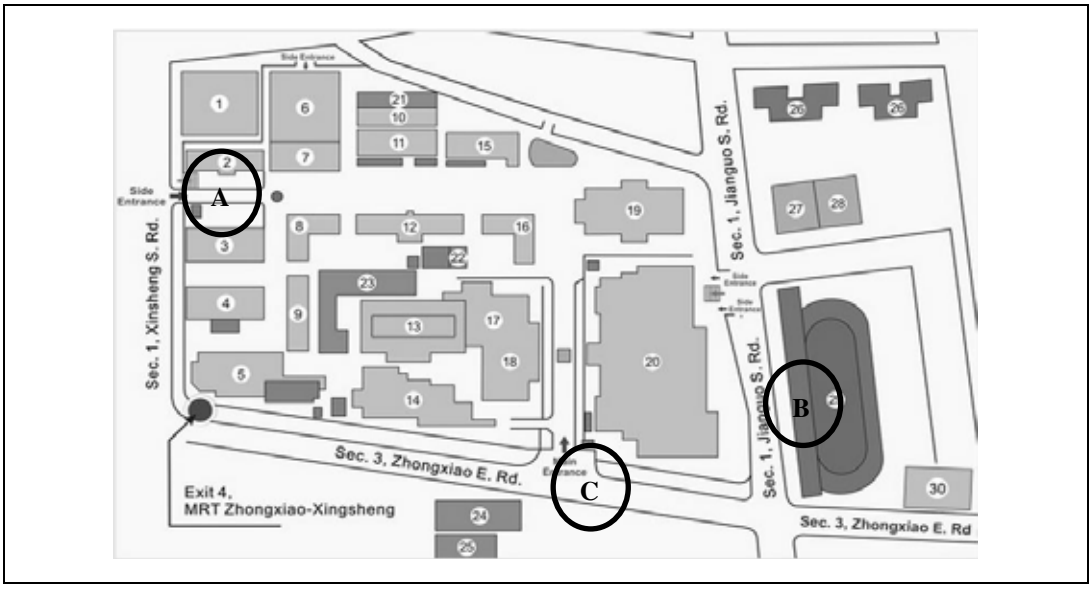

FIGURE 2
Sensor network schematic at National Taipei University of Technology campus

solid semiconductor sensor (Figaro, Japan) that can measure indoor air CO_2 concentrations in the range 350–10,000 ppm; the ZG01 CO_2 monitor module, a nondispersive infrared (NDIR) CO_2 gas sensor (ZyAura, Taiwan), whose sensor module and circuit board can be connected to function as an indoor air quality sensor for measuring CO_2 concentrations in the range 0–3,000 ppm; and the AZ7722 CO_2 sensor module (AZ instrument, Taiwan), which can measure CO_2 concentration in the range 0–2,000 ppm. The AZ7722 CO_2 sensor module is an NDIR sensor, which detects CO_2 and measures CO_2 concentration as it comes in contact with the sensor when it enters the device. In addition, it reacts quickly, is highly stable and compact, has a long use life, and warms up rapidly.

Standard gases with different CO_2 concentrations must be used for calibrating a CO_2-based sensor. In this study, a dynamic dilution method was used to adjust the standard gas concentrations (0, 500, 1200, 1800, 2500, and 3000 ppm). This enables the use of different CO_2 concentrations and offers continuous calibration. When performing multipoint sensor calibration, the difference between the readings of the sensor and the direct reading device must be calculated as an error percentage. The lower the error percentage, the more accurate the sensor results are. The maximum permitted error percentage is 10%.

$$\text{Error (\%)} = \frac{(\text{mean of sensor measurement} - \text{measurement of portable instrument}) \times 100\%}{\text{Mean of device measurement}}$$

AQWMN provisioning. The appropriate space for air quality measurement was determined on the basis of floor space, space allocation, and intensity of human activities. Accordingly, three rooms in the National Taipei University of Technology campus were selected for the field verification of the AQWMN: an environmental engineering and administrative research office (office A), a computer and information technology research office (office B), and an office of in the administration building of the Health, Safety, and Environment Center (office C). One indoor and one outdoor AQWMN and one host computer were placed in each room for collecting the sensor data. The sites of the sensors are shown in Fig. 2. A short-range ZigBee wireless transmission module with a maximum range of 100 m was used in this study. When locating the sensors, their representativeness was considered; all sensors were set at heights of more than 2 m (Table 1).

A sensor requires regular assessment using more precise instruments to determine whether the sensor readings are accurate. AKD AirBoxx, which directly measures the concentrations of pollutants such as CO_2 and CO and is equipped with temperature and humidity sensors, was used for comparing the readings of the gas sensor and the direct reading devices. It can be used for real-time control and continuous monitoring by conducting one measurement per minute.

TABLE 1
Basic information of the three sites

	Office A	Office B	Office C
Interior volume	195 m^3	459 m^3	127 m^3
Number persons	12	30	5

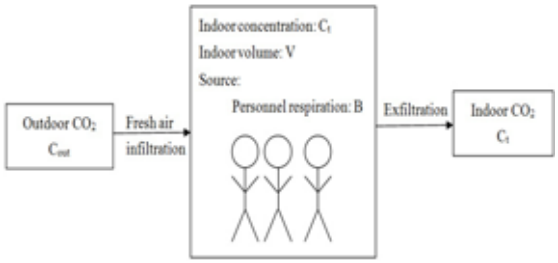

FIGURE 3
Indoor CO_2 prediction model

CO_2 prediction model. The indoor CO_2 concentration model is based on a mass balance model (Fig. 3). Parameters that affect indoor CO_2 concentration include indoor and outdoor CO_2 levels, indoor and outdoor exchange rates (airflow volume), number of people present, volume of the indoor space, and time of day. To simplify the prediction of CO_2 concentration, the model considers indoor CO_2 concentration, number of people present and in/out air exchange. Real-time indoor CO_2 and outdoor CO_2 concentration is necessary for the CO_2 prediction model. Outdoor CO_2 can affect indoor CO_2 through the In/Out air exchange.

For a given period, the mass balance equation for indoor CO_2 concentration, $C_{(t)}$,is:

Indoor concentration = human exhalation volume + outdoor concentration − indoor concentration

$$\frac{dc_{(t)}}{dt} = \frac{B \times P}{V} + \frac{QC_{out}}{V} - \frac{QC_{(t)}}{V} \quad (1)$$

According to Equation (1), the mass balance result can be deduced as follows:

$$C_{(t)} = k'e^{-\frac{Q}{V}t} + \frac{BP}{Q} + C_{out} \quad (2)$$

Assume that when nobody is present indoors, the indoor and outdoor CO_2 concentrations are equal. Thus, $C_{(t)} = C_{out}$. The final balance results are

$$C_{(t)} = \frac{BP}{Q}(1 - e^{-\frac{Q}{V}t}) + C_{out} \quad (3)$$

Where $C_{(t)}$ represents the indoor CO_2 concentration, which is a function of time (ppm); C_0 is the outdoor CO_2 concentration (ppm); t is the time (min); Q is the in/out air exchange flow (m^3/min); P is the number of people; B represents the human CO_2 production rate (m^3/person/min); and V is the volume of the indoor space (m^3).

In this study, an AQWMN system was used to predict the CO_2 concentrations in three sites (offices A, B, and C). The hourly indoor and outdoor CO_2 concentrations were used as the average hourly readings, and the actual or predicted number of people present was estimated. Considering that the doors to these rooms are sometimes open for long and other factors, in/out air exchange cannot be accurately calculated. The exchange rates for indoor and outdoor CO_2 concentrations, whose values affect the prediction, were calculated and input into the model for verification by continuously using the estimate for the highest number of people present and increasing the indoor and outdoor exchange to improve the indoor air quality. The mean absolute percentage error (MAPE) assessment of the predictive ability of the estimate is based on the four principles listed in Table 2.

TABLE 2
The mean absolute percentage error (MAPE) evaluation of the predictive ability of the model

MAPE range	Precision
MAPE＜10%	High
10%≦MAPE≦20%	High
20%≦MAPE≦50%	Acceptable
MAPE≧50%	Low

RESULTS AND DISCUSSION

Multipoint concentration measurement results of gas sensor module. Multipoint tests of the TGS4161, ZG01, and AZ7722 gas sensor modules were conducted using standard CO_2 concentrations (0, 500, 1200, 1800, 2500, and 3000 ppm). For TGS4161, the sensor output voltage (mV) response was converted to a voltage difference through an exponential regression curve for calculating the CO_2 concentration. For ZG01 and AZ7722, a CO_2 value is given and thus the voltage difference need not be calculated. Table 3 presents the results of the voltage difference regression for CO_2 concentration measurement by using TGS4161 and standard gas error (5.5%–30.7%). The average error percentage was 17.18%. The error for the ZG01 module ranged between 2.6% and 10.2% with an average of 6.88%, and that for the AZ772 ranged between 0.5% and 7.6% with an average of 3.88%. Thus, the average errors for both ZG01 and AZ7722 were less than 10%. Because the TGS4161 gas sensor module had an error percentage exceeding the gas standard defined in the Taiwan environmental regulations (10%), it was not used in this study. Thus, ZG01 and the AZ7722 gas sensor modules were used for the field tests.

TABLE 3
Gas sensor module testing results

TGS4161	Concentration setting(ppm)	0	500	1200	1800	2500	3000
	Sensor reading (ppm)	66	495	1469	1563	1989	2138
	Portable instrument (ppm)	75	524	1383	1973	2571	3085
	Error percentage (%)	11.7	5.5	6.2	20.8	22.7	30.7
	The average error (%)	**17.18**					
ZG01	Sensor reading (ppm)	24	527	1127	1628	2299	2844
	Portable instrument (ppm)	9	514	1216	1813	2514	3016
	Error percentage (%)	-	2.6	7.3	10.2	8.6	5.7
	The average error (%)	**6.88**					
AZ7722	Sensor reading (ppm)	31	524	1146	1714	2447	2997
	Portable instrument (ppm)	9	522	1229	1855	2522	3044
	Error percentage (%)	-	0.5	6.8	7.6	3.0	1.5
	The average error (%)	**3.88**					

Verification of the AWQMN system at 3 sites. The measurement results at the three sites were continuously compared for 24 h (short term) to determine whether the accuracy of the results were affected by field conditions. Moreover, a one-year long-term analysis was performed to determine whether drift occurs during long-term field use.

The 24-h indoor CO_2 measurements obtained using the ZG01 sensor module and the KD AirBoxx direct reading instrument had a correlation of 0.9722–0.9974 (Fig.4(a–c)). A similar correlation (0.9744–0.9984) was obtained for AZ7722 (Fig.4 (d–f)). For outdoor CO_2 measurements, ZG01 and KD AirBoxx showed a correlation of 0.7152–0.8145(Fig.5 (a–c)), and AZ7722 and KD AirBoxx showed a correlation of 0.6527–0.8595(Fig.5(d–f)). Because ZG01, AZ722, and KD AirBoxx are NDIR instruments, their measurement were highly correlated. The correlations when using these two gas sensor modules were higher for indoor measurements than they were for outdoor measurements, probably because the outdoor environment changes more rapidly than does the indoor environment; the NDIR readings are affected by the particulates present in the air and water vapor, thus reducing the correlation.

Table 4 presents a comparison of the one-year (long term) results at the three sites. The average error percentages of ZC01 and AZ7722 were less than 10%, which demonstrated that drift did not occur during long-term CO_2 measurements.

CO_2 prediction module verification. ACO_2 prediction model was used in this study. The prediction module considers several factors, such as the number of people present, in/out air exchange, time of day, and outdoor CO_2 concentration. Using these factors, a model can dynamically estimate indoor in/out air exchange and the maximum number of people present and thus predict the CO_2 concentration in real time. Moreover, the model can revise the CO_2 concentration estimation after such changes as in the number of people and in the in/out air exchange rate have been made.

In this study, ZG01 and AZ7722 sensor modules were used to measure indoor and outdoor CO_2 concentrations for predicting indoor in/out air exchange and verifying model feasibility. The results are listed in Table 5. The average in/out air exchange in offices A, B, and C obtained using ZG01 was 17.21, 17.22 and 14.02 m^3/min, and that obtained using AZ7722 was 16.36, 18.88 and 11.66 m^3/min, respectively. The predicted airflow volumes for offices A, B, and C obtained using ZG01 were 15.41, 6.69 and 7.30 $m^3/h/m^2$, and those obtained using AZ7722 were 14.65, 7.33 and 14.39 $m^3/h/m^2$, respectively.

According to the construction regulations of the Ministry of the Interior, Taiwan, In/out air exchange for private and public offices should be at least 8 and 10 $m^3/h/m^2$, respectively. Thus, offices A and C meet these specifications, whereas office B, which has a larger area, does not meet the requirements, thus necessitating further analysis and improvement.

TABLE 4
Verification of long-term monitoring results of ZG01 and AZ722 sensor modules at the three sites.(Error percentage, MAPE)

Sensor modules	Indoor			Outdoor		
	Office A	Office B	Office C	Office A	Office B	Office C
ZG01	2.2% (0~4%)	2.4% (0.1~8.8%)	2.4% (0.2~7.2%)	6.1% (0.2~18.2%)	6.6% (1.4~12.5%)	4.6% (0.2~9.7%)
AZ7722	3.4 % (0~7%)	2.3 % (0.3~5.7%)	3.4% (0.7~6.8%)	7.2% (0.2~20.6%)	5.8% (0.7~19.4%)	4.4% (0.4~7.1%)

TABLE 5
Estimated indoor and outdoor in/out air exchange for each site and the results of CO_2 prediction model verification

		Office A		Office B		Office C	
Sensor modules		ZG01	AZ7722	ZG01	AZ7722	ZG01	AZ7722
Site volume (V)		195 m^3		460 m^3		128 m^3	
Time		10:00~20:00		10:00-23:00		07:00~1700	
Number persons/hour (P)		5.2(1~9)		14.2(4~24)		3.2(1~5)	
In/out air exchange flow (m^3/min)		17.21 (12.4~29.8)	16.36 (11.5~29.4)	17.22 (10.9~22.5)	18.88 (13.8~26.3)	14.02 (8.3~22.8)	11.66 (8.0~17.2)
Air changes per hour, ACH		5.30 (3.8~9.0)	5.03 (3.5~9.0)	2.25 (1.4~2.9)	2.46 (1.8~3.4)	6.57 (3.8~10.7)	5.47 (3.7~8.1)
Verification of CO_2 concentration predication							
Estimate the amount of air changes per hour	MAPE Average	14.04%	12.71%	20.93%	19.02%	5.99%	6.97%
Estimate the average amount of in/out air exchange	MAPE Average	13.10%	11.64%	21.15%	18.58%	6.93%	7.03%

During indoor CO_2 concentration verification, MAPE provided the highest prediction results for office A (18%–23%) and the lowest for office C (5%–8%), thus demonstrating that the accuracy of the CO_2 concentration prediction model is high and acceptable, especially for small spaces or spaces with stable people number. These results showed that the highest error percentage caused by the use of average hourly indoor and outdoor exchange airflow volume and the average airflow volume to verify the prediction model is less than 1%. Thus, the indoor and outdoor in/out air exchange can be reliably estimated using the daily indoor and outdoor ventilation measurements.

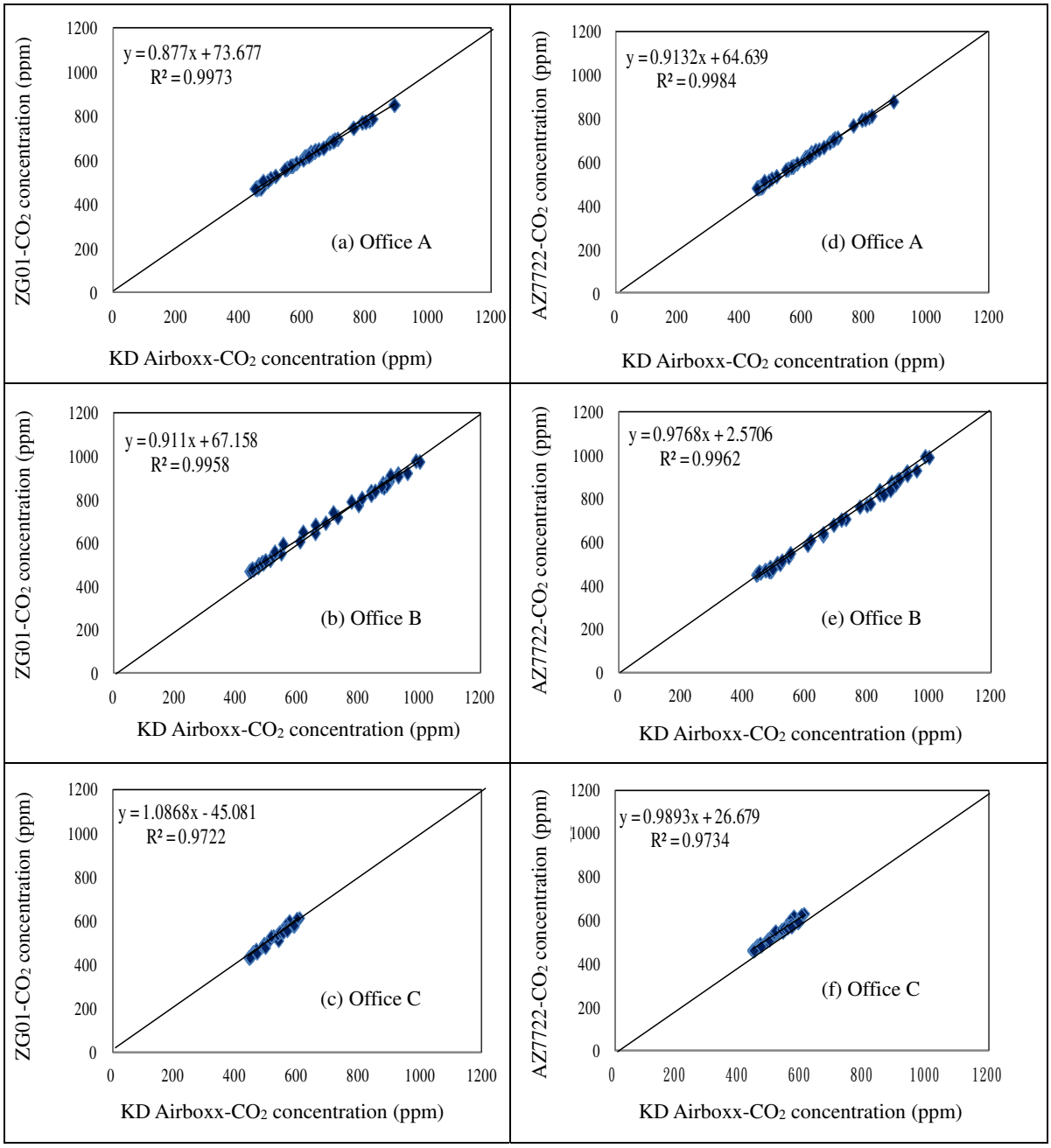

FIGURE 4
ZG01 and AZ7722 gas sensor module 24 hour indoor measurement comparison results

Estimation of the maximum number of people permitted. The CO_2 prediction model was used to predict the maximum number of people allowed at each site by using the outdoor CO_2 concentration and the estimated average in/out air exchange; the maximum permissible average indoor CO_2 concentration for 8 h was set to 1000 ppm. The results are given in Table 6. When more than 17, 18 and 12 people were in offices A, B and C, respectively, the indoor CO_2 concentration easily exceeds 1000 ppm. When the indoor CO_2 concentration exceeds the recommended level, sleepiness, fatigue and other symptoms can occur. Because these conditions affect work efficiency, windows and doors must be opened to increase in/out air exchange and reduce CO_2 concentration.

Improvements after installing in/out air exchange fans. The CO_2 prediction model was used to investigate the effects of different indoor and outdoor exchange volumes on CO_2 concentration at the three sites. To calculate the improvement in indoor air quality, time (t), number of people (n), outdoor CO_2 concentration (C_{out}) and in/out air exchange volume were used to predict the indoor CO_2 concentration by assuming that the indoor site allows the inflow of outdoor air.

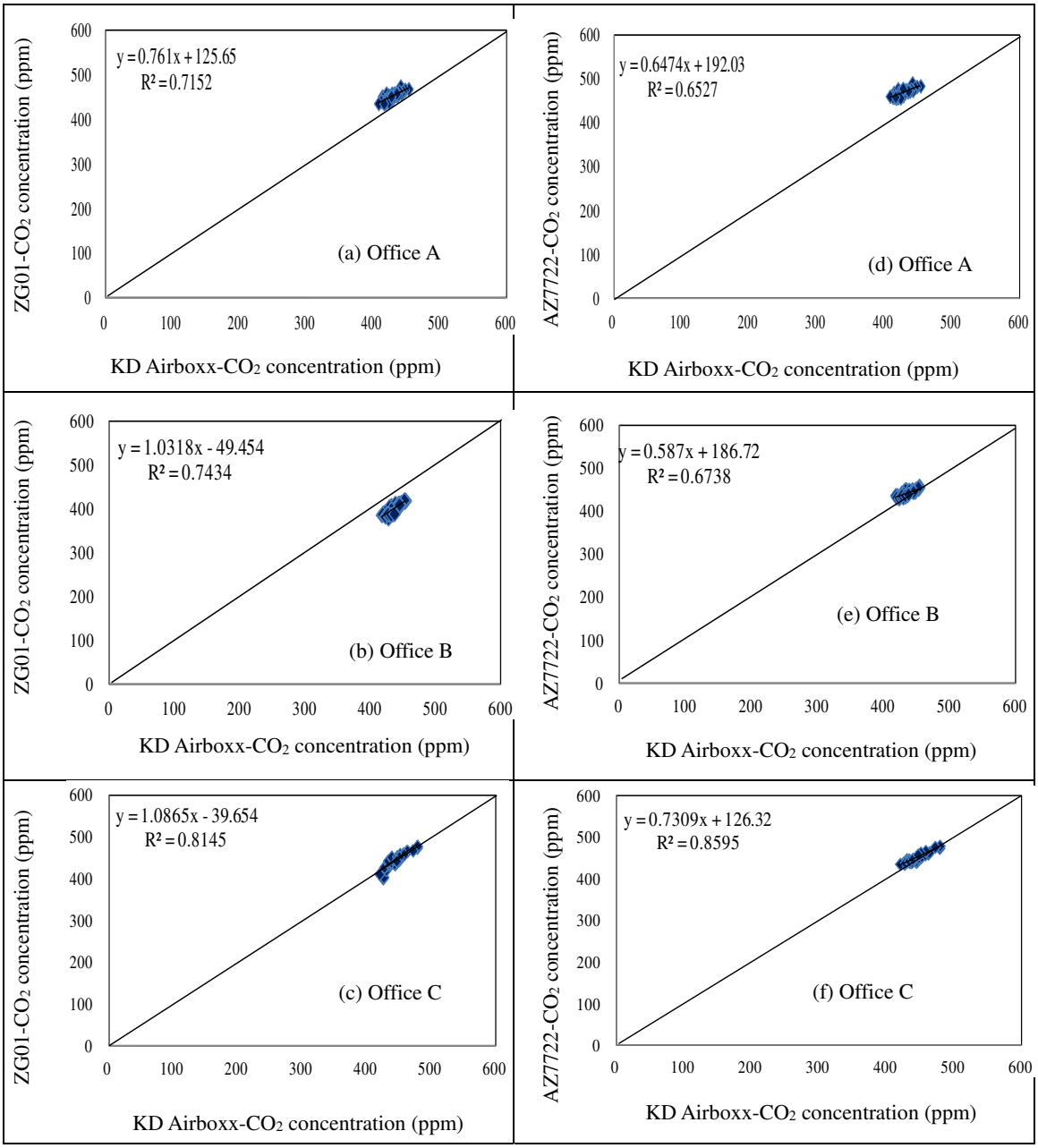

Notes. 1. Measurement period is from 3:30 pm Sept 7 to 4:00 pm Sept 8. 2. Data average taken every half hour

FIGURE 5
ZG01 and AZ7722 gas sensor module 24 hour outdoor measurement comparison results.

The results of installing one and two 14-in in/out air exchange fans at offices A, B and C to increase indoor in/out air exchange and reduce CO_2 concentration are shown in Table 7. In office A, the CO_2 concentration was predicted to be reduced by 8.9% ~ 9.1% after installing one fan and by 16.4% ~ 16.9% after installing two fans. In office B, the CO_2 concentration was predicted to be reduced by 9.5% ~ 12.1% after installing one fan and by 18.7% ~ 20.4% after installing two fans. In office C, the CO_2 concentration was predicted to be reduced by 12.8% ~ 16.9% after installing one fan and by 20.4% ~ 21.8% after installing two fans. These predicted results showed that all sites experienced approximately 9% ~ 13% reductions in CO_2 concentration after installing each exchange fan.

In addition, the accuracy of the prediction results was examined by installing one fan at office A. The ZG01 sensor module was placed in the office before and after installing the fan to measure the CO_2 concentration daily between 10:00 a.m. and 8:00 p.m. (Fig.6). The average CO_2 concentration in four days before the installation was 636 ppm; it reduced to 515 ppm four days after the installation of the fan, a reduction of approximately 19%.

TABLE 6
Prediction results for the maximum number of persons in each site

	Date (2013)	Sensor ZG01			Sensor AZ7722		
		Indoor (ppm)	Outdoor (ppm)	Number persons	Indoor (ppm)	Outdoor (ppm)	Number persons
Office A	10/19	640	442	19.21	651	448	18.07
	10/21	751	449	18.96	779	467	17.45
	10/25	555	452	18.86	569	460	17.66
	10/28	572	442	19.22	592	453	17.90
	10/31	629	456	18.73	645	459	17.72
Office B	11/15	691	439	19.31	691	443	21.03
	11/16	660	421	19.96	656	440	21.13
	11/17	678	428	19.71	676	448	20.86
	11/22	779	417	20.07	764	435	21.32
	11/23	738	454	18.82	740	456	20.54
Office C	10/5	705	459	15.18	683	444	12.96
	10/6	652	465	15.01	635	441	13.05
	10/12	721	443	15.62	700	431	13.28
	10/13	663	464	15.03	646	445	12.95
	10/17	652	458	15.20	671	440	13.05

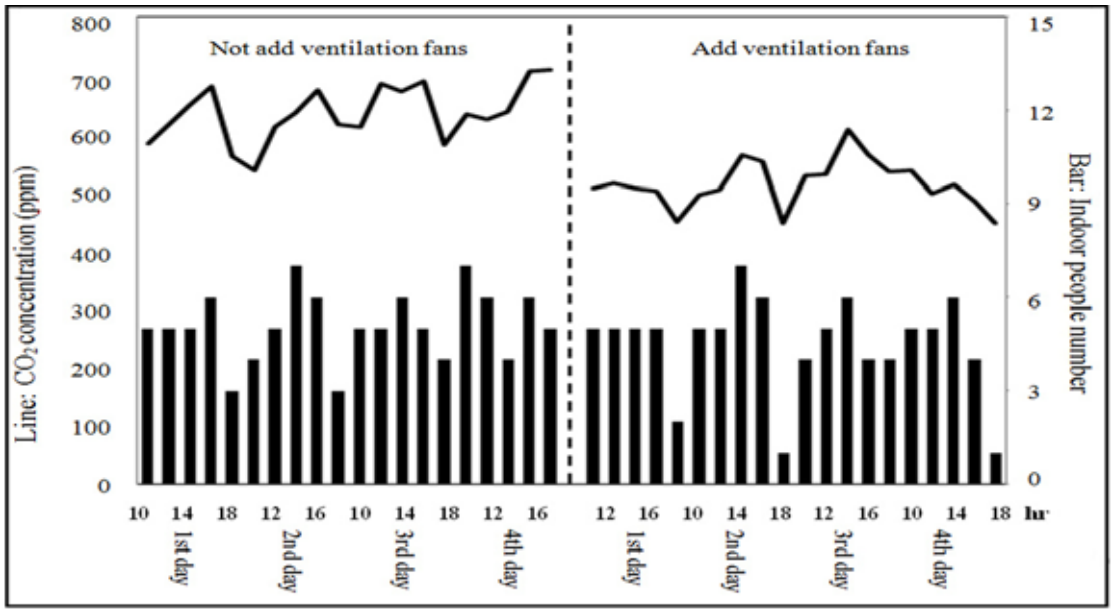

FIGURE 6
Office CO_2 monitoring concentrations before and after fan installation at office A

TABLE 7
Prediction results of CO_2 concentration after increasing in/out air exchange

Site		Office A		Office B		Office C	
Sensor modules		ZG01	AZ7722	ZG01	AZ7722	ZG01	AZ7722
Indoor concentration (ppm)		618	634	786	792	622	642
In/out air exchange (m^3/min)		17.21	16.36	17.22	18.88	14.02	11.66
Add one in/out air exchange fans	In/out air exchange (m^3/min)	29.33	28.38	29.34	31	26.14	23.78
	Indoor concentration (ppm)	563	576	712	696	543	531
	Reduce CO_2 concentration (%)	8.9%	9.1%	9.5%	12.1%	12.8%	17.2%
Add two in/out air exchange fans	In/out air exchange (m^3/min)	41.46	40.61	41.46	43.13	38.27	25.91
	Indoor concentration (ppm)	530	542	639	630	517	502
	Reduce CO_2 concentration (%)	16.4%	16.9%	18.7%	20.4%	16.9%	21.8%

CONCLUSIONS

An AQWMN and a CO_2 prediction model were constructed for indoor office use. After calibrating and testing three CO_2 measuring devices, TGS4161, ZG01, and AZ7722, ZG01 (7.13%) and AZ7722 (5.93%) had the lowest error percentage (the error percentage of TGS4101 was unacceptably high (20.75%)). The AQWMN was installed in three sites and their readings were compared against direct readings; the 24-h results showed a higher correlation with the direct readings for indoor air quality than for outdoor air quality. Long-term real-time comparisons showed an average difference of less than 10%. Indoor and outdoor exchange were calculated and the indoor CO_2 concentration was predicted using the CO_2 prediction model, number of people present, floor space, indoor and outdoor CO_2 measurements as model parameters. The verification results exhibited high accuracy and acceptability. The indoor CO_2 concentration prediction was more accurate when the volume of the space and the number of people were low. In addition, the maximum number of people allowed in order to not exceed the recommended CO_2 concentration was calculated; moreover, the improvement in air quality after increasing the in/out air exchange was predicted. The results showed that when the number of people in offices A, B and C exceeded 17, 18 and 12, respectively, the indoor CO_2 concentration exceeded 1000 ppm. The indoor CO_2 concentration was reduced by 10.4% and 17.3% after installing one and two fans, respectively. The extension of the system and the prediction model to other interior spaces require further examination of system stability and model prediction accuracy.

REFERENCES

[1] Ho, C.L. (2010). Design and implementation of indoor air quality monitoring system with wireless smart sensor networks. Master thesis, National Taipei University of Technology, Taiwan.

[2] Arampatzis, T., Lygeros, J. and Manesis, S. (2005). A Survey of applications of wireless sensors and wireless sensor networks. IEEE Computer Networks 719-724.

[3] Mahfuz, M.U. and Ahmed, K.M. (2005). A review of micro-nano-scale wireless sensor networks for environmental protection: prospects and challenges. Science and Technology of Advanced Materials 6: 302-306.

[4] Yick, J., Mukherjee, B. and Ghosal, D. (2008). Wireless sensor network survey. Computer Networks 52: 2292-2230.
[5] Warren, B.F. and Harper, N.C. (1991). Demand controlled ventilation by room CO_2 concentration: a comparison of simulated energy savings in an auditorium space. Energy and Buildings 17: 87-96.
[6] Lawrence, T.M. and Braun, J.E. (2007). A methodology for estimating occupant CO_2 source generation rates from measurements in small commercial buildings. Energy and Buildings 42: 623-639.
[7] Griffiths, M. and Eftekhari, M. (2008). Control of CO_2 in a naturally ventilated classroom. Energy and Buildings 40: 556-560.
[8] Yu, T.C., Lin, C.C., Chen, C. C., Lee, W.L., Lee, R.G., Tseng, C.H. and Liu, S.P. (2013). Wireless sensor networks for indoor air quality monitoring. Medical Engineering & Physic 35: 231-235.
[9] Malcolm, O.N., Qu, M., Zheng, P., Li, Z. and Hang, Y. (2011). CO_2-based demand controlled ventilation under new ASHRAE Standard 62.1-2010: a case study for a gymnasium of an elementary school at West Lafayette, Indiana. Energy and Buildings 43: 3216-3225.
[10] Hu, S. C., Wang, Y. C., Huang, C.Y. and Tseng, Y. C. (2011). Measuring air quality in city areas by vehicular wireless sensor networks. Journal of Systems and Software 84: 2005-2012.
[11] Chaudhary, D.D., Nayse, S.P. and Waghmare, L.M. (2011). Application of wireless sensor networks for greenhouse parameter control in precision agriculture. International Journal of Wireless & Mobile Networks 3: 1.
[12] Khoshnevisan, B., Rafiee, S., Omid, M. and Mousazadeh, H. (2013). Reduction of CO_2 emission by improving energy use efficiencyof greenhouse cucumber production using DEA approach. Energy 55: 676-682.
[13] Srbinovska, M., Gavrovski, C., Dimcev, V., Krkoleva, A. and Borozan, V. (2014). Environmental parameters monitoring in precision agriculture using wireless sensor networks. Journal of Cleaner Production 88: 297-307.

Received: **22.04.2015**
Accepted: **16.12.2015**

CORRESPONDING AUTHOR

Chao-Heng Tseng
Institute of Environmental Engineering and Management, National Taipei University of Technology, No.1,Sec. 3, Chung-Hsiao E. Rd., Taipei 106, Taiwan, R.O.C.

e-mail: jojeff@ms17.hinet.net

© by PSP Volume 25 – No. 10/2016, pages 3886-3894 Fresenius Environmental Bulletin

CUMULATIVE TOTAL DUST EXPOSURE CAUSES ACCELERATED CUMULATIVE ABNORMAL RATE OF PULMONARY FUNCTION IN COAL MINERS IN A CHINESE HAN POPULATION

Qing-Zeng Qian[1], Xiang-Ke Cao[2], Fu-Hai Shen[1,*], Qian Wang[1], Hai-Yan Liu[1], Jun-Wang Tong[1], Jie Zhou[3]

[1] College of Public Health, North China University of Science and Technology, Tang Shan 063000, China
[2] College of Life Sciences, North China University of Science and Technology, Tang Shan 063000, China
[3] Department of Obstetrics, Gynecology and Women's Health, University of Missouri School of Medicine, Columbia

ABSTRACT

To investigate the correlation between cumulative total dust exposures (CTE) and cumulative abnormal rate (CAR) of pulmonary function in coal miners in a Chinese Han population. Dust exposed coal miners (n = 359) and comparable non-dust exposed workers (n = 183) were respectively selected from a coal mine in Tangshan as observation group and control group, respectively. Pulmonary function test was conducted on each subject including forced vital capacity (FVC), forced expiratory volume in one second (FEV1), FEV1/FVC (FEV1%), maximal midexpiratory flow (MMEF), vital capacity (VC) and maximal ventilatory volume (MVV), to evaluate the CAR rate of pulmonary function in both two groups. FVC, FEV1.0, FEV1%, MMEF, VC and MVV in the observation group were significantly decreased compared with control group (all $P < 0.05$). The observation group presented with a higher CAR of pulmonary function than control group (all $P < 0.05$). FVC, FEV1, FEV1%, MMEF, VC and MVV were negatively correlated with CTE (all $P < 0.05$). CTE was positively correlated with the CAR of pulmonary function (all $P < 0.05$). Linear regression analysis showed that FVC, FEV1 and FEV1% were remarkably correlated with CTE (all $P < 0.05$). Our results demonstrated the positive correlation between CTE and CAR of pulmonary function, thus the increased CTE may aggravate the CAR of pulmonary function.

KEYWORDS:
Coal mine, coal miner, cumulative total dust exposures, cumulative abnormal rate of pulmonary function, dust exposure year, clinical symptoms, forced vital capacity, the first second of time vital capacity.

INTRODUCTION

Coal mining cast a considerable challenge for the respiratory health of coal miners worldwide due to the potential burden of pulmonary disease [1]. Respirable coal dust concentration in working area, cumulative total dust exposure (CTE) and free slica content are significant risk factors for pulmonary function abnormality [1]. It is widely accepted that cigarette smoking is an important risk factors for respiratory symptoms and pulmonary function abnormalities [2]. However, exposure to mineral dusts especially in underground mining, such as gold, coal, and uranium mining was reported to be implicated in multiple pulmonary diseases development, such as coal workers' pneumonectasis (CWP) and chronic obstructive pulmonary disease (COPD) [3-5]. Several documents reported the correlation between emphysema and COPD with coal dust exposure as well as the association between cumulative exposure and increased mortality from these diseases [1, 6]. In 2013, a total of 23,152 cases were reported in China to be related to occupational cases, among which coal mining activities were involved in more than 50% cases [7]. Currently, the working condition for coal miners was a major area of concern, implying that the working condition of coal miners still needs adequate protection for coal mine dust-related disease prevention [8].

Pulmonary function serves as an important predictor of morbidity and mortality from COPD and coronary heart disease [9]. Pulmonary function test (PFT) was applied to identify dysfunction and abnormalities of the respiratory system [10]. FEV1 (forced expiratory volume in one second after full inspiration) and FEV1/forced vital capacity (FVC) are widely used for pulmonary function examination [11, 12]. The level of FEV1 is a commonly used indicator of the presence and severity of airflow impairment, while a significantly decrease of FEV1 indicates the ongoing adverse health effects [13, 14]. An official

document of the American Thoracic Society (ATS) summarized that an increased risk of chronic cough, lower FEV1 and a lower FEV1/FVC (FEV1%) ratio was related to occupational exposures [15]. Evidence supported that CTE may lead to COPD, including chronic bronchitis and emphysema [1]. In addition, dust exposure was found to be associated with an increased yearly decline in FEV1 in workers of Norwegian silicon carbide plants [16]. However, little attention has been paid to the increase in prevalence and severity of the chronic pulmonary disease that results from CTE [1]. Therefore, the current study was performed to investigate the correlation between CTE and cumulative abnormal rate (CAR) of pulmonary function in coal miners in a Chinese Han population.

METHODS AND MATERIALS

Ethics Statement. The study was performed with the approval of the North China University of science and technology. The informed written consent was collected from each eligible worker and the whole study was performed based on the Declaration of Helsinki [17].

Subjects. A total of 359 male coal miners in one of the coal mine in Tangshan were enrolled as observation group with mean age of 45.7 ± 10.7 years (ranged from 20~60 years). Additionally, a sum of 183 male comparable healthy male workers in instrument and meter plant or electrical equipment factory were selected as control group with mean age of 42.0 ± 11.9 years (ranged from 21~61 years). The healthy controls were extracted from the same region with the coal miners in Tangshan. No statistical significance was detected among the differences of age, body weight, height, duration of employment, duration of smoking and smoking index between two groups (all $P > 0.05$) (Table 1). Subjects were enrolled in this study based on following criteria: exposure to dust for more than one year; dust exposure history in this coal mine accounts for more than 1/2 in one's whole dust exposure career; healthy results of physical examination within two years were provided; clear and complete records of work changes were supplied. Subjects were excluded from current study if they had any history of pulmonary damage and pulmonary injury caused by pulmonary infection, pulmonary tuberculosis, bronchial asthma or bronchiectasis.

Data Collection. An American Thoracic Society questionnaire form was used for data collection, which contains (1) dust exposure history and demography characteristics: age, gender, initial working time, work changes history, current occupation and retirement age; (2) pulmonary function abnormality: time of initial diagnosis, levels and complications; (3) dust exposure: dust concentration, dispersity and free silica content. The occupational histories were mainly extracted from the Capital and Labor Staff Database, supplementary by Occupational Health Examination Records. Any contradictory or difficult problem was settled by face to face interview to employed workers or telephone interview for retired workers. The information on pulmonary function abnormality was collected from the periodic check results in Occupational Diseases Prevention Institute of this coal miner and Capital and Labor Staff Database. Dust exposure data was calculated and collected from the files in Detection Department of Coal mine Ventilation and Administrative Department of Vocational Health in Tangshan. Pulmonary X ray were performed on each subject and characteristics of pulmonary X-rays were recorded.

TABLE 1
Comparisons on baseline characteristics between observation and control groups.

	Observation group (n = 359)	Control group (n = 183)	t/χ^2	*P*
Age (years)	45.7 ± 10.7	43.8 ± 11.5	1.862	0.064
Height (cm)	166.7 ± 5.4	165.8 ± 5.5	1.813	0.071
Weight (Kg)	67.1 ± 13.3	66.5 ± 13.4	0.494	0.622
Smoking (%)	185 (51.5)	90 (49.2)	0.025	0.875
Duration of employment (year)	21.6 ± 10.2	22.4 ± 9.8	0.886	0.376
Duration of smoking (year)	11.6 ± 4.8	10.9 ± 4.1	1.772	0.077
Smoking index (cigarettes/year)	164.5 ± 93.3	158.7 ± 85.6	0.723	0.470

Pulmonary Function Examination. A professional respiratory physician was employed to analyze the results of pulmonary function examination. Pulmonary function measurements were obtained with AS.507 spirometer (Minato, Osaka, Japan). FVC, FEV1, FEV1%, maximal midexpiratory flow (MMEF), vital capacity (VC) and maximal ventilatory volume (MVV) were employed as pulmonary function indexes, which were analyzed with percentages of observed values in predicted values. Before the examination, each subject was asked to rest for 5~10 min. After calmly breathed for 4~5 times, each subjects were told to deep inhale on the oral cavity of equipment and emphatically exhaled with the fastest speed. Special attention should be paid to following points: (1) use mouth to inhale and exhale while the nose was clipped; (2) the mouth should be tightened in case of gas escape; (3) inhale and exhale according to directions of doctors; (4) breath held at full inhalation and exhalation.

Evaluation Criteria. The evaluation criteria was based on the Assessment and Gradation of Disability Caused by Work Related Injuries and Occupational Diseases issued by People's Republic of China (GB/T 16180 2006). According to the tech and method of pulmonary function test, predicted values on healthy normal with the same age, weight, gender, ethnicity and work force were calculated. Above mentioned testing indices equal or higher than 80% of predicted values were considered as normal, otherwise it was regarded as abnormal.

The criteria set for dust exposure years were: a dust exposure year was defined as a whole year of dust exposure without any occupational changes, calculated from the first year. Dust exposure years were classified based on every 10 year, thus grouping into < 10 group, 10~20 year (10~years) group, 20~30 year (20~years) group and >30 years group [18].

CTE ($mg/m^3 \cdot years$) = $\sum Ci * Ti$ (Ci: time-weighted average of dust exposure years; Ti: dust exposure time).

Calculation of CAR of pulmonary function: cumulative abnormal rate = 1-cumulative normal rate; cumulative normal rate = (1-abnormal rate at the present range) × (1-abnormal rate at the higher range); abnormal rate = morbidity/number of adjusted; number of adjusted = (number of the beginning of the period-number of the end of the period)/2. The number of the beginning of the period refers to all the people consistent with the cumulative dust exposure, and the number of the end of the period refers to people consistent with the range of certain cumulative dust exposure.

Statistical Analysis. SPSS 20.0 software (SPSS Inc., Chicago, IL, USA) was applied for data analysis. Summary statistics for subject characteristics were constructed to establish a database and Epidata3.0 was employed for data input. Continuous data were presented with mean ± standard deviation (mean ± SD) and test by Student's *t* test and F test. Categorical data were expressed as percentage and frequency counts. A χ^2 test was employed to compare frequencies. Correlations analyses were calculated by the Pearson's tests. Linear regression analyses were conducted to exam the association between CTE and CAR of pulmonary function. A value of $P < 0.05$ was regarded statistically significant.

RESULTS

Comparisons on incidence of clinical symptoms, pulmonary X ray features, and indexes for pulmonary function. As shown in Figure 1 and Table 2, the percentages of chest tightness, breathlessness, cough and phlegm were respectively 20.9%, 12.0%, 24.0% and 17.8% among the 359 coal worker in observation group while 183 coal workers in control group presented the percentages of 2.2%, 1.6%, 10.9% and 7.7% respectively. This result demonstrated that the observation group presented with a high percentage of clinical symptoms compared with control group with statistical significance ($P < 0.05$). The frequency for increased lung markings, incrassate lung markings, dense lung markings, tortuous lung markings, thick reticular shadows and sparse reticular shadows in observation group were respectively 24.0%, 12.5%, 8.4%, 66.6%, 50.7% and 3.3% in contrast to control group with 7.1%, 4.9%, 3.8%, 8.2%, 4.4% and 0.5% respectively. Observation group had a greater chest X-ray changing frequency than that in control group ($P < 0.05$). The FVC, FEV1, FEV1%, MMEF, VC, MVV in control group were respectively 90.53 ± 7.12, 89.37 ± 6.25, 98.46 ± 1.13, 96.24 ± 19.25, 95.84 ± 24.21, 94.25 ± 18.25, which were all notably higher than 77.34 ± 8.09, 72.96 ± 10.31, 86.87 ± 6.49, 73.96 ± 28.85, 73.50 ± 25.85, 71.97 ± 26.75 in observation group. Those comparisons were statistically significant ($P < 0.05$) (Figure 2).

Pulmonary function indexes in coal miners with different dust-exposed years in observation group. As Table 3 had shown, the increase of dust exposure years were negatively correlated with the decrease of FVC, FEV1, FEV1%, MMEF, VC and MVV (all $P < 0.05$), implying that the pulmonary function was decreased with the increase of dust exposure years (Figure 3).

TABLE 2
Comparisons on incidence of clinical symptoms, pulmonary X ray features and index for pulmonary function between observation and control groups.

	Observation group	Control group	χ^2	*P*
Symptoms				
Chest tightness	75 (20.9%)	4 (2.2%)	34.01	< 0.001
Breathlessness	43 (12.0%)	3 (1.6%)	16.68	< 0.001
Cough	86 (24.0%)	20 (10.9%)	13.63	< 0.001
Phlegm	64 (17.8%)	14 (7.7%)	10,19	0.001
X ray changes				
Increased lung markings	86 (24.0%)	13 (7.1%)	23,06	< 0.001
Incrassate lung markings	45 (12.5%)	9 (4.9%)	7,84	0.005
Dense lung markings	30 (8.4%)	7 (3.8%)	3,17	0.049
Tortuous lung markings	239 (66.6%)	15 (8.2%)	165.9	< 0.001
Thick reticular shadows	182 (50.7%)	8 (4.4%)	114.3	< 0.001
Sparse reticular shadows	12 (3.3%)	1 (0.5%)	4,04	0.044
Pulmonary function indexes				
FVC	77.34 ± 8.09*	90.53 ± 7.12	-	-
FEV_1	72.96 ± 10.31*	89.37 ± 6.25	-	-
FEV_1%	86.87 ± 6.49*	98.46 ± 1.13	-	-
MMEF	73.96 ± 28.85*	96.24 ± 19.25	-	-
VC	73.50 ± 25.85*	95.84 ± 24.21	-	-
MVV	71.97 ± 26.75*	94.25 ± 18.25	-	-

Note: FVC: forced vital capacity; FEV_1: the first second of time vital capacity; FEV_1%: FEV_1/FVC; MMEF: maximal midexpiratory flow; VC: vital capacity; MVV: maximal ventilatory volume, *, compared with control group, $P < 0.05$.

TABLE 3
Comparisons on pulmonary function indexes among coal miners with different dust-exposed years in observation group.

Dust-exposed years	Cases (n)	FVC	FEV_1	FEV_1%	MMEF	VC	MVV
< 10	54	88.04 ± 5.19	87.36 ± 7.92	98.09 ± 1.34	93.71 ± 32.82	85.59 ± 30.31	78.98 ± 30.92
10～	106	80.96 ± 4.28*	79.21 ± 6.85*	90.28 ± 4.26*	80.24 ± 30.41*	81.03 ± 28.29*	75.60 ± 30.85*
20～	128	76.27 ± 5.83*#	71.01 ± 9.24*#	81.85 ± 6.37*#	68.70 ± 25.88*#	69.58 ± 23.36*#	70.29 ± 25.26*#
> 30	71	69.81 ± 7.26*#@	64.68 ± 10.37*#@	73.26 ± 7.98*#@	59.04 ± 24.97*#@	60.12 ± 22.52*#@	61.26 ± 23.15*#@

FVC: forced vital capacity; FEV_1: forced expiratory volume in one second after full inspiration; FEV_1%: FEV 1/FVC; MMEF: maximal mid expiratory flow; VC: vital capacity; MVV: maximal ventilatory volume; *: compared with < 10 groups, $P < 0.05$; #: compared with 10~groups, $P < 0.05$; @: compared with 20~groups, $P < 0.05$.

TABLE 4
Comparisons on pulmonary function between observation and control groups.

Groups	Cases (n)	Abnormal pulmonary function	Normal pulmonary function	χ^2	*P*
Control group	183	20 (10.9%)	163 (89.1%)	55.20	< 0.001
Observation group	359	152 (42.3%)	207 (57.7%)		

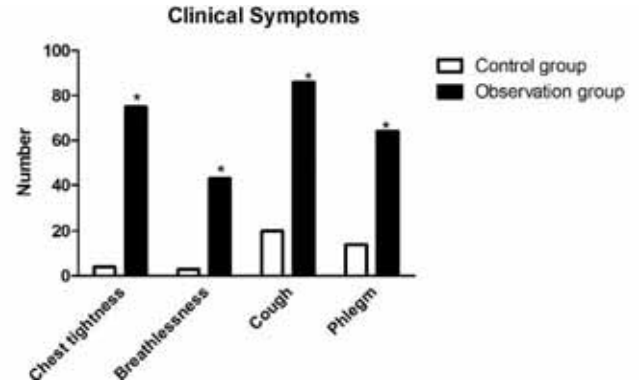

FIGURE 1
Comparisons on clinical symptoms between observation group and control group (*: observation group compared with control group, $P < 0.05$).

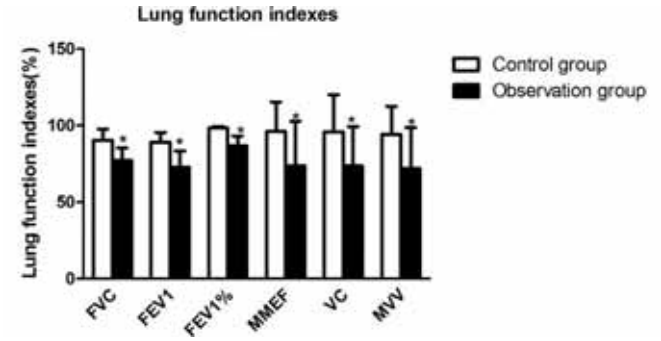

FIGURE 2
Comparisons on lung function indexes between observation group and control group (*: observation group compared with control group, $P < 0.05$).

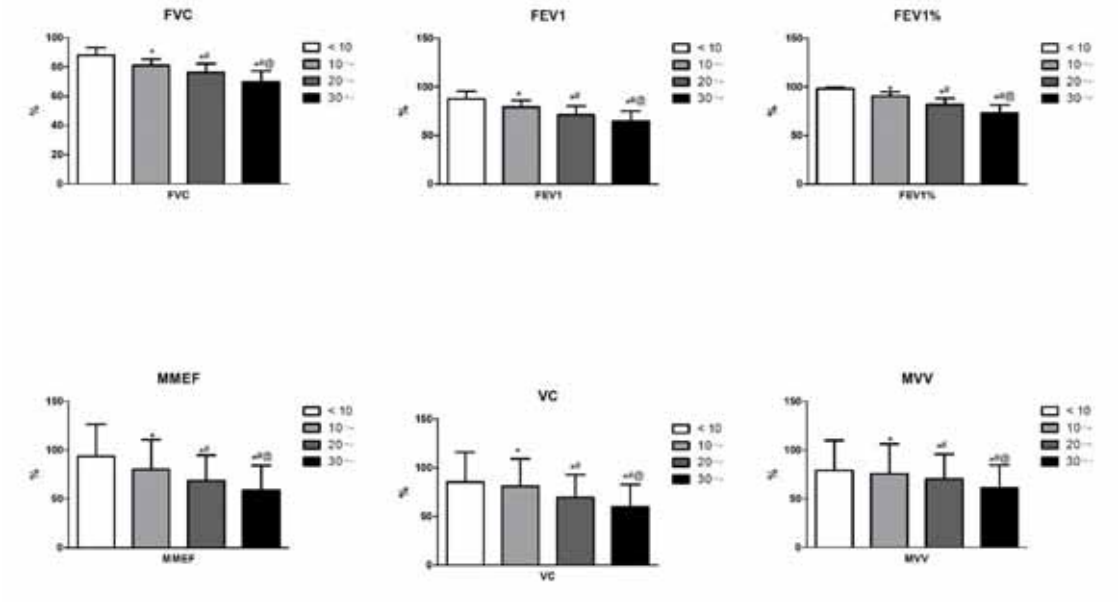

FIGURE 3
Comparisons on lung function indexes among coal workers with differenced dust exposure years in observation group (*: compared with < 10 group, $P < 0.05$; #: compared with 10~ group, $P < 0.05$; @: compared with 20~ group, $P < 0.05$).

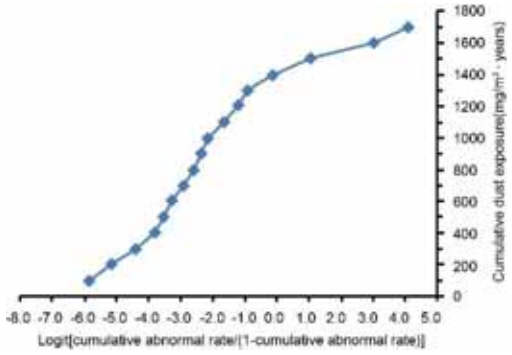

FIGURE 4
Curve diagram of Logit and cumulative dust exposure dose in observation group (Logit = cumulative abnormal rate/ (1 – cumulative abnormal rate)).

Comparisons on abnormal rate of Pulmonary Function. According to the examination results of pulmonary function, observation group had 152 (42.3%) cases of abnormal pulmonary function in contrast to 20 (10.9%) cases in control group (Table 4). The CAR of pulmonary function was remarkably higher in observation group compared with that in control group with statistical significance ($P < 0.001$).

Pulmonary injury levels among coal miners with different dust exposure years in observation group. The pulmonary injury rates in 10~ group, 20~ group and > 30 group were all significantly higher than that in < 10 group (all $P < 0.05$). Furthermore, > 30 group had an increased pulmonary injury rate compared to both 10~ group and 20~ group (both $P < 0.05$) while no significance was found between 10~ group and 20~ group ($P > 0.05$). As shown in Table 5, the dust exposure years were positively correlated with the severity of pulmonary injury, especially in coal miners with dust exposure years > 10 years. A total of 20 (74.1%) cases of severe pulmonary function injury were found in > 30 group while no severe pulmonary function injury was detected in < 10 group.

Comparison of CTE with Pulmonary Function Indexes. As demonstrated in Table 6, the abnormal rates of pulmonary function indexes with different cumulative dust exposure in observation group were all significantly higher than those in control groups (all $P < 0.01$). Moreover, the pulmonary function abnormalities in observation group were positively correlated with the CTE (all $P < 0.01$).

Correlation of CTE with CAR of Pulmonary Function in observation group. Current results revealed that the CAR of pulmonary function in observation group was positively correlated with CTE. CAR of pulmonary function was increased from 0.28% to 98.41% corresponding to the cumulative dust dose increased from 100mg/m^3·years~ group to 1700mg/m^3·years~ group. CAR of pulmonary function developed at high speed with cumulative dust dose ranged from 1000mg/m^3·years~ to 1700mg/m^3·years~ groups. The up limited value of each CTE as dependent variables and CAR of pulmonary function (Logit = cumulative abnormality rate/ (1 - cumulative abnormality rate)) as independent variable showed that the cumulative pulmonary function abnormalities in observation group were positively correlated with the cumulative dust dose (cumulative dust exposure = 178.25Logit+1232.9, $r^2 = 0.91$, $P < 0.001$) (Table 7, Figure 4).

Linear regression analysis on CTE and indexes of Pulmonary Function . As showed in Table 8, linear regression analysis showed that FVC, FEV1 and FEV1% were remarkably associated with CTE (all $P < 0.05$), while MMEF, VC and MVV showed no significant association with CTE of coal miners (all $P > 0.05$).

DISCUSSION

Dust refers to the small solid particles and has the ability to penetrate and deposit at different sites of the respiratory tract, which was usually inhaled through the mouth or the nose [19]. Dust inhalation in coal mine can lead to a variety of pulmonary diseases such as CWP, chronic alveolitis, and emphysema [4]. Thus it is of great importance to investigate the correlation between CTE and CAR of pulmonary function to provide an experimental basis for protective measurement for coal miners. Our results identified that coal miners had a high percentage of chest tightness, breathlessness, cough and phlegm compared with non-dust exposed workers, which may suggest that coal miners had a better chance of developing pulmonary disease. This result was in agreement with previous study showed that under-group exposure to dust cast a large burden of lung disease for coal miners all over the world [1, 20]. There is increasing recognition that both occupational exposure and tobacco use play curial role in the development of chronic obstructive lung disease and evidence showed that coal mine dust exposure is associated with progressive loss of lung function [21]. Even worse, a study by Graber JM et al demonstrated that exposure to coal mine dust and respirable silica could results in elevated mortality from respiratory diseases even in non-smokers [22]. Our study investigated the correlation between CTE and CAR of pulmonary function, which demonstrated that

dust-exposed coal miners had a significant CAR of pulmonary function compared with non-dust exposed workers. FEV1 and FEV1% were commonly used indices for lung function measurements [22]. Low FEV1% was used to evaluate the presence of airflow obstruction, while FEV1 classified the severity and the progression of dust-exposed lung disease [23]. In addition, MMEF was a physiological parameter that enables us to estimate the obstruction in small airways instead of larger airways [24]. In current study, our results demonstrated that aside from FEV1 and FEV1%, MMEF, VC and MVV were all remarkably decreased in dust-exposed coal workers compared with non-dust exposed workers, which suggested the negative correlation of exposure of dust with pulmonary function indexes and further confirmed CTE in coal mine was a significant risk factor for pulmonary function injury. A possible explanation could be that inhalable dusts breathing from nose or mouth can reach the respiratory tract anywhere from the nose to alveoli and cause effects throughout the entire respiratory system, while respirable dusts can enter the alveolar region of the pulmonary and cause fibrosis or pneumoconiosis that may be represented by changes in FVC [25]. The respirable dust in coal mine, such as quartz, asbestos fibers and dust will lead to fibrotic changes of the pulmonary parenchyma and restrictive spirometric changes, leading to a reduced FVC [26]. A previous study indicated a significant negative association of FEV1 and FEV1% with increasing exposure to crystalline quartz at the workplace [27]. In consistence with our results, a preview study in Norway demonstrated that increasing dust exposure in Norwegian smelting industry was negatively correlated with the annual changes in FEV1 [28]. A study conducted by Robert C. Stansbury demonstrated that compared to matched controls, the patients with mineral dust-related airway disease had remarkably decreased FVC and FEV1, suggesting that the pathologic lesions in the small airway had important functional consequences [29].

Our study also investigated the correlation between the CTE and the severity of pulmonary injury in dust-exposed coal miners. The results identified that coal miners with elevated dust exposure also presented with a high frequency of both pulmonary function injury rate and CAR of pulmonary function, indicating a positive correlation of CTE with lung injury rate. Furthermore, we also found that the CAR of pulmonary function increased rapidly with the CTE ranged from 1000mg/m^3·years~ to 1700mg/m^3·years~, indicating that 1000mg/m^3·years was a critical value for CAR of pulmonary function increase. Moreover, a study investigating the correlation between the mortality in British coal workers with respirable dust and quartz exposure confirmed the long term effect of dust exposure on mortality from respirable diseases, which found that the risk of mortality from respirable dust increases with the increased respirable dust exposure [30]. Agreed with the results in our results, a study reported that the prevalence and severity of coal mining related diseases were associated with the increasing mine working time [19]. Partially agreed with our results, a study of males with early COPD suggested that occupational exposure to fumes could play an important part in the increased rate of decline of lung function [31]. Moreover, a study investigating the beneficial effect of dust standards in prevalence and severity of CWP showed that the dust standards paly a certain part in reducing the prevalence and severity of CWP, after adjusting for the potentially confounding effects of age, years of mining, and smoking status [19], which suggested that age, mining years in coal mine and tobacco use as well as dust exposure were implicate in prevalence and severity of pulmonary dysfunction.

There are several highlight that should be noted in this text. Firstly, this is an innovative study with few study reporting similar results. Moreover, our conclusion was more comprehensive and convincible based on various indices, including FVC, FEV1, FEV1%, MMEF, VC and MVV. Additionally, as a tropical coal region, current study conducted in Tangshan may be of representative value for coal mine in China or even in the world. The potential limitation of this text should also be acknowledged. The first one was that only coal miners were investigated in current study and other occupations, like coal-mine drillers and coal porters were overlooked. Another limitation was that our included subjects were limited in one coal mine in Tangshan region. In summary, our study concluded that CTE was positively correlated with CAR of pulmonary function, thus long term exposure to coal mine dust increases the CAR of pulmonary function. We also found that under the certain range of CTE, the CAR of pulmonary function was rapidly increased. As we mentioned in our limitation, to further confirm our conclusion future studies are required to investigate the association of CTE with CAR of pulmonary function in other occupations of coal mine.

ACKNOWLEDGEMENTS

The authors would like to express their gratitude for reviewers for their helpful comments on this paper.

Running title: CTE and CAR of pulmonary function in coal miners

REFERENCES

[1] Petsonk, E.L., Rose, C. and Cohen, R. (2013) Coal mine dust lung disease. New lessons from old exposure. Am J Respir Crit Care Med. 187: 1178-1185.

[2] Vestbo, J., Hurd, S.S., Agusti, A.G., Jones, P.W., Vogelmeier, C., Anzueto, A., Barnes, P.J., Fabbri, L.M., Martinez, F.J., Nishimura, M., Stockley, R.A., Sin, D.D. and Rodriguez-Roisin, R. (2013) Global strategy for the diagnosis, management, and prevention of chronic obstructive pulmonary disease: GOLD executive summary. Am J Respir Crit Care Med. 187: 347-365.

[3] Mohner, M., Kersten, N. and Gellissen, J. (2013) Chronic obstructive pulmonary disease and longitudinal changes in pulmonary function due to occupational exposure to respirable quartz. Occup Environ Med. 70: 9-14.

[4] Lee, J.S., Shin, J.H. and Choi, B.S. (2015) Serum levels of IL-8 and ICAM-1 as biomarkers for progressive massive fibrosis in coal workers' pneumoconiosis. J Korean Med Sci. 30: 140-144.

[5] Santo Tomas, L.H. (2011) Emphysema and chronic obstructive pulmonary disease in coal miners. Curr Opin Pulm Med. 17: 123-125.

[6] Dey, T., Gogoi, K., Unni, B.G., Kalita, M., Bharadwaz, M., Bhattacharjee, M., Boruah, P.K., Bora, T., Ozah, D. and Kalita, M. (2014) Role of glutathione S transferase polymorphism in COPD with special reference to peoples living in the vicinity of the open cast coal mine of Assam. PLoS One. 9: e96739.

[7] Wu, B., Ji, X., Han, R., Han, L., Wang, T., Yang, J., Zhu, B. and Ni, C. (2014) GITR promoter polymorphism contributes to risk of coal workers' pneumoconiosis: a case-control study from China. Immunol Lett. 162: 210-216.

[8] Blackley, D.J., Halldin, C.N., Wang, M.L. and Laney, A.S. (2014) Small mine size is associated with lung function abnormality and pneumoconiosis among underground coal miners in Kentucky, Virginia and West Virginia. Occup Environ Med. 71: 690-694.

[9] Lash, T.L., Johansen, M.B., Christensen, S., Baron, J.A., Rothman, K.J., Hansen, J.G. and Sorensen, H.T. (2011) Hospitalization rates and survival associated with COPD: a nationwide Danish cohort study. Lung. 189: 27-35.

[10] Hyatt, R.E., Scanlon, P.D. and Nakamura, M. (2014) Interpretation of lung function tests. Lippincott Williams & Wilkins.

[11] Leaker, B.R., Barnes, P.J., Jones, C.R., Tutuncu, A. and Singh, D. (2015) Efficacy and safety of nebulized glycopyrrolate for administration using a high efficiency nebulizer in patients with chronic obstructive pulmonary disease. Br J Clin Pharmacol. 79: 492-500.

[12] Nishimura, M., Makita, H., Nagai, K., Konno, S., Nasuhara, Y., Hasegawa, M., Shimizu, K., Betsuyaku, T., Ito, Y.M., Fuke, S., Igarashi, T., Akiyama, Y., Ogura, S. and Hokkaido, C.C.S.I. (2012) Annual change in pulmonary function and clinical phenotype in chronic obstructive pulmonary disease. Am J Respir Crit Care Med. 185: 44-52.

[13] Celli, B.R., MacNee, W. and Force, A.E.T. (2004) Standards for the diagnosis and treatment of patients with COPD: a summary of the ATS/ERS position paper. Eur Respir J. 23: 932-946.

[14] Force, A.T.S.E.R.S.T. (2004) Standards for the diagnosis and management of patients with COPD, version 1.2. www.thoracic.org/go/copd.

[15] Eisner, M.D., Anthonisen, N., Coultas, D., Kuenzli, N., Perez-Padilla, R., Postma, D., Romieu, I., Silverman, E.K., Balmes, J.R., Committee on Nonsmoking Copd, E. and Occupational Health, A. (2010) An official American Thoracic Society public policy statement: Novel risk factors and the global burden of chronic obstructive pulmonary disease. Am J Respir Crit Care Med. 182: 693-718.

[16] Johnsen, H.L., Bugge, M.D., Foreland, S., Kjuus, H., Kongerud, J. and Soyseth, V. (2013) Dust exposure is associated with increased lung function loss among workers in the Norwegian silicon carbide industry. Occup Environ Med. 70: 803-809.

[17] Health, T.N.A.C.R.f.b.N.I.o. (2011) Guide for the Care and Use of Laboratory Animals. Washington (DC).

[18] Wu, Q.L., Ding, X.P., Xu, X.H., Wang, H.D. and Cheng, X.R. (2010) Investigation on lung functional indices in workers exposed to dust

in a coal mine industry group. China Occupational Medicine. 37: 261-262.

[19] Vallyathan, V., Landsittel, D.P., Petsonk, E.L., Kahn, J., Parker, J.E., Osiowy, K.T. and Green, F.H. (2011) The influence of dust standards on the prevalence and severity of coal worker's pneumoconiosis at autopsy in the United States of America. Arch Pathol Lab Med. 135: 1550-1556.

[20] Mehta, A.J., Miedinger, D., Keidel, D., Bettschart, R., Bircher, A., Bridevaux, P.O., Curjuric, I., Kromhout, H., Rochat, T., Rothe, T., Russi, E.W., Schikowski, T., Schindler, C., Schwartz, J., Turk, A., Vermeulen, R., Probst-Hensch, N., Kunzli, N. and Team, S. (2012) Occupational exposure to dusts, gases, and fumes and incidence of chronic obstructive pulmonary disease in the Swiss Cohort Study on Air Pollution and Lung and Heart Diseases in Adults. Am J Respir Crit Care Med. 185: 1292-1300.

[21] Stansbury, R.C., Beeckman-Wagner, L.A., Wang, M.L., Hogg, J.P. and Petsonk, E.L. (2013) Rapid decline in lung function in coal miners: evidence of disease in small airways. Am J Ind Med. 56: 1107-1112.

[22] Ong, B.A., Li, J., McDonough, J.M., Wei, Z., Kim, C., Chiavacci, R., Mentch, F., Caboot, J.B., Spergel, J., Allen, J.L., Sleiman, P.M. and Hakonarson, H. (2013) Gene network analysis in a pediatric cohort identifies novel lung function genes. PLoS One. 8: e72899.

[23] Hancock, D.B., Eijgelsheim, M., Wilk, J.B., Gharib, S.A., Loehr, L.R., Marciante, K.D., Franceschini, N., van Durme, Y.M., Chen, T.H., Barr, R.G., Schabath, M.B., Couper, D.J., Brusselle, G.G., Psaty, B.M., van Duijn, C.M., Rotter, J.I., Uitterlinden, A.G., Hofman, A., Punjabi, N.M., Rivadeneira, F., Morrison, A.C., Enright, P.L., North, K.E., Heckbert, S.R., Lumley, T., Stricker, B.H., O'Connor, G.T. and London, S.J. (2010) Meta-analyses of genome-wide association studies identify multiple loci associated with pulmonary function. Nat Genet. 42: 45-52.

[24] Mirsadraee, M., Boskabady, M.H. and Attaran, D. (2013) Diagnosis of chronic obstructive pulmonary disease earlier than current Global Initiative for Obstructive Lung Disease guidelines using a feasible spirometry parameter (maximal-mid expiratory flow/forced vital capacity). Chron Respir Dis. 10: 191-196.

[25] Shieh, T.S., Chung, J.J., Wang, C.J., Tsai, P.J., Kuo, Y.C. and Guo, H.R. (2012) Pulmonary function, respiratory symptoms, and dust exposures among workers engaged in early manufacturing processes of tea: a cohort study. BMC Public Health. 12: 121.

[26] Bruske, I., Thiering, E., Heinrich, J., Huster, K. and Nowak, D. (2013) Biopersistent granular dust and chronic obstructive pulmonary disease: a systematic review and meta-analysis. PLoS One. 8: e80977.

[27] Bruske, I., Thiering, E., Heinrich, J., Huster, K.M. and Nowak, D. (2014) Respirable quartz dust exposure and airway obstruction: a systematic review and meta-analysis. Occup Environ Med. 71: 583-589.

[28] Johnsen, H.L., Hetland, S.M., Benth, J.S., Kongerud, J. and Soyseth, V. (2010) Dust exposure assessed by a job exposure matrix is associated with increased annual decline in FEV1: a 5-year prospective study of employees in Norwegian smelters. Am J Respir Crit Care Med. 181: 1234-1240.

[29] Stansbury, R.C., Beeckman-Wagner, L.A., Wang, M.L., Hogg, J.P. and Petsonk, E.L. (2013) Rapid decline in lung function in coal miners: evidence of disease in small airways. Am J Ind Med. 56: 1107-1112.

[30] Miller, B.G. and MacCalman, L. (2010) Cause-specific mortality in British coal workers and exposure to respirable dust and quartz. Occup Environ Med. 67: 270-276.

Received: **20.01.2016**
Accepted: **10.05.2016**

CORRESPONDING AUTHOR

Fu-Hai Shen
Correspondence to: Professor Fu-Hai Shen
College of Public Health
North China University of Science and Technology
No. 57, South of Construction Road
North District of Tangshan Road
Tang Shan 063000, P.R. - CHINA

E-mail: shenfuhai804@126.com

© by PSP Volume 25 – No. 10/2016, pages 3895-3906 Fresenius Environmental Bulletin

THE FATE OF MERCURY DURING COAL COMBUSTION: OCCURRENCE MODE, TRANSFORMATION, EXISTENCE FORM AND EMISSION

Debo Li[1], Lili Fu[2], Qisheng Xu[1], Jie Gao[2], Jianyi Lu[2]*

[1]Electric Power Research Institute of Guangdong Power Grid co., Ltd., Guangzhou, 510080,Guangdong, P.R.China
[2]School of Environmental Science and Engineering, North China Electric Power University, Baoding, 071003, Hebei, P.R.China.

ABSTRACT

Mercury is an important toxic and hazardous substance in the natural environment, and is also one of HAPs in CAAA established by the United States. Source apportionment results show that the coal combustion process is one of the important source emission of mercury in the atmosphere. Based on the principle of material circulation and mass conservation, the occurrence mode and content of mercury in the coal before combustion was investigated, and its transformation and influence factors varied from temperature -time in the combustion process, as well as with speciation and mass distribution in the slag, fly ash, flue gas was discussed. According to the investigation, the emission control methods for mercury generated from coal combustion were proposed, and were generalized as pre-combustion control, in-combustion control, and post-combustion control. Pre-combustion control refers to the use of coal washing, heat treatment technology and improving quality of coal to reduce the mercury content in the coal; In-combustion control is the method of adjusting the combustion conditions and injection of additives during the combustion process to promote the adsorption of mercury or improve the formation of Hg^{2+}; Post-combustion control means that the mercury adsorbed by activated carbon, or corporately removal by SCR, ESP and WFGD from flue gas. Finally, the influence factors on the mercury removal are discussed, and some suggestions are put forward to reducing the mercury emission in coal-fired power plants.

KEYWORDS:
Mercury; Coal combustion; Transformation; Removal

INTRODUCTION

Mercury in the earth's crust can be emitted and released in several ways to water, air and soil. Mercury-containing rocks through natural weathering are continuous, allowing mercury to enter atmosphere, water and soil [1,2]. Meanwhile, geothermal activity and volcanic eruptions release mercury to our surrounding environment. Mercury is widespread in nature, through the respiratory tract, esophagus and skin into the human body, the vast majority of the general population intake mercury through diet. The human nervous system is mainly attacked by the mercury entering the body, especially in the central nervous system [3]. Due to the forms of mercury is different, the intensity of toxicity for human is different, which are organic mercury, inorganic mercury, elemental mercury, and within methyl mercury is most serious [4,5]. Mercury can be accumulated in organisms, and easily absorbed by skin, respiratory and digestive tract. Trace mercury exists in most animals and plants, as a result exists in our food and would be metabolized by the excretion as well as hair.

Mercury in the earth's crust, the total mercury reserves is about 160 billion tons. But 99.98% of the mercury is sparsely dispersed state, and only 0.02% of the mercury enriched in the ore can be mined [6]. Almost all of the earth elements are enriched in the process of long-term formation of coal, the average mercury content is 0.1mg/kg in coal [7,8]. Although the mercury content in coal is very low, as a result of the huge global consumption of coal, the coal combustion process is the most important sources of mercury in the atmosphere. The UNEP reported that coal burning was a continuing main source of emissions, about 475 tonnes of mercury emissions to air annually, of which about 10 tonnes from others fossil fuels combustion. The survey shows that more than 85% of emissions are from coal burning in power generation and other industrial uses [9].

The existence forms of mercury in the atmosphere are complex and varied. Due to its chemical properties, mercury in the atmosphere can be classified into three main forms: elemental mercury Hg^0, monovalent oxidized mercury Hg^+ and divalent oxidized mercury Hg^{2+}. The physical property decides two forms in the atmosphere: gaseous mercury Hg^0 and particulate mercury Hg^P. Hg^0 is the main element of the gaseous mercury, gaseous mercury are also formed by minority of monovalent and divalent mercury with strong volatility, such as $HgCl_2$, $HgBr_2$, CH_3HgCl,

$(CH_3)_2Hg$, et al [10]. Particulate mercury generally accounts for only 5% to 10% of the total atmospheric mercury [11], which refers to mercury combined with atmospheric particles (or aerosols). Both volatile mercury and its compounds are adsorbed on the surface of particles (such as Hg^0 and $HgCl_2$) and mercury is compounded with particles directly (such as Hg^0, HgS) [12].

In China, accompanied with the issuance of GB13223 "Thermal Power Plant Air Pollutant Emission Standards", people pay much more attention to the impact of atmospheric mercury on the daily production and life. It is the first time that mercury emissions has been taken into consideration for the pollutant emission control targets in the standards, and the standards require emissions of mercury and its compounds to meet the limit of 0.03 mg/Nm^3 after January 1, 2012.

OCCURRENCE MODE OF MERCURY IN COAL

During the course of geological history, increasing temperature and pressure spanning over millions of years, the plant and peat bogs have been converted to lignite, sub-bituminous coal, bituminous coal and anthracite. So the coal structure is more complex, the occurrence mode and content of mercury in coal varies from mine to mine. Higher mercury content (>1.0 mg/kg) is quite rare, but many authors cited higher values for coal [13,14]. Due to natural geological processes, the mercury content in coal is high. It depends on density, presence of sulfur, and analytical technique. And mercury content is connected with moisture in coal [15]. Both the logarithm of cumulative mass of Hg0 formed in soils and the reduction rate constants (k values) increased with moisture [16]. Previous research suggests that soil moisture drives adsorbed Hg0 into the soil air and also moves adsorbed Hg^{2+} into the soil water, where it can be reduced to Hg^0 [17, 18].

Mercury can be divided into organic mercury and inorganic mercury in the coal combustion, and mainly exists in the form of inorganic mercury [19]. Some studies indicated that mercury in coal mainly occur with pyrite. In the same coal samples, when the sub-samples of density are different, mercury distribution in pyrite is uneven. Pyrite-bound Hg can be released by pyrolysis only at a temperature of 400-600℃[20].

Mercury is a typical chalcophile element, most mercury in coal with solid phase exists in pyrite. Epigenetic pyrite probably has substantially greater mercury contents than the early-stage (syngenetic) pyrite does, such as framboidal pyrite [21]. Besides pyrite, it could also be found in other sulfides and selenides. As for the chemical properties of mercury, mercury mainly existed in the form of sulfide in nature, but the mercury proportion varied from different types of coal [22]. According to each era coal accounts for the weight of the country's coal reserves, Ren calculated the total resources of mercury in China coal, average content of 0.188 mg/kg is currently the most authoritative data about China's average content of mercury in coal [23].

In summary, the mercury in coal with a variety of the occurrence mode, its main occurrence mode is water soluble, exchangeable, organic bound, carbonate bound, silicate and sulfide bound. Most of the mercury exists in cinnabar, galena and sphalerite, especially sulfide of pyrite [23]. Material composition of coal is extremely complex, while the mercury content in coal is very low, in addition, highly volatile is also another feature of mercury, all of these lead to the relative difficulty for studying the occurrence mode of mercury in coal. Throughout the studies [16,24,25], it found that accumulation of mercury in coal is affected by many factors, the coal rank is just one of the factors which affect the coal formation process as well as post-depositional environment of coal, construction and other factors, and it also determines the level of mercury content in coal and the occurrence mode.

TRANSFORMATION AND REACTION MECHANISM OF MERCURY DURING COAL COMBUSTION

Coal-fired power plants are one of the largest anthropogenic sources of mercury emissions to the environment [26]. Defining the mercury species in coal may be useful in understanding its fate after combustion. Mercury will undergo complex physical and chemical changes during the coal combustion process, finally emit into atmosphere via the gas phase and aerosols. The kind of change is affected by many factors, such as the existence of oxidizing and reducing substances, the physical and chemical properties of fly ash, and the temperature of flue gas. These factors will eventually lead to different forms of mercury in flue gas outlet.

Transformation of mercury during coal combustion. During the coal combustion process in coal-fired power plants or industrial coal-fired boilers, the temperature is reduced from 1800K to 400K, mercury also undergoes a series of transformation accordingly. The transformations of Hg^0 oxidized forms are highly temperature dependent and predominantly occur below temperatures of 800 K [27]. With the advent of cooling process, elemental mercury undergo respectively through the following several different changes:

Part of gaseous elemental mercury undergoes physical adsorption, chemical adsorption and chemical reaction, and transform to particulate

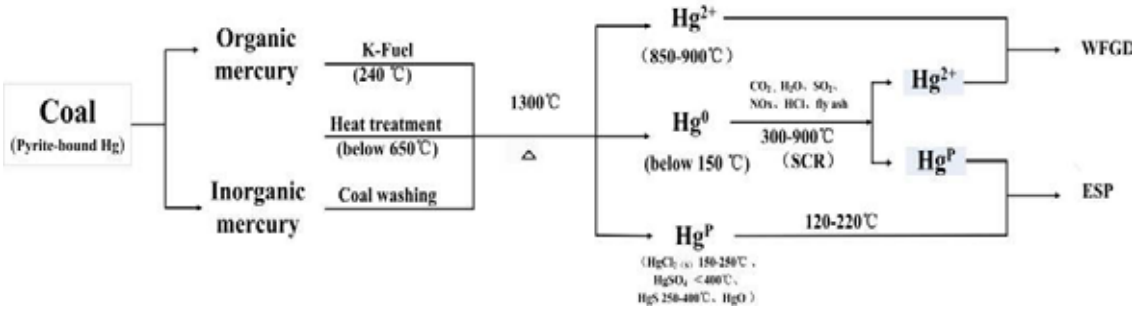

FIGURE 1
Mercury varied with the temperature -time in the coal combustion process

mercury (Hg^p), mainly includes $HgCl_2$, HgO,$HgSO_4$ and HgS, etc.; Part of gaseous elemental mercury occurs an oxidation reaction with the presence of chlorine, under the condition of flue gas temperature reduces to a certain range (the primary mercury oxidation product in flue gas is believed to be $HgCl_2$, part of mercury adsorbed by fly ash particles into particulate mercury) [25]; In the process of flue gas temperature decrease, part of gaseous elemental mercury undergoes catalytic oxidation of material in fly ash particles surface and generates gaseous bivalent mercury (Hg^{2+}) [28]; Part of gaseous elemental mercury remains invarible, along with the flue gas discharges.

Researchers [29] according to the experiments to calculate the results: each occurrence mode of mercury has its characteristic temperature range for mercury release. Hg^0 is below at 150℃, $HgCl_2$ or organic-bound Hg at 150-250℃, HgS or silicate-bound Hg at 250-400℃, and pyrite-bound Hg at 400-600℃. The research shows that [30] when the temperature is higher than 750℃, $Hg^0(g)$ is the only thermodynamically stable form of mercury; When the temperature of the flue gas is cooled to 400℃, $HgCl_2$ is the main existence forms of divalent mercury in the chlorine-containing flue gas [31]. However, due to practical combustion conditions the theoretical calculation may not fit well with the practical situation.

Reaction mechanism. At present, the studies about the reaction mechanism of mercury in coal combustion process mainly use quantum chemistry, chemical kinetics, and chemical thermodynamics. In a certain extent, mercury can be oxidized by different components and medias in flue gas, such as Cl, N, C, fly ash and SCR. The reaction mechanism schematic is illustrated as Figure 1.

Influence of halogen elements components. There are some materials can react with mercury in the flue gas, such as HCl (g), Cl_2 (g), HBr, HI,and the reaction intermediate of Cl(g). The formation processes of $HgCl_2$ and $Hg^0(g)$ are generally considered as the main mechanism of migration and transformation of mercury in the cooling flue gas. Halogen elements has important influence on the mercury oxidation, for it is easy to release in high temperature flue gas, so its content in flue gas increases with the increase of flue gas temperature, then the content of oxidized mercury increases accordingly. HCl(g) and $Cl_2(g)$ are the most important oxidizing agents of $Hg^0(g)$, in which $Cl_2(g)$ have a stronger oxidizing ability. After the coal was added Fe_2O_3, the concentration of $Cl_2(g)$ increased pathway may result from the Deacon reaction [32,33], the reaction requires the presence of an iron-based catalyst, as follows:

$$4HCl(g)+O_2(g)\rightarrow 2Cl_2(g)+2H_2O(g) \quad (1)$$

The influence of hydrogen chloride on mercury transformation. After the coal combustion, chlorine in coal mainly exists in the form of HCl, the content of HCl is far greater than the amount of Cl2, HCl has a promoting effect on the mercury oxidation [34,35]. The content of HCl directly affects the formation distribution of mercury in flue gas. The chemical equation of direct reaction by Hg and HCl is shown as the following:

$$Hg^0(g)+2HCl(g) \rightarrow HgC1_2(g)+H_2(g) \quad (2)$$

In Stolle's view, an increase in the HCl concentration led to higher oxidation activity for mercury. The highest sensitivity of the mercury oxidation activity to the HCl concentration was from 5 to 40 mg/m^3 [36]. The reaction is shown as the following:

$$Hg(g)+2HCl(g)+0.5O_2 \rightarrow HgCl_2(g)+H_2O(g) \quad (3)$$

The reaction mechanism that is relevant to this research is divided into the following categories:

One possible mechanism: In Sliger's view [37], on the one hand, $Hg^0(g)$ reacts with HCl(g) and generates HgCl(g); On the other hand, $Hg^0(g)$ reacts with dissociation of Cl(g) from HCl(g) and generates HgCl(g), then HgCl(g) reacts with HCl(g) and generates $HgCl_2(g)$, the reaction equations are as follows:

$$HCl(g)\rightarrow Cl(g)+H \quad (4)$$

$$Hg^0(g)+Cl(g)\rightarrow HgCl(g) \quad (5)$$

$Hg^0(g)+HCl(g)\rightarrow HgCl(g)+H$ (6)

$HgCl(g)+HCl(g)\rightarrow HgCl_2(g)+H$ (7)

The other reaction mechanism: Cl contained in coal is released in flue gas as HCl or Cl, which then reacts with mercury, producing oxidized Hg compounds [38].

The influence of chlorine gas on mercury transformation. Although it exists slightly in the flue gas, oxidized mercury in the flue gas is still positively correlated with Cl_2. Hall etc. [39,40]found that elemental mercury reacted with the flue gas of $O_2(g)$, HCl(g), and $Cl_2(g)$ rapidly, and generated mercuric oxide and mercuric chloride. The reaction rate of $Cl_2(g)$ with mercury was much faster than HCl(g). Laudal [41] and Agarwal [42] experiments also showed that, chlorine had strong oxidizability of mercury extremely in some cases. Sliger' s[37] study showed that the reaction took place between Hg^0 (g) and $Cl_2(g)$, which were as follows:

$Hg^0(g)+Cl_2(g)\rightarrow HgCl_2(g，s)$ （8）

This process includes two sections, the first section is that Hg^0 (g) reacts with $Cl_2(g)$ and generates intermediate Cl(g); the second section is that free state Cl(g) reacts with $Hg^0(g)$ rapidly:

$Hg^0(g) + Cl_2(g)\rightarrow HgCl(g)+Cl(g)$ （9）

$Hg^0(g)+Cl(g)\rightarrow HgCl(g)$ (react rapidly) （10）

$HgCl(g)+Cl(g)\rightarrow HgCl_2(g)$ （11）

In the process, $Cl_2(g)$ decomposes free state Cl (g) and promotes the progress of reaction:

$Cl_2(g)\rightarrow 2Cl(g)$ (12)

But in some cases, the chlorine content is not the decisive factors of the degree of mercury oxidation, the other components in flue gas may also affect the mercury oxidation, besides Cl_2 and HCl [43].

The influence of other halogen elements on mercury transformation. Under high temperature, bromine mainly is Br (g) and HBr (g). In the high temperature combustion area, Br (g) is a major form of bromine. Along with the temperature decreased, HBr (g) increases with the Br (g) to gradually reduce. The maximum formation of HBr(g) at the temperature of 825 ~ 925k. After the temperature dropped to 1000 k, can observe Br_2 (g) and BrCl (g).At 675k, the Br_2 (g) to achieve the greatest generation. When the temperature dropped to 500 k, BrCl (g) is the main form of flue gas in bromine [44].

The effects of HBr and HI on Hg oxidation were studied on some experiments [45,46]. Both HBr and HI are shown to be stronger mercury oxidants than HCl. At concentrations of 2 ppm, both HBr and HI oxidize more than 85% of the inlet elemental mercury. HBr causes a large amount of the oxidized mercury to be retained on the catalyst while HI desorbs previously retained mercury from the catalyst surface.

Influence of sulfur components. According to the theory about mercury was oxidized by S and Cl in flue gas, the reaction equations of SO_2 are as follows: [42]:

$SO_2(g)+O_2(g)+Hg^0(g)\rightarrow HgSO_4(g,s)$ (13)

$HgCl_2(g)+SO_2(g)+O_2(g)\rightarrow HgSO_4(s)+Cl_2(g)$ (14)

$Cl_2(g)+SO_2(g)\rightarrow SO_2Cl_2(g)$ (15)

$Hg^0(s, g)+SO_2(g)\rightarrow Hg^0(g)+SO_3(g)$ (16)

According to the above-mentioned reaction, $SO_2(g)$ both improve the formation rate of $Hg^{2+}(g)$ (Equation (13), (14)) and control the formation rate of $Hg^{2+}(g)$ (Equation (15), (16)). Furthermore, Agarwal's[42] research shows that Equation (13) and (14) are the main reaction mechanism, the $SO_2(g)$ content can promote the mercury oxidation. In the details, the high ratio of S/Cl can promote Equation (15) to increase the consumption of $Cl_2(g)$. Consequently, inhibiting the formation of $HgCl_2(g)$.

Mercury may also be adsorbed on fly ash components. $SO_3(g)$ competes for the active sites on the carbonaceous surface and inhibits Hg adsorption. $SO_3(g)$ cannot directly provide the active sites [47]. Besides, during combustion and along the flue gas path, $SO_3(g)$is formed from $SO_2(g)$ in a homogeneous gas phase reaction or in a heterogeneous, solids catalyzed reaction for example on iron oxides [48, 49]. The sulfur content of the coal affects directly the $SO_2(g)$ partial pressure and therefore indirectly the $SO_3(g)$ levels and is one of the most important parameters influencing the $SO_3(g)$ concentrations in the flue gas [50]. According to the above, due to the sulfur trioxide affects indirectly mercury transformation.

Influence of nitrogenous components. Reactions between NOx and Hg^0 in gas phase may give rise to different mercury nitrates that might condense on the surface of the char sorbents [51]. On the one hand, NO_x in flue gas has certain influence on the formation distribution of mercury, the formation of the different mercury nitrates could occur via the following reactions [52]:

$4Hg^0(g)+ 6NO_2(g)\rightarrow Hg_2(NO_3)_2 +Hg_2(NO_2)_2+2NO(g)$ (17)

$4Hg^0(g) +4NO_2(g)+O_2(g)\rightarrow Hg_2(NO_3)_2+Hg_2(NO_2)_2$ (18)

$4Hg^0(g)+6NO(g)+3O_2(g)\rightarrow Hg_2(NO_3)_2+Hg_2(NO_2)_2+2NO(g)$ (19)

$4Hg^0(g) +4NO(g)+3O_2(g)\rightarrow Hg_2(NO_3)_2+Hg_2(NO_2)_2$ (20)

In these mercury species, mainly $Hg_2(NO_3)_2$, and crystallizing from slightly acidified aqueous solutions in the form of dehydrate (the formation of HNO_2 (aq) and/or HNO_3 (aq) has been confirmed in

atmospheres containing NOx and H_2O[53].On the other hand, Agarwal's[42]experiment is that NO consumes $Cl_2(g)$ and inhibits the mercury oxidation via the following reaction:

$$2NO(g)+Cl_2(g)\rightarrow 2NOCl(g) \quad (21)$$

The point is that due to the following balance between NO(g) and $NO_2(g)$:

$$2NO(g)+O_2(g)\longleftrightarrow 2NO_2(g) \quad (22)$$

Thus NO_x both promote and inhibit the conversion of Hg^0 (g): When concentration of NO is low, the above balance proceed to the reverse reaction, the main reaction takes place between NO(g) and O_2, and promotes the mercury oxidation; when concentration of NO is high, the above balance react to the positive. The reaction takes place between $Hg^0(g)$ and NO_2, plays a dominant role, and inhibits the mercury oxidation. In actual reaction, the influence on Hg^0 transformation depends on its concentration in flue gas.

Influence of oxygen elements. The influence of oxygen element for mercury transformation mainly consists of two aspects:

(1) Direct reaction: Hall etc. [40] put forward that, when oxygen exists in flue gas, the oxidation reactions takes palace between $Hg^0(g)$ and oxygen quickly. With the amount of oxygen increasing, the conversion rate of Hg^0 also increased. By comparison, the activity of O_2 is poor than HCl, SO_2, and Cl_2.

(2) Indirect reaction: The existence of oxygen can affect a variety of balance to promote or inhibit the mercury oxidation.

For instance: Equation (22) shows that excess oxygen generated more NO_2. A small amount of O_2 in reaction, NO is more. O_2 can affect the transformation of mercury in above balance indirectly.

Influence of componential of carbonaceous substance. Reduction of oxidized mercury may be a migration transformation mechanism in the flue gas. Coal combustion produces a large amount of carbon dioxide, the reduction reaction between coal/coal tar and high concentrations of CO_2, and generates a large amount of CO (g). Hg^0 (s, g) will be reduced to Hg^0 (g) by the following reaction:

$$CO_2(g)+C(s)\rightarrow 2CO(g) \quad (23)$$

$$Hg^0(s,g)+CO(g)\rightarrow Hg^0(g)+CO_2(g) \quad (24)$$

Influence of fly ash. Controlled by the chemical kinetics, as well as the residence time in the flue gas, the homogeneous oxidation reaction between flue gas composition and $Hg^0(g)$ is under different degree of inhibition. However, when the inorganic substances and carbon exist in flue gas, the situation has changed. The influence of fly ash on the mercury transformation is mainly reflected in two aspects:

(1)Chemical absorption: By reaction with inorganic minerals and carbon-containing particle (active chemical components and oxidation catalyst), $Hg^0(g)$ is oxidized into $Hg^{2+}(g)$. There are mercury adsorption sites on the surface of fly ash particles [54,55]. Sulfur-rich fly ash may be reactants and adsorbent of $Hg^0(g)$ [56]. During the coal combustion, S is released in the form of $SO_2(g)$, and about 1-3% of SO_2 (g) are oxidized into SO_3 (g). When the temperature drop below sulfuric acid dew point, $H_2SO_4(l)$ condenses on the surface of fly ash particles and mercury may be adsorbed to the surface of $H_2SO_4(l)$. At the same time, sulfur compounds is adsorbed to the particles, the process may also produce the adsorption activity of Hg .Therefore, we often use adsorbent which are vulcanized to remove the mercury in flue gas.

(2) Physical absorption: Hall etc. [57] found that when temperature is between 100℃ and 300℃, oxygen can promote the adsorption of $Hg^0(g)$ by active carbon and fly ash. Laudal etc. [41] studied the influence of components in simulated flue gas (O_2, H_2O, N_2, SO_2, NO, NO_2, HF, HCl, Cl_2) on reaction of $Hg^0(g)$-fly ash and Hg^0 (g)-carbon, and found that the temperature is below 200 ℃, the existence of the $NO_2(g)$ can inhibit the adsorption of fly ash and carbon on $Hg^0(g)$, while promoting the formation of $Hg^{2+}(g)$. All above that, oxides and chlorides in the flue gas and oxidation catalyst on the surface of fly ash, which are critical factors for the adsorption and oxidation of Hg^0 (g) to Hg^p and $Hg^{2+}(g)$.

Influence of flue gas temperature. Combustion temperature affects the distribution and the volatilization of mercury in flue gas. With increasing flue gas temperature, Hg^{2+} decreased. At higher temperatures, most of the Hg are converted into Hg^0 (g), in other words, mercury conversion rate reduced [58].Elemental mercury is thermodynamically stable form of mercury at the highest temperature in combustion and gasification area, almost all mercury would evaporate into the gas phase, and the main form of mercury is elemental mercury in the relative reducing atmosphere of flue gas.

MERCURY EXISTENCE FORM IN COMBUSTION FLUE GAS

Mercury in flue gas can be divided into three kinds of forms [35]: zero-valent gaseous mercury (Hg^0), also known as gaseous mercury or gaseous

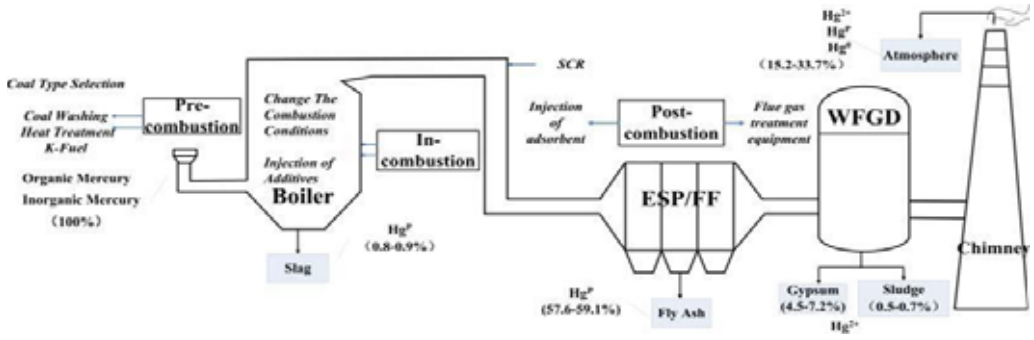

FIGURE 2
The fate of mercury during coal-fired power plants

elemental mercury, abounds when the temperature is greater than 600℃; gaseous oxidized mercury (Hg^{2+}), also known as gaseous divalent mercury, exists in the form of $HgCl_2$ when the temperature is below 400℃; particulate mercury (Hg^p), also called particles adsorbed mercury, do not distinguish between valence state.

Due to Hg^0 with chemical inertness, fairly low water solubility and effumability, it's difficult to be removed. And Hg^0 stays in the atmosphere longer than Hg^{2+} and Hg^P, and is much easier for long distance transportation. So it is the key problem of mercury removal from coal-fired flue gas. Lu etc. [59] found that the concentration of Hg^{2+} increased while the concentration of Hg^0 decreased in flue gas after the ESP. Besides, catalyst can also be used for converting $Hg^0(g)$ to $Hg^{2+}(g)$ in flue gas, thus improving the efficiency of mercury removal. Then Hg^{2+} can be dissolved in gypsum slurry of wet desulfurization and adsorbed on the gypsum granules. Finally, Hg^p can be removed via the capture of particulate matter [60]. In other words, raising the proportion of Hg^0 into Hg^{2+} can effectively control emissions of mercury form coal-fired power plant. The transformation of mercury is mainly influenced by the following several factors: coal, combustion temperature, combustion flue gas, components of flue gas.

The influence of coal. Coal is mainly divided into bituminous coal, anthracite and lignite. About 70% of mercury is divalent mercury in the combustion flue gas from bituminous coal; the proportion of oxidation mercury and element mercury is roughly in the combustion flue gas from anthracite; mercury exists mainly in the form of element mercury in the flue gas from lignite.

The influence of combustion temperature. Through thermodynamic calculation, common coal combustion temperature is about 1200 ℃, under this temperature, most of the mercury normally exists in the form of elements mercury. Decreasing the combustion temperature appropriately, for example dropping to 850-950℃, is beneficial to the formation of Hg^{2+}.

The influence of the flue gas atmosphere. According to the theory of chemical reaction, the oxygen content has a great influence on the transformation from Hg^0 to Hg^{2+}. Oxidizing atmosphere is in favor of the formation of Hg^{2+}, and reducing atmosphere is adverse to the formation of Hg^{2+}. At present most of the flue gas is reducing atmosphere, the main reason is that the element mercury accounted for the proportion of the total mercury is too high.

The influence of flue gas composition. The flue gas composition can affect the oxidative or reductive reactions of mercury after combustion, thereby affect the form of mercury in the exit of the chimney. For example, the existence of chlorine helps mercury oxidization [61].

CONTROL METHODS

Based on a series of studies on the speciation distribution, migration and transformation of mercury, as well as the mercury removal in coal-fired power plants, and integrated above discussion results, a systematic method for abating the formation and emission of mercury in coal-fired power plants was formulated. Furthermore, the emission control methods for mercury generated from coal combustion were proposed, and were generalized as pre-combustion control, in-combustion control, and post-combustion control. Besides, the mass distribution of mercury in coal-fired power plants during the migration process was speculated as well by citing some relevant data [62]. Finally, the fate schematic of mercury during the coal combustion in coal-fired power plants was drawn out and shown as Figure 2. The detailed discussion on emission control methods for mercury in coal-fired power plants is as follows.

Pre-combustion control. Coal washing. Coal washing is one of the most simple and effective way to reduce mercury emissions. Elemental mercury and other similar minerals mainly present in inorganic compounds. Adding organic flotation agents into slurry of pulverized coal, organic matter mainly become flotation, and inorganic minerals mainly become flotation waste, mercury and other heavy metals is heavily concentrated in the slag and then removed out. An average of 21% to 37% mercury is removed by coal flotation process. In addition, using chemical cleaners pickling coal, such as using two-step acid wash coal cleaning to remove mercury from coal [63]. Another study also showed that about 60% of mercury can be removed by the pretreatment before coal combustion [60].

As to the mercury removal before combustion, the coal washing method is greatly effective for inorganic mercury in coal, however, it can not remove the mercury which associated with the organic carbon structure in the coal [64].

Heat treatment. Heat treatment is known as mild or moderate pyrolysis gasification. Taking advantage of evaporation characteristics of mercury and other volatile harmful elements, the coal is isolated from air and heated to temperature lower than 650 ℃, then the volatile substances are produced by the thermal decomposition and expelled from the coal [65].With no loss of carbon, the mild pyrolysis of bituminous coal reduces emission amount of mercury after coal combustion [66]. Related studies show that the pyrolysis temperature is the main factor affecting the release of mercury during pyrolysis process, the higher pyrolysis temperature leads to the higher release rate of mercury. But when the pyrolysis temperature is higher than 800℃, the increase rate of mercury release is relatively low. At the same pyrolysis temperature, with the extension of residence time, the release of mercury in coal increased. So a mild pyrolysis treatment can be taken to remove part of the mercury from coal [22].

Improving quality of coal. Coal can be modified to improve quality on the basis of coal washing. An example of improving quality of coal is K- Fuel. K-Fuel is a new generation of cleaning coal technology, which utilizes treatment to reduce the mercury content of coal before coal combustion. The physical and chemical structures of the low-quality coal are changed by high temperature and pressure. The low-quality coal such as sub-bituminous coal and lignite converted into high-quality coal, while this process can remove a large amount of mercury and other heavy metals as well as sulfur and nitrogen [67].The process can also be called a multi-pollutant control technology before coal combustion, which includes the following two-step: First,using gravity separation process to remove pollutants (sulfur and mercury) and ash: second, using thermal processing vessel (240℃ and 340 kPa) treat at high temperature and pressure.

In-combustion control. The main methods for controlling mercury emissions in the combustion process can be summarized as circulating fluidized bed (CFB) combustion, low NOx combustion and furnace spray technology.

(1) In CFB combustion process, the emission of NOx, as well as mercury and other trace heavy metals can be decreased in flue gas. High chlorine bituminous coal (chlorine content of 0.42%) combustion test was performed in a fluidized bed combustor, in which almost all of the mercury is oxidized to $HgCl_2$. 15% of the secondary air was bubbled in the flue gas (based on the initial gas / coal ratio) .In favor of promoting Hg capture. About 55 % of Hg^{2+} was captured by fly ash. Only 4.5% of gaseous mercury Hg^0 in the coal diffused into the air [68].

(2) Furnace spray technology, in view of the mechanism that Hg^{2+} is easy to be absorbed and removed, so adding calcium chloride (or calcium bromine and other halogen compounds) in the coal combustion, the content of Hg^{2+} in flue gas increase a lot and amount of Hg^0 in flue gas can decrease due to the effect of catalytic transformation[69]. Therefore, development and employment the adsorption catalysts promote Hg^0 oxide into Hg^{2+}, so as to control mercury pollution.

(3) Low NOx combustion method is mainly used to inhibit the formation of NOx, which results in an increase of oxidized mercury content and then is easier for mercury removal in the subsequent purification equipment.

Post-combustion control. In coal-fired power plants, mercury emissions of flue gas to be processed after coal combustion, making mercury easily be captured by all kinds of equipments, such as dust removal, desulfurization and denitration devices. The study of post-combustion demercuration involves two aspects: First, using adsorbents to remove mercury with the existing adsorbents and modified or new adsorbents; second, using flue gas treatment equipments to remove mercury in the flue gas, and desulfurize and denitrate simultaneously. The present post-combustion control methods mainly include:

(1) Injection of adsorbent. Injecting adsorbent into the flue gas to absorb Hg^0, such as activated carbon, metal, and fly ash. Activated carbon injection (ACI) has been demonstrated on a number of full-scale systems and is a commercial technology currently. ACI must be combined with particulate matter (PM) control device (such as electrostatic precipitator (ESP) or fabric filter (FF)). Chemical treatment of activated carbon is routinely capable of over 90% mercury emission reduction,

and allows for lower carbon injection rates for the same amount of mercury removal than un-treated activated carbons [70]. Precious metals adsorbent, which can be regenerated, has a good adsorption ability to remove mercury, what's more, the captured mercury can be recycled as well.

(2) Multi-pollutant control. This method refers to use the existing control equipment to improve the efficiency of mercury removal while simultaneously control multiple pollutants without having to add new equipment. It is the most cost-effective method that has obvious advantage and application prospects. Taking advantage of existing dust removal, desulfurization and denitration devices can improve the utilization rate of equipment and reduce the pollution control technology costs. Such as SCR, ESP, WFGD collaborative remove mercury from flue gas.

Selective catalytic reduction (SCR) systems are not only used for flue gas denitration in coal-fired power plant, but also have an effect on demercuration in subsequent desulfurization systems [71]. Some scholars hold that the co-oxidation of elemental mercury (Hg) in SCR DeNOx reactors to water soluble oxidized species followed by co-removal in flue gas desulphurisation scrubbers is a promising way to reduce these emissions from fossil fuel fired power plants [36].And SCR can catalytically transform a part of the gaseous elemental mercury into oxidative mercury, thus improve the rate of mercury removal in WFGD. SCR combined with WFGD scrubber can remove 90% or more mercury, if there is sufficient oxidized Hg at the scrubber inlet [28]. Pudasainee [72] measured mercury distribution that 43.0% of Hg was collected in ESP fly ash, 49.4% in wet FGD by-products and effluents, 3.9% of Hg was removed in boiler bottom ash and 3.7% was released into the atmosphere.

Main factors influencing the mercury removal efficiency. Influence of mercury form. According to the above described, as a result of highly volatile and indissolvable in water, Hg^0 is relatively stable state of mercury, so it is too difficult to be captured by pollution control equipment. Inversely, $HgCl_2$ is easy to dissolve in the wet desulphurization device and eventually be removed. As a consequence, decreasing the proportion of Hg^0 in flue gas and enhancing the ratio of Hg^{2+} can be beneficial to the mercury removal efficiency. Therefore, in order to improve the mercury removal efficiency, a variety of physical and chemical methods can be used to affect the form of mercury in flue gas.

Influence of different flue gas treatment devices. ESP and FF can remove the particulate mercury which adsorbed by fly ash. Wet and semi-dry flue gas desulfurization device have an effect on oxidized mercury removal. Owing to additional gas–solid contact time for oxidation, the average of particulate mercury removal for fabric filters (FFs) are 58%, which is a little higher than ESP. Both wet and semi-dry flue gas desulfurization (FGD) systems have good performance of oxidized mercury removal, but are not capable of elemental mercury removal [60].

Coal species. Owing to the difference of coal species, the oxidation rate of Hg^0 into Hg^{2+} in coal combustion is significantly different, which is about 20%～95%(W/V). When chloride ions content is higher in coal, the proportion of the mercury oxidation is higher. But when content of calcium and alkaline composition is high, the alkaline gas reacts with chloride ions and the chloride ions content reduces, so does the oxidative mercury [60]. In addition, the content of residual mercury has a great relationship with the content of carbon in ash. When mass fraction of carbon accounts for about 5%, residual mercury is quite high, the value is about 80%～100%(W/V) [73].

Flue gas composition. Laudal etc. [41] researched the mercury oxidation existing in different gases, concluded that the proportions of oxidized mercury and elemental mercury differed from each other greatly in different flue gases. Different gas compositions have great influence on the efficiency of mercury removal due to the different contents in flue gas.

Influence of existing pollution control devices on mercury emission. Mercury removal process is affected by multiple variable factors. The removal efficiency is heavily dependent on the release of mercury in flue gas. The speciation distribution of mercury is influenced by many factors, such as coal species and distribution, type of burner, boiler operation condition and the arrangement of flue gas purification devices. Therefore, utilization of existing dust removal equipment to improve the efficiency of mercury removal is a good choice in the aspect of economy and technology.

Dust removal equipment. With the temperature decreasing, a part of the gaseous mercury in flue gas can be deposited on the surface of fly ash. ESP and fabric filter (FF) have effect on the speciation distribution of mercury in flue gas, which are mainly influenced on particulate mercury. Tang etc. [74] found that the average efficiency of mercury removal was 16% by ESP. Wang [75] reported that the concentration of the total gaseous mercury at the outlet of ESP was 18–30% lower than the inlet for some power plants in China. Zhou etc. [76] research shows that the ratio of total mercury decreased by 13.4% (after ESP),

and about 42.9% of particulate mercury were removed by ESP.

Desulfurization equipment. With the wide use of dry and wet scrubber systems for flue gas desulfurization, various amounts of Hg are captured by coal combustion byproducts, such as, FGD and WFGD. Adding limestone in coal makes the gaseous mercury transforming into solid mercury in flue gas is more conducive to the mercury emission control [76]. Senior etc. [34] research showed that the chlorine content in coal has a certain relationship with the efficiency of mercury removal in FGD system. Liu etc. [77] research is to identify the characteristic release temperatures for different Hg compounds in FGD gypsum, and to provide general information on the typical Hg species existing in FGD gypsums in China. Besides, FGD activated carbon is a commercial product developed for controlling heavy metal emissions from incinerators.

Denitration device. Research shows that SCR system has important effects on mercury forms and emission in flue gas [71].The oxidation of Hg^0 increased with increasing HCl content and decreasing flue gas flow rates in SCR system [78]. Srivastava etc. [79] research showed that frequently-used vanadium titanium oxide, catalysts and reducing agents can promote the formation of Hg^{2+} in SCR. And the existence of HCl of flue gas in SCR system, which is the key for the transformation of elemental mercury to oxidized mercury.

CONCLUDING REMARKS AND SUGGESTIONS

Based on the principle of material circulation and mass conservation, this paper firstly investigate the occurrence mode and content of mercury in the coal before combustion, and then discuss the mercury transformation and influence factors varied with temperature -time in the combustion process, as well as with morphology and mass distribution in the slag, fly ash and flue gas. Accordingly, the emission control methods for mercury generated from coal combustion were proposed, and were generalized as pre-combustion control, in-combustion control, and post-combustion control. Finally, the influence factors on the mercury removal are discussed. So, according to the above discussion, some management suggestions are put forward to reducing the mercury emission in coal-fired power plants.

(1) Strictly monitoring and governing the mercury emission from flue gas in coal-fired power plants according to the Thermal Power Plant Air Pollutant Emission Standards.

(2) Promoting the coal washing rate by formulating administrative regulations. And developing advanced coal washing technologies and new pretreatment processes.

(3) Stimulating the oxidation of mercury by catalysts mixing with coal or injecting into the furnace.

(4) Developing green chemicals with efficient, inexpensive and recyclable capability for mercury adsorption in flue gas.

(5) Improving and modifying the performance of the existing air pollutants control devices for mercury removal.

REFERENCES

[1] Fitzgerald, W.F., Lamborg, C.H.(2007).9.04-Geochemistry of Mercury in the Environment. Treatise on Geochemistry 9,1-47

[2] Canil, D., Crockford ,P.W., Rossin, R., Telmer, K. (2015). Mercury in some arc crustal rocks and mantle peridotites and relevance to the moderately volatile element budget of the Earth. Chemical Geology396, 134-142

[3] Berzas, N.J.J., et al. (2009).Mercury speciation analysis on cell lines of the human central nervous system to explain genotoxic effects. Microchem Journal 93, 12-16

[4] Rani,L., Basnet, B., Kumar, A. (2011).Encyclopedia of Environmental Health : Mercury Toxicity. Earth Systems and Environmental Sciences705-712

[5] Berlin,M.,Zalups, R.K.,Fowler, B.A. (2015).Chapter 46-Mercury. Handbook on the Toxicology of Metals (Fourth Edition) 46,1013-1075

[6] Zhang, J.Y.,,Ren, D.Y.,,Xu, D.W.and Zhao, F.H. (1999).Mercury in coal and its impact on the environment. Journal of environmental science03, 101-105

[7] Swaine, D. J. (1990).Trace Elements in Coal. Butterworth ,London

[8] Yudovich, Ya.E., Ketris, M.P.(2005).Mercury in coal: a review: Part 1.Geochemistry. Coal Geology62,107-34

[9] UNEP. (2013).Global Mercury Assessment 2013: Sources, Emissions, Releases and Environmental Transport. UNEP Chemicals Branch, Geneva, Switzerland

[10] Munthe, J., et al.(2001).Intercomparison of methods for sampling and analysis of atmospheric mercury species. Atmospheric Environment35,3007-3017

[11] Lindqvist,O.,et al. (1991). Mercury in the Swedish environment-recent research on causes , consequences and corrective methods. Water Air and Soil Pollution55,261

[12] Brosset, C. (1987). The behavior of mercury

in the physical environment. Water Air and Soil Pollution34, 145-166
[13] Finkelman,R.B.(2003). 7.08–Coal Formation and Geochemistry.Treatise on Geochemistry7,191-222
[14] Brownfield,M.E., et al.(2005). Geologic setting and characterization of coals and the modes of occurrence of selected elements from the Franklin coal zone, Puget Group, John Henry No. 1 mine, King County, Washington, USA. International Journal of Coal Geology63, 247-275
[15] Mukherjee, A.B.,et al. (2008).Mercury flow via coal and coal utilization by-products: A global perspective. Resources, Conservation and Recycling 52, 571-591
[16] Pannu,R., Siciliano, S.D., O'driscoll, N.J.(2014). Quantifying the effects of soil temperature, moisture and sterilization on elemental mercury formation in boreal soils. Environmental Pollution193,138-146
[17] Gustin, M.S., et al.(2006). Mercury exchange between the atmosphere and low mercury containing substrates. Applied Geochemistry21,1913-1923
[18] Schluter,K.(2000). Review: evaporation of mercury from soils. An integration and synthesis of current knowledge. Environmental Geology39,249-271
[19] Galbreath, K.C., Zygarlicke, C.J.(2000).Mercury transformation in coal combustion flue gas. .Fuel Processing Technology 65-66,289-310
[20] Luo G.Q., et al.(2013). Hg occurrence in coal and its removal before coal utilization. Fuel104,70-76
[21] Finkelman, R.B. (1994).Modes of occurrence of potentially hazardous elements in coal: levels of confidence. Fuel Processing Technology39,21-34
[22] Zheng,C.G.(2010). Emission and Control of Mercury from Coal Combustion. Beijing:Science Press 79-81
[23] Ren,D.Y., et al.(2006).Coal trace element geochemistry. Beijing: Science Press.
[24] Diehl S.F., et al. (2004).Modes of occurrence of mercury and other trace elements in coals from the warrior field, Black Warrior Basin, Northwestern Alabama. International Journal of Coal Geology59,193-208
[25] Kolker, A., et al.(2006).Mercury in coal and the impact of coal quality on mercury emissions from combustion systems. Applied Geochemistry21,1821-1836
[26] Rallo, M., et al.(2012). Mercury policy and regulations for coal-fired power plants. Environmental Science and Pollution Research19,1084-1096
[27] Kramlich, J.C.,Castiglone, L.(2009). The homogeneous Forcing of Mercury Oxidation to provide Low-Cost Capture. Department of Mechanical Eng, University of Washington, Seattle
[28] Hower,J.C., et al.(2010).Mercury capture by native fly ash carbons in coal-fired power plants. Progress in Energy and Combustion Science36,510-529
[29] Luo,G.Q., et al.(2011). Identifying modes of occurrence of mercury in coal by temperature programmed pyrolysis. Proceedings of the Combustion Institute33, 2763-2769
[30] Frandsen, F., Johansen, K.D., Rasmussen, P.(1994).Trace elements from combustion and gasification of coal-An equilibrium approach. Progress in Energy and Combustion Science20,115-138
[31] Senior, C.L., Helble, J.J., Sarofim,A.F. (2000).Predicting the speciation of mercury emissions from coal-fired power plants. Proceedings of the Air Quality Ⅱ: Mercury,Trace Elements,and Particulate Matter Conference, McLean,VA19-21
[32] Presto, A.A., Granite, E.J. (2006).Survey of Catalysts for Oxidation of Mercury in Flue Gas. Environmental Science and Technology40,5601-5609
[33] Mortensen,M., et al. (1996).A two-stage cyclic fluidized bed process for converting hydrogen chloride to chlorine. Chemical Engineering Science51, 2031-2039
[34] Senior ,C.L., et al.(2000).Gas-phase transformations of mercury in coal-fired power plants. Fuel Processing Technology 63,197-213
[35] Wang,Y.J., et al.(2009). Experimental study on mercury transformation and removal in coal-fired boiler flue gases. Fuel Processing Technology90,643
[36] Stolle, R., Koeser, H., Gutberlet, H.(2014). Oxidation and reduction of mercury by SCR DeNOx catalysts under flue gas conditions in coal fired power plants. Applied Catalysis B: Environmental144, 486-497
[37] Sliger, R.N., Kramlich, J.C., Marinov ,N.M. (2000).Towards the development of a chemical kinetic model for the homogeneous oxidation of mercury by chlorine species. Fuel Processing Technology65-66, 423-438.
[38] Kellie,S.,et al.(2005) Factors affecting mercury speciation in a 100-MW coal-fired boiler with low-NOx burners. Energy Fuels19,800-806
[39] Hall, B., Lindqvist, O., Ljungstrom, E. (1990).Mercury chemistry in simulated flue gases related to waste incineration conditions. Environmental Science and Technology24,108-111
[40] Hall, B., Schager, P., Lindqvist ,O.(1991).Chemical reactions of mercury in combustion flue gases. Water,Air and Soil

Pollution56,3-14
[41] Laudal, D.L., Brown ,T.D., Nott ,B.R.(2000). Effects of flue gas constituents on mercury speciation. Fuel processing Technology65-66,157-165
[42] Agarwal,H., Stenger, H.G., Wu, S., Fan ,Z.(2006). Effects of H2O, SO2, and NO on Homogeneous Hg Oxidation by Cl2. Energy&Fuels20,1068-1075
[43] Sliger,R.N. (2001).Development of a Chemical Kinetic Model for the Homogeneous Oxidation of Mercury by Chlorine Species: A Tool for Mercury Emissions Control. University of Washington,Washington
[44] Chen, S.K. (2013).Reaction mechanism study about impact of bromine on mercury's speciation transformation in flue gas. Chongqing University, Chongqing
[45] Eswaran,S., Stenger, H.G.(2008). Effect of halogens on mercury conversion in SCR catalysts. Fuel Processing Technology 89,1153-1159
[46] Lee,S.J., et al.(2004). Removal of gas-phase elemental mercury by iodine- and chlorine-impregnated activated carbons. Atmospheric Environment38,4887-4893
[47] He ,P., et al.(2012).Effect of SO3 on elemental mercury adsorption on a carbonaceous surface. Applied Surface Science 258, 8853-8860
[48] Srivastava, R.K., Miller, C.A., Erickson, C., Jambhekar, R.(2004). Emissions of sulfur trioxide from coal-fired power plants. Journal of the Air & Waste Management Association54,750-762
[49] Walsh,P.M., Mccain, J.D., Cushing, K.M. (2006).Evaluation and Mitigration of Visible Acidic Aerosol Plumes from Coal Fired Power Boilers, U.S. EPA final report.
[50] Fleig,D., K.A. and F.N., et al. (2011).SO3 Formation under Oxyfuel Combustion Conditions. Industrial and Engineering Chemistry Research50,8505-8514
[51] Rumayor,M., et al.(2015).Application of mercury temperature programmed desorption (HgTPD) to ascertain mercury/char interactions. Fuel Processing Technology132,9-14
[52] Fuente,C.A., et al.(2012). Retention of mercury by low-cost sorbents: influence of flue gas composition and fly ash occurrence. Chemical Engineering Journal 213,16-21
[53] Fernández,M.N., et al.(2014).Effect of oxy-combustion flue gas on mercury oxidation. Environmental Science and Technology48,7164-7170
[54] Xu,W.Q., et al.(2013).Mercury removal from coal combustion flue gas by modified fly ash. Journal of Environmental Sciences25,393-398
[55] Bhardwaj,R., Chen ,X.H., Vidic, R.D.(2009). Impact of Fly Ash Composition on Mercury Speciation in Simulated Flue Gas. Journal of the Air & Waste Management Association59, 1331-1338
[56] UNEP Chemicals Branch. (2008). The Global Atmospheric Mercury Assessment: Sources, Emissions and Transport
[57] Hall ,B., Schager, P., Weesmaa ,J.(1995). The homogeneous gas phase reaction of mercury with oxygen, and the corresponding heterogeneous reactions in the presence of activated carbon and fly ash. .Chemosphere30,611-627
[58] Linak ,W.P., Wendt ,J.O.L.(1994). Trace metal transformation mechanisms during coal combustion. Fuel Process Technology39,173-198
[59] Lu,Y.Q., et al.(2007). Characteristics of fly ashes from full-scale coal-fired power plants and their relationship to mercury adsorption. Energy & Fuels21,2112-2120
[60] Pavlish ,J.H., et al.(2003) Status review of mercury control options for coal fired power plants. Fuel Process Technology82,89-165
[61] Hall, B.(1995). The gas phase oxidation of elemental mercury by ozone. Water,Air and Soil Pollution80,301-305
[62] Lee,S.J., et al.(2006).Speciation and mass distribution of mercury in bituminous coal-fired power plant Atmospheric Environment40, 2215-2224
[63] April H.,et al.(2006). A two-step acid mercury removal process for pulverized coal. Fuel85,1166-1173
[64] Towler, B.F. (2014).Chapter 13-Coal and Clean Coal Technologies. The future of Energy273-299
[65] Yang,G. (2011).Research progress of mercury removal technologies in coal . Clean Coal Technology17,82-85
[66] Bian,W., Ren, A.L. (2008).Development of mercury emission control measures in coal-fired power plant. Hebei Journal of Industrial Science and Technology25, 401-404
[67] Black,V. (2003).Effective Mercury Reduction Strategy for Western Coal/K-Fuel Technology. Report to US EPA.
[68] Liu, K.L., et al.(2001). An investigation of mercury emission from FBC systems fired with high- chlorine coals. Energy&Fuels15,1173-1180
[69] Zhuang,Y., et al.(2007). Impact of calcium chloride addition on mercury transformations and control in coal flue gas.Fuel86,2351-2359
[70] UNEP. (2010).Process Optimization Guidance for Reducing Mercury Emissions from Coal Combustion in Power Plants , United Nations Environmental Program, Chemicals Branch, DTIE, Geneva, Switzerland

[71] Rallo, M., et al.(2012).Effect of SCR operation variables on mercury speciation.Chem Eng J.198-199, 87,2012.
[72] Pudasainee D., et al.(2012).Oxidation, reemission and mass distribution of mercury in bituminous coal-fired power plants with SCR, CS-ESP and wet FGD.Fuel93, 312
[73] Gibb, W.H., Clarke, F., Mehta ,A.K. (2000).The fate of coal mercury during combustion. Fuel Processing Technology65-66,365-377
[74] Tang,Q., et al.(2012). Distribution and fate of environmentally sensitive elements (arsenic, mercury, stibium and selenium) in coal-fired power plants at Huainan, Anhui, China . Fuel95,334-339
[75] Wang,S.X., et al.(2010).Mercury emission and speciation of coal-fired power plants in China. Atmospheric Chemistry and Physics10,1183-1192
[76] [76]Zhou,J.S. (2008).Research on mercury emission and control on boiler of 300 MW . Thermal Power Generation37,22-27
[77] Liu,X.L., et al.(2013).Speciation of mercury in FGD gypsum and mercury emission during the wallboard production in China. Fuel 111,621-62.
[78] Pudasainee,D., et al.(2012). Oxidation, reemission and mass distribution of mercury in bituminous coal-fired power plants with SCR, CS-ESP and wet FGD . Fuel 93,312-318
[79] Srivastava ,R.K.,et al.(2006). Control of mercury emissions from coal-fried electric utility boilers. Environment Science and Technology40,1385-1393

Received: **02.11.2015**
Accepted: **04.04.2016**

CORRESPONDING AUTHOR

Jianyi Lu
North China Electric Power University, Baoding, School of Environmental Science and Engineering, Baoding 071003, Hebei, P.R.CHINA

email: lujianyi@tsinghua.org.cn

© by PSP Volume 25 – No. 10/2016, pages 3907-3914 Fresenius Environmental Bulletin

EFFICIENT IN VITRO BULBLET REGENERATION FROM IMMATURE ZYGOTIC EMBRYOS OF *FRITILLARIA IMPERIALIS* AND *F. PERSICA*

Derya Cakmak[1], Cengiz Sancak[2], Cuma Karaoglu[3], Muhammad Aasim[4], Iskender Parmaksiz[5], Sebahattin Ozcan[2,*]

[1]Gazipaşa District Directorate, Ministry of Food, Agriculture and Livestock, Antalya, Turkey.
[2]Department of Field Crops, Faculty of Agriculture, University of Ankara, Ankara, Turkey.
[3]Central Research Institute for Field Crops, Ministry of Food Agriculture and Livestock, Ankara, Turkey
[4]Department of Biotechnology, Faculty of Science, Necmettin Erbakan University, Konya, Turkey
[5]Department of Molecular Biology and Genetics, Faculty of Science, Gaziosmanpasa University, Tokat, Turkey

ABSTRACT

In this study in vitro bulblet regeneration potential of immature zygotic embryo explants of *Fritillaria imperialis* L. and *F. persica* L. were investigated. Explants were cultured on Murashige and Skoog's (MS) media supplemented with 0.25-1.0 mg/l thidiazuron (TDZ), 0.25-0.5 mg/l α-naphthalene acetic acid (NAA), 1.0-4.0 mg/l 6-benzylaminopurine (BAP) and 0.5-2.0 mg/l kinetin (kin). Multiple bulblet regeneration from all culture media was recorded after 14 months of culture. The highest bulblet regeneration frequency was recorded on media containing TDZ and NAA combinations from *F. imperialis*. Maximum bulblets per explants from *F. imperialis* and *F. persica* were attained on media containing BAP and NAA, kinetin and NAA or TDZ-NAA respectively. Bulblets subjected to hardening showed longer roots of 8.19 cm in a medium containing agar and activated charcoal (AC) cultured at 23 °C and higher number of roots per bulblet in a medium solidified with gelrite. Rooted bulblets were directly transferred to pots and cultured under greenhouse conditions where plants developed new foliage and roots, and acclimatized successfully.

KEY WORDS:
Crown imperial, Persian lily, geophytes, micropropagation, bulblets

INTRODUCTION

Genus *Fritillaria* (Liliaceae) is an important geophyte of Europe and Middle East [1] including Turkey [2]. It has almost 100 species that show wide distribution in different climatic regions that ranged from Southern Europe to Middle East. Most *Fritillaria* species are either endemic or endangered and used as ornamental [1] or medicinal plant [3,4] due to presence of wide array of alkaloids [5].

Crown imperial (*Fritillaria imperialis* L.) and Persian lily (*Fritillaria persica* L.) are two important ornamental plants due to their attractive flowers available in different colours. They are commonly propagated through bulbs or seeds in natural environment (6). Low germination rate due to physiological dormancy [7] followed by weak seedlings, low survival rate and slow growth are the main problems associated with propagation through seeds. It takes normally 3-4 years to get mature bulb from seeds [1]. On the other hand, limited availability of bulblets [8] from the nature hinders the vegetative propagation. All these problems associated with propagation offer to develop more efficient and alternative means of propagation for commercial production of these valuable species.

Plant tissue culture techniques provide an alternative and efficient way of propagating geophytes or recalcitrant plants. Several successful regeneration protocols for different *Fritillaria* species has been reported [8-14] using different explants like immature/mature embryos, bulblets or bulbous scales. Immature embryos offers an alternative and efficient way of propagation of endemic or endangered plants and successfully employed for geophytes like *Sternbergia fischeriana* [15], *Muscari azureum* [16], *M. mirum* [17] and *M. muscarimi* [18]. In the present study, we targeted the use of immature embryo explants in order to in vitro propagate *F. imperialis* and F. *persica* species followed by rooting and acclimatization with objective to use protocol for commercial propagation.

MATERIALS AND METHODS

Immature fruits of *F. imperialis* and *F. persica* (originated from Mersin or Siverek provinces of Turkey) were collected from experimental field trial

area of Department of Field Crops, Faculty of Agriculture, Ankara University in May. Fruits containing immature embryos were surface sterilized with 80% commercial bleach for 20 min followed by 3 times rinsing with sterile top water. Following surface-sterilization seeds were squeezed gently using forceps until the immature zygotic embryos (approximately 1-2 mm in length) were released. Isolated Immature embryo explants of all *Fritillaria* species were then cultured on Murashige and Skoog's (MS) medium supplemented with 0.25-1.0 mg/l thidiazuron (TDZ) and 0.5 mg/l α-naphthalene acetic acid (NAA) (Table 1), 1.0-4.0 mg/l 6-benzylaminopurine (BAP) and 0.25-0.5 mg/l NAA (Table 2) or 0.5-2.0 mg/l kinetin (kin) and 0-0.5 mg/l NAA (Table 3). All regeneration media used in the study were based on MS medium supplemented with 3% sucrose and 0.65% agar. The pH of all the media were adjusted to ~5.8. BA and TDZ were added to culture medium prior to sterilization whereas, filter sterilized Kinetin was added after sterilization. All media were autoclaved at 118 kPa atmospheric pressure and 121 °C for 20 min. All cultures were kept at 24 °C with a 16 h photoperiod provided with cool fluorescent lamps. Data regarding frequency of bulblet regeneration, bulblets per explants and bulblet size were recorded after 14 months.

For hardening of in vitro regenerated bulblets, bulblets of *F. persica* (Siverek), they were cultured on MS medium containing 2.0% sucrose and solidified with agar (0.65%) or gelrite (0.25%) alone or in combination with 5 g/l activated charcoal (AC). They were then placed at different temperatures of 4, 16 and 23 °C. After 9 months of culture, data regarding rooting frequency, root length and number of roots were recorded and analysed statistically. For acclimatization, rooted bulblets were transferred to pots containing sterile peat moss, vermiculite, sand and perlite (2:1:1:1) and covered with polyethylene bags for 1-2 weeks. Pots were watered every 3 days in order to keep the moisture level at optimum conditions.

TABLE 1
Effects of different concentrations of TDZ-NAA on bulblet regeneration in *F. imperialis* and *F. persica.*

TDZ (mg/l)	NAA (mg/l)	Bulblet regeneration (%)			Bulblets per explant			Bulblet size (mm)		
		F. imperialis	*F. persica* (Siverek)	*F. persica* (Mersin)	*F. imperialis*	*F. persica* (Siverek)	*F. persica* (Mersin)	*F. imperialis*	*F. persica* (Siverek)	*F. persica* (Mersin)
0.25	-	47.5 b[1]	52.5 abc[1]	45.0[ns]	5.12 ab[2]	6.66 ab[2]	20.23 b[2]	4.02 a[1]	5.29 a[2]	5.300[ns]
0.25	0.5	45.0 b	47.5 bc	47.5	4.78 ab	10.19 a	28.93 a	3.37 ab	5.03 ab	4.83
0.5	-	52.5 b	37.5 c	45.0	7.12 a	7.96 ab	22.18 b	3.26 b	5.22 ab	5.12
0.5	0.5	95.0 a	72.5 a	40.0	7.22 a	3.96 b	30.85 a	3.72 ab	4.36 ab	4.59
1	-	85.0 a	50.0 bc	47.5	3.95 b	5.64 ab	20.20 b	3.95 ab	3.90 b	5.29
1	0.5	85.0 a	62.5 ab	45.0	5.92 ab	7.64 ab	19.02 b	4.15 a	5.02 ab	4.88

Each value is the mean of 4 replications with 10 explants; Values within a column followed by different letters are significantly different at the 0.01 (1) and 0.05 (2) level; ns: not significant

TABLE 2
Effects of different concentrations of BAP-NAA on bulblet regeneration in *F. imperialis* and *F. persica.*

BAP (mg/l)	NAA (mg/l)	Bulblet regeneration (%)			Bulblets per explant			Bulblet size (mm)		
		F. imperialis	*F. persica* (Siverek)	*F. persica* (Mersin)	*F. imperialis*	*F. persica* (Siverek)	*F. persica* (Mersin)	*F. imperialis*	*F. persica* (Siverek)	*F. persica* (Mersin)
1	-	72.5 a[1]	20.0 cd[1]	12.5 a[1]	4.81 ab[1]	5.33[ns]	17.50 a[2]	5.88 a[1]	5.15[ns]	3.90 a[2]
1	0.25	70.0 a	45.0 ab	2.5 b	4.07 abc	10.03	7.50 ab	5.46 ab	4.58	2.87 ab
1	0.5	65.0 ab	37.5 abc	0.0 b	7.16 a	9.87	0.00 b	6.06 a	4.95	0.00 b
2	-	67.5 ab	45.0 ab	0.0 b	3.67 bcd	10.90	2.50 b	4.96 ab	5.18	2.00 b
2	0.25	17.5 cd	52.5 a	0.0 b	3.67 bcd	8.09	0.00 b	6.04 a	5.38	0.00 b
2	0.5	42.5 bc	25.0 bcd	0.0 b	5.82 ab	7.12	0.00 b	3.51 b	3.74	0.00 b
4	-	17.5 cd	10.0 d	0.0 b	0.79 de	9.12	0.00 b	1.46 c	4.05	0.00 b
4	0.25	5.0 d	27.5 bcd	0.0 b	1.12 cde	7.99	0.00 b	0.98 c	4.28	0.00 b
4	0.5	0.0 d	25.0 bcd	0.0 b	0.00 e	7.99	0.00 b	0.00 c	4.85	0.00 b

Each value is the mean of 4 replications with 10 explants; Values within a column followed by different letters are significantly different at the 0.01 (1) and 0.05 (2) level; ns: not significant

TABLE 3
Effects of different concentrations of kinetin-NAA on bulblet regeneration in *F. imperialis* and *F. persica*

Kinetin (mg/l)	NAA (mg/l)	Bulblet regeneration (%)			Bulblets per explant			Bulblet size (mm)		
		F. imperialis	*F. persica* (Siverek)	*F. persica* (Mersin)	*F. imperialis*	*F. persica* (Siverek)	*F. persica* (Mersin)	*F. imperialis*	*F. persica* (Siverek)	*F. persica* (Mersin)
5	-	87.5 a[1]	22.5 b[2]	30.0 bc[1]	6.04 ab[1]	7.56 b[1]	11.41[ns]	6.18 a[1]	5.96[ns]	4.69 ab[2]
0.5	0.5	87.5 a	50.0 a	72.5 a	5.20 abc	8.05 ab	17.55	4.66 b	6.02	4.16 ab
1	-	82.5 a	22.5 b	30.0 bc	3.58 cd	11.12 ab	12.72	5.07 ab	6.57	5.19 a
1	0.5	62.5 b	32.5 b	52.5 ab	6.79 a	11.75 ab	19.72	5.28 ab	7.72	3.94 ab
2	-	57.5 c	15.0 b	20.0 c	4.25 bcd	12.62 a	20.31	4.35 b	6.56	3.06 b
2	0.5	40.0 c	22.5 b	50.0 b	2.25 d	12.50 a	18.72	2.57 c	7.20	4.18 ab

Each value is the mean of 4 replications with 10 explants; Values within a column followed by different letters are significantly different at the 0.01 (1) and 0.05 (2) level; ns: not significant

TABLE 4
Effects of gelling agents, activated charcoal and temperature on hardening of *F. persica* (Siverek)

Temperature +Gelling			Rooting frequency (%)	Root length (cm)	Number of roots
4 ° C	16 ° C	23 ° C			
A			100[ns]	2.13 d	4.83 b
	A		100	2.65 cd	7.25 ab
		A	91.7	1.71 d	4.94 b
A+AC			91.7	5.79 abc	5.58 ab
	A+AC		100	7.00 ab	7.92 ab
		A+AC	91.7	8.19 a	8.94 ab
G			93.3	2.49 cd	5.22 ab
	G		83.3	2.62 cd	9.75 a
		G	83.3	2.62 cd	8.17 ab
G+AC			100	5.17 abcd	6.67 ab
	G+AC		100	6.37 ab	8.27 ab
		G+AC	91.7	3.76 bcd	7.22 ab

Each value is the mean of 4 replications with 10 explants; Values within a column followed by different letters are significantly different at 0.05 level; ns: not significant; A=agar; G= gelrite; AC= activated charcoal

Each treatment had four replicates containing 10 explants for bulblet regeneration and three replicates with 4 explants for bulblet maturation and hardening experiments. Significance was determined by analysis of variance (ANOVA) and the differences between means were compared by Duncan's multiple range test. All given data presented in percentages were arranged to arcsine transformation [19].

RESULTS

The present study emphasized the successful use of immature embryos for multiple bulblet regeneration from *Fritillaria* species. Response of immature embryo explants from *Fritillaria* species was variable when subjected to different PGRs. Multiple shoot induction was recorded after 5-6 months of culture initiation irrespective of *Fritillaria* species or PGRs type and concentration (Fig. 1a and c) followed by bulblet induction after 10 months of culture. These explants were further awaited in the culture medium for increasing the bulblet regeneration and bulblet size (Fig. 1b and d). Results regarding frequency of bulblet regeneration, bulblets per explants and bulblet size were recorded and subjected to statistical analysis after 14 months of culture.

Data regarding efficacy of TDZ-NAA on in vitro bulblet formation in all *Fritillaria* species is presented in Table 1. Results clearly revealed the importance of TDZ-NAA on bulblet regeneration frequency ($p \leq 0.01$) in *F. imperialis* and *F. persica* (Siverek). Contrarily, *F. persica* (Mersin) showed insignificant effects of TDZ-NAA on bulblet regeneration frequency and bulblet size.

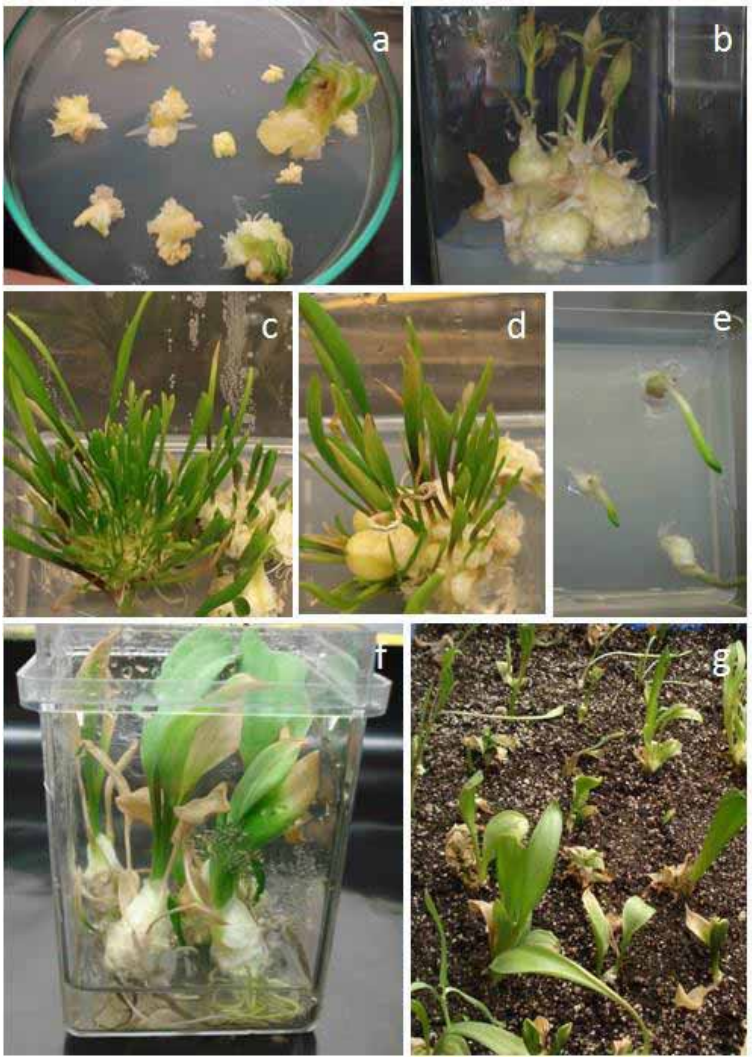

FIGURE 1

Multiple in vitro bulblet regeneration from immature zygotic embryos of *Fritillaria imperialis* and *F. persica*. (a) Callus Formation and shoot regeneration from *F. imperialis* embryos on MS medium containing 0.5 mg/l TDZ and 0.5 mg/l NAA after 5 months of culture. (b) Bulblet formation from *F. imperialis* embryos on MS medium containing 0.5 mg/l TDZ after 14 months of culture. (c) Multiple shoot induction from immature embryo explants of *F. persica* (Mersin) on MS medium containing 0.5 mg/l Kin and 0.5 mg/l NAA after 6 months and (d) multiple bulblet induction after 14 months of culture. (e) Rooting and hardening of *in vitro* regenerated bulbs of *F. persica* (Siverek). (f) Well-developed and Rooted bulblets of *F. persica* (Siverek). (g) Acclimatized *F. persica* (Siverek) plants with new foliage development.

The highest bulblet regeneration frequency for *F. imperialis* and *F. persica* (Siverek) was recorded on a medium containing 0.5 mg/l TDZ and 0.5 mg/l NAA. *F. imperialis* was more responsive to TDZ-NAA in terms of bulblet regeneration frequency compared to other species. However, *F. persica* (Mersin) regenerated 3 to 4-fold more number of bulblets per explants compared to other species (Table 1). Results revealed the need of low TDZ concentration for inducing larger bulblets of all three *Fritillaria* species. Mean bulblet size in response to TDZ-NAA was recorded as 3.26-4.15, 3.90-5.29 and 4.59-5.30 mm respectively for *F. imperialis, F. persica* (Siverek) and *F. persica* (Mersin). Presence of NAA in the culture medium with TDZ exerted variable effects on shoot regeneration behaviour that varied with concentration and *Fritillaria* species.

Bulblet regeneration behaviour of all three *Fritillaria* species in response to BAP and NAA is presented in Table 2. Results revealed the significant effects of BA-NAA on bulblet regeneration behaviour ($p \leq 0.01$) of *F. imperialis* and *F. persica* (Mersin). Contrarily, insignificant

effects of BAP-NAA on number of bulblets per explant and bulblet size of *F. persica* (Siverek) were recorded. *F. persica* (Mersin) induced bulblets only on medium containing 1.0 mg/l BAP with or without 0.25 mg/l NAA that resulted in 12.5% bulblet regeneration frequency and 17.50 bulblets per explant with average bulblet size of 3.90 cm. Contrarily, *F. imperialis* induced 0-72.5% shoot regeneration frequency and 0-7.16 bulblets per explant with the bulblet size ranged from 0.98 to 6.06 mm. Maximum number of bulblets per explant (7.16) with the highest bulblet size of 6.06 mm in *F. imperialis* was scored on medium containing 1.0 mg/l BAP and 0.5 mg/l NAA. On the other hand, shoot regeneration frequency, number of bulblets per explant with bulblet size for *F. persica* (Siverek) was recorded as 10.0-52.5%, 5.33-10.90 and 3.74-5.38 mm respectively. Presence of NAA in the culture medium exerted variable effects on bulblet regeneration behaviour and varied with concentration and *Fritillaria* species.

Results of kin and NAA showed statistically significant effects on bulblet regeneration frequency of all *Fritillaria* species (Table 3). However, kin-NAA exerted insignificant effects on bulblets per explant of *F. persica* (Mersin) and bulblet size of *F. persica* (Siverek). Maximum bulblet regeneration frequency in all three *Fritillaria* species was scored on medium containing 0.5 mg/l kin and 0.5 mg/l NAA. Comparing species, *F. imperialis* responded better than *F. persica* to kin-NAA and induced higher shoot regeneration frequency irrespective of concentration. Number of shoots per explants was recorded 2.25-6.79 for *F. imperialis,* 7.56-12.62 for *F. persica* (Siverek) and 11.41-20.31 for *F. persica* (Mersin). Comparing species, *F. persica* (Mersin) and *F. imperialis* was the most and the least responsive respectively in order to generate more number of bulblets per explants irrespective of kinetin and NAA concentrations. Mean bulblet size ranged 2.57-6.18 mm for *F. imperialis,* 5.96-7.72 mm for *F. persica* (Siverek) and 3.06-5.19 mm for *F. persica* (Mersin). Presence or absence of NAA in the culture medium with kin responded variably to shoot regeneration behaviour that also varied with concentration and species.

For hardening of *F. persica* (Siverek) bulblets, different gelling agents alone or in combination with AC at different temperatures were employed (Fig 1e). Gelrite alone was more suitable for inducing higher number of roots. Inclusion of AC exerted variable effects with different gelling agents and induced higher number of long roots. Maximum root length of 8.19 cm was scored on a medium containing agar and AC cultured at 23 °C (Table 4, Fig.1f). Hardened bulblets were then transferred to pots containing sterile peat moss, vermiculite, sand and perlite (2:1:1:1), and covered with polyethylene bags for 1-2 weeks for acclimatization in growth room. After acclimatization plants were transferred to greenhouse conditions that found to be beneficial for plant adaptation and their growth. During adaptation, old leaves and roots turned brown and replaced with new foliage development and root induction (Fig. 1g). A high number of plants successfully adapted to greenhouse conditions and continued their growth.

DISCUSSION

The study presents the successful use of immature embryos explants for in vitro bulblet regeneration potential of *F. imperialis and F. persica* species by exposing them to three different cytokinins (TDZ, BA and Kinetin) with or without different concentrations of NAA. TDZ, BA and Kinetin are most commonly used cytokinins for generating bulblets under *in vitro* conditions either alone or in combinations with auxins [20-23]. Mature or immature embryos are potent explants for bulblet induction of many geophytes [13, 15, 17, 18, 23, 24] especially for endemic [25] or endangered [8, 13, 26] bulbous species. The possible reason for preferring immature embryos is the presence of actively divided meristem regions in the embryos that response better to PGRs [18, 27] than other explants.

Bulblets from immature embryos were attained through indirect organogenesis irrespective of PGRs type, concentration and *Fritillaria* species with relatively longer time to induce callus which later on turned into shoot buds and induced shoots. It is generally reported that *in vitro* regeneration of bulbous plants took relatively more time for whole plant regeneration with increased bulblet size [15, 18, 28]. Results on bulblet regeneration frequency and bulblets per explants showed the clear relationship between species and PGRs [29-31]. Although explants response to different PGRs was species specific, *F. persica* (Mersin) was least responsive in terms of bulblet regeneration frequency to all PGRs used in the study. Karaguzel et al. [29] also emphasized the relationship between genotypes, explants and PGRs type and concentration for *in vitro* shoot regeneration of *Ornithogalum* species.

Results on effects of different PGRs revealed that all species responded better to TDZ and NAA concentrations for bulblet regeneration frequency. TDZ is very potent cytokinin type plant hormone that is used for the bulblet regeneration of recalcitrant plants [32] and has been successfully used for bulblet induction of other geophytes like *Curculigo orchiodes* [22], *Acampe praemorsa* [33], *Lilium longiflorum* [34] and Red Squill [28]. It was also interesting to note that all species required

relatively higher concentrations of TDZ to induce higher bulblet regeneration [22]. Contrarily, negative effects of TDZ on bulblet regeneration of *S. fischeriana* [15], *M. aucheri* and *M. azureum* [16, 21] and *L. longiflorum* [35] has also been reported. On the other hand, relatively lower concentration of kinetin was found suitable for inducing higher bulblet regeneration frequency [22]. Contrarily, higher kinetin concentration for gaining maximum bulblet regeneration frequency has been reported by Thomas and Maseena [36]. Results further revealed that higher BAP concentration was also detrimental for inducing maximum bulblet regeneration as reported by Rybczyński and Gomolińska [37] in *L. martagon*. Results on bulblets per explants showed the variable response of PGRs which was also species specific [38-40].

Presence or absence of NAA with cytokinins in the culture medium also played a significant role for bulblet induction frequency and bulblets per explants [22, 24, 36] but dependant to cytokinin type, concentration and species. Presence of NAA with all TDZ or kinetin concentrations exerted positive and statistically similar effects on bulblet regeneration frequency irrespective of species type [31]. Results also revealed the enhanced bulblet regeneration by the combination of BAP and NAA [17, 35, 41-44]. Contrarily, Rybczyński and Gomolińska [37] reported negative effects of BAP with NAA on bulblet regeneration of *L. martagon*. Use of gelling agents, AC and temperature showed positive effects on bulblet growth and hardening for better acclimatization [15, 27]. Results clearly showed the positive effects of gelling agents on the growth of bulblets [18, 45]. Gelrite alone was found more suitable as compared to agar alone [46] or in combination with AC in the culture medium [46, 47]. On the other hand, specific requirement of temperature is also important for bulblet growth and development and 16 °C was more suitable for gaining longer roots and more number of roots per bulblets [14].

Rooting and acclimatization of *in vitro* grown bulblets is an important step for successful regeneration protocol. It is common perception that *in vitro* grown bulblets failed to survive under greenhouse or field conditions due to dormancy, bulblet size or maturity [45] which exerts negative effects on plant growth [5] in their immediate environment. In these conditions, researchers developed or utilized different techniques like carbon source [48], basal mediums [49], temperature [50], phytohormones [28, 42], lighting system and photoperiod [48] and nitrogenous compounds [51] in order to increase bulblet size, hardening, breaking dormancy, rooting and acclimatization.

CONCLUSIONS

The present study reports the development of successful *in vitro* regeneration protocol for *Fritillaria imperialis and F. persica* species. In this study, regeneration potential of immature embryo explants was successfully checked on MS mediums provided with different cytokinins alone or in combination with NAA. After hardening process, in vitro grown bulblets were directly transferred to pots for successful acclimatization. In short, the study emphasized the use of simple, efficient and repeatable regeneration protocol that can be employed for other geophytes for their commercial propagation.

REFERENCES

[1] De HertogH A.A. and Lenard M. (1993) General chapter on spring flowering bulbs. In: De Hertogh A., Le Nard M. (Eds). The Physiology of Flower Bulbs. Elsevier, Amsterdam, pp 705-739.

[2] Bryan, J.E. (2002) Bulbs. Revised Edtion, Timber Press, Portland, Oregon, p 525.

[3] Ronsted, N., Law, S., Thornton H., Fay, M.F. and Chase, M.W. (2005) Molecular phylogenetic evidence for the monophyly of *Fritillaria* and *Lilium* (Liliaceae; Liliales) and the infrageneric classification of *Fritillaria.* Mol Phylogenet Evol 35, 509-527.

[4] Wang, S.Y., Gao, W., Chen, H. and Xiao, P. (2005) New starches from *Fritillaria* species medicinal plants. Carbohydrate Polymers 61: 111-114.

[5] Li, C.J. and Qin, Z.D. (1987) The relationship between physiological and biochemical changes and releasing dormancy of Fritillaria pallidiflora Schrenk. during low temperature treatment. Acta Bot Boreali-Occidential Sin 7: 23-28.

[6] Ulug, B., Korkut, V., Asli B. and Sisman E. (2010) Research on propagation methods of Persian lily bulbs (*Fritillaria persica* Linn.) with various vegetative techniques. Pak J Bot 42: 2785-2792.

[7] Baskin, J.M. and Baskin, C.C. (2004) A classification system for seed dormancy. Seed Sci Res 14: 1-16.

[8] Subotić, A., Trifunović, M., Jevremović, S. and Petrić, M. (2010) Morpho-histological study of direct somatic embryogenesis in endangered species *Frittilaria meleagri*. Biol Plantarum 54: 592-596.

[9] Sun, C.S., CHu, C.C. and Wang, D.Y. (1977) Callus formation and organ formation in the

tissue culture of *Fritillaria thunbergii* Miq. Acta Bot Sin 19: 161-162.

[10] Kukulezanka, K., Kromor, K. and Czastka, B. (1989) Propagation of *Fritillaria meleagris* L. through tissue culture. Acta Hort. 251: 147-153.

[11] Paek, K.Y. (1996) Several factors affecting bulblet regeneration from the culture of scale segment on none-bud in *Fritillary* as medicinal bulbous plant. Acta Hort. 440: 498-503.

[12] Paek, K.Y. and Murthy, H.N. (2002) High frequency of bulblet regeneration from bulb scale sections of *Fritillaria thunbergii*. Plant Cell, Tiss Org Cult 68: 247-252.

[13] Dehcheshmeh, M., Khalighi, A., Naderi, R., Ebrahimie, E. and Sardari, M. (2007). Indirect somatic embryogenesis from petal explant of endangered wild population of *Fritillaria imperialis*. Pak J of Biol Sci 10: 1875-1879.

[14] Kızıl, S. and Khawar, K.M (2014). The effects of plant growth regulators and incubation temperatures on germination and bulb formation of *Fritillaria persica* L. Propag Ornam Plants 14: 133-138.

[15] Mirici, S., Parmaksiz, I., Ozcan, S., Sancak, C., Uranbey, S., Sarhan, E.O., Gümüşçü, A., Gürbüz, B. and Arslan, N. (2005) Efficient in vitro bulblet regeneration from immature embryos of endangered *Sternbergia fischeriana.* Plant Cell, Tiss Org Cult 80: 239-246.

[16] Uranbey, S. (2010) Stimulating effects of different basal media and cytokinin types on regeneration of endemic and endangered *Muscari aucheri*. Arch Biol Sci Belgrade 62: 663-667.

[17] Nasırcılar, A., Mirici, S., Karagüzel, Ö., Eren, Ö. and Baktır, İ. (2011) In vitro propagation of endemic and endangered *Muscari mirum* from different explant types. Turk J Bot 35: 37-43.

[18] Uzun, S., Parmaksız, I., Uranbey, S., Mirici, S., Sarıhan, E.O., Ipek, A., Kaya, D.M., Gürbüz, B., Arslan, N., Sancak, C., Khawar, K.M. and Özcan, S. (2014) In vitro micropropagation from immature embryos of the endemic and endangered *Muscari muscarimi* Medik. Turk J Biol 38: 83-88.

[19] Snedecor, G.W. and Cochran, W.G. (1967) Statistical Methods. Ames, IA, USA: The Iowa State University Press.

[20] Podwyszynska, M. and Marasek, A. (2003) Effects of Thidiazuron and Paclabutrazol on regeneration potential of tulip flower stalk explants in vitro and subsequent shoot multiplication. Acta Societatis Bot Poloniae 72: 181-190.

[21] Uranbey, S., Ipek, A., Caliskan, M., Dundar, E., Cocu, S., Basalma, D., Guneylioglu, H. (2010) *In Vitro* bulblet induction from bulb scales of endangered ornamental plant *Muscari azureum*. Biotech Biotechnological Equip 24: 1843-1848.

[22] Thomas, T.D. (2007) High-frequency, direct bulblet induction from rhizome explants of *Curculigo orchioides* Gaertn., an endangered medicinal herb. In Vitro Cell Dev Biol-Plant 43: 442–448.

[23] Petrić, M., Subotić, A., Jevremović, S. and Trifunović, M. (2011) Somatic embryogenesis and bulblet regeneration in snakehead fritillary (*Fritillaria meleagris* L.). Afr J Biotechnol 10: 16181-16188.

[24] Rahimi, M., Daneshvar, M.H. and Heidari, M. (2014) Propagation and bulb formation of *Fritillaria* (*Fritillaria imperialis* l.) via in vitro culture. Int. J Plant, Animal and Environ Sci 4: 707-710.

[25] Carasso, V., Hay, F.R., Probert, R.J. and Mucciarelli M. (2011) Temperature control of seed germination in *Fritillaria tubiformis* subsp. moggridgei (Liliaceae) a rare endemic of the South-West Alps. Seed Sci Res 21: 33-38.

[26] Thomas, T.D. and Jacob, A. (2004) Direct somatic embryogenesis of *Curculigo orchioides* Gaertn., an endangered medicinal herb. J Plant Biotech 6: 193-197.

[27] Marija, P., Angelina, S., Slađana, J. and Milana, T. (2011) Somatic embryogenesis and bulblet regeneration in snakehead fritillary (*Fritillaria meleagris* L.) Afr J Biotechnol 10: 16181-16188.

[28] Aasim, M., Khawar, K.M. and Özcan, S. (2008) In vitro Regeneration of Red Squill Urginea maritima (L.) Baker. Using Thidiazuron, Biotechnol Biotechnological Equip 22: 925-928.

[29] Karaguzel, O., Kaya, A., Biner, B. and Aydinsakir, K. (2012) In vitro propagation of native *Ornithogalum species* in West Mediterrenean region of Turkey. Afr J Agric Res 7: 2669-2673

[30] Memon, N. (2012) In vitro Propagation of Gladiolus Plantlets and Cormels. J Hort Sci Ornam Plants 4: 280-291.

[31] Çiğ, A. and Başdoğan, G., (2015) In vitro propagation techniques for some geophyte ornamental plants with high economic value. Int J Secon Metabolite 2: 27-49.

[32] Huetteman, A. and E.J. Preece. (1993) Thidiazuron: a potent cytokinin for woody plant tissue culture. Plant Cell Tiss Org Cult 33: 105-119.

[33] Patnaik, S. and Rath, S.P. (1997) Direct shoot regeneration from foliar explants of an epiphytic orchid, Acampe Praemorsa (Roxb.) Blatter and McCann. Plant Cell Rep 16: 583-586.
[34] Nhut, D.T., Le, B.V., Minh ,T., De Silva, J.T., Fukai, S., Tanaka, M. and Van, K.T.T. (2002) Somatic embryogenesis through pseudobulblet thin cell layer of *Lilium longiflorum*. Plant Growth Reg 37: 193-198.
[35] Aslam, F., Naz, S., Tariq, A., Ilyas, S. and Shahzadi, K. (2013) Rapid multiplication of ornamental bulbous plants of *Lilium Orientalis* and *Lilium Longiflorum*. Pak J Bot 45: 2051-2055.
[36] Thomas, T.D. and Maseena, E.A. (2006) Callus induction and plant regeneration in *Cardiospermum halicacabum*n Linn. an important medicinal plant. Scientia Horticulturae 108: 332-336.
[37] Rybczyński, J.J. and Gomolińska, H. (1989) 6-benzyladenine control of the initial bulblets formation of wild *Lilium martagon* L. Acta Hort 251: 183-189.
[38] Han, B.H., Hee, J.Y., Byeoun, W.Y. and Kee, Y.P. (2004) In vitro micropropagation of *Lilium longiflorum* 'Georgia' by shoot formation as influenced by addition of liquid medium. Sci Horticulturae 103: 39-49.
[39] Sivanesan, I., Lim M.Y. and Jeong B.R. (2012) Micropropagation and green house cultivation of *Scrophularia takesimensis* nakai, A rare endemic medicinal plant. Pak J Bot 44: 1657-1662.
[40] Memon, N., Qasim, M., Jaskani, M.J., Khooharo, A.A., Hussain, Z. and Ahmed, I. (2013) Comparison of various explants on the basis of efficient shoot regeneration in Gladiolus. Pak J Bot 45: 877-885.
[41] Nakano, M., Tanaka, S., Kagami, S. and Saito, H. (2005) Plantlet regeneration from protoplast of *Muscari armeniacum* Leichtl. ex Bak. Plant Biotechnol 22: 249–251.
[42] Özel, A., Khawar, K.M. and Ünal, F, (2008) In vitro axillary bulblet regeneration of Turkish yellow grape hyacinth, (*Muscari macrocarpum* Sweet) from twin scale explants. Res J Agric Biol Sci 3: 924-929.
[43] Tang, Y.P., Liu, X.Q., Wahiti Gituru, R. and Chen, L.Q. (2010) Callus induction and plant regeneration from in vitro cultured leaves, petioles and scales of *Lilium leucanthum* Baker. Biotechnol Biotechnological Equip 24: 2071-2076.
[44] Skorić, M., Živković, S., Savić, J., Šiler, B., Sabovljević, A., Todorović, S. and Grubišić, D. (2012) Efficient one-step tissue culture protocol for propagation of endemic plant, *Lilium martagon* var. *cattaniae* Vis. Afr J Biotechnol 11: 1862-1867.
[45] Tsao, C. and Reed, B. (2002) Gelling agents, silver nitrate and sequestrene iron influence adventitious shoot and callus formation from Rubus leaves. In Vitro Cell Dev Biol-Plant 38: 29-32.
[46] Ebrahim, M.K. and Ibrahim, I.A. (2000) Influence of medium solidification and pH value on in vitro propagation of *Maranta leuconeura* cv. Kerchoviana. Sci Horticulturae 86: 211-221.
[47] Mohamed-Yasseen, Y. (2001) Influence of agar and activated charcoal on uptake of gibberellin and plant morphogenesis in vitro. In Vitro Cell Dev Biol-Plant 37: 204-205.
[48] Zhang, M. and Jia, G. (2014). The effects of sucrose concentration and light condition on lily's bulblet-in-tube production and incluson content. Pak J Bot 46: 307-315.
[49] Azad, M.A.K. and Amin, M.N. (2013) Effects of hormonal and basal nutrient medium on in vitro regeneration of an ornamental plant-*Muscari armeniacum* Leichtlin. ex Baker. Plant Tiss Cult Biotechnol 22: 113-126.
[50] Langens-Gerrits, M., De Klerk, G.J. and Croes, A. (2003) Phase change in lily bulblets regenerated in vitro. Physiol Plant 119: 590-597.
[51] Kumar, S., Avasthi, V., Kanwar, J.K. (2007) Influence of growth regulators and nitrogenous compounds on in vitro bulblet formation and growth in oriental lily. Horticultural Sci (Prague) 34: 77-83.

Received: **26.11.2015**
Accepted: **17.04.2016**

CORRESPONDING AUTHOR

Sebahattin Ozcan
Department of Field Crops Faculty of Agriculture
University of Ankara 06110, Ankara TURKEY

e-mail: ozcans@ankara.edu.tr

© by PSP Volume 25 – No. 10/ 2016, pages 3915-3922 Fresenius Environmental Bulletin

EFFECTS OF NITROGEN ADDITIONS ON SOIL SEED BANK OF A FRESHWATER MARSH IN SANJIANG PLAIN, NORTHEASTERN CHINA: A SHORT-TERM STUDY

Guodong Wang[1,*], Ming Wang[2], Ming Jiang[1]

1. Key Laboratory of Wetland Ecology and Environment, Northeast Institute of Geography and Agroecology, Chinese Academy of Sciences, Changchun, Jilin, 130102, China;
2. School of Geographical Sciences, Northeast Normal University, Changchun, Jilin, 130024, China;

ABSTRACT

Over the past five decades, the natural wetlands in Sanjiang Plain, Northeast China, have been extensively reclaimed for agriculture with a total loss of nearly 80% of the surface area and the un-drained ones have received a large amount of exogenous N input from the adjacent agricultural land because of fertilization. In the present study, the effects of nitrogen additions on seed germination and seedling biomass of *Calamagrostis angustifolia* freshwater marsh were tested in a greenhouse study. Seed bank soil was exposed to different N additions (0, 5, 10, 20 and 40 g/m^2) under non-flooded water regime. Results revealed that, low level of N additions (less than 10 g/m^2) did not significantly affect the species richness and seedling density, while the seedling biomass at 5 g/m^2 of N addition was higher than other nutrient conditions. But species richness, seedling emergence and biomass decreased significantly at high level of N additions (20-40 g/m^2). The responses were species-specific. High level of N additions had negative impacts on seed germination, seedling growth and biomass of dominant species *Eleocharis ovata*, *Calamagrostis angustifolia*, *Juncus effusus* in the seed bank. To protect and restore the wetland vegetation community in the Sanjiang plain, fertilization, irrigation and land management strategies will need to be implemented to reduce the nutrient input from the agricultural land to the wetlands.

KEYWORDS:

Nitrogen addition, freshwater marsh, seed bank, seed germination, seedling biomass, *Calamagrostis angustifolia*

INTRODUCTION

Increased input of nitrogen and phosphorus from agricultural, urban or atmospheric sources has caused the alteration of wetland plant community structure and composition, which are known to alter ecosystem function, such as primary production and nutrient cycling [1, 2], in a variety of habitats worldwide. Nutrient enrichment has also been shown to cause the expansion of dominant species and loss of community diversity in different types of wetlands [3-8]. Although wetland vegetation is often maintained by vegetative expansion of dominant species, moderate disturbance can create gaps allowing germination of the seeds, spores, and vegetative bodies present in the soil. If the seed bank composition is significantly different from standing vegetation, shifts in community composition following disturbance may be seen [9].

In areas of frequent disturbance due to fires or fluctuating water level such as in seasonally drying wetlands, seed bank composition and germination characteristics are necessary for modeling wetland vegetation composition over time [10]. Environmental factors such as water level, nutrient levels or temperature can affect which species are contributing to the seed bank, longevity of seeds, germination success, and seedling recruitment from the seed bank [10, 11]. These factors may be quite different than those that drive the composition of the standing vegetation [12].

Nitrogen (N) is commonly a limited nutrient in wetland ecosystems, and it directly affects the species composition and the productivity of the wetland [13]. Yet we still know little about how the exogenous nitrogen affect seed germination from soil seed banks, and further influence the

composition and productivity in the freshwater wetlands. Ket et al. [14] found that nitrogen additions could promote seed germination and seedling growth rate of the *Zizaniopsis miliacea* and further increase the primary production in a tidal freshwater marsh, Gerritsen and Greening [15] found that N addition could inhibit the germination of *Nymphaea*, while it has no significantly influence on other wetland species in the Okefenokee Swamp. The specific response may depend on the plant species, hydrology, soil nutrient status [15-17].

In recent decades, reclamation of natural wetlands has been one of the major land use changes in Northeast China. Sanjiang Plain, the largest freshwater marshland in China, has experienced intensive and extensive cultivation over the past 50 years [18]. An increasing number of marshes have been drained for conversion into agricultural lands, and the un-drained ones have received a large amount of exogenous N input from the adjacent agricultural land because of fertilization [19, 20]. Yet, there is no information about the response of soil seed bank to N enrichment in freshwater marsh ecosystems of Northeast China. So we conducted a germination experiment in the greenhouse to evaluate the effects of different N additions on the seed bank of *Calamagrostis angustifolia*-dominated freshwater marsh, which is a major component of wetlands in the Sanjiang Plain [18]. Results from this study shall provide important insight into the responses of wetland vegetation in mid-high latitudes to environmental disturbances such as increasing input of nitrogen from agricultural land. This information is important to the protection of aquatic plants and the restoration of impaired wetlands.

MATERIALS AND METHODS

Study site. The study site is located in a *C. angustifolia*-dominated freshwater marsh near the Sanjiang Mire Wetland Experimental Station (47°35′N, 133°31′E, 56 m a.s.l) in the Sanjiang Plain, Heilongjiang Province, northeastern China. *C. angustifolia*-dominated seasonally inundated wetland is one of the main wetland types in the Sanjiang Plain, as this ecosystem type accounts about 31% for the wetland area in this region [18]. The study site has a temperate continental monsoon climate with a mean annual (1990-2010) temperature of 2.53℃ (month range -20.4 to 21.6℃), a mean annual precipitation of 566 mm (approximately 60% fall in July and August) with growing season duration of 125 days per year. During the dry season marsh fires occur regularly. The soil type in the study site is meadow marsh soil and the soil properties are as below: the concentration of total organic C (TOC) and total N (TN) is 23.60 and 2.18 mg g^{-1}, respectively. Soil bulk density is 0.88 g cm^{-3}, and pH (H_2O) is 5.58.

The study sites are dominated by freshwater marsh with shallow and intermittent water levels, varying from no standing water to an average depth of approximately 12 cm. The flora mainly consists of *Calamagrostis angustifolia* Kom., with less dominant, but common species such as *Glyceria spiculosa* (Fr. Schmidt.) Rosh., *Phragmites australis* (Clav.) Trin., *Eleocharis ovata* (Roth.) Röem. et Schult., *Menyanthes trifoliate* L. and *Carex humida* Y.L.Chang.et Y.L.Yang.. We chose one 50 m×50 m area of *C. angustifolia* community as the sampling site to do soil samplings.

Seed bank collection. Sampling was conducted right after snow melt (6–8 May, 2012) to assess the seed bank present at the time of spring germination including both transient and persistent types of seeds. Note that transient seed banks are from seed produced in the previous year, which do not live until a second growing season. Persistent seed banks are comprised of seeds one or more year old [21, 22]. Soil samples from 20 replicate plots (25 cm×25 cm×5 cm) in natural site were taken and placed into soil bags. All samples were taken back to the greenhouse. In the laboratory, each soil sample was sieved to remove stones and plant fragments, and mixed thoroughly.

Seedling germination assays. Seed banks from the natural site were studied with one treatment factor: N addition. Five levels of N addition: 0, 5, 10, 20 and 40 g/m^2 were used. Nine replicates were used for each level of N addition, resulting in a total of 45 replicates.

The seedling germination assays were conducted in the greenhouse during 9-10 May, 2012. The greenhouse had a glass roof that did not significantly attenuate of disrupt visible or near-infrared radiation. It was also well ventilated to maintain an inside temperature comparable to

that of the outside. Monthly air temperature in the greenhouse during the study period ranged from 16.4℃ in May to 23.8℃ in July. Soil samples were divided into 45 equal parts. And then each part was spread as an even layer, 2 cm thick, in experimental pots (14 cm diameter and 11 cm depth) previously filled with washed vermiculite to an 8 cm depth, a procedure similar to that described by van der Valk and Rosburg [23] and Middleton [24]. All the pots were placed in a big tank randomly assigned to non-flooded (moist soil) water treatment. The tank was filled with distilled (DI) water from the bottom to keep the non-flooded water treatment, and water depths were maintained throughout the experiment with DI water. The total amount of N added was based on the amount applied in a year at a rate of 5, 10, 20 and 40 g m^{-2} $year^{-1}$, Nitrogen was added a total of six times in 20 day' intervals by injecting into the soil 10 mL of 0.25, 0.5, 1, 2 g N L^{-1} solution at five points in each pot in each treatment respectively. Nitrogen was added as ammonium nitrate (NH_4NO_3). Treatments without N were injected with DI water to control for the mechanical disturbance caused by injection. Pots were rotated weekly within the tank. Newly emerged seedlings were identified and counted each week. The seedling germination assays continued until no additional seedlings emerged. The germination assay lasted approximately 3 months. Nomenclature follows Yi et al. [25].

The height of each species in each pot was measured and then the above-ground biomass in each pot was sampled at the end of germination assay. Plant material was clipped above the soil surface of each pot, and was oven-dried at 80 °C until constant weight.

Data analysis. A one-way ANOVA and a subsequent Tukey's test were used to test the difference in mean number of species, the mean seedling density, number of seedlings of each species and the above-ground biomass among the N additions. Significance was determined at an alpha level of 0.05. Data of species richness, seedling density and biomass were transformed (log(x+1)) to satisfy the assumption of homogeneous variances. All statistics were conducted using SPSS version 16.0.

RESULTS

Effects of N addition on the species richness and seedling emergence. N addition significantly affected the number of species and seedlings germinated from seed banks (F=16.018, p<0.001; F=11.276, p<0.001). There was a weak increase in the number of species when the N addition

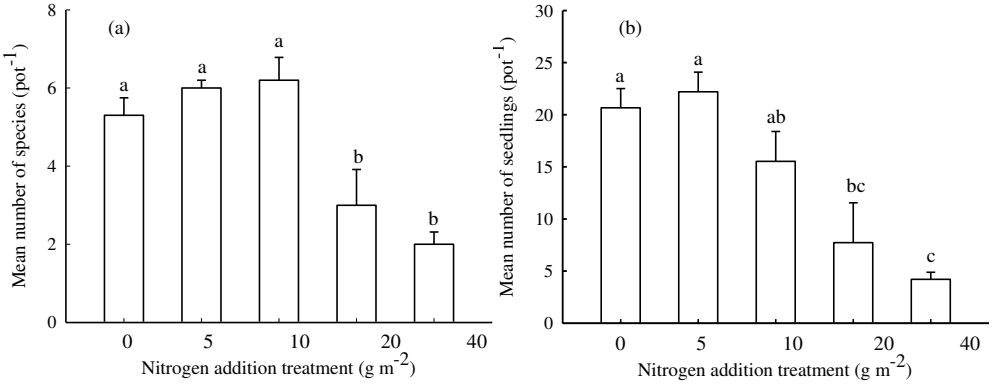

FIGURE 1

(a)Effects of N additions on the mean number of species emerging in the seed banks of the *Calamagrostis angustifolia* freshwater marsh in Sanjiang Plain. Values are means＋SE. Values followed by the same superscripted letter are not significantly different (Tukey's test; p>0.05; n=9 pots per treatment). (b) Effects of N additions on the mean number of seedlings emerging in the seed banks of the *Calamagrostis angustifolia* freshwater marsh in Sanjiang Plain. Values are means＋SE. Values followed by the same superscripted letter are not significantly different (Tukey's test; p>0.05; n=9 pots per treatment).

increased from 0 to 10 g/m^2, and it decreased significantly when the N addition increased from 10 to 40 g/m^2, the number of species was least in 40 g/m^2 of N addition (Fig. 1a).

There was a weak increase in the number of seedlings when the N addition increased from 0 to 5 g/m^2, and then it decreased significantly with increasing N addition. The number of seedlings in 20 and 40 g/m^2 was significantly lower than 0 g/m^2 of N addition, and it was least in 40 g/m^2 of N addition (Fig. 1b).

A total of 21 species germinated from the seed banks. Species responded differently to the addition of nutrient. The number of seedlings from *Eleocharis ovata* was high at 0-5 g/m^2 of N addition, and it decreased significantly at 10 g/m^2 of N addition, and it was lowest at 20-40 g/m^2 of N addition (Table 1). The number of seedlings from *Calamagrostis angustifolia*, *Juncus effuses*, *Poa palustris*, *Typha latifolia* was much lower at 20-40 g/m^2 of N addition than at 0-10 g/m^2 of N addition (Table 1). There was no significant difference among different N addition treatments for other species, as the numbers of seedling emergence were extremely low.

TABLE 1

Mean number of seedlings per pot in each N addition treatment in the Calamagrostis angustifolia community in Sanjiang Plain. Species are listed in order of decreasing abundance in the 0 g/m2 of N addition treatment. Values followed by the same superscripted letter were not significantly different (Tukey's test; p>0.05; n=9 pots per treatment).

	Nitrogen input (g/m^2)				
Species	0	5	10	20	40
Eleocharis ovata	7.22^a	8.89^a	3.44^b	2.0^c	1.67^c
Calamagrostis angustifolia	3.78^a	3.44^a	3.67^a	1.67^b	0.44^c
Juncus effusus	1.89^a	3^a	2.44^a	0.22^b	0^b
Poa palustris	1.56^a	2.44^a	2.22^a	1.22^b	0^b
Typha latifolia	1.11^a	0.89^a	0.89^a	0.22^b	0^b
Stachys baicalensis	0.89^a	0.33^a	0.56^a	0.84^a	0.33^a
Glyceria spiculosa	0.78^a	0.67^a	0.44^a	0.78^a	0.44^a
Echinochloa crusgalli	0.67^a	0.22^a	0.22^a	0^a	0^a
Sagittaria trifolia	0.67 ^{a}	0.67 ^{a}	0 ^{a}	0.33 ^{a}	0.44 ^{a}
Lysimachia thyrsiflora	0.56^a	0.67^a	0.22^a	0^a	0^a
Carex humida	0.33^a	0.22^a	0.22^a	0.11^a	0.22^a
Galium trifidum	0.33 ^{a}	0 ^{a}	0 ^{a}	0 ^{a}	0 ^{a}
Polygonum persicaria	0.22 ^{a}	0 ^{a}	0.22 ^{a}	0 ^{a}	0.44 ^{a}
Bidens bipinnata	0.22 ^{a}	0 ^{a}	0 ^{a}	0 ^{a}	0 ^{a}
Sium suave	0.11 ^{a}	0 .11^a	0 ^{a}	0 ^{a}	0 .11^a
Gnaphalium mandshuricum	0.11 ^{a}	0.22 ^{a}	0.44 ^{a}	0 ^{a}	0 ^{a}
Lycopus lucidus	0.11 ^{a}	0 .22^a	0 ^{a}	0 .11^a	0 ^{a}
Phragmites australis	0.11 ^{a}	0.44 ^{a}	0 ^{a}	0 ^{a}	0 ^{a}
Spiraea salicifolia	0 ^{a}	0 ^{a}	0.11 ^{a}	0 ^{a}	0 ^{a}
Saussurea amurensis	0 ^{a}	0.11 ^{a}	0.22 ^{a}	0.33 ^{a}	0.22 ^{a}
Rorippa palustris	0 ^{a}	0 ^{a}	0.22 ^{a}	0 ^{a}	0 ^{a}

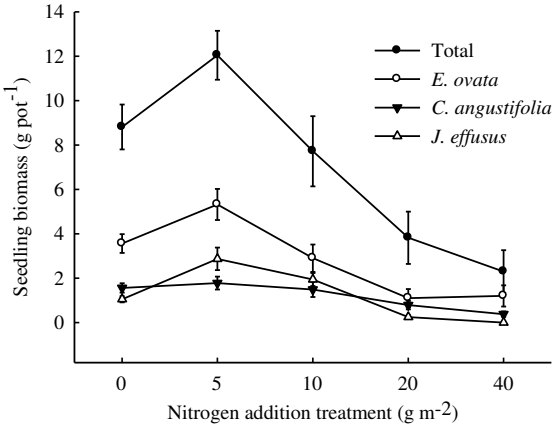

FIGURE 2

Effects of N additions on seedling biomass of the total species and three dominant species (*Eleocharis ovate*, *Calamagrostis angustifolia*, *Juncus effuses*) of the *Calamagrostis angustifolia* freshwater marsh in Sanjiang Plain. Values are means±SE. (n=9 pots per treatment).

Effects of N addition on seedling biomass. N addition significantly affected the seedling biomass. It showed similar response to the N addition with the seedling density (Fig. 2). The seedling biomass was highest as 5 g/m^2 of N addition, and decreased significantly when the N addition reached 10 g/m^2 or greater (Fig. 2). The seedling biomass was different among different N addition mainly because that the individual seedling biomass of three dominant species *Eleocharis ovate*, *Calamagrostis angustifolia*, *Juncus effuses* responded to N addition. For *Eleocharis ovate*, higher seedling biomass was found at low N addition, and it decreased significantly when the nutrient addition increased to 10 g/m^2 or more. For *Calamagrostis angustifolia* and *Juncus effuses*, seedling biomasses were much lower at 20-40 g/m^2 of N addition than at 0-10 g/m^2 of N addition (Fig. 2).

DISCUSSION

Boreal mire ecosystems are generally nutrient limited, and extra nitrogen could influence the community composition and plant production [13, 19]. Over the past five decades, the natural wetlands in Sanjiang Plain have been extensively reclaimed for agriculture with a total loss of nearly 80% of the surface area [26]. More and more marshes are being drained for conversion to agricultural production, whereas the still un-drained marshes often receive some leaching nitrogen during the agricultural activities (the total about 5.8 g N m^{-2}) or atmospheric deposition (wet deposition is about 0.8 g N m^{-2} yr^{-1}) and other inputs [19, 20]. This study tested seed germination and seedling responses to different N addition treatments in the freshwater marshes.

Nutrient addition significantly reduced the number of seedlings and species germinating from the seed banks, and the response is species-specific [15, 16, 27, 28]. In our study, Low level of nitrogen addition (less than 10 g/m^2) had no significant effects on the species richness and seedling density. But high level of nutrient addition (20-40 g/m^2) significantly decreased both the species richness and seedling density. High level of N additions suppressed the germination of the dominant species *Eleocharis ovate*, *Calamagrostis angustifolia*, *Juncus effuses*, *Poa palustris*, *Typha latifolia* from the seed bank, while it seemed to have no significant effect on other wetland species. Our findings are consistent with other studies. In other examples of nutrient enrichment effects on germination, N additions suppressed germination of *Nymphaea odorata* from Okfenokee seed banks [15]. Both Tilman [27] and Foster and Gross [28] have found negative correlations between N availability and seed germination. Nutrient addition reduced species richness by effectively preventing the seedling establishment and reduced the recruitment of *Andropogon gerardi* by inhibiting both germination and survival [28]. In freshwater herbaceous wetlands in Northern Belize, Nutrient addition reduced the number of seedlings of *Eleocharis Mimutissima* and *Chara* sp. from the seed bank [16]. But other study found that N addition did not have significant effects on the species richness and seedling density of wetland species from seed banks [29]. So nitrogen addition decreased the species richness and seedling density from the seed bank in our study, and level of nutrient addition may lead to different results.

Nitrogen is commonly a limited nutrient in wetland ecosystems, extra nitrogen is often very rapidly taken up by the plant, so it directly affects the productivity of the wetland [13]. Zhang et al.

[19] found that nitrogen addition significantly affected the growth of *C. angustifoila* in the freshwater marshes. The above-ground biomass and plant height are both significantly enhanced after low level of nitrogen addition. Other studies also found that Nitrogen appears to limit marsh plant growth and additions of nitrogen fertilizer increased plant production [14, 15, 28]. In our study, low level of N addition (5 g/m^2) increased the above-ground biomass by enhancing both the seed germination and seedling growth, especially for the *Eleocharis ovata* and *Juncus effuses*, low level of N addition increased the seedling density, seedling height (data not showed) and individual seedling mass, and thus the above-ground biomass were higher than other nutrient conditions. Rejmánková et al. [29] also found that *Eleocharis* sp. showed a similar response, low level of nutrient addition increased stem density and height and thus the overall above-ground biomass was much higher. High level of N addition (20-40 g/m^2), however, significantly decreased the above-ground biomass in our study. This is mainly because high level of nutrient addition suppressed seed germination and seedling growth, so the species richness and seedling density were lower than at low level of nutrient addition, which led to the lower above-ground biomass. Liu et al. [30] also found that high level of nutrient input significantly decreased the number of seedlings of some wetland species, and thus decreased the above-ground biomass in marshes in Xingkai Lake, China.

CONCLUSION

Our study revealed the negative impacts on seed germination, seedling growth and biomass by high level of N additions while low level of N addition had slight positive effects on the seed bank germination in Sanjiang Plain, Northeast China. And the responses to the nutrient additions were species-specific. Knowledge gained from this and similar studies will provide important insights into fertilizer use, irrigation and land management that should be paid more attention to sustain wetlands located in the agricultural lands.

ACKNOWLEDGEMENTS

We thank Dr. Beth Middleton for suggestions and English editing. This study was supported by National Natural Science Foundation of China (grant # 41501105, 41501090, 41271106), Science Foundation for Youths of Jilin Province (20160520059JH), and Fundamental Research Funds for the Central Universities (2412015KJ023).

REFERENCES

[1] J.J. Elser, M.M. Elser, N.A. Mackay, S.R. Carpenter, "Zooplankton-mediated transitions between N-limited and P-limited algal growth," Limnol. Oceanogr. vol. 33, pp.1-14, 1988.

[2] P. Vitousek, *Nutrient cycling and limitation: Hawaii as a model system*, Princeton University Press, Princeton, NJ, USA, 2004.

[3] Valeiela, J.M. Teal, W.J. Sass, "Production and dynamics of salt marsh vegetation and the effects of experimental treatment with sewage sludge," J. Appl. Ecol. vol. 12 , pp. 973-981, 1975.

[4] Y.J. Lou, G.P. Wang, X.G. Lu, M. Jiang, "Nitrogen and phosphorus content of vascular plant species in herbaceous marshes in the Sanjiang Plain, northeast China," Fresen. Environ. Bull. Vol. 21, pp. 3766-3772, 2012.

[5] R. Aerts, F. Berendse, "The effect of increased nutrient availability on vegetation dynamics in wet heathlands," Vegetatio, vol. 76, pp. 63-70, 1988.

[6] N.H. Urban, S.M. Davis, N.G. Aumen, "Fluctuations in sawgrass and cattail densities in Everglades Water Conservation Area 2A under varying nutrient, hydrologic and fire regimes," Aqua. Bot. vol. 46, pp. 203-223,1993.

[7] S.L. Miao, S. Newman, F.H. Sklar, "Effects of habitat nutrients and seed sources on growth and expansion of *Typha domingensis*," Aqua. Bot. vol. 68, pp. 297-311, 2000.

[8] F.H. Sklar, M.J. Chimney, S. Newman, P. McCormick, D. Gawlik, S.L. Miao, C. McVoy, W. Said, J. Newman, C. Coronado, G. Crozier, M. Korvela, K. Rutchey, "The ecological-societal underpinnings of Everglades restoration," Front. Ecol.

Environ., vol. 3, pp. 161-169, 2005.

[9] I.C. Wisheu, P.A. Keddy, "Seed banks of a rare wetland plant community, distribution patterns and effects of human-induced disturbance," J. Veg. Sci., vol. 2, pp. 181-188, 1991.

[10] M.I. Galinato, A.G. van der Valk, "Seed germination traits of annuals and emergents recruited during drawdowns in the Delta Marsh, Manitoba, Canada," Aqua. Bot., vol. 26, pp. 89-102, 1986.

[11] M.A. Leck, Wetland seed banks. In: M.A. Leck, V.T. Parker, R.L. Simpson (Eds.), *Ecology of soil seed banks*, Academic Press, San Diego, pp. 283-305, 1989.

[12] M. Tu, J.H. Titus, S. Tsuyuzaki, R. del Moral, "Composition and dynamics of wetland seed banks on Mount St. Helens, Washington, USA," Folia Geobot., vol. 32, pp. 3-16, 1998.

[13] W.J. Mitsch, J.G. Gosselink, *Wetlands*, Van Nostrand Reinhold Company Inc., New York, pp. 89-125, 2000.

[14] W.A. Ket, J.P. Schubauer-Berigan, C.B. Craft, "Effects of five years of nitrogen and phosphorus additions on a *Zizaniopsis miliacea* tidal freshwater marsh," Aqua. Bot., vol. 95, pp. 17-23, 2011.

[15] J. Gerritsen, H.S. Greening, "Marsh seed banks of the Okefenokee swamp: effects of hydrologic regime and nutrients," Ecology, vol. 70, pp. 750-763, 1989.

[16] S. Johnson, "Effects of water level and phosphorus enrichment on seedling emergence from marsh seed banks collected from northern Belize," Aqua. Bot., vol. 79, pp. 311-323, 2004.

[17] D. Song, Y. Wang, H. Li, L.Q. Shi, J. Mi, S. Deng, J.H. Zhan, X.J. Pan, "Vertical distribution of various forms of phosphorus in the sediments of Dianchi Lake, China," Fresen. Environ. Bull. Vol. 21, pp. 2191-2200, 2012.

[18] X.L. Song, X.G. Lu, Z.S. Zhang, Z.K. Chen, "Land use change in Naoli River Basin and its eco-environment effects during 1954-2005," Fresen. Environ. Bull. Vol. 21, pp. 3626-3635, 2012.

[19] L.H. Zhang, C.C. Song, D.X. Wang, Y.Y. Wang, "Effects of exogenous nitrogen on freshwater marsh plant growth and N_2O fluxes in Sanjiang Plain, Northeast China," Atmos. Environ., vol. 41, pp. 1080-1090, 2007.

[20] L.H. Zhang, C.C. Song, D.X. Wang, "CO_2, CH_4 and N_2O emissions to the atmosphere upon nitrogen addition in the swamp wetland," Acta Scientiae Circumstantiae, vol. 25, pp. 1112-1118, 2005. (in Chinese)

[21] C.C. Baskin, J.M. Baskin, *Seeds: Ecology, biogeography, and evolution of dormancy and germination*, Academic Press, San Diego, California, 2001.

[22] K. Thompson, J.P. Grime, "Seasonal variation in the seed banks of herbaceous species in ten contrasting habitats," J. Ecol., vol. 67, pp. 893-921, 1979.

[23] A.G. van der Valk, T.R. Rosburg, "Seed bank composition along a phosphorus gradient in the northern Florida Everglades," Wetlands, vol. 17, pp. 228-236, 1997.

[24] B.A. Middleton, "Soil seed banks and the potential restoration of forested wetlands after farming," J. Appl. Ecol., vol. 40, pp. 1025-1034, 2003.

[25] F.K. Yi, X.Y. Yi, Y.J. Lou, X. Wang, *Wetland Wild Vascular Plants in Northeastern China*, Science Press, Beijing, China, 2008. (in Chinese)

[26] Z.M. Wang, K.S. Song, W.H. Ma, C.Y. Ren, B. Zhang, D.W. Liu, J.M. Chen, C.C. Song, "Loss and fragmentation of Marshes in the Sanjiang Plain, Northeast China, 1954-2005," Wetlands, vol. 31, pp. 945-954, 2011.

[27] D. Tilman, "Community invisibility, recruitment limitation, and grassland biodiversity," Ecology, vol. 78, pp. 81-92, 1997.

[28] B.L. Foster, K.L. Gross, "Species richness in a successional grassland, effects of nutrient enrichment and plant litter," Ecology, vol. 79, pp. 2593-2602, 1998.

[29] E. Rejmánková, P. Macek, K. Epps, "Wetland ecosystem changes after three years of phosphorus addition," Wetlands, vol. 28, pp. 914-927, 2008.

[30] Q.Y. Liu, M. Jiang, G.D. Wang, X.G. Lu, M. Wang, Y.J. Lou, Y.X. Yuan, "Effects of exogenous phosphorus inputs on seed germination of soil seed bank in marshes in Xingkai Lake," Wetland Science, vol. 11, pp. 41-47, 2013. (in Chinese)

Received: **12.06.2015**
Accepted: **10.03.2016**

CORRESPONDING AUTHOR

Guodong Wang,
Key Laboratory of Wetland Ecology and Environment, Northeast Institute of Geography and Agroecology, Chinese Academy of Sciences, Changchun, 130102, China.

Email: wanggd@neigae.ac.cn

© by PSP Volume 25 – No. 10/2016, pages 3923-3940 Fresenius Environmental Bulletin

ERRATUM

LONG-TERM VARIABILITY OF TOTAL NITROGEN AND TOTAL PHOSPHORUS CONCENTRATION AND LOAD IN THE SOUTH PART OF THE BALTIC SEA BASIN

Piotr Ilnicki[1,*], Krzysztof Gorecki[1], Piotr Lewandowski[1], Ryszard Farat[2]

[1]Department of Entomology and Environmental Protection, Poznań University of Life Sciences, 60–594 Poznań, ul. Dąbrowskiego 159, Poland
[2]Institute of Meteorology and Water Management – State Research Institute, 51-616 Wrocław, ul. Parkowa 30, Poland

ABSTRACT

A high decrease was observed in concentrations and loads of nitrogen and phosphorus discharged from the Warta River (catchment area 54 519 km^2) to the Oder (catchment area 119 074 km^2). One half of the monitoring stations are strongly influenced by point sources, which allows for verifying the functioning of sewage treatment plants. Nitrogen compound concentrations are positively correlated with the river runoff, requiring the application of water years when studying river eutrophication. A high retention of nitrogen in the Warta River basin is documented. Calculated area-specific loads show that the Warta River introduced considerably less N and P than rivers discharging into the North Sea. Monthly loads of total nitrogen show a significant positive correlation with the river runoff. In 1992–2011, nitrogen and phosphorus load time trends were negative and statistically significant. The participation of non-point sources in the nutrient emission, used in the MONERIS model, is too high and of that of point sources is too low.

KEYWORDS:
Warta River, nitrogen, phosphorus, eutrophication, load, trend, Poland

INTRODUCTION

Intensification of human activities after 1950 led to widespread nutrient enrichment of surface waters, causing a range of environmental, social and economic problems encompassed under the term eutrophication [1-3]. In order to moderate high nutrient emissions into surface waters, governments organized in 1974 the International Helsinki Convention [4, 5] for protection of the Baltic Sea and the OSPAR Convention for the North Sea.

Determination of stream concentrations and transport of nitrogen (N) and phosphorus (P) are components of many monitoring programs and water quality studies, realized in Europe and the north-eastern United States. Most of the studies include periods shorter than ten to fifteen years. Notable inter-annual variation in loads, and the complexity of the mechanism underlying this variation, means that records of less than a decade are misleading and only long-term records can illustrate the process of change in conditions [6, 7]. Many investigations were realized in Poland in the two largest rivers Vistula and Oder (Behrendt et al., 2005[1, 3, 8-15]. Data for the Warta River, the third largest river in Poland, were studied in various periods: 1991–1994, 1993–1997, 1950–2000 by Behrendt et al. [8, 9], in 1993–1995, 1992–2002 by Ilnicki et al. [11, 16], and by Górecki and Olejnik [17]. In the Warta River basin for the periods 1993–1995 and in 1992–2000 for over six large rivers in this basin, longitudinal profiles present the TN and TP load changes along the analyzed rivers [11, 16]. Data for the Pilica River were published for a short period 2010/2011 [18]. In the most contaminated Ergene River in Turkey the TN and TP load were analysed in the period 1997-2010 by Bayrak et al. [19, 20] and in the Weihe River basin in the period 1995-2009 by Li et al. [21].

The aim of the present study is the determination of nitrogen and phosphorus concentrations and loads in the Warta River basin in a long period. We estimated loads (Mg) and area-specific loads (kg/ha/year) in five different rivers of this catchment area, compared them and examined the seasonal dynamics of nutrients in the longest available period 1992–2011. These data will allow for determining changes in the degree of river eutrophication which took place during the economic transformations in Poland over the past twenty years, in a region with a high population density and intensive agriculture. The inclusion of a catchment with a less intensive economic development (Drawa River) and with areas very densely populated (Ner River) allows for indicating

changes which have occurred in non-point and point emissions, as well as to determine the possible lowest eutrophication level representing a "good ecological status". This data could allow for improving mathematical models which have been elaborated assuming that the highest endangerment for rivers exist in the case of intensive agricultural management. The determination of the area-specific loads of nitrogen and phosphorus allows for comparing their amount with the changes in nitrogen surplus calculated according to the OECD method and with similar data from other countries.

STUDY AREA

The Warta River, a typical lowland river, is the largest right bank tributary of the Oder River (Fig. 1), including one half of its drainage basin. Most of the basin consists of unconsolidated soils with deep groundwater. A detailed description of the drainage basin was supplied by Ilnicki et al. [19]. It is a region of intensive agriculture, high population density, low specific runoff (4.03 l s^{-1} km^{-2}) and annual rainfall (544 mm). Eutrophication of river waters was investigated in the Warta River mouth (monitoring station in Kostrzyn and the gauge station in Gorzów Wlkp.), as well as in the central (gauge station in Oborniki) section below Poznań (550 000 inhabitants), in the Noteć River catchment area, the greatest tributary of the Warta River (Santok and Nowe Drezdenko gauge station) and its most natural tributary of the Drawa River (Łokacz and Drawiny gauge station) and also in two tributaries: Prosna (Bogusław gauge station) being under the influence of Kalisz (107 000 inhabitants) and Ner (Dąbie gauge station), which is strongly influenced by sewage from Łódź (729 000 inhabitants). The differentiated population density in these basins oscillates from 36 (Drawa), through 261 (Warta) to 1010 (Ner) inhabitants per km^{2}. Within the framework of state environment monitoring, studies were carried out in six water quality monitoring stations localized the closest to the gauge stations (Table 1). The method of land use in the catchment areas (Table 2) is differentiated. In the total Warta River basin, the arable land cover amounts to 48%, grassland 10.3% and forests cover 30.2%. The share of forests distinctly decreases above Oborniki. The Noteć River catchment has a distinctly smaller share of arable land (39.7%) but a very large area of forests (36.7%). The Drawa River basin (tributary of the Noteć River) shows the highest share of forests (50.9%) and lakes (3.8%), but the smallest number of inhabitants and therefore the least anthropogenic impact. The Prosna River and Ner River basins are characterised by almost no water reservoirs, by a high share of arable land (59.4% and 62.3%) and poor afforestation (12.0% and 19.2%). The waters of the Ner River are under the strong influence of Łódź because of the high population density. There is a smaller but distinct influence of point sources on the Prosna River (Kalisz) and on the Warta River in Oborniki (Poznań).

In 1997, wastewater in the Warta River basin was purified to 52.3% only with the first (mechanical) treatment, 23.1% sewage with second and 7.1% with tertiary treatment. In 2002, the analogical values were 34.6%, 38.5% and 21.7%, respectively. In the years 1993–2002, the amount of sewage from 20 large towns in Warta River basin locations decreased from 320.7 to 186.2 hm^3. Numerous sewage treatment plants with tertiary treatment were built. In 2002, Sewage Treatment Plants (STP) existed in 13 out of 20 of the largest towns [16]. In 2011, in the Warta River basin, 45% of sewage was purified with tertiary treatment and 10% with secondary. On the other hand, in all towns with more than 100 000 inhabitants, there existed STP with tertiary treatment [20]. The greatest STPs in the Warta River basin were rebuilt and modernized in Poznań in 1996–2001, in Łódź in 1997–2002 and in Kalisz in 2001–2003.

TABLE 1
Profiles of gauge stations.

River	Total river catchment area (km^2)	Gauge station					
		Name	River km	Catchment area km^2	Mean annual runoff (m^3 s^{-1}) in		Specific runoff in 1951–2010 (l $s^{-1}$$km^{-2}$)
					1951–2010	1992–2011	
Warta	54 519	Gorzów Wlkp.	56.4	52 365	211	207	4.03
		Oborniki	205.2	26 776	115[a]	111	4.29
Noteć	17 302	Nowe Drezdenko	37.7	25 926	73	70	4.59
Drawa	3 291	Drawiny	4.2	3 281	21.1[b]	21.0	6.43
Prosna	4 917	Bogusław	43.8	4 282	16.1	16.2	3.76
Ner	1 836	Dąbie	12.8	1 727	10.3	10.3	5.96

[a] for 1971–2010 [b] for 1956–2010

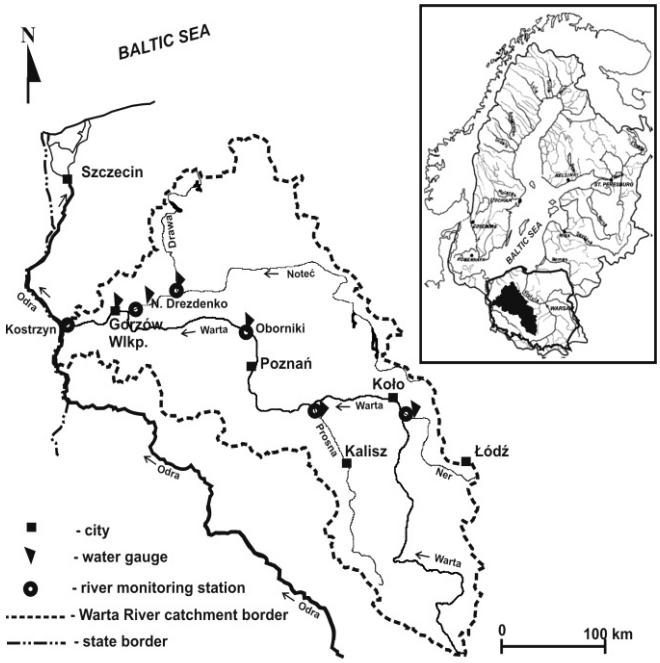

FIGURE 1
Map of the Warta River catchment area, with locations of gauge and water quality monitoring stations.

TABLE 2
Characteristics of river catchment areas and water quality stations.

River	Water quality station		Land use in the river catchment area (%)				Population density (people/ km^2)
	Name	River km	Arable land	Grass-land	Forest	Lakes and reservoirs*	
Warta	Kostrzyn	2.4	48.0	10.3	30.2	1.3	261
Warta	Oborniki	206.3	54.3	11.7	21.5	0.5	289
Noteć	Santok	0.5	39.1	10.6	36.7	2.0	62
Drawa	Łokacz	2.4	27.3	6.3	50.9	3.8	36
Prosna	Ruda Komorska	2.8	62.3	11.0	19.2	0.1	300
Ner	Chełmno	5.0	59.4	14.2	12.9	0.2	1010

* based on remote sensing acc. [8]

DATA

Runoff. It is a well-known fact, that the concentration and load of organic and inorganic substances in rivers can be strongly dependent on the runoff. The observed gauging stations (Table 1) provide information about daily runoff, which the authors received from the State Institute of Meteorology and Water Management. We used the data for water years 1992–2011 and for the comparison long-term annual mean values for 1951–2010, however for short periods for the Oborniki gauge (1971–2010) and Drawiny gauge (1956–2010). Monthly and annual runoffs were presented on the basis of daily data. The annual data were calculated for the water year starting on 1 November, the period usually used in Poland. In this respect water years better reflect the annual cycle of river discharge [6]. For the Warta River, the difference between the catchment area of the Gorzów Wlkp. gauge station and the nearest situated Kostrzyn monitoring station (mouth) was 4%, Noteć River 8%, Ner River 0.6% and Prosna River 1.3%. In the Warta (Oborniki) and Drawa rivers the areas were the same. In spite of these very small differences, the nutrient load in rivers could be calculated on the basis of runoff in the gauge station catchment and nutrient concentration in the water quality stations. The hydrologic characteristic of the Warta River is determined by

the gauge station in Gorzów Wlkp., situated 56.4 km upstream from the mouth, because of a very low slope and the influence of the Odra River downstream from them. A similar situation can be observed on the Noteć River, where the Nowe Drezdenko gauge station is situated 37.7 km upstream from the mouth.

Nutrient Concentration. All water quality data were taken from the laboratories of the Inspectorate for Environmental Protection in Poznań and Gorzów Wlkp., under the auspices of the National Monitoring Program. Both laboratories have Accreditation Certificates, which meet the requirements demanded by EN ISO/EC 17 025. Total nitrogen was determined according to the standard PN-73/C-04576.14, the total phosphorus by the spectrophotometric method according to the standard PN-EN ISO 6878:2006. Concentrations of total nitrogen (TN) and total phosphorus (TP) in water years of the period 1992–2011 were measured fortnightly before 1997, and later in monthly intervals (12 samples/year). In 2010, samples were taken only in the Ner River, but in 2011, no samples were analyzed in that river. In all rivers, data from 19 years were analyzed. Estimates of annual N and P transport based on regular sampling are more accurate than stratified sampling biased towards high-flow seasons. River sampling once a month for nutrient analysis is sufficient to produce annual transport estimates of satisfactory accuracy [14] and importantly, long–term records have diminished the risk of misinterpretation [6]. Short gaps in time series of observed concentration data were filled in by linear interpolation. Single outliers in the series were identified and removed.

Other Data. The land use, population density in watersheds and data about sewage treatment plants were published by Ilnicki et al. [16]. The population density was calculated on the basis of statistical publications for the year 2000, and the population of large cities for the year 2010. Data about monthly and annual precipitation and air temperature in nine meteorological stations (Bydgoszcz, Częstochowa, Gorzów Wlkp., Kalisz, Koło, Leszno, Łódź, Piła and Poznań) of the Warta River basin in 1951–2010 and 1991–2010 were obtained from the Institute of Meteorology and Water Management.

METHODS

The monthly analyses (TN, TP) were performed and the monthly runoff was determined. These data show significant oscillations connected with the building and modernization of STPs. In our study, we calculated the load in the river and not the emission in the watershed. From the monitoring data it is impossible to calculate the nutrient load from point (STPs) and nonpoint (landscape) sources. Only time trends from the total nutrient load for the six sites could be presented. So we present only the differences in time trends between sites with and without large point sources. For load calculations we used the monitoring stations and gauges situated nearest to the river mouth (Fig. 1).

In this study, nutrient load (Mg) was calculated by two different methods of runoff indices. In the first method (calculated load), the monthly riverine nutrient load was calculated by multiplying mean monthly concentrations and monthly runoff. The annual nutrient load is the sum of monthly loads in a water year started on 1 November. The second method applies the flow normalization use runoff from the reference period 1992–2011. This methods was applied also by the Baltic Sea Fifth Pollution Load Compilation [5] and the OSPAR–Convention for the North Sea [24]. Flow normalization of the observed riverine loads implies an attempt to estimate what the load would have been if the runoff had been equal to the average runoff for the analyzed period. Flow-normalized values can be calculated according to the formula (1) presented by Stålnacke et al. [14].

$$\hat{L}_{ij} = L_{ij} - (q_{ij} - \bar{q}_{ij})\hat{\beta}_{ij}, \quad i = 1, 2, \ldots, n, \quad j = 1, 2, \ldots, m, \quad (1)$$

where L_{ij} denotes the load during the jth season (month) of the ith year, q_{ij} is the runoff during the same period, $\bar{q}_{ij}$ is the average runoff and $\hat{\beta}_{ij}$ depicts parameter estimates obtained by employing the roughness penalty approach described above.

Temporal changes in flow-normalized loads can be regarded as indications of changes in the anthropogenic loading of the river [25]. Results are presented for the river as monthly and annual loads (Mg) in five analyzed rivers (six sites), and per unit area (kg/ha/year). The area-specific loads (similar to export coefficient) of TN and TP were calculated in all catchments by dividing the load through the catchment area of the gauge. This load is a good indicator, which informs about the population density, wastewater management and intensity of agriculture in the watershed. It was compared with specific loads in other catchments in Europe and in the north-eastern United States.

Basic statistical parameters, such as the mean and standard deviation of the monthly and annual time series for each of the six sites were calculated. The trend in time series between annual and monthly nutrient concentrations (TN, TP) versus the annual and monthly runoff in 1992–2011 were calculated by a simple linear regression gradient trend model, by Pearson's test and by Spearman's rank correlation (95% significance level). The results were similar. Annual and monthly slopes of

the regression were compared and the trend significance was evaluated. Correlation between mean yearly calculated and flow normalized load (TN, TP) versus the annual discharge were calculated by linear regression. Calculated and flow normalized monthly loads were tested for monotonous time trends by using the linear regression gradient, Mann-Kendall test [26] and Hydrospect software, version 2.0 [27, 28]. In comparison with other conventional parametric methods, the Mann-Kendall tests have an advantage as they allow for testing for all forms of monotonous trends, not only for linear trends, and in addition they are robust in terms of single outliers [14].

RESULTS

Runoff And Precipitation. In order to find whether the runoff of the studied rivers differed significantly in the water years 1992–2011 from the long-term values, they were compared with the values from 1951–2010. In this period the specific runoff of the Warta River (4.03 l $s^{-1}km^{-2}$) was the lowest among large Polish rivers; much higher in the case of the Drawa River (6.43 l $s^{-1}km^{-2}$) and Ner River (5.96 l $s^{-1}km^{-2}$). In the analyzed rivers, the mean annual runoff in 1992–2011 was only 2-4% lower than in the last 60 years (Table 1). The annual runoff in 1992–2011 shows distinct differences for the analyzed rivers (Fig. 2). In the Warta River basin, the wet years included 1994, 1999, 2002, 2010 and 2011, when the annual flow in the Gorzów Wlkp. gauge was 258–300 m^3s^{-1}, and for the Noteć River in Nowe Drezdenko, it was 71.9–96.8 m^3s^{-1}. The water years 1992, 1993, 2004, 2006 and 2009 can be regarded as dry years, when the flows in the Warta River showed only 136–157 m^3s^{-1}, and in the Noteć River only 49.4–61.2 m^3s^{-1}. In the Prosna River, in the June-October period of the dry year 1992, the flows were very small. The monthly runoffs showed very high oscillations, but in 1992–2011 deviate only to a small degree from the long-term mean. The lowest runoff usually occur in the June-September period. This monthly runoff variability of the Warta River in Gorzów Wlkp. has been illustrated for a dry, average, wet year and for the medium value in the period 1992–2011 (Fig. 3). The runoffs of the Drawa River basin area are the most equalized ones during the year, because of the high inflow of underground waters. Runoffs of winter half-years show a significantly higher variability than the very equalized flows of the June-October period.

The mean annual precipitation totals in water years 1951–2010 in the Warta River basin showed 546 mm (winter 206 mm, summer 340 mm), while in the years 1992–2011, it was slightly higher (560 mm), whereby the increase mainly occurred in winter half-year (223 mm). Mean annual precipitation totals in both analyzed sub-periods 1992–2000 and 2001–2011 were analogical. The annual precipitation totals in the water year 2011 showed 560 mm with high rainfall in November and December, after a very dry October of the preceding year. But in the calendar year 2011, the annual precipitation total showed only 473 mm, which indicates the importance of analyzing water years and not calendar years by nutrient load calculations. In nine representative meteorological stations localized in the Warta River basin, in the period 1951–2010, the mean annual air temperature showed 8.2°C and in the years 1992–2011, it increased to 8.8°C. In the years 2001–2011, it was by about 0.5°C higher than in the preceding nine years. The mean monthly temperature increased in the highest degree (from 0.7°C to 0.9°C) in the January–April period.

Nutrient Concentrations. The annual mean nutrient concentrations in the analyzed rivers are presented for two sub-periods 1992–2000 and 2001–2011 (Table 3). The diminishing nutrient concentration in this sub-periods in all rivers, was visible in particular since the building and modernization of STPs in Łódź (Ner River), Kalisz (Prosna River) and Poznań (Warta River in Oborniki). The highest concentration of TN (11.30 and in the later sub-period 6.60 mg N l^{-1}) and TP (1.58 and 0.45 mg P l^{-1}) was measured in the Ner River, which is the result of former bad sewage treatment of a great amount of sewage from Łódź and its suburbs. High concentrations of TN (6.07 and 5.35 mg N l^{-1}) and TP (0.37 and 0.53 mg P l^{-1}) in two sub-periods, were found also in the Warta River near Oborniki, the monitoring point being under the impact of a large STP from Poznań. The water of the best quality (1.34 and 1.16 mg N l^{-1} and 0.10–0.09 mg P l^{-1}) respectively, occurs in the Drawa River. In the mouth of the Warta River, the mean concentration decreased in two sub-periods from 3.07 to 2.65 mg N l^{-1} and from 0.34 to 0.21 mg P l^{-1} respectively.

The mean annual concentration variability of TN in 1992–2011 was low in the Noteć and Drawa rivers without large point sources in the catchment area (Fig. 4). In the Warta River, this variability was much higher in Oborniki (impact of Poznań) than in the mouth. High variability in the Prosna River is probably the result of in time different sewage clearing in the STP in Kalisz. In the Ner River, the concentration of TN rapidly decreased after the start of the STP in Łódź in 1999, and the higher concentrations in 2004 and 2006 have their source in this plant.

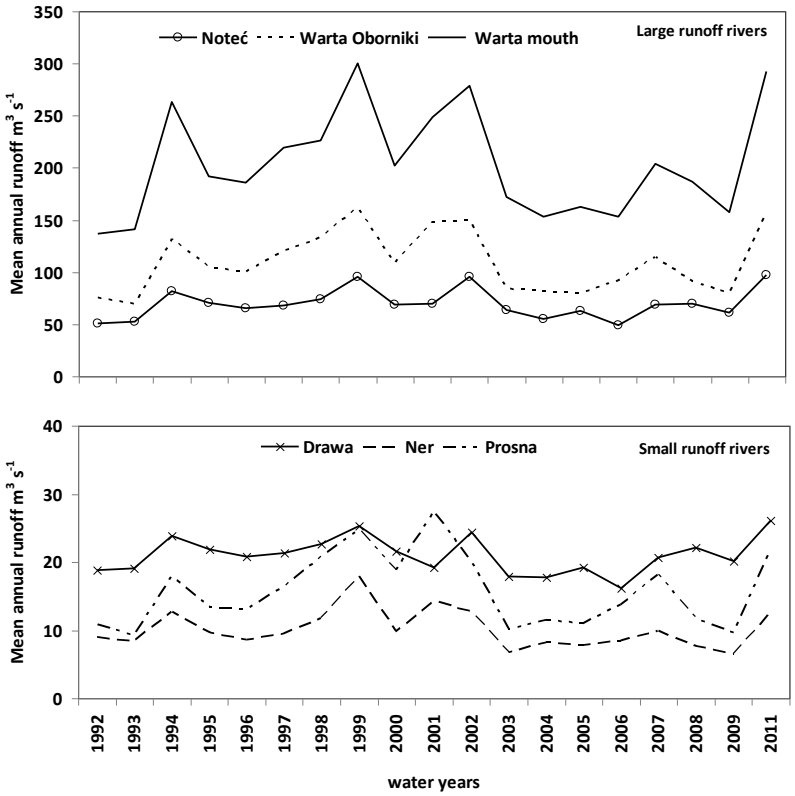

FIGURE 2
Mean annual runoff in the analyzed rivers in 1992–2011.

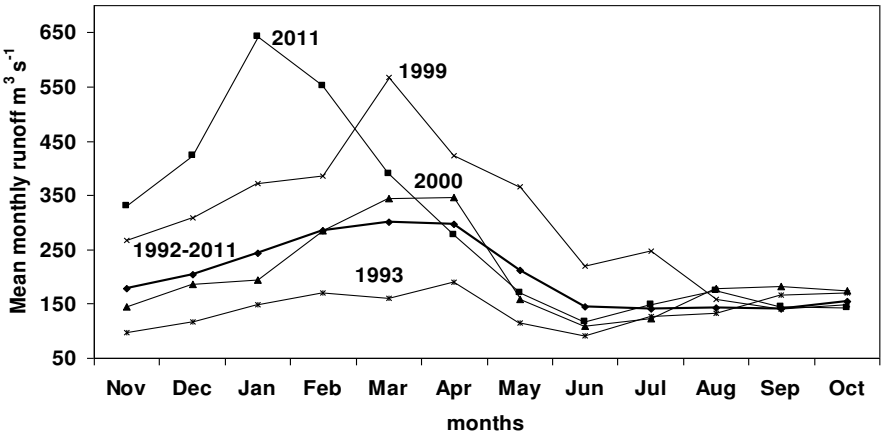

FIGURE 3
Mean monthly runoff in the Warta River in different years (wet years 1999 and 2011, dry year 1993, average year 2000) and the period 1992–2011.

The variabilities of the mean annual concentration of TP were different, through the impact of large point sources (Fig. 5). Without the STP in Łódź before 1999, the concentration of TP in the Ner River was very high (1–2.2 mg P l^{-1}), but later, it decreased to about 0.5 mg P l^{-1} in 2002–2007, and to 0.25 mg P l^{-1} in 2010. The TP concentration in the Prosna and the Warta rivers in Oborniki, being under the impact of sewage purification in Kalisz and Poznań, as well as at the Warta mouth in Kostrzyn, show a distinct, gradual decrease to the level of <0.2 mg P l^{-1} between the years 1992 and 2011. TP concentrations in the Noteć river indicate a slight decrease and in the Drawa River, they are always at the level of about 0.1 mg P l^{-1}. Changes in the mean annual concentration of phosphorus explicitly indicate that

their main source was sewage introduced into the rivers.

The mean monthly TN concentration at the Warta River mouth is highest between January and April (>4 mg N l^{-1}), in the period of the highest runoff (240–310 m^3s^{-1}). In Oborniki, in the same period, the above mentioned concentration reaches 7–8 mg N l^{-1}. The lowest TN concentration in the Warta River occurred in the June-October period, at the Warta River mouth 1.9–2.1 mg N l^{-1} and at Oborniki 3.4–4.6 mg N l^{-1}, by the lowest river runoff, showing respectively 140–160 m^3s^{-1} and 70–86 m^3s^{-1}.

TP concentrations at the Warta River mouth is the highest in the period June-September (0.32–0.37 mg P l^{-1}) by low runoff. In the Noteć River mouth, the TN concentration is the highest (>2 mg N l^{-1}) in the period January-March at high runoff (80–100 m^3s^{-1}) and they are the lowest (1.2–1.4 mg N l^{-1}) in the July-October period at low discharge (50–60 m^3s^{-1}). TP concentrations in the Noteć River show a small variability in the particular months and in the period June-September, it is slightly higher (0.18–0.21 mg P l^{-1}) than in spring. Similar changes can be found in the Drawa River. The Ner River presents a different picture with a very high concentration of TN (>7 mg N l^{-1}) that occurs almost the whole year, in spite of distinct oscillations in monthly runoff (5.6–17.5 m^3s^{-1}) and monthly TP concentrations show distinctly higher differences (0.52–1.55 mg P l^{-1}). In the Prosna River with records showing significant oscillations of monthly runoff, TN concentrations are the highest (7.0–8.2 mg N l^{-1}) in periods of the highest runoff (>14 m^3s^{-1}) (January-March) and are lowest (3.2–3.7 mg N l^{-1}) during low runoff (8.6–11.4 m^3s^{-1}) in the period June-October.

The correlation between TN and TP concentrations and the runoff was determined on the basis of mean annual and monthly values, using two methods and obtaining analogical results. Since the mean monthly runoffs better show the real situation, they were used for the purpose of conclusions. With the exception of the Ner River, in all rivers, the linear regression and Spearman's R show a positive and statistically significant correlations to TN (Table 4). Higher discharge connected with precipitation reflects the washing out of nitrogen compounds from the landscape and river bed. The mean monthly concentrations of TP are always negatively correlated with discharge and are statistically significant, which indicates the dilution of the relatively constant inflow of phosphorus, not easy washing out from the soil. Spearman's rank correlation is not significant only for TP in the Noteć and Prosna rivers, in which the correlation coefficient is also low.

TABLE 3
Mean annual nutrient concentrations in the analyzed rivers in two sub-periods of 1992–2011.

River	Period (water years)	Annual mean nutrient concentration (mg l^{-1})	
		TN	TP
Warta-mouth - Kostrzyn	1992–2000	3.07	0.34
	2001–2011	2.65	0.21
Warta- Oborniki	1992–2000	6.07	0.37
	2001–2011	4.72	0.22
Noteć - Santok	1992–2000	1.74	0.21
	2001–2011	1.57	0.14
Drawa - Łokacz	1992–2000	1.34	0.10
	2001–2011	1.16	0.09
Prosna - Ruda Komorska	1992–2000	5.35	0.53
	2001–2011	5.06	0.23
Ner - Chełmno	1992–2000	11.30	1.58
	2001–2010	6.60	0.45

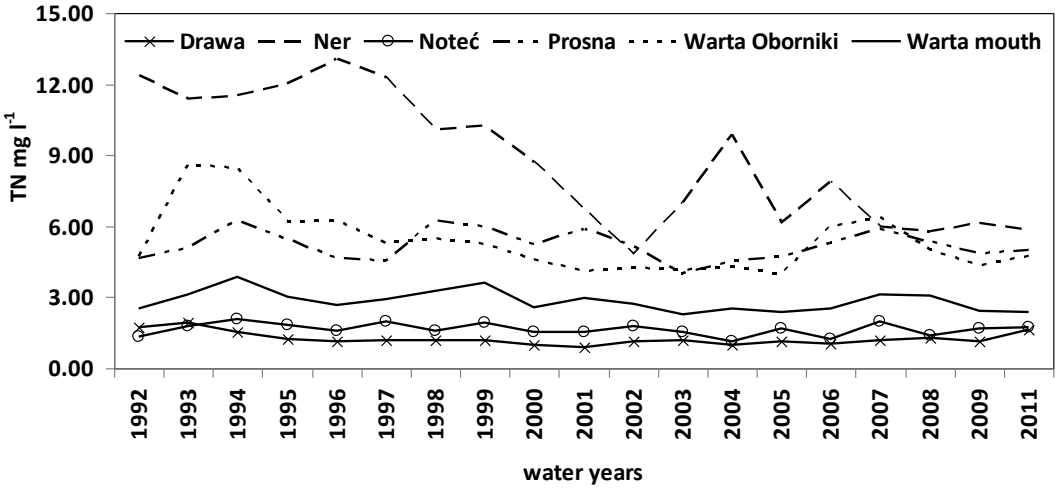

FIGURE 4
Mean annual concentration of total nitrogen in rivers in 1992–2011.

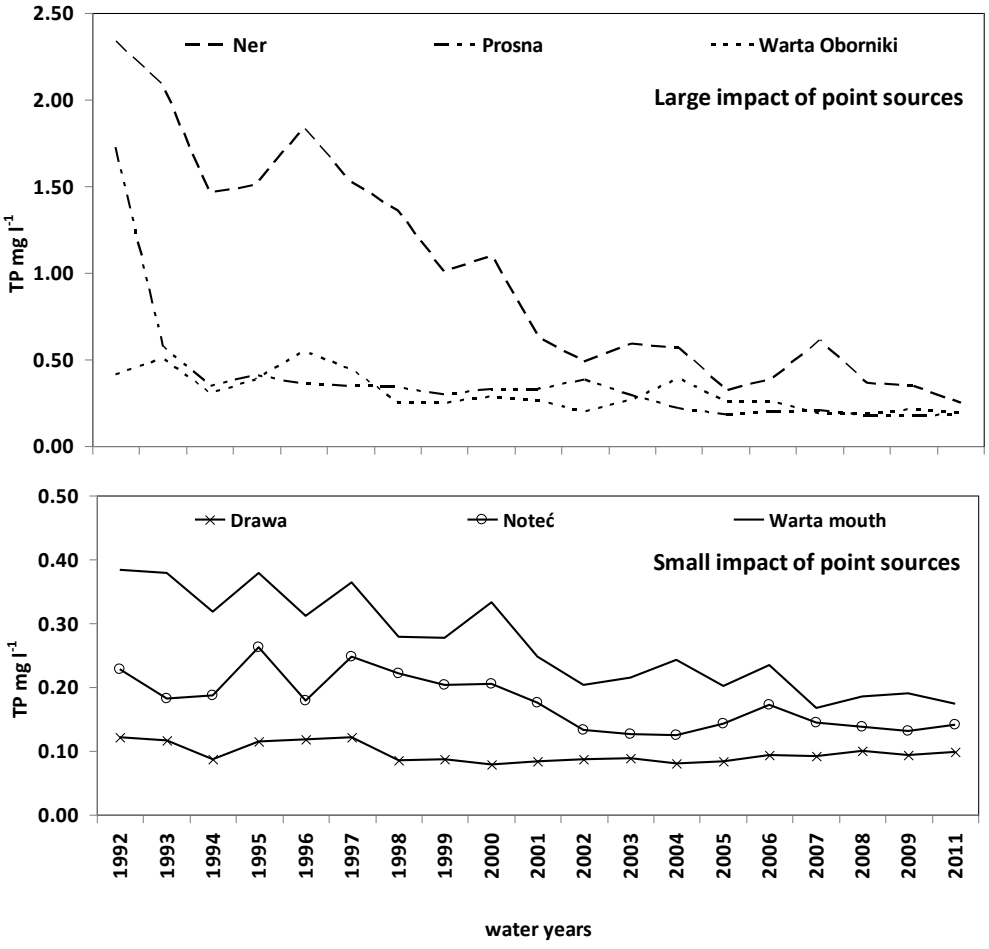

FIGURE 5
Mean annual concentration of total phosphorus in rivers in 1992–2011.

TABLE 4
Correlation between the mean annual and monthly concentrations of total nitrogen and total phosphorus versus the mean annual and monthly discharge in the analyzed rivers in 1992–2011, calculated by linear regression gradient trend model and Spearman's R.

River	Mean	Total nitrogen			Total phosphorus		
		r	Slope	R	r	Slope	R
Warta-mouth	annual	0.47*	0.004	-	-0.19	-0.0003	-
	monthly	0.66*	0.009	0.63*	-0.44*	-0.0005	-0.41*
Warta-Oborniki	annual	-0.07	-0.003	-	-0.39	-0.0014	-
	monthly	0.41*	0.018	0.39*	-0.39*	-0.0011	-0.36*
Noteć	annual	0.55*	0.010	-	-0.05	-0.0001	-
	monthly	0.58*	0.013	0.57*	-0.15*	-0.0004	-0.10
Drawa	annual	0.20	0.020	-	0.04	0.0002	-
	monthly	0.31*	0.023	0.37*	-0.36*	-0.0019	-0.46*
Prosna	annual	0.65*	0.076	-	-0.22	-0.0142	-
	monthly	0.67*	0.131	0.74*	-0.19*	-0.0070	-0.12
Ner	annual	0.06	0.072	-	0.10	0.0280	-
	monthly	0.05	0.030	0.15*	-0.25*	-0.0356	-0.24*

*significant 0.05

TABLE 5
Mean annual (Mg) and area specific (kg/ha/year) load of nitrogen and phosphorus in the Warta River basin in various periods calculated by two methods.

River	Period (water years)	Mean annual nutrient load							
		Total nitrogen				Total phosphorus			
		calculated		flow normalized		calculated		flow normalized	
		Mg	kg/ha/yea	Mg	kg/ha/yea	Mg	kg/ha/yea	Mg	kg/ha/yea
Warta –mouth	1992–2000	22 317	4.26	22 203	4.24	1 955	0.37	1 898	0.36
	2001–2011	19 781	3.78	19 840	3.79	1 204	0.23	1 246	0.24
Warta –Obornik	1992–2000	22 462	8.39	22 250	8.31	1 195	0.45	1 111	0.41
	2001–2011	18 502	6.91	18 589	6.94	747	0.28	772	0.29
Noteć	1992–2000	4 090	2.57	4 111	2.58	457	0.29	454	0.29
	2001–2011	3 704	2.33	3 685	2.32	305	0.19	307	0.19
Drawa	1992–2000	940	2.86	906	2.76	67	0.20	66	0.20
	2001–2011	776	2.36	806	2.46	56	0.17	58	0.18
Prosna	1992–2000	3 254	7.60	3 215	7.51	192	0.45	190	0.44
	2001–2011	3 104	7.25	3 136	7.32	119	0.28	117	0.27
Ner	1992–2000	3 761	21.78	3 533	20.46	458	2.65	438	2.54
	2001–2011	2 146	12.43	2 339	13.55	124	0.72	142	0.82

Nutrient Load. The mean calculated annual load of total nitrogen in the Warta River mouth for the period 1992–2011 was 20 982 Mg and its variability was very high (10 230–39 753 Mg). In the sub-period 2001–2011, in comparison with 1992–2000, the mean annual calculated nitrogen load diminished by 11.4% (Table 5). The highest loads were measured in 1994, 1999, 2008, 2011, and the lowest were in 1992 and in 2009 (Fig. 6). The positive correlation between TN concentration and runoff contributed to the fact that the highest loads were recorded in the years with the highest runoff (Fig. 2). In 1992–2011 the flow normalized mean annual load of nitrogen (20 959 Mg) at the Warta River mouth, was similar to the calculated load (20 982 Mg), but their annual variability was much lower (12 730–26 079 Mg).

Interesting is that in the Warta River in Oborniki, in the sub-periods mentioned above, the nitrogen loads were much higher (and not smaller!) to those at the river mouth. In 1992–2000 in the central and south part of the basin (26 776 km^2) the load was 8.39 kgN/ha/year and 0.45 kgP/ha/year, and near the river mouth (52 365 km^2) only 4.26

kgN/ha/year and 0.37 kgP/ha/year respectively. A comparison of nitrogen loads carried by the Warta River in Oborniki (205 km point) and at their mouth to the Oder River, shows that in Mg/year they are almost analogical, although their catchment area is almost doubled. This is much better visible by area specific load (kg/ha/year) comparison (Table 5). This is a consequence of the fact that in the lower and middle part of the Warta River basin (about 27 000 km^2) the amount of nitrogen and phosphorus emission into the river is similar per se to the retention in the basin discussed. This testifies to a very high retention in water courses of this basin.

In the large Noteć River, in the two analyzed sub-periods, the calculated nitrogen load diminished by 8%, and the phosphorus load decreased by 33%, respectively. In the Drawa River, the nitrogen load decreased by 17% and in the case of low population density, the phosphorus load decreased only by 16%. In the Prosna River, the nitrogen load decreased only by 5% and phosphorus by 38%. In the Ner River, thanks to the new STP in Łódź, the nitrogen load diminished by 43% and the phosphorus load by 73%.

The mean annual calculated load of total phosphorus at the Warta River mouth in the period 1992–2011 was 1560 Mg and its variability was lower (912–2502 Mg) than in the case of nitrogen. The mean annual flow normalized TP load was similar (1555 Mg) to the calculated one (Table 5 and Fig. 6). Between 1992–2000 and 2001–2011, the mean annual phosphorus load in both calculation methods decreased by about 30–38%, much higher than the nitrogen load.

A comparison of the river eutrophication degree and nutrient emission in the catchment areas requires the presentation of loads in the form of an area-specific load (kg/ha/year) (Table 5). Because the differences between two load calculation methods become very small, therefore, only the calculated loads were discussed. The area-specific nitrogen load in 2001–2011 was the lowest in the Noteć (2.33 kg N ha/year) and Drawa rivers (2.36 kg N ha/year), and the highest load was in the Ner River (12.43 kg N ha/year). In the Warta River mouth the load diminished in the two analyzed periods from 4.26 to 3.78 kg N ha/year. Monitoring stations with a high impact of point sources in the Warta (Oborniki), Prosna and Ner rivers showed the highest area-specific load of 6.91–12.43 kg N ha/year, which in the analyzed periods decreased by about 43% in the Ner River, by 18% In the Warta River at Oborniki and only by 5% in the Prosna River. The area-specific phosphorus load in 2001-2011 was the lowest in the Noteć (0.19 kg P ha/year) and Drawa rivers (0.17 kg P ha/year), and the highest in the Ner River (0.72 kg P ha/year). In the Warta River mouth the load diminished in the two analyzed periods from 0.37 to 0.23 kg P ha/year.

We analyzed the annual variability of total nitrogen and total phosphorus area-specific loads in the period 1992–2011. The differences between two load calculation methods in the analyzed years in the Warta River (mouth and Oborniki), Drawa and Ner Rivers show figure 7. In the Warta River mouth the variability and the loads were much smaller than in the Warta River at Oborniki. This proved to be the impact of the STP in Poznań, situated 35 km up-stream from Oborniki and the high catchment retention. A clearly visible area-specific load decrease of TN and especially of TP was shown by the Ner River after 2000, as a result of STP modernization in Łódź. In the Prosna River, the nitrogen load did not change significantly, but the TP load diminished visibly, after the start of STP in 1993 and its modernization in 2001–2003. The correlation between the mean calculated annual load and the mean annual runoff in the analyzed rivers in 1992–2011 was positive and significant for TN (Table 6). In terms of TP, this correlation was positive, but significant only in rivers without large point sources (Warta mouth, Noteć, Drawa).

The Mann-Kendall statistics for monotonous time trends for the period 1992-2011 in the annual calculated and flow-normalized loads of TN and TP for all sites are presented in Figure 8. Considering the length of the studied period, the test revealed statistically significant trends for total phosphorus in all sites and mostly for total nitrogen. Downward trends of the TP load in this period were the highest in the rivers Ner, Warta-Oborniki, and Prosna with large point sources and modernization of STPs. The negative significance of the TN load was high in the Ner, and Warta rivers. In the Noteć River, the trend of TN was not significant in the case of calculated load, but significant by flow normalized load and highly significant by flow-normalized load and TP loads. The trend of total nitrogen in the Prosna River was not significant in calculated and flow-normalized loads. This probably depends on a very low specific runoff (3.76 l s^{-1} km^{-2}) and problems with STP operation. In the Drawa River, with a high specific runoff (6.43 l s^{-1}km^{-2}), the flow normalized TN load was not and the calculated load was significantly correlated with the time. If we use the regression line method for these time trends, then in all rivers (except for the Drawa River) the trend for TP load is negative and significant, but for the TN load a significant negative trend is visible only in the Ner River.

Time trends of the nutrient loads in the period 1992–2011 illustrated the changes in the total emissions into the catchment area. The influence of much better sewage treatment in large cities is clearly visible. This shows that the highest nutrient load originate in point sources and not in the rural area.

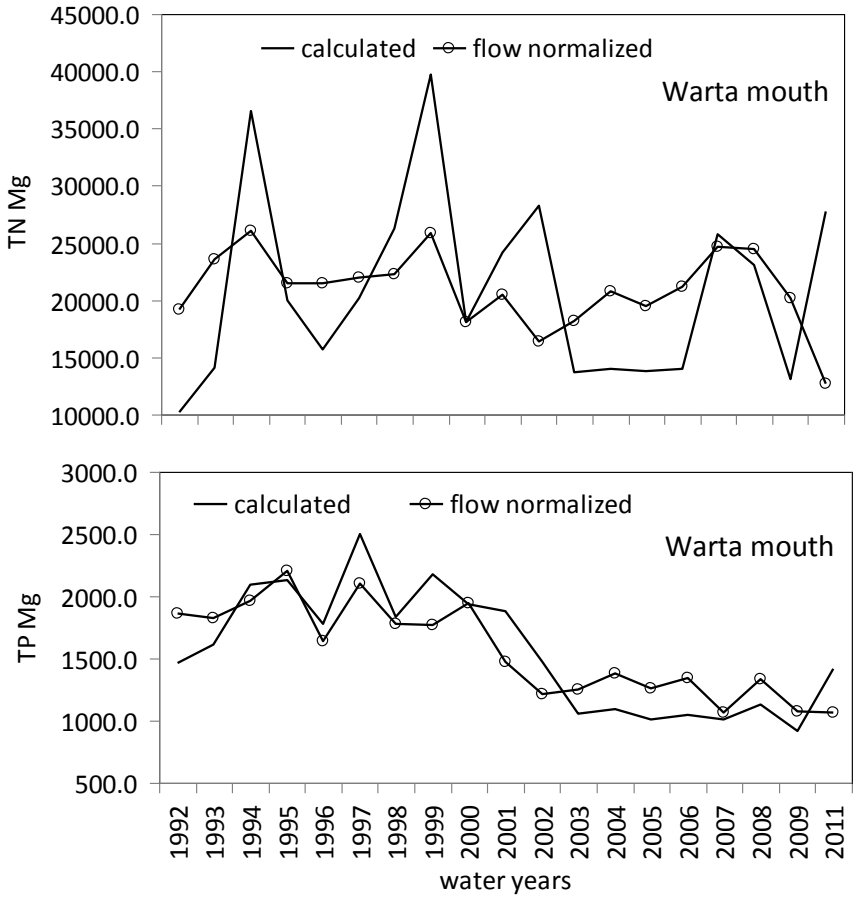

FIGURE 6
Annual load (calculated and flow normalized) of total nitrogen and total phosphorus in the Warta River mouth.

TABLE 6
Correlation between mean calculated annual load of total nitrogen and total phosphorus versus the mean annual discharge, calculated by linear regression gradient trend model.

River	Total nitrogen		Total phosphorus	
	r	Regression formula	r	Regression formula
Warta-mouth	0.91*	y=144x – 8424	0.50*	y=4.64x+609
Warta-Oborniki	0.68*	y=173x+1316	0.25	y=2.62x+645
Noteć	0.93*	y=88.6x–2128	0.57*	y=4.53x+62.3
Drawa	0.68*	y=60.8x–422	0.55*	y=2.43x+10.7
Prosna	0.91*	y=222x–348	0.32	y=4.73x+76.2
Ner	0.66*	y=231x+571	0.30	y=18.92x+91

*significant 0.05

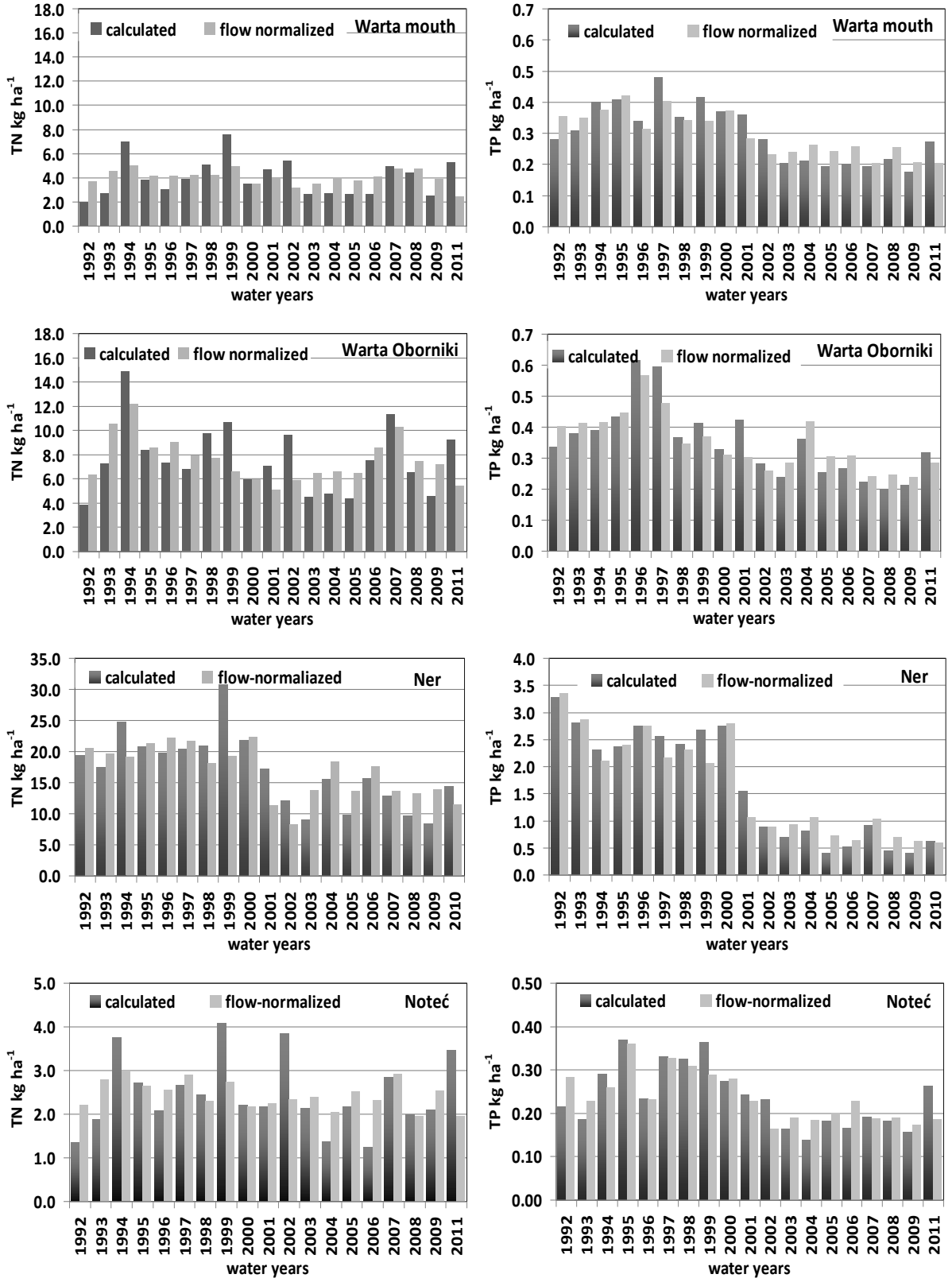

FIGURE 7
Calculated and flow normalized area-specific load of total nitrogen (TN) and total phosphorus (TP) in the Warta, Noteć and Ner rivers in 1992–2011.

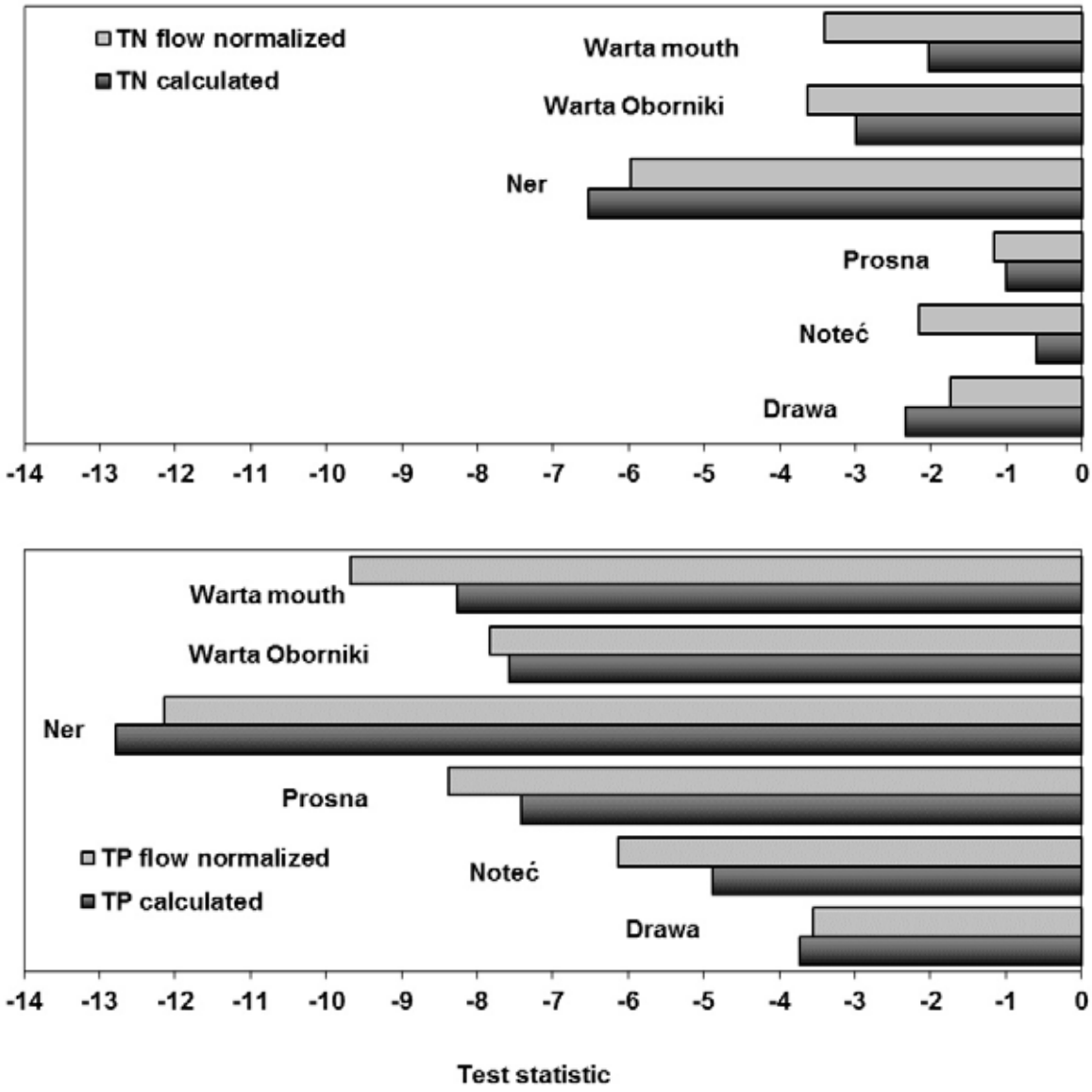

FIGURE 8
Mann-Kendall test statistics for monotonous trends in monthly calculated and flow-normalized loads of total nitrogen and total phosphorus in 1992–2011. The trend is statistically significant at the 0.05 level, if the test statistic is less than –2.

DISCUSSION

The mean annual TN and TP concentration in all analyzed rivers decreased visibly in the period 1992–2011 (Table 3, Figs. 4 and 5). In the 21st century, in the Warta River mouth, it was 2.65 mg N l^{-1} and 0.21 P l^{-1}, in the Noteć River only 1.57 mg N l^{-1} and 0.14 mg P l^{-1}. But in the analyzed point source dominated rivers (Warta–Oborniki, Prosna, Ner) the TN and TP concentrations were much higher (4.7–6.6 mg N l^{-1} and 0.22–0.45 mg P l^{-1}). The Drawa River (1.16 mg N l^{-1} and 0.09 mg P l^{-1}), could present a standard (good ecological status) for a clean water river in the Warta River basin. Compared with concentrations measured for the period 2005–2011 in the Oder River in Krajnik Dolny (3 mg N l^{-1} and 0.18 mg P l^{-1}) and in the Vistula River mouth in Kiezmark (2.1 mg N l^{-1} and 0.17 mg P l^{-1}), we can see lower N and slightly higher P concentrations in the Warta River than the Oder River [26]. In a range of 17 large European catchments, the mean P concentrations were 0.174 mg P l^{-1} (variation 0.014–0.591 mg P l^{-1}), being the highest in the northern and southern rivers [30]. In England, the average nitrogen concentration of nitrogen in the Great Ouse and Thames rivers, and those in East Anglia was 8.2–10.4 mg N l^{-1} [31]. The nitrogen concentrations in the Warta River basin are low compared with the Thames, Rheine, Seine and Elbe rivers, which are all between 5 and 8 mg N l^{-1} [1].

The correlation between monthly concentration of TN and runoff is positive and significant in all rivers except the Ner (Table 4), similar than in 1986–2004 in the Oder River [1]. In all rivers of the Warta River basin, between monthly (but not annual) concentration of TP and runoff, there is a negative significant correlation (Table 4).

The decrease in nutrient concentrations and loads in large point sources dominated rivers (Ner, Prosna, Warta in Oborniki) is much higher for phosphorus than for nitrogen (Tables 3 and 5). Unfortunately, monitoring data do not allow for calculating the nutrient load from point (STPs) and nonpoint sources. Rivers being point source dominated will show phosphorus concentrations which are the highest at low river flow, and become lower with increasing runoff due to dilution [31].

Because in the period 1960–2000, the observed decrease in N concentrations in the Oder and Vistula rivers is not ascribed to a drop in fertilizer use, but to nutrient removal in municipal STPs with the use of tertiary treatment facilities, the deposition of diffuse N sources from agriculture to the Baltic Sea might have been overestimated [1]. Similar conclusions can be found in the rivers Vltava [32] in Lithuania [33], Finland [34], Denmark [35], Thames in England [36] and in other research investigations [37-42]. The situation in the Warta River basin in 1992–2011 was similar. The nitrogen surplus [43] of 65.4 kg N ha/year in 2008–2011 in the Warta River basin (calculated acc. [23), had no visible connection with the observed area-specific nitrogen load of 3.78 kg N ha/year in 2001–2011.

Differences in long periods between calculated and flow normalized loads of nitrogen and phosphorus in all analyzed sites were low (Table 5), but in single years with very high or low runoff these differences were high, especially in the case of nitrogen (Fig. 6). The impact of better sewage treatment was visible in the reduction of the TP load.

The measured annual area-specific loads of total nitrogen and total phosphorus, are the best indicators of a potential environment degradation in the catchment, caused by land use and population density [28, 44]. This allows a comparison of different catchment areas. The natural background nitrogen flux of the landscape in regions with little human influence averages approximately 1 kg N ha/year [2]. Natural sources of P entering rivers are generally very small <0.1 kg P ha/year [45]. In our study, in point sources dominated rivers (Warta in Oborniki, Prosna and Ner), between two sub-periods 1992–2000 and 2001–2011, the calculated annual nitrogen area-specific load diminished in the Warta River in Oborniki by 1.48 kg N/ha, in the Prosna River only by 0.45 kg N/ha and in the Ner River by 9.35 kg N/ha. In the Warta River mouth and the Noteć River, this decrease was only about 0.50 kg N/ha and in the Drawa only 0.24 kg N/ha. The differences between clean water in the Drawa River and dirty water in the Ner River in 2001–2011 was 5.3 times by nitrogen and 4.2 times by phosphorus (Table 5). In other countries, the annual specific nitrogen loads show considerable oscillations between 2.29 (Finland) and 40 kg N/ha (England), mainly they are much higher than in the Warta River basin (Table 7). The annual N-flux in 1970s and 1980s in the North Sea region was 14.5 kg N/ha, in the Baltic Sea about 5 kg N/ha [43].

The calculated total annual phosphorus area-specific load decreased in the mentioned two sub-periods in the Warta River mouth from 0.37 to 0.23 kg P/ha and in Oborniki, from 0.45 to 0.28 kg P/ha. The smallest change was found in the most 'natural' Drawa River (from 0.20 to 0.17 kg P/ha). In 2010/2011 in the Pilica River the area specific load with 16.5 kg N/ha/year and 0.57 kg P/ha/year were much higher [18]. In 17 European catchments (250–11 000 km^2) this load was at mean 0.6 kg P/ha [29]. The highest P specific loads were measured in Europe in Belgium, Denmark and France (Table 7).

Retention is the difference between the input (emission) and riverine export (sinks in the landscape and in streams), the effect of various bio-geochemical processes responsible for N removal from the water phase, such as biological uptake, sedimentation, denitrification, and removal from the land phase [47, 48]. Riparian ecotones (wetland and peatland), lakes and water reservoirs increase retention in this context. Nitrogen retention in Finland was estimated to be in the range of 5–10 kg/ha in lakes and 0–1 kg/ha in peatlands [48], and the area of lakes and peatlands in the Noteć and Drawa rivers basin was high (Table 2). Also phosphorus was retained within the river systems, particularly under low runoff as a result of bio-geochemical and physical processes, and the retention rate differed between 10 and 60% [45]. In a great number of German rivers (including the Oder River basin), in 1993–2005, the retention was about 30–45% for N and 60–70% for P [49]. Hydro-geological conditions in the Warta River basin, large floodplains, many lakes in the northern part and long retention times favor the retention of nutrients. When we compare the total nitrogen load between the Warta River mouth (52 365 km^2) and Warta River in Oborniki (26 776 km^2), in the analyzed two sub-periods (Table 5), we can see that the loads were very similar because the N retention in the catchment between these points was very high. It should be noted that a very high retention was measured in the Warta River between Oborniki and Skwierzyna [17].

There is a close positive correlation between runoff and nitrogen load [1, 7, 24, 29, 35]. The highest runoff in the Warta River was between

TABLE 7
Annual area-specific loads of total nitrogen and total phosphorus in different rivers and periods.

Country	River/Lake	Catchment area km^2	Period	Area-specific load (kg/ha/year)		Source
				TN	TP	
Baltic Sea catchment area		1 729 000	1980–1993	4.78	0.24	[14]
Belgian	Scheldt	20 000	2000	20	0.80	[47]
Denmark	Baltic Sea catch.	-	1989–2002	13.9	0.38	[32]
England	Thames	9 850	1971–2008	40	-	[33]
Estonia	Lake Peipsi catch.	47 800	1992–2007	5.1	0.16	[48]
Europa	10 large rivers	>50 000	1993–1997	–	0.09–2.0	[27]
Finland	30 rivers	202 382	1993–1998	2.29	-	[45]
France	Seine	73 800	2000	18–20	1.8	[44]
Germany	Elbe	148 268	1992–2000	5.1–10.1	0.2-0.5	[49]
Latvia	Daugava	87 900	1977–1995	7.6	0.15	[7]
	Lielupe	17 600		9.3	0.17	
Lithuania	western, 15 rivers	-	1991–1996	15–30	0.15–0.45	[30]
Poland	Oder	118 861	1988–2008	ca 5.0	ca 0.4	[3]
	Warta	54 518	1993–1995	4.4	0.36	[11]
	Noteć	17 331		2.8	0.28	
Sweden	Göta	46 904	1971–1994	2.9[b]	-	[50]
U.S.A.[a]	16 rivers	248 326	1988–1993	3.1–17.6	-	[51]

[a]north-east U.S. coast from Maine to Virginia; [b] normalized load

January and May and the lowest runoff was between June and October (Fig. 3). The correlation between the mean calculated annual load of TN and the annual runoff in the Warta River basin was always positive and significant. A positive, significant correlation was also found between the calculated TP load and runoff in the Warta River mouth, Noteć and Drawa rivers. This correlation was positive but not significant in rivers with large point sources (Table 6). The Mann-Kendall test in the studied rivers revealed only downward statistically significant trends for total phosphorus and mostly total nitrogen load. Downward trends and modernization of numerous sewage treatment plants with tertiary treatment facilities. In the period 2001–2011, the annual mean concentrations in the Warta River mouth diminished to low values of 2.65 mg N l^{-1} and 0.21 mg P l^{-1}. With the exception of the Ner River, in all rivers the mean monthly runoff show a positive and statistically significant correlations to TN, but the concentrations of TP are mostly negative and statistically significant correlated, which indicates the dilution of the relatively constant inflow of phosphorus. The correlation between the mean calculated annual load and the mean annual runoff in the analyzed rivers in 1992–2011 was positive and significant for TN. In terms of TP, this correlation was positive, but significant only in rivers without large point sources.

The nutrient retention (difference between emission and riverine export) in the Warta River for TP and mostly for TN were the highest in rivers (Ner, Warta–Oborniki, Prosna) with large point sources and modernization of STPs.

CONCLUSIONS

In the period 1992–2011, the eco-chemical status of all analyzed rivers is constantly improving. TN and TP concentrations have decreased significantly, mainly because of the construction

catchment area is very high, particularly in their northern part. This is indicated by the fact that the nitrogen load in the Warta River at the mouth (52 365 km^2) and in Oborniki (26 776 km^2), in the analyzed periods was very similar, in spite of the fact that their catchment areas differ significantly, twice in size.

Annual area-specific loads of TN and TP, which express the net riverine load, are the best indication of potential environment degradation caused by land use and population density. In 2001–2011 in the Warta River mouth, there was 3.78 kg N ha/year and 0.23 kg P ha/year, in the Noteć River there were only 2.33 kg N ha/year and 0.18 kg P ha/year, but 12.4 kg N ha/year and 0.72 kg P ha/year were found in the point source dominated Ner River. Similar specific loads in North Sea countries were much higher in the 1990s.

The highest nutrient load originate in point sources and not in the rural area. These show that the participation of non-point sources in the nutrient emission used by calculations in the MONERIS model [8, 49] is too high.

REFERENCES

[1] Eriksson, H., Pastuszak, M., Löfgren, S., Mörth, C.M. and Humborg, C. (2007). Nitrogen budgets of the Polish agriculture 1960-2000 – Implications for riverine nitrogen loads to the Baltic Sea. Biogeochemistry. 85, 153–168. doi.10.1007/s10533- 007-9126-y.

[2] Howarth, R.W. (2008) Coastal nitrogen pollution: a review of sources and trends.globally and regionally. Harmful Algae. 8, 14–20. doi.10.1016/j.hal.2008.08.015.

[3] Pastuszak, M., Stålnacke, P., Pawlikowski, K. and Witek, Z. (2012) Response of Polish rivers (Vistula, Oder) to reduced pressure from point sources and agriculture during the transition period (1988–2008). J. Marine Syst. 94, 157–173. doi.10.1016/j.jmarsys.2011.11.017.

[4] Helcom (2006) Eutrophication in the Baltic Sea. Draft Helcom Thematic Assessment in 2006. Helcom Stakeholder Conference on the Baltic Sea Action Plan, Helsinki, Finland, 7 March 2006. pp. 29.

[5] PLC-5 (2011) Fifth Baltic Sea Pollution Load Compilation, Baltic Sea Environment Proceedings No. 128. Eds. Helsinki Commission, Baltic Marine Environment Protection Commission. Available from: http://www.helcom.fi.

[6] Burt, T.P., Howden, N.J.K., Worrall, F., Whelan, M.J. and Bieroza, M. (2010) Nitrate in United Kingdom rivers: policy and its outcome since 1970. Environ. Sci. Technol. doi.10.1021/es101395s.

[7] Laznik, M., Stålnacke, P., Grimvall, A. and Wittgren, H.B. (1999) Riverine input of nutrients to the Gulf of Riga –temporal and spatial variation. J. Marine Syst. 23, 11–25.

[8] Behrendt, H. and Dannowski, R. (eds) (2005) Nutrient and heavy metals in the Odra River system. Emissions from point and diffuse sources, their loads, and scenario calculations on possible changes. Weissensee Ökologie. pp. 353.

[9] Behrendt, H., Opitz, D., Kolanek, A., Korol, R. and Strońska, M. (2008) Changes of the nutrient loads of the Odra River during the last century – their causes and consequences. J. Water Land Dev. 12, 127-144. doi.10.2478/v10025-009-0010-0.

[10] Dannowski, R., Steidl, J., Mioduszewski, W. and Kajewski, I. (2002) GIS-based distributed analysis of subsurface nitrogen flow in the Odra basin. J. Water Land Dev. 6, 91–104.

[11] Ilnicki, P., Iwaniszyniec, P. and Korol, R. (2000) Stickstoff und Phosphorfrachten in der Oder und ihren Nebenflüssen, Z. Kulturtech. Landentw. 41, 211–217 (in German).

[12] Kowalkowski, T. and Buszewski, B. (2006) Emission of N and P in Polish rivers: past, present, and future in the Vistula River catchment. Environ. Eng. Sci. 23(4), 615–622.

[13] Kowalkowski, T., Pastuszak, M., Igras J. and Buszewski, B. (2012) Differences in emission of nitrogen and phosphorus into the Vistula and Oder basins in 1995–2008 – Natural and anthropogenic causes (MONERIS model). J. Marine Syst. 89, 48–60. doi.10.1016/j.jmarsys.2011.07.011.

[14] Stålnacke, P., Grimvall, A., Sundblad, K. and Tonderski, A. (1999) Estimation of riverine loads of nitrogen and phosphorus to the Baltic Sea, 1970-1993. Environ. Monit. Assess. 58, 173–200.

[15] Tonderski A. (1997) Control of nutrient fluxes in large river basins. University Studies in Arts and Science No 157, Thesis (Phd) Linköping University, Sweden. pp. 50.

[16] Ilnicki, P., Górecki, K. and Melcer, B. (2008) Eutrofizacja cieków wodnych zlewni rzeki Warty w latach 1992 –2002. Ed. Akademia Rolnicza Poznań. pp. 277 (in Polish).

[17] Górecki, K. and Olejnik, M. (2005) Changes in levels of nitrogen compounds in water of the Warta River on Oborniki-Skwierzyna stretch. Acta Sci. Pol. Circumiectus. 4 (2), 21–30.

[18] Kiedrzyńska, E., Kiedrzyński, M., Urbaniak, M., Magnuszewski, A., Skłodowski, M., Wyrwicka, A. and Zalewski, M. (2014) Point sources of nutrient pollution in the lowland river catchment in the context of the Baltic Sea eutrophication. Ecol. Eng. 70, 337–348.

[19] Bayrak Yilmaz G., Sivri N., Akgundogdu A. and Seker D.Z. (2014) The prediction of flow-rate and nutrient load in Ergene River basin through artificial neural networks. Fresen. Environ. Bull. 23, 12a, 3202-3211.

[20] Bayrak Yilmaz G., Sivri N., (2014) Estimation of nutrient loads in Ergene River basin through GIS. Fresen. Environ. Bull. 23, 12a, 3212-3221.

[21] Li JK., Li HE., Du J., Chen H., Shen B., (2014) Simulation studies on the effects of integrated management measures for reducing point source and non-point source pollution in the Weihe River basin. Fresen. Environ. Bull. 23, 8a: 1920-1933.

[22] Ilnicki P., Farat R., Górecki K. and Lewandowski, P. (2014) Impact of climate change on river discharge in the driest region of Poland. Hydrolog. Sci. J. 59(6), 1117–1134. http://dx.doi.org/10.1080/02626667.2013.831979.

[23] GUS (2012) Ochrona środowiska - Environment. Statistical information and elaborations. ed. D. Bochenek. Central Statistical Office, Warszawa.

[24] Guidelines for the compilation for waterborne pollution load to the Baltic Sea, 2006. (PLC-Water). Available from: http://www.helcom.fi/groups/monas/en_GB/plcwaterguide. PLC-5, pp 1-80.

[25] Stålnacke, P. and Grimvall, A. (2001) Semiparametric approaches to flow-normalization and source apportionment of substance transport in rivers, Environmetrics. 12, 233–250.

[26] Kendall, M.G. (1975) Rank correlation methods, 4th ed. Charles Griffin, London.

[27] Radziejewski, M. and Kundzewicz, Z.W. (2000) Hydrospect – software for detecting changes in hydrological data. In: Kundzewicz, Z.W. and Robson, A. ed. Detecting trend and other changes in hydrological data. 151–152 (appendix 2). World Climate Programme – Water, World Climate Data and Monitoring Programme, WCDMP-45, WMO/TD – No. 1013, Geneva.

[28] Radziejewski, M., and Kundzewicz, Z.W. (2004) Hydrospect, version 2.0. User's Manual.

[29] Pastuszak, M. and Igras, J. (eds.) (2012) Temporal and spatial differences in emission of nitrogen and phosphorus from Polish territory to the Baltic Sea. National Marine Fisheries Research Institute, Institute of Soil Science and Plant Cultivation–State Research Institute and Fertilizer Research Institute, Gdynia– Puławy. pp. 448.

[30] Kronvang, B., Vagstad, N., Behrendt, H., Bøgestrand, J. and Larsen, S.E. (2007) Phosphorus losses at the catchment scale within Europe: an overview. Soil Use Manage. 23(Suppl. 1), 104–116. doi.10.1016/j/jhydrol.2007.10.041.

[31] Neal, C., Davies, H. and Neal, M. (2008) Water quality, nutrients and the water framework directive in agricultural region: The lower Humber Rivers, northern England. J. Hydrol. 350, 232–245.

[32] Procházková, L., Blažka, P. and Kopácek, J. (1996) Impact of diffuse pollution on water quality of the Vltava River (Slapy Reservoir), Czech Republic. Water Sci. Technol. 33 (4-5), 145–152.

[33] Tumas, R. (2000) Evaluation and prediction of nonpoint pollution in Lithuania, Ecol. Eng. 14, 443–451.

[34] Räike, A., Pietiläinen, O.P., Rekolainen, S., Kaupilla, P., Pitkänen, H., Niemi, J., Raateland, A. and Vuoremaa, J. (2003) Trends of phosphorus, nitrogen and chlorophyll α concentrations in Finnish rivers and lakes in 1975–2000. Sci. Total Environ. 310, 47–59. Available from: www.sciencedirect.com.

[35] Kronvang, B., Jeppesen, E., Conley, D.J., Søndergard, M., Larsen, S.E., Ovesen, N.B. and Carstensen, J. (2005) Nutrient pressures and ecological responses to nutrient loading reductions in Danish streams, lakes and coastal waters. J. Hydrol. 304, 274–288. doi.10.1016/j.jhydrol.2004.07.035.

[36] Howden, N.J.K., Burt, T.P., Worrall, F., Whelan, M.J. and Bieroza, M. (2010) Nitrate concentrations and fluxes in the River Thames over 140 years (1868-2008): are increases irreversible? Hydrol. Proc. 23, 2657–2662. doi.10.1002/hyp.7835.

[37] Jarvie, H.P., Neal, C. and Withers, P.J.A. (2006) Sewage-effluent phosphorus: A greater risk to river eutrophication than agricultural phosphorus? Sci. Total Environ. 360, 246–253.

[38] Oenema, O., van Liere, L. and Schoumans, O. (2005) Effects of lowering nitrogen and phosphorus surpluses in agriculture on the quality of groundwater and surface water in the Netherlands. J. Hydrol. 304, 289–301. doi.10.1016/j.jhydrol.2004.07.044.

[39] Rankinen, K., Salo, T., Granlund, K. and Rita, H. (2007) Simulated nitrogen leaching, nitrogen mass field balances and their correlation on four farms in south-western Finland during the period 2000–2005. Agri Food Sci. 16, 387–406.

[40] Salo, T. and Turtola, E. (2006) Nitrogen balance as an indicator of nitrogen leaching in inland. Agri. Ecosyst. Environ. 113, 98–108.

[41] Stålnacke, P., Vandsemb, S.M., Vassiljev, A., Grimvall, A. and Jolankai, G. (2004) Changes in nutrient levels in some Eastern European rivers in response to large-scale changes in agriculture. Water Sci. & Technol. 49(3), 29–36.

[42] Vagstad, N., Stålnacke, P., Andersen, H-E., Deelstra, J., Jansons, V., Kyllmar, K., Loigu, E., Rekolainen, S. and Tumas, R. (2004) Regional variations in diffuse nitrogen losses from agriculture in the Nordic and Baltic Regions. Hydrol. Earth Syst. Sci. 8(4), 651–662.

[43] OECD (Organization for Economic Cooperation and Development) (2001) Environmental indicators for Agriculture. Methods and Results, Agriculture and Food. Paris, France. 3, 409.

[44] Salvai-Castellvi, M., Iffly, J.F., Borght, P.V. and Hoffmann, L. (2005) Dissolved and particulate nutrient export from rural catchments: a case study from Luxemburg. Sci. Total Environ. 344, 51–65.
[45] Withers, P.J.A. and Jarvie, H.P. (2008) Delivery and cycling of phosphorus in rivers: a review. Sci. Total Environ. 400, 379–395. doi.10.1016/j.scitotenv.2008.08.002.
[46] Howarth, R.W., Billen, G., Swaney, D., Townsend, A., Jaworski, N., Lajtha, K., Downing, J.A., Elmgren, R., Caraco, N., Jordan, T., Berendse, F., Freney, J., Kudeyarov, V., Murdoch, P. and Zhu-Zhao-Liang (1996) Regional nitrogen budget and riverine N, P fluxes for the drainages to the North Atlantic Ocean: Natural and human influence. Biogeochemistry. 35, 75–139.
[47] Billen, G., Garnier, J., Ficht, A. and Cun, C. (2001) Modeling the response of water quality in the Seine River Estuary to human activity in its watershed over the last 50 years. Estuaries. 24, 6B, 977–993.
[48] Lepistö, A., Granlund, K., Kortelainen, P. and Räike, A. (2006) Nitrogen in river basin sources, retention in the surface waters and peatlands, and fluxes to estuaries in Finland. Sci. Total Environ. 365, 238–259. doi.10.1016/j.scitotenv.2006.02.053.
[49] Fuchs, S., Scherer, U., Wander, R., Behrendt, H., Venohr, M., Opitz, D., Hillenbrand, T., Marscheider- Weidemann, F. and Götz, T. (2010) Calculation of emissions into rivers in Germany using the MONERIS model. Nutrients, heavy metals and polycyclic aromatic hydrocarbons. Umweltbundesamt Dessau-Rosslau, UBA Texte 46. pp. 173. Available from: http://www.uba.de/uba-info-medien-e/4018.html.
[50] Billen, G., Garnier, J. and Rousseau, V. (2005) Nutrient fluxes and water quality in the drainage network of the Scheldt basin over the last 50 years. Hydrobiologia. 540, 47–67.
[51] Buhvestova, O., Kangur, K., Haldna, M. and Möls, T. (2011) Nitrogen and phosphorus in Estonian rivers discharging into Lake Peipsi: estimation of loads and seasonal and spatial distribution of concentration. Est. J. Ecol. 60, 1, 18–38. doi.10.3176/eco.2011.1.03.
[52] Hussian, M., Grimvall, A. and Petersen, W. (2004) Estimation of the human impact on nutrient loads carried by the Elbe River. Environ. Monit. Assess. 96, 15–33.
[53] Stålnacke, P., Grimvall, A., Sundblad, K. and Wilander, A. (1999) Trends in nitrogen transport in Swedish Rivers, Environ. Monitor. Assess. 59, 47–72.
[54] Boyer, E.W., Goodale, C.L., Jaworski, N.A. and Howarth, R.W. (2002) Anthropogenic nitrogen sources and relationships to riverine nitrogen export in the northeastern U.S.A. Biogeochemistr., 57/58, 137–169.

Received: **22.07.2015**
Accepted: **18.01.2016**

CORRESPONDING AUTHOR

Prof. Dr.Piotr Ilnicki
Department of Entomology and Environmental Protection
Poznań University of Life Sciences
60–594 Poznań, ul. Dąbrowskiego 159, POLAND

e-mail: ilnickip@up.poznan.pl

© by PSP Volume 25 – No. 10/2016, pages 3941-3947 Fresenius Environmental Bulletin

STUDY OF THE MATRIX EFFECTS ON THE DETERMINATION OF IRON IN OILFIELD BRINES IN ALBANIA, USING AAS TECHNIQUE

Edlira Baraj[1], Valbona Celo[2], Alma Shehu[3], Rajmonda Totoni[1], *Besnik Baraj[3]

[1]Department of Chemistry, Faculty of Mathematical and Physics Engineering, University of Tirana, Tirana, Albania
[2]Environment Canada, Gatineau, Ontario, Canada
[3]Department of Chemistry, Faculty of Natural Sciences, University of Tirana, Tirana, Albania

ABSTRACT

The present article discusses the matrix interferences affecting the determination of Iron in brine waters. Chemical composition of brines, especially transition metals such as iron, cobalt and manganese, are useful indicators of petroleum and gas exploring. Owing to high salt content, the quantification of iron in brines is considered critical. In this work, chemical and background interferences of Na, K and Ca in Fe determination by AAS technique, has been studied. Experiments were carried out in synthetic samples, having similar composition with natural brine samples.

Two kinds of interferences were encountered at sodium content up to 30000 $mg.L^{-1}$: first, the scattering effect, which increased the signal value and the second, signal decrease due to formation of refractive compounds. Compared to Na, the scattering effect of Ca was more evident at concentrations up to 6000 $mg.L^{-1}$. The use of higher temperature flames, such as N_2O-C_2H_2, D_2 background correction as well as the method of standard additions were applied as alternatives in diminishing interferences during Fe determination by AAS. Extraction of iron's complex (sulfocianide form) in MIBK, followed by spectrophotometric determination was chosen as an alternative method of iron determination. Obtained results by different methods were compared by Analyses of Variance, ANOVA.

KEYWORDS:
Albanian oilfield brines, iron, matrix interferences, AAS, SF VIS

INTRODUCTION

Natural brines waters are known to have extremely high concentrations of dissolved constituent elements, ions, and molecules. Normally, brines are generated during oil and gas well drilling, completion and production operation. Brine is also produced along with crude oil as it is pumped from the reservoir and is separated from the oil-brine mixture by gravity in storage tanks [1, 2].

Chemical composition of brines provides a series of powerful tools regarding their origin, field development, exploring and production. Especially, transition metals, like iron, cobalt, manganese etc., are useful indicators for petroleum and gas exploring [2]. On the other hand, brines oilfield impact on fresh water stream is well known [3, 4]. Last decades different methods have been applied for heavy metal removal from aqueous solution [5, 6, 7].

Recently, in Albania an accident in the oilfield area of Patos-Marinz (Bankers Petroleum) happened causing severe damages, of which, the mixing of fresh waters with brines resulted in a heavy contamination.

Chemical analyses of some hundreds of brine samples from Albanian oilfield area have been accomplished and obtained results were used to estimate the distribution and nature of oil and gas. Also it helped for the distinction of hydrostratigraphic position of water sources in vertical sections. It was found that salt content of Albanian brines varies considerably from one formation to another and may also vary regionally, within a given formation [8].

From the analytical point of view, seawater and brines may be considered to be closely related systems in terms of matrix effects and analytical difficulties. However, brines represent, in some cases, even much higher salt concentration than seawater [9, 10]. AAS technique has shown to be a versatile laboratory technique on metals determination by application of flame or electrothermal atomisation [11, 12]. Analytical inaccuracies that arise from the high salt content are exacerbated by the low levels of trace metals, which require careful control of contamination during

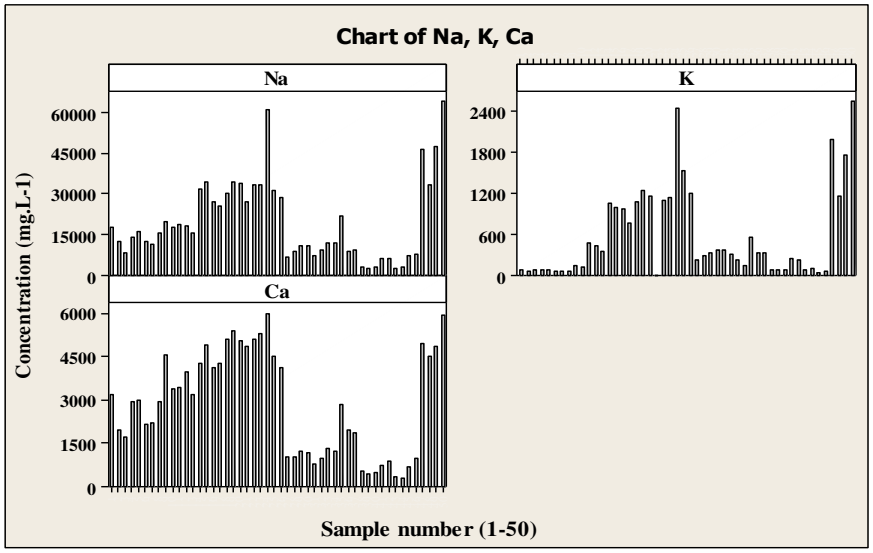

FIGURE 1
Content of different interfering elements in Albanian brines

sample collection and analysis and very sensitive analytical techniques. Many studies have been reported regarding pre-concentration, separation and isolation of trace elements from matrix constituents, which interfere on accuracy and precision [12, 13].

Iron is an important element, used by geochemists to determine the origin of oil field brines. However, the determination of iron in such complex samples suffers severe interferences, caused by high content of elements like sodium, potassium, calcium and magnesium [14]. Due to salt matrix interference and aiming the pre-concentration of trace elements, separation by ion exchange or MIBK extraction, after complexation with APDC, have been applied [15,16]. Sample dilution is also recommended in reducing matrix effects in brines and seawater, but sometimes this can lead to levels of the analyte below the detection limit of the method. In order to reduce the matrix-associated problems a number of approaches have been suggested, including matrix matching, standard addition and internal standardization methods [9]. However, these methods have not always been successful since the matrix problems appear still very complicated [17, 18].

In present study, the interferences of Na, K and Ca on Fe determination using AAS technique have been studied. Experimental work was carried out in synthetic samples, having similar composition with natural brine samples. Solutions were prepared with different concentration of interfering elements, while iron content remained constant (2 $mg.L^{-1}$). In figure 1, the levels of such elements, analysed in about 50 natural brine samples, are presented [19].

Determination of iron in natural samples, beside direct aspiration in the AAS technique, was also carried out by the spectrophotometric method, after the extraction of iron's complex (sulfocianide form) in MIBK [20, 21]. Analysis of Variance, ANOVA, was used for the assessment of significant differences between iron concentrations, obtained by different procedures applied [22].

MATERIALS AND METHODS

Instrumentation and reagents. A Pye-Unicam 240UV, UV-VIS spectrophotometer and a Varian AA10+ model spectrometer were used to determine iron concentration. In order to have the best sensitivity the instruments has been optimised before starting the measurements. All chemicals used were of analytical reagent grade, purchased from Merck. Acetylene-air as well as nitrogen oxide-acetylene flames were used for iron atomization.

Sample treatment. Brine samples collected in the oilfield area (usually 0.5 L) were stored in polyethylene bottles. Samples were filtered through 0.45-μm Millipore. For some of the oil well samples, it was necessary to prefilter the sample through a glass wool to prevent clogging by oil droplets. In most samples, especially those of limestone deposits, high amount of sulphides were found (up to 2000 $mg.L^{-1}$ H_2S) [8]. The high sulphides content indicate a reducing environment, which keeps iron, manganese etc. in their inferior oxidation states, being soluble into the water. However, if the water sample is non-acidified, notable changes were observed after collection. Due to oxidation process (by O_2 of air dissolved) the

TABLE 1
The intereference of Na on iron determination by AAS. (Fe 2 mg.L^{-1}).

mg.L-1 Na	0	1000	5000	10000	20000	30000
% Rel Abs	100	102	91	98	100	110
Blank	0	2	2	6	15	26
% Rel Abs – Blank	100	100	89	92	85	84
% Rel Abs (BC)	100	98	96	94	93	87
% Rel Abs (BC), N_2O- C_2H_2	32.5	32.5	32	33	33.5	32.5

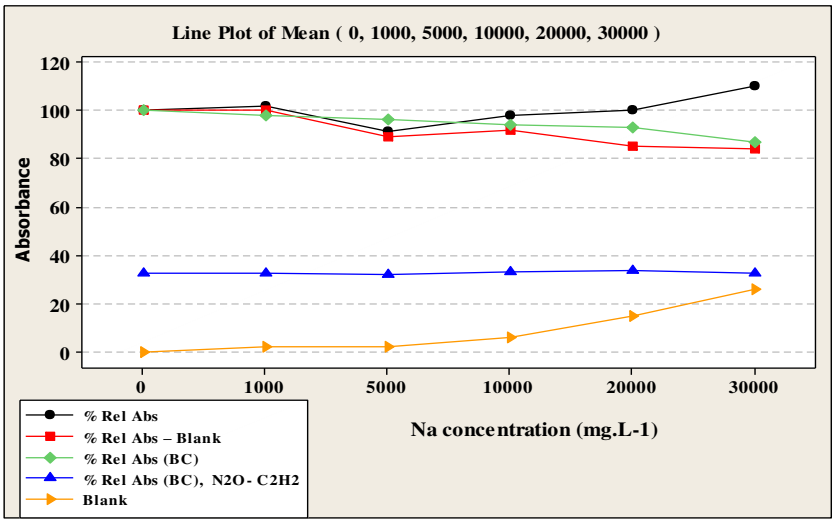

FIGURE 2
The influence of na on iron signal with aas technique

water had a yellowish-brown colour, as iron hydroxide precipitated and because sulphide is oxidized to sulphur. Sometimes, when the salt concentration was extremely high, discrete pulverisation was applied in order to mitigate salt effect on AAS aspiration system. For that 100 µL of sample solution was injected.

The filtered samples were acidified with 2 mL of ultrapure nitric acid. This treatment reduced the pH to about 1 and served to keep iron and other elements in oxidise form in solution.

Meanwhile, low concentrations of copper, lead and zinc were found in analyzed samples, which to our view, is due to the excess of hydrogen sulphide content, transforming them in sulphides of non-dissolved states (the data not shown in this paper) [8].

Procedures of iron determination. Given that brine analysis reflects considerable difficulties in establishing an accurate and precise method [15, 19], our work was focused into two aspects:

a) Evaluation of the interferences of Na, K, Ca and Mg during iron determination with AAS.

The relationship between the analyte concentration and the response of the instrument, especially in brine samples, depends on interference effects caused by matrix composition of the sample. Based upon previous experience of brine oilfield analysis carried out in Albania [5, 15], synthetic brine samples were prepared with different concentrations of macro constituents, respectively: Na (up to 30000 mg.L^{-1}, which is not the highest concentration found), K (up to 2000 mg.L^{-1}) and Ca (up to 6000 mg.L^{-1}), (Table 1).

b) The use of Analysis of Variance (one factor experiment) for assessing the interfering contribution of each element in the iron signal.

Natural brine samples were analysed by AAS technique (three procedures applied) and SF UV-VIS methods [19, 22]. The measurements with AAS were performed at 248.2 nm. Determination by SF VIS method was carried out after the formation of iron sulphocianyde $(Fe\text{-}SCN)^{+2}$ complex, at low pH, followed by the extraction of the complex with two portions of MIBK. The optimal wavelength used was at 495 nm [20, 21].

Results presented in Table 1 are measured in C_2H_2-Air flame, except of those shown in the last row. Finally, obtained results by four procedures applied were compared by the Analysis of Variance, ANOVA.

TABLE 2
The intereference of Ca on iron determination by AAS. (Fe 2 mg.L^{-1})

mg.L^{-1} Ca	0	400	800	2000	4000	6000
% Rel Abs	100	108	111	110	110	110
Blank	0	2	3	5	8	11.5
% rel Abs – Blank	100	106	108	105	102	98.5
% rel Abs (BC)	100	100	101	100	101	99

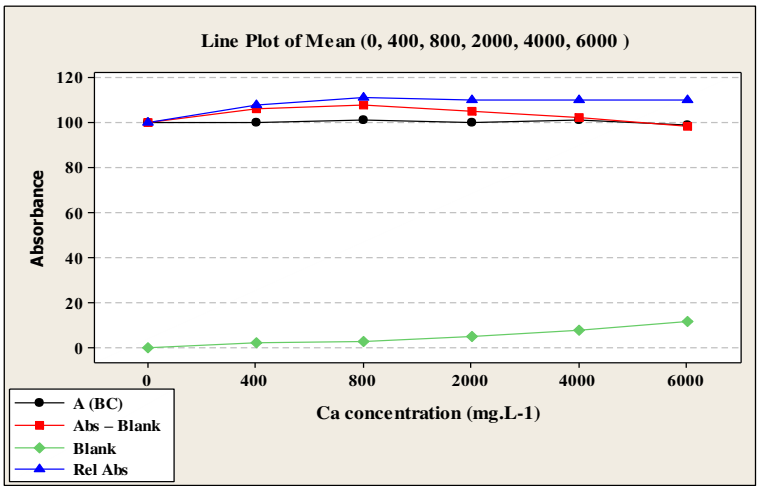

FIGURE 3
The influence of Ca on iron signal with AAS technique

RESULTS AND DISCUSSIONS

Study of the interferences. Using air acetylene flame, no interferences were observed at sodium concentration up to 1000 mg.L^{-1}. At 5000 mg.L^{-1} sodium, the absorbance of iron decreased, reaching a minimum value of 89 % (see Rel. Abs. – Blank row, in Table 1 and Figure 2). The decrease in signal in this case is due to the formation of a well known refractive compound, (Fe-O-Na), [20].

While the concentration of sodium increases, the scattering effect starts to contribute, which is due to the presence of small particles formed in the resonance beam. Such particles may remain because of the flame's inability to vaporize high dissolved solids content of the sample solution. Light scattering affects particularly those elements that absorb at lower wavelengths, such as the case of Fe, (248.2 nm). This is clearly shown looking the increasing absorbance values of blanks, (Table 1).

Scattering and refractive compounds effects have opposite contributions on the iron absorbance values. The scattering effect, in opposite with the previous one, increased the absorbance. Consequently, when sodium concentration is at 20000 mg.L^{-1}, increasing effect of scattering on the absorbance value is balanced by the decreasing effect of refractive compound (see Table 1 and Fig. 2).

At sodium concentration 30000 mg.L^{-1}, the scattering effect appeared predominant. The scattering increased the absorbance value up to 26% ,while the decreasing, due to formation of refractive compounds, resulted below 16%. In total, both effects produced a 10% increasing of iron absorbance signal. By using background correction, the relative absorbance of iron was decreased from 100 to 90 (for Na up to 30000 mg.L^{-1}), which means that scattering effect was almost eliminated, while chemical interference (refractive compound formed), was still evident (Table 1), [23]. In this case the blanks showed zero values.

To remove the interferences from molecular absorption spectra (refractive compounds), the use of higher temperature flames, such as N_2O-C_2H_2 was applied (Table 1, last row). In this case, a decrease in the method sensitivity was appeared, due to ionisation of iron atoms in high temperatures of this flame, but, no interferences affected the determination.

It is likely to admit that the interference elimination might be due to refractive compound destruction.

Calcium, in the concentrations used enhanced the signal of Fe up to 10 %, but the interfering effect disappeared by applying background correction (BC), which means that the interference is due to scattering effect, (Table 2). All the measurements were performed in an air-C_2H_2 flame.

Potasium, up to 1500 mg.L^{-1}, showed no interfere on iron determination by AAS.

TABLE 3
The iron concentration (mg.L^{-1}) in three oilfield water samples (triplicates a,b,c).

Sample Nr	AAS	AAS, SAM	AAS MIBK extraction	Fotometry UV-VIS
1-a	11.8	12.2	12.1	11.4
1-b	11.9	12.7	12.8	12.3
1-c	11.2	11.9	12.5	11.7
2-a	9.2	9.9	12.2	10.2
2-b	9.9	10.2	11.6	9.9
2-c	9.6	9.4	11.2	10.7
3-a	24.1	25.1	28.2	25.5
3-b	24.8	24.7	26.6	24.1
3-c	23.5	24.2	27.2	24.9

Iron determination by different methods. In Table 3 the results obtained on Fe determination in Albanian oilfield brine samples are presented. Because of the high concentration of Fe in natural brines, samples were diluted 10 to 20 times aiming to bring the iron concentration within the working range. This will also contribute to decrease the matrix effects due to high salt content.

Four different procedures were used to determine the iron concentration in three brine samples, presented in table 3. Respectively, in the first column results are obtained by AAS using simple calibration curve; in the second one, the standard addition method was followed by AAS measurements; in the third column results belong to iron AAS determination, after the complexation with SCN^- following the extraction with MIBK and in the last column, results obtained by the spectrophotometric UV-VIS method.

If we refer the data presented in Tables 3, regarding iron concentration in three samples by means of four different methods, it appears that results obtained by AAS, after extraction with MIBK, are systematically higher than those obtained with other procedures.

Applying one-way analysis of variance, it was confirmed that significant differences were evident between four procedures applied for the natural brines samples (Table 4). Excluding the results obtained with AAS after extraction with MIBK and applying ANOVA again, no significant differences were found. Despite the fact that the differences are relatively small, we do not recommend using AAS measurement after extraction with MIBK. On the other hand, by using SF VIS, the results did not show significant differences.

The sample dilution 10 or 20 times obviously diminished the matrix effects, which was observed much higher when Na and Ca were studied separately. Consequently, we recommend the AAS and SF VIS, as accurate methods for brine analysis. When it is possible, the dilution is preferred and for very high salty samples discrete pulverisation is advised [19]. However, it is likely that SAM provides more accurate results, because it looks that systematic constant error is not present, or at least is small [18].

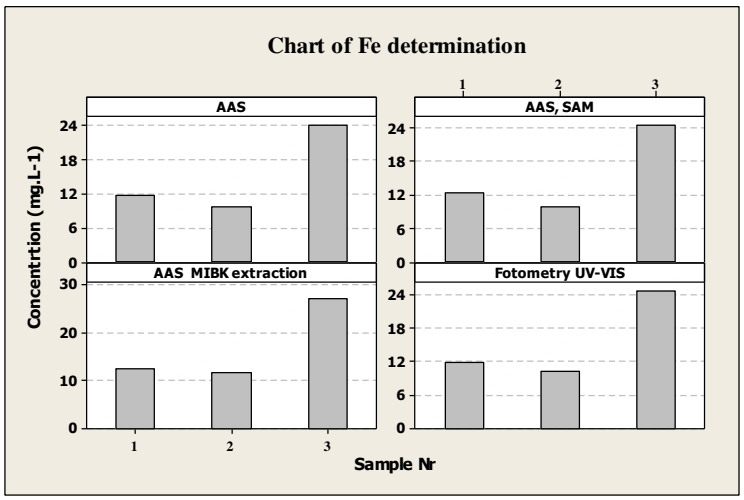

FIGURE 4
Iron concentration by four different methods

TABLE 4
Analyses of Variance, ANOVA

		Sample 1	Sample 2		Sample 3		
Source of Variation	F	P-value	F	P-value	F	P-value	F crit
Between methods*	**6.96**	0.02	**11.78**	0.01	**17.23**	0.00	**4.76**
Between methods**	**1.88**	0.23	**2.49**	0.16	**1.07**	0.40	**5.14**

*Four methods applied;
**Three methods applied, without SAA/MIBK

CONCLUSIONS

Investigation of systematic error is very crucial during the analyses of trace elements in samples which matrix effect cause severe interferences. Based on the type of systematic error, the right procedure of sample treatment and determination might be selected.

In present study, it was observed that determination of iron in brines is affected by two main factors: enhancement of absorbance due to scattering effect and decrease of absorbance because of refractive compounds formed. The matrix effect of brine constituents can be avoided by using a higher temperature flame, but the sensitivity in this case was decreased by almost three times. In such complex samples background correction should also be used during iron determination. The SAM method is also recommended as an alternative way in diminishing samples matrix effects.

REFERENCES

[1] P. E Drese and A. W. Rose. Chemistry and origin of oil and gas well brines in western Pennsylvania, Pennsylvania Geological Survey, fourth series, Open-File Report OFOG 10-01.0, (2010)

[2] Elsevier: Geochemistry of oilfield waters, A. G. Collins, New York, 1975.

[3] O. Obire, F. O. Amusan. The environmental impart of oilfield formation water on a freshwater stream in Nigeria. Journal of Applied Science & Environmental Manag., 7: 61-65., (2003)

[4] E. R.Daka, W. Amakiri., I.R Inyang. Surface and Groundwater Quality in Some Oil Field Communities in the Niger Delta. Research Journal of Environmental and Earth Sciences 6(2), 78-84. (2014).

[5] Jiunian Guan;Baixing Yan;Yingying Xu;Lixia Wang;Hui Zhu; Fresen. Environ. Bull., 24, 4, 1169-1175 (2015).

[6] Yu Li;Xianyuan Du;Qiao Zou;Yao Wang;Jianlin Liu;Yan Hu, Fresen. Environ. Bull., 21, 9a, 2772-2777 (2012).

[7] A Shehu; M Vasjari; E Baraj; R Lilo; R Allabashi Fresen. Environ. Bull., 25, 2, 525-533 (2016).

[8] P. Shtrepi, A. Çullaj, B. Baraj. "Buletini Nafta dhe Gazi"nr. 2, Albania, (1989).

[9] O.K. Galle. The Determination of Trace Elements in Brine by Atomic Absorption. Applied Spectroscopy, Vol 25, issue 6, pp 664 – 667, (1971)

[10] O. E. Troccoli. Heavy metals analysis in sea water and brines. Encyclopedia of Analytical Chemistry, (2006)

[11] Mustafa S. Dundar; Huseyin Altundag;Ozlem Yilmazcan;Sinem Kaygaldurak; Fresen. Environ. Bull., 22, 11, 3179-3183 (2013).

[12] G. Schaldach, H. Berndt. High performance flow flame atomic absorption spectrometry for interference-free trace determination. Fresenius Journal of Analytical Chemistry, Vol. 350, 7-9, 481-486, (1994).

[13] M. B. Shabani, A. Masuda. Determination of trace rhenium in sea water by inductively coupled plasma mass spectrometry with on-line preconcentration. Anal. Chem. 63, 2099-2105, (1991).

[14] APHA. Standard Methods for the examination of water and waste water, 1992, 18 edit.

[15] Price W . J., 1985, Spectrochemical analysis by AA. John Wiley & Sons, Britain.

[16] Sekhar C. K, Chary S. N., Tirumala K. C., Aparna V. Determination of trace metals in sea water by icp-ms after matrix separation. Acta Chim. Slov., 50, 409-418, (2003).

[17] Baraj B, Niencheski L F H., Trapaga R., Franca R G., Cocoli V, Robinson D. Study of Interference in the Flame Atomic Absorption Spectrometric Determination of Aluminum by Using Factorial Design. Fresenius J Anal Chem, 364, 678-681, (1999).

[18] Baraj B., Cocoli V, Karayannis, Robinson D., 1994, Models in Chemistry, 131(5), pp 597-605.

[19] Cocoli V., 1992, Thesis for Ph.D, Tirana University, Albania.

[20] Marcenko E., Fotometriceskoje opredjeljenie elementov, 1971, Mir, Moskva
[21] Interscience Publishers, Inc., N.Y. Colorimetric determination of traces metals, E.B. Sandell, 1959
[22] Elsevier, Netherland. Massart D. Chemometrics, . L., Vandeginste B. G. M., Deming S. N., Michotte Y., Kaufman L., 1988,
[23] F.G. Kirkbright, M. Sargent. Atomic absorption and fluorescence spectroscopy, London, (1974)

Received: **27.07.2015**
Accepted: **10.12.2015**

CORRESPONDING AUTHOR

Besnik Baraj
Department of Chemistry, Faculty of Natural Sciences, University of Tirana, Blv "Zogu I", 1001, Tirana, Albania

e-mail: besnik_baraj@fshn.edu.al

© by PSP Volume 25 – No. 10/2016, pages 3948-3954 Fresenius Environmental Bulletin

IDENTIFICATION OF PHARMACEUTICAL WASTEWATER CHARACTERISTICS BASED ON PARTICLE SIZE DISTRIBUTION, BIODEGRADABILITY AND ACUTE TOXICITY

Shan Liu[1], Zhe Qin[1], Chunxia Zhao[1], Da Lu[1], Shu-xuan Liang[1*], Jianbing Li[2]

[1]College of Chemistry and Environmental Science, Hebei University; Key Laboratory of Analytical Science and Technology of Hebei Province, Baoding 071002, P. R. China

[2]Environmental Engineering Program, University of Northern British Columbia, Prince George, British Columbia, Canada V2N 4Z9

ABSTRACT

The characteristics of pharmaceutical wastewater were identified based on its particle size distribution (PSD), biodegradability and acute toxicity. The PSD profiles were determined through physical segregation experiments using membrane discs with varying pore sizes between 2 and 3000 nm. The biodegradability was evaluated using readily biodegradable COD (S_S) and soluble inert COD (S_I) contents in wastewater, and the acute toxicity was assessed based on luminescent bacteria test. Domestic sewage samples were used for control experiments. The results indicated that PSD-based COD fractionation profiles could serve as effective fingerprints for identifying the characteristics of pharmaceutical wastewater. The COD component in pharmaceutical wastewater was found mainly as the S_I with size of below 2 nm, while little SI was found in domestic sewage. The biodegradability characteristics of the domestic and pharmaceutical wastewaters exhibited clear difference. The level of acute toxicity in pharmaceutical wastewater is relatively higher than domestic sewage. Also, the acute toxicity of the wastewater decreased after sewage treatment process.

KEYWORDS
Pharmaceutical wastewater, COD fractionation, particle size distribution, biodegradability, acute toxicity.

INTRODUCTION

The pharmaceutical industry often generates wastewaters of high pollutant concentration with varying characteristics and quantities, depending upon the products and related manufacturing processes [1]. Generally, such wastewater contains complex compositions which can be non-biodegradable and toxic. Even after wastewater treatment, many pharmaceutically active compounds, solvents, metabolites and other pollutants can still be transported to surface water [2,3]. Thus, the identification of wastewater characteristics is of fundamental importance for developing effective management strategies for pharmaceutical industrial effluents.

The size distribution of pollutants in wastewater has long been recognized as an important indicator for the interpretation of wastewater characteristics, the assessment of appropriate treatment technologies and the estimation of treatment process performance [4]. Recently, the particle size distribution (PSD)-based partitioning of contaminants between particulate, colloidal and soluble size ranges has been introduced as supportive information to examine the state and fate of wastewater components. The division of chemical oxygen demand (COD) into different size categories has been used to investigate the reaction mechanisms during the treatment of wastewater from a wide range of sources [5-7], including agricultural purposes [8], industrial food processing [9], municipal infrastructure [10,11], olive oil mills [12], pulp and paper mills [13], polymer industry [14], tanneries [15], and textile industry [16]. Based on their biodegradability and solubility, organic matters in wastewater can be divided into four categories, including readily biodegradable COD (S_S), slowly hydrolysable COD (X_S), soluble inert COD (S_I) and particulate inert COD (X_I) [17]. A variety of biochemical methods have been proposed for the quantitative characterization of these COD fractions in domestic wastewater, but most of them are time-consuming which generally require acclimated biomass [18-22]. In comparison, the physicochemical method has been applied as a fast approach for the determination of readily biodegradable soluble COD [23-25], and it can achieve a good correlation with biochemical methods [26]. The wastewater characteristics can

also be examined through the measurement of toxicity, including acute, sub-acute, and chronic toxicity [27.28]. However, acute toxicity tests can identify the pathways of toxic substances and determine the relationship between dosage and effect. The acute toxicity of wastewater can be rapidly and cost-effectively evaluated by measuring the reduction of light output of luminescent bacteria (e.g., marine and freshwater bacteria) [29].

In this paper, pharmaceutical wastewater characteristics, including the size distribution profiles of COD, dissolved organic matter (DOC), UV254 fractions, biodegradability and acute toxicity, was investigated. As control subjects, domestic wastewater received same determination. The objective of this study was to offer insights into complex bio-refractory component and successively find pertinent treatment methods.

Samples were collected from the influent and effluent of a pharmaceutical wastewater treatment plant (WWTP-A) in northern China. Samples were also collected from a domestic wastewater treatment plant for comparison. The collected samples were subject to sequential filtration/ultrafiltration tests and COD/DOC/UV_{254} analyses, as well as biodegradability and acute toxicity assessments.

MATERIAL AND METHODS

Wastewater sample collection. The pharmaceutical wastewater samples were collected from WWTP-A which is located in an economic and technological development zone in Shijiazhuang city of northern China. Many large pharmaceutical companies are located in this zone and their pre-treated wastewater is discharged into plant A which has a treatment capacity of 50000 $m^3 \cdot d^{-1}$. The influent of this plant flows into a regulating tank, followed by an anaerobic tank, an aerobic tank, an oxidation ditch, a sedimentation tank, and a biochar filtration facility. The treated water is finally discharged into a local river. In order to compare the characteristics of pharmaceutical wastewater with those of domestic sewage, wastewater samples were also collected from a municipal wastewater treatment plant (called WWTP-B in this study) which is located in Baoding city northern China.

Sequential filtration and ultrafiltration. The collected wastewater samples were subject to a sequential filtration and ultrafiltration. Solvent filters were used as the filtration units, and were operated under positive pressure (0.1 MPa, vacuum pump). All ultrafiltrations were carried out in a continuously-stirred cell (Amicon, Model 8200) under positive pressure (maximum recommended pressure is 0.483 MPa; for membranes with MWCO 100 kDa, the maximum recommended pressure is 0.069 MPa; N_2 as the inert gas). Samples were filtered sequentially through conventional filters with pore sizes of 1000~3000 nm (Quantitative filter paper, slow), 450 nm, and 220 nm (Xing Ya Shanghai). Permeates from the 220 nm membrane were then filtered successively through ultrafiltration membranes with nominal molecular weight cut-off (MWCO) values of 100, 30, 10, 5, 3 and 1 kDa (PL series, Millipore, MA), respectively. A volume of at least 80 mL of filtrates from each successive filtration step were collected for COD, TOC, and UV_{254} measurements. The COD was analyzed by the traditional dichromate method. The TOC was measured on a TOC analyzer (Apollo 9000) according to the standard (HJ501-2009). The UV_{254} measurement was conducted on a UV-visible Spectroscopy system (Agilent 8543). The measurements of COD, TOC, and UV_{254} were also carried out for the raw wastewater samples without sequential filtration and ultrafiltration (homogenized without settling and filtration).

Biodegradability test. In most cases, the effluent COD of WWTP does not satisfy the discharge requirements because of the dissolved organic matter [11]. As mentioned above, the organic matter can be divided into four categories, including S_S, S_I, X_S, and X_I. Three categories of wastewater can then be obtained based on the measured total COD of wastewaters (COD_T), total truly soluble COD (COD_{sol}), and S_I:

$$COD_T = S_S + S_I + (X_I + X_S) \quad (1)$$

$$COD_{sol} = S_S + S_I \quad (2)$$

In order to determine COD_{sol}, 1 mL of 100 g/L zinc sulfate solution was added to a 100 mL wastewater sample. The sample was then mixed vigorously with a magnetic stirrer for about 1 min. The pH of the mixed sample was adjusted to about 10 with 6 mol/L sodium hydroxide solution. The sample was then allowed to settle quiescently for a few minutes, and about 30~40 mL of clear supernatant was withdrawn with a pipette. The supernatant was passed through a 0.45 μm filter membrane. The COD of the supernatant filtrate was then measured to represent COD_{sol}. In order to determine S_I which is equal to the truly soluble effluent COD from an activated sludge plant at a mean cell retention time (MCRT) > 3 days, raw wastewater sample and sludge were placed into a batch reactor and aerated for 3 days. After batch treatment, the water sample was gone through similar procedures of measuring COD_{sol}, and the COD of the supernatant filtrate was determined as S_I. The value of S_S was then calculated as the difference between COD_{sol} and S_I as shown in Eq. (2).

Acute toxicity test. Luminescent bacterium emits luminescence in clear water. Toxic pollutants

in wastewater can destroy the bacteria's metabolic process and inhibit luminescence. The inhibition extent is correlated with the concentration of toxic pollutants, which can then be used to evaluate the wastewater's toxicity. The acute toxicity test of wastewater samples was conducted according to the national standard of "determination of the acute toxicity - luminescent bacteria test" (GB/T 15441-1995, China). It was carried out using a BHP9511 water quality toxicity analyzer (Beijing HAMAMATSU, China). A suspension of 0.05 mL freshwater luminescent bacterium (*V. qinghaiensis* sp. Nov. A) and 2 mL wastewater sample were thoroughly mixed in a test tube, and the relative light intensity of the mixed sample was then recorded after 15 min.

RESULTS AND DISCUSSION

COD removal efficiency of pharmaceutical WWTP. The influent and effluent COD of the study pharmaceutical WWTP-A were monitored from March to May 2013, and Fig. 1 presented the results. It can be found that the influent and effluent COD were nearly stable with an average value of 341 and 135 mg·L^{-1}, respectively. The influent COD was quite lower than the COD discharge standard in China (1000 mg·L^{-1}) (GB8978-1996, China) because the wastewater received by the pharmaceutical WWTP has already been pre-treated by pharmaceutical companies. However, the effluent COD was relatively higher and did not meet the discharge requirement for municipal WWTP in China (50 mg·L^{-1}) (GB18918-2002, China), and this can be caused by the pharmaceutical WWTP process design and influent characteristics.

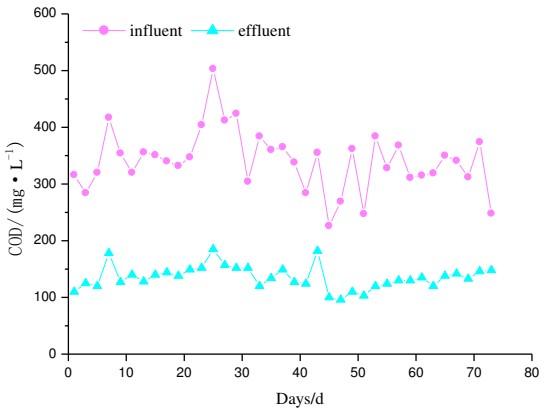

FIGURE 1
COD of influent and effluent from WWTP-A.

Particle size distribution (PSD)-based COD fractionation. As mentioned above, filtrate from each sequential filtration treatment of the pharmaceutical wastewater sample was subject to COD, TOC, and UV_{254} measurements. The wastewater samples were collected from the study pharmaceutical WWTP during April to June 2013, and the results indicated similar variation pattern of these water quality parameters. These three parameters showed strong correlations, with R^2 values being listed in Table 1.

COD is an important parameter for design and analysis, and can reflect the total organic content of wastewater sample. For these reasons, only the parameter of COD is discussed in the following analysis. Table 2 lists the particle size distribution (PSD) based COD fractionation. In this study, the total COD represents the sum of COD in the size ranges of settleable (> 1000 nm), colloidal (2~1000 nm), and soluble (< 2 nm) portions. The cumulative COD value for a given filter size reflects the COD of the filtrate, and it defines the total COD below that filter size. The differential COD represents the COD with size between the two consecutive filter sizes, and it is the difference of the two cumulative COD values.

TABLE 1
Correlation analysis for COD, TOC, and UV_{254} of the influent and effluent samples.

Water quality parameter	Influent			Effluent		
	TOC	COD	UV_{254}	TOC	COD	UV_{254}
TOC	1	0.868	0.769	1	0.811	0.964
COD		1	0.924		1	0.868
UV_{254}			1			1

TABLE 2
Particle size distribution of organic pollutants from pharmaceutical WWTP (plant A) and domestic sewage WWTP (plant B).

Separation technique	Particle size (nm)	Cumulative COD (mg·L^{-1})			Size range (nm)	Differential COD (mg·L^{-1})		
		Plant A		Plant B influent		Plant A		Plant B influent
		influent	effluent			influent	effluent	
Total		355	182	1306				
Filtration								
Filter paper	1000~3000	275	178	178	＞1000	80	4	1128
Solvent filter	450	252	148	120	450~1000	23	30	58
Solvent filter	220	245	140	110	220~450	7	8	10
Ultrafiltration								
100kDa	13	243	138	102	13~220	2	2	8
30 kDa	8	240	137	99	8~13	3	1	3
10 kDa	5	236	133	91	5~8	4	4	8
5 kDa	4	233	132	76	4~5	3	1	15
3 kDa	3	221	130	72	3~4	12	2	4
1 kDa	2	172	118	66	2~3	49	12	6
					＜2	172	118	66

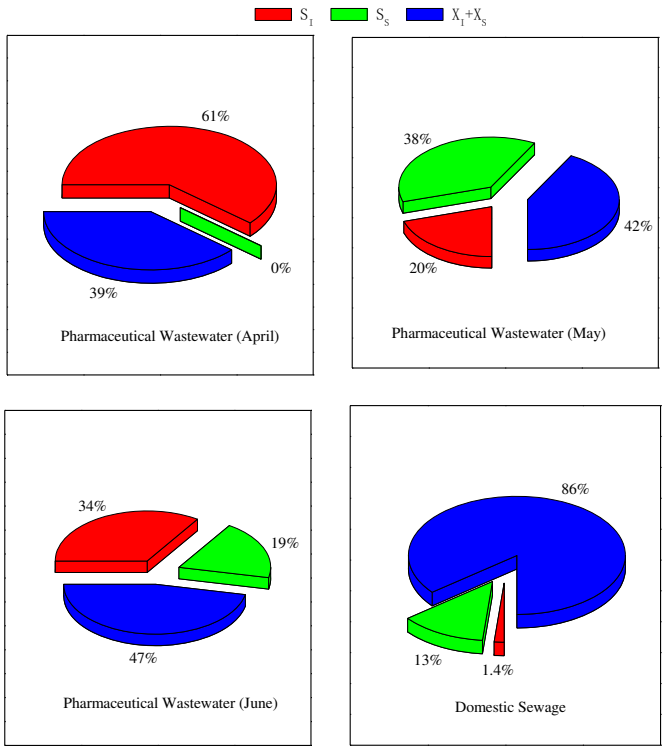

FIGURE 2
Biodegradability assessment of influent characteristics for WWTP-A and WWTP-B.

It can be found that the main COD components of the pharmaceutical WWTP influent are settleable and soluble, accounting for 22.5% and 48.5% of the total influent COD respectively. However, the COD content of effluent exhibited different size distribution, where its main COD component is dissolved organic matter, accounting for 64.8% of the total effluent COD, while the settleable COD only accounted for 2.20%. Such difference can be caused by the partial adsorption of the settleable COD fraction onto activated sludge and its partial conversion to dissolved organic matter during biological treatment in the pharmaceutical WWTP. The soluble COD fractions are only partially degraded by microorganisms in the activated sludge, and the non-biodegradable soluble COD fractions and microbial metabolites remain in the WWTP effluent. Table 2 also presents the comparison of the PSD-based COD fractionation between the pharmaceutical WWTP and domestic sewage WWTP influents. It can be found that these two types of wastewater exhibited an obvious variation of PSD-based COD fractionation. The majority (86.4%) of the COD in domestic sewage consisted of particulate organic matter (> 1000 nm), and only 5.1% of its COD was soluble (< 2 nm). The COD size distribution profile for pharmaceutical wastewater is more complex, where its COD fractions were well partitioned across the entire size ranges as found in Table 2. Its highest COD fraction (48.5%) appeared in the soluble range, but the particulate (22.5%) and the 2~3 nm size range (13.8%) also accounted for a significant COD fraction.

Biodegradability assessment. Fig. 2 presents the biodegradability assessment results of pharmaceutical wastewater and domestic sewage, and an obvious difference of characteristics between these two types of wastewater was found, especially when comparing the result of pharmaceutical wastewater in April with that of domestic sewage. It can be found that the COD in pharmaceutical wastewater in April mainly consisted of the S_I (around 61%). The X_S and $_I$ accounted for 39% of the COD, while almost no readily biodegradable COD (S_S) was observed. On the other hand, the COD in domestic sewage mainly consisted of X_I and X_S (around 86%), followed by S_S (13%) and S_I (1%). The X_I which consists of suspended solids and dead microorganisms, can be adsorbed onto activated sludge and then discharged into the WWTP effluent along with residual activated sludge. When there is a low percentage of biodegradable COD (S_S), or when S_S is mostly degraded, the X_I can be hydrolyzed outside the cells. However, the S_I flows out along with effluent, which is not considered as being degraded by microorganisms. It was found from Fig. 4 that the main component of WWTP-A influent was S_I (i.e. accounting for 61%, 20% and 34% of the total influent COD), which could lead to high COD value of pharmaceutical WWTP effluent.

Acute toxicity assessment. Fig. 3 presents the relative light intensity (RLI) result for both pharmaceutical wastewater and domestic sewage. It can be found that the RLI of the pharmaceutical WWTP effluent is higher than that of its influent, which indicates that the acute toxicity of pharmaceutical wastewater was decreased after treatment. It was also observed that the pharmaceutical wastewater samples were not stable as compared with domestic sewage, particularly for the samples collected in June. Furthermore, the acute toxicities of both treated and untreated pharmaceutical wastewater were higher than those of domestic sewage.

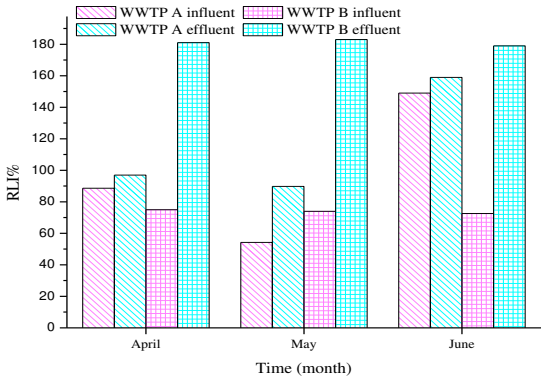

FIGURE 3
Acute toxicity of wastewater from WWTP-A and WWTP-B.

CONCLUSION

The PSD-based COD fractionation serves as fingerprints for pharmaceutical wastewaters. The main components of WWTP A influent are particulate and soluble portions, while the bulk of the COD in effluent consists of dissolved organic matter, with almost no settleable portion. Comparing with domestic sewage, the PSD-based COD fractionation of pharmaceutical wastewater is more complex, with the main contribution in the soluble range.

The pharmaceutical wastewater mainly consists of S_I, which is considered as not being degraded by microorganisms. The level of acute toxicity in pharmaceutical wastewater is relatively higher than domestic sewage. The acute toxicity of the wastewater decreased after sewage treatment process of WWTP A.

ACKNOWLEDGEMENTS

This work was supported by the National 12th Five-Year Major Science and Technology Projects on Control and Prevention of Water Pollution (NO. 2012ZX07203-003) and The National Natural Science Youth Fund (No. 51308179).

REFERENCES

[1] Cokgor, E.U., Karahan, O., and Orhon, D. (2008) The effect of mixing pharmaceutical and tannery wastewaters on the biodegradation characteristics of the effluents. J. Hazard. Mater. 156, 292-299.

[2] Gotvajn, A.Z. and Koncan, J.Z. (2003) Hazard identification of pharmaceutical wastewaters using biodegradability studies. Water Sci. Technol. 47, 197-204.

[3] Fernández, R.F., Martínez, L. and Villaverde, S. (2012) Membrane bioreactor for the treatment of pharmaceutical wastewater containing corticosteroids. Desalination 300, 19-23.

[4] Dulekgurgen, E., Dogruel, S., Karahan, O., Orhon, D. (2006) Size distribution of wastewater COD fractions as an index for biodegradability. Water Res. 40, 273-282.

[5] Chang, C.N., Chao, A., Lee, F.S. and Zing, F.F. (2000) Influence of molecular weight distribution of organic substances on the removal efficiency of DBPS in a conventional water treatment plant. Water Sci. Technol. 41, 43-49.

[6] Nguyen, H.V, Shin, J.K., Hur, J. (2011) Multivariate analysis for spatial distribution of dissolved organic matters in a large river-type dam reservoir. Environ. Monit. Assess. 183, 425-436.

[7] Lin, Y.H. (2012) Molecular weight distribution of organic matter by ozonation and biofiltration. Water Sci. Technol. 66, 2604-2612.

[8] Chavez, A., Jimenez, B. and Maya, C. (2004) Particle size distribution as a useful tool for microbial detection. Water Sci. Technol. 50, 179-186.

[9] Sophonsiri, C. and Morgenroth, E. (2004) Chemical composition associated with different particle size fractions in municipal, industrial, and agricultural wastewaters. Chemosphere 55, 691-703.

[10] Esparza-Soto, M., Fox, P. and Westerhoff, P. (2006) Transformation of molecular weight distributions of dissolved organic carbon and UV-absorbing compounds at full-scale wastewater-treatment plants. Water Environ. Res. 78, 253-262.

[11] Doğruel, S. (2012) Biodegradation characteristics of high strength municipal wastewater supported by particle size distribution. Desalin. Water Treat. 45, 11-20.

[12] Beccari, M., Carucci, G., Lana, A.M., Majone, M. and Petrangeli-Papini, M. (2002) Removal of molecular weight fractions of COD and phenolic compounds in an integrated treatment of olive oil mill effluents. Biodegradation 13, 401-410.

[13] Leiviskä, T., Nurmesniemi, H., Poykio, R., Ramo, J., Kuokkanen, T. and Pellinen, J. (2008) Effect of biological wastewater treatment on the molecular weight distribution of soluble organic compounds and on the reduction of BOD, COD and P in pulp and paper mill effluent. Water Res. 42, 3952-3960.

[14] Doğruel, S., Cokgör, E.U., Ince, O., Sözen, S. and Orhon, D. (2013) Potential of ultrafiltration for organic matter removal in the polymer industry effluent based on particle size distribution analysis. Environ. Sci. Pollut. Res. 20, 340-350.

[15] Karahan, Ö., Dogruel, S., Dulekgurgen, E. and Orhon, D. (2008) COD fractionation of tannery wastewaters -particle size distribution, biodegradability and modeling. Water Res. 42, 1083-1092.

[16] Doğruel, S., Dulekgurgen, E. and Orhon, D. (2006) Effect of ozonation on chemical oxygen demand fractionation and color profile of textile wastewaters. J. Chem. Technol. Biotechnol. 81, 426-432.

[17] Spérandio, M. and Espinosa, M.C. (2008) Modelling an aerobic submerged membrane bioreactor with ASM models on a large range of sludge retention time. Desalination 231, 82-90.

[18] Ziglio, Z., Andreottola, G., Foladori, P. and Ragazzi, M. (2001) Experimental validation of a single-OUR method for wastewater RBCOD characterization. Water Sci. Technol. 43, 119-126.

[19] Sari, S., and Tas, D.O. (2014) Anaerobic degradation of diclofenac under mesophilic conditions. Fresen Environ. Bull. 23(12a), 3048-3053.

[20] Orhon, D. and Okutman, D. (2003) Respirometric assessment of residual organic matter for domestic sewage. Enzyme Microb. Technol. 32, 560-566.

[21] Járová, K., Vávrová, M., Jírová, A., and Oborná, J. (2014) Assessment of contamination level of aquatic ecosystem in the Svratka and the Svitava Rivers (Czech Reoublic) by selected pharmaceuticals, Fresen Environ Bull. 23(12b), 3265-3271.

[22] Alper, N., Bulent, K. and Ergun, Y. (2005) Mathematical modelling of the activated sludge process-the Erzincan case. Process

Biochem. 40, 2467-2473.
[23] Mamais, D., Jenkins, D and Pitt, P. (1993) A rapid physical-chemical method for the determination of readily biodegradable soluble COD in municipal wastewater. Water Res. 27, 195-197.
[24] Gao, C., Jiao, E., Li, H., Wang, W.X., and Wang, S.Y. (2013). Filamentous sludge bulking in A/O process treating domestic sewage of low carbon/nitrogen ratio. Fresen Environ. Bull., 22(12 a), 3607-3613.
[25] Hu, Z.Q., Chandran, K. and Smets, B.F. (2002) Evaluation of a rapid physical-chemical method for the determination of extant soluble COD. Water Res. 36, 617-624.
[26] Fall, C., Flores, N.A., Espinoza, M.A., Vazquez, G., Loaiza-Návia, J., van Loosdrecht, M.C.M. and Hooijmans, C.M. (2011) Divergence between respirometry and physicochemical methods in the fractionation of the chemical oxygen demand in municipal wastewater. Water Environ. Res. 83, 162-172.
[27] Deryabin, D. and Aleshina, E. (2008) Natural and recombinant luminescent microorganisms in biotoxicity testing of mineral waters. Appl. Biochem. Micro. 44, 378-381.
[28] Babuna, F.G., Avsar, E., Iskender, G., Darcan, B. (2014) Fate of paracetamol production wastewater under aerobic and anaerobic treatment. Fresen Environ Bull. 23(12a), 3232-3236.
[29] Ye, Z.F., Zhao, Q.L., Zhang, M. and Gao, Y.C. (2011) Acute toxicity evaluation of explosive wastewater by bacterial bioluminescence assays using a freshwater luminescent bacterium, *Vibrio qinghaiensis* sp. Nov. J. Hazard. Mater. 186, 1351-1354.

Received: **30.07.2015**
Accepted: **25.12.2015**

CORRESPONDING AUTHOR

Shu-xuan Liang
College of Chemistry and Environmental Science
Hebei University
No.180 Wusi East Road, Lianchi District
071002 Baoding, Hebei Province
P.R. CHINA

E-mail: liangsx168@126.com

© by PSP Volume 25 – No. 10/2016, pages 3955-3961 Fresenius Environmental Bulletin

AN ASSOCIATION BETWEEN AMBIENT POLLUTANTS AND HOSPITAL ADMITTED RESPIRATORY CASES IN AHVAZ, IRAN

Mehran Khaefi[1], Gholamreza Goudarzi[2], Ahmad Reza Yari[3], Sahar Geravandi[4,5], Sina Dobaradaran[6], Esmaeil Idani[7], Parviz Javanmardi[8,5], Farid Youesfi[9,5], Bayram Hashemzadeh[10], Arman Shahriari[11], Mohammad Javad Mohammadi[12,13,5] *

[1]M.SC Environmental Engineering, Environmental & Occupational Health Center, Ministry of health medical & education, Tehran, Iran
[2]Associate professor, Department of Environmental Health Engineering, School of Public Health, Environmental Technologies Research Center, Ahvaz Jundishapur University of Medical Sciences, Ahvaz, Iran
[3]Research Center for Environmental Pollutants, Qom University of Medical Sciences, Qom, Iran.
[4]M.SC Nursing, Islamic Azad University, Tehran Medical Sciences Branch, Tehran, Iran
[5]Razi Teaching Hospital, Clinical Research Development Center, Ahvaz Jundishapur University of Medical Sciences, Ahvaz, Iran
[6]Associate Professor Department of Environmental Health Engineering, Faculty of Health & the Persian Gulf Marine Biotechnology Research Center, the Persian Gulf Research Center, Bushehr University of Medical Sciences, Bushehr, Iran.
[7]Associate professor, Department of Internal medicine, Ahvaz Jundishapur University of medical sciences, Ahvaz, Iran
[8]M.SC Environmental Engineering, Department of Environmental Engineering, School of Agricultural, Islamic Azad University, Ahvaz Sciences Branch, Ahvaz, Iran
[9]Assistant professor, Infectious and Tropical Diseases Research Center, Ahvaz Jundishapur University of Medical Sciences, Ahvaz, Iran
[10]Department of Environmental Health, Khoy School of Nursing, Urmia University of Medical Sciences, Urmia, Iran
[11]Assistant professor, Gastrointestinal and Nephrology Research Center, Ahvaz Jundishapur University of Medical Sciences, Ahvaz, Iran
[12]Student Research Committee, Department of Environmental Health Engineering, School of Public Health AND Environmental Technologies Research Center, Ahvaz Jundishapur University of Medical Sciences, Ahvaz, Iran
[13]Abadan school of Medical Sciences, Abadan, Iran

ABSTRACT

Air pollutants have harmful effects on human health and can intensify rates hospital admissions, asthma attacks, mortality and disease. One of the most reliable and valid approach to assess the health effects of air pollution is statistical modeling. Emissions from anthropogenic sources such as transportation, industries and dust storm are two major concerns of air pollution in Ahvaz. The aim of this study to assess hospital admissions respiratory disease of exposure Particle matter (PM_{10}), Sulfur dioxide (SO_2), Nitrogen dioxide (NO_2), and Ground Level Ozone (GLO) in Ahvaz city (located in south-western Iran), during 2012. Daily concentrations of PM_{10}, SO_2, NO_2, and GLO were used to evaluate the health effects of human exposure to these pollutants. Raw data processing by Excel software and after the impact of meteorological parameters was converted as input file to the model. Finally, were calculated the hospital admissions respiratory diseases of exposure PM_{10}, SO_2, NO_2, and GLO in Ahvaz, in 2012. The results showed that the concentration of PM_{10}, SO_2, NO_2, and GLO were related to Ahvaz with annual average 727, 160, 37 and 211 $\mu g/m^3$ in 2012. Findings showed that cumulative cases of hospital admissions respiratory diseases which attributed to PM_{10}, SO_2, NO_2, and GLO were 2675, 15, 25 and 58 persons, respectively. The higher percentage of these health point perhaps could be the result of higher average this pollutants or because of sustained high concentration days in Ahvaz. In Ahvaz city environmental concerns, most industries and dust storm phenomena are that required to decrease in source produce Air pollutants. Pollution prevention and control measures that reduce pollutants can very useful for expected to reduce people's exposures to Sulfur dioxide.

KEYWORDS:
Particle matter, Sulfur dioxide, Nitrogen dioxide, Ground Level Ozone, Hospital admissions, Ahvaz.

INTRODUCTION

Deferent study has been asserted a consistent increased the rate of harmful on human health and major environmental risk to health disease versus to the air pollution [1-3]. The many studies have showed relationship between health effects on human such as hospital admissions, asthma attacks, cardiovascular and repository disease, lungs cancer,

causing permanent DNA mutation, number of the years of life lost (YOLLs) and mortality with short and long term effects exposure to air pollutants [4-13]. In recent decades, one of the important sources of air pollution is from anthropogenic sources such as fossil fuel, deforestation, power plants, synthetic fertilizers, motor vehicles and industrial emissions [14-21]. Based on result studies done in Europe have reported that the daily cardiovascular mortality raises with increase in GLO exposure [22]. Katsouyanni estimates in 12 European cities of increase in daily mortality for an increase of 50 μg/m^3 in concentrations of Sulfur dioxide and particulates were 3% and 2% respectively [23]. Martuzzi in this study in the eight major Italian cities showed that with an increase of 30 μg/m3 concentration PM_{10}, 3500 cases in mortality and morbidity were attributable [24]. In another study which was conducted in Taiwan, there was an association between Nitrogen dioxide levels and in hospital admission in patients suffered from chronic obstructive pulmonary disease and asthma exacerbation [25]. In similar works Mohammadi et al studied the association between Chronic obstructive pulmonary disease (COPD) attributed to the NO_2 [15]. in another study Geravandi et al studied the effects of SO_2 and NO_2 on Respiratory Mortality in Ahvaz [26]. and hospital admissions respiratory disease and PM_{10} in the Ahvaz in 2013[27]. Also Goudarzi et al studied the association between hospital admissions respiratory disease and PM_{10} in the Ahvaz in 2012 [28], cardiovascular death cases associated with sulfur dioxide Exposure in Ahvaz 2012 [29] and COPD attributed to the PM_{10} emission in Ahvaz city in 2012 [30]. In the last decade, with the dust storm, rapid economic growth in Ahvaz, the level of air pollution from both motor vehicles and industrial emissions has drastically increased. Furthermore, health effect of air pollution in terms of PM_{10}, SO_2, NO_2, and GLO levels in most of megacities particularly Ahvaz was reported.

The objective of this study was to evaluating the association between fluctuations in ambient PM_{10}, SO_2, NO_2, and GLO concentrations with hospital admissions respiratory disease in Ahvaz city (located in south-western Iran) during year 2012.

MATERIALS AND METHODS

Study population and exposure assessment. The present study is an epidemiological and used model study. Using both methods (AirQ and epidemiologic) with the same pollutants data, they would tend to the same points in term ofType equation here. mortality and morbidity. In this study, was used to assess the potential effects of PM_{10}, SO_2, NO_2, and GLO exposure on human health in Ahvaz city (located in south-western Iran) during year 2012. Data's was taken from Ahvaz Department of Environment (ADoE). In Ahvaz there were 4 sampling point for measure air pollutants. Sampling was performed for 24 hours in 4 stations. Method of sampling and analysis were performed according to EPA guideline. In this study for pollutants 35040 samples of Ahvaz's air was taken and collected in during year 2012.

To make input file PM_{10}, SO_2, NO_2, and GLO data based on gravimetric unit which is required for health effects model several steps were taken in the recent work. The most important part of analysis is data processing that encompasses conversion was conducted by ideal gas formula, modification of temperature and pressure on the basis of meteorological data, primary processing, secondary, formulation and filtering.

$$\frac{P_1V_1}{T_1} = \frac{P_2V_2}{T_2}$$

Where P is atmospheric pressure, V is gas volume and T is ambient temperature in Kelvin.

Afterward we ran a program to achieve PM_{10}, SO_2, NO_2, and GLO values that would be convenient and consistent as well as compatible with model. For estimated of hospital admissions respiratory disease attributable to the exposure of air pollution on the target population using AirQ model, that estimate the this impacts to specific air pollutants on a resident population in a certain area and period.

The standard of air pollutants according to national ambient air quality standard (NAAQS) and World Health Organization (WHO) guidelines are PM_{10} (24-hour) 150 μg/m^3 [31], SO_2 (24-hour) 150 μg/m^3 [31], NO_2 (24-hour) 100 μg/m^3 [31] and GLO (8-hour) 100μg/m^3[32].

Geographical features of Ahvaz. For assessing of health impacts related to PM_{10}, SO_2, NO_2, and GLO exposure in the ambient air of Ahvaz we need population of city, coordination (latitude and longitude), number of station and their data set [29, 33]. Ahvaz city, with a population of 1 million approximately, with an area of 8152 square kilometers, the capital city of Khuzestan Province is located between 48 degree to 49°29′ east of Greenwich meridian and between 31 degrees and 45 minutes to the north of the equator [27, 28, 34]. Data was taken from Ahvaz Department of Environment (ADoE). Stations were "Naderi", "BehdashtGhadim", "Havashenasi" and "Mohitzist".

Data analysis. In terms of epidemiological parameters, relative risk, baseline incidence and

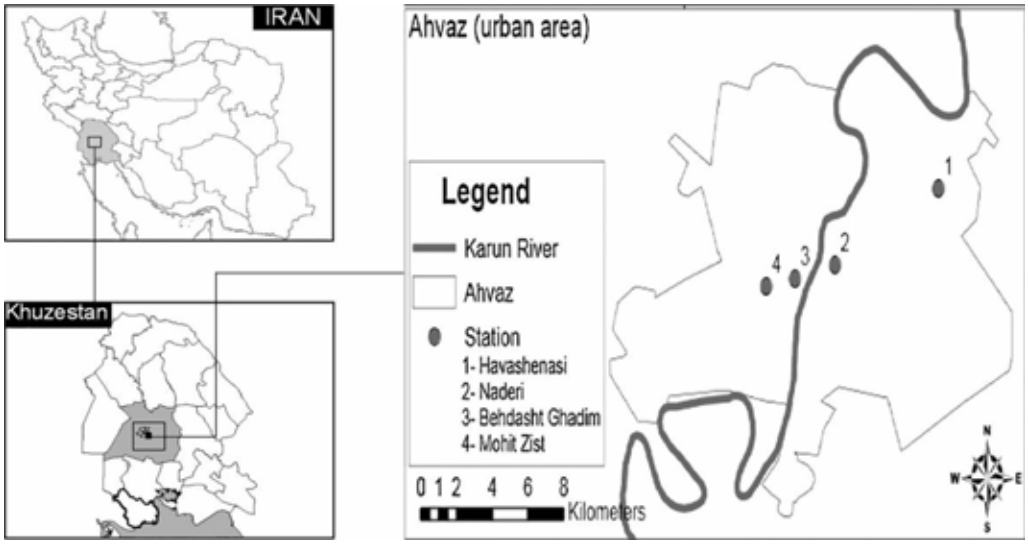

FIGURE 1
Location of the study area and sampling station in the Khuzestan Province (Ahvaz city), in the south west of Iran

TABLE 1
PM_{10}, SO_2, NO_2, and GLO concentrations (µg/m^3) in Ahvaz during 2012

Study Years / Parameters	PM_{10}	Nitrogen dioxide	Ozone maximum8-hour	Sulfur dioxide
Annual mean	**727**	**37**	**102.27**	**160**
Spring mean	**985**	**17**	**56.21**	**32**
Summer mean	**646**	**21**	**41.79**	**46**
Autumn mean	**348**	**50**	**111.03**	**120**
Winter mean	**922**	**58**	**135.79**	**173**
Annual 98 percentile	**2663**	**152**	**171.55**	**171**

attributable proportion were calculated based on previous studies around the world and also following formulas [15]. For instance, attributable proportion was calculated as below formula:

$$AP= SUM \{[RR(c)-1] \times p(c)\} /SUM [RR(c) \times p(c)]$$

Where p(c) is the proportion of Ahvaz population in category c of exposure and RR is the relative risk of disease.

Relative risk (RR) is the risk of an event (or of developing a disease) relative to exposure [30].

RR = Incidence in the exposed / Incidence in the non-exposed

Generally, incidence or certain frequency of an outcome particularly hospital admissions respiratory disease in Ahvaz community is obvious but in rare cases it can be assumed. Attributable proportion was multiplied at baseline incidence and divided to 10^5. Obtained value should be multiplied at population (10^6). The results will be the excess cases of hospital admissions respiratory disease associated with given pollutant (PM_{10}, SO_2, NO_2, and O_3).

RESULTS AND DISCUSSION

The annual mean, spring mean, summer mean, Autumn mean, winter mean and 98 percentile of PM_{10}, SO_2, NO_2, and GLO concentrations in these stations has presented in table 1. Table 1 shows that annual mean of PM_{10}, SO_2, NO_2, and GLO in Ahvaz was 727, 160, 37 and 102.27 µg/m^3 in 2012. Based on results in this table average concentrations maximum Nitrogen dioxide, Ground Level Ozone and Sulfur dioxide were in winter season.

Relative risk and estimated attributable proportion percentage for hospital admissions were estimated in table 2. Baseline incidence (BI) of these health endpoints were calculated per 10^5. The number of hospital admissions estimated by model

TABLE 2
Relative risks, attributable proportions and number of people suffering from hospital admissions respiratory disease due to PM_{10}, SO_2, NO_2, and GLO exposure

Hospital admission to respiratory diseases	RR, 95% CI	AP (%)	Estimated number of excess cases (persons)
PM_{10}	1.0080 (1.0048 - 1.0112)	16.8569	2675
Sculpture dioxide	1.0044 (1-1.011)	4.0350	25
Ozone	1.0080 (1.004 -1.012)	9.1654	58
Nitrogen dioxide	1.0038 (1.0004 - 1.0094)	2.1694	15

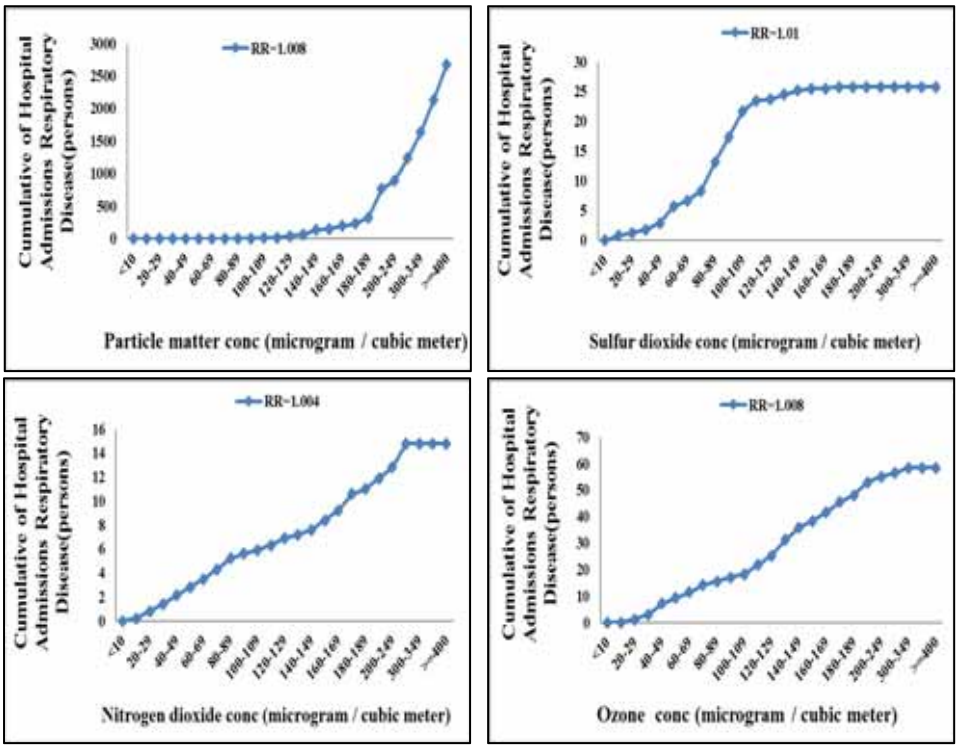

FIGURE 2
Relationship between cumulative of hospital admissions respiratory disease related to PM_{10}, SO_2, NO_2, and GLO

at centerline of relative risk were (RR=1.0080 and AP=16.8569%), (RR=1.01 and AP=4.0350%), (RR=1.004 and AP=2.1694%) and (RR=1.0080 and AP=9.1654%) for PM_{10}, SO_2, NO_2, and O_3.

Figure 2 show that despite the relative risk of health effects of PM_{10}, SO_2, NO_2, and GLO. particle matter concentrations below 30µg/m^3 due to lack of contact with the population concentration is zero, In other words, no one day in 2012 has been reaches the particle matter concentration below 30µg/m^3. Estimated cases which attributed to sulfur dioxide for hospital admissions at central of RR were 25, respectively. Hospital admissions respiratory disease versus nitrogen dioxide concentration has shown in figure 5. 61% of this number has occurred in the days with concentrations lower than 110µg/m^3. Fifteen persons were estimated by the model as total cumulative number of hospital admissions respiratory disease within one year of exposure. Cumulative cases of hospital admissions attributed to GLO concentrations has illustrated in Figure 2 with three ranges of relative risk central. 57 percent of these cases have occurred in days with GLO levels not exceeding 150µg/m^3.

In recent decades, air pollution is considered to be a serious threat to the environment, and quality of life and health of people. Ahvaz is located in an arid area in south west of Iran with long and hot summertime. In this study, we estimate hospital admissions respiratory disease were associated with short and long term fluctuations in concentrations of PM_{10}, SO_2, NO_2, and GLO, using AirQ model in Ahvaz, Iran. Breathing PM_{10}, SO_2, NO_2, and GLO can increase a variety of health effects such as increase rates hospital admissions respiratory disease, chronic

obstructive pulmonary, myocardial infarction, bronchitis, emphysema, asthma, respiratory mortalities, cardiovascular disease and death [5, 6, 26, 30, 35, 36, 16, 8, 9]. Based on the results of our study, in Ahvaz, case of hospital admissions attributed to PM_{10}, SO_2, NO_2, and GLO in case of respiratory and cardiovascular were 2675, 15, 25 and 58 persons, respectively. These values are correspondent to 16, 4, 2 and 9 in term of AP as well as 1.0080, 1.004, 1.0038 and 1.008 for RR, respectively. It should be noted that, High percentage of the observed health endpoints related to PM_{10} in compared to SO_2, NO_2, and GLO was associated with high concentration of measured PM_{10} and existing heavy industry and dust storm in Ahvaz. Approximately 15, 3.6, 4.2 and 6.7 % of the total hospital admissions respiratory disease were attributed to respiratory PM_{10}, SO_2, NO_2, and GLO. Study Tominz et al in Trieste, Italy showed that 1/8 percent of all respiratory mortality were attributed to inhalation concentrations over 20µg/m^3 [37]. Ballester and Associates to estimate the respiratory of SO_2 in Valencia city during 2001, Spain [38]. Based on the results of this study, increase in the 10µg/m^3 of SO_2 was associated with an increase 3 percent in respiratory diseases. Based on report centers for disease chronic in the United States, approximately 6.3% of the adult population, has been diagnosed with COPD attributed to Nitrogen dioxide [39]. Based on result study Bell et al a 10-ppb increase in ozone concentration was related to a 0.52% increase in daily deaths [40]. Gryparis et al found that there is revealed significant effects were observed during the warm season with an increase ozone concentration [41]. According to result study Biggeri and Baccini, increase in 10µg/m^3 of sulfur dioxide levels was relationship with an increase 2.8 percent in cardiovascular disease [42]. In a similar work, Lipmann et al estimated the air pollution hygienic effects in Detroit, USA. Their showed that an increase in the sulfur dioxide levels of 10µg/m^3 can be increased approximately 2% in the rate of hospital admissions [43]. Glad et al in 2012 conducted a work to find the relation between asthma ED and exposed to concentrations of ozone. The results this study shows that 2.5% increase was in asthma ED visits for each 20µg/m^3 increase in the 1-hour maximum ozone level [44].

Finally, it was supposed to study cumulative cases of hospital admissions respiratory disease related to PM_{10}, SO_2, NO_2, and GLO in present work but it should be mentioned that all morbidities such as respiratory disease, COPD, myocardial infarction, bronchitis, emphysema, asthma and cardiovascular disease can be at paramount of importance in standpoint of health effect attributed to PM_{10}, SO_2, NO_2, and GLO.

CONCLUSION

This study was conducted to estimate cumulative case of hospital admission to respiratory diseases versus PM_{10}, SO_2, NO_2, and GLO in Ahvaz, Iran. The number of cases of the health effects attributed to PM_{10} was relatively higher because of the greater PM_{10} concentration in Ahvaz during a year (2012). Larger relative risks for air pollution were mostly found in the elderly except for PM_{10}, SO_2, NO_2, and GLO and for cause hospital admissions respiratory disease which showed larger relative risk. Careful monitoring of air pollution, reduce exposure of general population, cost-effective measures and management schemes should be considered to subside air pollution concentrations, reduced by limiting emissions of pollutants from various sources such as changing modes of transport and reducing energy consumption especially which are based on combustion sources is necessary to reduce health risk.

Conflict of Interests. Authors have no conflict of interests.

Acknowledgment. The authors would like to thank student Research committee, Ahvaz Jundishapur University of Medical Sciences for providing financial supported by grant: (95s16) of this research.

Funding/Support. This work was financially supported by grant: (95s16) from Vice- Chancellor for research Affairs of Ahvaz Jundishapur University of Medical Sciences.

REFERENCES

[1] Di Nardo F, Laurenti P. Respiratory Diseases and Health Disorders Related to Indoor and Outdoor Air Pollution. A Systematic Review of Key Issues in Public Health. Springer; 2015;3: 109-27.

[2] Rad HD, Babaei AA, Goudarzi G, Angali KA, Ramezani Z, Mohammadi MM. Levels and sources of BTEX in ambient air of Ahvaz metropolitan city. Air Quality, Atmosphere & Health. 2014;7(4):515-24.

[3] Hoek G, Krishnan RM, Beelen R, Peters A, Ostro B, Brunekreef B et al. Long-term air pollution exposure and cardio-respiratory mortality: a review. Environ Health. 2013;12(1):43.

[4] Chen C-H, Chan C-C, Chen B-Y, Cheng T-J, Guo YL. Effects of particulate air pollution and ozone on lung function in non-asthmatic children. Environmental research.

2015;137:40-8.
[5] Frampton MW, Pietropaoli A, Dentler M, Chalupa D, Little EL, Stewart J et al. Cardiovascular effects of ozone in healthy subjects with and without deletion of glutathione-S-transferase M1. Inhalation Toxicology. 2015;27(2):113-9.
[6] Franklin BA, Brook R, Pope CA. Air pollution and cardiovascular disease. Current Problems in Cardiology. 2015.
[7] Kariisa M, Foraker R, Pennell M, Buckley T, Diaz P, Criner GJ et al. Short-and Long-Term Effects of Ambient Ozone and Fine Particulate Matter on the Respiratory Health of Chronic Obstructive Pulmonary Disease Subjects. Archives of environmental & occupational health. 2015;70(1):56-62.
[8] Pride KR, Peel JL, Robinson BF, Busacker A, Grandpre J, Bisgard KM et al. Association of short-term exposure to ground-level ozone and respiratory outpatient clinic visits in a rural location – Sublette County, Wyoming, 2008–2011. Environmental Research. 2015;137(0):1-7.
[9] Sheffield PE, Zhou J, Shmool JLC, Clougherty JE. Ambient ozone exposure and children's acute asthma in New York City: a case-crossover analysis. Environmental Health. 2015;14(1):25.
[10] Skouloudis AN, Kassomenos P. Combining environment and health information systems for the assessment of atmospheric pollution on human health. Science of The Total Environment. 2014;488–489(0):362-8.
[11] Wang N, Guo H, Jiang F, Ling Z, Wang T. Simulation of ozone formation at different elevations in mountainous area of Hong Kong using WRF-CMAQ model. Science of The Total Environment. 2015;505:939-51.
[12] Goudarzi G, Geravandi S, Foruozandeh H, Babaei AA, Alavi N, Niri MV et al. Cardiovascular and respiratory mortality attributed to ground-level ozone in Ahvaz, Iran. Environmental monitoring and assessment. 2015;187(8):1-9.
[13] Neisi A, Goudarzi G, Akbar Babaei A, Vosoughi M, Hashemzadeh H, Naimabadi A et al. Study of heavy metal levels in indoor dust and their health risk assessment in children of Ahvaz city, Iran. Toxin Reviews. 2016;35(1-2):16-23.
[14] Li T, Yan M, Ma W, Ban J, Liu T, Lin H et al. Short-term effects of multiple ozone metrics on daily mortality in a megacity of China. Environmental Science and Pollution Research. 2015:1-9.
[15] Mohammadi MJ, Godini H, Khak MT, Daryanoosh SM, Dobaradaran S, Goudarzi G. An Association Between Air Quality and COPD in Ahvaz, Iran. Jundishapur J Chronic Dis Care. 2015;4(1):e26621.
[16] Mraihi R, Harizi R, Mraihi T, Bouzidi MT. Urban air pollution and urban daily mobility in large Tunisia′ s cities. Renewable and Sustainable Energy Reviews. 2015;43:315-20.
[17] Goudarzi G, Geravandi S, Vosoughi M, javad Mohammadi M, sadat Taghavirad S. Cardiovascular deaths related to Carbon monoxide Exposure in Ahvaz, Iran. Iranian Journal of Health, Safety and Environment. 2014;1(3):126-31.
[18] Taghavirad S, Davar H, Mohammadi MJ. The a study on concentration of BETX vapors during winter in the department of ports and shipping located in one of the southern cities of Iran. Inte J Cur Life Sci. 2014;4(9):5416-20.
[19] Mohammadi MJ, Goudarzi G, Geravandi S, Yari AR, Ghalani B, Shirali S et al. Dispersion Modeling of Nitrogen Dioxide in Ambient Air of Ahvaz City. Health Scope. 2016;5(2):e32540.
[20] Geravandi S, Goudarzi G, Soltani F, Salmanzadeh S, Ghomeishi A, Zalaghi E et al. The cardiovascular and respiratory deaths attributed to sulfur dioxide in Kermanshah. Journal of Kermanshah University of Medical Sciences 2016;19(6):319-26.
[21] Dobaradaran S, Geravandi S, Goudarzi G, Idani E, Salmanzadeh S, Soltani F et al. Determination of Cardiovascular and Respiratory Diseases Caused by PM10 Exposure in Bushehr, 2013. Journal of Mazandaran University of Medical Sciences. 2016;26(139):42-52.
[22] Boyce CP, Goodman JE, Sax SN, Loftus CT. Providing perspective for interpreting cardiovascular mortality risks associated with ozone exposures. Regulatory Toxicology and Pharmacology. 2015;72(1):107-16.
[23] Katsouyanni K, Samet JM, Anderson H, Atkinson R, Le Tertre A, Medina S et al. Air pollution and health: a European and North American approach (APHENA). Research report (Health Effects Institute). 2009(142):5-90.
[24] Martuzzi M. Health impact of PM10 and ozone in 13 Italian cities. WHO Regional Office for Europe; 2006.
[25] Yang C-Y. Air pollution and hospital admissions for congestive heart failure in a subtropical city: Taipei, Taiwan. Journal of Toxicology and Environmental Health, Part A. 2008;71(16):1085-90.
[26] Geravandi S, Goudarzi G, Mohammadi MJ, Taghavirad SS, Salmanzadeh S. Sulfur and Nitrogen Dioxide Exposure and the Incidence of Health Endpoints in Ahvaz, Iran. Health Scope. 2015;4(2):e24318.

[27] Geravandi S, Goudarzi G, Vosoughi M, Mohammadi MJ, Salmanzadeh S, Zallaghi E. Relationship between Particulate matter less than 10 microns exposures and health effects on humans in Ahvaz, Iran. Archives of Hygiene Sciences. 2015;4(2):23-32.
[28] Goudarzi G, Geravandi S, Mohammadi MJ, Ghomaishi A, Salmanzadeh S. Cardiovascular death, Respiratory mortality and Hospital Admissions Respiratory Disease related to PM10 Exposure in Ahvaz, Iran. Iranian Journal of Health, Safety and Environment. 2014;1(4):159-65.
[29] Goudarzi G, Geravandi S, Salmanzadeh S, Mohammadi MJ, Zallaghi E. The Number of Myocardial Infarction and Cardiovascular Death Cases Associated with Sulfur Dioxide Exposure in Ahvaz, Iran. Archives of Hygiene Sciences. 2014;3(3):112-9.
[30] Goudarzi G, Geravandi S, Mohammadi MJ, Salmanzadeh S, Vosoughi M, Sahebalzamani M. The relationship between air pollution exposure and chronic obstructive pulmonary disease in Ahvaz, Iran. Chronic Diseases Journal. 2015;3(1):14-20.
[31] Agency UEP. National Ambient Air Quality Standards (NAAQS): for air pollutant. US Environmental Protection Agency. wwwepagov. 2014.
[32] Organization WH. Ambient (outdoor) air quality and health. Fact sheet N. 313. World Health Organization, Geneva. 2014.
[33] Mohammadi MJ, Geravandi S, Goudarzi G, Malihi R, Yousefi F, Soltani F et al. Estimation of the chronic obstructive pulmonary disease from exposure to particulate matter in Ahvaz, Southwest Iran. International Journal of Infectious Diseases. 2016(45):232-3.
[34] Zallaghi E, Goudarzi G, Geravandi S, Mohammadi MJ. Epidemiological Indexes Attributed to Particulates With Less Than 10 Micrometers in the Air of Ahvaz City During 2010 to 2013. Health Scope. 2014;3(4):e22276.
[35] Jane C, Fanny W. Air pollution: Its impact on adult patients with respiratory conditions. The Cover Shot. 2015;20(1):12.
[36] Loomis D, Grosse Y, Lauby-Secretan B, Ghissassi FE, Bouvard V, Benbrahim-Tallaa L et al. The carcinogenicity of outdoor air pollution. The lancet oncology. 2013;14(13):1262-3.
[37] Tominz R, Mazzoleni B, Daris F. [Estimate of potential health benefits of the reduction of air pollution with PM10 in Trieste, Italy]. Epidemiologia e prevenzione. 2004;29(3-4):149-55.
[38] Ballester F, Tenias J, Perez-Hoyos S. Air pollution and emergency hospital admissions for cardiovascular diseases in Valencia, Spain. Journal of epidemiology and community health. 2001;55(1):57-65.
[39] Control CfD, Prevention. Chronic obstructive pulmonary disease among adults--United States, 2011. MMWR Morbidity and mortality weekly report. 2012;61(46):938.
[40] Bell ML, Dominici F. Effect modification by community characteristics on the short-term effects of ozone exposure and mortality in 98 US communities. American journal of epidemiology. 2008;167(8):986-97.
[41] Gryparis A, Forsberg B, Katsouyanni K, Analitis A, Touloumi G, Schwartz J et al. Acute effects of ozone on mortality from the "air pollution and health: a European approach" project. American journal of respiratory and critical care medicine. 2004;170(10):1080-7.
[42] Biggeri A, Baccini M. [Short-term effects of air pollution in Italy: risk heterogeneity from 1996 to 2005]. Epidemiologia e prevenzione. 2008;33(6 Suppl 1):95-102.
[43] Lippmann M, Ito K, Nadas A, Burnett R. Association of particulate matter components with daily mortality and morbidity in urban populations. Research report (Health Effects Institute). 2000(95):5-72, discussion 3-82.
[44] Glad JA, Brink LL, Talbott EO, Lee PC, Xu X, Saul M et al. The relationship of ambient ozone and PM2. 5 levels and asthma emergency department visits: Possible influence of gender and ethnicity. Archives of environmental & occupational health. 2012;67(2):103-8.

Received: **08.01.2016**
Accepted: **23.07.2016**

CORRESPONDING AUTHOR

Mohammad Javad Mohammadi
Department of Environmental Health Engineering, School of Public Health, Ahvaz Jundishapur University of Medical Sciences, Ahvaz, Iran

e-mail: javad.sam200@gmail.com

© by PSP Volume 25 – No. 10/2016, pages 3962-3970 Fresenius Environmental Bulletin

STRUCTURAL PROPERTIES OF TiO_2/Sb NANOPARTICLES WITH DIFFERENT MOLAR RATIOS AND INVESTIGATION THE PHOTOCATALYTIC DEGRADATION OF AZO DYES UNDER UV IRRADIATION IN DIFFERENT CONDITION

Maryam Nozari, Shahram Moradi Dehaghi*

Department of Chemistry, Tehran North Branch, Islamic Azad University, Tehran, Iran

ABSTRACT

Photocatalytic activity of metal doped semiconductors can be influenced by various factors. TiO_2 and TiO_2/Sb nano photocatalysts were prepared using sol-gel method. The synthesized nano photocatalysts were characterized by Fourier Transform Infrared (FT-IR) and Raman spectroscopy, X-ray diffraction (XRD), Field Emission Scanning Electron Microscopy (FE-SEM) equipped with Energy-dispersive X-ray (EDX) spectroscopy and Brunauer-Emmet-Teller (BET) techniques.

Different molar ratios of Sb doped TiO_2 were prepared and their photocatalytic activities were investigated under UV irradiation for degradation of methyl orange (MO) solution as a model of azo dye pollutant. The degradation abilities of the best sample evaluate in different pH (2, 5, 7, 9). In each condition, photodegradable ability of TiO_2 and TiO_2/Sb were determined and compared. The results showed that antimony doped titania nano photocatalyst with molar ratio of 0.00136:1 had better photocatalytic activity comparing with the others and the photocatalytic degradation of the sample was the best at pH≈5.

KEYWORDS:
TiO_2/Sb; Nano Photocatalyst; Sol-Gel; Methyl Orange

INTRODUCTION

By increasing the organic pollutant in the environment and their harmful effects on the earth and human's health, elimination of these compounds become the most scientists' attention [1-7].

Among organic pollutant, azo dyes are stable and the biological degradation methods are not effective on destroying them [8], so degradation of azo dyes becomes a challenge [8].

Many ways for degradation of azo dyes have been investigated. Among them semiconductor photocatalysts have been used extensively [9]. Among these semiconductors, TiO_2 has been widely used because of its low cost, thermal stability and high photocatalytic activity [10, 11]. The photocatalytic activity arises from the photo oxidation of TiO_2 which produces electron-hole pairs. These species can migrate to the surface of the photocatalyst and perform the oxidation reduction reactions or can combine with each other and release energy [5]. The efficiency of the photocatalytic activity depends on the competition between these two processes [3, 5]. Adsorbed oxygen atoms are the traps for the electrons and produce superoxide anion species ($O^{-\bullet}_2$); on the other hand hydroxyl ions (OH^-) act as the traps for the holes and produce hydroxyl radicals ($OH^\bullet$), so the life time of the charge carriers will increase and the recombination rate will decrease [5, 9, 12, 13], on the other hand these species are active types of molecules for the degradation of the pollutant.

Because of the large band gap of TiO_2 (3.2 ev), using UV irradiation is necessary for excitation of TiO_2 [9, 12, 13]. So, researchers trying to find different ways to shift the absorption field to visible region [9, 12-14].

For solving this problem, modification of TiO_2 by doping with noble metals such as Au, Ag, Pt, transition metals such as Fe, Cu, Mn and non-metal elements such as N, C, S, F has been studied [4, 9, 12,15-21]. Few studies relating to Sb doped TiO_2 for degradation of organic pollutants has been investigated. Moon *et al.* [22] synthesized the Sb-doped TiO_2 by co-precipitation method and investigated the photodegradation of methylene blue. Luo *et al*. [23], synthesized Sb doped on the TiO_2 lattice by co-precipitation method and investigated their photocatalytic activity under visible light irradiation [23].

Important parameters deals with the photocatalytic activity of TiO_2 including: the particles size, surface area, and the energy of the band gap and the composition of the produced

crystals [24]. However, an optimum concentration of dopant metal ions is another considerable factor.

Among different methods for production of metal doped TiO_2 such as sol-gel, hydrothermal deposition, impregnation, flame reactor, ion implantation, and pulsed laser deposition and so on, the sol-gel method shows good adoption for metal doping of TiO_2 because it can incorporate dopant into TiO_2 lattice and finally, obtain materials with sufficient optical and catalytic properties [9, 14, 25].

This paper deals with synthesis of TiO_2 nano photocatalyst and Sb doped TiO_2 by the sol-gel method. Different molar ratios of Sb doped TiO_2 were prepared and characterized by the analysis techniques, then their photocatalytic activities were investigated under UV irradiation for degradation of methyl orange solution in the batch reactor and the photodegradation of the best sample was investigated at different pH (2, 5, 7, 9).

MATERIALS AND METHODS

Materials and Methods. Titanium tetraisopropoxide (TTiP >98%), HNO_3 (65%), C_2H_5OH (EtOH 99%), and Methyl Orange (MO) are all from Merck Chemical Company. $SbCl_3$ (>99%) and Hydroxypropyl Cellulose (HPC) were purchased from Sigma-Aldrich company.

Preparation of the Samples. TTiP was dissolved in EtOH with the molar ratio of 1:75 respectively then 0.01 g of HPC was added to the solution and then stirred for 15 min [6, 26]. Then a mixture of EtOH, HNO_3 and deionized water with the molar ratio of 43:0.2:1 was added drop wise into the precursor solution and stirring for 45 min to achieve the transparent sol. Different amounts of alcoholic solution of $SbCl_3$ to TTiP with molar ratios of 5.44 E^{-5} :1, 2.72 E^{-4}:1, 1.36 E^{-3}:1 , 2.72 E^{-3}:1, 8.18 E^{-3}:1 were prepared and added to the last solution (Sample 1–5 respectively). The solution was stirred for 45 min and then homogenized at 20000 rpm for 30 min. The achieved sol was aged for 48 h to form a gel, then calcinated at 550 ^oC in an electric furnace for 4 h. TiO_2 nano photocatalyst was prepared using the same method, but without addition of $SbCl_3$.

Characterization. FT-IR spectra of the samples were determined using Thermo Nicolet Nexus 870 FT-IR spectroscopy at the range of 400-4000 cm^{-1}. Raman spectra of TiO_2 and TiO_2/Sb samples were obtained using Thermo Nicolet 960 FT Raman spectrometer. The phase characterization of the nano photocatalyst was obtained by XRD using SCIFERT-3003 PTS X-ray diffractometer with CuKα radiation from 0 to 100. The morphology of the samples obtained by using FE-SEM (MIRA3 TESCAN) equipped with EDX analyzer. UV-Vis spectrophotometer model Cary UV-Vis 100 was used to determine the photocatalytic degradation.

Photocatalytic Activities. Photocatalytic degradation experiments were carried out using a UV-C pencil lamp (Hach Company, USA) which was placed in the quartz reactor. Methyl Orange solution with an initial concentration of 5 ppm was prepared and 0.01 g of the synthesized nano photocatalyst was added into 25 ml of it. After reading the initial absorption at the maximum absorbance (λ_{max} = 465 nm for the neutral solution), the reaction started by UV irradiation. Another suspension consists of 0.01 g nano photocatalyst and 25 ml of distilled water was used as blank solution. The absorption was read by means of UV-Vis spectrophotometer during 10 min intervals.

RESULTS

FT-IR Spectroscopy. FT-IR spectra of the TiO_2 and TiO_2/Sb nano photocatalyst with different molar ratios were obtained and the results are shown in Figure 1. The peaks at 400 and 1400 cm^{-1} were attributed to the vibration mode of Ti-O and Ti-O-C that the Ti-O-C may result from the presence of organic polymer [5, 27] and those at 1240, 1160 and 1080 cm^{-1} related to Ti-OH band [5]. The peaks at 550 and 700 cm^{-1} can be assigned to symmetric stretching vibration of the Ti-O-Ti bond and O-Ti-O flexion vibration respectively [5, 27-29]. The peak at 1650 cm^{-1} resulted from the adsorbed H_2O molecules, which were not removed completely after sol-gel synthesis [5, 29, 30]. During the hydrolysis of TTiP, large amount of ethanol, lead to the appearance of hydroxyl bond, so the wide peak at 3304-3269 cm^{-1} was attributed to the OH stretching vibration of surface hydroxyl group [5, 31]. In addition, the peak around 1620-1635 cm^{-1} can be assigned to the stretching mode of the physically adsorption of hydroxyl group [5, 31]. As it can be seen further increasing in Sb concentration lead to decrease in O-Ti-O band [5].

Raman Spectroscopy. Structural properties of the synthetic nano photocatalyst can be investigated by Raman spectroscopy [32]. Doping of an atom can affect the vibration of the lattice of TiO_2 [33] and decrease in particle size can be observed by vibration in Raman spectra [32]. Figure 2 shows the Raman spectra of TiO_2 and Sb doped TiO_2 with different concentration. The peaks at 144, 197, 399, 513, 519, 639 cm^{-1} related to anatase form of TiO_2 [32- 35].

Sb_2O_3 has a peak at 712 cm^{-1} and Sb_2O_4 containing Sb^{5+} and Sb^{3+} has several peaks at 831, 759, 722, 658, 616 cm^{-1} [36]. The tiny peak at 181

cm^{-1} can be assigned to Sb-O stretching mode associated with the combination of Sb and O in TiO_2 matrix [37]. The Raman peak at 138 cm^{-1} is related to the interaction between two Sb atoms as Sb-Sb bond [38]. Decreasing in nanoparticles lead to the band broadening and shift of the bands to the higher wavenumber and decrease the intensity of the peak [32].

XRD Pattern. XRD diffractogram is the proper technique to characterize the crystallinity of the samples. The phase content and the change in the structure of the samples after doping can be identified by using XRD pattern [15].

The XRD pattern of TiO_2 and Sb incorporated TiO_2 nano photocatalyst shows in Figure 3. The XRD peaks at 25˚, 37.5˚, 48˚, 53.8˚, 54.9˚, 63.0˚ assigned to the anatase form of TiO_2 [39] and the peaks at 25.36˚, 31.7˚ assigned to Sb doped TiO_2 [40]. As it can be seen the major phase in all of the samples is anatase. Doping of Sb ions can inhibit the transformation of anatase TiO_2 to rutile form, but the exact mechanism was not identified completely [15, 41].

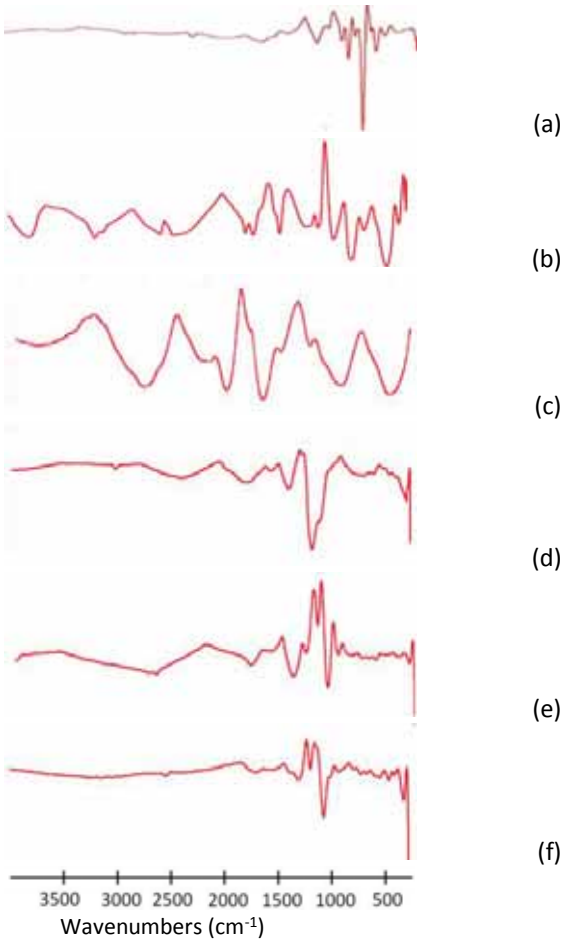

FIGURE 1
FT-IR spectra of (a) TiO_2, (b) Sample 1, (c) Sample 2, (d) Sample 3, (e) Sample 4, (f) Sample 5

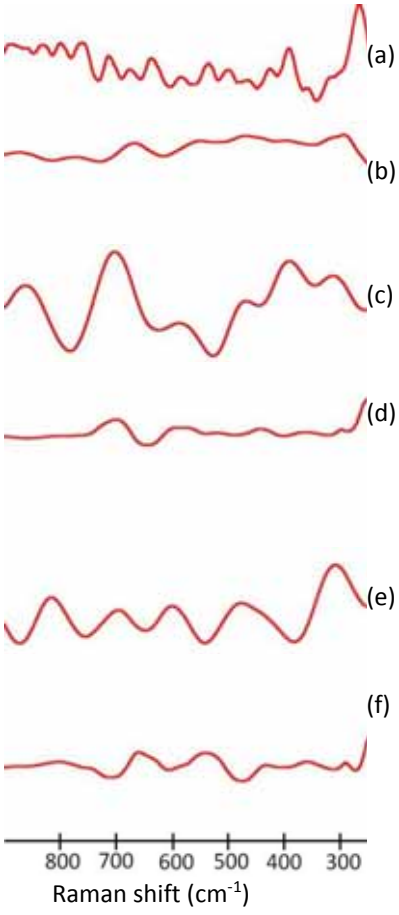

FIGURE 2
Raman spectra of (a) TiO_2, (b) Sample 1, (c) Sample 2, (d) Sample 3, (e) Sample 4, (f) Sample 5

SEM Images. SEM is one of the promising techniques for the topography study of the samples and it gives important information regarding the growth mechanism, shape and size of the particles. The surface morphology of the synthesized nano photocatalyst has been studied and their SEM images are shown in Figure 4.

Figure 4a shows TiO_2 nano photocatalyst, without adding any $SbCl_3$. It is seen that pure nano TiO_2 does not show a regular surface and the agglomeration of tiny particles can be observed. Figure 4 (b-f) shows the TiO_2/Sb nano photocatalyst with different molar ratios of Antimony (III) chloride solution. Addition of dopant can affect the morphology of the TiO_2. There is no agglomeration in the nanoparticle products. Also, the entire SEM images clearly show the average size of the nano particles is of the order of nanometer size. X- Ray Mapping images of TiO_2 and TiO_2/Sb prove that Sb was incorporated into the TiO_2 nano photocatalyst.

As it can be seen the distribution of the Sb nano particles is uniform in the matrix of the TiO_2 lattice in all of the samples.

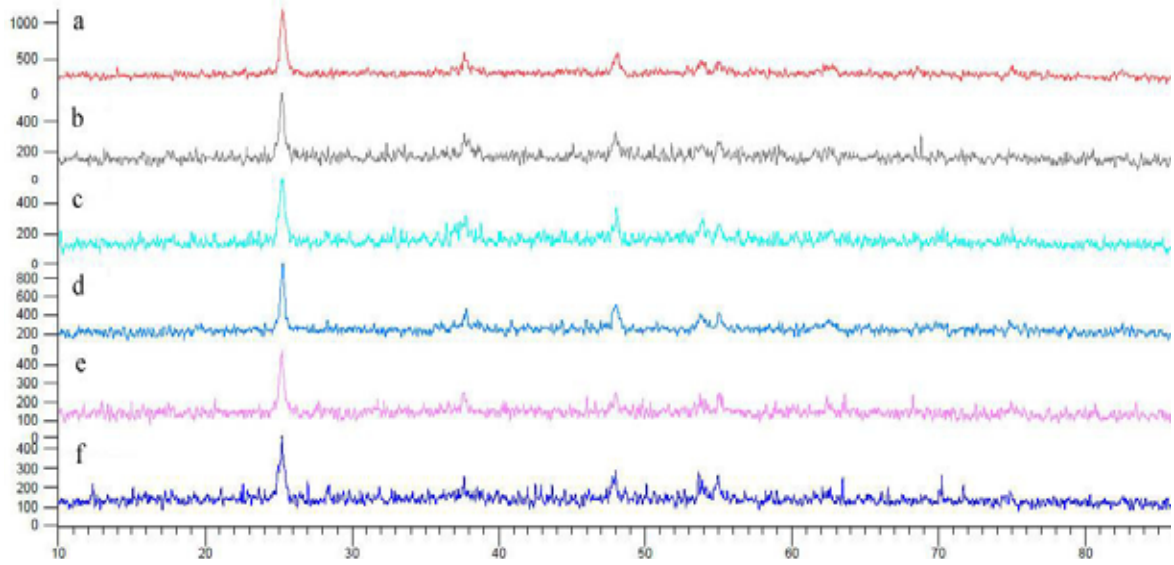

FIGURE 3
XRD pattern of (a) TiO_2, (b) Sample 1, (c) Sample 2, (d) Sample 3, (e) Sample 4, (f) Sample 5

TABLE 1
EDX analysis of the samples

Samples	TiO_2(wt%)	Sb (wt%)
Sample 1	99.71	0.29
Sample 2	99.23	0.77
Sample 3	98.99	1.01
Sample 4	97.96	2.04
Sample 5	96.65	3.35

EDX is used for elemental analysis and can identify the chemical characterization of the samples by emission of X-ray from the species [15]. The existence of the other elements except Ti and Sb atoms were omitted to simplify the comparison between the samples. The EDX analyses of the samples are as Table 1. As it can be seen by increasing the dopant concentration, the amount of Sb will increase in the EDX analysis.

Particle size and the surface area are the effective parameters in photocatalytic activities of the nano particles. By decreasing the particle sizes, large surface area will obtain which increase the photocatalytic degradation [42]. So the surface area of the synthetic catalysts was obtained by BET method and the results are shown in Table 2.

Photocatalytic activity of TiO_2/Sb samples. Different molar ratios of TiO_2/Sb were evaluated for understanding the best concentration of the dopant metal. Table 3 shows the time needed for the degradation of methyl orange solution with different samples under UV irradiation. The characterization of dopant atom, the situation of the experiment, the concentration of the dopant and the method of producing nano photocatalyst affect the photocatalytic activity of TiO_2 after doping [24].

During this phenomenon, Sb make new trapping site so, Sb nanoparticles accept the photogenerated electrons and transfer them to the oxygen species on the surface of TiO_2 and produce $O^{-\bullet}_2$, so the recombination rate decrease and the photocatalytic activity increase [10]. By increasing the dopant concentration, separation of the charge carriers occurred, so the degradation time decreases [22, 10], but at higher concentration of the dopant, the energy level become lower than the energy level of O_2, so after the acceptance of electrons by the dopant, it can't migrate them to the oxygen atoms on the surface of the TiO_2, so the photocatalytic activity decreases [10]. On the other hand, multiple trapping of charge carriers increase the recombination of electron- holes and lead to the reduction of the photocatalytic activity [10, 22].

As it can be seen the photocatalytic activity of sample 3 is the best comparing with the other samples in degradation of methyl orange solution. After this step, sample 3 was candidate to evaluate the other conditions.

Effect of pH on the photocatalytic activities. The effect of pH on the photocatalytic degradation of dye solution in the range of 2–9 was investigated. The pH of the reaction mixture was adjusted by adding adequate amount of HCl (0.001 M) or NH_3 (0.05 M). Figure 5 compares the results of the photocatalytic degradation of methyl orange solution under different pH condition.

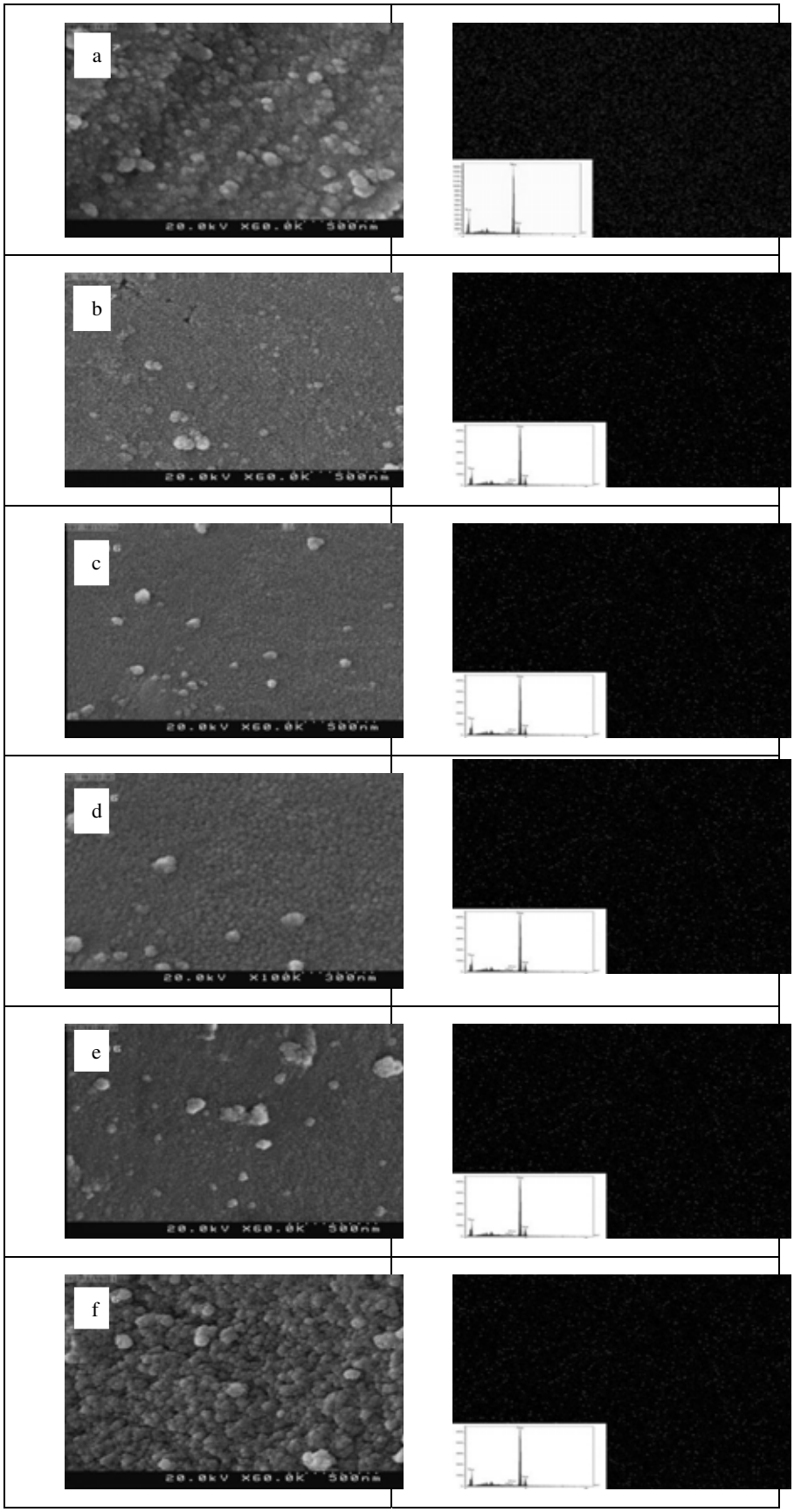

FIGURE 4
SEM and X- Ray Mapping images of (a) TiO_2, (b) Sample 1, (c) Sample 2, (d) Sample 3, (e) Sample 4, (f) Sample 5 (Black spots: TiO_2 nanoparticles, White spots: Sb nanoparticles)

TABLE 2
Surface area of the samples

Samples	TiO_2	Sample 1	Sample 2	Sample 3	Sample 4	Sample 5
Surface area (m^2/g)	165	168	223	247	196	190

TABLE 3
Photocatalytic activities of TiO_2 and Antimony doped TiO_2 samples

Samples	TiO_2	Sample 1	Sample 2	Sample 3	Sample 4	Sample 5
Time (min)	65	63	60	43	45	60

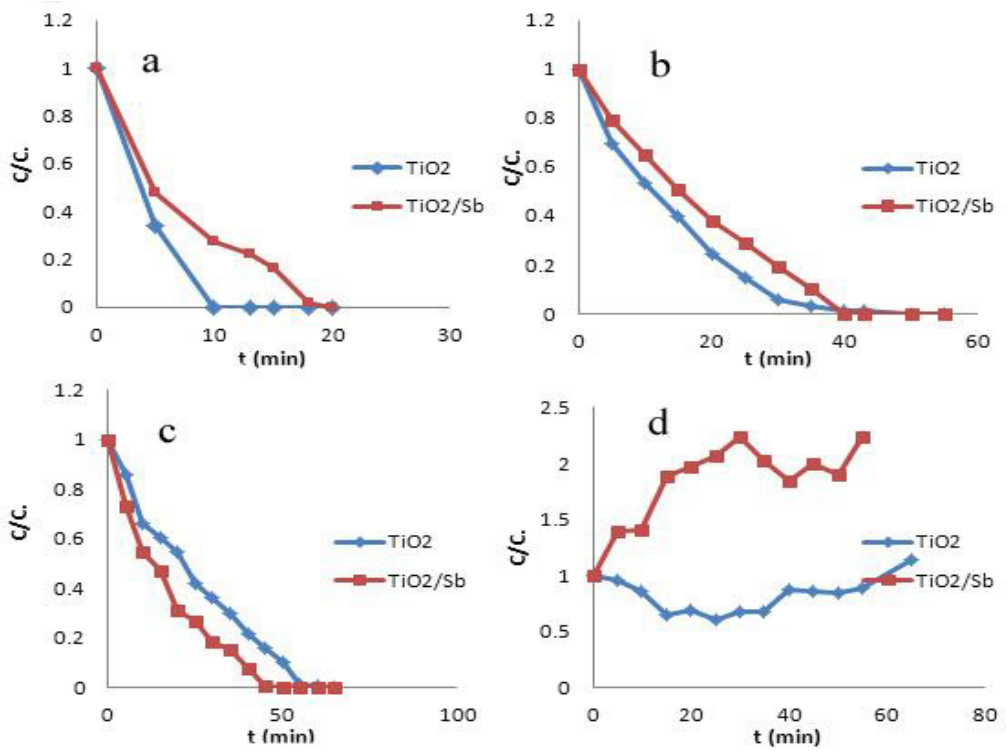

FIGURE 5
Photocatalytic degradation of MO solution at different pH, a: pH≈ 2, b: pH≈5 c: pH≈7, d: pH≈9

Chemical properties of the compounds are changing in different pH [24]. The pH of the solution can affect the zero point charge (Pzc) of the nano photocatalyst [24].

At Pzc of TiO_2, the minimum interaction between the surface of the nano photocatalyst and the solution has occurred, because there is no more electrostatic force [24].

By lowering the pH under Pzc, TiO_2 particles are positively charged and they can adsorb the anionic group (SO_3^-) of MO, so the degradation activity increased [3, 24, 43].

These reactions can be described as below [24]:

1) pH < Pzc $TiOH + H^+ \rightarrow TiOH_2^+$
2) pH > Pzc $TiOH + OH^- \rightarrow TiO^- + H_2O$

At alkaline pH, TiO_2 particles become negatively charged and the electrostatic repulsion occurred between the surface of the nano photocatalyst and the OH^- species, so the degradation performance decreased [3,43] and the degradation process does not show the regular pattern.

As it shows in the figures, the TiO_2/ Sb sample shows better degradation performance comparing with TiO_2 at pH ≈ 5 and 7 and the best degradation time for TiO_2/Sb achieved at pH~5 that is about 40 min. At alkaline pH, the formation of TiOH,

decreases the photocatalytic activity. It is clear that lower pH causes the increase of dye degradation.

DISCUSSION AND CONCLUSIONS

TiO_2/Sb nano photocatalysts were prepared with different molar ratios by using sol-gel method and their characterization and photocatalytic activities were evaluated. The XRD pattern showed that the major phase in all of the samples were the anatase and the average size of the particles decreased by increasing the dopant concentration until reached the optimum amount of doping and after that the particle size increased. BET analysis proved that sample 3 had the highest amount of BET and of course the smallest particle size. The SEM images of the particles showed that Sb doped TiO_2 samples have no aggregation comparing with TiO_2 and the distribution of the dopant is uniform in all of the samples. The photocatalytic activities of the prepared samples were investigated by decolorization of methyl orange solution and the best sample which showed the shortest degradation time was selected to investigate the effect of pH on the decolorization of the azo pollutant. The result showed that the photocatalytic activity of Sb doped TiO_2 with molar ratio of 0.00136:1 was the best comparing with the other molar ratios of the dopant and the efficiency of TiO_2/Sb nano particles were better than TiO_2 at pH ≈ 5.

REFERENCES

[1] Coleman, H. M., Eggins, B. R., Byrne, J. A., Palmer, F. L., King, E. (2000) Photocatalytic degradation of 17-β-oestradiol on immobilized TiO_2, Appl. Catal. B: Environ. 24, L1-L5.

[2] Rui, X., Jia, L., Jun, W., Xiaofang, W., Binliu, B. W., Xiaoyu, L., Xiangdong, Z. (2010) Photocatalytic degradation of organic dyes under solar light irradiation combined with Er^{3+}: $YAlO_3$/Fe- and co-doped TiO_2 coated composites, Sol. Energ. Mat. Sol. C., 94, 1157- 1165.

[3] Moradi dehaghi, S. , Ghasemi Mobtaker, H., Ahmadi, S. J., Aberoomand azar, P. (2012) Investigation of coupled system effect on photocatalytic activity of TiO_2/M nano composite, Fresen. Environ. Bull., 21, 1-7.

[4] Thiruvenkatachari. R., Vigneswaran, S., Moon, II S., (2008) A review on UV/TiO_2 photocatalytic oxidation process, J. Chem. Eng., 25, 64- 72.

[5] Moradi, S., Aberoomand–Azar, P., Raeis-Farshid, S., Abedini- Khorrami, S., Givianrad, M. H. (2012) The effect of different molar ratios of ZnO on characterization and photocatalytic activity of TiO_2/ZnO nanocomposite, J. Saudi. Chem. Soci, in press.

[6] Nozari, M., Moradi Dehaghi, S. (2015) Synthesis, characterization and photocatalytic activity of pure and Sb co-doped TiO_2 nano photocatalyst, Fresen. Environ. Bull., 24, 3505- 3514.

[7] Demir, E.; Turna, F., Burgucu, D., Kilic, Z., Burunkaya, E., Kesmez, Ö., Yesil, Z., Akarsu, M., Kaya, B. (2013) Genotoxicity of different nano-sizes and ions of silica nanoparticles, Fresen. Environ. Bull, 22, 2901-2909.

[8] Naderpour, H., Noroozifar, M., Khorasani-Motlagh, M. (2013) Photodegradation of methyl orange catalyzed by nanoscale zerovalent iron particles supported on natural zeolite, J. Iran. Chem. Soc., 10, 471-479.

[9] Umar, K., Haque, M.M., Muneer, M., Harada, T., Matsumura, M. (2013) Mo, Mn and La doped TiO_2: Synthesis, characterization and photocatalytic activity for the decolourization of three different chromophoric dyes, J. Alloy. Comb., 578, 431-438.

[10] Liu, Y., Wang, Z., Fan, X., Geng, Z., Feng, L. (2014) Enhancement of the photocatalytic performance of Ni- loaded TiO_2 photocatalyst under sunlight, Ceram. Int., 40, 3887-3893.

[11] Wang, S., Wu., L., Yu, H., Gao, X., (2012) Visible-light-induced degradation of indoor formaldehyde over TiO_2 thin film co-doped with iron (III) and nitrogen**,** Fresen. Environ. Bull, 12b.

[12] Zhang, H., Zhu, H. (2012) Preparation of Fe-doped TiO_2 nanoparticles immobilized on polyamide fabric, Appl. Surf. Sci., 258, 10034-10041.

[13] Liu, B., Wang, X., Cai, G., wen, L., Song, Y., Zhao, X. (2009) Low temperature fabrication of V- doped TiO_2 nanoparticles, structure and photocatalytic studies, J. Hazard. Mater., 169, 1112-1118.

[14] Xiaoliang, S., Xingyong, Y., Sheng, W., Qiaoxin, Z., Yufu, W. (2010) Photocatalytic degradation of Rhodamine B dye with high purity anatase nano-TiO_2 synthesized by a hydrothermal method, J. Wuhan University of Technology-Mater. Sci. Ed., 26. 600-604.

[15] Montazer, M., Behzadnia, A., Pakdel. E., Rahimi, M.K., Mameni Moghadam, M. (2011) Photo induced silver on nano titanium dioxide as an enhanced antimicrobial agent for wool, J. Photochem. Photobiol. B., 103, 207-214.

[16] Hakoda, T., Matsumoto, K., Mizuni, A., Hiroto, K. (2009) Role of metals loaded on a TiO_2 surface in the oxidation of xylene in air using an electron beam irradiation/ catalytic process, Appl. Catal. A: General, 357, 244-249.

[17] Sun, S., Ding, J., Bao, J., Gao, C., Qi, Z. M., Yang, X. Y., He, B., Li, C. X. (2012)

Photocatalytic degradation of gaseous toluene on Fe-Tio_2 under visible light irradiation: a study on the structure, activity and deactivation mechanism, Appl. Surf. Sci., 258, 5031- 5037.

[18] Riaz, N., Chong, F. K., Dutta, B. K., Man, Z. B., Khan, M. S., Nurlaela, E. (2012) Photodegradation of orange II under visible light using Cu-Ni/TiO_2: effect of calcination temperature, Chem, Eng. J., 185-186, 108-119.

[19] Nogawa, T., Isobe, T., Matsushito, S., Nakajim, A. (2012) Preparation and visible-light photocatalytic activity of Au- and Cu-modified TiO_2 powders, Mater. Lett., 82, 174-177.

[20] Peng, Y. H., Huang, G. F., Huang, W. Q. (2012) Visible-light absorption and photocatalytic activity of Cr-doped TiO_2 nanocrystal films, Adv. Powder. Technol., 23, 8- 12.

[21] Deng, Q. R., Xia, X. H., Guo, M. L., Gao, Y., Shao, G. (2011) Mn- doped TiO_2 nanopowders with remarkable visible light photocatalytic activity, Mater. Lett., 65, 2051-2054.

[22] Moon, J., Takagi, H., Fujishiro, Y., Awano, M., Preparation and characterization of the Sb-doped TiO_2 photocatalysts, J. Mater. Sci., 2001, 36, 949- 955.

[23] Luo, L., Li, T., Ran, X., Wang, P., Guo, L. (2014) Probing photocatalytic characteristics of Sb-doped TiO_2 under visible light irradiation, J. Nano. Mater., 2014, 1-6, Article ID 947289.

[24] Ahmed, S., Rasul, M. G., Brown, R., Hashib, M. A. (2011) Influence of parameters on the heterogeneous photocatalytic degradation of pesticides and phenolic contaminants in wastewater: A short review, Environ, Environ. Manage., 92, 311- 330.

[25] Akpan, U. G., Hameed, B. H. (2010) The advancements in sol-gel method of doped-TiO_2 photocatalysts, Appl. Catal. A-Gen., 375, 1- 11.

[26] Zhao, G., Tian, Q., Liu, Q., Han, G. (2005) Effects of HPC on the microstructure and hydrophilisity of sol-gel-derived TiO_2 films, Surf. Coat. Tech., 198, 55- 58.

[27] Moradi, S., Aberoomand Azar, P., Raeis Farshid, S., Abedini Khorrami, S., Givianrad, M. H. (2012) Effect of additives on characterization and photocatalytic activity of TiO_2/ZnO nanocomposite prepared via sol-gel process, J. Nano. Mater., 2012, 1-5, Article ID 215373.

[28] Sava, B. A., Diaconu, A., Elisa, M., Grigorescu, C. E. A., Vasiliu, C., Manea, A. (2007) Structural characterization of the sol-gel oxide powders from the ZnO-TiO_2-SiO_2 system, Superlattices. Microst., 42, 314-321.

[29] Karthik, K., Kesava Pandian, S., Victor Jaya, N. (2010) Effect of nickel doping on structural, optical and electrical properties of TiO_2 nanoparticles by sol-gel method, Appl. Surf. Sci., 256, 6829-6833.

[30] Liao, S., Donggen, H., Yu, D., Su, Y., Yuan, G. (2004) Preparation and characterization of ZnO/TiO_2 and SO_4^{2-}/ ZnO/ TiO_2 photocatalyst and their photocatalysis, J. Photochem. Photobiol. A., 168, 7-13.

[31] Oseghe, E. O., Ndungu, P. G., Jonnalagadda, S. B. (2015) Synthesis of mesoporous Mn/TiO_2 nanocomposites and investigating the photocatalytic properties in aqueous solution, Environ. Sci. Pollut. Res., 22, 211-222.

[32] Choi, H. C., Jung, Y. M., Kim, S. B. (2005) Size effects in the raman spectra of TiO_2 nanoparticles, Vib. Spectrosc., 37, 33-38.

[33] Truijen, I., Haeldermans, I., Van Bael, M. K., Van den Rul, H., D' Haen, J., Mullens, J., Terryn, H., Goossens, V. (2007) Influence of synthesis parameters on morphology and phase composition of porous titania layers prepared via water based chemical solution deposition, J. Eur. Ceram. Soc. 27, 4537-4546.

[34] Miao, L., Tanemura, S., Toh, S., kaneko, K., Tanemura, M. (2004) Fabrication, characterization and raman study of anatase-TiO_2 nanorods by a heating-sol-gel template process, J. Cryst. Growth, 264, 246-252.

[35] Ren, D., Bei, Z., Shen, J., Cui, X., Yang, X., Zhang, Z. (2005) The structure change and the superhydrophilicity of the Sb-doped titanium dioxide thin film, J. Sol-gel. Sci. Techn., 34,123-126.

[36] Ikeda, T., Nomoto, T., Eda, K., Mizutani, Y., Kato, H., Kudo, A., Onish, H. (2008) Photoinduced dynamics of TiO_2 doped with Cr and Sb, J. Phys. Chem: C., 112, 1167- 1173.

[37] Roy, A., Komatsu, M., Matsuaishi, K., Onari, S. (1997) Raman spectroscopic studies on Sb nanoparticles in SiO_2 matrix prepared by rf-cosputtering technique, J. Phys. Chem. Solids., 58, 741-747.

[38] Guerreto-Pérez, M. O., Fierro, J. L. G., Vicente, M. A., Baňnares, M. A. (2002) Effect of Sb/V ratio and of Sb/V coverage on the molecular structure and activity of alumina-supported Sb-V-O catalysts for the ammoxidation of propane to acrylonitrile, J. Catal., 206, 339-348.

[39] Aberoomand–Azar, P., Moradi Dehaghi, S., Samadi, S., Saber Tehrani, M., Givianrad, M. H. (2011) Effect of CMC and HPC mixture on the photocatalytic activity of Nd-TiO_2/SiO_2

film under visible light irradiation, Turk. J. Chem., 35, 37-44.
[40] SÖnmezoğlu, S., Akin, S. (2013) Current transport mechanism of antimony-doped TiO_2 nanoparticles based on MOS device, Sensor. Actuat A., 199, 18-23.
[41] Shi, J. W., Zheng, J. T., Wu, P. (2009) Preparation, characterization and photocatalytic activity of holmium-doped titanium dioxide nanoparticles, J. Hazard. Mater., 161. 416-422.
[42] Xinshu, N., Sujuan, L., Huihui, C., Jianguo, Z. (2011) Preparation, characterization of Y^{3+}-doped TiO_2 nanoparticles and their photocatalytic activities foe methyl orange degradation, J. Rare. Earth., 29, 225-229.
[43] Karimi, L., Zohoori, S., Yazdanshenas, M. E. (20141) Photocatalytic degradation of azo dyes in aqueous solutions under UV irradiation using nano-strontium titanate as the nanophotocatalyst, J. Saudi. Chem. Soci.,18, 581-588.

Received: **05.08.2015**
Accepted: **07.12.2015**

CORRESPONDING AUTHOR

Shahram Moradi Dehaghi
Islamic Azad University,
Faculty of Chemistry,
Tehran North Branch,
Tehran, Iran

e-mail: shm_moradi@yahoo.com

© by PSP Volume 25 – No. 10/2016, pages 3971-3980 Fresenius Environmental Bulletin

HYBRIDIZATION OF MoO_3 WITH BN NANOSHEETS FOR IMPROVING SOLAR-LIGHT-DRIVEN PHOTOCATALYSIS

Junjie Yuan[1], Liang Liu[2], Hui Xu[2,*] Huaming Li [2]

[1]School of Agricultural Equipment Engineering, Institute of Agricultural Engineering, Jiangsu University, Zhenjiang 212013, P. R. China
[2]Institute for Energy Research, Jiangsu University, Zhenjiang 212013, P. R. China

ABSTRACT

Pure MoO_3 photocatalyst was prepared and simultaneously modified with graphene-like BN by a facile method which had attracted much attention. The samples were characterized by using X-ray diffraction (XRD), scanning electron microscopy (SEM), X-ray photoelectron spectroscopy (XPS), UV-vis diffuse reflectance spectroscopy (DRS), Fourier transform infrared spectra (FT-IR). The hybrids showed higher photocatalytic activity toward the decomposition of the RhB molecules under visible light irradiation than the pure MoO_3, and the results indicated that the optimal loading amount of graphene-like BN was 3 wt%. The results of the photocurrent and impedance analysis manifested that a small amount of graphene-like BN was beneficial for the separation of photogenerated electrons and holes, and then could enhance the photoactivity of graphene-like BN/MoO_3. Based on the experimental results, a possible visible-light photocatalytic degradation mechanism was also discussed.

KEYWORDS:
Photoactivity, MoO_3, Graphene-like BN, Degradation

INTRODUCTION

At present, a great number of researches have focused on the photodegradation of organic pollutants [1]. Semiconductor-based photocatalysis is efficient and environmentally and friendly, as it shows potential application in pollution controls [2, 3]. Among the different photocatalysts, TiO_2 has been demonstrated exactly to be the most outstanding photocatalyst for the decomposition of many organic compounds under UV irradiation. However, its relatively wide band gap (3.2 eV) and high ionic character (58%) limit its application in the visible light regions [4, 5]. Generally, in order to utilize the visible light, the band gap of the photocatalyst material should be narrow or up to 3.0 eV with a percentage ionic character ranging between 20-30% [6]. Molybdenum trioxide (MoO_3), with a band gap of 2.8-3.2 eV (analogous to TiO_2) [7], is one of the most promising n-type semiconductor photocatalysts because of its exceptional optical and electronic properties. High photocatalysis efficiency under visible light is prerequisite to the far-ranging application of MoO_3, but hindered due to some drawbacks, for instance, very poor response to visible light and the photocorrosion, which make it necessary to employ new photocatalysts to meet the requirements of future applications. So, in order to improve its photocatalytic efficiency in the practical chemical reaction process, traditional method is often used by doping with metal or metal oxide such as Ag, TiO_2 et al. [8, 9]. The improvement of photocatalytic activity can be attributed to the formation of heterostructure, but it is a pity that these photocatalysts can't achieve a wide range of practical applications due to the mixture with metal elements. So, we consider whether composite non-metal materials can also achieve the same effect.

In recent years, layered materials have intensely attracted scientific and technological attention [10], boron nitride (BN) nanomaterials, such as born nitride nanotubes and nanosheets, have exhibited remarkable properties. BN is similar to graphite in crystallographic parameters, possessing layered structure and hydrophobic nature [11], but it has some unique properties compared to graphite, such as electrical-insulating properties, a wide band gap, high stability, and good chemical inertness [12-15]. In addition, a series of reports have been released about the good performance of boron-nitride-based catalysts for photocatalytic applications. For instance, Wang et al. [11] prepared a high yield of boron nitride submicron-boxes for the degradation of MO under visible light irradiation. Tang et al. [16] improved the photocatalytic reduction of TiO_2 using the intrinsic electrostatic potential of BN nanotubes. Chen et al. [17, 18] successfully synthesized h-BN/TiO_2 and h-BN/ZnO composites under the

ball milled hexagonal BN condition, which promoted the photocatalytic activity for degradation of dye molecules. In one word, graphene-like BN is few-layer material with a large surface [19], and can change the absorption edge or restrain the recombination of photogenerated electrons (e^-) and hole (h^+) so as to improve the photocatalytic activity further.

Many of literatures have reported that graphene-like BN deposited on a metal surface can be strongly corrugated and form a nanomesh superstructure because of the mismatch between the lattice parameters of BN and metal [20-22]. Such a nanomesh is considered to be a promising template for the formation of ordered arrays of adsorbed molecules [23, 24]. Therefore, Graphene-like BN/MoO_3 composites via a facile calcination process were prepared in this work, and the effects of the loading amount of graphene-like BN on the photocatalytic degradation of RhB dyes were studied. Moreover, it verified that modification of MoO_3 with suitable proportion boron nitride was significant for reducing the rapid recombination of photogenerated electron-hole pairs that related directly to highly efficient photocatalytic activity. A possible mechanism for enhancing photocatalytic activity of graphene-like BN/MoO_3 was also proposed in this work.

EXPERIMENTAL SECTION

Sample Preparation. To prepare the graphene-like boron nitride (BN): The graphene-like BN was prepared via the method of Rao et al.[25] The typical experimental measure included boric acid/urea being dissolved in 40 mL of distilled water and heated at 65℃ until the evaporation of water was complete. The dried mixtures were heated at 900℃ for 5 h in a N_2 atmosphere.

To prepare graphene-like BN/MoO_3 hybrid materials: Obtain pure MoO_3 Sample by Calcining 3g of ammonium molybdate at 500℃ for 2h in a flowing N_2 atmosphere. Then, 0.495 g of the as-obtained MoO_3 powder and 0.005g of the graphene-like BN was first dispersed into 50 mL of ethanol by ultrasonication for 2h to form a white suspension. And the resultant suspension was at 100°C in an oven for 8h. Subsequently, the above as-obtained mixture heated at 300°C for 6h. Using this same method, different mass ratios of the graphene-like BN/MoO_3 samples were obtained and denoted as the graphene-like BN/MoO_3 (1 wt%), the graphene-like BN/MoO_3 (3 wt%) and the graphene-like BN/MoO_3 (5 wt%), respectively.

Sample Characterization. The crystal structures of the graphene-like BN/MoO_3 hybrid materials were characterized by X-ray diffraction (XRD) on a Bruker D8 diffractometer with Cu Kα radiation (λ=1.5418Å) in the range of 2θ=10-80°. The field-emission scanning electron microscopy (SEM) measurements were carried out with a field-emission scanning electron microscope (JEOL-JSM-7001F) equipped with an energy-dispersive X-ray spectroscope (EDS). Ultraviolet-visible (UV-vis) diffuse reflection spectra (DRS) were collected at room temperature with a UV-vis spectrophotometer spectrophotometer (Shimadzu UV-2450, Japan) in the range of 200-800 nm. The Fourier transform infrared spectra (FT-IR) of the samples were obtained using a Nicolet Nexus 470 spectrometer. The elemental compositions were determined using X-ray photoelectron spectroscopy (XPS) analysis, which was performed on an ESCALab MKII X-ray photo-electron spectrometer using Mg Kα radiation.

Catalytic Activity Test. The photocatalytic activity of the sample was evaluated by the degradation of RhB dye under a 300W Xe lamp with a 400 nm cutoff filter. Firstly, 0.050 g of the photocatalysts was added into 50 mL of RhB (10mg/L) in a Pyrex photocatalytic reactor. Before irradiation, the suspensions were magnetically stirred in the dark for about 30 min to ensure the establishment of an adsorption-desorption equilibrium between the surfaces of the catalysts and RhB dye. Every certain irradiation interval, 4 mL of the suspension was sampled and centrifuged to remove the photocatalyst particles. Then the filtrates was analyzed by recording variations of the absorption band maximum (553 nm) in the UV-vis spectra of RhB by using a UV-vis spectrophotometer (UV-2450 Shimadzu) with deionized water as a reference sample. The photocatalytic degradation efficiency (E) of RhB was obtained by the following formula:

$$E= (1-C/C_0) *100\%= (1-A/A_0)*100\% \quad (1)$$

Where C is the concentration of the RhB solution at the reaction time t, C_0 is the adsorption-desorption equilibrium concentration of RhB (at reaction time 0), and A and A_0 are the corresponding absorbance values. The active species generated in the photocatalytic system could be detected through trapping by tert-butyl alcohol (t-BuOH) and ethylenediaminetetraacetic acid disodium salt (EDTA-2Na).

Photoelectrochemical measurements. The photocurrents were measured with an electrochemical analyzer (CHI660B, Chen Hua Instruments, Shanghai, China). A standard three-electrode cell with a platinum wire as counter

electrode, a saturated calomel electrode (SCE) as reference electrode, and an indium-tin oxide glass (ITO) as working electrode were employed, respectively. A 500 W Xe arc lamp was utilized as the light source. A 0.1M Na_2SO_4 aqueous solution was used as the electrolyte solution. The modified electrode was prepared as follows: 20 μL of a 5.0 mg/mL graphene-like BN/MoO_3 aqueous solution was dropped onto the pretreated ITO with a 1 cm×0.5 cm area and dried in air at room temperature to form graphene-like BN/MoO_3-modified ITO (denoted as graphene-like BN/MoO_3/ITO). In a similar manner, the electrochemical impedance spectroscopy (EIS) measurements were performed. 5 mM $Fe(CN)_6^{3-}$/$Fe(CN)_6^{4-}$was used as the impedance liquid, and 5 mg graphene-like BN/MoO_3 was dispersed in the 1 mL EG solution as-prepared photocatalyst.

RESULTS AND DISCUSSION

XRD analysis. The XRD patterns of the as-prepared graphene-like BN/MoO_3 composites with various graphene-like BN contents and the pure MoO_3 were presented in Fig. 1. The diffraction peaks of the synthesized samples could be ascribed to the (002) plane of the graphene-like BN matching well with the standard data (JCPDS No. 34-0421). The diffraction peaks of pure MoO_3 appearing at 12.78º, 23.33º, 25.70º, 25.88º, 27.34º, 38.97º corresponded to (020), (110), (040), (120), (021) and (060) crystal planes (JCPDF 35-0609), respectively [26]. For the graphene-like BN/MoO_3 hybridizations, by comparing with the XRD pattern of the pure MoO_3, showed that there was no change in MoO_3 crystal structure. Moreover, neither diffraction peaks of the graphene-like BN were observed, which was due to the relatively small amount and low diffraction intensity of the graphene-like BN, nor other diffraction peaks were observed in the pattern, demonstrating that no new species were formed during the synthesis process.

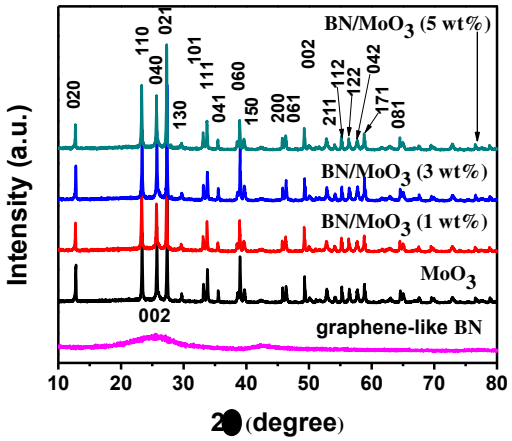

FIGURE 1
X-ray diffraction patterns of graphene-like BN, MoO3 and graphene-like BN /MoO3.

SEM analysis. Fig. 2 showed SEM images of pure MoO_3 and the graphene-like BN/MoO_3 (3 wt%). From Fig. 2A, it could be observed that MoO_3 nanocrystals were obvious bright irregular particles. From Fig. 2B, MoO_3 nanocrystals were attached mostly to the surface of graphene-like BN. The contact region was highly expected to improve the separation of photoinduced electrons and holes. Besides, comparing to pure MoO_3, the graphene-like BN/MoO_3 had a large surface. The results manifested the coexistence of graphene-like BN and MoO_3 was conducive to photocatalytic reaction.

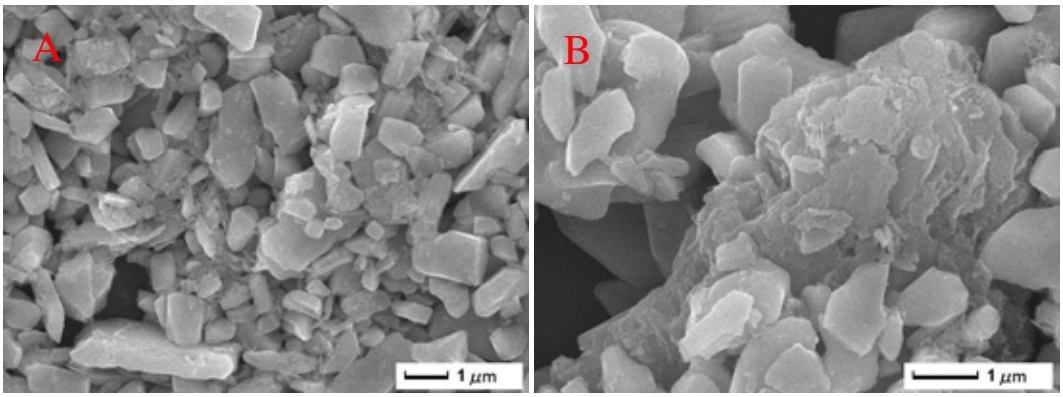

FIGURE 2
SEM images of pure MoO3 and graphene-like BN/MoO3 (A and B).

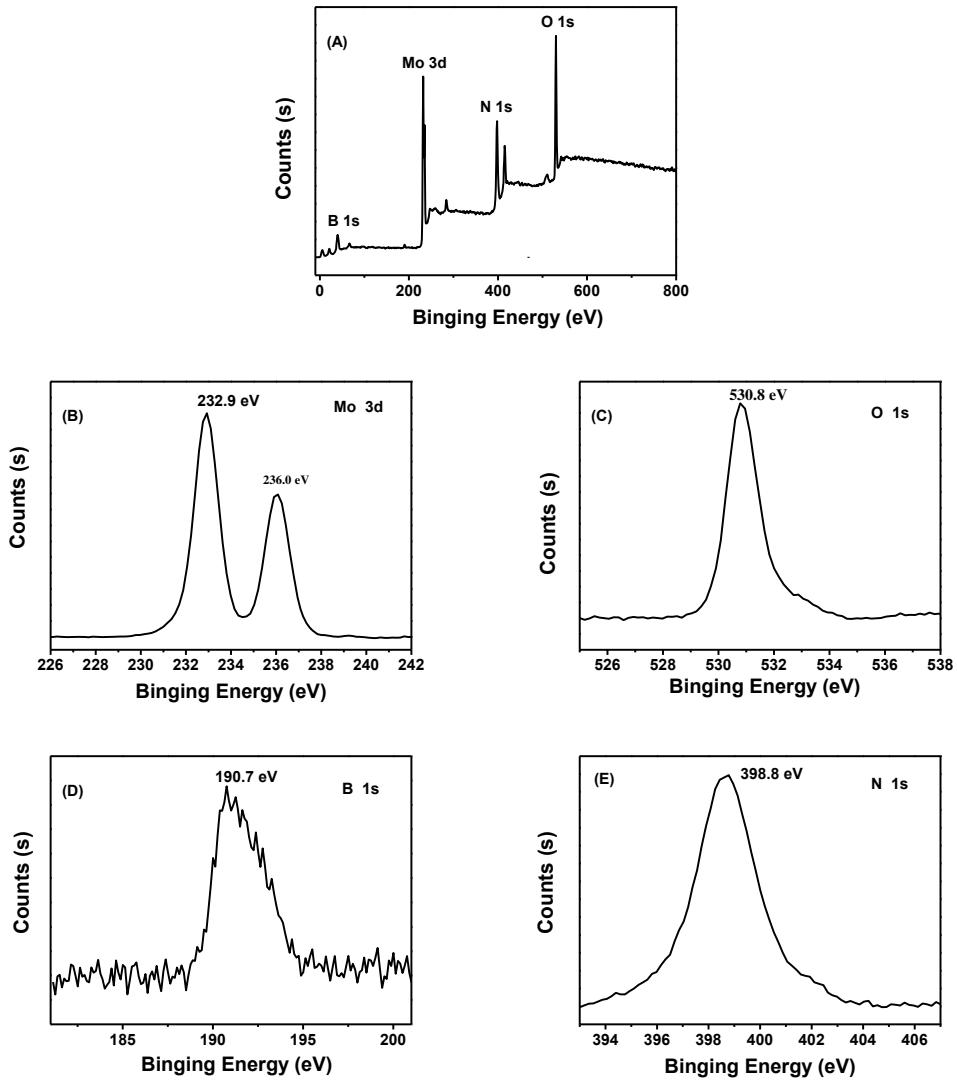

FIGURE 3
XPS spectra of the samples: (A) graphene-like BN/MoO3 (3 wt%) hybrid material, (B) Mo 3d, (C) O 1s, (D) B 1s and (E) N 1s of graphene-like BN/MoO3 (3 wt%) hybrid material.

XPS analysis. To investigate the compositions and element chemical states of the samples, XPS analysis (Fig. 3) was performed. Fig. 3A showed the XPS survey spectrum of the as-obtained graphene-like BN/MoO_3 composites (3 wt%), specifying the presence of B, N, Mo, and O elements in the samples. High resolution spectra of Mo 3d, O 1s, B 1s, and N 1s were shown in Fig. 3B-E. As depicted in Fig. 3B, the binding energy values of Mo 3d5/2 and Mo 3d5/2 were observed at 232.9 eV and 236.0 eV, respectively, which were consistent with the XPS results provided by the literatures reported for MoO_3 [27]. The O 1s peak (Fig. 3C) centering at 530.8 eV was associated with the O^{2-} in the MoO_3. Peaks of B 1s and N 1s appeared at 190.7 eV and 398.8 eV (Fig. 3 D and E), respectively, which correlated well with previously reported values for the graphene-like BN [28, 29]. On the basis of the XPS measurement, the experimental results showed that the successful preparation of graphene-like BN/MoO_3 samples.

FT-IR analysis. Fig. 4 showed the FT-IR spectra of the pure MoO_3, graphene-like BN and a series of graphene-like BN/MoO_3 photocatalysts. For the pure graphene-like BN, two main characteristic absorption bands could be observed at approximately 1378 cm^{-1} and 805 cm^{-1}. The former could be attributed to the stretching vibration of the B-N bond, while the latter belonged to the B-N-B out-of-plane bending vibrations [30]. For the pure MoO_3, three main characteristic absorption bands could be observed at approximately 607 cm^{-1},873 cm^{-1} and 992 cm^{-1}, which corresponded to O-Mo-O, Mo-O-Mo and Mo=O stretching vibration [31]. For different percentages of graphene-like BN/MoO_3, Mo-O-Mo and O-Mo-O stretching vibration absorption peaks shifted slightly in the complex

system. This phenomenon might be because of the interaction of graphene-like BN and MoO_3. As above results, indicated that graphene-like BN might not destroy but affected the MoO_3 particles. This results also manifested the heterojunction structure was formed in the composites possibly.

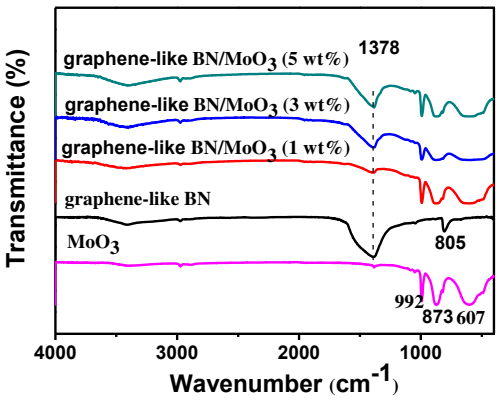

FIGURE 4
FT-IR spectra of graphene-like BN, MoO3 and graphene-like BN/MoO3.

DRS analysis. The UV-Vis diffuse reflectance spectra of the pure MoO_3 and graphene-like BN/MoO_3 photocatalysts were revealed in Fig. 5A. The absorption bands of all the samples were located at approximately 200-800 nm. It could be seen that the absorption edge of pure MoO_3 was determined to be 420 nm (Eg =2.92 eV). The optical absorption of graphene-like BN/MoO_3 (3 wt%) in the visible-light region was significantly enhanced. The red shift of the absorption wavelength indicated that the photocatalysts could absorb more visible light and produce more electron-hole pairs, which would be favorable for a photocatalytic reaction.

Photocatalytic activity. As observed in Fig. 6A, the photoactivities of graphene-like BN/MoO_3 materials were evaluated by degradation of RhB dye in aqueous solution under visible-light irradiation. The results confirmed that degradation without a catalyst didn't occur, indicating that RhB was a stable molecule and the photolysis could be ignored. It was apparent that all the graphene-like BN/MoO_3 exhibited much higher photocatalytic activity than that of pure MoO_3. Additionally, the amount of graphene-like BN had a crucial effect on the photocatalytic activity of the composite. As the graphene-like BN content increased to 3 wt%, the highest photocatalytic activity was achieved, and 62% of RhB was removed after 50 min irradiation. However, the pure MoO_3 could degrade RhB by 22% under the same conditions. When further increasing the content of the graphene-like BN (5 wt%) led to decreasing degradation efficiency of RhB under the same conditions. This result was attributed to excess graphene-like BN might cover part of the active site of MoO_3. By comparison, the photocatalysts of Degussa P25 was obtained under the same conditions. It could be observed that P25 exhibited almost no photocatalytic activity for degradation of RhB after 50 min irradiation.

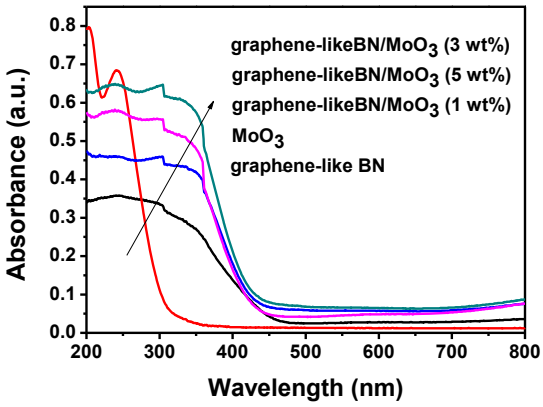

FIGURE 5
UV-vis diffuse reflectance spectra of graphene-like BN/MoO3 hybrid materials (A).

The evolution of the absorption spectra of RhB with reaction time was shown in Fig. 6C-D. The absorption of RhB decreased steadily as the reaction proceeded, and the color of the RhB solution changed from rose to and light rose. In addition, the absorption peak of RhB became weaker in the case of graphene-like BN/MoO_3 hybrids, which indicated that the chromophoric structure of the RhB dye was decomposed.

Kinetics. To quantitatively investigate the reaction kinetics of the RhB degradation, the experimental data were fitted by a first-order model as expressed by the formula:

$$-\ln (C/C_0) = kt \quad (3)$$

Where C_0 and C are the dye concentrations in solution at times 0 and t, respectively, and k is the apparent first-order rate constant. Fig. 6B shows the pseudo-first-order rate constants (k) for RhB degradation with pure MoO_3 and different proportions of the graphene-like BN/MoO_3 composites under visible light irradiation, and the corresponding kinetic constants (k) and regression coefficients (R^2) were calculated and are listed in Table 1. In the graphene-like BN/MoO_3 system, the corresponding degradation rate constants (k) were estimated to be 0.00451 min^{-1}, 0.00809 min^{-1}, .

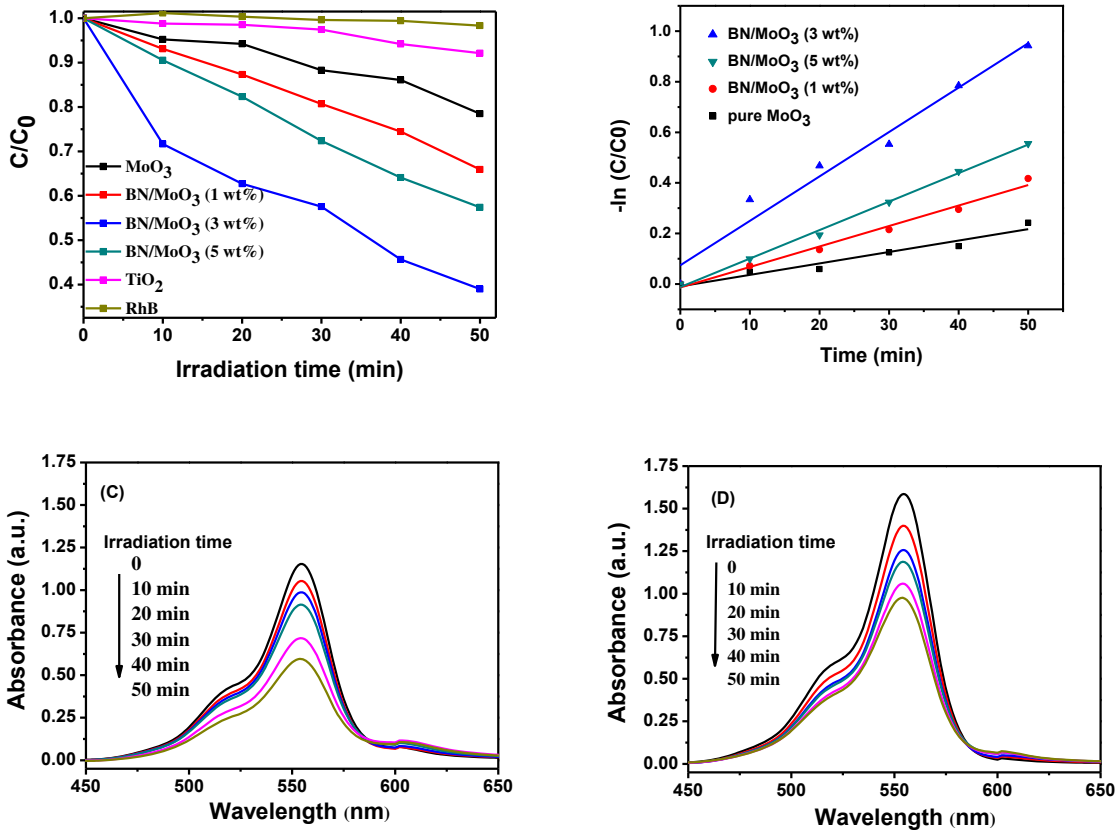

FIGURE 6
Photocatalytic degradation of RhB by pure MoO3 (C) and graphene-like BN/MoO3 hybrids (3 wt%) (D) under visible light irradiation.

0.01757 min^{-1} and 0.01127 min^{-1}, respectively. Besides, the rate constant of the graphene-like BN/MoO_3 (3 wt%) photocatalyst was 3.9 times as high as that of pure MoO_3.

TABLE 1
Kinetic constants and regression coefficients of RhB degradation under visible light irradiation

sample	kinetic constant	R^2
MoO_3	0.00451	0.93853
BN/MoO_3 (1 wt%)	0.00809	0.98431
BN/MoO_3 (3 wt%)	0.01757	0.96238
BN/MoO_3 (5 wt%)	0.01127	0.99683

Photocurrent analysis. The separation efficiency of electrons and holes playing a crucial role in the photocatalytic system was widely accepted [32]. In order to evaluate the electronic interaction between the graphene-like BN and pure MoO_3, photocurrents were measured for pure MoO_3 and graphene-like BN/MoO_3 (3 wt%) electrodes. The results were presented in Fig. 7A. It could be found that the pure MoO_3 exhibited a weak photocurrent response. On the contrary, the graphene-like BN/MoO_3 hybrid materials exhibited a dramatical photocurrent under visible light irradiation, which was 3.9 times as high as that of pure MoO_3. This result could be attributed to the synergetic effect in hybridization.

EIS analysis. EIS measurement was employed to investigate the charge transfer resistance and the separation efficiency between the photogenerated electrons and holes. From Fig. 7B, it could be seen that the diameter of the Nyquist circle of the graphene-like BN/MoO_3 (3 wt%) composite was smaller than that of pure MoO_3. It indicated that the graphene-like BN/MoO_3 (3 wt%) composite had lower resistance than that of MoO_3. This result demonstrated that the introduction of graphene-like BN into MoO_3 could enhance the separation and transfer efficiency of photogenerated electron-hole pairs. Thus, the EIS result further supported that

loading with graphene-like BN facilitates the charge separation.

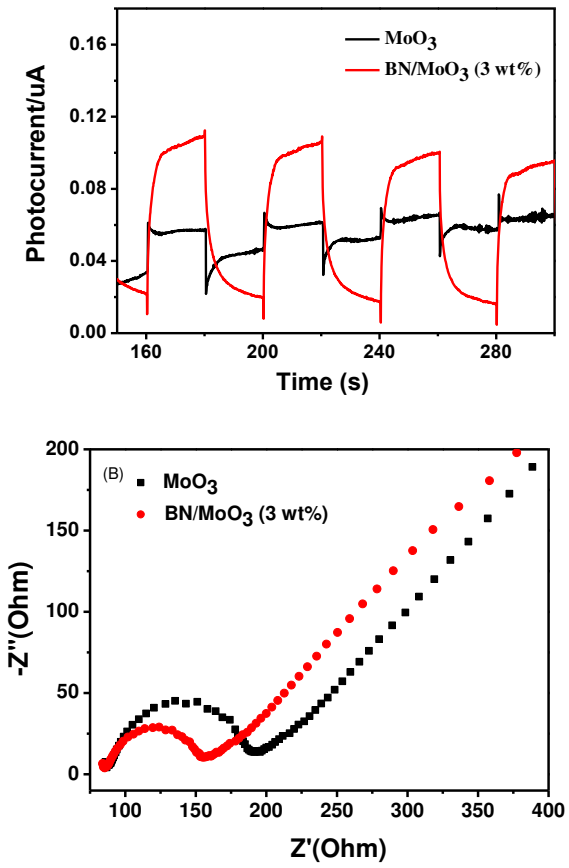

FIGURE 7
Transient photocurrent responses and the electrochemical impedance spectra of MoO3 and graphene-like BN/MoO3 (3 wt%) observed under visible light irradiation(A and B).

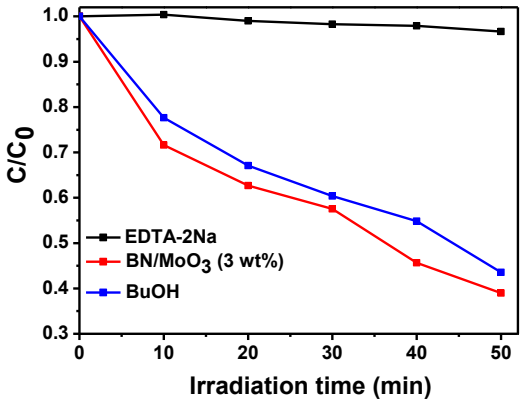

FIGURE 8
Plots of photogenerated carriers trapping in the BN/MoO3.

Possible photocatalytic mechanism. Photocatalytic activity was affected by some crucial factors, such as the phase structure, optical absorption, adsorption ability, and separation efficiency of photogenerated electrons and holes. It was imperative to detect the main oxidative species in the photocatalytic process, which could be detected through the trapping experiments of radicals and holes using t-BuOH (radical scavenger) [34] and EDTA-2Na (hole scavenger) [35], respectively. The trapping experiments of radicals and holes were only performed on graphene-like BN/MoO_3 (3 wt%) photocatalyst. From Fig. 8, it can be observed that the photodegradation of RhB was obviously suppressed after the injection of EDTA-2Na. But the addition of t-BuOH had no effect on graphene-like BN/MoO_3 (3 wt%) photocatalyst. This result suggested that holes were the main oxidative species in this system.

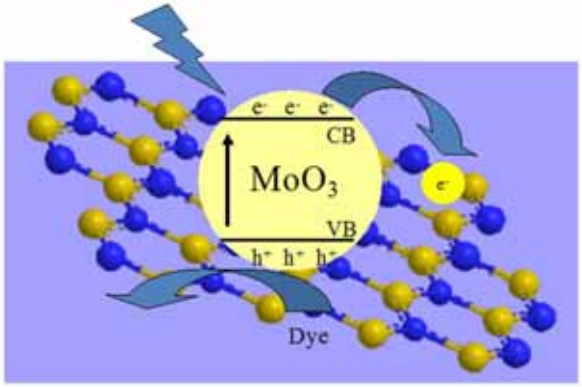

FIGURE 9
Proposed mechanism for the photodegradation of RhB on BN/MoO3 composites.

According to these discussions, the possible reasons for the prominent photocatalytic activity of graphene-like BN/MoO_3 (3 wt%) were as follows: Firstly, the graphene-like BN interaction with MoO_3 lead to passivation surface barrier, reduce the surface energy, and then effectively restrain the recombination of electron-hole pairs[36]. Secondly, the hydrophobic property of graphene-like BN makes RhB concentrate around the MoO_3 nanoparticles. This good contact is beneficial to enhance the photocatalytic efficiency of graphene-like BN/MoO_3. Moreover, a similar mechanism about the Cu_2O/h-BN [37], h-BN/TiO_2 [38], h-BN/ZnO [18], BN/CdS [39] and other materials has also been put forward. Based on the analysis of the above, the graphene-like BN/MoO_3 photocatalysts exhibit a high photocatalytic activity under visible light irradiation. The reason for this behavior may be attributed to synergetic effect between graphene-like BN and pure MoO_3. The possible mechanism of the visible light activity of BN/MoO_3 is proposed and illustrated in Fig. 9.

CONCLUSION

In the summary, novel graphene-like BN/MoO_3 hybridization photocatalysts via a calcination method has been prepared. The hybridization displays an enhancement of photocatalytic activity, which induced 62% degradation of RhB within 50 min under visible light irradiation, while pure MoO_3 only induced 22% in the same conditions. The enhanced photocatalytic activity is attributed to the synergy effect between graphene-like BN and pure MoO_3, which was beneficial for suppressing the combination of photogenerated electrons and holes.

ACKNOWLEDGEMENTS

The authors genuinely appreciate the financial support of this work from the National Nature Science Foundation of China. The authors genuinely appreciate the financial support of this work by the National Nature Science Foundation of China (21476097, 21476098 , 21407065 and 21406094), the Natural Science Foundation of Jiangsu Province (BK20131207 and BK2012717, BK20140533).

REFERENCES

[1] Hoffmann, M.R., Martin, S.T., Choi, W., Bahnemann, D.W. (1995) Environmental applications of semiconductor photocatalysis. Chemical Reviews. 95, 69-96.

[2] Aarthi, T., Narahari, P., Madras, G. (2007) Photocatalytic degradation of Azure and Sudan dyes using nano TiO2. Journal of Hazardous Materials. 149, 725-734.

[3] Cui, W.Q., Liu, Y.F., Liu, L., Hu, J.S., Liang, Y.S. (2012) Microwave-assisted synthesis of CdS intercalated K4Nb6O17 and its photocatalytic activity for hydrogen production. Applied Catalysis A. 417, 111-118.

[4] Kazuya, N., Tachikawa, T., Fujitsuka, M. and Majima, T. (2009) Photoreactivity of As-Fabricated Au Clusters at the Single-Cluster Level. Journal of the American Chemical Society. 131, 934-936.

[5] Issac, A., Jin, S., Lian, T. (2008) Intermittent electron transfer activity from single CdSe/ZnS quantum dots. Journal of the American Chemical Society. 130, 11280-11281.

[6] Mahesh, G., Viswanathan, B., Viswanath, R.P. and Varadarajan, T.K. in the book (2007) Photoelectrochemistry and photobiology in the environment energy and Fuel. 11, 321-358.

[7] Shakir, I., Shahid, M. and Kang, D.J. (2010) MoO3 and Cu0.33MoO3 nanorods for unprecedented UV/Visible light photocatalysis. Chemcial Communications. 46, 4324-4326.

[8] Gao, H., He, G., Wei, M., Yu, X., Huo, P., Wang, D., Cao, K., Li, S., Yan, Y. (2013) Effect of silver doped into MoO3 photocatalyst on degration of methylene blue. Fresen. Environ. Bull.. 22, 2682-2688.

[9] Da, Z., Huo, P., Wang, H., Yan, Y., Pan, J., Li, H., Wu, X., Huang, W. (2011) Preparation of MoO3/TiO2/fly-ash cenosphere photocatalysts and photocatalytic decolorization of methylene blue solution under visible light. Fresen. Environ. Bull.. 20, 2179-2186.

[10] Neto, A.H.C., Novoselov, K. (2011) New directions in science and technology: two-dimensional crystals. Reports on Progress in Physics. 74, 82501-82509.

[11] Wang, M., Li, M., Xu, L., Wang, L., Ju, Z., Lia, G. and Qian, Y. (2011) High yield synthesis of novel boron nitride submicro-boxes and their photocatalytic application under visible light irradiation. Catalysis Science & Technology. 1, 1159-1165.

[12] Wu, J., Han, W.Q., Walukiewicz, W., Ager III, J.W., Shan, W., Haller, E.E. and Zettl, A. (2004) Raman spectroscopy and time-resolved photoluminescence of BN and BxCyNz nanotubes. Nano Letters. 4, 647-650.

[13] Watanabe, K., Taniguchi, T. and Kanda, H. (2004) Direct-bandgap properties and evidence for ultraviolet lasing of hexagonal boron nitride single crystal. Nature Materials. 3, 404-409.

[14] Kubota, Y., Watanabe, K., Tsuda, O. and Taniguchi, T. (2007) Deep ultraviolet light-emitting hexagonal boron nitride synthesized at atmospheric pressure. Science, 317, 932-934.

[15] Macnaughton, J.B., Moewes, A., Wilks, R.G., Zhou, X.T., Sham, T.K., Taniguchi, T., Watanabe, K., Chan, C.Y., Zhang, W.J., Bello, I. and Lee, S.T. (2005) Electronic structure of boron nitride single crystals and films. Physical Review B. 72, 195113.

[16] Tang, C.C., Li, J.G., Bando, Y., Zhi, C.Y., Golberg, D. (2010) Improved TiO2 photocatalytic reduction by the intrinsic electrostatic potential of BN nanotubes. Chemistry-An Asian Journal. 5, 1220-1224.

[17] Fu, X.L., Hu, Y.F., Yang, Y.G., Liu, W., Chen, S.F. (2013) Ball milled h-BN: an efficient holestransfer promoter to enhance the photocatalytic performance of TiO2. Journal of Hazardous Materials. 244, 102-110.

[18] Fu, X.L., Hu, Y.F., Zhang, T., Chen, S.F. (2013) The role of ball milled h-BN in the enhanced photocatalytic activity: a study based on the model of ZnO. Applied Surface Science. 280, 828-835.

[19] Grad, G.B., Blaha, P., Schwarz, K., Auwärter, W., Greber, T. (2003) Density Functional Theory Investigation of the Geometric and Spintronic Structure of h-BN/Ni (111) in View of Photoemission and STM Experiments. Physical Review B. 68, 085404.

[20] Lin, Y., Connell, J.W. (2012) Advances in 2D Boron Nitride Nanostructures: Nanosheets, Nanoribbons, Nanomeshes, and Hybrids with Graphene. Nanoscale. 4, 6908-6939.

[21] Corso, M., Auwarter, W., Muntwiler, M., Tamai, A., Greber, T., Osterwalder, J. (2004) Boron Nitride Nanomesh. Science. 303, 217-220.

[22] Vinogradov, N.A., Zakharov, A.A., Ng, M.L. Mikkelsen, A., Lundgren, E., Martensson, N., Preobrajenski, A.B. (2012) One-Dimensional Corrugation of the h-BN Monolayer on Fe (110). Langmuir. 28, 1775-1781.

[23] Yazyev, O.V., Pasquarello, A. (2010) Metal Adatoms on Graphene and Hexagonal Boron Nitride: Towards Rational Design of Self-Assembly Templates. Physical Review B. 82, 045407.

[24] Koch, H. P., Laskowski, R., Blaha, P., Schwarz, K. (2012) Adsorption of Small Gold Clusters on the h-BN/Rh (111) Nanomesh. Physical Review B. 86, 155404.

[25] Nag, A., Raidongia, K., Hembram, K.P.S.S., Datta, R., Waghmare, U.V., Rao, C.N.R. (2010) Graphene analogues of BN: novel synthesis and properties. ACS Nano. 4, 1539-1544.

[26] Chen, Y.P., Lu, C.L., Xu, L., Ma, Y., Hou, W., Zhu, J.J. (2010) Single-crystalline orthorhombic molybdenum oxide nanobelts: synthesis and photocatalytic properties. Crystengcomm. 12, 3740-3747.

[27] Teng, Y., Wang, A.Y., Li, X., Xie, J., Wang, Y., Hu, Y. (2009) Preparation of high-performance MoP hydrodesulfurization catalysts via a sulfidation-reduction procedure. Journal of Catalysis. 266, 369-379.

[28] Ci, L., Song, L., Jin, C., Jariwala, D., Wu, D.X., Li, Y.J., Srivastava, A., Wang, Z.F., Storr, K., Balicas, L. (2010) Atomic layers of hybridized boron nitride and graphene domains. Nature Materials. 9, 430-435.

[29] Nazarov, A.S., Demin, V.N., Grayfer, E.D., Bulavchenko, A.I., Arymbaeva, A.T., Shin, H.J., Choi, J.Y., Fedorov, V.E., (2012) Functionalization and dispersion of hexagonal boron nitride (h-BN) nanosheets treated with inorganic reagents. Chemsity -An Asian Journal. 7, 554-560.

[30] Song, L., Ci, L., Lu, H., Sorokin, P.B., Jin, C.H., Ni, J., Kvashnin, A,G., Kvashnin, D.G., Lou, J., Yakobson, B.I. (2010) Large scale growth and characterization of atomic hexagonal boron nitride layers. Nano Letters. 10, 3209-3215.

[31] Sinaim, H., Ham, D.J., Lee, J.S., Phuruangrat, A., Thongtem, S., Thongtem, T., (2012) Free-polymer controlling morphology of alpha-MoO3 nanobelts by a facile hydrothermal synthesis, their electrochemistry for hydrogen evolution reactions and optical properties. Journal Alloys and Compounds. 516, 172-178.

[32] Jiang, J., Zhang, X., Sun, P.B., Zhang, L.Z., (2011) ZnO/BiOI heterostructures: photoinducedcharge-transfer property and enhanced visible-light photocatalytic activity. Journal of Physical Chemistry C. 115, 20555-20564.

[33] Xiang, Q.J., Yu, J.G., Jaroniec, M., (2011) Preparation and enhanced visible-light photo-catalytic H2-production activity of graphene/C3N4 composites. Journal of Physical Chemistry C. 115, 7355-7363.

[34] Lee, H., Choi, W. (2002) Photocatalytic oxidation of arsenite in TiO2 suspension: kinetics and mechanisms. Environmental Science and Technology. 36, 3872-3878.

[35] Zhou, J.H., Deng, C.Y., Si, S.H., Shi, Y., Zhao, X.L. (2011) Study on the effect of EDTA on thephotocatalytic reduction of mercury onto nanocrystalline titania using quartzcrystal microbalance and differential pulse voltammetry. Electrochimica Acta. 56, 2062-2067.

[36] Shanmugam M., Jacobs-Gedrim R., Durcan, C., Yu, B. (2013) 2D layered insulator hexagonal boron nitride enabled surface passivation in dye sensitized solar cells. Nanoscale. 5, 11275-11282.

[37] Huang, C.J., Ye, W.Q., Liu, Q.W., Qiu, X.Q. (2014) Dispersed Cu2O octahedrons on h-BN nanosheets for p-nitrophenol reduction. Applied Materials Interfaces. 6, 14469-14476.

[38] Fu, X.L., Hu, Y.F., Yang. Y.G., Liu, W., Chen, S.F. (2013) Ball milled h-BN: an efficient holes transfer promoter to enhance the photocatalytic performance of TiO2. Journal of Hazardous Materials. 244, 102-110.

[39] Zhang, R.Z., Wang, J., Han, P. (2015) Highly efficient photocatalysts of Pt/BN/CdS constructed by using the Pt as the electron acceptor and the BN as the holes transfer for H2-production. Journal Alloys and Compounds. 637, 483-488.

Received: **28.08.2015**
Accepted: **26.12.2015**

CORRESPONDING AUTHOR

Hui Xu
Institute for Energy Research, Jiangsu University, Zhenjiang 212013, P. R. China

E-mail address: xh@ujs.edu.cn

© by PSP Volume 25 – No. 10/2016, pages 3981-3986 Fresenius Environmental Bulletin

EFFECTS OF BENSULFURON-METHYL ON CELL MORPHOLOGY OF *A.AZOTICA*

Li Li.Guo[1], Jin Zhi. Liao[1], Jian Ying. Shen[1*], Qiu Guang. Shen[2]

[1] Department of Environmental Science and Resource, Shanghai Jiaotong University, Shanghai
[2] Agricultural Productor Quality and Safety Testing Center of Shanghai

ABSTRACT

Application of bensulfuron-methyl produced a stimulative effect on growth and heterocyst formation at low concentrations but an inhibition effect at high concentrations. Presence of the sulfonylurea herbicide bensulfuron-methyl at 0.001 to 10 mg/L affected the growth and cell morphology of the nitrogen-fixing cyanobacteria (*Anabaena azotica*), high concentration of bensulfuron-methyl (1 mg/L and 10 mg/L) obviously inhibited the growth of *A.azotica*, especially vegetative cells and heterocyst. And at the same time lots of cell disintegrated and inclusions dissolved. Presenting in 0.001 to 0.1 mg/L, the effect of bensulfuron-methyl on cell morphology was not significant. Cells can grow well and vegetative cell and heterocyst number increased notly. Our findings support the view that low concentrations stimulate growth and cell maintain good morphological structure while high dose inhibited.

KEYWORDS:
A.azotica, Bensulfuron-methyl, Cell morphology, Heterocyst, Vegetative cells

INTRODUCTION

Nitrogen is a very rich element in the nature, but due to the fact that free forms of ammonia nitrogen in the air is quite stable, it cannot be used by the vast majority of plants directly. Nitrogen-fixing cyanobacteria is a kind of high nitrogen-fixing quantity organism, it can simultaneously make photosynthesis and nitrogen fixation [1]. It is prokaryote, breeding on the basis of cell division and contains heterocyst. Nitrogen-fixing cyanobacteria continuously produce amino acids, sugars, peptides and small amounts of hormone and other nitrogen compounds and active substances during the growing process [2]. In addition, nitrogen-fixing cyanobacteria can release a large amount of ammonia nitrogen after death, which greatly increased the soil fertility [3, 4].

Heterocyst is a unique nitrogen fixing cell of some certain filamentous cyanobacteria, a major place for nitrogen fixing, and they are differentiated from some vegetative cells of cyanobacteria. In a lot of cyanobacteria, heterocyst arranged in a certain interval in filaments and they linked together with the vegetative cells by plasmodesmata which exist at the micro and exchange material [5].

Anabaena azotica is a beneficial cyanobacteria without toxins, it can improve soil fertility by fixing nitrogen from atmosphere and was widely used in the weed control and clean energy [6]. Bensulfuron-methyl (3-(4,6-dimethoxy pyrimidine-2-base)-1-(2-methoxy methyl benzyl) sulfonylurea)) is a sulfonylurea herbicide, which is widely used in agriculture for nearly 30 years [7]. Sulfonylurea herbicides destruct the synthesis of valine, leucine and isoleucine by inhibiting the acetolactate synthase in plants, thereby inhibiting protein synthesis, hinder cell division, and eventually lead to the death of plants [8]. Long-term usage of sulfonylurea herbicide has caused serious effect on *A.azotica* [9].

The study showed that high dose herbicide significantly inhibited growth, photosynthesis and nitrogenase activity of three kinds of nitrogen-fixing cyanobacteria, and low concentration sometimes stimulate growth [10]. The research for toxicity of bensulfuron-methyl to *A.azotica* addressed that low dose concentration improved growth (for instance, cell numbers, photosynthetic pigments and so on) while high dose inhibited [11,12]. Bensulfuron-methyl has effect on antioxidant enzyme activity of *A.azotica* during different concentrations of herbicide [13]. But the influence of herbicide on cell morphology was not reported. So we conducted the research of bensulfuron-methyl on cell morphology and vegetative cells and heterocyst of *A.azotica*.

MATERIALS AND METHODS

Bensulfuron-methyl was provided by Jiangsu Kuaida Agrochemical Co., Ltd. and was dissolved in a mixture of double distilled water. The fresh concentrate was sterilized and added to the culture medium to result in the final desired bensulfuron-methyl concentrations. *A.azotica* was obtained from the Institute of Hydrobiology of the Chinese Academy of Sciences in Wuhan, China. Axenic cultures were grown in a liquid medium (Aquatic 111) pH 7.2 at 32℃ under constant fluorescent light at an intensity of 36.8 μmol/m^2/s. Aquatic 111 consists of $MgSO_4$ (0.125g/L)、$CaCO_3$ (0.1g/L)、NaOH (1.5ml/L)、Molybdate (5 drops/L)、Citric acid (0.5ml/L)、Citric acid iron (0.5ml/L)、K_2HPO_4 (0.075g/L) and so on [14]. Cultures were grown in 250 mL flasks containing 100 mL culture medium and 0.5 million cells/ml. Continuous training 1-2d at full illumination to adapt to grow well and then added the concentrate to the culture medium to result in 0.001, 0.01, 0.1, 1 and 10mg/L bensulfuron-methyl in the test samples. Control experiment was carried out using sterilize water.

Samples was suspended in 1 mL sterilized water and centrifuged at 12,000 g for 1 min. The supernatant was discarded and the cells were washed twice with 1 ml sterilized water. Cells were suspended in 1 mL sterilized water and 10 μL of the cell suspension was spotted onto a cover glass. Then the cell morphology of *A.azotica* was observed using optical microscope (400X). And take photos of cell structure. Transmission electron microscopy (sem) specimens were made as follows:

1) Sampling: Sucking up 10 mL from the culture medium and added to the test tube.

2) Fixing: Using 2.5% glutaraldehyde and phosphate to fixation for about 2h or more; and 0.1Mphosphorus acid bleaching lotion rinsing for 15min; and 0.1M phosphoric acid bleaching lotion rinsing for 15min.

3) Dehydrating: 50% ethanol dehydration for 15-20 minutes; 70% alcohol for 15 to 20 minutes; 90% ethyl alcohol for 15 to 20 minutes; 90% acetone + 90% ethanol (1:1) for 15-20 minutes; 90% acetone dehydration for more than 15-20 minutes, all above are conducted in 4℃ freezer; 100% acetone for 15 to 20 minutes at room temperature.

4) Soaking and embedding: Pure acetone + embedding fluid (2:1) for 3 to 4 hours at room temperature; Pure acetone + embedding fluid (1:2) at room temperature for all night; Pure embedding liquid at 37 degrees for 2-3 hours.

5) Slicing: Ultra-thin microtome sliced for 50-60nm.

6) Dyeing: 3% acetic acid uranium - lead citrate double staining

7) Observing: Transmission electron microscopy (11000X, 60000X)

Various cell numbers were obtained using cyanobacterial cell counting method and analyzed using ANOVA. Significant differences were determined using Duncan's test at a significance level of $p = 0.05$ (PROC GLM; SAS; Origin).

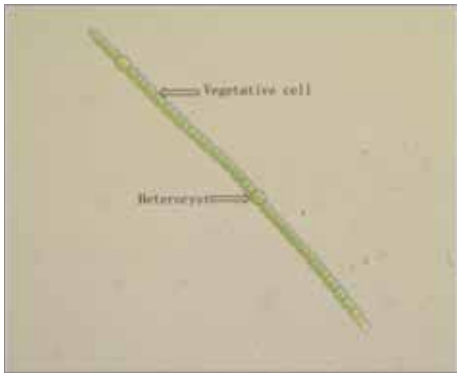

FIGURE 1
The vegetative cell, heterocyst of A. azotica (×400)

RESULTS

A. Normal morphological characteristics of *A.azotica*

A.azotica, belongs to *Cyanophyceae*, *Nostocaceae*, *Anabaena.* Its filaments arrange closely in the colloid. *A.azotica* can differentiate into vegetative cells and heterocyst (Fig.1). A single cyanobacteria body is 2.5-7.3μm long and 2.3-5.6μm wide, vegetative cells contain uniform particles. Heterocyst is differentiated from vegetative cell, to be larger and more transparent than vegetative cells. Cyanobacteria filament includes one or more heterocyst, which is the key place for biological nitrogen fixation and don't contain chlamydospore. Vegetative cells provide regular growth for *A.azotica* and cover transparent colloid substances on the periphery which is called colloid sheath. The colloid sheath is the natural barrier of cells to resist external environment damage caused by stress.

Fig.2 and Fig.3 illustrate the ultrastructure of vegetative cell and heterocyst of *A.azotica*. The vegetative cell has a three-layer structure (Fig.2). The inner layer is composed of cellulose. The middle and outer layer are made of pectic substances. From outer to inner, the color gradually deepened. The membrane structure is complete and distinct. No real nucleus, nuclear membrane and nucleolus, in the central area with karyoplasm. Cells have no chromatophore and pigments dispersion in the cytoplasm, including chlorophyll, lutein, carotene and phycocyanobilin, etc.

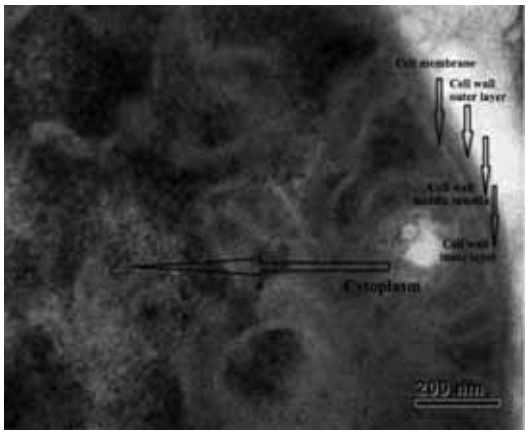

FIGURE 2
The vegetative cell of *A. azotica* (×60000)

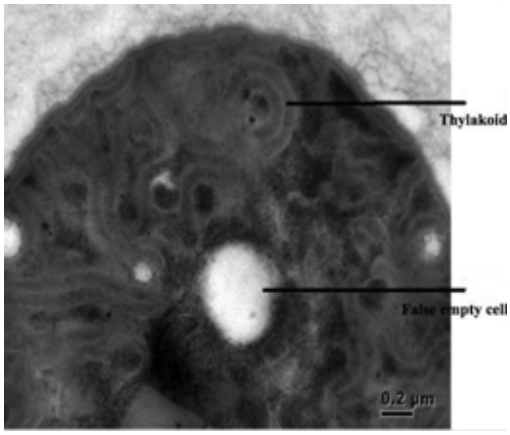

FIGURE 3
The heterocyst of *A. azotica* (×60000)

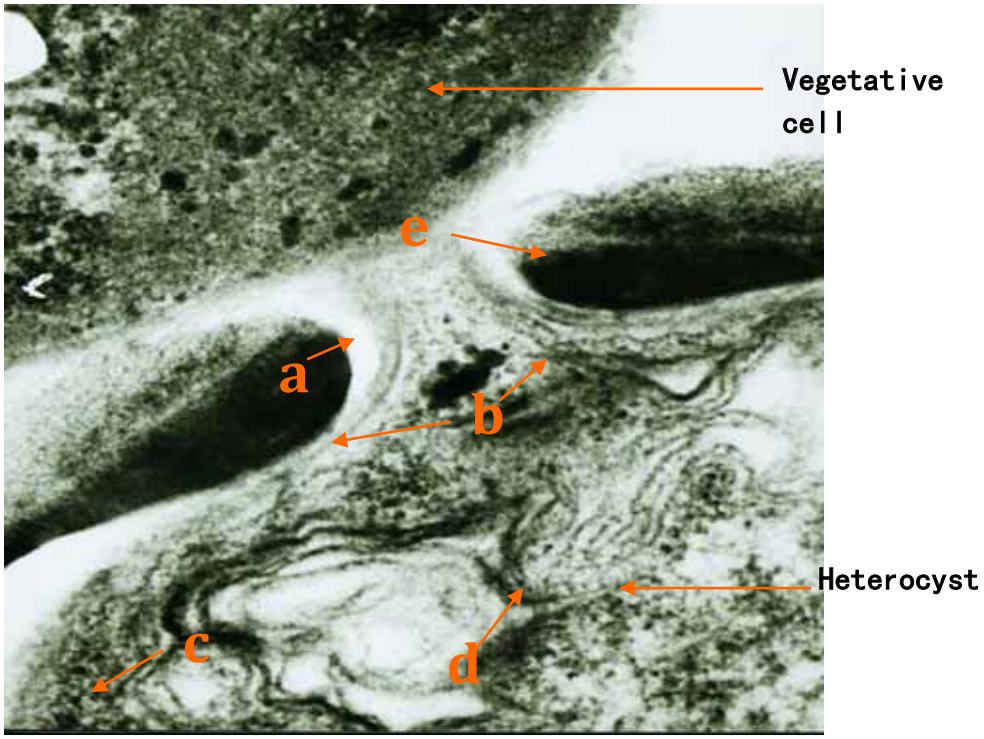

FIGURE 4
Ultrastructure of cellular linkage between heterocyst and vegetative cell (10.5k×)
a) Cell orifice b) Layered layer c) Cytoplasm wall d) Thylakoids e) Homogeneous matter

Interestingly, the heterocyst of *A.azotica* has extremely abundant thylakoid structure (Fig.3), and its numbers are obviously more than that of vegetative cells. They are arranged like a mesh and focused on the poles and formatting a typical semi crystalline lattice structure. In the middle of the cell, a larger false empty cell (also called bubbles) formed, with the effect of regulating buoyancy.

Fig.4 depicted the connected vegetative cell and heterocyst. In the central section of heterocyst possess a copolymer which is made up of arginine and aspartic, and also have pore canal, plasmodesmata and the adjacent vegetative cell.

Under the suitable condition of light, moisture and nutrition (no external environmental stress), *A.azotica* grow well. Vegetative cells and heterocyst are full, and the inclusions of vegetative cells are clear, and the color is green. Cell has a vigorous vitality.

B. The damaged (added different concentrations of bensulfuron-methyl) morphological characteristics of *A.azotica*

Low concentration (0.001-0.1 mg/L) of bensulfuron-methyl has no significant effect on cell morphology of *A.azotica* and cyanobacteria cells grow well and present a good status.

Bensulfuron-methyl doesn't affect the growth of vegetative cell and heterocyst of *A.azotica* after applying, moreover, that is the low dose herbicide as exogenous nutrient supply the cell growth.

But high concentration (1 mg/L and 10 mg/L) bensulfuron-methyl significantly affect the growth of both vegetative cells and heterocyst of *A.azotica*. Cyanobacteria cells constantly etiolation, death, disintegration and so on. Compared with normal cells, cells grow severely malnourished and there are lots of cellular debris around cyanobacteria filaments. At 10d all cells completely disintegrated. High dose bensulfuron-methyl accelerated the etiolation and death of *A.azotica,* leading to the reduction of heterocyst, shorter and irregular of filaments, the smaller of cells.

Observe the cyanobacteria cell morphology under the electron microscope, plasmodesmata of vegetative cell disappeared. Cells became into a single individual, with wall structure damaged and the pseudo empty cells increased. And the reticular formation in the heterocyst ceased to exist, cell inclusions shows irregular filiform, and internal structure damaged. Pseudo empty cell disappeared, lacking of cell membrane, with cell inclusion partly flew out and gelatinous sheaths damaged.

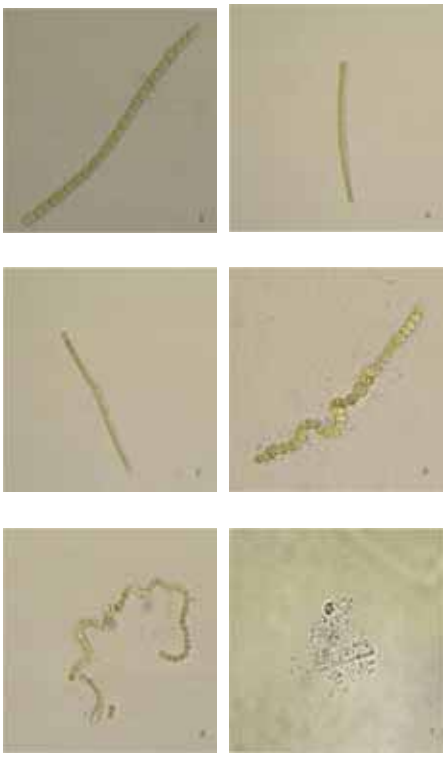

FIGURE 5
Effect of bensulfuron-methyl on vegetative cell and heterocyst of *A.azotica* (X400) a, b, c, d, e and f represent the concentration of 0.001mg/L, 0.01mg/L, 0.1mg/L, 1mg/L, 10mg/L bensulfuron-methyl and 10mg/L bensulfuron-methyl after 10d treatment

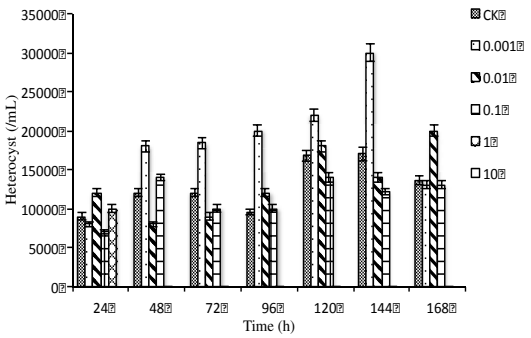

FIGURE 6
Changes of heterocyst numbers of *Anabaena azotica* under different bensulfuron-methyl

C. The number of heterocyst and etiolation of *A.azotica*

Heterocyst is the key of biological nitrogen fixation of *A.azotica*. Differentiated from normal vegetative cells, the numbers of cellular changes directly represent the dynamic state of *A.azotica*. Different concentrations of bensulfuron-methyl on cyanobacteria heterocyst number of *A.azotica* is shown in fig.6, high concentration of bensulfuron-methyl inhibit the formation of heterocyst in the culture cycle, only 1 mg/L bensulfuron-methyl stimulate a small amount of heterocyst at 24h, then the number of heterocyst rapidly decreased. Under 10 mg/L treatment that observed a little existence of heterocyst. All these proved that high concentration of bensulfuron-methyl significantly inhibited the differentiation characteristics of vegetative cell, leading to its unable to form heterocyst, make it have a low or no nitrogen fixation activity.

Low concentration of bensulfuron-methyl (0.001to 0.1 mg/L) had an impact on the heterocyst number of *A.azotica*, heterocyst number present a wave change of decreasing after rising first and then increased again. The heterocyst number increased 11%-33% compared with control at 24h under low concentrations (0.001to 0.1 mg/L); At 72h, 0.001 mg/L heterocyst quantity increased 53%, and heterocyst quantity is restrained at 168h, the inhibition rate is 4%. In general, low concentration of bensulfuron-methyl did not significantly affect the heterocyst number of *A.azotica*, even in the early stage of culture, promoting the formation of heterocyst, and stimulating the ability of nitrogen fixation.

Different concentrations of bensulfuron-methyl lead to the etiolation of *A.azotica* (Fig. 7). To adapt to the new environment, *A.azotica* cells grow well and the number of etiolation cells are less at the first 48h; yellow cells largely changed since the third day.

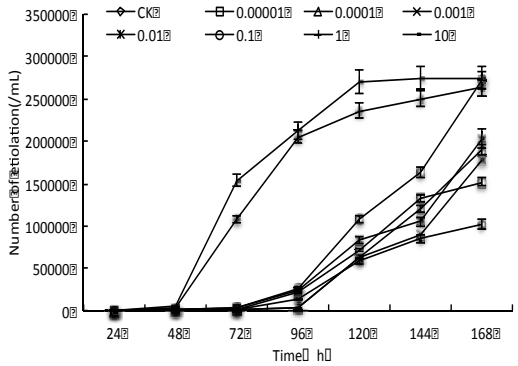

FIGURE 7
Changes of etiolation numbers of *Anabaena azotica* under different bensulfuron-methy

High concentrations significantly inhibit the growth of cells, contributing to a large number of etiolation.

Low concentration treatments (0.001to 0.1 mg/L), the etiolation cells is less at 72h, yellow cells significantly increased since the fourth day, under 0.001 to 0.1 mg/L, the number of yellow cells of *A.azotica* were increased 78%, 82% and 97% compared with control. Then with the extension of incubation time, the etiolation numbers clearly increasing, and significantly higher than control.

DISCUSSION

The stimulative effect of bensulfuron-methyl on *A.azotica* growth observed on low dose of this study is similar to that reported by Shen [10] for monosulfuron on three cyanobacteria species. Low concentrations (0.001 to 0.1 mg/L) of bensulfuron-methyl had no obviously effect on cell morphology of *A.azotica*. Cells present a good growth condition and have complete membrane structure, clear inclusions and more heterocyst and photosynthetic pigment is present in the cytoplasm (Fig.2). PJ Oberholster [15] found that unstrained *Anabaena* sp. had an integrated structure under microscope observing but strained were not. Under external environment stimulation, cyanobacteria cells structure changed. Takashi Osanai [16] observed that *sigE* overexpression affect the cell division and morphology of cyanobacteria and made the cell structure ambiguous. Shen [10] had described the similar results about cyanobacteria structure under high concentrations of monosulfuron. In our research we had found that high concentrations of bensulfuron-methyl inhibit the cell division and destroy cell structure, etiolation and disintegration (Fig.5 (E), (F)). Cyanobacteria cell inclusions outflowed, thylakoid damaged and cytochrome disappeared.

The heterocyst numbers represent the vitality of cell growth. Low dose bensulfuron-methyl had stimulated the heterocyst number of *A.azotica* for that making this herbicide as carbon source to supply their growth and heterocyst numbers present a wave change trend, especially 0.001mg/L significantly higher than control after 48h. But high concentrations (1 mg/L and 10 mg/L) significantly inhibited the heterocyst number of *A.azotica* and it's hardly to see heterocyst during the whole experiment. Etiolation cell represent a steady increasing trend with time extending. Under low concentration stimulation, etiolation numbers of *A.azotica* appeared steady growth after 96h. Etiolation cells began to grow rapidly after 48h at high concentrations of bensulfuron -methyl.

The study results demonstrated that the effect of bensulfuron-methyl on cell growth of *A.azotica* was similar to the phenomenon of cell morphology. Low concentrations stimulate the growth and had no significantly effect on cell structure. And high dose inhibited the heterocyst and cell structure was severely damaged.

CONCLUSION

The high dose herbicide bensulfuron-methyl affected cell morphology, which may have inhibited the growth of *A.azotica* by destroying the cell structure of membrane and thylakoid. Cell membrane was destructed and pigment content decreased and finally led to the etiolation and disintegration of cyanobacteria cells. Low concentrations (0.001 to 0.1 mg/L) had no significant effect on cell morphology. Cell structure was completed and grew well. Bensulfuron-methyl had different effect on heterocyst and etiolation numbers of *A.azotica*. High dose bensulfuron-methyl had inhibited the numbers of heterocyst and contributed to the etiolation of cells. Low concentrations present a wave change trend on cell numbers, heterocyst number decreased after increasing quickly and then increasing again. But etiolation numbers keeping rising after 48h under high concentrations of bensulfuron-methyl; and significantly increased after 96h at low dose treatments.

REFERENCES

[1] Boison, G., Steingen, C., Stal, L. J., et al. (2006) The rice field cyanobacteria *Anabaena azotica* and *Anabaena* sp. CH1 express

vanadium-dependent nitrogenase. Archives of Microbiology, 186:367-376.
[2] Shen, J., Ditommaso, A., Shen, M., et al. (2009) Molecular Basis for Differential Metabolic Responses to Monosulfuron in Three Nitrogen-Fixing Cyanobacteria. Weed Science, 57:133-141.
[3] Irisarri, P., Gonnet, S., Monza, J. (2001) Cyanobacteria in Uruguayan rice fields: diversity, nitrogen fixing ability and tolerance to herbicides and combined nitrogen. Journal of Biotechnology, 91:95-103.
[4] Dai, G., Deblois, C. P., Liu, S., et al. (2008) Differential sensitivity of five cyanobacterial strains to ammonium toxicity and its inhibitory mechanism on the photosynthesis of rice-field cyanobacterium Ge–Xian–Mi (Nostoc). Aquatic Toxicology, 89:113-121.
[5] [5]. Meeks, J. C. (2015) Systems Level Approaches to Understanding and Manipulating Heterocyst Differentiation in Nostoc Punctiforme: Sites of Hydrogenase and Nitrogenase Synthesis and Activity.
[6] Tiwari, A., Pandey, A. (2012) Cyanobacterial hydrogen production-A step towards clean environment. International Journal of Hydrogen Energy, 37:139-150.
[7] Brusa, T., Ferrari, F., Bolzacchini, E., et al. (2001) Study on the Microbiological Degradation of Bensulfuron-methyl, Ann Microbiol, 51, 189.
[8] Yang, C., Wang, Y., Li, J. (2011) Plant Species Mediate Rhizosphere Microbial Activity and Biodegradation Dynamics in a Riparian Soil Treated with Bensulfuron-methyl. Clean-soil, air, Water 39:338-344.
[9] Manjunatha, K. B., Hanumanthappa, M., Nagesha, L., et al. (2013) Effect of New Herbicide Molecules on Growth and Yield of Transplanted Rice (Oryza sativa L.) in Coastal Karnataka. Mysore J Agric Sci, 47(2):292-295.
[10] Shen, J. Y., Luo, W. (2011) Effects of Monosulfuron on Growth, Photosynthesis, and Nitrogenase Activity of Three Nitrogen-Fixing Cyanobacteria. Arch Environ contam Toxicol, 60:34-43.
[11] Guo, L. L., Huang, R. S., Chen X. H., Liao, J. Z., Shen, J. Y. (2015) Toxicity Testing of Bensulfuron-methyl to *Anabaena azotica*. 2015 Seventh International Conference on Measuring Technology and Mechatronics Automation, 333:1366-1369.
[12] Zheng, P. Z. (2011) Cloning and Functional Analysis of ALS and the Toxicity of its Inhibitors to *A.azotica*. Shanghai: Shanghai Jiaotong University.
[13] Guo, L.L., Huang, R.S., Chen, X.H., et al. (2015) Toxicity Testing of Bensulfuron-Methylto Anabaena azotica. International Conference on Measuring Technology & Mechatronics Automation. IEEE, 1363-1366.
[14] Shen, Y. W., Li, S. H. (1993) Cultivation and Application of the Nitrogen-fixing Blue-green Algae: Results and Prospects. Acta Hydrobiologica Sinica, 84(11):1234-1242.
[15] Oberholster, P. J., Jappie, S., Cheng, P. H., Botha A. M., Matthews, M. W. (2015) First report of an Anabaena Bory strain containing microcystin-LR in a freshwater body in Africa. African Journal of Aquatic Science, 40(1):21-36.
[16] Osanai, T., Kuwahara, A., Iijima, H., et al. (2013) Pleiotropic effect of *sigE* overexpression on cell morphology, photosynthesis, and hydrogen production in Synechocystis sp. PCC 6803. Plant Journal, 76(3):456–465.

Received: **14.09.2015**
Accepted: **24.01.2016**

CORRESPONDING AUTHOR

Jian Ying Shen
Department of Environmental Science and Resources, College of Agriculture and Life Science, Shanghai Jiaotong, University, Shanghai 200240, China

e-mail: jyshen88@sjtu.edu.cn

© by PSP Volume 25 – No. 10/2016, pages 3987-3992 Fresenius Environmental Bullet

A COMPARATIVE STUDY OF FENTON AND ELECTRO-FENTON TREATMENT FOR COD REMOVAL FROM COKING INDUSTRY WASTEWATER

Ruichao Peng, Ping Yu *, Yunbai Luo

College of Chemistry and Molecular Sciences, Wuhan University, Wuhan 430072, Hubei, People's Republic of China

ABSTRACT

Effluents of the coking industry after conventional biological treatment processes contain high concentration of non-biodegradable and refractory organic matters, which should be treated in order to satisfy the strict water quality discharge standards (COD < 150 mg·L^{-1}, NH_3–N < 25 mg·L^{-1}). In this comparative study, the post-treatment of coking industry wastewater was treated by Fenton and electro-Fenton methods. Chemical oxygen demand (COD) was selected as the target parameter. The effect of initial pH values, dosages of Fenton reagent and reaction time on the COD removal efficiency by both the Fenton and Electro-Fenton were compared. Under the optimum operating conditions, COD was removed more efficiently in E-Fenton system (90%) compared with that in Fenton method (61.96%). It was also determined that the both two COD removal methodologies followed first-order reaction kinetics. Furthermore, the operating costs for the studied treatments were evaluated and compared. The total operating cost in E-Fenton system is more than twice higher than that in Fenton system.

KEYWORDS:
coking wastewater, chemical oxygen demand, electro-Fenton, Fenton treatment

INTRODUCTION

Nowadays, due to industrial proliferation and urbanization, pollution of water bodies is increasing drastically. [1, 2] As a complex industrial wastewater, coking wastewater is generated from coal coking plants. Traditionally, the biological treatment is regarded as the main coking wastewater treatment technology due to the relatively low cost and higher efficient mineralization of pollutants [3]. However, high concentration of non-biodegradable pollutant makes coking wastewater much recalcitrant.[4, 5] Most of compounds such as phenols, polycyclic aromatic compounds, ammonia, sulfide, cyanide, are highly concentrated and should be treated through properly to prevent long-term environmental and ecological impacts[5, 6]. For example, the coking wastewater coming from one factory in Wuhan was treated by anaerobic–anoxic–oxic (A^2O). However, unfortunately it didn't meet current effluent discharge standards (COD < 150 mg·L^{-1}, NH_3–N < 25 mg·L^{-1}), especially the chemical oxygen demand (COD). Thus, the depth processing of the coking wastewater is the major concern for the discharge of the wastewater into the environment

Recently, advanced oxidation processes (AOPs) are receiving great attention for treating refractory compounds owing to the large amount of residual of the hard-to-biodegrade organics in the wastewater [7-13]. Among various AOPs, Fenton reactions, based on the generation of hydroxyl radicals (·OH) through the reaction between hydrogen peroxide (H_2O_2) and ferrous ion (Fe^{2+}) [14, 15], are frequently used to oxidize complex organic constituents found in wastewaters. [16, 17]. The hydroxyl radical (•OH) is known as one of the most active oxidant with a wide variety of organic pollutants in water. Several kinds of technologies based on the Fenton reaction, including classic Fenton treatment, photo-assisted Fenton reaction, electrochemical Fenton treatment have been applied to the treatment of various hazardous organic compounds[9, 15-17]. Due to the easy operation, high reactivity and no discharge of toxic chemical to the environment, electro-Fenton was considered as an ideal method for degradation of various kinds of wastewater.[16, 21-26].

The use of electro-Fenton method was proposed as an alternative process. One approach consists of either adding ferrous iron or reducing ferric iron electrochemically with the simultaneous produce of hydrogen peroxide upon the reduction of oxygen on several electrodes. The other approach utilized sacrificed iron anode to provide ferrous while the H_2O_2 was added externally to form Fenton's reagent.[27]

In order to compare the treatment efficiency and operating costs of the Fenton and E-Fenton progress, the deep degradation of coking industry wastewater by direct Fenton and E-Fenton was studied. A kinetic model of COD removal was

established under the optimum conditions predetermined in this study. The treatment efficiency and operating costs of the Fenton reagent and E-Fenton were compared so as to provide some additional information for Industrial use.

TABLE 1
Characterization of effluents of the coking wastewater used in the study

Parameter	Average value
pH	7~8
COD (mg·L^{-1})	700~900
Turbidity（NTU）	58
Chromaticity color	178
Conductivity(μS/cm)	500-600
ss(mg•L-1)	43

MATERIALS AND METHODS

Wastewater source and characteristics. The coking wastewater employed in this study was taken with polyethylene bottles from the outlet of a biological treatment unit of a full-scale wastewater treatment plant of a cokes-making plant in a steel company in Wuhan, Hubei province, China. Its characteristics on average are shown in Table1.

Experimental apparatus and procedure. Oxidation of wastewater by Fenton Reagent. A glass beaker (500ml) containing 400ml sample wastewater was employed as a reactor for direct Fenton method. The acidic condition on the reactor was controlled by using 1M sulfuric acid and 10M sodium hydroxide. A selected quantity of granular ferrous sulfate was added in a single step, and then defined amount of hydrogen peroxide was added to initiate the reaction. Mixing was provided by a magnetic stirrer (Model HJ-3, China). Samples were taken at pre-selected time intervals with syringe and neutralized to approximately pH 7.5–8.0 by 3M NaOH solution. After leaving alone for 30min, the supernatant was taken to measure the COD value.

Oxidation of wastewater by Electro-Fenton progress. The E-Fenton experiment was also carried out in a 500 mL beaker. Four plate electrodes (two iron plate anodes and two stainless steel cathodes) with dimensions of (20 x 80 x 2 mm) were used in the study. The current of electrolysis was supplied by a laboratory DC power supply) and was controlled at 7 V. Mixing was provided by a magnetic stirrer (Model HJ-3, China). 400 ml of wastewater was used in each trial. When turning on the power supply, the electrolysis was started. A suitable amount hydrogen peroxide was added to study its effects on COD removal for the optimization experiments. The electro-Fenton oxidation lasted usually less than 120 min. After the first drop of hydrogen peroxide poured into the vessel, the electric power was turned on simultaneously to start the oxidation process. At different time intervals, COD value was measured by the method as Fenton above. All experiments were performed at room temperature.

Analytical methods. The solution pH was monitored by a portable pH meter (Metteler-Toledo Instruments Co. Ltd., Shanghai). Chemical oxygen demand (COD) was determined using a closed reflux spectrophotometric method based on the Standard of the People's Republic of China for Environmental Protection (HJ-T 399-2007). The percentage removal efficiency of COD was calculated using the following equation:

$$\text{Percentage removal efficiency (\%)} = \left(\frac{C0-C}{C0}\right) \times 100 \quad (1)$$

RESULT AND DISCUSSION

Effect of initial pH on COD removal. In both Fenton and E-Fenton treatment, the pH has been observed to be a very important factor. It was found that the Fenton reaction and E-Fenton occurs in optimal acidic conditions (pH=2-3). As higher production of hydroxyl radical in the pH range of 2–4 by a reaction involving the organometallic complex where either hydrogen peroxide is regenerated or reaction rates are increased[27]. So both Fenton and E-Fenton experiments were carried out with initial pH=3. To explore the application performance of Fenton and E-Fenton progress, the pH range of 3 and 6 were tested. [18] Tab.2 showed the effect of pH on the COD removal efficiencies. It indicated that low pH has high removal efficiency for Fenton's reagent (pH=3, 90% of COD removal). As the initial pH increases above 3, there was a rapid decrease of COD removal both in Fenton and E-Fenton.The present results agree with previous studies on the degradation of organic compounds.[13, 27]

Effects of H_2O_2 concentration on COD removal. The dosage of H_2O_2 is an important operating factor of Fenton and E-Fenton oxidation. Fig. 1 shows the effect of H_2O_2 dosage for a fixed Fe (II) to Fenton oxidation and for E-Fenton oxidation on COD removal, respectively. An obvious increase of the rate of COD decay was observed by adding into solution and raising initial H_2O_2 concentrations from 2000 mg·L^{-1} to 5000 mg·L^{-1}. As we can see after 120 min of electrolysis the COD removals were 90% for the initial H_2O_2 concentrations of 5000 mg·L^{-1} and the voltage of 7V. But when the H_2O_2 concentration increased to 7000 mg·L^{-1}, the COD abatement might decrease, and only 84.09% of the COD was removed after

TABLE 2
Effect of initial pH on the COD removal.

Treatment process	pH	Reaction time (h)	H_2O_2 dosage (mgL^{-1})	Influent COD (mgL^{-1})	Effluent COD (mgL^{-1})	COD removal (%)
Fenton	3	2	5000	780	475	61.96
	6	2	5000	780	266	35.10
Electro-Fenton	3	2	5000	800	80	90.00
	6	2	5000	800	247	69.13

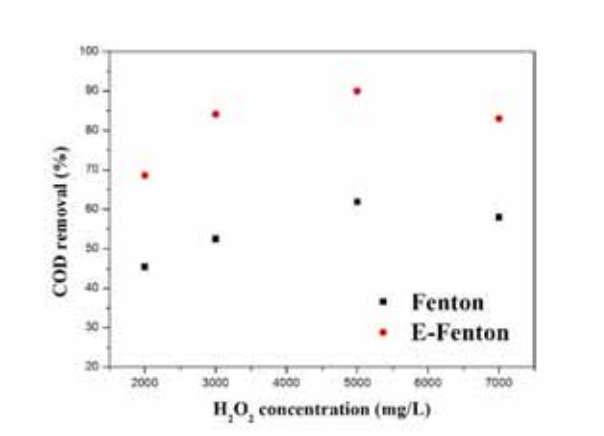

FIGURE 1
Effects of H_2O_2 concentration on the COD removal
(Fenton: Initial pH=3, $[FeSO_4]$ =1000 mgL^{-1}, Reaction time=2 h;
E-Fenton: Initial pH=3, Cell voltage=7 V, $[Na_2SO_4]$ =500 mgL^{-1}; Reaction time=2 h)

120 min of electrolysis. This agreed with the fact that the Fe^{2+} transform into Fe^{3+}. (Fe^{2+} + ·OH → Fe^{3+} + OH^-) As a result, the continuous production of oxidizing ·OH was regulated by the small catalytic amount of regenerated Fe^{2+} in the medium. Consequently the suitable concentration of H_2O_2 and voltage was an important prerequisite in the electro-Fenton reaction

Effects of reaction time on COD removal. In order to determine an experimental condition for further research, the reaction time effect on both Fenton and E-Fenton process was tested. Figure4 showed the change of COD removal as a function of reaction time.it is evident that an increase of the treatment time by 180min, increased COD removal from 30.45% to 60.10% by direct Fenton reagent, and in E-Fenton the overall removal of COD removal increased from 32.50% to 90.30%. After reacted for 120min, the dosed H_2O_2 were run out, so the increase of COD removal was limited.

Rate constants for direct Fenton and EF-Fenton. In order to investigate the decay kinetics of COD, in the Fig.3 and 4, where C_0 is the initial COD value of the target wastewater in the solution; C is the remained COD value of wastewater in the solution. With both methods, the decay kinetics of COD always followed a pseudo-first-order reaction. As we can see in Fig.3 and 4, all of the values for the pseudo-first-order reaction rate constant (k) were calculated from the linear regression of the pseudo-first-order kinetic model with related coefficients higher than 0.95. In the Fenton and EF-Fenton systems, the rate constants are clearly proportional to the reaction time.

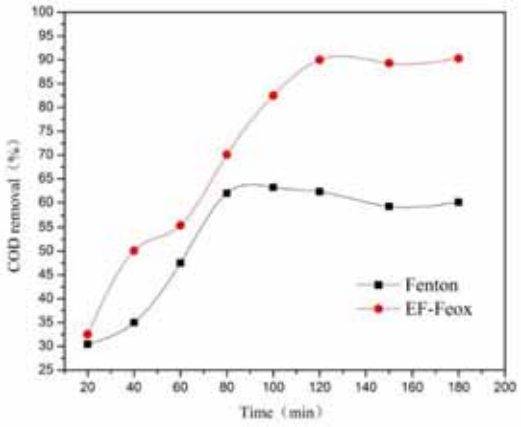

FIGURE 2
Effects of reaction time on the COD removal
(Fenton: Initial pH=3, $[FeSO_4]$ =1000 $mg·L^{-1}$, $[H_2O_2]$ = 5000 $mg·L^{-1}$, Reaction time=120 min;
E-Fenton: Initial pH=3, Cell voltage=7 V, $[H_2O_2]$ = 5000 $mg·L^{-1}$, $[Na_2SO_4]$ =500 mgL^{-1} Reaction time=120min)

Comparison of operating costs between the Fenton and E-Fenton. With regards to electrochemical oxidation technology, one of the most important parameters that affect the application of any method of water and wastewater treatment greatly is the operating cost. It is a useful parameter for evaluating its practical application value from the economic point of view.

In this study, the data derived from the experiments on the COD removal of coking wastewater allowed a rough estimation of operating costs taking into account the costs of chemicals and energy. The operating costs (OCs) of the Fenton

process and E-Fenton processes were calculated by including the material cost (mainly electrodes), utility cost (mainly electrical energy), chemicals, as

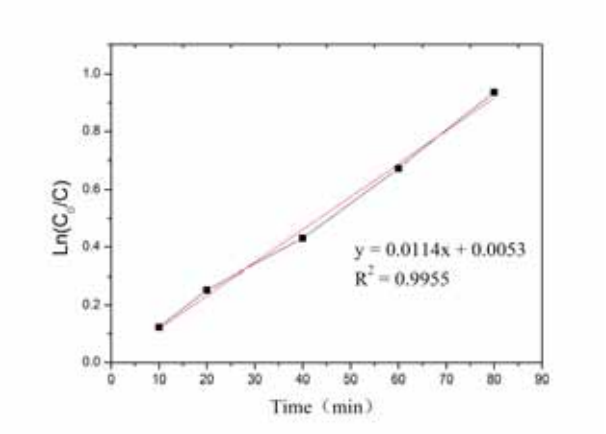

FIGURE 3
The pseudo-first-order removal of COD via Fenton
(Initial pH=3, [$FeSO_4$] =1000 mg·L^{-1}, [H_2O_2] = 5000 mg·L^{-1}, Reaction time=80min)

well as labor, maintenance and other fixed costs. In this study, the energy, electrode material and chemicals costs were taken into account as major cost items in the calculation of the OC as \$/m^3 for the treatment of coking industry wastewater[31, 32].

$$OC = xC_{energy} + yC_{electrode} + zC_{chemicals} \quad (2)$$

In equation (10), $C_{chemicals}$ is consumption quantities of chemicals (kg/m3) of the wastewater treated. The constants x , y and z in Equation（2） provided by the China market in September, 2014 were values of electrical energy price (0.1\$/kWh), electrode price (\$0.6/kg) and chemical costs (\$0.9/kg for H_2O_2 , \$0.35/kg for Na_2SO_4 and \$0.363/kg for H_2SO_4),respectively. According to the equations, operating costs for Fenton, and E-Fenton treatments for 90% removal of COD are calculated and presented in Table 3.

Apparently, as can be seen from Table 3, the E-Fenton method not only presents excellent COD removal ability and catalytic activity, but also possesses remarkable electrochemical properties for economic consumption in wastewater treatment. The total operating cost in E-Fenton system is more than twice higher than that in Fenton system. However, it is worth pointing out that the depreciation fee of equipment and maintenance cost are not considered here.

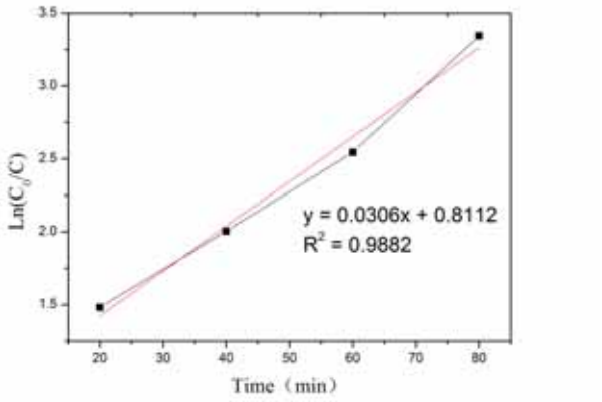

FIGURE 4
The pseudo-first-order removal of COD via E-Fenton
(Initial pH=3, Cell voltage=7V, [H_2O_2] = 5000 mg·L^{-1}, Reaction time = 80 min).

CONCLUSION

In this comparative study, the performance and cost-effectiveness of Fenton process and E-Fenton for treating industrial wastewater for COD removal were evaluated. The evaluations of treatment performance were conducted for different H_2O_2 dosage, initial pH value and reaction time. Based on the experimental results presented above, the following conclusions are drawn.

1) E-Fenton, in general, has a remarkable higher treatment performance than that of Fenton. Compared with direct Fenton and EF- Fenton processes, the results indicate that more than 90% of COD removal using the electro-Fenton method, but only 61.96% of COD was removed by Fenton's method.

2) At the initial pH=3, it showed a much higher COD removal efficiency either in Fenton system or in E-Fenton system than other initial pH.

3) The pseudo-first-order treatment kinetics of COD was observed for both Fenton and E-Fenton process.

4) Calculation of operating costs has shown that the E-Fenton process is high in economic consumption. It is necessary to adopt appropriate operating conditions to make this process cost-effective.

TABLE 3
Comparison of operating costs between the direct Fenton and E-Fenton

Treatment process	Fe (Ⅱ) cost (\$$m^{-3}$)	Na_2SO_4 cost (\$$m^{-3}$)	Electrode (\$$m^{-3}$)	H_2O_2 cost(\$$m^{-3}$)	Energy cost (\$$m^{-3}$)	Total cost (\$$m^{-3}$)
Fenton	1.19	0	0	0.82	0	2.01
E-Fenton	0	2.85	1.1	0.43	0.51	4.89

REFERENCE

[1] Rajkumar, D., Palanivelu, K., Electrochemical treatment of industrial wastewater, Journal of Hazardous Materials113(2004)123-129.

[2] Oller, I., Malato, S., Sánchez-Pérez, J. A., Combination of Advanced Oxidation Processes and biological treatments for wastewater decontamination—A review, Science of The Total Environment409(2011)4141-4166.

[3] Li, H., Cao, H., Li, Y., Zhang, Y., Liu, H., Innovative biological process for treatment of coking wastewater, Environmental Engineering Science27(2010)313-322.

[4] Zhu, X., Tian, J., Liu, R., Chen, L., Optimization of Fenton and electro-Fenton oxidation of biologically treated coking wastewater using response surface methodology, Separation and Purification Technology81(2011)444-450.

[5] Güçlü, D., Şirin, N., Şahinkaya, S., Sevimli, M. F.,Advanced treatment of coking wastewater by conventional and modified fenton processes, Environmental Progress & Sustainable Energy 32(2013)176-180.

[6] Zhu, X., Ni, J., Lai, P., Advanced treatment of biologically pretreated coking wastewater by electrochemical oxidation using boron-doped diamond electrodes,Water Research 43(2009) 4347-4355.

[7] Irmak,S.,Yavuz,H. I., Erbatur,O., Degradation of 4-chloro-2-methylphenol in aqueous solution by electro-Fenton and photoelectro-Fenton processes, Applied Catalysis B: Environmental63(2006) 243-248.

[8] Chou,S.,Huang,Y.-H., Lee, S.-N., Huang, G.-H.,Huang,C., Treatment of high strength hexamine-containing wastewater by electro-Fenton method,Water research33(1999) 751-759.

[9] Brillas, E., Sirés, I., Oturan, M. A., Electro-Fenton Process and Related Electrochemical Technologies Based on Fenton's Reaction Chemistry,Chemical Reviews109(2009) 6570-6631.

[10] Lin, S. H., Chang, C. C., Treatment of landfill leachate by combined electro-Fenton oxidation and sequencing batch reactor method,Water Research34(2000)4243-4249.

[11] Removal of basic red 9 in wastewater using green Fenton reaction , Azize Alayli Gungor*, Neslihan Celebi, Hayrunnisa Nadaroglu*,Fresenius Environmental Bulletin, （2015）01.05.

[12] Enhancement of waste activated sludge aerobic digestion with combined fenton oxidation and electrochemical pretreatment method , Haiping Yuan;Qingji Wang;Shengjuan Guo;Jie Yao;Nanwen Zhu*;Yi Gong Fresenius Environmental Bulletin（2015）01.09.

[13] Removal of residual organics in coking wastewater under different electrolytic conditions using three-dimensional system, Hao Wang*;Lin Chen;Zhiguo You;Yong Yang;Lei Zhang， Fresenius Environmental Bulletin，（2013）01.02.

[14] Pérez, M., Torrades, F., García-Hortal, J. A., Domènech, X., Peral, J., Removal of organic contaminants in paper pulp treatment effluents under Fenton and photo-Fenton conditions, Applied Catalysis B: Environmental 36 (2002)63-74.

[15] Benitez, F. J., Acero, J. L., Real, F. J., Rubio, F. J., Leal, A. I.,The role of hydroxyl radicals for the decomposition of p-hydroxy phenylacetic acid in aqueous solutions, Water Research35(2001)1338-1343.

[16] Zhu, X., Logan, B. E., Using single-chamber microbial fuel cells as renewable power sources of electro-Fenton reactors for organic pollutant treatment, Journal of Hazardous Materials252–253(2013)198-203.

[17] Boye, B.; Dieng, M. M.; Brillas, E., Degradation of Herbicide 4-Chlorophenoxyacetic Acid by Advanced Electrochemical Oxidation Methods, Environmental science & technology36(2002)3030-3035.

[18] Qiang, Z., Chang, J.-H., Huang, C.-P., Electrochemical regeneration of Fe^{2+} in Fenton oxidation processes,Water Research37 (2003)1308-1319.

[19] Yuan, S., Fan, Y., Zhang, Y., Tong, M., Liao, P., Pd-catalytic in situ generation of H_2O_2 from H_2 and O_2 produced by water electrolysis for the efficient electro-Fenton degradation of rhodamine B, Environmental science & technology 45(2011)8514-8520.

[20] Zhao, H.-Z., Sun, Y.,Xu, L.-N.; Ni, J.-R., Removal of Acid Orange 7 in simulated wastewater using a three-dimensional electrode reactor: Removal mechanisms and dye degradation pathway,Chemosphere78(2010)46-51.

[21] Wang, Y., Zhao, H., Chai, S., Wang, Y., Zhao, G.,Li, D., Electrosorption enhanced electro-Fenton process for efficient mineralization of imidacloprid based on mixed-valence iron oxide composite cathode at neutral pH,Chemical Engineering Journal223(2013)524-535.

[22] Ding, X., Ai, Z., Zhang, L., Design of a visible light driven photo-electrochemical/electro-Fenton coupling oxidation system for wastewater treatment, J Hazard Mater239-240 (2012)233-40.

[23] Liu, W., Ai, Z., Zhang, L., Design of a neutral three-dimensional electro-Fenton system with foam nickel as particle electrodes for

wastewater treatment, J Hazard Mater243 (2012)257-64.
[24] Zhang, H., Ran, X., Wu, X., Electro-Fenton treatment of mature landfill leachate in a continuous flow reactor, J Hazard Mater241-242(2012)259-66.
[25] Fan, Y., Ai, Z., Zhang, L., Design of an electro-Fenton system with a novel sandwich film cathode for wastewater treatment, Journal of hazardous materials176(2010)678-684.
[26] Ozcan, A., Sahin, Y., Oturan, M. A., Complete removal of the insecticide azinphos-methyl from water by the electro-Fenton method--a kinetic and mechanistic study, Water Reseach 47(2013)1470-9.
[27] Wang, Q., Lemley, A. T., Oxidation of diazinon by anodic Fenton treatment,Water Research36(2002)3237-3244.
[28] Li, R., Yang, C., Chen, H., Zeng, G., Yu, G., Guo, J., Removal of triazophos pesticide from wastewater with Fenton reagent, Journal of hazardous materials167(2009)1028-1032.
[29] Bouasla, C., Samar, M. E.-H., Ismail, F., Degradation of methyl violet 6B dye by the Fenton process,Desalination254 (2010)35-41.
[30] Sedlak, D. L.,Andren, A. W., Oxidation of chlorobenzene with Fenton's reagent, Environmental science & technology25(1991)777-782.
[31] Kobya, M., Delipinar, S., Treatment of the baker's yeast wastewater by electrocoagulation, Journal of Hazardous Materials 154(2008)1133-1140.
[32] Akyol, A., Can, O. T., Demirbas, E., Kobya, M., A comparative study of electrocoagulation and electro-Fenton for treatment of wastewater from liquid organic fertilizer plant, Separation and Purification Technology112(2013)11-19.

Received: **24.09.2015**
Accepted: **20.05.2016**

CORRESPONDING AUTHOR

Ping Yu
College of Chemistry and Molecular Sciences, Wuhan University,
Wuhan 430072, Hubei, People's Republic of China

E-mail: yuping@whu.edu.cn

© by PSP Volume 25 – No. 10/2016, pages 3993-4003 Fresenius Environmental Bulletin

MODIFICATION MECHANISM OF AMPHOTERIC MODIFIER BS–12 ON TWO DIFFERENT CLAYS

Wenbin Li[1], Zhaofu Meng[1,2*], Qiong Wu[1], Dan Bai[1], Shaoe Xu[3], Yu Lu[1]

[1]Department of Natural Resource and Environment, Northwest A&F University, Yangling, Shaanxi, 712100, China
[2]Key Laboratory of Plant Nutrition and Agri–Environment in Northwest China, Ministry of Agriculture, Yangling 712100, China
[3]Department of Biological and Agriculture Engineering, University of Arkansas, Fayetteville 72707, US

ABSTRACT

To explore the modification mechanism of BS–12 (dodecyl dimethyl betaine) on different clay, this study chose bentonite and kaolin as the subjects. The modification mechanism was determined via the changes in the S_{BC} (sum of BS–12 and $Ca^{2+}/2$ adsorbed on clay) curves. This mechanism was verified through the Vanselow ionic selectivity coefficients, adsorption isotherms and superficial characteristics such as TOC (total organic carbon) content, XRD (x–ray diffraction) and S_{BET} (specific surface–area). Results indicated that: 1) Ion exchange and hydrophobic bonds coexisted in the process of bentonite and kaolin modification with BS–12, and the hydrophobic modification began to appear at BS-12 modification ratios of 40.09% and 29.11% CEC (cation exchange capacity) of bentonite and kaolin, respectively. After 85.30% and 78.44% CEC of bentonite and kaolin, respectively, hydrophobic modification was stronger than ion exchange and became the main modification mechanism. 1) $\mathrm{Ln}K_v$ [(the natural logarithm for K_v (Vanselow selectivity coefficients)] of two clays were all greater than 1, indicating that the adsorption preferences for BS–12 were greater than Ca^{2+}, meanwhile the Ln*Kv* values increased significantly with the increase in BS–12 modification ratios. 3) Adsorption isotherms increased sharply before an inflection point occurred at the modification ratio of 60% (bentonite) and 40% (kaolin) CEC of clay, then the ascensional range decreased after this modification ratio. Lastly, both rapidly rose again after the modification ratio of 100% CEC of the two clays. 4) TOC content, d_{001} of two clays and S_{BET} of bentonite all showed no significant distinction between bentonite and 25%BS bentonite, S_{BET} had significant differences between kaolin and 15%BS kaolin. On the other hand, characteristics of 50% and 100%BS bentonite, 30% and 60%BS kaolin all significantly increased (for TOC and d_{001}) or reduced (for S_{BET}) compare with that of 25%BS bentonite and 15%BS kaolin, respectively.

KEYWORDS:
Ion exchange, hydrophobic bond, Vanselow selectivity coefficients, adsorption isotherm, superficial characteristics.

INTRODUCTION

Clays are easily modified [1–2], and their adsorption ability on organic and some heavy metal contaminants can be greatly increased after modification [3–5]. Thus studying the modification mechanisms of different modifiers on clays is the basis and core aspect of eliminating soil contaminations with modified clays [6–8].

When clay is modified by cationic surfactants, the positive charges on the hydrophilic end quickly combine with the negative charges on the clay surface by ionic exchange effect [6, 9, 10], and the hydrophobic chain is exposed to the soil surface [11–13]. Studies proposed Ionic exchange is the level of surfactant within a certain ratio of the cation exchange capacity (CEC) of soil [14, 15], and clay surfaces present hydrophobic aggregation of carbon chain through increasing loading level of cationic surfactant, making the CEC ratio more than the certain ratio [16]. Data suggested that hydrophobic modification began to form in the range of 20% to 28% CEC of Lou Soil [17] and about 70% CEC of vermiculitic subsoil [18], whereas all began to dominate after 100% CEC of soil. X–ray diffraction and thermogravimetric analyses of modified bentonite presented great changes at the modification ratio of 50% and 100% CEC of clay [19, 20].

In previous studies, experiments on clays

modified with cationic surfactant were common, and soil adsorption ability for organic and anionic heavy metal pollutants was found to increase sharply [21, 22]. Meanwhile, the mechanism for clay modified with cationic surfactant was first assessed [17]. For adsorbing both organic and anionic and cationic heavy metal pollutants, amphoteric surfactants were proposed to modify Lou Soil, and the absorption ability of modified soil was improved [23, 24]. Thus, the exploration of the modification mechanisms of amphoteric modifiers is significant for the repair of various soil pollutions.

In this paper, the "S_{BC}" (sum of BS–12 and $Ca^{2+}/2$ adsorbed on clay) curve was used to study the modification reaction characteristics of amphoteric modifier (BS–12 (dodecyl dimethyl betaine)] on two different clays (bentonite and kaolin). Linear fitting, Vanselow ion exchange model, adsorption experiment and superficial characteristics such as TOC (total organic carbon) content, XRD (x–ray diffraction), S_{BET} (specific surface–area) were discussed as evidence to verify the mechanism of the exchange reaction.

MATERIALS AND METHODS

Materials. Amphoteric modifier. Dodecyl dimethyl betaine (BS–12) with 30% (w/v) concentration in water solution was chosen in this experiment as the amphoteric modifier. This analytical reagent was provided by the Xingguang Auxiliary Factory, Tianjin City, China. Fig 1 presented the structural formula of BS–12.

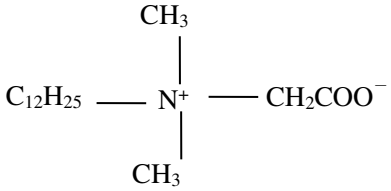

FIGURE 1
Structural formula of BS–12.

Clays. Two types of clay were selected, namely, bentonite and kaolin. Bentonite was collected from Xinyang City, Henan Province, China. Kaolin was purchased from Alibaba Net Guangzhou Rio Trade Co., Ltd. The raw bentonite was purified by wet cleaning process [25] before use. Table 1, 2 show the basic characteristics of the two clays after purification.

Experimental design and methods. Ion exchange between BS–12 and Ca^{2+}.

1) Preparation of Ca^{2+}–saturated clays: First, about 300 g of clay was saturated six times with 300 mL of $CaCl_2$ solution (0.50 mol L^{-1}) via stirring for 3 h in a magnetic stirrer to ensure that Ca^{2+} was completely saturated. The clay sample was then washed with dH_2O (distilled water) using a suction filter until the chloride ions derived from the $CaCl_2$ solution were undetectable, and dialyzed using dH_2O until the conductivity was similar to dH_2O. Lastly, the clay samples were dried at 60 °C for 12 h and then passed through a 0.25 mm sieve.

2) Defining the mole fraction of BS–12: The mole fraction of BS–12 was calculated using the following formula:

$$X_{(BS-12)} = n\ (BS-12) \ /\ [n\ (Ca^{2+}/2) + n\ (BS-12)]$$

Where n is the amount of substance (mol), and the basic unit forms of the substance are shown in the brackets.

A series of total modification proportions at 20%, 40%, 60%, 40%, 100%, and 200% CEC of clays was prepared for calculating the initial total ion exchange concentration, which is a mixture of BS–12 and $Ca^{2+}/2$ (referred to as total molar concentration). With each molar concentration, different $CaCl_2/2$ and BS–12 solutions were further prepared, and a series of mixed solution kept the total molar concentrations of BS–12 + $1/2Ca^{2+}$ unchanged. The molar fractions of BS–12 ($X_{(BS-12)}$) were set at 0.1, 0.25, 0.4, 0.5, 0.6, 0.85, and 0.95, and the weight of BS–12 or $CaCl_2$ in the solution was calculated in 2.4.1.

3) Experimental method of ion exchange: Approximately 0.2000 g of Ca^{2+}–saturated bentonite (0.5000 g of kaolin) (W_1) was divided into seven 50 mL centrifuge tubes, and the total weight of the centrifuge tube and clay sample (W_2) was obtained. In each centrifuge tube, approximately 20.00 mL of each BS–12 and $1/2Ca^{2+}$ mixed solution with different BS–12 molar fraction series was added, and the tubes were capped tightly. Equilibrium was reached by shaking the suspensions for 24 h at 20 °C using the batch method with a temperature–regulated thermostat shaker, and the samples were centrifuged at 4800 rpm for 20 min.

TABLE 1
Basic physical and chemical properties of bentonites.

Clays	swelling volume /mL g^{-1}	pH value	Methylene blue adsorption/%	Montmorillonite content/wt%	CEC /mmol kg^{-1}
raw	40.0	8.97	16.0	36.4	767.94
purified	98.5	8.49	38.9	88.6	1003.32

TABLE 2
Basic physical and chemical properties of kaolin.

CEC/mmol kg^{-1}	pH value	Fe_2O_3 /%	Al_2O_3/%	SiO_2/%
88.69	6.7–7.6	≤0.3	36±0.5	47±0.5

Lastly, the Ca^{2+} (C_1) and BS–12 concentrations in the supernatant were measured. The amount of BS–12 adsorbed by the clay was calculated as the difference between the initial and final concentrations of BS–12 in the supernatant.

After separating the supernatant from the centrifuge tube, the total weight of the centrifuge tube, clay sample, and residual supernatant (W_3) was obtained. The weight of residual supernatant (W_{rs}) was based on the weight difference (W_3–W_2). About 15 mL of NaCl (10%) solution was then added into the centrifuge tube for desorbing Ca^{2+} on the surface of clays via shaking for 24 h under the same condition. The tubes were centrifuged at 4800 rpm for 20 min. The Ca^{2+} concentration (C_2) of the supernatant was again measured, and the amount of Ca^{2+} adsorbed on the clay surface was calculated as the difference between the desorbed Ca^{2+} $(C_2\times 15+C_2\times W_{rs})/(W_1)$ and Ca^{2+} in the supernatant residues $(C_1\times W_{rs})/(W_1)$. Each step was performed in triplicate.

BS–12 equilibrium adsorption. A series of modification concentration of 10%, 20%, 40%, 60%, 80%, 100%, 150%, and 200% CEC of clay was designed, and the weight of BS–12 in solution was calculated using the equation in 2.4.1. Each process was determined using three replicates.

Ca^{2+}–saturated bentonite (0.2000 g) or kaolin (0.5000 g) was weighed and then placed in seven separate plastic centrifuge tubes. The weight of single clay and total weight of the centrifuge tube and clay were obtained and recorded. Approximately 20.0 mL of BS–12 solutions with modification concentration ranging from 20% to 200% CEC of clay minerals was added to the tubes. The tubes were shaken in a thermostat shaker for 24 h at 20 °C, and centrifuged at 4800 rpm for 20 min to separate the solid and liquid phases. The BS–12 concentration in the supernatant was measured, and the amount of BS–12 adsorbed on the clay was calculated using the subtraction method.

Superficial characteristics. The TOC concentration was analyzed using a Shimadzu TOC–VCPH analyzer. S_{BET} was determined by the BET method (Analyzer ASAP2400, Micromeritics) by N_2 gas adsorption at liquid nitrogen temperature. Powder XRD patterns were recorded between 1° and 20 ° (2h) at a step size of 0.0167 using a Bruker D8 Advance diffractometer with Cu Ka radiation (40 kV and 40 mA), and the Interlayer spacing(d_{001}) was calculated by the Bragg equation ($2d\sin\theta=\lambda$).

Determination method. Ca^{2+} concentration in the supernatant was determined via flame atomic adsorption spectrometry with a Hitachi Z–5000 atomic absorption spectrometer. Background absorption was corrected by the Zeeman effect.

Meanwhile, BS–12 concentration in the supernatant was measured through the gold orange II method [26] with a SP–2100 UV–VIS spectrophotometer. A reagent blank was used to adjust the absorbance to zero. In brief, at room temperature, 25.0 mL of a certain concentration of BS–12 solution was added into a 125 mL separatory funnel with a pipette. 5.0 mL of acetic acid sodium acetate buffer solution (pH 4.3) and 3.0 mL of golden orange II solution were mixed in

order and blended uniformly, and 10.0 mL of chloroform was used for extraction by continuous shaking for 2 min. The lower extract was moved to a 25.0 mL volumetric flask and then extracted three times with 5.0, 4.0, and 4.0 mL chloroform. The four extracts were combined and diluted with chloroform to 25 mL. 25.0 mL of water was used with the same steps as the blank solution. The absorbance values of the blank and extracts were measured 10 min later at the wavelength of 485 nm.

Data processing. Computation of BS–12 or $CaCl_2$. The weight of BS–12 or $CaCl_2$ for a certain quality of clays can be obtained using the following equation:

$W = m \times CEC \times M \times 10^{-6} \times R/b$

Where W is the weight of BS–12 or $CaCl_2$, g; m is the weight of the clays that will be modified, g; CEC is the CEC of the clays, mmol kg^{-1}; M is the molecular mass of BS–12 or $CaCl_2/2$, g mol^{-1}; R is the proportion of modification; and b is the product content of modifier (mass fraction).

Calculation of the Vanselow selectivity coefficients for ion exchange reaction. The commutative adsorption between Ca^{2+}-saturated soil sample and BS–12 (BS in the equation) is shown in the following reaction:

$$2BS_{aq} + Ca^{2+}{}_{\text{Soil}} \Leftrightarrow Ca^{2+}{}_{aq} + 2BS_{\text{Soil}}$$

The Vanselow selectivity coefficient [27] is obtained as follows:

$$K_V = \frac{[BS_{Soil}]^2 \cdot (Ca^{2+})_{aq}}{[Ca^{2+}{}_{Soil}]^2 \cdot (BS)_{aq}} \cdot \frac{1}{[BS_{Soil} + Ca^{2+}{}_{Soil}]}$$

Where BS_{Soil} and $Ca^{2+}{}_{\text{Soil}}$ are the amounts of BS–12 and Ca^{2+} adsorbed on the soil surface, respectively; [ ] is the amount of substance concentration, mol kg^{-1}; $(BS)_{aq}$ and $(Ca^{2+})_{aq}$ are the quantities of BS–12 and Ca^{2+} in water phase, respectively; and ( ) is the activity, mol L^{-1}.

$$(Ca^{2+})_{aq} = [Ca^{2+}]_{aq} f_{Ca}$$

$$(BS)_{aq} = [BS]_{aq} f_{BS}$$

Where f_{Ca} and f_{BS} are the activity coefficients of Ca^{2+} and BS–12, respectively.

The molecular diameter of BS–12 cannot be obtained, and the activity coefficient can be calculated using the Davies formula:

$$-\log f_i = AZ_i^2 \cdot \left(\frac{\sqrt{I}}{1+\sqrt{I}} - 0.3I\right)$$

The value of A is 0.5070 at 20 °C.

Meanwhile, the ionic strength is calculated as follows:

$$I = \frac{1}{2}\sum (c_i \cdot Z_i^2)$$

Where C_i is the concentration of ions in the solution, and Z is the charges of the ions. BS–12 has both positive and negative charges, and the charge strength is determined by the pH of the reaction mixture, so the charge numbers of BS–12 should be 1.

Processing software. The Curve Expert 1.3 fitting software was used in linear fitting, and Sigmaplot 10.0 software was adopted to improve the plotting.

RESULTS AND DISCUSSION

Ion exchange reaction of clays modified with BS–12. Changes in different S_{BC} curves. Previous studies showed that the surface modifiers on clay surface include ion exchange and hydrophobic bond reactions [28], and the ion exchange appeared at an equal charge and equal amount of substance [18, 29]. If the occurrence of BS–12 on the clay surface is in the ion exchange reaction form, then the equal amount of BS–12 would be able to replace the equal amount of $Ca^{2+}/2$ on the clay surface. Under the precondition of the same total molar concentration, the amount of BS_{Soil} + $(Ca^{2+}/2)_{Soil}$ should remain constant, despite the change in the molar fraction of BS–12 in additive solution.

Hydrophobic adsorption means molecular aggregation by the hydrophobic chains, and the accumulation on clay surface will increase rapidly by hydrophobic bonding. In a hydrophobic bond reaction, the amount of BS_{Soil} + $(Ca^{2+}/2)_{Soil}$ should increase with increasing molar fraction of BS–12. Hence, BS_{Soil} + $(Ca^{2+}/2)_{Soil}$ can be used as an indicator to determine the form of modification reactions on clay surfaces. For simplicity, the symbol "S_{BC}" is used to represent the total amount of BS_{Soil} + $(Ca^{2+}/2)_{Soil}$ adsorbed on the clays. If the slope of the S_{BC} curve is almost zero, the total amount of BS_{Soil} + $(Ca^{2+}/2)_{Soil}$ is unchanged by the ion exchange reaction. With increasing S_{BC} slopes, hydrophobic bonding begins to appear and finally goes beyond the ion exchange mode, becoming the dominant mode.

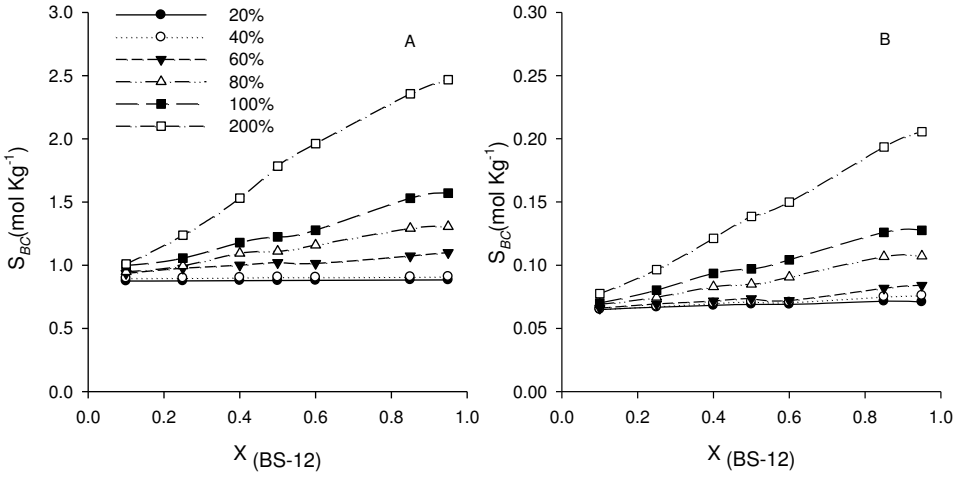

FIGURE 2

S_{BC} curve for bentonite (A) and kaolin (B) under different modified proportions (20%, 40%, 60%, 80%, 100%, and 200%) of BS-12 at 20 °C. $X_{(BS-12)}$ is the molar fraction (0.1, 0.25, 0.4, 0.5, 0.6, 0.85, and 0.95) of BS–12 in the mixture of BS–12 and $Ca^{2+}/2$, and S_{BC} is the sum of BS–12 and $Ca^{2+}/2$ adsorbed on the clays.

Combining the results in Fig. 2, under different modification proportions of bentonite, total amounts of BS_{Soil} + $(Ca^{2+}/2)_{Soil}$ were different and had different S_{BC} curves. The S_{BC} curves showed no change with increasing mole fraction of BS–12 at the total concentrations of 20% and 40% CEC of bentonite, and this confirmed that BS–12 modification on the clay surface was given priority to the ion exchange. When the total modification concentration reached 60% CEC of bentonite, the S_{BC} curve started to rise with increasing molar fraction of BS–12, and this showed the appearance of hydrophobic bond mode as BS–12 combined with bentonite, and the rising tendency of the S_{BC} curves gradually increased with increasing total concentration. However, the modification mode given the priority to the ion exchange reaction with the total proportion of 20% CEC of kaolin, and the S_{BC} curves began to rise after the 40% CEC total concentration of kaolin, exhibiting a hydrophobic pattern.

In addition to the ion exchange reaction, hydrophobic adsorption appeared after a certain modification concentration, and the modification concentration was different between bentonite and kaolin. As shown by the S_{BC} curves, the turning point that began to appear in hydrophobic bonding was between the total concentration of 40% and 60% CEC for bentonite and 20% to 40% CEC for kaolin, which was consistent with the findings reported by Meng [17], but different from those presented by Xu [18] because of the differences in modifiers and clay samples.

Turning point calculation using the slope of different S_{BC} curves. The turning point at which hydrophobic bonding began to appear was roughly estimated using the shape of the S_{BC} curve above. To determine the accurate critical proportion, each S_{BC} curve was linearly fitted (Table 3). The slope (K) and total modification proportion (R) were calculated, followed by linear regression ($K = k \times R + y$). The results after regression were listed in Table 3.

Each S_{BC} curve of the two clay samples was linearly fitted, and all fitted results showed significant correlations. The slope of each S_{BC} curve increased with increasing total modification ratio (total concentration). Combining the aforementioned analysis of ion exchange mechanism, if surface modification is only by the ion exchange form, then the slope of the line between S_{BC} and x-axis would be almost 0. Hence, when the K value was 0, the critical proportion at which the hydrophobic bond began to appear on clay modified with BS–12 could be determined. By contrast, when BS–12 was more than $Ca^{2+}/2$ adsorbed on clay surfaces, hydrophobic bonding became the dominant mode, and the slopes (K) of the S_{BC} curve approximately equaled to the

adsorbed amount of BS–12 on clay surfaces. Thus when K value reached the CEC/2 of clay, hydrophobic bonding became the dominant mode.

The results of R values calculated by the equation $K=k \times R + y$ are listed in Table 3. R_0 values (when K=0) were 40.09% and 29.11% for bentonite and kaolin, respectively. After the turning point, a hydrophobic modification pattern began to appear, and the slope of S_{BC} curve gently increased. When the modification ratios reached 85.30% CEC (bentonite) and 78.44% CEC (kaolin) of clay, the second turning point appeared as modification mechanisms were dominated by the hydrophobic combination, and presented a significant increase in the S_{BC} curve after the second turning point. These results could verify that at relatively low loadings of surfactant, most of the surfactants were absorbed on the cation sites of soil only via the ion–exchange mechanism [18]. When the concentration of the surfactant exceeded 100% CEC of clays, surfactant molecules adsorbed on clay were by hydrophobic aggregation [17]. All these results were consistent with the findings of Meng [17] and Xu [18].

Selectivity of ion exchange between BS–12 and Ca^{2+}. The Vanselow ion exchange model (see 1.4.1) was used to calculate the selectivity coefficients (K_v) of soil samples in the ionic exchange process. Table 4 showed the selectivity results (LnKv) of soil samples between BS–12 and Ca^{2+} in the ion exchange process. And if the LnKv>1, adsorption preference for BS–12 on soil samples was far greater than that for Ca^{2+}, and the opposite when LnKv<1. So LnKv could be used to demonstrate adsorption preference for BS–12 and Ca^{2+}.

TABLE 3
Results of linear regression equation $K = k \times R + y$, where K is the slope of the S_{BC} curve, r is the correlation coefficient, and R_0 and $R_{CEC/2}$ are the values of R (when K = 0 and CEC/2 of clay minerals) calculated by the equation ($K= k \times R + y$).

Clays	Modification Proportion /R (%)	$K = k \times R + y$						
		S_{BC} Slopes / K	Correlations / r	k	y	Correlations / r	R values R_0, $R_{CEC/2}$ / %	
Bentonite	20	0.0108	0.9745**	0.0111	-0.4451	0.9990**	(R_0)	($R_{CEC/2}$)
	40	0.0146	0.9702**				40.09	85.30
	60	0.1798	0.9863**					
	80	0.4395	0.9948**					
	100	0.7087	0.9916**					
	200	17.740	0.9965**					
Kaolin	20	0.0072	0.9656**	0.0009	-0.0262	0.9963**	(R_0)	($R_{CEC/2}$)
	40	0.0124	0.9879**				29.01	78.44
	60	0.0207	0.9678**					
	80	0.0476	0.9928**					
	100	0.0700	0.9959**					
	200	0.1541	0.9991**					

Note: **indicates that the correlation coefficient is significant at the p = 0.01 level (r = 0.765 when the degree of freedom f = 8 and the level of significance p = 0.01).

TABLE 4
Electivity of ion exchange between BS–12 and Ca^{2+}. LnK_v is the natural logarithm for K_v (Vanselow selectivity coefficients).

Modification	LnK_v	
Proportion / %	Bentonite	Kaolin
20	1.06–9.23	6.74–10.89
40	3.15–11.28	9.64–13.22
60	5.06–12.71	10.45–16.89
80	6.18–10.61	9.28–17.56
100	10.47–12.67	9.99–16.98
200	11.63–12.58	13.01–19.08

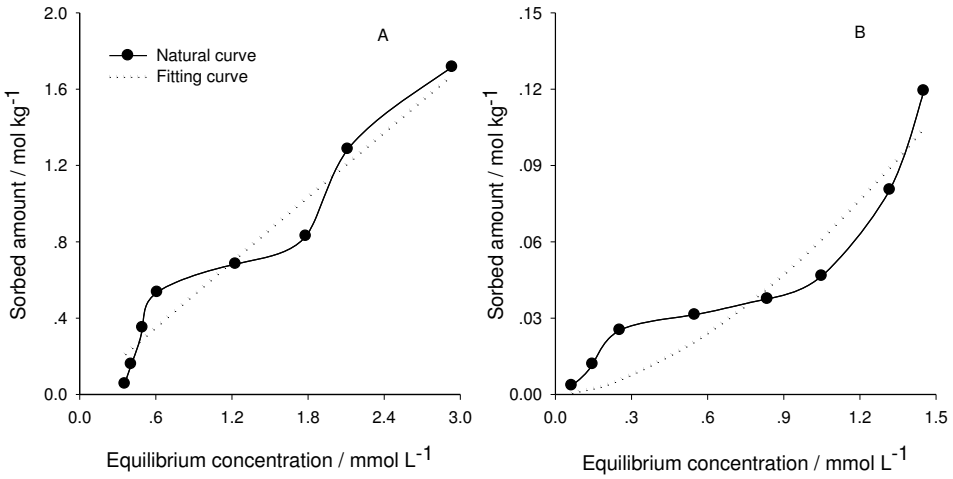

FIGURE 3
Adsorption isotherms of BS–12 at 20 °C on bentonite (A) and kaolin (B). Solid curve means the natural value, and dotted curve is the isotherm fitted by the Freundlich equation. The black dot represents the modified series (10%, 20%, 40%, 60%, 80%, 100%, 150%, 200%).

Ln*Kv* values of bentonite and kaolin samples were 1.06–12.71 and 6.74–19.08, respectively, all greater than 1. The adsorption preference for BS–12 of the two kinds of clay was all far greater than that for Ca^{2+}. The Ln*Kv* values increased significantly with an increase in BS–12 modification ratios, and this was mainly because that the inorganic cations on clay surfaces were easily replaced by organic cations [30], and the ion exchange reaction exhibited a larger trend, leading to larger affinity of soil surface to BS–12, and the form of organic phases. Meanwhile, the organic phase formed by hydrophobic effects showed repulsion to Ca^{2+}. These results conformed to a previous study [31, 32].

Adsorption isotherms of BS–12 on clays. The adsorption isotherms for BS–12 of the two kinds of clays were displayed as "LS" and "S" forms, respectively (Fig. 3). Compared with kaolin, the adsorption ability of BS–12 on bentonite increased noticeably in the modification range from 10% to 60% CEC of clay (equilibrium concentration: 0.41–0.61 mmol L^{-1}, the same as follows), The adsorption ability began to decrease after the modification ratio of 60% CEC of bentonite (0.61 mmol L^{-1}), but rapidly increased again after the modification ratio of 100% CEC of bentonite (1.78 mmol L^{-1}). For kaolin, after the modification ratio of 40% CEC (0.25 mmol L^{-1}), the adsorption ability began to increase with small increments until 100% CEC. After 100% CEC

(1.05 mmol L^{-1}) modification, the adsorption ability increased greatly again.

In the initial stage, the adsorption of BS–12 was mainly by electrostatic adsorption via negative charge points on the surface and with strong affinity adsorption. When the modification ratio reached 40% CEC (kaolin) and 60% CEC (bentonite), the negative charge points on the soil surface decreased and began to form the organic phase, thereby decreasing the adsorption affinity. After the modification ratio of 100% CEC, the organic phase on the soil surface began to accumulate on clay surfaces. Adsorption by the hydrophobic bond mode played a leading role, and made the adsorption affinity increase again.

The fitted curve in Fig. 3 showed distributive adsorption of bentonite and synergistic adsorption type of kaolin modified with BS–12, and this indicated kaolin were easy to appear hydrophobic adsorption when modified with BS–12, and electrostatic adsorption stage of kaolin was shorter than that of bentonite, and quickly began to form organic phases. Nevertheless, the hydrophobic bond mode was the main form until the modification proportion of 100% CEC in the two clays. These findings were evidences to the changes in S_{BC} curves and results of linear regression.

Superficial characteristics of BS–12 modified clays. Compared with raw clay, differently modified clay all had different changes in TOC content, Interlayer spacing (d_{001}) and specific surface–area (S_{BET}) (Table 5). TOC content, d_{001} of the two clays and S_{BET} of bentonite all showed no significant distinction between bentonite and 25%BS bentonite, as well as kaolin and 15%BS kaolin. S_{BET} of kaolin had significant differences between kaolin and 15%BS kaolin. The result presented that enhanced modification in the ion exchange mode was weak. However, the 50% and 100%BS bentonite, 30% and 60%BS kaolin all increased (TOC and d_{001}) or reduced (S_{BET}) more than 25%BS bentonite and 15%BS kaolin, respectively. This showed enhanced modification of hydrophobic effect as BS–12 was modified on clay surfaces. These results corresponded to the results that 25% (bentonite) and 15% (kaolin) modification were in the ion exchange mode, and the hydrophobic modification appeared when the added amount of BS–12 was over 50% (bentonite) and 30% (kaolin) CEC. Previous results of the superficial characteristic on modified clay also indicated strong changes at the modification ratio of around 50% and 100% CEC of clay [23, 33–36].

Two different kinds of clay minerals were compared in this study, and some differences in the adsorption mechanism were observed. Compared with kaolin, the clay structure of bentonite was layered with interlayer space and had high specific surface areas and CEC values [37]. Thus, bentonite showed larger amount of BS–12 by the ion exchange mode. On the other hand, kaolin had low CEC values and small interlayer space, only a small amount of BS–12 entered the kaolin interlayer by the ion exchange mode. The amount of charge sites on clay surfaces determined the adsorption of modifiers on clay minerals [31]. The results reasonably explained the difference of BS–12 modification ratios at which hydrophobic modification appeared. The more amount of BS–12 on clay surfaces by ion exchange, the larger tendency of hydrophobic interaction appeared, presenting different adsorption amount of the two clays.

TABLE 5
TOC, Interlayer spacing (d_{001}) and specific surface–area of BS–12 modified clays.

Clays	Modification Proportion/CEC%	Total organic carbon contents/%	Interlayer spacing /nm	Specific surface–area/(m2/g)
Bentonite	CK	0.46±0.02c	1.43±0.00c	50.61±1.50a
	25BS	5.21±0.12c	1.45±0.01c	43.85±1.07b
	50BS	13.17±0.68b	1.57±0.02b	11.87±0.50c
	100BS	18.52±2.03a	1.96±0.03a	6.25±0.14d
Kaolin	CK	0.01±0.00c	0.71±0.00b	10.12±0.07a
	15BS	0.09±0.01c	0.71±0.01b	10.02±0.18a
	30BS	0.32±0.03b	0.72±0.00a	9.70±0.06b
	60BS	0.62±0.03a	0.72±0.01a	8.27±0.10c

Note: The different lowercase letters indicate significant difference among treatments at 0.05 levels respectively.

CONCLUSIONS

Hydrophobic modification of BS−12 began to appear on bentonite and kaolin at 40.09% and 29.11% CEC of clay minerals, respectively, and became the dominant modification mode at modification ratios of 85.30% and 78.44% CEC for bentonite and kaolin, respectively. LnK_v of the two clays were all greater than 1, indicating greater adsorption preferences for BS−12 than Ca^{2+}, and LnKv values (adsorption preferences) increased significantly with increasing BS−12 modification ratios. Adsorption isotherms increased sharply before the inflection point occurred at the modification ratio of 60% (bentonite) and 40% (kaolin) CEC of clay. The upward tendency began to decrease after this modification ratio, and rapidly rose again after the modification ratio of 100% CEC of the clay. TOC content and d_{001} of the two clays and S_{BET} of bentonite all showed no significant distinction between bentonite and 25%BS bentonite, as well as kaolin and 15%BS kaolin. In addition, S_{BET} of kaolin had significant differences between kaolin and 15%BS kaolin. The characteristics of 50% and 100%BS bentonite, and 30% and 60%BS kaolin significantly increased (for TOC and d_{001}) or reduced (S_{BET}) compared with that of 25%BS bentonite and 15%BS kaolin, respectively. The results provided good evidences for the modification mechanisms.

ACKNOWLEDGEMENTS

The authors wish to acknowledge and thank the financial assistance from the National Natural Science Foundation of P.R. China (No. 41271244), Social Development Project (No. 2013K0105), and Agricultural Science and Technology Project (No. 2012K0215) in Shaanxi Province.

Conflict of intrests. The authors declare that they have no conflict of interest.

REFERENCES

[1] Faiza, B., Gerhard, L., 2001. Surface modification of clay minerals. Appl. Clay Sci. 19(1), 1-3.

[2] Zha, F., Huang, W.Y., Wang, J.Y., Chang, Y., Ding, J., Ma, J., 2013. Kinetic and thermodynamic aspects of arsenate adsorption on aluminum oxide modified palygorskite nanocomposites. Chem. Eng. J. 215/216, 579-585.

[3] Bowman, R.S., Li, Z., Roy, S.J., Burt, T., Johnson, T.L., Johnson, R.L., 2002. Physical and Chemical Remediation of Contaminated Aquifers. In: Smith JA, Burns S (Eds.), Kluwer Academic Pulishers, pp. 161-163

[4] Chen, H., Zhou, W., Zhu, K., Zhan, H., Jiang, M., 2004. Sorption of ionizable organic compounds on HDTMA-modified loess soil. Sci. Total. Environ. 326(1-3), 217-223.

[5] Gus'kov, V.Y., Gainullina, Y.Y., Ivanov, S.P., Kudasheva, F., 2014. Thermodynamics of organic molecule adsorption on sorbents modified with 5-hydroxy-6-methyluracil by inverse gas chromatography. J. Chromatogr. A. 1356, 230-235.

[6] Bhattacharyya, K.G., Gupta, S.S., 2008. Adsorption of a few heavy metals on natural and modified kaolinite and Bentonite: A review. Adv. Colloid Interface Sci. 140(2), 114-131.

[7] Gonzalez, M., Mingorance, M.D., Sanchez, L., Pena, A., 2008. Pesticide adsorption on a calcareous soil modified with sewage sludge and quaternary alkyl-ammonium cationic surfactants. Environ. Sci. Pollut. Res. Int. 15(1), 8-14.

[8] Ma, J.F., Qi, J., Yao, C., Cui, B.Y., Zhang, T.L., Li, D.L., 2012. A novel bentonite-based adsorbent for anionic pollutant removal from water. Chem. Eng. J. 200/202, 97-103.

[9] Li, Z., Bowman, R.S., 2001a Retention of inorganic oxyanions by organo-kaolinite. Water Res. 35(16), 3771-3776.

[10] Li. Z., Alessi, D., Zhang, P., Bowman, R.S., 2002. Organo-illite as a low permeability sorbent to retard migration of anionic contaminants. J. Environ. Eng. 128(7), 583-587.

[11] Zhou, W., Zhu, K., Zhan, H., Jiang, M., Chen, H., 2003. Sorption behaviors of aromatic anions on loess soil modified with cationic surfactant. J. Hazard. Mater. 100, 209-218.

[12] Bosco, S.M.D., Jimenez, R.S., Vignado, C., Fontana, J., Geraldo, B., Figueiredo, F.C.A., Carvalho, W.A., 2006. Removal of Mn(II) and Cd(II) from wastewaters by natural and modified clays. Adsorption. 12(2), 133-146.

[13] Lee, S.M., Tiwari, D., 2012. Organo and inorgano-organo-modified clays in the

remediation of aqueous solutions: An overview. Appl. Clay Sci. 59/60, 84-102.
[14] McBride, M.B., 1994. Environmental Chemistry of Soils. Oxford University Press, New York, pp. 363.
[15] Alkaram, U.F., Mukhlis, A.A., Al-Dujaili, A.H., 2009. The removal of phenol from aqueous solutions by adsorption using surfactant-modified bentonite and kaolinite. J Hazard Mater. 169(1-3), 324-332.
[16] Li, Z.H., Zhang, T., Dai, H.Y., Liu, G.H., Wang, H.B., Sun, Y.Y., Zhang, Y., Ge, Z.M., 2007. Involvement of endoplasmic reticulum stress in myocardial apoptosis of streptozocin-induced diabetic rats. J. Clin. Biochem. Nutr. 41(1), 58-67.
[17] Meng, Z.F., Gong, N., Li, R.H., Zhang, Z.Q., Zhang, Y.P., 2008a. Ionic Exchange Modification Mechanism Between Organic Modifier and Lou Soil. Environ. Sci. 29(5), 1412-1417, In Chinese.
[18] Xu, S.H., Boyd, S.A., 1995. Cationic surfactant sorption to a vermiculitic subsoils via hydrophobic bonding, Environ. Sci. Technol. 29(5), 312-320.
[19] Chen, B.L., Zhu, L.Z., Zhu, J.X., Xing, B.S., 2005. Configurations of the bentonite-sorbed myristylpyridinium cation and their influences on the uptake of organic compounds. Environ. Sci. Technol. 39(16), 6093-6100.
[20] Zhu, J.X., Qing, Y.H., Wang, T., Zhu, R.L., Wei, J.M., Tao, Q., Yuan, P., He, H.P., 2011. Preparation and characterization of zwitterionic surfactant-modified Bentonites. J. Colloid Interface Sci. 360(2), 386-392.
[21] Bonczek, J.L., Nkedi-Kizza, P., 2007. Using surfactant-modified clays to determine sorption mechanisms for a representative organic base, quinoline. J Environ. Qual. 36(6), 1803-1810.
[22] Wu, Y., Luo, H.J., Wang, H., Wang, C., Zhang, J., Zhang, Z.L., 2013. Adsorption of hexavalent chromium from aqueous solutions by graphene modified with cetyltrimethylammonium bromide. J. Colloid Interface Sci. 394, 183-191.
[23] Meng, Z.F., Zhang, Y.P., Wang, G.D., 2007. Sorption of heavy metal and organic pollutants on modified soils. Pedosphere. 17(2), 235-245.
[24] Meng, Z.F., Zhang, Y.P., Zhang, Z.Q., 2008b. Simultaneous adsorption of phenol and cadmium on amphoteric modified soil. J. Hazard. Mater. 159(2-3), 492-498.
[25] Wang, Z.M., Zhou, F.Q., Ma, X.F., Qiu, L.M., 1999. The purification and application of bentonite, Non-Metallic Mines. 22, 19-20.
[26] Sun, W., Yv, B., 2004. Microanalysis of sulfitobetaine. J. Nanjing Univ. Technol. 26(2), 88-91, In Chinese.
[27] Jiang, Y.C., Zhang, Y.P., 1993. The physical chemistry of soil chemical processes. China Science and Technology Press, Peking, pp. 117-203, In Chinese.
[28] Bektaş, N., Soysal, D., 2004. Kinetics of phosphate removal using surfactant modified clinoptilolite. Fresen Environ Bull. 13(4), 366-369.
[29] Xu, S.H., Boyd, S.A., 1994. Cation exchange chemistry of hexadecyltrimethylammonium in a subsoil containing vermiculite. Soil Sci. Soc. Am. J. 58(5), 1382-1391.
[30] Solomon, H.D., Devine, T.M., 1983. Duplex Stainless Steels, Proceedings of Conference on Duplex Stainless Steels, Metal Park, pp. 693-756.
[31] Wang, X.R., Wu, S.N., Li, W.S., Sheng, G.Y., 1997. Contaminated environment remediation with organoclay minerals. Environ. Chem. 16(1), 1-13.
[32] Kyziol-Komosinska, J., 2009. Influence of properties of selected metal ions on their sorption onto neogene clays. Fresen Environ Bull. 18(7), 1080-1085.
[33] Anirudhan, T.S., Ramachandran, M., 2007. Surfactant-modified bentonite as adsorbent for the removal of humic acid from wastewaters. Appl. Clay Sci. 35(3), 276-281.
[34] Meng, Z.F., Zhang, Y.P., Guo, Z.Y., 2008c. Surface characteristics of organic modified soil I.CEC and specific surface area. Acta Pedologica Sinica. 45(2), 370-374, In Chinese.
[35] Slade, P.G., Gates, W.P., 2004. The swelling of HDTMA smectites as influenced by their preparation and layer charges. Appl. Clay. Sci. 25(s1-2), 93-101.
[36] Shen, Y.H., 2004. Phenol sorption by organoclays having different charge characteristics. Colloid Surf. A. 232, 143-149.
[37] Tanabe, K., 1981. Catalysis Science and Technology, Springer Verlag, New York, pp. 86-182.

Received: **21.09.2015**
Accepted: **25.12.2015**

CORRESPONDING AUTHOR

Dr. Zhaofu Meng
Department of Natural Resource and Environment, Northwest A&F University, and Key Laboratory of Plant Nutrition and Agri–Environment in Northwest China Ministry of Agriculture
Yangling, Shaanxi, 712100, P R - CHINA

E-mail: zfmeng@hotmail.com

© by PSP Volume 25 – No. 10/2016, pages 4004-4012 Fresenius Environmental Bulletin

ESTIMATION OF THE LONGITUDINAL DISPERSION COEFFICIENT FOR RIVER NETWORKS USING A DIFFERENTIAL EVOLUTION ALGORITHM

Xiaodong Liu[1, 2], Shengcheng Mei[1], Li Gu[1, 2], Qile Tu1, Zulin Hua[1, 2,*]

[1]Key Laboratory of Integrated Regulation and Resource Development on Shallow Lake of Ministry of Education, College of Environment, Hohai University, Nanjing 210098, P.R. China
[2]National Engineering Research Center of Water Resources Efficient Utilization and Engineering Safety, Nanjing 210098, P.R. China

ABSTRACT

Parameter estimation for river network systems is an important issue in environmental science and has attracted increasing interest from various research fields, it could be essentially formulated as a multidimensional optimization problem. As a novel evolutionary computation technique, differential evolution (DE) algorithm has attracted much attention and wide applications owing to its simple concept, easy implementation and quick convergence. In this paper, a new parameter identification model based on a DE algorithm coupled with a water quality model was constructed for the determination of longitudinal dispersion coefficients for river networks. It concluded that a DE algorithm has better global convergence than a standard genetic algorithm in the solution of De Jong function F2. The method was validated by a river network numerical test which was composed of nine channels. The computational results indicated that the model could give good identification precision results.

KEYWORDS:
River network; Differential evolution (DE); Parameter identification; Optimization; Water quality model

INTRODUCTION

The prediction of pollutant concentration downstream of its disposal into a stream is crucial for maintaining a suitable water quality standard. The longitudinal dispersion coefficient (LDC) is a fundamental parameter in hydraulic modeling of river pollution, as it is a measure of the intensity of the mixing of pollutants in natural streams and is, therefore, of great interest to river managers, environmental engineers, institutional researchers, among others, who are involved in river water pollution control. For streams in which mixing and dispersion characteristics are unknown, the dispersion coefficient can only be estimated using empirical equations, theoretical equations or tracer test methods. Each approach has its own merits and demerits. Theoretical derivation of the LDC is a classic method using velocity profiles[1]. The theoretical method requires detailed measurement of velocity distribution along three Cartesian coordinate systems, and usually has difficulties in natural streams. Thus, the theoretical method is not encouraging in terms of data requirement. A number of investigators have developed empirical equations for predicting the dispersion coefficient based on experimental and field data[7]. They have developed relationships for dispersion coefficient in terms of the known hydraulic characteristics of the stream. But since most studies have been conducted based on specific assumptions and channel conditions, the behavior of existing equations varies widely even for the same flow conditions and streams[5]. Thus, Gokmen Tayfur[15] derived an expression for prediction of the LDC in natural rivers using a genetic algorithm optimized model. He observed that the performance of the model was better than existing equations. Riahi-Madvar et al.[16], developed a new flexible tool to predict the LDC using the adaptive neuro-fuzzy inference system (ANFIS). They found that dispersion coefficient values predicted by the ANFIS model satisfactorily compared with the measured values and also provides better prediction than published relationships. Comparatively, the tracer test method is thought to be more accurate and reliable. The LDC can be obtained by using curves of the temporal variation of concentration (C–t curves) at one or more station downstream of the injection point. Many research achievements on tracer test methods have been published, such as the moment

method[4], routing procedure[17], optimization method [18] and genetic algorithm[20]. However, they need a tracer test which is very expensive. The above mentioned methods have been successfully applied to predict LDC of a single natural steam. However, they are difficult to apply on producing water quality parameters for a river network model. River networks are one of the most widespread and recognizable features of Earth's landscapes[21]. In general, a river network model has many stream segments and each segment includes unknown parameters. The determination of the unknown parameters generally requires a great deal of effort because they are dependent on complex physical and hydraulic factors of different streams. The popular method of parameter selection is a trial-and-error method that adjusts parameters continuously until there is an optimal agreement between predicted values and measured data. This method needs a subjective and laborious step in the water quality model calibration process because water quality state variables and model parameters are cross-related to each other. This requires high computational cost and expert practical ability. To overcome these difficulties and obtain reliable water quality model performance, more efficient and robust processes are required.

Many optimization methods are employed to estimate unknown parameters. The Gauss-Newton method is considered the most effective and popular method due to the fact that it does not require the calculation of the Hessian matrix and the rate of convergence is superior when compared to other methods[22]. However, the Gauss-Newton method cannot converge in certain conditions because it requires a modification of the algorithm[24]. A traditional optimization algorithm has the ability to converge from a wider range of initial guesses but its solution usually converges to local minimum points, thus sometimes the optimum solution cannot be obtained. This limits their application in multi-parameter identification for complicated models. To address this, many new intelligent optimization algorithms have been tried to predict the parameters of water-quality models[25]. Recently, a new evolutionary technique, differential evolution (DE), has been proposed for unconstrained continuous optimization problems[26]. Although the original objective in the development of DE was for solving the Chebychev polynomial problem, it has been found to be an efficient and effective solution technique for complex functional optimization problems. Due to the simple concept, easy implementation and quick convergence, nowadays the DE algorithm has attracted much attention and wide applications[27]. However, to the best of our knowledge, there is no published work on DE for estimating parameters of water quality models. In this paper, a DE approach is applied to estimate the parameters of a river network model. Numerical cases and comparisons demonstrate the effectiveness and robustness of DE. Moreover, the effect of population size on the optimization performances is also investigated.

MATERIAL AND METHODS

Water quality model for river network. Governing equation. The evolvement of pollution in rivers includes advection, dispersion, attenuation, etc. Basically, the general equation for solute transport considering advection-dispersion is as follows:

$$\frac{\partial(AC)}{\partial t}+\frac{\partial(QC)}{\partial x}=\frac{\partial}{\partial x}(AE_x\frac{\partial C}{\partial x})-AKC+S \quad (1)$$

Where A is a cross-sectional area of river, C is cross-sectional average concentration, Q is flow discharge, E_x is LDC, K is pollutant degradation coefficient, x is longitudinal coordinate, t is time, S is net source term.

Only under conditions of instantaneous source with steady uniform flow, can the analytic solution of the equation be obtained. Numerical methods must be used to solve the above equation in other conditions. So finite differential method (FDM) is adopted here. The studied river is divided into N sections. Each term of equation (1) is obtained by the upwind implicit scheme:

$$\frac{\partial(AC)}{\partial t}=\frac{(AC)_i^{k+1}-(AC)_i^k}{\Delta t} \quad (2)$$

$$\frac{\partial(QC)}{\partial x}=\frac{(QC)_i^{k+1}-(QC)_{i-1}^{k+1}}{\Delta x_{i-1}} \quad (3)$$

$$\frac{\partial}{\partial x}(AE_x\frac{\partial C}{\partial x})=\left[\frac{(AE_x)_i^{k+1}C_{i+1}^{k+1}-(AE_x)_i^{k+1}C_i^{k+1}}{\Delta x_i}-\frac{(AE_x)_{i-1}^{k+1}C_i^{k+1}-(AE_x)_{i-1}^{k+1}C_{i-1}^{k+1}}{\Delta x_{i-1}}\right]\frac{1}{\Delta x_{i-1}} \quad (4)$$

$$KAC-S=\overline{K}_{d,i-1}^{k+1}(AC)_i^{k+1}-\overline{S}_{i-1}^{k+1} \quad (5)$$

Where $\overline{K_d}$ represents the degradation coefficient of the river section. Details about the upstream

scheme can be found in the literature[29]. From this scheme, the discrete equations can be given as:

$$a_i C_{i-1} + b_i C_i + c_i C_{i+1} = z_i \quad (6)$$

Where the subscripts i and i+1 denote the locations of the current and next micro-section.

Water quality junction equation. The water quality conditions at the junctions can be expressed by mass conservation equations. The continuity equation can be written as

$$\sum_{l=1}^{m} (QC)_{jl} = A_j C_j (\frac{dz_j}{dt})$$

where j is the junction, m is all channels that link to the junction j, A_j is storage area of the junction j. Upstream boundary conditions are mostly given in the form of discharge time series Q_1(t) and variables concentration time series C_1(t), and the initial condition C(0) is known. The equations and boundary conditions can constitute cyclic tri-diagonal equations, which can be solved by the chase-after method. The detailed calculation can be found in Chu, 1994[30], and Zhang et al., 2008[31].

Parameter identification model based on differential evolution. The trial-and-error method can only partially adjust the parameters for the numerical models of river network, since the capacity of the modeler is finite. If this problem is addressed by automated means, the convergence criterion of the model can be easily assigned and the adjustment can cover all the rivers in the network. The majority of previous research into parameter estimation in river network models has centered on calibrating Manning coefficient (n) of river networks hydrodynamic model automatically[32]. The identification of LDC for water quality model is studied here.

If there is spatial variation of LDC, as was found in many river networks, there must be an optimal group of parameter values to match the computational results with the field data. So the parameter calibration problem can be addressed as an optimization problem. The agreement between the measured results and simulated values is one of the most important indicators as to how well a model is calibrated. A target function J is used to measure the agreement and can be expressed mathematically as follows:

$$J(C,E) = \int_0^T \frac{1}{2} \left\| C - C^* \right\|^2 dt \quad (7)$$

Where, $X = (x_1, x_2, ..., x_n)$ and is the parameter vector, n is the number of parameters to be identified, C^* is measured concentration vector, and C is the simulated value corresponding to C^*. In parameter identification, model parameters are adjusted to achieve satisfactory agreement between the measurements and simulation for all variables simultaneously. This process can be described mathematically as follows:

$$\text{Minimize } J = f(x_1, x_2, ..., x_n) \quad (8)$$

$$\text{Subject to } x_{ilow} \le x_i \le x_{iup} \quad i = 1, 2, ..., n \quad (9)$$

where, x_{ilow} and x_{iup} represent the lower bound and upper bound of the parameter x_i. The extreme value problem can be solved by a DE algorithm coupled with FDM water quality model for river networks.

In DE, the jth individual in the d-dimensional search space at generation t can be represented as X_j, j=1, 2,…, NP, where NP denotes the size of the generation. The procedure of the parameters identification model can be summarized as follows:

Step 1. *Initialization*: the initial population is generated from specified ranges of parameters by random methods, although there may be different methods for specific problems. Random selection is usually preferred for keeping a suitable balanced distribution in the initial population. $x_i^0 = x_{ilow} + rand \times (x_{iup} - x_{ilow})$, where *rand* is a random number between 0 and 1 which can be given by random function.

Step 2. *Designation of the fitness function*: since the DE can only make the individual evolution in the direction where the fitness increases, the DA can only be applied to seek a maximum point rather than a minimum point. Hence, there is a need to rewrite Eq. (8)

$$Fit(X) = \begin{cases} J_{\max} - J(X) & \text{when } J(X) < J_{\max} \\ 0 & \text{otherwise} \end{cases} \quad (10)$$

where $Fit(X)$ is the fitness function for the DA

and $J_{\max}$ is the given maximum of $J(X)$.

Step 3. *Calculation of fitness*: C_k is simulated by the FDM model, and C_k^* is obtained by measurement. Calculate the fitness of the current *X*. Check the fitness whether it has satisfied termination criterion (for example, $T > T_m$, where *T* is the number of generation). If so, output the current value of *X* as the final parameter estimation results. Otherwise continue.

Step 4. *Mutation*. For each target individual $X_j(t)$, according to the mutation operator, a mutant vector $V_j(t+1) = (v_1(t+1),...,v_n(t+1))$ is generated by adding the weighted difference between a defined number of individuals randomly selected from the previous population to another individual, which is described by the following equation:

$$V_j(t+1) = X_{r1}(t) + F(X_{r2}(t) - X_{r3}(t)) \qquad (11)$$

Where $r1, r2, r3$ are randomly chosen and mutually different and also different from the current index *j*. $F \in [0,2]$ is a constant called scaling factor which controls amplification of the differential variation $X_{r2}(t) - X_{r3}(t)$, and NP is at least 4 so that the mutation can be applied.

Step 5. *Crossover*. The crossover operator is applied to increase the diversity of the population. Thus, for each target individual $X_j(t)$, a crossover vector $U_j(t+1) = (u_1(t+1),...,u_n(t+1))$ is generated by the following equation:

$$u_j(t+1) = \begin{cases} v_i(t+1), & \text{if } (rand(i) \le CR) \text{ or } i = randn(j) \\ x_i(t), & otherwise \end{cases} \quad i = 1,2,...,n \qquad (12)$$

Where $rand(i)$ is the *i*th independent random number uniformly distributed in the range of [0,1]. $randn(j)$ is a randomly chosen index from the set $\{1,2,...,n\}$. $CR \in [0,1]$ is a constant called crossover parameter that controls the diversity of the population.

Step 6. *Selection*. After the crossover operation, the selection arises to decide whether the vector $U_j(t+1)$ would be a member of the population of the next generation. For a minimum optimization problem, $U_j(t+1)$ is compared to the initial target individual $X_j(t)$ by the following one-to-one based greedy selection criterion:

$$X_j(t+1) = \begin{cases} U_j(t+1), & \text{if } f(U_j(t+1)) \le f(X_j(t)) \\ X_j(t), & otherwise \end{cases} \qquad (13)$$

where *f* is the objective function under consideration, $X_j(t+1)$ is the individual of the new population. After this go back to step 3.

The flow chart of the parameter identification model can be seen in Fig.1.

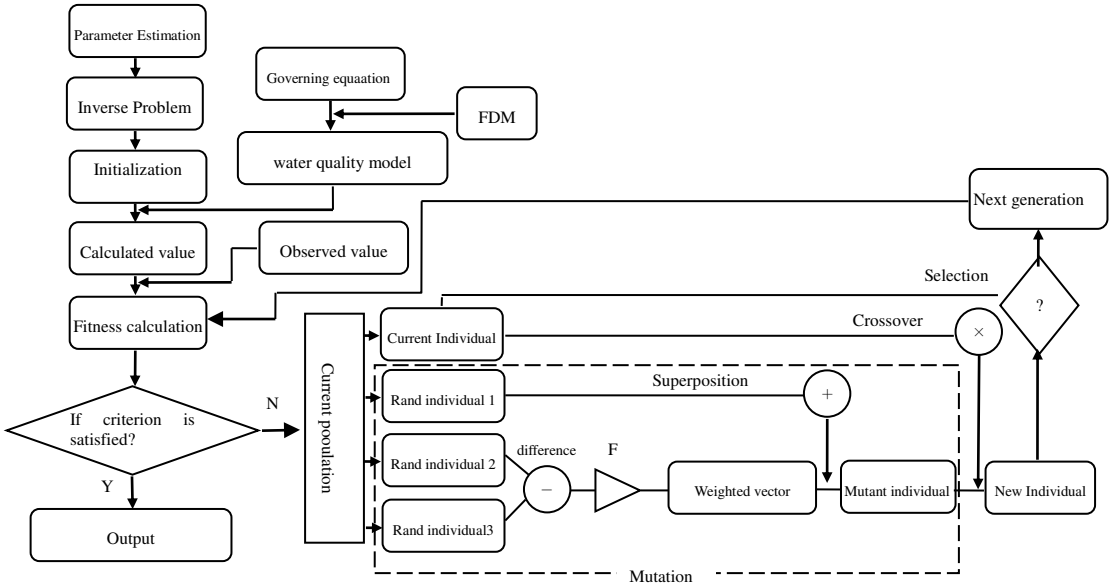

FIGURE 1
Flow chart diagram for the parameter identification model

TABLE 1
computed results between DE and SGA

algorithm	evolutional generation	population size	x_1	x_2	f_2
SGA	100	10	0.7556	0.5693	0.0600
	1000	100	0.9653	0.9316	0.0012
DE	100	10	1.0009	1.0019	0.0000
	200	10	1.0000	1.0000	0.0000

RESULTS AND DISSCUSION

Two cases are used for method verification. Case 1 is applied to verify the performance of the DE algorithm. Case 2 is applied to verify the parameter identification model based on DE.

Case 1. De Jong function *F2* is usually applied to verify the performance of optimization algorithms. The function has a global minimum point $f_2(1.0,1.0) = 0.0$, which can't be searched by local optimization algorithms. De Jong function *F2* can be written as:

$$f_2(x_1, x_2) = 100(x_1^2 - x_2)^2 + (1 - x_1)^2 \quad x_i \in [-5.12, 5.12]$$

For algorithm verification, the results of DE are compared to the results of the standard genetic algorithm[33] (SGA), which are showed in Table I.

The results show SGA converges to local optimal solution when population size is 10 (Fig.2), this is called premature convergence. To restrain the premature convergence, population size has to be expanded to 100. Then an approximate solution is obtained (Fig.3). Nevertheless, DE can converge to global optimal solution even when population size is 10 (Fig.4). Computed results show that DE has better global convergence than SGA.

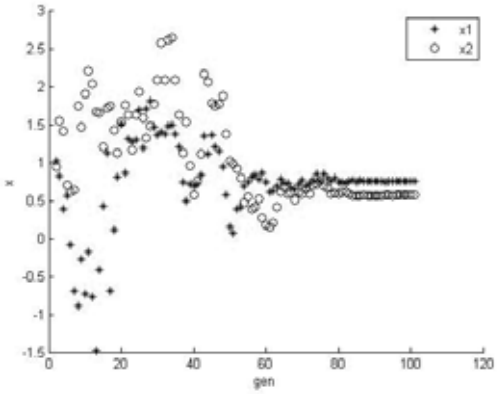

FIGURE 2
SGA evolution process when population size is 10

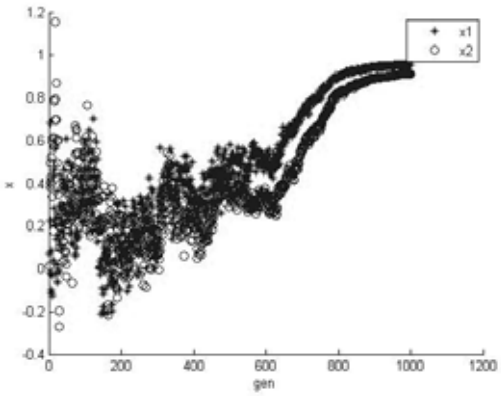

FIGURE 3
SGA evolution process when population size is 100

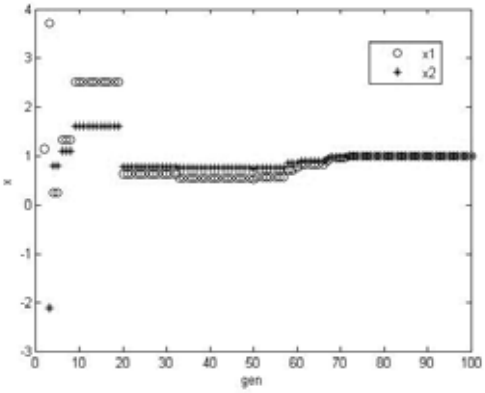

FIGURE 4
DE evolution process when population size is 100

Case 2. Test data are taken from the literature[32]. The case was a numerical test, not an actual test. The river network composed of nine channels, which is shown in Fig.5. Initial concentration in the studied river is assumed to be 0 mgL^{-1}. The inflow discharge is 10 m^3/s, and upstream concentration C_0=10 mgL^{-1}. The denoted LDCs and velocities of the channels are shown in Table 2. Then the concentrations of the final section of nine segments can be obtained by a water quality model, data shown in Table 3. The LDCs of the six sections are supposed to be unknown parameters, which should be identified by parameter identification model if the proposed model is correct.

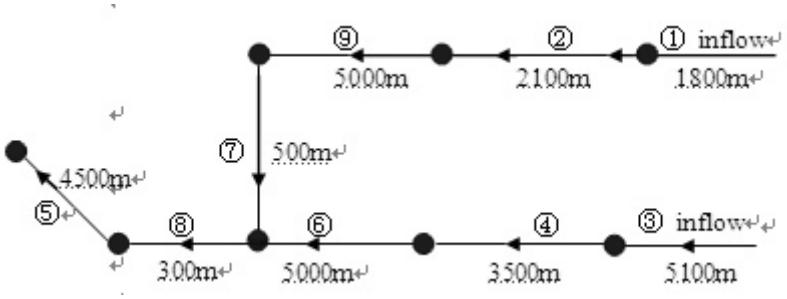

FIGURE 5
River network

TABLE 2
Computational coefficients

Stream number	LDC (m^2/s)	velocity (m/s)	Stream number	LDC (m^2/s)	Velocity (m/s)
1	25	3.62	6	50	2.40
2	30	2.71	7	55	2.36
3	35	2.67	8	60	2.37
4	40	2.36	9	65	2.84
5	45	2.56			

TABLE 3
Concentration values used in parameter identification (mg/l)

t/min	Steam section number								
	1	2	3	4	5	6	7	8	9
10	8.64	7.25	6.41	4.60	2.38	2.90	4.57	3.62	4.81
20	9.80	9.37	8.68	7.52	5.16	5.79	7.65	6.62	7.82
30	9.96	9.84	9.49	8.90	7.22	7.72	9.05	8.33	9.13
40	9.98	9.94	9.77	9.50	8.47	8.80	9.59	9.17	9.63
50	9.98	9.95	9.88	9.73	9.14	9.35	9.79	9.55	9.80
60	9.98	9.96	9.91	9.83	9.48	9.61	9.85	9.72	9.86

TABLE 4
estimation result of parameters by DE

Channel number	True value (m^2/s)	Calculated value (m^2/s)	Relative error
1	25	25.738	2.95%
2	30	30.726	2.42%
3	35	35.692	1.98%
4	40	42.203	5.51%
5	45	43.202	4.00%
6	50	50.840	1.68%
7	55	53.087	3.48%
8	60	58.669	2.22%
9	65	65.362	0.56%

Denoting the data in Table 3 as measured concentration, the parameters of all channels can be estimated by the parameter identification model based on DE. The key parameters in DE are NP (size of population), F (scaling factor) and CR (crossover parameter). Proper configuration of the above parameters would achieve a good tradeoff between the global exploration and the local exploitation so as to increase the convergence velocity and robustness of the search process. In general, NP is choosing from 5*n* to 10*n* (*n*-number of dimensions). F and CR lie in the range of [0.4,1.0] and [0.1,1.0], respectively. In this case, NP=50, F=0.8, and CR=0.8.

The calculated results are shown in Table 4. These values are very close to the assumed values and the maxim error is only 5.51%. It is concluded that satisfactory results can be obtained.

CONCLUSION

DE is a population-based evolutionary computation technique, which uses a simple differential operator to create new candidate solutions and a one-to-one competition scheme to greedily select new candidates. The theoretical framework of DE is very simple and is easy to be coded and implemented by computer. Besides, it is computationally inexpensive in term of memory requirements and CPU times. Compared with SGA, the DE algorithm has better global convergence in the solution of De Jong function *F2*.

To avoid the shortcomings of traditional optimization algorithms, a new multi-parameters estimation model based on DE coupled with river network water quality model was proposed in this paper. The calculated result shows that it has high accuracy for estimation of LDCs.

ACKNOWLEDGEMENTS

This research was supported by the National Nature Science Foundation of China (Grant No. 51479064, 51379058, 51379060), a Project Funded by the Priority Academic Program Development of Jiangsu Higher Education Institutions（PAPD） and Qing Lan Project.

REFERENCES

[1] Taylor, G. I. 1953. The dispersion of soluble matter in solvent flowing through a tube. Proceedings of Royal Society of London 219A, 186–203.

[2] Taylor, G. I. 1954.The dispersion of matter in turbulent flow through a pipe. Proceedings of Royal Society of London 23A, 446–468.

[3] Elder, J. W.□1959 The dispersion of markedfluid in turbulent shear flow. *Journal of Fluid Mechanics* 5(4), 544–560.

[4] Fischer, H. B., List, E. J., Koh, R. C. Y., Imberger, J. & Brooks, N. H. 1979 *Mixing in Inland and Coastal Waters.* Academic Press, New York.

[5] Seo, I. W. & Cheong, T. S. 1998. Predicting longitudinal dispersion coefficient in natural streams. *Journal of Hydraulic Engineering* 24(1), 25–32.

[6] Ahmad, Z. 2003. Estimation of longitudinal dispersion coefficients. Journal of *Hydraulic Engineering* 9(1), 14–28.

[7] McQuivey, R. S. & Keefer, T. N. 1974. Simple method for prediction dispersion in streams.Journal of Environment Engineering 100, 997–1011.

[8] Sooky, A. A. 1969. Longitudinal dispersion in open channels. *Journal of Hydraulic Division*

95(4), 1327–1346.

[9] Magazine, M. K., Pathak, S. K. & Pande, P. K. 1988. Effect of bed and side roughness on dispersion in open channels. Journal of Hydraulic Engineering114(7), 766–782.

[10] Asai, K., Fujisaki, K. & Awaya, Y. 1991. Effect of aspect ratio on longitudinal dispersion coefficient. In: Environmental Hydraulics (J. H. W. Lee & Y. K. Cheung, eds). Balkema, Rotterdam, pp. 493–498.

[11] Ahmad, Z., Kothyari, U. C. & Ranga Raju, K. G. 1999. Longitudinal dispersion in open channel flows. J*ournal of Hydraulic Engineering* 5(2), 1–21.

[12] Deng, Z. Q., Singh, V. P. & Bengtsson, L. 2001 Longitudinal dispersion coefficient in straight rivers. *Journal of Hydraulic Engineering*127(11), 919–927.

[13] Kashefipour, S. M. & Falconer, R. A. 2002. Longitudinal dispersion coefficients in natural streams. *Water Research* 36,1596–1608.

[14] Sahay, R. R. & Dutta, S. 2009 Prediction of longitudinal dispersion coefficients in natural rivers using genetic algorithm. *Hydrology Research*40(6), 544–552.

[15] Gokmen Tayfur. 2009 GA-optimized model predicts dispersion coefficient in natural channels *Hydrology Research* 40(1), 65-78.

[16] Riahi-Madvar, H., Ayyoubzadeh, S. A., Khadangi, E. &Ebadzadeh, M. M. 2009 An expert system for predicting longitudinal dispersion coefficient in natural streams by using ANFIS. *Expert Systems with Applications*36, 8589–8596.

[17] Gu L. , Hua Z. L., He W. 2007 Routing-optimization method for determination of longitudinal dispersion coefficient in river, Journal of Hydraulic Engineering 38(11), 1421-1425. (in Chinese)

[18] Ho D. T., Schlosser P., and Caplow T. 2002 Determination of longitudinal dispersion coefficient and net advection in the tidal Hudson River with a large-scale, high resolution SF6 tracer release experiment. *Environmental Science & Technology* 36(15) : 3234-3241.

[19] Liu X.D., Hua Z.L., Xue H.Q., Gu L. and Xie Z.F.(2011) Inverse optimization method to determine longitudinal dispersion coefficient and selection of sampling time in tracer test. *Fresen. Environ. Bull.* 20 (5), 1149-1154.

[20] Liu X.D.**,** Zhou Y.Y., Hua Z.L., Chu K.J., Wang P., Gu L., and Chen L.Q., Parameter identification of river water quality models using a genetic algorithm, *Water Science & Technology*, 2014, 69(4):687-693.

[21] J. T. Perron,P. W. Richardson,K. L. Ferrier, M. Lapôtre, 2012 The root of branching river networks. *Nature* 492, 100–103.

[22] Bard, Y. 1970 Comparison of gradient methods for the solution of nonlinear parameter estimation problems. SIAM Journal of Numerical Analysis, 7(1) ,157-186.

[23] Yeh, W. W. G. 1986 Review of parameter identification procedures in groundwater hydrology: The inverse problem. *Water Resources Research*, 22(2), 95-108.

[24] Kim T. and Sheng Y. P. 2010 Estimation of Water Quality Model Parameters *Journal of Civil Engineering* 14(3),421-437.

[25] Toprak Z. F., and Cigizoglu H. K. 2008 Predicting longitudinal dispersion coefficient in natural streams by artificial intelligence methods. *Hydrological Processes* 22(20), 4106-4129.

[26] Storn R, Price K. 1997 Differential evolution – a simple and efficient heuristic for global optimization over continuous spaces. *J Global Optim*11,341–59.

[27] Khazraee SM, Jahanmiri AH, Ghorayshi SA 2010 Model reduction and optimization of reactive batch distillation based on the adaptive neuro-fuzzy inference system and differential evolution. *Neural Comput Applic* 20(2),239–248.

[28] Peng B., Liu B., Zhang F.Y., Wang L. 2009 Differential evolution algorithm-based parameter estimation for chaotic systems. *Chaos, Solitons and Fractals* 39,2110–2118.

[29] Tang H.W., Xin X.K., Dai W.H., Xiao Y. 2010 Parameter identification for modeling river network using a genetic algorithm. *Journal of Hydrodynamics Ser.B*,22(2),246-253.

[30] Chu J. D. 1994 Solution and application of convection transport problem for river networks. *Journal of Hydraulic Engineering*, (10): 14-23 (in Chinese).

[31] Zhang M.L., Shen Y.M., Guo Y.K. 2008 Development and application of a eutrophication water quality model for river networks. Journal of Hydrodynamics, Ser. B, ,20(6),719-726.

[32] Zhang C., Mao G.H., Zhang T.Q., Zhu S., Cheng W.P. 2008 Inversion of roughness

parameter of river network based on BP-Bayesian method. *Journal of Jiangsu University* 29(1),47-51.

[33] Liu X.D., Xue H.Q., Xie Z.F.,Yao Q. Genetic Algorithm for Determination of LongitudinalDispersion Coefficient in River for tracer test. *2010 Sixth International Conference on Natural Computation*. 2010,8.

Received: **27.10.2015**
Accepted: **23.01.2016**

CORRESPONDING AUTHOR

Zulin Hua
College of Environment Hohai University(HHU)
Xikang Road 1 Nanjing 210098 P.R. CHINA

E-mail: zulinhua00@163.com

© by PSP Volume 25 – No. 10/2016, pages 4013-4025 Fresenius Environmental Bulletin

BENTHIC DIATOMS AS INDICATORS OF WATER QUALITY IN THE ACARLAR FLOODPLAIN FOREST (NORTHERN TURKEY)

Tugba Ongun Sevindik[1]*, Fatma Kucuk[2]

[1]Sakarya University, Faculty of Arts and Science, Department of Biology, 54187, Adapazarı, Turkey
[2]Atatürk University, Faculty of Fisheries, 25240, Erzurum, Turkey

ABSTRACT

The structure and diversity of the epilithic and epiphytic diatom community and their relationship with the physicochemical parameters of the Acarlar Floodplain Forest were studied. Also, diatom indices and their applicability as a tool for estimating the floodplain water quality were tested. Diatoms were sampled monthly from February 2011 to January 2012 at three sites. A total of 94 taxa were identified. Approximately 76% of the diatom taxa are cosmopolitan distribution for Turkey. The diatom ecological indicator values, Trophic Diatom Index (TDI), Saprobic Index (SI), Swiss Diatom Index (DI-CH), the ‘‘Indice de polluo-sensibilite´ spe´cifique’’, also named IPS and Trophic Diatom Index for Lakes (TDIL) were evaluated. TDI, SI and TDIL showed good relationships with environmental variables. A principal component analysis (PCA) was performed on environmental data. The results of PCA separated the second station with high specific conductance, hardness and NO_3-N concentrations. It also showed that physicochemical parameters were affected by temperature and water level. Canonical Correspondence Analysis (CCA) was carried to determine the relationship between the diatom distributions and environmental variables. The results of CCA bi plot showed that specific conductance, hardness, turbidity, pH, dissolved oxygen, oxygen saturation and nutrients were significantly correlated with species distribution. According to the CCA result, two diatom groups were separated.

KEYWORDS:
Acarlar, floodplain forest, diatom, diatom indices, ecological quality, environmental parameters.

INTRODUCTION

Increased pollution caused by industrial, urban and agricultural contaminants threats aquatic environments all over the world. Numerous different methods have been developed to determine the condition of these systems. Besides the physicochemical parameters, biotic parameters should be used to determine the condition of wetlands. Biotic parameters as a water quality measurements provide better evaluation of environmental changes, because community development integrates a period of time reflecting conditions that might no longer be present at the time of sampling and analysis [1]. Community indices, such as diversity and evenness, have been used to monitor the impact of disturbance and pollution on aquatic systems and have been discussed by many authors [2, 3]. While several researchers have reported that diversity decreases with pollution [4], some have stated that diversity values increase with pollution [5].

Other methods consist of the application of ‘‘biotic indices’’ that express as a single, a dimensional, numeric value the general ecological status of a water mass [6]. Diatoms are well suited for water quality assessments [7, 8] because they have a short generation time and many species have a specific sensitivity to ecological characteristics [9]. The species composition of diatoms depends on many biochemical and physical factors [10, 11] and they provide information about characteristics like trophic state and pH [12]. Water quality monitoring especially in rivers, based on diatom indices have been applied for more than a decade in several European countries [13-15], but is a new topic in Turkey, especially after the 2000s, and is becoming increasingly important each day [16].

The Acarlar Floodplain Forest (AFF) is one of the two important floodplain forests (Longoz Forest) of Turkey. It is a wetland system that firstly originated as a stream and gradually transformed into a lagoon in quaternary [17]. However, it is a unique ecosystem that is neither exactly a lagoon nor exactly a stream because of the major changes in water level during dry and wet periods. It appears like a channel rather than a lagoon in the dry period. The most important feature is that the majority of the area is covered with forest. The area is preserved as a “Wildlife Protection Area", however its surroundings and water withdrawal areas undergo intensive agricultural activity in the

dry period as do other wetlands of Turkey. Furthermore, incoming sewage water from settlements is another effective contaminant. Previously, taxonomical and ecological studies have been carried out with bird composition [18] and epiphytic algal composition on three different macrophytes [19]. The first aim of this study is to determine the relationships between both the structure and diversity of the epilithic and epiphytic diatom community and the physicochemical parameters of AFF water using statistical analyses, diversity indices, Principal Component Analysis (PCA) and Canonical Correspondence Analysis (CCA). As most described diatom indices were developed and applied for running waters [20], applications for lakes are sporadic and in many cases doubtful [21]. However, AFF isn't exactly a lentic system (or exactly a lotic system); therefore we used diatom indices for both a lotic system (the diatom ecological indicator values, TDI, SI, DI-CH, IPS) and a lentic system (TDIL) and their applicability as a tool for estimating the floodplain water quality.

MATERIALS AND METHODS

Study Area. The Acarlar Floodplain Forest, located between the towns of Karasu and Kaynarca, both in the county of Sakarya, lies 60 km north of the city centre (Turkey) (Figure 1). AFF (41° 05' N - 30° 30' E) lies at 5 m above the sea level. The area stretches along the western side of the Sakarya delta and is approximately 2 km away from the Black Sea. AFF was formed at the estuary of one of the branches of the Sakarya River and is 6 km away from the western part of the Sakarya River, where it flows into the Black Sea. Acarlar extends 12 km east to west and empties into the River Sakarya via the Gölköprü Stream. This territory, with a size of 7.200 hectares, becomes a canal when the water level goes down in the summer. In the winter it covers a large area as it overflows and forms floodplain. A 1.576.06 hectare of the AFF lies within the boundaries of the town of Kaynarca and the rest within the boundaries of the town of Karasu. In 1976, this part was declared a "Wildlife Protection Area" in order to protect the pheasants and waterfowls, later the rest of this particular area was also announced a "Wildlife Protection Area". Freshwater swamp forest is other peculiar feature of the area. The forest, consisting of ash trees (*F. angustifolia* Vahl), alders (*A. campestre* L.) and willows (*S. alba* L.) is a very convenient shelter for bird species. Most of the southern part covered with reeds, sedge and various water plants [19].

The first station was determined near the village of Zonguldik, while the second station was selected near the village of Taşlıgeçit. These areas become a canal when the water level goes down in the summer and water withdrawal areas are used for agricultural purposes. Water levels are maximum (2 m) in winter and minimum (0.50 m) in summer. The third station was chosen near the villages of Karamüezzin and Denizköy. This area is used for recreational purposes. Water levels are maximum (3 m) in winter and minimum (1.5 m) in summer.

Diatom analysis. Sampling was carried out monthly at three stations between February 2011 and January 2012. For the determination of epiphytic diatoms, submerged leaves of vascular aquatic plants (*Typha sp.)* were collected. Leaves were not separated to the vertical sections and the choosen section was about 30 cm long for ech leaves. Epiphytic algae were removed manually using a toothbrush. Epilithic diatoms were collected by scraping of the upper surfaces of three submerged stones in a tray using a toothbrush.

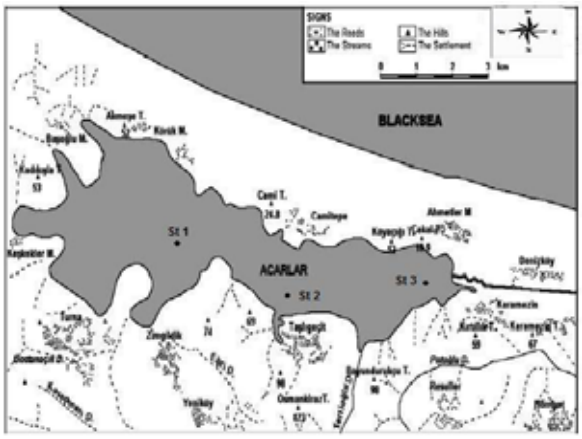

FIGURE 1
The map of the Acarlar Floodplain Forest and the location of sampling stations.

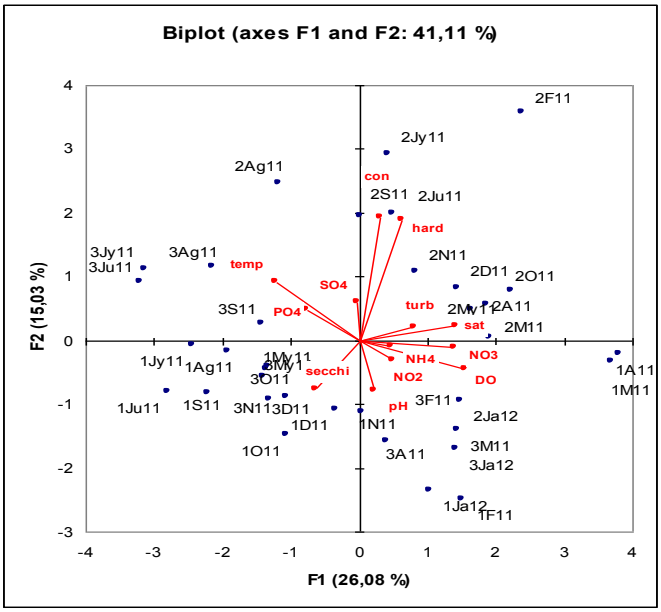

FIGURE 2

Principal component analysis performed on environmental parameters. Cumulative percentage variance explained by axes: I - 26.08%; I+II - 41.11%. Station codes: First character corresponds to the sampling site (1 - first station, 2-second station, 3 - third station) and subsequent ones to month and year of survey (1 - 2011, 2 - 2012). Environmental variables: temp: water temperature; pH; DO: dissolved oxygen concentration; sat: oxygen saturation, NO_3: nitrate-nitrogen concentration; NO_2: nitrite-nitrogen concentration; NH_4 ammonium-nitrogen concentration; PO_4: orthophosphate, SO_4: sulphate, con: specific conductance, secchi: secchi disk depth, turb: turbidity, hard: hardness).

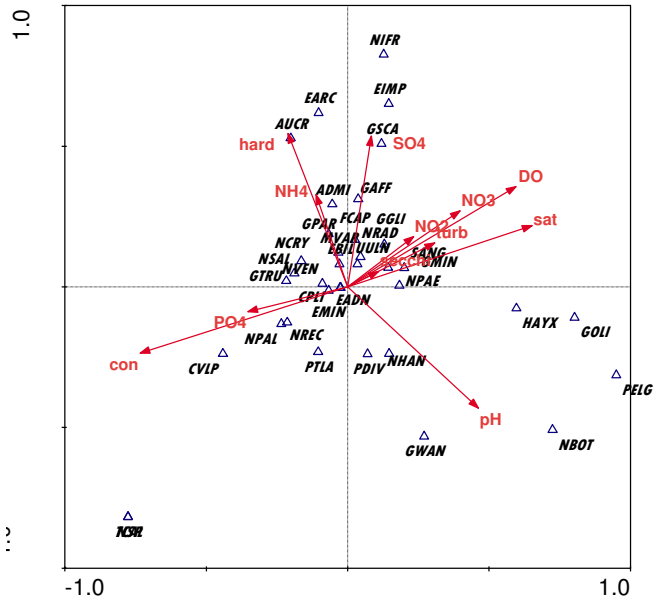

FIGURE 3

Bi plot of scores of environmental variables and species scores of the Canonical Correspondence Analysis (CCA). Full taxon names are given in Appendix. Environmental variables: temp: water temperature; pH; DO: dissolved oxygen concentration; sat: oxygen saturation, NO_3: nitrate-nitrogen concentration; NO_2: nitrite-nitrogen concentration; NH_4 ammonium-nitrogen concentration; PO_4: orthophosphate, SO_4: sulphate, con: specific conductance, secchi: secchi disk depth, turb: turbidity, hard: hardness).

Stone substrata of uniform size and flatness were selected. Samples were washed with distilled water yielding a compound sample of 100 mL fixed with 4% formaldehyde. After this procedure, the compound sample was well mixed and an aliquot of 50 mL was separated for analysis. Samples for diatom analysis were digested following a protocol by Round [22]. Cleaned diatom suspensions were dried onto glass coverslips and mounted in Entellan. Permanent slides were made for each sample. At least 300 diatom valves were counted on random transects across each slide. Diatoms were examined and identified using an Olympus BX51 compound microscope (1000× magnification). Taxa were identified mainly according to Round et al. [23]; Kramer and Lange-Bertalot [24-28]; Sims [29].

Physical and chemical analyses. Water temperature (Temp), pH, specific conductance (Con), dissolved oxygen (DO) and oxygen saturation (Sat) were measured from 10 cm below the surface using a Hach-Lange water quality instrument. Water transparency was measured on each sampling date using a Secchi disk. Concentrations of nitrate-nitrogen (NO_3-N), nitrite-nitrogen (NO_2-N), ammonium-nitrogen (NH_4-N), orthophosphate (PO_4-P) and sulphate (SO_4) were determined spectrophotometrically according to Strickland and Parsons [30] and Technicon Industrial Methods [31, 32], while hardness was determined by EDTA titrimetric method and turbidity was analysed by nephelometric method as described by APHA [33]. Chemical analyses were carried out at SASKİ (Sakarya Metropolitan Municipality Water and Sewage Administration).

Data analysis. Species diversity index and evenness were calculated using the equations developed by Shannon and Weaver [34]. The physicochemical datas were compared among sampling stations and seasons by analysis of variance (ANOVA). The existence of temporal and spatial differences of species diversity, richness, and evenness of the diatoms was also determined by ANOVA. Pearson correlations between the physicochemical parameters and species richness, diversity and evenness were determined using the SPSS 15.0 programme. A principal component analysis (PCA) was performed on environmental data to determine which variables were correlated and to summarize sampling sites environmental characteristics in an ordination diagram by using XLSTAT software [35]. Canonical Correspondence Analysis (CCA) was carried out using CANOCO software [36]. To determine the relationship between the diatom distributions and environmental variables, CCA was carried out on the log-normal transformed abundance data. Statistical significance of the environmental predictor variables was assessed by 999 restricted Monte Carlo permutations. The diatom ecological indicator values [saprobity (*S*), oxygen requirements (*O*), trophic state (*T*), nitrogen uptake metabolism (*N*), moisture (*M*), pH (*R*), and salinity (*H*)] of each station were obtained from scores of weighted averages of the diatom assemblages based on values compiled by Van Dam et al. [37]. The Trophic Diatom Index (TDI) according to Kelly and Whitton [38] and Kelly [14], Saprobic Index (SI) according to Rott et al. [39], Swiss Diatom Index (DI-CH) according to Buwal [40], the ''Indice de polluo-sensibilite´ spe´cifique'', also named IPS according to Cemagref [41] and Trophic Diatom Index for Lakes (TDIL) according to Stenger-Kova´cs et al. [21] were evaluated. Pearson correlations between TDI, SI, DI-CH, IPS and TDIL were also determined.

RESULTS

Physicochemical parameters. The average concentrations, standard deviations, maximums and minimums of measured physicochemical variables are listed in Table 1. Temp, pH, DO, Sat, NH_4-N, PO_4-P and SO_4 values were significantly different among seasons ($p < 0.001$), although were not significantly different among sampling stations ($p > 0.05$). However, the second station differed significantly ($p < 0.001$) from the other stations with higher specific conductance and hardness. NO_3-N values are both significantly different among seasons ($p < 0.05$), and among the second and the third stations ($p < 0.05$).

PCA ordination of environmental variables and sampling sites is presented in Figure 2. The first and the third stations of May 2011, and both stations of June, July, Agust, September 2011 were gathered near the PO_4-P, Temp, Con, hardness and SO_4 values. The second station samples were most closely associated with Con and hardness, while others with PO_4-P and Temp. Both stations of February, March, April, October, November, December 2011, January 2012, and the second station of May 2011 were gathered near to DO, Sat, NO_3-N, NO_2-N, NH_4-N, turbidity, secchi disk depth and pH. However, the second station samples, except January 2012, were most closely associated with turbidity, NO_3-N and DO; while, the first and the third stations of October, November, and December 2011 were associated with secchi disk depth.

Diatom taxa and abundances. A total of 94 diatom taxa belonging to 32 genera were recorded among the three sampling sites: 72 taxa recorded in epiphytic diatoms and 69 taxa recorded in epilithic diatoms. The list of the diatom taxa are presented in the Appendix.

TABLE 1
The mean, Standard Deviation (SD), minimum and maximum values of physical and chemical variables measured at the sites on the Acarlar Floodplain Forest water.

	Station 1		Station 2		Station 3	
Variable	**Mean±SD**	**Min.-Max.**	**Mean±SD**	**Min.-Max.**	**Mean±SD**	**Min.-Max.**
Temp(ºC)	17.6±7.35	5-28.6	17.9±6.55	6-28.8	17.6±6.7	7-28.9
pH	7.62±0.49	6.8-8.5	7.61±0.41	6.75-8.18	7.64±0.42	7.1-8.5
Con (μScm^{-1})	438.25±95.3	269-631	653.5±106.6	439-793	495.6±84.5	329-612
Sat (%)	67.24±15.2	40.8-96	83.9±12.2	61.8-108	57.1±14.4	25.9.1980
DO(mgL^{-1})	6.96±2.7	3.79-10.8	7.56±1.94	3.11-9.6	5.71±2.1	2.12-9.2
Secchi disk(m)	0.92±0.32	0.5-1.6	0.76±0.25	0.5-1.25	0.89±0.19	0.6-1.25
Hardness(Fsº)	16.9±2.13	13.65-21.3	26.9±5.4	22-43.2	20.02±2.13	16.7-23.5
Turbidity(NTU)	11.6±5.5	5.86-23.5	11.65±6.5	2-23.1	9.2±4.8	1.3.2020
NO_3–N(mgL^{-1})	4.61±2.99	2.10.1995	6.43±2.27	3.1-10.4	3.21±2.54	1.9.1937
NO_2–N(mgL^{-1})	0.014±0.012	0.001-0.04	0.016±0.021	0.002-0.077	0.021±0.012	0.01-0.046
NH_4–N(mgL^{-1})	0.085±0.05	0.01-0.16	0.11±0.18	0.01-0.56	0.082±0.077	0.02-0.3
PO_4-P(mgL^{-1})	0.14±0.05	0.1-0.2	0.16±0.06	0.1-0.25	0.16±0.06	0.08-0.25
SO_4 (mgL^{-1})	19.21±10.1	6.1-33.73	20.53±9.5	10.15-42.9	17.46±9.09	5.1-37.2

TABLE 2
Mean (M) and Standard Deviation (SD) of epiphytic and epilithic diatom diversity characteristics in the sampling stations.

		Richness		Diversity		Evenness	
Station		**M**	**SD**	**M**	**SD**	**M**	**SD**
Epiphytic	St 1	10	7	1,58	0.64	0.81	0.1
	St 2	10	6	1,27	0.76	0.58	0.31
	St 3	14	8	1,80	0.43	0.76	0.22
Epilithic	St 1	9	4	1,68	0.49	0.85	0.11
	St 2	11	5	1,86	0.61	0.83	0.21
	St 3	14	6	2,03	0.62	0.79	0.19

TABLE 3
Pearson correlation coefficients between environmental variables and species richness, diversity, and evenness (* P < 0.05; ** P < 0.01).

	Richness		Diversity		Evenness	
	Epiphytic	**Epilithic**	**Epiphytic**	**Epilithic**	**Epiphytic**	**Epilithic**
Temperature	0.083	0.027	-0.178*	-0.025	-0.367*	-0.002
pH	-0.239	-0.172	-0.019	-0.1	0.224	-0.107
Spesific conductance	-0.036	-0.048	-0.327	-0.017	-0.517**	0.055
Dissolved oxygen	0.106	-0.121	0.266	0.339*	0.355*	0.395*
Turbidity	0.056	-0.106	0.085	-0.045	0.099	-0.030
Nitrate–nitrogen	0.127	0.002	0.068	-0.245	0.085	-0.447**
Nitrite–nitrogen	0.134	0.095	0.070	-0.011	0.008	-0.219
Ammonium–nitrogen	-0.122	0.388*	0.184	0.276	0.324	0.033
Orthophosphate	0.039	0.09	-0.078	0.293	-0.269	0.302
Sulphate	0.001	0.239	-0.146	0.150	-0.137	0.024

TABLE 4
Mean values of twelve diatom indicator values in sampling stations (*R* pH, *H* Salinity, *N* Nitrogen uptake metabolism, *O* Oxygen requirements, *S* Sabrobity, *T* Trophic state, *M* Moisture, TDI Trophic diatom index, SI Sabrobic index, DI-CH Swiss Diatom Index, TDIL Trophic diatom index for lakes, IPS Specific pollution sensitivity index).

		R	*H*	*N*	*O*	*S*	*T*	*M*	TDI	SI	DI-CH	TDIL	IPS
Epiphytic	St 1	3.67	2.12	1.91	2.21	2.25	4.62	2.36	61.5	1.86	4.99	2.55	3.36
	St 2	3.71	2.05	1.86	2.26	2.33	4.8	2.19	67	1.8	4.58	2.45	3.73
	St 3	3.59	2.02	1.82	2.18	2.23	4.43	2.25	56.75	1.74	4.47	2.66	3.56
Epilithic	St 1	3.53	2.25	1.97	2.43	2.55	5	2.52	55.75	1.84	4.91	2.63	3.24
	St 2	3.66	2.08	1.94	2.36	2.35	5	2.44	57.5	2.07	5.19	2.79	3.32
	St 3	3.68	2.02	1.94	2.38	2.28	4.8	2.49	45.5	1.99	5.32	2.91	2.96

Planothidium lanceolatum (Brébisson ex Kützing) Lange-Bertalot was abundant in all the stations, however especially abundant in the second station for both epiphytic and epilithic diatoms. *Cocconeis placentula* var. *lineata* (Ehrenberg) Van Heurck was the second most abundant consistent species occurring in high abundance in epiphytic diatoms. Its abundance increased with a mean relative abundance of 51.2% in the second station. However, abundance of this species was low in epilithic diatoms. *Ulnaria ulna* (Nitzsch) Compère was another significant diatom with high percentages, especially in the third station for both epiphytic and epilithic diatoms. In epiphytic diatoms, high abundances were also observed for *Eunotia bilunaris* (Ehrenberg) Schaarschmidt, while *Navicula cryptocephala* var. *veneta* (Kützing) Rabenhorst, *Nitzschia hantzschiana* Rabenhorst, *Navicula bottnica* Grunow and *Gomphonema parvulum* (Kützing) Kützing were abundant in epilithic diatoms.

Diatom richness, diversity and evenness. The mean value and the standard deviation for species richness, diversity, and evenness of epiphytic and epilithic diatoms in the sampling stations are presented in Table 2. Evenness values of epiphytic diatoms were significantly high in the first station compared to the second station ($p < 0.05$), while species richness of epilithic diatoms were significantly low in the first station compared to the third station ($p < 0.05$). Correlations between environmental variables and species richness, diversity, and evenness are given in Table 3.

Diatom indices. Indices values of epiphytic diatoms were highly correlated with indices values of epilithic diatoms ($p < 0.01$). Saprobity (*S*) indicator values were slightly higher in the first and the second stations than the third station (Table 4). Oxygen metabolism indicator (*O*) values and Trophic state (*T*) indicator values followed similar trends to that of saprobity. Similarly, lower Nitrogen uptake metabolism (*N*) and lower salinity (*H*) indicator values were seen in the third station than the other stations. However, Moisture indicator (*M*) values were low in the second station. pH (*R*) indicator values varied, but indicated circumneutral pH in all the stations (Table 4). Significant correlations were found between the indices ($p < 0.05$). According to TDI and SI, all the stations were determined within the III quality class (mesotroph and β-mesosaprobic). According to DI-CH, all the stations were classified as quality class V (eutroph), while IPS and TDIL indicated moderate pollution in all the stations (Table 4).

Canonical Correspondence Analysis. The CCA was used to analyse relationships between the relative abundance of diatoms and environmental variables. The results showed that the distribution of diatoms was affected by 11 environmental variables (Figure 3). Species occurrences with relative abundance of 10% or more at least one sample, were included in this analysis. The first two CCA axes had eigenvalues of 0.244 and 0.190, respectively. Diatoms-environmental correlations were higher than 0.99 for both axes and explained collectively 37.1% of the diatom-environmental variations. The first axis of CCA explained 20.8% of the total variance in diatom taxa, while the second axis explained 16.3% of the total variance. Axis 1 is most closely associated with NO_2-N, NO_3-N, DO, Sat, turbidity, PO_4-P and Con. Axis 2 was associated with hardness, SO_4, NH_4 and pH. *C. placentula* var. *lineata, Epithemia adnata* (Kützing) Brébisson and *Encyonema minutum* (Hilse) Mann were placed near the origin of the ordination diagram. *Gomphonema minutum* (Agardh) Agardh, *G. angustatum* (Kützing) Rabenhorst, *G. olivaceum* (Hornemann) Brébisson, *Nitzschia paleacea* Grunow, *N. hantzschiana*, *Navicula bottnica, Gyrosigma wansbeckii* (Donkin) Cleve, *Pinnularia divergens* W. Smith, *Placoneis elginensis* (Gregory) Cox and *Hantzschia amphioxys* (Ehrenberg) Grunow seemed to be related with higher NO_2-N, NO_3-N, DO, Sat, turbidity and pH. *Nitzschia recta* Hantzsch Ex Rabenhorst, *N. palea*

(Kützing) W.Smith, *N. frustulum* (Kützing) Grunow, *Cavinula lapidosa* (Krasske) Lange-Bertalot, *Gomphonema truncatum* Ehrenberg, *G. parvulum, G. grovei var. lingulatum* (Hustedt) Lange-Bertalot, *G. affine* Kützing, *Navicula cryptocephala* Kützing, *N. cryptocephala* var. *veneta, N. salinarum* Grunow, *N. radiosa* Kützing, *U. ulna, E. bilunaris, Melosira varians* Agardh, *Aulacoseira crenulata* (Ehrenberg) Thwaites, *Gyrosigma scalproides* (Rabenhorst) Cleve, *Fragilaria capucina* Desmazières, *P. lanceolatum, Achnanthidium minutissimum* (Kützing) Czarnecki, *Eunotia arcus* Ehrenberg, *E. implicata* Nörpel, Lange-Bertalot and Alles were associated with higher level of hardness, Con, SO_4, NH_4 and PO_4-P.

DISCUSSION

Just like in many other wetlands, the AFF is under pressure due to intensive agricultural activity and sewage waters from settlements. Besides these, intervention to the water level, wrong water management strategies and destruction of forested lands for agricultural purposes are other problems of the AFF [42].

The seasonal variation of physical and chemical water parameters in AFF was essentially determined by temperature and water level. During the dry period, Con, hardness, SO_4 and PO_4-P concentrations were high and secchi disk depth, DO, Sat were low in all stations as a result of increasing temperature and decreasing water level. Besides these, Con and hardness values were significantly higher in the second station than the others in this period. Con values can be related to increasing ionic concentration due to evaporation, increasing mineralisation of organic matter and low water level in the dry period at this station [43]. During the wet period, secchi disk depth, DO, Sat, pH, NO_2-N, NO_3-N were high in all the stations. Moreover, NO_3-N, Sat and turbidity were higher in the second station during this period especially in spring months. Higher concentrations of nitrogen compounds were probably entered this site due to increasing fertilizing in these months.

Approximately 76 % of the diatom taxa recorded in the AFF are cosmopolitan distribution for Turkey [44, 45]. Diversity and evenness values of epilithic diatoms were slightly high compared to epiphytic diatoms. Diversity values were low in the second station compared to other stations. High specific conductance, hardness and NO_3-N concentrations of this station might affect the diversity. Especially low evenness values of epiphytic diatoms in the second station occurred as a result of the dominance of *C. placentula* var. *lineata* during the study period. Dominancy of this species could be due to herbivory [46] and scouring effects [47]. Varieties of *Cocconeis* are attached to the substrate along the entire valve and they are more resistant to scour and grazing [48]. *C. placentula* was also found most abundant and consistent species on *Potamogeton pectinatus* L. in Lake Liman [49]. This species was also placed near the origin of the CCA diagram, meaning that this algae were present in all samples and were not associated to one or more particular environmental variables. The correlation between diatom diversity measures and environmental variables were generally weak. However, increasing Temp and Con and decreasing DO affected the diversity negatively during the dry period. Biodiversity was correlated with higher quality water, and reduced when water quality was lower [4]. Although, physiochemical dynamics affects the diversity measures, other factors such as interactions and competition with other micro-algae, bacteria, protozoa, and grazers [50] and physical disturbances as a result of human activities [51], should be considered.

Significant correlations were observed between the diatom indicator values and most environmental variables. For example, pH (*R*) indicator values indicated circumneutral pH in all the stations and it is correlated with the measured data in the AFF. Also oxygen requirements (*O*) indicator values indicated fairly high (above 75% saturation) in all the stations and the measured values of Sat in the AFF were mostly close to this level. Indices values of epiphytic diatoms are highly correlated with indices values of epilithic diatoms. This is supported by other studies in which values of trophic and saprobic diatom indices did not differ no matter whether they were derived from epilithon, epipelon, or epiphyton [52, 53]. Among diatom indices, four indices (TDI, SI, IPS and TDIL) indicate that all the stations are mesosaprobic and under eutrophication threat. Measured physicochemical parameters and species composition support the indices results. TDI and TDIL correlated well; althought one of them was used for lotic, other one was used for lentic system. According to the results of TDI, SI and TDIL, the second station was slightly more polluted than the other station. High Con, hardness and NO_3-N concentrations of the second station support these three indices. However, IPS showed that the second station was slightly less polluted. Therefore, it is considered that TDI, SI and TDIL could be better reflecting the trophic state of AFF. Furthermore, results of Saprobity (*S*) indicator values and Trophic state (*T*) indicator values support TDI, SI and TDIL. DICH indicate eutrophic condition, although high numbers of species in the AFF weren't involved to the calculation of DICH (only 188 species was used in this index), might cause deviation in the result. In fact, TDI, SI, TDIL and diatom ecological indicator values were developed for the United Kingdom, Austria, Hungary and the

Netherlands, respectively [14, 21, 37, 38, 39]; they suited well for AFF. Although Turkey has a temperate climate with a typically Mediterranean climate zone, the AFF is located in the north of the country, which is under the influence of the Black Sea climate. In other studies carried out in Turkey; firstly, TDI, SI, GI and DAIpo indices were used by Gürbüz and Kıvrak [54] in the Karasu River, and they indicated that TDI and SI were better suited to physicochemical parameters. TDI was used in the Orhaneli Stream by Dalkıran et al. [55] and they stated that TDI reflected the water quality in the studied system. However, Kalyoncu et al. [56] determined that DI-CH and TI better reflected the changes in the Isparta and Darıören stream's water quality, while DESCY seems to be the best for the Akçay stream [57], and there was a high correlation between physicochemical parameters and BDI in the Düden waterfall [58]. Furthermore, IDAP, WAT, CEE and IPS indices had a high correlation with physicochemical parameters in the Felent stream [59] and Kızılırmak River [60].

Multivariate analyses (CCA) demonstrated a significant effect of water quality variables (con, hardness, turbidity, pH, DO, Sat and nutrients) on the distribution of diatom taxa. According to CCA results, two diatom groups were separated. The first group, including *G. minutum*, *G. angustatum*, *G. olivaceum*, *N. paleacea, N. hantzschiana, N. bottnica, G. wansbeckii, P. divergens*, *P. elginensis* and *H. amphioxys* seemed to be related with higher NO_2-N, NO_3-N, DO, Sat, turbidity and pH. *N. bottnica* and *N. hantzschiana* were important species with high abundance especially in the third station during the wet period in epilithic diatoms. *N. hantzschiana* is reported as oligosaprobic [37]. It is also significant that the abundance of *G. minutum* was increased with the elevated concentrations of NO_3-N during the spring in the second station. It is also significant that the abundance of *G. minutum* was increased with the elevated concentrations of NO_3-N during the spring in the second station. Other species were mainly abundant during the wet period and were considered moderately tolerant to pollution, oligosaprobic to α- mesosaprobic [21, 37, 61].

The second group, including *N. recta, N. palea, N. frustulum, C. lapidosa*, *G. truncatum, G. parvulum, G. grovei var. lingulatum, G. affine, N. cryptocephala, N. cryptocephala* var. *veneta, N. salinarum, N. radiosa, U. ulna, E. bilunaris, M. varians, A. crenulata, G. scalproides, F. capucina, P. lanceolatum, A. minutissimum, E. arcus, E. implicata* were associated with higher level of hardness, Con, SO_4, NH_4 and PO_4-P. *P. lanceolatum* was abundant in all the stations and tended to increase in the second station. *P. lanceolatum* are considered as α or β- mesosaprobic [37]. The abundance of *G. parvulum* was significant, especially in the second station during the dry period in epilithic diatoms. *G. parvulum* has been considered both α-mesosaprobic and polysaprobic [62]. Kobayasi and Mayama [63] stated that this taxa is highly tolerant to organic pollution in studies carried out in the rivers of Japan. *U. ulna* was another significant diatom with high percentages, especially in the second and the third stations. This species occurred during the study period; however, its abundance was increased with elevated concentrations of nitrogen compounds in spring months. *U. ulna* is considered very tolerant to pollution and indicators for a wide range of conditions, varying from α-mesosaprobic to polysaprobic [24, 37, 64]. Within this group, high abundances were also observed for *E. bilunaris* in the first and in the third stations and *N. cryptocephala* var. *veneta* in the second and in the third stations. *E. bilunaris* showed a wide tolerance [65] and is considered β-mesosaprobic; however *N. cryptocephala* var. *veneta* was considered α-mesosaprobic and polysaprobic [37]. *N. palea* is described as an indicator species of polysaprobic or hyper-eutrophic environments, occurring in waters with low concentrations of dissolved oxygen, according to Van Dam et al. [37]. Licursi and Gomez [66] noted that this species has an affinity for water of higher conductivity. In the present study, *N. palea* was found in all the samples, especially in the second station; however its densities were not so high during the studied period. However, this species were found dominant in eutrophic Porsuk River [67]. Other species were mainly abundant during the dry period and were considered moderately tolerant to pollution, β- to α-mesosaprobic [21, 37, 61].

In summary, gradients of environmental parameters and abundance of the dominant species wasn't increased gradually over the stations as expected, such as running waters. However, Con, hardness and NO_3-N values were significantly different in the second station. Dominant species, *C. placentula* var. *lineata, P. lanceolatum* and *G. parvulum,* were more abundant than the other stations, explained by the lowest evenness values in this station. Especially the high values of Con and hardness and the presence of *G. parvulum* and *P. lanceolatum* were significantly correlated in the CCA. Temp and water level were the determinant for the seasonal variation of physical, chemical and biological parameters. Both PCA and CCA indicated that physical, chemical and biological parameters were divided into two parts as a result of dry and wet periods. The results of CCA showed that Con, hardness, turbidity, pH, DO, Sat and nutrients were significantly correlated with species distribution. Generally, the AFF was dominated by β -mesosaprobous and α -mesosaprobous taxa that tolerate increased levels of organic pollution, declining levels of oxygen saturation and circumneutral levels of pH. Diatom indices results

indicated the same points. Although the AFF is not exactly a running water system, results of physicochemical parameters and indices give an idea about the availability of these indices in the northern regions of Turkey and this type of wetland ecosystem and can be used as a proxy for water quality.

ACKNOWLEDGMENTS

This research was supported by Sakarya University Research Foundation (Project No: 2012-02-20-012). The authors would like to thank Cüneyt Nadir SOLAK and Özden FAKIOĞLU for their advice on diatom indices. SASKİ (Sakarya Metropolitan Municipality Water and Sewage Administration) and Sakarya Forestry and Water Works Directorate were also acknowledged for their helps in chemical analyses and transportation to the field.

APPENDIX
The list of species codes and their full species names.

Code	Species name	Epiphytic	Epilithic
ADMI	*Achnanthidium minutissimum* (Kützing) Czarnecki		+
ABKM	*Adlafia brockmannii* (Hustedt) Bruder & Hinz		+
AEXM	*Amphora eximia* J.R.Carter	+	+
AOVA	*A. ovalis* (Kützing) Kützing		+
APED	*A. pediculus* (Kützing) Grunow ex A.Schmidt		+
AUCR	*Aulacoseira crenulata* (Ehrenberg) Thwaites	+	
CVLP	*Cavinula lapidosa* (Krasske) Lange-Bertalot		+
CAPS	*Caloneis alpestris* (Grunow) Cleve		+
CSIL	*C. silicula* (Ehrenberg) Cleve		+
CPLA	*Cocconeis placentula* (Ehrenberg)	+	
CPLI	*C. placentula* var. *lineata* (Ehrenberg) van Heurck	+	+
CMEN	*Cyclotella meneghiniana* Kützing	+	+
CAFF	*Cymbella affinis* Kützing	+	
CCIS	*C. cistula* (Hemprich & Ehrenberg) O.Kirchner	+	
CLAN	*C. lanceolata* (C.Agardh) C.Agardh	+	+
CHEL	*C. helvetica* Kützing	+	
CHUS	*C. hustedtii* Krasske	+	
CTUM	*C. tumida* (Brébisson) van Heurck		+
CBAM	*Cymbopleura amphicephala* (Nägeli) Krammer	+	
DVUL	*Diatoma vulgaris* Bory de Saint-Vincent	+	+
EMIN	*Encyonema minutum* (Hilse) D.G.Mann	+	+
ESLE	*E. silesiacum* (Bleisch) D.G.Mann	+	+
EADN	*Epithemia adnata* (Kützing) Brébisson	+	+
ETUR	*E. turgida* (Ehrenberg) Kützing	+	+
EARC	*Eunotia arcus* Ehrenberg	+	
EBIL	*E. bilunaris* (Ehrenberg) Schaarschmidt	+	+
EFOR	*E. formica* Ehrenberg	+	
EIMP	*E. implicata* Nörpel, Lange-Bertalot & Alles	+	
EPUN	*E. pectinalis* var. *undulata* (Ralfs) Rabenhorst	+	
FCAP	*Fragilaria capucina* Desmazières	+	+
GACU	*Gomphonema acuminatum* Ehrenberg	+	+
GAFF	*G. affine* Kützing	+	+
GANG	*G. angustatum* (Kützing) Rabenhorst	+	+
GCLA	*G. clavatum* Ehrenberg	+	
GGRA	*G. gracile* Ehrenberg	+	+
GGLI	*G. grovei* var. *lingulatum* (Hustedt) Lange-Bertalot		+
GMIN	*G. minutum* (C.Agardh) C.Agardh	+	+
GOLI	*G. olivaceum* (Hornemann) Brébisson	+	+
GPAR	*G. parvulum* (Kützing) Kützing	+	+

GPSA	*G. pseudoaugur* Lange-Bertalot	+	
GTRU	*G. truncatum* Ehrenberg	+	+
GYAC	*Gyrosigma acuminatum* (Kützing) Rabenhorst	+	+
GSCA	*G. scalproides* (Rabenhorst) Cleve		+
GWAN	*G. wansbeckii* (Donkin) Cleve	+	+
HAYX	*Hantzschia amphioxys* (Ehrenberg) Grunow	+	+
MVAR	*Melosira varians* C.Agardh	+	+
NSP	*Navicula sp.*		+
NAAN	*N. angusta* Grunow	+	
NBOT	*N. bottnica* Grunow		+
NCIN	*N. cincta* (Ehrenberg) Ralfs	+	
NCRY	*N. cryptocephala* Kützing	+	+
NVEN	*N. cryptocephala* var. *veneta* (Kützing) Rabenhorst	+	+
NDSL	*N. densilineolata* (Lange-Bertalot) Lange-Bertalot	+	
NDIG	*N. digitoradiata* (Gregory) Ralfs	+	+
NAEP	*N. expecta* S.L.VanLandingham		+
NGRE	*N. gregaria* Donkin	+	
NLAN	*N. lanceolata* Ehrenberg	+	
NLIB	*N. libonensis* Schoeman		+
NPHY	*N. phyllepta* Kützing	+	+
NRAD	*N. radiosa* Kützing	+	+
NRCS	*N. recens* (Lange-Bertalot) Lange-Bertalot	+	+
NSAL	*N. salinarum* Grunow	+	+
NSPD	*N. splendicula* Van Landingham	+	
NTPT	*N. tripunctata* (O.F.Müller) Bory de Saint-Vincent	+	+
NTRV	*N. trivialis* Lange-Bertalot	+	+
NVRO	*N. viridula* var. *rostellata* (Kützing) Cleve	+	+
NEAM	*Neidium ampliatum* (Ehrenberg) Krammer		+
NDUB	*N. dubium* (Ehenberg) Cleve		+
NEPR	*N. productum* (W.Smith) Cleve		+
NALP	*Nitzschia alpina* Hustedt	+	
NIFR	*N. frustulum* (Kützing) Grunow		+
NHAN	*N. hantzschiana* Rabenhorst	+	+
NZLT	*N. linearis* var. *tenuis (W.Smith) Grunow*	+	
NPAL	*N. palea* (Kützing) W.Smith	+	+
NPAE	*N. paleacea* Grunow	+	+
NREC	*N. recta* Hantzsch ex Rabenhorst	+	+
NSUA	*N. subacicularis* Hustedt	+	
PDIV	*Pinnularia divergens* W. Smith	+	+
PTLA	*Planothidium lanceolatum* (Brébisson ex Kützing) Lange-Bertalot	+	+
PELG	*Placoneis elginensis* (Gregory) E.J. Cox	+	
RABB	*Rhoicosphenia abbreviata* (C.Agardh) Lange-Bertalot	+	
RGIB	*Rhopalodia gibba* (Ehrenberg) Otto Müller		+
SPUP	*Sellaphora pupula* (Kützing) Mereschkovsky	+	+
STGR	*Stauroneis gracillima* Hustedt	+	+
SNOB	*S. nobilis* Schumann	+	+
SPHO	*S. phoenicenteron* (Nitzsch) Ehrenberg		+
SANG	*Surirella angusta* Kützing	+	+
SBRE	*S. brebissonii* Krammer & Lange-Bertalot	+	+
TACM	*Tryblionella acuminata* W.Smith		+
TCAL	*T. calida* (Grunow) D.G. Mann		+
UACU	*Ulnaria acus* (Kützing) M. Aboal	+	+
UCAP	*U. capitata* (Ehrenberg) P. Compère	+	+
UDEL	*U. delicatissima* (W.Smith) M. Aboal & P.C.Silva	+	
UULN	*U. ulna* (Nitzsch) P.Compère	+	+

REFERENCES

[1] Lobo, E.A., Callegaro, V.L.M. and Bender, P. (2002) Utilização De Algas Diatomáceas Epilíticas Como İndicadoras Da Qualidade Da Água Em Rios E Arroios Da Região Hidrográfica Do Guaíba, Rs, Brasil. Santa Cruz Do Sul: Edunısc. 127 P.

[2] Podani, J. (1992) Monitoring System. In: Kovacs M. (eds): Biological Indicators In Environmental Protection. 12–18, UK: Ellis Horwood Series İn Environmental Management, Science and Technology.

[3] Stewart, P.M., Butcher, J.T. and Gerovac, P.J. (1999) Diatom (Bacillariophyta) Community Response To Water Quality and Land Use. Natural Areas Journal, 19, 155–165.

[4] Rott, E. and Pfister, P. (1988) Natural epilithic algal communities in fast-flowing mountain streams and rivers and some man-induced changes. Verhandlungen Internationale Vereinigung fur Theoretische und angewandte Limonologie, 23, 1320–1324.

[5] Izsak, C.A., Price, R.G., Hardy, J.T. and Basson, P.W. (2002) Biodiversity of periphyton (diatoms) and echinoderms around a refinery effluent, and possible associations with stability. Aquatic Ecosystem Health & Management, 5, 61–70.

[6] Blanco, S. and Bécares, E. (2010) Are Biotic Indices Sensitive To River Toxicants? A Comparison of Metrics Based on Diatoms and Macro-Invertebrate. Chemosphere, 79, 18–25.

[7] Passy, I.S. and Bode, R.W. (2004) Diatom model affinity (DMA), a new index for water quality assessment. Hydrobiologia, 524, 241-251.

[8] Salomoni, S., Rocha, O., Callegoro, V.L. and Lobo, E.A. (2006) Epilithic Diatoms As İndicators Of Water Quality İn The Gravataı´ River, Rio Grande Do Sul, Brazil. Hydrobiologia, 559, 233-246.

[9] Stevenson, R.J. and Pan, Y. (1999) Assessing Environmental Conditions İn Rivers And Streams With Diatoms. In: Stoermer E.F. &Smol J.P. (eds): The Diatoms: Applications For The Environemental And Earth Sciences. 11-40. Cambridge University Press, Cambridge, UK.

[10] Simonsen, R. (1962) Untersuchungen Zur Systematik And Okologie Der Boden Diatomeen Der Westlichen Ostsee. Int. Rev. Ges. Hydrobiol. Syst. Beih., 1, 94-97.

[11] Juggins, S. (1992) Diatoms in the Thames Estuary, England: Ecology, Paleoecology and Salinity Transfer Function. Bibl. Diatomol. Bd., 25, 1-216.

[12] Cholnoky, B.J. (1968) Die Okologie Der Diatomeen İn Binnengewassern. J. Cramer Verlag, Vaduz. 699 P.

[13] Descy, J.P. and Coste, M. (1991) A test of methods for assessing water quality based on diatoms. Verhandlungen der Internationale Vereinigung fu¨r theoretische und Angewandte Limnologie, 24, 2112–2116.

[14] Kelly, M.G. (1998) Use of the Trophic Diatom Index to monitor eutrophication in rivers. Water Research, 32, 236-242.

[15] Prygiel, J. and Coste, M. (2000) Guide Me´thodologique pour la mise en oeuvre de l'Indice Biologique Diatome´ es. NF T 90–354. Etude Agences de l'Eau-Cemagref Bordeaux, March 2000, Agences de l'Eau: 134

[16] Solak, C.N. and Àcs, É. (2011) Water Quality Monitoring in European and Turkish Rivers Using Diatoms. Turkish Journal of Fisheries and Aquatic Sciences, 11, 329-337.

[17] Bilgin, T. (1984) Adapazarı Ovası ve Sapanca Oluğunun Alüviyal Morfolojisi ve Kuaternerdeki Jeomorfolojik Tekamülü, İstanbul Üniversitesi Edebiyat Fakültesi Yayınları, Edebiyat Fakültesi Matbaası, İstanbul.

[18] Uzun, A., Tabur, M.A. and Ayvaz, Y. (2008) Birds of Lake Acarlar and Environmental Problems. Ekoloji, 17, 1-14.

[19] Tunca, H., Ongun Sevindik, T., Bal, D.N., Arabacı, S. (2014) Community structure of epiphytic algae on three different macrophytes at Acarlar floodplain forest (northern Turkey). Chinese Journal of Oceanology and Limnology, 32, 845-857.

[20] Brabecz, K. and Szoszkiewicz, K. (2006) Macrophytes and diatoms – major results and conclusions from the STAR project. Hydrobiologia, 566, 175–178.

[21] Stenger-Kova´Cs, C., Buczko, K., Hajnal, E. and Padisak, J. (2007) Epiphytic, littoral diatoms as bioindicators of shallow lake trophic status: Trophic Diatom Index for Lakes (TDIL) developed in Hungary. Hydrobiologia, 589, 141–154.

[22] Round, F.E. (1953) An investigation of two benthic algal communities in Malharm Tarn, Yorkshire. Journal of Ecology, 41, 97-174.

[23] Round, F.E., Crawford, R.M. and Mann, D.G. (1990) The Diatoms: Morphology and biology of the genera. Cambridge University Press, Cambridge. 747 P.

[24] Krammer, K. and Lange-Bertalot, H. (1986) Bacillariophyceae: Naviculaceae. In: Ettl, H., Gerloff, I., Heynig, H. and Mollenhauer, D. (eds): Süsswasserflora Von Mitteleuropa. Stuttgart: G. Fischer. 876 P.

[25] Krammer, K. and Lange-Bertalot, H. (1991a) Bacillariophyceae. 3. Centrales, Fragilariaceae, Eunoticeae. In: Süβwasserflora von Mitteleuropa, 2/3. Gustav Fischer Verlag, Stuttgart, New York. 577 P.

[26] Krammer, K. and Lange-Bertalot, H. (1991b) Bacillariophyceae. 4. Achnanthaceae, Kritische Ergänzungen zu Navicula (Lineolatae) und Gomphonema Gesamtliteraturverzeichnis. In: Süβwasserflora von Mitteleuropa, 2/4. Gustav Fischer Verlag, Stuttgart, New York. 437 P.

[27] Krammer, K. and Lange-Bertalot, H. (1999) Bacillariophyceae. 2. Epithemiaceae, Surirellaceae. In: Süβwasserflora von Mitteleuropa, 2/2. Gustav Fischer Verlag, Stuttgart, New York. 596 P.

[28] Krammer, K. and Lange-Bertalot, H. (2003) Diatoms of Europe. Volume 4: Cymbopleura, Delicata, Navicymbula, Gomphocymbellopsis, Afrocymbella. A.R.G. Gantner Verlag K.G., Koeltz Scientific Books. 530 P.

[29] Sims, P.A. (1996) An Atlas of British Diatoms. Biopress Ltd., London. 601 P.

[30] Strickland, J.D.H. and Parsons, T.R. (1972) A practical handbook of seawater analysis. 2nd Edition. Bull. Fish. Res. Bd Can. 167 P.

[31] Technicon Industrial Methods (1977a) Nitrate and nitrite in water and wastewater. No. 158–71, W/A.

[32] Technicon Industrial Methods (1977b) Phosphate and silicate analysis in water and seawater. No. 253–280 E. Application note, p.5 – 7, U.K.

[33] APHA (American Public Health Association) (1995) Standard methods for the examination of water and wastewater. 19th Edition, Washington, D.C.

[34] Shannon, C.E. and Weaver, W. (1963) The Mathematical Theory of Communication. University of Illinois Press, Urbana: 210–360.

[35] Fahmy, T. (2013) XLSTAT, version (2013). Addinsoft, Paris.

[36] Ter Braak, C.J.F. and Smilauer, P. (2002) CANOCO reference manual and CanoDraw for Windows user's guide: software for canoinical community ordination (version 4.5). Ithaca (NY, USA): Microcomputer Power. 500 P.

[37] Van Dam, H., Mertens, A. and Sinkeldam, J. (1994) A coded checklist and ecological indicator values of freshwater diatoms from the Netherlands. Netherlands Journal of Aquatic Ecology, 28, 117–133.

[38] Kelly, M.G. and Whitton,B.A. (1995) The Trophic Diatom Index: A New İndex for Monitoring Eutrophication in Rivers. Journal of Applied Phycology, 7, 433-444.

[39] Rott, E., Hofmann, G., Pall, K., Pfister, P. and Pipp, E. (1997) Indikationslisten Für Aufwuchsalgen İn Österreichischen Fliessgewässern. Teil 1: Saprobielle Indikation. Wasserwirtschaftskataster. Bundesminsterium Für Land-Und Forstwirtschaft. Stubenring 1. 1010 Wein. Austria. 248 P.

[40] Buwal (Bundesamt Für Umwelt, Wald Und Landschaft) (2002) Methoden Zur Untersuchung Und Beurteilung Der Fließgewässer: Kieselalgen Stufe F (Flächendeckend) Entwurf Stand January, Bern.

[41] Cemagref, (1982) Etude des méthodes biologiques quantitatives d'appréciation de la qualité des eaux. Rapport Q.E. Lyon - A.F.B. Rhône-Méditerranée-Corse. 218 P.

[42] Ustaoğlu, B. (2012) Spatiotemporal analysis of land cover change patterns in western part of the Sakarya River Delta and its surroundings in Turkey. Enery Education Science and Tecnology Part A: Energy Science and Research, 29, 721-730.

[43] Kıvrak, E. (2006) Seasonal and long term changes of the phytoplankton in the Lake Tortum in relation to environmental factors, Erzurum, Turkey. Biologia, 61, 339-345.

[44] Aysel, V. (2005) Check-List of the Freshwater Algae of Turkey. Journal of the Black Sea/Mediterranean Environment, 11, 1-124.

[45] Solak, C.N., Ector, L., Wojtal, A.Z., Ács, É. and Morales, E.A. (2012) A review of investigations on diatoms (Bacillariophyta) in Turkish inland waters. Nova Hedwigia, 141, 431–462.

[46] Steinman, A.D. (1996) Effects of Grazers on Freshwater Benthic Algae In: Stevenson R.J., Bothwell M.L. and Lowe R.L. (eds): Algal Ecology: Freshwater Benthic Ecosystems. 341-373, Academic Press, New York.

[47] Peterson, C.G. and Stevenson, R.J. (1990) Post-spate development of epilithic algal communities in different current regimes. Canadian Journal of Botany, 63, 2092-2102.

[48] Yallop, M. (2008) A Study of the Diatom Assemblages in Grazing Marsh Ditches: Application to Assessment of Ecological and Conservation Status, Part 1: Gwent and Somerset Levels. Buglife - The Invertebrate Conservation Trust.

[49] Soylu EN, Maraşlıoğlu F, Gönülol A. (2011) Liman Gölü (Bafra-Samsun) Epifitik Diatome Florası, Ekoloji, 20, 57-62.

[50] Elber, F. and Schanz, F. (1990) Algae, other than diatoms, affecting density, species richness and diversity of diatom communities in rivers. Archiv fu¨r Hydrobiologie, 119, 1–14.

[51] Triest, L., Lung'ayia, H., Ndiritu, G. and Beyene, A. (2012) Epilithic diatoms as indicators in tropical African rivers (Lake Victoria catchment). Hydrobiologia, 695, 343–360.

[52] Rott, E., Duthie, H.C. and Pipp, E. (1998) Monitoring organic pollution and

eutrophication in the Grand River, Ontario, by means of diatoms. Can. J. Fish Aquat. Sci., 55, 1443–1453.
[53] Kitner, M. and Pouli-Ckova, A. (2003) Littoral diatoms as indicators for the eutrophication of shallow lakes. Hydrobiologia, 506–509, 519–524.
[54] Gürbüz, H. and Kıvrak, E. (2002) Use of epilithic diatoms to evaluate water quality in the Karasu River of Turkey. J. Environmental Biology, 23, 239-246.
[55] Dalkıran, N., Karacaoğlu, D., Dere, Ş. and Şentürk, E. (2008) Orhaneli Çayı'nın Kirlilik Düzeyinin Diyatomelere Dayandırılarak Saptanması. 19. Ulusal Biyoloji Kongresi Özet Kitapçığı, Trabzon, Türkiye, 23-27 Haziran 2008.
[56] Kalyoncu, H., Çiçek, N.L., Akköz, C. and Yorulmaz, B. (2009) Comparative performance of diatom indices in aquatic pollution assessment. African Journal of Agricultural Research, 4, 1032-1040.
[57] Solak, C.N., Fehér, G., Barlas, M. and Pabuçcu, K. (2007a) Use of epilithic diatoms to evaluate water quality of Akçay Stream (Büyük Menderes River) in Mugla/Turkey. Archiv Für Hydrobiologie Suppl., 161 (3-4), Large Rivers, 17, 327-338.
[58] Solak, C.N., Ács, É. and Pabuçcu, K. (2007b) BDI (Biyolojik Diyatome İndeksi) İndeksine Göre Düden Şelalesi (Antalya) Su Kalitesinin Durumu. 10-13 Eylül 2007, 7. Ulusal Ekoloji ve Çevre Sempozyumu, Özet Kitapçığı, Malatya.
[59] Solak, C.N., Àcs, É. and Dayıoglu, H. (2009) The application of diatom indices in Felent Creek (Porsuk-Kütahya). Diatomededlingen, 33, 107-109.
[60] Akbulut, N., Akbulut, A., Günsel, S. and Solak, C.N. (2010) Use of epilithic diatoms to evaluate water quality of Kızılırmak River. Hacettepe University Fund, No: 0701601006, Final Report, in Turkish.
[61] Lobo, E.A. and Callegaro, V.L.M. (2000) Avaliac¸a˜o da qualidade de a´ guas doces continentais com base em algas diatoma´ceas epilı´ticas: Enfoque metodolo´ gico. In: Tucci, C.E. and Marques, D.M. (eds): Avaliac¸a˜o e Controle da Drenagem Urbana. 277–300. Porto Alegre: ed. Universidade/ UFRGS.
[62] Lobo, E.A., Da Costa, A.B. and Kirst, A. (1999) Avaliac¸a˜o da qualidade da a´gua dos arroios Sampaio, Bonito e Grande, municı´pio de Mato Leita˜ o, RS, Brasil, segundo a resoluc¸a˜o do CONAMA 20/86. Revista Redes, 4, 129–146.
[63] Kobayasi, H. and Mayama, S. (1989). Evaluation Of River Water Quality By Diatoms. The Korean Journal of Phycology, 4, 121-133.
[64] Nevo, E. and Wasser, S.P. (2000) Biodiversity of Cyanoprocaryotes, Algae and Fungi of Israel: Cyanoprocaryotes and Algae of Continental Israel. A.R.A. Gantner Verlag, Ruggell. 629 P.
[65] Patrick, R. and Reimer, C.W. (1966) The diatoms of the United States. Academy of Natural Sciences. Philadelphia. 688 P.
[66] Licursi, M. and Go´Mez, N. (2002) Benthic diatoms and some environmental conditions in three lowland streams. - Ann. Limnol. - International Journal of Limnology, 38, 109–118.
[67] Bingöl N.A., Özyurt M.S., Dayıoğlu H., Yamık A. and Solak C.N. (2007) Yukarı Porsuk Çayı (Kütahya) Epilitik Diyatomeleri, Ekoloji, 15, 23-29.

Received: **04.10.2015**
Accepted: **26.01.2016**

CORRESPONDING AUTHOR

Tugba Ongun Sevindik
Sakarya University
Faculty of Arts and Science
Department of Biology
54187, Adapazarı - TURKEY

E-mail: tsevindik@sakarya.edu.tr

© by PSP Volume 25 – No. 10/2016, pages 4026-4035 Fresenius Environmental Bulletin

COMPOSTING OF MUNICIPAL OPEN MARKET WASTES WITH DIFFERENT MATERIALS

Kamil Ekinci[1,*], Barbaros Salih Kumbul[1], Davut Akbolat[1], İbrahim Erdal[2], Berk Bitrak[3]

[1]Department of Agricultural Machinery and Technologies Engineering, Faculty of Agriculture, Suleyman Demirel University, 32260 Isparta, Turkey
[2]Department of Soil Science and Plant Nutrition, Faculty of Agriculture, Suleyman Demirel University, 32260 Isparta, Turkey
[3]Department of Environmental Engineering, Faculty of Engineering, Suleyman Demirel University, 32260 Isparta, Turkey

ABSTRACT

Composting of municipal open market wastes (MOMW) with rose oil processing wastes (ROPW), dairy manure (DM), and straw was investigated. Three compost mixes were prepared based on the initial measured carbon/nitrogen (C/N) ratios of 9.9, 12.4, and 15.9 for Mix-1, 2, and 3, respectively. The composting experiment was conducted in an open type composting bin with three sections. During the composting process, temperature, O_2 concentration, CO_2 and H_2O emissions, moisture, pH, electrical conductivity, total carbon, total nitrogen, and organic matter were measured. The experiment lasted for 44.75 days. The results revealed that the highest temperature recorded during composting was 62, 67, and 66 °C at 6, 6, and 10th days of composting for Mix-1, 2, and 3, respectively. The highest organic matter loss (55.9 %) occurred for Mix-3 having the mixing ratio of 0.37, 0.25, 0.23, and 0.15 (kg kg^{-1}, dry mass basis) of MOMW, ROPW, DM, and straw, respectively. Results on CO_2 and water emissions from the surface of piles during composting process supported that the highest degradation occurred at Mix-2 and Mix-3. The resultant pH of mixes ranged from 7.51 to 8.35. The compost with the final C/N ratios of 7.4, 7.9, and 9.5 for Mix-1, Mix-2, and Mix-3, respectively met the criteria for the mature compost and could be utilized for plant growing. In conclusion, the results showed that composts with the adequate amount of nutrients for plant growing could be produced with these wastes.

KEYWORDS:
Composting; municipal open market wastes, rose oil processing wastes;

INTRODUCTION

Some of agricultural products (fruit and vegetable) are marketed in municipal open places in Turkey and leftovers, which are called “municipal open market wastes (MOMW)” from agricultural products are collected from market places by the municipal authority. The amount of MOMW have been increased due to increase in population. MOMW are sold to livestock owners for free or collected by municipalities for landfilling. At the other side, in 2013, approximately 8481 tons of rose (*Rosa damascena* Mill) oil flower were produced in Isparta province accounting 78.8 % of Turkey’ production [1]. Rose oil processing wastes (ROPW), which is emerged form rose oil processing, are mainly disposed nearby rose oil facilities, and either sold or given for free of charge after a 4-5 months drying period because of its high moisture content (90% wet basis, (w.b.)). The estimated amount of ROPW was 18234.7 tons in 2013 [1,2]. The ROPW is pile up for natural decomposition or utilized in stoves for cooking and heating applications in rural areas. Additionally, it is directly applied to land to increase soil organic matter content. These kinds of waste disposal methods are resulted in not only ecological problems [3,4]; but also penalty fine by officials such as environmental protection agencies [2]. Animal manure, which is a by-product of animal production have been increased due to increase in agricultural production in Turkey. There has been a dramatic increase in farm size thereby the amount of manure accumulated for the recent years. Most of the animal farms in Turkey don’t have engineered structure to store animal manure existing from barn. Animal manure which is accumulated outside emits greenhouse gases during storage. Therefore, improper management and utilization of animal manure cause environmental problems and threatens human and animal health. On the other side, Turkish farmers have insufficient financial and technical capacities to collect, transport, and safely treat and dispose of animal manures, consequently waste management remains one of the agricultural problems [5]. Therefore, sustainable management of wastes, which is a major challenge being faced by agricultural and industrial sectors in Turkey, is required.

Composting is a decomposition of organic materials and a process of which physical, chemical, and biological factors interact

TABLE 1
Physical and chemical properties of ROPW, MOMW, DM, and straw used in the mixes.

Parameters	MOMW	ROPW	DM	Straw
Moisture (%, w.b.)	88.35±0.47	28.68±6.62	59.79±8.13	26.44±0.24
Organic matter (%)	92.47±1.41	77.87±7.44	48.75±6.55	94.14±0.41
pH	4.70±0.03	6.76±0.44	8.26±0.11	6.05±0.06
EC (dS m^{-1})	3.53±0.75	2.38±0.88	3.67±0.52	1.34±0.06
C (%)	51.37±0.79	43.26±4.13	27.09±3.64	52.3±0.23
N (%)	1.95±0.11	5.20±0.09	2.93±0.05	0.66±0.04
C/N	26.31±1.07	8.31±0.65	9.24±1.07	78.89±4.54
P (%)	0.29±0.01	0.39±0.031	0.80±0.036	0.40±0.00
K (%)	2.10±0.07	0.95±0.04	1.84±0.02	0.63±0.03
Ca (%)	0.56±0.02	3.20±0.15	2.54±0.08	0.28±0.02
Mg (%)	0.17±0.00	0.56±0.04	0.744±0.02	0.082±0.01
Fe (mg kg^{-1})	223.00±14.00	2825.00±40.00	2809.00±122.00	28.50±1.13
Cu (mg kg^{-1})	7.40±0.45	170.20±2.50	61.30±2.20	5.80±0.40
Zn (mg kg^{-1})	29.50±2.40	104.00±11.00	236.10±6.10	40.30±1.20
Mn (mg kg^{-1})	25.80±1.50	257±2.00	267.30±7.60	28.50±1.13

simultaneously [6]. At the end of composting process, the new and economic products (humus like materials) are produced. Compost is used in open fields, orchards, vineyards, urban landscapes, and nursery to improve soil fertility, to increase water holding capacity of soils, and to prepare potting mixes [7]. The objective of this study is to investigate the evolution of parameters describing the mixture of municipal open market wastes with rose oil processing wastes, animal manure, and straw using windrow composting.

MATERIALS AND METHODS

The study was carried out at a farm (Gürelli Farm) located in Isparta province. This study involved MOMW, ROPW, dairy manure (DM), and straw. MOMW was collected from Isparta Municipality open market. The ROPW was obtained from Biolandes Rose Oil Factory in Isparta province. The DM and straw were supplied from a farm in Isparta province. Chemical analyses of MOMW, ROPW, and DM are given in Table 1. MOMW had C/N of 26.31 and organic matter of 92.47 % while ROPW had C/N of 8.31 and organic matter of 77.87 %. DM had a total nitrogen content of 2.93 % on a dry mass basis. DM was rich in concentration of P, Ca, Mg, Fe, Zn, and Mn while ROPW had high initial nutrient concentration in terms of Ca, Mg, Fe Cu, and Mn. [8] reported that the initial nutrient concentration of ROPW for N, P, K, Ca, Mg, Fe, Zn, and Mn as 3.7%, 0.099%, 2.4%, 1.6%, 0.5%, 2000 mg kg^{-1}, 85 mg kg^{-1}, 171 mg kg^{-1}. MOMW is rich only in K concentration. The straw is poor in initial nutrient concentration of K, Ca, Mg, Fe, and Cu compared to the other raw materials. ROPW was stored at the farm for one year (Table 1).

Compositions of reactor feed at the beginning of experiment are given in Table 2. Mixing ratios for MOMW, ROPW, DM, and straw are given on a dry mass basis. Straw was used as carbon amendments to balance of the C/N ratios and to form free air space (FAS). Two initial (i) C/N ratios were evaluated during the study. They were: $[C/N]_{ia}$, where a is the calculated ratio of C/N in compost at time = 0 based on mixing ratios and laboratory analyses of parent materials before mixing and $[C/N]_{ib}$, where b is the measured ratio of carbon to nitrogen in compost at time = 0 based on laboratory analysis of blended ingredients after mixing. The amount of MOMW used in the mixtures increased from (0.04 kg kg^{-1}) for Mix-1 to (0.37 kg kg^{-1}) for Mix-3. Conversely, the amount of ROPW used in mixes decreased from (0.47 kg kg^{-1}) for Mix-1 to (0.25 kg kg^{-1}) for Mix-3. C/N ratios of the mixtures were determined according to C and N values of parent materials. FAS values of compost mixes were obtained from the equation given by [9]. FAS values of Mix-1, 2, and 3 were 27.28%, 31.69%, and 34.51%, respectively.

Composting experiment was carried out in an open type composting bin having three sections. There different mixtures of MOMW, ROPW, DM, and straw were prepared for each cone-shaped windrow separately. Mix-1, Mix-2, and Mix-3 had a total mass of 520.46 kg, 571.86 kg, and 673.40 kg, respectively. Each windrow was built by mixing raw

TABLE 2
Compositions of feedstocks and amendments used to formulate feed and initial physical and chemical analysis of mixtures in windrow

	MOMW (kg kg^{-1})	ROPW (kg kg^{-1})	DM (kg kg^{-1})	Straw (kg kg^{-1})	$[C/N]_{ia}$ -	$[C/N]_{ib}$ -	pH -	FAS (%)
Mix-1	0.04	0.47	0.39	0.10	10.23	9.85±0.04	7.73±0.11	27.28
Mix-2	0.19	0.30	0.34	0.16	13.35	12.42±0.02	6.68±0.36	31.69
Mix-3	0.37	0.25	0.23	0.15	15.62	15.88±0.62	6.76±0.03	34.51

materials by shoveling. Particle size of MOMW was reduced by an industrial shredder. Compost temperature in each windrow was monitored with a hand-held digital thermometer (Model HH-21, Omega). Compost temperature was measured at one point at the center of heap (1 m down from top of the heap) once a day.

O_2 concentrations as a function of time were analyzed by a portable analyzer (MODEL 902P, Quantek Instruments). O_2 concentration was measured from the point at the center of heap (25 cm down from top of the heap) once a day. The process was also monitored for C/N ratio, moisture content, and organic matter content, EC, and pH as a function of time. Triplicate samples were analyzed for moisture content, organic matter, pH, and EC. Moisture content of compost materials was determined at 105 ºC for 24 hours [10]. Organic matter was analyzed at 550 °C for 4 hours [10]. pH and EC measurements were performed in the water-compost extract 1:10 (w v^{-1}). Samples were analyzed for total N content [10]. Secondly, carbon contents were calculated using organic matter contents of materials [11]. The composting experiment lasted for 44.75 days. The piles were remixed at 4.75, 7.75, 9.75, 15.75, 23.75, and 36.75th days of composting by shoveling. The sampling of compost materials was performed for all the remixing days except for 4.75 and 7.75th days of composting.

Mineral contents of MOMW, ROPW, DM, straw and mixes were analyzed by spectrophotometer for P and atomic absorption spectrophotometer (Perkin-Elmer AA800) for K, Ca, Mg, Zn, Cu, Fe, and Mn after digestion in HNO_3 65% in a microwave. The initial and final mineral contents of samples were made for all mixes [12].

Losses of organic matter (OML) were calculated from the initial (X_1) and final (X_2) ash contents according to the following equations (Eq.1) [13]:

$$OML\ (\%) = 100 - 100\frac{[X_1(100-X_2)]}{[X_2(100-X_1)]} \quad (1)$$

The soil CO_2 flux system (PP Systems, Hitchin, UK) was used for in-situ composting CO_2 emissions. The flux system are comprised of CO_2 analyzer, H_2O sensor, soil respiration chamber, and thermocouple [14]. Net CO_2 flux from the soil respiration chamber was measured considering CO_2 concentrations of influent and effluent air and the flow rate under normal composting atmosphere. The accuracy of measurements of CO_2 and H_2O concentrations are better than 1% and 2%, respectively. Three recordings were randomly taken from different locations on each heap. The CO_2 flux chamber (21 cm in diameter and 12 cm in height) was located on the top of the piles, which was randomly selected. It was inserted to 1.5 cm deep on top of the heap isolating from the ambient atmosphere. The measurements were performed once a day. CO_2 flux was expressed in $gCO_2\ m^{-2}\ h^{-1}$. Composting piles established in the open space were covered with plastic cover to protect them from outer effects. However, the plastic cover was opened during the data recording.

RESULTS AND DISCUSSION

Temperature evolution. The composting temperature development is an indication of microorganism activity during decomposition of organic wastes [9]. The temperature profiles in all the experimented windrows are shown in Fig.1. An increase of temperature from starting temperature points for all mixes to the level of 42 °C was resulted from the activity of mesophilic flora within half days for all mixes. The highest temperature recorded was 62°C, 67°C, and 66 °C at 6, 6, and 10th days of composting for Mix-1, 2, and 3, respectively. It was observed that thermophilic phase lasted for 14, 21, and 23 days for Mix-1, 2, and 3, respectively with high fluctuation due to remixing process for all mixes. Consequently, temperature histories showed variation based on the composted mixtures. The aeration of the windrows by shoveling and the moistening decreased the temperature. However, the temperature rose back to the previous level immediately due to microbial activity after mixing. Since readily available nutrients were depleted during thermophilic phase, the temperature of compost tended to decline [15]. Then, temperature approached to the ambient level. At this stage, the composted substrates reached the end of the bio-oxidative phase [16].

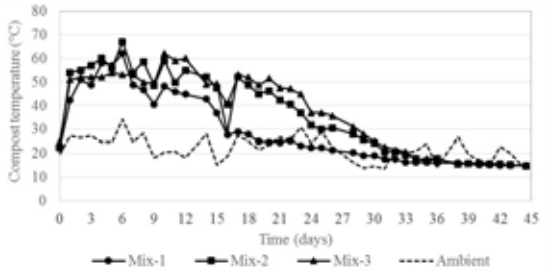

FIGURE 1
Temperature profiles during composting of Mix-1, 2, and 3

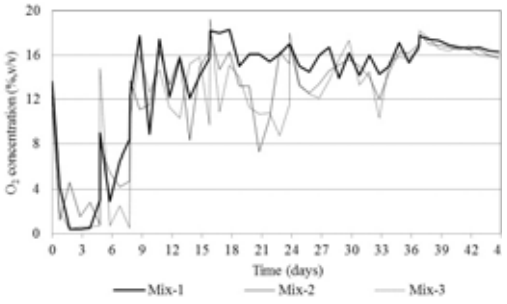

FIGURE 2
O_2 concentration histories during composting

It should be monitored temperature of Mix-1 usually was lower than that of Mix-2 and Mix-3 at all stages due to probably very low C/N ratio compared to that of Mix-2 and Mix-3.

O_2 evolution and CO_2 flux emission. Figure 2 shows change of O_2 concentration varying with time during process. Oxygen concentration for Mix-1 was measured as 0.4-0.5% between 1.75th and 3.75th days of composting showing scarcity of O_2 levels in the compost matrix. After the first remixing, oxygen concentration was measured as 2.9% at 5.75th days of composting. Then it never dropped below 5%, which is reasonable level [17]. O_2 concentration in Mix-2 dropped to 1.2% at 1.75th days and 2.8% at 3.75th days of composting. As for Mix-3, oxygen concentration was measured as 0.4-0.6 % between 1.75th and 3.75th days of composting. After the first remixing, the oxygen concentration was measured as 0.7% at 5.75th days of composting. Then before second remixing, O_2 concentration was 0.5% at 7.75th days. For all mixes, O_2 concentration was higher than 7.3% at 13.75th days of composting indicating that the composting processes were all aerobic. Through the end of composting, all mixes showed an increase in oxygen level up to 16% at the end of 44.75th days.

Figure 3 presents CO_2 emission changing with time for all mixes. The CO_2 emission histories reflected both temperature and O_2 concentration histories. Furthermore, the change of compost temperatures, O_2 concentration, and CO_2 emissions became stable after the 34th day. While the CO_2 emissions of the Mix-2 and Mix-3 reached their peak values (35.1, and 36.9 g m^{-2} h^{-1}) at the end of the 1st day, Mix-1 reached its peak value (32.4 g m^{-2} h^{-1}) at the end of 7th day. When each of three mixes ranked from minimum to maximum, Mix-1, Mix-2, and Mix-3 followed one another and the compositions of mixes were found to be effective on CO_2 emissions. After reaching the peak values of CO_2, the values began to decrease gradually. Carbon dioxide emissions of the Mix-1 decreased to a value under 1.0 (g m^{-2} h^{-1}) after 30th day. The CO_2 emissions of the other mixes decreased to values under 1.0 (g m^{-2}h^{-1}) at 34th day.

Throughout the composting period (44.75 days), depending on the mixes, cumulative CO_2 emissions for Mix-1, Mix-2, and Mix-3 were 5.89, 8.76 and 9.57 kg m^{-2}, respectively (Figure 4). It should be pointed out that increase in initial C/N in all mixes increased cumulative CO_2 emission from heaps.

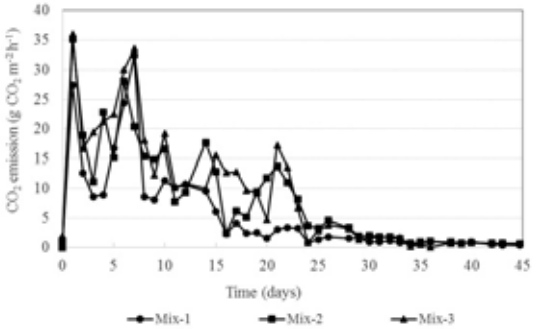

FIGURE 3
Evolution of CO_2 emission during composting

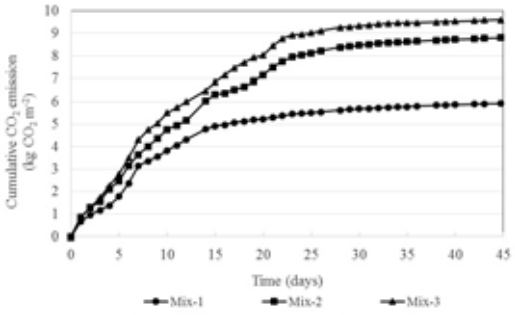

FIGURE 4
Cumulative CO_2 emission as a function of time

Moisture content variation and water evaporation. No water was added to the initial mixes thereby yielding the initial moisture content of 58.61±2.09, 69.67±2.03, and 78.75±0.45 for Mix-1, Mix-2, and Mix-3, respectively (Figure 5). Initial moisture contents of Mix-2 and 3 was higher than that of reasonable limits [17] due to initial moisture contents of MOMW used in the mixes.

The compost materials were remixed (1) to avoid moisture limitation (2) to maintain homogeneity in terms moisture and (3) to eliminate compaction during composting [18]. It was reported that a fair amount of water can be lost due to evaporation and water addition is necessary to maintain optimum moisture content for microbial activity [19]. Therefore, 40, 40, and 10 kg of water was added to Mix-1, Mix-2, and Mix-3, respectively to avoid moisture limitation at 9.75th days of composting. The second water addition was at 23.75th days at the amount of 20 and 10 kg for Mix-1 and Mix 2, respectively.

Evaluating moisture transport is important because of the significant quantity of energy transferred during the evaporation of water from compost matrix. This moisture transfer also leads to significant drying, which eventually inhibits microbial activity due to lack of moisture and excessive cooling [18]. 0.5 to 0.6 g H_2O of metabolic water is produced per g volatile solids decomposed [20]. The heat generated during composting evaporate significantly more water than is produced and tend to dry the material out [21]. Therefore, water emission from the surface of pile is closely related with the change of compost moisture during composting. Water emission and cumulative water evaporation from the surface of compost heaps for all mixes are given in Figure 6 and 7, respectively. While the highest water evaporation value reached at 6th day for Mix-1 and 2, Mix-3 reached that value 10th day of composting. Water emission value is defined as the amount of water evaporated from the surface of compost heap. Therefore, it is reasonable to expect that the highest cumulative water emission occurred from Mix-3 (Figure 7). Water emission was under 1.0 g m^{-2} h^{-1} for the three treatments at 44.75th day of composting.

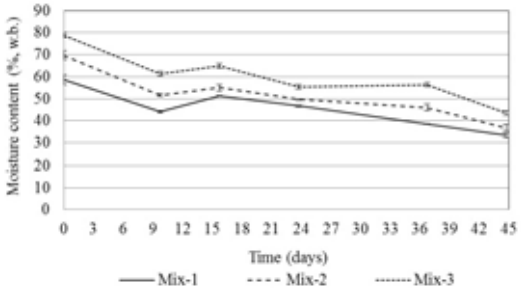

FIGURE 5
Changes of moisture content with time for all mixes (mean ± standard deviation)

Organic matter degradation. The starting organic matter content differed based the composition of the windrows (Table 2). The organic matter of composts declined during the composting process in all the three mixtures (Figure 8).

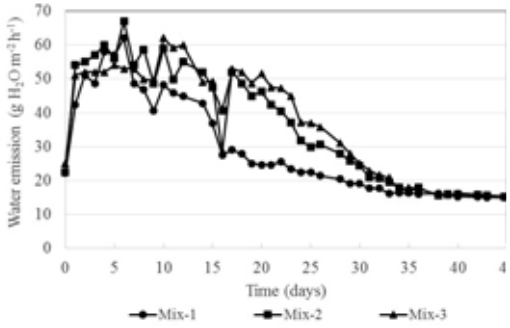

FIGURE 6
Evolution of water emission during composting

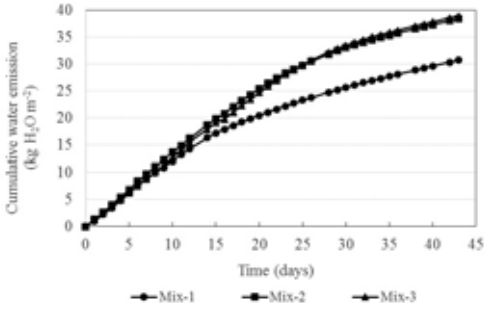

FIGURE 7
Cumulative water emission from the surface of compost piles

Furthermore, results showed that the highest OM degradation occurred during the thermophilic stage due to microbial activity [22]. This findings supports the temperature evolution of mixes. The levels of organic matter decomposition of three mixtures were different. This may be as a result of the mineralization of unstable organic compounds which mainly occurred during the thermophilic stage [16]. Among the well-composted materials, Mix-2 and Mix-3 exhibited OML of 55.17±3.96 and 55.93±8.62 (%), respectively. On the other hand, little changes of OM contents were measured for Mix-1 having a low level of OML (18.08±7.70 %) due to 47% of ROPW in the initial composition of mixture, which is probably as a consequence of initially having low C/N ratio. The trend observed in cumulative CO_2 emission as a function of time is parallel to those found in organic matter degradation. Higher OM losses and higher values of biodegradability were observed in Mix-2 and Mix-3 mixtures [11].

pH variations. Figure 9 shows changes of pH of tree mixes during the composting process. pH of Mix-1 decreased from 7.88 to 7.47 at 15.75th day of composting. This decrease could be attributed to the production of organic acids from the readily available carbon sources. Then, pH increased due to result of the biodegradation of acids as the

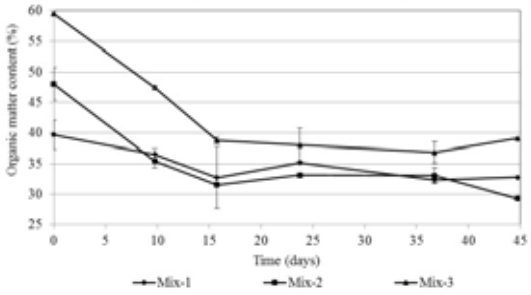

FIGURE 8
Evolution of organic matter content of the mixes during composting (mean ± standard deviation)

mineralization of organic compounds to inorganic compounds [23]. Finally, in Mix-1, the pH decreased, up to the value of 7.51. As for Mix-2 and Mix-3, pH increased from 6.68 and 6.76 to the values of 8.44 and 8.43 at 9.75th days of composting, respectively. Then, it decreased to 7.92 and 8.35 at the end of composting experiment. The final pH values were slightly higher in the mixtures probably due to ammonium evolution and N losses [24].

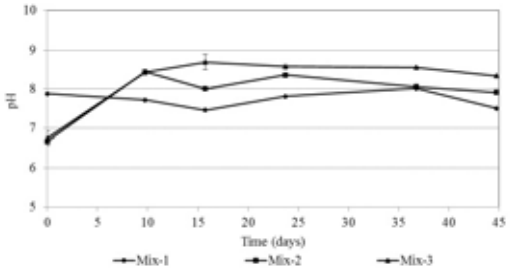

FIGURE 9
Changes of pH for all mixes (mean ± standard deviation)

EC variation.EC of mixes increased due to the ionic concentrations resulted from the mass loss of compost except for that of Mix-1 (Table 3). The EC of the Mix-1 decreased at the end of the process probably due to the volatilization of ammonia [25,16]. Conversely, the EC of Mix-2 and Mix-3, increased from initial value of 4.14 and 4.08 to final of 4.46 and 5.16, respectively. This is in agreement with those reported by other authors [26, 27,16]. As reported by [26], this pattern could be attributed to the increase in ion concentration because of mass loss in windrow. Even if with different absolute EC values of mixes, the final EC value of Mix-1 was less than 4 dS m^{-1}and classified as non-saline soil while the final EC values of Mix-2 and Mix-3 were 4.46±0.04 and 5.16±0.91 dS m^{-1}, which is classified as low-saline soils [28].

C/N pattern. C/N ratio is one of the most influential parameters for composting process and it can be controlled at the beginning of the process.

TABLE 3
Electrical conductivity at the initial and the final stages of composting

Mixes	Electrical conductivity (dS m^{-1})	
	Initial time	Final time
Mix-1	3.62±0.33	2.86±0.42
Mix-2	4.14±0.33	4.46±0.04
Mix-3	4.08±0.38	5.16±0.91

It was reported that initial optimum C/N ratio for composting was between 25 and 30 [29]. However, there have been researches concerning the low initial C/N ratios for example, C/N ratios of 9.15, 12.47, 12.67, 20.04, and 21.41 for co-composting of rose oil processing waste with caged layer manure [30] and C/N ratios of 14.5 for composting of chicken litter [31].

Initial C/N values were 9.85±0.35, 12.42±0.16, and 15.88±0.62 for Mix-1, Mix-2, and Mix-3, respectively. As shown in Fig. 10, as composting proceeded, the C/N ratio declined for all the mixes [32,16]. The initial C/N of mixes decreased to 7.43±0.27, 7.87±0.48, and 9.48±0.17 at the end of the biodegradation process for Mix-1, Mix-2, and Mix-3, respectively. The change of C/N ratio for Mix-1 was small due to probably the excess of N. The final C/N of compost alone cannot be used to determine whether compost is mature. On the other hand, the final values of C/N ratios for all mixes in this study could be well enough for compost to be utilized for plant growing [33,34,15].

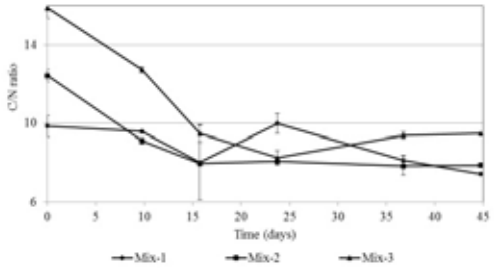

FIGURE 10
Changes of C/N ratios as a function of time for all mixes (mean ± standard deviation)

Mineral concentration. The concentrations of P, K, Ca, Mg, Fe, Cu, Zn, and Mn were determined at the initial and final stages of composting (Table 4). The results showed a significant increase of the minerals. Average increase for all mixes in P, K, Ca, Mg, Fe, Cu, Zn, and Mn was determined as 37, 16, 80, 32, 38, 40, 26, and 32%, respectively. Similarly, the study conducted by [35] showed that concentration of P, K, Fe, Zn, Mn, and Cu of composted material increased about 33, 30, 21, 29, 34, and 20%, respectively comparing to raw material. In another study, increases of P, K, Ca, Mg, Zn, Cu, Mn, and Fe in composted material were found as

TABLE 4
Mineral composition of before (t_i) and after composting (t_f)(values calculated on the dry mass basis)

Nutrients	Mix-1		Mix-2		Mix-3	
	t_i	t_f	t_i	t_f	t_i	t_f
P (%)	0.41±0.05	0.60±0.08	0.55±0.07	0.61±0.05	0.29±0.03	0.45±0.08
K (%)	1.29±0.08	1.50±0.19	1.63±0.19	1.99±0.07	2.12±0.20	2.31±0.19
Ca (%)	2.53±0.38	3.87±0.34	1.72±0.16	3.71±032	2.11±0.33	3.60±0.38
Mg (%)	0.31±0.02	0.36±0.04	0.20±0.19	0.36±0.03	0.17±0.02	0.29±0.03
Fe (mg kg^{-1})	2276±15	2611±14	1803±26	2353±40	1239±41	2095±50
Cu (mg kg^{-1})	48.75±3.11	63.75±2.11	37.50±2.20	55.00±40	38.75±20	54.60±3.00
Zn (mg kg^{-1})	52±12	71±10	65±6	79±8	75±11	91±7
Mn (mg kg^{-1})	374±38	468±29	330±15	461±40	281±41	365±36

TABLE 5
Estimated and measured initial nutrient concentration of mixtures

Nutrients	Estimated nutrient contribution to the mixes				Total	Measured initial nutrient concentration of mixtures	Matching rate (%)
	MOMW	ROPW	DM	Straw			
Mix-1							
P (%)	0.012	0.19	0.31	0.04	0.55	0.41	74.5
K (%)	0.084	0.45	0.72	0.06	1.31	1.29	98.5
Ca (%)	0.024	1.50	0.99	0.022	2.53	2.53	100
Mg (%)	0.007	0.26	0.29	0.008	0.57	0.31	54.4
Fe (mg kg^{-1})	8.9	1328.0	1096.0	2.9	2436.0	2276.0	93.4
Cu (mg kg^{-1})	0.3	80.0	23.9	0.58	104.8	48.75	46.5
Zn (mg kg^{-1})	1.2	48.9	92.1	4.0	146.2	52.0	35.6
Mn (mg kg^{-1})	1.0	120.8	104.3	2.9	229.0	374.0	61.2
Mean							70.5
Mix-2							
P (%)	0.05	0.12	0.27	0.06	0.50	0.55	90.1
K (%)	0.40	0.29	0.63	0.10	1.42	1.63	87.1
Ca (%)	0.10	0.96	0.86	0.04	1.90	1.72	90.5
Mg (%)	0.03	0.17	0.25	0.01	0.46	0.20	43.4
Fe (mg kg^{-1})	42.4	848.0	955.0	4.6	1850.0	1803.0	97.5
Cu (mg kg^{-1})	1.4	51.0	20.8	0.9	74.1	37.5	50.6
Zn (mg kg^{-1})	5.6	31.2	80.3	6.5	123.6	65.0	52.6
Mn (mg kg^{-1})	4.9	77.1	90.9	4.6	177.5	330.0	53.8
Mean							79.6
Mix-3							
P (%)	0.11	0.10	0.18	0.06	0.45	0.29	65.9
K (%)	0.78	0.24	0.42	0.09	1.53	2.12	72.2
Ca (%)	0.21	0.80	0.58	0.04	1.63	2.11	77.3
Mg (%)	0.06	0.14	0.17	0.01	0.38	0.17	44.7
Fe (mg kg^{-1})	83	706	646	4	1439	1239	86.1
Cu (mg kg^{-1})	2.7	42.6	14.1	0.9	60.3	38.78	64.3
Zn (mg kg^{-1})	11	26	54	6	97	75	77.3
Mn (mg kg^{-1})	10	64	61	4	139	281	49.5
Mean							67.2

59, 22, 77, 50, 20, 70, 29, and 37%, respectively [36]. In this study, the initial mineral nutrient concentrations of raw materials used for composting had significant effect on final nutrient concentration of mixes. For example, initial concentration of Ca, Mg, Fe, Cu and Mn of Mix-1 was higher than that of the other mixes. This led to the higher final concentration of these minerals in Mix-1 compared to the other mixes. On the other hand, the opposite was valid for Mix-3. Therefore, in order to obtain a compost which have high final nutrient concentration, the raw materials, which is rich in terms of mineral nutrient concentration, should be used. [37] found that final nutrient concentrations of compost mixes varied between 0.45-0.61 for P (%); 1.50-2.31 for K (%); 3.60-3.87 for Ca (%), 0.29-0.36 Mg (%), 2095-2611 mg kg^{-1} for Fe, 54.6-63.75 mg kg^{-1} for Cu, 71-91 mg kg^{-1} for Zn and 365-468 mg kg^{-1} for Mn. Similarly, [38] reported the results of final nutrient concentration of nine composts as 0.85-2.13%, 0.27-0.40%, 0.12-0.63%, 0.2-5.8%, 0.04-0.67%, 8-50 mg kg^{-1}, 12-88 mg kg^{-1} and 85-270 mg kg^{-1} for N, P, K, Ca, Mg, Zn, Fe, and Mn, respectively.

Estimated and measured initial nutrient concentrations of the mixtures are presented in Table 5. Table 5 was prepared based on initial nutrient concentrations of raw materials (Table 1) and compositions of the mixes (Table 2). Matching rate was calculated considering measured and estimated initial nutrient concentrations of the mixtures. Furthermore, the range of matching rate of 35.6-100%, 50.6-97.5%, 44.7-86.1% for Mix-1, Mix-2, and Mix-3, respectively, were calculated. The average matching rates of mixes were 70.5%, 79.6%, and 67.2%, respectively. This shows that initial nutrient concentration of raw materials was effective on initial nutrient concentration of the mixes considering composition of mixes.

CONCLUSIONS

Composting of municipal open market wastes with rose oil processing wastes, animal manure, and straw was experimented. The results showed that the composting process could solve the disposal problem of wastes such as municipal open market wastes, and rose oil processing wastes produced in Isparta province. The results indicated that composting of these wastes produces composts with the adequate amount of nutrients to maintain plant growth suggesting that composting is a viable approach for recycling these wastes. Furthermore, temperature evolution and organic matter degradation of Mix-1 yielded that initial C/N ratio of 9.2 was so low that the lowest organic matter loss of 18% occurred comparing to that of 55.2% and 55.9% for Mix-2 and 3, respectively. The findings of both CO_2 and water emission from the surface of piles during composting process confirmed that the highest degradation occurred for Mix-2 and Mix-3. Although the resultant EC values of Mix-1 was less than 4 dS m^{-1} and classified as non-saline soil while the final EC values of Mix-2 and Mix-3 were 4.46±0.04 and 5.16±0.91 dS m^{-1}, which is classified as low-saline soils based on Turkish regulation on the implementation of the Law on Soil Preservation and Land Utilization. Even though all mixes were not suffered from the scarcity of water in the compost matrix, O_2 concentration measured from piles showed that process was carried out under partially anaerobic conditions due to reasonable O_2 level (5%). It can be concluded that the composts with the final C/N ratios of 7.4, 7.9, and 9.5 for Mix-1, Mix-2, and Mix-3, respectively can be utilized for plant growing.

ACKNOWLEDGEMENT

This research was supported by Suleyman Demirel University and Gurelli farm in Isparta Turkey.

REFERENCES

[1] TUIK (2013) Turkish Statistical Institute, Plant Production Report. Available at http://www. turkstat.gov.tr.

[2] Tosun, İ. (2003) Compostability of rose processing wastes with organic fractions of municipal solid wastes (in Turkish). Ph.D. Thesis, Yildiz Technical University.

[3] Huang, G.F., Wong, J.W.C., Wu, Q.T. and Nagar, B.B. (2004) Effect of C/N on composting of pig manure with sawdust. Bioresource Technology, 24: 805-813.

[4] Castaldi, P., Santona, L., Melis, P., 2006. Evolution of heavy metals mobility during municipal solid waste composting. Fresenius Environ. Bull. 15, 1133–1140.

[5] Atılgan, A., Erkan M., Saltuk, B. and Ekinci, K. (2004) Manure Management and Current Situation of Manure Storage Facilities in Dairy Farms In Adıyaman Region. 3. Ulusal Gübre Kongresi, Tokat, 11-13 Ekim.

[6] Keener, H.M., Marugg, C., Hansen, R.C. and Hoitink, H.A.J. (1993) Optimizing the efficiency of the composting process. In: Hoitink, H.A.J., Keener, H.M. (Eds.), Science and Engineering of Composting: Design, Environmental, Microbiological and Utilization Aspects. Renaissance Publications, Ohio, pp. 59-94.

[7] Keener, H.M., Dick, W.A. and Hoitink, H.A.J. (2000) Composting and beneficial utilization of composted by-product materials, in: Power, J.F., Dick, W.A., Kashmanian, R.M., Sims, J.T., Wright, R. J., Dawson, M. D., Bezdicek, D. (Eds.), Beneficial Uses of Agricultural, Industrial and Municipal By-products. Soil Science Society of America. Madison, Wisconsin, pp. 315-341.

[8] Tosun, İ., Gönüllü, M. T. and Arslankaya, E. (2005) Gül Sanayi Proses Atıkları Özelliklerinin Belirlenmesi. Yıldız Teknik Üniversitesi Çevre Mühendisliği Bölümü, İstanbul. http://www.yildiz.edu.tr/~gonul/bildiriler/b82.pdf

[9] Epstein, E. (1997) The Science of Composting. CRC Press LLC.

[10] APHA (1995) Standard Methods for the Examination of Water and Wastewater. APHA, AWWA, WEF, 19th Ed.

[11] Haug, R.T. (1993) The Practical Handbook of Compost Engineering. Lewis Publishers, Boca Raton, FL.

[12] Kacar, B. and İnal, A. (2010) Plant Analysis. Nobel Press, Ankara

[13] Paredes, C., Bernal, M.P., Roig, A. and Cegarra, J. (2001) Effects of olive mill wastewater addition in composting of agroindustrial and urban Wastes. Biodegradation. 12, 225-234.

[14] Akbolat, D., Evrendilek, F., Coskan, A. and Ekinci, K. (2009) Quantifying soil respiration in response to short-term tillage practices: a case study in southern Turkey. Acta Agriculturae Scandinavica, Section B-Plant Soil Science. 59: 50-56.

[15] Sellami, F., Jarboui, R., Hachicha, S., Medhioub, K. and Ammar, E. (2008) Co-composting of oil exhausted olive-cake, poultry manure and industrial residues of agro-food activity for soil amendment. Bioresource Technology. 99: 1177-1188.

[16] Montemurro, F., Diacono, M., Vitti, C., Debiase, G., 2009. Biodegradation of olive husk mixed with other agricultural wastes. Bioresource Technology. 100: 2969-2974.

[17] Rynk, R. (1992). On farm composting handbook. NRAES-54, Cooperative Extension Service, Northeast Regional Agricultural Engineering Services, Ithaca NY, USA.

[18] Keener, H.M., Elwell, D.L., Das, K. and Hansen, R.C. (1996) Remix scheduling during composting based on moisture control. Transactions of the ASAE. 39: 1839-1845.

[19] Bernal, M.P., Alburquerque, J.A. and Moral, R. (2009) Composting of animal manures and chemical criteria for compost maturity assessment. A review. Bioresour.Technol. 100: 5444-5453.

[20] Miller, F.C. (1991) Biodegradation of solid wastes by composting. In: Martin, A.M. (ed.). Biological Degradation of Wastes. Elsevier Applied Science. London. pp. 1-31.

[21] Nakasaki, K., Kato, K., Akiyama, T. and Kubota, H. (1987) A new composting model and assessment of optimum operation for effective drying of composting material. Journal of Fermentation Technology. 65, 441-447.

[22] Ekinci, K., Keener, H.M. and Elwell, D.L. (2000) Composting short paper fiber with broiler litter and additives. Part I: Effects of initial pH and carbon/nitrogen ratio on ammonia emission. Compost Science and Utilization. 8: 160-172.

[23] Baeta-Hall, L., Sàagua, M.C., Bartolomeu, M.L., Anselmo, A.M. and Rosa, M.F. (2005) Biodegradation of olive husks in composting aerated piles. Bioresource Technology. 96: 69-78.

[24] Nakasaki, K., Yaguchi, H., Sasaki, Y. and Kubota, H. (1993). Effect of pH control composting of garbage. Waste Manage. Research. 11: 117-125.

[25] Wong, J.W.C., Li, S.W.Y. and Wong, M.H. (1995) Coal fly ash as a composting material for sewage sludge: effects on microbial activities. Environ. Technol. 58: 309-313.

[26] Sánchez-Monedero, M.A., Roig, A., Paredes, C. and Bernal, M.P. (2001) Nitrogen transformation during organic waste composting by the Rutger system and its effects on pH, EC and maturity of the composting mixtures. Biores. Technol.78: 301–308.

[27] Canet, R., Pomares, F., Cabot, B., Chaves, C., Ferrer, E., Ribò, M. and Albiach, R. (2008) Composting olive mill pomace and other residues from rural southeastern Spain. Waste Management. 28: 2585–2592.

[28] OG (2005) The Official Gazette of Republic of Turkey. Regulation on the implementation of the Law on Soil Preservation and Land Utilization (In Turkish). Law Nr: 5403, Republic of Turkey, Official Gazette, No: 26024.

[29] Fong, M., Wong, J.W.C. and Wong, M.H. (1999) Review on evaluation of compost maturity and stability of solid waste. Shanghai Environ. Sci.18: 91–93.

[30] Onursal, E. (2006) A research on determination of optimum C/N ratio of composting of rose processing wastes (in Turkish). Master Thesis. Suleyman Demirel University.

[31] Tiquia, S.M. and Tam, N.F.Y. (2000) Fate of nitrogen during composting of chicken litter. Environmental Pollution, 110: 535-541.

[32] Paredes, C., Bernal, M.P., Cegarra, J. and Roig, A. (2002) Bio-degradation of olive mill wastewater sludge by its co-composting with agricultural wastes. Biores. Technol. 85: 1–8.
[33] Abid, N. and Sayadi, S. (2006) Detrimental effect of olive mill wastewater on the composting process of agricultural wastes. Waste Manage. 26: 1099–1107.
[34] Hachicha, S., Sellami, F., Medhioub, K., Hachicha, R. and Ammar, E. (2008) Quality assessment of composts prepared with olive mill wastewater and agricultural wastes. Waste Management. 28: 2593–2603.
[35] Ahmad, R., Khalid, A., Arshad, M., Zahir, Z.A. and Naveed, M. (2006). Effect of raw (un-composted) and composted organic waste material on growth and yield of maize (Zea mays L.). Soil & Environment. 25: 135-142.
[36] [Roca-Pérez, L., Martínez, C., Marcilla, P. and Boluda, R. (2009) Composting rice straw with sewage sludge and compost effects on the soil–plant system. Chemosphere. 75: 781–787.
[37] López, M., Huerta, O., Valero, J., and Soliva, M. (2004) 11th International Conference of the FAO ESCORENA Network on Recycling of Agricultural, Municipal and Industrial Residues in Agriculture. Murcia, October 2004.
[38] Yüksel, A. (2006) The Effects of different compost processes on two different growing environments on clover and onion plant's growing plant nutrient elements uptake and Mycorrizae infection quality (in Turkish). Master Thesis, University of Çukurova.

Received: **07.10.2015**
Accepted: **25.07.2016**

CORRESPONDING AUTHOR

Kamil Ekinci
Department of Agricultural Machinery and Technologies Engineering, Faculty of Agriculture, Suleyman Demirel University,32260 Isparta-TURKEY

e-mail: kamilekinci@sdu.edu.tr
kamil_ekinci@yahoo.com

© by PSP Volume 25 – No. 10/2016, pages 4036-4044 Fresenius Environmental Bulletin

ANAEROBIC OXIDATION OF LANDFILL CH_4 AND N_2O EMISSIONS BY AGED REFUSE AND COVER SOIL: EFFECTS OF ENVIRONMENTAL FACTORS

Chaoran Li [1], Houhu Zhang [2,*], Shaojun Jiao[2], Zhehua Zhao[2]

[1]College of Life and Environmental Sciences, MinZu University of China
No.27 S. Zhongguancun St, Haidian District, Beijing, China, 100081
[2]Nanjing Institute of Environmental Sciences of the Ministry of Environmental Protection of P.R. China. Nanjing, Jiangsu, 210042, P. R. China

ABSTRACT

Anaerobic oxidation of CH_4 (AOM) and the rate of N_2O emissions were investigated using aged refuse, landfill cover soil and two mineral soils (sandy and clay soils). The influences of particle size, temperature and soil moisture content were also evaluated. The maximum AOM rate in incubated aged refuse was 0.12 μmol/g/h, which was several times higher than AOM rates of the three soils and two to three orders of magnitude higher than rates reported in previous studies. The average CH_4 oxidation rate for aged refuse with water contents in the range of 10–30% was 1.97 μmol/(g·d), which was 1.61 ($P<0.01$), 1.84 ($P<0.01$), and 3.05 ($P<0.01$) times more than those of the cover soil, clay soil, and sandy soil, respectively. The conversion ratios of CH_4 to CO_2 were 43.8–52.3%, 26.5–50.5%, 23.4–49.6%, and 20.9–49.5% for aged refuse, cover soil, clay soil, and sandy soil, respectively. The average CH_4-to-CO_2 ratio for the four sample types followed the order of aged refuse > cover soil > clay soil > sandy soil. Additionally, the average N_2O emission rate for aged refuse was 3.79 ($P<0.01$), 3.82 ($P<0.01$) and 5.50 ($P<0.01$) times more than those of the cover soil, clay soil, and sandy soil, respectively. The environmental implications of these findings are that application of an aged refuse bio-cover to a municipal solid waste landfill can reduce CH_4 emissions, which would significantly reduce the effect on global warming of solid waste management operations.

KEYWORDS:
anaerobic oxidation of CH_4, aged refuse, cover soil, N_2O emissions.

INTRODUCTION

Methane (CH_4) is a powerful greenhouse gas (GHG) with a global warming potential 25 times higher than carbon dioxide over a 100-year timeframe [1]. Methane production in landfills and the resulting emissions to the atmosphere represent the second largest anthropogenic methane source, and have been frequently evaluated in the past [1, 2]. Not all landfills produce sufficient biogas volumes for viable energy recovery, yet the release of CH_4 emissions from these sites still contributes to atmospheric GHG accumulation. The recent Working Group III assessment report by the IPCC (Intergovernmental Panel on Climate Change) has listed bio-covers and bio-filters as key technologies and practices for the mitigation of fugitive and low-calorific emissions from landfills [3]. As CH_4 transits through the landfill cover, methanotrophic bacteria use it as a substrate and oxidize it to CO_2 and H_2O.

To date, the majority of studies examining the potential of soils and other media for aerobic oxidation of landfill CH_4 are well known, and different factors, mainly moisture, temperature, and nutrient supply, as well as the availability of the substrates CH_4 and O_2, have been suggested to govern oxidation efficiency. Numerous studies have reported that landfill cover soils can oxidize up to 100% of the CH_4 emissions [4–9]. Under certain conditions, the landfill cover can even consume atmospheric CH_4, rather than emit CH_4 to the atmosphere [5, 10]. However, anaerobic oxidation of landfill CH_4 (particularly for landfill cover soils) has not been elucidated.

Anaerobic oxidation of methane (AOM) is a process that was first reported to occur in deep anoxic marine sediments [11]. In this environment, CH_4 is oxidized using sulfate (SO_4^{2-}) as the terminal electron acceptor. It is mediated by a syntrophic consortium formed by SO_4^{2-}-reducing bacteria and anaerobic CH_4-oxidizing archaea, or by the latter alone. Since this landmark discovery, AOM has been found to occur in other environments including freshwater lake sediments and water columns [12,13], mud volcanoes [14], landfill leachate [15], deep buried Holocene sediments and hydrocarbon contaminated aquifers [16,17] . As the bottom layer of landfill cover soil is becoming recognized as a fundamental biogeochemical redox

boundary in methane- and sulfate-rich environments, these findings raise the question of whether AOM is existent in landfill cover soils.

Furthermore, nitrous oxide (N_2O) has a global warming potential that is 298 times greater than CO_2 and it accounts for 6% of the anthropogenic greenhouse effect. Only CO_2 and CH_4 emissions have a greater impact [1, 18]. Nitrous oxide is produced predominantly by microbial processes in soils, as a by-product of nitrification and as an intermediate product of denitrification. In landfills, N_2O emissions are attributed to the primary nitrification and denitrification processes in the cover soil and, in some cases, landfill N_2O emissions have been shown to be at least one or two orders of magnitude greater than emissions from forests and agricultural fields [7, 18–20]. Thus, the properties of landfill cover material used to support anaerobic oxidation of CH_4 may also be important for N_2O emissions through denitrification processes. However, there is less information on N_2O emissions by active bio-cover materials, particularly as they relate to the AOMs.

The primary objectives of this study were to investigate the influences of environmental factors on AOM and N_2O emissions by aged refuse and landfill cover soil. Specifically, we sought to (i) compare AOM rates in aged refuse with cover soil in order to determine how it is regulated by environmental factors; (ii) elucidate the relationship between AOM rates and CO_2 emission potential and (iii) assess the potential N_2O emissions after field-scale applications. To evaluate these factors, we used aged refuse in laboratory batch assays and compared it with three different types of soils.

MATERIALS AND METHODS

Aged refuse and soil samples. The aged refuse for this study was excavated in 2010 from a single enclosed chamber at the Shuige municipal solid waste (MSW) landfill in Nanjing City that had been covered for 10 years. Currently landfilled refuse is comprised of (wet weight basis) food waste (60%); plastics (20%); organic matter, such as bamboo, wood, paper and textiles (15%); and inorganic matter, such as stone, sand, metals and other materials (5%). The excavated sample of aged refuse was air-dried in the laboratory after which large non-degradable matter (e.g., stones, glass bottles, plastic film, plastic bags and rubber) was removed by manual sorting. The cover soil was taken from the bottom layer (-80cm) in a 4-year closed unite within the same MSW landfill site. The soil samples for the comparative study were taken from a paddy field and from the base of a mountain located in the Taihu Lake basin, Jiangsu Province, China (31°29'N, 119°59'E), which were named as Clay soil and Sandy soil, respectively. Each sample was immediately placed in a plastic vacuum bag and excess air was removed by suction prior to sealing the bag. All samples were characterized by selected chemical properties. Air dried subsamples were sieved through 2.00 mm screens to remove large particulate matter. The physicochemical properties of the aged refuse and the three soil samples are shown in Table 1.

Anaerobic methane oxidation rate. The AOM rates by the aged refuse and soil samples were determined in triplicate at an incubation temperature of 25°C and a moisture content of 20%, unless otherwise specified. The aged refuse and soil samples were air-dried for 48 h to a moisture content of approximately 8% dry weight. Distilled water was then added to the dried samples to reach the desired water content. After overnight storage (25°C), 20 g samples were placed in 250 mL serum bottles, which were then closed with rubber stoppers and sealed with aluminum crimps.

TABLE 1
Physicochemical properties of aged refuse and soil samples (n= 3)

Physicochemical properties	Aged refuse	Cover soil	Clay soil	Sandy Soil
pH($CaCl_2$)	7.25±0.23	6.94±0.15	7.43±0.14	7.50±0.17
Cation exchange capacity (cmol kg^{-1})	68.62±1.84	58.37±2.09	49.27±1.78	43.68± 1.63
Specific surface area (m^2 g^{-1})	0.73±0.11	0.77±0.20	0.82±0.16	0.84± 0.18
D_{50} (μm)	152	144	136	148
Organic matter content (%)	10.36±2.72	11.77±2.31	4.58±0.88	2.31± 0.20
NH_4^+-N content (mg kg^{-1})	17.73±0.14	14.83±0.52	14.06±1.33	8.79± 0.95
NO_3^--N content (mg kg^{-1})	56.43±0.66	30.75±1.70	16.24±2.71	12.25±0.63
SO_4^{2-} content (mg kg^{-1})	143.21±1.13	42.68±2.22	15.89±0.47	9.56±0.21
Clay (in mass, %)	-	33.5	41.5	24.6
Silt (in mass, %)	-	22.1	33.2	28.5
Sandy (in mass, %)	-	44.4	25.3	46.9

At least four replicates were used in each treatment. Gases and liquids were transferred through replaceable thermo-green butyl rubber septa using a 20 mL syringe. Syringes were sealed before removal from the septa to maintain gas partial pressure. Prior to incubation experiments, bottles were evacuated to –67 kPa and then over-pressurized with N_2 to 135 kPa. This process was repeated at least ten times for each bottle, with gentle shaking between each repetition. Each bottle was then overfilled with N_2 and slowly allowed to equilibrate to external atmospheric pressure through a syringe filled with O_2-free deionized H_2O.

In order to ensure anoxic conditions, bottles were allowed to equilibrate for 24 h to consume any remaining O_2. Bottles were kept in the dark at 20°C and the headspace atmosphere for each was sampled using a consistent technique after 0, 5, 10, 15, and 20 days. Typically, five gas samples totaling 10 mL were taken from each closed bottle at every sampling. The CH_4, CO_2, and N_2O concentrations in the bottles were plotted as a function of time, and the initial consumption or generation rates were determined from the best fit model using the method of Börjesson and Zhang [7, 21]. The results were expressed as dry weights.

To evaluate the effects of temperature and moisture content on AOM, a set of incubation experiments were conducted to determine the potential for applying results to field conditions. Previous measurements of field-scale MSW landfill covers in eastern China by Zhang were used to select the incubation temperatures of between 30°C and 45°C (i.e., hot summer), 20–25°C (spring and autumn) and 4–10°C (winter) and soil moisture contents ranging from 10% to 20% by mass [19].

Analytical methods for the gas and soil samples. The gas samples from the headspace in each incubation bottle were analyzed for CO_2, N_2O and CH_4 using a gas chromatograph (Agilent 7890A, Palo Alto, California, USA) fitted with an electron capture detector and flame ionization detector. The operational temperatures for the injection port, the oven and the detector were 55°C, 200°C and 360°C, respectively. The physicochemical properties of the soil and aged refuse were determined according to the Chinese Soil Society Guidelines [22]. The ammonium nitrogen (NH_4^+-N) and nitrate-nitrogen (NO_3^--N) were extracted from the aged refuse and soil samples by first shaking a 10 g sample in 50 mL of 2 mol/L KCl for 1 h, then filtering the mixture and analyzing the filtrate using a 765 UV-VIS spectrophotometer (Shanghai Precision & Scientific Instrument Co., Ltd., Shanghai, China). The sulfate concentration was determined by ion exchange chromatography (ICS-3000, Dionex, California, USA). The organic carbon content in samples was measured using the potassium dichromate-volumetric method, and the soil organic matter content was calculated by multiplying the soil organic carbon content by 1.732 [22].

Data analysis. All statistical analyses were performed using SPSS 14.0 software (SPSS Inc. 2005, Chicago, IL, USA). Statistical analyses to evaluate the performance differences were conducted using a two-sample *t*-test and analysis of variance (ANOVA). The performance differences were confirmed at the 95% confidence level.

RESULTS

The initial CH_4 concentrations. The influence of the initial CH_4 concentrations on AOM rates is shown in Fig 1a. The AOM rates of aged refuse and soil samples were maximal at the 10% initial CH_4 concentration. The maximum AOM rate of aged refuse was 2.44 μmol/(g·d), which was 1.56, 1.78, and 2.94 times more than the maximum AOM rates for cover soil, clay soil and sandy soil, respectively. Similar to AOM rates, the CO_2 emission rate was maximal at the 10% initial CH_4 concentration. The average CO_2 emission rate of aged refuse was 0.82 μmol/(g·d), which was 1.59, 1.97, and 3.62 times more than the AOM rates for cover soil, clay soil and sandy soil, respectively ($P<0.05$). The conversion ratio of CH_4 to CO_2 was 43–56% for aged refuse.

In contrast to CH_4 oxidation and CO_2 emissions, N_2O emission rates of aged refuse and soil samples were maximal at the 15% initial CH_4 concentration (Fig. 1c). The maximum N_2O emission rate of aged refuse was 2.54 ($P>0.05$), 3.68 ($P<0.01$), and 4.67 ($P<0.05$) times more than that of cover soil, clay soil and sandy soil, respectively.

Influence of particle size. Suitable soil porosity promotes good conditions for gas distribution and exchange, thus fostering high levels of CH_4 consumption. The AOM rate, and CO_2 and N_2O emission rates of the medium-sized particles ($0.25\ mm<d<2\ mm$) were obviously higher than the large-sized particles ($2\ mm<d<4mm$, $P<0.05$) and small-sized particles ($d<0.25$ mm, $P<0.05$) (Fig 2). The AOM rate of medium-sized aged refuse particles was about 30% higher than those of refuse samples comprised of large-sized and small-sized particles (Fig. 2a). For the sandy soil, the AOM rate of medium-sized particles was about 3.36 and 1.38 times as high as those of large-sized and small-sized particles (Fig. 2a). The CO_2 and N_2O emission rates of the samples with medium-sized particles were 20–65% as high as those of samples comprised of large-sized and small-sized particles.

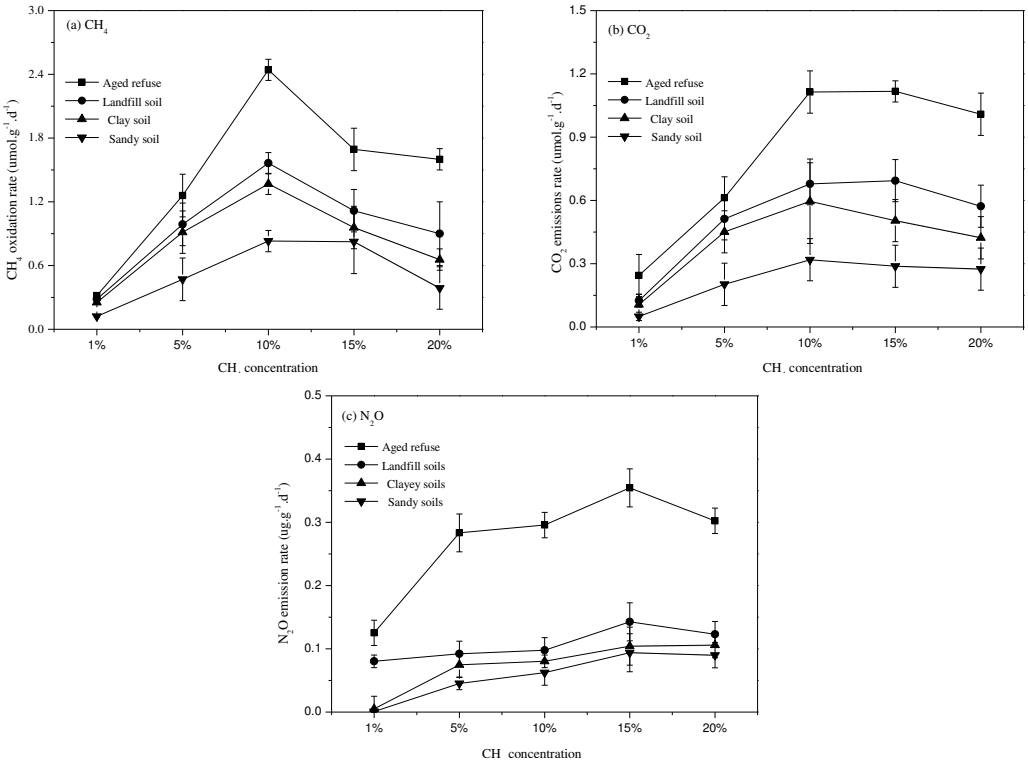

(a)The influence on CH_4 oxidation rate of the initial concentration of CH_4
(b) The influence on CO_2 emission rate of the initial concentration of CH_4
(c) The influence on N_2O emission rate of the initial concentration of CH_4

FIGURE 1
The influence of the initial CH_4 concentrations on CH_4 oxidation rate and CO_2 and N_2O emission rates

The moisture content. The maximum AOM rate in aged refuse was directly proportional to the moisture content below 20% (Fig. 3a). Conversely, the maximum AOM rates in the three soil samples occurred at 15% moisture content. The average CH_4 oxidation rate for aged refuse with water contents of 10–30% was 1.97 μmol/(g·d), which was 1.61 ($P<0.01$), 1.84 ($P<0.01$) and 3.05 ($P<0.01$) times more than those of the cover soil, clay soil and sandy soil, respectively.

The maximum CO_2 emission rates did not occur simultaneously with the maximum AOM rate for any of the four sample types (Fig. 3b). The maximum CO_2 emission rates in aged refuse and clay soil occurred at a moisture content of 20%, while those in the cover soil and sandy soil were observed at 25% moisture content. The CH_4 to CO_2 ratios were 43.8–52.3%, 26.5–50.5%, 23.4–49.6%, and 20.9–49.5% for the aged refuse, cover soil, clay soil, and sandy soil, respectively. The average conversion ratio of CH_4 to CO_2 for the four sample types was in the following order: aged refuse > cover soil > clay soil > sandy soil. The maximum N_2O emission rates in the four sample types all occurred at 20% moisture content (Fig. 3c). In contrast to the AOM rate and CO_2 emission rate, the N_2O emission rate in aged refuse was 5.12 ($P>0.05$), 4.48 ($P>0.05$), and 8.44 times ($P<0.05$) higher than those for cover soil, clay soil, and sandy soil, respectively.

Incubation temperature. The AOM rates in the four types of samples were directly proportional to the incubation temperature below 35°C (Fig. 4a). The average CH_4 oxidation rate for aged refuse at incubation temperatures of 5–45°C was 1.74 μmol/(g·d), which was 1.61 ($P<0.01$), 1.91 ($P<0.01$) and 3.00 ($P<0.01$) times more than those of the cover soil, clay soil and sandy soil, respectively.

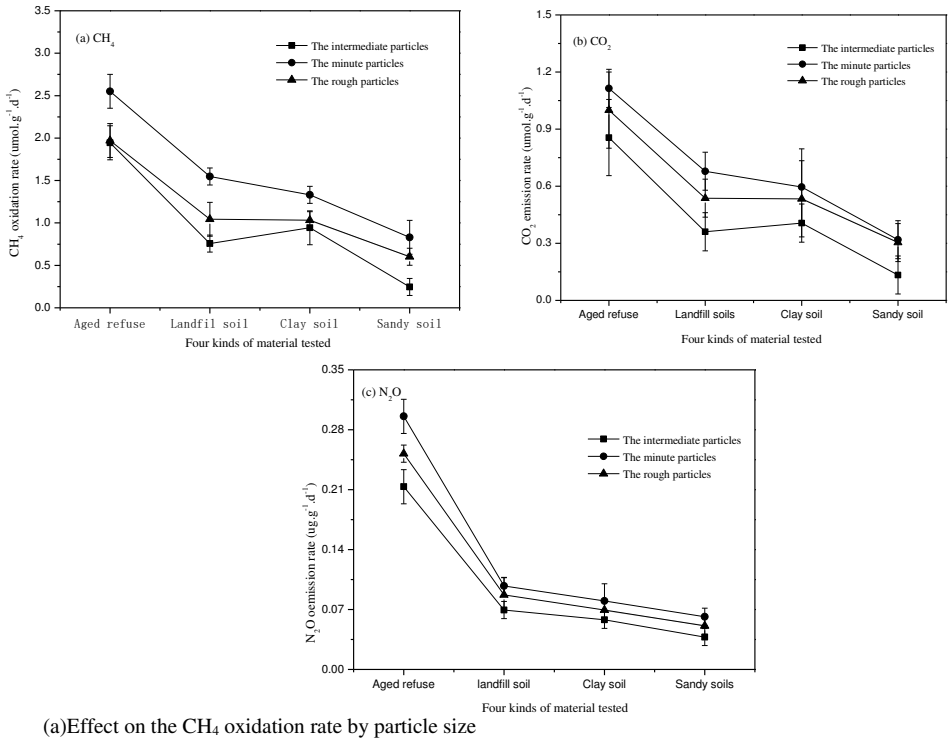

(a)Effect on the CH_4 oxidation rate by particle size
(b) Effect on CO_2 emission rate by particle size
(c) Effect on N_2O emission rate by particle size

FIGURE 2
Influence of particle size on anaerobic oxidation of CH_4 by aged refuse, landfill, clay and sandy soil samples (10% initial CH_4 concentration (v/v))

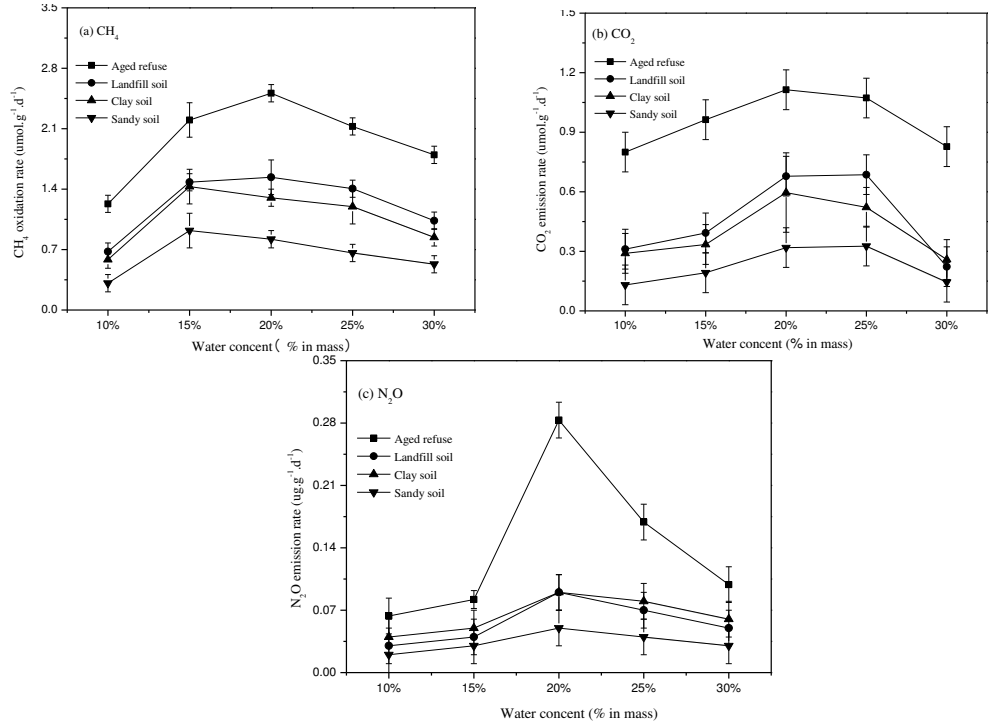

(a)Effect on the CH_4 oxidation rate by moisture content
(b) Effect on CO_2 emission rate by moisture content
(c) Effect on N_2O emission rate by moisture content

FIGURE 3
Effects of moisture content on the anaerobic oxidation of CH_4 by aged refuse, landfill, clay and sandy soil samples (10% initial CH_4 concentration (v/v))

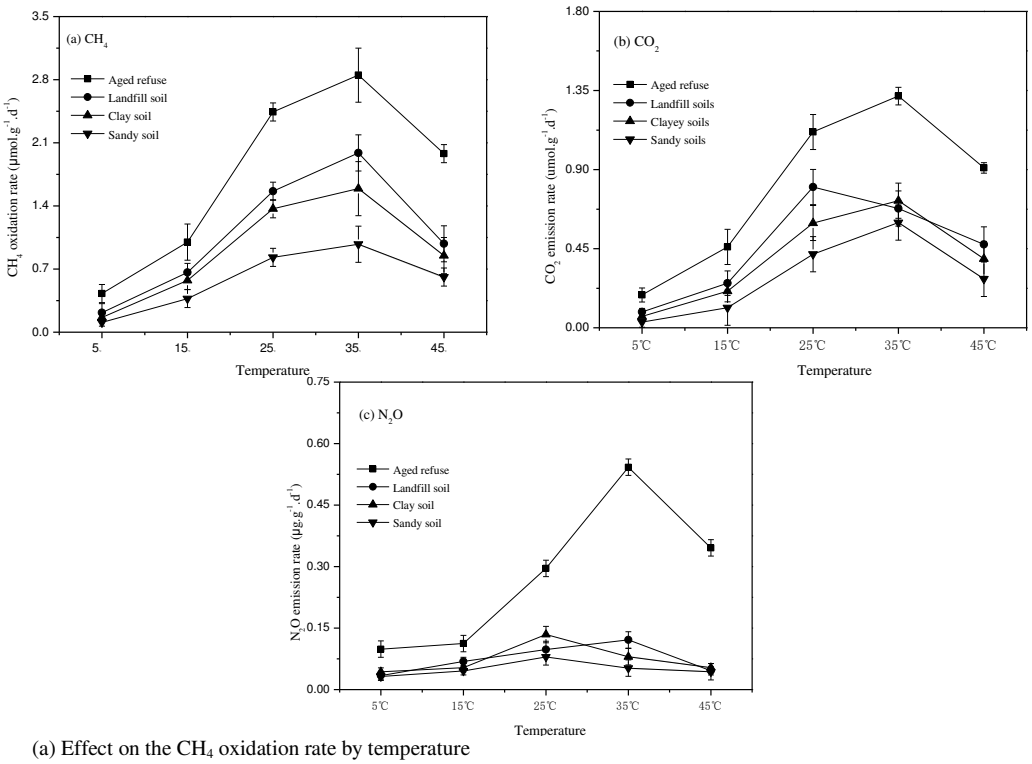

(a) Effect on the CH_4 oxidation rate by temperature
(b) Effect on CO_2 emission rate by temperature
(c) Effect on N_2O emission rate by temperature

FIGURE 4
Influence of temperature on the anaerobic oxidation of CH_4 by aged refuse, landfill, clay and sandy soils (10% initial CH_4 concentration (v/v))

At incubation temperatures of 25–35°C, the maximum CO_2 emission rates in aged refuse were observed to be 1.19–1.32 μmol/(g·d), with a conversion ratio of CH_4 to CO_2 of 43–56% (Fig. 4c). The average CO_2 emission rate for aged refuse was 1.74 ($P<0.01$), 2.01 ($P<0.01$) and 2.76 ($P<0.01$) times more than those of the cover soil, clay soil and sandy soil, respectively. The maximum N_2O emission rates of the three soil samples were all below 0.15 μg/(g·d) when the incubation temperature ranged from 5–45°C (Fig. 4c). The maximum N_2O emission rate in aged refuse was almost 5.5 times more than that of the minimum value. The average N_2O emission rate for aged refuse was 3.79 ($P<0.01$), 3.82 ($P<0.01$) and 5.50 ($P<0.01$) times more than those of the cover soil, clay soil and sandy soil, respectively.

DISCUSSION AND CONCLUSIONS

Anaerobic oxidation on landfill methane. The aged refuse used in this study was comprised of residual material that was excavated from an MSW landfill after more than 10 years of stabilization, and contained abundant nutrients and microorganisms [6, 23]. With its large variation in particle sizes, the initial CH_4 concentrations, and other environmental factors (Fig. 1–4), the aged refuse exhibited excellent AOM performance when compared with that of cover soil, clay soil and sandy soil. The organic matter, sulfate and nitrate contents in the aged refuse were several times higher than those in the three soil samples. Previous studies have established strong relationships between methanotrophic activity (and/or diversity) and organic matter, sulfate and nitrate contents [4, 23]. Although methanotrophs use CH_4 rather than organic C as their energy supply, increasing the organic matter content of soil should enhance the overall microbial activity and increase nutrient cycling, with subsequent positive effects on methanotrophs [17]. Our results agree with both field observations at landfills and results from laboratory studies that have demonstrated that the AOM in mineral soil can be enhanced by adding organic material, such as sewage sludge and compost [4, 8, 9]. However, the extent to which CH_4 oxidation rate is influenced by other constituents of aged refuse (including sulfate, nitrite content and heavy metals) should be further investigated.

N_2O is formed in the soil during the biological nitrification and denitrification processes, the latter of which were reported to be responsible for the large emission fluxes [18, 19]. Due to the high concentrations of microorganisms, carbon and nitrogen substrates, N_2O emissions were several times higher from the aged refuse than from the

TABLE 2
Comparison of anaerobic CH_4 oxidation rate by aged refuse with other document data

Materials	CH_4 oxidation rate (μmol/g d.w./h)	Initial CH_4 contents (% in v/v)	Source
Aged refuse (10 years)	0.12	10%	This study
Aged refuse (10 years)	0.03	2.0%	[24]
Landfill cover soil	0.064	10%	This study
Clay soil	0.059	10%	This study
Sandy soil	0.038	10%	This study
Peat land soil	$1.1*10^{-3}$	2.0%	[17]
Acid sulfate soil	$0.06*10^{-3}$	2.0%	[17]
Deep-sea sediments	0.14	20%	[16]
Mud volcanoes	$0–0.42*10^{-3}$	-	[14]

TABLE 3
Comparison of aerobic CH_4 oxidation rate by aged refuse with other document data

Materials	CH_4 oxidation rate (μmol/g d.w./h)	Initial CH_4 contents (% in v/v)	Source
Aged refuse (10 years)	12.45	1.0%	[20]
Waste bio-cover soil (3–5 years)	9.03	10–30 %	[6]
Chipped yard waste compost	7.02	12%	[5]
Clay soil	5.52	1.0%	[20]
Sandy soil	1.91	1.0%	[20]
Interim sandy clay soil	1.8	12%	[5]
Landfill cover soil samples	1.17–1.57	5.0%	[25]
Aged refuse (5 years)	0.44	1.2–1.4%	[20]

three soil samples (Figs. 1–4). Equally, the results presented here confirm the observations from plot experiments conducted on the same sites from which soil was collected for this laboratory study under aerobic conditions [19].

Anaerobic vs. aerobic oxidation of landfill CH_4. Results from the present study indicated that the rate of anaerobic oxidation of CH_4 in incubated aged refuse, with a maximum of 0.12 μmol/g/h, was similar to that in deep-sea sediments reported by Zhang [16], four times greater than the adsorbed levels reported by Zhou (0.3 μmol/g/h) [24], two orders of magnitude greater than the adsorbed levels reported by Gauthier (1.1 nmol/g/h) [17], and 200–300 times greater than rates from acid sulfate soil reported by Gauthier (0.6 nmol/g/h) [17] and mud volcanoes reported by Niemann (0.42 nmol/g/h) [14] (Table 2).

The high rates of AOM that we observed may be due to the aged refuse used in our experiments having been collected from a 14-year-old solid waste landfill; the refuse samples had thus been exposed to a high concentration of CH_4. Compared to the oxidation of CH_4 under anaerobic conditions, AOM is generally assumed to be a slow process. In our experiments, the anaerobic oxidation of CH_4 rate in incubated aged refuse was almost two orders of magnitude lower than the aerobic oxidation rate of the same material under different incubation conditions (Table 2 & Table 3). This observation was in agreement with results from a previous study on peatland soil and acid sulfate soil by Gauthier [17].

N_2O and CO_2 emissions. Global warming potentials of 298 times for N_2O and 25 times for CH_4 were used to convert N_2O and CH_4 emissions to CO_2-equivalents so that their greenhouse impacts could be compared (IPCC, 2007). In previous research, landfill CH_4 flux has been determined to be approximately one to two and two to three orders of magnitude higher than CO_2 and N_2O emissions, respectively, in MSW landfill sites when calculated on a CO_2-equivalent basis [18, 19]. The reported CO_2-equivalent for the CH_4 flux accounted for more than 90% of the total three greenhouse gas emissions (CH_4, CO_2 and N_2O) [19]. The increase in the N_2O and CO_2 emissions and the reduction in CH_4 emissions arising from a bio-cover comprised of aged refuse could thus be used to reduce the overall effect and production of global warming gases during MSW landfill operation.

The effects of environmental factors on anaerobic oxidation of landfill CH_4 and N_2O emissions rate were investigated using an aged

refuse and three different soil samples. The influence of particle size, temperature and soil moisture content was also evaluated. CH_4 oxidation rate in the aged refuse was several times higher than it was in the cover soil, clay soil and the sandy soil. Additionally, the emissions of N_2O from the aged refuse during the batch incubation were several times greater than the emissions from the clay soil and almost one order of magnitude greater than the emissions from the sandy soil. The rate of anaerobic oxidation of CH_4 in incubated aged refuse, at a maximum of 0.12 μmol/g/h, was several times higher than that in the three soil samples and approximately two to three orders of magnitude higher than previously reported AOM rates. In addition, anaerobic oxidation of CH_4 was shown to be almost two orders of magnitude lower than the aerobic oxidation rate of the same refuse material. The extent to which CH_4 oxidation is influenced by other constituents of aged refuse (including sulfate, nitrite content and heavy metals) should be further investigated.

ACKNOWLEDGEMENTS

This study was supported financially by the National and Jiangsu Provincial Natural Science Foundation of China (grant Nos. 41375161 & BK20151101), and the 'Strategic Priority Research Program-Climate Change: Carbon Budget and Relevant Issues' of the Chinese Academy of Sciences (grant No. XDA05020602).

REFERENCES

[1] Intergovernmental Panel on Climate Change (IPCC), (2007). Climate change 2007-the physical science basis. In: Solomon, S., Qin, D., Manning, M., Marquis, M., Averyt, K., Tignor, M.M.B., Miller, H.L., Chen, Z. (Eds.), Contribution of Working Group I to the Fourth Assessment Report of the Intergovernmental Panel on Climate Change. Cambridge University Press, UK.

[2] United States Environmental Protection Agency (USEPA), (2007). Inventory of US Greenhouse Gas Emissions and Sinks: 1990-2005. US Environmental Protection Agency, Washington, pp. 1-16.

[3] Bogner, J., Abdelrafie Ahmed, M., Diaz, C., Faaij, A., Gao, Q., Hashimoto, S., Mareckova, K., Pipatti, K. and Zhang, T. (2007). Waste Manag., In: Metz, B., Davidson, O.R., Bosch, P.R., Dave, R., Meyer, L.A. (Eds.), Climate Change 2007: Mitigation. Contribution of Working Group III to the Fourth Assessment Report of the Intergovernmental Panel on Climate Change. Cambridge University Press, Cambridge, United Kingdom and New York, NY, USA.

[4] Barlaz, M.A., Green, R.B., Chanton, J.P., Goldsmith, C.D. and Hater, G.R. (2004). Evaluation of a biologically active cover for mitigation of landfill gas emissions. Environ. Sci. Technol., 38, 4891-4899.

[5] Abichou, T., Mahieu, K., Yuan, L., Chanton, J. and Hater, G. (2009). Effects of compost biocovers on gas flow and methane oxidation in a landfill cover. Waste Manag., 29, 1595-1601

[6] Wang, J., Xia, F.F., Bai, Y., Fang, C.R., Shen, D.S. and He, R., (2011). Methane oxidation in landfill waste biocover soil: Kinetics and sensitivity to ambient conditions. Waste Manag., 31, 864-870.

[7] Zhang H.H., Yan, X.F., Cai, Z.Z. and Zhang, Y. (2012). Effect of rainfall on the diurnal variations of CH_4, CO_2, and N_2O fluxes from a municipal solid waste landfill. Sci. Total Environ., 442, 73-76.

[8] Zhang, H.H., Cai, B.C., Zhang, Y., Liu, J.T. and Ao, H.Y., (2015), The effects of aged refuse and sewage sludge on landfill CH_4 oxidation and N_2O emissions: Roles of moisture content and temperature. Ecol. Eng., 74, 345-350.

[9] Yue, B., Lin, Y., Wang, Q., Huang, Z.C., Huang, Q.F., Yang, X. and Zhang, W. (2011). Research on methane oxidation capacity of landfills cover materials and its impact factors. J. Environ. Eng., 1, 57-62.

[10] Berger, J., Fornés, L.V., Ott, C., Jager, J., Wawra, B. and Zanke, U. (2005). Methane oxidation in a landfill cover with capillary barrier. Waste Manag., 25, 369-373.

[11] Reeburgh, W.S., (1976). Methane consumption in Cariaco Trench waters and sediments. Earth Planet. Sci. Lett., 28, 337-344.

[12] Eller, G., Käanel, L., Krüger, M., Ka, L. and Kru, M. (2005). Co-occurrence of aerobic and anaerobic methane oxidation in the water column of Lake Plußsee. Appl. Environ. Microbiol., 71, 8925-8928.

[13] Raghoebarsing, A.A., Pol, A., van de Pas-Schoonen, K.T., Smolders, A.J.P., Ettwig, K.F., Rijpstra, W.I.C., Schouten, S., Sinninghe Damst, J.S., Op den Camp, H.J.M., Jetten, M.S.M. and Strous, M. (2006). A microbial consortium couples anaerobic methane oxidation to denitrification. Nature, 440, 918-921.

[14] Niemann, H., Duarte, J., Hensen, C., Omoregie, E., Magalhâs, V.H., Elvert, M., Pinheiro, L.M., Kopf, A. and Boetius, A. (2006). Microbial methane turnover at mud volcanoes of the Gulf of Cadiz. Geochim. Cosmochim. AC., 70, 5336-5355.

[15] Grossman, E.L., Cifuentes, L.A. and Cozzarelli, I.M. (2002). Anaerobic methane oxidation in a landfill-leachate plume. Environ. Sci. Technol., 36, 2436-2442.
[16] Zhang, Y., Henriet, J.P., Bursens, J. and Boon, N. (2010). Stimulation of in vitro anaerobic oxidation of methane rate in a continuous high-pressure bioreactor. Bioresour. Technol., 101, 3132-3138.
[17] Gauthier, M., Bradley, R.L. and Simek, M. (2015), More evidence that anaerobic oxidation of methane is prevalent in soils: Is it time to upgrade our biogeochemical models? Soil Biol. Biochem., 80, 167-174.
[18] Rinne, J., Pihlatie, M., Lohila, A., Thum, T., Aurela, M., Tuovinen, J., Laurila, T. and Vesala, T. (2005). Nitrous oxide emissions from a municipal landfill. Environ. Sci. Technol., 39, 7790-7793.
[19] Zhang, H.H., He, P.J. and Shao, L.M. (2009). N_2O emissions at municipal solid waste landfill sites: Effects of CH_4 emissions and cover soil. Atmos. Environ. 43, 2623-2631.
[20] Zhang, Y., Zhang, H.H., Jia, B., Wang, W., Zhu, W., Huang, T.Y. and Kong, X. (2012). Landfill CH_4 oxidation by mineralized refuse: Effects of NH_4^+-N incubation, water content and temperature. Sci. Total Environ., 426, 406-413.
[21] Börjesson, G., Sundh, I. and Svensson, B. (2004). Microbial oxidation of CH_4 at different temperatures in landfill cover soils. FEMS Microbiol. Ecol., 48, 305-312.
[22] Lu, R.K. (2000). Methods for soil agrochemistry analysis. China Agricultural Science and Technology Press, Beijing. pp. 62-141.
[23] Lou, Z.Y., Wang, L. and Zhao, Y.C. (2011). Consuming un-captured methane from landfill using aged refuse bio-cover. Bioresour. Technol., 102, 2328-2332.
[24] Zhou, H.Y. and Dan, H. (2011). New way for natural mitigation in domestic waste landfill sites: Co-oxidation of anaerobic and aerobic oxidation. Environ. Sanitat. Engin., 19, 50-62 (In Chinese).
[25] Börjesson, G., Sundh, I. and Svensson, B. (2004). Microbial oxidation of CH_4 at different temperatures in landfill cover soils. FEMS Microbiol. Ecol., 48, 305-312.

Received: **09.10.2015**
Accepted: **01.02.2016**

CORRESPONDING AUTHOR

H.H. Zhang
Nanjing Institute of Environmental Sciences,
Ministry of Environmental Protection,
Jiangsu Nanjing, No 8, Jiang-wang-miao Street,
Nanjing, Jiangsu, 210042, China

e-mail: zhanghouhu2008@163.com

© by PSP Volume 25 – No. 10/2016, pages 4045-4051 Fresenius Environmental Bulletin

MORPHOLOGICAL AND MERISTIC DIFFERENCES AMONG FRESHWATER FISH, *CYPRINION KAIS* (CYPRINIDAE) POPULATIONS IN TIGRIS RIVER OF SOUTHEAST TURKEY

Serbest Bilici [1]*, Arif Baysal [2], Tarık Cicek [3,] Ersin Uysal [4], Erhan Unlu [3]

[1] Department of Animal Science, Faculty of Agriculture, Şırnak University, Şırnak, Turkey
2 Department of Biology, Faculty of Science, Kafkas University, Kars, Turkey
3 Department of Biology, Section of Hydrobiology, Faculty of Science, Dicle University, Diyarbakır, Turkey.
4 Department Of Technical Programmers, Vocational School, Dicle University, Diyarbakır, Turkey

ABSTRACT

In this study, morphometric and meristic characteristics of *Cyprinion kais* samples which is obtained from different locality in Tigris River were carried out. In order to determine the morphological and meristic variation among populations, discriminant function can be detected, intergroup discrimination with the help of this function are the most distinctive variables affecting the availability of discriminant analysis , has benefited from the descriptive features.

Success rate of classifying the groups according to the result of discriminant analysis of morphometric characteristics of *C. kais* individuals belonging to 3 different locality of Tigris River is manifested as 96.1%. According to the results of classifications, morphometric characteristics of the individuals of Kulp and Kayser Stream and Tigris River are different. Success rate of classifying the groups according to the discriminant analysis of meristic characteristics of *C. kais* individuals appeared as 70.6%. Kulp and Kayser Stream from the locality groups showed similarity. It is determined that there is high variation between the locality groups belonging the samples of *C. kais* according to the morphometric and meristic characteristics.

KEYWORDS:
Cyprinion kais, Tigris River, morphometric , meristic, Discriminant analysis.

INTRODUCTION

Fish populations are affected by many environmental factors such as temperature, salinity, radiation, dissolved oxygen, water depth, current flow [1] and large dams which are constructed on rivers lead to phenotypic and genotypic differences by preventing fish mobility in stream basin [2]. Measurement of morphological and meristic characteristics applied widely to the fish taxonomy to determine the hybrids, differences and similarities of any populations [3, 4]. Large dams which are constructed on Tigris River bring big risks of reproduction of the fishes by preventing migration of the fish species that are migrating to the reproduction field [5].

Five nominal species have been described in genus *Cyprinion* from western Syria/Tigris Euphrates drainage and western Iran [6]. From these, *C. kais* (Heckel, 1843) shows a wide distribution in the Tigris and Euphrates Basins from Turkey, Iraq, Iran and Syria [7, 8, 9, 10, 11]. Beside the morphologic and meristic characteristics about species definition given in many researches [6, 11] that deal with morphological differences among populations are not found. Meristic and morphometric characteristics are strong means to measure and differentiate the relations between the stocks [13].

It is hypothesized that different localities on the Tigris River isolated because of the barrier characteristics of the barrage sets and in which reproduction between species is impossible; characteristics like aliment, physico-chemical structure of water, flow rate of water and structure of bed can also be different. Samples of the same fish species can prove different adaptations in different conditions. Therefore we aimed to explore the morphometric and meristic variations which can exist morphologically and their importance between the samples of *C. kais* species that is obtained from 3 different localities belonging to Tigris River system.

MATERIALS AND METHODS

A total of 51 specimens of *C. kais* were collected from 3 different localities: Kulp Stream, Kayser Stream and Tigris River by using gill nets of various mesh size (18X18mm, 24X24mm) and a

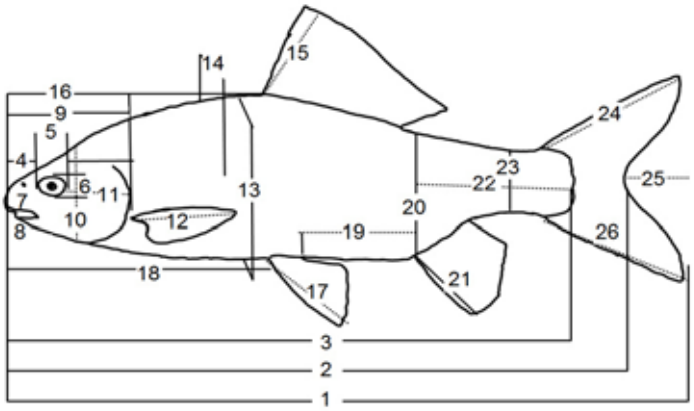

FIGURE 1
Morphometric measurement performed upon *C. kais*.
1. TL: Total Length 2. FL: Fork Length, 3. SL: Standard Length 4. SNL: Snout Length 5. OHD: Horizontal Ocular Diam 6. OVD: Vertical Ocular Diam 7. USL: Upper Lip Length 8. LJL: Lower lip Length 9. HL: Head Length 10. HD: Head Height 11. POHL: Post Ocular Head Length 12. PFL: Pectoral Fin Length 13. BD: Body Height 14. BW: Body Width 15. DFL: Dorsal Fin Length 16. PDFL: Predorsal Length 17. Pelvic Fin Length 18. PPEFL: Prepelvik Length. 19. DPA: Distance Between Pelvik and Anal Fin 20. BDA Body Height In Anal Level 21. Anal Fin Length 22. CPL: Caudal Pedunculus Length 23. LD: Body Height in Caudal Pudunculus Area 24. LUCFL: Upper Lab Length of Caudal Fin 25. LMCFR: Caudal Fin's Fork's Length 26. LLCFL: Length of Lower Lab of Caudal Fin.

fish shocker. Material was preserved in 4% formaldehyde solution. In the laboratory, 26 morphometric characteristics are measured to the nearest 0.01 mm with an electronic compass (Fig. 1). Truss network method has been used to construct a network on fish body [14, 15, 16, 17].

For meristic characteristics, totally 13 different variances have been used: DFRS (A): number of dorsal fin rays (spine), DFRS (A): number of dorsal fin rays (branched), VFRS (A): number of ventral fin rays (spine), VFRS (B): number of ventral fin rays (branched), AFRS (A): number of anal fin rays (spine), AFRS (B): number of anal fin rays (branched), PFRSA (L): number of pectoral fin rays (left part branched), PFRSA(R): number of pectoral fin rays (right part spine), PFRSB(R): number of pectoral fin rays (right part branched), GRS: number of gill rakers L.L.S.(L): lateral line scales (left part), L.L.S.(R): lateral line scales (right part).

The percentage ratios of morphometric characters in relations to standard length (SL) were calculated to eliminate variations that are derived from length. Transformed morphometric characters are subjected to discriminant analysis and according to grouping model, discriminant function numbers and morphologic variation between populations with respect to their importance of explaining total variation are determined. Features that provide the classifications and their effective functions were determined. In two dimensions; based on two different discriminant functions, the place of discriminant functions are determined. The features of classification and their influential functions are determined with stepwise analysis. With the help of canonical discriminant function, the limit maps of the groups in a two dimensional platform are created. Among the distinguished groups, the place of group medium (group centers) is detected [15, 17]. Similar applications about discriminant analysis are also applied for countable meristic characters. Morphometric and meristic variations between *C. kais* populations are shown on plot charts. Furthermore, morphometric differences between populations are analyzed with variation analysis and F test.

RESULTS AND DISCUSSION

The standard lengths of the samples are between 43 - 125 cm and the lengths differences between populations were statistically insignificant ($p>0.05$). Descriptive data for the morphometric characters that are calculated as the percentage of standard length in the sampled specimens and meristic characters are given Table 1.

From the morphometric characters: SL/LJL, SL/HL, SL/PDFL, SL/PPEFL, SL/LMCFL, SL/LLCFL, OVD/OHD, HL/HD, PFL/PEFL were more determinant to reveal the variations. This variation is originated from all three locality groups. From 13 countable meristic characters belonging to populations, 2 of them GRS and L.L.S.(R) differed from the others among populations.

TABLE 1
Morphometric and meristic characteristics of different C. kais populations in Tigris River (SD= Standard deviation).

Morphometric characters	Kulp (n=15) Mean±SD	Kayser (n=27) Mean±SD	Tigris (n=9) Mean±SD	Meristic characters	Kulp (n=15) Mean±SD	Kayser (n=27) Mean±SD	Tigris River (n=9) Mean±SD
TL/SL	1.385±0.38	1.294±0.03	1.299±0.01	DFSR-A	4.0±0.00	4.00±0.00	4.00±0.00
FL/SL	1.218±0.32	1.124±0.01	1.149±0.03	DFSR-B	13.8±0.41	13.96±0.19	13.44±0.52
SL/SNL	11.517±1.8	12.187±1.6	12.964±1.0	VFRS-A	1.00±0.00	1.00±0.00	1.00±0.00
SL/OHD	15.036±2.0	15.872±0.7	17.935±1.7	VFRS-B	8.00±0.00	8.00±0.00	8.00±0.00
SL/OVD	15.687±2.3	15.393±1.1	18.035±1.5	AFRS-A	3.00±0.00	3.00±0.00	3.00±0.00
SL/UJL	10.268±1.9	12.216±2.1	14.285±2.8	AFRS-B	7.00±0.00	7.00±0.00	7.00±0.00
SL/LJL	6.116±0.89	6.578±0.48	7.534±0.46	PFRSA-L	1.00±0.00	1.00±0.00	1.00±0.00
SL/HL	4.098±0.66	4.236±0.17	4.468±0.20	PFRSB-L	13.00±0.0	13.00±0.00	13.00±0.00
SL/HD	6.059±0.93	6.177±0.31	6.201±0.47	PFRSA-R	1.00±0.00	1.00±0.00	1.00±0.00
SL/POHL	9.278±1.43	9.194±0.55	9.554±0.43	PFRSB-R	13.00±0.0	13.00±0.00	13.00±0.77
SL/PFL	4.638±0.69	4.933±0.28	5.033±0.19	GRS	26.47±0.5	27.37±0.92	25.67±1.50
SL/BD	3.349±0.50	3.498±0.37	3.372±0.13	LLS-L	37.53±1.6	37.52±1.6	39.33±086
SL/BW	4.999±0.80	5.082±0.42	5.300±0.49	LLS-R	37.47±2.0	37.48±1.42	40.11±1.27
SL/DFL	4.32±0.68	4.691±0.31	4.622±0.40				
SL/PDFL	1.817±0.26	1.883±0.10	1.895±0.07				
SL/PEFL	4.884±0.72	5.009±0.29	5.180±0.28				
SL/PPEFL	1.828±0.23	1.866±0.08	1.905±0.05				
SL/DPA	4.546±0.76	4.668±0.24	4.118±0.27				
SL/BDA	5.045±0.77	5.321±0.44	5.143±0.34				
SL/AFL	4.642±0.73	5.014±0.47	4.890±0.47				
SL/CPL	5.716±0.81	6.050±0.49	6.1626±0.6				
SL/LD	8.806±1.24	9.176±0.34	9.331±0.42				
SL/LUCFL	3.117±0.46	3.364±0.24	3.549±0.19				
SL/LMCFR	7.670±1.40	8.733±0.99	8.529±0.19				
SL/LLCFL	3.15±0.45	3.341±0.23	3.562±0.21				
OVD/OHD	0.961±0.04	1.035±0.07	0.994±0.04				
HL/HD	1.480±0.87	1.458±0.05	1.389±0.11				
UJL/LJL	0.603±0.61	0.550±0.07	0.543±0.09				
BD/BDA	1.505±0.54	1.525±0.67	1.526±0.11				
BD/LD	2.634±0.96	2.644±0.21	2.769±0.14				
PFL/DFL	0.931±0,54	0.953±0.07	0.918±0.07				
PFL/PEFL	1.054±0.05	1.016±0.05	1.029±0.04				
PFL/AFL	1.001±0.05	1.019±0.10	0.973±0.10				
LUCFL/LLCFL	1.012±0.02	0.993±0.02	1.003±0.02				

TABLE 2
Discriminant functions (DF1. DF2) that is formed by using morphometric and meristic characteristics.

Morfometric character	DF 1	DF2	Meristic character	DF1	DF2
PFL/AFLa	0.305*	-0.033	GRS	0.710*	0.705
SL/LJL	-0.276*	0.193	LLS-R [a]	-0.641	0.767*
SL/BDA a	-0.191*	0.102	L.L.S.(L) [a]	0.087	0.199*
SL/DPA a	0.187*	0.050	DFSRB [a]	0.053	-0.134*
SL/UJL a	-0.181*	0.035			
BD/BDA a	-0.172*	0.133			
HL/HD a	0.153*	-0.067			
SL/OVD a	-0.135*	-0.048			
SL/PEFL a	-0.130*	0.113			
PFL/DFL a	0.116*	0.035			
SL/HL a	-0.112*	0.096			
SL/BD a	-0.108*	0.048			
UJL/LJL a	0.089*	0.012			
OVD/OHD	0.009	0.397*			
SL/LMCFL	-0.043	0.318*			
SL/PFL a	-0.144	0.258*			
SL/DFL a	-0.054	0.245*			
SL/BW a	-0.087	0.242*			
PFL/PEFL	0.017	-0.241*			
SL/OHD a	-0.158	0.238*			
SL/POHL a	0.004	0.220*			
SL/AFL a	0.134	0.175*			
SL/LD a	-0.034	0.174*			
SL/LLCFL	-0.148	0.173*			
SL/CPL a	-0.142	0.166*			
FL/SL a	-0.048	-0.151*			
TL/SL a	-0.047	-0.139*			
BD/LD a	0.124	0.138*			
SL/LUCFL a	-0.114	0.138*			
SL/PDFL	-0.040	0.125*			
LUCFL/LLCFL a	-0.115	0.118*			
SL/PPEFL	-0.060	0.079*			
SL/SNL a	0.007	-0.079*			
SL/HD a	-0.019	0.055			

*:Largest absolute correlation between eaach variable any discriminant function
[a] : This variable not used in the analysis

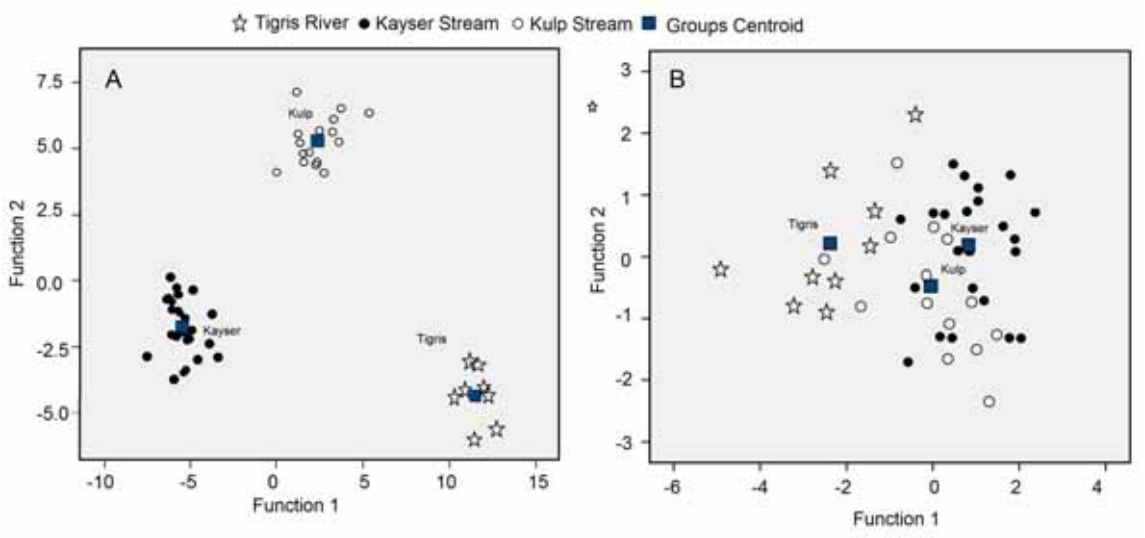

FIGURE 2
The difference between populations and graphing charts of function first and second function scores found as a result of discriminant analysis. A. morphometric characters, B. meristic characters.

As a result of being subjected to discriminant analysis of morphometric characters, two discriminant functions provided 100% of total variation. According to discriminant functions (Table 2), first function (DF1) formed 79.3% of total variation (Canonical Correlation = 0.964). Second function (DF2) formed 20.7% (Canonical Correlation = 0.801) Canonical discriminant parameters in DF1: -3.933, in DF2: 3.278. In discriminant analysis, in 1stfunction (DF1) PFL/AFL, SL/LJL, SL/BDA, SL/DPA, SL/UJL, BD/BDA, HL/HD, SL/OVD, SL/PEFL, PFL/DFL, SL/HD, SL/BD, UJL/LJL. 2. OVD/OHD, SL/LMCFR, SL/PFL, SL/DFL, SL/BW, PFL/PEFL, SL/OHD, SL/POHL, SL/AFL, SL/LD, SL/LLCFL, SL/CPL, FL/SL, TL/SL, BD/LD, SL/LUCFL, SL/PDFL, LUCFL/LLCFL, SL/PPEFL, SL/SNL, SL/HD were significant.

DF_1 and DF_2 scores which are obtained from morphometric and meristic characters in discriminant analysis are given in Figure 2. It can be seen that the individuals belonging to Tigris River and Kayser Stream are different than the other populations and they are also different from each other. The success of discriminant analysis is 96.1% in terms of morphometric separation of populations. Success rate of separating locality groups in terms of meristic characters is 70.6. Tigris River stood in its own group, 1 of them passed to Kulp Stream and other 2 passed to Kayser Stream. The representation rate of the samples brought from Tigris River to be in its own group is 66.7%. From the 15 samples brought from Kulp Stream, 7 of them are represented in its own group, 7 of them represented in Kayser and 1 of them represented in Tigris group. The representation rate of the samples brought from Kulp to be in its own group in terms of studied samples is 46.7%. From 27 samples brought from Kayser Stream, 23 of them are stayed in its own group and the rest (4 samples) passed to Kulp Stream. The representation rate of the samples brought from Kayser Stream to be in its own group is 85.2%.

As a result of countable meristic characteristics belonging to *C. kais* subjection to discriminant analysis, second function is considered and the first of them forms 91.4% of total variation. While the first one forms 91.4% of total variation (canonical correlation: 0.690), DF2 forms 8.62% (canonical correlation: 0.281) of total variation.

In the discriminant analysis, GRS was important for (DF1), L. L.S.(R), L.L.S.(L), DFSRB for (DF2). According to grouping graph (Figure 2B; in terms of meristic characters, Tigris River and Kayser Stream localities are different than Kulp Stream localities at the least.

The separation success rate of localities group in term of morphometric features is 83%. In the evaluation results about separation analysis: While 9 of the 9 samples brought from Tigris stayed in its own group, possibility of the samples brought from Tigris River to be in its own group in terms of studied characters is 100%, while 14 of 16 samples brought from Kulp stayed in its own group, 2 samples transferred to Kayser group. Possibility of the samples brought from Kulp to be in its own group in terms of studied characters is 87.5%.

All samples brought from Kayser stayed in its own group. Possibility of the samples brought from Kayser to be in its own group in terms of studied characters is 100%. In the analysis made according to the meristic characters belonging to *C. kais* (Heckel, 1843) samples brought from 3 different regions, success rate of separating localities groups in terms of meristic characters is 70.6%. In the evaluation results about discriminant analysis;

while 6 of 9 samples brought from Tigris River stays in its own group, 1 of them transferred to Kulp and 2 of them transferred to Kayser. Possibility of the samples brought from Tigris in terms of studied characters is 66.7%.

From the 15 samples brought from Kulp Stream, 7 of them stays in its own group, 7 of them transferred to Kayser and 1 of them transferred to Tigris group. The possibility of the samples brought from Kulp to be in its own group in terms of studied samples is 46.7%. From 27 samples brought from Kayser Stream, 23 of them stayed in its own group and the rest (4 samples) passed to Kulp Stream. The possibility of the samples brought from Kayser Stream to be in its own group is 85.2 %. According to the results; in terms of meristic characters while Tigris individuals represented separately clustering, Kayser and Kulp individuals mixed as one cluster (Figure 2B). According to the discriminant analysis of C. *kais* individuals belonging to 3 different localities in Tigris River; in terms of morphometric characters all of the locality groups found to be different to a large extent, only between Kulp Stream and Kayser Stream locality groups some similarity is seen at the least.

Locality groups show closer dispersion in terms of meristic characters than morphometric characters. Kulp Stream and Kayser Stream's localities groups are further similar. Morphometric characters are more effective than meristic characters in terms of revealing variations. It is thought that important morphometric characters mostly belong to head's front parts features and this is because of the possibility of being related to be swimmer and studied fish species to be in flowing waters. Although groups showed far grouping in grouping graphes in terms of morphometric and meristic characters, it seems that Kulp Stream and Kayser Stream locality groups are closer to each other than Tigris River locality groups. Kulp Stream and Kayser Stream's similarity in terms of characters like flow regime, stream bed and water quality makes Tigris River locality group that is different regarding these characters distinctive.

From the 15 samples brought from Kulp Stream, 7 of them are represented in its own group, 7 of them represented in Kayser and 1 of them represented in Tigris group. The representation rate of the samples brought from Kulp to be in its own group in terms of studied samples is 46.7%. From 27 samples brought from Kayser Stream, 23 of them are represented in its own group and the rest (4 samples) passed to Kulp Stream. The representation rate of the samples brought from Kayser Stream to be in its own group is 85.2 %.

The results of the present study revealed that *C. kais* populations surveyed had morphologically forms using discriminant methods. Some related morphological studies have been recently done in the region on the native fishes [12-17]. Discriminant Function Analysis could be a useful method to distinguish different stocks of a same species [12, 15]. Because of not attaining any similar studies about this species, there was no possible way to compare the data. Bilici et al. [12] studied on *C. macrostomus* success rate of categorizing the groups was 83% for morphometric characters and 76.6% for meristic characters in 5 different localities belonging to Tigris River. Between the dispersion of 3 locality groups in this study and the same locality groups in the study of Bilici et al. [12], parallelism was found. In our study, it was shown up that the rate was 83% for morphometric characters and 70.6% for meristic characters.

CONCLUSIONS

Morphometric and meristics characteristics of *C. kais* vary between populations on the same river system. This may be related to different environmental factors such as dams which causes of genetic isolation. As a result, morphometric characters are more successful than meristic characters in terms of revealing the existing variations. From the morphometric characters, many of the characters reflecting the differences seem to be in the head part. It is considered that this may be the result of swimming in the waters, which has high flow rates. Discriminant analysis is also regarded as an important method to distinguish these populations.

REFERENCES

[1] O'reilly, K.M. and Horn, M,H. (2004) Phenotypic variation among populations of Atherinops affinis (Atherinopsidae) with insights from a geometric morphometric analysis. J. Fish Biol. 64: 1117-1135.

[2] Dynesius, M. and Nilsson, C. (1994) . Fragmentation and flow regulation of river systems in the northern third of the world. Science 266:753-763.

[3] Pepin, P. and Carr, S. M. (1993) Morphological, meristic, and genetic analysis of stock structure in juvenile Atlantic cod (Gadus morhua) from the New found land shelf. Can. J. Fish. Aquat. Sci. 50(9), 1924-1933.

[4] Thorpe, R.S. and Baez, M. (1987) Geographic variation within an island: univariate and multivariate contouring of scalation, size and shape of the lizard, Gallotia galloti. Evolution, 41:256-268.

[5] Ünlü E. 2012. Fisheries and Aquaculture in the Euphrates and Tigris Basin in Turkey. In:

FAO. 2014. Report of the Expert Meeting on the Review of Fisheries and Aquaculture Activities in the Tigris Euphrates Basin, Erbil, Iraq, 11–12 November 2012. FAO Fisheries and Aquaculture Report No. 1079. Rome. 125 pp. p 19-58.

[6] Banarescu P.M. and Herzig-Straschil B. (1995) A revision of the species of the Cyprinion macrostomus-group (Pisces: Cyprinidae). Annal. Naturhist. Mus. Wien. 97, 411-420.

[7] Coad, B.W. (1998) Systematic biodiversity in the freshwater fishes of Iran. Italian J. Zool. 65: 101-108.

[8] Nasri, M. Keivany, Y. and Dorafshan, S. (2013) Comparative osteology of lotaks, Cyprinion kais and C. macrostomum (Cypriniformes, Cyprinidae), from Godarkhosh River, western Iran. J. Ichthyol. 53: 455-463.

[9] Kuru, M. Yerli, S.V. Mangıt, F. Ünlü, E. And Alp, A. (2014) Fish Biodiversity in inland waters of Turkey. J. Acad. Doc. Fish. Aquacult. 3: 93-120.

[10] Coad, B.W., (2010) Freshwater fishes of Iraq. Pensoft Series Faunistica, 93, 274.

[11] Ünlü, E., (1999) A study on the taxonomy and distribution of Cyprinion macrostomus Heckel, 1843 and Cyprinion kais Heckel, 1843 (CYPRINIDAE). IX. National National Fisheries Science Symposium. 20-22 September 1999, Adana, Vol II, 688-697.

[12] Bilici, S. Cicek, T. Baysal, A. Ünlü, E. and Alp A. (2015) Morphological differences among the Cyprinion macrostomus (Cyprinidae) populations in the Tigris River. J. Surv. Fish. Sci. 2: 57-67.

[13] Ihssen P.E, H.R. Booke., J. Mcasselman (1981) Stock identification: materials and methods Can. J. Fish. Aquat. Sci. 38:1838-1855.

[14] Schaefer, S.A. (1991) Morphometric investigations in Cyprinid biology. In: Winfield, I. J. & J. S. Nelson (eds.), Cyprinid fishes: Systematics, biology and exploitation. Chapman and Hall, London. Pp. 55-82.

[15] Turan, C. Ergüden, D. Gülek, M. Başusta, N. and Turan, F. (2004) Morphometric structuring of the Anchovy (Engraulis encrasicolus L.) Black Sea, Aegean Sea and northeastern Mediterranean Sea. Turk. J. Vet. An. Sci., 28:865-871.

[16] Tzeng, T.D. (2004) Morphological variation between populations of spotted mackerel (Scomber australasicus) of Twain. Fish. Res. 68: 45-55.

[17] Çakmak, E. and Alp, A. (2010) Morphological differences among the mesopotamian spiny eel, Mastacembelus mastacembelus (Banks and Solander 1794), Populations. Turkish J. Fish. Aquat. Sci. 10: 87-92.

Received: **01.10.2015**
Accepted: **11.05.2016**

CORRESPONDING AUTHOR

Serbest Bilici
Department of Animal Science, Faculty of Agriculture, Şırnak University, Şırnak, Turkey

E-mail: serbestbilici@hotmail.com.tr

© by PSP Volume 25 – No.10/2016, pages 4052-4059 Fresenius Environmental Bulletin

RESPONSES OF MULTIPLE BIOMARKERS IN THE FISH *HOPLOSTERNUM LITTORALE* AFTER EXPOSURE TO CHROMIUM AND LEAD

Analía Ale[1], Carla Bacchetta[1], Jimena Cazenave[1,2*]

[1]Laboratorio de Ictiología, Instituto Nacional de Limnología (INALI-CONICET-UNL), Santa Fe, Argentina
[2]Facultad de Humanidades y Ciencias, Universidad Nacional del Litoral (FHUC-UNL), Santa Fe, Argentina

ABSTRACT

We studied the effect of chromium (Cr) and lead (Pb) and their combination using the freshwater fish *Hoplosternum littorale*. After 15 days, we analyzed the responses of multiple biomarkers, such as morphometric and hematological parameters, hepatic and renal enzymes activities (aspartate and alanine aminotransferases, alkaline phosphatase) and oxidative stress markers (antioxidant enzymes activities and lipid peroxidation). Cr caused a decrease in glucose levels and tissue damage in liver and kidney. Pb caused changes in hematological parameters, tissue damage in liver and kidney and induced liver lipid peroxidation. The metal combination modified hematological parameters and increased the hepatic injury biomarkers. According to multivariate statistical analysis, fish exposed to the mixture showed a differential physiologic profile to those exposed to individual metals. Thus, *H. littorale* has demonstrated to be sensitive for biomarkers response and suitable as potential test species. Our results suggest deleterious effects of sublethal concentrations of heavy metals and support the usefulness of a multi-biomarker approach for the characterization of toxicological mechanisms induced by the exposure to a combination of Cr and Pb.

KEYWORDS:
fish; heavy metals; hematology; oxidative stress; transaminases

INTRODUCTION

Heavy metals occur naturally in the environment and they are found in both ground and surface waters. Fish can absorb metals through the skin, the gill epithelium and the gastroinstestinal tract. They are accumulated mainly in kidney, liver and gills, which anatomical and physiological features make them key target organs of toxic substances [1].

Chromium (Cr) and lead (Pb) have been found in water bodies of Argentina [2-4] and in native species tissues [1, 5]. Low concentrations of Cr can generate morphological abnormalities in fish liver and gills [6]. As regards Pb, it has caused cellular abnormalities by micronucleus formation [7] and inhibits the activity of the δ-aminolevulinic acid dehydratase enzyme in aquatic organisms [8].

Although toxicity of individual metals has been extensively studied in fish [9, 10], data about the effects of their mixtures on fish biomarkers are scarce. Some laboratory studies have investigated the effects of mixtures such as lead and cadmium [11], zinc and cadmium [12], chromium and nickel [13]. To our knowledge, this is the first report of a multi-biomarker assessment carried out on fish exposed to combined Cr + Pb.

The combined use of a set of complementary biomarkers can detect exposure to contaminants and quantify their impact on living organisms. Consequently, the multi-biomarker approach has gained considerable interest in ecotoxicological research, and has been recently applied in field and laboratory studies [14-16].

Hoplosternum littorale (Pisces, Callichthyidae) is a neotropical fish species widely distributed in South America. Because they are easy to collect and maintain in laboratory conditions [17-18], *H. littorale* is proposed as test species.

This study is aimed at evaluating multi-biomarker responses in *H. littorale*, after controlled exposure to an environmental concentration of Cr and Pb alone, and in combination. The multi-biomarker approach focuses on morphometric indexes, hematological responses, tissue damage markers and oxidative stress parameters.

MATERIALS AND METHODS

Fish. Adult *H. littorale* (n = 32; 9.38 ± 0.77 cm standard length; 21.95 ± 4.82 g) were obtained from an aquarium trade. For acclimation purpose, fish were held in 150-L tanks containing aerated dechlorinated water for two weeks, and fed once daily with dry commercial pellets. Both acclimation

and experimental periods were carried out in 12:12 h light–dark cycles and temperature was 25 ± 1 °C.

Experimental design. Based on previous reports of heavy metal concentrations in water bodies of Argentina [4, 19], *H. littorale* were exposed to relevant environmentally concentrations of Cr (100 µgCr·L^{-1}), Pb (100 µgPb·L^{-1}) and their combination (100 µgCr·L^{-1} + 100 µgPb·L^{-1}). According to previous studies, the mixture was defined as the addition of the two individual concentrations [9, 16, 20]. A group kept in tap water served as the control.

Metal stock solutions were prepared by dissolving appropriate amount of $K_2Cr_2O_7$ and $Pb(NO_3)_2$ (analytical grade, Merk) in distilled water, and the nominal test concentration of each metal or combination were obtained by adding appropriate aliquots of each stock solution to the aquaria. Levels of Cr and Pb in aquaria were measured by anatomic absorption spectrophotometer (Perkin Elmer Analyst).

Tests were conducted in glass aquaria containing 5 L of test solution and one fish. A control and three treatments were replicated eight times. The aquarium solutions were renewed every two days by transferring the fish to another aquarium.

After 15 days, fish were anesthetized and measured, weighted, sacrificed and dissected. Liver and kidney were immediately frozen in liquid nitrogen and stored at -80°C. All experiments were conducted in accordance with national and institutional guidelines for the protection of animal welfare.

Biomarkers. Morphometric and hematological parameters. The condition factor (CF) and the liver somatic index (LSI) were calculated according to Goede and Barton [21]. Blood was rapidly extracted from the caudal vessel by dissection of the caudal peduncle. Red blood cells (RBC), hemoglobin concentration (Hb) and hematocrit (Ht) were calculated according to Cazenave et al. [22]. Mean cell volume (MCV), mean cell hemoglobin (MCH) and mean cell hemoglobin concentration (MCHC) were calculated from primary indices. Plasma was separated by centrifugation at 1409 *g* for 10 min. The glucose concentration (GL) and the total proteins (TP) were calculated employing commercial kits (Wiener Lab®). A drop of freshly collected blood was smeared on clean slides to estimate the total white blood cells (WBC) counts and for determination of leukocyte frequency according to Tavares-Dias and de Moraes [23].

Transaminases and alkaline phosphatase. Samples of liver and kidney were homogenized in phosphate buffer (pH 7.4). The homogenate was centrifuged at 25,000 *g* at 4 °C for 10 min, and supernatant was collected. Aspartate aminotransferase (AST) and alanine aminotransferase (ALT) activities were estimated according to Reitman and Frankel. [24]. Alkaline phosphatase (ALP) (Orthophosphoric monoester phosphohydrolase) activity was determined colorimetrically using a commercial kit (Wiener Lab®). Each sample was measured by triplicate and the enzymatic activity was calculated in terms of protein content [25].

Oxidative stress markers. Antioxidant enzyme extracts from liver and kidney were prepared according to Cazenave et al. [14]. The activity of glutathione S-transferase (GST) was determined according to Habig et al. [26]. Gluthation reductase activity (GR) was assayed according to Tanaka et al. [27]. The activity of glutathione peroxidase (GPx) was determined according to Drotar et al. [28]. Catalase activity (CAT) was determined according to Beutler. [29]. All enzymatic assays were carried out in triplicate and the enzymatic activity was calculated in terms of the sample protein content [25].

Liver lipid peroxidation (LPO) levels were determined according to Fatima et al. [30]. The LPO activity was expressed as nanomoles of TBARS formed per hour, per milligram of proteins (nmol TBARS· h^{-1}·mg $prot^{-1}$). Protein content of each sample was determined according to Bradford [30].

Statistical Analysis. All data are reported as mean ± standard error. Shapiro–Wilks test was applied to evaluate normality while Levene test was used to test the homogeneity of variance. Variables that had not a normal distribution and/or homogeny of variance were transformed using Log_{10} and tested again, prior to parametric analysis. For statistical comparisons of data among treatments, one way analysis of variance (ANOVA) followed by a Multiple Comparison Test (Tukey) were performed. *P*-values below 0.05 were regarded as significant. In addition, principal component analysis (PCA) was performed in order to get a comprehensive view of the results, and to define the most important parameters involved in metal toxicity. Multivariate analysis was carried out taking into account four cases (individuals with 30 variables measured). All statistical analysis was performed by the InfoStat software [31].

RESULTS AND DISCUSSION

Morphometric and hematological parameters. Morphometric and hematological biomarkers in control and exposed fish are summarized in Table 1. CF and LSI did not show

variation among treatments. These results are in agreement with Lombardi et al. [1], who observed no changes in *Prochilodus lineatus* collected from a river contaminated with Pb, Cd, Cu and Zn. *H. littorale* exposed to Pb and the mixture showed an increase in MCH (p=0.05) and MCHC (p=0.01). These results are in agreement with Ates et al. [32], who observed higher MCH levels in *Oncorhynchus mykiss* exposed to Pb and Cu individually for 72 hours.

Besides, fish exposed to Cr showed a decrease in glucose levels (p=0.03) (Table 1). This result coincides with Mehrim [33], who observed the same response in *Oreochromis niloticus* exposed to Cr for 12 weeks by diet treatment. The decrease of glucose caused by Cr may due to the utilization of glucose as an energetic substrate for repairing the damage caused by the metal, or homeostasis mechanisms related to glycogenolysis and glyconeogenesis that tend to keep glucose at normal levels [34].

An alteration in differential leucocytes count was showed in fish exposed to Pb compared with the control group; there was an increase in neutrophils (p=0.016) and a decrease in eosinophils (p=0.0232) (Table 1). Pb is involved in irreversible effects on cells due to their interaction with cellular macromolecules [35]. On the other hand, neutrophils function as phagocytes to salvage debris from injured tissues [36]. So, neutrophilia observed in our study could indicate an increased phagocytic action in order to eliminate cellular debris. As regards eosinophils, low concentrations have been widely reported in fish, but their function is not clear [37].

Transaminases and alkaline phosphatase. AST and ALT are enzymes involved in the metabolism of amino acids, and their alterations allow the identification of tissue damage in organs such as the liver and kidney [38]. Inductions of AST (p=0.0003) and ALT (p=0.0004) were observed in the liver of fish exposed to the mixture (Fig. 1A). In kidney, an induction of AST was observed in the Cr-exposed fish (p=0.0003) (Fig. 1B). These results agree with those found by other authors in the liver of fish exposed to heavy metals in field and laboratory studies [39, 40]. Thus, transaminases resulted in sensitive indicators of cellular damage, and an increase of their activity could be related to hepatic problems [38].

ALP activity was increased in the liver of fish exposed to the three treatments (p<0.0001) (Fig. 1A). This result correlates with other authors who exposed *O. niloticus* to Pb and Zn + Cd [20, 41]. However, in kidney decreased ALP activity was shown in fish exposed to all treatments (p=0.04) (Fig. 1B). ALP enzyme is very important for detoxification, and any alteration of its activity could cause biochemical deficiency, cellular dysfunction and tissue damage [20].

Oxidative stress biomarkers. Antioxidant enzymes activities in control and exposed fish are summarized in Table 2. CAT activity was decreased in the liver of fish exposed to Cr and Pb individually (p=0.0002). This coincides with Atli and Canli [42], who observed a decrease of CAT activity in liver of *O. niloticus* exposed to sublethal concentrations of Cr for 2 and 20 days. Other authors observed the same response in kidney of Cr-exposed fish [43, 44]. CAT inhibition may be

TABLE 1

Morphometric and hematological parameters of *H. littorale* exposed to chromium (100 µgCr ·L^{-1}) and lead (100 µgPb ·L^{-1}) individually, and in combination (Cr + Pb), for 15 days. The values are expressed as means ± SE. Means sharing the asterisk (*) are significantly different at p<0.05.

Parameter	Control	Cr	Pb	Cr + Pb
LSI	1.54 ± 0.07	1.52 ± 0.12	1.40 ± 0.19	1.59 ± 0.15
CF	1.27 ± 0.03	1.22 ± 0.04	1.26 ± 0.02	1.22 ± 0.02
RBC (10^6·µL^{-1})	1.80 ± 0.13	1.79 ± 0.37	1.81 ± 0.15	1.42 ± 0.15
Ht (%)	30.67 ± 2.03	28.97 ± 2.91	30.31 ± 2.41	26.51 ± 1.87
Hb (g·dL^{-1})	4.89 ± 0.44	4.56 ± 0.75	5.75 ± 0.69	5.54 ± 0.84
MCV (µm^3)	174.89 ± 12.53	180.43 ± 14.68	168.55 ± 7.53	191.50 ± 9.22
MCH (pg)	28.13 ± 2.97	27.33 ± 3.54	31.80 ± 2.82	39.71 ± 2.84 *
MCHC (%)	15.85 ± 0.66	15.19 ± 1.36	18.67 ± 1.06 *	21.18 ± 1.86 *
GL (g·L^{-1})	0.59 ± 0.04	0.37 ± 0.05 *	0.52 ± 0.07	0.68 ± 0.12
TP (g·dL^{-1})	3.00 ± 0.10	2.65 ± 0.30	3.23 ± 0.20	2.78 ± 0.27
WBC (µL)	10530 ± 1351	17449 ± 5062	11721 ± 2740	8650 ± 704
Lymphocytes (%)	65.02 ± 5.05	72.54 ± 4.44	64.23 ± 4.69	68.58 ± 2.99
Neutrophils (%)	7.45 ± 1.67	5.31 ± 0.96	16.53 ± 1.94 *	7.94 ± 1.01
Eosinophils (%)	20.56 ± 1.68	14.26 ± 2.64	5.80 ± 1.41*	16.66 ± 1.65
Monocytes (%)	4.88 ± 1.29	7.90 ± 2.50	7.31 ± 1.54	6.58 ± 0.89

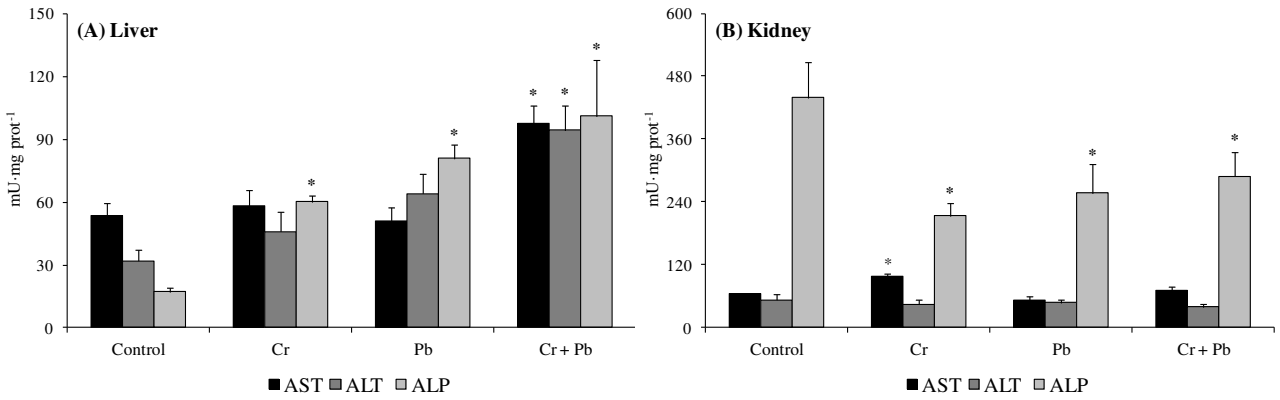

FIGURE 1

Aspartate aminotransferase (AST), alanine aminotranferase (ALT), and alkaline phosphatase (ALP) activities in liver and kidney of *H. littorale* exposed to chromium (100 µgCr ·L^{-1}) and lead (100 µgPb ·L^{-1}) individually, and in combination (Cr + Pb), for 15 days. Means sharing the asterisk (*) are significantly different at $p<0.05$.

related to the accompanied direct binding of metal ions to sulfhydryl groups on the enzyme molecule. Reduced CAT activity may increase cellular H_2O_2, and this molecule has the potential of inducing oxidative stress and starting the LPO process [45]. Such response was observed in the liver of *H. littorale* exposed to Pb individually, in which the inhibition of CAT was accompanied by an increased in LPO levels (p=0.0198) (Table 2).

Many authors have found a positive correlation between the increase of LPO levels and the inhibition of CAT activity in fish exposed to different xenobitics [46, 47]. Oliva et al. [48] found an increase in LPO levels in the liver of *Solea senegalensis* inhabiting a river contaminated with metals. However, Campana et al. [49] observed a decrease in LPO levels in the liver of *Halobratrachus didactylus* exposed to Pb for 7 days. Thus, the results observed in *H. littorale* exposed to Pb could indicate that the liver suffered an oxidative damage that the antioxidant defense system could not prevent.

Multi-biomarker approach. Many authors suggest that the selection of an appropriate battery of biomarkers and their integral analysis are important to determine deleterious effects caused by both complex mixtures of pollutants and chronic situation of contamination [15, 16, 48]. When a wide number of biomarkers are measured, many approaches are used to analyze their results. The principal component analysis (PCA) is one of the techniques usually employed [50]. In the present

TABLE 2

Oxidative stress markers in liver and kidney of *H. littorale* exposed to chromium (100 µgCr ·L^{-1}) and lead (100 µgPb ·L^{-1}) individually, and in combination (Cr + Pb), for 15 days. The values of antioxidant enzyme activities (nkat mg prot^{-1}) and lipid peroxidation (nmol TBARS· h^{-1}·mg prot^{-1}) are expressed as means ± SE. Means sharing the asterisk (*) are significantly different at $p<0.05$.

		Control	Cr	Pb	Cr + Pb
Liver					
	GST	9.85 ± 0.81	8.06 ± 0.43	7.76 ± 1.04	9.13 ± 0.98
	GR	0.49 ± 0.05	0.51 ± 0.06	0.57 ± 0.06	0.53 ± 0.05
	GPx	3.95 ± 0.24	4.39 ± 0.48	4.12 ± 0.38	3.80 ± 0.34
	CAT	552.24 ± 34.76	338.88 ± 25.64 *	355.52 ± 35.33 *	657.13 ± 28.24
	LPO	0.06 ± 0.01	0.07 ± 0.01	0.12 ± 0.01*	0.04 ± 0.02
Kidney					
	GST	4.94 ± 0.36	4.27 ± 0.24	4.64 ± 0.37	3.55 ± 0.31
	GR	0.98 ± 0.11	0.74 ± 0.13	0.80 ± 0.07	0.68 ± 0.12
	GPx	6.58 ± 0.65	6.01 ± 0.27	6.28 ± 0.57	5.17 ± 0.66
	CAT	106.33 ± 18.87	87.73 ± 6.07	103.08 ± 6.53	104.72 ± 12.87

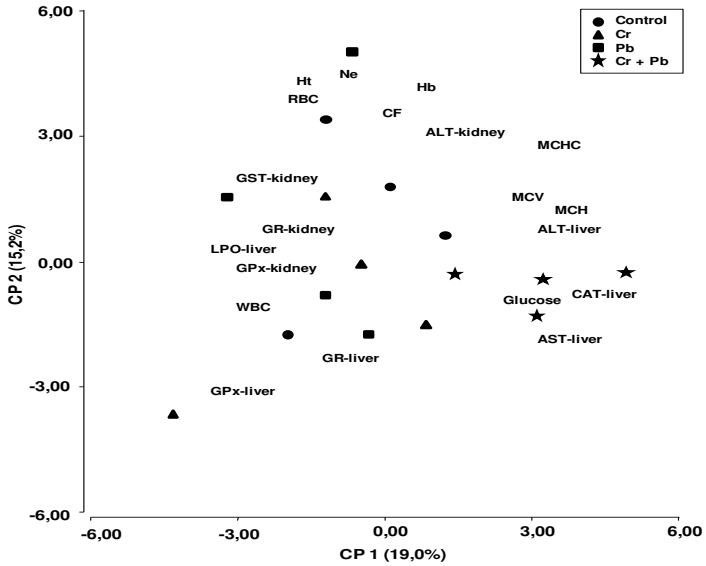

FIGURE 2
Representation of the biomarkers (in letters) and individuals (in forms, n = 4 per treatment) onto the first factorial plane of the principal component analysis (PCA). Biomarkers with correlation coefficients >0.5 were represented in the PCA. Biomarkers abbreviations are explained in the text with the exception: Ne (neutrophils).

study, two components were extracted by applying the PCA (Fig. 2). According to Legendre and Legendre [51], interpretation of principal components may be done for eigenvalues of the data matrix higher than 1. The PCA indicated that 10 eigenvalues were higher than 1; moreover correlation coefficients are significant when they are higher than $\sqrt{d/n}$, d being the number of principal components and n the number of variables. Therefore, correlation coefficients >0.5 were indicative of a good representation of the variables with principal component axes. The components accounted for 34.2% of the original dataset variance. The first principal component (PC1) explained 19.0% of the variance, and showed significant positive loadings for glucose, MCV, MCH, MCHC, AST, ALT and CAT in liver. On the contrary, a negative correlation was found in WBC, GST, RBC and GPx in kidney, and GPx and LPO in liver. The second principal component (PC2) explained 15.2% of the variance, and showed positive correlations for the CF, Ht, Hb, neutrophils and ALT in kidney, but negative correlations for GPx and RBC in liver. Thus, Figure 2 represents that PC1 separated clearly fish exposed to Cr + Pb from the other treatments and PC2 shows the great variability of individual physiologic responses (independently of the treatment).

The increase of both transaminases activities and oxidative damage found in our study suggests that the liver is a target organ under the action of the metal combination. These results are in agreement with many authors, who claimed that the liver is more sensitive to metal exposure than the kidney [42].

CONCLUSIONS

In summary, our results showed different effects on *H. littorale* exposed to individual metals and their combination. Cr produced nutrients mobilization by a decrease in plasma glucose, tissue damage in liver and kidney, and an inhibition of an antioxidant enzyme (CAT). On the other hand, hematological alterations, tissue damage in liver and kidney and evident hepatic oxidative stress were found in fish exposed to Pb. The combination of metals caused changes in hematological parameters and damages in tissues. The multi-biomarker approach based on a wide array of physiological parameters showed that fish exposed to Cr + Pb had a different physiologic profile to those exposed to individual metals. Thus, this work underscores the need for new studies to explore how complex mixtures affect aquatic organisms.

ACKNOWLEDGEMENTS

This work was supported by grants from CONICET and Universidad Nacional del Litoral (CAI+D).

REFERENCES

[1] Lombardi, P.E.; Peri, S.I.; Verrengia Guerrero, N.R. (2010) Trace metal levels in *Prochilodus lineatus* collected from the La Plata River, Argentina. Water Air Soil Pollut. 160, 47-59.

[2] Gagneten, A.M.; Gervasio, S.; Paggi, J.C. (2007) Heavy metal pollution and eutrophication in the Lower Salado River Basin (Argentina). Water Air Soil Pollut. 178, 335-349.

[3] Marchese, M.; Rodriguez, A.R.; Pave, P.J.; Carignano, M.R. (2008) Benthic invertebrates structure in wetlands of a tributary of the middle Parana River (Argentina) affected by hydrologic and anthropogenic disturbances. J. Environ. Biol. 29, 343-348.

[4] Peluso, L.; Abelando, M.; Apartín, C.D.; Almada, P.; Ronco, A.E. (2013) Integrated ecotoxicological assessment of bottom sediments from the Paraná basin, Argentina. Ecotox. Environ. Safe. 198, 179-186.

[5] Giarratano, E.; Duarte, C.A.; Amin, O.A. (2010) Biomarkers and heavy metal bioaccumulation in mussels transplanted to coastal waters of the Beagle Channel. Ecotox. Environ, Safe. 73, 270-279.

[6] Antón, A.; Serrano, T.; Angulo, E.; Ferrero, G.; Rallo, A. (2000) The use of two species of crayfish as environmental quality sentinels: the relationship between heavy metal content, cell and tissue biomarkers and physic-chemical characteristics of the environment. Sci. Total Environ. 247, 239-251.

[7] Ferraro, M.V.M.; Fenocchiol, A.S.; Mantovani, M.S.; Oliveira Ribeiro, C.; Cestari, M.M. (2004) Mutagenic effects of tributyltin and inorganic lead (Pb II) on the fish *H. malabaricus* as evaluated using the comet assay and the piscine micronucleus and chromosome aberration tests. Genet. Mol. Biol. 27(1), 103-107.

[8] Lombardi, P.E.; Peri, S.I.; Verrengia Guerrero, N.R. (2010) ALA-D and ALA-D reactivated as biomarkers of lead contamination in the fish *Prochilodus lineatus*. Ecotox. Environ. Safe. 73, 1704-1711.

[9] Firat, Ö.; Cogun, H.Y.; Aslanyavrusu, S.; Kargin, F. (2008) Antioxidant responses and metal accumulation in tissues of Nile Tilapia *Oreochromis niloticus* under Zn, Cd and Zn plus Cd exposures. J. Appl. Toxicol. 29, 295-301.

[10] Pandey, S.; Parvez, S.; Ahamd Ansari, R.; Ali, M.; Kaur, M.; Hayat, F.; Ahmad, F.; Raisuddin, S. (2008) Effects of exposure to multiple trace metals on biochemical, histological and ultrastructural features of gills of a freshwater fish, *Channa punctata* Bloch. Chem. Biol. Interac. 174, 183-192.

[11] Birceanu, O.; Chowdhury, M.J.; Gillis, P.L.; McGeer, J.C.; Wood, C.M.; Wilkie, M.P. (2008) Modes of metal toxicity and impaired branchial ion regulation in rainbow trout exposed to mixtures of Pb and Cd in soft water. Aquat. Toxicol. 89, 222-231.

[12] Firat, Ö. and Kargin, F. (2009) Biochemical alterations induced by Zn and Cd individually or in combination in the serum of *Oreochromis niloticus*. Fish Physiol. Biochem. 36(3), 647-653.

[13] Palaniappan, P.L.R. and Karthikeyan, S. (2009) Bioaccumulation and depuration of chromium in the selected organs and whole body tissues of freshwater fish *Cirrhinus mrigala* individually and in binary solutions with nickel. J. Environ. Sci. 21, 229-236.

[14] Cazenave, J.; Bacchetta, C.; Parma, M.J.; Scarabotti, P.A.; Wunderlin, D.A. (2009) Multiple biomarkers responses in *Prochilodus lineatus* allowed assessing changes in the water quality of Salado River basin (Santa Fe, Argentina). Environ. Pollut. 157, 3025-3033.

[15] Cazenave, J.; Bacchetta, C.; Rossi, A.; Ale, A.; Campana, M.; Parma, M.J. (2014) Deleterious effects of wastewater on the health status of fish: A field caging study. Ecol. Ind. 38, 104-112.

[16] Bacchetta, C.; Rossi, A.; Ale, A.; Campana, M.; Parma, M.J.; Cazenave, J. (2014) Combined toxicological effects of pesticides: A fish multi-biomarker approach. Ecol. Ind. 36, 532-538.

[17] Affonso, E.D.; Polez, V.L.P.; Correa, C.; Mazon, A.F.; Araujo, M.R.R.; Moraes, G.; Rantin, F.T. (2004) Physiological responses to sulfide toxicity by the air-breathing catfish, *Hoplosternum littorale* (Siluriformes, Callichthyidae). Comp. Biochem. Physiol. 139(4), 251-257.

[18] Rossi A., Cazenave J., Bacchetta C., Campana M., Parma M.J. (2015) Physiological and metabolic adjustments of *Hoplosternum littorale* (Teleostei, Callichthyidae) during starvation. Ecol. Ind. 56: 161-170.

[19] Topalián, M.L.; Castañé, P.M.; Rovedatti, M.G.; Salibián, A. (1999) Principal component analysis of dissolved heavy metals in water of the Reconquista river (Buenos Aires, Argentina). Bull. Environ. Contam. Toxicol. 63, 484-490.

[20] Firat, Ö. and Kargin, F. (2010) Individual and combined effects of heavy metals on serum biochemistry of Nile Tilapia *Oreochromis niloticus*. Arch. Environ. Contam. Toxicol. 58, 151-157.

[21] Goede, R.W. and Barton, B.A. (1999) Organismic indices and autopsy-based

assessment as indicators of health and condition of fish. Am. Fish Soc. Symp. 8, 93-108.
[22] Cazenave, J.; Wunderlin, D.A.; Hued, A.C.; Bistoni, M,Á. (2005) Haematological parameters in a neotropical fish, *Corydoras paleatus* (Jenyns, 1842) (Pisces, Callichthyidae) captured from pristine and polluted water. Hydrobiologia. 53, 25-33.
[23] Tavares-Dias, M. and Ruas de Moraes, F. (2007) Leukocyte and thrombocyte reference values for channel catfish (*Ictalurus punctatus* Raf), with an assessment of morphhologic, cytochemical, and ultrastructural features. Vet. Clin. Path. 36, 49-54.
[24] Reitman, S. and Frankel, F. (1957) A colorimetric method for the determination of serum glutamic oxaloacetic and glutamic pyruvic acid transaminase. Am. J. Clin. Path. 28, 56-63.
[25] Bradford, M.M. (1976) A rapid and sensitive method for the quantification of microgram quantities of proteins utilizing the principle of protein-dye binding. Anal. Biochem. 72, 248-254.
[26] Habig, W.H.; Pabst, M.J.; Jakoby, W.B. (1974) Glutathione S-transferases. The first step in mercapturic acid formation. J. Biol. Chem. 249, 7130-7139.
[27] Tanaka, K.; Sano, T.; Ishizuka, K.; Kitta, K.; Kawamura, Y. (1994) Comparison of properties of leaf and root glutathione reductases from spinach. Physiol. Plant. 91, 353-358.
[28] Drotar, A.; Phelps, P.; Fall, R. (1985) Evidence for glutathione peroxidase activities in cultured plant cells. Plant Sci. 42, 35-40.
[29] Beutler, E. (1982) Catalase. In Red Cell Metabolism, a Manual of Biochemical Methods, 3rd Ed.; Grune and Stratton Inc.: New York, 105-106 pp.
[30] Fatima, M.; Ahmad, I.; Sayeed, I.; Athar, M.; Raisuddin, S. (2000) Pollutant-induced over-activation of phagocytes is concomitantly associated with peroxidative damage in fish tissues. Aquat. Toxicol. 49, 243-250.
[31] Di Rienzo, J.A.; Casanoves, F.; Balzarini, M.G.; Gonzalez, L.; Tablada, M.; Robledo, C.W. InfoStat versión 2012. Grupo InfoStat, FCA, Universidad Nacional de Córdoba, Argentina. http://www.infostat.com.ar (accessed Oct 2013)
[32] Ates, B.; Orun, I.; Talas, Z.S.; Durmaz, G.; Yilmaz, I. (2008) Effects of sodium selenite on some biochemical and hematological parameters of rainbow trout (*Oncorhynchus mykiss* Walbaum, 1792) exposed to Pb^{2+} and Cu^{2+}. Fish Physiol. Biochem. 34, 53-59.
[33] Mehrim, A.I.M. (2014) Physiological, biochemical and histometric responses of Nile tilapia (*Oreochromis niloticus* L.) by dietary organic chromium (chromium picolinate) supplementation. J. Adv. Res. 5(3), 303-310.
[34] Ricard, A.C.; Daniel, C.; Anderson, P.; Hontela, A. (1998) Effects of subchronic exposure to cadmium chloride on endocrine and metabolic functions in rainbow trout *Oncorhynchus mykiss*. Arch. Environ. Contam. Toxicol. 34, 377-381.
[35] Heath, A. G. (1995) In Water pollution and fish physiology, 2nd Ed. CRC Press Inc.: Boca Raton, Florida, 373 pp.
[36] Witko-Sarsat, V.; Rieu, P.; Descamps-Latsha, B.; Lesavre, P.; Halbwachs-Mecarel, L. (2000) Neutrophils: molecules, functions and pathophysiological aspects. Lab. Invest. 80, 617-653.
[37] Takashima, F. and Hibiya, T. (1995) In: An atlas of fish histology. Normal and pathological features. Kodansha Ltd Inc., Tokio, 192 pp.
[38] Ramaiah, S.K. (2007) A toxicologist guide to the diagnostic interpretation of hepatic biochemical parameters. Food Chem. Toxicol. 45, 1551-1557.
[39] Levesque, H.M.; Moon, T.W.; Campbell, P.G.C.; Hontela, A. (2002) Seasonal variation in carbohydrate and lipid metabolism of yellow perch (*Perca flavescens*) chronically exposed to metals in field. Aquat. Toxicol. 60, 257-267.
[40] Ibrahim, S.A. and Mahmoud, S.A. (2005) Effect of heavy metals accumulation on enzyme activity and histology in liver on some nile fish in Egypt. Egypt. Aquat. Biol. Fish. 9, 203-219.
[41] Atli, G. and Canli, M. (2007) Enzymatic responses to metal exposures in a freshwater fish *Oreochromis niloticus*. Comp. Biochem. Physiol. 145(C), 282-287.
[42] Atli, G. and Canli, M. (2010) Response of antioxidant system of freshwater fish *Oreochromis niloticus* to acute and chronic metal (Cd, Cu, Cr, Zn, Fe) exposures. Ecotox. Environ. Safe. 73, 1884-1889.
[43] Atli, G.; Alptekin, O.; Tükel, S.; Canli, M. (2006) Response of catalase activity to Ag^{+}, $Cd^{2+,}$ Cr^{6+}, Cu^{2+} and Zn^{2+} in five tissues of freshwater fish *Oreochromis niloticus*. Comp. Biochem. Physiol. 143(C), 218-224.
[44] Lushchak, O.V.; Kubrak, O.I.; Lozinsky, O.V.; Storey, J.; Storey, K.B.; Lushchak, V.I. (2009) Chromium (III) induces oxidative stress in goldfish liver and kidney. Aquat. Toxicol. 93, 45-52.
[45] Kong, X.; Wang, S.; Jiang, H.; Nie, G.; Li, X. (2010) Responses of acid/alkaline phosphatase, lysozyme, and catalase activities and lipid peroxidation to mercury exposure

during the embryonic development of goldfish *Carassius auratus*. Aquat. Toxicol. 120-121, 119-125.
[46] Atif, F.; Ali, M.; Kaur, M.; Rehman, H.; Raisuddin, S. (2005) Modulatory effect of cadmium injection on endosulfan-induced oxidative stress in the freshwater fish *Channa punctata* Bloch. Bull. Environ. Contam. Toxicol. 74, 777-784.
[47] Ferreira, D.; Costa da Motta, A.; Kreutz, L.C.; Toni, C.; Loro, V.L.; Barcellos, L.J.G. (2010) Assessment of oxidative stress in *Rhamdia quelen* exposed to agrochemicals. Chemosphere. 79, 914-921.
[48] Oliva, M.; Vicente, J.J.; Gravato, C.; Guilhermino, L.; Galindo-Riano, M.D. (2010) Oxidative stress biomarkers in Senegalsole, *Solea senegalensis*, to assess the impact of heavy metal pollution in a Huelva estuary (SW Spain): Seasonal and spatial variation. Ecotox. Environ. Safe. 75, 151-162.
[49] Campana, O.; Sarasquete, C.; Blasco, J. (2003) Effect of lead on ALA-D activity, metallothinein levels, and lipid peroxidation in blood, kidney and liver of the toadfish *Halobatrachus didactylus*. Ecotox. Environ. Safe. 55, 116-125.
[50] Wepener, V. (2008) Application of active biomonitoring within an integrated water resources management framework in South Africa. S. Afr. J. Chem. 104, 367-373.
[51] Legendre, L. and Legendre, P. (1979) Ecologie numérique. 2-la structure desdonnées écologiques. Chapitre 8. In: *L'ordination en espace r duit*. Les Presses de l'Universit du Qu bec, Masson, Paris, New York, 101-146 pp.

Received: **26.10.2015**
Accepted: **19.02.2016**

CORRESPONDING AUTHOR

Jimena Cazenave
Laboratorio de Ictiología, Instituto Nacional de Limnología (INALI-CONICET-UNL), Paraje El Pozo, Ciudad Universitaria UNL, 3000 Santa Fe, Argentina

e-mail: jcazenave@inali.unl.edu.ar

© by PSP Volume 25 – No. 10/2016, pages 4060-4066 Fresenius Environmental Bulletin

EVALUATION OF SULFANILIC ACID REMOVAL FROM AQUEOUS SOLUTIONS BY ACTIVATED CARBON AND POLYMERIC RESINS

Yue Sun*, Deqiang Yin, Junfen Luo, Yan Xu

School of Civil Engineering, Southeast University, Nanjing, 210096, China

ABSTRACT

The feasibility of using granular activated carbon (GAC), weakly basic anion-exchanger (D301) and aminated hypercrosslinked polymeric resin (AH-1) to remove sulfanilic acid (SA) from water was investigated. Adsorption isotherms, kinetics, effects of solution pH and coexisting NaCl, as well as regeneration tests were carried out through batch method. Most favorable adsorption was observed at solution pH around 3, and further increase or decrease of solution pH resulted in a reduction of sorption capacity, while the polymeric sorbents AH-1 and D301 were more sensitive to solution pH than GAC. Equilibrium adsorption data fitted well to the Langmuir isotherm, and the maximum uptakes decreased in the following order: D301 > AH-1 > GAC. All the sorption kinetic data followed the pseudo-second-order rate equation well, and AH-1 possessed the fastest sorption rate. Coexisting NaCl exerted a negative effect on the adsorption process, and relatively better salt-resistance property of AH-1 as well as GAC than that of D301 could enable AH-1 and GAC to be used effectively in removal of SA from aqueous solution at a high salinity level. Moreover, AH-1 and D301 were amenable to an entire regeneration by NaOH solution, whereas only about 50% regeneration efficiency was observed for GAC. Results of column adsorption tests reinforced the feasibility of AH-1 for potential industrial application, and SA could be readily recovered by further treatment of the concentrated regenerant solution.

KEYWORDS:
activated carbon, polymeric resin, sulfanilic acid, adsorption

INTRODUCTION

In the past decades, water pollution by organic compounds has been of increasing concern in many countries. One of the largest sources of organic pollutants is the industrial effluent accompanying the manufacture of organic chemicals. Sulfonated aromatic amines, as a family of the widespread environmental pollutants with high toxicity and carcinogenicity, are used extensively in the production of dyes, pharmaceuticals, pesticides, ion exchange resins and optical brightners [1-3]. Another important source of sulfonated aromatic amines is formed during the biodegradation of several sulfonated nitrogen containing organic compounds such as azo dyes under anaerobic conditions [4]. Sulfanilic acid (SA) is a representative compound of sulfonated aromatic amines, and produced in large quantities and easily enters the surface waters because of its high water solubility [5]. Due to environmental and health concerns, SA-contaminated wastewaters need to be treated prior to their discharge.

The removal of SA from its waste effluents has been accomplished mainly by advanced oxidation and biodegradation [6-12]. However, SA can be very slowly destroyed by strong oxidants such as ozonation and Fenton reagent, and the negatively charged sulfonate group on aromatic ring is known to suppress biodegradation by most heterotrophic microorganisms due to the low permeability of SA through bacterial membranes. It has been demonstrated in many cases that sorption is an effective and economical approach to remove many pollutants from wastewaters, and activated carbon has been widely employed for removal of aromatic contaminants from waste streams. In the past few decades, polymeric resins have been gradually used as an alternative to activated carbon in field applications to remove aromatic pollutants from wastewaters. But up to now, only few studies about SA removal using some common adsorbents were published [5, 13], and it is unclear whether the conventional adsorbents are effective for SA removal from water or not. Therefore, it is necessary to understand which adsorbent should be used to effectively eliminate it once water is polluted by SA.

The aim of this work is to compare the sorption behavior of SA on the different adsorbents including

activated carbon and polymeric resins, and evaluate their feasibility for SA removal from aqueous solutions. The sorption isotherms and kinetics for SA using the granular activated carbon (GAC), weakly basic anion-exchanger (D301) and aminated hypercrosslinked polymeric resin (AH-1) were examined in detail, and the effect of solution pH and coexisting NaCl on the performance of the tested sorbents was particularly concerned. Moreover, the regeneration performance of the three sorbents as well as the column adsorption for SA removal from industrial wastewater by AH-1 was also investigated.

MATERIALS AND METHODS

Materials. Sulfanilic acid (SA) and other reagents were purchased from Shanghai Chemical Reagent Plant (China) in A.R. grade. The weakly basic anion-exchanger D301 and the aminated hypercrosslinked polymeric resin AH-1 were kindly provided by Nange Environmental Technology Co. (China), and the coconut-shell granular activated carbon (GAC) was purchased from Jinbei Fine Chemical Co. (China).

Method. ***Batch adsorption experiments*****.** Batch adsorption tests were carried out in 250 mL glass flasks. 0.100 g of adsorbent was introduced to a 100 mL solution containing known initial concentration of SA. The flasks were completely sealed and placed in a constant temperature shaker at 298 K and shaken at 150 rpm for 24 h to ensure the adsorption process reaching equilibrium. Diluted HCl or NaOH solution was used to adjust the solution pH and NaCl was introduced into the flask before adsorption when necessary. As for kinetic study, 0.500 g of adsorbent and 500 mL of SA solution at an initial concentration of 1000 mg/L were introduced into a 1000 mL conical flask quickly and shaken at a speed of 150 rpm at 298 K continuously, and a 0.2 mL aliquot of solution was sampled from the flasks at various time intervals to determine adsorption kinetics. Adsorbent from the kinetic study was transferred to another flask after filteration and 500 mL of 1.0 M NaOH solution was used for desorption at 318 K. The amount of solute loaded on the adsorbent particles was calculated by conducting a mass balance on the solute before and after the test.

Column tests. Column experiments were carried out with a glass column (32 mm diameter and 360 mm length) equipped with a water bath to maintain a constant temperature. A 100 mL portion of AH-1 was packed into the column for further use. A Lange-580 pump (China) was used to ensure a constant flow rate. After adsorption, 2.0 bed volumes (BV) of 1.0 M NaOH solution followed by 3.0 BV deionized water was used for desorption at 318 K. The SA industrial effluent was passed through the column at a flow rate of 2.0 BV/h, and the desorption flow rate was controlled at 1.0 BV/h.

Analyses. Surface area and pore size distribution of adsorbents were determined by using a Micromertics 2010C automatic analyzer (Australia). X-ray photoelectron spectroscope (XPS) was used to determine the protonation degree of tertiary amino group on AH-1 when the sorbent was placed in solution with different pH values. After being separated from solutions, the sorbent samples were vacuum-dried in an oven at 313K until constant weights. The analysis was made with an ESCALB MK-II X-ray spectrometer (U.K.) equipped with Mg K_α X-ray source (1253.6 eV protons). In batch sorption test, content of SA in water was determined at the wavelength of 240 nm using a Helious Betra UV-vis spectrophotometer (U.K.). Before analysis, pH values of all the samples were adjusted to 12±0.5 to minimize the disturbing effect of solution pH. While in column test, content of SA was determined by use of HPLC (Waters 600, USA, Nov-Pak C_{18} column, flow phase: methanol/0.1 M phosphoric acid = 50/50, wavelength: 240 nm, flow rate: 1 mL/min).

TABLE 1
Characteristics of adsorbents

Property	GAC	AH-1	D301
BET surface area (m^2/g)	897.4	822.7	31.8
Micropore surface area (m^2/g)	489.5	491.3	2.7
Pore volume (cm^3/g)	0.609	0.679	0.279
Tertiary amino group (mmol/g)	0	1.51	3.78
Average pore diameter (nm)	2.72	3.30	16.62

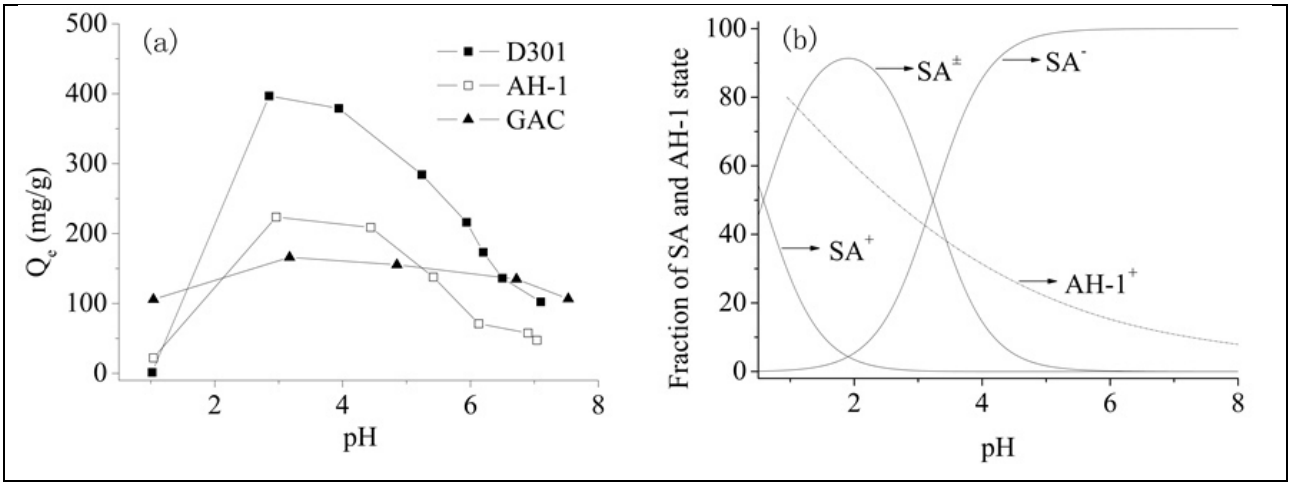

FIGURE 1
Effect of pH on sorption of SA onto sorbents (a) and correlation of pH with fraction of molecular state of SA and protonation degree of tertiary amino group on AH-1 (b).

RESULTS AND DISCUSSION

Characteristics of adsorbents. Some characteristics of the tested adsorbents are presented in Table 1. Both AH-1 and GAC had large specific surface area, pore volume, micropore region and small average pore diameter. Furthermore, compared to GAC, the two polymeric adsorbents possessed stronger polarity for the presence of the tertiary amino group on their network.

Effect of solution pH on SA sorption. The pH-dependent trend of the sorption capacity at an initial SA concentration of 1000 mg/L is shown in Fig. 1a. It can be seen that the adsorption capacity of either AH-1 or D301 was very sensitive to solution pH and the uptake initially increased notably with raising pH up to about 3 and then decreased dramatically with the further increasing solution pH. In the case of GAC, the maximum sorption amount also reached at about pH 3, but the uptake changed very gradually with varying solution pH.

According to p*K*a1 (0.59) and p*K*a2 (3.23) of SA in aqueous solution, the values of molar percentages of SA present in different form as a function of pH are predicted in Fig. 1b. The cationic species $^+NH_3$-Ar-SO_3H (SA^+) dominates at lower pH values, the zwitterion form $^+NH_3$-Ar-SO_3^- ($SA^{\pm}$) is the principal species in moderate acidic medium, and the anionic species NH_2-Ar-SO_3^- (SA^-) is the main form at higher pH values. In general, two parallel adsorption mechanisms, namely dispersive interaction and electrostatic interaction were reported to explain the adsorption of organic compounds on activated carbons [14]. The fact that SA uptake of GAC changed slightly with varying solution pH, indicated electrostatic interaction did not play a predominant role in this case. AH-1 had the similar surface area and pore structure to GAC, thus its significantly different pH-dependent sorption trend from GAC could be explained in terms of its surface chemical property. As shown in Fig. 1b, the results of XPS analysis revealed that the protonation degree of the functional group, i.e. $-N(CH_3)_2$ on AH-1 decreased remarkably with increasing solution pH. In the mild acidic media, for example pH 3, AH-1 had quite a few net positive charge due to protonation of $-N(CH_3)_2$ on it (denoted as $AH\text{-}1^+$), and effectively adsorbed deprotonated form of adsorbate ($SA^{\pm}$ and SA^-) through electrostatic attractive interaction. With the solution pH value further increasing, the net positive charge of AH-1 decreased obviously, which led to the reduction of the uptake. Contrarily, when pH values were lower than about 3, with the solution pH value decreasing, net positive charge of AH-1 increased, in the meanwhile, positive charge density of SA molecule increased, which casued against adsorption because of electrostatic repulsion between the net positively charged sorbent surface and protonated amino group of SA. Thereafter, maximum sorption capacity of SA onto AH-1 was observed at about pH 3, and further increasing or decreasing solution pH would be unfavorable to adsorption. D301 had the same functional group as AH-1, thus it showed the similar pH-dependent sorption characteristic.

Adsorption isotherms. Fig. 2 shows the equilibrium adsorption isotherms of SA onto the adsorbents at 298 K. The equilibrium adsorption data were fit into the Freundlich and Langmiur equations

TABLE 2
Regression parameters of Freundlich and Langmuir isotherm equations at 298 K.

Sorbent	Freundlich constants			Langmuir constants		
	n	K_F	R^2	Q_m (mg/g)	K_L (L/g)	R^2
GAC	2.094	7.096	0.9795	204.8	4.642	0.9936
AH-1	4.801	59.18	0.9093	224.7	39.42	0.9995
D301	4.103	90.43	0.9520	396.4	53.06	0.9983

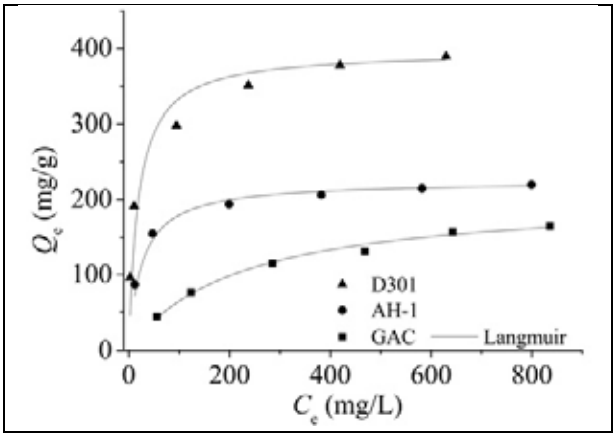

FIGURE 2
Adsorption isotherms of SA onto sorbents at 298 K.

respectively as [15]

$$\ln Q_e = \ln K_F + 1/n \ln C_e \quad (1)$$

$$C_e / Q_e = C_e / Q_m + 1 / (K_L Q_m) \quad (2)$$

where Q_e is the equilibrium adsorption capacity of the adsorbent (mg/g); C_e is the equilibrium concentration of adsorbate (mg/L); K_F, n, Q_m and K_L are the characteristic constants. The correlative relevant parameters and correlation coefficient (R^2) of both the isotherm equations are listed in Table 2.

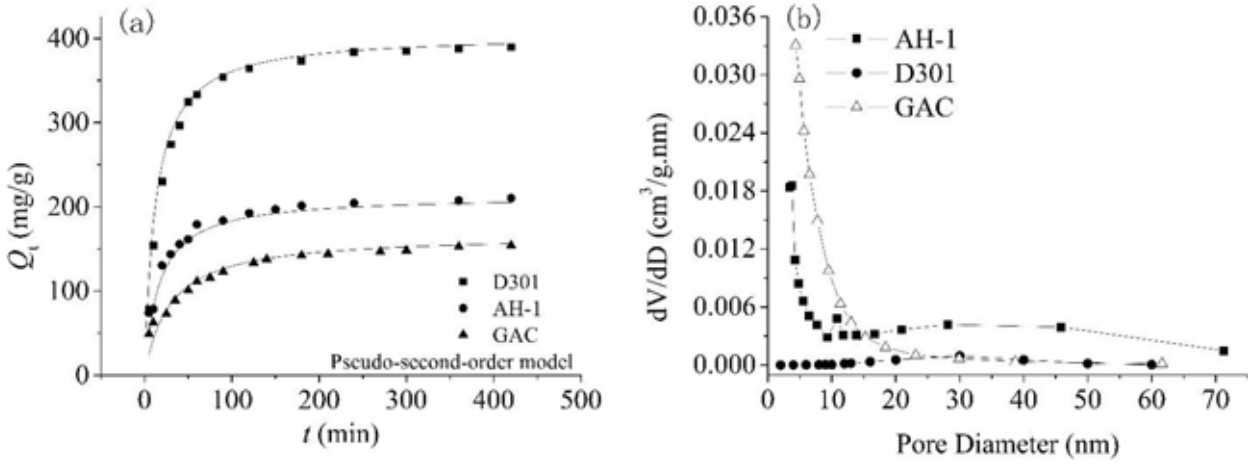

FIGURE 3
Sorption kinetic curves of SA on sorbents (a) and pore size distribution of sorbents (b).

TABLE 3
Kinetic parameters for adsorption of SA onto adsorbents at 298 K.

Adsorbent	Pseudo-first-order model		Pseudo-second-order model			
	k_1 (min^{-1})	R^2	$10^4 k_2$ (g/mg·min)	Q_e (mg/g) Calculated	Q_e (mg/g) Experimental	R^2
D301	0.0072	0.8596	2.000	405.1	401.3	0.9950
AH-1	0.0066	0.8529	2.865	213.2	217.7	0.9854
GAC	0.0057	0.9121	2.072	166.9	164.3	0.9889

As can be seen from table 2, Langmuir equations were more reliable than Freundlich equations because all the correlation factors (R^2) of the former were greater than those of the latter. The values of Q_m, the maximum monolayer coverage of adsorbent in the Langmiur theory, indicated that the adsorption capacity towards SA decreased in the following order: D301 > AH-1 > GAC. Taken into account their similar surface area and pore structure, higher adsorption capacity of AH-1 than that of GAC could be attributed to the chemical surface heterogeneity of the two sorbents. It was reasonable that the largest amount loaded on D301 was owing to the largest amount of tertiary amino groups on its network, and electrostatic interaction played a predominant role in this case.

Adsorption kinetics. Fig. 3a presents the plot of SA removal versus contact time for the three adsorbents at initial concentration of 1000 mg/L within a total contact time of 420 min.

The kinetic data for all the adsorbents were represented by the pseudo-first-order and pseudo-second-order model [15]

$$\ln (1 - Q_t / Q_e) = - k_1 t \quad (3)$$

$$1 / (Q_e - Q_t) = k_2 t + 1 / Q_e \quad (4)$$

where Q_t is the adsorption uptake (mg/g) of SA at time t and Q_e is the equilibrium uptake (mg/g), k_1 and k_2 are the pseudo-first and pseudo-second order equation rate constants, respectively. The values of the rate constants and the relevant parameters are listed in Table 3.

Higher correlation coefficients of the pseudo-second order model and the calculated Q_e values close to the experimental data indicated that SA sorption could be interpreted as a pseudo-second order process. The k_2 values in Table 3 showed that AH-1 possessed the fastest adsorption. The average pore diameter of AH-1 was larger than that of GAC, additionally, as shown in Fig. 3b, AH-1 had larger macropore and mesopore region than GAC, which could act as diffusion channel for adsorbate, leading to a larger rate constant of AH-1 than that of GAC. The average pore diameter of D301 was larger than that of AH-1, but the sorption rate of the former was smaller than that of the latter. Notably, the average pore diameter was measured using dry sorbent beads, but in aqueous solution, the tertiary amino group on sorbent matrix would extend as well as adsorb water then build up "water clusters" due to its hydrophilic character, which might lead to a decrease of the accessibility of the pores and then diffusion would slow down [16]. The tertiary amino group content on D301 was about 2.5 times of that on AH-1, so AH-1 possessed better kinetic character than D301, although average pore diameter of the latter was larger.

Effect of NaCl on SA sorption. Taken into account the fact that inorganic salts always coexist with sulfonated aromatic amines at a relatively high level in the industrial wastewaters, selective sorption properties of adsorbents are of particular importance for their application. Here, we tested the effect of NaCl as a representative of competitive inorganic salts on the uptake of SA onto the three sorbents. As shown in Fig. 4, the SA uptake decreased significantly with adding NaCl in solution, and gradually reached to a magnitude when further raising the NaCl content. Less effect of salinity on AH-1 and GAC sorption than D301 might be attributed to the enhanced sorption of SA driven by dispersion force corresponding to their larger specific surface area. The relatively better salt-resistance property of AH-1 and GAC thus enabled them to be used effectively in the removal of SA from wastewater with a high strength of inorganic salts.

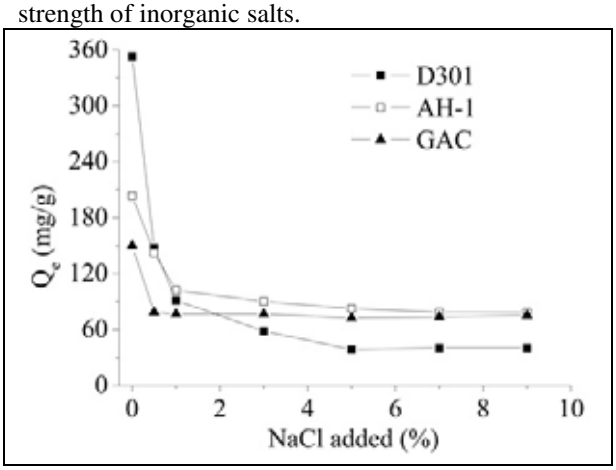

FIGURE 4
Effect of NaCl on sorption of SA onto adsorbents.

Desorption. The adequate regeneration of the exhausted adsorbent is essential from the economic point of view. The results of regeneration tests showed that SA anions were rapidly desorbed from AH-1 as well as D301 by addition of 1.0 M NaOH solution, and a desorption equilibrium was approximately achieved within 60 min, while that for GAC was nearly 180 min. The desorption efficiencies of AH-1, D301 and GAC within 180 min were 99.4%, 97.4% and 51.7%, respectively. The high desorption efficiencies and rates ensured both the polymeric sorbents could be used repeatedly.

Column treatment of SA chemical effluent. The main properties of the SA chemical effluent

generated in the production process of sulfonamide from Changshou Chemical Plant (China) were as follows: pH, 1; SA, 5600 mg/L; NaCl, 8%. AH-1 was selected to test its reliability for SA removal from the chemical effluent due to its large capacity in aqueous solution at a high salinity level and satisfactory regeneration behavior. The effluent pH was first adjusted to about 3 by diluted NaOH solution and filtered for AH-1 adsorption. Fig. 5 depicts the breakthrough adsorption curve of a fixed-bed column packed with AH-1 for a feeding solution. After adsorption, leakage of SA appeared at 12 BV, and the SA removal efficiency was over 96%. Fig. 5 also gives the elution curve of SA from AH-1. A complete column regeneration of AH-1 was readily achieved by 2 BV of 1.0 M NaOH solution followed by rinsing with 3 BV of water.

The spent NaOH effluent containing high content SA in anionic form was then subjected to acidification, filtration and desiccation for SA recovery, and more than 90% of SA in the industrial effluent could be recovered as a raw product (> 90% in purity). Continuous adsorption-regeneration runs of an identical AH-1 bed were also performed to test its stable applicability. The superposition of SA breakthrough curves in the 1st and 5th run (Fig. 5) indicated that AH-1 could be effectively regenerated for repeated use with no capacity loss.

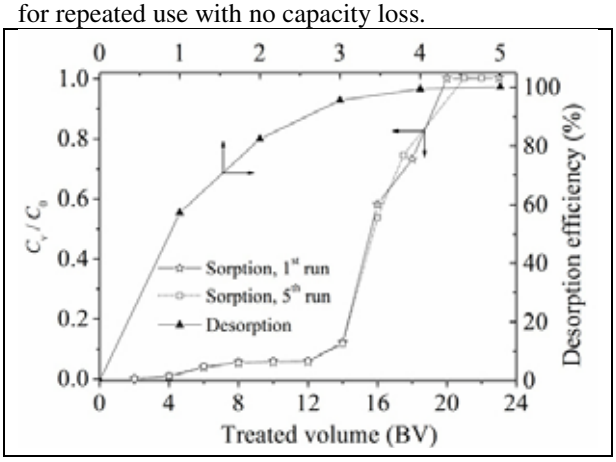

FIGURE 5
Sorption and desorption curves of AH-1 towards SA.

CONCLUSIONS

Adsorption isotherms, kinetics, effects of solution pH and coexisting NaCl, as well as regeneration experiments were carried out through batch method to compare the sorption behavior of SA on three different types of sorbents including granular activated carbon GAC, weakly basic anion-exchanger D301 and aminated hypercrosslinked polymeric resin AH-1. Most favorable adsorption was observed at solution pH around 3, and the polymeric sorbents AH-1 and D301 were more sensitive to the solution pH than GAC. Adsorption isotherms were found to be well fitted by the Langmuir equation, and sorption kinetic data followed the pseudo-second-order rate equation well. Although, coexisting NaCl exerted a negative effect on all the adsorption processes, AH-1 was the one which was least affected. Desorption study showed that both the polymeric sorbents were amenable to a nearly entire regeneration by NaOH solution. Among the tested sorbents, AH-1 possessed considerable adsorption capacity, high adsorption rate, relatively good salt-resistance property and efficient regeneration performance. Column test results further demonstrated that AH-1 was capable of effectively removing SA from industrial wastewater at a high salinity level.

ACKNOWLEDGEMENTS

We greatly acknowledge the financial support by National Natural Science Foundation of China (No. 51578131), Natural Science Foundation of Jiangsu Province, China (No. BK20131287) and the Project Funded by the Priority Academic Program Development of Jiangsu Higher Education Institutions.

REFERENCES

[1] Cleotilde J.R., Juvencio G.M., Nora R.O., Oswaldo R.M., Fortunata S.T. and Héctor P.V. (2015) Steady-state inhibition model for the biodegradation of sulfonated amines in a packed bed reactor. New Biotechnology 32, 379-386.

[2] Prashant B., Arti T., Taruna J. and Sanjeev G. (2011) Application of a novel bacterial consortium for mineralization of sulphonated aromatic amines. Bioresource Technology 102, 765-771.

[3] Wang J., Liu G.F., Lu H., Jin R.F. and Zhou J.T. (2013) Degradation of 1-amino-4-bromoanthraquinone-2-sulfonic acid using combined airlift bioreactor and TiO_2-photocatalytic ozonation. Journal of Chemical Technology and Biotechnology 88, 970-974.

[4] Chen G., Cheng K.Y., Ginige M.P. and Kaksonen A.H. (2012) Aerobic degradation of sulfanilic acid using activated sludge. Water Research 46, 145-151.

[5] Wei M.C., Wang K.S., Lin I.C., Hsiao T.E., Lin

Y.N., Tang C.T., Chen J.C. and Chang S.H. (2012) Rapid regeneration of sulfanilic acid-sorbed activated carbon by microwave with persulfate. Chemical Engineering Journal 193-194, 366-371.

[6] Abdellatif E.G., José A.G., Francesc C., Conchita A., Pere L.C., Rosa M.R. and Enric B. (2012) Electro-Fenton and photoelectro-Fenton degradation of sulfanilic acid using a boron-doped diamond anode and an air diffusion cathode. The Journal of Physical Chemistry A 116, 3404-3412.

[7] Farokhi S.A. and Nandibewoor S.T. (2009) Mechanistic studies of osmium (VIII) catalysed oxidation of sulfanilic acid by hexacyanoferrate (III) in alkaline medium. Catalysis Letters 129, 207-214.

[8] Faria P.C.C., Órfão J.J.M. and Pereira M.F.R. (2008) Catalytic ozonation of sulfonated aromatic compounds in the presence of activated carbon. Applied Catalysis B: Environmental 83, 150-159.

[9] Abdellatif E.G., Sergi G.S., Rosa M.R., Enric B., Mohamed S.E.B. and Ben A.A. (2012) Optimization of the electro-Fenton and solar photoelectro-Fenton treatments of sulfanilic acid solutions using a pre-pilot flow plant by response surface methodology. Journal of Hazardous Materials 221-222, 288-297.

[10] Gan H.M., Shahir S., Ibrahim Z. and Yahya A. (2011) Biodegradation of 4-aminobenzenesulfonate by Ralstonia sp. PBA and Hydrogenophaga sp. PBC isolated from textile wastewater treatment plant. Chemosphere 82, 507-513.

[11] Wang Y.Q., Zhang J.S., Zhou J.T. and Zhang Z.P. (2009) Biodegradation of 4-aminobenzenesulfonate by a novel Pannonibacter sp. W1 isolated from activated sludge. Journal of Hazardous Materials 169, 1163–1167.

[12] Biala S., Chadha P. and Saini H.S. (2014) Biodegradation of 4-aminobenzenesulfonate by indigenous isolate shinella yambaruensis SA1 and its validation by genotoxic analysis. Biotechnology and Bioprocess Engineering 19, 1034-1041.

[13] Faria P.C.C., Órfão J.J.M., Figueiredo J.L. and Pereira M.F.R. (2008) Adsorption of aromatic compounds from the biodegradation of azo dyes on activated carbon. Applied Surface Science 254, 3497-3503.

[14] Radovic L.R., Silva I.F., Ume J.I., Menéndez J.A., Leon y Leon C.A. and Scaroni A.W. (1997) An experimental and theoretical study of the adsorption of aromatics possessing electron-withdrawing and electron-donating functional groups by chemically modified activated carbons. Carbon 35, 1339-1348.

[15] Wang G., Zhou Y., Chai X., Wang X., Liu J. and Deng N. (2010) Adsorption behavior of azo dye Acid Red R in aqueous solution onto β-cyclodextrin-grafted chitosan. Fresenius Environmental Bulletin 19, 811-817.

[16] Kato Y., Machida M. and Tatsumoto H. (2008) Inhibition of nitrobenzene adsorption by water cluster formation at acidic oxygen functional groups on activated carbon. Journal of Colloid and Interface Science 322, 394-398.

Received: **30.10.2016**
Accepted: **06.06.2016**

CORRESPONDING AUTHOR

Sun Yue
School of Civil Engineering
Southeast University
Nanjing 210096 - P.R. CHINA

E-mail: sycyseu@163.com

© by PSP Volume 25 – No. 10/2016, pages 4067-4077 Fresenius Environmental Bulletin

COMBINED TOXIC EFFECTS OF FIVE ESTROGENS ASSESSED BY YEAST ESTROGEN SCREEN ASSAY

Zhaohan Zhang[1,2], Peng Gao[2], Lin Nan[2], Binyu Lu[2], Yujie Feng[2*], Wei Liu[1], Nanqi Ren[2]

1. Heilongjiang River Fisheries Research Institute, Chinese Academy of Fishery Sciences, No 43, Songfa Street, Daoli District, Harbin 150001, China
2. State Key Laboratory of Urban Water Resource and Environment, Harbin Institute of Technology, No73, Huanghe Road, Nangang District, Harbin 150090, China

ABSTRACT

Due to the wide presence of estrogens in aquatic environment and their negative ecological effects on wildlife and humans, they have become a major concern worldwide. However, the joint effect and reaction mechanism are not very clear, especially for various estrogens coexisting as a mixture at environmental levels. This study investigated the single and combined effects of five estrogens at different toxic units and molar ratios by employing the estrogen receptor binding as the endpoint. The results showed that all chemicals studied at single exposure could bind with estrogen receptor with a relative estrogenic effect of E_2>EE_2>DES>E_1>E_3>OP>NP>BPA. The combined effects of binary, ternary, quaternary and quinary mixture were assessed by toxic unit, additive index and mixture toxicity index method. The result indicated that the types and strengths of combined effects were related to kinds and contents of chemicals in the mixture. Most estrogens mixture in this study exhibited a synergic effect. However, for EE_2-E_1 mixture, it exhibited partial addition effect at EE_2/E_1 toxic unit ratio of 1:1 and 1:4, while antagonistic effect at ratio of 4:1. We also found that the strength of synergic effect did not always increase with estrogen numbers in the mixture. The present study will provide useful information and reference for the ecological effect research and risk assessment of estrogens in actual aquatic environment.

KEYWORDS:

Estrogen; Combined exposure; Toxic unit; Yeast estrogen screen assay; Synergic effect

INTRODUCTION

Estrogens are essential hormones for all vertebrates, and mainly used for adjusting the endocrine system, including natural and synthetic estrogens. Natural estrogens, such as estrone (E_1), 17β-estradiol (E_2) and estriol (E_3) are mainly excreted by terrestrial and aquatic vertebrates through urine and feces in either free forms or conjugated with glucuronide or sulfate groups [1,2]. Synthetic xenoestrogens, including 17α-ethinylestradiol (EE_2) and diethylstilbestrol (DES), are primarily used in the contraceptive pill and hormone replacement therapy [3]. There are a variety of ways for estrogens entering aquatic environments, such as runoff, infiltration and sewage discharges, etc [4]. However, raw and sewage discharges are considered as the primary source of estrogens to natural waters [5,6]. Estrogens have extensive distribution in aquatic environments and have been detected in sewage influents and effluents, rivers, lakes, oceans, estuaries, groundwater, septic system discharges and even drinking water, with the concentrations from low ng/L to as high as μg/L[7,8]. Although estrogen concentration in aquatic environment was very low, due to their high estrogenicity, these chemicals could cause serious environmental problems and pose threats to ecological security and human health. Previous researches showed that estrogen in sub-nanogram per liter could disrupt the normal growth and development of aquatic organisms, decrease the sperm reproduction in humans, and cause the feminization of male fish [9-11].

Various methods are developed to investigate the environmental effects of estrogens, including *in vivo* assays such as uterotrophic assay, vitellogenin induction assay and pubertal onset assay, and *in vitro* assays such as MCF-7 breast cancer cell

proliferation assay and yeast estrogen screen assay [12-16]. Although yeast estrogen screen assay cannot fully predict the adverse effects of pollutants on human and wildlife, due to the advantages of simple operation, rapid detection and high sensitivity, it has been developed quickly and widely used in environmental engineering field, including screening estrogenic active compounds, pollution levels analysis of various water samples, toxicity assessment, etc [17-19]. However, less research is conducted with this method to study the combined pollution of estrogens and its action mechanisms.

There are always several estrogens coexisting in the real aquatic environment. It is important for ecological security to clarify how these estrogens react with each other and what the combined action effect is. Up to now, several indexes, such as, cell proliferation, vitellogenin induction and estrogenic receptor activation are used as endpoints to assess the combined effect of estrogens. Suzuki et al assessed the binary effect of natural and synthetic estrogen including E_2, E_1, BPA, butyl benzylphthalate, endosulfan, methoxychlor and pentachlorophenol by E-SCREEN assay, and found mixture of E_2 and BPA exhibited apparent synergistic effect, while other eight binary mixtures gave additive, antagonistic or weakly synergistic effects [20]. Sun et al took the plasma vitellogenin (VTG) induction in male adult Japanese medaka as the endpoint, and found that E_2, NP and BPA had a common mechanism for inducing VTG synthesis and no significant interactions was observed in binary mixture [21]. Li et al found a relative binding order of BPA>OP>NP>DCP by yeast estrogen screen assay, and all the mixture exhibited an antagonistic effect [22]. Rajapakse et al found that mixtures involving 8 and 12 estrogenic chemicals assessed by yeast estrogen screen agreed well with concentration addition effect [23]. However, present studies usually focus on the joint action of two chemicals in the mixture. Few reports are about the combined action effect of more than three estrogenic chemicals, and the influence of estrogen ratios in mixture on action effect are also not very clear, especially for yeast two-hybrid estrogen screen assay.

The objectives of this study were summarized as follows: (1) to investigate the single estrogenic effect of natural and synthetic estrogens normally detected in aquatic environment; (2) to study the combined effect of binary estrogen mixture and the role of estrogen content ratio; (3) to assess the joint effect of ternary, quaternary and quinary mixture system, and develop a feasible assessment method for combined effect, providing the useful information and reference for estrogenic ecological effect study in actual environment.

MATERIALS AND METHODS

Reagents and chemicals. Target estrogens, such as E_1, E_2, EE_2, E_3, DES, BPA, NP and OP, were all of chromatographic pure (>99%) and purchased from Sigma, China. Due to the lower water solubility of studied estrogens, individual stock solutions (1.0 mmol/L) of each estrogens were prepared in dimethyl sulfoxide (DMSO) and stored in amber glass vials at −20 °C until using, which could remain stable for at least three months. DMSO, yeast nitrogen base (YNB) and various kinds of amino acid used in yeast estrogen screen were ultra-pure grade and obtained from Difco Company. Other chemicals and solvents were all of analytical reagent grade from Benchmark Regent Ltd, China. High-purity water was used to prepare yeast culture solution, which was produced by a MilliQ Plus system (Millipore, USA).

YES assay procedure. Recombinant human estrogen receptor gene yeast cells were kindly provided by Dr. Zijian Wang at Research Center for Eco-Environmental Sciences, China. The yeast assay was carried out as described by Ma et al with some modifications [24]. Yeast strains were grown in selective solution (SC) prepared according to the procedures of Gaido et al overnight at 30 °C on a shaker (130 rpm) [25], which was diluted to the OD_{600nm} of 0.30 with the SC medium before using. All tests were conducted in triplicates and each plate contained a positive control (E_2) and a negative control (DMSO). 5 μL of serial dilutions of single or mixture estrogens were added into 995μL of medium with 5×10^3 yeast cell/mL to form the test culture. 200 μL of test cultures were transferred into the 96-well plate and incubated at 30 °C with vigorous orbital shaking (800 rpm) for 2 h. Then, the cell density in the culture was measured at 595 nm with an ELIASA reader (BIO-TEK EL808). After throwing away 150 μL test culture, 120 μL Z-buffer and 20μL chloroform were added into each well, and the plate was carefully mixed 15 min at 1200 rpm. 40 μL o-nitrophenyl-β-D- galactopyranoside (ONPG, 13.3 mmol/L, dissolved in Z-buffer) was added into each

well to initiate the enzyme reaction. After incubating at 30 ºC for 60 min, 100 μL Na_2CO_3 (1.0 mol/L) were injected into the plate which was mixed at 800 rpm for 10 min to terminate the reactions. Then 200 μL of the supernatant was transferred into a new 96-well plate and the absorbance at 420 nm was determined by the ELIASA reader. The β-galactosidase activity was calculated according to the following equation, and expressed as the mean values and standard deviations of the triplicate results:

$$U = \frac{OD_{420} - OD_{420}^{'}}{t \times V \times OD_{595}} \quad (1)$$

Where U was β-galactosidase activity; t was the enzyme reaction time (min) after adding ONPG; V was the volume of test culture (mL); OD_{595} was the cell density of test culture; OD_{420} and $OD_{420}^{'}$ were the absorbance of the enzyme reaction supernatant of the sample and blank, respectively.

The dose-response curve of test sample was fitted well by four-parameter logistic model with the sigmaplot software:

$$U = \frac{U_{\max} - U_{\min}}{1 + (EC_{50} / c)^{\gamma}} + U_{\min} \quad (2)$$

Where c was the concentration of test sample; EC_{50} was the sample concentration producing a half of maximum β-galactosidase activity; γ was the slope of regression curve at the mid-point; U_{max} and U_{min} were the maximum and background values of β-galactosidase activity, respectively.

The 17β-estradiol equivalents (EEQs) of other compounds could be described with the following equation:

$$EEQ = \frac{EC_{50,E_2}}{EC_{50,comp}} \quad (3)$$

Where $EC_{50,E2}$ was the EC_{50} value of E_2; $EC_{50,comp}$ was the EC_{50} value of other tested compounds.

Experimental design. According to the pilot trial, the concentrations of eight estrogens were set in the range of 0.001-2 nmol/L (E_2), 0.001-10 nmol/L (EE_2), 0.001-50 nmol/L (E_1), 0.0001-30 μmol/L (E_3), 0.001-5 nmol/L (DES), 0.01-100 μmol/L (BPA), 0.001-50 μmol/L (NP and OP), which contained at least eight concentration gradients. The EC_{50} value represented the estrogenicity could be obtained from the dose-response curve. Based on the single action effect, five estrogens (E_2, EE_2, E_1, E_3 and DES) with higher estrogenicity were selected to conduct the binary and multivariate combination effect experiments. In the binary experiments, each mixture comprised of five groups at different molar ratios including 1:4, 2:3, 3:2, 4:1 and 1:1, and three groups at different toxic unit ratios containing 1:4, 4:1 and 1:1, respectively. The multivariate experiments including ternary, quaternary and quinary mixture were conducted at the equal toxic unit ratio. The mixture was prepared at higher concentrations according to the above designed ratios, then diluted to at least eight concentration levels, which could maintain the component ratio constant in each diluted sample. The EC_{50} value of each component could be calculated from the dose-response curve of the mixture, which was further used to assess the combined effect.

Assessment methods for combined effects. The combined effects of mixture generally involve synergistic (larger than the sum of individual effects), antagonistic (less than the sum of individual effects), and additive (equal to the sum of individual effects) toxicity effects [26]. It also contains partial additive and irrelevant toxicity effects (the same as the strongest individual effect) for mixture species larger than two. Three methods including toxic unit (TU), additive index (AI) and mixture toxicity index (MTI) methods were selected to quantitatively analyze the joint action effects of binary and multiple estrogen mixture.

Toxic unit was firstly proposed by Spargue, who thought that the relative toxicological strength of each mixture component could be expressed by scaling the individual concentrations (C_i) of the single components for their respective toxicity [27]. TU was defined as:

$$TU_i = \frac{c_i}{EC_{50_i}} \quad (4)$$

The total toxicological effect of an estrogen mixture could be calculated by summing up the TUs of the individual mixture components i,

$$S = \sum_{i=1}^{n} TU_i = \sum_{i=1}^{n} \frac{c_i}{EC_{50_i}} \quad (5)$$

$$S_0 = \frac{S}{\max(TU_i)} \quad (6)$$

Where c_i was the concentration of estrogen i in the mixture; EC_{50i} was the EC_{50} value of estrogen

TABLE 1
Combined action effects assessed by TU, AI and MTI methods

Action effects	Toxic unit method	Additive index method	Mixture toxicity index
Synergism	S <1	AI>0	MTI>1
Addition	S =1	AI=0	MTI =1
Partial addition	S_0>S>1	-	1>MTI >0
Irrelevant action	S =S_0	-	MTI =0
Antagonism	S >S_0	AI<0	MTI <0

i; TU_i was the toxic unit of estrogen i in the mixture; S was the total toxic unit of the mixture; max(TU_i) was the maximum toxic unit value in mixture. S and S_0 could be used to determine the type of combined effect caused by the mixture, as shown in Table 1.

Based on the concept of toxic unit, Marking defined the additive index as follows [28]:

When S ≤1, $AI = 1/S - 1.0$ (7)

When S >1, $AI = 1.0 - S$ (8)

Where S was the sum of the toxic unit and could be calculated by equation (5); AI was the additive index. The relationship between combined effect type and AI was also given in Table 1.

The MTI was a method for assessing the combined effect of multiple compounds, which was firstly reported by Konemann [29], and could be described as the following equation:

$$MTI = 1 - \frac{LgS}{LgS_0} \quad (9)$$

Where S and S_0 were described as above and could be calculated using Equation (5) and (6); MTI was the toxicity index of the mixture.

RESULTS AND DISCUSSION

Single estrogenic effect. Fig 1 shows the concentration-response data for single estrogen and their estimated regression curves. There was significant S type correlation between the β-galactosidase activity (Y axis) and the test estrogen concentration. It indicated that all test estrogens could express the reporter gene by mediating of estrogen receptor in a certain concentration range, which led to the increase of β-galactosidase activity with the increase of estrogen dose. Maximum β-galactosidase activity and γ represented the binding ability and sensitivity of compound and estrogen receptor. E_3 and OP had the strongest and weakest binding ability with estrogen receptor in our test, with the maximum β-galactosidase activity of 160.9 and 38.6 u, respectively. The γ value had the order of E_3>E_1> DES>E_2>EE_2>BPA>OP>NP, indicating that this method was most sensitive for E_3.

The corresponding best-fit model parameters are listed in Table 2. EC_{50} value is always used to describe the chemical potency. Natural steroid E_2 was the most potent estrogen tested, with an EC_{50} of 18.25 ng/L, which was 1.3 times more potent than synthetic EE_2, with EC_{50} of 23.71 ng/L. E_1, E_3 and DES were 10.2, 740 and 16.7 times less potent than E_2, with EC_{50} values of 0.329, 13.5 and 0.183 μg/L, respectively. Three xenoestrogens, including BPA, NP and OP, were the least potent chemical tested, with an EC_{50} of 4.51, 0.164 and 0.138 mg/L, which were 2.48×10^5, 9.01×10^3 and 7.58×10^3 times less potent than E_2. Leroy et al found EC_{50} of E_2, EE_2 and DES with YES assay was 57, 86 and 51ng/L, while that of NP was 64 mg/L, which was 3.1, 3.6, 0.28 and 464 times in this experiment, respectively[30]. Elisabete et al used a breast cancer cell proliferation assay to assess the estrogenic activity of chemical, and found that EC_{50} of E_2, EE_2, E_1, E_3, DES and BPA was 6.5, 4.5, 75.7, 147.1, 42.9 and 1.39×10^5 ng/L, which was much lower and only 0.36, 0.19, 0.23, 0.01, 0.23 and 0.03 times in our experiments[31]. The difference might be caused by test method, exposure microorganism and conditions, etc. However, the estrogenic activity of test compounds with different methods was almost in the same order.

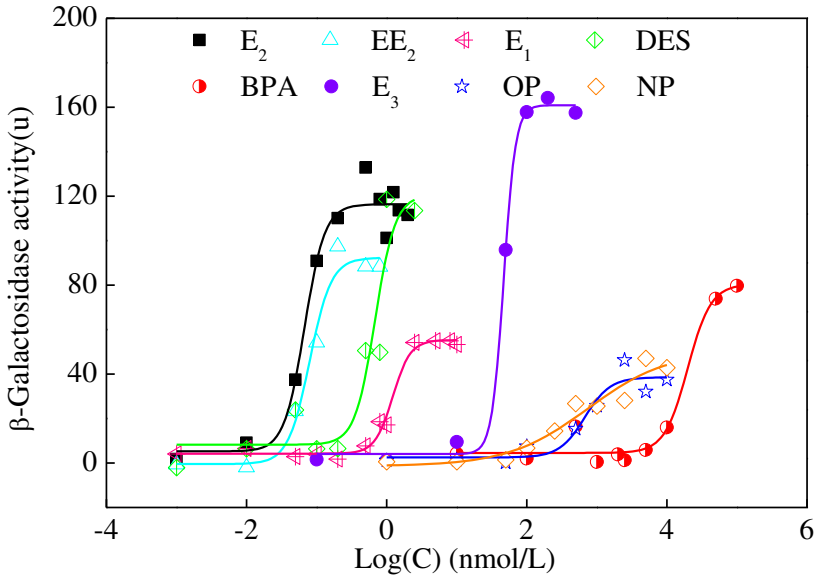

FIGURE 1
Dose-response curves of eight estrogens in single action

TABLE 2
Parameters of eight estrogens in single action obtained from four-parameter logistic model

Compounds	U_{max}	U_{min}	γ	EC_{50}		R^2	EEQ
				nmol/L	ng/L		
E_2	116.4	5.2	-3.00	0.067	18.25	0.973	1
EE_2	92.3	4.5	-2.85	0.080	23.71	0.981	0.77
E_1	55.3	4.2	-3.43	1.217	329.08	0.989	0.06
E_3	160.9	4.0	-5.14	46.8	1.35×10^{4}	0.998	1.35×10^{-3}
DES	120.5	8.2	-3.04	0.683	183.28	0.943	0.10
NP	49.0	1.6	-0.83	746.4	1.64×10^{5}	0.942	1.11×10^{-4}
OP	38.6	2.5	-2.40	672.2	1.38×10^{5}	0.933	1.32×10^{-4}
BPA	80.4	4.5	-2.62	19771.8	4.51×10^{6}	0.979	4.04×10^{-6}

Combined action of two estrogens at different molar ratio. E_1, E_2 and EE_2 were selected to conduct the exposure experiments of binary estrogens at different molar ratios, and EC_{50} of each estrogen were calculated from the dose-effect curves, as shown in Table 3. The EC_{50} in binary mixture was all much smaller than that in single reaction. For example, in mixture of E_1 and EE_2, EC_{50} was in the range of 0.0086-0.1128 nM for E_1 and 0.0282-0.059 nM for EE_2, which were only 0.007-0.093 and 0.35-0.74 times of that in single reaction, respectively. In the other two mixtures, the similar results were obtained. It indicated that lower concentration of estrogen was needed in mixture to obtain the same estrogenic effect.

Joint action effects of binary estrogen at different molar ratio were analyzed by three methods, and the results were showed in Table 3. For toxic unit method, the total toxic unit (S) in E_1-E_2, E_1-EE_2 and E_2-EE_2 mixture were in the range of 0.147-1.041, 0.436-0.771 and 0.31-1.349, respectively, indicating that three mixtures at most molar ratios exhibited synergic effect. Meanwhile, the synergic effect was stronger at lower S value. It was obtained that 3:2, 2:3 and 4:1 of E_1-E_2, E_1-EE_2 and E_2-EE_2 mixture produced the strongest synergism effect in the five studied ratios, respectively. However, for 1:1 of E_1-E_2 and 3:2 of E_2-EE_2 mixture, the S value was 1.041 and 1.349, which were above 1.0 and lower than S_0, exhibiting the partial additive effect. Therefore, reaction effect

TABLE 3
Combined action of binary mixture of E1, E2 and EE2 at different molar ratio assessed by TU, AI and MTI methods

Compounds	Ratio	EC_{50}(nmol/L)		TU method			AI method		MTI method	
		M_1	M_2	S	S_0	Effect	AI	Effect	MTI	Effect
E_1+E_2	1:4	0.082	0.0205	0.373	1.22	SYN	1.678	SYN	5.95	SYN
	2:3	0.057	0.038	0.614	1.083	SYN	0.629	SYN	7.147	SYN
	1:1	0.045	0.045	1.041	1.055	PAD	0.411	SYN	7.427	SYN
	3:2	0.0063	0.0095	0.147	1.037	SYN	5.804	SYN	54.48	SYN
	4:1	0.0102	0.0406	0.614	1.014	SYN	0.628	SYN	36.47	SYN
E_1+EE_2	1:4	0.1128	0.0282	0.445	1.263	SYN	1.246	SYN	4.467	SYN
	2:3	0.0171	0.0341	0.440	1.033	SYN	1.271	SYN	26.29	SYN
	1:1	0.0401	0.0401	0.534	1.066	SYN	0.872	SYN	10.85	SYN
	3:2	0.0394	0.0591	0.771	1.044	SYN	0.299	SYN	7.06	SYN
	4:1	0.0086	0.0343	0.436	1.016	SYN	1.295	SYN	51.81	SYN
E_2+EE_2	1:4	0.0067	0.0268	0.435	1.299	SYN	1.299	SYN	4.187	SYN
	2:3	0.0185	0.0278	0.624	1.795	SYN	0.604	SYN	1.808	SYN
	1:1	0.0115	0.0115	0.315	1.838	SYN	2.171	SYN	2.897	SYN
	3:2	0.058	0.0387	1.349	1.559	PAD	-0.349	ANT	0.325	PAD
	4:1	0.0172	0.0043	0.31	1.209	SYN	2.221	SYN	7.153	SYN

of binary estrogen was related to the types and proportions in the mixture. For additive index method, except for 3:2 of E_2-EE_2 mixture, the AI values for E_1-E_2, E_1-EE_2 and E_2-EE_2 mixture were in the range of 0.411-5.804, 0.299-1.295 and 0.604-2.221, respectively, and were all above 0, indicating that they exhibited synergic effect, which had the same results with the toxic unit method. However, the calculated AI value for 3:2 of E_2-EE_2 mixture was -0.349, indicating that it exhibited antagonism effect. For MTI method, the MTI value for most mixtures except 3:2 of E_2-EE_2 were all above 1.0, exhibiting synergic effect, which obtained the same action effect with the former two methods. MTI value for 3:2 of E_2-EE_2 mixture was 0.325, locating in range of 0-1.0, and exhibited partial additive effect, which was the same as toxic unit method. For most ratios of binary estrogen mixture, the three methods obtained the same action effects, indicating that it was feasible to assess the action effect of estrogen mixtures with these methods.

Combined action of two estrogens at different toxic unit. Five estrogens with higher activity were selected to study the binary action effect at different toxic unit ratios, and EC_{50} of each estrogen was calculated from the dose-effect curves, as shown in Table 4. EC_{50} of each estrogen in all ten group mixtures was smaller than that in single exposure at the three studied toxic unit ratios. For example, in E_2-EE_2 mixture, EC_{50} of E_2 and EE_2 was in the range of 0.0125-0.0245 nM and 0.0073-0.0593 nM, which were only 0.19-0.37 and 0.09-0.74 times of that in single action. While EC_{50} of E_2 and E_1 in binary mixture were only 0.05-0.59 and 0.15-0.61 times of that in single exposure. The other binary mixtures also had the same phenomenon, indicating that it needed smaller estrogen in binary exposure to produce the same action effect with the single one.

Table 4 also listed the assessment results of three methods. Except for EE_2-E_1 mixture, the other binary mixture all produced a synergic effect, indicating that coexisting of different type estrogen might produce a much larger estrogenic effect than its single action. Moreover, different ratio of the binary mixture also influenced the strength of action effect. For example, in E_2-EE_2 mixture, the strength of synergic effect increased with E_2 content, indicating that the estrogen with higher estrogenicity might contribute more for the combined effect. The E_2-DES, E_1-DES and E_3-DES mixture also produced the same trend with E_2-EE_2 mixture. However, in other mixture (E_2-E_1, E_2-E_3, EE_2-DES and E_1-E_3), different results were

TABLE 4
Combined action of binary estrogen mixture at different toxic unit ratio assessed by TU, AI and MTI methods

Compounds	Ratio	EC_{50} (nmol/L)		TU method			AI method		MTI method	
		M_1	M_2	S	S_0	Effect	AI	Effect	MTI	Effect
E_2+EE_2	1:1	0.0245	0.0293	0.732	2.0	SYN	0.366	SYN	1.45	SYN
	1:4	0.0125	0.0592	0.927	1.253	SYN	0.079	ADD	1.336	SYN
	4:1	0.0244	0.0073	0.455	1.25	SYN	0.545	SYN	4.529	SYN
E_2+E_1	1:1	0.0284	0.5159	0.848	2.0	SYN	0.180	SYN	1.238	SYN
	1:4	0.0034	0.7431	0.661	1.082	SYN	0.512	SYN	6.263	SYN
	4:1	0.0397	0.1802	0.741	1.25	SYN	0.259	SYN	2.345	SYN
E_2+E_3	1:1	0.0255	17.832	0.762	2.0	SYN	0.313	SYN	1.392	SYN
	1:4	0.0078	21.553	0.577	1.252	SYN	0.733	SYN	3.45	SYN
	4:1	0.0417	7.288	0.778	1.251	SYN	0.222	SYN	2.122	SYN
E_2+DES	1:1	0.0248	0.2534	0.741	1.997	SYN	0.349	SYN	1.433	SYN
	1:4	0.0038	0.1531	0.281	1.254	SYN	2.560	SYN	6.6	SYN
	4:1	0.0045	0.0114	0.084	1.254	SYN	0.916	SYN	11.95	SYN
EE_2+E_1	1:1	0.0494	0.7501	1.234	1.997	PAD	-0.234	ANT	0.696	PAD
	1:4	0.0232	0.9449	1.066	1.374	PAD	-0.066	ANT	0.799	PAD
	4:1	0.0936	0.2388	1.366	1.168	ANT	-0.366	ANT	-1.01	ANT
EE_2+E_3	1:1	0.0098	5.7399	0.245	1.992	SYN	3.079	SYN	3.041	SYN
	1:4	0.0079	18.426	0.493	1.251	SYN	0.508	SYN	4.155	SYN
	4:1	0.0501	7.324	0.783	1.251	SYN	0.278	SYN	2.093	SYN
EE_2+DES	1:1	0.0234	0.2001	0.585	1.997	SYN	0.708	SYN	1.775	SYN
	1:4	0.0030	0.1037	0.189	1.243	SYN	0.811	SYN	8.647	SYN
	4:1	0.0139	0.0297	0.217	1.247	SYN	3.603	SYN	7.918	SYN
E_1+E_3	1:1	0.3606	13.867	0.593	2.0	SYN	0.687	SYN	1.752	SYN
	1:4	0.0627	9.646	0.258	1.252	SYN	0.742	SYN	7.019	SYN
	4:1	0.7621	7.328	0.783	1.251	SYN	0.277	SYN	2.093	SYN
E_1+DES	1:1	0.2362	0.133	0.388	2.0	SYN	1.576	SYN	2.366	SYN
	1:4	0.0761	0.1707	0.312	1.248	SYN	0.688	SYN	6.257	SYN
	4:1	0.5948	0.0834	0.611	1.249	SYN	0.637	SYN	3.212	SYN
E_3+DES	1:1	5.2338	0.0776	0.227	1.991	SYN	3.398	SYN	3.153	SYN
	1:4	1.9552	0.1137	0.208	1.253	SYN	0.792	SYN	7.962	SYN
	4:1	17.859	0.0651	0.477	1.249	SYN	1.097	SYN	4.333	SYN

obtained. Therefore, the type and strength of combined effects for binary mixture were related to the type, content and estrogenic potencies of coexisting estrogens in mixture. Previous studies also reported that some lower estrogenic compounds might produce synergic effect when coexisted with others. Arnold et al found that combinations of two weak environmental estrogens (such as dieldrin, endosulfan or toxaphene) produced 1000 times potency in hER-mediated transactivation as that in any chemical alone [32]. Sumpter et al also found that estrogenic potency of BPA, NP and DDT mixture detected by vitellogenin analysis was evidently enhanced by comparing with the single reaction [33]. Up to now, the mechanism of synergism effect is not very clearly. Synergism effect not only strengthened the binding ability of estrogen and receptor, but also improved the biological reaction activity mediated by estrogen. Due to estrogenic effect was produced by the binding of estrogen and receptor, synergic effect in mixture system might be leaded by competitively

inhibiting the binding of estrogen and some receptors[34].

For EE_2-E_1 mixture, TU and MTI method obtained the same results. It exhibited partially additive effect at EE_2/E_1 toxic unit ratio of 1:1 and 1:4, while antagonism effect at ratio of 4:1. However, AI method obtained that EE_2-E_1 mixture exhibited antagonism effect for all three toxic unit ratios, which might be caused by that AI method did not contain the partial addition and irrelevant action effect. The results also indicated that the estrogen content could influence the action effect in binary mixture. Antagonism effect might be caused by the different affinity of EE_2 and E_1 with estrogen receptor. When they coexisted on the surface of cells or active sites in metabolic system, they might compete for estrogen receptor and less potent E_1 inhibited the binding of EE_2 with receptor, which reduced the activity expression of mixture.

Combined action of multiple estrogens. E_2, EE_2, E_1, E_3 and DES were selected to investigate the combined action effect of ternary, quaternary and quinary estrogen mixtures at same molar ratio, and the results were shown in Table 5. The calculated EC_{50} of each estrogen in mixture were much smaller than that in single action. For example, in E_2-EE_2-E_1 mixture, EC_{50} of E_2, EE_2 and E_1 were 0.022, 0.0262 and 0.398 nM, which were approximately 1/3 of that in single system. While in E_2-EE_2-E_1-E_3 mixture, EC_{50} of four estrogens were 0.0098, 0.0117, 0.1774 and 6.815 nM, which was only 0.15 times of that in single system. The other ternary and quaternary mixture all had the same phenomena. For the only one quinary system, EC_{50} of each estrogen in mixture was only 0.122 times of that in single system, indicating that it needed much less estrogen in this mixture to produce the same estrogenic effect.

The reaction effects of multiple estrogens assessed by three methods were all obtained as synergic effect, as listed in Table 5, indicating that the estrogenic potency was strengthened when multiple estrogens coexisted in one system. In all ternary mixture, the total S was in the range of 0.334-0.983, indicating that E_2-EE_2-E_1 and E_2-EE_2-DES system produced the weakest and strongest synergic effect, respectively. While the total S of quaternary mixture ranged from 0.303 to 0.594, which was much smaller than that in ternary

TABLE 5
Joint action of multiple estrogen mixtures at same molar ratio assessed by TU, AI and MIT methods

Compounds	EC_{50} (nmol/L)					TU method			AI method		MIT method	
	M_1	M_2	M_3	M_4	M_5	S	S_0	Effect	AI	Effect	MIT	Effect
E_2+EE_2+E_1	0.0220	0.0262	0.398	-	-	0.983	3	SYN	0.017	SYN	1.016	SYN
E_2+EE_2+E_3	0.0170	0.0202	11.815	-	-	0.758	3	SYN	0.319	SYN	1.252	SYN
E_2+EE_2+DES	0.0075	0.0089	0.0761	-	-	0.334	3	SYN	1.994	SYN	1.998	SYN
E_2+E_1+E_3	0.0091	0.1655	6.354	-	-	0.408	3	SYN	1.451	SYN	1.816	SYN
E_2+E_1+DES	0.0122	0.2225	0.1251	-	-	0.549	3	SYN	0.821	SYN	1.546	SYN
E_2+E_3+DES	0.0177	12.346	0.18	-	-	0.791	3	SYN	0.264	SYN	1.213	SYN
EE_2+ E_1+E_3	0.0193	0.2938	11.283	-	-	0.724	3	SYN	0.381	SYN	1.294	SYN
EE_2+ E_1+DES	0.0160	0.2432	0.1367	-	-	0.600	3	SYN	0.667	SYN	1.465	SYN
EE_2+ E_3+DES	0.0197	11.516	0.1679	-	-	0.738	3	SYN	0.355	SYN	1.277	SYN
E_1+ E_3+DES	0.2518	9.6838	01414	-	-	0.621	3	SYN	0.61	SYN	1.434	SYN
E_2+EE_2+E_1+E_3	0.0098	0.0117	0.1774	6.8148	-	0.583	4	SYN	0.715	SYN	1.389	SYN
E_2+EE_2+E_1+DES	0.0099	0.0119	0.1804	0.1014	-	0.594	4	SYN	0.684	SYN	1.376	SYN
EE_2+ E_1+E_3+DES	0.0061	0.0922	3.5392	0.0518	-	0.303	4	SYN	2.3	SYN	1.861	SYN
E_2+E_1+E_3+DES	0.0082	0.1482	5.6923	0.0833	-	0.487	4	SYN	1.053	SYN	1.519	SYN
E_2+EE_2+E_3+DES	0.0095	0.0113	6.5958	0.0965	-	0.565	4	SYN	0.77	SYN	1.411	SYN
E_2+EE_2+E_1+ E_3+DES	0.0082	0.0098	0.1490	5.7231	0.084	0.612	5	SYN	0.634	SYN	1.305	SYN

system, indicating that the synergic effect was much stronger in quaternary system. The total S for quinary mixture was 0.612, indicating that its synergic effect was weaker than any group of quaternary mixture. It also suggested that the strength of synergic effect was changed with the type and number of estrogens in mixture. Warne et al reported that the toxicity of mixture increased with the number of compounds, which was proved by the E_2-EE_2-E_1 and E_2-EE_2-E_1-E_3 mixture [36]. While Thomulka et al found that the toxicity of mixture was not only related to the dose and composition of mixture, also with tested microorganism, which was not always increasing with compounds number [36].

CONCLUSIONS

Yeast estrogen screen assay was established and used to assess the single and combined effects of estrogens normally detected in aquatic environment. Eight studied chemicals could evidently bind with estrogen receptor in yeast cell and their estrogenic effect in single exposure were found in the order of E_2>EE_2> DES>E_1>E_3>OP>NP>BPA. Most binary mixture at different toxic unit ratios and molar ratios all exhibited synergic effect, and its strength was related to estrogen kinds and contents in the mixture. However, in EE_2-E_1 mixture, it exhibited partial addition effect at toxic unit ratio of 1:1 and 1:4, while antagonism effect at ratio of 4:1. For ternary, quaternary and quinary mixtures, they all produced synergic effects at same molar ratio and their strengths were found not always increasing with estrogen numbers of mixture. For most cases, same effects were obtained by the methods of toxic unit, additive index and mixture toxicity index, which were proved as effective methods for combined effects assessment.

ACKNOWLEDGEMENT

This research was supported by National Natural Science Foundation of China (51308150, 51125033), Specialized Research Fund for the Doctoral Program of Higher Education (20132302120072), State Key Laboratory of Urban Water Resource and Environment, Harbin Institute of Technology (2016TS05), China Postdoctoral Science Foundation funded project (2013M541396), Basic Research Operating expenses Program of Heilongjiang River Fisheries Research Institute.

REFERENCES

[1] Hutchins S. R., White M. V., Hudson F. M. and Fine D. D. (2007) Analysis of lagoon samples from different concentrated animal feeding operations for estrogens and estrogen conjugates. Environ Sci Technol 41, 738-744.

[2] Hartel A., Pertl C., Wierer M. and Meyer H. H. D. (2004) Endocrine disrupting chemicals - Assaying androgenicity by quantitating the induced expression levels in two different prostate cell lines: Human prostate carcinoma cells 22RV1 and normal primary porcine epithelial cells. Fresen Environ Bull 13, 1129-1138.

[3] Koh Y. K. K., Chiu T. Y., Boobis A., Cartmell E., Scrimshaw M. D. and Lester J. N. (2008) Treatment and removal strategies for estrogens from wastewater. Environ Technol 29, 245-267.

[4] Khanal S. K., Xie B., Thompson M. L., Sung S. W., Ong S. K. and Van Leeuwen J. (2006) Fate, transport, and biodegradation of natural estrogens in the environment and engineered systems. Environ Sci Technol 40, 6537-6546.

[5] Griffith D. R., Soule M. C. K., Matsufuji H., Eglinton T. I., Kujawinski E. B. and Gschwend P. M. (2014) Measuring Free, Conjugated, and Halogenated Estrogens in Secondary Treated Wastewater Effluent. Environ Sci Technol 48, 2569-2578.

[6] Yang X. L., Li G. P., Chen M., Shen D. Q., Fu D. F. and Song H. L. (2012) Occurrence and removal of steroid estrogens in three sewage treatment plants in nanjing, china. Fresen Environ Bull 21, 3836-3841.

[7] Soto A. M., Calabro J. M., Prechtl N. V., Yau A. Y., Orlando E. F., Daxenberger A., Kolok A. S., Guillette L. J., le Bizec B., Lange I. G. and Sonnenschein C. (2004) Androgenic and estrogenic activity in water bodies receiving

cattle feedlot effluent in eastern Nebraska, USA. Environ Health Persp 112, 346-352.

[8] Huang B., Wang B., Ren D., Jin W., Liu J. L., Peng J. H. and Pan X. J. (2013) Occurrence, removal and bioaccumulation of steroid estrogens in Dianchi Lake catchment, China. Environ Int 59, 262-273.

[9] Jobling S., Casey D., Rodgers-Gray T., Oehlmann J., Schulte-Oehlmann U., Pawlowski S., Baunbeck T., Turner A. P. and Tyler C. R. (2003) Comparative responses of molluscs and fish to environmental estrogens and an estrogenic effluent. Aquat Toxicol 65, 205-220.

[10] Caldwell D. J., Mastrocco F., Hutchinson T. H., Lange R., Heijerick D., Janssen C., Anderson P. D. and Sumpter J. P. (2008) Derivation of an aquatic predicted no-effect concentration for the synthetic hormone, 17 alpha-ethinyl estradiol. Environ Sci Technol 42, 7046-7054.

[11] Turker H. and Takemura A. (2013) Priming effects of xenoestrogen treatments on vitellogenin synthesis under in vitro and in vivo conditions in the mozambique tilapia. Fresen Environ Bull 22, 3236-3242.

[12] Barlas N., Ozer S. and Karabulut G. (2014) The estrogenic effects of apigenin, phloretin and myricetin based on uterotrophic assay in immature Wistar albino rats. Toxicol Lett 226, 35-42.

[13] Korner W., Hanf V., Schuller W., Kempter C., Metzger J. and Hagenmaier H. (1999) Development of a sensitive E-screen assay for quantitative analysis of estrogenic activity in municipal sewage plant effluents. Sci Total Environ 225, 33-48.

[14] Zacharewski T. (1997) In vitro bioassays for assessing estrogenic substances. Environ Sci Technol 31, 613-623.

[15] Balsiger H. A., de la Torre R., Lee W. Y. and Cox M. B. (2010) A four-hour yeast bioassay for the direct measure of estrogenic activity in wastewater without sample extraction, concentration, or sterilization. Sci Total Environ 408, 1422-1429.

[16] Kaptaner B., Kankaya E. and Unal G. (2009) Effects of 17 alpha-ethynylestradiol on hepatosomatic index, plasma vitellogenin levels and liver glutathione-s-transferase activity in lake van fish (chalcalburnus tarichi pallas, 1811). Fresen Environ Bull 18, 2366-2372.

[17] Inoue D., Nakama K., Sawada K., Watanabe T., Matsui H., Sei K., Nakanishi T. and Ike M. (2011) Screening of agonistic activities against four nuclear receptors in wastewater treatment plants in Japan using a yeast two-hybrid assay. J Environ Sci-China 23, 125-132.

[18] Bistan M., Podgorelec M., Logar R. M. and Tisler T. (2012) Yeast Estrogen Screen Assay as a Tool for Detecting Estrogenic Activity in Water Bodies. Food Technol Biotech 50, 427-433.

[19] Citulski J. and Farahbakhsh K. (2012) Overcoming the toxicity effects of municipal wastewater sludge and biosolid extracts in the Yeast Estrogen Screen (YES) assay. Chemosphere 87, 498-503.

[20] Suzuki T., Ide K. and Ishida M. (2001) Response of MCF-7 human breast cancer cells to some binary mixtures of oestrogenic compounds in-vitro. J Pharm Pharmacol 53, 1549-1554.

[21] Sun L. W., Zha J. M. and Wang Z. J. (2009) Interactions between estrogenic chemicals in binary mixtures investigated using vitellogenin induction and factorial analysis. Chemosphere 75, 410-415.

[22] Li Z.Y., Zhang H.L., Gibson M. and Li J.L. (2012) An evaluation on combination effects of phenolic endocrine disruptors by estrogen receptor binding assay. Toxicol in Vitro 26, 769-774.

[23] Rajapakse N., Silva E. and Kortenkamp A. (2002) Combining xenoestrogens at levels below individual No-observed-effect concentrations dramatically enhances steroid

hormone action. Environ Health Persp 110, 917-921.

[24] Ma M., Li J. and Wang Z. J. (2005) Assessing the detoxication efficiencies of wastewater treatment processes using a battery of bioassays/biomarkers. Arch Environ Con Tox 49, 480-487.

[25] Gaido K. W., Leonard L. S., Lovell S., Gould J. C., Babai D., Portier C. J. and McDonnell D. P. (1997) Evaluation of chemicals with endocrine modulating activity in a yeast-based steroid hormone receptor gene transcription assay. Toxicol Appl Pharm 143, 205-212.

[26] Koutsaftis A. and Aoyama I. (2007) Toxicity of four antifouling biocides and their mixtures on the brine shrimp Artemia salina. Sci Total Environ 387, 166-174.

[27] Sprague J. B. (1969) Measurement of pollutant toxicity to fish I. Bioassay methods for acute toxicity. Water Res 3, 793–821.

[28] Marking L. L. (1977) Method for assessing additive toxicity of chemical mixtures. Aquat toxicol hazard eval 634, 99-108.

[29] Könemann H. (1981) Fish toxicity tests with mixtures of more than two chemicals: A proposal for a quantitative approach and experimental results. Toxicology 19, 229-238.

[30] Folmar L. C., Hemmer M. J., Denslow N. D., Kroll K., Chen J., Cheek A., Richman H., Meredith H. and Grau E. G. (2002) A comparison of the estrogenic potencies of estradiol, ethynylestradiol, diethylstilbestrol, nonylphenol and methoxychlor in vivo and in vitro. Aquat Toxicol 60, 101-110.

[31] Silva E., Rajapakse N., Scholze M., Backhaus T., Ermler S. and Kortenkamp A. (2011) Joint Effects of Heterogeneous Estrogenic Chemicals in the E-Screen-Exploring the Applicability of Concentration Addition. Toxicol Sci 122, 383-394.

[32] Arnold S. F., Klotz D. M., Collins B. M., Vonier P. M., Guillette L. J. and McLachlan J. A. (1996) Synergistic activation of estrogen receptor with combinations of environmental chemicals. Science 272, 1489-1492.

[33] Sumpter J. P. and Jobling S. (1995) Vitellogenesis as a Biomarker for Estrogenic Contamination of the Aquatic Environment. Environ Health Persp 103, 173-178.

[34] Simons S. S. (1996) Environmental estrogens: Can two "alrights" make a wrong? Science 272, 1451-1451.

[35] Warne M. S. J. and Hawker D. W. (1995) The Number of Components in a Mixture Determines Whether Synergistic and Antagonistic or Additive Toxicity Predominate - the Funnel Hypothesis. Ecotox Environ Safe 31, 23-28.

[36] Thomulka K. W. and Lange J. H. (1996) A mixture toxicity study employing combinations of tributyltin chloride, dibutyltin dichloride, and tin chloride using the marine bacterium vibrio harveyi as the test organism. Ecotox Environ Safe 34, 76-84.

Received: **29.10.2015**
Accepted: **23.02.2016**

CORRESPONDING AUTHOR

Yujie Feng
State Key Laboratory of Urban Water Resource and Environment, Harbin Institute of Technology, No73, Huanghe Road, Nangang District, Harbin 150090, China

E-mail: hitzzh@hit.edu.cn

© by PSP Volume 25 – No. 10/2016, pages 4078-4087 Fresenius Environmental Bulletin

SYNTHESIS AND CHARACTERIZATION OF TiO_2 AND TiO_2/CeO_2 MICRO-SPONGE HETERO STRUCTURE: PHOTOCATALYTIC APPLICATIONS UNDER UV LIGHT

Ali Imran Vaizogullar[1*], Mehmet Ugurlu[2], Ibrahim Kula[2]

[1] Vocat Sch Health Care, Med Lab Programme, Muğla Sıtkı Koçman University, Muğla, Turkey
[2]Department of Chemistry, Faculty of Science, Muğla Sıtkı Koçman University, 48000 Muğla, Turkey

ABSTRACT

TiO_2 nanoparticles which synthesized a sol–gel method were decorated with CeO_2 by means of a chemical precipitation technique. We used activated carbon (AC) to prevent the agglomeration and disordered forms of TiO_2. X-ray diffraction (XRD), infrared (FTIR) spectra, scanning electron microscopy (SEM-EDAX), and BET techniques were used to evaluate the structure and morphology. The structural characterization by XRD confirms the formation of anatase TiO_2 and fluorite-structured CeO_2 phases in the Ti/Ce500 and Ti/Ce700 particles. The interaction between TiO_2 and CeO_2 affected the degradation efficiency. Due to its high surface area and porosity, the Ti/Ce700 micro-sponge photocatalyst exhibited a much higher photocatalytic effect than the pure TiO_2 and Ti/Ce500 catalyst for the degradation of Methylene Blue (MB). The optimum conditions for MB degradation were found to be pH=9, 0.5 g catalyst dosage and 10 mg/L initial MB concentration. From our point of view Ti/Ce700 micro-sponge photocatalyst can be envisaged as material for treatment of industrial waste waters.

KEYWORDS:
Micro-sponge, photocatalytic degradation, TiO_2/CeO_2, methylene blue, water treatment

INTRODUCTION

Much industrial waste such as rubber paper plastics and food cause environmental pollution because of the azo-dyes [1]. These azo-dyes significantly affect the water quality [2], and they caused some diseases such as cancer which affect the health of people and other living things [3]. The recently discovered photocatalytic degradation method is the most remarkable method which enables the elimination of organic pollutants [4].

This method is carried out with semiconductor metal oxides and the most commonly used metal oxides are TiO_2 because of nontoxicity, chemical stability and low cost [5]. Its utility is constrained due to a narrow absorption band which is limited to the UV range of the solar spectrum, low quantum efficiency and high probability for recombination of the e-/h+ pairs [6,7]. Many researchers have expressed that composite TiO_2 such as TiO_2/ZnO, TiO_2/ZrO_2, TiO_2/CeO_2 and SiO_2/TiO_2 is better than bare TiO_2 for the removal of organic pollutants [8]. Among these composite materials, TiO_2/CeO_2 is an attractive option because of CeO_2 and its significant properties such as high oxygen storage capacity, thermal stability, and high absorption of UV light [9]. Jiang and co-workers reported that when comparing the photoactivity of TiO_2/CeO_2 and CeO_2/TiO_2 composite materials, it was found that a CeO_2/TiO_2 catalyst was better than a TiO_2/CeO_2 [10]. Liu and a co-worker reported a photocatalytic mechanism of CeO_2-TiO_2 composite particles and they also found that TiO_2–CeO_2 films present better photocatalytic activity than the pure TiO_2 films under UV irradiation [11].

In all photocatalysts, the catalyst absorbs light for excitation from the valence band to the conduction band for the formation of electron/hole pairs and this pair creates a redox reaction on the catalyst surface resulting in the degradation of the toxic pollutant [12]. In this case, the shape of the catalyst plays an important role because the catalyst can be synthesized as nanotube, microsphere, nanosphere, hollow structure and core-shell form which affects the degradation of organic pollutants. The objective of this study was to synthesize TiO_2 and TiO_2/CeO_2 micro-sponge structure particles and to investigate the photocatalytic degradation efficiency. To the best of our knowledge, this is the first study to use a micro-sponge phenomenon on photocatalytic research.

Experimental. Preparation of TiO_2. The TiO_2 micro-sponge particles were synthesized by using the sol–gel method. 10 ml TBOT and 25 ml absolute ethanol were mixed into 50 ml deionized water and 0,2g activated carbon (AC). The mixture was stirred for 4 h, after that solutions were separated by centrifugation, the particles washed with deionized water and ethanol dried at 80 ◦C for 4 h. AC substrates could prevent TiO_2 agglomerating; for the formation of the micro-

sponge structure activated carbon was removed by calcination at 500 ◦C for 3 h.

TiO_2/CeO_2 composite particles. The TiO_2/CeO_2 composite hetero-structure particles were prepared by means of chemical precipitation method. Firstly, 1.0 g TiO_2 micro-sponge particles and 1.5 g $Ce(NO_3)_3 \cdot 6H_2O$ were dissolved into 100 ml water which contained 0.2 g CTAB. The solution pH value was adjusted to about 10 by using 0.1 mol L^{-1} NaOH solution. The mixed solution was stirred for 4 hours and aged for 2 hours, after that it was filtered and washed with deionized water, then dried at 80 ◦C for 4 hours. The prepared catalyst was separated into two portions and calcined at 500°C and 700 °C for 3h.

Nomenclature

TBT	Titanium tetra butoxide
$Ce(NO_3)_2.6H_2O$	Cerium nitrate hexahydrate
CTAB	Cetryl trimetil ammonium bromide
AC	Activated carbon
MB	Methylene blue
k	Pseudo-first order kinetic rate constant (min^{-1})
IEP	Isoelectric point
C	Concentration in solution at time t (mg L^{-1})
C_o	Initial concentration of MB
t	Time
R^2	Linear regression coefficient

Characterization. The crystalline phase was examined by XRD (Rigaku Dmax 350) using copperK radiation (λ = 0.154056 nm). The IR spectrum analysis of the catalyst was carried out by the IR measurement system Thermo-Scientific, (Nicolet IS10-ATR). The microstructure and shape of the particle were investigated using SEM (JEOL JSM-7600F). The element was determined with (JEOL JSM-7600F) EDAX analyzer with SEM measurement. The Brunauer-Emmett-Teller (BET), pore volume, and pore size were measured using ASAP2010 (Micromeritics Instrument Corporation, USA) with N_2 adsorption at 77.35 K.

The crystallite size of TiO_2 and Ti/Ce500 and Ti/Ce700 particles was calculated using the Scherer equation;

$$d = \frac{B\lambda}{\beta_{1/2} Cos\,\theta} \qquad (1)$$

Where d is the average particle size, B is the Scherer constant (0,91), λ is the wavelength of the X-Ray, $\beta_{1/2}$ is full width at half maximum of the diffraction peak and θ is the diffraction angle.

Surface physical properties of the prepared catalyst including pore volume, surface area, and surface morphology have been examined and the results are summarized in Table 1.

Photocatalytic Experiments

In photolytic experiments, a specially designed UV reactor was used. This reactor consists of a closed system having a UV lamp, properties of fixed mixing and cooling and oxygen entry (Fig.1). A 36 W medium pressure mercury vapor lamp was used as UV light. Prior to irradiation, to allow adsorption/desorption equilibrium mixture was stirred for 60 min in the dark. The color of MB was analyzed by using a Dr. Lange Spectro-Photometer and the maximum wavelength in the visible area was determined to be 664 nm. Then, all color changes were investigated at this wavelength. The amount of degradation was calculated by taking 5 ml of MB solution every 5 minutes. The degradation percentage of MB is calculated in the below equation:

$$\%Degradation = \frac{Co - C}{Co} \times 100 \qquad (2)$$

Where Co is the initial concentration of MB and C is the MB concentration at time.

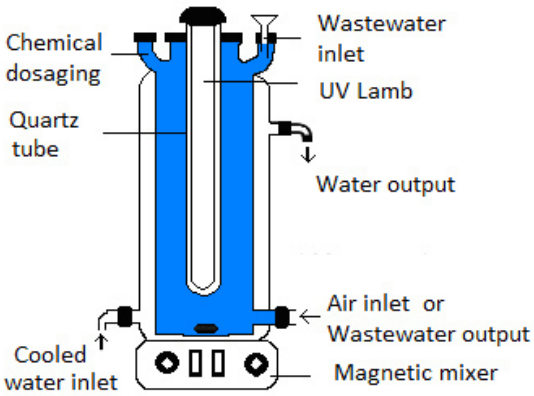

FIGURE 1
Schematic of UV reactor used at the experimental study

RESULTS AND DISCUSSION

FTIR analysis. Figure 2 shows the FTIR spectrum of TiO_2, CeO_2 and Ti/Ce500, Ti/Ce700 particles.

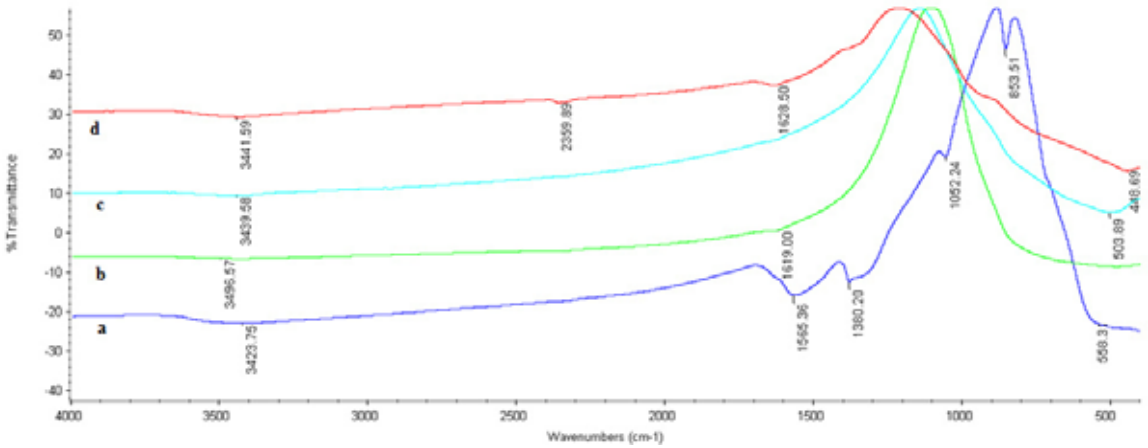

FIGURE 2
FTIR spectrum of particles (a) CeO_2 (b) Ti/Ce500 (c) TiO_2, (d) Ti/Ce700

In all spectrums, the broad peaks at 3423 cm^{-1}, 3496cm^{-1}, 3439cm^{-1} and 3441cm^{-1} are the stretching vibrating peaks of O-H bond in the surfaced hydroxyl in water. In Figure 2a, the FT-IR spectrum positions of the CeO_2 particles were found at about 1565, 1380, 1052, and 853 cm^{-1} that are similar to the FTIR bands of CeO_2 as reported literature. The band at below 700 cm^{-1} was attributed to the stretching frequency of Ce–O bonds [13]. The band at 1619 cm^{-1} and 1628 cm^{-1} corresponds to Ce=O stretching (Fig. 2b,d). The band at 503 cm^{-1} is assigned to the Ti–O stretching vibration (Fig. 2c). During the condensation reaction Ti-OH groups provide Ti-O-Ce bridges between surfaces of the TiO_2. The band at 448 cm^{-1} is assigned to the stretching modes of Ti–O–Ce bridges (Fig. 2d) [14]. The characteristic peaks of the Ti/Ce700 catalyst is seen more clearly than Ti/Ce500 catalyst (Fig 2b,d).

SEM and EDAX Analysis. The morphology of TiO_2, Ti/Ce500, and TiCe700 micro-sponge particles were observed by SEM image (Fig.3). TiO_2 was in irregular sizes, shapes and porous structure as shown in Figure 3a. Both Ti/Ce500 and Ti/Ce700 particles were in irregular sizes and shapes like TiO_2, but Ti/Ce500 particles were smooth in structure and CeO_2 spread on TiO_2 porous homogeneously (Fig.3b). Figure 3c displayed the SEM image of the Ti/Ce700 composite catalyst. It could be observed that a congested CeO_2 are spread over TiO_2 surface and pores. With the increase of the calcination temperature, the surface area and the average pore diameter increased because of CeO_2 entered into the pores of TiO_2 (Fig. 3c). Compared with the pore diameter of TiO_2 (~300nm) that of Ti/Ce500 (~250nm) the composite particles was much wider. Therefore, we can say that CeO_2 particles could be deposited on the inner surface of TiO_2 particles.

In addition, the EDAX spectrum also showed beside SEM image. The main elements were Ti, Ce, O which was good agreement with target products.

XRD Analysis. The XRD patterns of catalysts are shown in Figure 4. The diffraction peaks appearing at 2θ: 25.28°, 37.78°, 43.79°, 47.88°, 54.50° and 63.32°correspond to the anatase and rutile phase (Fig. 4a) [15]. In addition, a mixture of anatase and rutile catalyst, predominantly in the anatase phase was obtained after the calcination process. In Figure 4b and c the XRD patterns of Ti/Ce500 and Ti/Ce700 show peaks appearing at 2θ: 28.42°, 33.46°, 47.36° attributed to the cubic fluorite structure of CeO_2 [16]. Peaks of TiO_2 and CeO_2 could be seen in Figure 4b and c. We could say all the diffraction peaks can be attributed mainly to a mixture of TiO_2 and CeO_2 in Ti/Ce500 and Ti/Ce700 micro-sponge particles. As the calcination temperature increased, the stability of the anatase phase was enhanced, which indicated that CeO_2 prevented the phase transforming from anatase to rutile (Fig. 4c). In Figure 4c, we observed the broad line width of the diffraction peaks of components which are due to the smaller crystallite size of Ti/Ce500 catalyst. The crystallite size (*d*) for the TiO_2, Ti/Ce500 and Ti/Ce700 micro-sponge particles were determined by equation 1. The XRD patterns for the three samples the size of the TiO_2, Ti/Ce500 and Ti/Ce700 micro-sponge particles are around 21.5, 8.38 and 21.3 nm respectively. Increasing the calcination temperature to 700◦C, the peaks become somewhat sharpness, indicating that the crystallite size increased.

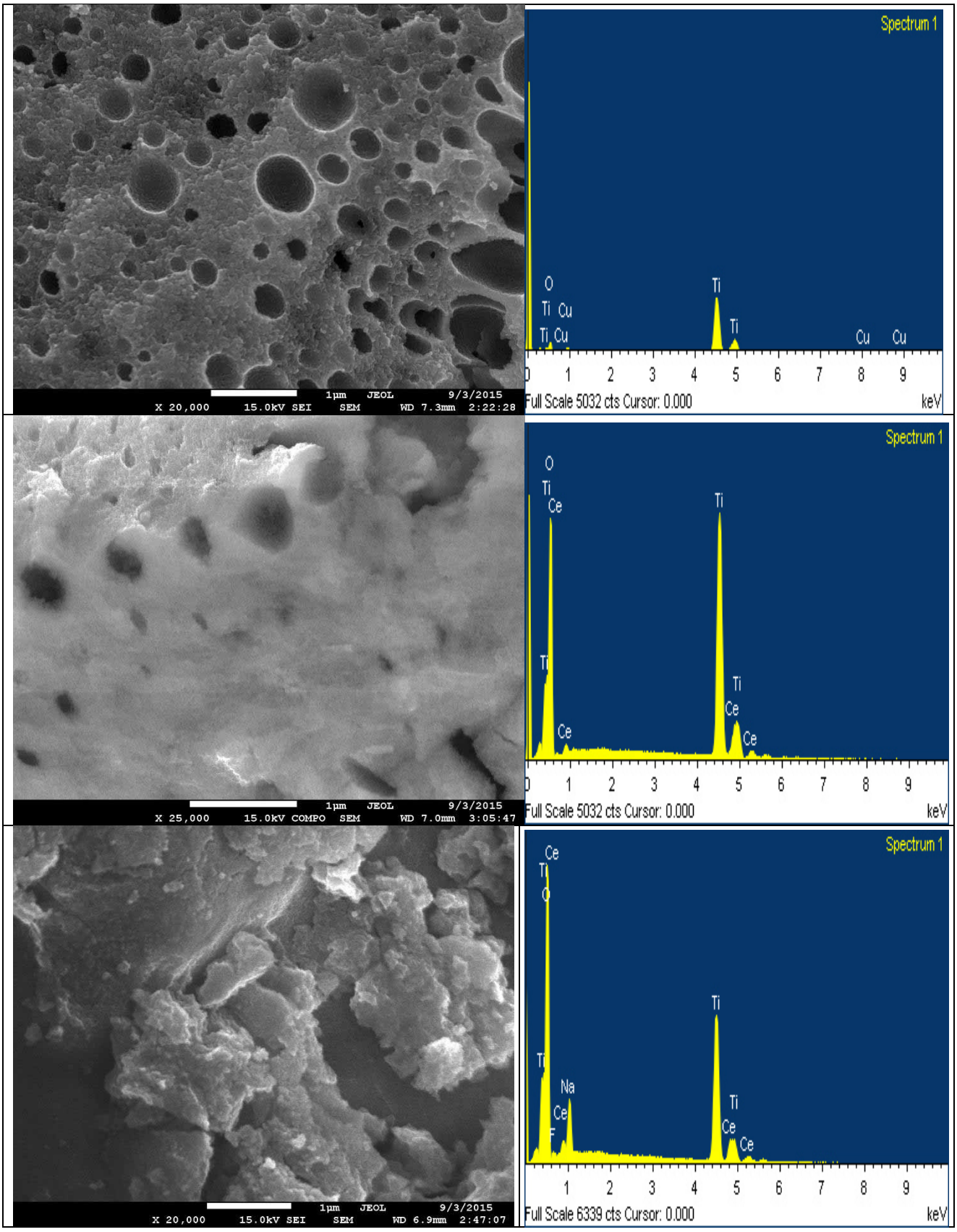

FIGURE 3
SEM and EDAX analyses of (a) TiO_2 (b) Ti/Ce500 (c)Ti/Ce700 particles

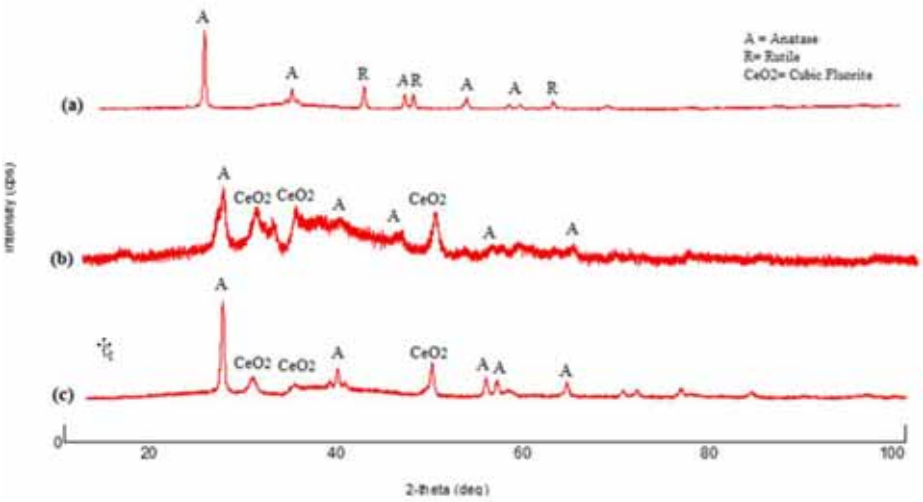

FIGURE 4
XRD pattern for (a) TiO_2 (b) Ti/Ce500 (c) Ti/Ce700 particles

A decrease in the crystalline size could be attributed to the broadening effect due to the incorporation of CeO_2 into TiO_2 matrix and preventing agglomerated CeO_2 crystals (Fig.4b). In addition, the un-shifted anatase peak at 25.28° (101) showed that CeO_2 did not confuse the TiO_2 lattices [17].

To characterize the specific surface area and porosity of as-prepared samples, N_2 adsorption analyses were carried out. From Table 1, BET surface area, pore size and pore volume increased with CeO_2 and calcination temperature. Compared to the pure TiO_2, the surface area for Ti/Ce500 and Ti/Ce700 micro-sponge particles increased. It was considered that porosity of the TiO_2 structure inhibited the agglomeration of CeO_2 on the TiO_2 surface [18].

Photocatalytic Applications. Effect of pH. pH is the most important factor affecting the surface charge of the catalyst [19]. Therefore, the activity of Ti/Ce700 particles was studied for degradation of MB. The initial dye concentration of 10 mg/L and the amount of the catalyst 0.2g was examined within the pH range of 2-9. The degradation percentage of MB was found to be 78%, 91%, 99% at pH 5,7,9 respectively. We obtained a maximum degradation percentage of 99% at pH 9 (Fig. 5). 10 mg/L of MB can be completely decomposed in 60 min by Ti/Ce/700. Usually, in pH > 3.0 conditions, cationic dyes are more easily adsorbed into the catalyst surface by the catalyst than anionic dyes [20]. Fig. 6 shows zeta point charge for Ti/Ce/700 catalyst. From the figures it appears that zeta potential values of the Ti/Ce700 catalyst were always negative at each pH point. The shape of the graph demonstrates that the surface charge of Ti/Ce/700 is negative and the IEP of the catalyst is below pH=2. Therefore, we could be saying the catalyst surface is negatively charged in the pH 3-12 range. In basic solutions more OH^- ions are present around the catalyst surface and it is because of the formation of more hydroxyl radicals resulting in increased the photoactivity. In addition zeta potential values of the Ti/Ce700 catalyst is -26 mV, -29 mV and -24 mV at pH 5,7,9 respectively. There is a clearly defined pattern to the figure and this can be taken to mean that repulsion force is stronger at pH=9 therefore the Ti/Ce700 catalyst has good dispersion stability at pH=9 which enhances photoactivity. When the solution pH was more acidic (pH=2) the photocatalytic degradation percentage of MB decreased because of the positive charge of the catalyst surface that occurs in electrostatic repulsion.

TABLE 1
Physiochemical properties of catalyst

Catalyst	BET (m^2/g)	Pore size (nm)	Pore volume (cm^3/g)	Langmuir Surface area (m^2/g)	Crystallite size (nm)
TiO_2	10.02	11.99	0.030	17.01	21.5
Ti/Ce500	16.12	13.34	0.053	20.73	8.38
Ti/Ce700	31.99	20.91	0.167	41.54	21.3

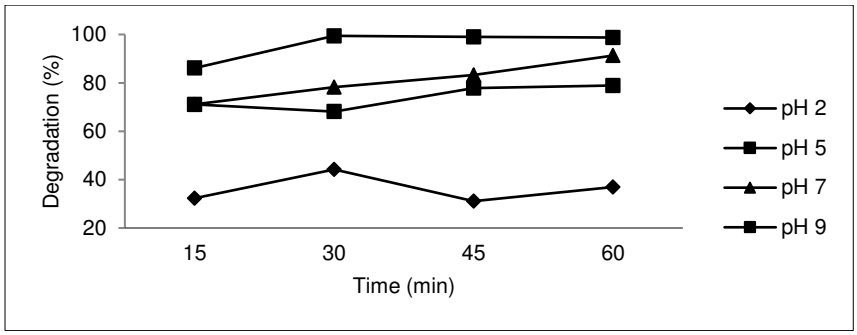

FIGURE 5
The effect of pH for degradation of MB using Ti/Ce700 catalyst (Amount of catalyst 0.2g and initial concentration of MB dye 10 mg/L)

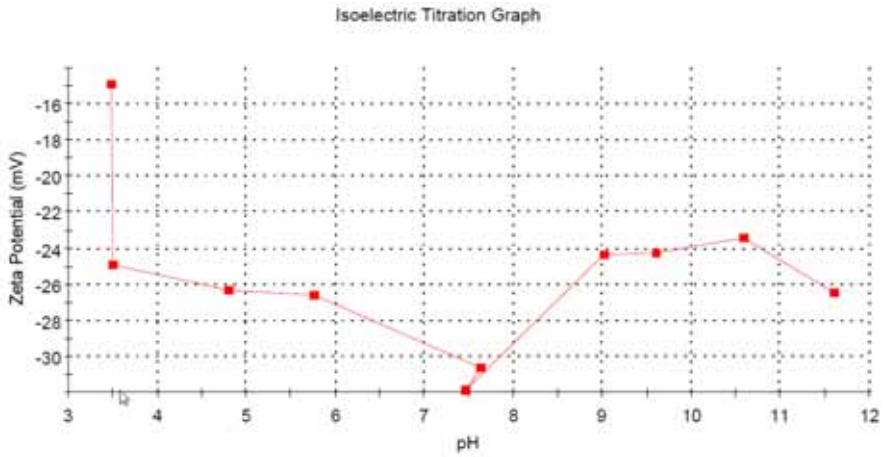

FIGURE 6
Zeta potential measurement for Ti/Ce700 catalyst

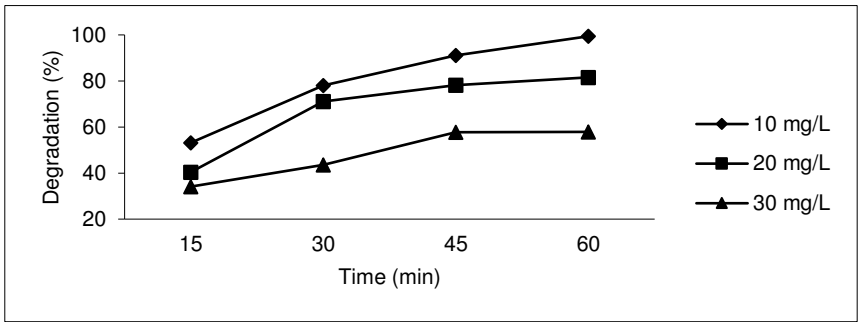

FIGURE 7
The effect of initial MB concentration for degradation of MB using Ti/Ce700 catalyst, (Amount of catalyst 0.1g/50 mL and solution pH 9).

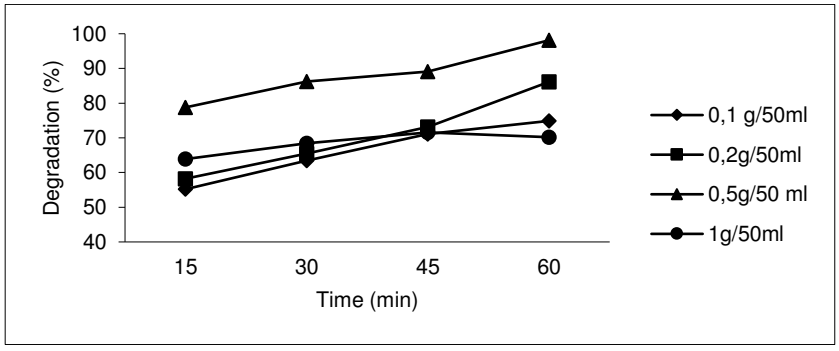

FIGURE 8
The effect of catalyst dosage for degradation of MB using Ti/Ce700 catalyst (Concentration of MB dye 10 mg/L pH 9).

Effect of initial MB concentration. In order to determine optimum initial dye concentration, 10 mg/L, 20 mg/L and 30 mg/L of MB concentration was studied using a Ti/Ce700 catalyst. The amount of catalyst and pH were 0.2g and 9 respectively (Fig.8).

Figure 7 shows that when the concentration of MB increased, the percentage degradation of MB decreased. Thiscan be explained by the increasing MB concentration which caused an increase of dye molecules on the catalyst surface. This affected the photoactivity of the catalyst. An increase in the concentration of the dye solution reduces the light path of the photons which enter into the dye solution. In higher dye concentrations, the dye molecules absorb a large part of light instead of the catalyst and this may also reduce the catalytic activity [21].

Effect of catalyst dosage. A series of experiments were carried out by varying the amount of the catalyst in the range of 0.1-1g with an initial dye concentration of 10 mg/L and pH 9. Figure 8 shows the effect of catalyst concentration on the degradation of MB. It could be clearly seen that the greatest degradation percentage was found at 0.5g catalyst dosage and the color removal rates achieved the maximum percentage (99%). At a higher than 0.5 g catalyst dosage, the color removal rates decrease. This can be explained by the light scattering and reduction in light penetration through the solution, caused by the lightproof suspended catalyst [22].

Kinetic Studies. The pseudo first order equation can be used to explain the kinetics of photocatalytic degradation of MB. The first order kinetic rate k (1/min) for MB degradation can be calculated by plotting $\ln(\frac{Co}{C})$ versus time (t) (Eq.4). In this investigation, the photodegradation of MB was evaluated at a constant initial pH of 9, catalyst dosage of 0.5 g, initial MB concentration of 10 mg/L and within reaction time 75 min.

$$\ln\left(\frac{Co}{c}\right) = k.t \qquad (4)$$

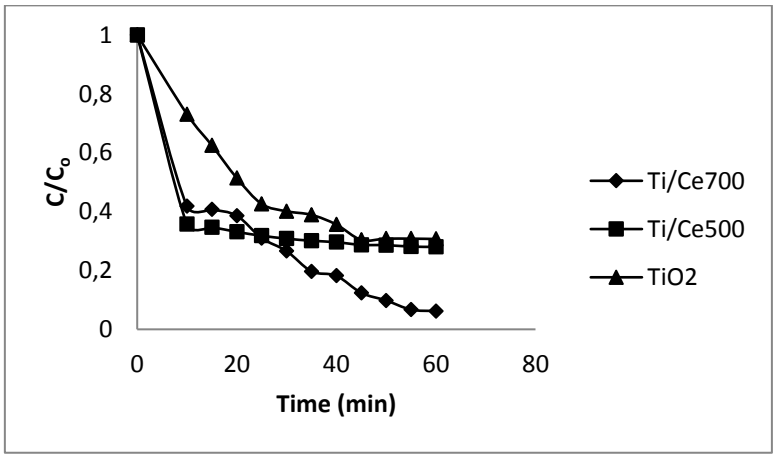

FIGURE 9. Photodegradation of MB by Ti/Ce700, Ti/Ce500, TiO_2

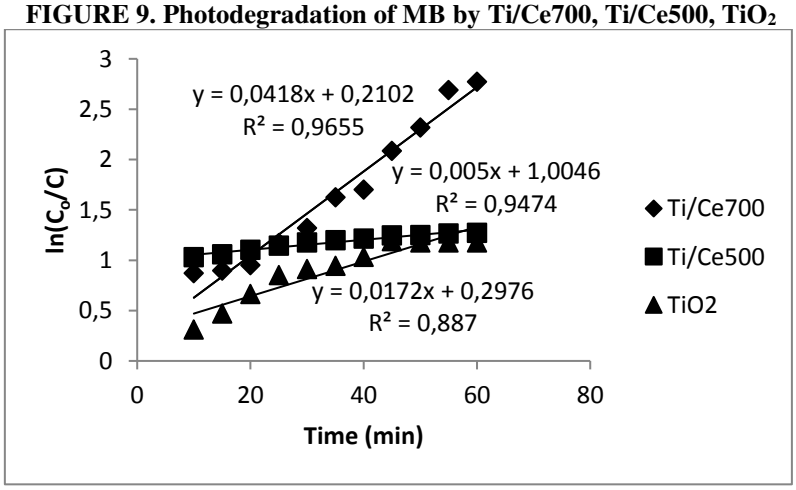

FIGURE 10
Plots of ln(C_o/C) versus the irradiation time (t)

The kinetic results revealed that Ti/Ce700 has the higher photoactive than other It has an almost completely degraded MB within a period of 60 min (Fig. 10). For our experimental conditions, data was in good agreement with the pseudo first-order isotherm for the Ti/Ce700 catalyst by Figure 11. The correlation constant for the lines was calculated to be R^2=0.96.

TABLE 2
Reaction rate constant (k) and correlation coefficient (R^2)

Catalyst	$kx10^{-3}$ (1/min)	R^2
Ti/Ce700	41.8	0.96
Ti/Ce500	5	0.94
Ti500	17.2	0.88

The k value of Ti/Ce700 in Table 2 represents a good measurement of the other. Ti/Ce700 has a faster degradation rate than about two times from Ti/Ce500 and eight times from Ti/Ce500. The activity of the catalyst is influenced by its crystallinity, surface area, crystal size, crystal phase and other. Tian and co-worker [23] also reported that the higher surface area and pore volumes have more surface active sites and channels that allowed rapid diffusion of reactants resulting in increased photoactivity. It can be seen from the Table 1, that the surface areas are 10.02 m^2/g, 16.12 m^2/g and 31.99 m^2/g for TiO_2, Ti/Ce500 and Ti/Ce700 respectively. In photocatalytic experiments, the Ti/Ce700 catalyst showed the highest photocatalytic activity. This was due to the fact that Ti/Ce700 showed better crystallization. This may be attributed to the larger specific surface area and bimodal mesoporous structures. Moreover, CeO_2 is not photoactive material; therefore TiO_2/CeO_2 composites are less photoactive when the amount of CeO_2 is increased. Why photoactivity of TiO_2/CeO_2 is higher than TiO_2? This is explained by better crystallinity which reveals fewer lattice defects which act as a recombination center [24].

In addition, the catalytic activity of TiO_2/CeO_2 composite materials can be explained as follows: UV light can excite both TiO_2 and CeO_2 and that reveals photogenerated electron-hole pairs (e^-/h^+) in their valence band (VB) and conductivity band (CB). The CB electrons of CeO_2 transfer to the CB of TiO_2 due to its electronegativity. In this case, surface O_2 easily convert to O_2^- anion. The VB electrons of TiO_2 transfer to the VB of CeO_2 because of higher VB level resulting in the appearance of OH^* radicals. The production of this reactive species in which OH^* radicals and O_2^- anion are responsible for oxidizing organic molecules to CO_2, H_2O etc. Finally, (i) regular porosity caused enhanced surface area because of preventing agglomeration forming large clusters while the formation of composite structures and (ii) minimizing of charge carriers because of Ce^{+3} and Ce^{+4} ions which prevent recombination of e-/h+ pairs.

CONCLUSIONS

Sol-gel and a chemical precipitation process were applied to synthesize TiO_2 and TiO_2/CeO_2 catalysts. AC was used to prevent the agglomeration and disordered forms of TiO_2. The activities of catalysts on the degradation of MB in aqueous solutions were evaluated. Compared with pure TiO_2, composite micro-sponge Ti/Ce particles were more active. The surface area of catalysts increased with calcination temperature.

The optimum condition was found to be pH 9, 0.5 g of catalyst dosage and 10 mg/L of initial concentration for the degradation of MB using a Ti/Ce700 catalyst. The enhancement in the photocatalytic activity was mainly due to the high surface area, anatase TiO_2, and low diffusion resistant of Ti/Ce700.

The arguments given above prove that Ti/Ce700 is a good catalyst for organic dye removal in wastewater treatment. It can be an alternative material along with a nanotube, microsphere, nanosphere, a hollow structure and core-shell form. To sum up, the above discussion has attempted to synthesize a new material structure and provide enhanced photactivity.

REFERENCES

[1] Gnanaprakasam, A., Sivakumar V.M., Sivayogavalli, P.L., & Thirumarimurugan M. (2015). Characterization of TiO2 and ZnO nanoparticle sand their applications in photocatalytic degradation of azo dyes Ecotoxicology and Environmental Safety 121,121-125.

[2] Pirzada, B. M. Mir, N.A., Qutub, N., Mehraj, O., Sabir, S., & Muneer, M. (2015). Synthesis, characterization and optimization of photocatalytic activity of TiO2/ZrO2nanocomposite hetero structures Materials Science and Engineering B, 193 ,37–145

[3] Li, Z., Hou, B., Xu, Y., Wu, D., & Sun, Y.Y., (2005). Hydrothermal synthesis, characterization and photocatalytic performance of silica – modified titanium dioxide nanoparticles. Journal of Colloid Interface Science, 288,149–154.

[4] Zhang, M., An, T., Hu, X., Wang, C., Sheng, G., & Fu, J. (2004). Preparation and photocatalytic properties of a nanometer ZnO–SnO2coupled oxide, Applied Catalysis A: Geneneral, 260,215–222.

[5] Wang, Y., Zhu, S., Chen, X., Tang, Y.Y., Peng, J., & Z. Wang H. (2014). One-step template-free fabrication of mesoporous ZnO/TiO2 hollow microspheres with enhanced photocatalytic activity, Applied Surface Science, 307, 263–271.

[6] Rajbongshi, B.M., Samdarshi, S. K., & Boro B. (2015). Multiphasic bi-component TiO2–ZnO nanocomposite: synthesis, characterization and investigation of photocatalytic activityunder different wavelengths of light irradiation, Materials Science: Material Electron, 26,377–384.

[7] Behnajady, M.A., Modirshahla, N., Daneshvar, N., & Rabbani. M. (2007). Photocatalytic degradation of C.I. Acid Red 27 by immobilized ZnO on glass plates incontinuous mode, Journal of Hazardous Material, 140,257–263.

[8] Zhou, W., Liu, K., & Fu H. (2008). Multi-modal mesoporous TiO2– ZrO2 composites with high photocatalytic activity and hydrophilicity, Nanotechnology, 19,035610–035616

[9] Ameen, M.S., Akhtar, H.K., Seo, H-S. & Shin. (2014). Solution-processed CeO2/TiO2 nanocomposite as potent visible light photocatalyst for the degradation of bromophenol dye, Chemical Engineering Journal, 247,193–198.

[10] Jiang, B., Zhang, S., Guo, X., Jin, B., & Tian. Y. (2009). Preparation and photocatalytic activity of CeO2/TiO2 interface composite film, Applied Surface Science, 255,5975–5978

[11] Liu, B., Zhao, X., Zhang, N., Zhao, Q., He, X., & Feng. J. (2005). Photocatalytic mechanism of TiO2-CeO2 films prepared by magnetron sputterning under UV and visible light, Surface Science, 595,203–211.

[12] Batista, M.M., Ballari, A., Kubacka, A.E., Cassano, O.M., Alfano, M., F. & García, F. (2014). Acetaldehyde degradation under UV and visible irradiation using CeO2–TiO2 composite systems Evaluation of the photocatalytic efficiencies, Chemical Engineering Journal 255, 297–306.

[13] Zuas , O., Abimanyu, H., & Wibowo. W. (2014). Synthesis and characterization of nanostructured CeO2 with dyes adsorption property, Processing and Application of Ceramics, 8,39-46.

[14] Bhosale, A.K., Kulal, S.R., Gurame,V.M., & Patil, P.S. (2015). Spray deposited CeO2–TiO2 counter electrode for electrochromic devices. Bulletin of Materials Science, 38,483–491

[15] Sherbiny, S.E., Morsy, F., Samir, M., & Fouad. O.A. (2014). Synthesis, characterization and application of TiO2 nanopowders as special paper coating pigment, Applied Nanoscience, 4,305–313.

[16] Qua, X., Xiea , D., Caob, L., & Dua, F. (2014). Synthesis and characterization of TiO2/ZrO2 coaxial core–shell composite nanotubes for photocatalytic applications, Ceramics International, 40,12647–12653.

[17] Zuas, O., & Hamim, N. (2013). Synthesis, characterization and properties of CeO2-doped TiO2 Composite Nanocrystals Materials Science 19,4.

[18] Guzmán, C., Angel, G.D. Gomez R., Galindo, F., Zanella, R., Torres, G., Ángeles-Chávez, C., & Fierro. J. L.G. (2009). Gold Particle Size Determination on Au/TiO2-CeO2 Catalysts by Means of Carbon Monoxide, Hydrogen Chemisorption and Transmission Electron Microscopy, Journal of Nano Research, 5,13-23.

[19] Tedla H. Díaz, I. Kebedea, T.A. (2015). Synthesis, characterization and photocatalytic activity of zeolite supported ZnO/Fe2O3/MnO2 nanocomposites, Journal of Environmental Chemical Engineering, 3, 1586–1591.

[20] Chun, H., Yizhong, W., & Hongxiao, T. (2001). Preparation and characterization of surface bond-conjugated TiO2/SiO2 and photocatalysis for azo dyes, Applied Catalysis B: Environmental 30, 277–285.

[21] Sobana, N., Selvam, K., & Swaminathan, M. (2008). Optimization of photocatalytic degradation conditions of Direct Red 23 using nano-Ag doped TiO2, Separation and Purification Technology, 62,648–653

[22] Zhu, C., Wang, L., Kong, L., Yang, X,. Wang, L., Zheng, S., Chen F., MaiZhi, F., & Zong H. (2000). Photocatalytic degradation of Azo dyes by supported TiO2 + UV in aqueous solution, Chemosphere, 41,303-309

[23] Tian, G., Fu, H., Jing, L., Xin, B. & Pan,K. (2008). Preparation and Characterization of Stable Biphase TiO2 Photocatalyst with High Crystallinity, Large Surface Area, and Enhanced Photoactivity, Journal of Physics Chememistry, 112, 3083-3089.

[24] Cao,T., Li,Y., Wang,C., Wei,L., Shao,C., & Liu,Y. (2010) Fabrication, structure, and enhanced photocatalytic properties of hierarchical CeO2 nanostructures/TiO2 nanofibers heterostructures, Materials Research Bulletin, 45, 1406–1412.

Received: **04.11.2025**
Accepted: **11.05.2016**

CORRESPONDING AUTHOR

Ali Imran Vaizogullar
Vocat Sch Health Care, Med Lab Programme, Muğla Sıtkı Koçman University, Muğla, Turkey

Email: vaizogullar@yahoo.com

© by PSP Volume 25 – No. 10/2016, pages 4088-4092 Fresenius Environmental Bulletin

DEGRADATION AND ITS CAUSES OF INFLUENZA A VIRUS IN EUTROPHIC FRESHWATER

Mingjun Liao, Wei Liu, Kai Cheng, Yijun Zhao*

Key Laboratory of Ecological Remediation for Lakes and Rivers and Algal Utilization of Hubei Province, Wuhan, China, 430068
College of Resources and Environmental Engineering, Hubei University of Technology, Wuhan, China, 430068

ABSTRACT

Avian Influenza (AI) can cause extremely high mortality in infected fowls, and the factors affecting its maintenance and infectivity in aquatic environment is still unclear. In this study, effects of ultraviolet (UV) irradiation, heat-sensitive materials and particle materials on influenza A virus infectivity in aquatic environment were analysed under laboratory condition. Influenza A virus was sensitive to both of the ultraviolet B (UVB) radiation and ultraviolet A (UVA) radiation. UVB may led to viral inactivation through both of the genome and protein damage, while UVA may inactive the influenza A virus through endogenous indirect inactivation. Heat-sensitive materials plays important role in influenza A virus decay process and contributed 8.7-25% to viral decay ratio. The particle material concentrations significantly affected the influenza A virus decay process. With the particle material concentrations increased 5 and 10 fold, the decay ratio increased from 22.56±2.35% to 55.67±2.08% and 70±2% respectively.

KEYWORDS:
Influenza A virus; Decay ratio; Ultraviolet radiation; Heat-sensitive substances; Particle materials

INTRODUCTION

As a subtype of influenza A virus, bird flu (Avian Influenza, AI) is recognized as a disease which caused extremely high mortality in infected fowls since its outbreak for the first time in 1878 [1] . All known subtypes of influenza A virus could be isolated from feral birds, especially ducks and geese [2]. Most avian influenza virus were excreted at high levels in feces, thus we could isolate influenza virus from lake water even without concentration. [3-5].

Without host, the influenza virus could not initiate the infection and replication, but at low-temperature, the virus could remain infectious in aquatic system even more than 207 days[6], thus the influenza virus could re-infect ducks in the next spring[7].

Many environmental factors can result in viral inactivity, such as protozoon grazing, attachment to labile colloids, degradation by heat-sensitive and high molecular weight dissolved material, and disinfection by the UV component of solar radiation[8]. In previous study, solar UV irradiation, especially UVB, is considered to be the dominant factor in controlling viral infectivity in the aquatic environments [9-12]. However, most of these studies were focused on aquatic original virus, such as bacteriophage and cyanophage. Only a few research investigated the effect of pH, temperature and salinity on persistence of avian influenza viruses in water [6, 13, 14]. Influence of most factors affecting virioplankton infectivity on the influenza A virus maintenance and infectivity in aquatic environment is still unclear. In this study, the decay of influenza A virus and its causes in eutrophic freshwater were analysed. The results may help us to understand the epidemic of influenza A virus in aquatic environment.

MATERIALS AND METHODS

Virus propagation. The influenza A virus (H1N1) was originally obtained from Hubei Provincial Center for Disease Control and Prevention. The virus was inoculated to 18-day-old embryonated chicken eggs through the allantoic cavity. After 48 h of incubation at 35°C, the allantoic fluid was collected and the virus was prepared as described by Tang et al.[15]. Viral titer was tested by the hemagglutination (HA) assay using freshly prepared 1% chick red blood cells. HA assay was performed according to the WHO guidelines[16].

Viral decay caused by UV radiation. Influenza A virus suspension was mixed at ratio of 1:7 with natural water sampled from Honghu Lake (29°53'56.48" N, 113°15'44.60" E), a shallow eutrophic lake in Hubei Province of China，and the viral titer of the mixture was assayed as initial titer. Six Petri dishes without lid were infilled with 5 mL viral mixture, respectively. Three dishes containing

viral mixture were placed under an ultraviolet A (UVA) lamp (8.216-8.268 mw cm^2), and 3 dishes containing viral mixture were placed under an ultraviolet B (UVB) lamp (6.18-6.28 μw cm^2). The UV irradiation intensity was approximately equal to the solar UV intensity of sampling site. All dishes were placed under room temperature and 0.1 mL sample was collected from each mixture for HA test at 0 min, 30 min, 60 min, 90 min, 120 min, 150 min, 180 min and 240 min. Comparing to the initial titer, the percentage of viral titer decrease at each sampling time was denoted as the decay ratio caused by UV irradiation (%).

Viral decay caused by heat-sensitive substances. Influenza A virus suspension was mixed at ratio of 1:7 with natural water sampled from Honghu Lake， and the viral titer of the mixture was assayed as initial titer. Three Petri dishes without lid were infilled with 5 mL viral mixture, respectively. Dishes containing viral mixture as the test group were incubated at 22 ºC in water bath in the dark, and 0.1 mL sample was collected from each dish every 24 hours for titer assay. In the control group (for measuring the decay ratio caused by heat-stable substances), influenza A virus suspension was mixed at ratio of 1:7 with natural water restrained the heat-sensitive substances, and the other operations were the same as the test group. The heat-sensitive substances in water samples were restrained by heated to 70 ºC and maintained for 45 min, and then cooled to room temperature.

The viral decay ratios were calculated as the percentage of viral titer decrease at sampling time. The decay ratio of test group is the total decay ratio, and the decay ratio of control group is the decay ratio caused by heat-stable substances. The difference between the decay ratio of test and control groups was the decay ratio caused by heat-sensitive substances.

Viral decay caused by particle materials. Particle materials in the water samples were concentrated by 5 and 10 folds respectively through centrifugation at 8000 ×g for 30 minutes. The concentrated water samples were used to test the effect of particle materials on viral decay, and the un-concentrated water samples were applied as control. For each group, triplicate 7 mL water samples were mixed with 1 mL influenza A virus suspension, respectively. The mixtures were incubated at 22 ºC in water bath in the dark, and 0.1 mL sample was collected from each mixture every 2 hours for titer assay. The decay ratio was denoted as the percentage of viral titer decrease at the sampling time.

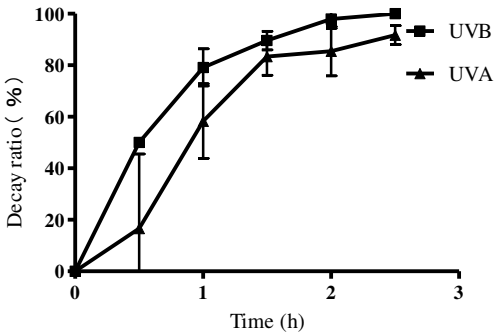

Decay ratio (mean ± SD) caused by UVA and UVB radiation

FIGURE 1
Influenza A virus suspension was mixed at ratio of 1:7 with natural water sample, and the mixture were divided into Petri dishes and exposed to ultraviolet A (UVA) radiation (8.216-8.268 mw cm^2) or ultraviolet B radiation (UVB) lamp (6.18-6.28 μw cm^2). The viral titer was monitored during the exposure, and the decay ratio (%) was calculated as the percentage decrease of viral titer.

RESULTS

Influence of UVA and UVB irradiation on viral decay. Results of UV radiation caused viral decay are shown in Fig. 1. UV radiation exposure led to rapid viral decay at the beginning time: viral decay ratio caused by UVB and UVA in 1.5 hour exposure was 89.6±3.6% and 83.3 ±7.2% respectively. The increases of viral decay ratio slowed down with the extended UV exposure, and at the end of exposure, the UVB and UVA caused viral decay ratio was 100% and 91.7±3.6%, respectively. Comparing the two treatment groups, the UVB caused viral decay ratio is significantly higher than that of UVA under the same exposure time ($P<0.05$, One-way ANOVA).

Influence of heat-sensitive substances on viral decay. Influence of heat-sensitive and heat-stable substances on viral decay is shown in Fig. 2. The viral decay process performed an average decay rate of 0.97%·h^{-1} and caused 95.87±3.58% of viral inactivation at the end. The viral decay ratio caused by heat-stable materials was significantly higher than that of heat-sensitive substances ($P<0.05$, One-way ANOVA). At the first 24 hours, heat-sensitive substances showed almost no influence on viral infectivity, and heat-stable materials contributed 100% to the total decay ratio. But after that, the contribution of heat- sensitive substances increased and maintained at a decay ratio of 8.4-16.6%, which was about 8.7-25% of total decay ratio.

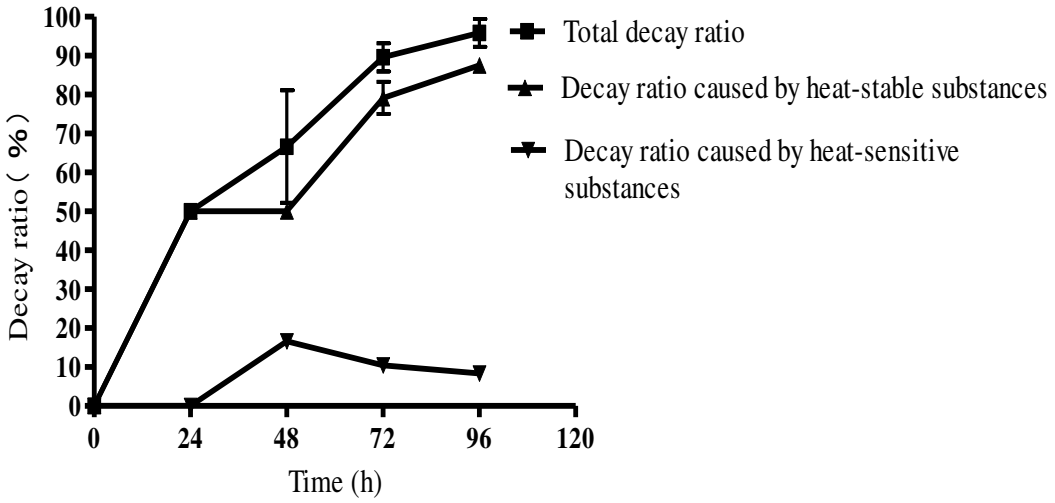

Decay ratio (mean ± SD) caused by UVA and UVB radiation

FIGURE 2

The heat-sensitive substances in water samples were restrained by heated to 70 ºC and maintained for 45 min. Influenza A virus suspension was mixed at ratio of 1:7 with both water samples with and without heat-sensitive substances. The mixtures were incubated in the dark, and the viral titer was monitored during the incubation, and the decay ratio (%) was calculated as the percentage decrease of viral titer. The total decay ratio was denoted as the viral decay ratio in water with heat-sensitive substances, the decay ratio caused by heat-stable substances was denoted as the viral decay ratio in water without heat-sensitive substances, and the difference between the two decay ratios was denoted as the viral decay ratio caused by heat-sensitive substances.

Influence of particle materials on viral decay. The viral decay ratio at different particle material concentrations varied significantly and increased with particle material concentrations ($P<0.05$, One-way ANOVA) (Fig. 3). The final viral decay ratios under three particle material concentrations were 22.56±2.35%, 55.67±2.08% and 70±2% respectively. Regression analysis indicated that the viral decay ratio was highly correlated to the particle material concentrations ($P<0.05$, $r^2=0.997$).

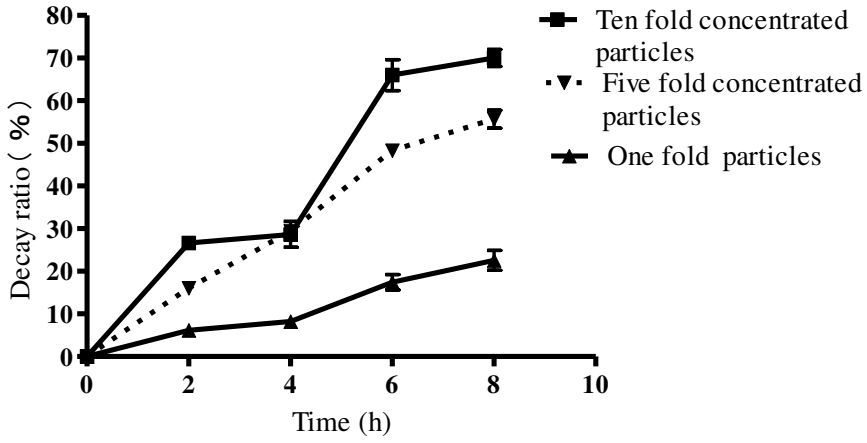

Decay ratio (mean ± SD) caused by UVA and UVB radiation

FIGURE 3

Particle materials in the water samples were concentrated by 5 and 10 folds respectively through centrifugation, and the un-concentrated water sample was applied as control. Influenza A virus suspension was mixed at ratio of 1:7 with above water samples and incubated in the dark. The viral titer was monitored during the incubation, and the decay ratio was denoted as the ratio (%) between the decreased viral titer at sampling time and the initial titer.

DISCUSSION AND CONCLUSIONS

Decay caused by UV irradiation. Our results indicated influenza A virus was sensitive to both of UVB and UVA. During a 2.5 hour period of irradiation, UVB and UVA equal to solar UV level led to a viral decay ratio of 100% and 91.7 ±3.6% respectively. The solar UV irradiation caused damage, especially the solar UVB caused dimes in the viral dsDNA was considered to be the main reason responsible for the loss of virioplankton infectivity [9, 17-19]. As to ssRNA virus like influenza A, the UV damage mechanism may be different. Research in human adenovirus type 2 (HAdV2) indicated UVB radiation was the major environmental factor challenging viral activation while UVA showed indirect photo-inactivation effect on HAdV2 [20]. Another research about HAdV2 demonstrated that genome damage induced by UVC light caused efficient inactivation, while the contribution of protein damage to the disinfection process was relevant for UVA combining exogenous sensitizer, and the full-spectrum sunlight may cause viral inactivation through both of genome and protein damage [21]. As to influenza A virus in this study, UVB may led to viral inactivation through both of genome and protein damage. However, UVA radiation alone also showed extensive inactivation effect, indicating that influenza A virus may contain endogenous sensitizers that could contribute to endogenous indirect inactivation.

Decay caused by non-light factors. In the absence of sunlight, heat-sensitive materials (especially heat-sensitive microparticles) [17] and heat-sensitive colloidal dissolved organic matter (DOM)[9] seemed to be an important factor regulating the viral infectivity. Our results indicated that heat-sensitive materials contributed 8.7-25% to influenza A virus decay. The proportion was close to that of viral decay observed in seawater (20% in average) [9]. The recent research in deep sea indicated that the extracellular enzymes controlled the virial decomposition through hydrolyzing the proteins of the viral capsids [22]. This suggests that the effect of heat-sensitive substances should be considered in assessing the maintenance of influenza A in eutrophic freshwaters.

Our results indicate that the viral decay ratio was highly correlated to the particle material concentrations. Similar phenomenon was observed in the Adriatic Sea. By studying the viral decay rates along a trophic gradient in the north Adriatic Sea, Bongiorni *et al* found out that particles appeared responsible for more than 56% of the total dark decay rate in eutrophic waters, while in oligotrophic waters the number was less than 6.6% [23]. The mechanism of this effect was contributed to the aggregate of virus and particles, since the viral recovery efficiency from the aggregate was very low [17]. These indicates that it will be more difficult for influenza A to maintain infectivity in eutrophic water than in oligotrophic water.

Influenza A virus was sensitive to both of UVB and UVA. UVB may led to viral inactivation through both of genome and protein damage, while UVA may inactive the influenza A virus through endogenous indirect inactivation. Heat-sensitive materials and particle material concentrations also play important role in influenza A virus decay process

ACKNOWLEDGEMENTS

This study was financially supported by the NSFC (National Science Foundation of China, No. 31370148) and .the Open Project Program of Engineering Research Center of Eco-environment in Three Gorges Reservoir Region, Ministry of Education, China Three Gorges University (KF2013-01).

REFERENCES

[1] Lupiani, B. and S.M. Reddy, (2009). The history of avian influenza. Comparative Immunology Microbiology and Infectious Diseases, 32(4): p. 311-323.

[2] Alexander, D.J., (2000). A review of avian influenza in different bird species. Veterinary Microbiology, 74(1-2): p. 3-13.

[3] Webster, R.G., et al., (1978). Intestinal Influenza - Replication and Characterization of Influenza-Viruses in Ducks. Virology, 84(2): p. 268-278.

[4] Hinshaw, V.S., R.G. Webster, and B. Turner, (1980).The Perpetuation of Orthomyxoviruses and Paramyxoviruses in Canadian Waterfowl. Canadian Journal of Microbiology, 26(5): p. 622-629.

[5] Murti, K.G., et al., (1992). Composition of the helical internal components of influenza virus as revealed by immunogold labeling/electron microscopy. Virology, 186(1): p. 294-299.

[6] Stallknecht, D.E., et al., (1990). Effects of pH, temperature, and salinity on persistence of avain influenza- virusese in water. Avian Diseases, 34(2): p. 412-418.

[7] Webster, R.G., et al., (1992). Evolution and ecology of influenza - A viruses. Microbiological Reviews, 56(1): p. 152-179.

[8] Wommack, K.E. and R.R. Colwell, (2000). Virioplankton: Viruses in aquatic ecosystems. Microbiology and Molecular Biology Reviews, 64(1): p. 69-114.

[9] Noble, R.T. and J.A. Fuhrman, (1997). Virus decay and its causes in coastal waters. Applied and Environmental Microbiology, 63(1): p. 77-83.
[10] Cheng, K., et al., (2007). Solar radiation-driven decay of cyanophage infectivity, and photoreactivation of the cyanophage by host cyanobacteria. Aquatic Microbial Ecology, 48(1): p. 13-18.
[11] Jassim, S.A.A. and R.G. Limoges, (2013). Impact of external forces on cyanophage-host interactions in aquatic ecosystems. World Journal of Microbiology & Biotechnology, 29(10): p. 1751-1762.
[12] Weinbauer, M.G., et al., (1999). Sunlight-induced DNA damage and resistance in natural viral communities. Aquatic Microbial Ecology, 17(2): p. 111-120.
[13] Brown, J., et al., (2014). Survivability of Eurasian H5N1 Highly Pathogenic Avian Influenza Viruses in Water Varies Between Strains. Avian Diseases, 58(3): p. 453-457.
[14] Davis-Fields, M.K., et al., (2014). Effects of Temperature and pH on the Persistence of Avian Paramyxovirus-1 in Water. Journal of Wildlife Diseases, 50(4): p. 998-1000.
[15] Tang, S., et al., (2014). Improved methods for isolation of avian influenza virus. Journal of Virological Methods, 210: p. 22-25.
[16] World Health Organization (WHO), (2002). Manual on animal influenza diagnosis and surveillance. Department of Communicable Disease Surveillance and Response,WHO Global Influenza Programme.
[17] Suttle, C.A. and C. Feng, (1992). Mechanisms and rates of decay of marine viruses in seawater. Applied and Environmental Microbiology, 58(11): p. 3721-3729.
[18] Wommack, K.E., et al., (1996). Effects of sunlight on bacteriophage viability and structure. Applied and Environmental Microbiology, 62(4): p. 1336-1341.
[19] Liao, M.-J., et al., (2010). Assessment of UV-B damage in cyanophage PP. Aquatic Microbial Ecology, 58(3): p. 323-328.
[20] Carratala, A., et al., (2013). Environmental effectors on the inactivation of human adenoviruses in water. Food and Environmental Virology, 5(4): p. 203-214.
[21] Bosshard, F., et al., (2013). Mechanisms of human adenovirus inactivation by sunlight and UVC light as examined by quantitative PCR and quantitative proteomics. Applied and Environmental Microbiology, 79(4): p. 1325-1332.
[22] Dell'Anno, A., C. Corinaldesi, and R. Danovaro, (2015). Virus decomposition provides an important contribution to benthic deep-sea ecosystem functioning. Proceedings of the National Academy of Sciences of the United States of America, 112(16): p. E2014-E2019.
[23] Bongiorni, L., et al., (2005). Viral production, decay rates, and life strategies along a trophic gradient in the north Adriatic sea. Applied and Environmental Microbiology, 71(11): p. 6644-6650.

Received: **04.11.2015**
Accepted: **09.02.2016**

CORRESPONDING AUTHOR

Yijun Zhao
College of Resources and Environmental engineering,
Hubei University of Technology,
Wuhan, China

e-mail: Zhaoyj2000@163.com

© by PSP Volume 25 – No. 10/2016, pages 4093-4102 Fresenius Environmental Bulletin

FRACTAL OF RANDOM PORE AND DIRECTIVITY OF SOIL SEEPAGE

Sun, Jichao[1*], Liao, Qian[2]

[1]School of Water Resource & Environment, China University of Geosciences, Beijing 100083, China
[2]Department of Civil & Environmental Engineering, University of Wisconsin, Milwaukee 53211, United States

ABSTRACT

Simply and rapidly obtaining the permeability coefficient of rock and soils is the requirement in geotechnical, geological and environmental engineering. A kind of threshold parameter in gray image of rock/sols is put forward, some stable fractal dimension pictures of soil porosity is generate, so the relationship formula of soil fractal dimension and permeability coefficient is established. The way in which the permeability coefficient is obtained by picture's fractal dimension is simple and rapid. The permeability coefficient of soil sampling in same random field, is different in x and y direction with the increasing of the sampling angles relative to the rock/soil layer. The discreteness of the permeability coefficient in x and y direction increases with the increasing of the permeability coefficient variance. So the sample needs increasing the density in this rock/soil. Secondly, the angle between rock/soil layer and seepage path is studied. The permeability coefficient in x and y direction has linear relationship when angle is $\pi/4$ while the relationship is confusion when angle is 0. So the sampling in 0 angle needs more rigorous measurement and test procedures.

KEYWORDS:

Permeability coefficient, random field, rock layer angle, directional permeability.

INTRODUCTION

The accurate and easy obtain of the rock and soils permeability coefficient is an important work in research and engineering, such as the unsaturated soil water evaporation and temperature coupling analysis[1], the cracking of rock and soils[2], the influence factors of permeability coefficient in numerical simulation about soil liquefaction[3], the plant roots absorbing water [4, 5], ocean engineering construction[6], underground sediment transport[7, 8], landslide disaster[9] and the embankment cracking and collapsed[10, 11], and the radioactive pollution of the groundwater[12].

There are many methods that can be used to obtain the permeability coefficient. The general method is to make experiment in laboratory to the sample from the field[13]. The Hazen formula, Kozeny-Carman formula, Pavchich formula, and Shahabi et al. formulas were used to predict the coefficient of permeability of nonplastic soils [14] too. Fitting parameters method[15], and neural network model[6, 16] is used to estimate the permeability coefficient of soils. These methods are very complicated, and sometimes inaccurate[6]. This paper is dedicated to simplify the cumbersome process, save cost, find and get some questions when sampling in fields, and put forward some matters needing attention to provide the reference and help in obtaining the permeability coefficient of rock and soils in future.

The work in the paper has two parts. (1) The fractal dimension is obtained by processing the picture of rock and soils. The permeability coefficient is gotten by numerical simulating the seepage of the rock and soils. Then the connection between the permeability coefficient and the fractal dimension of soils picture is set up. In this way, the permeability coefficient is represented by the fractal dimension to simplify the experiment process. (2) The second part is to study the relationship between the angle of rock layer/the seepage direction, and the standard deviation of the permeability coefficient. The random data field of the permeability coefficient under the four different standard deviation (0.1,0.2,0.3,0.4) is rotated 200 different angles. The permeability coefficient in x and y direction is gotten in the random data field. In another simulation, 500 different random data fields

are rotated four different angles (0, π/6, π/4, π/3). At same time, the two direction permeability coefficients are obtained. By analyzing the phenomenon and laws, many considerations are set up.

Fractal dimension of soils. Soils have the self-similar fractal structure characteristics in a statistical sense. Using the similar method to quantitative descript the fractal features of soil complicated seepage, and to reveal the physical properties of soil behavior, is an important means to study the soil seepage from micro to macro[17].

Soil is composed of tiny particles and pore, pore is filled with water, and water flows in the pore. There is a transition zone between pore and soil particles. The seepage channel is a grey area of open and closed. At this time, the permeability coefficient is between the maximum and the minimum. A grey parameter r characterizes the transition. There are many different relationship between r and the permeability coefficient. It is linear or hyperbolic. In the paper, the linear relationship is chosen. That is K=0 when n=0; K=rr×K_{max}, when $n\in$[0,1]; K=Kmax when n=1.

The physical parameters in the transitional zone are not clear and the seepage is complex, since the pore and the transitional zone position is random. So the permeability coefficient is the macro effect of soil seepage. The relationship between the macro seepage and the microstructure in soils is very complex too. In these two reasons, the permeability coefficient is difficult to analytical analysis.

A good ways to solve the above problems is fractal dimension method in mathematics. The box fractal dimension of soil connecting the microstructure with macro characteristics, can not only reflect the features of soil porosity and soil particle microstructure, but also reflect the overall seepage characteristics of soil in the macro. The box fractal dimension has nothing to do with the scale parameter.

This box dimension method[18] is used to obtain the relationship between the soil particles/pore in the paper. Grassberger adopted commonly grid method (Box counting method)[19] to get the box dimension of soils. The basic idea is to use a different length of the square grid to cover soil. There is a change when the length of a square grid ε, the grid number N(ε) covered the measured soil changes. Eq. (1) is established according to the fractal theory:

$$N(\varepsilon)\propto\varepsilon^{-D} \quad (1)$$

When the length of a square grid is ε_1, ε_2, ε_3,……, ε_k, the number of the square grid covered the measured soil is N(ε_1), N(ε_2), N(ε_3), ……, N(ε_k). Take logarithm of Eq. (1) both sides, then

$$\lg N(\varepsilon)=-D\lg\varepsilon+A \quad (2)$$

Where A is a undetermined constant, D is the fractal dimension of soils, which is the absolute value of the slope.

Random soils model. Soil is composed of a large amount of soil particles and pores. As different physical properties of these particles and soil pore, soil is heterogeneous. In this section, stochastic soil structure is established by the computer, and different physical parameters are given for the subsequent calculation.

The main soil parameter is the permeability coefficient K, which is control by the void ratio or the porosity[7, 20], that is $K=n(\gamma_w/\mu)(d^2_0/32)$, $d_0=2.67n/(1-n)\times D_h/\alpha$, $D_h=1/\sum(\Delta S_i/Di)$; where α is the shape coefficient, 6 when the soil granular is treated as a ball; n is the porosity; and K is the seepage coefficient; μ is the viscosity of water, 1.01×10^{-3} pa·s when the temperature is 20°C; γ_w are the unit weight of water and d_0 is the minimum pore diameter. Di is the average diameter in the ith interval of the particle size distribution curve of the sample considered and Si is the weight of grains in the ith interval divided by the total weight of the sample.

The permeability coefficient is a function of porosity. Soil with the random structure can be established by random porosity within a certain range. The process can be run by computer. Random coordinates have random number porosity matrix. The random coordinate is (X_R,Y_R,N_R), Where $X_R=(x_{max}-x_{min})$Rand(), $Y_R=(y_{max}-y_{min})$Rand(), $N_R=N_{max}$Rand(); rand() generates the random number within (0,1); x_{max},x_{min},y_{max},y_{min} are the maximum and the minimum in studied area; N_{max} is the maximum porosity in the area.

Random porosity generated in the random coordinates, since coordinates are random and not equally spaced equidistant grid or a rectangular area, can not be assigned to the porosity of the above mentioned soil. Voronoi diagram can to solve this problem.

Voronoi diagram[21, 22] (shown in Fig.1) is a division of a plane. Any two points in the control point set P ={p1, p2, ..., pn} is not co-located, and there is no four points on a circle[23]. The distance from any point in an arbitrary convex polygons

(Voronoi polygons), to any control points pi, is less than the distance from the point to any other control points pj. Any vertex in Voronoi polygons is the center of the triangle circumcircle.

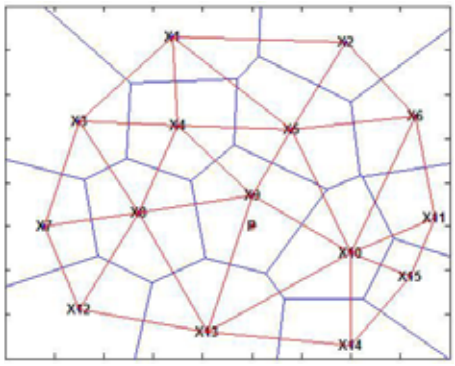

FIGURE 1
Voronoi diagram.

As shown in Fig. 1, X_i is the random coordinate and porosity, the neighboring Xi points can be connected into the red triangle by straight lines. Then these triangles perpendicular bisector for each side is drawn. Some perpendicular bisectors near X_i form a polygon. The porosity of the X_i represent the porosity of the polygon area, namely the whole polygon zone has the same porosity. As shown in Fig. 2, a random porosity soils are generated.

Relationship between fractal dimension and permeability coefficient. The fractal dimension of soils can be obtained by analysizing the soils picture. And the permeability coefficient of soils is gotten by the numerical simulation. Then the connection between the fractal dimension and the permeability coefficient is established. In this way, the permeability coefficient can be skimpily obtained.

A series of coordinate porosity data, maximum porosity at 1, the minimum porosity at 0, 2, are generated, as shown in Fig. 2. The permeability coefficient and connected parameters along the seepage path AC are shown in Fig.2. The position with the max porosity can be treated as air, and the water can directly flow through it. The position with the min porosity is close-grained. The place between the 0 and 1 is the transition zone.

In order to study the relationship between the permeability coefficient in random field and fractal dimension of soil, a threshold is established to obtain a soil grayscale.

In a same random field, random numbers are changing with the distance, shown in Fig. 3 upper curve. The different threshold *Th* is proposed to cut off the curve. The upper of the *Th* is the pore which water can flow through. The lower of the *Th* is the soil. The black-white line is set up at the bottom of the Fig. 3, which is the pattern on a plane shown in Fig. 4.

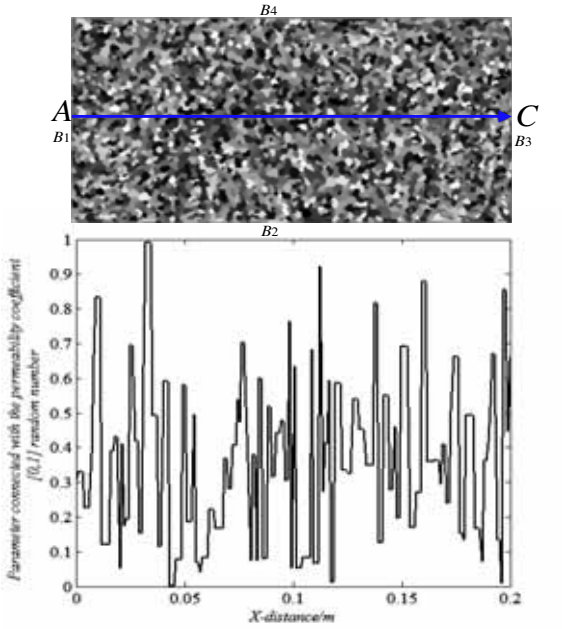

FIGURE 2
Random porosity of soils.

The top figure shows the random porosity of soils, white position represents the porosity is 1, and black position represents the porosity is 0. The bottom figure is the parameter connected with the permeability coefficient on Line *AC* in top figure. The length of the *B*1, *B*3 is 0.1m. The length of the *B*2, *B*4 is 0.2m.

The advantages of using the threshold are: (1) The fractal dimension has the good gradation stability; (2) The random field has certain seepage flow stability. So the fractal dimension and the seepage characters have good regularity.

According to the Eq. (2), the box dimension of the picture in Fig. 4 is calculated.

The fitting curve equation of Fig. 4A is $\lg N=-1.561883\lg r+11.6963$ when $Th=0.6$. The correlation coefficient R=0.9991. $\lg N=-1.544394\lg r+11.6058$ when $Th=0.62$. The correlation coefficient R=0.9990.

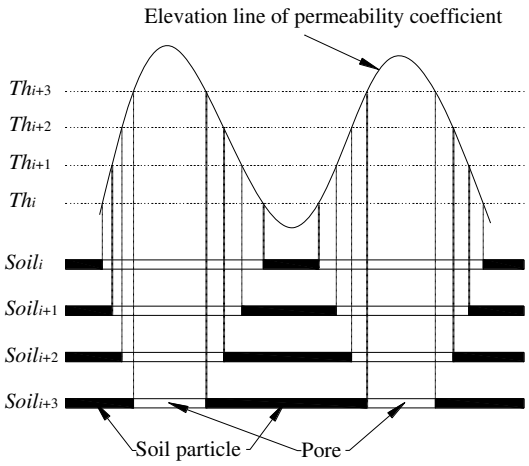

FIGURE 3
Relationship between permeability coefficient and porosity threshold.

The seepage and fractal dimension of soils in Fig. 4 ~~to get the~~ is calculated. The porosity, B3 (In Fig. 3) output flow flux, *K*eq, and fractal dimension are shown in Table 1. And fit the number in Table 1, the formula is,

$$Ked\times 1e3=6.27e^{10.0321\times(Fd-1)}+572 \quad (3)$$

The equation parameters of other *Th* is in table 1. In Table 1, the pressure on the Boundary *B*1 is 10000 *Pa*, *Th* is the thresholds of porosity, *Fd* is the fractal dimension of soils, the pressure gradient is 5.102041 that has no unit, and *Keq* is the equivalent permeability coefficient. The correlation coefficient of *Por* and *Fd* is 0.9957, that is the two parameters are highly correlated.

Soil fractal dimension and porosity have a direct relationship. As shown in Figure 5A, the porosity and the fractal dimension have a linear relationship. And at the same time, the porosity and the permeability coefficient have the close relationship, as shown in Fig. 5B.

Eq. (3) is the final formula describing the connection between the soil fractal dimension and the permeability coefficient. The process is, the image processing of soil, calculation of the fractal dimension according to the Eq. (2), and the soil permeability coefficient obtention according to the Eq. (3). This way is a simple method to obtain the soil permeability coefficient.

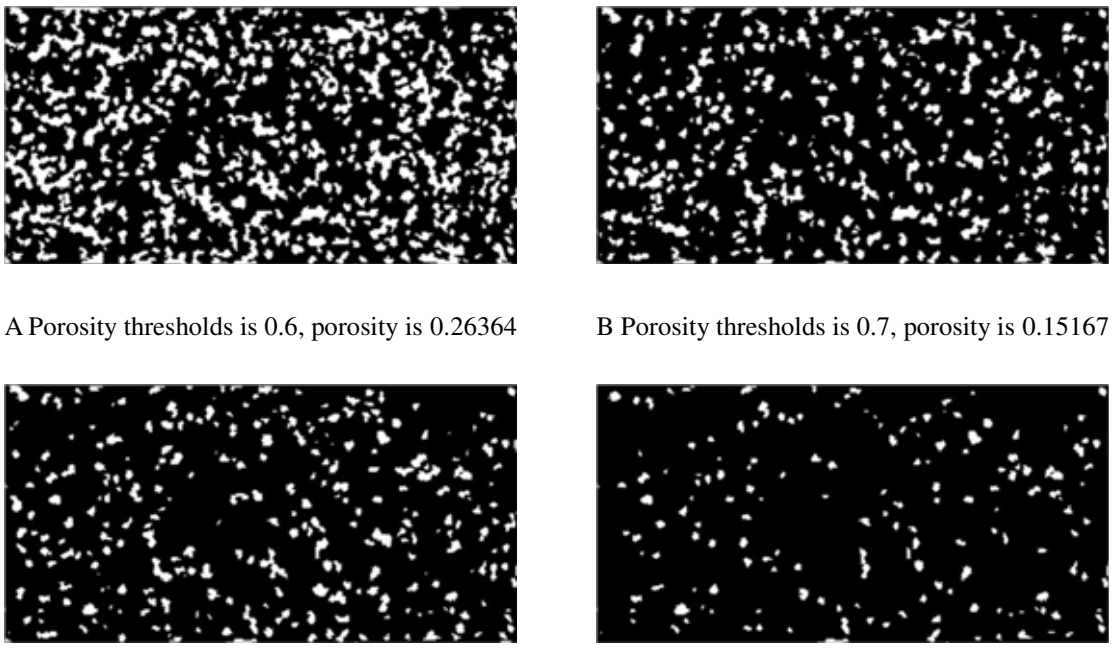

A Porosity thresholds is 0.6, porosity is 0.26364

B Porosity thresholds is 0.7, porosity is 0.15167

C Porosity thresholds is 0.8, porosity is 0.10449

D Porosity thresholds is 0.9, porosity is 0.052428

FIGURE 4
The porosity picture under different thresholds.

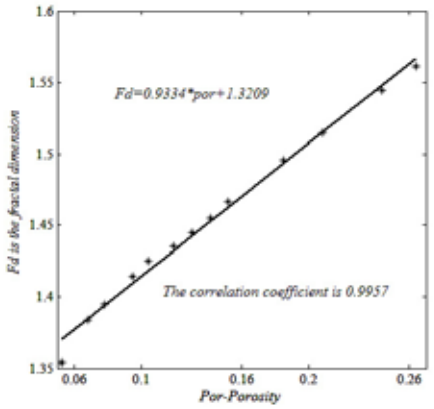

A Correlation between the porosity and the fractal dimension

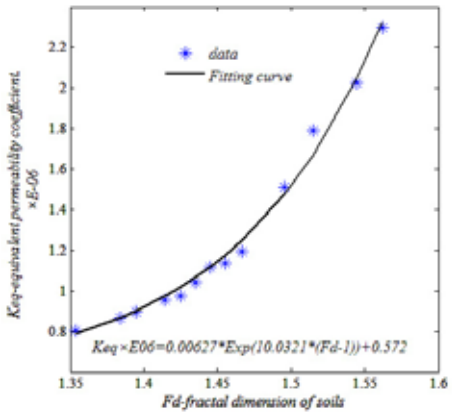

B Relationship between permeability coefficient and porosity

FIGURE 5
Correlation of porosity, permeability coefficient and fractal dimension.

TABLE 1
The fractal dimension and equivalent permeability coefficient of the soils.

Sample	Th	Por	Fd	Fig.4	Flux on B3	Keq
1	0.60	0.263641	1.561883	Fig.4A	1.1733E-06	2.29961E-06
2	0.62	0.243309	1.544394		1.0348E-06	2.02822E-06
3	0.65	0.208255	1.514720		9.1465E-07	1.79271E-06
4	0.67	0.18497	1.495602		7.7121E-07	1.51157E-06
5	0.70	0.15167	1.466492	Fig.4B	6.0916E-07	1.19395E-06
6	0.72	0.141381	1.455220		5.7925E-07	1.13533E-06
7	0.75	0.130216	1.444802		5.6838E-07	1.11403E-06
8	0.77	0.119085	1.435179		5.3164E-07	1.04201E-06
9	0.80	0.104492	1.424822	Fig.4C	4.9788E-07	9.75844E-07
10	0.82	0.095027	1.414511		4.8618E-07	9.52917E-07
11	0.85	0.078264	1.394431		4.5749E-07	8.96685E-07
12	0.87	0.068201	1.383661		4.4161E-07	8.65547E-07
13	0.90	0.052428	1.353855	Fig.4D	4.1025E-07	8.04100E-07

Directivity function of permeability coefficient. During sampling in field for obtaining the soil permeability coefficient, the rock/soils itself has a certain stratification with different permeability of each layer. When there is an angle between the seepage path and rock/soil layer, the seepage perhaps is different. So it is great significant that study the seepage of rock/soil with this angle. In this section, a random seepage field is set up, rotated an little angle, then the seepage is calculated to get the permeability coefficient in X and Y direction. In this way, the permeability coefficient in two directions and the rotate angle are considered to find some regularity.

The soil permeability coefficient is normally distributed[24, 25] because of the random solid particles and structures[26]. The probability density function for the normal distribution is,

$$f(x)=\frac{1}{\sqrt{2\pi\sigma}}\exp\left(-\frac{(x-\mu)^2}{2\sigma^2}\right)$$

$$\begin{bmatrix} x_{11} & x_{12} & \cdots & x_{1n} \\ x_{21} & x_{22} & \cdots & x_{2n} \\ \vdots & \vdots & \vdots & \vdots \\ x_{m1} & x_{m1} & \cdots & x_{mn} \end{bmatrix}, \begin{bmatrix} x_{1j}\sim N(\mu_1,\sigma_{1j}) \\ x_{2j}\sim N(\mu_2,\sigma_{2j}) \\ \vdots \\ x_{mj}\sim N(\mu_m,\sigma_{mj}) \end{bmatrix}, \begin{bmatrix} \mu_1 \\ \mu_2 \\ \vdots \\ \mu_m \end{bmatrix} \sim N(\mathrm{U},\Omega) \quad (4)$$

Point A (x0, y0), around the origin (0, 0), is clockwise rotated α. The last point is A'(x1, y1). The rotation function of the coordinates is,

$x_1=x\cos\alpha-y\sin\alpha$, $y_1=y\cos\alpha+x\sin\alpha$ (5)

According to the Eq. (4) and (5), a example is given. The parameters U=0.7, Ω=0.5, σ_{ij}=0.08. In area, $0\le x\le 0.2, 0\le y\le 0.1$. The rotate angle is α=0, π/6, π/4, π/3. The random field is shown in Fig. 6.

The permeability coefficient K is the only parameter describing the soil/rock seepage in the previous research. But the rock/soil is not completely homogeneous and has a normal random distribution. Therefore the permeability coefficient should contain σ in the normal distribution N(μ,σ). μ is the K. These two parameters, μ and σ, constitute the physical parameters of rock and soil, which represent the seepage of rock/soil.

Research on how to get the normal parameters connected with the permeability coefficient, is great significant to study the stratum permeability. Since the rock/soil permeability is random to some degree, the process is very complex if the traditional method is used. Proposing a more concise scientific methods to obtain these parameters, through the test sample as little as possible, it is of great value in engineering.

Kx is the permeability coefficient in X direction, *Ky* is the permeability coefficient in Y direction. The goodness of fitting line is $R=1-[\sum(y-y^*)^2/\sum y^2]^{0.5}$. R is nearer 1 means the fitting is better.

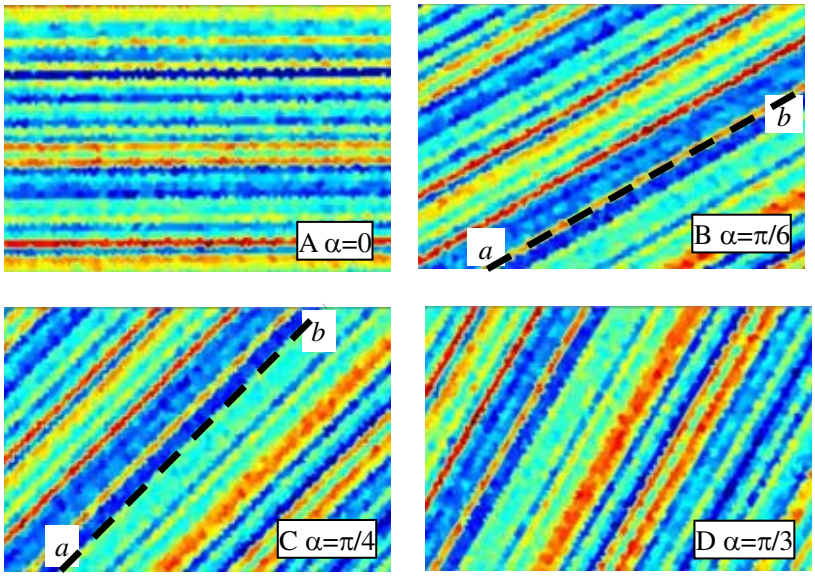

FIGURE 6
Rotating random field of permeability coefficient.

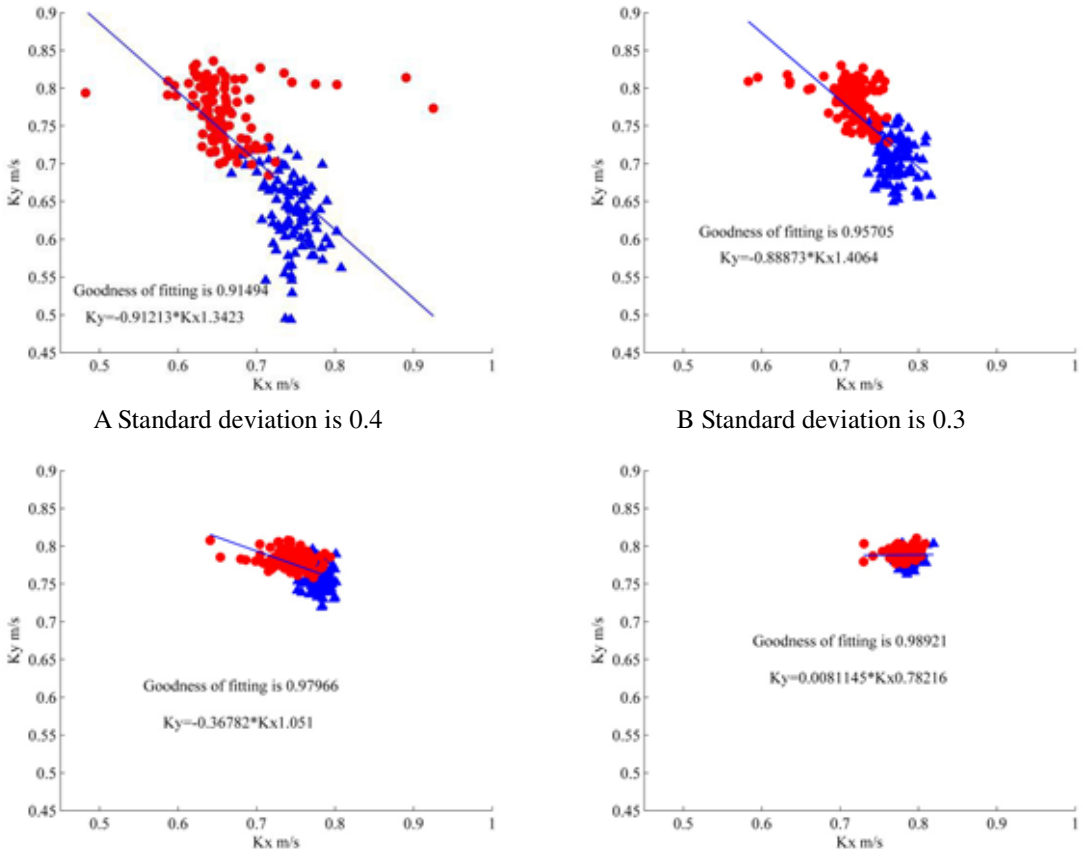

A Standard deviation is 0.4 B Standard deviation is 0.3

C Standard deviation is 0.2 D Standard deviation is 0.1

FIGURE 7
The points (*Kx*, *Ky*) under 200 different angles.

The seepage field is not completely homogeneous, has a certain directionality and has a strong penetration stratification. The seepage field is like the rock/soil layer. The two orthogonal directions in the seepage field is X^k and Y^k. The permeability coefficient for each point in the direction of X^k is normal distributed $N(\mu,\sigma)$ and has a certain stratification. The parameters of the permeability coefficient in the direction of Y^k is μ_j and σ_j. Namely the permeability coefficient of every point in random field is normal distributed $N(\mu_j,\sigma_j)$, where j characterizes the different rock layers.

In Fig. 7, $K\sim N(\mu_j,\sigma_j)$, $\mu_j\sim N(\mu_0,\sigma_0)$, where $K\sim N(\mu_j,0.08)$,$\mu_j\sim N(0.8, \sigma_0)$, namely $\sigma_j=0.08$, $\mu_0=0.8$, $\sigma_0=0.1,0.2,0.3,0.4$. *Kx* is the permeability coefficient in X direction, *Ky* is the permeability coefficient in Y direction. The goodness of fitting line is $R=1-[\sum(y-y^*)^2/\sum y^2]^{0.5}$. R is nearer 1 means the fitting is better. An random field is established, then is rotated an angle $i\pi/400$, where $i\in 1,2,\ldots,200$. There are 200 points. Fig. 7 ▲ points are 1-100, and the corresponding rotation angle is from $\pi/400$ to $\pi/4$. ● points are 101-200, and the corresponding rotation angle is from $\pi/4$ to $\pi/2$. The sample size is 0.2m×0.1m. When the angle is 0, the permeability direction in X and Y directions and seepage rock layer direction coincides.

From Fig. 7, the laws and the corresponding mechanism are as follow,

(1) With the increase of the rotation angle, the ● point in figure gradually move up and to the left. While the ▲ point moves down and to the right with the decrease of the rotation angle. With the increase of the rotation angle, the permeability coefficient K_x decreases, while K_y increases, namely the direction of the dominant permeability coefficient transfers from *x* direction to *y* direction. The natural reason is that the direction of the rock/soil layer changes with the rotation of the random field. And the permeability coefficient in rock/soil layer is more than that between layers.

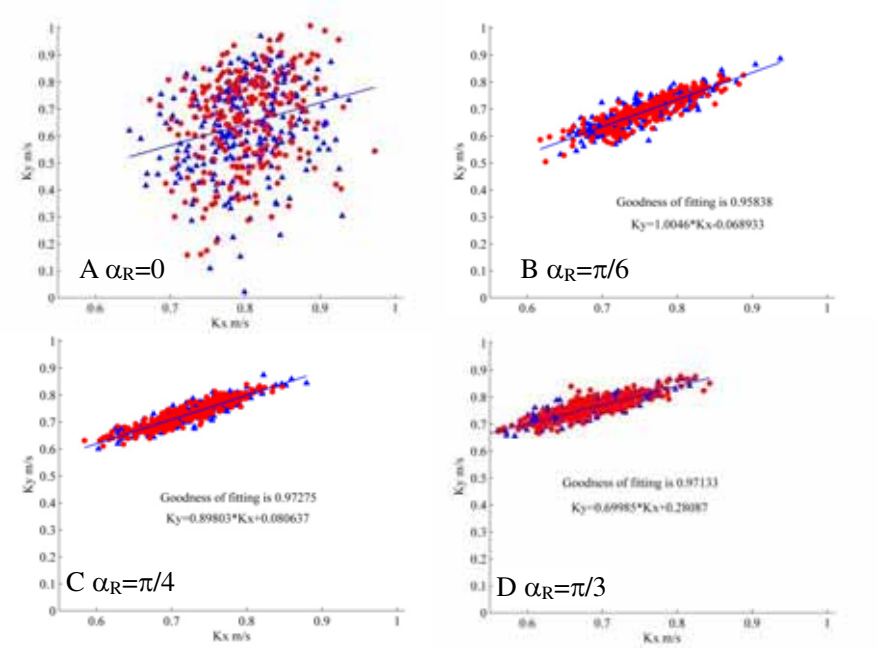

FIGURE 8
Points (*Kx*, *Ky*) of 500 random fields under 4 rotation angles (α_R).

(2) With the standard deviation increasing, the permeability points in Fig. 7 gradually diverging. While with the standard deviation decreasing, permeability coefficient points become more centralized. The reason is that the average permeability coefficient of each layer are normally distributed, N(0.8, σ_0). When σ_0 is larger, the volatility of the permeability coefficient is greater, and the difference between the layer permeability coefficients is greater. When rock/soil layer rotates a certain angle, rock/soil layer with larger permeability coefficient cuts through along y direction, so the *ky* becomes larger. Similarly, when the cut-through layer with less permeability coefficient, the *ky* becomes less. Thus rock/soil layer with high permeability coefficient cutting through or not, will increase and decrease K_y.

(3) Under the same standard deviation, with the increase of the rotation angle, the divergence of points is also enhanced. The reason is that as the angle increases, some layers in y direction is gradually penetrating, for example, in Fig. 6B and 6C , layer *ab* doesn't penetrate when π/6, while penetrate when π/4. If the permeability coefficient μ of *ab* layer is larger, the K_y significantly increases, and K_x significantly reduced.

The calculation process in Fig. 8 and Fig. 7 is almost same. But *Kx* and *Ky* in Fig. 7 is gotten from the 4 porosity random fields with 200 different rotation angles. But *Kx* and *Ky* in Fig. 8 is gotten from the 500 porosity random fields with the rotation angles of 0,π/6,π/4 and π/3. In Fig. 8, the parameters are K~N(μ_j,0.08), μ_j~N(0.8, 0.03), namely σ_j=0.08,μ_0=0.8,σ_0=0.3.

In Fig. 8 ▲ points are the first 250 points, and● points represents 250 points behind. From the figure, the following regularity and the mechanisms are:

(1) ▲ points and ● points are intermixed, and no significant separation, which means 500 sampled regions, has good porosity randomness.

(2) Under the sampling angle π/6, π/4 and π/3 except 0, *Kx* and *Ky* show a significant linear relationship.

In different porosity random fields, since the permeability coefficient is normally distributed at 0 angle, different layer has great difference and has no connection. So the permeability layer in x direction becomes the aquifuge in y direction. While the aquifuge layer in x direction becomes permeable in y direction. The *Kx* and *Ky* have no linear relationship.

Under the angle π/6, π/4 and π/3, some parts of rock/soil cuts through in x and y direction, as layer *ab* shown in Fig. 7B. Since layer *ab* cuts through seepage path, *Kx* and *Ky* is larger if the

layer *ab* is more permeable. Otherwise, *Kx* and *Ky* is smaller. *Kx* and *Ky* have the linear relationship.

(3) From Fig. 8A to 8B, then to 8C, and from Fig. 8D to 8C, the deviation degree from the straight line decreases. Namely, when the angle is nearer $\pi/4$, all points are nearer the straight line and the linear extent becomes more significant.

Mechanism: With the rotation angle approaching $\pi/4$, more rock/soil layers cut through in the X and Y direction, and the impact of rock itself permeability coefficient on *Kx* and *Ky* is more. *Kx* and *Ky* will be more closely linked to the rock/soil permeability coefficient. The *Kx* and *Ky* has good linear relationship. Therefore, better linearization between *Kx* and *Ky* is appears when the angle is closer to $\pi/4$.

CONCLUSION

(1) The permeability coefficient of rock/soil can be obtained by the picture fractal dimension of rock/soil. Gray images of rock and soil mass have fractal properties. The fractal dimension of rock/soil is connected with the rock/soil porosity. The rock/soil porosity and the fractal dimension have a specific relationship. In the paper, the equation of the grey picture fractal dimension and permeability coefficient is established. The model can be referred. The formula is somewhat different, but the form of the formula is same.

(2) In a stable random field, sampling angles effect on *Kx* and *Ky*. The affection sampling angle on *Kx* and Ky is different, namely. *Ky* increases but *Kx* decreases with the angle increasing. The sampling times can be reduced by understanding the angle. The fact the discrete is great standards deviation is great, so the sampling needs to strengthen.

(3)There is and angle between the seepage direction and the rock/soil layer direction. When the angle is small and far from $\pi/4$, the permeability coefficient has great discrete and instability. In this conditions, the angle is important for obtaining *Kx* and *Ky*. The three parameters the angle, *Kx* and *Ky* need to be strictly measured. When the angle is close to $\pi/4$, the three parameters can be gotten in less samples and experiments.

(4)The rock/soil permeability coefficient is normally distributed, $K \sim N(\mu_j, \sigma_j)$, $\mu_j \sim N(\mu_0, \sigma_0)$. There are 7 parameters of μ_j, σ_j, μ_0, σ_0, α, *Kx* and *Ky* which describe the rocl/soil seepage. The 7 parameters have some certain relationship. Some can de deduced by others. For example σ_j, μ_0, σ_0 and α are enough. These parameters characterize the seepage characteristics of rock/soil. These parameters can help researchers to enhance understanding the permeability coefficient of rock/soil.

ACKNOWLEDGEMENTS

This work is supported by the National Natural Science Foundation of China (No. 51179177) , China State Scholarship Found (No.: 201208110444).

REFERENCES

[1] Sun J.C., Gao Q.C., Wang H.B., Li Y.M. Numerical simulation of coupled rainfall and temperature of unsaturated soils. Key Engineering Materials, 2006, 306-308(2): 1433-1438.

[2] Sun Jichao, Wang Guangqian, Sun Qicheng. Crack spacing of unsaturated soils in the critical state. Chinese Science Bulletin, 2009, 54(12): 2008-2012.

[3] Rahmani A., Fare O. G., Pak A. Investigation of the influence of permeability coefficient on the numerical modeling of the liquefaction phenomenon. Scientia Iranica, 2012, 19(2): 179-187.

[4] Sun Jichao, Liao Qian, Wang Guangqian. Not light or gravity but water guiding root to grow. Optik-International Journal for Light and Electron Optics, 2016, 127(8): 3834-3839.

[5] Sun Jichao, Liao Qian, Wang Guangqian. Root Absorbing and Seepage Model in Weightless Environment and Space. Bangladesh Journal of Botany, 2015, 44(5): 779-786.

[6] Park H. I. Development of Neural Network Model to Estimate the Permeability Coefficient of Soils. Marine Georesources & Geotechnology, 2011, 29(4): 267-278.

[7] Sun Jichao. Mathematical model coupling seepage and sedimentation of solid particles in porous media. Fresenius Environmental Bulletin, 2015, 24(5): 1735-1741.

[8] Sun Jichao Wang Guangqian. Transport model of underground sediment in soils. Scientific World Journal, 2013, Articale Number: 367918.

[9] Chandrasekaran S. S., Owaise R. S., Ashwin S., Jain R. M., Prasanth S., Venugopalan R. B.

Investigation on infrastructural damages by rainfall-induced landslides during November 2009 in Nilgiris, India. Natural Hazards, 2013, 65(3): 1535-1557.
[10] Sun Jichao. The phenomenon of the floating riverbank collapse by water scouring. International Journal of Ground Sediment and Water, 2014, 1(1): 5-8.
[11] Sun J.C. Wang G.Q. Riverbank Collapse Mechanism Under Scouring. 2010, Germany: VDM Publishing House.
[12] Sun Jichao Wang Guangqian. Research on underground water pollution caused by geological fault through radioactive stratum. Journal of radioanalytical and nuclear chemistry, 2013, 297(1): 27-32.
[13] Horseman S. T., Harrington J. F., Noy D. J. Swelling and osmotic flow in a potential host rock. Physics and Chemistry of the Earth, 2007, 32(1-7): 408-420.
[14] Dolzyk K. Chmielewska I. Predicting the Coefficient of Permeability of Non-Plastic Soils. Soil Mechanics and Foundation Engineering, 2014, 51(5): 213-218.
[15] Gui M. W. Hsu C. S. Generalized Fitting Parameters of Three Permeability Functions for Predicting Water Coefficient of Permeability of Lateritic Soil. Geotechnical Testing Journal, 2009, 32(5): 418-427.
[16] Yilmaz I., Marschalko M., Bednarik M., Kaynar O., Fojtova L. Neural computing models for prediction of permeability coefficient of coarse-grained soils. Neural Computing & Applications, 2012, 21(5): 957-968.
[17] Gimenez D., Allmaras R. R., Nater E. A., Huggins D. R. Fractal dimensions for volume and surface of interaggregate pores - Scale effects. Geoderma, 1997, 77(1): 19-38.
[18] Bird N., Diaz M. C., Saa A., Tarquis A. M. Fractal and multifractal analysis of pore-scale images of soil. Journal of Hydrology, 2006, 322(1-4): 211-219.
[19] Grassberger Peter. On Efficient Box Counting Algorithms. International Journal of Modern Physics C, 1993, 4(4): 515-523.
[20] Indraratna Buddhima Radampola Sujeewa. Analysis of critical hydraulic gradient for particle movement in filtration. Journal of Geotechnical and Geoenvironmental Engineering, 2002, 128: 347-350.
[21] Guibas L. Stolfi J. Primitives for the manipulation of general subdivisions and the computation of voronoi diagrams. Acm Transactions on Graphics, 1985, 4(2): 74-123.
[22] Aurenhammer F. Voronoi diagrams - a survey of a fundamental geometric data structure. Computing Surveys, 1991, 23(3): 345-405.
[23] Rieger J. H. Voronoi Diagrams of Real Algebraic Sets. Geometriae Dedicata, 2003, 98(1): 81-94.
[24] Xie Yonghua, Huang Guanhua, Zhao Lixin. Spatial Variability of Field Soil Properties. Journal of China Agricultural University, 1998, 3(2): 41-45.
[25] Huang Guanhua. A Review of Experimental Study on Spatial Variability of Soil Hydraulic Properties. Advances in Waterence, 1999, 10(4): 450-457.
[26] Sun Jichao. Ground Sediment Transport Model and Numerical Simulation. Polish Journal of Environmental Studies, 2016, 25(4): 1691-1697.

Received: **06.11.2015**
Accepted: **23.04.2016**

CORRESPONDING AUTHOR

Sun, Jichao
School of Water Resource & Environment
China University of Geosciences
Beijing 100083 - CHINA

E-mail: jichao@email.com

© by PSP Volume 25 – No. 10/2016, pages 4103-4110 Fresenius Environmental Bulletin

THE GENETIC HETEROGENEITY OF FACULTATIVE ALKALIPHILIC BACILLUS SPECIES ISOLATED FROM SODA LAKE

Cumhur Avsar [1], Zeynep Yegin [2*], Seyhan Civek [1], Ismet Berber [1]

[1] Department of Biology, Faculty of Science and Arts, Sinop University, Sinop, 57000, Turkey
[2] Medical Laboratory Techniques Program, Vocational School Of Health Services, Sinop University, Sinop, Turkey

ABSTRACT

In this study, the genotypic diversity of 26 *Bacillus* strains, including 24 facultative alkaliphilic isolates from the waters and surrounding soils of Lake Van, Turkey and 2 reference strains were investigated. Plasmid profiling and RAPD-PCR were used to determine the genetic variability of the isolates. The plasmid profiling analysis confirmed all the isolates had plasmids and 20 isolates were allocated into three major groups excluding the ones with unique plasmids. A total of six oligonucleotide primers were used for RAPD amplification, which generated a total of 505 fragments, all of them were polymorphic. A numerical analysis of the DNA band profiles with 6 different primers was generated by unweighted pair group method with arithmetic mean (UPGMA). The genetic distances among the isolates using the primers M13-10, M13-14, OPL3, OPL12, RAPD12, and RPO2 were at percentage similarities between 16 to 100%, 12 to 100%, 28 to 94%, 4 to 100%, 31 to 100% and 8 to 80% respectively. The results of the study suggested that RAPD-PCR technique can provide rapid and efficient approach to solve taxonomic difficulties among the facultative alkaliphilic *Bacillus* isolates at the strain level.

KEYWORDS:
Bacillus spp., RAPD-PCR, Lake Van, dendrogram, heterogeneity

INTRODUCTION

Lake Van which is located at 1,648 m above sea level, with a maximum depth of 450 m and a volume of 607 km^3 is known as the largest soda lake on Earth. It also has a much lower salinity of 2.17% compared to other soda lakes (5% up to saturation, approximately 30%) contributed mainly by calcium, sodium, chlorine, and carbonate ions and by sulfate, potassium and magnesium minorly [1]. Soda lakes are natural alkaline environments defined with large amounts of soda (Na_2CO_3) that may be present in the form of natron (Na_2CO_3) or trona ($Na_2CO_3/NaHCO_3$) [2]. Soda lakes were asserted as the potential origin of microbial diversity [3]. Turkey with two soda lakes called as Lake Van and Lake Salda is among twenty countries that harbour soda lakes and soda deserts worldwide [4]. Soda Lake Van Gram-positive members include close relatives of alkaliphilic hydrocarbon-degrading *Planococcus* and *Bacillus* strains or related environmental sequences together with other microorganisms [1].

Alkaliphilic bacteria grow over the pH range 7.5-11.5 and can be divided into two groups as obligate alkaliphiles (growth pH: 9.0-11.5) and facultative alkaliphiles (growth pH: 7.5-11.2) [5]. The genus *Bacillus* consists of a large number of species and at least six phylogenetically distinct groups based on the molecular analyses of 16S rRNA sequences [6]. Alkaline-stable enzymes derived from alkaliphilic microorganisms have led to the application of enzymes mostly in laundry and dishwashing detergents, as well as leather tanning, paper pulp bleaching, production of cyclodextrins, and treatment of agricultural wastes from food processing industries [7]. Thus, alkaliphilic Bacillus species may also have industrial applications that stem from their potentials to produce alkaline enzymes such as protease, cyclomaltodextrin glucanotransferase and cellulose [8]. Alkaline proteases are the most suitable members as detergent additives since they can digest proteinaceous stains. Protease idea was first initiated by Röhm (German Patent GP283923, 1913) with incorporation of pancreatic enzymes into a detergent and the first detergent containing bacterial protease was on the markets in the 1960s. The used enzyme was subtilisin Carlsberg from *Bacillus licheniformis* and the compatible nature of the enzyme with detergent matrices has led to the development of new proteases with better washing performance as detergent additives worldwide [9]. Though alkaline proteases are the most produced, other alkaline enzymes such as alkaline cellulases, alkaline amylases, and alkaline lipases also act as detergent additives to improve cleaning efficiency. Enzymes derived from *Bacillus* species including the alkaliphilic ones cover nearly half of the total industrial enzyme market [10]. Biotechnological potential of the applications together with relatively easy cultivation conditions have attracted the

interest of a vast number of workers and much effort has focused on *Bacillus* spp. as an alkaliphilic microorganism.

Several methods have been used for the molecular identification of bacterial species involving random amplified polymorphic DNA (RAPD), 16S-23S rRNA internal transcribed spacer-PCR (ITS-PCR), repetitive sequence element (REP-PCR) and amplified ribosomal DNA restriction analysis (ARDRA) [11]. In the analysis of microbial communities, RAPD fingerprinting is a very useful technique. The elimination of culture dependent procedures makes RAPD a favorable candidate for the representation of the entire microbial community [12].

RAPD assay also referred to as arbitrary primed (AP)–PCR takes advantage of using synthetic primers of 10 bases in length. While fluorescent probes and PCR offer powerful approaches as genotypic characterization methods, these methods require sequence information of the investigated organisms. On the other hand, RAPD-PCR uses arbitrary primers and can detect polymorphisms with no prior knowledge of the specific sequence information. Thus, even closely related strains of the same species can be differentiated at molecular level with the generation of polymorphic genomic fingerprints [13-14].

The aim of the presented study was to analyse the genotypic biodiversity of 26 *Bacillus* strains, including 24 native isolates from Lake Van, Turkey and 2 reference strains according to plasmid DNA contents and RAPD-PCR profiles.

MATERIALS AND METHODS

Bacillus Strains, Culture Conditions, and Initial Identification. Reference strains *Bacillus alcalophilus* ATCC 27647 and *Bacillus halodurans* C125 were kindly supplied from Dr. Arthur A. Guffanti and Dr. Terry A. Krulwich (Department of Biochemistry, Mont Sinai School of Medicine of the City University of New York, 10029 New York, USA). New facultative alkaliphilic *Bacillus* strains were isolated from the water and surrounding soil of Lake Van according to the isolation procedure of the reference authors [15] with PYA Agar medium (1% soluble starch (Difco), 0.5% polypeptone (Difco), 0.5% yeast extract (Difco), 0.1% K_2HPO_4, 0.02% $MgSO_4$ x $7H_2O$, 0.5% Na_2CO_3, 2% Agar, pH 10.5). Isolated strains were identified by conventional microbiological methods [15-17]. Morphological and physiological characteristics previously revealed that the strains were members of *Bacillus* genus. Besides, the strains were defined as facultative alkaliphilic since they were cultivated in nutrient broth at pHs between 6.8 and 10.5, and optimum pH was found at 9 [18].

Isolation of Chromosomal DNA. *Bacillus* spp. samples were activated with incubation at 37ºC for 24 hours. Recovered bacteria were centrifuged at 3.000 rpm for 5 min and cell pellets were resuspended in 500 µl TE buffer (10 mM Tris-HCl pH 8.0, 1 mM EDTA). Pellets were then incubated at 55ºC for 30 min following the addition of 50 µl SDS (10%) and 25 µl proteinase K (20 mg/ml). Total DNA was recovered by sequential extractions with phenol and chloroform. Initially, 575 µl phenol/chloroform (1:1) was added, tubes were inverted and centrifuged at 14.000 rpm for 10 min. The aqueous upper layer (500 µl) was carefully transferred into a fresh tube and again treated with 500 µl phenol/chloroform (1:1). Tubes were inverted a few times and incubated on ice for a few minutes, then centrifuged at 14.000 rpm for 10 min. After centrifugation, upper layer (500 µl volume) was transferred into a new eppendorf tube and treated with 50 µl sodium acetate (3M, pH: 5.2) and 330 µl isopropanol (100%). Tubes were gently inverted and DNA was precipitated by centrifugation at 14.000 rpm for 10 min followed by washing with 70% (v/v) ethanol, dried, resuspended with 100 µl TE buffer containing 2 µl RNase. DNA samples were stored at -20ºC until further used for the RAPD analysis.

Plasmid Analysis. The extrachromosomal DNAs of the strains were extracted according to the method of Sambrook et al. with some modifications [19]. *Bacillus* spp. samples were inoculated into 5 ml NB (Nutrient Broth) medium from a single colony and incubated overnight at 37ºC. Then, 1.5 ml culture was transferred into an eppendorf tube and centrifuged at 10.000 rpm for 1 min. The upper layer was discarded and bacteria in the pellet were resuspended in 100 µl cold Solution I (50 mM glucose, 25 mM Tris-HCl pH 8.0, 10 mM EDTA pH: 8.0) and vortexed. Samples were then treated with 200 µl Solution II (1% SDS, 0.2 N NaOH), mixed throughly by inverting and incubated on ice for 15 min. Following incubation, samples were centrifuged at 10.000 rpm for 7 min and the upper layers were transferred into sterile eppendorf tubes. The application of phenol/chloroform at equal volumes was folllowed with vortexing and centrifugation at 10.000 rpm for 5 min and the supernatant was transferred into a clean eppendorf tube. This application was repeated twice in order to eliminate the protein residues from plasmid DNA. The supernatant was mixed with cold pure ethanol that is double volume of the sample and kept on ice for 15 min. Plasmid DNA was precipitated by centrifugation at 10.000 rpm for 10 min followed by washing with 70% (v/v) cold ethanol, dried, and resuspended in 50 µl TE buffer containing RNase. The plasmids were separated by agarose gel electrophoresis (0.7% agarose gel in 1X TBE buffer: 5X stock contained 0.45 M Tris, 0.45

M boric acid, 0.5 M EDTA, pH: 8.0, and mixed with 0.5 µg/ml ethidium bromide). The plasmid sizes were determined with a molecular weight marker (O' Gene Ruler 1 kb DNA Ladder, ready-to-use, Thermo Scientific, USA).

TABLE 1
Random primers used for RAPD analysis of *Bacillus* spp. Isolates

Primer name	Oligonucleotide sequence
M13-10	5′-CCGCAGCCAA-3′
M13-14	5′-GAGGGTGGCGGTTC-3′
OPL3	5'-CCAGCAGCTT-3'
OPL12	5'-GGGCGGTACT-3'
RAPD12	5'-AGCCCCCAAG-3'
RPO2	5′-GCGATCCCCA-3′

RAPD-PCR Analysis. RAPD-PCR analysis was performed using six different oligonucleotide primers (Table 1). PCR was carried out in a reaction volume of 50 µl containing 1X PCR buffer, 1.5 mM $MgCl_2$, 200 µM each deoxynucleotide triphosphates (dNTPs), 100 pmol primer, 1.25 U of Taq DNA polymerase (Thermo Scientific, USA) and 3 µl genomic DNA. Techne TC-5000 thermal cycler (California, USA) was used for all amplification reactions and amplification conditions included an initial denaturation step at 94ºC for 3 min, 34ºC for 1 min and 72ºC for 1 min during one cycle. This initial denaturation step was followed by denaturation at 94ºC for 30 sec, primer annealing at 34ºC (with the exception of M13 primer at 54ºC) for 30 sec, extension at 72ºC for 30 sec during 30 cycles and final extension at 72ºC for 5 min. PCR completion reaction mixtures were stored at 4ºC until electrophoresis was performed. RAPD-PCR products were analyzed by agarose gel (1%) electrophoresis with a molecular size marker (O' Gene Ruler, 1 kb DNA Ladder, ready-to-use, Thermo Scientific, USA) and DNA bands were visualized under UV light.

Statistical Analysis. The gels of plasmid profiles and RAPD-PCR of genomic DNAs were visualized under UV transilluminator (Cleaver-MicroDOC, UK) and the photographs were documented. The molecular weights of each band were calculated with Total Lab 1D Manual R11.1, UK programme. Following installation of the gel images into the programme, the bands were determined with their pixel positions and their molecular weights were scored according to the molecular size marker. The data collected were further subjected to cluster analysis by using unweighted pair group method using arithmetic averages (UPGMA) based on Jaccard's similarity coefficient with the Phoretix 1D-Pro (Total lab, UK) programme and dendrograms were generated.

RESULTS AND DISCUSSION

The plasmid profiles of all tested strains are given in Fig. 1A and 1B. Agarose gel electrophoresis analysis showed that the strains harbored at least one or more plasmids. Four isolates (numbered by 19, 34, 108, and 109)

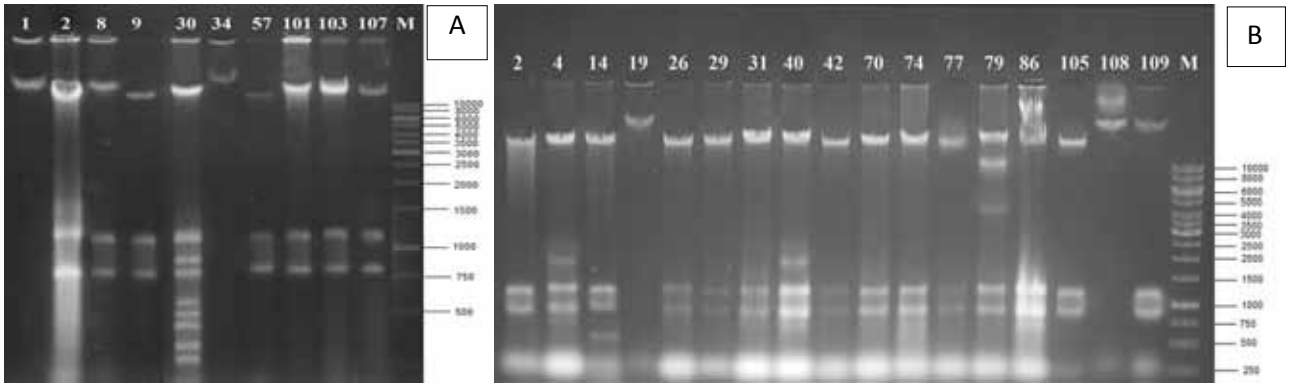

FIGURE 1
Plasmid patterns of *Bacillus* spp. isolates
A/Lanes: 1: *Bacillus alcalophilus* ATCC 27647, 2: *Bacillus halodurans* C125, 3: Isolate number 8, 4: Isolate number 9, 5: Isolate number 30, 6: Isolate number 34, 7: Isolate number 57, 8: Isolate number 101, 9: Isolate number 103, 10: Isolate number 107, 11: Molecular weight marker
B/Lanes: 1: *Bacillus halodurans* C125, 2: Isolate number 4, 3: Isolate number 14, 4: Isolate number 19, 5: Isolate number 26, 6: Isolate number 29, 7: Isolate number 31, 8: Isolate number 40, 9: Isolate number 42, 10: Isolate number 70, 11: Isolate number 74, 12: Isolate number 77, 13: Isolate number 79, 14: Isolate number 86, 15: Isolate number 105, 16: Isolate number 108, 17: Isolate number 109, 18: Molecular weight marker

TABLE 2
Characteristics of the bands amplified using six primers in the analyzed variants

No	Primer	No of bands	Polymorphic	Monomorphic
1	M13-10	110	110	0
2	M13-14	72	72	0
3	OPL3	93	93	0
4	OPL12	98	98	0
5	RAPD12	48	48	0
6	RPO2	84	84	0
TOTAL		505	505	0

were regarded to have unique plasmid profiles due to displaying completely different plasmid profiles. The remaining 20 isolates were subdivided into three groups, each containing isolates that shared the same plasmid pattern. Group I members included the isolates number 8, 101, 103, and 107 and their plasmid profiles consisted of the same bands of 20.400 bp, 1.109,1 bp, and 809,3 bp. Group II members included the isolates number 9, 57, 26, 29, 31, 42, 70, 74, 77, 105 and reference strain 2. Their plasmid profiles consisted of the same bands of 14.800 bp, 1.109,1 bp, and 809,361 bp. Group III members included only two isolates number 4 and 40 and their plasmid profiles consisted of the same bands of 14.800 bp, 1.975,4 bp, 1.109,1 bp and 809,4 bp. When compared with group II members, isolate number 14 had one extra, isolate number 30 had six extra, isolate number 79 had two extra, and isolate number 86 had two extra plasmids than group II and since these isolates share at least three plasmids in common, they can be accepted as derivatives of group II. As mentioned above, group II members resembled to reference strain 2 according to their plasmid profiles. Whereas, the isolate marked by 34 with a unique plasmid profile was closer to reference strain 1. RAPD-PCR did not confirm the plasmid analysis results except for 2 isolates that generated the similar bands with M13-10 primer. Isolates 70 and 77 produced the same bands of 1.540 bp and 946 bp and their plasmid profiles were completely similar.

RAPD-PCR method was used to analyze the interspesific genomic polymorphism among *Bacillus* spp. with 6 oligonucleotide primers. *Bacillus alcalophilus* ATCC 27647 (numbered by 1), *Bacillus halodurans* C125 (numbered by 2) and 24 isolates were analyzed by RAPD-PCR using independently prepared template DNAs. The RAPD-PCR profiles of 24 isolates were compared with those of reference strains. Primers used for RAPD-PCR are listed in Table 1. The six primers examined produced a total of 505 scorable bands. The greatest numbers of bands (110) were produced with M13-10 primer and the lowest numbers of bands were produced with RAPD12 primer (Table 2).

A total of 22 strains generated DNA fragments with primer M13-10. The molecular weights of the DNA bands produced with M13-10 primer ranged from 2.775 bp to 305 bp for the isolates (Fig. 2A). In the dendrogram in fig. 2A, the isolates were separated into two major clusters (A and B) at similarity levels between 16 and 100%. The cluster A consists of two groups, namely A_1 and A_2 at similarity levels of 24% or above. The cluster B had only two strains numbered by 14 and 19. The molecular weights of the DNA bands produced with M13-14 primer ranged from 2.219 bp to 311 bp for the isolates (Fig. 2B). In the dendrogram in fig. 2B, the isolates were scattered into two major clusters (C and D) at similarity levels between 12 and 100%. The cluster C consists of two groups, namely C_1 and C_2 at similarity levels of 24% or above. The cluster C_2 had only one strain numbered by 77. Cluster C_1 was further discriminated into two sub-clusters ($C_1(1)$ and $C_1(2)$) at similarity levels of 47% or above. Sub-cluster $C_1(2)$ had two strains numbered by 8 and 57. The molecular weights of the DNA bands produced with OPL3 primer ranged from 3043 bp to 233 bp for the isolates (Fig. 2C). In the dendrogram, the isolates were separated into two major clusters (E and F) at similarity levels between 28 and 94%. Both cluster E and F were further divided into two sub-clusters. E_1 and E_2 sub-clusters displayed similarity levels of 29% or above. Sub-clusters F_1 and F_2 had similarity levels of 47% or above. Sub-cluster E_2 had only one strain numbered as 14 while sub-cluster E_1 formed the major group of cluster E. Sub-cluster F_1 contained the isolates numbered as 103 and 31 and sub-cluster F_2 consisted of three isolates numbered as 4, 26, and 79. The molecular weights of the DNA bands produced with OPL12 primer ranged from 3.209 bp to 251 bp for the isolates (Fig. 2D). In the dendrogram in fig. 2D, the isolates were separated into two major clusters (G and H) at similarity levels between 4 and 100%. Cluster H had only one strain numbered as 29. Cluster G had two sub-clusters (G_1 and G_2) at similarity level 9% or above and sub-cluster G_2 had only two strains numbered as 30 and 107. Sub-cluster G_1 was further divided into two sub-clusters ($G_1(1)$ and $G_1(2)$ at similarity level 17% or above. While sub-cluster $G_1(1)$ was the major sub-cluster that consists

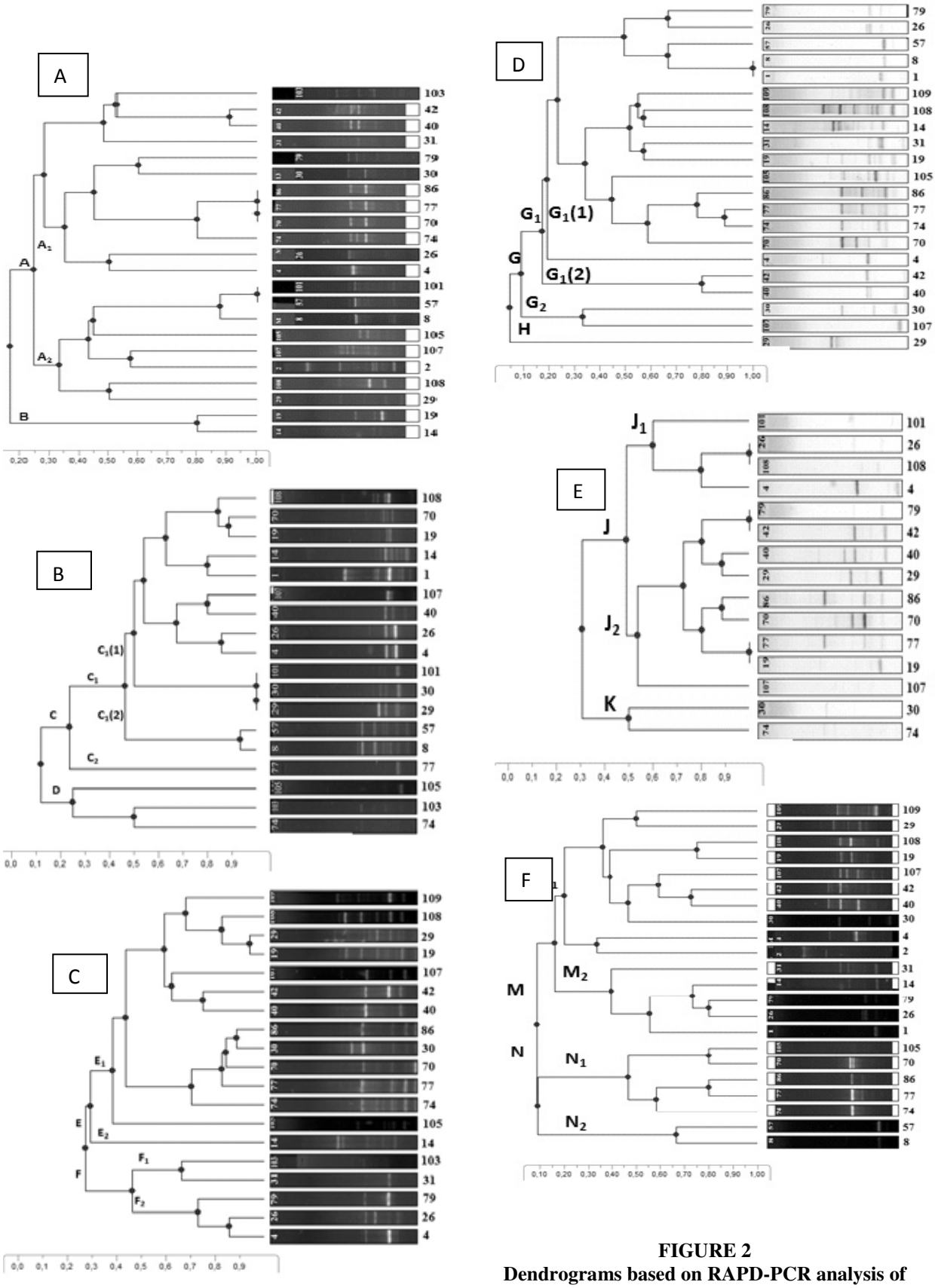

FIGURE 2
Dendrograms based on RAPD-PCR analysis of M13-10 (A), M13-14 (B), OPL3 (C), OPL12 (D), RAPD12 (E), and RPO2 (F)

of 16 members, sub-cluster $G_1(2)$ had only two members numbered as 40 and 42. The molecular weights of the DNA bands produced with RAPD12 primer ranged from 3.500 bp to 262 bp (Fig. 2E). In the dendrogram, the isolates were scattered into two major clusters (J and K) at similarity levels between 31 and 100%. Cluster K had only two strains numbered as 30 and 74. Cluster J was separated into two sub-clusters (J_1 and J_2) at similarity level 49% or above. The molecular weights of the DNA bands produced with RPO2 primer ranged from 3.752 bp to 201 bp (Fig. 2F). In the dendrogram in fig. 2F, the isolates were separated into two major clusters (M and N) at similarity levels between 8 and 80%. Both cluster M and N were further divided into two sub-clusters. Cluster M had two sub-clusters (M_1 and M_2) at similarity level of 16% or above and sub-cluster N had two sub-clusters (N_1 and N_2) at similarity level of 9% or above. Sub-cluster N_2 had only two strains numbered as 8 and 57.

Our study indicates that RAPD provides a high degree of discrimination among *Bacillus* spp. isolates. Genetic distances among the isolates according to primers M13-10, M13-14, OPL3, OPL12, RAPD12, and RPO2 were found at percentage similarities between 16 to 100%, 12 to 100%, 28 to 94%, 4 to 100%, 31 to 100% and 8 to 80% respectively. Thus, it was demonstrated that OPL12 primer provided better distinction than the other tested primers and RPO2 primer followed this.

RAPD-PCR pattern that was generated with RPO2 primer offering second better discriminative profile was also more consistent with SDS-PAGE of whole-cell protein profiles. In the previous study [18], whole-cell protein profiles of the reference and new facultative alkaliphilic *Bacillus* strains were analysed with SDS-PAGE and dendrograms generated were divided into four basic clusters (I-IV) and two subclusters for IV (IVa and IVb) including the two reference strains *B. megaterium* GCM 1842 and *B. megaterium* DSM 32. In the dendrogram generated with RPO2 primer, the members of N_2 sub-cluster (isolates 8 and 57) were in the subgroup IVa and the members of N_1 sub-cluster (isolates 105, 70, 86, 77, and 74) were in the subgroup IVb though two other members of subgroup IVb (isolates 42 and 79) were not compatible with the RAPD profile sub-cluster and were in the major cluster M. Besides, isolates 70 and 77 in the same sub-cluster IVb in terms of protein bands shared interesting features as mentioned above. Their plasmid profiles were completely similar and their RAPD profiles generated with M13-10 primer produced the same two bands. In terms of similar characteristics revealed, the isolates can be accepted as a single clone genetically.

The molecular approach related with the division of *Bacillus* into several phylogenetically distinct genera has started in the 1990s. The genus *Bacillus* comprises both phenotypically and phylogenetically heterogeneous species [20-21]. The utilization of RAPD protocol on *Bacillus* comprises of different researches mainly focusing on thermophilic *Bacillus* species. Indeed, controlling and identifying thermophilic bacilli in dairy processing and especially in milk powders have been an issue of interest. The results of two pioneering studies on this issue corroborate each other. The four strains of thermophilic bacilli from thermophilic isolates in milk powders which were identified by using RAPD have been determined as *Geobacillus stearothermophilus*, *Anoxybacillus flavithermus*, *Bacillus licheniformis*, and *Bacillus subtilis* and these species accounted for 96.8-98% of all isolates investigated. Also the most variable strain was defined as *B. licheniformis* since it is more representative of the diversity of soil, compost and silage origins [11, 22]. RAPD-based analysis of thermophilic bacilli in milk powders with these two primary studies also seems compatible with one of the most recent studies which identified the thermophilic bacilli in milk powders with whole cell protein profiles and partial 16S rDNA. *Bacillus licheniformis*, *Anoxybacillus flavithermus* and *Geobacillus stearothermophilus* comprised 80.5% of all isolates [23]. RAPD fingerprinting method has also used for the identification of thermophilic *Bacillus* species in composts and 76.1% of the isolates positively assigned by their RAPD profiles belonged to two species; *Bacillus thermodenitrificans* which is the dominant member and *B. licheniformis*. The utilized RAPD methodology enables to the discrimination of closely related species by 16S rDNA gene sequences and accurate identification below the species level [24]. A very recent study has focused on the identification of genetic variability of alkaline protease producing bacteria isolated from soil of India with RAPD and 16S rDNA analysis methods. A total of 21 primers was tested for RAPD screening of 20 bacteria producing alkaline protease; 17 primers generated 100% polymorphic band patterns while the other three primers generated both mono and polymorphic band patterns. RAPD patterns revealed a high degree of polymorphism; 258 of 261 bands (90%) were polymorphic. Among these 20 isolates, 5 of them were identified as *Bacillus* spp. based on the similarity of 16S rRNA gene sequences and their RAPD amplification profiles displayed 100% polymorphism [25]. The results of this study seem supportive of us (see Table 2) in terms of the wide heterogeneity of the genus *Bacillus.* However, as summarized above most of the genetic variability studies on *Bacillus* have centered upon the isolates from food additives and soils from different

geographical regions. To the best of our knowledge, the detailed genetic variability studies on the genus *Bacillus* seem to be absent in soda lakes and the filling of the holes in this scientific field is desirable. Some of the studies focusing on alkalophilic bacteria in soda lakes are either related with a newly identified *Bacillus* species or mostly with enzymatic activities of the isolates. So, the limited information on this field does not permit us making comparisons among different soda lakes for the present.

In conclusion, we suggest that genotyping of bacteria with RAPD analysis is a sensitive and an efficient molecular approach and can allow the discrimination of even the closely related strains. For this purpose, the choice of the most discriminatory primers can help us to separate the isolates. In addition, the combination of molecular methods rather than a single classification method can strengthen our point of view. The data resulting in all the fragments amplified with different primers in our study generated polymorphic bands are small but supportive steps in terms of reflecting the genomic diversity of facultative alkaliphilic *Bacillus* spp. in soda Lake Van. A better understanding of the microbial diversity in such ecosystems not only increases our conception about organisms of the extreme limits, but also may direct us to novel studies to take advantage of these biomolecules in biotechnological applications.

REFERENCES

[1] López-García P, Kazmierczak J, Benzerara K, Kempe S, Guyot F, Moreira D. (2005) Bacterial diversity and carbonate precipitation in the giant microbialites from the highly alkaline Lake Van, Turkey. Extremophiles, 9(4):263-74.

[2] Hashim SO, Delgado O, Hatti-Kaul R, Mulaa FJ, Mattiasson B. (2004) Starch hydrolysing Bacillus halodurans isolates from a Kenyan soda lake. Biotechnol Lett, 26(10):823-8.

[3] Zavarzin GA. (1993) Epicontinental soda lakes as probable relict biotopes of terrestrial biota formation. Microbiology (Moscow), 68:503–521.

[4] Grant WD. (2006) Alkaline Environments and Biodiversity, in Extremophilies [Eds. Charles Gerday, and Nicolas Glansdorff], in Encyclopedia of Life Support Systems (EOLSS), Developed under the Auspices of the UNESCO, Eolss Publishers, Oxford ,UK, [http://www.eolss.net].

[5] Dimroth P, Cook GM. (2004) Advances in Microbial Physiology, 49, UK: Ed. Robert K. Poole, Elsevier Ltd.

[6] Carrasco IJ, Márquez MC, Xue Y, Ma Y, Cowan DA, Jones BE, Grant WD, Ventosa A. (2007) Bacillus chagannorensis sp. nov., a moderate halophile from a soda lake in Inner Mongolia, China. Int J Syst Evol Microbiol, 57(9):2084-8.

[7] Martins RF, Davids W, Abu Al-Soud W, Levander F, Rådström P, Hatti-Kaul R. (2001) Starch-hydrolyzing bacteria from Ethiopian soda lakes. Extremophiles, 5(2):135-44.

[8] Nogi Y, Takami H, Horikoshi K. (2005) Characterization of alkaliphilic Bacillus strains used in industry: proposal of five novel species. Int J Syst Evol Microbiol, 55(6):2309-15.

[9] Saeki K, Ozaki K, Kobayashi T, Ito S. (2007) Detergent alkaline proteases: enzymatic properties, genes, and crystal structures. J Biosci Bioeng, 103(6):501-8.

[10] Fujinami S, Fujisawa M. (2010) Industrial applications of alkaliphiles and their enzymes-past, present and future. Environ Technol, 31(8-9):845-56.

[11] Ronimus RS, Parker LE, Turner N, Poudel S, Rückert A, Morgan HW. (2003) A RAPD-based comparison of thermophilic bacilli from milk powders. Int J Food Microbiol, 85(1-2):45-61.

[12] Franklin RB, Taylor DR, Mills AL. (1999) Characterization of microbial communities using randomly amplified polymorphic DNA (RAPD). J Microbiol Methods, 35(3):225-35.

[13] Welsh J, McClelland M. (1990) Fingerprinting genomes using PCR with arbitrary primers. Nucleic Acids Res, 18(24):7213-8.

[14] Williams JG, Kubelik AR, Livak KJ, Rafalski JA, Tingey SV. (1990) DNA polymorphisms amplified by arbitrary primers are useful as genetic markers. Nucleic Acids Res, 18(22):6531-5.

[15] Horikoshi K, Akiba T. (1982) Alkalophilic Microorganisms: a New Microbial World, Tokyo: Japan Scientific Societies Press.

[16] Fritze D, Flossdorf J, Claus D. (1990) Taxonomy of alkaliphilic Bacillus strains. Int J Syst Bacteriol, 40(1): 92-7.

[17] Slepecky RA, Hemphill HE. (1992) The Genus Bacillus-nonmedical. In: The Prokaryotes, 2nd. Ed. A. Balows et al (eds). Springer-Verlag, New York Inc. Secaucus, New Jersey, Chapter 76.

[18] Berber I, Berber S. (2006) Numerical analysis of SDS-PAGE protein patterns of facultative alkaliphilic Bacillus species isolated from Lake Van, Turkey. Fresenius Environmental Bulletin, 15(5):409-416.

[19] Sambrook J, Fritsch EF, Maniatis T. (1989) Molecular cloning: a laboratory manual, Cold Spring Harbor Laboratory, Cold Spring Harbor, New York.

[20] Ash C, Farrow JAE, Wallbanks S, Collins MD. (1991) Phylogenetic heterogeneity of the genus

Bacillus revealed by comparative analysis of small-subunit-ribosomal RNA sequences. Letters in Applied Microbiology, 13:202–206.
[21] Ivanova EP, Vysotskii MV, Svetashev VI, Nedashkovskaya OI, Gorshkova NM, Mikhailov VV, Yumoto N, Shigeri Y, Taguchi T, Yoshikawa S. (1999) Characterization of Bacillus strains of marine origin. Int Microbiol, 2(4):267-71.
[22] Rückert A, Ronimus RS, Morgan HW. (2004) A RAPD-based survey of thermophilic bacilli in milk powders from different countries. Int J Food Microbiol, 96(3):263-72.
[23] Yuan DD, Liu GC, Ren DY, Zhang D, Zhao L, Kan CP, Yang YZ, Ma W, Li Y, Zhang LB. (2012) A survey on occurrence of thermophilic bacilli in commercial milk powders in China. Food Control, 25(2):752–757.
[24] Zhang YC, Ronimus RS, Turner N, Zhang Y, Morgan HW. (2002) Enumeration of thermophilic Bacillus species in composts and identification with a Random Amplification Polymorphic DNA (RAPD) protocol. Syst Appl Microbiol, 25(4):618-26.
[25] Saxena S, Verma J, Shikha, Modi DJ. (2014) RAPD-PCR and 16S rDNA phylogenetic analysis of alkaline protease producing bacteria isolated from soil of India: Identification and detection of genetic variability. JGEB, 12:27-35.

Received: **02.11.2015**
Accepted: **10.04.2016**

CORRESPONDING AUTHOR

Zeynep Yegin, Dr.
Medical Laboratory Techniques Program, Vocational School Of Health Services, Sinop University, Sinop, Turkey

E-mail: zyegin@sinop.edu.tr

© by PSP Volume 25 – No. 10/2016, pages 4111-4117 Fresenius Environmental Bulletin

STAGE-DISCHARGE RELATIONSHIP IN TIDAL RIVERS FOR TIDAL FLOOD CONDITION

Mohammad Sadegh Sadeghian[1], Meysam Salarijazi[2*], Iman Ahmadianfar[3], Mohammad Heydari[4]

1-Assistant Professor, Civil Engineering Dept., Faculty of Engineering, Tehran Central Branch, Islamic Azad University, Iran.
2-Assistant Professor, Department of Water Engineering, Gorgan University of Agricultural Sciences and Natural Resources, Gorgan, Iran.
3-Assistant Professor, Department of Civil Engineering, Behbahan Khatam Alanbia University of Technology, Behbahan, Iran.
4-PhD candidate, Dept of Civil Engineering, Faculty of engineering, University of Malaya, Kuala Lumpur, Malaysia

ABSTRACT

Estimation of the water level in river's tidal reach is a suitable tool for the tidal flood risk and environmental management and design for rivers that are located in coastal area. The reaches of the river that affected by river flow and tidal wave are called as tidal limit and water level in this limit is a function of flood discharge and water level in upstream and downstream, respectively. In tidal limit, tidal waves propagate along the river to the upstream and combination of these waves and upstream flood discharge leads to an increase in water level. This mechanism increases flood plain limit and potential of damage and the risk. In this study, the reach between Ahvaz and Khorramshahr in Karun River in Iran is selected as case study and different linear models for the prediction of water level in tidal flood condition are investigated. Results show that the simple linear regression is not acceptable because of its variable variance of residuals. Transformed nonlinear models that are a form of linear models are used for modeling too. Two equations (Logarithmic and Power) with improved coefficient of determination, relatively constant variance and normal distribution of residuals of models are concluded from detailed analysis. These selected models are used for prediction. Prediction's results confirm the acceptability of these models considering their simplicity.

KEYWORDS:
Flood Discharge, Water Level, Tidal Limit, Tidal Flood

INTRODUCTION

Estimation of the extremes of the river water level is extraordinary important in the design of environmental projects along the river [1]. The rivers located in coastal areas are simultaneously under influence of upstream discharge and downstream tide level. The upstream and downstream of these rivers are under influence of flood discharge and tide phenomena while the middle limit, known as tidal limit, are under influence of combination of both tide and river flood. In different studies, the water level in middle limit is predicted by different equations based on water level of tide in downstream and/or the river's flow in upstream. Linear regression is used to determine the Stage-discharge relationship in tidal rivers in Canada and concluded the accuracy of these equations [2]. Li *et al*. [3] first used some models for prediction of water level at three stations in Changjiang Estuary in China and then investigated adding discharge data of upstream to the model. They concluded improvement in prediction of model because of using further inputs. Harmonic and developed harmonic analysis used to calculate water level in River estuary of several past years and analyzed calculation errors [4, 5]. Structural curves (an especial type of discharge-stage curve) and related regression equations developed by using of discharge of fluvial flow in the upstream and tidal height in the downstream [6]. Artificial neural networks (ANN) are investigated by researchers to predict water level in tidal interaction limit [7, 8, 9, 10, 11]. They concluded good accuracy of these models beside their limitation to present explicit equation. With respect to the literature, this research investigates the acceptability of linear models for water level prediction in tidal limit. The main goal of this study is answering to two questions. First: Is there any significant relation between flood discharge and water level in tidal interaction limit during tidal flood? Second: Can linear or non-linear models apply to predict water level in tidal limit as a function of flood discharge of the upstream?

MATERIAL AND METHODS

Study Area. Karun River is the most important river in Iran and is located in Karun and Dez watershed. The downstream of Karun has the tidal regime while the river regime in the upstream is dominant. However, three stations i.e. Ahvaz, Khorramshahr and Darkhoein located respectively

in upstream, downstream and tidal limit of the river are selected. The generalized extreme value distribution is fitted to the water level dataset and based on partial duration series analysis, the value of 392 *cm* above sea level is determined as threshold value of tidal flood water level. According to the determined threshold value, 206 pairs of recorded data are extracted.

Simple Linear Regression Model. The equation of simple linear regression is:

$$y_i = \beta_0 + \beta_1 x_i + \epsilon_i i = 1,2,\dots,n \quad (1)$$

Where y_i is the *i*th observation of the dependent variable, $x_i$is the *i*th observation of the independent variable, $\beta_0$is the intercept, $\beta_1$is the slope, $\epsilon_i$is the random error or residual for the *i*th observation, and n is the sample size. The ϵ_i is independent of x_i. For this study the required assumptions are: *i*) The model form is correct and *y* has linear relation with *x*. *ii*) Data used to fit the model are representative of data of interest. *iii*) The variance of the residuals is constant. It does not depend on *x* or on anything else (e.g. time). *iv*) The residuals are normally distributed [12]. The parameters of the model are estimated by following equations:

$$\bar{x} = \frac{\Sigma x_i}{n} \quad (2)$$

$$\bar{y} = \frac{\Sigma y_i}{n} \quad (3)$$

$$b_1 = \frac{\Sigma x_i.y_i - \frac{(\Sigma x_i)(\Sigma y_i)}{n}}{\Sigma x_i^2 - \frac{(\Sigma x_i)^2}{n}} \quad (4)$$

$$b_0 = \bar{y} - b_1\bar{x} \quad (5)$$

The Coefficient of Determination

It is a scale free one-number summary of the strength of the relationship between x_i and y_i in the data and can be written as:

$$R^2 = \frac{[\Sigma x_i.y_i - \frac{(\Sigma x_i)(\Sigma y_i)}{n}]^2}{[\Sigma y_i^2 - \frac{(\Sigma y_i)^2}{n}][\Sigma x_i^2 - \frac{(\Sigma x_i)^2}{n}]} \quad (6)$$

The mentioned assumptions must be consider in addition to ANOVA and coefficient of determination analysis because in some cases, a good results with respect to some mentioned criteria may be not acceptable according to analysis of residuals [12, 13].

Nonlinear Models. Some assumptions may not be satisfied in application. In such situations, nonlinear models may be useful. However, there are some mathematical transformations to convert nonlinear models to linear ones. Some of such transformed models are presented in Table 1.

TABLE 1
The linear and non-linear models of study

No	Non-Linear Form	Transformation	Linear Form
1	---	---	$y = b_0 + b_1 x$
2	$y = b_0 x^{b_1}$	$\acute{y} = \log y, \acute{x} = \log x$	$\acute{y} = \log b_0 + b_1 \acute{x}$
3	$y = b_0 e^{b_1 x}$	$\acute{y} = \ln y$	$\acute{y} = \ln b_0 + b_1 x$
4	$y = b_0 + b_1 \log x$	$\acute{x} = \log x$	$y = b_0 + b_1 \acute{x}$
5	$y = \frac{x}{b_0 x - b_1}$	$\acute{y} = \frac{1}{y}, \acute{x} = \frac{1}{x}$	$\acute{y} = b_0 + b_1 \acute{x}$

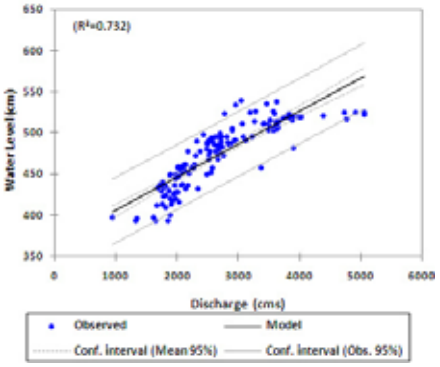

FIGURE 1(a)
Fitted Model No 1

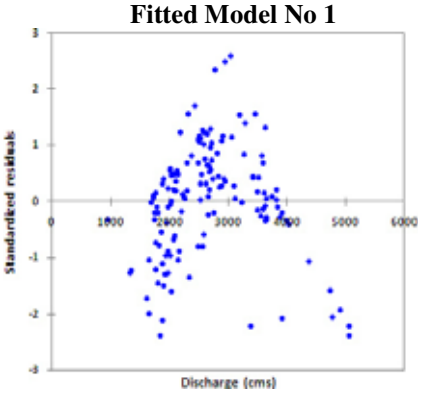

FIGURE 1(b)
Residuals-Independent Variable Model No 1

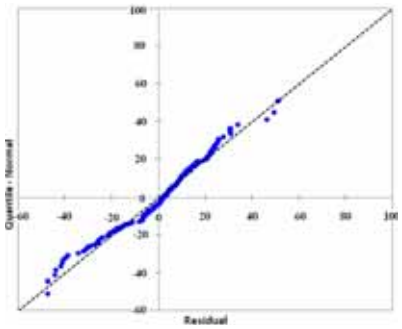

FIGURE 1(c)
Q-Q Plot of Residuals Model No 1

RESULTS AND DISCUSSION

The Mann-Kendall test (Mann, 1945; Kendall, 1975) is suitable tool to investigate monotonic trend of considered data sets (Marofi *et al.* 2012; Moazed *et al.* 2012; Salarijazi *et al.* 2012) [14, 15, 16, 17, 18]. The results of this test confirmed there is no significant trend in investigated dataset. Dataset is divided to two parts. The first part, 70 percent of data, used for modeling and the second part, 30 percent remaining data, is dedicated to the prediction. In the first step, the simple linear model (i.e. Model No.1) is applied to the data. The result of this model is illustrated in Fig. 1 and Table 2. Results of Table 2 show a significant linear equation in 99% confidence level and Fig. 1(a) illustrates a relatively suitable fitness of the model. The variation of residuals against independent variable in Fig. 1(b) reveals that the variance of residuals is not constant and therefore the model No. 1 is not suitable. The approximate normal distribution of the residuals can be recognized by Fig. 1(c).

TABLE 2
Analysis of variance for Model No. 1

Source	DF	Sum of squares	Mean of squares	F	Pr> F
Model	1	152543.889	152543.889	387.384	< 0.0001
Error	142	55916.750	393.780		
Corrected Total	143	208460.639			

$$\text{Water Level}(cm) = 366.077 + 0.04\text{Q}\left(\frac{m^3}{s}\right) \quad , \quad R^2 = 0.732$$

TABLE 3
Analysis of variance for Model No.2

Source	DF	Sum of squares	Mean of squares	F	Pr> F
Model	1	0.145	0.145	552.412	< 0.0001
Error	142	0.037	0.000		
Corrected Total	143	0.182			

$$\log\big(\text{Water Level}(cm)\big) = 1.838 + 0.245\log\left(Q\left(\frac{m^3}{s}\right)\right) \quad , \quad R^2 = 0.796$$

TABLE 4
Analysis of variance for Model No.3

Source	DF	Sum of squares	Mean of squares	F	Pr> F
Model	1	0.692	0.692	362.103	< 0.0001
Error	142	0.271	0.002		
Corrected Total	143	0.963			

$$\ln\big(\text{Water Level }(cm)\big) = 5.928 + 8.5 \times 10^{-5}\left(Q\left(\frac{m^3}{s}\right)\right) \quad , \quad R^2 = 0.718$$

TABLE 5
Analysis of variance for Model No.4

Source	DF	Sum of squares	Mean squares	F	Pr> F
Model	1	167138.876	167138.876	574.364	< 0.0001
Error	142	41321.763	290.998		
Corrected Total	143	208460.639			

$$\text{Water Level }(cm) = 425.509 + 263.788\log\left(Q\left(\frac{m^3}{s}\right)\right) \quad , \quad R^2 = 0.802$$

TABLE 6
Analysis of variance for Model No.5

Source	DF	Sum of squares	Mean squares	F	Pr> F
Model	1	0.000	0.000	520.236	< 0.0001
Error	142	0.000	0.000		
Corrected Total	143	0.000			

$$\frac{1}{\text{Water Level }(cm)} = 0.002 + 1.262\left(\frac{1}{Q\left(\frac{m^3}{s}\right)}\right) \quad , \quad R^2 = 0.786$$

Considering the figures of the results, it is concluded that maybe nonlinear transformed to linear models can be appropriate to improve the results of modeling. Another important issue that leads to investigation of nonlinear models is the physical basis of the phenomena. The results of modeling based on different nonlinear models are presented in following parts.

The results of tables 2 to 6 show that different investigated models are significant in 99% confidence level. In addition, consideration of the coefficient of determination can be resulted to the better fitness of Model 2 and Model 4 among five different linear models. Investigations of the distributions of residuals of different models show approximately normal distributions for Model 2 and Model 4. Constant variation of residuals is another assumption that should be investigated. Residual plot of Model 1 shows change in variance clearly. The residual plots of different nonlinear transformed to linear models show that the variances of the residuals are approximately constant for Model 2, Model 4 and Model 5. The selected models (i.e. Model 2 and Model 4) are used for prediction using remaining 62 pairs of dataset. The results of predictions are illustrated in Fig. 6. Results confirm the efficiency of selected models for prediction of water level.

CONCLUSION

Water level predictions in tidal rivers are complicated because of effects of two important mechanisms. The first one is upstream river discharge and the second one is downstream tide. Despite of dominant effects of these mechanisms in upstream and downstream but middle reach is under influence of both mechanisms. However prediction of water level during flood condition is essential for environmental risk management. Using simple models are important because they do not require different type of input variables. To predict water level in tidal limit during tidal flood condition, long term recorded data for Karun River in Ahvaz-Khorramshahr reach is considered. Using partial duration series analysis, flood condition data is extracted. Simple linear model and four transformed linear models are evaluated for prediction of water level in tidal limit as a function of upstream flood discharge. Considering the mentioned results lead to the selection of logarithmic and power models for calibration step. The results confirm that the transformation improves the model and approximately satisfy related assumptions of linear model. Consideration validation results reveal that the selected models can be acceptable for the prediction of water level in tidal limit during tidal flood condition considering their simplicity.

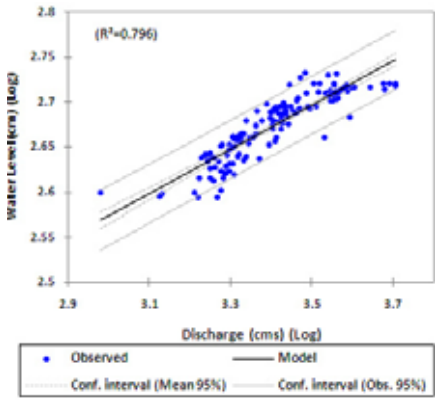

FIGURE 2(a)
Fitted Model No 2

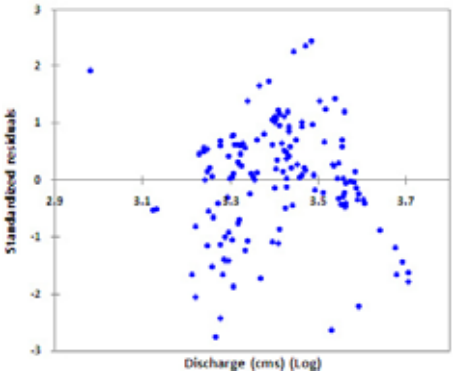

FIGURE 2(b)
Residuals-Independent Variable Model No 2

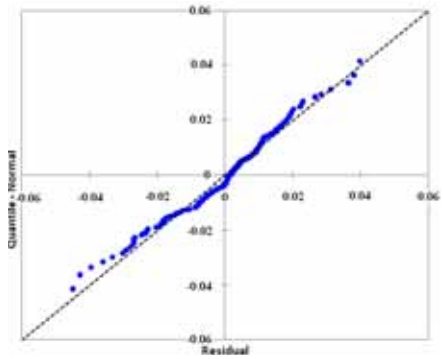

FIGURE 2(c)
Q-Q Plot of Residuals Model No 2

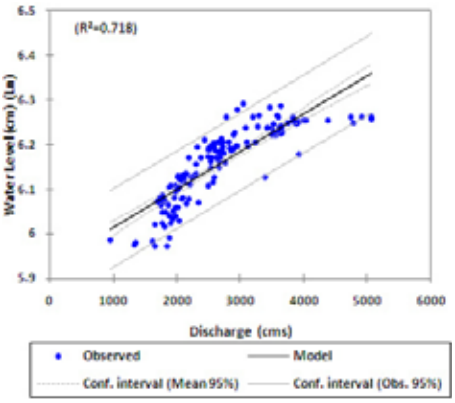

FIGURE 3(a)
Fitted Model No 3

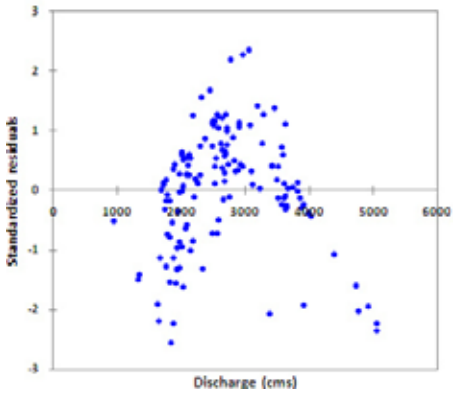

FIGURE 3(b)
Residuals-Independent Variable Model No 3

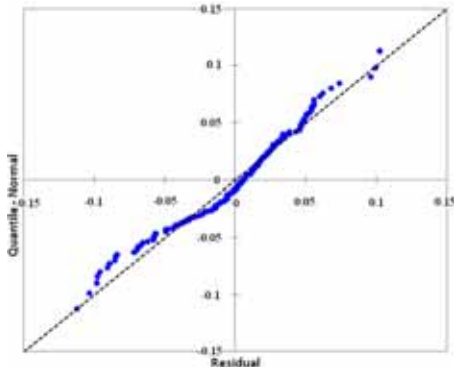

FIGURE 3(c)
Q-Q Plot of Residuals Model No 3

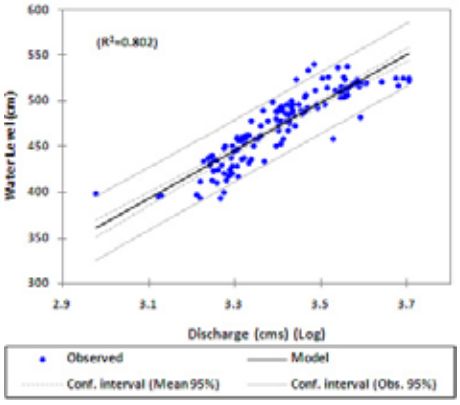

FIGURE 4(a)
Fitted Model No 4

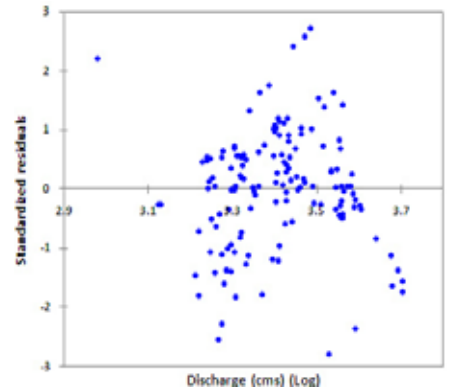

FIGURE 4(b)
Residuals-Independent Variable Model No 4

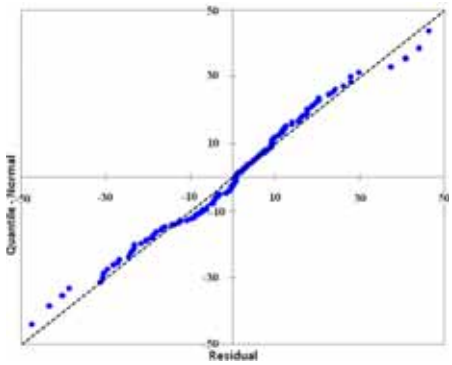

FIGURE 4(c)
Q-Q Plot of Residuals Model No 4

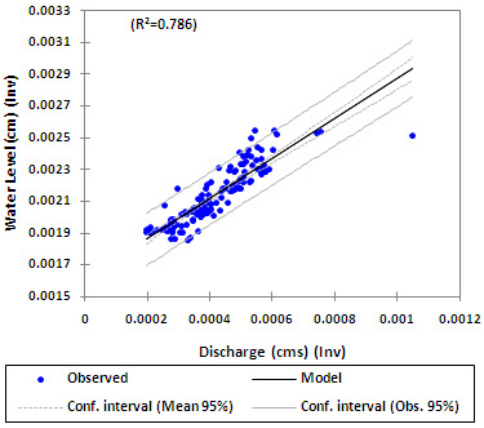

FIGURE 5(a)
Fitted Model No 5

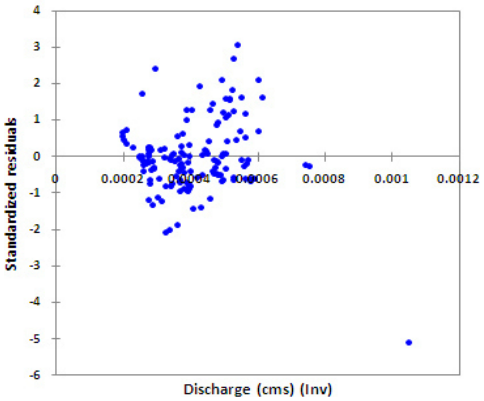

FIGURE 5(b)
Residuals-Independent Variable Model No 5

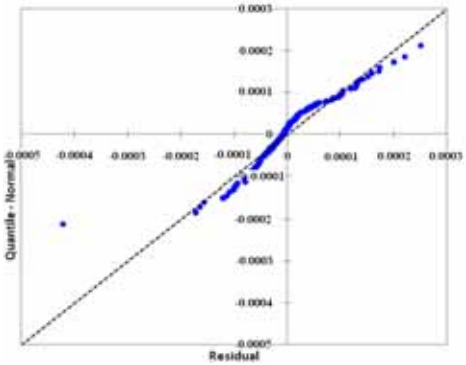

FIGURE 5(c)
Q-Q Plot of Residuals Model No 5

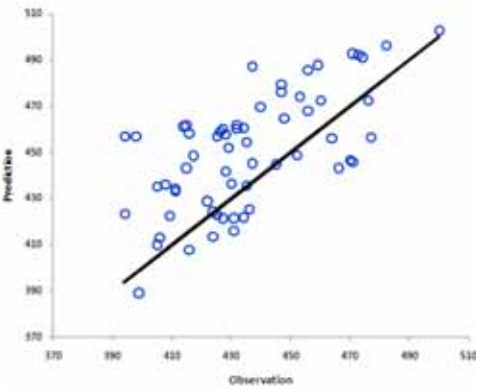

FIGURE 6(a)
Result of Prediction by Model No 2

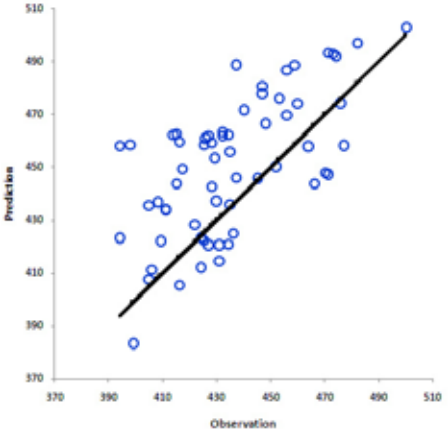

FIGURE 6(b)
Result of Prediction by Model No 4

ACKNOWLEDGEMENTS

Authors gratefully acknowledge the Khuzestan Water and Power Organization for Preparation of dataset.

REFERENCES

[1] Salarijazi, M. (2013). Assessment of the Flooding Risk for River with Tidal Interaction Zones. PhD Thesis. Shahid Chamran University of Ahvaz. 155 pages.

[2] El-Jabi, N., Wakim, G., and Sarraf, S. (1992). Stage-discharge relationship in tidal rivers. Journal of waterway, port, coastal, and ocean engineering,118(2): 166-174.

[3] Li, G. F., Tan, Y., and Zhang, X. J. (2006). Influence of upstream discharge in tidal level prediction for tidal reaches. Journal of Hohai University (Natural Sciences),34(2):144-147.

[4] Ya, L. G. W. W. T., and Jie, W. U. (2009). Study on Tidal Level Forecasting and Real-time Correction Model for Yangtze River Estuary [J].Water Resources and Power,2, 015.

[5] Li, G., Xiang, X., Wu, J., and Tan, Y. (2011).Long-Term Water-Level Forecasting and Real-Time Correction Models in the Tidal Reach of the Yangtze River. Journal of Hydrologic Engineering,18(11):1437-1442.

[6] Adib, A. (2010). Extraction of structural curves, regression relations and structural regression relations in the tidal limit of the Karun River. Indian Journal of Science and Technology, 3(5), 530-536.

[7] Hidayat, H., Hoitink, A. J. F., Sassi, M. G., & Torfs, P. J. J. F. (2014). Prediction of Discharge in a Tidal River Using Artificial Neural Networks. Journal of Hydrologic Engineering, 19(8), 04014006.

[8] Tsai, C. P., and Lee, T. L. (1999).Back-propagation neural network in tidal-level forecasting. Journal of Waterway, Port, Coastal, and Ocean Engineering,125(4):195-202.

[9] Supharatid, S. (2003). Application of a neural network model in establishing a stage–discharge relationship for a tidal river. Hydrological processes, 17(15), 3085-3099.

[10] Adib, A. (2008). Determining water surface elevation in tidal rivers by ANN. Proceedings of the ICE-Water Management,161(2):83-88.

[11] Kisi, O., and Çobaner, M. (2009). Modeling River Stage-Discharge Relationships Using Different Neural Network Computing Techniques. CLEAN-Soil, Air, Water,37(2):160-169.

[12] [12]- Helsel, D. R., & Hirsch, R. M. (1992). Statistical methods in water resources(Vol. 49). Elsevier. ISBN-13: 978-0444814630. 522 pages

[13] Von Storch, H., & Zwiers, F. W. (2002). Statistical analysis in climate research. Cambridge University Press. ISBN-13: 978-0521012300. 496 pages.

[14] Mann, H. B. (1945). Nonparametric tests against trend. Econometrica: Journal of the Econometric Society, 245-259.

[15] Kendall MG (1975). Rank Correlation Methods. Charles Griffin, London. 202 pp.

[16] Marofi, S., Soleymani, S., Salarijazi, M., & Marofi, H. (2012). Watershed-wide trend analysis of temperature characteristics in Karun-Dez watershed, southwestern Iran. Theoretical and Applied Climatology, 110(1-2), 311-320.

[17] Moazed, H., Salarijazi, M., Moradzadeh, M., & Soleymani, S. (2012). Changes in rainfall characteristics in Southwestern Iran. African Journal of Agricultural Research, 7(18), 2835-2843.

[18] Salarijazi, M., Akhond-Ali, A. M., Adib, A., & Daneshkhah, A. (2012). Trend and change-point detection for the annual stream-flow series of the Karun River at the Ahvaz hydrometric station. African Journal of Agricultural Research, 7(32), 4540-4552.

Received: **24.09.2015**
Accepted: **10.05.2016**

CORRESPONDING AUTHOR

Meysam Salarijazi
Department of Water Engineering, Gorgan University of Agricultural Sciences and Natural Resources, Gorgan, Iran.

email: meysam.salarijazi@gmail.com

© by PSP Volume 25 – No. 10/2016, pages 4118-4129 Fresenius Environmental Bulletin

POTABLE WATER QUALITY ASSESSMENT IN AL-HASSA, EASTERN REGION OF SAUDI ARABIA

El-Sayed A Badr[1,2,*], Ahmed A Al-Naeem[1]

1 Environment and Natural Resources Department, College of Agricultural & Food Sciences, King Faisal University, Al-Hassa, Saudi Arabia
2 Environmental Sciences Department, Faculty of Science, Damietta University, New Damietta City, Egypt

ABSTRACT

Drinking water should be of sufficient quantity and meet certain water quality guidelines. Main sources of potable water supply in Saudi Arabia are groundwater wells and desalinated sea water. The aim of this research was to assess potable water quality in Al-Hassa, KSA. The study focused on drinking water quality criteria including nitrate, fluoride (NO_3, F) and related physiochemical parameters such as turbidity, pH, EC, TDS, residual chlorine, hardness, anions and cations. Approximately 59 sampling sites have been selected and water samples were collected twice (May and December 2013) from groundwater wells, mixing plant, distribution networks and consumers. The results revealed that, TDS concentrations for the water samples collected averaged 1196 ± 599 mg/l; with lower values reported in central towns compared to relatively higher values within villages. NO_3 and F concentrations were mainly averaged 4.64 ± 1.99 mg/l and 0.76 ± 0.31 mg/l, respectively. These findings reflect high nitrate inputs from anthropogenic sources within the study area. Average concentrations of major anions including Cl, HCO_3 and SO_4 were 383 ± 235 mg/l, 164 ± 45.1 mg/l and 314 ± 167 mg/l, respectively. On the other hand, average concentrations of major cations including Na, K, Ca and Mg were 207 ± 127 mg/l, 14.3 ± 9.13 mg/l, 130 ± 57.7 mg/l and 41.4 ± 22.3 mg/l, respectively. Fe and Mn were in the range of 33.4 – 381 μg/l, and 12.3 – 116 μg/l, respectively. Higher values of these ions were observed in water samples collected from northern and eastern villages relative to those collected from central towns; reflecting higher concentrations of these ions in groundwater wells. The research outcomes contribute to a robust view of the current potable water quality and putting recommendations for improving water quality.

KEYWORDS:
Potable water quality, Pollution, groundwater, Al-Hassa, nitrate and fluoride

INTRODUCTION

Water is a common chemical substance that is essential for the survival of all known forms of life [1]. Drinking water is important for human health where water constitutes approximately 75 % of our body and all biochemical reactions in the body occur in a water medium [2]. Groundwater plays an important role in water management worldwide and is the sole source of potable water in many areas [3]. Main sources of Potable water supply in Saudi Arabia are groundwater wells, mixed with desalinated sea water [4,5]. Potable water quality is strongly affected by the characteristics of the main groundwater resources from which potable water derives [2,6]. In Saudi Arabia, water demands are continuously increasing due to increasing population, urbanization, agricultural activities and industrialization; as well as improving living standards [4,7,8].

Potable water should be of sufficient quantity and meet certain water quality criteria, in order to maintain adequate public health [9,10]. Water purification for human consumption is the process of removing undesirable chemical and biological contaminants from raw water [11]. Increases in human activities have led to significantly enhanced anthropogenic inputs and leaching of contaminants into groundwaters; resulting in marked changes in water quality [12-14]. Groundwater quality varies widely depending on hydrological conditions, abstraction rates, types and characteristics of soil, depth of aquifer and human activities within the catchment area [3]. For instance the massive expansion in agricultural production in the Kingdom of Saudi Arabia resulted in extensive use of fertilizers and reuse of treated wastewater, and subsequent contamination of groundwater [4]. Moreover, drinking water might get contaminated through the distribution networks. Main environmental problems within drinking water distribution networks include corrosion of pipeline materials, contamination from external sources, and participation of iron, manganese and carbonate. These might lead to changes in the physical, chemical and biological characteristics of drinking water, as well as biological contamination

from sewage [3,15]. Hence, evaluation of potable / drinking water quality has been studied by several investigators [2,4,8,11,13,16,17]

High levels of nitrate, fluoride and TDS (total dissolved salts) are among main environmental problems affecting groundwater quality. Nitrate is the most obvious chemical contaminant in the world's groundwater [5,16]. Contamination of drinking water with nitrate presents a health hazard because nitrate ion (NO_3) can be reduced to nitrite (NO_2) ion in the gastrointestinal tract [2]. Nitrite causes methemoglobinemia, a sometimes fatal disease to which infants are susceptible [10]. High levels of nitrate in groundwater are widespread which introduced from a variety of sources including agricultural activities, seepage from the urban sewage system, leaching from solid waste disposal locations, intensive farming, use of nitrogen fertilizers and dissolution of nitrogen from the atmosphere [16]. The maximum contaminant level (MCL) of nitrate in potable water have been set to be 10 mg-N/L (or 50 mg-NO_3/L) [18-20].

Fluoride is found naturally in all waters with groundwater having appreciable levels as compared with surface water [21]. High or low levels of fluoride in drinking water sources have been found to cause adverse health effects [21-23]. Excessive amounts of fluoride in water result in dental and skeletal fluorosis, whereas low levels result in diminishing caries reduction [21,22]. The Optimal fluoride level in water was estimated to be 0.8 – 1.5 mg/L [18] in order to produce the greatest protection against caries with the least risk of fluorosis. Generally, the Saudi Arabian Standards Organisation[18] developed drinking water standards (SASO) for both bottled and un-bottled water to define a quality of water that is safe and acceptable to public health. These standards set limits for the maximum contaminant level (MCL) of chemical elements. Moreover, the international guidelines for drinking water include WHO (2011), USEPA (2012) and EU (1998).

The objective of the current study is to report one of the first systematic studies on assessing spatial and temporal variations in potable water quality of Al-Hassa Oasis, Eastern Region of Saudi Arabia, and to compare these results with the drinking water standards set by SASO and other international guidelines. The proposed research is very significant in term of assessing quality of Potable water supply, which closely related to public health and water scarcity. Moreover, there are no detailed comprehensive studies on the nitrate and fluoride levels in the potable water supplies of the Eastern Region.

MATERIALS AND METHODS

Study area. The study area has a desert climate, characterized by high temperatures during the day and low temperatures at night. The hottest temperatures are in June – August, averaging 40°C; whereas winter temperatures are normally below than 20 °C, the lowest temperature are in December and January. The average rainfall is within 60 mm / year mostly in the winter months [24].

The main source of drinking water in Al-Hassa Oasis is a mixture of groundwater with desalinated sea water coming from Desalination Treatment Plant in Khobar. Groundwater is coming from 31 wells (14 first stage and 17 second stage) located at Riyadh Road in Owisa without any pre-treatment techniques and total dissolved salts (TDS) is estimated to be approximately 1000 ppm. Whereas desalinated sea water coming from Khobar is approximately salts free and thus mixing take place to get domestic/drinking water with TDS averaging 700 – 800 ppm; with the addition of chlorine as disinfectant. The daily amount of water coming from desalinated plant at Khobar is estimated to be 50 thousand cubic meter, whereas the amount of water coming from Owisa wells is estimated to be 160 thousand cubic meter. Northern and Eastern villages within Al-Hassa Oasis are using potable water coming directly from groundwater wells; after addition of a disinfectant in some cases.

Sample collection. The current study was conducted twice during summer and winter seasons to investigate whether there are seasonal variations in the quality of Potable water supply. Hence two field surveys were carried out in May 2013 and December 2013. In each survey, 59 sampling sites were chosen throughout the study area to investigate spatial variations. Four water samples were collected from supplying groundwater wells (referred as 1W – 4W) in Owisa, and another 4 water samples were collected from the main mixing plant at various stages (1P – 4P) in Mahasen. Then geographically representative samples were collected from the distribution network system and consumers in Al-Hassa Oasis. Approximately 29 water samples were collected from the central region of Al-Hofuf and Al-Mubarraz towns (1 – 29); 11 water samples were collected from the Northern villages (1N – 11N) and another 11 water samples were collected from the Eastern villages (1E – 11E) (as shown in Figure 1). The geographical location of sampling sites has been recorded using GPS. A well planned sampling protocol was implemented to minimize changes in sample composition. All glassware used was first acid-washed in 10% HCl for 24 h, and then rinsed 3 – 5 times with distilled water and water sample before use. The water samples were collected from the

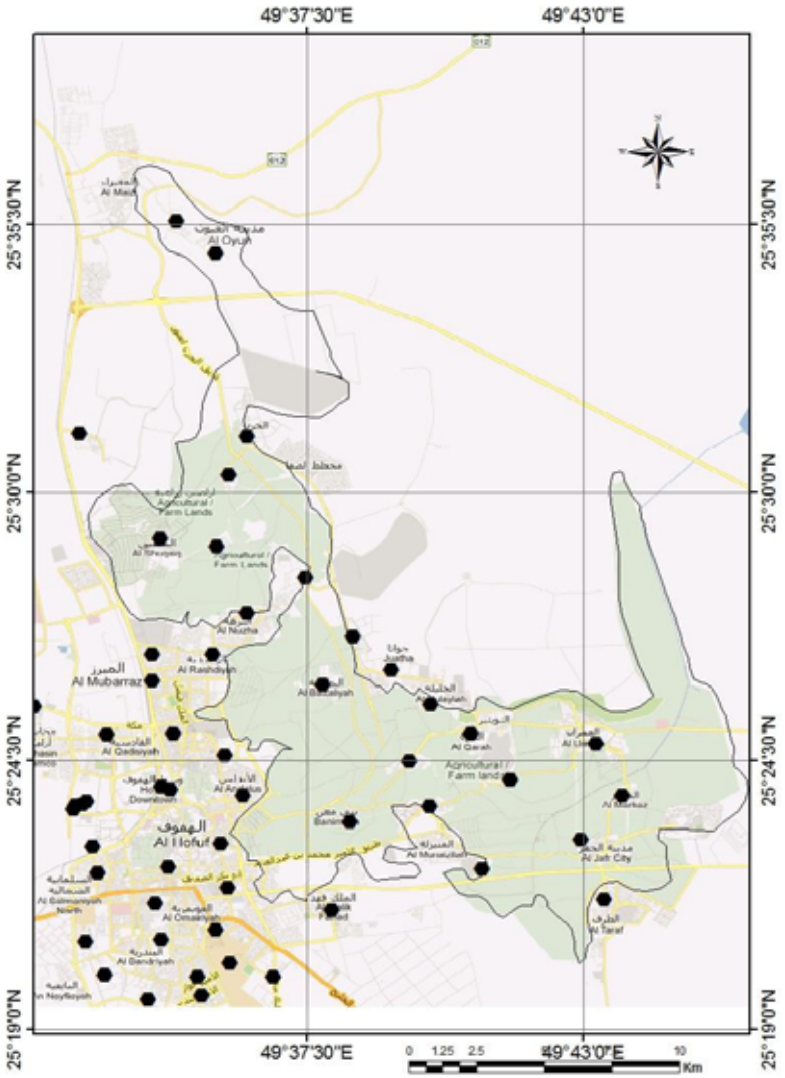

FIGURE 1
Geographic map of the Al-Hassa Oasis, KSA indicating location of the sampling sites

chosen sampling sites into 1 litre HDPE (high density polyethylene) bottles; after the pipes have been cleaned of any stagnant water. This research focused on assessment of NO_3 and F characterization within Potable water. Moreover, the following physiochemical parameters were measured; including pH, TDS, electrical conductivity (EC), turbidity, residual chlorine, hardness, anions (Cl, CO_3, HCO_3, SO_4), cations (Na, K, Ca, Mg), Fe and Mn.

Sample analysis. Master water quality variables, which measured in situ, include temperature, pH, EC, TDS and residual chlorine. Measurements of pH and temperature were performed in situ using a pH meter (model HI 9124, Hanna Instruments Ltd, Germany). EC and TDS were measured using Portable Conductivity / TDS meter (model 470-Digital, Jenway- UK). Residual chlorine was measured based on DPD colorimetric method using Portable colorimeter (C301, OAKTON). Turbidity was measure using Turbidity meter (model HI 88703, Hanna Instruments Ltd, Germany).

All water samples analysis has been conducted in the laboratory according to a well-established method in accordance to the American Standards for Water and Wastewater Examination Manual [25]. NO_3, F and SO_4 were measured in the collected water samples using spectrophotometer methods (UV-direct method, SPADNS method and Turbid-metric method, respectively) with the aid of UV-Vis Spectrophotometer (UV-1650, Shimadzu) [25-27]. Ions such as Cl, HCO_3, Ca, and Mg (hardness) were measured using trimetric methods (Mohr's method, HCl method and EDTA method, respectively) [26]. Na and K were measured using flame emission photometric method (Flame Photometer, Jenway). Fe and Mn were measured using atomic absorption spectrophotometer (AA6650F, Shimadzu) [25].

TABLE 1
Average ± standard deviation of the measured parameters in water samples collected from Al-Hassa Oasis, KSA in comparison with drinking water quality standards

Parameters	All Data		Desalinised water	Ground water wells	Mixing unit	Urban samples	Rural Samples	Permissible limits		
	Average ± SD	Min. – Max.	(1P, 2P)	(1W–4W)	(3P, 4P)	(1–29)	(1N–11N, 1E–11E)	SASO (2009)	WHO (2011)	USEPA (2012)
Temperature	26.6±2.6	21.7–32.5	24.0±0.36	24.4±0.97	24.2±0.75	26.2±2.21	28.0±2.68	-	-	
pH	7.72±0.27	7.10–8.25	7.90±0.05	7.52±0.08	7.69±0.15	7.82±0.26	7.62±0.27	6.5–8.5	6.5–8.5	6.5–8.5
TDS (mg/l)	1196±599	69.5–3365	98.9±24.9	1051±26.7	701±64.3	909±345	1748±505	500	1000	500
EC (µS/cm)	1995±997	116–5575	165±41.9	1752±45.9	1168±106	1514±578	2915±835	-	-	2500
Turb.(NTU)	0.35±0.26	0.11–2.10	0.46±0.21	0.38±0.30	0.27±0.08	0.33±0.30	0.38±0.19	5	5	1
Cl_2 (mg/l)	0.16±0.18	0.03–0.78	0.10±0.06	0.04±0.00	0.59±0.19	0.23±0.19	0.05±0.02	0.2–1	0.2–0.5	0.8
NO_3 (mg-N/l)	4.64±1.99	0.01–9.27	0.14±0.11	6.81±0.15	3.75±0.68	4.80±1.59	4.53±2.13	50-NO_3	50-NO3	10-N
F (mg/l)	0.76±0.31	0.03–1.55	0.07±0.05	0.74±0.09	0.48±0.07	0.62±0.23	1.03±0.19	0.8–1.5	1.5	2
Cl (mg/l)	383±235	7.94–1362	21.2±10.3	319±26.7	197±21.6	273±113	589±238	250	250	250
HCO_3 (mg/l)	164±45.1	26.1–252	41.1±5.17	186±6.94	126±9.05	145±34.5	200±22.7	-	125-350	-
SO_4 (mg/l)	314±167	1.09–836	6.41±5.81	293±13.7	146±31.6	229±106	475±114	200	250	250
Na (mg/l)	207±127	5.49–729	9.39±4.02	147±12.8	115±6.82	146±67.5	325±116	100	200	200
K (mg/l)	14.3±9.13	0.09–52.2	0.37±0.26	8.90±2.72	5.66±0.79	9.81±5.23	23.2±7.12	-	12	-
Ca (mg/l)	130±57.7	7.31–324	15.6±2.80	126±10.4	78.9±9.17	106±36.2	176±53.4	200	100	-
Mg (mg/l)	41.4±22.3	2.25–108	3.58±0.95	44.0±3.82	26.7±4.49	28.9±14.2	62.2±16.6	150	50	-
Hardness	494±225	36–1172	53.6±8.47	496±14.3	307±36.7	384±128	696±191	200	200	-
Fe (µg/l)	141±71.1	33.4–381	77.8±44.7	131±104	136±59.5	148±72.4	140±65.0	300	300	300
Mn (µg/l)	58.0±25.3	12.3–116	43.2±6.54	58.4±18.8	60.7±2.85	57.1±25.8	60.2±27.9	100	100	50

The analytical data quality was guaranteed through the implementation of laboratory quality assurance and quality control methods. These include the use of standard operating procedures, calibrations with standards, blank determination and triplicate analysis of water samples. The linear regression coefficient of calibration curves was ≥ 0.999 (n = 6), indicating good linearity between concentrations of measured parameters and absorbance. The coefficient of variation (CV) or precision was typically < 3 – 5 %. Basic statistical analysis of the resulted data such as mean, maximum, minimum, average, standard deviation and coefficient of variance were conducted. Moreover, plotting charts, diagrams, investigations of correlation matrix and regressions between measured water quality parameters were used. Hence, correlations (Pearson's product moment) between pairs of water quality parameters were calculated using the SPSS software package (version 17.0) in order to identify any statistically significant correlations ($p < 0.01$ "the 99% confidence level", n = 118), and thus aid interpretation of the data. Paris of variables with positive Pearson correlation coefficients tends to increase together. If the Pearson correlation coefficient is negative, one variable tends to decrease as the other increases.

RESULTS AND DISCUSSION

Physico-chemical characteristics. The water temperature varied between 21.7 and 32.5 ºC; with an average value of 26.9 ± 2.6 ºC. It has been noticed that temperature values of water samples collected from villages were relatively higher compared to temperature values of those collected from central towns (Figure 2). Water sources in the villages include groundwater wells and the use of storage tanks. As shown in Figure 2 and Table 1, pH values of the collected water samples ranged between 7.10 and 8.25, with an average value of 7.72 ± 0.27. PH is an important indicator of water quality and the extent of pollution. The results of pH values recorded in this study fall within the range of international and Saudi standards (6.5 – 8.5).

Values of TDS ranged between 69.5 – 3365 mg/l with average of 1196 ± 599 mg/l. Higher TDS values were observed in water samples collected from northern and eastern villages (averaged 1748 ± 505 mg/l) relative to those water samples collected from central towns (averaged 909 ± 345 mg/l), (Figure 2). In comparison, TDS values of water distribution networks in Riyadh City ranged 226 – 580 mg/L [5].

Of the 118 water samples tested 8 samples (6.8 %) comprised the best water quality (TDS < 500 mg/l), whereas 9 samples (7.6 %) comprised the highest salinity water samples (TDS > 2000 mg/l). Moreover, 35.6 %, 30.5 % and 19.5 % of the collected water samples have TDS values in the range of 501 – 1000 mg/l, 1001 – 1500 mg/l and 1501 – 2000 mg/l, respectively. Hence, the results revealed that 57.6 % of the examined water samples have TDS values exceeding the permissible limit of 1000 mg/l [19]. High salinity levels (TDS > 1200 mg/l) may be objectionable to consumers because of the excessive scale formation in boilers and household equipment [28]. It is reported, in similar study, that the majority of groundwater wells in central and eastern part of KSA are highly saline [17].

EC concentrations ranged between 116 and 5575 µS/cm with an average value of 1995 ± 997µS/cm. A relatively higher average values of EC were reported for water samples collected from villages (2915 ± 835 µS/cm) compared to those water samples collected from central towns (1514 ± 578 µS/cm) (Table 1 and Figure 2). The main source of Potable water in central towns is the municipal distribution networks, which includes groundwater, mixed with desalinized water. Northern and eastern villages depend on private groundwater wells with higher salt contents. It has been reported that elevated groundwater salinity in different region of the country such as Al-Hassa Oasis and Al-Qassim region resulting from excessive pumping, over exploitation, soil weathering and agricultural drainage [4,7].

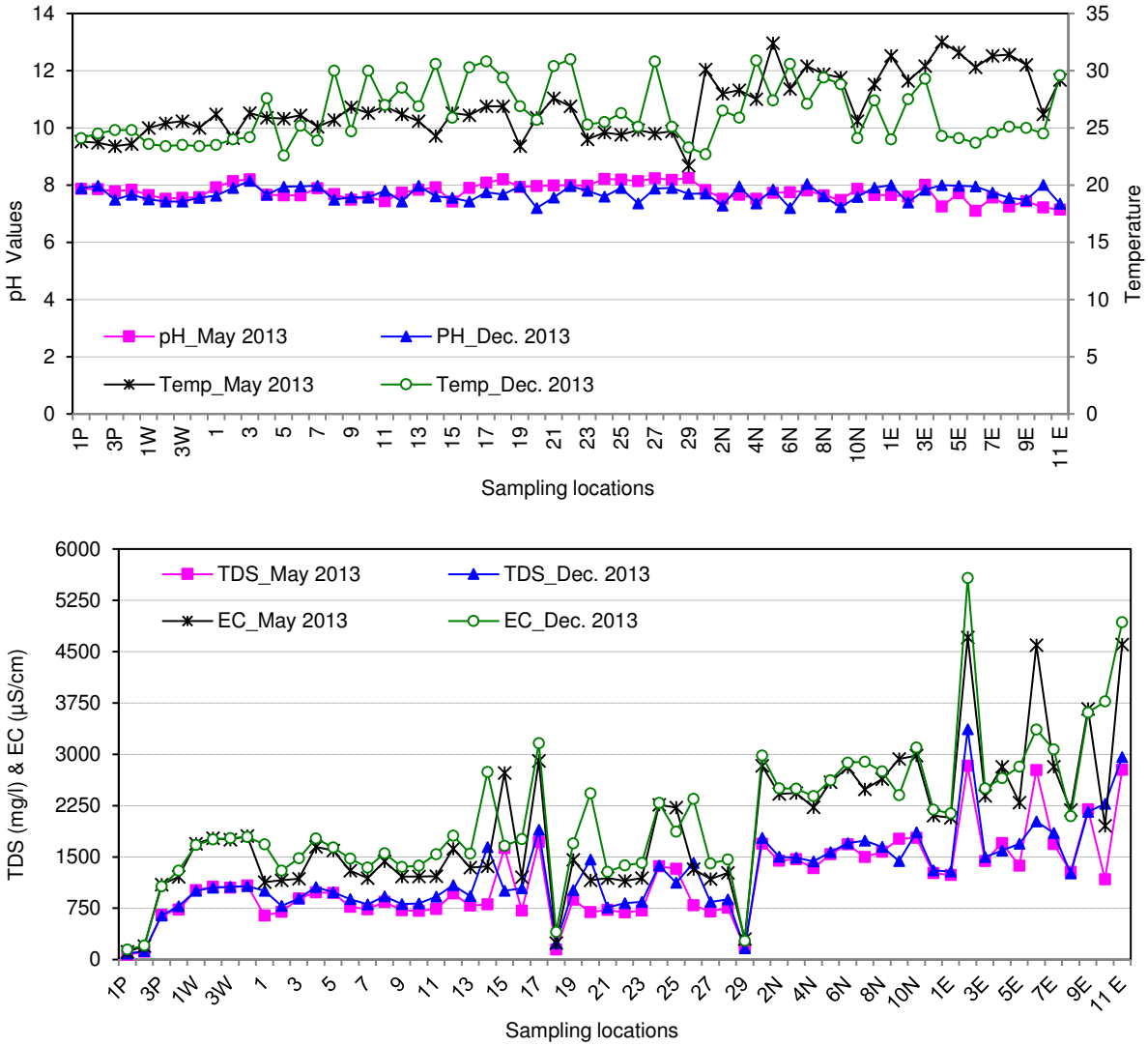

FIGURE 2

Values of temperature (°C), pH, TDS (mg/l) and EC (µS/cm) in water samples collected from Al-Hassa Oasis, KSA

Note: Water samples were collected from water mixing plant in Mahasen (1P – 4P), groundwater wells in Owisa (1W – 4W), Al-Hofuf and Al-Mubarraz towns (1 – 29), Northern villages (1N – 11N) and Eastern villages (1E – 11E)

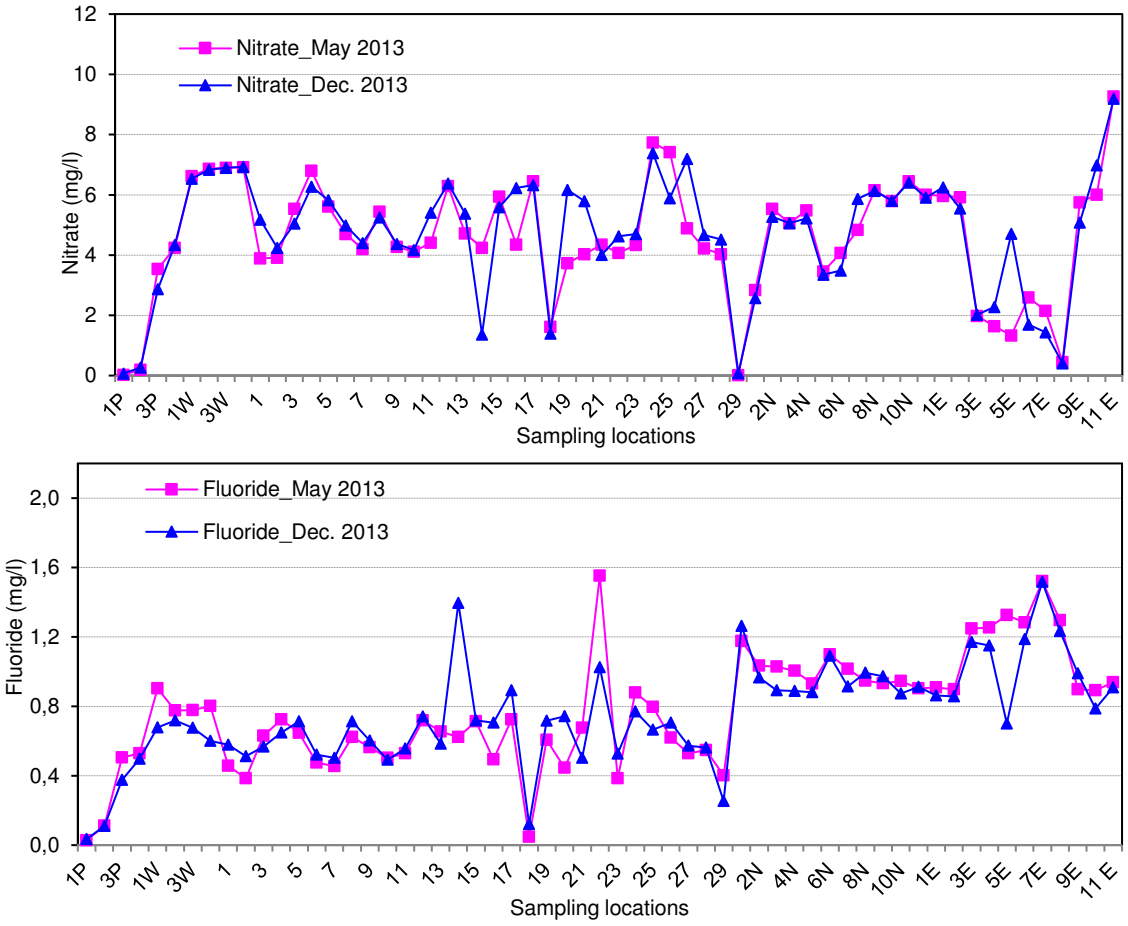

FIGURE 3
Concentrations nitrate and fluoride (mg/l) in water samples collected from Al-Hassa Oasis, KSA

The turbidity values of the water samples ranged between 0.11 – 2.10 NTU, with average value of 0.35 ± 0.26 NTU (Table 1). Concentrations of free chlorine (Cl_2) ranged between 0.03 – 0.78 mg/l, with very lower values ≤ 0.10 mg/l for water samples collected from villages and groundwater wells and higher values of average 0.5 mg/l for those water samples collected from central towns (Table 1). In villages, groundwater is used without addition of chlorine as disinfectant.

Nitrate and fluoride. Nitrate concentrations in the collected water samples were mainly averaged 4.64 ± 1.99 mg-N/l; with the range 0.01 – 9.27 mg-N/l. As shown in Figure 3, highest values up to 9.27 mg/l were reported for water samples collected from villages. Moreover, values of nitrate in water samples collected from groundwater wells averaged 6.81 ± 0.15 mg-N/l (Table 1). Approximately 50% the collected water samples have nitrate concentrations greater than 5 mg-N/l. The findings of the current study reflect relatively high nitrate concentrations due to extensive anthropogenic activities within the study area. The increased anthropogenic pressure is due to the rapid development of population and related activities such as urbanization, agriculture and industry [29,30]. The average value of nitrate in water samples collected from the urban area of Al-Hassa is 4.80 mg-N/l, which is higher than the average nitrate concentration in Riyadh distribution network of 0.994 mg-N/l [5]. In general, the nitrate concentrations in the collected water samples are below the recommended guideline of 10 mg-N/l. An examination of the seasonal variations, revealed no significant changes between nitrate values of water samples collected during May 2013 and nitrate values of those water sample collected during December 2013 (Table 1and Figure 3).

Concentrations of fluoride in the collected water samples were averaged 0.76 ± 0.31 mg/l, with the range 0.03 – 1.55 mg/l. Higher fluoride values were observed in water samples collected from northern and eastern villages (averaged 1.03 ± 0.19 mg/l) relative to those water samples collected from central towns (averaged 0.62 ± 0.23 mg/l) (Table 1 and Figure 3). In comparison to Riyadh City, the range of fluoride levels in the influent to water treatment plants was 0.63 – 1.6 mg/l, with lower fluoride range

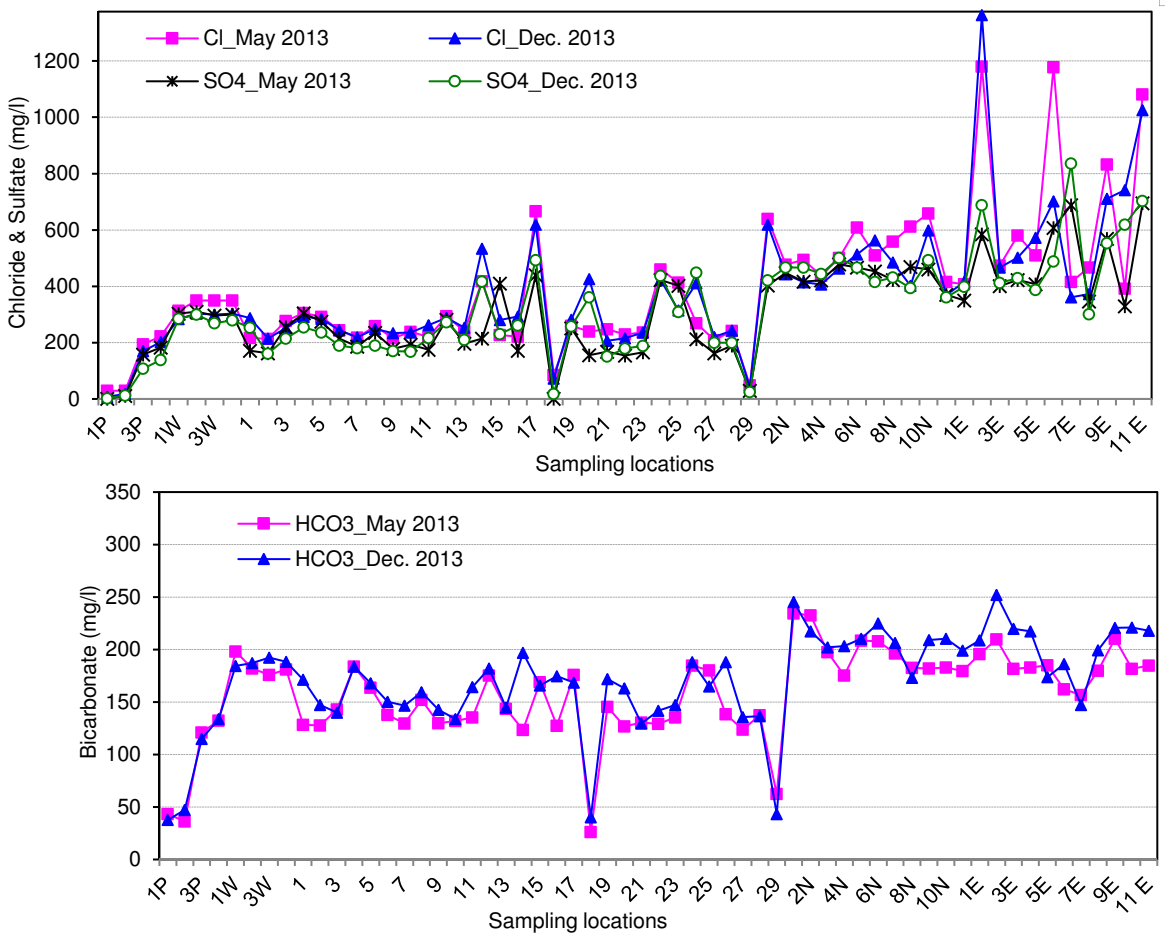

FIGURE 4
Concentrations chloride, sulfate and bicarbonate (mg/l) in water samples collected from Al-Hassa Oasis, KSA

of 0.01 – 0.50 mg/l in Riyadh water distribution network [22]. An examination of the seasonal variations in fluoride concentrations in the collected water samples revealed no significant seasonal trend (Figure 3). The study revealed that almost 59% of the collected water samples have fluoride concentrations below the optimum recommended level of 0.8 – 1.5 mg/l [18]. It is recommended that fluoridation should be considered in water purification plant.

Major anions and cations. Chloride (Cl) concentrations were in the range of 7.94 – 1362 mg/l, with average of 383 ± 235 mg/l. Lower chloride values were observed in water samples collected from central towns (averaged 273 ± 113 mg/l) relative to those water samples collected northern and eastern villages (averaged 598 ± 238 mg/l) (Table 1 and Figure 4). Almost 67 % of the collected water samples have chloride concentrations greater than the permissible limit of 250 mg/l [18]. Generally, carbonate ion is mostly absent in majority of collected water samples. Concentration range of bicarbonate measured in the collected water samples were 26.1 – 252 mg/l, with average concentrations of 164 ± 45.1 mg/l. Lower bicarbonate values of 26.1 – 196 mg/l were reported for water samples collected from central towns; relative to higher values of 147 – 252 mg/l reported for those water samples collected from villages (Figure 4).

On the other hand, average concentrations of sulfate were 314 ± 167 mg/l, with the range 1.09 – 836 mg/l. As shown in Table 1 and Figure 4, highest values up to 836 mg/l (average 475 ± 114 mg/l) were reported for water samples collected from villages, relative to average values of 229 ± 106 mg/l reported for those water samples collected from central towns. Elevated levels of sulfate concentrations may adversely affect human health [16]. Sulfate is a major ionic constituents with approximately 70.3 % of the 118 samples tested having concentrations greater than the recommended guidelines of 200 mg/l [18]. In similar study, the average concentration of sulfates in groundwater collected from Khamis Mushait (KSA) was 524 ± 125 mg/l, with 60 % of water samples above the permissible limit of sulfates (200 mg/l) [6]. Thompson (2003) reported high level of sulfate (mean of 712 mg/l) in groundwater supplies in Saskatchewan, Canada, where 25% of samples tested with sulfate concentrations greater than 1000 mg/l. In contracts, Al-Redhaiman and Abdel Magid (2002)

reported sulfate concentration range 48 – 360 mg/l, with a mean value of 160 mg/l in drinking water of Al-Gassim region. An examination of the seasonal variations revealed that average values of bicarbonate and sulfate in water samples collected during May 2013, were relatively lower than average bicarbonate and sulfate values of those water sample collected during December 2013 (Figure 4).

Concentration ranges of sodium and potassium measured in the collected water samples were 5.49 – 729 mg/l and 0.09 – 52.2 mg/l respectively, with relatively higher values reported for water samples collected from villages (Figure 5). Average concentrations of sodium and potassium were 207 ± 127 mg/l and 14.3 ± 9.13 mg/l, respectively (Table 1). Approximately 43% of the collected water samples contained concentrations of sodium above the permissible limit of 200 mg/l [18]. Concentrations of calcium and magnesium in the collected water samples were averaged 130 ± 57.7 mg/l and 41.4 ± 22.3 mg/l, respectively. Approximately 7.6 % of the collected water samples have calcium concentration above the standard limit of 200 mg/l [18]. Higher calcium and magnesium values were observed in water samples collected from villages (averaged 176 ± 53.4 mg/l and 62.2 ± 16.6 mg/l) relative to those water samples collected from central towns (averaged 106 ± 36.2 mg/l and 28.9 ± 14.2 mg/l, respectively).

Total hardness (as calcium carbonate) concentrations in the collected water samples averaged 494 ± 225 mg/l. The current study revealed that groundwater suppliers in rural area of Al-Hassa Oasis are quit hard (696 ±191 mg/l); where almost 93.2% of water samples tested had a measured total hardness greater than the recommended guidelines of 200 mg/l [18]. In similar study, 79% of tap water samples collected from Al-Hassa City exceeds the permissible limit of 200 mg/l [8].

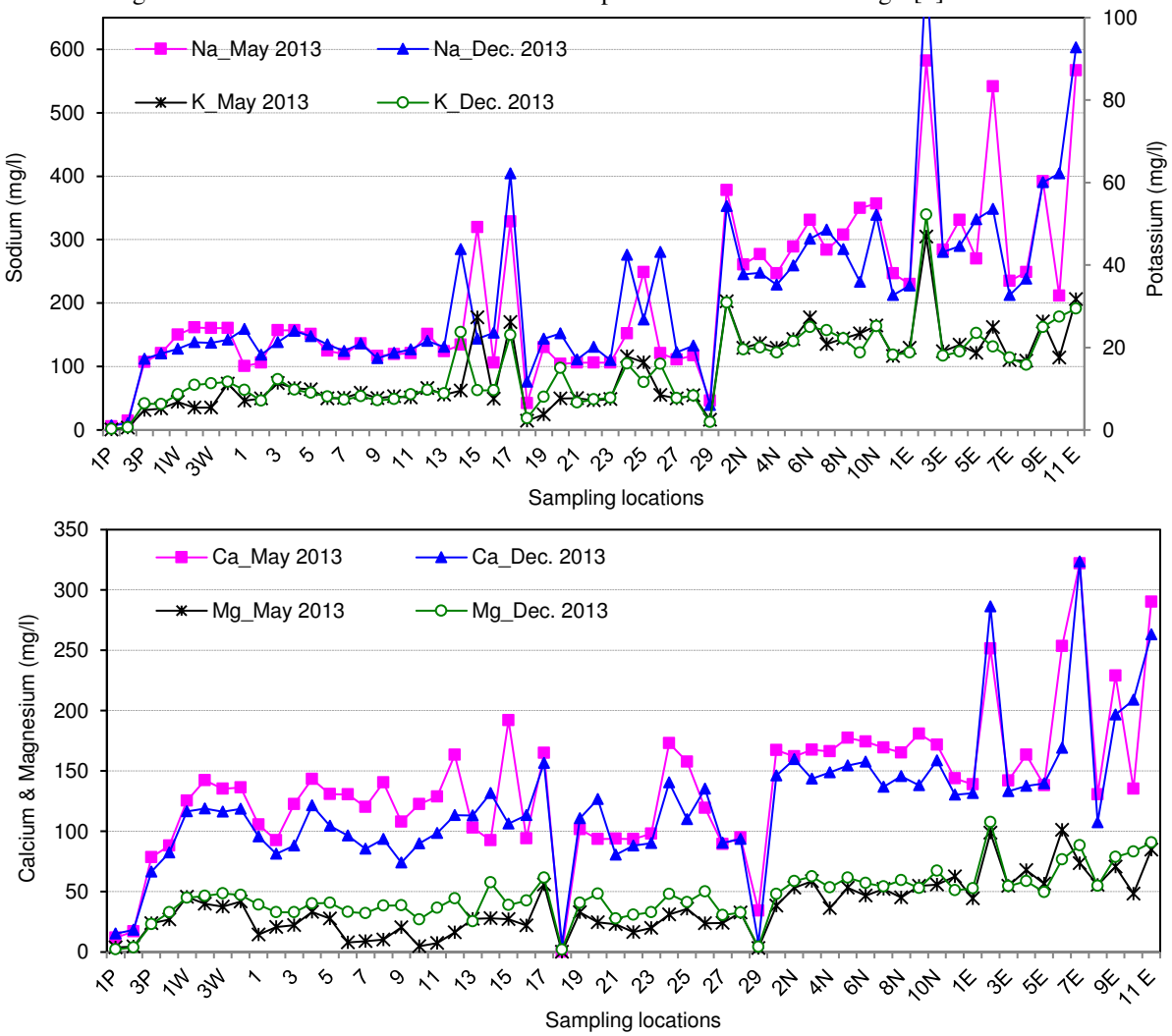

FIGURE 5
Concentration of sodium, potassium, calcium and magnesium (mg/l) in water samples collected from Al-Hassa Oasis, KSA

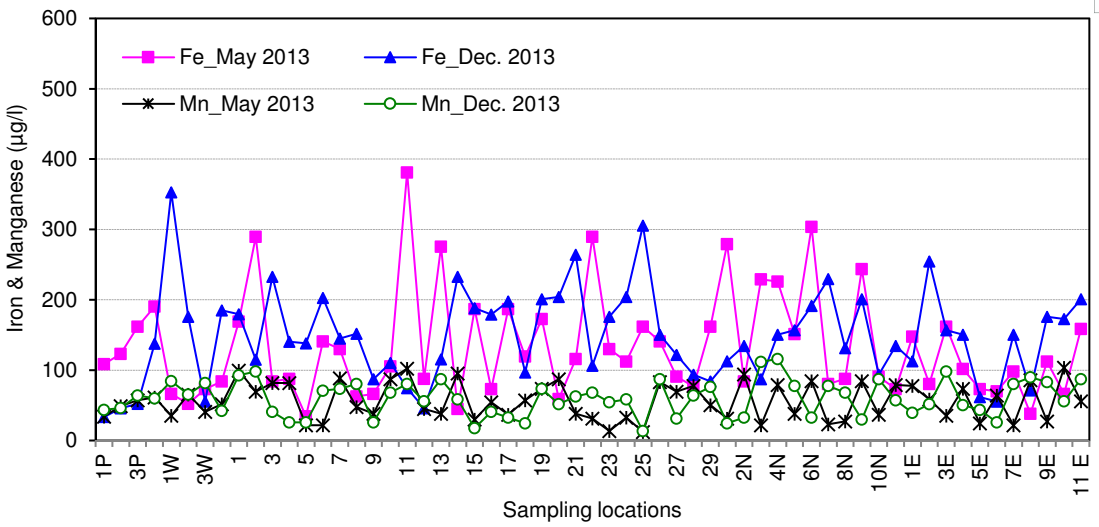

FIGURE 6
Concentrations iron and manganese (µg/l) in water samples collected from Al-Hassa Oasis, KSA

Even though, 46.6% of collected water samples tested in the current study had a total hardness greater than 500 mg/l. Water hardness of more than 500 mg/l is considered excessive for potable water and results in high soap consumption and scale in heating vessels [4]. As shown in Figure 5, an examination of the seasonal variations revealed that calcium values in water samples collected during May 2013 were relatively higher than calcium values of those water samples collected during December 2013. In contrast, relatively higher magnesium values were reported in water samples collected during December 2013.

Iron and manganese concentrations were in the range of 33.4 – 381 µg/l, and 12.3 – 116 µg/l, respectively. Average concentrations of iron and manganese were 141 ± 71.1 µg/l and 58 ± 25.34 µg/l, respectively (Table 1). A few water samples tested (4%) had iron and manganese concentrations greater than the maximum permissible limits of 300 µg/l, and 100 µg/l, respectively [18]. Iron and manganese at higher concentrations in potable water supplies can cause adverse health effects such as neurotoxin and tend to stain laundry and plumbing fixture [28,31]. There is no clear trend of the spatial / temporal variation of iron and manganese concentrations (Figure 6).

Generally, concentrations of TDS, anions (Cl, NO_3, HCO_3, SO_4) and cations (Na, K, Ca, Mg) in the collected water samples were relatively high in comparison with household water characteristics from different zones in Riyadh [5,22], and ground water characteristics in Dakhla Oasis, Egypt [3]. Similarly, Higher levels of physico-chemical parameters were reported in groundwater samples collected from Khamis Mushait (KSA) as compared to Saudi standards [6]. Moreover, higher values of pH, turbidity, TDS, hardness, Na, Cl and SO_4 were reported in household drinking water of Al-Hassa (KSA); these values exceeds the permissible limits set by WHO (2011) [8]. The current study revealed the following ionic dominance order of $Cl^- > SO_4^{2-} > HCO_3^- > NO_3^-$ and $Na^+ > Ca^{2+} > Mg^{2+} > K^+$. This Ionic order might indicate lithogenic origin of these ions in ground water [3]. Relatively, high concentrations of Cl, Na and TDS might indicate the intrusion of seawater into the aquifers, as a result of the excessive extraction of groundwater [2].

Correlation between water quality variables.
Pearson's correlation analysis was applied to analyse the relationships between different ion species (Table 2). There were significant positive correlation between TDS (EC) and the following ions: sodium, potassium, calcium, magnesium, chloride, fluoride, bicarbonate and sulfates with correlation coefficients of r = 0.684 – 0.971 (P < 0.01). These strong correlations reflect the significant contributions of these ions to the acquisition of groundwater mineralisation. Moreover, all the above mentioned ions were strongly correlated with each other (r = 0.605 – 0.969, P < 0.01) (Table 2). For instance, significant positive correlations were observed between fluoride and other ions (Cl, HCO_3, SO_4, Na, K, Ca, and Mg). The strong correlations among these variables suggest that they were influenced by the same environmental factors. There was a weak, but significant, positive correlation (r = 0.362, p < 0.01) between nitrate and TDS (including related ions). Also, turbidity was related to iron with correlation coefficient of 0.313 (P < 0.01). There was a weak, but significant, negative correlation (r = - 0.398, p < 0.01) between pH and TDS (including related ions) (Table 2).

TABLE 2
Correlations matrix for the measured parameters in water samples collected from Al-Hassa Oasis, KSA

	Temp	pH	TDS	Turbid	Cl_2	NO_3	F	Cl	HCO_3	SO_4	Na	K	Ca	Mg	Fe	Mn
Temp	1.00															
pH	**-.383**	1.00														
TDS	**.381**	**-.398**	1.00													
Turbid	.013	-.093	-.006	1.00												
Cl_2	*-.203*	*.213*	**-.438**	-.057	1.00											
NO_3	-.002	*-.197*	**.362**	-.128	-.127	1.00										
F	**.463**	**-.295**	**.684**	-.025	**-.388**	.073	1.00									
Cl	**.374**	**-.354**	**.961**	.000	**-.382**	**.310**	**.605**	1.00								
HCO_3	**.291**	**-.357**	**.775**	-.074	**-.397**	**.507**	**.729**	**.692**	1.00							
SO_4	**.370**	**-.369**	**.936**	-.036	**-.484**	**.344**	**.766**	**.847**	**.780**	1.00						
Na	**.404**	**-.366**	**.971**	.012	**-.414**	**.293**	**.620**	**.969**	**.708**	**.869**	1.00					
K	**.390**	**-.306**	**.932**	-.017	**-.439**	**.268**	**.640**	**.912**	**.750**	**.858**	**.946**	1.00				
Ca	**.365**	**-.379**	**.886**	-.038	**-.337**	**.383**	**.707**	**.812**	**.700**	**.941**	**.814**	**.790**	1.00			
Mg	**.350**	**-.409**	**.924**	-.018	**-.495**	**.286**	**.716**	**.867**	**.757**	**.904**	**.861**	**.816**	**.811**	1.00		
Fe	.068	-.014	.146	**.313**	.097	.156	.107	.101	.174	.124	.143	.174	.114	.060	1.00	
Mn	-.042	-.096	-.015	*.199*	.109	.016	-.038	-.019	.036	-.002	-.021	-.041	-.021	.042	.004	1.00

Bold correlations are significant at $p < 0.01$, *Italic and underline* correlations are significant at $p < 0.05$, (N = 96)

CONCLUSION

Main sources of Potable water supply in Eastern Regions of Saudi Arabia are groundwater wells and desalinated sea water. The purpose of this work was to evaluate Potable water quality in Al-Hassa Oasis. This study provides in depth information about the current situation of Potable water quality in Al-Hassa Oasis with regard to nitrate, fluoride and related physiochemical characteristics. High spatial variations were found in the nitrate, fluoride and related physiochemical characteristics within Potable water supply in Al-Hassa Oasis. Higher values of measured water quality parameters were reported for rural areas of Al-Hassa (Northern and Eastern Villages), while lower values were reported for urban towns (Al-Hofuf and Al-Mubarraz). Where, the water distribution network in urban areas contains groundwater mixed with desalinized water. On the other hand, the sources of potable water in rural areas are groundwater from private wells (with higher salts content) and transported vehicles. Approximately, 50% of the collected water samples have nitrate concentrated greater than 5mgN/L. Moreover, 59% of the collected water samples have fluoride concentrated below the optimum recommended level of 0.8 – 1.5 mg/L. Many of the collected water samples had elevated levels of ions (TDS, Cl, SO_4, Na and total hardness) in excess of the recommended guidelines set by SASO, WHO, EU and USEPA.

In the other hand, no clear trends of seasonal variability were observed in most of the measured potable water quality parameters. The average values of bicarbonate, sulfate and magnesium in water samples collected during December 2013, were relatively higher than average bicarbonate, sulfate and magnesium values of those water sample collected during May 2013. In contrast, average calcium values in water samples collected during May 2013 were relatively higher. Therefore, Potable water quality assessment in Al-Hassa Oasis with respect to nitrate, fluoride and related physiochemical characteristics is essential to ensure the adequacy of water resources for drinking, irrigation and domestic purposes.

The main problems related to potable water quality in Al-Hassa are associated with the characteristics of water supply networks, contamination of groundwater, absence of water purification techniques, as well as scarcity of groundwater. Moreover, it is recommended that a fluoridation process to be used within AL-Hassa potable water distribution networks to increase the fluoride contents in areas with low level of fluoride. Due to the high content of total dissolved salts especially in northern and eastern villages, the sources of potable water are not suitable directly for drinking. Hence, some purification techniques such as reverse osmosis should be installed and used in order to reduce dissolved ions in AL-Hassa potable water. Finally, chemical disinfectants such as sodium

hypochlorite should be used to prevent bacterial contamination.

ACKNOWLEDGEMENTS

The authors would like to thank the Environment and Agricultural Natural Resources Department, King Faisal University in conducting this research. This work was funded by the Deanship of Scientific Research (KFU), Research Project NO 130088.

REFERENCES

(1) Badr,E.A. (2010). The consideration of water resources within environmental impact assessment in Egypt. The International Journal of Environmental Sciences (CATRINA) 5, 31-39.

(2) Karavoltsos,S., Sakellari,A., Mihopoulos,N., Dassenakis,M., and Scoullos,M.J. (2008). Evaluation of the quality of drinking water in regions of Greece. Desalination 224, 317-329.

(3) Soltan,M.E. (1999). Evaluation of ground water quality in Dakhla Oasis (Egyptian Western Desert). Environmental Monitoring and Assessment 57, 157-168.

(4) Al-Redhaiman,K.N. and Abdel Magid,H.M. (2002). The applicability of the local and international water quality guidelines to Al-Gassim region of central Saudi Arabia. Water Air and Soil Pollution 137, 235-246.

(5) Alabdulaaly,A.I. (1997). Nitrate concentrations in Riyadh, Saudi Arabia drinking water supplies. Environmental Monitoring and Assessment 47, 315-324.

(6) Al-Otaibi,E.L. and Zaki,M.S. (2009). Physico-chemical Quality of Drinking Water at Mushait, Aseer, South-Western, Saudi Arabia. African Journal of Clinical and Experimental Microbiology 10, 117-127.

(7) Al-Naeem,A.A. (2015). Monitoring of Groundwater Salinity for Water Resources Management in Irrigated Areas of Al-Jouf Region, Saudi Arabia., 9: 256-269. Research Journal of Environmental Sciences 9, 256-269.

(8) Al-Zarah,A.I. (2014). Evaluation of Household Drinking Water Quality in Al-Ahsa City, Saudi Arabia. Research Journal of Environmental Sciences 8**,** 62-77.

(9) El-Ezaby,K.H., El-Sonbati,M.A., and Badr,E.A. (2010). Impact of fish cages on the Nile water quality at Damietta Branch. Mansoura Journal of Environmental Sciences 39, 329-344.

(10) Cidu,R., Frau,F., and Tore,P. (2011). Drinking water quality: Comparing inorganic components in bottled water and Italian tap water. Journal of Food Composition and Analysis 24, 184-193.

(11) Massoud,M.A., Al-Dakheel,Y.Y., Hussein,A.H., and El-Mahmoudi,A.S. (2011). Spatial Decision Support System for Drinking Water Quality Monitoring and Evaluation in Al-Hassa. International Journal of Water Resources and Arid Environments 1, 457-468.

(12) Giuliano,G. (1995). Ground water in the Po basin: some problems relating to its use and protection. The Science of The Total Environment 171, 17-27.

(13) Robins,N.S. (2002). Groundwater quality in Scotland: major ion chemistry of the key groundwater bodies. The Science of The Total Environment 294, 41-56.

(14) Masoud,A.A., Koike,K., Mashaly,H.A., and Gergis,F. (2016). Spatio-temporal trends and change factors of groundwater quality in_بan arid area with peat rich aquifers: Emergence of water environmental problems in Tanta District, Egypt. Journal of Arid Environments 124, 360-376.

(15) Ikem,A., Osibanjo,O., Sridhar,M.K.C., and Sobande,A. (2002). Evaluation of groundwater quality characteristics near two waste sites in Ibadan and Lagos, Nigeria. Water Air and Soil Pollution 140, 307-333.

(16) Thompson,T.S. (2003). General chemical water quality of private groundwater supplies in Saskatchewan, Canada. Bulletin of Environmental Contamination and Toxicology 70, 447-454.

(17) Sadiq,M. and Hussain,G. (1997). Drinking Water Quality in Saudi Arabia - an overview. Arabian Journal for Science and Engineering 22**,** 153-164.

(18) SASO (2009). Bottled and Unbottled Drinking Water. Standard No. 409. SASO (Saudi Arabian Standards Organization). Riyadh, Saudi Arabia.

(19) WHO (2011). Guidelines for Drinking Water Quality. World Health Organization, Geneva, Switzerland, pp. 1-541.

(20) USEPA (2012). Drinking Water Standards and Health Advisories. USEPA (United States Environmental Protection Agency). EPA 822-S-12-001, 1-12. Washington D.C.

(21) Gupta,M.K., Singh,V., Rajwanshi,P., Agarwal,M., Rai,K., Srivastava,S., Shrivastav,R., and Dass,S. (1999). Groundwater quality assessment of Tehsil Kheragarh, Agra (India) with special reference to fluoride. Environmental Monitoring and Assessment 59, 275-285.

(22) Alabdulaaly,A.I. (1997). Fluoride content in drinking water supplies of Riyadh, Saudi Arabia. Environmental Monitoring and Assessment 48, 261-272.

(23) Srikanth,R., Viswanatham,K.S., Kahsai,F., Fisahatsion,A., and Asmellash,M. (2002). Fluoride in groundwater in selected villages in Eritrea (North East Africa). Environmental Monitoring and Assessment 75, 169-177.
(24) Abderrahman, W. A. (2006). Groundwater Resources Management in Saudi Arabia. Khober, Saudi Arabia, Special Presentation and Water Conservation Workshop.
(25) APHA (2005). Standard Methods for the Examination of Waters and Wastewaters. American Public Health Association (APHA), Washington, DC, USA.
(26) Adams,V.D. (1990). Water & Wastewater Examination Manual. Lewis Publishers, Michigan, USA, pp. 01-247.
(27) Hanrahan,G., Gardolinski,P., Gledhill,M., and Worsfold,P. (2002). Environmental monitoring of nutrients. In, Environmental monitoring handbook (F.R.Burden, I.D.Mckelvie, U.Forstner, and A.Guenther, Eds.). McGraw-Hill, New York, p. 8.1-8.16.
(28) Al-Ghanim,K.A., Abd El-Salam,M.M., and Mahboob,S. (2014). Assessment of Water Quality for Some Roof Tanks in Alkharj Governorate, KSA. Pakistan Journal of Zoology 46, 1003-1012.
(29) Ali,S.M., Sabae,S.Z., Fayez,M., Monib,M., and Hegazi,N.A. (2011). The influence of agro-industrial effluents on River Nile pollution. Journal of Advanced Research 2, 85-95.
(30) Elewa,H.H. (2010). Potentialities of Water Resources Pollution of the Nile River Delta, Egypt. The Open Hydrology Journal 4, 1-13.
(31) Masoud,A.A., Koike,K., Mashaly,H.A., and Gergis,F. (2016). Spatio-temporal trends and change factors of groundwater quality in_بan arid area with peat rich aquifers: Emergence of water environmental problems in Tanta District, Egypt. Journal of Arid Environments 124**,** 360-376.

Received: **11.11.2015**
Accepted: **10.03.2016**

CORRESPONDING AUTHOR

El-Sayed A. Badr
Environment and Natural Resources Department, College of Agricultural & Food Sciences, King Faisal University, Al-Hassa, Saudi Arabia

E-mail: sobadr@kfu.edu.sa, ebadr@du.edu.eg

© by PSP Volume 25 – No. 10/2016, pages 4130-4140 Fresenius Environmental Bulletin

ENHANCING BIOGAS PRODUCTION FROM ORGANIC FRACTION OF MUNICIPAL SOLID WASTE BY CO-DIGESTION WITH THICKENED WASTE ACTIVATED SLUDGE AND RICE STRAW

Zaidun Naji Abudi[1,3], Zhiquan Hu[1,*], Bo Xiao[1], Nagham Rajaa[2,3], Song Chen[1]

1. School of Environmental Science and Engineering, Huazhong University of Science and Technology, Wuhan, 430074, P R China
2. School of Civil Engineering and Mechanics, Huazhong University of Science and Technology, Wuhan, 430074, P R China.
3. Al-Mustansiryiah University, College of Engineering, Baghdad, Iraq

ABSTRACT

The characteristics of anaerobic co-digestion of organic fraction of municipal solid waste (OFMSW), thickened waste activated sludge (TWAS) and rice straw (RS) were investigated in this study. The batch experiment was conducted under mesophilic (37±1ºC) conditions in two groups, that is, (OFMSW with TWAS co-digestion), and (OFMSW, TWAS, and RS co-digestion) along with three different (volume basis) ratios of (1:3, 1:1, and 3:1) and (1:1.5:1.5, 1:0.5:0.5, and 3:0.5:0.5), respectively.The batch test evaluated the biogas potential, and biogas production rate of the OFMSW co-digestion with TWAS with/without RS at different mixing ratios. The first-order kinetic model and modified Gompertz model were also introduced to predict the biogas yield and evaluate the kinetic parameters.The optimum mixing ratios of OFMSW with TWAS and TWAS and RS were 3:1 and 3:0.5:0.5, the cumulative biogas yields (CBY) were 552.9 and 536.1 mL/g VS_{added},which is greater by (153.4% and 185.9%) and (145.7%, 177.2% and 128.7%) than that of digesting OFMSW, TWAS and RS alone, respectively. The modified Gompertz model (R^2: 0.993–0.999) showed a better fit to the experimental results and the calculated parameters indicated that the co-digestion of OFMSW, TWAS with/without RS markedly improved the biogas production rate.

KEYWORDS:
Anaerobic co-digestion; OFMSW; TWAS; Rice straw; Kinetic study.

INTRODUCTION

The rapid economic growth and improving living conditions in most countries over the world have led to rapidly increasing energy consumption. Due to the same reasons, the production of municipal solid waste (MSW) increased rapidly too. The organic fraction of municipal solid waste (OFMSW) is a large and renewable potential energy source that can be exploited on a sustained basis if treated under controlled conditions[1]. Conventional OFMSW management has focused on disposal by aerobic composting or anaerobic digestion. The anaerobic digestion of OFMSWseems to be especially attractive for the renewable energy production and reduction of the greenhouse gas emissions and decrease of the energy dependency on fossil fuels [2]. However; one of the problems most frequently found during digestion processing of OFMSW is the high C:N ratio of these residues[3].

To address this issue, co-digestion of OFMSW with other substrates has been proposed. Athanasoulia et al. reported that the biogas production from the co-digestion of OFMSW and sewage sludge was significantly higher than those of OFMSW and sludge alone [4]. The technical feasibility of anaerobic co-digestion with three types of organic wastes (OFMSW, industrial sludge, and cattle manure) was evaluated under mesophilic conditions[5]. Their results showed that co-digestion can utilize the nutrients and bacterial diversities in various wastes to optimize the digestion process and increase the biogas yield.

Although successful co-digestion of OFMSW with different wastes has been reported in the literature, to our knowledge, there is no information on co-digestion of OFMSW with thickened waste activated sludge (TWAS) and agricultural straw. In the present work, co-digestion of OFMSW, TWAS, and rice straw (RS) was examined under mesophilic (37±1ºC) fermentation conditions. The main aim of this work is to evaluate the effect of TWAS and RS added as co-substrates on OFMSW anaerobic digestion. For this purpose, batch anaerobic digestion tests were performed in order to check the biochemical methane potential (BMP) under different mixing ratios. Two sets of BMP assays were conducted, one for the co-digestion of OFMSW and TWAS and the other for the OFMSW, TWAS and RS anaerobic co-digestion. Furthermore,

the first-order kinetic model and modified Gompertz model were introduced to predict the methane yield and evaluate the kinetic parameters of co-digestion of OFMSW, TWAS and RS.

MATERIALS AND METHODS

Feedstocks and inoculum. Organic fraction of municipal solid waste (OFMSW), thickened waste activated sludge (TWAS), and rice straw (RS) were used as substrate in this study. OFMSW was prepared in the lab with constituents which simulate green bin waste or kitchen waste. Instead of using actual kitchen waste, a sample OFMSW was used in this study in order to maintain consistent homogenous waste compositions throughout the whole study. The OFMSW, which mainly consisted of rice, vegetable and meats, was crushed with electrical blender. The crushed OFMSW was sealed in a plastic bag and stored in a refrigerator at (4ºC). The waste was allowed to reach room temperature prior to the testing. Rice straw (RS) was obtained from a rural area in Wuhan, China. The RS was completely dried in an oven at 105ºC for more than 20 hr. The dried RS was ground to (<5 mm) particles by a hammer mill and then used as the co-substrate.

TWAS and inoculum were obtained from a local full-scale municipal wastewater treatment plant (Wuhan, China). Collected sludge and inoculum were stored at 4ºC for subsequent experiments.

Batch experimental setup. The biochemical methane potential (BMP) assays were conducted according to the procedures described in the literature [6]. OFMSW, TWAS, RS, and their mixtures were separately examined, in mono-digestion or co-digestion, respectively. The assays were carried out in three groups.The first group was mono-digestion of substrates (reactors A, B, and C for OFMSW, TWAS, and RS, respectively), while the second group of the batch experiments was performed to assay the BMP of the various mixture ratios of co-digestion of OFMSW and TWAS (reactors D, E, and F for 1:3, 1:1, and 3:1 as volume basis, respectively). In the third group, the batch anaerobic co-digestion of OFMSW, TWAS, and RS was carried out in three mixture ratios (reactorsG, H, and I for 1:1.5:1.5, 1:0.5:0.5, and 3:0.5:0.5, as volume basis, respectively). In the three BMP experiments, the mixtures of substrates and inocula were transferred to 250 mL septum top glass bottles with a working volume of 180 mL. The TS content in each reactor was adjusted to 5% and the working volume was composed of 80% substrate and 20% inoculum. Before seeding, the inoculum was placed in an incubator for ~10 d until biogas production ceased to minimize the contribution from the residual organic materials contained in the inoculum [7]. After adding the required amounts of inoculum and substrate, each bottle was filled with distilled water to reach the desired volume. Assays with inoculum alone were also used as the control samples. The initial pH of the mixed liquor in each digester was adjusted to 7.0±0.1 by using 1 M HCl or 1 M NaOH[8].

After adding the substrates, the bottles were purged with nitrogen for 2-5 min to eliminate oxygen. The bottles were then immediately capped tightly with rubber stoppers. Then bottles were placed in a water bath shaker to provide continual homogeneous mixing of the mixtures at approximately 100 rpm and to incubate the bottles at the mesophilic temperature of 37±1ºC. During the digestion period, biogas productions were determined daily. After biogas production stopped, the digestates were finally sampled to determine pH, TS, VS, VFA, alkalinity and total and soluble COD, in order to analyze the treatment efficiencies.

Biogas volume measurement, composition analysis, and calculation. Biogas production yield was measured daily by the water displacement method and transferred to the standard condition. Assay bottle (250 ml volume) was removed from the incubator and allowed to cool to room temperature prior to biogas volume measurement, after that it was connected to a 1-L gas collection glass bottle and a 250-mL liquid collection cylinder (Fig. 1). Once the digestion bottle was connected to the gas collection glass bottle, biogas was directly distributed into the gas collection bottle which was filled with a saturated sodium chloride solution [9], and then an equivalent volume of liquid to the produced biogas was displaced to the liquid collection cylinder. Biogas produced from the inoculum was subtracted from the sample assays.

The CH_4 gas content was analyzed via gas chromatography (SP-2100, China) equipped with a thermal conductivity detector (TCD) and a packed column. For the calibration, standard gases (H_2, O_2, N_2, CH_4, CO_2: purity >99.9%) were used. The temperature of injector port, column and detector was increased from 70 ºC, 50 ºC and 70 ºC to 120 ºC, 95 ºC and 150 ºC, respectively. Argon was used as the carrier gas at a flow rate of 40ml/min.

The simulated biogas yield (SBY) of the mixtures was introduced to evaluate the effect of co-digestion. SBY was calculated based on the weighted average biogas yield from each of the individual single substrates and the portion of each waste co-digested in the assay. If there is no effect of co-digestion, the cumulative biogas yield as measured for the particular mixture should be the same as SBY value, as shown in Eq. (1):

$$SBY_i = BY_{OFMSW,mono,i} \times Y_1\% + BY_{TWAS,mono,i} \times Y_2\% + BY_{RS,mono,i} \times Y_3\% (1)$$

where i = the digestion time (d); SBY_i = the simulate biogas yield of mixture at the ith day (mL/g VS_{added}); $BY_{OFMSW,mono,i}$ = biogas yield of OFMSW at the ith day (mL/g VS_{added}); $Y_1\%$ = the percentage of OFMSW in mixture (%);$BY_{TWAS,mono,i}$ = biogas yield of TWAS at the ith day (mL/g VS_{added}); $Y_2\%$ = the percentage of TWAS in mixture (%), $BY_{RS,mono,i}$=biogas yield of RS at the ith day (mL/g VS_{added}); $Y_3\%$ = the percentage of RS in mixture (%).

The fed TS and VS removal rate during the batch test was calculated based on total mass removal from the testing reactors and the blank reactors following of Kafle et al. [10].

$$TS_{removal} = \frac{(F+I)\times a - I\times b}{F} \times 100\% \ (2)$$

$$VS_{removal} = \frac{(F+I)\times a - I\times b}{F} \times 100\% \ (3)$$

where F = TS_{feed} or VS_{feed} added to reactor (g); I = $TS_{inoculum}$ or $VS_{inoculums}$ added to reactor (g); a = calculated TS or VS removal of feed plus inoculums based on total initial and final TS or VS present in the reactor(%); b = calculated TS or VS removal of inoculum in blank reactor (%).

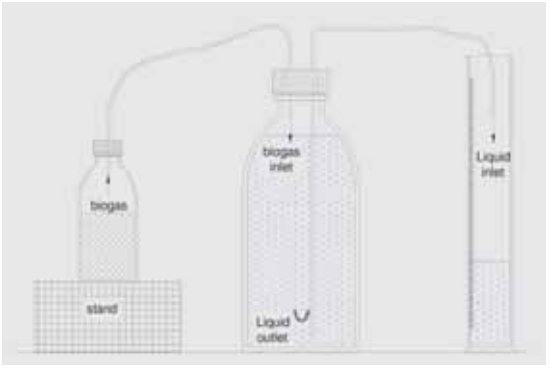

FIGURE 1
Schematic representation of the batch experimental setup

Analytical methods. All analyses were duplicated, and the results given are mean values. The total solids (TS), volatile solids (VS), and total chemical oxygen demand (TCOD) contents of OFMSW, TWAS, RS and inoculum and digestate were determined according to the Standard Methods [11]. The pH was determined with a pHS-25C pH meter (Shanghai Precision & Scientific Instrument Co., Ltd., China). The carbon and nitrogen analysis was conducted using a Vario EL element analyzer (Elementar Analysensysteme GmbH,Germany).

To determine VFA, alkalinity, and the soluble chemical oxygen demand (SCOD) samples from substrates and reactors were filtered through a filtration membrane with a pore size of 0.45μm, then the filtrates were diluted 10 times with distilled water [12]. Total VFA and alkalinity were determined through a two-step titration method [13]. SCOD was analyzed according to the Standard Methods [11].The biogas yield of each substrate and mixture at the end of each test was calculated by dividing the cumulative gas volume by the mass of VS in the feedstock loaded into the reactors at start-up.

Kinetic model. The kinetics of biogas fermentation of several organic materials is calculated by the use of the first-order kinetic model [14]. The biogas fermentation of OFMSW, TWAS, and RS can be described by the first-order kinetic model. The biogas yield from anaerobic co-digestion of (OFMSW and TWAS) and (OFMSW, TWAS, and RS) can be predicted using Eq.(4) [10].

$$G(t) = G_{mas} \times (1 - e^{-Kt}) (4)$$

By linearization, Eq. (4) becomes Eq. (5), which is representing an equation of a straight line with a slope whose magnitude is the hydrolysis rate constant. The slope was obtained by plotting $\ln\left[1 - \frac{G(t)}{G_{max}}\right]$ versus time and performing linear regression [15].

$$-Kt = \ln\left[1 - \frac{G(t)}{G_{max}}\right] (5)$$

Where G(t) is the cumulative biogas yield at time t (mL/g VS_{added}); G_{max} was the potential maximum biogas yield (mL/g VS_{added}); K is hydrolysis rate constant (d^{-1}) and t is the time (d). The parameters K, correlation coefficient (R^2), and predicted maximum biogas yield (G_{max}) were obtained from the batch experiments by using the SigmaPlot 12.3 software.

Apart from the specific biogas yield and the cumulative biogas yield, the duration of the lag phase is also an important factor in determining the efficiency of anaerobic digestion. The lag phase (λ) can be calculated with the modified Gompertz model as follows [10]:

$$G(t) = G_{max} exp\left\{-exp\left[\frac{R_{max}e}{G_{max}}(\lambda - t) + 1\right]\right\} (6)$$

where G(t) is the cumulative biogas yield at time t (mL/g VS_{added}); G_{max} is the biogas potential maximum production (mL/g VS_{added}); R_{max} is the maximum biogas production rate (mL/g VS-d); λ is the lag phase (d); t is the duration of the assay (d); and e is the exp(1) = 2.7183.

RESULTS AND DISCUSSION

Characteristics of feedstocks and inoculum. The environmental characterization data for the individual substrates (OFMSW, TWAS, RS and inoculum), (pH, TS, VS, TCOD, sCOD, alk, TC

TABLE 1
Characteristics of feedstocks and inoculum

Parameters	OFMSW	TWAS	RS	Inoculum
pH	3.51±0.04	6.40±0.00	6.22±0.02	6.54±0.05
T.S (%)	23.30±0.34	14.18±0.16	92.59±0.31	2.25±0.39
V.S (%)	20.15±0.26	6.72±0.09	70.37±0.22	1.35±0.35
V.S / T.S	88.48	47.39	76.00	60.00
TCOD (mg/l)	210667±3581	37040±1332	ND	19040±1351
sCOD (mg/l)	110050±1610	12800±750	ND	5600±452
sCOD/TCOD	52.24	34.60	ND	29.40
alk (mg/l CaCO3)	500±12	1500±21	ND	667±14
Total Carbon (%/TS)	ND	ND	40.95±1.1	ND
Total Nitrogen (%/TS)	ND	ND	0.72±0.04	ND

Note: ND, not determined

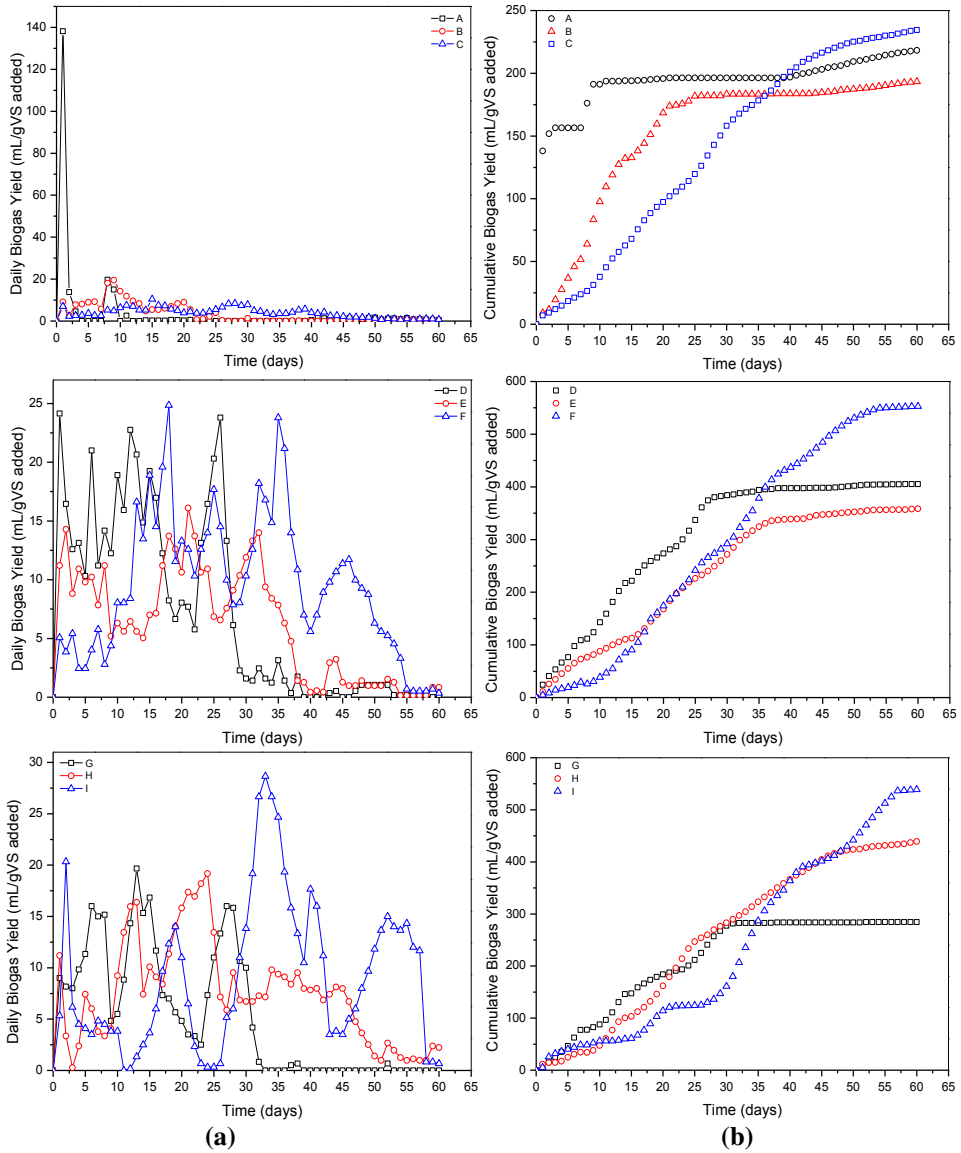

FIGURE 2
(a) Daily and (b) Cumulative biogas yields during anaerobic digestion of reactors A, B, C, D, E, F, G, H, and I

and TN) are listed in Table 1. Rice straw (RS) had the highest TS and VS percentage (92.59% and 70.37%, respectively), followed by OFMSW (23.30% and 20.15%, respectively), and TWAS (14.18% and 6.72%, respectively). The inoculum had the lowest TS and VS percentage values (2.25% and 1.35%, respectively). The pH of OFMSW was the lowest (3.51), and inoculum had the highest pH (6.54), followed by TWAS and RS (6.40 and 6.22, respectively).

Biogas production. The daily and cumulative biogas yields of OFMSW, TWAS, RS, co-digestion (OFMSW/TWAS), and co-digestion (OFMSW/TWAS/RS) are shown in Fig.2. The biogas production processes ran for about 60 days.All the assays were finished when the biogas production was below 5% of the total cumulative production [16]. Biogas production started immediately from the first day for all digestion tests. For reactors A, B and C, peaks of the daily biogas yield occurred on day 1 (138.16 mL/g VS-d), day 9 (19.50 mL/g VS-d), and day 15 (10.43 mL/g VS-d), respectively. For co-digestion of OFMSW/TWAS, the highest biogas production rate was obtained at reactor F, with a peak daily biogas production rate of (24.85 mL/g VS-d), which was 1.5-fold higher than that of the digestion system with other mixing ratios. For the co-digestion of OFMSW/TWAS/RS, the highest biogas production rate was obtained at reactor I, which was 1.89-fold higher than that of the reactor G.

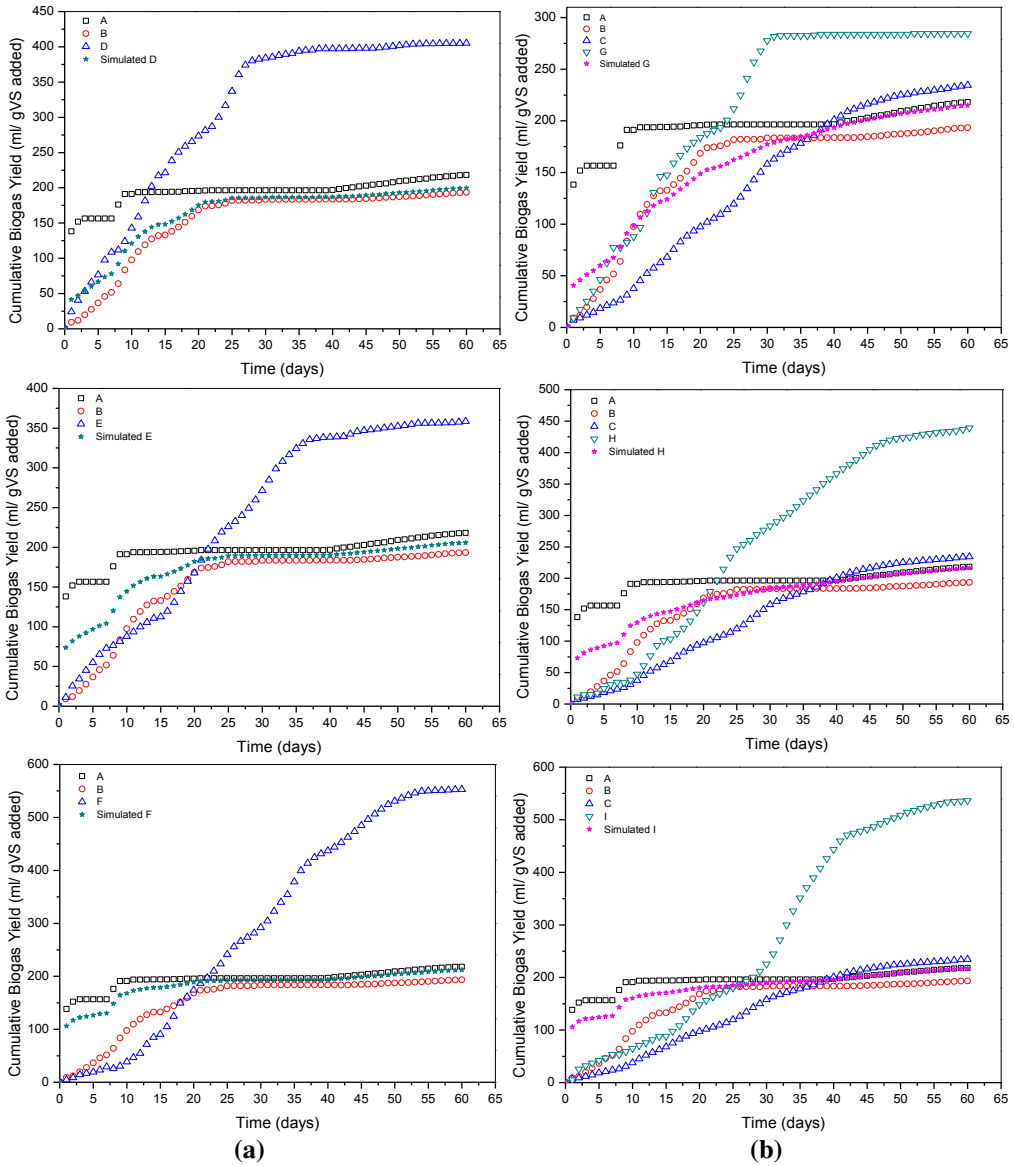

FIGURE 3
(a) Reactors D, E, and F and (b) Reactors G, H, and I in comparison with reactors A, B, and C (b)

From Fig.2-b, it can also be seen that at the end of the digestion process the total biogas yields were 218.19, 193.43, and 234.46 mL/g VS_{added} for the reactors A, B, and C, respectively.The total biogas yields were 405.25, 358.53, and 552.93 mL/g VS_{added} for the reactors D, E, and F, respectively, while the total biogas yields were 284.33, 439.17, and 538.75 mL/g VS_{added} for the reactors G, H, and I, respectively. Approximately 90.0%, 94.8%, 67.4%, 94.7%, 75.7%, 49.5%, 97.6%, 64.4%, and 29.9% of the total biogas yields were obtained after first 30 days of digestion, for reactors A, B, C, D, E, F, G, H, and I, respectively. The percentage of cumulative biogas to the total was used to indicate the completeness of biogasification. From the percentages of cumulative biogas yield to the total, it can be seen that reactors G, B, D, and A exhibited a faster biogas production rate than other reactors.

The cumulative biogas yields from reactors D, E, F, G, H, and I compared with that of cumulative biogas yields from reactors A, B, and C individually and simulated biogas yields (SBY) were shown in Fig.3. Reactors D, E, and F showed a higher biogas yields of 64.3-153.39% and 85.37-185.88% than reactors A and B, respectively (Fig.3-a). Moreover, cumulative biogas yields were more than 2.0, 1.7,and 2.6 times higher than SBY, for reactors D, E, and F, respectively (Fig.3-a and Table 2). From Fig.3-b,reactors G, H, and I had increasing percent of 30.29–146.88%, 47–178.54, and 21.24–129.72% more than reactors A, B, and C, respectively. The cumulative biogas yields in the reactors G, H, and I were increased by 32.2%, 103.3%, and 148.1% more than the simulated yields (Fig.3-b and Table 2).

Table 2 summarizes the analyses for co-digestion mixtures of OFMSW, TWAS and RS, depicting the differences between the biogas yields from co-digestion samples and the SBYs calculated from mono-digestion biogas yields. The data however shoes that the co-digestion of OFMSW with TWAS or with both TWAS and RS is synergistic, since biogas yields are (103%, 74.2%, 160.8%, 32.2%, 103.2%, and 148.1%) for the reactors D, E, F, G, H, and I higher than their SBY. Synergistic effects may arise from the contribution of additional alkalinity, trace elements, nutrients, enzymes, or any other amendment which a substrate by itself may lack, and could result in an increase in substrate biodegradability, and biogas potential.

Volatile solids removal. One of the most useful parameters for evaluating the efficiency of anaerobic digestion is the reduction in volatile solids (VS). As shown in Fig.4-a, reactor G obtained the highest rate of VS destruction at 78.85%, while reactor B had the lowest at 34.39%. Similarly, Takashima (2008) reported only 30-40% of the organic matter content in waste active sludge was degraded in mesophilic temperature conditions.VS reduction of reactor A in this experiment (43.27%) was relatively lower than the VS reduction (65.2%) achieved by L. Martín-González et al.[17], but Cabbai et al. [18] presented a similar VS reduction of 33%. With respect to the reactor C,VS reduction in this study (58%) was higher than the VS reduction (51.53%) achieved by Ye et al.[2]. For reactors D, E, F, G, H, and I as illustrated in Fig.4-a, with increasing the amount of OFMSW percent in feedstock, the VS reduction increased.

Based on proportions of OFMSW, TWAS and RS in the mixtures and the VS removal rates of OFMSW, TWAS and RS, the simulated VS removal rates for the reactors D, E, F, G, H, and I were (36.61%, 38.83%, 41.05%, 45.46%, 44.73%, and 44.00%), respectively. The actual VS removal rates for the reactors D, E, F, G, H, and I increased by 61.8%, 73.4%, 78.2%, 5.9%, 64.3%, and 79.2% more than their simulated values, respectively (Fig.4-a).

TABLE 2
Synergistic effect evaluation of co-digestion of OFMSW, TWAS and RS

Reactor	BY (ml/gVS)	SBY (ml/gVS)	Differential (BY-SBY)	Increasing rate of biogas yield (%)	Synergistic effect
A	218.2	218.2	--	--	--
B	193.4	193.4	--	--	--
C	234.5	234.5	--	--	--
D	405.30	199.62	205.68	103.04	Synergistic
E	358.50	205.81	152.69	74.19	Synergistic
F	552.90	212.00	340.90	160.80	Synergistic
G	284.30	215.01	69.29	32.23	Synergistic
H	439.20	216.07	223.13	103.27	Synergistic
I	536.08	217.13	318.95	146.89	Synergistic

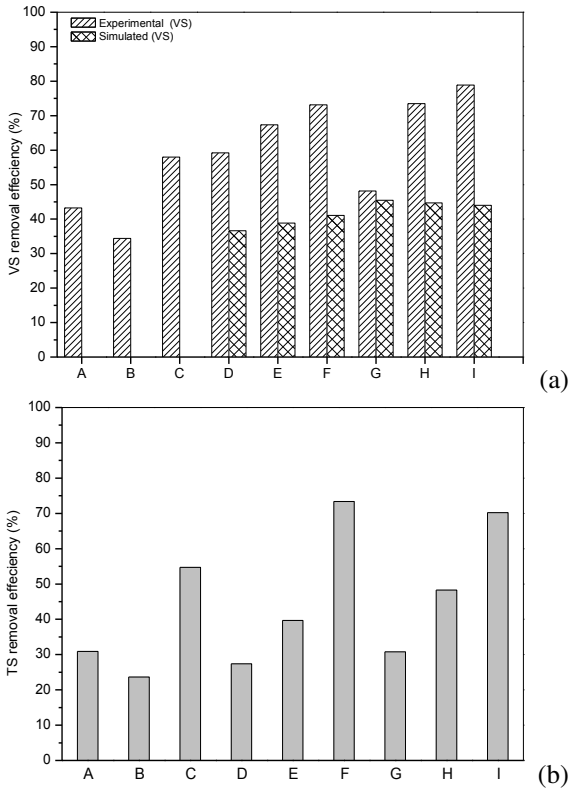

FIGURE 4
(a) Volatile solids removal efficiency (b) Total solids removal efficiency

Degradation of organic solid content. Biogas is recognized to be produced through the conversion of organic matters by anaerobic microorganisms. With the conversion of organic matters into biogas, the amount of organic dry matters would be reduced accordingly. Based on the mass balance concept, the removals of TS are illustrated in Fig.4-b. It was observed that the removal rates for TS were affected by substrates mixing ratios. Highest TS removal rates of (73.37% and 70.23%) were achieved with the reactors F and I, respectively, while relatively low TS removal efficiency of 23.63% and 27.37% found with reactors B and D, respectively.

CH_4 content. The average methane contents of biogas produced from reactors A, B, C, D, E, F, G, H, and Iare shown in Fig. 5. The highest methane content of 68.0% was observed in the reactor A. With the addition of TWAS and RS, methane content of the biogas started to decrease.Reactor C had the lowest methane content of 53.2%. The higher methane content at higher composition ratios of OFMSW was probably caused by the high protein content contained in the OFMSW. Compared with carbohydrate-rich feedstocks, such as lignocellulosic green waste, methane content in the biogas produced during the degradation of protein-rich materials was higher [19]. Liu et al. reported higher methane contents in the biogas were achieved from digestion of food waste than from green waste and the mixture (50% food waste and 50% green waste, based on VS)[20].

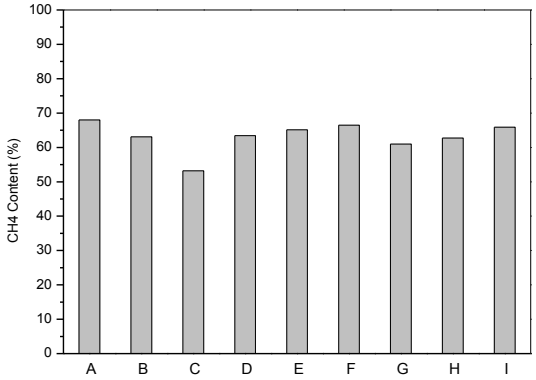

FIGURE 5
Average methane content

Kinetic study results. Tables3 and 4 and Figure 6 summarize the results of a kinetic study for reactors A, B, C, D, E, F, G, H, and I, by using a first-order kinetic model and the modified Gompertz model.

Figure 6-a shows the plot of Eq. (5) for all scenarios of OFMSW, TWAS, and RS combinations evaluated with the batch assays. The slopes of the linear regression lines correspond to hydrolysis constants (K). The biogas production rate constant (K) for reactors A, B, and Cwere calculated to be (0.047, 0.077, and 0.078 day^{-1}), respectively. For reactors D, E, and F, (K) values were (0.121, 0.098, and 0.091day^{-1}), respectively, with increase in (K) values by approximately (1.9-2.6 and 1.2-1.6) compared to A and B reactors, respectively (Table 3). The K values for reactors G, H, and I, were increased by approximately (1.7-3.3, 1.0-2.0, 1.0-2.0) compared to reactors A, B, and C, respectively (Table 4). This suggests that co-digestion significantly increased the bioavailability of the organic content in all substrates.

From Tables 3 and 4, R_{max} (the maximum biogas production rate) values estimated by modified Gompertz model, for reactors A, B, and C were (53.22, 10.92, and 6.93mL/g VS-d), respectively. These tables also showed that the R_{max} was improved by (8.24-54.38%)for reactors D, E, and F, than reactor B. With respect to reactors G, H, and I, the R_{max} was improved by (8.1-52.6%) and (70.3-140.4%), respectively than that of reactors B and C. This reflected that co-digestion of OFMSW, TWAS, and RS significantly accelerated the mixing substrate's conversation rate.The other important indicator of substrate biodegradability and utilization rate was the digestion time [8]. The technical digestion time (T_{90}) is defined as the time taken to achieve 90% of maximum cumulative

biogas production [10]. The effective biogas production period (T_{ef}) was calculated by subtracting the lag time (λ) from T_{90} (Tables 3 and 4). The T_{ef} value for reactor B was found to be lower than that for reactors A and C. The T_{ef} for reactors D, E, F, G, H, and I was increased when OFMSW fraction increased in the mixed feedstock. One possible reason for the increased T_{ef} under co-digestion conditions could be the VFA's inhibition to methanogens due to OFMSW's rapid acidification. Based on the parameters obtained from the model, the high biogas production rate and the increased effective biogas production time were obtained in the systems of co-digestion of OFMSW, TWAS, and RS.

As shown in Tables 3 and 4, the difference between the predicted and measured methane yields in the first-order kinetics model was (0.94-6.34%), (0.07-2.07%) and (0.01-8.20%) for mono– and co–digestions, respectively. While for the modified Gompertz model (0.00-0.73%), (0.35-4.31%), and (0.40-9.01%) for mono- and co-digestions, respectively. To evaluate the soundness of the model results in the modified Gompertz model, the predicted values of methane yield were plotted against the measured values, as plotted in Fig.6-b. The correlation coefficients R^2 values fell within the ranges of (0.868–0.998), (0.993-0.997), and (0.993-0.998) for mono- and co-digestions, respectively.

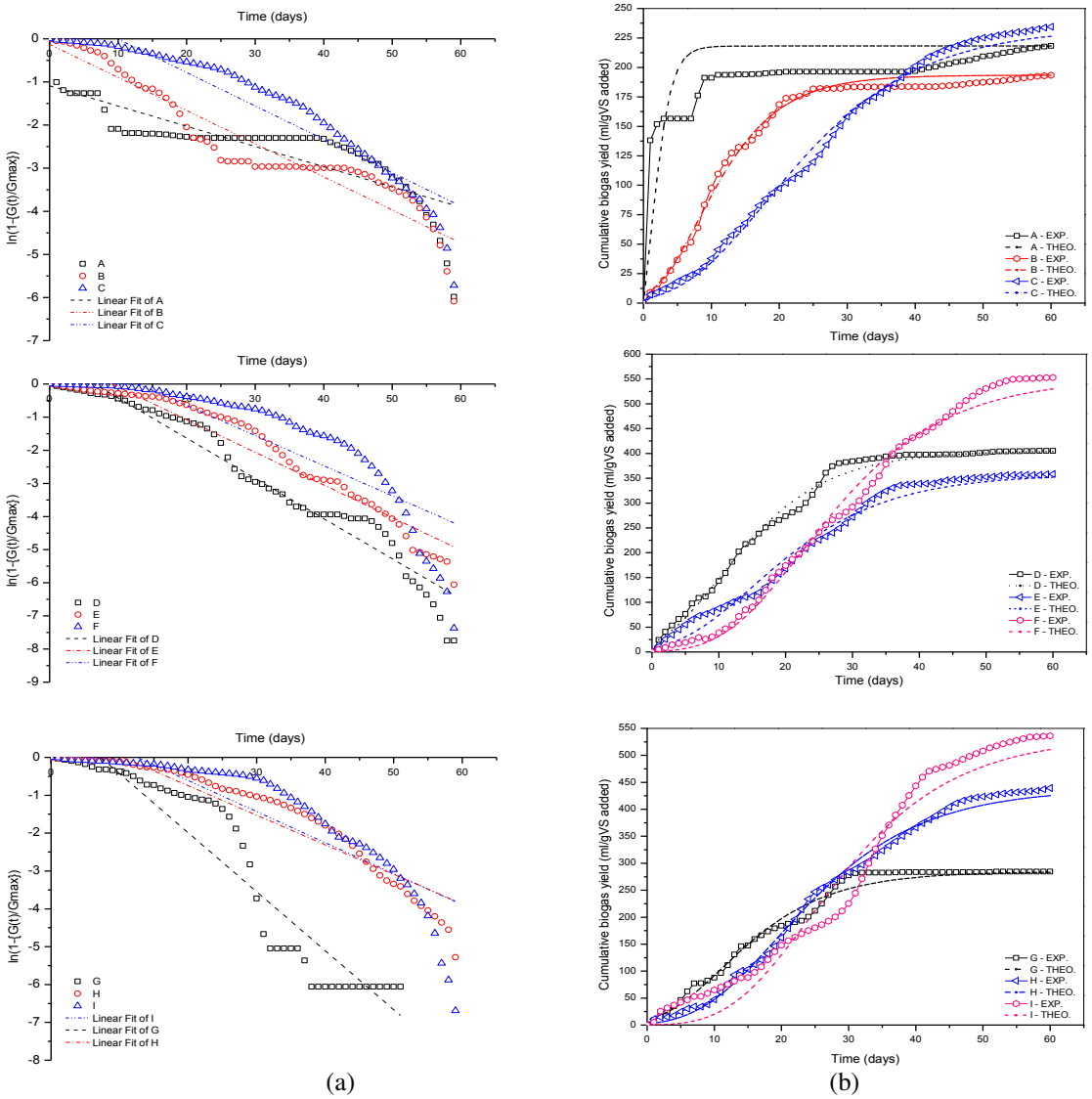

(a) (b)

FIGURE 6

(a) Linear regression fits for estimation of hydrolysis constants (k) from the batch assay data for reactors A, B, C, D, E, F, G, H, and I (b) Modified Gompertz equation to the batch dates for reactors A, B, C, D, E, F, G, H, and I

(b)

TABLE 3
Model parameters of the first-order kinetic model and the modified Gompertz model for reactors A, B, C, D, E, and F

Parameter	A	B	C	D	E	F
First order kinetic model						
correlation coefficient R^2	0.707	0.908	0.889	0.948	0.931	0.752
K (1/day)	0.047	0.077	0.078	0.121	0.098	0.091
predicted biogas yield (ml/g VS_{added})	205.18	191.52	232.28	404.96	357.53	550.58
Measure biogas yield (ml/g VS_{added})	218.19	193.43	234.46	405.25	358.53	552.93
Difference between measured and predicted biogas yield (%)	6.34	1.00	0.94	0.07	0.28	0.43
Modified Gompertz model						
correlation coefficient R^2	0.868	0.997	0.998	0.997	0.993	0.996
R_{max} (mL/g VS-d)	53.22	10.92	6.93	16.85	11.82	17.16
λ (d)	0.00	1.61	5.64	1.23	3.92	10.63
T_{90} (d)	22	22	43	27	35	48
T_{ef} (d)	22.00	20.39	37.36	25.77	31.08	37.38
Predicted biogas yield (mL/g VS_{added})	218.19	193.36	226.52	403.82	352.18	530.10
Measure biogas yield (mL/g VS_{added})	218.19	193.43	234.46	405.25	358.53	552.93
Difference between measured and predicted biogas yield (%)	0.00	0.04	3.51	0.35	1.80	4.31

TABLE 4
Model parameters of the first-order kinetic model and the modified Gompertz model for reactors G, H, and I

Parameter	G	H	I
First order kinetic model			
correlation coefficient R^2	0.897	0.890	0.775
K (1/day)	0.156	0.078	0.082
predicted biogas yield (ml/g VS_{added})	284.31	435.10	532.19
Measure biogas yield (ml/g VS_{added})	284.33	439.17	536.08
Difference between measured and predicted biogas yield (%)	0.01	0.94	0.73
Modified Gompertz model			
correlation coefficient R^2	0.993	0.998	0.986
R_{max} (mL/g VS-d)	11.80	13.72	16.66
λ (d)	2.20	7.62	12.27
T_{90} (d)	28	44	56
T_{ef} (d)	25.80	36.38	43.73
Predicted biogas yield (mL/g VS_{added})	283.19	425.43	491.79
Measure biogas yield (mL/g VS_{added})	284.33	439.17	536.08
Difference between measured and predicted biogas yield (%)	0.40	3.23	9.01

CONCLUSIONS

The characteristics of anaerobic co-digestion of OFMSW, TWAS and RS were evaluated in this study. The biogas yields were improved by (64.3-153.3% and 85.3-185.8%), and (30.2-146.8%, 47-178.5, and 21.2-129.7%), respectively, for co-digestion of OFMSW/TWAS and OFMSW/TWAS/RS, compared with the digestion of OFMSW, TWAS, and RS alone. The VS removal rates were increased by (36.9-69% and 72.2-112.6%) and (11.2-82.2%, 40.0-129.2%, and 4.8-35.9%), for co-digestion of OFMSW/TWAS and OFMSW/TWAS/RS, respectively.The parameters obtained from the modified Gompertz model and the first-order kinetic model indicated that the co-digestion of OFMSW, TWAS, and RS greatly improved the biogas production rate.

ACKNOWLEDGEMENTS

The authors would like to acknowledge the financial supports of Iraqi scholarship foundation from Ministry of Higher Education and Scientific Research of Iraq, Fundamental Research Funds for the Central Universities (2015TS113), Wuhan International Science and technology cooperation project (No. 2015030809020369) and SRF for ROCS, SEM, China. We thank to the Analytical and Testing Center of Huazhong University of Science and Technology (HUST), Wuhan, P.R. China for carrying out the analyses of biomass samples.

REFERENCES

[1] Shahriari H, Warith M, Hamoda M, Kennedy KJ (2012) Anaerobic digestion of organic fraction of municipal solid waste combining two pretreatment modalities, high temperature microwave and hydrogen peroxide. Waste Management 32: 41-52.

[2] Ye J, Li D, Sun Y, Wang G, Yuan Z, et al. (2013) Improved biogas production from rice straw by co-digestion with kitchen waste and pig manure. Waste Management 33: 2653-2658.

[3] Gómez X, Cuetos MJ, Cara J, Morán A, Garcia AI (2006) Anaerobic co-digestion of primary sludge and the fruit and vegetable fraction of the municipal solid wastes: Conditions for mixing and evaluation of the organic loading rate. Renewable energy 31: 2017–2024.

[4] Athanasoulia E, Melidis P, Aivasidis A (2012) Optimization of biogas production fromwaste activated sludge through serial digestion. Renewable Energy 47: 147-151.

[5] Capela I, Rodrigues A, Silva F, Nadais H, Arroja L (2008) Impact of industrial sludge and cattle manure on anaerobic digestion of the OFMSW under mesophilic conditions. Biomass and Bioenergy 32: 245-251.

[6] Owen WF, Stuckey DC, Healy JB, Young LY, McCarty PL (1979) Bioassay for monitoring biochemical methane potential and anaerobic toxicity. Water research 13: 485-492.

[7] Zhang W, Wei Q, Wu S, Qi D, Li W, et al. (2014) Batch anaerobic co-digestion of pig manure with dewatered sewage sludge under mesophilic conditions. Applied Energy 128: 175-183.

[8] Xie S, Lawlor PG, Frost JP, Hu Z, Zhan X (2011) Effect of pig manure to grass silage ratio on methane production in batch anaerobic co-digestion of concentrated pig manure and grass silage. Bioresource Technology 102: 5728-5733.

[9] Salam B, Islam M, Rahman MT. Biogas from anaerobic digestion of fish waste; 2009. pp. 1-3.

[10] Kafle GK, Kim SH, Sung KI (2013) Ensiling of fish industry waste for biogas production: a lab scale evaluation of biochemical methane potential (BMP) and kinetics. Bioresource technology 127: 326-336.

[11] APHA (1998) Water Environment Federation (1998) Standard methods for the examination of water and wastewater. Washington, DC.

[12] Wang K, Yin J, Shen D, Li N (2014) Anaerobic digestion of food waste for volatile fatty acids (VFAs) production with different types of inoculum: Effect of pH. Bioresource technology 161: 395-401.

[13] Voß E, Weichgrebe D, Rosenwinkel K (2009) FOS/TAC—Deduction, Methods, Application and Significance. Internationale Winenschaftskonferenz “Biogas Science.

[14] Rao MS, Singh SP, Singh AK, Sodha MS (2000) Bioenergy conversion studies of the organic fraction of MSW: assessment of ultimate bioenergy production potential of municipal garbage. Applied Energy 66: 75-87.

[15] Parameswaran P, Rittmann BE (2012) Feasibility of anaerobic co-digestion of pig waste and paper sludge. Bioresource technology 124: 163-168.

[16] Ferreira L, Nilsen P, Fdz-Polanco F, Pérez-Elvira S (2014) Biomethane potential of wheat straw: Influence of particle size, water impregnation and thermal hydrolysis. Chemical Engineering Journal 242: 254-259.

[17] Martín-González L, Colturato L, Font X, Vicent T (2010) Anaerobic co-digestion of the organic fraction of municipal solid waste with FOG waste from a sewage treatment plant: recovering a wasted methane potential and enhancing the biogas yield. Waste Management 30: 1854-1859.

[18] Cabbai V, Ballico M, Aneggi E, Goi D (2013) BMP tests of source selected OFMSW to evaluate anaerobic codigestion with sewage sludge. Waste Management 33: 1626-1632.

[19] Weiland P (2010) Biogas production: current state and perspectives. Appl Microbiol Biotechnol 85: 849-860.

[20] Liu G, Zhang R, El-Mashad HM, Dong R (2009) Effect of feed to inoculum ratios on biogas yields of food and green wastes. Bioresource technology 100: 5103-5108.

Received: **23.09.2015**
Accepted: **25.03.2016**

CORRESPONDING AUTHOR

Zhiquan Hu
School of Environmental Science and Engineering,
Huazhong University of Science and Technology
Wuhan 430074 P. R. China

e-mail :huzq@hust.edu.cn

© by PSP Volume 25 – No. 10/2016, pages 4141-4147 Fresenius Environmental Bulletin

A RESEARCH ON THE SENSITIVITY OF TROUTS (*Oncorhynchus mykiss*) TO SOME METALS ($HgCl_2$, $ZnSO_4$, $PbCl_2$)

Bülent Verep[1,*], Ertugrul Terzi[1], E. Sibel Besli[2]

[1]Recep Tayyip Erdoğan University, Faculty of Fisheries and Aquatic Sciences, Department of Basic Fisheries Sciences, 53100 Rize, Turkey
[2]Giresun University, Tirebolu Mehmet Bayrak Vocational School, Giresun, Turkey

ABSTRACT

The aim of this study is to investigate the sensitivity of (*Oncorhynchus mykiss*, Walbaum, 1792), a salmonid fish species, to some toxic metal substances (Mercuric chloride; $HgCl_2$, Zinc sulfate; $ZnSO_4$, and Lead chloride; $PbCl_2$) for aquatic ecosystems. The fishes were taken from local trout farms (Rize-Turkey) for bioassay experiments. The 96-h LC_{50} values for Rainbow trout were estimated, and their variations for each metal discussed. Lead chloride and zinc sulfate were less toxic for Rainbow trout as 20.21 mgL^{-1} and 1.69 mgL^{-1} respectively; however the most toxic metal was mercuric chloride (LC_{50}: 0.81 mgL^{-1}).

KEYWORDS:
Metals, acute toxicity, Rainbow trout, Oncorhynchus mykiss, water pollution

INTRODUCTION

Aquatic pollution in freshwater and other sites causes serious toxicological hazards to animals and eco toxicological problems for aquatic ecosystems. To solve the environmental and ecotoxicological problems, the dimensions of pollution sources, as well as ecological properties of aquatic media have been discussed consistently. The determination of toxic compounds in the aquatic environment and their effects on fish are the basic issues in aquatic toxicology [1], preferably evaluated by mortality or bioassay experiments [2].

Mercury exists in three forms: elemental mercury, inorganic mercury compounds (primarily mercuric chloride), and organic mercury compounds (primarily methyl mercury). All forms of mercury are quite toxic, and each form exhibits different health effects for biota [3]. Mercury compounds are very toxic and all forms of mercury are possible human carcinogens [4]. Mercuric chloride; $HgCl_2$ has been used in agriculture as fungicide, in medicine as a topical antiseptic and disinfectant. Mercuric chloride; $HgCl_2$ is commonly used both for industrial, scientifically and agricultural purposes around the world including Turkey.

Zinc is a necessary element to all forms of life. It is a normal part of metabolism in all living organisms. Zinc is widely distributed in plants, animals and soils, and is normally present in food. Zinc salts include three pesticide active ingredients: zinc chloride, zinc oxide, and zinc sulfate monohydrate (or zinc sulfate). Zinc salts are used as herbicides to control the growth of moss on structures, walkways, patios and lawns in rainy areas [5]. Acute symptoms of oral zinc poisoning are primarily gastrointestinal. Symptoms include nausea, vomiting, abdominal pain, diarrhea, and hematemesis. Fever is also reported. With supportive care, zinc toxicity usually is self-limited, and resolution of symptoms occurs in a matter of hours or days [6, 7].

Lead is a natural metal occurring found in small amounts in the earth's crust. Lead compounds can be found in all parts of the environment; for example, in plants and animals (consumed as food), air, drinking water, rivers, lakes, oceans, dust, and soil. Lead, which is widely used in industry, comes from mined ores or from recycled scrap metal. Its main use is in the manufacture of storage batteries. Other uses include the production of chemicals, including paint, gasoline additives, and various metal products. Lead is a potentially toxic chemical that may be directly ingested by man or indirectly through aquatic animals like fish and shellfish [8].

Rainbow trout is a common culture fish for aquaculture in the world. The toxicity of many metal compounds to the rainbow trout, *Oncorhynchus mykiss*, was first studied in detail. Among a variety of available species, it was distinguished with the following properties: amenable to life in the laboratory, a fish of considerable commercial importance and sensitive to most toxic pollutants and reacts more quickly than most species to adverse environmental conditions [9, 10, 11, and 12]. In this research, the comparison of three heavy metal substances toxic effects on Rainbow trout (*Oncorhynchus mykiss*) and its responses to these aquatic pollutants have been discussed respectively.

In this work, the three common pollutant in aquatic environment as heavy metal, Mercuric chloride; $HgCl_2$, Zinc sulfate; $ZnSO_4$, and Lead chloride; $PbCl_2$ were selected for the bioassay experiments. This study was carried out to determine the sensitivity of Rainbow trout (*Oncorhynchus mykiss*) to these heavy metals (Mercuric chloride; $HgCl_2$, Zinc sulfate; $ZnSO_4$, and Lead chloride; $PbCl_2$) using acute bioassay tests. Rainbow trout was selected for bioassays because it can easily be obtained from local trout farms throughout the year, and its growth is excellent under laboratory conditions.

MATERIALS AND METHODS

Rainbow trout (*Oncorhynchus mykiss*) (weights: 18.14 ± 4.53 g, lengths: 12.43 ± 1.06 cm) were obtained from the local trout farms in Rize province, Turkey. Fish were carried with tanks and brought to the laboratory within 20 min in plastic buckets with sufficient air. After acclimatization (12 days), the fish were placed into the maintenance aquarium of 250-L capacity. Temperature was regulated at 12 ± 1 °C. Except for dosing, all aquaria were aerated. Test chambers were filled with 40 L of tap-water. Physicochemical characteristics of aquarium water are listed in Table 1.

Following the preliminary experiments, all determinations were repeated three times. The groups of experimental animals, each consisting of 10 individuals, were selected randomly and placed into the aerated aquaria. After 48 h of adaptation, different concentrations of metal substances were added (Mercuric chloride; $HgCl_2$, Zinc sulfate; $ZnSO_4$, and Lead chloride; $PbCl_2$). Metal substances were obtained from the chemicals market, and prepared by diluting them in deionize water to give stock material. Dosing solutions were then prepared by dilution with water (see Table 2).

TABLE 1
Physicochemical properties of the test water used.

Parameter	Bioassay experiments medium
Temperature (°C)	12±1°C
pH	7.33-8.2
Dissolved oxygen (mg L^{-1})	5.89-8.20
Conductivity (µS cm^{-1})	60.1-65.9
Total hardness (as mg $CaCO_3L^{-1}$)	64-65
TDS (mg L^{-1})	29-32

During the last 24 h of adaptation, and throughout the experiment, animals were not fed. Mortality was controlled at 24, 48, 72, and 96 h after start of tests. Dead individuals were removed immediately. Behavioural changes were recorded in detail at 1-6 hours and every 12 h during tests.

The bioassay system was described in standardized methods [13] and the national regulation [14]. The LC_{50} confidence limits were calculated by a computer program [15, 16].

RESULTS

A static bioassay system were used to measure the acute toxicity values of Rainbow trout (*Oncorhynchus mykiss*). The calculated 96-h acute LC_{50} values (95% confidence limits) with regard to the following metals were 0.808 µg L^{-1} (0.682-0.922) for Mercuric chloride; $HgCl_2$, 1.695 mg L^{-1} (0.974-2.491) for Zinc sulfate; $ZnSO_4$ and 20.21 mg L^{-1} (16.604-23.994) for Lead chloride; $PbCl_2$. Control mortalities were zero in each test. The results show that Mercuric chloride is highly toxic,

TABLE 2
The concentrations of some metals used for bioassay experiments (mg L^{-1}).

Metals	Concentrations					
Mercuric Chloride	0	0.28	0.56	0.84	1.12	1.40
Zinc Sulfate	0	1.07	1.78	2.85	3.57	4.99
Lead Chloride	0	0.15	0.60	2.40	9.60	19.20

TABLE 3
Acute 96-h toxicity of some metals in Rainbow trout (*Oncorhynchus mykiss*).

Concentration (mg L^{-1})	Points*								
	$LC_{1.00}$	$LC_{5.00}$	$LC_{10.00}$	$LC_{15.00}$	$LC_{50.00}$	$LC_{85.00}$	$LC_{90.00}$	$LC_{95.00}$	$LC_{99.00}$
$HgCl_2$	0.49	0.57	0.61	0.65	**0.81**	1.01	1.07	1.15	1.34
$ZnSO_4$	0.02	0.08	0.16	0.25	**1.69**	11.51	18.10	35.41	124.68
$PbCl_2$	0.18	0.26	4.67	5.23	**20.21**	17.14	23.28	38.75	48.43

*Note: Control group (theoretical spontaneous response rate = 0.0000).

TABLE 4
Summary table of lethal concentrations (LC_{50}) on the acute toxicity of Mercuric chloride to different fish species.

Common Name	Scientific Name	Duration d (days) h (hours)	Concentration (mg L^{-1})	References
Chub	*Leuciscus cephalus*	96 h	0.55	Gül et al., 2004 [20]
	Oncorhynchus mykiss	96 h	0.670-0.855	Terzi and Verep, 2012 [24]
	Salmo gairdneri	96 h	0.28	Wobeser, 1975 [25]
Rainbow trout	*(Oncorhynchus mykiss)*	48 h	0.21	Matida et al., 1971 [26]
	Oncorhynchus mykiss	96 h	0.193	Buhl and Hamilton, 1991 [23]
	Oncorhynchus kisutch	96 h	0.282	Buhl and Hamilton, 1991 [23]
Guppy	*Poecilia reticulata*	96 h	0.16	Sarikaya et al., 2003 [21]
	Poecilia reticulata	96 h	0.26	Khangarot and Ray, 1987 [27]
White sucker	*Catostomus commersoni*	96 h	0.687	Duncan and Klaverkamp,1983 [22]
Arctic grayling	*Thymallus arcticus*	96 h	0.218	Buhl and Hamilton, 1991 [23]
Rainbow trout	*Oncorhynchus mykiss*	96h	0.81	This study

TABLE 5
Summary table of lethal concentrations (LC_{50}) on the acute toxicity of Zinc sulfate to different fish species.

Common Name	Scientific Name	Duration d (days) h (hours)	Concentration (mg L^{-1})	References
Guppy	*Poecilia reticulata*	96 h	30.83	Gül et al., 2009 [28]
Guppy	*Poecilia reticulata*	8 d	55	Khangarot et al., 1981 [29]
Guppy	*Lebistes reticulatus*	48 h	75	Khangarot and Ray, 1987 [27]
Flagfish	*Jordanella floridae*	96 h	1.5	Spehar, 1976 [30]
Australian Rainbowfish	*Melanotaenia fluviatilis*	24 h	0.51	Williams and Holdway, 2000 [31]
Ten spotted live-bearer	*Cnesterodon decemmaculatus*	24 h	93.2	Gomez et al., 1998 [32]
Milkfish	*Chanos chanos*	96 h	25	Herrera et al., 1995 [33]
Chinook salmon	*Oncorhynchus tshawytscha*	96 h	39-122	Finlayson and Verrue, 1982 [34]
Mottled sculpin	*Cottus bairdii*	96 h	0.156	Woodling et al., 2002 [35]
Mottled sculpin	*Cottus bairdii*	96 h	0.439	Brinkman and Woodling, 2005 [36]
Bluegill	*Lepomis macrochirus*	96 h	5.46	Pickering and Henderson, 1966 [37]
Rainbow trout	*Oncorhynchus mykiss*	24 h	2.1	Cairns et al., 1978 [38]
Fathead minnow	*Pimephales promelas*	96 h	9	Mount, 1966 [39]
Perch	*Perca fluviatilis*	5 d	16	Ball, 1967 [40]
Channel catfish	*Ictalurus punctatus*	14 d	8.2	Reed et al., 1980 [41]
Rainbow trout	*Oncorhynchus mykiss*	96 h	1.69	This study

whereas Zinc sulfate and Lead chloride are moderately toxic to fish (Table 3).

The control group showed normal behavior during the test period for all metal substances in this study. The changes in behavioral response of Rainbow trout to Mercuric chloride was discussed in a preceding paper [17]. Zinc sulfate; $ZnSO_4$ was also moderately toxic to Rainbow trout (*Oncorhynchus mykiss*), which did not showed very high sensitivities to Zinc sulfate; ZnSO4 and Lead chloride; $PbCl_2$ in mg L^{-1} levels, but a very high one to Mercuric chloride; $HgCl_2$ as 0.81 mg L^{-1}. The 96-h LC_{50} value of Mercuric chloride in Rainbow trout was found to 0.81 mg L^{-1} in the present work. In aquatic toxicology, if LC_{50} (mg L-1) concentration is smaller than 1 mg L^{-1}, the pollutant is highly toxic, and if it is between 1-10 mg L^{-1}, then it is considered to be a moderately toxic [18].

Boening (2000) declared that the toxicity rate of inorganic mercuric substances for aquatic life is less than organic mercury salts and the LC_{50} value of mercuric chloride for different fish species range between 0.16 mg L^{-1} and 0.855 mg L^{-1} [19]. According to some studies (Table 4), the values that acute toxicity of mercuric chloride as an inorganic mercury salts for rainbow trout are between 0.193-0.855 mg L^{-1}. Gül et al. (2004) determined the 96-h fish LC_{50} value of mercuric chloride in chub (L. cephalus) to be 0.55 mg L^{-1}[20]. In some bioassay test results, acute toxicity 96-h LC_{50} value of

mercuric chloride on guppy (*Poecilia reticulata*) were observed between 0.16-0.26 mg L^{-1} (Table 4). Sarıkaya et al. (2003) reported 96-h fish LC_{50} values are like the followings: guppy (*Poecilia reticulata*), 0.16 mg L^{-1} [21]; white sucker (*Catostomus commersoni*), 0.687 mg L^{-1} [22]; arctic grayling (*Thymallus arcticus*), and 0.218 mg L^{-1} [23] for mercuric chloride.

In some bioassay test results, acute toxicity 96-h LC_{50} value of lead chloride on rainbow trout (*Oncorhynchus mykiss*) were observed between 1.04-2.4 mg L^{-1} (Table 5). Tabche et al.(1990) reported 72-h fish LC_{50} values as follows tilapia fish (*Oreochromis hornorum*), 202 mg L^{-1}; and streaked prochilod (*Prochilodus lineatus*) [42], 95 mg L^{-1} [43]; blue gill (*Lepomis macrochirus*), 442 mg L^{-1} [37] for lead chloride. Other results in several different duration for fathead minnow and lead are shown in Table 6.

On the other hand, the LC_{50} value of zinc substances for fish range between 0.156 mg L^{-1} and 122 mg L^{-1}. Acute toxicity of zinc salts to a freshwater fish as guppies, *Poecilia reticulata*, was investigated by Gül et al. (2009), and they reported a 96-h LC_{50} value of 30.83 mg L^{-1} [28]. Khangarot et al. (1981) determined zinc toxicity to *P. reticulata* as LC_{50} = between 55-75 mg L^{-1} [29]. Zinc toxicity to *Oncorhynchus tshawytscha* was found to be as LC_{50} between 39-122 mg L^{-1} [34] , whereas that of Cairns et al.(1978) to fry rainbow trout (*Oncorhynchus mykiss*) was examined to be 24-h LC_{50} = 2.1 mg L^{-1} [38]. This study's results are in good agreement with the reports of other investigators using different fish species (Table 4, 5 and 6).

DISCUSSION AND CONCLUSION

Heavy metals or the alternative term as toxic metals occur naturally in the ecosystem with large variations in concentration. Heavy metals that have an important role in environmental pollution due to anthropogenic sources have been introduced to the ecosystem leisurely [50]. In the monitoring of aquatic environmental pollution, an important issue is metal bioaccumulation in aquatic animal tissue and metal toxicology on fish or other organisms. Bioassay test results have been used for determining of toxicological metal concentrations in aquatic environments [51]. Mercury, lead and zinc substances are the best known metals for toxicological problems and bioaccumulation in aquatic food web [6, 52, and 53].

Sensitivity of organisms to toxic metals varies in terms of species and kinds of toxic metals [54]. According to this work's results, most toxic metal in this study was mercury to rainbow trout (*Oncorhynchus mykiss*). Others (Zinc and Lead) were less toxic metal for rainbow trout. Toxicity levels of metals for rainbow trout in this study are in the following order, mercury>zinc>lead, separately (Table 3). Another species like chub (*Leuciscus cephalus*, LC_{50}:0.55 mg L^{-1}), guppy (*Poecilia reticulate*, LC_{50}:0.16 mg L^{-1}), white sucker (*Catostomus commersoni*, LC_{50}:0.687 mg L^{-1}) and arctic grayling (*Thymallus arcticus*, LC_{50}:0.218 mg L^{-1}) are more sensitive to mercuric chloride than rainbow trout (*Oncorhynchus mykiss,* LC_{50}:0.81 mg L^{-1}) in preceding papers (Table 4). On the other hand, the results of lethal toxicity of zinc to rainbow trout's bioassay experiment don't point out same situation. The main reason is that except for mottled sculpin (*Cottus sp.*), flagfish (*Jordanella floridae*)

TABLE 6
Summary table of lethal concentrations (LC_{50}) on the acute toxicity of Lead chloride to different fish species.

Common Name	Scientific Name	Duration d (days) h (hours)	Concentration (mg L^{-1})	References
Tilapia Fish	*Oreochromis hornorum*	72 h	202	Tabche et al., 1990 [42]
Streaked prochilod	*Prochilodus lineatus*	96 h	95	Martinez, 2004 [43]
Bluegill	*Lepomis macrochirus*	96 h	442	Pickering and Henderson, 1966 [37]
Rainbow trout	*Salmo gairdneri*	96 h	471-542	Davies et al., 1976 [44]
Rainbow trout	*Oncorhynchus mykiss*	96 h	1.04	Rogers et al., 2003 [45]
Rainbow trout	*Salmo gairdneri*	21 d	2.4	Hodson et al., 1978 [46]
Fathead minnow	*Pimephales promelas*	96 h	482	Pickering and Henderson, 1966 [37]
Fathead minnow	*Pimephales promelas*	96 h	0.293	Mager et al., 2011 [47]
Fathead minnow	*Pimephales promelas*	96 h	0.052	Grosell et al., 2006 [48]
Fathead minnow	*Pimephales promelas*	10 d	0.043	Grosell et al., 2006 [48]
Fathead minnow	*Pimephales promelas*	30 d	0.039	Grosell et al., 2006 [48]
Fathead minnow	*Pimephales promelas*	96 h	0.041-3.598	Esbaugh et al., 2011 [49]
Rainbow trout	*Oncorhynchus mykiss*	48h	20.21	This study

and Australian rainbowfish (*Melanotaenia fluviatilis*), the most sensitive fish species for zinc sulfate is rainbow trout according to lethal toxicity values (LC_{50}) (Table 5). In Table 6, it can show that some species like fathead minnow (*Pimephales promelas*), are more sensitive species to lead chloride than rainbow trout in terms of lethal concentration. But tilapia fish (*Oreochromis hornorum*), bluegill (*Lepomis macrochirus*) and streaked prochilod (*Prochilodus lineatus*) are more resistant species.

Although, metals are biologically bio accumulate and upsurge in aquatic organism's tissues in food chain, because of the lack of risk assessments and monitoring environmental pollution during the use of metalloids in the aquatic or other environments, there may be unexpected potential risks on the environments. On the other hand, if it concern acute, chronic, mutagenic and carcinogenic effects of heavy metals, special consideration should be given to acute levels of metals in environmental pollution and the residues in food and bioaccumulation rate in non-target organisms including man in food chain.

ACKNOWLEDGEMENTS

Thanks to the US EPA for the acute toxicity testing probity analysis computer program on the web. The study was supported by Recep Tayyip Erdoğan University, Research Project Fund (Project No: 2009103011).

REFERENCES

[1] Bolis, C.L. Piccolella, M. Dalla Valle, A.Z. And. Rankin, J.C, (2001) "Fish as Model in Pharmacological and Biological Research". *Pharmacological Research*, 44, 265-280.

[2] Svobodova, Z., Luskova, V., Drastichova, J., Svobodova, M., Zlabek, V., (2003) "Effect of Delta-methrin on Hematological Indices of Common Carp (*Cyprinus carpio* L.)", *Acta Vet. Brno,* 72, 79-85.

[3] U.S.E.P.A. (2006) Regulatory Impact Analysis of the Final Clean Air Mercury Rule, United States Environmental Protection Agency, Office of Air Quality Planning and Standards, Research Triangle Park, N.C. 27711.

[4] A.T.S.D.R. (2001) Toxicological Profile for Malathion (Draft for Public Comment), Contract 205-1999-00024, Syracuse, NY: Syracuse Research Corporation (for the Agency for Toxic Substances and Disease Registry).

[5] U.S. E.P.A. (1992) Reregistration Eligibility Documents: Zinc Salts, Office of Prevention, Pesticides and Toxic Substances, United States Environmental Protection Agency.

[6] Newman, M.C., Diamond, G.L., Menzie, C., Moya, J., Nriagu, J., (2004) Issue Paper on Metal Exposure Assessment, US Environmental Protection Agency (USEPA), Risk Assessment Forum, 50 pp.

[7] Bat, L., Gündoğdu, A., Sezgin, M., Çulha, M., Gönlügür, G., Akbulut, M., (1999) "Acute toxicity of zinc, copper and lead to three species of marine organisms from the Sinop Peninsula, Black Sea", Turkish Journal of Biology, 23, 537-544.

[8] Langmuir, D., Chrostowski, P., Vigneault, B., Chaney, R., (2004) Issue Paper on Environmental Chemistry of Metals, US Environmental Protection Agency (USEPA), Risk Assessment Forum, 106 pp.

[9] Bernstein, Y. and Montgomery, W.L., (2008) Rainbow Trout (Oncorhynchus mykiss; Walbaum, 1792): a technical conservation assessment. [Online]. USDA Forest Service, Rocky Mountain Region.

[10] Pandey, S., Kumar, R., Sharma, S., Nagpure, N.S., Srivastava, S.K., Verma, M.S., (2005) "Acute toxicity bioassays of mercuric chloride and malathion on air-breathing fish *Channa punctatus* (Bloch)", *Ecotoxicology and Environmental Safety*, 61, 114-120.

[11] Molony, B., (2001) Environmental requirements and tolerances of Rainbow trout (Oncorhynchus mykiss) and Brown trout (*Salmo trutta*) with special reference to Western Australia: A review, Government of Western Australia, Department of Fisheries, Fisheries Research Division, WA Fisheries Research Laboratories, Fisheries Research Report, No: 13, North Beach, Western Australia.

[12] Abel P.D., (1996) Water Pollution Biology. CRC Press, 2nd Edition, 296 pp, London.

[13] APHA, AWWA, WEF, (1985) Standard Methods for the Examination of Water and Wastewater. *APHA, AWWA, WEF*, 16th ed. APHA, Washington, DC.

[14] T.O.G., (1991) Turkish Official Gazette Methods for Water Analysis in Water Pollution and Control Regulations (In Turkish). No: 20106, 7.1.1991, Ankara.

[15] U.S.E.P.A., (1999) EPA Probity Analysis Program Used for Calculating LC/EC Values, Version 1.5, Ecological Monitoring Research Division, Environmental Monitoring Systems Laboratory, US Environmental Protection Agency, Cincinnati, OHIO, 45628.

[16] Finney D.J., (1971) Probity Analysis, 3rd ed., Cambridge University Press, Cambridge, UK.

[17] Verep, B., Beşli, E.S., Altınok, İ., Mutlu, C., (2007) "Assessment of mercuric chloride toxicity on Rainbow trout (Oncorhynchus

mykiss) and Chubs (*Alburnoides bipunctatus*)", Pakistan Journal of Biological Sciences, 10 (7): 1098-1102.

[18] Louis, A.H., Diana, L.W., Patricia H. and Elizabeth R.S., (1996) Pesticides and Aquatic Animals: A Guide to Reducing Impacts on Aquatic Systems, Virginia Cooperative Extension, Virginia State University, Virginia, 24 p.

[19] Boening D.W., (2000) "Ecological effects, transport, and fate of mercury: a general review", Chemosphere, 40(12):1335-1351. Available: http://www.fs.fed.us/r2/projects/scp/assessments/rainbowtrout.pdf

[20] Gül, A., Yılmaz, M., Selvi, M., (2004) "The study of the toxic effects of mercury-II-chloride to chub *Leuciscus cephalus* (L., 1758)". *G.U. Journal of Science. 17(4): 53-58.*

[21] Sarıkaya, R., Selvi, M., Yılmaz, M., Gül, A. ve Erkoç, F., (2003) "Civa-II-Klorür'ün Poecilia reticulata Üzerindeki Akut Toksik Etkisinin Araştırılması ve Davranış Değişimlerinin İncelenmesi", Türk Sucul Yaşam Dergisi (Turkısh Journal of Aquatic Life), Yıl 1, Sayı 1, 83-89.

[22] Duncan, D.A., Klaverkamp, J.F., (1983) "Tolerance and resistance to cadmium in white suckers (C*atostomus commersoni*) previously exposed to cadmium, mercury, zinc or selenium", *Can. J. Fish. Aquat. Sci.* 40:128-138.

[23] Buhl KJ., Hamilton SJ., (1991) "Relative sensitivity of early life stages of arctic grayling, coho salmon and rainbow trout to nine inorganics". Ecotoxicology and Environmental Safety 22(2): 184-197.

[24] Terzi, E. and Verep, B., (2012) "Effects of water hardness and temperature on the acute toxicity of mercuric chloride on rainbow trout (Oncorhynchus mykiss)". *Toxicology and Industrial Health: An International Journal, 28(6):499-505.*

[25] Wobeser, G., (1975) "Prolonged oral administration of methylmercury chloride to rainbow trout (*Salmo gairdneri*) Fingerlings", *J. Fish. Res. Board. Can.* 32: 2015-2023.

[26] Matida, Y., Kumada, H., Kimura, S., Saiga, Y., Nase, T., Yokota, M., Kawatsu, H., (1971) "Toxicity of mercury compounds to aquatic organisms and accumulation of the compounds by the organisms", *Bull. Fresh. Fish. Lab*. 21: 197-227.

[27] Khangarot, B.S., and Ray, P.K., (1987) "Correlation between heavy metal acute toxicity values in Daphnia and fish". Bulletin of Environmental Contamination and Toxicology 38(4): 722-726.

[28] Gül, A., Yılmaz, M. and Isilak, Z., (2009) "Acute Toxicity of Zinc Sulphate (ZnSO4.H2O) to Guppies (*Poecilia reticulata* P., 1859)", G.U. Journal of Science. 22(2): 59-65.

[29] Khangarot, B.S., Durve, V.S., Rajbanish, V.K., (1981) "Toxicity of interaction zinc-nickel, copper-nickel and zinc-nickel-copper to a freshwater teleost, Lebistes reticulatus (Peters)", Acta Hydrochim Hydrobiol., 9 (5): 495-503.

[30] Spehar, R.L., (1976) "Cadmium and zinc toxicity to flagfish *Jordanella floridae*", Fish-Res-Board Can., 33 (9): 1939-1945.

[31] Williams, N.D., Holdway, D.A., (2000) "The Effects of pulse-exposed cadmium and zinc on embryo hatchability larval development and survival of Australian crimson spotted rainbow fish (Melanotaenia fluviatilis)", Environmental Toxicology, 15 (3): 165-173.

[32] Gomez, S., Villar, C., Benotto, C., (1998) "Zinc toxicity in the fish *Cnesterodon decemmaculatus* in the Parana River and Rio de la Plata Estuary", Environmental Pollution, 99 (2): 159-165.

[33] Herrera, A.A., Amparado, E.A., Santos, M.D., (1995) "Laboratory studies on the effect of heavy metals (Zn and Cu) and on organophosphate (Gustation) on *Chanos chanos*", Third-National-Symposium in-Marine-Science-of-the-Philippine-Association of- Marine-Science, Palms Philippines.

[34] Finlayson, B.J., Verrue, K.M., (1982) "Toxicities of copper, zinc and cadmium mixture to juvenile chinook salmon", Trans. Am Fish Soc., 111: 645- 650.

[35] Woodling, J., Brinkman, S, Albeke, S. (2002) "Acute and chronic toxicity of zinc to the mottled sculpin (*Cottus bairdii*)". Environ Toxicol Chem, 21:1922–1926.

[36] Brinkman S. and Woodling J., (2005) "Zinc Toxicity to the Mottled Sculpin (*Cottus bairdii*) in High-Hardness Water". Environ Toxicol Chem 24:1575–1517.

[37] Pickering, Q, H. and Henderson, C., (1966) "The acute toxicity of some heavy metals to different species of warm water fishes". International Journal of Air and Water Pollution 10:453-463.

[38] Cairns, J., Buikema, A. L., Heath, A. G. and Parker, B. C., (1978) Effects of temperature on aquatic organism sensitivity to selected chemicals. Center for Environmental Studies, Virginia Polytechnic Institute and State University, Bulletin 106.

[39] Mount, D. I., (1966) "The effect of total hardness and pH on acute toxicity of zinc to fish". International Journal of Air and Water Pollution v. 10:49-56.

[40] Ball, I. R., (1967) "The relative susceptibilities of some species of fresh-water fish to poisons-II, Zinc". Water Research v. 1:777-783.

[41] Reed, P., Richey, D. and Roseboom D., (1980) "Acute toxicity of zinc to some fishes in high alkalinity water". Illinois State Water Survey Circular 142,21 p.
[42] Tabche, L.M., Martínez, M. and Sánchez-Hidalgo E., (1990) "Comparative study of toxic lead effect on gill and haemoglobin of tilapia fish". J. Applied Toxicol. 10, 193-195.
[43] Martinez, C. B. R., Nagae, M. Y., Zaia, C. T. B. V. and Zaia, D. A. M., (2004) "Acute Morphological and Physiological Effects of Lead in the Neotropical Fish Prochilodus lineatus". Braz. J. Biol 64(4): 797-807.
[44] Davies, P.H., Goetl, J.P., Sinley, J.R., Smith, N.F., (1976) "Acute and chronic toxicity of lead to rainbow trout Salmo gairdneri, in hard and soft water". Water Res. 10, 199–206.
[45] Rogers J.T., Richards, J.G., and Wood, C.M., (2003) "Ion regulatory disruption as the acute toxic mechanism for lead in the rainbow trout (Oncorhynchus mykiss)". Aquatic Toxicology 64 .215-/234.
[46] Hodson, P.V., Blunt, B.R., Spry, D.J., (1978) "Chronic toxicity of waterborne and dietary lead to rainbow trout (*Salmo gairdneri*) in Lake Ontario water". Water Res. 12, 869/878.
[47] Mager, E. M. Esbaugh, AJ. Brix, KV, Ryan, AC and Grosell, M. (2011) Influences of water chemistry on the acute toxicity of lead to Pimephales promelas and *Ceriodaphnia dubia*. Comparative Biochemistry and Physiology, Part C 153. 82–90.
[48] Grosell, M., Gerdes, R., and Brix KV., (2006) Influence of Ca, humic acid and pH on lead accumulation and toxicity in the fathead minnow during prolonged water-borne lead exposure. Comparative Biochemistry and Physiology, Part C. 143. 473–483.
[49] Esbaugh, AJ. Brix, KV, Mager, EM and Grosell, M., (2011) Multi-linear regression models predict the effects of water chemistry on acute lead toxicity to Ceriodaphnia dubia and Pimephales promelas. Comparative Biochemistry and Physiology, Part C. 154. 137–145.
[50] Valavanidis, A. and Vlachogianni, T., (2010) "Metal Pollution in Ecosystems, Ecotoxicology Studies and Risk Assessment in the Marine Environment", Science advances on environment, toxicology and ecotoxicology issues, www.chem-tox-ecotox.org.
[51] Verep B., (2006) "Acute toxicity of malathion on European chub", Indian Veterinary Journal, 83, 2006.
[52] McGeer, J., Henningsen, G., Lanno, R., Fisher, N., Sappington, K., Drexler, J., (2004) Issue Paper on the Availability and Bioaccumulation of Metals, US Environmental Protection Agency (USEPA), Risk Assessment Forum, 122 pp.
[53] Clearwater, S., (2002) "Metals in the Aquatic Food Web: Bioavailability and Toxicity to Fish, Fact Sheet on Environmental Risk Assessment", International Council on Mining and Metals (ICMM), No: 6, 7 pp.
[54] Khangarot, B.S., (1981) "Lethal effects of zinc and nickel on freshwater teleost", Acta Hydrochim Hydrobiol., 9: 297-302.

Received: **18.11.2015**
Accepted: **12.08.2016**

CORRESPONDING AUTHOR

Bülent Verep
University of Recep Tayyip Erdoğan, Faculty of Fisheries and Aquatic Sciences, Department of Basic Fisheries Sciences 53100 Rize, Turkey

E-mail: bulent.verep@erdogan.edu.tr
verepoglu@hotmail.com

© by PSP Volume 25 – No. 10/2016, pages 4148-4156 Fresenius Environmental Bulletin

PROMOTIONAL EFFECT OF Ce DOPING ON V_2O_5/TiO_2-SnO_2 CATALYSTS FOR SELECTIVE CATALYTIC REDUCTION OF NO by NH_3

Yaping Zhang, Kai Shen*, Wei Xiang, Haitao Xu, Kai Shen, Changcheng Zhou, Linjun Yang

Key Laboratory of Energy Thermal Conversion and Control, Ministry of Education, School of Energy and Environment, Southeast University, Nanjing 210096, P.R. China

ABSTRACT

Series of V_2O_5/TiO_2-SnO_2, CeO_2/TiO_2-SnO_2 and V_2O_5-CeO_2/TiO_2-SnO_2 catalysts were prepared by the impregnation method for selective catalytic reduction of NO by NH_3. Various characterization techniques, like BET, XRD, H_2-TPR, HRTEM and in situ FT-IR were employed to investigate the promotional effect CeO_2 doping and the interaction of cerium and vanadium oxides in the V_2O_5-CeO_2/TiO_2-SnO_2 catalysts. It was found that the quadric-component catalyst with lower ceria content had the better catalytic activity in the wide temperature range (250~450 °C) with above 85% NO conversion than the tertiary oxides counterparts. The combination of characterization techniques revealed the strong interaction of V_2O_5 and CeO_2 existing in such quadric-oxide complex, which could be confirmed from that (1) The introduction of CeO_2 strengthened the synergy between Ti and Sn while V_2O_5 reduced slightly the dispersion of cerium on the Ti-Sn support; (2) V_2O_5 and CeO_2 jointly decreased the H_2 reduction temperature and improve the reducibility while CeO_2 was the main promoter; (3) the asymmetric deformation vibration of ammonia adsorbed on Lewis acid sites(~1585 cm^{-1}) increased considerately in the Ce-contained samples, which favored the low-temperature SCR reaction but hinder the high-temperature activity.

KEYWORDS:
Vanadium; Cerium; Interaction; TiO_2-SnO_2; NO; Selective catalytic reduction

INTRODUCTION

Following extensive researches in the last decades, catalytic reduction of nitric oxide is a feasible technology for commercial applications. Among the various non-catalytic and catalytic processes developed to eradicate NO_x, the selective catalytic reduction of NO_x by NH_3 (NH_3-SCR) in the presence of excess oxygen is by far the most important commercial process today for removing NO_x from flue gas.[1-3] V_2O_5-based catalysts are industrially important catalysts used for the selective reduction of NO_x because of its high SCR activity and excellent resistance of SO_2 poisoning. However, this catalyst system also suffers from disadvantages such as the narrow activity temperature window of 300 – 400 °C and the toxicity of vanadium pentoxide.[4] Dozens of studies investigated the modification of many metal oxides, like CeO_2, Fe_2O_3, MnO_2, ZnO_2, MoO_3, WO_3 and Ga_2O_3, on the V_2O_5/TiO_2 catalysts and found that the composite metal oxides had significant effects on the activity and selectivity of V_2O_5/TiO_2.[5-11] Cerium oxide has attracted extensive concerns due to its high "oxygen storage capacity" and excellent activity in the low-temperature SCR reaction.[12] Xu et al. proved that Ce/TiO_2 still showed high activity in the presence of H_2O and remained 85% NO conversion even in the co-existence of H_2O and SO_2.[13]

It is well-known that TiO_2 (anatase) can be obtained only with a relatively low specific surface area and less thermal and mechanical resistance than other oxides, such as silica.[14] The anatase phase generally has much higher catalytic activity than rutile, but anatase/rutile contacts may increase the activity, as in the case of P25 (Degussa) which is often considered as a benchmark in photocatalysis.[15] For further improving the performance of TiO_2, several chemical and structural modifications of this material have been studied, such as the use of doped TiO_2-ZrO_2 and TiO_2-Al_2O_3 catalysts.[16, 17] Among the studied dopant cations, TiO_2-SnO_2 system (hereafter denoted as Ti-Sn) has been reported with the formation of anatase – rutile mixtures of titania by the incorporation of Sn^{4+} into the TiO_2 lattice.[18, 19]

TiO_2 and SnO_2 could form homogeneous solid solution in a wide range of Sn concentration under suitable condition. In most cases, multiphase Ti-Sn solid solution are found a higher activity than undoped TiO_2 for the photocatalytic oxidation (PCO) of methylcyclohexane and toluene vapours, which is attributable to the incorporation of Sn promoting the anatase to rutile transformation and the decrease of the size of rutile crystallites.[20] Ti-Sn nano-particles could reduce SO_2 and NO by CO to produce S and N_2 simultaneously. The catalyst shows extremely high activity for the reduction of SO_2 alone by CO, 98% the conversion rate of SO_2 whilst for the NO reduction by CO，its catalytic activity is rather low with 50% of NO conversion, indicating the existence of SO_2 promotes the reduction of NO by CO.[21] All these merits possessed by Ti-Sn nano-particles might provide the solution of SO_2 related problems on traditional V_2O_5/TiO_2 or V_2O_5-WO_3/TiO_2 catalysts as there is sufficient SO_2 in the smog, which could enhance the conversion of NO_x.

In this study, series of V_2O_5-CeO_2/Ti-Sn, CeO_2/Ti-Sn and V_2O_5/Ti-Sn catalysts were prepared with different CeO_2 content by the impregnation method. The interaction of V_2O_5 and CeO_2 in the quadric-component V_2O_5-CeO_2/Ti-Sn for the removal of NO_x was investigated by using various characterization techniques of BET, XRD, HRTEM, H_2-TPR and FT-IR, and the SCR characteristics were evaluated in a gas-solid fixed bed.

METHODS

Catalyst preparation. The Ti-Sn (1:1, mole ratio) mixed oxide was prepared by a co-precipitation method from $TiCl_4$ and $SnCl_4$ aqueous solutions. Ammonium hydroxide was dropped slowly to the mixture on the condition of ice-water bath and then the obtained solution was kept in stirring for 30 minutes until pH =9.0-10.0. The mixture kept overnight was filtered and washed by deionized water until no $Cl^{-1}$was detected. The precipitate was dried at 110 °C for 12 h and calcined at 500 °C under continuous airflow (150 mL • min^{-1}) for 4h.

CeO_2/Ti-Sn catalysts and 1 wt% V_2O_5/Ti-Sn were prepared by impregnating Ti-Sn support with an aqueous solution containing the required amount of Ce $(NO_3)_3$ • $6H_2O$ and NH_4VO_3, respectively. Then the mixture was kept stirring at 20 °C first for 2 h, then at 85 °C for 4 h. The precipitate obtained was dried at 110 °C for 12 h and calcined at 500 °C under continuous airflow (150 mL • min^{-1}) for 4h. For short, CeO_2/Ti-Sn catalysts and V_2O_5/Ti-Sn samples were denoted as x CeO_2/Ti-Sn and V/Ti-Sn in the following text, where x repented the molar ratio of Ce to Ti-Sn support.

V_2O_5-CeO_2/Ti-Sn catalysts with 1 wt % of V_2O_5 loading was synthesized by impregnating 2 g of CeO_2/TiO_2-SnO_2 with the NH_4VO_3 solution. The resulting mixture was dried at 110 ° C overnight before calcined in fowing air (150 mL/min) at 500 °C for 4 h. The obtained samples were denoted as x Ce-V/Ti-Zr, where x represented the molar ratio of Ce to Ti-Sn support.

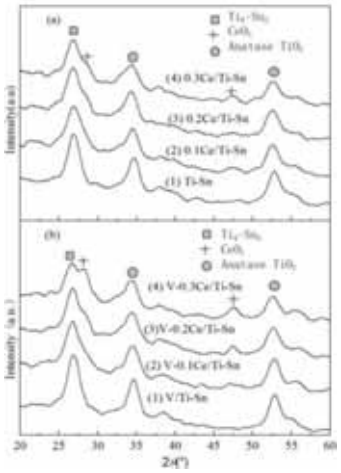

FIGURE 1
X-ray powder diffractions of series of (a)Ce/Ti-Sn and (b) V_2O_5-modified samples

Catalysts characterization. The BET surface area and pore size were measured by nitrogen adsorption at 77 K using an F-Sorb 3400 (Beijing JinAiPu) instrument. X-ray diffraction (XRD) patterns were obtained with Beijing PEPSEE XD-3 diffractometer using nickel-filtered Cu Ka (0.15406nm) radiation source and a scintillation counter detector. H_2-TPR was carried out in a quartz U-tube reactor connected to a thermal conduction detector (TCD) with H_2-Ar (7.3% H_2 by volume) as reductant. TPR started from room temperature to 700 °C at a rate of 10 °C/min. A Nicolet 5700 FT-IR instrument (Thermo Electron Corporation, USA) was employed to record the in situ FT-IR spectra, running in the range of wave numbers 400-4000 cm^{-1}at 4 cm^{-1}resolution. The size and morphology of all the samples were measured with a JEM-2100 (JEOL, Japan) high resolution transmission electron microscope (HRTEM).

Catalytic activity tests. SCR activity measurements of different catalysts were carried out in a gas-solid fixed bed reactor at 80-300 °C containing 0.3 g of catalyst with a gas hourly space velocity (GHSV) of 24,000/h. Typically, the total

gas flow was 100 mL/min, which was pre-mixed in a gas mixer to obtain the simulated gas of 800 ppm of NO, 800 ppm of NH3, 5% of O2 and balanced by N2. The mixed gas was then flown in to the reactor. The NO and NO2 concentrations were continually monitored by flue gas analyzer (Testo 330-2 L).

TABLE 1
BET surface area and pore volume of samples

Samples	S_{BET} (m^2/g)	V_p (cm^3/g)
Ti-Sn	74	0.20
0.1Ce/Ti-Sn	73	0.18
0.2 Ce/Ti-Sn	62	0.16
0.3 Ce/Ti-Sn	50	0.15
V/ Ti-Sn	73	0.17
V-0.1 Ce/Ti-Sn	69	0.17
V-0.2 Ce/Ti-Sn	51	0.15
V-0.3 Ce/Ti-Sn	63	0.17

RESULTS AND DISCUSSION

XRD spectroscopy. Figure 1 presented the powder XRD profiles of series of Ce/Ti-Sn and V_2O_5-modified quadric-component samples. Figure1(a) and Figure1(b) showed the similar changes with the ceria content increasing, i.e.(1) characteristic peaks ascribed to crystalline CeO_2 appeared gradually while they could not be noted when the catalyst contained 10% or 20% CeO_2, indicating that CeO_2 was in an X-ray amorphous form and highly dispersed on the surface of the Ti-Sn support since the CeO_2 content was lower than 20%; (2) characteristic peaks due to crystalline TiO_2 and binary compounds such as Ti_6Sn_5 were weakened, implying that there might be a strong interaction among Ce, Ti and Sn, thus reducing the crystallinity of the support. However, it was worth noting that the addition of V_2O_5 to the Ce/Ti-Sn catalysts showed some different changes in the diffraction patterns, as shown in Figure1 (b). The significant peaks corresponding to CeO_2 became clearer and stronger for the V_2O_5-modified samples, suggesting that vanadium oxide had an influence on the dispersion of cerium oxide on the surface of the support. No independent diffraction lines of crystalline V_2O_5 were noted for all samples, indicating an X-ray amorphous form of V_2O_5.

From the above analysis, it could be concluded that the introduction of CeO_2 strengthened the interaction between Ti and Sn while V_2O_5 had an adverse effect on the cerium oxide dispersion, which might influence the catalytic performance.

BET surface area and pore volume. The BET surface area and pore volume of different samples were presented in Table1. They were 74 m^2/g and 0.2 cm^3/g, respectively, for the Ti-Sn carrier, whereas they dwindled after Ce was loaded and decreased gradually with the loading of cerium oxide increasing. Combined with the XRD results discussed earlier, it could be inferred that the amorphous (low content) and crystalline CeO_2 (high content) were dispersed on the surface of Ti-Sn and occupied the original pores, hence resulting in the decline of specific surface area.

As the vanadium oxide impregnated on the series of Ce/Ti-Sn catalysts, a decrease in the specific surface area and pore volume was noted. It was mainly due to the penetration of the active oxides into the pores of the support and solid state reaction between the dispersed active oxide and the supporting oxides.[22] Hence the pore diameter of the support was narrowed and some of the micropores were blocked. Interestingly, V-0.3Ce/Ti-Sn showed larger surface area and pore volume than V-0.2Ce/Ti-Sn. It might form new micropores caused by the large amount of cerium oxides.

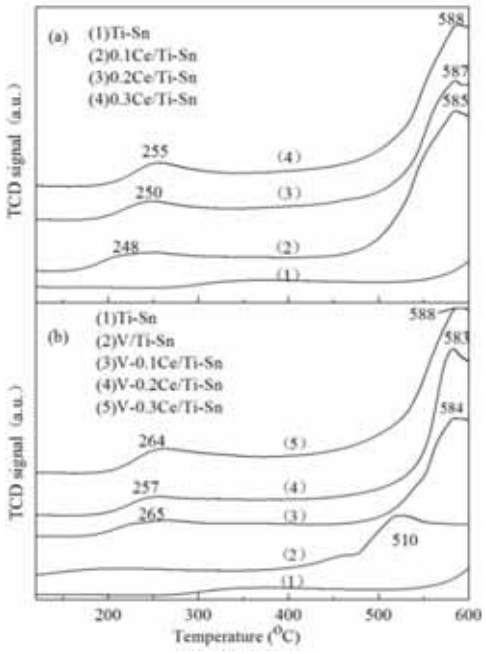

FIGURE 2
TPR profiles of series of (a) Ce/Ti-Sn and (b) V-Ce/Ti-Sn samples

Reducible properties of the catalysts. Figure 2 showed the TPR profiles of series of (a) Ce/Ti-Sn and (b) V-Ce/Ti-Sn samples. The result showed a weak and broad reduction peak for Ti-Sn starting at

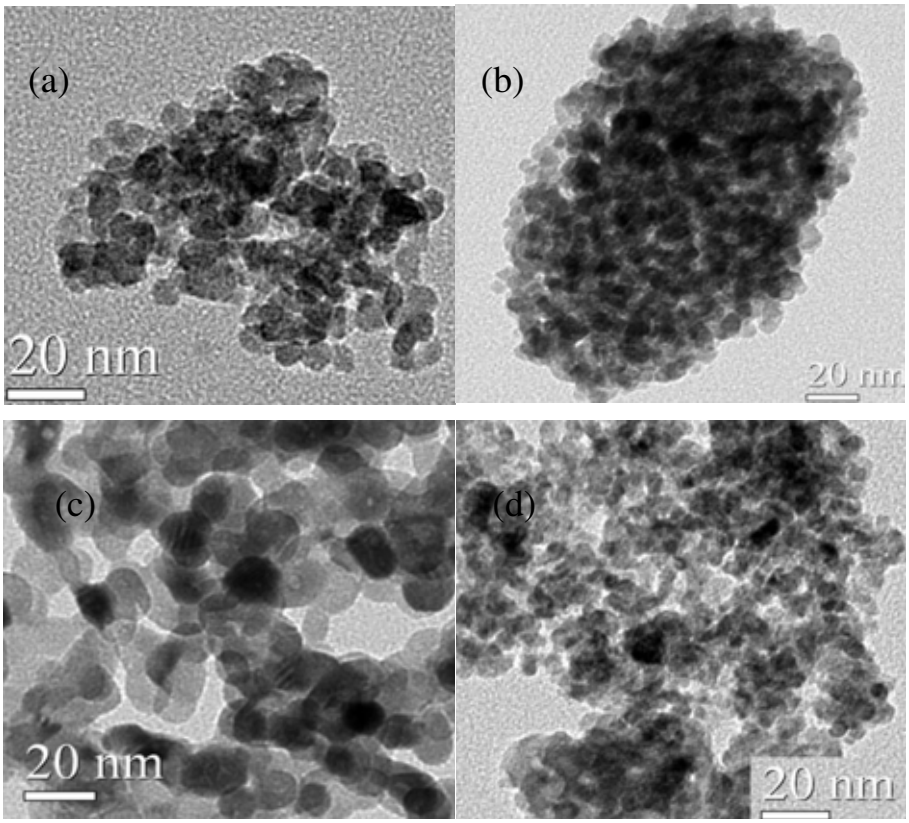

FIGURE 3
HRTEM profiles of (a)0.1Ce/Ti-Sn; (b) 0.3Ce/Ti-Sn; (c) V-0.1Ce/Ti-Sn and (d) V-0.3Ce/Ti-Sn

about 580 ºC could be detected, which was consistent with the previous research. As loading small amount of V_2O_5, the V/Ti-Sn sample showed a sharp peak (~510 ºC), which was quite different TPR profile with that for the Ti-Sn support. Jia and his coworkers had declared that the reduction peak of pure TiO_2 and SnO_2 could not be clearly observed below 700 ºC, indicating both metal oxides are quite stable and hard to be reduced, while the $Sn_{0.8}Ti_{0.2}O_2$ sample exhibited a sharp reduction peak at ~560 ºC, resulting in the increased reducibility of the Ti-Sn mixed oxides.[23] Pure V_2O_5 was reduced by hydrogen in four consecutive/parallel steps, which might be: $V_2O_5 \rightarrow V_6O_{13} \rightarrow VO_2 \rightarrow V_nO_{2n-1} \rightarrow V_2O_3$ ($4 < n < 8$).[24] Hence, it could be concluded that the decreased reduction temperatures of the V/Ti-Sn sample could be caused by the support effect from the Ti-Sn. Generally, the crystal size, combined with crystal orientation dominates the reduction behavior of the oxides. As showed in the literature, the unsupported V_2O_5 had a random orientation of various crystallographic planes exposed to the reduction gas mixture, whereas the supported V_2O_5 displayed a preferred orientation and exhibited better reducibility.[24] Accordingly, the dispersed vanadium over the Ti-Sn support was expected to reduce NO at a lower temperature than the unsupported bulk V_2O_5.

For all the Ce-contained tertiary oxides, i.e. Ce/Ti-Sn, they exhibited similar profiles including a strong peak at ~ 585 ºC and a relatively weak one at ~ 250 ºC. Reduction of bulk CeO_2 was facile and known to reduce at lower temperatures. Bulk ceria also exhibited at least three reduction peaks due to the removal of adsorbed oxygen on the surface as (~416 ºC) well as surface and bulk reduction of $CeO_2 \rightarrow Ce_2O_3$.(~680 ºC and ~940 ºC, respectively).[25] Similar to V/Ti-Sn sample, the reduction temperatures of Ce/Ti-Sn samples had also been shifted to lower temperatures. However, the reduction temperatures of all the peaks were increased with the CeO_2 content rising. This peculiar reduction phenomenon had been reflected in the changes of their catalytic activities, which was being dealt in the later paragraphs.

Series of V-Ce/Ti-Sn samples also displayed similar patters consisting of a broad and well-defined reduction peak (~585 ºC) and another weak and broad peak(~260 ºC). These profiles were almost identical with those of Ce/Ti-Sn samples except that the latter peaks were shifted to a little higher temperatures(~260 ºC), primarily due to the

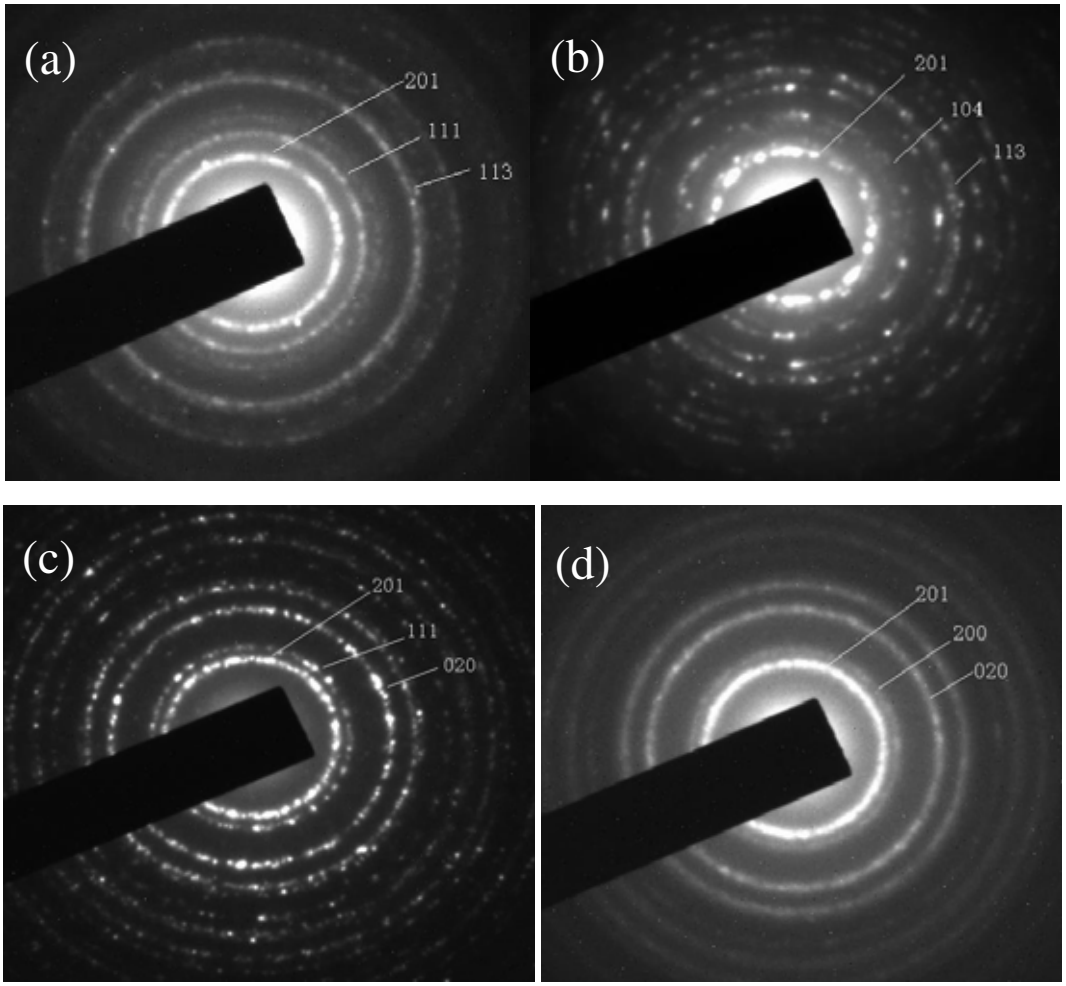

FIGURE 4
Electron diffraction profiles of (a) 0.1Ce/Ti-Sn; (b) 0.3Ce/Ti-Sn; (c) V-0.1Ce/Ti-Sn and (d) V-0.3Ce/Ti-Sn

reduction of the dispersed ceria-vanadia mixed oxide phase over the Ti-Sn support, which was formed owing to solid-state reactions between them.

HRTEM results. Figure 3 showed the HRTEM images of 0.1Ce/Ti-Sn, 0.3Ce/Ti-Sn, V-0.1Ce/Ti-Sn and V-0.3Ce/Ti-Sn to analyze their micro-scale constructions, and Figure 4 presented electron diffraction profiles.

It could be seen from the HRTEM images that the average particle size of the prepared nano-size catalysts was about 9 nm 0.1Ce/Ti-Sn which was in a highly dispersed state with more uniform particles, while particles in the 0.3Ce/Ti-Sn sample agglomerated easily. After loading a spot of vanadium oxide, the two V-Ce/Ti-Sn complexes displayed clearly better dispersion than the tri-oxide counterparts, while the latter showed more agglomeration.

Diffraction rings observed in Figure4 implied the existence of polycrystalline, possibly caused by the tin and titanium oxide. We compared the measured distance between different crystal surfaces (d_{hkl}) and standard ones to find out that the ring 201 stood for Ti_6Sn_5, 111, 113 and 020 represented different crystal planes of TiO_2 species, while the rings of 104 and 200 meant the existence of CeO_2, which were in good agreement with the abovementioned XRD results.

NH_3-adsorbed in situ FT-IR. In situ IR of ammonia adsorption was employed for further study of the interaction between vanadium–cerium and mixed oxide support. FT-IR spectra of various samples at 50 °C were presented in Figure 5. The vibration of N-H deformation of absorbed ammonia molecule, ranging from 1000 to 1700 cm^{-1}, was an important indicator to distinguish the Lewis and Brønsted acid.[26-28] Alejandre et al. had reported that the band at about 1600 cm^{-1} was due to the asymmetric deformation vibration of ammonia adsorbing on Lewis acid site, and the band with two split components at 1222 cm^{-1} and 1155 cm^{-1} was attributed to the symmetric deformation of this type of adsorbed ammonia.[26] Furthermore, many

studies confirmed that the bands at 1450 and 1650 cm^{-1} were attributed to the asymmetric and symmetric deformation of NH_4^+ ($\delta_{as}(NH_4^+)$ and $\delta_s(NH_4^+)$) bound to Brønsted acid sites, respectively.[27, 28]

For the Ti-Sn sample, several weak but broad peaks at 1637, 1450 and 1175 cm^{-1} could be detected, indicating the coexistence of two kinds Brønsted acid sites (marked as B1 and B2, respectively) and one kind of Lewis acid site (marked as L1). Since TiO_2 was purely Lewis acid, the weak Brønsted acid sites observed over the Ti-Sn binary oxides must be related to the tin oxides deposited on TiO_2 supports. While impregnating the vanadium on the Ti-Sn carrier, both the B1 and B2 sites weakened while the L1 sites became stronger, might resulting from the fact that vanadium centers were slightly more Lewis acidic than titanium centers, and coordinated NH_3 was more perturbed on the V_2O_5-based catalysts than on TiO_2.

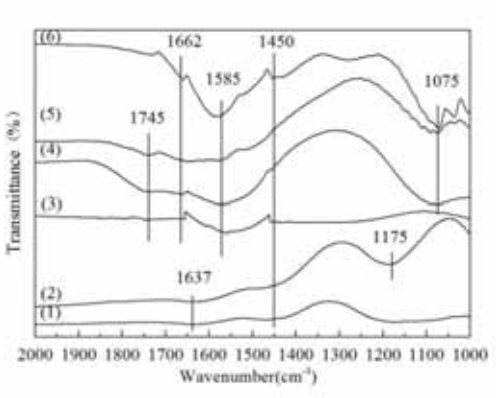

FIGURE 5
FT-IR spectra of various samples at 50 °C of (1) Ti-Sn; (2) V/Ti-Sn; (3) 0.1 Ce/Ti-Sn; (4) V-0.1Ce/Ti-Sn; (5) 0.3Ce/Ti-Sn and (6) V-0.3Ce/Ti-Sn

For the cerium-contained ternary catalyst, two new peaks at 1745 and 1585 cm^{-1} appeared, while the peak at 1175 cm^{-1} disappeared. With reference to the above literatures, the band at 1745 cm^{-1} was ascribed to the weakly adsorbed NH_3 or gas-phase NH_3, while the latter peak was assigned to the asymmetric deformation of NH_3 (δ_{as}-(NH_3)) coordinated to Lewis acid sites, indicating the existence of a new kind of Lewis acid sites, marked as L2. Meanwhile, the peak at 1637 cm^{-1} shifted to 1662 cm^{-1} as well as the band at 1175 cm^{-1} shifted to 1075 cm^{-1}. As the formation mechanism of the new Lewis acid sites was similar as that in V/Ti-Sn, we also marked it as L1. The combination of moderately strong monodentate and bidentate nitrate species, along with a split in the symmetric deformation of NH_3 coordinated to Lewis acid sites, appeared to be important for high activity and selectivity.[29] The peak resulting from the vibrational mode of ammonia adsorbed on Lewis acid sites, which was located at ~1170 cm^{-1}, was believed to be important in facilitating hydrogen abstraction to form amide species that react with bidentate nitrates.

As for the quadric-component sample with lower CeO_2 content, i.e., V-0.1Ce/Ti-Sn, it exhibited quite similar profile of ammonia adsorption FT-IR spectra as that of 0.1Ce/Ti-Sn except that the broad band at 1075 cm^{-1} appeared. Additionally, all the peaks ascribed to Lewis acid sites were obviously broadened while those bands due to Brønsted acid sites (B1 and B2) peaks got slightly weakened, indicating the Lewis acid sites increased considerably and became the dominant acid sites. While for the V-0.3Ce/Ti-Sn sample, it had identical pattern of FT-IR spectra with that of the counterpart with lower cerium loading but all the intensities of peaks weakened and the B2 site was almost invisible, indicating the surface acidity of such sample decreased.

According to the above analysis, it could be concluded that (1) for all the samples studied except the Ti-Sn support, Lewis acid sites are the main acid sites; (2) the minute amount of Brønsted acid sites showed no apparent changes for the Ce-contained samples; (3) the CeO_2-doped samples possessed larger amount of Lewis acid sites.

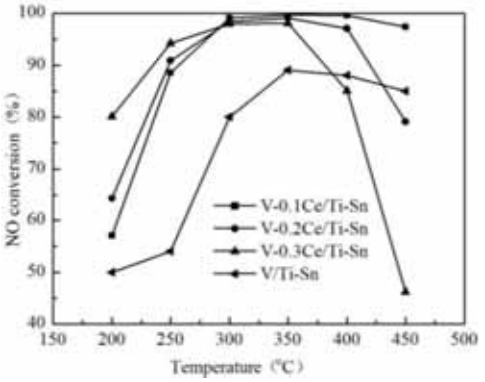

FIGURE 6
NO conversion of V/Ti-Sn and Ce-doped compounds samples

Activity tests. Figure 6 showed the NO conversion comparison of V/Ti-Sn and V-Ce/Ti-Sn samples. In the middle-temperature range of 200~350 °C, all Ce/Ti-Sn samples exhibited much better catalytic performance than the V/Ti-Sn sample, indicating that cerium oxide could drastically promote the catalytic activity, especially at the lower temperature window of 200~350 °C, while such improvement did not exist for the two cerium-modified samples with highest ceria content in the high temperature range(>350 °C). Additionally, at the lower temperature window, the

catalytic activity of three Ce-contained samples increased with the cerium content increased, and then showed almost 100% NO conversion at 300 ºC, while only 80% for V/Ti-Sn. However, as the temperature continued increasing to 450 ºC, their NO conversions declined despite increasing the cerium loading. It was obviously concluded that cerium can promote the lower-temperature (below 350 ºC) activity but hinder that at the high temperature window (above 350 ºC), probably resulting from complete coverage of vanadium oxide by high loading of ceria. Hence, the sample with lowest loading of ceria exhibited the poor low-temperature catalytic performance (below 250 ºC) but best medium and high temperature activity(250~400 ºC).

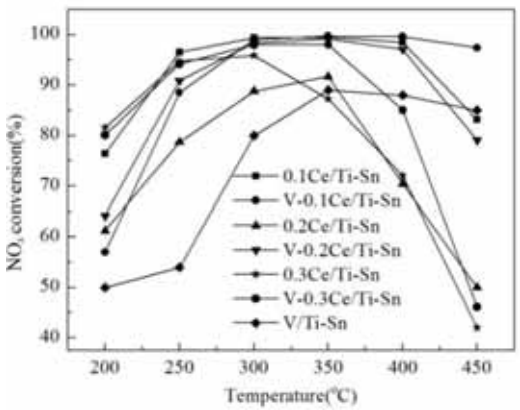

FIGURE 7
NO conversion of series of Ce/Ti-Sn and V-Ce/Ti-Sn

Figure 7 presented the NO conversion comparison between series of V-Ce/Ti-Sn and Ce/Ti-Sn samples with different Ce content. For all the Ce/Ti-Sn samples, the NO conversions displayed the similar trend with those for the V-Ce/Ti-Sn counterparts, as shown in Figure7. Upon loading 1 wt % V_2O_5, the catalytic activities of almost all samples investigated were clearly improved within the whole temperature range, except that of the V-0.1Ce/Ti-Sn sample at the lower temperature window (<300 ºC). Moreover, such improvement was more transparent in the high temperature range, in particular, for the samples with higher ceria loading, indicating the better activity of vanadium oxide.

It can be concluded from the combination of Figure 6 and Figure 7 that cerium manifested better low-temperature catalytic performance while vanadium showed excellent activity at the high temperature window, which were in well consistence with previous researches. Hence, the stable quadric-oxide catalyst with higher activity can be obtained with low loading of the two active metal oxides.

Recall the discussion about NH_3-adsorbed in situ FT-IR, V/Ti-Sn displayed the lowest low-temperature catalytic activity but better high-temperature performance, which might be due to its stable and larger amount of Brønsted acid sites (~1452 cm^{-1}) and Lewis acid sites (~ 1175 cm^{-1}). The V-0.1Ce/Ti-Sn samples generally exhibited outstanding catalytic performance in the wide temperature range, might being attributed to the comparatively stable and considerate amount of Lewis acid sites (~1585 and ~1075 cm^{-1}). Whereas, the V-0.3Ce/Ti-Sn samples together with the 0.3Ce/Ti-Sn, though having better performance at the low-temperature window, presented the worst activity at the high-temperature window. At this temperature, two kinds of Lewis acid sites existed, located at 1585 and 1160 cm^{-1}, respectively. The former band was broad and strong while the latter was sharp and weak. Therefore, we could conclude that the considerable Lewis acid sites in the high wave number region, which were favorable for the low-temperature SCR reaction, might caused the terrible high-temperature activity of such catalyst.

There were still other factors contributing to the excellent performance of the V-0.1Ce/Ti-Sn samples. Larger BET specific surface area and pore volume, low crystalline, strengthened redox properties also are important.

CONCLUSIONS

A quadric-component V_2O_5-CeO_2/TiO_2-SnO_2 was prepared and applied in the SCR reaction. The tertiary-oxide V/Ti-Sn exhibited higher high-temperature catalytic activity (>300 ºC), while the Ce/Ti-Sn catalyst showed the better low-temperature catalytic performance. The quadric-component V-Ce/Ti-Sn catalysts with low Ce content manifested excellent and stable catalytic activity in the wide temperature range (250~450 ºC) due to the interaction of cerium and vanadium oxides. Lewis acid sites (~1585cm^{-1}) increased in Ce-contained samples, favoring low-temperature reaction. The synergy of CeO_2 and V_2O_5 promoted the redox properties of catalysts.

ACKNOWLEDGEMENTS

The authors acknowledge the financial support of the National Natural Science Foundation of China (Grant No. 51306034), Key Research and Development Program of Jiangsu Province （BE2015677）and the National Basic Research Program of China (973 Program, 2013CB228505)are gratefully acknowledged.

REFERENCES

[1] Liu Z. M, Zhang S. X, Li J. H, Zhu J. Z., Ma L. L. (2014) Novel V_2O_5-CeO_2/TiO_2 Catalyst With Low Vanadium Loading For Theselective Catalytic Reduction Of NO_x By NH_3. *Appl. Catal. B: Environ*, *158*, 11-19.

[2] Ning P., Song Z., Li H., Zhang Q., Liu X., Zhang J., Tang X., Huang Z. (2015)Selective Catalytic Reduction Of No With NH_3 Over CeO_2-ZrO_2-WO_3 Catalysts Prepared By Different Methods. *Appl. Surf. Sci*, *332*, 130-137.

[3] Lou X., Liu P., Li J., Li Z., He K. (2014) Effects Of Calcination Temperature On Mn Species And Catalytic Activities Of Mn/Zsm-5 Catalyst For Selective Catalytic Reduction Of No With Ammonia. *Appl. Surf. Sci*, *307*, 382-387.

[4] Chen L., Li J., Ge M. (2010) Drift Study On Cerium-Tungsten/Titiania Catalyst For Selective Catalytic Reduction Of NO_x With NH_3. *Environ. Sci. Technol*, *44*, 9590-9596.

[5] Liu Z. M., Li Y., Zhu T. L., Su H., Zhu J. Z. (2014) Selective Catalytic Reduction Of NO_x By NH_3 Over Mn-Promoted V_2O_5/TiO_2 Catalyst. *Ind. Eng. Chem. Res*, *53*, 12964-12970.

[6] Chen L., Li J., Ge M. (2009) Promotional Effect Of Ce-Doped V_2O_5-WO_3/TiO_2 With Low Vanadium Loadings For Selective Catalytic Reduction Of NO_x By NH_3. *J. Phys. Chem.* C, 113, 21177-21184.

[7] Lu X., Song C., Chang C., Teng Y., Tong Z., Tang X. (2014) Manganese Oxides Supported On TiO_2–Graphene Nanocomposite Catalysts For Selective Catalytic Reduction Of NO_x With NH_3 At Low Temperature. *Ind. Eng. Chem. Res*, *53*, 11601-11610.

[8] Boningari T., Pappas D. K., Ettireddy P. R., Kotrba A., Smirniotis P. G. (2015) Influence Of SiO_2 On M/TiO_2 (M= Cu, Mn And Ce) Formulations For Low-Temperature Scr Of NO_x With NH_3: Surface Properties And Key Components In Relation With Activity Of NO_x Reduction. *Ind. Eng. Chem. Res*, *54*, 2261-2273.

[9] Granger P., Parvulescu V. I. (2011) Catalytic NO_x Abatement Systems For Mobile Sources: From Three-Way To Lean Burn After-Treatment Technologies. *Chem. Rev. 111*, 3155-3207.

[10] Chang H., Jong M. T., Wang C., Qu R., Du Y., Li J., Hao J. (2013) Design Strategies For P-Containing Fuels Adaptable CeO_2-MoO_3 Catalysts For $DeNO_x$: Significance Of Phosphorus Resistance And N_2 Selectivity. *Environ. Sci. Technol. 47*, 11692-11699.

[11] Yu W. C., Wu X. D., Si Z. C., Weng D. (2013) Influences Of Impregnation Procedure On The Scr Activity And Alkali Resistance Of V_2O_5-WO_3/TiO_2 Catalyst. *Appl. Surf. Sci*, *283*, 209-214.

[12] Gao R., Zhang D., Maitarad P., Shi L., Rungrotmongkol T., Li H., Zhang J., Cao W. (2013) Morphology-Dependent Properties Of MnO_x/ZrO_2-CeO_2 Nanostructures For The Selective Catalytic Reduction Of No With NH_3. *J. Phys. Chem. C*, *117*, 10502-10511.

[13] Xu W. Q., Yu Y. B., Zhang C. B., He H. (2008) Selective Catalytic Reduction Of No By NH_3 Over A Ce/TiO_2 Catalyst. *Catal. Commun*, *9*, 1453-1457.

[14] Caraba R., Masters S., Eriksen K. M., Parvulescu V., Fehrmann R. (2001) Selective Catalytic Reduction Of No By NH_3 Over High Surface Area Vanadia-Silica Catalysts. *Appl. Catal. B: Environ*, *34*, 191-200.

[15] Fresno F., Tudela D., Maira A. J., Rivera F., Coronado J. M., Soria J. (2006) Triphenyltin Hydroxide As A Precursor For The Synthesis Of Nanosized Tin - Doped TiO_2 Photocatalysts. *Appl. Oganomet. Chem*, *20*, 220-225.

[16] Zhang Y. P., Zhu X., Shen K., Xu H., Sun K. Q., Zou C. C. (2012) Influence Of Ceria Modification On The Properties Of TiO_2-ZrO_2 Supported V_2O_5 Catalysts For Selective Catalytic Reduction Of No By NH_3. *J. Colloid Interf. Sci*, *376*, 233-238.

[17] Li Y. H., Zhao F., Zou J. Y., Liu H., Zhang Y. (2015) Research On Denox-Scr Over Pd/TiO_2/Al_2O_3 Under Simulated Post Euro-Iv Diesel Exhaust Conditions. *Adv. Mater. Res. 1*:52-55.

[18] Tang Y., Wu D., Chen S., Zhang F., Jia J., Feng X. (2013) Highly Reversible And Ultra-Fast Lithium Storage In Mesoporous Graphene-Based TiO_2/SnO_2 Hybrid Nanosheets. *Energ. Environ. Sci*, *6*, 2447-2451.

[19] Hirano M., Kono T. (2011) Hydrothermal Synthesis Of Rutile - Type Complete Solid Solution Nanoparticles In The TiO_2-SnO_2 System Under Acidic Conditions. *J. Am. Ceram. Soc*, *94*, 3319-3326.

[20] Fresno F., Hernandez-Alonso M. D., Tudela D., Coronado J. M., Soria J. (2008) Photocatalytic Degradation Of Toluene Over Doped And Coupled (Ti,M)O(2) (M = Sn Or Zr) Nanocrystalline Oxides: Influence Of The Heteroatom Distribution On Deactivation. *Appl. Catal. B: Environ*, *84*, 598-606.

[21] Liu Z. Q., Ma J., Yang X. Y. (2004) SnO_2-TiO_2 Solid Solution Catalyst For Simultaneous Reduction Of SO_2 And No By Co Iii. Catalyst Active Sites And Reaction Mechanism. *Chinese. J. Catal*, *25*, 624-632.

[22] Reddy B. M., Lakshmanan P., Khan A. (2004) Investigation Of Surface Structures Of Dispersed V_2O_5 On CeO_2-SiO_2, CeO_2-TiO_2, And CeO_2-ZrO_2 Mixed Oxides By Xrd, Raman, And Xps Techniques. *J. Phys. Chem. B*, *108*, 16855-16863.

[23] Jia Y. R., Jiang X. Y., Zheng X.M. (2006) $CuO/Sn_{0.8}Ti_{0.2}O_2$ Catalyst: Characterization And Catalytic Performance In No Plus Co Reaction. *Chinese J. Inorg. Chem*, *22*, 525-532.

[24] Koranne M. M., Goodwin J. G., Marcelin G. (1994) Partial Oxidation Of Methane Over Silica-And Alumina-Supported Vanadia Catalysts. *J. Catal*, *148*, 388-391.

[25] Shyu J. Z., Otto K. (1989) Characterization Of Pt/Gamma-Alumina Catalyst Containing Ceria. *J. Catal*, *115*, 16-23.

[26] Gutierrez-Alejandre A., Ramirez J., Busca G. (1998) A Vibrational And Spectroscopic Study Of WO_3/TiO_2-Al_2O_3 Catalyst Precursors. *Langmuir*, *14*, 630-639.

[27] Naito N., Katada N., Niwa M. (1999) Tungsten Oxide Monolayer Loaded On Zirconia: Determination Of Acidity Generated On The Monolayer. *J. Phys. Chem. B*, *103*, 7206-7213.

[28] Larrubia M. A., Ramis G., Busca G. (2000) An Ft-Ir Study Of The Adsorption Of Urea And Ammonia Over V_2O_5-MoO_3-TiO_2 Scr Catalysts. *Appl. Catal. B: Environ*, *27*, 145-151.

[29] Pena D. A., Uphade B. S., Reddy E. P., Smirniotis P. G. (2004) Identification Of Surface Species On Titania-Supported Manganese, Chromium, And Copper Oxide Low-Temperature Scr Catalysts. *J. Phys. Chem. B*, *108*, 9927-9936.

Received: **18.11.2015**
Accepted: **24.03.2016**

CORRESPONDING AUTHOR

Kai Shen
Ministry of Education of Key Laboratory of Energy Thermal Conversion and Control, School of Energy and Environment, Southeast University,Nanjing 210096, P.R. China.

e-mail: amflora@seu.edu.cn

© by PSP Volume 25 – No. 10/2016, pages 4157-4162 Fresenius Environmental Bulletin

ASSESSMENT OF SOME HEAVY METALS IN CANNED FISHES FOR HUMAN HEALTH

Metin Caglar, Ozgur Canpolat*

Firat University, Fisheries Faculty, 23119 Elazig, Turkey

ABSTRACT

Information on the metal content in canned fish is important to ensure that the fish consumed is safe for human consumption. In this study, the concentrations of some heavy metals in were determined in seven different brands (A, B, C, D, E, F and G) of canned tuna fish samples available in local food markets of Elazig (Turkey). Only copper (Cu), iron (Fe), zinc (Zn) and cadmium (Cd) were detected in canned tuna fish samples analysed. Nickel (Ni), and chromium (Cr) were found to be undetectable levels in the all samples. The heavy metals were found to be in the range of 13.08–22.35 mg/kg for iron, 9.05–16.76 mg/kg for zinc, 0.23–0.38 mg/kg for copper and 0.046–0.058 mg/kg for cadmium. These results show that heavy metal levels in canned tuna fish samples were under the dangerous limits given by WHO and FAO and their is no any risk for public health by consuming.

KEYWORDS:
Canned fish, heavy metals, food safety.

INTRODUCTION

Fish is widely consumed in many parts of the world because it has high protein content, low saturated fat and also contains omega fatty acids known to support good health (Ikem and Egiebor, 2005; Mahalakshmi, 2012). Fish are constantly exposed to chemicals in polluted and contaminated waters. So the heavy metals content in fishery products need to be well established. Since fish is the last link in the aquatic food chain, the heavy metal concentrations in many fish species have been determined in relation to the metal content of the aquatic environment (Mahalakshmi, 2012).

In this study aims to take stock of some heavy metals (copper, iron, zinc, cadmium, nickel and chromium) in the edible portion of seven different brands of canned tuna fish from markets in Turkey.

MATERIALS AND METHOD

Canned tuna samples were purchased from popular supermarkets in Elazığ, Turkey, during March–May 2010. Seven different Turkish brands (ten individuals from each brands) tuna cans were used in this study. A total of 70 samples were collected.

All reagents were of analytical grade unless otherwise stated. Distilled water was used for the preparation of solutions. All the plastic and glassware were cleaned by soaking, with contact, overnight 0.1 N nitric acid solution and then rinsed with distilled water prior to use. HNO_3 used for digestion are supplied by Merck. The concentrations of copper, iron, zinc, cadmium, nickel and chromium were determined by ICP (Perkin Elmer Optima 5300 DV).

After opening, each cans oil was drained off and the meat was homogenized thoroughly in a food blender with stainless steel cutters. Each sample was then taken and digested promptly as follows: For the determination of selected heavy metals, about 10±0.001 g of homogenized sample were weighed into a 200 ml beaker and 10 ml of concentrated HNO_3 were added. The beaker was covered with a watch glass, and after most of the sample was dissolved by standing overnight, it was then heated on a hot plate with boiling until any vigorous reaction had subsided. The solution was allowed to cool, transferred into a 50 ml volumetric flask and diluted to the mark with distilled water. For each run, a triplicate sample, spiked samples for recovery and two blanks were carried through the whole procedure. Diluted samples and blank solutions were analyzed by ICP (Perkin Elmer Optima 5300 DV) for determination of Cu, Fe, Zn, Cd, Ni and Cr levels (APHA, 1985).

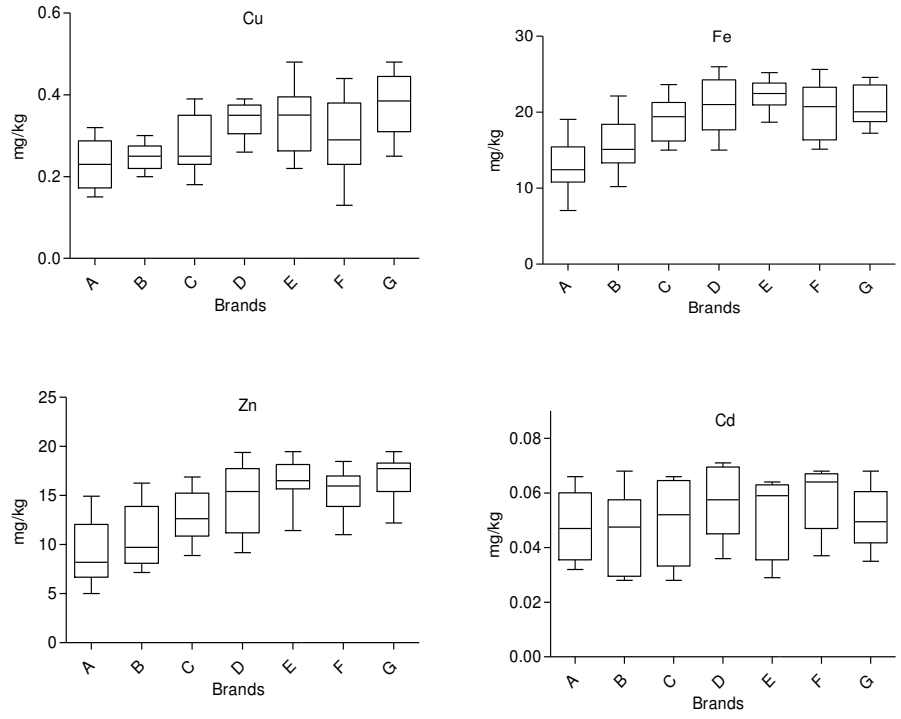

FIGURE 1
Box-Whisker diagram dissemination of some heavy metals concentration in canned tuna fish.

TABLE 1
The concentrations of heavy metals in seven different brands of canned tuna fish.

		A	B	C	D	E	F	G
Fe	Min	7.07	10.21	15.0	15.02	18.88	15.15	17.23
	25%	10.82	13.34	16.20	17.70	20.95	16.36	18.76
	Median	12.44	15.12	19.41	21.00	22.46	20.73	20.08
	75%	15.44	18.43	21.28	24.26	23.84	23.30	23.58
	Max.	19.06	22.13	23.64	25.99	25.22	25.65	24.59
	Mean	13.08	15.80	19.04	20.97	22.35	20.24	20.76
	Std. Dev.	2.87	3.49	2.92	3.78	1.93	3.79	2.60
	Std. Error	0.60	0.97	0.92	1.26	0.52	1.34	0.92
Cu	Min	0.15	0.20	0.18	0.28	0.22	0.13	0.25
	25%	0.17	0.22	0.23	0.31	0.26	0.23	0.31
	Median	0.23	0.25	0.25	0.35	0.35	0.29	0.39
	75%	0.29	0.28	0.35	0.38	0.40	0.38	0.45
	Max.	0.32	0.30	0.39	0.35	0.48	0.44	0.48
	Mean	0.23	0.25	0.28	0.34	0.34	0.29	0.38
	Std. Dev.	0.062	0.032	0.070	0.046	0.082	0.092	0.078
	Std. Error	0.022	0.011	0.021	0.015	0.026	0.028	0.025
Zn	Min	5.00	7.15	8.89	9.18	11.43	11.0	12.20
	25%	6.67	8.09	10.87	11.20	15.68	13.90	15.42
	Median	8.21	9.71	12.63	15.41	16.50	15.96	17.74
	75%	12.08	13.89	15.23	17.74	18.16	16.98	18.31
	Max.	14.92	16.26	16.88	19.38	19.46	18.47	19.46
	Mean	9.05	10.90	12.86	14.60	16.38	15.41	16.76
	Std. Dev.	2.97	2.25	2.56	3.27	2.24	2.17	2.18
	Std. Error	0.74	0.81	0.60	0.75	0.65	0.60	0.61
Cd	Min	0.032	0.028	0.028	0.036	0.029	0.037	0.035
	25%	0.035	0.029	0.033	0.045	0.036	0.047	0.041
	Median	0.047	0.047	0.052	0.058	0.059	0.064	0.49
	75%	0.060	0.058	0.065	0.069	0.063	0.067	0.061
	Max.	0.066	0.068	0.066	0.071	0.064	0.068	0.068
	Mean	0.047	0.046	0.050	0.056	0.051	0.058	0.051
	Std. Dev.	0.013	0.015	0.016	0.013	0.015	0.013	0.011
	Std. Error	0.005	0.006	0.007	0.005	0.007	0.006	0.005

Graphpad Prisim 5.0 package programs were used to graph of the data obtained during the research. The experiments were triplicated (n=3). Data were subjected to one-way analysis of variance (ANOVA). A significant difference was used at 0.05 probability level. All statistical analyses of data were performed using SPSS 11.5 software.

RESULTS

Only Cu, Fe, Zn and Cd were detected in canned tuna fish samples analysed (Fig. 1 and Table 1). Co, Ni, Hg and As were found to be undetectable levels in the all samples.

DISCUSSION

Some metals, such as cadmium and lead in any concentration, can damage the kidneys and may cause symptoms of chronic toxicity, including impaired kidney function, poor reproductive capacity, hypertension, tumors and hepatic dysfunction (Abou-Arab *et al*., 1996; Tarley *et al*., 2001). On the other hand, chromium, copper, iron, zinc and manganese are essential for human health. However, for these metals called micronutrients, there are "xed allowed levels for an adequate dietary intake (Tarley *et al*., 2001).

Iron is a mineral essential for life and for our diets. However, it is also known that when their intake is excessively elevated the essential metals can produce toxic effects (Ashraf *et al*., 2006; Mol, 2010). Therefore, Republic of Turkey Ministry of Agriculture (2002) proposed 15 mg/kg Fe as limit for canned foods. In this study, the mean Fe concentration was under the 15mg/kg in only sample brand A, it was found over 15mg/kg in all other brands. Ikem and Egeibor (2005) reported the mean content of Fe in canned tuna, from Georgia and Alabama, as 15.8 mg/kg, but they mentioned that some samples may contain this metal up to 88.4 mg/kg, as well. Mol (2010) reported the mean content of Fe in canned tuna fish from Turkey as 34.4 mg/kg for the samples of brand A, 38.7 mg/kg for brand B, 26.70 mg/kg for brand C, 20.20 mg/kg for brand D. Therefore, it is obvious that Fe levels of some canned tuna samples are above the limits.

Zinc is an essential trace element for both animals and humans, but the excess may be harmful and the maximum zinc level permitted for fish is 50 mg/kg (Turkish Food Codex, 2002). The recommended daily allowance is 10 mg/day in growing children and 15 mg/day for adults. A deficiency of zinc is marked by retarded growth, loss of taste and hypogonadium, leading to decreased fertility (Celik and Oehlenschlager, 2007). In this study, the mean concentration of Zn were estimated between 9.05-16.76 mg/kg for samples of brands and none of the samples exceeded the recommended limit. In Kingdom of Saudi Arabia, and in US, the mean concentrations of Zn in canned tuna were found to be 10.4 mg/kg, and 4.78 mg/kg, respectively (Ashraf *et al*., 2006; Ikem and Egeibor, 2005). Likewise, Tuzen and Soylak (2007) reported the mean Zn value as 17.8 mg/kg for canned tuna, commercialized in Turkey. However, Celik and Oehlenschlager (2007) analyzed three samples of canned tuna from two different Turkish brands and reported higher amount of Zn than the limits. Mol (2010) reported the mean content of Zn in canned tuna fish from Turkey as 10.5 mg/kg for the samples of brand A, 8.20 mg/kg for brand B, 9.50 mg/kg for brand C, 12.40 mg/kg for brand D. It might be concluded that the amounts of trace metals in canned fish must be controlled comprehensively and periodically with respect to the consumer health.

It is known that seafoods are good source of dietary copper, which is an essential element available to humans. However, Cu is very toxic when consumed excessively, and the presence of Cu in seafoods was limited by the Turkish Food Codex (Anonymous, 1997) 20.0 mg/kg, and by the FAO (1983) for fish and fishery products to 30.0 mg/kg. In this study, the mean concentration of Cu were estimated between 0.23-0.38 mg/kg for samples of brands. It is clear that all samples contained lower amount of Cu than these limits. Mean Cu contents in canned tuna from Kingdom of Saudi Arabia, US, and Turkey were reported as 1.02 mg/kg (Ashraf *et al*., 2006), 0.25 mg/kg (Ikem and Egeibor, 2005), 2.50 mg/kg (Tuzen and Soylak, 2007), and 0.55 mg/kg (Mol, 2010) respectively. All these studies showed that there is no risk with respect to the concentrations of Cu in canned tuna fish.

The recommended daily intakes of zinc and copper are 15 mg Zn for adult males and 12 mg Zn for adult females and 1.5–3.0 mg Cu (Anonymous, 2002). The maximum heavy metal levels permitted in Turkey are 0.1 mg/kg (100 µg/kg) for cadmium, 20.0 mg/kg for copper, 50.0 mg/kg for zinc according to Turkish Food Codex (Anonymous, 1997) the regulations of the European Union permit a limit for cadmium of 0.1 mg/kg wet weight for bonito, common two-banded seabream, eel. European anchovy, grey mullet, horse mackered or scad, sardine, sardinops, tuna and wedge sole; and 0.05 mg) kg wet weight for all others (Atta *et al*., 1997).

The comparison of the present values for canned fish with international data was given in Table 2. Levels of Zn and Cd showed a wide variation world over, ranging from 2.10 to 19.9 µg-g^{-1} and from 0.006 to 1.03 µg-g^{-1}. Our results also lie within the limits laid down by United States

TABLE 2
Comparison of present mean values (mg/kg) in seven different brands canned fish with values of others.

	Present work values		References
	Brands	mg/kg	
Fe	A	13.08	6.0 in USA (Dudek et al.1989)
	B	15.80	2.95 in Pakistan (Tariq and Jaffar, 1993)
	C	19.04	2.94-6.80 in Kingdom of Saudi Arabia (Dudek et al. 1989)
	D	20.97	20.96-88.83 in Brazil (Tarley et al. 2001)
	E	22.35	4.83-29.2 in USA (Ikem and Egeibor, 2005)
	F	20.24	8.04-48.18 in Nigeria (Chukwujindu et al. 2009)
	G	20.76	31.07 in Korea (Islam et al. 2010)
			3.000 in WHO limit
Zn	A	9.05	11.0 in USA (Dudek et al.1989)
	B	10.90	2.10 in Pakistan (Tariq and Jaffar, 1993)
	C	12.86	19.9 in Nigeria (Onianwa et al., 2001)
	D	14.60	16.6-36.09 in Brazil (Tarley et al. 2001)
	E	16.38	11.45 in USA (Ikem and Egeibor, 2005)
	F	15.41	10.38-16.15 in Kingdom of Saudi Arabia (Ashraf et al. 2006)
	G	16.76	0.09-4.63 in Nigeria (Chukwujindu et al. 2009)
			38.35 in Korea (Islam et al. 2010)
			0.0526-1.5472 (Dallatu et al., 2013)
			2.000 in WHO limit
Cu	A	0.23	1.10 in Pakistan (Tariq and Jaffar, 1993)
	B	0.25	2.25 in Nigeria (Onianwa et al. 2001)
	C	0.28	0.50-1.75 in USA (Ikem and Egeibor, 2005)
	D	0.34	1.02-2.26 in Kingdom of Saudi Arabia (Ashraf et al. 2006)
	E	0.34	3.13-0.63 in Korea (Islam et al. 2010)
	F	0.29	0.0558-0.2329 (Dallatu et al., 2013)
	G	0.38	0.0030 in WHO limit
Cd	A	0.047	0.01-0.02 (Mol, 2010)
	B	0.046	0.0091-0.0297 (Dallatu et al., 2013)
	C	0.050	
	D	0.056	
	E	0.051	
	F	0.058	
	G	0.051	

Environmental Protection Agency in fish, i.e. for Cu (120 $\mu g\text{-}g^{-1}$) and Zn (480 $\mu g\text{-}g^{-1}$), (Ashraf *et al*., 2006).

The concentration of these metals in canned fish varies, depending on the type and origin of food, pH of the canned product, oxygen concentration in the headspace, quality of the inside lacquer coating of cans, storage place, etc (Tarley *et al*., 2001).

According to both, Turkish Food Codex and European Union regulations, seven different brands of canned tuna fish samples investigated in this study had heavy metals concentrations were below the permitted levels.

Globally, further reduction in the levels of environmental contaminants emanating from power plants and other industrial emissions and effluent discharges are highly needed to reduce contaminant inputs into the aquatic environments. More research and assesments of seafood quality is needed in many countries to provide more data and help safeguard the health of humans (Ikem and Egeibor, 2005).

REFERENCES

[1] Abou-Arab, A.A.K., Ayesh, A.M., Amra, H.A., Naguib, K., 1996. Characteristic levels of some pesticides and heavy metals in imported fish. *Food Chemistry*, 57: 487-492. doi:10.1016/S0308-8146(96)00040-4,

[2] Anonymous, 1997. Regulation of setting maximum levels for certain contaminants in foodstuffs. Official Gazette, Iss: 23172.

[3] Anonymous, 2002. Regulation of setting maximum levels for certain contaminants in foodstuffs. Official Gazette, Iss: 24908.
[4] APHA, 1985. Standart Methods for Examination of Water and Wastewater. 16th ed. American Public Health Assosiciation, Washington.
[5] Ashraf, W., Seddigi, Z., Abdulkibash, A., Khald, M., 2006. Levels of selected metals in canned fish consumed in Kingdom of Saudi Arabia. *Environmental Monitoring and Assessment*, 117:271-279. doi: 10.1007/s10661-006-0989-5
[6] Atta, M.B., El Sebaie, L.A., Noaman, M.A. and Kassab, H.E. 1997. The effect of cooking on the content of heavy metals in fish (*Tilapia nilotica*). *Food Chemistry*, 58(1-2):1-4.
[7] Celik, U., Oehlenschlager, J., 2007. High contents of cadmium, lead, zinc and copper in popular fishery products sold in Turkish supermarkets. *Food Control*, 18:258-261.doi: 10.1016/j.foodcont.2005.10.004
[8] Chukwujindu, M.A.I., Nwajei, G.E., Arimoro, F.O., Eguavoen, O., 2009. Characteristic levels of heavy metals in canned sardines consumed in Nigeria. *Environmentalist*, 29:431-435.doi:10.1007/s10669-009-9233-5
[9] Dallatu, Y.A., Abechi, S.E., Abba, H., Mohammed, U.S. and Ona, E.C., 2013. Level of heavy metals in fresh and canned foods consumed in North Central Nigeria. *Scholarly Journal of Agricultural Science*, 3(6), 210-213.
[10] Dudek, J.A., Elkins, E.R., Burman, S.C., Egelhofer, D., Hagen, R.E., 1989. Effects of cooking and canning on the mineral content of selected sea food. *Journal of Food Composition Analysis*, 2:273-285.doi:10.1016/0889-1575(89)90024-0
[11] EU 2005. Commission regulation as regards heavy metals. Amending Regulation 466/2001, N:78/2005.
[12] FAO (Food and Aqriculture Organization), 1983. Compilation of legal limits for hazardous substances in fish and fishery products. FAO Fish Circular No:464:5-100.
[13] Galitsopoulou, A., Georgantelis, D., Kontominas, M.G., 2009. Cadmium content in fresh and canned squid (*Loligo* opalescens) from the Pacific coastal waters of California (USA). *Food Additives and Contaminants Part B*, 2(1):38-43. doi: 10.1080/0265203 0902824956
[14] Ikem, A., Egiebor, N.O., 2005. Assessment of trace elements in canned fishes (mackerel, tuna, salmon, sardines and herrings) marketed in Georgia and Alabama (United States of America). *Journal of Food Composition and Analyses*, 18:771-787.doi: 10.1016/j.jfca.2004.11.002
[15] Islam, M.M., Bang, S., Kyoung-Woong, K., Ahmed, M.K., Jannat, M., 2010. Heavy metals in frozen and canned marine fish of Korea. *Journal of Scientific Research*, 2(3):549-557.
[16] Khansari, F.E., Ghazi-Khansari, M., Abdolabi, M., 2005. Heavy metal content of canned tuna fish. *Food Chemistry*, 93:293-296. doi.org/10.1016/j.foodchem.2004.09.025
[17] Larsen, E.H., Anderson, N.L., Moller, A., Petersen, A., Mortenson, G.K., Peteren, J., 2002. Monitoring the contents and intake of trace elements from food in Denmark. *Food Additives and Contaminants*, 19(1):33-46. doi:10.1080/02652030110087447
[18] Mahalakshmi, M., Balakrishnan, S., Indira, K., Srinivasan, M., 2012. Characteristic levels of heavy metals in canned tuna fish. *Journal of Toxicology and Environmental Health Science*, 4(2):43-45. doi:10.5897/JTEHS11.079.
[19] Mol, S., Ozden, O., Oymak, S.A., 2010. Trace metal contents in fish species from Atatürk Dam Lake (Euphrates, Turkey). *Turkısh Journal of Fisheries and Aquatic Sciences*, 10:209-213. doi: 10.4194/trjfas.2010.0208
[20] Onianwa, P.O., Adeyemo, A.O., Idowu, O.E., 2001. Copper and zinc contents of Nigerian foods and estimates the adult dietary intakes. *Food Chemistry*, 72:89-95.
[21] Tariq, J., Jaffar, M., 1993. Selected trace metals in fish, sediments and water from freshwater Tarbella reservoir, Pakistan. *Toxicological Environmental Chemistry*, 39:201-205.
[22] Tarley, C.R.T., Coltro, W.K.T., Matsushita, M., de Souza, N.E., 2001. Characteristic levels of some heavy metals from Brasilian canned sardines (*Sardinela brasiliensis*). *Journal of Food Composition and Analyses*, 14:611-617.
[23] Turkish Food Codex 2002. Su Ürünleri Yönetmeliği. Official Gazette, No: 24936, Ankara, Turkey.
[24] Tuzen, M., Soylak, M., 2007. Determination of trace metals in canned fish marketed in Turkey. *Food Chemistry*, 101:1378-1382. doi: 10.1080/02772249309357918
[25] WHO (World Health Organization) 1996. Health criteria other supporting informaion: guidelines for drinking water quality. 2nd edn. WHO, Geneva, 31-388.
[26] Zahari bin, A.H., Mamat, M., Embong, S., 1987. Cadmium, mercury and lead contents of canned seafoods in Malaysia. *Journal of Micronutrient Analysis*, 3(2):129-135.

Received: **24.11.2015**
Accepted: **24.03.2016**

CORRESPONDING AUTHOR

Ozgur Canpolat
Firat University, Fisheries Faculty, 23119 Elazig, Turkey

Email: ocanpolat@firat.edu.tr

© by PSP Volume 25 – No. 10/2016, pages 4163-4170 Fresenius Environmental Bulletin

ISOLATION, CHARACTERIZATION AND PATHOGENICITY OF BACTERIA FROM *OLIGONYCHUS UNUNGUIS* (JACOBI) (ACARI: TETRANYCHIDAE)

Nurcan Albayrak Iskender[1*], Yasar Aksu[2]

[1] Faculty of Health Sciences, Artvin Coruh University, 08000, Artvin, Turkey
[2]Artvin Regional Forestry Management, 08000, Artvin, Turkey

ABSTRACT

This study was conducted to isolate and characterize pathogenic bacteria for possible use in the biocontrol of Spruce Spider Mite *Oligonychus ununguis* and to determine their pathogenicity. *O. ununguis* were collected from Savsat Forests, in Artvin and transported to the laboratory to be used in the experiments. According to the results of our study; eight bacteria species belonging to seven genera of *O. ununguis* were isolated. Some morphological,biochemical and other phenotypic properties of bacterial isolates were determined by routine and conventional methods (API 20E, API 50 CH and API Staph kits). In addition, 16S rRNA gene region also was sequenced. Based on studies, bacterial isolates were identified as *Methylobacterium* sp. (Ou1), *Bacillus thuringiensis* (Ou2), *Staphylococcus chromogenes* (Ou3), *Pseudomonas oleovorans* (Ou4), *Streptomyces* sp. (Ou6), *Paenibacillus apiarius* (Ou7), *Mycobacterium* sp. (Ou8) and *Bacillus cereus* (Ou9). All these bacteria were tested against adults of *O. ununguis* within ten days. *Bacillus thuringiensis* (Ou2) was found to be causing the highest pathogenicity (40.7%).

KEYWORDS:
Oligonychus ununguis, pest, bacterial flora, isolation, pathogenic bacteria, biological control.

INTRODUCTION

The Spruce Spider Mite, *Oligonychus ununguis*, (Jacobi) (Acari: Tetranychidae), is one of the most important destructives pests of spruce forests in various regions of the world. It is reported to be found in spruce trees in the Eastern Black Sea Region of Turkey. The pest reduces photosynthesis areas of the trees by absorbing chlorophyll and honeydew of the leaves and it is particularly an important obstacle to the development of seedlings [1].

In the literature, it is reported that the use of chemical pesticides in the existing control strategies of mites in spruce trees causes varying levels of toxicity and effects [2]. In contrast to insect pathogens, the information about pathogens of the mites are still insufficient. In this regard, there are also some microbial control studies about some bacteria and fungi. Aksoy et al. [3] have investigated the effects of *Pseudomonas putida* biotype B on twospotted spider mite *Tetranychus urticae* (Acari: Tetranychidae) and found that it causes high rates of mortalities on *T. urticae.* In addition, it is also reported that *Bacillus thuringensis* kills adults and larvae of Tetranychid mites [4] as well as some Mesostigmata and Prostigmata species [5]. *B. thuringensis* strains were isolated from the bee mite, but its pathogenicity could not be identified [6]. Furthermore, some studies related to the use of entomopathogenic fungi in the microbial control of harmful mites have been conducted in recent years [7,8].

Surprisingly, although *O. ununguis* is a very harmful species around the world, bacterial pathogens of this mite have not been investigated yet. In this study, bacterial flora was investigated for the first time to be used in the biological control of *O. ununguis* and their pathogenicity against adults of this pest was also determined.

MATERIALS AND METHODS

Isolation of bacteria. The acari were surface sterilized in 70% alcohol and then washed three times with sterile distilled water and homogenized in nutrient broth media by using a glass tissue grinder. Suspensions were diluted and 0.1ml suspension was plated on nutrient agar. Plates were incubated at 30ºC for 2-3 days. After the incubation period, the plates were examined and bacterial colonies were selected. The colonies determined were purified by subculture on the plates. Bacterial strains were maintained for long-term storage in nutrient broth with 15% glycerol at -80 ºC.

Identification of bacterial isolates. Some morphological (cell morphology, endospore

formation, parasporal crystals and mobility) and biochemical properties (gram reaction, oxidase, catalase, and reduction of nitrate) of bacterial isolates were examined by routine and conventional methods. The commercially available API 20E, API 50 CH and API Staph kits (bioMerieux) also was used to determine other phenotypic properties according to the manufacturer's instructions.

16S rRNA gene sequencing. Bacterial colonies were inoculated into nutrient broth and incubated approximately 18 h at 30 ^{0}C in order to extract DNA from bacterial isolates. At the end of incubation time, the bacterial cells were collected by centrifuging from the culture medium. Then, genomic DNA was isolated with Genomic DNA Purification Kit (Promega, Germany) in accordance with the manufacturer's recommendations. 16S rRNA gene sequences of the bacterial isolates were performed with the following universal primers: UNI16S-L: 5'-ATT CTA GAG TTT GAT CAT GGC TCA -3' as forward and UNI16S-R: 5'ATG GTA CCG TGT GAC GGG CGG TGT GTA-3' as reverse. PCR conditions were adjusted according to the instructions of Weisburg et al. [9]. The amplified 16S rRNA gene product was sent to RefGen Biotechnology Laboratory (Ankara, Turkey) for sequencing. The sequences obtained were used for identification of the isolates and phylogenetic analyses.

Phylogenetic relationship of the bacterial isolates. The sequences obtained were used to perform BLAST searches using the NCBI GenBank database to confirm isolate identification [10]. Evolutionary relationships of the eleven bacterial isolates were evaluated. Cluster analyses of the sequences were performed using BioEdit (version7.09) with Clustal W followed by neighbor joining analysis on aligned sequences performed with MEGA 6.0 software [11]. Reliability of dendograms was tested by bootstrap analysis with 1000 replicates using MEGA 6.0.

The acaricidal effects of bacterial isolates. Adults of *O. ununguis* were used for the acaricidal assay of bacterial isolates. All of the bacterial isolates were tested as overnight cultures after removing the growth medium. Bacterial isolates were incubated for 18 hours (72 h for *Bacillus* to sporulation) at 30ºC in the nutrient broth medium. After incubation, bacterial cells were centrifuged at 3000 rpm for 10 min [12]. The pellet was resuspended by adding sterile PBS. The optical density of the cells was adjusted to 1.89 at OD (optical density)$_{600}$ [13]. Fresh spruce exiles were

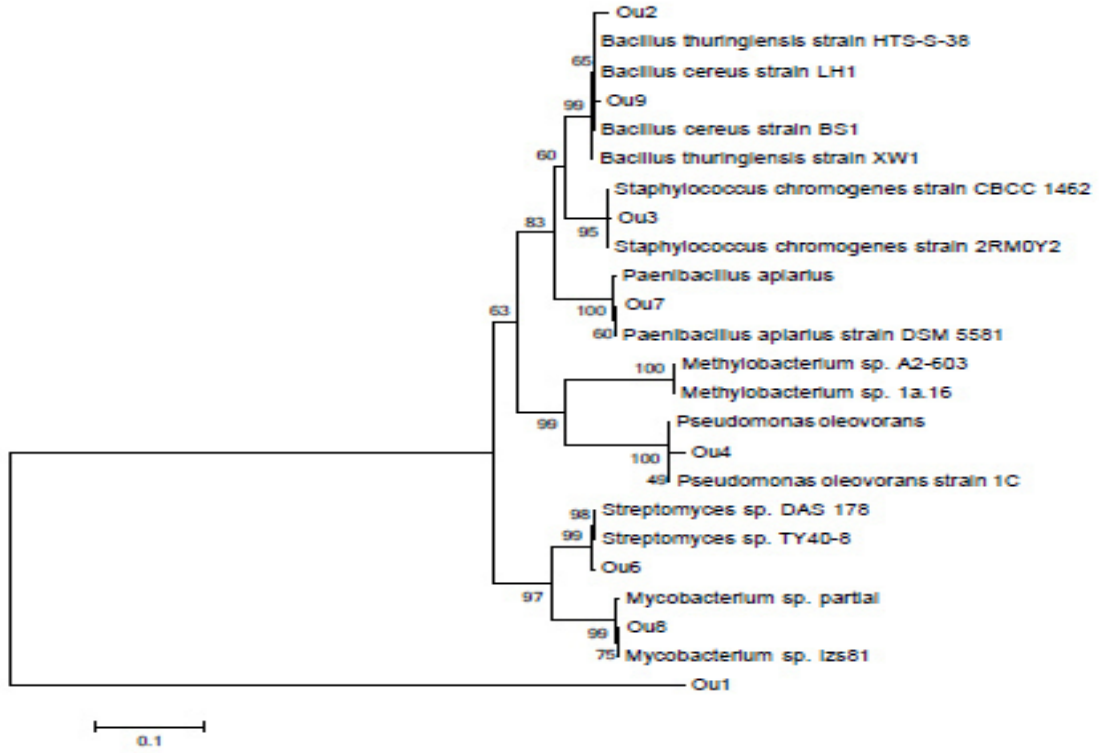

FIGURE 1

Neighbor-joining tree of bacterial isolates from *O. ununguis* and their closely related 16 bacterial species. The dendrogram was constructed by MEGA 6.0 software based on the partial sequences of the 16S rRNA gene. Bootstrap values shown next to nodes are based on 1000 replicates. The scale on the bottom of the dendrogram shows the degree.

TABLE 1
Some morphological and biochemical characteristics of bacterial isolates.

Isolates	Ou1	Ou2	Ou3	Ou4	Ou6	Ou7	Ou8	Ou9
Colony color	Pale red	Cream	Melon yellow	Yellow	Cream	Cream	Orange	Cream
Shape	Bacil	Bacil	Coccus	Bacil	Bacil	Bacil	Bacil	Bacil
Gram stain	-	+	+	-	+	+	+	+
Endospore	-	+	-	-	-	+	-	+
Parasporal cyristals	-	+	-	-	-	-	-	-
Motility	+	+	-	+	-	+	-	+
Nitrate reduction	-	+	+	-	-	+	+	+
Catalase test	+	+	+	+	+	+	+	+
Oxidase test	+	-	-	+	+	-	nd	-

nd: not determined

inoculated by dipping them into the bacterial suspensions and placed in a sterile plastic box (150ml). The control group was treated with sterile PBS. Ten adult mites were placed into each box and fresh spruce exile was provided in each day for ten days. These boxes were incubated at 26±2ºC and 60% RH during 12 h L: 12 h D photoperiod. Mortality was recorded ten days later. All experiments were repeated three times.

Mortalities were corrected according to Abbott's formula [14]. The data were subjected to ANOVA and subsequently to LSD multiple comparison test to compare isolates against the control group and to determine differences among isolates using SPSS 15.0 statistical software.

RESULTS

According to the results of the study, a total of 8 bacterial strains belonging to 7 genera and 5 species were isolated and characterized. All of the isolates were bacilli except *Staphylococcus chromogenes* Ou3. Two isolates (*Methylobacterium* sp. Ou1 and *Pseudomonas oleovorans* Ou4) were Gram negative while the other isolates were Gram positive. Some morphological and biochemical characteristics of bacterial isolates are summarized in Table 1. API test results are listed in Tables 2, 3 and 4, respectively.

TABLE 2
The results of API 20E test system of bacteria isolated from *O. ununguis*

	Isolate number							
Tests	Ou1	Ou2	Ou3	Ou4	Ou6	Ou7	Ou8	Ou9
β-galaktosidase	-	-	-	+	+	-	-	-
Arginine dihydrolase	-	+	+	-	-	-	+	wp
Lysine decarboxylase	-	-	-	-	-	-	-	-
Ornithine decarboxylase	-	-	-	-	-	-	-	-
Trisodium citrate	-	+	+	+	-	-	-	+
H_2S(sodium thiosulfate)	-	-	-	-	-	+	+	-
Urease	+	-	+	-	-	wp	wp	-
L-tryptophan	-	-	-	-	-	-	-	-
Indole	+	-	-	-	-	-	-	-
VP (sodium pyruvate) test	-	+	-	-	-	-	+	+
Gelatinase	-	+	-	+	+	+	-	+
Glucose fermentation	-	+	+	+	-	+	-	+
D-mannitol fermentation	-	-	+	-	-	-	wp	-
Inositol fermentation	-	-	-	-	-	+	+	-
D-sorbitol fermentation	-	-	-	-	-	-	wp	-
L-rhamnose fermentation	-	-	-	-	-	-	-	-
D-saccharose fermentation	-	-	+	-	-	+	+	-
D-melibiose fermentation	-	-	-	-	-	-	-	-
Amygdaline fermentation	-	-	-	-	-	+	-	-
L- arabinose fermentation	-	-	-	+	-	-	-	-

+ positive, - negative, wp: weak positive

TABLE 3
The results of API 50CH test system of bacteria isolated from *O. ununguis*

	Isolate number				
Tests	Ou2	Ou3	Ou7	Ou8	Ou9
Glycerol	+	+	-	+	+
Erythritol	-	-	-	+	-
D-Arabinose	-	-	-	-	-
L-Arabinose	-	-	-	-	-
D-Ribose	+	+	+	-	+
D-Xylose	-	-	-	+	-
L-Xylose	-	-	-	-	-
D-Adonitol	-	-	-	+	-
Methyl-βD-xylopyranoside	-	-	-	-	-
D-Galactose	-	+	-	-	-
D-Glucose	+	+	+	-	+
D-Fructose	+	+	-	+	+
D-Mannose	wp	+	-	+	-
L-Sorbose	-	-	-	-	-
L-Rhamnose	-	-	-	-	-
Dulcitol	-	-	-	-	-
Inositol	-	-	+	-	-
D-Mannitol	-	+	-	-	-
D-Sorbitol	-	-	-	-	-
Methyl-αD-mannopyranoside	-	-	-	-	-
Methyl-αD-glucopyranoside	-	-	+	-	-
N-Acetylglucosamine	+	+	+	-	+
Amygdalin	-	-	+	-	-
Arbutin	+	-	-	-	+
Esculin-ferric citrate	+	-	+	-	+
Salicin	+	-	+	-	+
D-Celiobiose	+	-	+	-	wp
D-Maltose	+	+	+	-	+
D-Lactose (bovine origin)	-	+	-	-	-
D-Melibiose	-	-	-	-	-
D-Saccharose	wp	+	+	-	-
D-Trehalose	+	+	+	+	+
Inulin	-	-	-	-	-
D-Melezitose	-	-	+	-	-
D-Raffinose	-	-	+	-	-
Starch	+	+	+	-	-
Glycogen	+	-	-	-	+
Xylitol	-	-	-	-	-
Gentiobiose	-	-	-	-	wp
D-Turanose	-	-	-	-	-
D-Lyxose	-	-	-	-	-
D-Tagatose	-	-	-	-	-
D-Fucose	-	-	-	-	-
L-Fucose	-	-	-	-	-
D-Arabitol	-	-	-	-	-
L-Arabitol	-	-	-	-	-
Potassium gluconate	-	-	+	-	-
Potassium 2-ketogluconate	-	-	-	-	-
Potassium 5-ketogluconate	-	-	+	-	-

+ positive, - negative, wp: weak positive

TABLE 4
The results of API Staph test system of Ou3 isolate

Tests	Isolate
Glucose	+
Fructose	+
Mannose	+
Maltose	+
Lactose	+
Trehalose	+
Mannitol	+
Xylitol	-
Melibiose	-
Nitrate to nitrite	+
Alkaline phosphatase production	+
Acetyl methyl carbinol production	-
Raffinose	-
Xylose	-
Saccharose	+
Acid from alpha-methylglucoside	-
Acid from N-acetylglucosamine	+
Arginine dihydrolase ADH	+
Urease	+

+ positive, - negative, wp: weak positive

16S rRNA gene sequence analysis results of isolates are given in Table 5. The 16S rRNA partial gene sequences generated in this study have been deposited with the GenBank database under the accession numbers KP128697, KP128698, KP128699, KP128700, KP128701, KP128702, KP128703, and KP128704, respectively. Phylogenetic tree was constructed by using Neighbor Joining method (Figure 1). The similarities between isolates were ranged between 98%- 99% compared to other species.

Based on the study and 16S rRNA sequencing, isolates were identified as *Methylobacterium* sp. (Ou1), *Bacillus thuringiensis* (Ou2), *Staphylococcus chromogenes* (Ou3), *Pseudomonas oleovorans* (Ou4), *Streptomyces* sp. (Ou6), *Paenibacillus apiarius* (Ou7), *Mycobacterium* sp. (Ou8) and *Bacillus cereus* (Ou9). All these bacteria were tested against *O. ununguis*. The highest acaricidal activity %40.7 was obtained from *B. thuringiensis* ($p<0.05$), whereas the lowest acaricidal activity 11.1% was obtained from *Methylobacterium* sp. within ten days. Acaricidal activity of the remaining isolates (Ou3, Ou4 and Ou6 the same, Ou7 and Ou9 the same, Ou8) were as follows; 18.5%, 22.2%, 25.9%, and 14.8%, respectively. The acaricidal activity of the isolates on *O. ununguis* adults are shown in Figure 2.

TABLE 5
Conclusion identification and GenBank Accession numbers of bacterial isolates according to the partial 16S rRNA gene sequence.

Isolates	GenBank	Conclusion	16S rRNA similarity(%)	Accesion numbers
Ou1	KP128697	*Methylobacterium* sp.	99	KF441619
Ou2	KP128698	*Bacillus thuringiensis*	99	EU545396
Ou3	KP128699	*Staphylococcus chromogenes*	99	NR036901
Ou4	KP128700	*Pseudomonas oleovorans*	98	AY623816
Ou6	KP128701	*Streptomyces* sp.	99	AB918658
Ou7	KP128702	*Paenibacillus apiarius*	99	NR040890
Ou8	KP128703	*Mycobacterium* sp.	99	KC355359
Ou9	KP128704	*Bacillus cereus*	99	KC248212

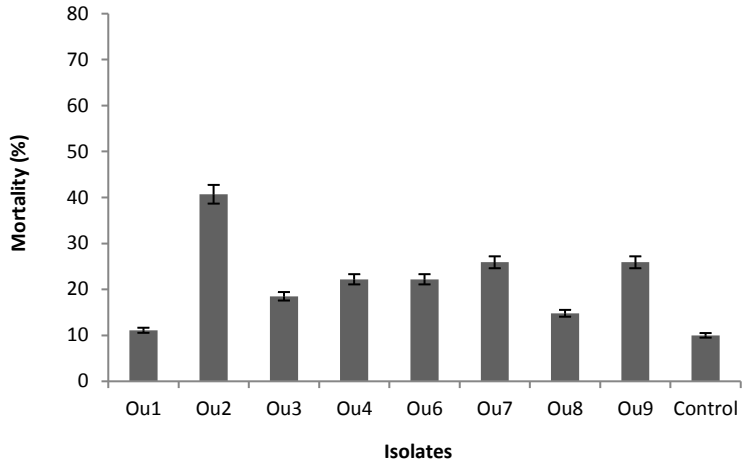

FIGURE 2
Mortality of bacterial isolates from *O. ununguis* on this pest within ten days. Ou1, *Methylobacterium* sp.; Ou2, *Bacillus thuringiensis*; Ou3, *Staphylococcus chromogenes*; Ou4, *Pseudomonas oleovorans*; Ou6, *Streptomyces* sp.; Ou7, *Paenibacillus apiarius*; Ou8, *Mycobacterium* sp.; Ou9, *Bacillus cereus*.

DISCUSSION AND CONCLUSION

In contrast to insect pathogens, the information about pathogens of the mites are still insufficient. Although *O. ununguis* is one of the most important destructives pests of spruce forests, no attempt was done to find its bacterial flora and their potentials as a biocontrol agent. In this study, we determined the culturable bacterial flora of *O. ununguis* and we also investigated their availability in the control of this pest for the first time.

The presence of *Bacillus thuringiensis* [15], *Bacillus cereus* [16,17], *Staphylococcus chromogenes* [18] and *Mycobacterium* [19] with acari has previously been demonstrated. However, to our knowledge, this is the first documentation of *Methylobacterium, Pseudomonas oleovorans, Streptomyces* sp. and *Paenibacillus apiarius* from any acari.

In the literature, there are several studies investigated *Bacillus* species that are isolated from the mite [19,20,21]. *B. thuringiensis* was isolated from the mite species and was investigated the pathogenicity in previous studies [22,23]. *B. thuringiensis* (Ou2) was found to be causing the highest pathogenicity rates (40.7%) within ten days in adults of *O. ununguis*. But, *B. cereus* has shown a mortality rate of 25.9% against the pest.

Methylobacterium strains are reported to be isolated from environments such as freshwater, soil, dust, sediments, air or hospitals, where they are very widespread [24]. In this study, the lowest acaricidal activity 11.1% was obtained from *Methylobacterium* sp.

Staphylococcus chromogenes (Ou3), a Gram positive, member of the bacterial genus *Staphylococcus* and associated with mastitis in dairy animals [25]. We found that it has 18.5% acaricidal effect on adults of *O. ununguis*.

Bacteria belonging to the *Pseudomonas* species were isolated from dust and oribatid mites [19,26,27]. We determined that it has mortality 22.2% against the pest.

The isolation of *Streptomyces* sp. from mites was not observed; however, Takahashi et al. [28] have reported acaricidal and antitumor activity of *Streptomyces* species isolated from sea mud. In this study, acaricidal activity of *Streptomyces* sp. (Ou6) against the pest was determined as 22.2%.

The genus *Paenibacillus* have been determined in a variety of environments such as: soil, water, rhizosphere, vegetable matter, forage and insect larvae [29,30,31]. In this study, it was found that *Paenibacillus apiarius* (Ou7) isolated from the mites for the first time has the same mortality rate as the Ou2 isolates (25.9%).

Bacteria belonging to *Mycobacterium* genus contains a number of absolute (*M. tuberculosis*, *M. leprae* etc.) and opportunistic pathogens (such as *M. avium, M. simiae, M. kansasii*) that afflict humans and animals alike [32]. In the previous studies, *Mycobacterium* sp. (Ou8) was isolated from mites with no pathogenicity identification and determined to have low mortality rates against the pest (14.8%).

In conclusion, this is the first study on the bacterial flora of *O. ununguis* and pathogenicity of isolates as well as adults of *O. ununguis*. Our results indicated that *B. thuringiensis* Ou2 can be considered as a candidate microbial control agent that can be used against *O. ununguis.* Further studies will be directed to determine the effectiveness of the isolate in the field.

ACKNOWLEDGEMENTS

This work was supported by the Artvin Coruh University Research Foundation (ACU-BAP 2012.F15.02.22).

REFERENCES

[1] Yüksel, B. (1999). Doğu Karadeniz bölgesinde ladin örücü akarı (*Oligonychus ununguis*, Jacobi)'nin zararı ve mücadelesi. Orman Mühendisliği Dergisi, 36, 28-31.

[2] Shetlar, D.J. and Herms, D. (1999. Insect and mite control on woody ornamentals and herbaceous perennials. Ohio State Univ. Ext. Bull. 83.

[3] Aksoy, H.M., Ozman-Sullivan, S.K., Ocal, H., Celik, N. and Sullivan G. T. (2008). The effects of *Pseudomonas putida* biotype B on *Tetranychus urticae* (Acari: Tetranychidae). Exp. Appl. Acarol., 46, 223-230.

[4] Hall, I.M., Hunter, D.K., Arakawa, K.Y. (1971). The effect of the β-exotoxin fraction of *Bacillus thuringiensis* on the citrus red mite. J. Invertebr. Pathol. 18, 359-362.

[5] Chandler, D., Sunderland, K.D., Ball, B.V. and Davidson, G. (2001). Prospective biological control agents *Varroa destructor* n.sp., an important pest of the european honeybee. Biocontrol Sci. Techn. 11, 429-448.

[6] Glinski, Z.F. and Jarosz, J. (1990). Microorganisms associated fortuitously with *Varroa Jacobsoni*. Microbios, 62, 59-68.

[7] Chandler, D., Davidson, G., Pell, J.K., Ball, B.V., Shaw, K., Sunderland, K.D. (2000). Fungal biocontrol of acari. Biocontrol Sci. Techn. 10, 357-384.

[8] Roy, H.E., Steinkraus, D.C., Eilenberg, J., Hajek, A.E. and Pell, K.J. (2006). Bizarre interactions and endgames: entomopathogenic fungi and their arthropod hosts, Annu. Rev. Entomol, 51, 331-357.

[9] Weisburg, W.G., Barns, S.M., Pelletier, D.A. and Lane, D.J. (1991). 16S ribosomal DNA amplification for phylogenetic study. J Bacteriol. 173, 697-703.

[10] Altschul, S.F., Gish, W., Miller, W., Myers, E.W. and Lipman, D.J. (1990). Basic local alignment search tool. J Mol. Biol. 215, 403-410.

[11] Tamura, K., Stecher, G., Peterson, D., Filipski, A. and Kumar, S. (2013). MEGA6: Molecular evolutionary genetics analysis version 6.0. Mol. Biol. Evol. 30, 2725-2729.

[12] Ben-Dov, E., Boussiba, S. and Zaritsky, A. (1995). Mosquito larvicidal activity of *Escherichia coli* with combinations of genes from *Bacillus thuringiensis* subsp. israelensis. J. Bacteriol. 10, 2581-2587.

[13] Moar, W.J., Pusztzai-Carey, M., Mack, T.P. (1995). Toxity of purified proteins and the HD-1 strain from *Bacillus thuringiensis* againts lesser cornstalk borer (Lepidoptera: Pyralidae). J. Econ. Entomol. 88, 606-609.

[14] Abbott, W.S. (1925). A method of computing the effectiveness of aninsecticide. J. Econ. Entomol. 18, 265–267.

[15] Jung, Y.C., Mizuki, E., Akao, T. and Cote, J.C. (2007). Isolation and characterization of a novel *Bacillus thuringiensis* strain expressing a novel crystal protein with cytocidal activity against human cancer cells. J. Appl. Microbiol. 103, 65-79.

[16] Oh, H., Ishii, A., Tongu, Y. and Itano, K. (1986). Microorganisms associated with the house dust mite, Dermatophagoides. Jpn. J. Sanit. Zool. 37, 229-235.

[17] Hubert, J., Erban, T., Nesvorna, M. and Stejskal, V. (2011). Emerging risk of infestation and contamination of dried fruits by mites in the Czech Republic. Food Addit. Contam. Part A Chem. Anal. Control Expo. Risk Assess. 28, 1129-1135.

[18] Hogg, J.C. and Lehane, M.J. (1999). Identification of bacterial species associated with the sheep scab mite (*Psoroptes ovis*) by using amplified genes coding for 16S rRNA. Appl. Environ. Microbiol. 65, 4227-4229.

[19] Wolf, M.M. and Rockett, C. L. (2009). Habitat changes affecting bacterial composition in the alimentary canal of oribatid mites (acari: oribatida). Int. J. Acarol. 10, 209-215.

[20] Yoon, C., Indiragandhi, P., Anandham, R., Cho, S., Sa, T.M. and Kim, G.H. (2010). Bacterial diversity and distribution from the whole mite extracts in acaricide resistant and susceptible populations of twospotted spider mite-*Tetranychus urticae* (Acari: Tetranychidae). J. Korean Soc. Appl. Bı. 53, 446-457.

[21] Gazeta, G.S., Norberg, A.N., Aboud-Dutra, A.E. and Serra-Freire, N.M. (2000). *Tyrophagus putrescentiae* (Schrank, 1781) as a vector of pathogenic bacteria: laboratory observation. Entomologia y Vectores, 7, 49-55.

[22] Neal, J.W., Lingquist, R.K., Gott, K.M. and Casey, M.L. (1987). "Activity of the thermostable beta-exotoxin of *Bacillus thuringiensis* Berliner on Tetranychus urticae and Tetranychus cinnabarinus". J. Agr. Entomol. 4, 33-40.

[23] Royalty, R.N., Hall, F.R. and Taylor, R.A.J. (1990). Effects of *B. thuringiensis* on *Tetranychus urticae* (Acari: Tetranychidae) mortality, fecundity and feding, J. Econ. Entomol. 83, 792-798.

[24] Green, P.N. (2006). *Methylobacterium*. In: Prokaryotes, 3rd edn. (eds Dworkin, M., Falkow, S., Rosenberg, E., Schleifer, K.H. and Stackebrandt, E.) Springer. New York, 257-265.
[25] Nickerson, S.C. (2009). "Control of heifer mastitis: antimicrobial treatment an overview", Vet. Microbiol. 134, 128-135.
[26] Ushijima, H., Park, R., Yoshino, K., Ohta, K. Fuji, R. and Kobayashi, N. (1983). Microorganisms in house-dust mites in Kawasaki disease. Paediatr. Jpn. 25,127-129.
[27] Kato, H., Fujimoto, T., Inoue, O., Kondo, M., Koga, Y.,Yamamoto, S., Shingu, M., Tominaga, K. and Sasaguri, Y. (1983). Variant strain of *Propionibacterium acnes*: a clue to the aetiology of Kawasakidisease. Lancet, 2, 1383-1387.
[28] Takahashi, A., Kurasawa, S., Ikeda, D., Okami, Y. and Takeuchi, T. (1989). Altemicidin, a new acaricidal and antitumor substance, I. Taxonomy, fermentation, isolation and physico-chemical and biological properties. J. Antibiot. 42, 1556-1561.
[29] Lal, S., Tabacchioni, S. (2009). Ecology and biotechnological potential of *Paenibacillus polymyxa*: a minireview. Indian J. Microbiol. 49, 2-10.
[30] McSpadden Gardener, B.B. (2004). Ecology of *Bacillus* and *Paenibacillus* spp. in Agricultural Systems. Phytopathology. 94, 1252-1258.
[31] Montes, M.J., Mercade, E., Bozal, N. and Guinea, J. (2004). *Paenibacillus antarcticus* sp. nov., a novel psychrotolerant organism from the Antarctic environment. Int. J. Sys. Evol. Microbiol. 54, 1521-1526.
[32] Rastogi, N., Legrand, E. and Sola, C. (2001). The mycobacteria: an introduction to nomenclature and pathogenesis. Rev. Sci. Tech. 20, 21-54.

Received: **25.11.2015**
Accepted: **28.04.2016**

CORRESPONDING AUTHOR

Nurcan Albayrak Iskender
Faculty of Health Sciences
Artvin Coruh University
08000 Artvin-Turkey

e-mail: nurcaniskender25@hotmail.com

© by PSP Volume 25 – No. 10/2016, pages 4171-4183 Fresenius Environmental Bulletin

FLOW BEHAVIOUR AND RHEOLOGICAL ASSESMENT OF KAOLINITE/PDMS PASTES VIA CAPILLARY RHEOMETER

Zurriye Gunduz[1,*], Mahir Alkan[2], Mehmet Dogan[2]

[1]Balıkesir University, Engineering and Architecture Faculty, Environmental Engineering, Balıkesir, Turkey
[2]Balıkesir University, Science and Art Faculty, Department of Chemistry, Balıkesir, Turkey

ABSTRACT

An improved understanding of the influence of some parameters such as solid:liquid ratio, particle size and temperature on the rheology of kaolinite/silicone oil AK 60 000 pastes is needed so that new application areas of this clay can be brought into existence. Kaolinite/PDMS paste forms were used to measure the rheological properties with high pressure capillary rheometer. All pastes were exhibited non-Newtonian, pseudoplastic shear-thinning behaviour under experimental conditions. The viscosity decreased with an increase in temperature and particle size and with a decrease in solid:liquid ratio. Herschel-Bulkley model is capable of predicting the extrusion behaviour of the whole pastes.

KEYWORDS:
Kaolinite/PDMS paste, non-Newtonian, Herschel-Bulkley model, High Pressure Capillary Reheometer.

INTRODUCTION

A suspension consists of solid particles dispersed in a solution. The addition of particles affects the flow field and rheological properties of the fluid. Characterization of concentrated suspension has been conducted extensively [1]. Suspensions of solid particles in viscous fluids are often encountered in various applications such as paints, polymer, ceramics, pharmaceutical products, drilling muds and food products.

Rheology is a science dealing with the mechanical behaviour of fluids and plastic bodies when subjected to external stresses. However, its technical application has been more conventionel in chemical industry, e. g. food science, polymer research, but uncommon in soil mechanics, yet [2]. The term “paste” is not precisely defined and there are many definitions in common use most of which focus upon the perceived mechanical response. For example, one of the definitions is ‘any composition and mixture containing just enough moisture to render itself soft and plastic’[3]. Pastes, or highly filled suspensions, are important intermediates in the manufacture of a wide range of products, including catalysts, agrochemicals and ceramics [4]. The ceramic paste flow is different from molten polymers or metals because the flow behaviour is dependent on the properties of solid and liquid components. Theoretical analysis and prediction of paste rheology have been studied by many workers. The origins of theoretical analysis of paste rheology can be found from Benbow [5] who used a capillary attached to a ram extruder [6]. Rheological studies of pastes are required to develop novel extrusion applications, and to improve product quality and process optimization [7]. The rheological properties of suspension of solid particles in polymeric matrices (pastes) are important in analyzing the processing of such materials, which are encountered in several industries. The flow behaviour of these composite systems depends on the particle shape, size and size distribution, volume fraction of particles, particle-particle and particle-matrix interactions, matrix rheology, and measurement conditions such as temperature and shear rate [8].

Clay minerals are extensively used in a wide range of applications. They are a key component in the formulation of ceramic products, cement, drilling fluids, moulding sands, paints and paper, among others [9]. An important characteristic that clay minerals are able to provide in such applications is adequate particle dispersion, which is necessary to obtain a uniform and stable system. Under certain conditions the clay particles may become aggregated, which leads to the variation of important properties required for a particular function. In drilling fluids, for example, the flow behaviour of the system is of utmost importance due to its circulation around the wellbore [10]. The aggregation of the clay particles under varying conditions of temperature and electrolytes leads to strong variations of the flow properties. It becomes necessary therefore to add certain additives, or polymers, to stabilise the clay particles and prevent this behaviour.

As indicated in literature [1], a suspension consists of solid particles dispersed in a solution and its characterization has been performed widely. However, it remains a challenge as the flow behaviour of concentrated suspension is complicated by the microstructural change with the

occurence of particle migration and wall slip, as well as yield stress. There is a wide range of studies on rheological properties of kaolinite dispersions, however, few of which involve kaolinite pastes. Kaolinite mineral is an environmentally safe material with no adverse health problems as long as the fine particle dust is controlled. Paste is an intimate mixture of particulate solids and liquids. The rheological behaviour of pastes is not nearly so well defined as that of pure fluids, be they Newtonian fluids or macromolecular-based, non-Newtonian fluids [11]. Numerous empirical and theoretical models have been proposed to describe the rheological behaviour of pastes [12]. Establishing the optimal amount of fluid is particularly important for ceramic pastes. Not only are pastes important in agriculture, food, cosmetics, construction, pharmacy, and ceramics, but their behaviours can be extremely complex due to the relative movement of the liquid phase within the solid matrix [13]. Theoretical rheological flow models applied to pastes are currently not adequate to predict the material flow properties under extrusion process conditions. Therefore, these properties usually must be measured experimentally [14]. Capillary extrusion flow has been very often utilised for a wide variety of paste-like materials in an attempt to characterize their bulk intrinsic rheology as well as their wall interface boundary conditions. The wall slip phenomenon is basically the occurence of apparent relative velocity between the wall and the fluid at the wall. However, since the fluid is continuum, even in concentrated suspensions there is no 'true slip'. It is in reality an 'apparent slip' created by a region of high velocity gradient close to the wall compared to the bulk. This appears as an apparent slippage of the suspension through a thin liquid-rich layer (slip layer) of thickness δ at the wall [15]. The flow of paste-like materials invariably involves interactions at the interface between the material and the processing engine wall [16]. This wall influence, which generally reduces shear strength of the particle network, extends from the wall to a distance of approximately a few particle diameters. At sufficiently high shear loadings the particle structure collapses in the layer of paste near the wall, causing formation of a thin film, which allows the paste to flow via slip along the wall [12]. The relative slip velocity changes with increase in temperature. In general, the behaviour of the particulate pastes during extrusion depends on:1. the amount and rheological properties of liquid phase, 2. the interference between particles, 3. the extrusion conditions, and 4. the time scale of the experiments [17]. Lin et al. designed a study to measure the yield stress, thixotropy, and viscosity at different shear rates of commercially available screen-printing pastes and self-prepared pastes by using a rheometer. Their results showed that commercial pastes are not totally suitable for application in screen-printing process [18].

Previously, work in this field has been confined to capillary rheometry of chemical additives/silicone oil pastes and no consideration of has been given to the rheological behaviour of kaolinite/ PDMS (silicone oil AK 60 000) pastes. The aim is to investigate flow behaviour and rheological characteristics of kaolinite/silicone oil AK 60 000 pastes via capillary rheometry. This paper is a part of a research project focused on rheological characteristics of kaolinite/silicone oil pastes. Doğan et al. [11] reported the flow behaviour of kaolinite/silicone oil AK 1 000 000 paste as a non-Newtonian and time-dependent material.

EXPERIMENTAL

Materials. Kaolinite paste consists of a combination of kaolinite powders having a particle size less than 25 μm (obtained from Kalemaden, a local mining corporation) and commercial silicone oil. Kaolinite, a natural geological sample and one of the most versatile industrial clay mineral, have a chemical formula $Al_2O_3.2SiO_2.2H_2O$ and its specific gravity is 2.62. As received, the kaolinite was in powder form and light cream in colour. The particle size distribution of the kaolinite was determined using fine sieves having diameter size between 0 and 25, 25 and 50, and 50 and 75 μm, corresponding to upper- and lower-size fractions. Silicone oil used as binder material is polydimethylsiloxane (PDMS) which is known for low weight, good thermal stability, inert, nontoxic and a water-repellent surface. The surface hydrophobicity of PDMS prevents the formation of a continuous water band on the surface. This leads to improved insulator performance, even in extreme enviroments [11]. Silicone oil (trademark name: silicone oil AK 60 000) supplied generously by Wacker-Chemie GmbH was utilized as continuous phase.

Paste Preparation. Processed kaolinite powders were mixed thoroughly in the dry state prior to adding the silicone oil in a kneader (IKA HKD-T0,6 kneader) and then the liquid phase, silicone oil, was added to solid phase. Aforementioned ingredients were mixed thoroughly batchwise for 4 h to ensure favorable homogenization. All of pastes were prepared in accordance with same procedure. The IKA high-efficiency laboratory kneader is suitable for processing nonflowable, highly viscous media. The uniform mixing is based on intensive processing by means of wide-bladed kneading elements. The kneading medium is moved within the trough both horizontally and vertically. Additional media

TABLE 1
Paste parameters prepared for the rheological measurements (solid:kaolinite, liquid:silicone oil).

solid:liquid ratio (g:g)	particle size (µm)	temperature (ºC)
75:25:00 77:23:00 80:20:00	0-25	25
77:23:00	0-25 25-50 50-75	25
77:23:00	0-25	25 50 75

quantities may be added during the kneading operation. The double-walled kneading chamber allows cooling or heating of the product. The product temperature was measured directly behind the kneading blades. In the experiments, kaolinite-silicon oil pastes were prepared in different silicon oil content in the range of 0-25, 25-50, and 50-75 µm [19]. Table 1 shows the compositions and particle sizes of six pastes prepared for these experiments with the dies of various L/D ratios, respectively [11].

Apparatus and Methodology. Capillary rheometry is a pressure-driven technique which mimics flow through an extruder die or injection moulding nozzle, capable of providing shear and extensional rheological properties of the melt at rates experienced during processing [20]. Besides this, capillary rheometry is a standart experimental technique for paste characterization and used to determine rheological characteristics of the pastes as a function of shear rate. [11]. Also it is the simplest and most popular system to measure the viscosity of fluids at high shear rates and, because of this, it is normally used to simulate industrial processes in the polymer processing industry. Thus, traditionally the rheometers have been equipped with high pressure transdusers, which means that they present some limitations in the characterization for low viscosity (lower than 0 (10^1) Pa s) fluids [21].

The shear rheology of all pastes prepared with four different silicone oils was studied employing twin bore (RH10) precision advanced capillary rheometer (Malvern Instruments, UK) using Flowmaster version 8.3.10 control software. Figure 1 shows a cross-section of such a rheometer with barrel diameter D_0, die land diameter D, and die land length L. A common crosshead is used to drive twin pistons at a range of speeds causing paste to flow at known flow rate through capillary dies. Pressure drop at the entrance of each capillary die was monitored by the control software. The inner diameter and length of the barrel used were15 and 240 mm, respectively. One barrel of the rheometer was fitted with a capillary die of L/D ratio 16 and the other bore was fitted with an orifice die. The bore diameter of both capillary dies was 1 mm, with die entry angle of 180°, whilst the lengths were 16 and less than 0.25 mm for long and orifice dies, respectively. Twin bore capillary rheometers allow two geometries of die to be examined simultaneously, thus corrected shear viscosity can be measured during a single test. In addition to measuring vicosity, capillary rheometry can, through the use of specialist test equipment, provide information relating to time dependent behaviour, die swell (a measure of elasticity), melt fibre strength, wall slip velocity and P-V-T data. Capillary dies, made from tungsten carbide-cobaltalloy in order to maintain tight geometrical integrit, were fitted into the bottom of the barrels and pressure transducers located directly above the dies [20].

The barrel could be fitted with different orifice and capillaries (or dies) of different diameters; an orifice is a capillary of negligible length. The arrangement used consisted of orifice and capillary of diameter was 1.0 mm, and the length of the capillary was 16 mm. The paste compounded in the kneader was fed into both bore of the barrel and manually compressed before the test was started. All pastes were extruded from capillary rheometer at a wide shear rate range. The shear viscosity and shear stress of pastes were measured as a function of shear rate. [11]

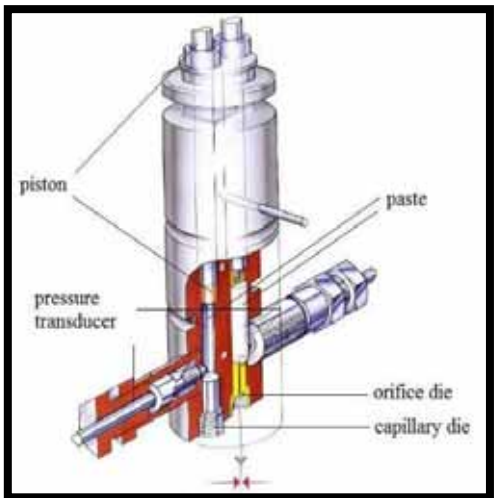

FIGURE 1
Outlines of a twin bore capillary rheometer.

RESULTS AND DISCUSSION

Structural and Morphological Characterization. XRD diffractogram obtained for the kaolinite/silicone oil paste is reported in Fig. 2. Patterns of the kaolinite and silicone oil are also represented to determine whether adding silicone oil affected the interlayer spacing. Characteristic maxima of the kaolinite were observed located at 2θ=12.42°, 20.89°, 24.93° and 26.68° (very intense, sharp and narrow peaks), which referred to the basal spacing of the kaolinite (Table 2). After dispersion in silicone oil, considerable changes occured in the XRD diffractogram compared to kaolinite. The peaks at 2θ=20.89°, 24.93° and 26.68° in the original kaolinite greatly shifted in the intercalates to small reflection angles (2θ=22.37°, 26.38° and 28.12°) originated by presence of silicone oil. As seen in Figure 2c significant difference occured at the 2θ=12.42° peak of kaolinite. This peak disappeared completely due to kaolinite-silicon oil intercalating. The diffraction pattern presented in Figure 2c illustrated that some kaolinite layers were delaminated, whereas certain layers retained their basal spacing. It can be concluded from these results that kaolinite-silicone oil composite material was obtained because of the dispersing of kaolinite into the polymer matrix of silicone oil.

The DTA peak temperatures are characteristic for each mineral, and DTA curves are applicable for the identification and determination of many types of clay. As seen from Figure 3, the DTA pattern of the crude clay exhibits characteristic endothermik and exothermic peaks of kaolinite at 523 and 1008 ºC, respectively. [22,23] In the first step of transformation in the range of 400-620 ºC, kaolinite, due to dehydroxylation and predehydration, was transformed to metakaolinite phase with loss of structural hydroxyl groups. In the second step, metakaolinite decomposes and forms Al-Si spinel phase generally during heating around the exothermic peak temperature [24].

Scanning electron microscopy (SEM) was also used in order to more closely observe the dispersion of the kaolinite in the silicone oil and to provide further confirmation of morphology. SEM micrographs of kaolinite and kaolinite/silicone oil paste presenting the microstructure are shown in Figs. 4,5. The formation of dispersion of kaolinite clay layers in the matrix can be said with the aid of these SEM micrographs.

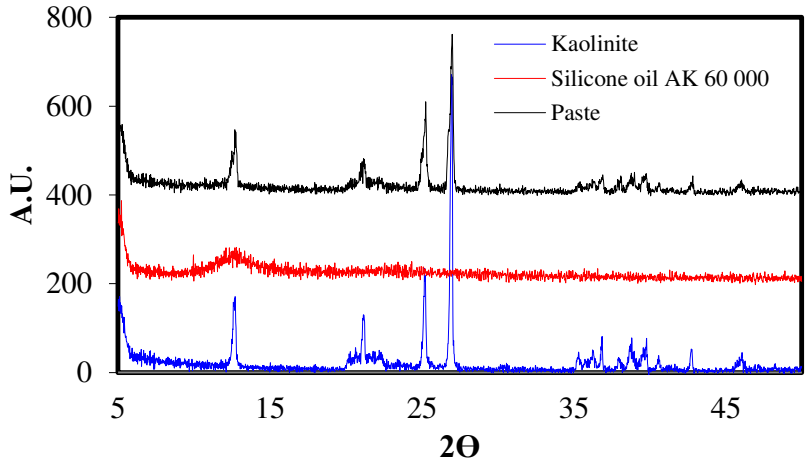

FIGURE 2
X-ray diffraction results of kaolinite, silicone oil AK 60 000 and the paste.

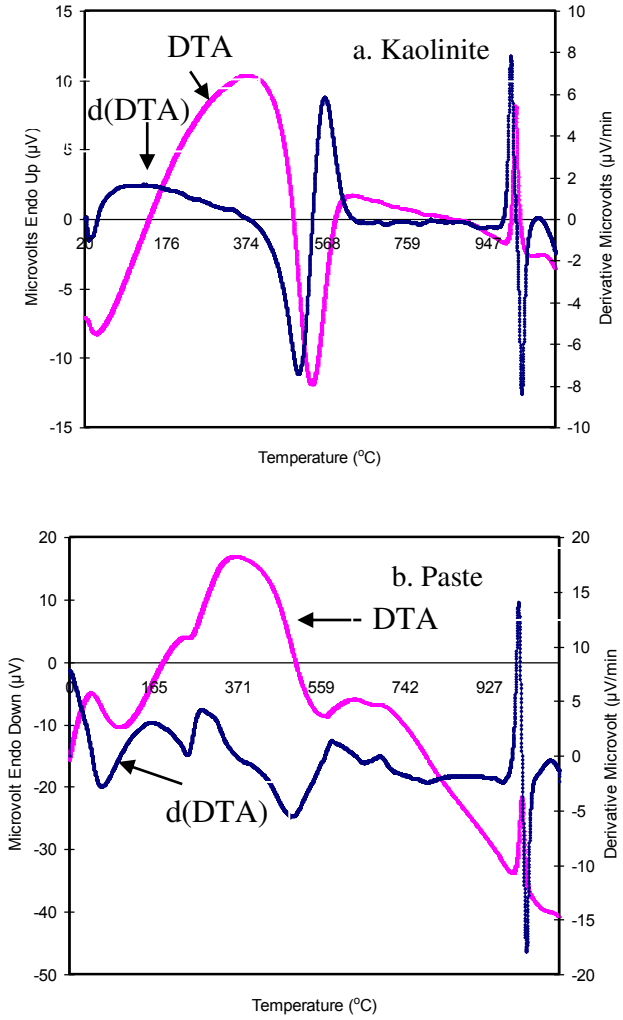

FIGURE 3
DTA spectra of kaolinite and paste.

TABLE 2
XRD data of kaolinite, silicone oil AK 60 000 and the paste.

Sample	2θ	d (Å)	% relative intensity
Kaolinite	12,678	6,977	21,75
	21,210	4,185	15,41
	25,209	3,529	28,75
	26,982	3,302	100,00
Silicone oil AK 60 000	5,206	16,960	100,00
Paste	12,787	6,917	24,64
	21,219	4,184	14,60
	25,264	3,522	49,26
	26,734	3,312	36,77
	27,012	3,298	100,00

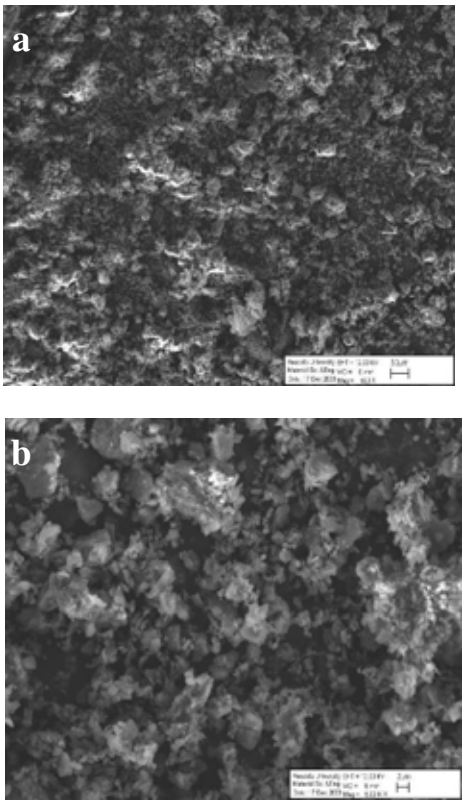

FIGURE 4
SEM image of kaolinite: a) 500 and b) 5000.

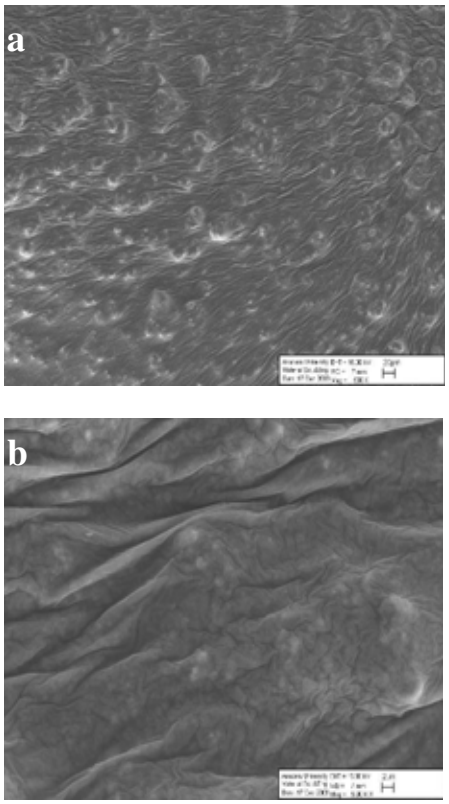

FIGURE 5
SEM image of kaolinite/silicone oil AK 60 000 paste: a) 500 and b) 5000.

Rheological Characterization of Pastes. Flow Behaviour of Pastes. The flow processes that occur during extrusion are very complex. Many effects are apparent, some of which are difficult to separate, e.g. shear flow with yield point, wall slippage with slippage limit, elastic and time effects such as thixotropy. These effects should be identifiable in measuring processes. The capillary rheometer can be used to determine such effects [25]. Fluids and pastes may be studied by subjecting them to continuous shearing at a constant shear rate. One of the fundamental parameters that characterizes flow behaviour of liquid and semiliquid materials is viscosity, which is an intrinsic parameter and a measure of a fluid's resistance to flow when a shearing stress is applied. The flow behaviour of these materials under applied stresses classifies them as Newtonian or non-Newtonian, a classification that is based on their stress-strain relationship [26]. The majority of the pastes do not show Newtonian behaviour. For non-Newtonian liquid, the viscosity or shear stress is a function of the shear rate, meaning that for an applied shear rate the corresponding shear stress remains constant provided the shear rate has not changed. [27,28]. A non-Newtonian fluid is any fluid that doesn't obey the Newtonian relationship (shear stress is linearly proportional to shear strain rate) between the shear stress and shear rate, as seen from Figs. 6-8,a [29]. Flow plots of shear stress versus shear rate do not exhibit a linear relationship. In this case, it can be said that the paste is a non-Newtonian material. When the material exhibits a diminish in viscosity as shear rate increases, it is called shear thinning or pseudoplastic [27,28]. Flow plots of shear viscosity versus shear rate point out that paste in the studied shear rate ranges displays a non-Newtonian and pseudoplastic behaviour [30]. A pseudoplastic material is one in which viscosity decreases with increasing shear rate. Pseudoplastic or shear thinning fluids have a lower shear viscosity at higher shear rates. It is generally supposed that the large molecular chains tumble at random and affect large volumes of fluid under low shear but that they gradually align themselves in the direction of increasing shear and produce less resistance [31].

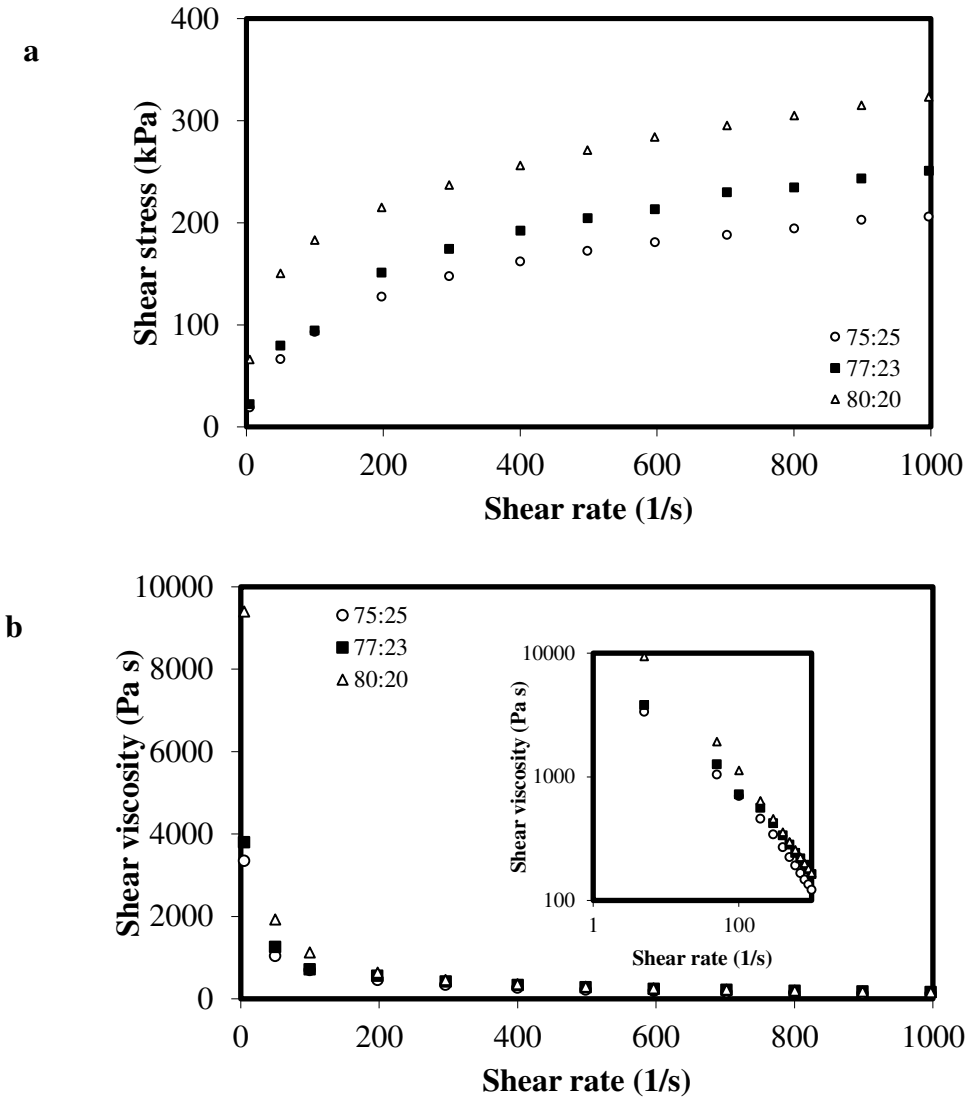

FIGURE 6
The plots of shear stress (a) and shear viscosity (b) versus shear rate for pastes with different solid:liquid ratios. (L/D=16 mm/1 mm).

Effect of Rheological Parameters. Various factors affect the flow behaviour of clay suspensions. Naturally, the clay concentration will bring about an increase of all rheological properties. Additionally, a rise of the temperature increases the interparticle attractive forces, which in turn, leads to enhanced particle-particle interactions affecting yield stress and suspension viscosity. The suspension viscosity also depends to a great extent on the viscosity of the medium, which is also a function of temperature [32]. The effects of rheological parameters such as solid:liquid ratio, particle size and temperature on the flow of kaolinite/silicone oil AK 60 000 pastes through the capillary dies as function of shear rate will be presented in this section.

Figure 6 presents the comparison of kaolinite/silicone oil AK 60 000 pastes with three different solid:liquid ratios for the die dimension of L/D=16mm/1mm. Curve plotted shear stress versus shear rate for the paste changes systematically which proceed below that of lower solid:liquid ratios and above that of higher solid:liquid ratios. The pattern and magnitude of the flow curves of the pastes based on silicone oil are strongly dependent on the solid concentration. A higher solids fraction tends to cause a paste to display more plastic characteristics [33].

Figure 7 reports experimental findings of the influence of shear rate and particle size on shear stress and shear viscosity. One of the parameters affects the flow behaviour is particle size of kaolinite powder used for the pastes. Three different groups of particle size were employed and incorporated with silicone oil in the kneader for the capillary rheometric measurements. Maintaining a

constant mass of particles in a suspension while reducing the particle size of the solid phase leads to an increase in the number of particles in the system. In general, a higher number of smaller particles results in more particle-particle interactions and an increased resistance to flow. Clearly as shear rate increases, this effect becomes less marked, suggesting that any particle-particle interactions are relatively weak and broken down at high shear rates. As particle size increases, shear stress values decrease regularly. Besides viscosity decreased with increasing shear rates, showing only a marginal decrease thereafter. The same scenario was found in the temperature change of the pastes. As shown in Fig. 8, the shear stress decreased by increasing temperature. The viscosity of a fluid is affected by the binding between molecules that make up the solution or the relationship between the solvent and the solute, both factors which are affected by solution concentration or temperature [11]. Besides, Rha noted that the decrease in viscosity with increasing shear rate is related to the increasing alignment of constituent molecules [34].

Wall Slip Analysis. For determining the wall slip behaviour of extrusion pastes, the high-pressure capillary rheometry equipped with a computer for data acquisition is particularly well-suited. Figs. 9-11 show the plots of wall slip velocity versus shear stress as a function of solid:liquid ratio, particle size and temperature, respectively. The shear stress values for all pastes during capillary flow changes systematically when the amounts of liquid or solid are altered. The corrected shear stress has decreased with an increase in the amount of solid. As seen from Figs. 9-11, V_{slip} for all paste samples have increased at high shear stress values. The change in slip velocity indicates that the surface layer properties rely on the amount of solid or liquid. Al pastes depending on the solid:liquid ratio show low wall slip velocity in the shear stress range of 0-100 kPa, but wall slip velocity has significantly increased at above 100 kPa (Fig. 9).

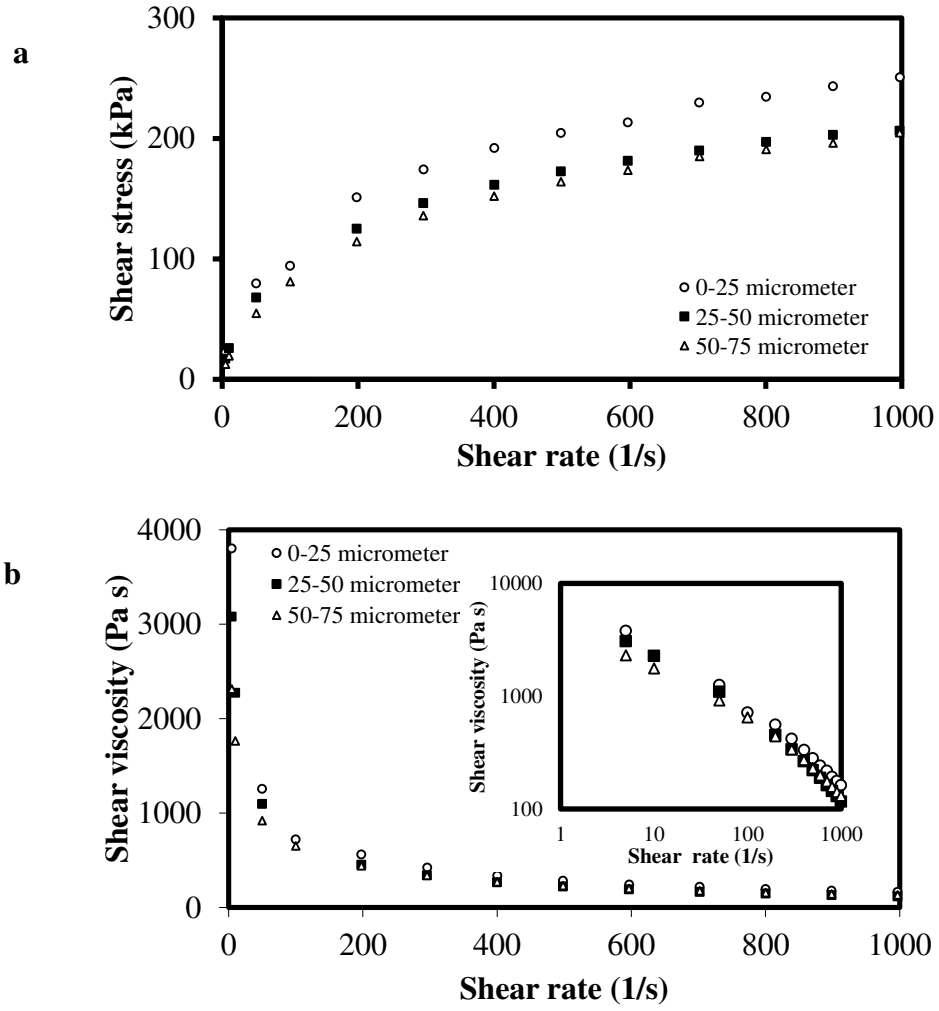

FIGURE 7
The plots of shear stress (a) and shear viscosity (b) versus shear rate for pastes with different particle sizes. (L/D=16 mm/1 mm).

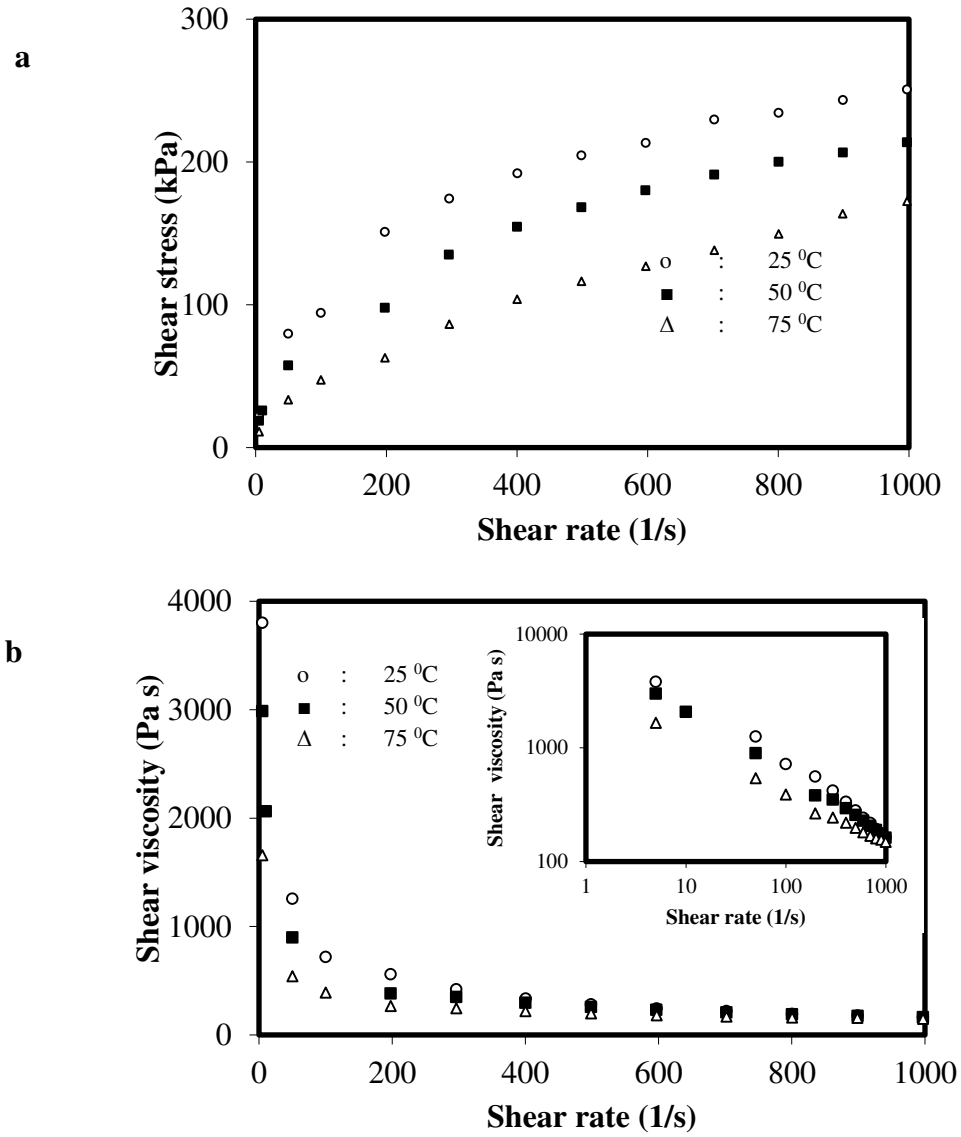

FIGURE 8
The plots of shear stress (a) and shear viscosity (b) versus shear rate for pastes with different temperatures. (L/D=16 mm/1 mm).

This may be a result of phase separation for pastes. Some degree of phase seperation is essential for paste flow as wall slip is often caused by the presence of a liquid rich-layer of material at the wall which deforms preferentially to the bulk material (sometimes called *apparent slip*: the layer is thin as evidenced by imaging) [35,36]. To examine the effect of particle size on wall slip velocity, the volume fraction was preserved constant at 77:23 of the maximum volume fraction during the experiments. As seen from Fig.10, as particle size increases, the wall slip velocity values are low and the wall slip velocity has not significantly changed until a shear stress value is 100 kPa. But at high shear stress values above 100 kPa (Fig.10) the wall slip velocity increases markedly for all particle sizes. This indicates that the shear stress values of process conditions of pastes are lower than 100 kPa. Since the kinetic energy of molecules increases with temperature, the interaction between the kaolinite and silicone oil reduces and phase migration can ocur more easily. The relationship between shear stress and V_{slip} with increasing temperature is shown in Fig. 11, indicating that wall slip has a significant contribution to the flow of the paste through the capillary die. Besides, it represents that the wall slip velocity of pastes increases with increasing temperature.

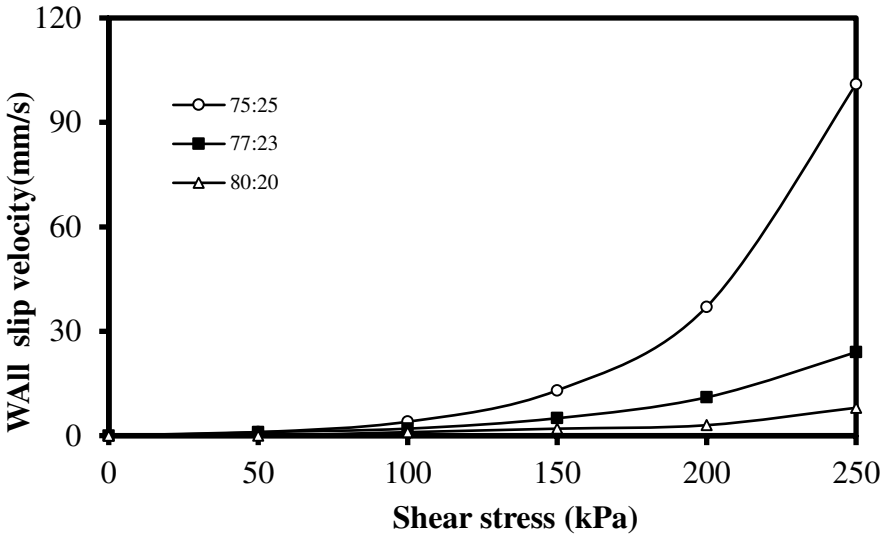

FIGURE 9
Wall slip velocity versus shear stress for different solid:liquid ratios.

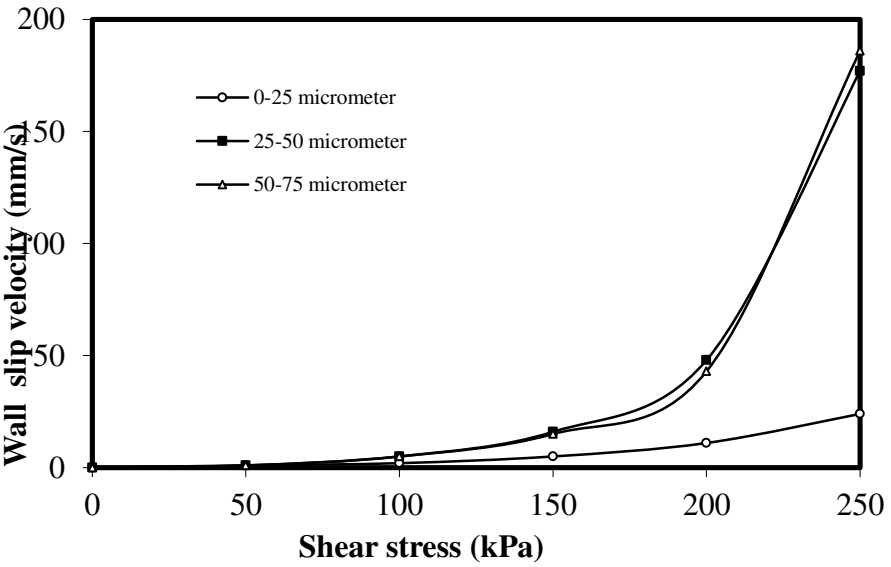

FIGURE 10
Wall slip velocity versus shear stress for different particle sizes.

Rheological Models. Aqueous clay suspensions that possess a relatively high particle concentration have been described traditionally in accordance to the Bingham theory of plastic flow [37]. The Bingham model postulates that a finite stress must be applied to initiate flow and at greater stresses the flow will be Newtonian. The resistance of the suspension to flow can therefore be considered as consisting of two parts: a Newtonian part in which the shear stress is proportional to the shear rate and a non-Newtonian part in which the shear stress is constant irrespective of the shear rate. The equation for the Bingham model is:

$$\tau = \tau_0 + \mu_\infty \dot{\gamma} \quad (1)$$

Where μ_∞ is the plastic viscosity, defined as the slope of the curve, and τ_0 is the bingham yield stress normally taken as the intercept of the flow curve at high shear rates. Very dilute clay suspensions or drilling fluids that contain polymers behave as pdeudoplastic fluids, which may be described by the power –law equation [38]:

$$\tau = K\dot{\gamma}^n \quad (2)$$

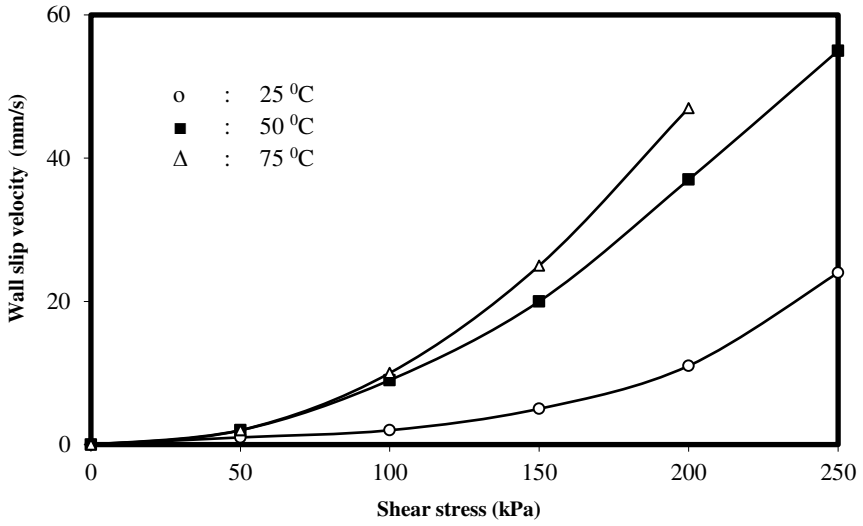

FIGURE 11
Wall slip velocity versus shear stress for different temperature values.

$$\tau^{1/2} = \tau_0^{1/2} + \mu_\infty^{1/2}\dot{\gamma}^{1/2} \quad (3)$$

and the Herschel-Bulkley equation [40]

$$\tau = \tau_0 + K(\dot{\gamma})^n \quad (4)$$

Both Eqs. (3) and (4) have been used to describe the consistency curves of drilling fluids, with the Herschel-Bulkley equation being the most suitable. In both cases, the suspension has an initial yield stress at low shear rates, and afterwards presents pseudoplastic or 'shear-thinning' type behaviour at higher shear rates. In the last case, the viscosity decreases with shear rate.

The model parameters obtained by fitting the experimental shear stress-shear rate data of kaolinite-silicone oil pastes to the Power Law, Casson, Bingham and Herschel-Bulkley (HB) models as a function of particle size, solid/liquid ratio, and temperature are given in Table 3. The coefficients of determination (R^2) obtained were high, which confirms the HB model to be adequately suitable for describing the flow behaviour of the pastes within the range studied. In all cases, R^2 values were higher than 0.994. The results showed that the shear stress-shear rate relationship at all experimental conditionals are nonlinear, indicating that these pastes behave as a non-Newtonian fluid. From the values of the HB model parameters, reported in Table 3, it can be seen that the consistency coefficient and the yield stress of kaolinite pastes increased with an increase in solid concentration and particle size and decrease in temperature. Similarly, Rao and Tattiyakul[41] showed that an increase in the starch concentration would increase the volume fraction of solids in starch dispersion and this led to an increase in yield stress. The yield stress, which represents a finite stress required to achieve flow, is an important factor that plays a vital role during mechanisation of paste preparation. Below the yield stress a material exhibits solid-like characteristics. This characteristic is highly crucial in process design and quality assessment for materials. Furthermore, the fact that (n) values were less than unity indicates that these products are pseudoplastic materials. The smaller the (n) values, the greater the departure from Newtonian behaviour. All pastes exhibited a shear thinning behaviour because the values of flow behaviour index (n) were less 1 for all pastes.

CONCLUSIONS

The shear viscosity of the suspension decreased with increased loading of silicone oil.

At a certain particle size distribution the shear viscosity of paste increases with the increase of solid concentration.

It was found that the pastes behaved as a non-Newtonian, shear-thinning fluid in the temperature range of 25-75 °C.

The extrusion behaviour of concentrated pastes was found to be strongly affected by slip at the wall at a

high shear stress.

All pastes were successfully described by the Herschel-Bulkley model.

The consistency coefficient of pastes increases greatly upon increasing the solid level and decreasing temperature.

TABLE 3
Model parameters calculated for the kaolinite/silicone oil AK 60 000 pastes.

Parameters			Rheological models												
Die dimension (L/D) (mm/mm)	Variable factors		Power Law			Casson			Bingham			Herschel-Bulkley			
			n	K ($kPas^n$)	R^2	τ_0 (kPa)	μ_∞ (kPa s)	R^2	μ_∞ (kPa s)	τ_0 (kPa)	R^2	τ_0 (kPa)	K_H ($kPas^n$)	n_H	R^2
16/1	Solid:liquid ratio (g::g)	75:25	0,4	10,9	0,98	35,1	0,09	0,89	0,16	73,5	0,83	13	21,1	0,3	0,994
		77:23	0,5	12	0,99	37,9	0,12	0,91	0,2	82,4	0,85	15	22,7	0,4	0,994
		80:20	0,3	44,8	0,99	94,9	0,08	0,9	0,21	147	0,83	16	55,7	0,3	0,998
16/1	Particle size (μm)	0-25	0,5	12	0,99	37,9	0,12	0,91	0,2	82,4	0,85	11	22,7	0,4	0,994
		25-50	0,5	9,1	0,99	25,6	0,11	0,91	0,18	60,3	0,84	16	23,7	0,3	0,999
		50-75	0,5	6,2	0,99	20,4	0,12	0,92	0,18	52,8	0,87	19	24,5	0,4	0,999
16/1	Temperature (°C)	25	0,5	12	0,99	37,9	0,12	0,91	0,2	82,4	0,85	11	22,7	0,4	0,994
		50	0,5	8,9	1	21,2	0,12	0,96	0,19	50,2	0,91	9	14,8	0,4	0,996
		75	4,4	0,5	1	11,4	0,1	0,99	30,35	0,2	0,97	7	4,9	0,5	0,995

ACKNOWLEDGEMENTS

The authors would like to acknowledge the financial support of TUBITAK (The Scientific and Technical Research Council of Turkey) (TBAG-2455 106T539).

REFERENCES

[1] Lam, Y.C., Wang, Z.Y., Chen, X., Joshi, S.C., Wall slip of concentrated suspension melts in capillary flows, Powder Technology 177 (2007) 162-169.

[2] Markgraf, W., Horn, R., Peth, S., "An approach to rheometry in soil mechanics-Structural changes in bentonite, clayey and silty soils", Soil&Tillage Research, (2006) 91, 1.

[3] Khan, A. U., Briscoe B.J., Luckham P.F., "Evaluation of slip in capillary extrusion of ceramic pastes", Journal of the European Ceramic Society, (2001) 21, 483.

[4] Amarasinghe A. D. U. S. and Wilson, D. I., "Interpretation of paste extrusion data, Trans IChemE, Vol 76, Part A, January 1998.

[5] Benbow, J. J. "The dependence of output rate on die shape during catalyst extrusion", Chemical Engineering Science (1971) 26, 1467-1473.

[6] Li, Y.Y. and Bridgwater, J., "Prediction of extrusion pressure using an artificial neural network", Powder Technology (2000) 108, 65-7

[7] Martın, P. J. and Wilson, D. I., Bonnett, P. E., "Rheological study of a talc-based paste for extrusion-granulation", Journal of the European Ceramic Society, (2004) 24, 3155.

[8] Gülmüş, S. A., Yılmazer, Ü., "Effect of volume fraction and particle size on wall slip in flow of polymeric suspensions", Journal of Applied Polymer Science, (2005) 98, 439.

[9] Grim, R.E., Clay Minerology, 2nd ed., McGraw-Hill, NY, 1968, pp.596.

[10] Darley, H.C.H., Gray, G.R., Composition and Properties of Drilling and Completion Fluids, 5th edn., Gulf Publ. Co., TX, USA, 1988.

[11] Doğan, M., Yılmaz, Z., Alkan, M., "Characterization and Rheological Properties of Kaolinite-Silicon Oil Pastes", Ind. Eng. Chem. Res., (2008) 47, 8218.

[12] Graczyk, J., Buggisch, H., Güner, S., "Wall Slip Behavior of Alumina-Silicon Oil Pastes During Extrusion", Chem. Eng. Technol. (2001), 24 (5), 489-491.

[13] Chandler, H. W.; George, S. D.; Liddle, J. "Deformation and Flow of Stiff Pastes: Review of Rheology of Some Soft Solids", Br. Ceram. Trans.,(2002), 101 (2), 47.

[14] Buggisch, H.; Graczyk, J. Rheometrical Methods for Studying Flow Behavior of Pastes. International Congress for Particle Technology; Nuremberg, Germany, March 2001.

[15] Vand, V., 1948. Viscosity of solutions and suspensions I. Theory. J. Phys. Colloid Chem. 52, 277-299.

[16] Khan, A. U., Briscoe B.J., Luckham P.F., "Evaluation of slip in capillary extrusion of ceramic pastes", Journal of the European Ceramic Society, (2001) 21, 483.

[17] Benbow, J. J., Blackburn, S., Mills, H., "The effects of liquid-phase rheology on the extrusion behaviour of paste", Journal of Materials Science, (1998) 33, 5827.

[18] Lin, H.W., Chang, C.P., Hwu, W.H., Ger, M.D., "The Rheological Behaviours of

Screen-Printing Pastes" Journal of Materials Processing Technology, (2008) 197, 284-291.
[19] Doğan, M., Graczyk, J., Buggisch, H., "Kapillarrheometrische Charakterisierung der Extrusionseigenschaften Von Pasten". Wissenschaftliche Abschlussberichte 38; Internationales Seminar, Universitat Karlsruhe, Karlsruhe-Germany, (2003).
[20] Paradkar, A., Kelly, A., Coates, P., York, P., " Shear and Extensional Rheology of Hydroxypropyl cellulose Melt using Capillary Rheometry" Journal of Pharmaceutical and Biomedical Analysis (2009) 49, 304-310.
[21] Barroso, E.G., Duarte, F.M., Couto, M., Maia, J.M., "High Strain Rate Rheological Characterization of Low Viscosity Fluids", Polymer Testing (2010) 29, 419-424.
[22] Alkan, M., Kalay, B., Doğan, M., Demirbaş, O., "Removal of copper ions from aqueous solutions by kaolinite and batch design", J. Hazard. Mater., (2008) 153, 867.
[23] Kakali, G., Perraki, T., Tsivilis, S., Badogiannis, E., "Thermal treatment of kaolin: The effect of mineralogy on the pozzolanic activity", Appl. Clay Sci., (2001) 20(12), 73.
[24] Alkan, M., Yılmaz, Z., Hopa, Ç., Güler, H., "The effect of reaction temperature and time on the zeolitisation of natural kaolinite", Fresen Environ Bullet, (2009) 18(3), 240-248.
[25] Händle F. (Ed.), Extrusion in Ceramics, Springer, 2007, pp.175.
[26] Bhattacharya, S.N., Rheology: Fundamentals and Measurements; Royal Melbourne Institute of Technology: Melbourne, Australia, 1997.
[27] Daubert, C.R.; Foegeding, E.A. Rheological Principles for Food Analysis. In Foof Analysis, 3rd ed.; Nielsen, S. S., Ed.; Kluwer Academic/ Plenum Publishers, nc.; New York, 2003, pp.507-508.
[28] Tabilo-Munizaga, G., Barbosa-Canovas, G.V. Rheology for the Food Industry.
[29] Skelland AHP, Non-Newtonian Flow and Heat Transfer, New York:John Wiley and Sons Inc; 1967.
[30] Razavi, S. M. A., Najafi, M. B. H., Alaee, Z., "The time independent rheological properties of low fat sesame paste/date syrup blends as a function of fat substitutes and temperature", Food Hydrocolloids, (2007) 21, 198.
[31] Mezger, T. G., The Rheology Handbook, Vincentz Network: Hannover, (2006).
[32] Luckham, P.F., Rossi, S., "The colloidal and Rheological Properties of Bentonite Suspensions", Advances in Colloid and Interface Science 1999, 82, 43-92.
[33] Benbow, J. J., Bridgewater J., Paste Flow and Extrusion, Clarendon Press, Oxford, (1993), s. 28.
[34] Rha, C., Theories and Principles of Viscosity Theory in Determination and Control of Physical Properties of Food Materials, Ed. Reidel, Inc. Dordrecht, The Netherlands, , s. 7-249, 1975.
[35] Götz, J., Kreibich, W. and Peciar, M., "Extrusion of pastes with a piston extruder for the determination of the local solid and fluid concentration, the local porosity and saturation and displacement profiles by means of NMR imaging", Rheol. Acta, 2002, 41(1-2), 134-143.
[36] Barnes, E.C., Wilson, D.I. and Johns, M.L., "Velocity profiling inside a ram extruder using magnetic resonance (MR) techniques", Chem. Eng. Sci., 2006, 61(5), 1357-1367.
[37] Bingham, E.C., Fluidity and Plasticity, McGraw-Hill, 1922.
[38] Metzner, A.B., Non-Newtonian Technology: Fluid Mechanics and Transfers, Adv. Chem. Eng., Acad. Pres, 1956.
[39] Casson, N., in: C.C. Mills (Ed.), Rheology of Disperse Systems, Pergam, 1959, p.84.
[40] Herschel, W., Bulkley, J., Test of Materials, Proc. Am. Soc., 26 (1926) 621.
[41] Rao, M.A., Tattiyakul, J., "Granul Size and Rheological Behaviour of Heated Tapioca Starch Dispersions", Carbohydr. Polym., 1999, 38, 123.

Received: **26.11.2015**
Accepted: **12.08.2016**

CORRESPONDING AUTHOR

Zurriye Gunduz
Balıkesir University
Engineering and Architecture Faculty
Environmental Engineering
Balıkesir - TURKEY

E-mail: zyilmaz@balikesir.edu.tr

© by PSP Volume 25 – No. 10/2016, pages 4184-4191 Fresenius Environmental Bulletin

THE INFLUENCE OF THE EM-A PREPARATION ON THE PROPERTIES OF STRUCTURE IN ARABLE MINERAL SOILS

Piotr Gajewski[1*], Zbigniew Kaczmarek[1], Wojciech Owczarzak[1], Bartłomiej Glina[1] Agnieszka Mocek – Płociniak[2], Eliza Gawęł[3], Mieczysław Grzelak[4], Dariusz Swierk[5]

[1]Poznań University of Life Sciences, Department of Soil Science and Land Protection, Poznań, Poland.
[2]Poznań University of Life Sciences, Department of General and Environmental Microbiology, Poznań, Poland.
[3]Department of Forage Crop Production, Institute of Soil Science and Plant Cultivation – State Research Institute, Puławy, Poland
[4]Poznań University of Life Sciences, Department of Grassland and Natural Landscape Sciences, Poznań, Poland.
[5] Poznań University of Life Sciences, Department of Landscape Architecture, Poznań, Poland.

ABSTRACT

The paper presents results of the research which tested the influence of two doses of activated form of microbial inoculants known as "Effective microorganisms" (EM-A) on the properties of epipedones of two lessive soils (Luvisols). "The soil primary aggregates models" (in the further text they are called "aggregates") in the form of intact soil cores of 1 cm^3 volume was taken (cut) from experimental fields in two consecutive years: 2008 and 2009. Apart from basic soil physical properties such as: texture, and porosity other soil traits as its static and dynamic water-resistance, secondary aggregation after static and dynamic water action, the compression strength of aggregates, maximal and minimal capillary water capacity, swelling of the aggregates and the speed of maximal and minimal capillary rise were also determined. The addition of EM-A into the soil had a visible, yet minor influence on parameters of the aggregate structure. The positive influence of EM-A addition on secondary aggregation, both after static and dynamic water action was noticed. In the case of other soil structure parameters, application of the EM-A preparation seems groundless.

KEYWORDS:
EM-A preparation, water resistance, secondary aggregation

INTRODUCTION

Microbial communities can be considered as architects of soils [1]. Other authors noticed that the soil matrix as well as chemical and physical properties of soils, like quality and amount of soil organic matter have an influence on the microbial communities [2]. What is emphasized in the literature, is the influence of microorganisms on the soil structure properties [3]. Schluz *et al*. [4] noticed a loss of soils quality. The authors underline a need to develop a strategies for sustainable protection of soils. Application of bio-fertilizers are frequently recommend for improving biological, and physical properties of soil as well as for sustainable agriculture. [5,6]. One of the world's most commonly used biofertilizers are effective microorganisms [7]. The author claims that EM is a specially selected composition of naturally occurring microorganisms. Among others, the inoculums consists of lactic acid bacteria, photosynthetic bacteria, actinobacteria and a filamentous fungus. The aim of the study was the assessment of the effects of EM-A preparation on the physical features of structure of two arable mineral soils under field conditions.

MATERIAL AND METHODS

The object of the research was an individual farm in Poland, in Małachowo (Wielkopolskie voivodeship, gnieźnieński district, 52°26′56″N, 17°44′51″E, Witkowo commune – 52°26′20″N, 17°46′27″E). The field experiment, was conducted in this farm, within its natural production cycle, in 2008 - and 2009 years. Two arable fields were used (field A and field B) which were located on broad areas of Luvisols. Texture of the arable-humus horizon of field A was characteristic to sandy loam (SL), whereas that of the corresponding level of field B – to loamy sand (LS) [8] (Table 1). In both experimental fields, (300m long and 60m wide), three stripes were marked: A0, A0+EM1, A0+EM2 and B0, B0+EM1, B0+EM2. Soil aggregates were collected from two depths: 7 and 20 cm.

A0 and B0 were the control areas – without EM-A addition. Two other stripes were sprayed with various doses of the preparation (EM-A = 1 dm^3 of EM1 concentrate + 1 dm^3 of treacle + 20 dm^3 of water). EM1 was produced by *Greenland*

TABLE 1
Texture of investigated soils

Soil	Depth (m)	Percentage content of fraction on diameter (mm):								Texture acc. FAO/USDA [8]
		2.0 - 0.50	0.50 - 0.25	0.25 - 0.10	0.10 - 0.05	0.05 - 0.02	0.02 - 0.005	0.005 - 0.002	< 0.002	
A	0.05-0.10	5.93	20.65	30.42	15	8	7	6	7	SL
	0.15-0.20	5.88	21.42	31.70	13	7	6	7	8	SL
B	0.05-0.10	8.12	25.61	31.27	12	7	7	4	5	LS
	0.15-0.20	9.08	26.56	29.36	13	6	8	4	4	LS

Technologies EM. In 2008 and 2009 the fields were sprayed with EM-A twice: in April, before sowing, and in October, before winter ploughing. On A0+EM1 and B0+EM1 stripes the dose of 100 dm^3 of EM-A/ha was applied, whereas on A0+EM2 and B0+EM2 stripes – of 200 dm^3 of EM-A/ha. Spraying was done with a sprayer of 1500 dm^3 capacity and <3atm pressure. In 2008, sugar beet was grown in field A, and spring barley in field B. In 2009 corn was grown on both fields. From each treatment intact soil cores, later called aggregates (diameter 11.28 mm, height 10 mm, volume 1 cm^3) were taken from two depths: 7 and 20 cm. In these cores, after air drying, the following parameters were determined [9]:

- static water resistance (SW) of soil aggregates was determined in a plastic container with nylon threads spread every 0.6 cm, on which aggregates was placed, and next the container was filled with water. The determination of this trait consists in the assessment of the breakup time [s] ("soaking time") of the aggregates submerged in the water.

- dynamic water resistance (DW) of soil aggregates was determined using a dynamic water resistance analyzer. The determination of this trait consists in the measurement of the energy needed to break up a soil aggregate by the impact of water drops of 0.05 g weight falling from the height of 1m at 1 second long intervals (kinetic energy of 1 drop – $E= 4.905 \cdot 10^{-4}$ J).

- the secondary aggregation following the dynamic (DSW) and static (ASW) water action was determined using the sieve method in the wet state on a set of sieves with mesh diameters: 7, 5, 3, 1, 0.5 and 0.25mm. The sieves were submerged in the water where, as the result of horizontal and vertical movements and then aggregates were segregated into fractions.

- the speed of water transfer within aggregates, their minimum (Vkmin) and maximum (Vkmax) capillary water capacity, and swelling (Pmin) of aggregates at Vkmin as well as swelling (Pmax) at Vkmax were determined on a filtration set placed on the Petri dish and flooded up with water to the level the filter paper. Swelling of aggregates was determined as the difference (+ or -) between capillary water capacities and porosities.

- the compression strength of aggregates (Rc) – determined by crushing method. The test consisted basically of crushing an individual aggregates between two flat parallel plates and recording the force required to break it.

Texture of aggregates were determined using Cassagrande method modified by Prószyński [10]; total porosity at: Rc (Pc1); DW (Pc2); SW (Pc3); Vkmax (Pc4); Vkmin (Pc5) from bulk and specific densities [11] The content of total carbon was determined with a Makro Elemental Analyzer (Vario Max CNS). The statistical analysis was conducted with Duncan's test at the statistical significance of $\alpha = 0.05$. The significance of differences between combinations deriving from a particular soil and depth and specific research year (eg. A07, 2008 or B020, 2009) was tested. This model was applied because of the large variability between individual properties of both soils (A and B) as well as depths (7 and 20 cm).

RESULTS AND DISCUSSION

Content of total carbon in both years ranged between 10.2 and 16.2 $g \cdot kg^{-1}$ (in soil A) and from 5.3 to 10.2 $g \cdot kg^{-1}$ (in soil B) (Figure 1). In most cases the addition of EM-A preparation significantly influenced on total C content in tested treatments. Although from practical agricultural point of view those changes could be recognized as negligible. Similar observations were also made by van Vliet *et al.* [12] Some authors, however, showed the decrease of organic matter after EM applications [13].

Only slight (although usually statistically significant) influence of the inoculums on porosity of aggregates was noticed. The variability of this parameter between the treatments within the individual soil was very small, regardless of the applied EM-A dose (Table: 2, 3, 4).

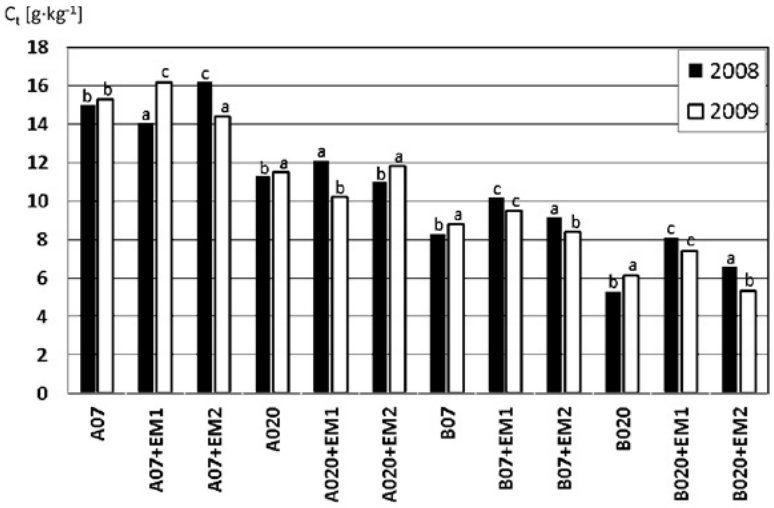

FIGURE 1
Content of the total carbon in years 2008-2009.
An explanation of abbreviations were given in the chapter: Material and Methods. Mean values with the same letter (a,b,c) do not differ significantly (see Material and Methods)

TABLE 2
Static resistance of aggregates models and their secondary aggregation.

Treatment	Poro-sity (Pc3) (%v/v)	Aggre-gates destru-ction time (s)	Content of various fractions of the secondary aggregates (%) Diameter of sieve (mm)						Percentage of aggregates > 0.25 mm
			7	5	3	1	0.5	0.25	
Year 2008									
A07	36.3a	147a	0.00a	0.00a	0.00a	2.71a	11.52b	36.01a	50.2a
A07+EM1	39.3c	191b	0.00a	0.00a	0.00a	4.90b	8.64a	39.12b	52.7b
A07+EM2	38.2b	249c	0.00a	0.00a	0.00a	5.49c	12.35c	36.14a	54.0c
A020	32.1a	90a	0.00a	0.00a	0.00a	2.93a	9.24a	38.71c	50.9a
A020+EM1	33.6b	104b	0.00a	0.00a	0.59b	3.42c	15.93c	33.53a	53.5b
A020+EM2	34.7c	212c	0.00a	0.00a	0.00a	3.28b	12.61b	38.05b	53.9b
B07	40.3a	131a	0.00a	0.00a	0.00a	4.47b	13.92b	35.76b	54.2a
B07+EM1	41.1b	143a	0.00a	0.00a	0.00a	3.12a	13.54a	38.06c	54.7a
B07+EM2	41.4b	160b	0.00a	0.00a	0.58b	6.27c	16.15c	34.02a	57.0b
B020	37.3a	180a	0.00a	0.00a	1.68c	3.61a	13.13a	34.47a	52.9a
B020+EM1	38.8c	196a	0.00a	0.00a	0.71b	4.69b	14.25b	34.73a	54.4b
B020+EM2	38.4b	219b	0.00a	0.00a	0.00a	7.88c	14.33b	34.33a	56.5c
Year 2009									
A07	37.4a	87a	0.00a	0.00a	1.59c	3.39a	7.42a	39.51b	51.9a
A07+EM1	40.8c	101b	0.00a	0.00a	1.15b	5.64c	18.68c	38.03a	63.5b
A07+EM2	38.9b	133c	0.00a	0.00a	0.00a	3.77b	17.64b	45.04c	66.5c
A020	35.9a	59a	0.00a	0.00a	0.43b	4.46c	15.73c	32.83a	53.5a
A020+EM1	37.4b	176c	0.00a	0.00a	0.00a	4.26b	9.39b	44.98b	58.6b
A020+EM2	38.2c	120b	0.00a	0.00a	0.77c	3.51a	8.45a	47.31c	60.0c
B07	40.7a	304c	0.00a	0.00a	0.32a	5.83b	2.42a	35.46b	44.0a
B07+EM1	41.8b	226b	0.00a	0.00a	0.55b	6.25c	7.01b	33.70a	47.5b
B07+EM2	42.6c	134a	0.00a	0.00a	0.67c	2.60a	11.36c	37.35c	52.0c
B020	36.1a	204b	0.00a	0.00a	2.61c	4.59b	9.24a	30.59a	47.0a
B020+EM1	39.2b	219c	0.00a	0.00a	0.84a	2.35a	14.77c	33.21b	51.2b
B020+EM2	41.4c	98a	0.00a	0.00a	1.53b	4.74b	11.80b	38.86c	56.9c

An explanation of abbreviations were given in the chapter: Material and Methods.
Mean values with the same letter (a,b,c) do not differ significantly (see Material and Methods)

One of the most important properties of an aggregate structure is the resistance of the aggregates to water action (water resistance). Under field conditions, a stable aggregate structure protects against excessive compaction, ensures a favorable content of capillary pores [14]. Water resistance markings are most often conducted measurements connected with the structure of soil's arable layer. Water action in the process of soil's aggregate structure devastation may occur either as dynamic (raindrops action) or static action – as a result of scouring and decomposition of flimsy soil nubs. Both types of destruction often occur simultaneously [9].

Water resistance to static water action in soil A ranged between 90s (A020) and 249s (A07+EM2) – in the first year of the study – and from 59s (A020) to 176s (A020+ EM1) – in the second year. Introduction of EM-A to soil A caused 2- or 3-fold significant increase of water resistance. In the case of soil B, an increase (up to 20%) of water resistance was observed only in the first year, but in 2009 a 2-fold decrease was found (Table 2) after the application of the higher dose of EM-A. Those differences were usually significant. Positive influence of soil microorganisms on soil structure's parameters was observed by Feeney *et al*. [15]. Oades [16] claimed that the impact of soil microorganisms on structure's state is more visible in soils with low content of colloids, where the influence of moisturization and drying as well as swelling and contraction processes is limited. Bonds between biomass of soil microorganisms and the stability of structures was also reported by Cosentino *et al*. [17]. Lynch and Bragg [18] tried to explain the mechanism of improvement of structure by microorganisms. These authors observed clear connection: soil microorganisms – organic matter – structure's state. They suggest that the positive impact of organic matter would not be visible without microorganisms. Moreover, they claim that a huge role in the stabilization of structure is also played by the mechanical actions of hypha.

TABLE 3
Dynamic resistance of aggregates models and their secondary aggregation also mechanical resistance of aggregates

Treatment	Poro-sity (Pc1) (%v/v)	Poro-sity (Pc2) (%v/v)	Com-pres-sion stren-gth of aggre-gates (MPa)	Dyna-mic resis-tance ($J \cdot 10^{-2}$)	Content of various fractions of the secondary aggregates (%) Diameter of sieve (mm)						Percen-tage of aggre-gates > 0.25 (mm)
					7	5	3	1	0.5	0.25	
Year 2008											
A07	34.1a	35.1a	0.98b	2.80c	0.00a	0.00a	0.78b	1.99a	11.97a	36.37b	51.1a
A07+EM1	37.9c	37.4b	0.56a	1.77a	0.00a	0.00a	0.00a	2.78b	14.46c	35.56a	52.8b
A07+EM2	34.8b	38.2c	0.84b	2.21b	0.00a	0.00a	0.00a	2.82b	13.75b	37.75c	54.3c
A020	30.7a	30.9a	1.21c	3.34c	0.00a	0.00a	0.49a	2.70a	9.53a	36.77b	49.5a
A020+EM1	34.5c	32.8b	0.67a	2.26a	0.00a	0.00a	0.59b	3.08b	10.26b	38.45c	52.4b
A020+EM2	33.6b	34.4c	0.95b	2.99b	0.00a	0.00a	0.93c	6.18c	12.93c	36.15a	56.2c
B07	39.8b	36.9a	0.25a	1.72ab	0.00a	0.00a	0.00a	3.67b	10.93a	27.34a	41.9a
B07+EM1	36.1a	38.0b	0.34b	1.86b	0.00a	0.00a	0.24b	2.65a	11.02a	29.63b	43.5b
B07+EM2	40.2b	40.3c	0.38b	1.52a	0.00a	0.00a	0.00a	2.70a	12.67b	32.23c	47.6c
B020	36.2a	36.1a	0.47a	1.96c	0.00a	0.00a	0.00a	2.76b	10.71a	31.33b	44.8a
B020+EM1	37.4b	37.6b	0.48a	1.67b	0.00a	0.00a	0.00a	3.39c	14.83c	26.92a	45.1a
B020+EM2	36.6a	37.3b	0.51a	1.47a	0.00a	0.00a	0.00a	2.45a	13.76b	32.17c	48.4b
Year 2009											
A07	32.7a	35.9a	0.88c	3.68b	0.00a	0.00a	1.80c	3.82b	6.37a	41.30a	53.3a
A07+EM1	34.6b	37.4b	0.75a	2.60a	0.00a	0.00a	0.46a	2.76a	9.32b	50.36c	62.9b
A07+EM2	33.1a	40.1c	0.84b	2.40a	0.00a	0.00a	0.69b	2.86a	12.63c	48.69b	64.9c
A020	32.4a	34.4a	1.14b	3.63c	0.00a	0.00a	1.07a	4.16b	6.72b	52.23c	64.2c
A020+EM1	34.3c	36.3b	0.87a	2.26b	0.00a	0.00a	1.37b	4.78c	9.06c	40.89a	56.1a
A020+EM2	33.2b	36.6b	0.91a	2.11a	0.00a	0.00a	1.52c	2.39a	5.97a	48.68b	58.6b
B07	37.4a	37.6a	0.32a	1.96a	0.00a	0.00a	0.33b	2.71a	6.40a	23.54a	33.0a
B07+EM1	38.6b	38.4b	0.37b	2.35c	0.00a	0.00a	0.00a	3.46b	7.14b	33.29c	43.9b
B07+EM2	37.8a	40.3c	0.39b	2.06b	0.00a	0.00a	2.41c	4.83c	8.62c	29.43b	45.3c
B020	36.4a	34.6a	0.52a	1.91a	0.00a	0.00a	0.00a	4.15b	6.89a	32.95a	44.0a
B020+EM1	37.4b	36.9b	0.54a	2.26b	0.00a	0.00a	1.20b	3.26a	7.17a	36.33b	48.0b
B020+EM2	37.2b	41.4c	0.58b	2.11b	0.00a	0.00a	1.68c	4.76c	8.33b	36.81c	51.6c

An explanation of abbreviations were given in the chapter: Material and Methods.
Mean values with the same letter (a,b,c) do not differ significantly (see Material and Methods)

Whereas, Chenu and Cosentino [19] reported a structure forming role of polysaccharides emitted by bacteria and fungi. According to these authors, these formations are "an aggregate bond" and enhance cohesion of aggregates. . They also claim that fungi enhance the growth of aggregates resistance to soaking, as they emit hydrophobic substances. Dynamic water action in field conditions has limited possibilities of destroying the aggregate structure as it is only limited to its devastating action on aggregates on the soil surface or in the uppermost soil layer. Aggregates dissoluted by raindrops take part in the development of a crust of low permeability [20]. It is a highly disadvantageous phenomenon as it may reduce infiltration and consequently increase erosion and soil degradation [21]. The resistance of aggregates to raindrops action also forms the state of erosion risk and superficial flow [22]. The application of EM-A to soil A caused a significant decrease of the dynamic water resistance, especially in 2009 (up to 40%). However, there was no clear trend in the case of soil B where a significant decrease up to 25% in 2008, but a significant increase up to 20% in 2009 were noticed (Table 3). Such an ambivalent "response" of the analyzed soils to the application of effective microorganisms might have result from numerous factors which form the activeness and, what follows, also the effectiveness of microorganisms in soils. Some authors notice that microorganisms act in little capacities ($1\mu m^3$) by forming the bond with the soil and their own life environment [23]. Its changes are followed by brisk changes in microbiological biodiversity [24, 25] and probably also in the influence of microorganisms on structure's properties.

The formation of secondary aggregation from the primary soil aggregates after dynamic water action is a very important phenomenon. When assessing the state of secondary aggregation, not only the total amount of water aggregates bigger than 0.25mm (so called state of original aggregates dissolution) should be considered. What is also crucial, is the way of the dissolution – percentage content of each fraction of emerging secondary aggregates [28]. The fraction – 0.5-0.25mm – was dominated in all combinations. Aggregates of A and B soils modified with EM-A doses – regardless of the year of conducted field research – dissolved as a result of water action and formed secondary aggregates of various diameters. In most of the examined treatments (except A020; 2009), EM-A addition led to percentage growth of the sum of secondary aggregates >0,25mm when compared it to the control. In 2008 it ranged from 3.32 to 6.70% (*av*.4,9) for EM1, and from 6.26 to 13.60% (*av*.10.3) for EM2. In 2009 the EM-A preparation increased the percentage of secondary aggregates from 9.09 to 33.03% (*av*.20.04) for EM1 and from 17.27 to 37.27 (av.25.5) for EM2 (Table 3). In most cases above mentioned differences were statistically significant.

Secondary aggregates are also produced as an effect of disintegration of original aggregates in water, under static water action. Also, in case of this type of water resistance, what is important in the assessment of the state of secondary aggregation, is both the stadium and the character of this dissolution, i.e. percentage content of each fraction. As a result of static water action on primary aggregates in soils A and B, the aggregates became dissolved (disintegrated) into secondary aggregates. In majority, this process resulted in the appearance of four different fractions of the secondary aggregates: 5-3mm; 3-1mm;1-0.5mm; 0.5-0.25mm. This tendency was visible in nearly all treatments in the second year and in four combinations in the first year of research. Positive influence of EM-A on percentage of soil in the form of secondary aggregates >0.25 mm could be observed in both years and both soils. An increase of percentage of secondary aggregates under the influence of EM-A addition in 2008, ranged from 0.92 to 5.1% (*av.* 3.5%) for EM1 and from 5.2% to 7. 6% (*av.* 6.4%) for EM2 (Table 2). In 2009 EM1 increased the percentage of secondary aggregates by 7.9-22.3% (*av.* 12.2%), and EM2 by 12.1-28.1% (*av.* 19.9%). In most cases above mentioned differences were statistically significant. This positive change, was probably a result of bonding microaggregates into macroaggregates. This phenomenon was described by Six *et al*. [26]. Six *et al.* [27] also tried to explain complicated mechanism of the formation of macroaggregates from microaggregates. According to the authors, an important role in the process is played by hyphae and polysaccharides produced (synthetized) by microorganisms.

Two types of inner forces (pulling and repulsive) act between soil particles as well as between the soil aggregates. Pulling and repulsive forces are equal when they act between two neighboring particles in a balanced state. When applying outer force tangent to the surface of their contact and causing resistance called the soil cohesion resistance, one moves the particles. The finer texture, the larger number of particles and bonds within a capacity unit – the stronger soil cohesion appears. Therefore, as a result of compression (squashing) force in the aggregate there are generated tensions which lead to its dissolution into smaller parts at a critical point [9]. A defined compression strength of aggregates in the examined treatments showed values typical for the soils of similar texture and genesis [28]. Changeability of these values as a result of the application of the tested inoculums, was minor.

TABLE 4
Minimum and maximum capillary water capacity of aggregates and their swell abilities

Treatment	Porosity (Pc5) (%v/v)	Porosity (Pc4) (%v/v)	Time of minimal capillary rise*(s)	Water capacity		Swelling of aggregates (%v/v)	
				Vkmin (%v/v)	Vkmax (%v/v)	Pmin	Pmax
Year 2008							
A07	35.9a	36,6a	65b	42,42c	55,24c	+6,52c	+18,64c
A07+EM1	39.3c	40,1c	55a	34,12b	55,16b	-5,18b	+15,06b
A07+EM2	38.2b	38,5b	76c	31,85a	50,06a	-6,35a	+11,56a
A020	34.0c	32,8a	90b	40,12c	57,11b	+6,12c	+24,31c
A020+EM1	33.6b	37,0c	68a	32,14b	57,76c	-1,46a	+20,76b
A020+EM2	32.8a	33,6b	88b	31,96a	53,84a	-0,84b	+20,14a
B07	37,4a	37,8a	34c	36,43b	41,13a	-0,97c	+3,33a
B07+EM1	39,7b	38,5b	28b	37,15c	50,35b	-2,55a	+11,85b
B07+EM2	39,7b	37,8a	24a	33,85a	53,62c	-5,85a	+15,82c
B020	37,0a	38,2c	25a	32,54a	47,10a	-4,46a	+8,90a
B020+EM1	38,5c	36,6b	24a	35,16b	52,38b	-3,34b	+15,78b
B020+EM2	37,8b	35,9a	32b	36,41c	52,56c	-1,39c	+16,46c
Year 2009							
A07	35.7a	34.6	71b	42.64c	56.24c	+6.94c	+21.64c
A07+EM1	38.4b	38.8b	53a	35.12b	55.93b	-3.28a	+17.13b
A07+EM2	35.7a	34.2a	84c	32.86a	50.83a	-2.84b	+16.63a
A020	33.5b	33.5a	88b	39.74c	57.74b	+6.28c	+24.24c
A020+EM1	33.8b	38.0c	66a	32.65b	59.25c	-1.15a	+21.25b
A020+EM2	32.9a	36.1b	93c	31.75a	51.33a	-0.25b	+15.23a
B07	38.8a	36.9a	42b	32.16a	41.81a	-6.64a	+4.91a
B07+EM1	39.2b	37.3a	31a	37.83c	50.62b	-1.37c	+13.32b
B07+EM2	39.9c	36.9a	34a	34.84b	54.13c	-5.06b	+17.23c
B020	36.9b	36.9c	32c	33.54a	48.08a	-3.36a	+11.18a
B020+EM1	37.6c	35.7b	26a	35.83b	52.68b	-1.77b	+16.98b
B020+EM2	36.1a	34,2a	29b	37.14c	52.94c	+1.04c	+18.74c

*the time of maximum capillary rise was assumed at 86400s
An explanation of abbreviations were given in the chapter: Material and Methods.
Mean values with the same letter (a,b,c) do not differ significantly (see Material and Methods)

However a significant decrease of this parameter was observed in soil A, whereas its significant increase (except B020; 2008) was visible in soil B (Table 3).

In order to conduct a complex analysis of physicochemical properties of soil aggregates, it is crucial to define such traits as: the speed of water flow in the aggregate, its minimal and maximal water capacity, and the capacity changes which may occur as a result of capillary rise. Filing an aggregate up to its minimal and maximal capacity occurs within a given period. It is marked as *Tkmin* for the minimal capillary rise and as *Tkmax* – for the maximal one [9]. The addition of the EM inoculum caused significant shortening of capillary rise after the application of the lower (smaller) dose of EM-A into soil A. When the larger dose was applied – the time of capillary rise was usually significant longer. In case of soil B, the addition of the inoculants caused irregular (normally significant) changes in the speed of capillary rise (Table 4). Such changes in the speed of water flow in an aggregate may prove major quality changes in the structure of differential porosity. In order to define the speed of water flow in the aggregate and its capillary water capacity, it is vital to define its minimal (Vkmin) and maximal (Vkmax) capillary water capacity of aggregates. During the analysis of Vkmin of the aggregates, the following directions of the discussed changes were observed. As a result of EM-A addition to soil A, the minimal capillary water capacity was lower than that in the control samples, in the case of both years and both soil depths (7 and 20 cm). At Vkmax of soil aggregates

collected from the depth of 7cm, in both years a drop of this property was observed when compared to Vkmax of a control sample (A07). Other, irregular (usually significant) changes occurred in Vkmax in aggregates collected from the depth of 20cm (Table 4). The positive influence of EM-A addition on Vkmax and Vkmin was also usually observed in the case of soil B. Whereas a positive influence of effective microorganisms on water retention capacity was observed by Valarini *et al.* [13].

During a capillary rise, soil aggregates are being moisturized gradually. The amount of absorbed water usually depends on such parameters as: moisture, compaction and texture. If the amount of absorbed water exceeds the original porosity of an aggregate, its capacity grows by the capacity which is a difference between the capacity of the absorbed water and the original capacity of aggregate's pores. The growth of the original capacity of an aggregate is called aggregates free swelling [9]. After the minimal capillary rise, aggregates swelled sporadically; the process occurred mainly in the aggregates collected from the control. Whereas in case of maximal capillary rise, almost all the aggregates swelled. After the application of EM-A, a significant decrease of swelling was observed in soil A, whereas its significant increase – in soil B (Table 4).

CONCLUSIONS

1. Application of EM-A into soils under field conditions had a visible yet minor influence on the parameters of the soil structure.

2. In most cases the addition of EM-A preparation significantly influenced on total C content in the tested treatments. Although from agricultural point of view those changes could be recognized as negligible.

3. The positive impact of EM-A addition on secondary aggregation both after static and dynamic water action should be emphasized. In the case of other soil structure's parameters, the inoculants application seems unjustified.

REFERENCES

[1] Rajendhran J. and Gunasekaran P. (2008) Strategies for accessing soil metagenome for desired applications. Biotechnol. Adv., 26, 576-590.

[2] Lombard N., Prestat E., van Elsas J.D. and Simonet P. (2011) Soil specific limitations for access analysis of soil microbial communities by metagenomics. FEMS, Microbiol. Ecol., 78, 31-49.

[3] Pirmordian N., Sepaskhah A.R., and Hajabbasi M.A. (2005) Application of fractal theory to quantify soil aggregate stability as influenced by tillage treatments. Biosyst. Eng., 90 (2), 227-234.

[4] Schulz S., Brankatschk R., Dümig A., Kögel-Knabner I., Schloter M. and Zeyer J. (2013) The role of microorganisms at different stages of ecosystem development for soil formation. Biogeosc., 10, 3983-3996.

[5] Singh J.S., Pandey V.C., Singh P.D. (2011) Efficient soil microorganisms: A new dimension for sustainable agriculture and environmental development (review). Agriculture, Ecosystem and Environment 140, 339-353.

[6] Dehghani I., Kordlaghari Panahi K. and Mohamadinia G. (2013) Effect of effective microorganisms activate (EMa) on growth, yield and components of corn in Firozabad region. Ann. of Biol. Res., 4 (4), 126-129.

[7] Higa T. (2002) Eine Revolution zur Rettung der Erde. Mit Effektiven Mikroorganismen (EM) die Probleme unserer Welt lösen. 4th edn. Organischer Landbauverlag, Xanten.

[8] FAO. (1977). Guidelines for soil profile description. Land and Water Development Division, FAO. Rome. 66 p.

[9] Rząsa S. and Owczarzak W. (1983) Modeling of soil structure and examination methods of water resistance, capillary rise and mechanical strength of soil aggregates. Ann. of Poznan Agriculture

[10] University, Scientific Disserations, 135p.

[11] Lamorski K, Bieganowski A. and Sławiński C. (2013) Soil data from Poland. In: European Hydropedological Data Inventory (Eds. Joint Research Centre of the European Commission). Institute for Environment and Sustainability, 80-82.

[12] Houšková M. (2013) Soil data from Slovakia. In: European Hydropedological Data Inventory (Eds. Joint Research Centre of the European Commission). Institute for Environment and Sustainability, 93-94.

[13] Van Vliet P.C.J., Bloem J. and de Goede R.G.M. (2006) Microbial diversity, nitrogen loss and grass production after addition of effective microogranisms (R) (EM) to slurry manure. Appl. Soil Ecol., 32, 188-198.

[14] Valarini, P.J., Alvarez, D., Gascó J.M., Guerrero F. and Tokeshi H. (2003) Assessment of soil properties by organic matter and EM-microorganism incorporation R. Bras. Ci. Solo, 27, 519-525.

[15] Paluszek J. (2013) Assessment of soil structure of Luvisols developed from loess classified in various complexes of agricultural suitability. Soil Scien. Ann., 64 (2), 41-48.

[16] Feeney D. S., Hallet. P.D., Rodger, S., Bengough, A.G. White N.A. and Young, I.M. (2006) Impact of fungal and bacterial biocides on microbial induced water repellency in arable soil. Geoderma, 135, 72-80.
[17] Oades J.M. (1993) The role of biology in the formation, stabilization and degradation of soil structure. Geoderma, 56, 377-400.
[18] Cosentino D., Chenu C. and Le Bissonnais Y. (2006) Aggregate stability and microbial community dynamics under drying- wetting cycles in a silt loam soil. Soil Biology. & Biochem., 38, 2053-2062.
[19] Lynch J.M. and Bragg E. (1985) Microorganisms and soil aggregate stability. Advan. in Soil Scien., 2, 133-171.
[20] Chenu C. and Cosentino D. (2011) Microbial regulation of soil structural dynamics. Ritz, K., Young, I.M. (ed). The architecture and biology of soils: life in inner space. CABI, Oxford University Press, chapter 3, 37-70.
[21] Green R.S.B. and Hairsine P.B. (2004) Elementary processes of soil-water interactions and thresholds in soil surface dynamics: a review. Earth Surface Processes and Landforms, 29, 1077-1091.
[22] De Pierri Castilho S.C., Cooper M. and Juhász C.E.P. (2011) Influence of crust formation under natural rain on physical attributes of soils with different textures. R. Bras. Ci. Solo, 35, 1893-1905.
[23] Fristensky A.J. and Grismer, M.E. (2009) Evaluation of ultrasonic aggregate stability and rainfall erosion resistance of disturbed and amended soils in the Lake Tahoe Basin, USA. Catena, 79, 93-102.
[24] Totsche, K.U., Rennert, T., Gerzabek, M.H., Kögel –Knabner I., Smalla, K., Spiteller M. and Vogel H.J. (2010) Biogeochemical interfaces in soil: The interdisciplinary challenge for soil science. J. of Plant Nutrition and Soil Scien., 173, 88-99.
[25] Sharma S., Mehta R., Gupta R. and Schloter M. (2012) Improved protocol for the extraction of bacteria mRNA from soils. J. of Microb. Meth., 91, 62-64.
[26] Simon C. and Daniel R. (2011) Metagenomic analyses: past and future trends Applied and Environmental Microbiology, 77, 1153-1161.
[27] Six, J., Elliott, E.T. and Paustian, K. (2000). Soil macroaggregate turnover and microaggregate formation: a mechanisms for sequestration under no tillage agriculture. Soil Biology & Biochem., 32, 2099-2103.
[28] Six J., Bossuyt, H., Degryze, S. and Denef K. (2004) A history of research on the link between (micro)aggregates, soil biota and soil organic matter dynamics. Soil & Till. Res., 79, 7-31.
[29] Rząsa S. Owczarzak W. (2004) The structure of the mineral soils. (in Polish). August Cieszkowski Agricultural University in Poznań Publisher. 394 p.

Received: **24.06.2015**
Accepted: **10.12.2015**

CORRESPONDING AUTHOR

Piotr Gajewski
Department of Soil Science and Land Protection University of Life Sciences ul. Szydłowska 50 60-656 Poznań Poland.

E-mail: gajewski@up.poznan.pl

© by PSP Volume 25 – No. 10/2016, pages 4192-4196 Fresenius Environmental Bulletin

DIFFERENTIAL RESPONSE OF GROWTH, PHOTOSYNTHETIC PIGMENTS AND ANTIOXIDANT ENZYMES TO UV-B RADIATION IN TOMATO (*SOLANUM LYCOPERSICUM* L.) SEEDLINGS

Kadriye Uruc Parlak*

Ibrahim Cecen University, Faculty of Arts and Sciences, Department of Moleculer Biology and Genetic, Agrı, TURKEY

ABSTRACT

The affect of UV-B radiation (UV-B, 280~320 nm) on growth, biochemical and antioxidant enzyme activity was investigated in tomato (*Solanum lycopersicum* L.). Tomato seedlings were grown on perlite in an 14 h day/10 h dark cycle for 2-8 days. The supplementary UV-B radiaiton significantly decreased the growth and chlorophyll amount. Enzymatic antioxidant system activity generally decreased after UV-B supplementation. Activation of APX in tomato increased in SOD activity, proline and TBARS contents. From the results obtained ROS accumulated despite higher engagement of the enzymatic antioxidant system, and that proline can protect cells against damage induced by ultraviolet radiation.

KEYWORDS:
Proline, lipid peroxidation, catalase, asorbate peroxidase, superoxide dismutase

INTRODUCTION

Increasing levels of ultraviolet-B (UV-B) radiation on the Earth's surface led to stratospheric ozone layer depletion [1,2]. A few studies have shown that additional UV-B radiation can harmfully influence physiological duration and extensive growth in several plant species [3,4]. Lately, Agrawal et al. (2004) informed the adverse effects of UV-B on various physiological and biochemical processes in two cultivars of *Triticum aestivum* L. leading to decrease in biomass and grain yield [5]. Composed of cells for example nucleic acids and proteins absorb this radiation, therefore biomass decrease, photosynthesis and other chloroplast functions damage, protein synthesis reduce and DNA is impaired [6-8].

Plants have improved distinctive mechanisms so they can prevent injuries, which changing ROS into less-toxic products. These defense mechanisms are based on metabolic compounds and enzymes [9, 10]. The present study was designed to investigate (I) chorophyll amounts and growth parameters (ii) markers of oxidative stress such as proline and TBARS contents, (iii) the activities of enzymatic antioxidants (SOD, CAT, and APX) in *S. lycopersicum*.

MATERIALS AND METHODS

Plant growth conditions and Photosynthetic pigments. The experimental material consisting of seedlings of *Solanum lycopersicum* grown on perlite under controlled growth conditions: 25°C, 14 h photoperiod, and 120 µmol m^{-2} s^{-1} photon flux density (400–700 nm). Ten-day-old seedlings were subjected to UV-B radiation supplied by Philips TL 20 W/01 RS lamps, max. 315 nm, 16 kJ m^{-2} day^{-1} intensity, for 8 h per day (3.25 µmol m^{-2} s^{-1} photon flux density) for 2–8 days. The amount of chlorophyll was determined according to the method described by Wintermans and De Mots (1965) [11].

Lipid peroxidation. The level of lipid peroxidation was estimated following the method of Razinger et al. (2008) with modifications [12].

Determination of catalase (CAT), superoxide dismutase (SOD) and ascorbate peroxidase (APX). CAT activity was measured according to Aebi method [13].

The activity of SOD (EC 1.15.1.11) was assayed by measuring the inhibition of the photochemical reduction of nitroblue tetrazolium (NBT) [14].

The APX activity was determined according to Nakano and Asada (1981) by the decrease in the absorbance of ascorbate at 290 nm [15].

Proline. The amount of proline was determined according to the method described by

TABLE 1
Effects of UV-B radiation on shoot length, fresh weight and dry weight in *Solanum lycopersicum* seedlings. Values are the mean±SE of three replicates. *Significant at the level of P < 0.05.

Day(s)	Treatments	Plant height (cm)	Fresh weight (g plant^{-1})	Dry weight (g plant^{-1})
2	Control	3.8±0.01	0.17±0.01	0.12±0.02
	UV-B	4.1±0.02	0.19*±0.01	0.13±0.02
4	Control	6.3*±0.03	0.26±0.02	0.18*±0.01
	UV-B	5.6±0.03	0.22±0.01	0.15±0.02
8	Control	9.1*±0.03	0.31*±0.02	0.21*±0.01
	UV-B	7.2*±0.03	0.26*±0.03	0.18*±0.03

Bates *et al*. (1973) [16].

Statistical analysis. Data were expressed as means ± standard error (SE) for UV-B radiation. Differences were analyzed with one-way of variance (ANOVA) and least significant difference Tukey test. *P* values of ≤ 0.05 were considered to be significant.

RESULT AND DISCUSSION

Growth Parameters and chlorophyll contents. After 2–8 days of UV-B treatment the shoot length, fresh weight and dry weight were reduced to 20.9%, 17.2% and 14.3% respectively (Table 1). In the study the supplemental UV-B radiation significantly reduced the chlorophyll content (20.1%) throughout the study period except during the initial period (Fig. 1.). Thus indicating a possible damage in the photosynthetic capacitiy of chloroplasts cause harm cell and tissue in the upper [17, 18]. Similar results were also reported by Feng et al (2007) and Krause et al. (2007) [19, 20].

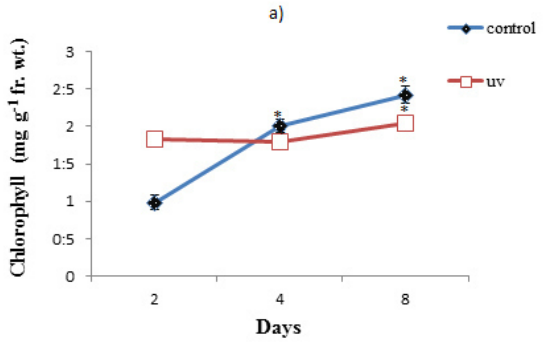

FIGURE 1
Effect of UV-B radiation on chlorophyll content in *Solanum lycopersicum* L. seedlings. Values are the mean±SE of 5 replicates. *Significant at the level of P < 0.05.

Effect of UV-B on lipid peroxidation. The level of malondialdehyde (MDA) is used to assess the extent of oxidative stress in plants, and its level is increased under stress conditions (Liu et al., 2009). The effect of UV-B on MDA content is presented in Fig. 2. According to control, the content of MDA was higher in *S. lycopersicum* seedlings subjected to 2, 4 and 8 day (Fig. 2). Cell membranes stability has been greatly used to discriminate stress tolerant and sensitive cultivars of many crops [22, 23] and in some cases higher membrane stability could be correlated with better performance [24].

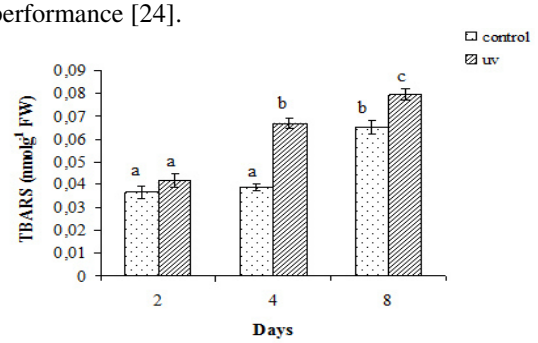

FIGURE 2
Effect of UV-B treatments on in *Solanum lycopersicum* L. seedlings lipid peroxidation. Values represent mean ± S.E. (n = 5). Different letters indicate significantly different values P < 0.05

Effect of UV-B on Enzymes (CAT, SOD and APX). Because of the fact that these enzymes acted as anti-oxidant compounds to reduce photo-oxidative damage in plant leaves, SOD, APX and CAT activities had been associated with UV-B exposure as well. Earlier studies results concerning the influence of UV-B radiation show that the antioxidant response have important differences between plant tissues and plant species [25-27]. CAT activity (about %50 rate) decreased with increasing of UV-B treatments in tomato seedlings. But this situation is different in controls (Fig. 3). A similar result was reported in the leaves of *T. chinensis* var. *mairei* by Gao and Zhang, the activity of CAT was slightly decreased by UV-B treatment [28].

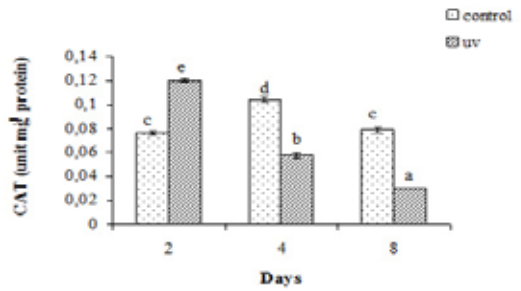

FIGURE 3
Effect of UV-B treatments on in *Solanum lycopersicum* L. seedlings CAT activities. Values represent mean ± S.E. (n = 5). Different letters indicate significantly different values P < 0.05.

The differences in superoxide dismutase (SOD) content between the control and the UV-B treatments were statistically significant ($p < 0.05$). SOD content differed between control and fourth day but the difference was not statistically (Fig. 4). SOD has implicated as essential defense mechanisms against the potent toxicity of oxygen [29]. The reduction was watched in SOD activity leading to O_2^- accumulation and so could be responsible for TBARS increase.

The activity of APX increased with rising UV-B radiation stress application time as compared with the controls in *S. lycopersicum* . However, the activity for *S. lycopersicum* has decreased on the eighth day compared with the fourth day activity (Fig. 5). CAT was significantly increased in the present study although APOX activity remained unaltered CAT has suggesting they have an important role in the control of endogenous H_2O_2 content. Activities of peroxidase-related enzymes and increases in reactive oxygen species by UV-B radiation have been sighted in several species involving sugar beet [30], *Arabidopsis thaliana* [31], *Anacystis nidulans* [32] and cucumber [33].

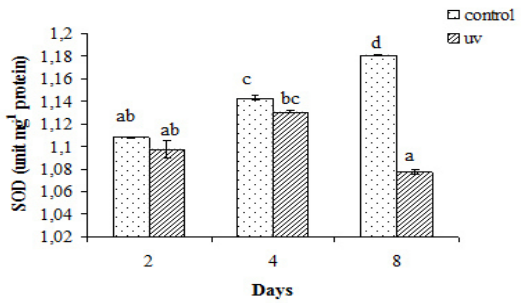

FIGURE 4
Effect of UV-B treatments on in *Solanum lycopersicum* L. seedlings SOD activities. Values represent mean ± S.E. (n = 5). Different letters indicate significantly different values P < 0.05

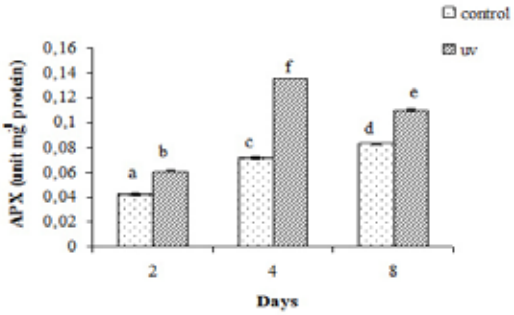

FIGURE 5
Effect of UV-B treatments on in *Solanum lycopersicum* L. seedlings APX activities. Values represent mean ± S.E. (n = 5). Different letters indicate significantly different values P <0.05

Effect of UV on Proline. In this study, the accumulation of proline increased with increasing of UV-B treatments in tomato seedlings. (Fig. 6). The existent binding is in acceptance with the results of Demir (2000) and Amal et al. (2006) [34, 35]. The important increase in proline contents was a significant cause for giving higher tolerance to plant species treated UV radiation.

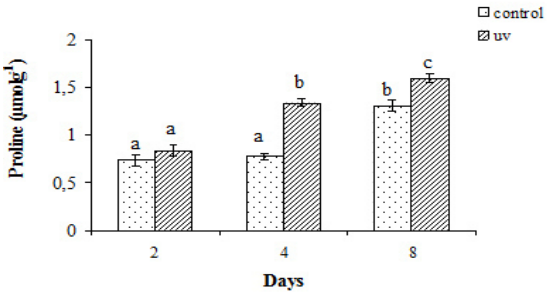

FIGURE 6
Effect of UV-B treatments on in *Solanum lycopersicum* L. seedlings proline. Values represent mean ± S.E. (n = 5). Different letters indicate significantly different values P < 0.05.

Our results show that after eight days of treatment, *S. lycopersicum* exhibits a different sensibility to supplemental UV-B radiation. UV-B adversely affected the growth parameters and photosynthetic pigments. UV-B radiation doses caused the antioxidant defenses, protecting the plant in contrast to major harmful effects of activated oxygen species. Then, thanks to these radicals augment in TBARS content harm was restricted. Despite the fact that SOD, CAT and APX activity decreased, the amount of proline in tomato seedlings increased.

ACKNOWLEDGEMENTS

This work was supported by Agrı Ibrahim Cecen University.

REFERENCES

[1] Aebi, H., 1984. Catalase in vitro. Methods Enzymol. 105, 121-176.

[2] Agrawal, S.B., Rathore, D., Singh, A., 2004. Combined effects of enhanced UV-B radiation and additional nutrients on two cultivars of wheat (*Triticum aestivum* L.). Physiol. Mol. Biol. Plants. 10, 99-108.

[3] Amal, A., Dina, Z., Abd Elghafar, M., 2006. Metabolic responses of soybean (*Glycine max*) plant to in increasing UV (A+B) radiation. Assiut. Univ. J. Bot. 35 (2), 107-125.

[4] Bates, L., Waldren, R.P., Teare, I.D., 1973. Rapid determination of free proline for water-stress studies. Plant and Soil. 39, 205-207.

[5] Beauchamp, C., Fridovich, I., 1971. Superoxide dismutase: improved assays and an assay applicable to acrylamide gels. Anal. Biochem. 44, 276-287.

[6] Caldwell, M.M., Bjorn, L.O., Bornman, J.F., Flinta, S.D., Kulandaivelu, G., Teramura, A.H., Tevini, M., 1998. Effects of increased solar ultraviolet radiation on terrestrial ecosystems. J. Photochem. Photobiol. B: Biol. 46, 40-52.

[7] Demir, Y., 2000. Growth and proline content of germinating wheat genotypes under ultraviolet light. Turk. J. Bot. 24, 67-70.

[8] Dohler, G., Drebes, G., Lohmann, M., 1997. Effect of UV-A and UV-B radiation on pigments, free amino acids and adenylate content of *Dunaliella tertiolecta* Butcher (Chlorophyta). J. Photochem. Photobiol. B: Biol. 40, 126–131.

[9] Feng, H., Shiwen Li., Xue L., An, L., 2007. Xunling wang, The interactive effects of enhanced UV-B radiation and soil drought on spring wheat, South African Journal of Botany, 73, 429-434.

[10] Frohnmeyer, H., Staiger, D., 2003. Ultraviolet-B radiation-mediated responses in plants. Balancing damage and protection. Plant Phys. 133, 1420-1428.

[11] Gao, Q., Zhang, L.X., 2008. Ultraviolet-B-induced oxidative stress and antioxidant defense system responses in ascorbate-deficient vtc1 mutants of *Arabidopsis thaliana*. J. Plant Physiol. 165, 138-148.

[12] Gonzáleza, J.A., Rosab, M., Parradoc, M.F., Hilalb, M., Prado, F.E., 2009. Morphological and physiological responses of two varieties of a highland species (*Chenopodium quinoa* Willd.) growing under near-ambient and strongly reduced solar UV-B in a lowland location. J. Photochem. Photobiol. B: Biol. 96, 144-151.

[13] Hou, W., Chen, X., Song, G., Wang, Q., Chang, C.C., 2007. Effect of copper and cadmium on heavy metal polluted water body restoration by duckweed (*Lemna minor*). Plant Physiol. Biochem. 45, 62-69.

[14] Iriti, M., Guarnieri, S., Faoro1, F., 2007. Responsiveness of *Lycopersicon pimpinellifolium* to acute UV-C exposure: histo-cytochemistry of the injury and DNA damage. Acta Biochim. Pol. 54, 273-280.

[15] Jordan, B.R., 1996. The effects of ultraviolet-B radiation on plants: a molecular perspective. Adv. Bot. Res. 22, 97-162.

[16] Kakani, V.G., Reddy, K.R., Zhao, D., Sailaja, K., 2003. Field crop response to ultraviolet-B radiation: a review. Agro. Forest Meterol. 120, 191-218.

[17] Krause, G.H., Jahns, P., Vigor, A., Garcia, M., Aranda, J., Wellmann, E., Winter K., 2007. Photoprotection, photosynthesis and growth of tropical tree seedlings under near-ambient and solar reduced solar ultraviolet-B radiation, Journal of Plant Physiology, 164, 1311-1322.

[18] Liu, Z.J., Zhang, X.L., Bai, J.G., Suo, B.X., Xu, P.L. and Wang, L. (2009) Exogenous paraquat changes antioxidant enzyme activities and lipid peroxidation in roughtstressed cucumber leaves. Sci. Hortic., 121, 138–143.

[19] Madronich, S., McKenzie, R.L., Caldwell, M.M., Bjorn,L.O., 1995. Changes in ultraviolet radiation reaching the earth's surface. Ambio. 24, 143-152.

[20] Malanga, G., Calmanovici G., Puntarulo, S., 1997. Oxidative damage to chloroplasts from *Chlorella vulgaris* exposed to ultraviolet-B radiation, Physiol. Plant 101, 455-462.

[21] Nakano, Y., Asada K. 1981. Hydrogen Peroxide is Scavenged by ascorbate-specific Peroxidase in Spinach Chloroplasts. Plant Cell Physiol. 22, 867-880.

[22] Premachandra, G.S., Saneoka, H., Kanaya, M., Ogata, S., 1991. Cell membrane stability and leaf surface wax content as affected by increasing water deficits in maize. J. Exp. Bot. 42, 167–171.

[23] Qaderi, M.M., Reid, D.M., 2005. Growth and physiological responses of canola (*Brassica napus)* to UV-B and CO_2 under controlled environment conditions. Physiol. Plant. 125, 247-259.

[24] Rathore, D., Agrawal, S.B., Singh, A., 2003. Influence of supplemental UV-B radiation and mineral nutrients on biomass, pigments and yield of two cultivars of wheat (*Triticum aestivum* L.). Int. J. Biotronics 32,1-15.

[25] Razinger, J., Dermastia, M., Koce, J.D.,

Zrimec, A., 2008. Oxidative stress in duckweed (*Lemna minor* L.) caused by short-term cadmium exposure. Environ. Pollut. 153, 687-694.
[26] Scandalios, J.G., 1993. Oxygen stress and superoxide dismutases. Plant Physiol. 101, 7-12.
[27] Scandalios, J.G., 2002. The rise of ROS. Trends in Biochemical Sciences. 27,483-486.
[28] Sudhakar, C., Lakshmi, A., Giridarakumar, S., 2001. Changes in the antioxidant enzyme activities in two high yielding genotypes of mulberry (*Morus alba* L.) under NaCl salinity. Plant Sci. 161, 613–619.
[29] Teramura, A.H., Sullivan, J.H.,1994. Effects of UV-B radiation on photosynthesis and growth of terrestrial plants. Photosynth. Res. 39, 463-473.
[30] Tevini, M., 2000. UV-B effects on plants. In: Agrawal S.B., Agrawal M. (eds), Environmental Pollution and Plant Responses. 83-97. Lewis Publishers, Boca Raton, U.S.A.
[31] Walz, C., Juenger, M., Schad, M., Kehr, J., 2002. Evidence for the presence and activity of a complete antioxidant defence system in mature sieve tubes. Plant J. 31, 189-97.
[32] Wintermans, J.F., De Mots, A., 1965. Spectrophotometric characteristics of chlorophylls a and b and their pheophytins in ethanol, Biochim. Biophys. Acta 109, 448-453.
[33] Xiong, F.S., Day, T.A., 2001. Effect of solar ultraviolet-B radiation during springtime ozone depletion on photosynthesis and biomass production of antarctic vascular plants. Plant Physiol. 125, 738-751.
[34] Yanarelli, G.G., Noriega, G.O., Batlle, A., Tomaro, M.L., 2006. Heme oxygenase up-regulation in ultraviolet-B irradiated soybean plants involves reactive oxygen species. Planta. 224, 1154-1162.

Received: **27.11.2015**
Accepted: **16.07.2016**

CORRESPONDING AUTHOR

Kadriye Uruc Parlak
Ibrahim Cecen University, Faculty of Arts and Sciences, Department of Moleculer Biology and Genetic, Agrı, TURKEY

e-mail: uruckadriye@gmail.com

© by PSP Volume 25 – No. 10/2016, pages 4197-4201 Fresenius Environmental Bulletin

NEAR-INFRARED SPECTROSCOPY ANALYSIS OF VFA IN ANAEROBIC BIOLOGICAL TREATMENT OF HIGH CARBON-NITROGEN WASTEWATER WITH INTERVAL PARTIAL LEAST SQUARES REGRESS

Jian Huang[1,2], Jian-yu Zhou[2], Qing-ye Sun[1,*], Hua Zhang[2], Yong Zhang[2], Meng Wang[2], Ling Ling[2]

[1]School of Resources and Environmental Engineering, Anhui University, Hefei, 230601, China
[2]Anhui Jianzhu University, Key Laboratory of Anhui Province of Water Pollution Control and Wastewater Reuse, Hefei, 230601, China

ABSTRACT

To realize the rapid detection of volatile fatty acids (VFA) in anaerobic biological treatment of high carbon nitrogen wastewater, the calibration model of VFA was established with interval partial least squares regress (IPLSR) based on the near-infrared spectroscopy technology in anaerobic sequencing batch reactor (ASBR). The running results of ASBR illustrate that COD concentrations of influent and effluent are 10250 mg·L^{-1}and 2100 mg·L^{-1}, and the removal rate of COD is 79.5%. The concentration of VFA keeps accumulating from 400 mg·L^{-1} to 508 mg·L^{-1} in 0~16 h, and decreasing from 508 mg·L^{-1} to 383 mg·L^{-1} in 16~96 h. The raw near-infrared spectra of water samples are preprocessed with wavelet threshold denoising method, and the redundant information is effectively removed. The calibration model of VFA is established with IPLSR method based on the preprocessed near-infrared spectra, the results show that the correction coefficient (r_c) of the calibration model of VFA is 0.9417 with root mean square errors of cross validation (RMSECV) being 0.5567. Consequently, the calibration model of VFA is tested, and the test result indicates that the prediction coefficient (r_p) is 0.9658 and the root mean square error of prediction (RMSEP) is 0.0942. The results show that the calibration model of VFA is effective on prediction of VFA concentration. This study will provide theoretical basis and technical support for the rapid detection of VFA concentration using near-infrared spectroscopy.

KEYWORDS:
Interval partial least squares, near-infrared spectroscopy, high carbon-nitrogen wastewater, anaerobic sequencing batch reactor, volatile fatty acids.

INTRODUCTION

High carbon-nitrogen wastewater has such characteristics as high COD, high nitrogen and difficult biodegradability. Volatile fatty acid (VFA), produced in the treatment of high carbon-nitrogen wastewater, has important indication function for the stable operation of anaerobic sequencing batch reactor (ASBR)[1]. Excessive accumulation of VFA may inhibit the activity of methanogens in anaerobic reaction, and further influence normal operation of the process[2-3]. In addition, chemical measure method of VFA concentration is complex, energy-intensive, and easily causes new environmental pollution[4]. Therefore, establishing timely and accurate measure method of VFA concentration is very important, which can not only effectively understand the process of organic degradation, but also timely regulate the operation of ASBR.

Near-infrared spectroscopy is an excellent technique in water quality measurement, which is characterized with high efficiency, non-pollution, and low cost[5-8]. Previous studies have shown that the composition and concentration of chemical substances can be quantitatively analyzed with multivariate statistical analysis methods based on near-infrared spectroscopy [9-12]. However, these researches mainly focus the substances in nature water, manual configuration water, and treated effluent, but related researches in the whole process of wastewater treatment have been less reported relatively. Especially, the study on rapid measurement of VFA concentration in the process of ASBR has been seldom reported with multivariate statistical analysis methods based on near-infrared spectroscopy.

Near-infrared spectroscopy can reflect the chemical composition and concentration of the chemical substances, but it can be influenced by the physical properties such as viscosity, particle size, density and so on. In order to improve the accuracy of model predictions, raw near-infrared spectra needs to be preprocessed before establishing quantitative analytical model of some chemical substances, which aimed to remove the redundant information and get more useful spectral data in modeling. Researches show that wavelet threshold

denoising method is an effective method of spectrum preprocessment[13].

In this work, the method of wavelet threshold denoising is used to preprocess the raw near-infrared spectra, and then the preprocessed spectra are divided into a number of intervals. Then interval partial least squares regress (IPLSR) is utilized for regression analysis in every interval, and obtaining a number of regression models and corresponding root mean square errors of cross validation (RMSECV). After that, the interval with the minimum RMSECV is selected as spectrum band of high signal to noise ratio (SNR). The quantitative analytical calibration model (hereafter refers to calibration model of VFA) for rapid detection the concentration of VFA is developed in high SNR spectrum band with IPLSR in the process of ASBR. In addition, the accuracy of the calibration model of VFA is also tested and the feasibility and validity of the model in the process of ASBR was further discussed.

EXPERIMENTAL MATERIALS AND ANALYTICAL METHODS

Experimental materials and water quality. The reactor, made of organic glass, has an available volume of 6.3 L. The influent flow was controlled by a peristaltic pump, and the mixture of wastewater and active sludge was achieved by the magnetic stirring machine at the bottom of the reactor. The temperature was maintained at 34℃ in the reactor, and the oxidation reduction potential was observed on-line. The experimental cycle was 96 h, during which the influent flow was 2.1 L/h, and the drainage ratio was one third. Water sample was collected every 8 h in a cycle.

The composition of original wastewater quality was illustrated by the following elements: COD, 10250 $mg \cdot L^{-1}$; total nitrogen, 320 $mg \cdot L^{-1}$; ammonia nitrogen, 280 $mg \cdot L^{-1}$, pH, 7.1. The sludge that inoculated in the reactor was taken from the anaerobic sludge pool of a sewage treatment plant.

Instruments and detection methods. COD is measured by fast digestion-spectrophotometric method, ammonia nitrogen is measured by nessler's reagent spectrophotometry, total nitrogen is measured by alkaline potassium persulfate digestion UV spectrophotometric method, pH is measured by pH meter and VFA is measured by gas chromatography. Near-infrared spectroscopy is detected by transform infrared spectrometer (Germany), the scanning wave number range and resolution are 4000-12500 cm^{-1} and 8 cm^{-1}. The gas chromatography is Agilent 6890N (USA), whose chromatographic column model is DBFFAP. The samples are all filtered by 0.45 μm filters before detected by gas chromatography and near-infrared spectroscopy.

Method of establishing and testing the calibration model of VFA. The 84 water samples were collected from 7 stable cycles in ASBR, in which 60 water samples (in 5 stable cycles) were used as calibration set to establish the calibration model of VFA, and 24 water samples (in 2 stable cycles) were used as test set to test the accuracy of the calibration model of VFA. Each water sample was divided into two groups, one group was measured to get VFA concentrations with chemical method by gas chromatography, and the VFA concentrations were used as concentration matrix in modeling; The other group was used to get raw near-infrared spectral data, and then the raw near-infrared spectra were preprocessed with wavelet threshold denoising method, these preprocessed spectral data were used as absorbance matrix. The calibration model of VFA, between the concentration matrix and absorbance matrix, was established by IPLS method using the calibration set. The calibration model of VFA was evaluated through RMSECV and correlation coefficient (r_c).

The calibration model of VFA was further tested in 24 water samples from other operational cycle time. The preprocessed spectral data of 24 samples were input the calibration model of VFA, and then the validity of the calibration model of VFA was evaluated by the root mean square error of prediction (RMSEP) and correlation coefficient (r_p).

RESULTS AND ANALYSIS

Changes of COD, ammonia nitrogen, total nitrogen and VFA in stable cycle. Figure 1 shows the changes of COD, ammonia nitrogen, total nitrogen during the stable cycles in ASBR. COD concentration in the influent is 10250 $mg \cdot L^{-1}$, which dramatically reduces to 2100 $mg \cdot L^{-1}$ after 90 h, with the COD removal rate of 79.5%. It indicates that ASBR has good degradation ability for high carbon-nitrogen wastewater. Meanwhile, the concentration of ammonia nitrogen in the effluent is 344 $mg \cdot L^{-1}$, which increases by 23%. The increase of ammonia nitrogen concentration is due to the deamination reaction of organic nitrogen in wastewater under anaerobic conditions. In most cases, anaerobic reactor faces the risk of acidification in high concentration wastewater treatment, but ammonia nitrogen can be used as buffer material of pH regulation by neutralizing a part of VFA, which is conducive to the anaerobic reaction, and can reduce the dosage of alkalinity.

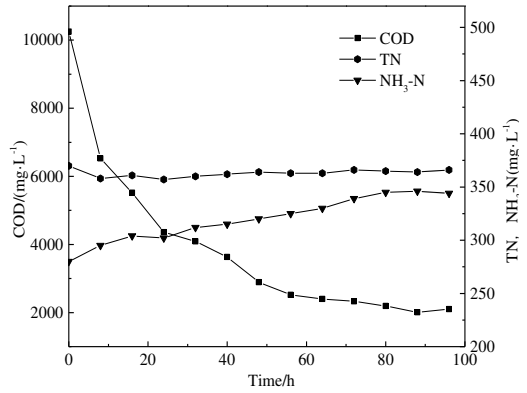

FIGURE 1
Changes of COD, ammonia nitrogen, total nitrogen in stable cycle.

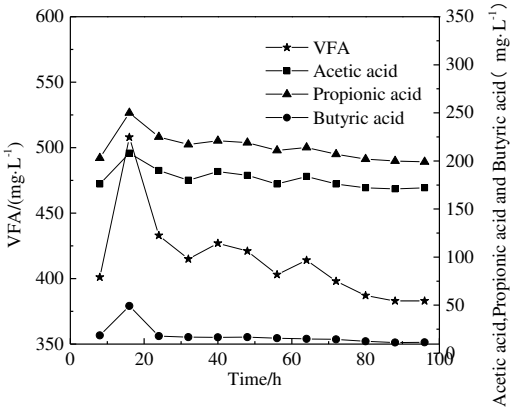

FIGURE 2
Change of VFA in stable cycle.

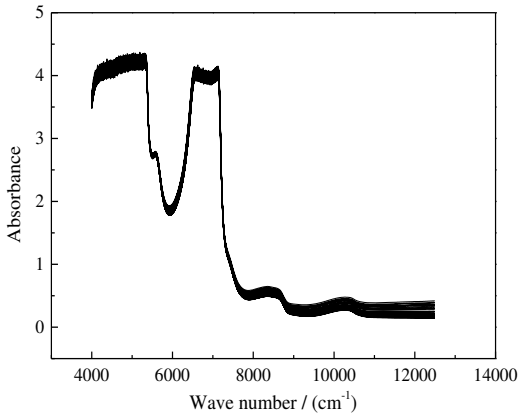

FIGURE 3
Raw near-infrared spectra of water samples.

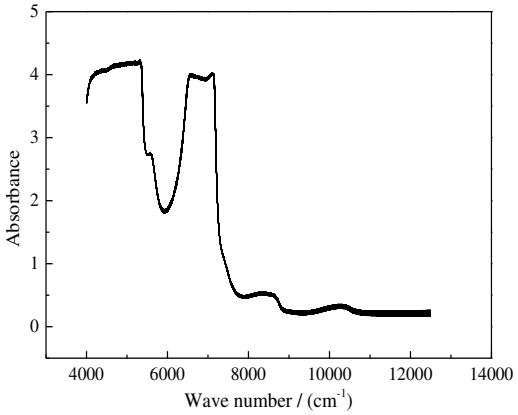

FIGURE 4
Spectra after filtering noise.

Figure 2 shows the change of VFA concentrations (calculated as acetate acid) in ASBR. The concentration of VFA keeps accumulating from 400 mg·L^{-1} to 508 mg·L^{-1} with fermentation reaction in 0~16 h, and decreasing from 508 mg·L^{-1} to 383 mg·L^{-1} in 16~96 h with the reaction proceeding. This indicates that acid-produced reaction is obvious in 0~16 h, and then VFA is consumed by methanogen with hydraulic detention time increasing.

Near-infrared spectra of water samples. Figure 3 shows raw near-infrared spectra of 60 water samples collected in five stable cycles. These near-infrared spectroscopic absorption data are extract in the full wavelength range of 4000~12500 cm^{-1} (every 3.858 cm^{-1} is recorded). Each spectrum shows the same trend, however, the noisy parts mainly locate in wavelength of 4000~5200 cm^{-1} and 6300~7200 cm^{-1}. Therefore, in order to improve the accuracy and stability of the calibration model of VFA, it is necessary to preprocess the raw near-infrared spectra and exclude the redundant information before establishing the calibration model of VFA.

The preprocessed near-infrared spectra with wavelet threshold denoising method are shown in Figure 4. From Figure 4, the preprocessed spectra can be seen smoother than raw spectra, while the shapes of the spectra are not changed obviously, these show that the effective information of the raw spectra is preserved.

Establishment of the calibration model of VFA. In order to select high SNR interval, the full wavelength of preprocessed spectra are divided into 20 intervals. Each of the first 19 intervals contains 110 data and the last interval contains 113 data. After that, IPLS is used for regression analysis in each interval, as shown in Figures 5 and 6. By IPLS command 20 IPLS models are calculated, all of which are cross validated and mean centered, and then up to 8 PLS components (PLSC) are calculated (Figure 5), a minimum RMSECV is seen in a global model. The IPLS plots are made for the global model (Figure 6). As shown in figure 6, the optimal number of PLSC and consequent RMSECV in each internal are shown with italic numbers on each bar, and the RMSECV of the global model with 8 PLSC is shows in dotted lines. As seen from Figure 6, the

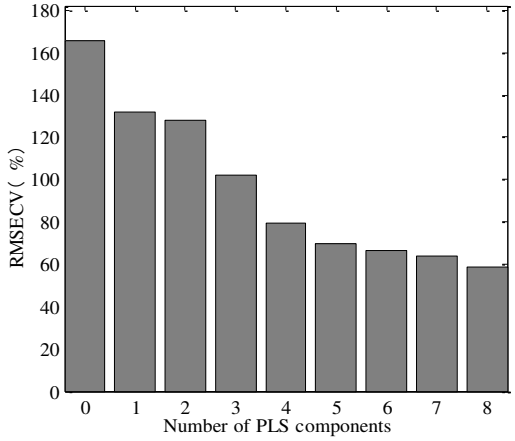

FIGURE 5
RMSECV of different PLS component.

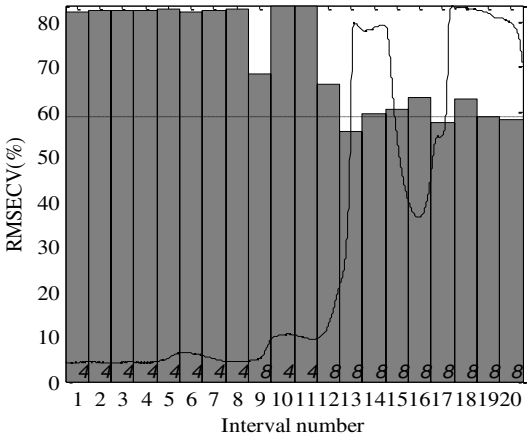

FIGURE 6
RMSECV of each interval in iPLS.

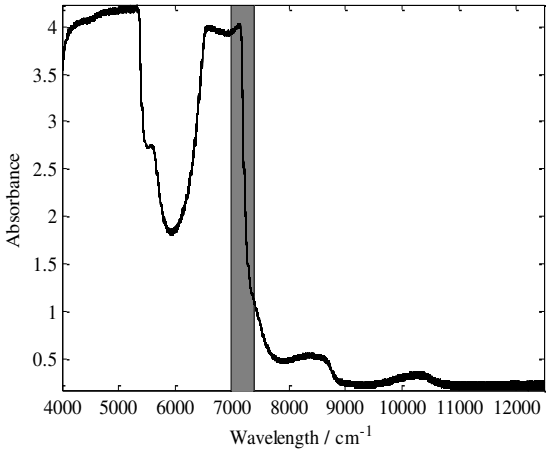

FIGURE 7
Wavelengths of interval number 13.

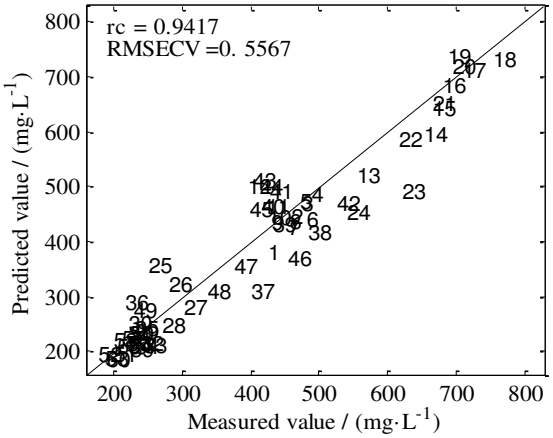

FIGURE 8
Establishment of the calibration model of VFA.

plot interval 13 performs better than the global model. So interval 13 with the minimum RMSECV is selected as high SNR interval to establish calibration model. Horizontal ordinate can be expressed with wavelengths as shown in Figure 7, the main wavelength range of interval 13 locates in 6969.87~7390.3 cm^{-1}.

The calibration model of VFA is established in high SNR interval, as shown in Figure 8. The correction coefficient (r_C) and consequent RMSECV of the model is 0.9417 and 0.5567, which shows better correlations between the measured values of VFA and the calibration values of VFA.

Test of the calibration model of VFA. In order to test the accuracy of the calibration model of VFA, the 24 water samples taken from two stable cycles are used as test set. The predicted results of VFA by the calibration model of VFA are shown in Figure 9. As seen from Figure 9, the predicted values of VFA fit well with the measured values, with r_p=0.9658, RMSEP=0.0942. It shows that the calibration model of VFA is feasible for the rapid detection of VFA concentration.

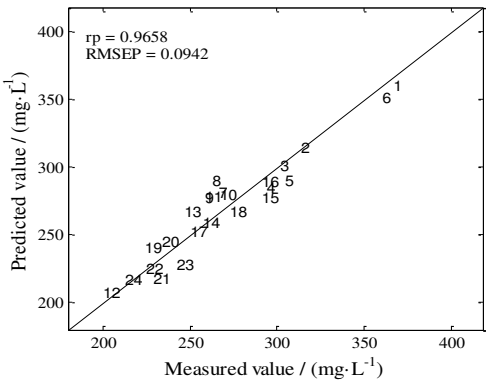

FIGURE 9
Test of calibration model of VFA.

CONCLUSION

The results show that steady and good treatment efficiency are achieved in treating high carbon-nitrogen wastewater with ASBR. The concentration of COD significantly reduces from 10250 $mg \cdot L^{-1}$ to 2100 $mg \cdot L^{-1}$ with removal rate of

79.5%. The concentration of VFA keeps accumulating from 400 mg·L^{-1} to 508 mg·L^{-1} with fermentation reaction in 0~16 h, and decreasing from 508 mg·L^{-1} to 383 mg·L^{-1} with methanation reaction in 16~96 h.

Raw near-infrared spectra of VFA are pretreated with wavelet threshold denoising method, the preprocessed spectra are smoother than raw near-infrared spectra, which can effectively remove the redundant information. The calibration model of VFA is established with IPLS, the correction coefficient (r_C) and consequent RMSECV of the model is 0.9417 and 0.5567. The results show better correlations between the measured values of VFA and the calibration values of VFA.

Near-infrared spectroscopy of 24 water samples are used to test the calibration model of VFA, the result shows that the predicted values of VFA have good correlation with the measured values of VFA, the correction coefficient (r_p) and consequent RMSECP of the model is 0.9658 and 0.0942. The result indicates that the calibration model performs better in the prediction of VFA.

ACKNOWLEDGEMENTS

The Natural Science Project for Colleges of Anhui Province (KJ2016A817), Major Science and Technology Program for Water Pollution Control and Treatment of China (2014ZX07405-003-03).

REFERENCES

[1] Ingrid H. Franke W, Andreas W ,Christian Ebner,Heribert Insam. (2014) Investigation into the effect of high concentrations of volatile fatty acids in anaerobic digestion on methanogenic communities. *Waste Management*, 34(11):2080–2089.

[2] Xiao K K , Guo C H, Zhou Y, et, al. (2016) Acetic acid effects on methanogens in the second stage of a two-stage anaerobic system. *Chemosphere*, 2016, 144:1498–1504.

[3] Smola N , Urleb U. Qualitative and quantitative analysis of oxytetracycline by near-infrared spectroscopy. *Analytica Chimica ACTA,* 2000, 410(1-2): 203-210.

[4] Yu L, Mahesh B, Ma J W, Zhao Q B. (2014) Craig Frear, Shulin Chen. Enhancing volatile fatty acid (VFA) and bio-methane production from lawn grass with pretreatment. *Bioresource Technology*, 162:243–249.

[5] Helena I. Mota,Maria Joana Neiva Correia,,João C.M. (2015) Bordado. Multivariate near infrared spectroscopy models to monitor polycondensation production process reactions. *European Polymer Journal*, 66(3): 12–17.

[6] Chen T, Chang Q R, Clevers L. (2015) Kooistra. Rapid identification of soil cadmium pollution risk at regional scale based on visible and near-infrared spectroscopy. *Environmental Pollution*, (11):217–226.

[7] Yu X. Liu Q. Wang Y. B. et, al. (2016) Evaluation of MLSR and PLSR for estimating soil element contents using visible/near-infrared spectroscopy in apple orchards on the Jiaodong peninsula. *CATENA*, 137(2):340-349.

[8] Boyan K, Tekin Y, Abdul M. (2015) Comparison between artificial neural network and partial least squares for on-line visible and near infrared spectroscopy measurement of soil organic carbon, pH and clay content. *Soil and Tillage Research* Part B, (3): 243–252.

[9] Liu H X, Zhang J, Wang B G, et al. (2009) No-chemical monitoring and fast analysis on total nitrogen in water. *Optics and Precision Engineering*, 17(3): 525-530.

[10] Liu H X, Zhang J, Wang B G, et al. (2008) Investigation on the non-chemical method for monitoring total phosphate in water, *Journal of Analytical Science*, 24(6): 664-666.

[11] Li H, Yao Z X, Li G L, et al. (2011) Determination of COD in biological and chemical wastewater by near infrared spectrometry. *Chinese Journal of Spectroscopy Laboratory*, 28(6): 3040-3043.

[12] Zhang G L, Li D, Zhang X J, et al. (2014) Delay aeration effect on low temperature ammonia nitrogen SBR nitrosation and recovery. *China Environment Science*, 34(8): 1998-2002.

[13] Li T H, Shi G Y, Wei M, et al. (2013) Wavelet denoising in prediction model of tomato vitamin C content using NIR spectroscopy. *Transaction of the Chinese Society for Agricultural Machinery*, 44(z1): 200-204.

Received: **08.01.2016**
Accepted: **12.08.2016**

CORRESPONDING AUTHOR

Qing-ye Sun
School of Resources and Environmental Engineering
Anhui University
Hefei, 230601 - CHINA

E-mail: sunqingye@ahu.edu.cn

© by PSP Volume 25 – No. 10/2016, pages 4202-4208 Fresenius Environmental Bulletin

NaCl PRIMING ALLEVIATES THE INHIBITING EFFECT OF SALINITY DURING SEEDLING GROWTH OF PEAS (*PISUM SATIVUM* L.)

Bulent Senturk, H Ozkan Sivritepe*

Department of Horticulture, Faculty of Agriculture, Uludag University,Gorukle Campus, Nilufer, Bursa 16059, Turkey

ABSTRACT

This study was conducted to determine the availability of NaCl priming for increasing salt tolerance at different viability levels and to evaluate the effects of NaCl priming on emergence and seedling establishment of peas (*Pisum sativum* L.) grown under long term salinity conditions. Seeds of pea 'cv. Bolero' were divided into two parts. The first part of the seed was reserved as the original (*i.e.*, the high viability seed lot). The low viability seed lot was obtained by ageing the seeds for 5 days at 60°C. Then, the seeds were primed with 150 mM NaCl for 2 days at 16°C. After priming, seeds were dehydrated for 50 hours at 20°C until the original seed moisture content was reached. Non-primed and primed seeds were sown in plastic trays. The trays were irrigated with 5 different saline solutions (0.3, 2.0, 4.0, 6.0 and 8.0 dSm^{-1}). Increasing salinity levels negatively affected growth of the seedlings derived from both high and low viability seeds. However, in each viability and salinity level, NaCl priming diminished the inhibiting effect of salinity on growth of pea seedlings. Total emergence, germination index, seedling vigour index, chlorophyll content, leaf relative water content, seedling length and dry weight of plants derived from primed seeds tended to be higher than those of the non-primed ones. Primed seeds emerged faster and therefore decreased mean emergence time. Then all the parameters were correlated with total emergence to determine a useful indicator for peas. The highest correlation was obtained between total emergence and emergence index.

KEYWORDS:
Seed viability, priming, salinity, seedling emergence and correlation matrix.

INTRODUCTION

Salinity is one of the major problems that adversely affect production of most crops worldwide [1] and which lower physiological processes resulting as reduced growth and yield in plants [2, 3]. Plant salt tolerance is a complex phenomenon and it depends on different factors [4]. Increased tolerance to salinity stress in crop plants is necessary in order to increase productivity with limited water supplies and high salinity. There are many investigations with the degree of salt tolerance and the associated mechanisms in different crops, e.g., cucumber [5], pea [6], radish [7], turnip [8] and eggplant [9].

One of the mechanisms plants used to withstand salt stress is by regulating osmotic potential of the cell, especially if salinity increase gradually from mild stress to severe one. It has been reported that the seedlings derived from primed seeds emerge faster, grow more vigorously and perform better under sub-optimal conditions. Like many other leguminous crops, the production of pea is affected by salinity stress [10]. Low osmotic potential, salt stress, nutritional facts, or a combination of these three adversely affect growth [11, 12].

Seed priming is a well-known pre-germination strategy that improves seed performance and seedling quality. Seed priming technique has been used to accelerate synchronized seed germination, improve seedling establishment and stimulate vegetative growth and crop yield. Seed priming, especially with NaCl, has improved germination and growth of many crops under salinity stress conditions [13, 14, 15, 16, 17, 18].

It is known that the plants are able to develop adaptive response to salinity not only during the first phases of germination, but also during the seedling growth stage [16]. However, the beneficial effects of NaCl priming on field performance of peas under salinity stress has not yet been investigated. Therefore, this research was conducted to determine the availability of the NaCl priming for increasing the salt tolerance of high and low viability seed lots and to evaluate the effects of NaCl priming on the emergence and seedling establishment of peas (*Pisum sativum* L.) grown under long term salinity conditions.

MATERIALS AND METHODS

Seeds of pea 'cv. Bolero' (obtained from MayAgro Seed Corporation in Bursa, Turkey) were used in this study. In order to compare the effects of salinity in high and low viability seeds, the original seed lot was divided into two parts. The high viability seed lot was maintained as the original (*i.e.*, 92.5% normal germination). The low viability seed lot (*i.e.*, 82.0% normal germination) was obtained by ageing the seeds in hermetically sealed laminated aluminium foil packets for 5 days at 60°C. The viability levels of the non-aged and aged seeds were determined by germination tests at 20°C according to the ISTA Rules [19]. Before starting the experiments, seeds were sterilized with 5% NaOCl for 10 min. Then they were washed for 3 min with tap water and rinsed with distilled water.

Priming Treatments. Pea seeds were primed with 150 mM NaCl solution for 2 days at 16°C as described by Senturk and Sivritepe [20]. After priming, seeds were put in a wire mesh strainer and washed with tap water for 3 min and then rinsed with distilled water. Following this, seeds were dehydrated for 50 hours at 20°C until the original seed moisture content was reached.

Growing of Seedlings in the Greenhouse. Non-primed (NP) and primed (P) seeds were sown in plastic trays (40 x 30 x 10 cm) filled with a mixture of soil, sand, sphagnum peat and farmyard manure (2:1:1:1, v/v). The trays were placed in an unheated polyethylene greenhouse where temperature ranged between 16 to 25°C and seedling growth period continued until the flowering stage for a period of 6 weeks. There were 4 replicates in each treatment group and 50 seeds in each replicate. The trays irrigated with 5 different saline solutions, which were derived from tap water by the use of NaCl. Electrical conductivities at 25°C of five salinity levels were 0.3, 2.0, 4.0, 6.0 and 8.0 dS m^{-1}. The trays were irrigated every other they (*i.e.*, when the soil water content decreased) during seedling growth period. Leaching fraction about 30% ensured that the EC of the drain water (that was monitored) was practically the same as the EC of the salinity treatments. The fertigation solutions were applied by the use of a commercial water-soluble fertiliser (Nutribella 20-20-20 NPK, Turkey).

Measurements. The trays were inspected daily and seedling emergence recorded. Total number of emerged seedlings in each replicate was determined and evaluated as percentage, in calculation of total emergence (TE).

Mean emergence time (MET) was calculated according to the equation of Ellis and Roberts [21]:

$MET = \sum Dn / \sum n$

n: The number of seeds germinated on day D
D: Days counted from the beginning of germination

Emergence index (EI) was calculated according to the equation of Copeland and McDonald [22]:

$EI = \sum n / d$

n: The number of normal seedlings on day D
d: Days counted from the beginning of germination

Seedling vigour index-1 (SVI-1) was calculated by the equation of Butola and Badola [23]:

SVI-1= MDW / MET x 100

MDW: Mean dry weight per seedling (mg)
MET: Mean emergence time (day)

Seedling vigour index-2 (SVI-2) was calculated by the equation of Abdul-Baki and Anderson [24]:

SVI-2 = (RL + SL) x TE

RL: Root length (cm)
SL: Shoot length (cm)
TE: Total emergence (%)

Seedlings were harvested after 6 weeks, in order to evaluate their response to salinity. At harvest, the plants were dissected into shoots and roots. Shoot length (SL), root length (RL) and total seedling length (TSL) of each plant were also recorded. Then all the samples were dried at 70°C for 24 hours to a constant weight and the dry matter of shoots (SDW), roots (RDW) and total seedling (TSDW) were recorded. Fully-expanded mature leaves from the mid-shoot area of each sampled plant were measured 2 days before plant harvesting. Chlorophyll content (CC) was measured with a portable leaf chlorophyll meter (SPAD-502, Minolta) and the data represented were the means of ten readings from each sampled plant of each replicate. Measurements of leaf relative water content (LRWC) were calculated according to Yamasaki and Dillenburg [25].

Statistical Evaluations. The layout of the experiment was a Factorial Randomised Plots Design. All the results were subjected to a three way ANOVA (NaCl concentration x Seed viability level x NaCl priming). For discrimination of significant differences, means were compared by LSD test at $P \leq 0.05$. Then all the parameters were subjected to correlation matrix analyses. JMP 7.0 software was used in all the analyses.

RESULTS AND DISCUSSION

Salinity is a major abiotic stress factor that seriously decreases productivity in arid and semi-arid regions of the world. On the other hand, decrease in viability causes a delay in metabolic activities of seeds. However, salt tolerance could be increased by NaCl priming of seeds before sowing [20]. Seed priming with NaCl stimulates the germination by regulating some metabolic activities. In general, increase in NaCl levels and decrease in seed viability cause reductions in

TABLE 1
The effects of NaCl concentrations, initial seed viability and NaCl priming on total emergence (TE), mean emergence time (MET), emergence index (EI), seedling vigour index-1 and 2 (SVI-1 and SVI-2), chlorophyll content (CC) and leaf relative water content (LRWC) of pea seedlings.

NaCl Conc. (dS m^{-1})	Viability	NaCl Priming	TE (%)	MET (days)	EI	SVI-1	SVI-2	CC (SPAD)	LRWC (%)
0.3	High	NP	84.5 bc*	11.3 j	15.2 b	4749.9 c	54.7 b	46.4 b	92.3 ab
		P	89.0 a	10.4 l	17.5 a	5918.2 a	62.2 a	47.8 b	94.5 a
	Low	NP	73.5 fgh	12.6 e	11.9 fgh	3904.5 f	45.7 d	41.1 ef	85.9 def
		P	79.5 de	11.7 hi	13.7 c	4815.9 c	53.9 bc	43.2 de	90.8 b
2.0	High	NP	83.0 bcd	12.2 gh	13.8 c	3974.3 f	51.8 bc	47.0 b	86.8 de
		P	86.5 ab	10.4 l	17.1 a	5215.2 b	58.9 a	52.0 a	93.3 a
	Low	NP	70.0 hi	12.6 e	11.3 gh	3449.3 h	41.2 ef	45.8 bc	84.3 efg
		P	79.5 de	12.2 gh	13.4 cd	4165.2 e	50.3 c	50.3 a	92.1 ab
4.0	High	NP	77.0 ef	12.5 ef	12.5 ef	3150.1 j	42.4 def	39.4 f	85.9 def
		P	82.0 cd	11.0 k	15.3 b	4343.1 d	50.6 bc	44.2 cd	92.3 ab
	Low	NP	64.0 j	12.9 cd	10.1 i	2633.9 l	32.3 h	34.0 hij	83.7 fg
		P	72.5 gh	12.3 g	12.1 fg	3616.5 g	38.6 fg	36.8 g	87.8 cd
6.0	High	NP	73.0 fgh	13.1 c	11.3 gh	2834.7 k	34.9 gh	35.6 ghi	82.8 gh
		P	76.0 efg	12.0 h	13.0 de	3719.8 g	43.2 de	37.3 g	90.0 bc
	Low	NP	51.5 l	12.8 cd	7.8 k	2640.1 l	22.7 i	31.8 kl	82.1 gh
		P	65.5 j	13.3 b	10.3 i	3285.2 ij	31.3 h	36.9 g	86.2 de
8.0	High	NP	66.5 ij	13.3 b	10.1 i	2609.4 l	25.3 i	33.9 ijk	80.8 h
		P	72.0 gh	12.7 de	11.5 gh	3233.1 i	33.4 h	36.0 gh	83.3 g
	Low	NP	46.5 m	13.6 a	6.9 l	2303.7 m	15.7 j	30.3 l	80.3 h
		P	58.5 k	13.3 b	8.8 j	2871.7 k	24.6 i	33.2 jk	82.4 gh

* Values not associated with the same letter are significantly different (P≤ 0.05).

physiological parameters such as seedling emergence, leaf characteristics, root and shoot lengths and dry weights. However, in the present study, it was also concluded that NaCl priming alleviated the inhibiting effects of salinity during seedling emergence and growth. The effects of NaCl concentrations, initial seed viability, NaCl priming and their interaction were significant on total emergence, mean emergence time, emergence index, seedling vigour indexes (SVI-1 and SVI-2), chlorophyll content and leaf relative water content (Table 1).

Salinity delayed or inhibited seed germination and seedling growth by creating low osmotic potential in irrigation water. Total emergence of seedlings derived from both NP and P seeds decreased with increasing NaCl salinity and low viability. However, this reduction in total emergence was higher for NP seeds, compared to P seeds. Meanwhile, total emergence in seedlings of the P group at each salinity and viability level was higher than those of the NP ones. The beneficial effect of NaCl priming on TE was more obvious in low viability than in high viability seed groups. P groups had lower MET compared with NP groups. Increased NaCl concentrations and low viability caused an increase in MET of seedlings derived from NP and P seeds. Previous works have proved that salinity causes a decrease or a delay in germination of seeds and emergence of seedlings [26, 27]. Primed seeds has better efficiency for water absorption from growing mixture [28, 29]. Also priming can homogenize seed germination in a short period of time and metabolic activities commence much earlier [12, 15, 16, 30]. Our results show that in pea seedlings TE decreases while MET increases due to the effect of increasing NaCl salinity and decreasing viability levels.

The emergence index reflects the speed and uniformity of seedling emergence. In primed groups, EI was significantly higher than those of the non-primed ones under salinity stress conditions. Moreover, sharp decreases in EI were observed above 4.0 dSm^{-1} treatment groups. The EI decreased with the effect of low viability and increasing salinity concentrations.

The seedling vigour index can be defined as representation of the germination capacity and growing tendency of seedlings. Similar results in seedling vigour index by dry weights (SVI-1) and seedling vigour index by lengths (SVI-2) were obtained under different concentrations of NaCl and viability levels. Vigour of seedlings derived from both NP and P seeds decreased with increasing NaCl salinity and low viability. However, this reduction in vigour was higher for NP groups compared to P groups.

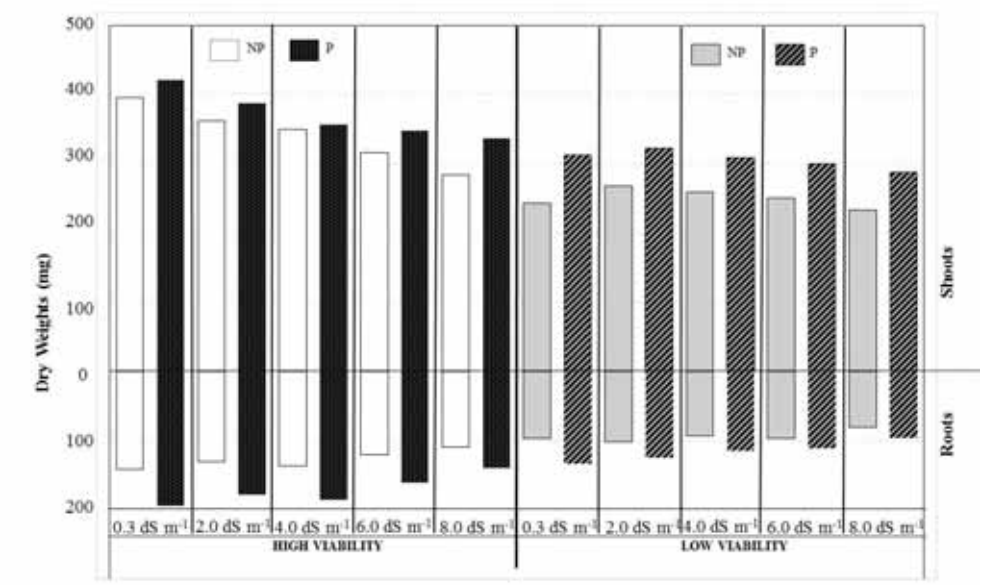

FIGURE 1
The effects of NaCl concentrations, initial seed viability and NaCl priming on root dry weight and shoot dry weight of pea seedlings.

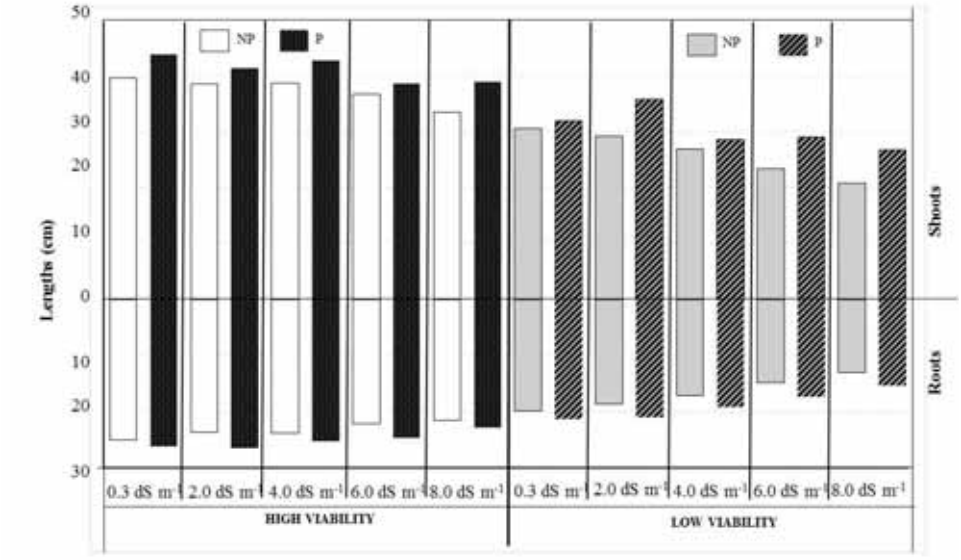

FIGURE 2
The effects of NaCl concentrations, initial seed viability and NaCl priming on root length and shoot length of pea seedlings.

Sharp decreases in SVI-1 were observed above 4.0 dSm^{-1} treatment groups. The trend of SVI-2 values were also similar to SVI-1. These findings further indicate that the seedlings derived from P seeds had higher seedling vigour indexes than those of the NP ones under saline conditions.

In order to maintain seedling quality, chlorophyll and leaf relative water contents were observed in pea seedlings. Salt stress affects physiological growth parameters and water status in leaves [31, 32, 33]. Probably the osmotic adjustment was not sufficient to avoid NaCl stress in pea seedlings derived from NP seeds. Thus, there was a decrease in chlorophyll and leaf relative water contents. The relative chlorophyll content of leaves increased up to 2.0 dSm^{-1} salinity in all groups. The injurious effect of salinity started with the 4.0 dSm^{-1} treatment. However, it was more destructive in low viability groups. The P groups resulted in higher relative chlorophyll content of leaves in each salinity and viability level. Contrarily, increasing NaCl salinity and low viability caused significant decreases in leaf relative water contents.

Mineral nutrient uptake and ion contents can be altered in plants with the effect of salinity. Thus, length and biomass reduction can be attributed to mineral nutrient deficiency. Salinity reduces

TABLE 2
The correlation matrix arranged by the use of different physiological parameters of pea seedlings affected by NaCl concentrations, initial seed viability and NaCl priming.

	TE	MET	EI	SVI-1	SVI-2	CC	LRWC	SL	RL	TSL	SDW	RDW	TSDW
TE	1.00												
MET	-0.83	1.00											
EI	0.96	-0.94	1.00										
SVI-1	0.83	-0.94	0.92	1.00									
SVI-2	0.94	-0.88	0.95	0.91	1.00								
SPAD	0.81	-0.79	0.83	0.83	0.87	1.00							
LRWC	0.77	-0.87	0.84	0.87	0.83	0.78	1.00						
SL	0.79	-0.81	0.83	0.95	0.88	0.80	0.80	1.00					
RL	0.81	-0.88	0.88	0.96	0.89	0.84	0.85	0.89	1.00				
TSL	0.82	-0.86	0.87	0.98	0.91	0.84	0.84	0.98	0.96	1.00			
SDW	0.85	-0.83	0.87	0.88	0.97	0.84	0.80	0.87	0.87	0.89	1.00		
RDW	0.81	-0.77	0.81	0.84	0.93	0.81	0.77	0.84	0.84	0.87	0.92	1.00	
TSDW	0.85	-0.82	0.87	0.88	0.97	0.85	0.80	0.87	0.87	0.90	0.99	0.97	1.00

biosynthesis of phytohormones [18] and causes a decrease in photosynthetic activities by lowering plant height and biomass [34]. Total height and biomass of seedlings derived from both NP and P seeds decreased with low viability and increasing NaCl salinity. However, this reduction was higher for NP groups, compared to P groups (Figures 1 and 2). Our results are in parallel to those of Conrath et al. [35] who reported that the primed plants display a faster and stronger activation to various abiotic stresses.

On the other hand, in this study, vigour of pea seedlings has been assessed through mean emergence time, emergence index, seedling vigour index by dry weights (SVI-1) and seedling vigour index by lengths (SVI-2). Moreover, the important growth parameters such as chlorophyll content and leaf relative water content of pea seedlings were investigated. Then the results of these physiological parameters were correlated with total emergence (Table 2). The highest correlation value was observed between TE and EI as 0.96. On the other hand, SVI-2, SDW, TSDW, MET and SVI-1 were also good indicators of pea seedling emergence, respectively.

CONCLUSIONS

In conclusion, previous works suggest that long-term NaCl stress produces irreversible effects on germination, emergence, growth, chlorophyll content, leaf water relations and seedling vigour. However, the information was lacking with regard to the comparative evaluation of the mechanisms for high and low viability seed lots subjected to NaCl priming that triggers the changes in the processes of seedling emergence and growth under saline conditions. The results of the present study showed for the first time that in different seed viability levels, seed priming with NaCl can markedly improve seedling emergence and early seedling growth of pea under long term salinity. Therefore, NaCl priming could serve as a promising method to increase salt tolerance of peas during seedling stage. Our studies are in progress to investigate the possible beneficial effects of NaCl priming in the later growth and development stages of pea plants under long term salinity.

ACKNOWLEDGEMENTS

We are highly indebted to Uludag University Scientific Research Projects Unit [UUBAP -Project №: OUAP (Z) 2012/6] for their financial support. We are grateful to MayAgro Seed Corporation in Bursa, Turkey for supplying seeds of pea 'cv. Bolero'.

REFERENCES

[1] Ashraf, M. 2009. Biotechnological approach of improving plant salt tolerance using antioxidants as markers. Biotechnol. Adv., 27: 84-93.

[2] Ashraf, M., Harris P.J.C. 2004. Potential biochemical indicators of salinity tolerance in plants. Plant Sci., 166: 3-16.

[3] Munns, R., Tester M. 2008. Mechanisms of salinity tolerance. Annu. Rev. Plant Biol., 59: 651-681.

[4] Ashraf, M., Akram N.A., Arteca R.N., Foolad M.R. 2010. The physiological, biochemical and molecular roles of brassinosteroids and salicylic acid in plant processes and salt

tolerance. Crit. Rev. Plant Sci., 29: 162-190.
[5] Shi, K., Huang Y.Y., Xia X.J., Zhang Y.L., Zhou Y.H., Yu J.Q. 2008. Protective role of putrescine against salt stress is partially related to the improvement of water relation and nutritional imbalance in cucumber. J. Plant Nutr., 31: 1820-1831.
[6] Noreen, Z., Ashraf M. 2009a. Assessment of variation in antioxidative defense system in salt treated pea (*Pisum sativum* L.) cultivars and its putative use as salinity tolerance markers. J. Plant Physiol., 166: 1764-1774.
[7] Noreen, Z, Ashraf M. 2009b. Changes in antioxidant enzymes and some key metabolites in some genetically diverse cultivars of radish (*Raphanus sativus* L.). Environ. Exp. Bot., 67: 395-402.
[8] Noreen, Z., Ashraf M., Akram N.A. 2010. Salt-induced regulation of some key antioxidant enzymes and physio-biochemical phenomena in five diverse cultivars of turnip (*Brassica rapa* L.). J. Agron. Crop Sci., 196: 273-285.
[9] Abbas, W., Ashraf M., Akram N.A. 2010. Alleviation of salt-induced adverse effects in eggplant (*Solanum melongena* L.) by glycinebetaine and sugarbeet extracts. Sci. Hort., 125: 188-195.
[10] Maas, E.V. 1990. Crops salt tolerance. Agriculture Salinity Assessment and Management. American Society Civil Engineers, In: K.K. Tanji, New York. p. 262-334.
[11] Ashraf, M. 1994. Breeding for salinity tolerance in plants. Crit. Rev. Plant Sci., 13(1): 17-42.
[12] Zhu, J.K. 2002. Salt and drought stress signal transduction in plants. Annu. Rev. Plant Biol., 53:247–273
[13] Passam, H.C., Kakouriotis D. 1994. The effects of osmoconditioning on the germination, emergence and early plant growth of cucumber under saline conditions. Sci. Hort., 57: 233-240.
[14] Sivritepe, H.O., Eris A., Sivritepe N. 1999. The effects of priming treatments in melon seeds. Acta Hortic., 492: 287–295.
[15] Sivritepe, N., Sivritepe H.O., Eris A. 2003. The effects of NaCl priming on salt tolerance in melon seedlings grown under saline conditions. Sci. Hort., 97: 229–237.
[16] Sivritepe, H.O., Sivritepe N., Eris A. and Turhan E. 2005. The effect of NaCl pre-treatments on salt tolerance of melons grown under long-term salinity. Sci. Hort., 106: 568-581.
[17] Ashraf, M., Foolad M.R. 2005. Presowing seed treatment, a shotgun approach to improve germination, growth and crop yield under saline and non-saline conditions. Advances in Agronomy, 88: 223-271.
[18] Cuartero, J., Bolarin M., Asins M.J. and Moreno V. 2006. Increasing salt tolerance in the tomato. J. Exp. Bot., 57: 1045-1058.
[19] ISTA. 2012. International Rules for Seed Testing. Edition 2012. International Seed Testing Association, Bassersdorf, Switzerland.
[20] Senturk, B. and Sivritepe H.O. 2015. Determination of Optimum Protocol for NaCl Priming in Pea (*Pisum sativum* L.) Seeds. J. Agric. Fac. Uludag Univ., 29(2): 95-105.
[21] Ellis, R.H., E.H. Roberts. 1981. The Quantification of ageing and survival in orthodox seeds. Seed Sci. Technol., 9: 373-409.
[22] Copeland, L.O. and McDonald M.B. 2001. Principles of seed science and technology. Kluwer Academic Publishers, Norwell, MA.
[23] Butola, J.S., Badola H.K. 2004. Effect of pre-sowing treatment on seed germination and seedling vigour in *Angelica glauca*, a threatened medicinal herb. Current Science, 87(6): 796-799.
[24] Abdul-Baki, A.A. and Anderson J.D. 1973. Vigor determination in soybean by multiple criteria. Crop Sci., 13: 630-633.
[25] Yamasaki, S. and Dillenburg L. R. 1999. Measurements of leaf relative water content in *Araucaria angustifolia.* Revista Brasileira de Fisiologia Vegetal, 11(2):69-75.
[26] Levitt, J. 1980. Responses of plants to environmental stresses Volume II. (Physiological Ecology), Academic Pres, New York. p. 365-490.
[27] Franco, J.A, Esteban C., Rodriguez C. 1993. Effects of salinity on various growth stages of muskmelon 'cv. Rev'. J. Hort. Sci., 68(6): 899-904.
[28] Hopper N.W., Overholt J.R., Martin J.R. 1979. Effect of cultivar, temperature and seed size on the germination and emergence of soy beans (*Glycine max* L. Merr.). Ann. Bot., 44: 301-308.
[29] Bajehbaj, A.A., 2010. The effects of NaCl priming on salt tolerance in sunflower germination and seedling grown under salinity conditions. African J. Biotechnol., 9: 1764-1770.
[30] Khaje-Hoseini M, Powell A.A., Bingham I.J. 2003. The interaction between salinity stress and seed vigour during germination of soybean seeds. J. Seed Sci. Technol, 31:715-725.
[31] Alarco´n, J.J., Sa´nchez-Blanco M.J., Bolari´n M.C., Torrecillas A. 1993. Water relations and osmotic adjustment in *Lycopersicon esculentum* and *L. pennellii* during short-term salt exposure and recovery. Physiol. Plant., 89: 441-447
[32] Ortiz, A., Martinez V., Cerda´ A. 1994. Effects of osmotic shock and calcium on growth and solute composition of *Phaseolus vulgaris* plants. Physiol. Plant., 91: 468-476.

[33] Torrecillas, A, Guillaume C., Alarco´n J.J., Ru´iz-Sa´nchez M.C. 1995. Water relations of two tomato species under water stress and recovery. Plant Sci., 105: 169-176.
[34] Afkari B.A., Qasimov N., Yarnia M. 2009. Effects of drought stress and potassium on some of the physiological and morphological traits of sunflower (*Helianthus annuus* L.) cultivars. J. Food Agric. Environ., 7 (3&4): 132-135.
[35] Conrath, U., Beckers G.J.M., Flors V., García-Agustín P., Jakab G., Mauch F., Newman M.A., Pieterse C.M.J., Poinssot B., Pozo M.J., Pugin A., Schaffrath U., Ton J., Wendehenne D., Zimmerli L., Mauch-Mani B. 2006. Priming: getting ready for battle. Mol. Plant-Microbe Interact., 19: 1062-1071.

Received: **04.12.2015**
Accepted: **17.06.2016**

CORRESPONDING AUTHOR

H. Ozkan Sivritepe
Department of Horticulture, Faculty of Agriculture, Uludag University, Gorukle Campus, Nilufer, Bursa 16059, Turkey

E-mail: ozkan@uludag.edu.tr

© by PSP Volume 25 – No. 10/2016, pages 4209-4216 Fresenius Environmental Bulletin

COMPARATIVE INFLUENCES OF ORGANIC AND CONVENTIONAL HAZELNUT ORCHARD ON THE SOIL WATER CONTENT, ELECTRICAL CONDUCTIVITY, AND TEMPERATURE IN WESTERN BLACK SEA REGION OF TURKEY

Selcuk Ozmen[1,2,*]

Düzce University, Department of Biosystem Engineering, 81620, Düzce, Turkey
University of California, Department of Agricultural and Biological Engineering, 95616, Davis, CA, USA

ABSTRACT

The present study aimed to investigate the comparative influences of organic and conventional hazelnut orchard on soil water content (SWC), electrical conductivity (SEC), and temperature (ST) in Western Black Sea Region of Turkey. SWC, SEC and ST variations were monitored hourly between 3 July and 3 September 2014 at four soil layers (0-30, 30-60, 60-90 and 90-120 cm) under the canopy of selected trees for the both orchards by using ECH_2O-5TE probe. The results show that the values of SWC and SEC at each soil layer were higher in conventional treatment of hazelnut orchard than organic treatment used hazelnut orchard during Julian days. However, organic treatment of hazelnut orchard has higher ST values at each soil layer except at 0-30 cm soil layer. It can be concluded that the hazelnut orchard under the organic treatment consumes more water from soil or has higher evapotranspiration rates. Therefore, organic agriculture could be a productive alternative for development of reduced irrigation strategies in the regions in higher rainfall.

KEYWORDS:
ECH_2O-5TE probe, hazelnut tree, organic agriculture, Black Sea Region of Turkey

INTRODUCTION

Hazelnut (*Corylus avellana L.*) is an important product in Turkey since about 80% of the world total 878 ha of hazelnut orchard area is in Turkey. Moreover, Turkey has been the largest hazelnut exporter in the world with exports total of $ 2.0 billion in 2014 [1]. Most of hazelnut trees are fed by rain especially in the Black Sea Coast Region in Turkey. Düzce Province located in the Western Black Sea Region of Turkey is one of the most important areas in terms of hazelnut production with approximately 10% of total hazelnut area of Turkey [2]. Hazelnut orchards are mostly grown under the conventional conditions with a seldom practice of organic farming in Düzce Province as well as other areas in Turkey. Organic products are being grown in the total area of 842 ha with 208 different varieties in Turkey. Hazelnut is one of the most important organic exports products with 11% of total organic exports product of Turkey [3]. Organic hazelnut farming areas are cited inadequate to meet the demand in Turkey despite the rich ecologically suitable natural background for organic farming [4, 5].

There are a number of problems in conventional agriculture, such as excessive inputs of chemical fertilizers, soil degradation, frequent pesticide applications, and the presence of pesticide residues in food. Therefore, organic farming was offered as an alternative process to overcome these challenges [6]. Organic farming has gained importance and expanded in the last decade in parallel to the environmental, economic and social concerns in the world [7].

Soil moisture content measurement is one of the most important abiotic factors to determine plant growth and water regime in the soil profile [8]. Moreover, Qiu et al. [9] has identified that soil moisture is also a key factor to identify infiltration, surface runoff and evapotranspiration, especially irrigation systems. To obtain satisfactory results, it is important to avoid over irrigation and minimizes water stress for plants, and understand plant root water uptake mechanism [10]. To develop a successful irrigation scheduling program in the future studies and applications, it should be understand to have a working knowledge of the irrigation practices and its relation with plant water use and soil moisture status [11]. Therefore, it is important to monitor soil water content continuously.

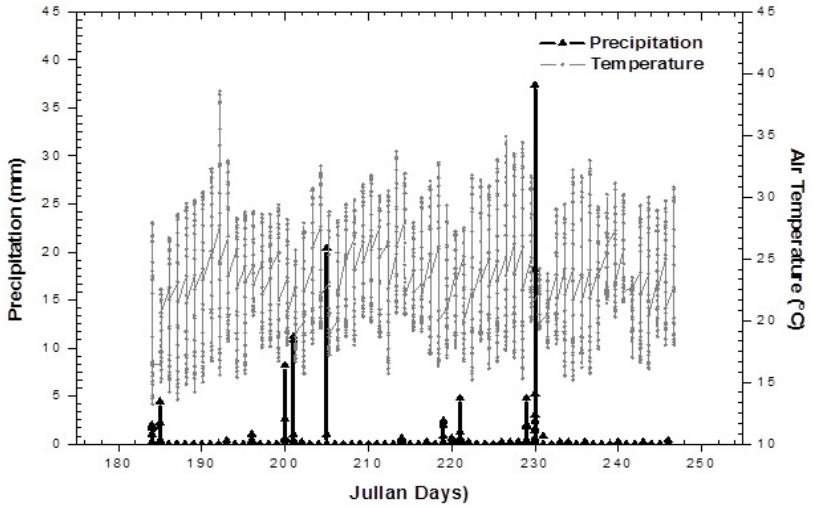

FIGURE 1
Hourly precipitation and temperature during experimental period

One of the most advance systems which monitor soil water content is the employment of the electronic devices. However, there is wide variety of electronic systems for such purpose [12] and capacitance technique is regarded as an efficient in situ nondestructive method to measure soil water content [13]. This method takes advantage of the high dielectric constant of water, compared to that of soil, to quantify its volumetric water content. Despite the fact that all dielectric sensors are relatively easy to use, they are noted to require calibration for each soil and sometime also for each sensor [14]. Kizito et al. [15] have pointed out that the recent development of the ECH_2O-5TE probe (Decagon Device Inc.) could allow for detailed monitoring of soil water content, solute concentration, and temperature in their study in the fields of soil science and hydrology, without extensive calibration. In hazelnut orchard managing, measuring of parameters such as soil water content, soil electric conductivity and soil temperature in response to organic practice are critical particularly in the context of limited water resources with the global warming.

This study was aimed to observe the comparative influences of organic and conventional hazelnut orchard on the soil water content, temperature, and electrical conductivity using ECH_2O-5TE probe in Western Black Sea Region of Turkey.

MATERIALS AND METHODS

Organic and conventional field works were conducted on the hazelnut orchard established and maintained of RALILA Gıda Company and Karslıoğlu Farm, Düzce in Western Black Sea Region of Turkey, respectively (Figure1).

The organic experimental orchard had an area of approximately 1.0 ha and was located at latitude 40° 53' N, longitude 31° 03' E, at an altitude of 205 m while the conventional experimental orchard had an area of approximately 0.5 ha and was located at latitude 40° 54' N, longitude 31° 06' E, at an altitude of 165 m. The distance between experimental areas was approximately 2 km. Average annual precipitation and temperatures for last 40 years in Düzce were 814 mm and 13.2 °C, respectively. Maximum temperature and minimum precipitation occurred in July during a year [16]. In this study, hourly precipitation and temperature from meteorological station which was gathered from the experimental areas are given in Figure 2.

FIGURE 2
Location of Düzce Area of the Western Black Sea Region in Turkey

A number of physical and chemical characteristics for the both experimental orchards [17] were analyzed and given in Table 1. Organic experimental orchard had soil properties of clay-loam containing 32% sand, 36% clay and 32% silt in the upper 120 cm profile while conventional experimental orchard had soil identified as clay containing 32% sand, 41% clay and 41% silt in the

TABLE 1
Physical and chemical characteristics of two experimental orchards

	Organic				Conventional			
	Soil depth, cm				Soil depth, cm			
	0-30	30-60	60-90	90-120	0-30	30-60	60-90	90-120
Saturation Point, %	68.00	68.00	62.00	58.00	77.00	73.00	70.00	60.00
Sand, %	35.00	31.00	31.00	31.00	31.00	31.00	33.00	33.00
Clay, %	33.00	37.00	37.00	37.00	42.00	46.00	40.00	34.00
Silt, %	32.00	32.00	32.00	32.00	27.00	23.00	27.00	33.00
Texture	CL	CL	CL	CL	C	C	C	CL
Total Salt, %	0.021	0.035	0.017	0.011	0.041	0.029	0.037	0.017
pH	5.69	6.41	6.29	6.35	5.68	6.05	6.67	6.52
As, g*cm^{-1}	1.20	1.25	1.28	1.27	1.21	1.24	1.26	1.22
FC, %	30.87	29.82	30.26	29.69	42.82	38.21	42.50	27.41
PWP%)	19.49	18.36	17.03	16.52	21.56	18.63	24.18	10.33

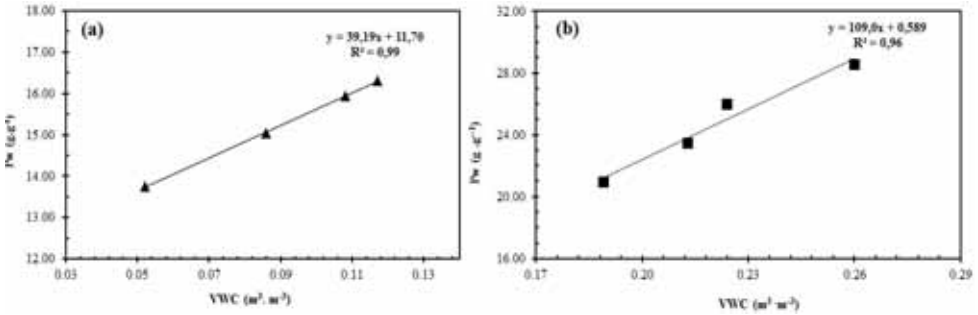

FIGURE 3
ECH$_2$O-5TE calibration curve for the organic (a) and conventional (b) hazelnut orchards soils

upper 120 m profile. Soil bulk densities of organic and conventional experimental orchards were ranged from 1.20 to 1.27 g/cm^3 and 1.21 to 1.26 g/cm^3, respectively. Topography of the both orchards was non-problematic. All analyses were performed via Richards' methods [18], which were shown in Table 1.

In this study, Kara variety of hazelnut trees (*Corylus avellana L.)* with a 4 × 3-m planting distance was established for the both of experimental sites. This type of hazelnut that is widely grown in Turkey has the roots which can grow 80 cm from the trunk under conventional conditions in the coast of Black Sea Region of Turkey [19]. The organic and conventional experimental hazelnut orchards were 10 and 18 years old, respectively, when the study was conducted. Additionally, it should be noticed that these orchards were not irrigated during summer season of 2014.

The hazelnut trees in the both experimental sites, which were organic and conventional, had similar canopy properties. Nutrient management and other cultural practices for the organic and conventional experimental hazelnut were monitored by using the standard practices of RALILA Gıda Company (producers of organic products) and Provincial Agriculture Directorship of Düzce, respectively.

In the each experimental orchard, SWC, SEC and ST parameters were measured hourly in an area assigned to a tree for the both treatments. Measurements were done before the start of repining nut with the higher evapotranspiration and at the end of the growing period, which corresponded to leaf freshening and leaf shades times between 3 July 2014 and 3 September 2014. Measurements were performed using ECH$_2$O-5TE probe (Decagon Device Inc.) every 30 cm and gravimetric methods every 30 cm of soil depth to maximum depth of 120 cm [20, 14]. Probes were installed vertically under the canopy area of hazelnut tree for the both of organic and conventional conditions [11, 14]. All readings were obtained at soil depth intervals of 0-30 cm, 30-60 cm, 60-90 cm, and 90-120 cm from each selected point. During the study, all readings were saved in the data logger and then download weekly. ECH$_2$O-5TE readings were converted to volumetric water content using a calibration curve obtained using the method given by Kinzli et al. [21] (Figure 3). Probes readings and samples of gravimetric soil were obtained at the same time from the four different soil layers in each of the organic and conventional experimental plots. All measured values for the both treatments were compared for significant differences using *Student's t*-test analysis [22].

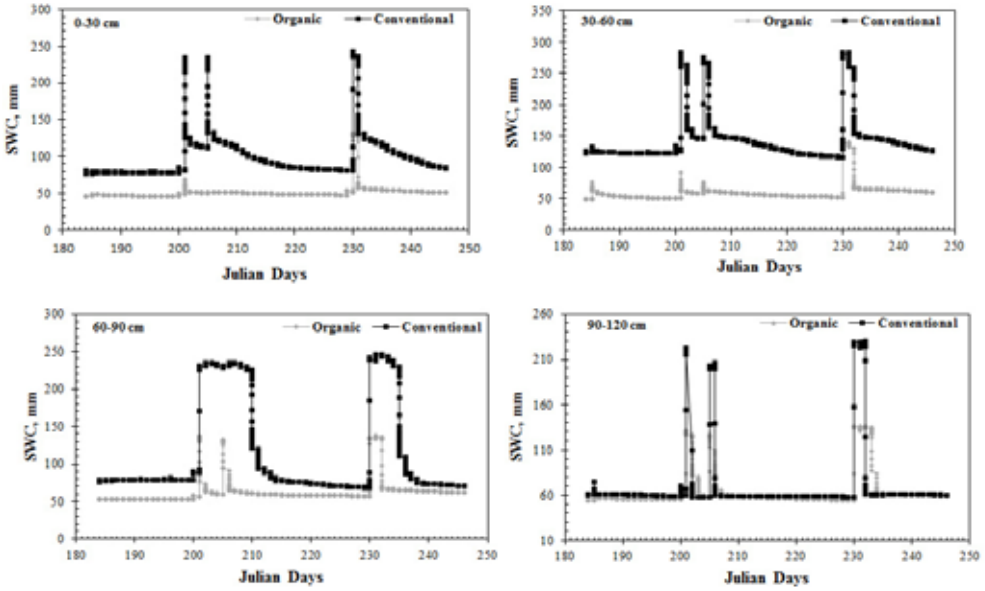

FIGURE 4
Changes in SWC at the different soil layers (0-30; 30-60; 60-90; 90-120 cm) in the soil profile (120 cm) for organic and conventional hazelnut orchards during the Julian days

RESULTS AND DISCUSSION

Soil Water Content (SWC). SWC has an important impact on many fundamental biophysical processes, such as the germination of seeds, plant growth and nutrition, microbial decomposition of the soil organic matter, nutrient transformations in the root zone, as well as heat and water transfer at the land–atmosphere interface [23]. In this work, the results of SWC measurements for organic and conventional treatment used hazelnuts in Düzce Province are presented in Figure 4. The results for the both treatments show that SWC values were higher at 201, 205 and 230 of Julian days. The reason of these results are clearly due to higher precipitation and a decline trend starting with increasing air temperature and no precipitation (Figure 1) at 201 to 230 and 230 to 250 Julian days (Figure4).SWC of conventional treatment shows hard decline for all soil layers except at the 60-90 soil layer in the soil profile after precipitation occurred at 200 to 230 and 230 to 250 of Julian days while this situation did not occurred in the organic hazelnut treatments. Moreover, the highest mean values of SWC were observed at 30-60 cm and 90-120 cm soil layers for conventional and organic hazelnut orchard treatments, respectively (Table 2). These results could be attributed to the organic application process and differences of cultural applications between the treatments. This might be related to the different type of soil texture between the treatments.

As shown in Figure 4, findings for each soil layer in the soil profile clearly show that SWC values were higher under the conventional treatment of hazelnut orchard than the organic treatment during the observed Julian days. The difference between two treatments was found to be highly significant ($p < 0.01$) according to using *Student*'s *t*-test statistical analysis. The results shows that obtained values of SWC in the conventional treatment is higher when compared to the organic treatment for all layers of the soil profile (Table 2). This difference could be attributed to higher evapotranspiration in the organic treatments. Similar impressions were also obtained by Odindi and Kakembo [24]. Chen et al. [25] have indicated that higher evapotranspiration capacity has strong correlation with plantation forest and shrub vegetation results in a lower soil moisture content and even a drier layer. Thereby, it can be concluded that organic hazelnut could consume more water than conventional hazelnut according to SWC results. This conclusion is compatible by literature [26].

Soil Electrical Conductivity (SEC). All irrigation water contains at least some salt which impact yields of irrigated land by causing long term damage to the land itself. For this reason, learning the salt concentration in soil water and soil have great importance to preserve the productivity of irrigated land. SEC is a very effective way of measuring salt concentrations in soil since the

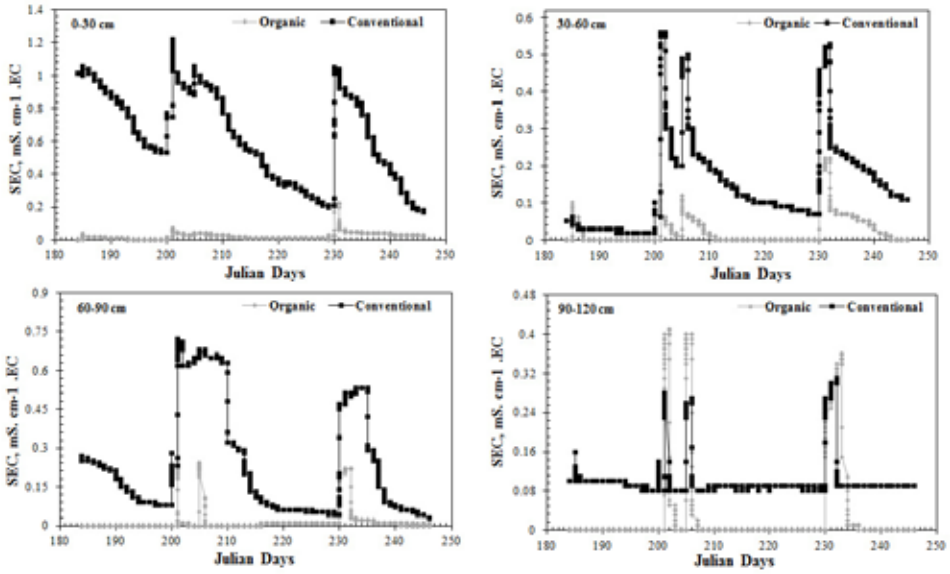

FIGURE 5
Changes in SEC at the different soil layers (0-30; 30-60; 60-90; 90-120 cm) in the soil profile (120 cm) for organic and conventional hazelnut orchards during the Julian days

concentration of salts directly affects its conductivity. The results of SEC meaurements in this study were depicted in Figure 5. It was found that the SEC values is directly in related to results of SWC. Thereby, SEC values show similar tendency for the conventional and organic hazelnut orchard treatments during studied days of Julian as shown Figure 5. The results of SEC in the conventional treatment was higher in all layers of the soil profile when compared by those of organic treatment. Additionally, these results were verified by *Student*'s *t*-test analysis ($p< 0.01$) as shown in Table 2. As shown in Table 2, there was no mean values of SEC in the organic treatment of hazelnut orchard when the mean values of SEC were obtained for all soil layers. The highest value of SEC was observed at 0-30 cm soil layer for the conventional treatment of hazelnut orchard (Table 2). The results presented in this work are in agreement with the previous results reported by Kodešová et al. [13]. SEC values listed in Table 2 were low at low moisture content and increased as the outer viscous water layer developed with higher moisture content. Additionally, there was a clear jump in SEC values when the free unboundwater starts to fill the pores between the mineral grains. The results of this work were quite similar with the studies reported by Topp et al. [27] and Saarenketo [28]. The results in this work had direct outcomes for organic application process and differences in cultural applications between tratments as reported by Stockdale et al. [6]. This might be related to diferent type of soil texture between treatments as Wang et al. [29] pointed out in their study.

Soil Temperature (ST). Plant development process is also quite related to ST during each groving season for the all type of crops as discussed by Bittelli [23]. Therefore, ST is another important factor, especially, to effect plant water uptake from soil. ST could be affected mostly by soil texture, air temperature and farm management such as cultural practices and organic process [30, 31]. In this study, the measured values of ST were shown in Figure 6. As shown in this figure, ST values for each soil layer in the soil profile obviously display that the organic treatment of hazelnut orchard had higher ST values than conventional treatment of hazelnut orchard in the Julian days for all soil layer depths except 0-30 cm soil layer (Figure 6). Similar results were also described by Mead et al. [30]. The reason of higher ST values for the conventional treatment in the first soil layer (30 cm) in contrast with other soil layers (60, 90 and 120 cm) could be due to higher soil temperature fluctuation caused by the solar radiation for the near-surface soil. The conclusion of ST values in this study are quite comparable with the results reported by Koèárek and Kodešová [14].

Significant differences between the organic and conventional practices were observed in ST values ($p<0.01$) except results at 0-30 cm soil layer where the values were higher in the conventional practices. Furthermore, the mean values of soil temperature become lower for deeper soil depths independently of hazelnut treatment (Table 2). Verhoef et al. [32] reported the similar results for the relation between soil temperature and soil depth. On the other hand, ST values were not strongly affected after precipitation occurred at 200 to 230 and 230 to 250 of Julian days. Additionally, determining lines for each soil layer in the both treatments show sigmoidal increment in the Julian days (Figure 6). This can attribute to the variation in the atmospheric temperature during recorded days (Figure 1).

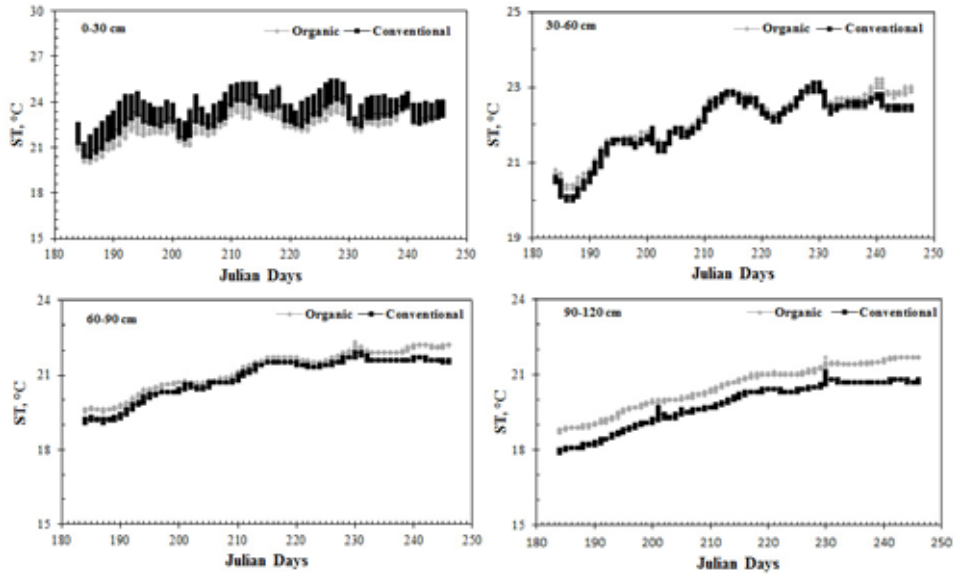

FIGURE 6
Changes in ST at the different soil layers (0-30; 30-60; 60-90; 90-120 cm) in the soil profile (120 cm) for organic and conventional hazelnut orchards during the Julian days

TABLE 2
Using *Student*'s *t*-test statistical analysis to compare of SWC, SEC, and ST between organic and conventional treatments of hazelnut orchard

Soil Depths (cm)	Mean Values of Organic Treatment	Mean Values of Conventional Treatment	Mean Difference	*t*	df	P (2 tailed)
SWC, mm						
0-30	50.9	97.4	-46.5	-63.1	1816	<0.01
30-60	59.8	142.3	-82.5	-82.2	1929	<0.01
60-90	62.7	113.6	-51.0	-29.2	1707	<0.01
90-120	64.4	69.7	-5.3	-4.6	2336	<0.01
SEC, mS.cm^{-1}.EC						
0-30	0.0	0.6	-0.6	-85.1	1538	<0.01
30-60	0.0	0.1	-0.1	-36.7	1837	<0.01
60-90	0.0	0.2	-0.2	-38.5	1642	<0.01
90-120	0.0	0.1	-0.1	-24.9	2098	<0.01
ST, °C						
0-30	23.0	23.4	-0.4	-14.2	3018	<0.01
30-60	22.1	22.0	0.1	4.4	3022	<0.01
60-90	21.2	20.9	0.3	9.3	3022	<0.01
90-120	20.5	19.8	0.7	21.6	3022	<0.01

df: degrees of freedom, *t*: statistical test, P: confidence

The differences between the results obtained from the both treatments could be due to organic practice or different cultural practices. Additionally, different types of soil texture for the both hazelnut treatments could be another reason of the different ST results.

CONCLUSION

In this study, the effects of the organic and conventional hazelnut treatments on the soil parameters, which were SWC, SEC and ST, were investigated for different soil layers (0-30, 30-60, 60-90 and 90-120 cm) by using ECH$_2$O-5TE probe. The measurements were performed in the organic and conventional hazelnut orchard in Western Black Sea Region of Turkey. The results of measurements show that the conventional treatment of hazelnut orchard had higher SWC and SEC values for each soil layer than the organic treatment of hazelnut orchard during studied days of Julian. However, the measured values of ST were higher in organic treatment of hazelnut, except the results at 0-30 cm soil layer, than the conventional treatment

of hazelnut orchard. By considering these results, it can be concluded that the soil water depletion and ST (except the values at 0-30 cm soil layer) were increased by applying the organic agriculture to hazelnut orchard. This conclusion can be stated that organic hazelnut orchard consumed more water or has higher evapotranspiration when compared by those of conventional hazelnut orchard. Moreover, another important result in this study is that organic agriculture is a good alternative practice in rainfed regions where have difficulties to irrigate field (e.g. Black Sea Coast of Turkey) or no irrigation water supplies.

ACKNOWLEDGEMENTS

The author thanks DÜBAP (Düzce University Scientific Research Projects: 2013.23.01.131 and 2013.23.01.196) for its financial support of this study. Furthermore, the author thanks Mrs. Yasemin KARSLIOĞLU-who is owner of Karslıoğlu Farm and Mr. Rahmi AYDIN-who is the owner of RALILA Gıda Company to open their farms for this study.

REFERENCES

[1] CTM, Activity Report of General Directorate of Cooperative in Customs and Trade Ministry (CTM) of Turkey, 2015. [In Turkish]
[2] DPDA, Activity Report of Düzce Provincial Directorate of Agriculture, Düzce Provincial Directorate of Agriculture (DPDA), Turkey, 2015. [In Turkish]
[3] C. Sayin, R.G. Brumfield, B. Ozkan, N.M. Mencet, "The Organic Farming Movement in Turkey", HortTechnology, 15 (2005) 864-871.
[4] (www.tuik.gov.tr.), Last access on 09.13.15. [In Turkish]
[5] Y. Ataseven, "A comparison of organic farming support policies in Turkey and the EU", Revista De Cercetare Interventie Social, 44 (2014) 199-211.
[6] E.A. Stockdale, N.H. Lampkin, M. Hovi, R. Keatinge, E.K.M. Lennartsson, D.W. MacDonald., S. Padel, F.H. Tattersall, M.S. Wolfe, C.A. Watson, "Agronomic and environmental implications of organic farming systems", Advances in Agronomy 70 (2001) 261-327.
[7] A.S.F. Araujo, V.B. Santos, R.T.R. Monteiro, "Responses of soil microbial biomass and activity for practices of organic and conventional farming systems in Piaui state, Brazil", European Journal of Soil Biology 44 (2008) 225-230.
[8] M.M. Chen, G. Su, Y.H. Zhu, D. Chen, B.J. Fu, P. Marschuer, "Effects of soil moisture and plant interactions on the soil microbial community structure", European Journal of Soil Biology 43 (2007) 31-38.
[9] Y. Qiu, B. Fu, J. Wang, L. Chen, "Spatial variability of soil moisture content and its relation to environmental indices in a semi-arid gully catchment of the Loess Plateau, China", Journal of Arid Environment 49 (2001) 723-750.
[10] C. M. K. Gardner, K.B. Laryea, P.W. Unger, "Soil Physical Constraints to Plant Growth and Crop Production," Land and Water Development Division Food and Agriculture Organization of the United Nations, Rome, Italy, 1999.
[11] V. Francesca, F. Osvaldo, P. Stefano, R.P. Paola, "Soil moisture measurements: comparison of instrumentation performances", Journal of Irrigation Drainage Engineering 136 (2010) 81-89.
[12] N. Czarnomski, G. Moore, T. Pypker, J. Licata, B. Bond, "Precision and accuracy of three alternative instruments for measuring soil water content in two forest soils of the Pacific Northwest", Canadian Journal of Forest Research 358 (2005) 1867-1876.
[13] R. Kodešová, V. Kodeš, A. Mráz, "Comparison of two sensors ECH$_2$O EC-5 and SM200 for measuring soil water content", Soil and Water Research 6 (2011) 102-110.
[14] M. Koèárek, R. Kodešová, "Influence of temperature on soil water content measured by ECH2O-TE sensors", International Agrophysics 26 (2012) 259-269.
[15] F. Kizito, C.S. Campbell, G.S. Campbell, D.R. Cobos, B.L. Teare, B. Carter, J.W. Hopmans, "Frequency, electrical conductivity and temperature analysis of a low-cost capacitance soil moisture sensor", Journal of Hydrology 352 (2008) 367-378.
[16] S. Özmen, "Irrigation water use and water table in Düzce area," Düzce University Journal of Science and Technology 1(2013) 47–57. [In Turkish]
[17] A. Tüzüner, "The Handbook of Soil and Water Analyzes Laboratory", The Publications of General Directorate of Rural Services Ankara, Turkey (1990) 375. [In Turkish]
[18] L.A. Richards, "Diagnosis and Improvement of Saline and Alkali Soils", Agriculture Handbook, Washington, D.C., United States Department of Agriculture (1954) 60.
[19] (http://www.ezob.org.tr/findik.pdf) [In Turkish], Last accessed on 09.16.15.
[20] S. E. Burnett, M.W.V. Iersel, "Morphology and irrigation efficiency of *Gaura lindheimeri* grown with capacitance sensor-controlled irrigation", HortScience, 43 (2008)1555-1560.
[21] K. Kinzli, N. Manana, R. Oad, "Comparison of

laboratory and field calibration of a soil-moisture capacitance probe for various soils", Journal of Irrigation and Drainage Engineering 138 (2012) 310-321.
[22] (http://pareonline.net/getvn.asp?v=18&n=10), Last access on 10.10.15.
[23] M. Bittelli, "Measuring soil water content: A review", HortTechnology 21 (2011) 293-300.
[24] J.O. Odindi, V. Kakembo, "The hydrological response of Pteroniaincana-invaded areas in the Eastern Cape Province, South Africa", Ecohydrology 4 (2011) 832-840.
[25] L.D. Chen, J.P. Wang, W. Wei, B.J. Fu, D.P. Wu, "Effects of landscape restoration on soil water storage and water use in the Loess Plateau Region, China", Forest Ecology and Management 259 (2010) 1291-1298.
[26] A. Kaur, Y. G. Garcia, "Enhancing Water-Holding Capacity of Soils with Organic and No-till Production Practices," Field Days Bulletin, Wyoming Agricultural Experiment Station WAES, Wyoming, USA (2012) 175-177.
[27] G.C. Topp, J.L. Davis, A.P. Annan, "Electromagnetic determination of soil water content: measurements in coaxial transmission lines", Water Resources Research 16 (1980) 574-582.
[28] T. Saarenketo, "Electrical properties of water in clay and silty soils", Journal of Applied Geophysics 40 (1998) 73-88.
[29] B. Wang, F. Wen, J. Wu, X. Wang, Y. Hu, "Vertical profiles of soil water content as influenced by environmental factors in a small catchment on the Hilly-Gully Loess Plateau", PLoS ONE 9 (2014) e109546. doi: 10.1371/journal.pone.0109546.
[30] R.M. Mead, R.W.O. Soppe, J.E. Ayars, "Capacitance probe observations of daily soil moisture fluctuations," Proc. Int. Conf. Evapotranspiration and Irrigation (Eds: C.J. Camp, E.J. Sadler, R.E. Yoder), November 3-6, San Antonio, TX, USA, 1996.
[31] (http://www.decagon.com/appnotes/echo_analysis.pdf), Last access on 11.06.15.
[32] A. Verhoef, J. Fernández-Gálvez, A. Diaz-Espejo, B.E. Main, M. El-Bishti, "The diurnal course of soil moisture as measured by various dielectrid sensors: Effect of soil temperature and the implication for evapotranspiration estimates", Journal of Hydrology 321 (2006) 147-162.

Received: **11.12.2015**
Accepted: **25.04.2016**

CORRESPONDING AUTHOR

Selçuk Ozmen
Düzce University, Faculty of Agriculture and Natural Sciences, Department of Biosystem Engineering, 81620, Düzce, Turkey

E-mail: selcukozmen@hotmail.com

© by PSP Volume 25 – No. 10/2016, pages 4217-4223 Fresenius Environmental Bulletin

EVALUATION OF EFFECTIVENESS OF GROUND IMPROVEMENT BASED ON RANDOM FIELD THEORY

Jun Lin[1], Guojun Cai[1,*], Songyu Liu[1], Anand J Puppala[2], Haifeng Zou[1]

[1]Institute of Geotechnical Engineering, Southeast University, Nanjing 210096, China

[2]Department of Civil Engineering, The University of Texas at Arlington, Arlington, Texas 76019, USA

ABSTRACT

Vibro-compaction is a technique most commonly used to improve soil in situ. Piezocone penetration test (CPTU) obtains soil profiles with three measurements of cone tip resistance (q_t), sleeve friction (f_s), and pore pressure (u_2). This study is a result of experimental studies performed on a liquefaction-susceptible site located in the east of China before and after using vibro-compaction method. To evaluate the geotechnical characterization of liquefaction foundation improved by the vibro-compaction method, a set of CPTU tests were performed on the ground unimproved and improved in the construction activity of highway in Suqian, China. The changes of geotechnical properties of liquefaction-susceptible soil, including relative density (D_r), effective frictional angle (φ') and compressive modulus (E_s), were assessed based on CPTU data. Given relatively high sampling frequency of cone tip resistance in the vertical direction, vertical random field parameters are determined by employing the random field theory before and after vibro-compaction. And the changes of vertical spatial variability were also discussed. The results show that relative density, effective frictional angle and compressive modulus have been improved in different degrees, and the soil profiles become more homogeneous after vibro-compaction.

KEYWORDS:
Vibro-compaction, piezocone penetration test, liquefaction, random field model.

INTRODUCTION

Vibro-compaction technique can be effectively used to improve factor of safety against liquefaction. Vibro-compaction is commonly utilized to densify loose silty soils to improve in-situ soil properties in the fields with liquefaction risk [1, 2]. CPTU tests are particularly useful for effectiveness evaluation during ground improvement because they allow a quick contrast in comparing the before and after measured parameters with depth [3].

Based on CPTU data, Massarsch and Fellenius discussed the variation of coefficient of earth pressure in normally consolidated and over-consolidated soil, and effect of soil compaction on the change of the horizontal effective stress [4]. Using CPTU test and equipment specially developed for vibro-compaction, Massarsch presented the most important factors governing the compaction process [5]. Galy and Nollet proposed a new approach, based on limit equilibrium theory, pseudo-static and pseudo-dynamic concepts, to estimate the bearing capacity of reinforced soils under seismic conditions [6]. Accompany with the new approach, two finite difference models were built to verify the validity of the proposed procedure.

The objective of this study is to evaluate the liquefaction-susceptible soil improved by vibro-compaction method using CPTU tests. The vibro-compaction method is presented in detail along with the geologic setting of the liquefaction-susceptible soil. The changes of geotechnical properties of the liquefaction-susceptible soil before and after vibro-compaction are discussed. After a review of random field theory (RFT), vertical random field parameters of liquefaction-susceptible soil before and after vibro-compaction are determined with CPTU data. In this study, the random field model characterization differs from those previously reported.

SITE DESCRIPTIONS AND VIBRO-COMPACTION METHOD

The site situates in a construction activity of highway in Suqian, Jiangsu Province, China. Adopting china standard soil classification method for CPTU testing [7], the subsoil is composed of 1.5m of a plain fill, underlain by

4.5m of a silty clay, underlain in turn by 9.5m of a silty sand and underlain in the end a sand, as shown in Figure 1. The liquefaction-susceptible soil is the silty sand layer, which is mainly studied in this paper. The average thickness of liquefaction-susceptible soil is 9.5m. Liquefaction index ranges from 3.7 to 9.0.

The vibro-compaction equipment has vibrator with powerpack, cross-shaped vibro-wing and base machine (carrier), as shown in Figure 2. The cross-shaped vibration wing is made up of two perpendicular steel and a probe. The vertical oscillation is generated by the hydraulically driven vibrators. Vibration frequency can be tumbled varying from 0 to 20 Hz during ground improvement. In practice, the optimal compaction frequency is 15~17Hz. The vibro-wing is lowered into the soil at a rate of 2.0 m/min, and pulled out of the soil at a rate of 1.2 m/min.

GEOTECHNICAL CHARACTERIZATION OF LIQUEFACTION- SUSCEPTIBLE SOIL

CPTU test is one of the most popular in-situ testing methods used to investigate soil properties. In order to characterize subsurface soil conditions, D_r, φ', and E_S are chosen to assess changes of soil index of liquefaction-susceptible layer before and after compaction.

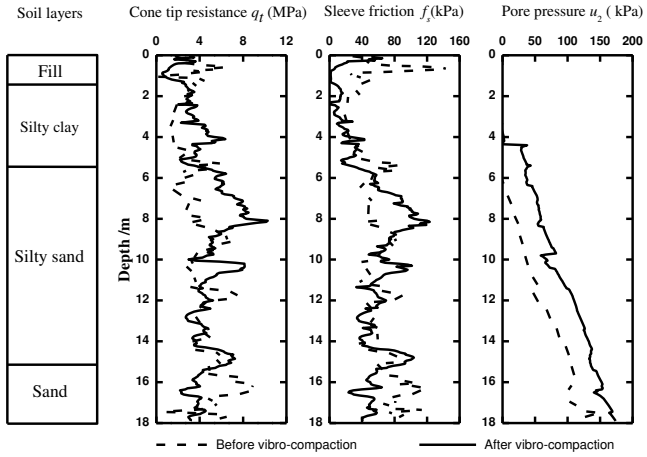

FIGURE 1
Soil layers and typical CPTU profiles in the test site.

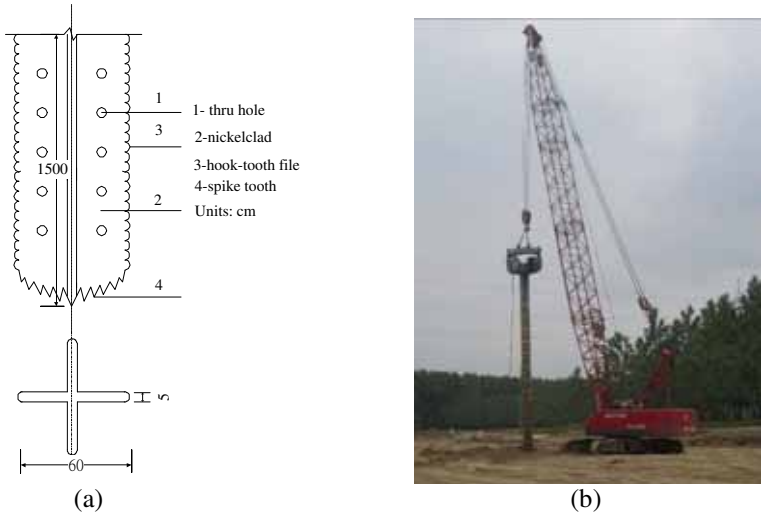

FIGURE 2
The cross-shaped vibration equipment: (a) crisscross section vibratory probe (b) base machine in the field [8].

Relative Density. For cohesion1ess soi1s, D_r expresses the degree of compactness with respect to both the loosest and the densest states [8]. Jamiolkowski summarized the experience gained interpretation of CPTU tests for assessment of geotechnical and technical properties of sands [9].

During vibro-compaction, particles of granular soil can be rearranged by vibrator in a higher density state. In this study, D_r is determined by the method proposed by Jamiolkowski [10]. Considering the influence of the vertical effective stress σ'_{v0}, the relation between q_t and σ'_{v0} can be described as:

$$D_r = 100\left[0.268\ln\frac{q_t/\sigma_{atm}}{\sqrt{\sigma'_{v0}/\sigma_{atm}}} - 0.675\right] \quad (1)$$

In which $\sigma'_{v0} =$ is the vertical effective stress, KPa; and $\sigma_{atm} =$ normal atmospheric pressure.

Effective Frictional Angle. Lots of correlations for φ' have been developed relying on cone penetration test (CPT), pressuremeter test (PMT), and dilatometer test (DMT). Among all those methods, the CPT relationships are perhaps the best-estimation. According to the equation proposed by Kulhawy [11], φ' can be gotten from the normalized cone tip resistance q_{t1}, as

$$\phi' = 17.6^\circ + 11\lg q_{t1} \quad (2)$$

Where $q_{t1} = \left(q_t/\sigma_{atm}\right)\Big/\left(\sigma'_{v0}/\sigma_{atm}\right)^{0.5}$;

$\sigma_{atm} =$ normal atmospheric pressure.

Compressive Modulus. Compressibility parameters for cohesion1ess soils can be obtained by carrying out CPTU test. In this study, E_s of liquefaction-susceptible soils can be determined from the relation between q_t and E_s proposed by Lunne [12], as

$$\left.\begin{aligned} E_s &= 5q_t \quad q_t < 50\text{MPa} \\ E_s &= 250\text{MPa} \quad q_t > 50\text{MPa} \end{aligned}\right\} \quad (3)$$

Assessment of Geotechnical Characterization Parameters. The geotechnical characterization parameters of liquefaction-susceptible soil determined from CPTU data are listed in Table 1. Vibro-compaction will increase D_r, φ' and E_s values of liquefaction-susceptible soil deposit, as listed in Table 1. Inducing from the calculated result in Table 1, the liquefaction-susceptible soil parameters seem to be improved in different degrees. D_r and E_s increase remarkably with 24.8% and 38.4% respectively after vibro-compaction. With an increasing in D_r, an increase in E_s follows. The value of φ' increases 2°, not as remarkably as the increase in D_r and E_s. The increases in D_r, φ' and E_s are highly desirable results of vibro-compaction.

TABLE 1
Evaluation results of D_r, φ' and E_s.

Soil types	D_r (%)	φ' (°)	E_s (MPa)
Before vibro-compaction	34.42	35.74	20.3
After vibro-compaction	42.96	37.25	27.8

RANDOM FIELD THEORY

RFT is a powerful framework for the assessment of soil spatial variability [13]. It provides useful statistical results for planning exploration, sampling strategies, generating inferences, and inclusion of spatial variation of soils [14]. Now, RFT is introduced to evaluate the spatial variability of liquefaction-susceptible soil before and after vibro-compaction. Due to strongly correlation of soil properties in the vertical direction, only the vertical spatial variability in direction is considered in this study [15].

CPTU Data Process Procedure. The spatial variability of soil parameters can be described with the mean, the variance or coefficient of variation (COV), and the scale of fluctuation (δ). The procedure of performing random field theory on CPTU data includes trend removal, determination of the best-fit correlation structure of sample autocorrelation function and corresponding δ, and estimation of COV.

In this study, the q_t profiles of liquefaction-susceptible soils are chosen to be performed random field model on in the vertical direction. Requiring statistically homogenous data may be perceived as an undue burden in the setting of design projects [16, 17]. As a result, the chosen CPTU profile can be performed random field theory to get the δ and COV values of liquefaction-susceptible soil before and after compaction.

Trend Removal. The CPTU measurements, $g(z)$, can be separated into two parts: a deterministic trend, $t(z)$, and residual fluctuating about the trend, $x(z)$, as

$$g(z) = t(z) + x(z) \quad (4)$$

In which $t(z)$ = trend removal function, and $x(z)$ = fluctuating about the trend.

The trend function can be removed by least square regression analysis [18, 19]. However, the statistical estimation uncertainty in the parameters of trend function will increase as the flexibility of trend function becomes greater [14, 20]. In this paper, the linear trend removal technique was adopted. The trend removal and residual results are shown in Figure 3 and Figure 4.

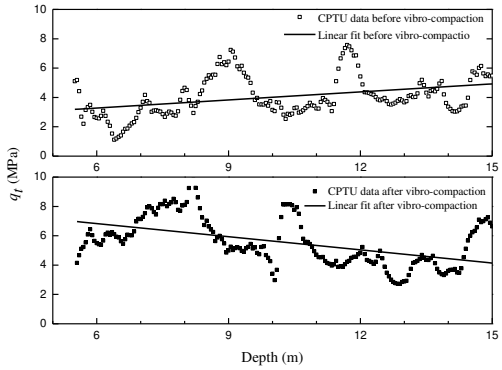

FIGURE 3
Trend removal curve of liquefaction-susceptible soil.

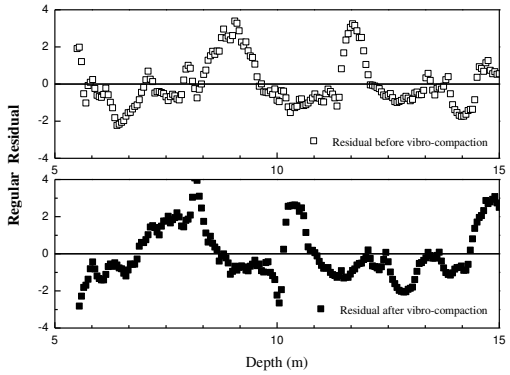

FIGURE 4
Regular residual of liquefaction-susceptible soil.

Fitting of Sample Autocorrelation Models. The correlation of a parameter may be readily compared across disparate soil units using δ, as well as by using the autocorrelation function (ACF). The ACF describes the change in autocovariance of selected parameter with separation distance (τ), normalized with respect to the autocovariance at zero separation [17]. There are many different methods used to estimate δ, such as expeditive method, variance reduction function, autocorrelation model fitting, and intersection of the sample ACF.

In this study, the autocorrelation model fitting of ACF method is used to estimate δ value. The ACF method employs typical curve fitting procedures to fit the parameter sample ACF. The autocorrelation models are adopted herein including the single-exponential (SNX), binary noise (BIN), cosine exponential (CSX), second-order Markov (SMK), and squared exponential (SQX) models [16, 20]. The five model formulations and corresponding δ values are presented respectively in Table 2. Uzielli suggests fitting the autocorrelation models only to the initial part of the sample ACF with coefficients exceeding Bartlett's limits [16]:

$$r_B = 1.96/\sqrt{n_d} \quad (5)$$

In which $n_d = q_t$ data sample number.

The fitting results of q_t sample ACF with SNX, BIN, CSX, SOM, SQX curves before and after vibro-compaction are given out in Figure 5 and Figure 6. The corresponding δ values of the q_t sample ACF are listed in Table 3.

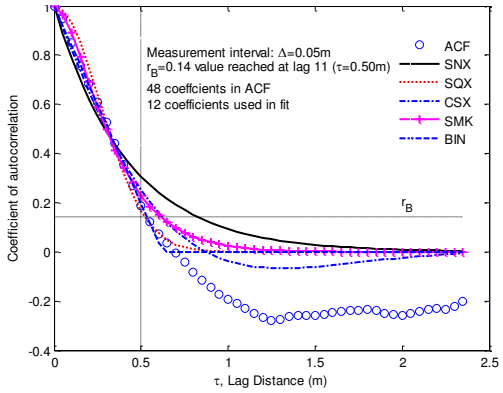

FIGURE 5
The results of fitting the q_t sample ACF before vibro-compaction.

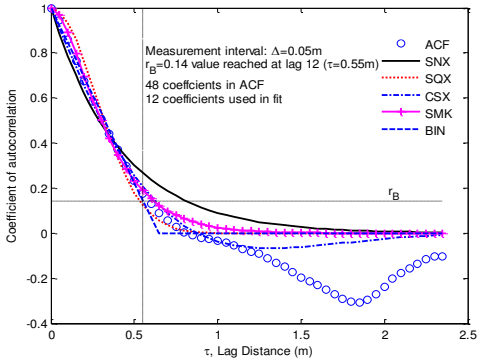

FIGURE 6
The results of fitting the q_t sample ACF after vibro-compaction.

TABLE 2
Autocorrelation models and corresponding δ values[19].

Autocorrelation model	Equation	δ
Single exponential	$R(\tau) = \exp(-\lambda\|\tau\|)$	$\delta = 2/\lambda$
Binary noise	$R(\tau)=\begin{cases}1-c\|\tau\| & \|\tau\| \le 1/c \\ 0 & otherwise\end{cases}$	$\delta = 1/c$
Cosine exponential	$R(\tau) = \exp(-b\|\tau\|)\cos(b\tau)$	$\delta = 1/b$
Second-order Markov	$R(\tau) = (1+d\|\tau\|)\exp(-d\|\tau\|)$	$\delta = 4/d$
Squared exponential	$R(\tau) = \exp[-(a\tau)^2]$	$\delta = \pi /a$

Coefficient of Variation. Phoon and Kulhawy provided typical values for various soils and design parameters and recommended using the coefficient of variability rather than the variance [21], defined as

$$\mathrm{COV}(z) = \sigma_w(z)/t(z) \qquad (6)$$

Where $t(z) =$ mean soil property trend in the observed parameter, and $\sigma_w(z) =$ standard deviation of the fluctuating component for a statistically homogenous soil layer.

Determination of variability required a careful consideration as the COV and δ decreases with an increase in the order of polynomial trend removal [20, 22]. The COV value would be overestimated if the deterministic trend in the soil data is not removed, which is known as total variability analysis.[23].

Assessment of Random Field Model Parameters. It can be seen that trend removal profiles show opposite results before and after vibro-compaction, as show in Figure 3. Before vibro-compaction, the removal trend profile increases with an increase of depth; while after vibro-compaction, the removal tend profile decreases with an increasing of depth. As is shown in Figure 4, the residual is zero-mean weakly stationary overall. The residuals consist with the requirement of the fluctuations of CPTU measurements about a mean trend function modeled as a zero-mean stationary random field [20, 24].

Based on the results of each coefficient of determination (R^2) in Table3, it can be observed that SQX model is the best fitting of the q_t sample before and after vibro-compaction. The coefficients of determination of SQX model are 0.989 and 0.995 respectively before and after vibro-compaction. This result is different from the previously reported result that the SNX model is mostly used [19].

TABLE 3
The δ and corresponding R^2 values of SNX, BIN, CSX, SOM, SQX.

Autocorrelation model	δ (m)		R^2	
	Unimproved	Improved	Unimproved	Improved
SNX	0.80	0.81	0.938	0.957
BIN	0.64	0.68	0.951	0.944
CSX	0.66	0.68	0.973	0.9626
SOM	0.54	0.55	0.968	0.961
SQX	0.70	0.71	0.988	0.995

TABLE 4
The δ, COV and mean q_t values of liquefaction-susceptible soil.

Soil type	δ (m)	COV (%)	Mean q_t (MPa)
Before vibro-compaction	0.70	31.35	4.06
After vibro-compaction	0.71	25.94	5.56

As listed in Table 4, the vertical δ values of SQX model are 0.70m and 0.71m respectively before and after vibro-compaction. This result indicates that δ values change little after vibro-compaction. As listed in Table4, the COV values are 31.35% and 25.94% respectively before and after vibro-compaction. The comparison of δ and mean q_t are also listed in Table4. The COV values decreases with an increase of mean q_t values. The obtained results mean that spatial variability of soil profiles reduces and liquefaction-susceptible soil becomes more homogeneous after vibro-compaction.

SUMMARY AND CONCLUSIONS

This paper presents a brief evaluation of geotechnical characterization and random field modeling of liquefaction-susceptible layer improved by the vibro-compaction method. The changes of geotechnical properties (such as D_r, φ', E_s) and spatial variability in the vertical direction are evaluated before and after vibro-compaction based on CPTU data. This study yields some valuable conclusions for liquefaction-susceptible soil improved by vibro-compaction method. The results can be summarized as follows:

After vibro-compaction, D_r, φ', and E_s of liquefaction-susceptible soil seemed to be improved in different degrees. D_r and E_s increased remarkably while φ' increased only a little. Before vibro-compaction, the removal trend increased with an increase of depth. While after vibro-compaction, the removal trend decreased with an increase of depth. The best fitting autocorrelation function of q_t sample was SQX model for liquefaction-susceptible soil before and after compaction. After vibro-compaction, the vertical δ values changed little while the COV values decreases notably. There was also an increase in mean q_t values after vibro-compaction.

ACKNOWLEDGEMENTS

Majority of the work presented in this paper was funded by the Foundation for the New Century Excellent Talents of China (NCET-13-0118), the Foundation of Jiangsu Province Outstanding Youth (Grant No. BK20140027), the Foundation for the Author of National Excellent Doctoral Dissertation of PR China (Grant No. 201353), and the High Level Talent Project of Peak of Six Talents in Jiangsu Province (Grant No. 2015-ZBZZ-001). These financial supports are gratefully acknowledged.

REFERENCES

[1] Castelli, R J. Vibratory Deep Compaction of Underwater Fill. In Deep Foundation Improvements: Design, Construction, and Testing, ASTM STP, 1089, Melvin I. Esrig and Robert C Bachus, Eds., ASTM, Philadelphia, pp. 279-319, (1991)

[2] Hussin, J D. Methods of Soft Ground Improvement. In The Foundation Engineering Handbook, Taylor & Francis Group, New York, pp. 525-569, (2006)

[3] Mayne, P. W. Cone penetration testing: A synthesis of highway practice. Project 20-5. Transportation Research Board, Washington DC, NCHRP synthesis 368, pp. 3-4, (2007)

[4] Massarsch, K R, Fellenius, B H. Vibratory compaction of coarse-grained soils. Canadian Geotechnical Journal, **39**(3), pp. 695-709, (2002)

[5] Massarsch, K. R., and Fellenius, B. H.. Deep vibratory compaction of granular soils. In Ground Improvement Case Histories, Buddhima Indraratna and Jian Chu, Eds., Elsevier Publishers, **3**(19), pp. 633– 658, (2005)

[6] Galy, B., Nollet, M. J., LeBoeuf, D., and Lessard, D. Influence of the Vibro Stone Column Reinforcement on The the Seismic Bearing Capacity of a Surface Shallow Footing. In 15th World Conference on Earthquake Engineering, Lisboa, (2014).

[7] Liu S., Cai G., and Zou H.. China standard soil classification method based on piezocone penetration testing. Chinese Journal of Geotechnical Engineering, **35**(10), pp.1765-1776, (2013)

[8] Cheng, Y., Liu, S., Liu, Z., and Cai, G. Seismic Cone Penetration Test Assessment of Vibratory Probe Compaction for Liquefaction Mitigation. Bridges, **10**, pp.1898-1907, (2014)

[9] Burmister, D M. The importance and practical use of relative density in soil mechanics, In Proceedings-American Society for Testing and Materials, 48, West Conshohocken, pp. 1249-1268, (1948)

[10] Raju, V. R., and Valluri, S.. Practical Application of Ground Improvement, In Symposium on Engineering of Ground & Environmental Geotechnics, Hyderabad, India, (2008)

[11] Jamiolkowski, M., Lo Presti, D. C. F., and Manassero, M. Evaluation of relative density and shear strength of sands from CPT and DMT, In Soil behavior and soft ground construction, ASCE, pp. 201-238, (2003)

[12] Kulhawy, F H, and Mayne, P W. Manual on

estimating soil properties for foundation design, In Electric Power Research Institute, Palo Alto, Report EL-6800, pp. 306-307, (1990)
[13] Lunne, T. In situ testing in offshore geotechnical investigations, In Proc. Int. Conf. on In Situ Measurement of Soil Properties and Case Histories, pp. 61-81, (2001)
[14] Goldsworthy, J. S., Jaksa, M. B., Fenton, G. A., Kaggwa, W. S., Griffiths, V., and Poulos, H. G. Effect of sample location on the reliability based design of pad foundations. Georisk, **1**(3), pp 155-166, (2007)
[15] Baecher, G B, Christian, J T. Reliability and statistics in geotechnical engineering. John Wiley & Sons Inc., New York, pp. 216-217, (2003)
[16] Wu, S. H., Ou, C. Y., Ching, J., and Juang, C. H. H. Reliability-based design for basal heave in an excavation considering spatial variability, In GeoFlorida, ASCE, Atlanta, pp. 1914-1923, (2010)
[17] Uzielli, M., Vannucchi, G., and Phoon, K. K. Random field characterisation of stress-nomalised cone penetration testing parameters. Géotechnique, **55**(1), pp 3-20, (2005)
[18] Stuedlein, A. W., Kramer, S. L., Arduino, P., and Holtz, R. D.. Geotechnical characterization and random field modeling of desiccated clay. Journal of Geotechnical and Geoenvironmental Engineering, **138**(11), pp 1301-1313, (2012)
[19] Kulhawy, F H, Birgisson, B, Grigoriu, M D. Reliability-based foundation design for transmission line structures: Transformation models for in-situ tests. Report EL-5507(4), Electric Power Research Institute, Palo Alto, pp 46-48, (1992)
[20] Phoon, K. K., Quek, S. T., and An, P. Identification of statistically homogeneous soil layers using modified Bartlett statistics. Journal of Geotechnical and Geoenvironmental Engineering, **129**(7), pp 649-659, (2003)
[21] Phoon, K. K., and Kulhawy, F. H. Characterization of geotechnical variability. Canadian Geotechnical Journal, **6**(4), pp 612-624, (1999)

Received: **11.09.2015**
Accepted: **11.05.2016**

CORRESPONDING AUTHOR

Guojun Cai
Institute of Geotechnical Engineering
Southeast University
Nanjing 210096 - CHINA

E-mail: focuscai@163.com

© by PSP Volume 25 – No. 10/2016, pages 4224-4226 Fresenius Environmental Bulletin

ACUTE LETHAL TOXICITY TO THE MARINE COPEPOD *ACARTIA TONSA* OF THE REFERENCE ITEM 3,5-DICHLOROPHENOLE (3,5-DCP) ACC. TO ISO 14669 : 1999 (E)

Martina Noack*, Monika Koenig, Thomas Nowakowski, Udo Noack

DR.U.NOACK-LABORATORIEN, Kaethe-Paulus-Str. 1, 31157 Sarstedt, Germany

ABSTRACT

The purpose of the test series of acute lethal toxicity tests to the marine copepod *Acartia tonsa* with the reference item 3,5-Dichlorophenole in the years 2014 and 2015 was to determine the sensitivity of the copepods and the conformity of the procedure. The copepods originate from DHI (Denmark) were cultured at the test facility. Copepods from a healthy and stable culture stock were exposed to different concentrations of the reference item under static conditions. LC_{50}-values of 3,5-DCP were determined for each study after 24 and 48 hours of exposure by sigmoidal dose-response regression. The recommended range of validity of the ISO guideline is 0.5 - 1.5 mg/L. The investigations achieved a $LC_{50\ (48\ h)}$ of 0.5 mg/L (standard deviation of 0.1 mg/L).

KEYWORDS:
Acute Toxicity, Marine Copepod, Acartia tonsa, 3,5-Dichlorophenole

INTRODUCTION

The lethal effects of 3,5-DCP on the marine copepod *Acartia tonsa* have been determined in a test series of 10 studies in the years 2014 and 2015. The studies were carried out as dose-response tests.

MATERIALS AND METHODS

Test system and culture. Acartia tonsa DANA (1879) is one of the recommended species of the test guideline and is bred at the test facility. The test system originates from DHI (Agern Allé 5, DK-Hørsholm, Denmark). The test system is cultured in glass flasks (> 2 L capacity) with approximately 2 L culture medium, at 20 ± 3°C, in an incubator, 16 hours illumination; light intensity of max. 2200 lx at the water surface, dissolved oxygen concentration above 80 % air saturation, pH 8.0 ± 0.3. M7 medium, according to ISO/DIS 16778, Annex A (2015), with a salinity of 20 ± 2 S (before 09/2015) or 32 ± 2 S (since 09/2015) is used. The culture copepods are fed at least 5 times per week ad libitum with a suspension of the Chryptophyceae Rhodomonas salina. The algae are cultured at the test facility and originates also from DHI.

The culture is frequently renewed with eggs produced from healthy culture stocks which are hatched under culture conditions.

Preparation of the test solutions and application technique. A 100 mg/L stock solution of the reference item 3,5-DCP PESTANAL® (SIGMA) was prepared in demineralised water or M7 medium and mixed thoroughly by manual agitation. The stock solution was further diluted with M7 medium to different concentration levels to achieve clear and true solutions.

The following nominal concentration ranges were tested [mg/L]:

0.128 - 0.320 - 0.800
0.125 - 0.250 - 0.500 - 1.00 - 2.00
0.257 - 0.463 - 0.833 - 1.50 - 2.70
0.257 - 0.463 - 0.833 - 1.50
0.257 - 0.463 - 0.833

As a control, the test medium without reference item was tested under the same conditions as the test groups.

The studies carried out before October 2015 were carried out at a salinity of 20 ± 2 S. Thereafter, for the culture stock and for the tests M7 medium with a salinity of 32 ± 2 S was used.

Test conditions (acc. to ISO 14669 : 1999 (E)[1]). The studies were carried out under static conditions over a period of 48 hours in glass beakers with a capacity of 50 mL (low shape) which were loosely covered with watch glasses. The test volume was 25 mL. 20 large copepodids (stage 5) or adults per concentration level and control, divided into 4 replicates with 5 copepods each, were used. The copepods were not fed during the test.

TABLE 1
LC_{50}-values (48 h) of 3,5-DCP for *Acartia tonsa* in the Years 2014 and 2015 at different salinities

Reference item: 3,5-DCP			
Study date	Nominal test concentrations [mg/L]	Salinity [S]	**$LC_{50, 48\ hours}$ [mg/L]**
2014-06-24 to 2014-06-26	0.257 - 0.463 - 0.833 - 1.50 - 2.70	20	**0.5**
2014-07-31 to 2014-08-02	0.257 - 0.463 - 0.833 - 1.50 - 2.70	20	**0.6**
2014-08-06 to 2014-08-08	0.257 - 0.463 - 0.833	20	**0.3**
2014-08-12 to 2014-08-14	0.257 - 0.463 - 0.833 - 1.50	20	**0.4**
2014-12-02 to 2014-12-04	0.257 - 0.463 - 0.833 - 1.50 - 2.70	20	**0.5**
2014-12-08 to 2014-12-10	0.257 - 0.463 - 0.833 - 1.50 - 2.70	20	**0.6**
2015-07-28 to 2015-07-30	0.125 - 0.250 - 0.500 - 1.00 - 2.00	20	**0.5**
2015-10-12 to 2015-10-14	0.128 - 0.320 - 0.800	32	**0.3**
2015-10-19 to 2015-10-21	0.128 - 0.320 - 0.800	32	**0.4**
2015-10-26 to 2015-10-28	0.128 - 0.320 - 0.800	32	**0.5**
Mean ± Standard deviation			**0.5 ± 0.1**
Number of studies			10

Range of validity acc. to ISO 14669 : 1999 (E): 0.5 - 1.5 mg/L

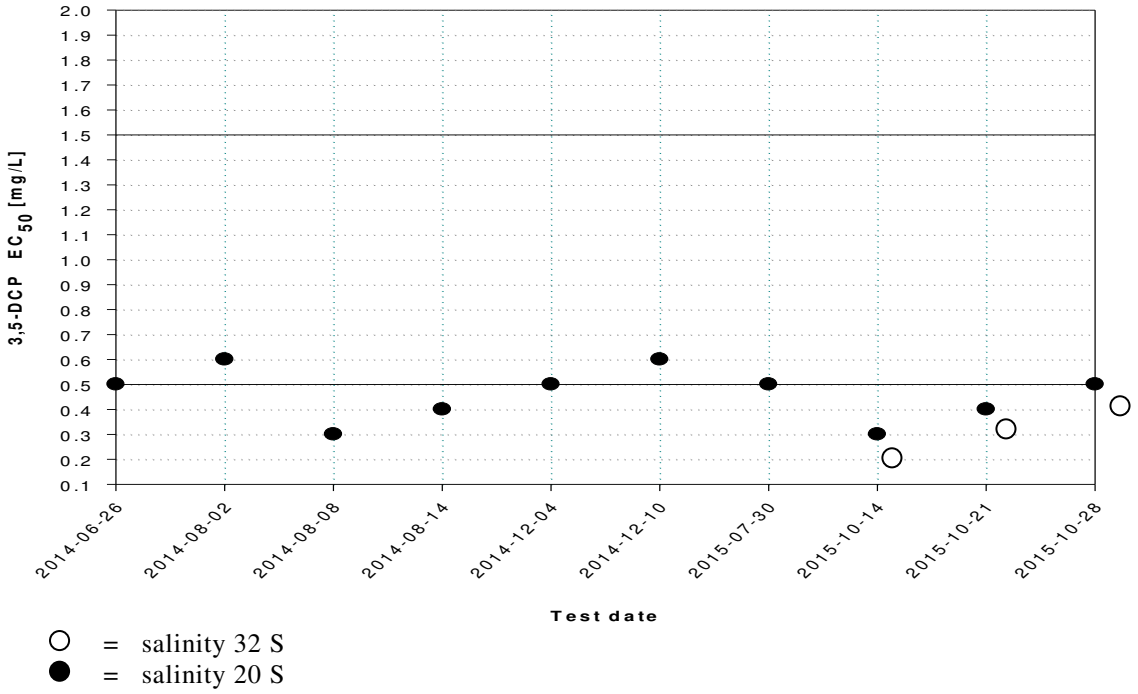

FIGURE 1
LC_{50}-values (48 h) of 3,5-DCP for *Acartia tonsa* (n = 10) at different salinities
Range of validity acc. to ISO 14669 : 1999 (E): 0.5 - 1.5 mg/L

Incubation conditions were similar to the culture conditions: 20 ± 2 °C, diffuse light (max. 2200 lx at the water surface), 16/8 hours light/dark cycle. The test medium was the same as the culture medium: M7 medium, according to ISO/DIS 16778, Annex A [2], with a salinity of 20 ± 2 S or 32 ± 2 S, dissolved oxygen concentration above 80 % air saturation, pH 8.0 ± 0.3.

The effects of 3,5-DCP were determined after 24 and 48 hours of exposure. An animal was considered to be dead, if it is showing no swimming or appendage movements within an observation period of 10 seconds

Evaluation. The LC_{50}-values were calculated by sigmoidal dose-response regression. Respective 95 % confidence limits were calculated from the standard error and the t-distribution. All calculations were carried out from the best-fit values with the software GraphPad Prism5.

RESULTS

Environmental conditions. Environmental conditions (pH-value, dissolved oxygen concentration, incubation temperature, light conditions) were determined to be in the acceptable limits.

Effects of 3,5-DCP. The effects of 3,5-DCP are summarised in Tables 1 and Figure 1.

CONCLUSIONS

The studies performed in the years 2014 and 2015 result in a mean $LC_{50\ (48\ h)}$ of 0.5 mg/L with a standard deviation of 0.1 mg/L of the reference item 3,5-DCP.

The variation between the studies were very low independent from the tested concentration range and the salinity (20 S and 32 S) of the test solutions. The good reproducibility of the reference test shows the constant sensitivity of the copepods and the conformity of the procedure.

Therefore, we come to the conclusion, that the range of validity of 0.5 - 1.5 mg/L which is recommended by the guideline should be reconsidered.

REFERENCES

[1] ISO 14669 (1999): Water Quality - Determination of Acute Lethal Toxicity to Marine Copepods (Copepoda, Crustacea).

[2] ISO/DIS 16778 (2015), Annex A Water quality -- Calanoid copepod early-life stage test with *Acartia tonsa*

Received: **16.12.2015**
Accepted: **15.06.2016**

CORRESPONDING AUTHOR

Martina Noack
DR.U.NOACK-LABORATORIEN, Kaethe-Paulus-Str. 1, 31157 Sarstedt, Germany

email: mn@noack-consultants.eu

© by PSP Volume 25 – No. 10/2016, pages 4227-4234 Fresenius Environmental Bulletin

THE INFLUENCE OF TEMPERATURE ON THE ATMOSPHERE-EXPOSED BIOFILM SYSTEM PROCESSING CHARACTERISTICS AND THE MICROBIAL COMMUNITY

Dong Nie[1], Ming-Ji Jin[2*], Ming-Zhe Xu[2]

1. Sciences College of Yanbian University, Yanji Jilin 133000, China
2. Agricultural College of Yanbian University, Yanji Jilin 133000, China

ABSTRACT

The influence of temperature on the processing characteristics of the Atmosphere-Exposed Biofilm (AEB) system and the microbial community was investigated by employing PCR-DGGE with cloning and sequencing. Our results indicated that the chemical oxygen demand (COD) and total phosphorus (TP) removal rate increased with an increase in temperature from 10°C to 35°C, while the total nitrogen (TN) removal rate declined after first increasing with a maximum removal rate at 30°C. The temperature coefficients of COD, TN, and TP were 1.0062, 1.0727, 1.0336, respectively, indicating that the influence of temperature on the TN removal was greatest. During the entire process, significant changes were observed in the microbial community shifts. The dominant strains were *Flavobacterium oncorhynchi* and *Parachlamydia acanthamoebae UV-7* at low-temperatures, while *Uncultured bacterium TB127-12*, *Undibacterium parvum,* and *Uncultured bacterium bf1-54* were significant dominant strains at medium to high temperatures. The results have the potential to form a basis for the optimization, application, and popularization of the AEB system.

KEYWORDS:

Atmosphere-Exposed Biofilm; Temperature; Temperature coefficient; PCR-DGGE; dominant strains; Microbial community structure

INTRODUCTION

The development of biofilm production systems has led to their increasing use in wastewater treatment. One such new Atmosphere-Exposed Biofilm (AEB) system has the advantages of convenient operation, low investment and low management costs owing to its novel structural features. The filter in the AEB system is directly in contact with air, microorganisms on the filter can absorb oxygen directly; this abolishes the need for artificial aeration and reduces operation costs because oxygen strongly influences microbial activity, which has significant effects on processing characteristics. In addition, the AEB system uses a new soft fiber hanging bio-contactor (HBC) ring, which is a coil made of polyvinyl chloride wire that provides large specific surface area for the microorganism adhesion and growth and improves absorbance by microorganisms.

Many factors affect processing characteristics of biofilm production systems, such as substrate type and concentration, pH, temperature, and biofilm thickness [1]. Among these, temperature significantly influences rates of microbial growth and substrate metabolism,it also has an important influences in the composition and structure of the microbial communit

Therefore, this study investigated the influence of temperature on processing characteristics of the AEB system by analyzing changes in the microbial community at different temperatures and by identifying dominant strains by polymerase chain

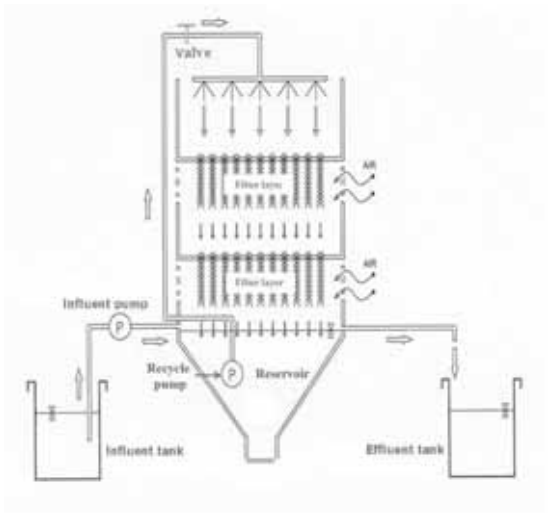

FIGURE 1
Schematic of the Atmosphere-Exposed Biofilm system

reaction (PCR)-density gradient gel electrophoresis (DGGE) combined with cloning and sequencing methods. The findings of this study have the potential to form a basis for the optimization, application, and popularization of the AEB system.

MATERIALS AND METHODS

Experimental setup. The reactor of AEB system was made of poly methyl methacrylate (Perspex). It was composed of a reservoir, two filter layers, and a water-circulation device (Fig. 1). The reservoir had a working volume of 19 L, each filter layer (volume, 9 L) had two vents on both sides to maintain internal ventilation. HBC rings of length 0.12 m were hung in the filter layers with a packing rate of 600 m/m^3. The water-circulation device was composed of a circulating pump, turret spray, and valve in the upper region of the reactor.

Operating conditions. The synthetic waste -water used in this study contained beef extract (150 mg/L), peptone (150 mg/L), yeast extract (150 mg/L), K_2HPO_4 (20 mg/ L), $CaCl_2$ (20 mg/L), $MgSO_4 \cdot 7H_2O$ (20 mg/L), NaCl (6 mg/L), $ZnSO_4$ (10 mg/L), $MnSO_4$ (0.2 mg/L), and $FeCl \cdot 6H_2O$ (2.5 mg/L).

The inoculate sludge was collected from the secondary sedimentation tank of a municipal wastewater treatment plant (Yanji city of jilin province in China). Biofilm formation occurred under closed and recirculating conditions.

Six stages were operated with different temperature of 10°C, 15°C, 20°C, 25°C , 30°C, and 35°C, respectively. The AEB systems were operated in a continuous mode with a daily capacity of 10 L, the hydraulic retention time was 24 h, the organic loading and surface loading rates was 0.33 kg chemical oxygen demand (COD)$\cdot m^{-3} \cdot d^{-1}$ and 17.0 $m^3 \cdot m^{-2} \cdot d^{-1}$, respectively.

Water quality analysis. Chemical oxygen demand (COD) , total nitrogen (TN), and total phosphorus (TP) were measured using standard methods of water quality analysis as described previously [2].

Microbial sampling and DNA extraction. Microbial samples were collected from initial and final layers in different reactors. Two samples from different filter layers in the same reactor were mixed to form a new sample for DNA extraction.

Total DNA was extracted from samples by using the Soil DNA Kit (Omega Bio-tek, Norcross, GA), and DNA quality was evaluated by agarose gel (0.8%) electrophoresis.

PCR amplification. The total bacteria universal primers (GC-338 f : attaccgcggctgctgg and 518 r : cctacgggaggcagcag) were used for amplification [3]. PCR was conducted as follows: 5 min at 94°C; 30 cycles, 1 min at 94°C; 45s at 55°C; 1 min at 72°C; and 10 min extension at 72°C. The PCR mixture (50 μL) consisted of 50 ng template DNA, 5 μL of 10× PCR buffer, 0.4 μL of rTaq (5 μ/μL), 2.5 μL dNTP (2.5 mM), 1 μL upstream and downstream primers (20 μM), and ddH2O. Amplicon size was evaluated by agarose gel (2%) electrophoresis.

DGGE analysis. The PCR products were separated by DGGE on a polyacrylamide gel with a 35%–55% linear gradient. After the gel curdled, 10 μL PCR products were added. Gels were run at 60°C and 150 V for 5 h in 1× TAE buffer. After electrophoresis, the gel was stained using the silver staining method and imaged using the Gel-Doc 2000 (Bio-Rad, Hercules, CA). Desired bands were recovered from the amplification products and sequenced (Yimingbio Co. Ltd., Beijing, China). Sequences were analyzed using DNAstar and Cluster, and valid sequences were compared using the GenBank database to obtain the sequence with highest homology and identify reference strains.

Temperature coefficient. The Phelps equation was used to obtain a generalized estimate of the influence of temperature on kinetics in the AEB system (Eq.(1)).

$$K_T = K_{20}\theta^{T-20} \quad (1)$$

where K_T is the removal rate of COD ($mgCOD \cdot m^{-3} \cdot d^{-1}$), TN ($mgTN \cdot m^{-3} \cdot d^{-1}$), or TP ($mgTP \cdot m^{-3} \cdot d^{-1}$) at T °C; K_{20} is the removal rate of the substrate at 20°C; and θ is the temperature coefficient. To estimate the temperature coefficient (θ) of the AEB system, equation (1) was converted to equation (2), and logarithmic transformation was applied to equation (2) to obtain equation (3).

$$K_T / K_{20} = \theta^{T-20} \quad (2)$$

$$\mathrm{Ln}(K_T / K_{20}) = (T - 20)\mathrm{Ln}\,\theta \quad (3)$$

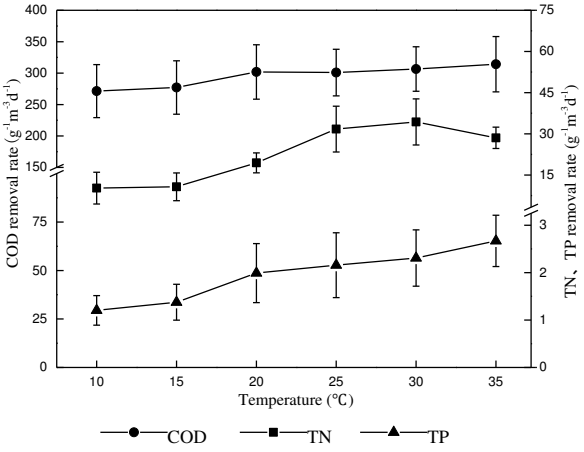

FIGURE 2

The average removal rate of COD, TN, and TP at different temperatures.

RESULTS AND DISCUSSION

Influence of temperature on system processing characteristics. The processing characteristics of the AEB system (COD, TN and TP) in all operating conditions were shown in Fig. 2. The microbial activity and average removal rate of COD, TN, and TP generally increased, respectively, in a range of temperature.

Maximum changes in COD and TP removal rates were 24.71 $g \cdot m^{-3} \cdot d^{-1}$ and 0.61 $g \cdot m^{-3} \cdot d^{-1}$, respectively, when the operating temperature raising from 15°C to 20°C. The COD removal efficiency was more than 80%(81.3% to 89.9%), which suggested that the influence of temperature on COD removal was not significant, it possibly because heterotrophic microorganisms involved in COD removal were abundant and capable of adapting to a wide range of temperatures. The TP removal efficiency increased from 27.0% to 59.2% and the change in the TP removal efficiency was greater than COD, which suggested that the influence of temperature on TP removal efficiency was significant. Some studies have indicated that most phosphorus-accumulating bacteria were psychrophilic which could adapt to the temperatures below 20°C while maintaining good phosphorus removal efficiency [4]. However, the phosphorus removal efficiency at 10°C and 15°C was 27.0% and 30.9%, respectively, in the AEB system

As temperature rise, the TN removal rate declined after first increasing. It was indicated that the operating temperature had a significant effect on the TN removal rate. There was a positive effect on the TN removal rate when the operating temperature roes from 10°C to 30°C; The maximum removal rate was observed at 30°C (12.3 $g \cdot m^{-3} \cdot d^{-1}$), which was consistent with results of a previous study [5].

Nitration was mainly conducted by autotrophic bacteria which were more sensitive to the change of temperature compared with heterotrophic bacteria. The optimum temperature for nitrifying and denitrifying bacteria was 22°C–37°C [6-7]. When the temperature of water was 35°C in the reservoir, the heat produced by microbial slightly increased the internal temperature of the layer compared to the surface of layer; this increase of temperature affected enzyme activity and inhibited denitrification.

Determination of the temperature coefficient. In the same system, the influence of temperature on processing characteristics was different among the different range of temperature, for examples, the TN removal rate in the AEB system declined after first increasing with the increase of temperature. Therefore, different temperature ranges were chosen to determine the temperature coefficient (θ) of individual processing characteristics. The temperature range of 10℃ -35℃ which showed the upward trend of the COD and TP removal rates was selected to determine the temperature coefficient (θ) of COD and TP, while the temperature range chosen for TN was 10°C -30°C. When the temperature exceeds 30°C , the TN removal rate decreased obviously. Combined with the results, $Ln\ (K_T/K_{20})$ was estimated as a function of (T–20), while $Ln\theta$ was the slope (Fig.3);

TABLE 1
Specific Shannon-Wiener index values and evenness and richness values calculated from density gradient gel electrophoresis profiles at different temperatures

	Initial	10°C	15°C	20°C	25°C	30°C	35°C
Shannon-Wiener	3	2.69	3.04	3.08	2.74	2.77	2.78
Evenness	0.98	0.95	0.98	0.98	0.97	0.98	0.98
Richness	21	17	22	23	17	17	17

thus, the corresponding temperature coefficient (θ) was obtained. The temperature coefficient (θ) of COD, TP and TN was 1.0062, 1.0336 and 1.0727 respectively. In the AEB system, the influence of temperature on the TN was the highest, followed by TP; the influence on COD was the lowest, which was consistent with the previous analysis of processing characteristics.

The temperature coefficient (θ) was different when the treatment processes was different. The organic matter was removed, θ_{COD} was 1.0062, which was lower than that in the traditional activated sludge process (1.04, range 1.00–1.08) and the traditional biological membrane method (1.035, range 1.02–1.08) [8]. This finding indicated that the AEB system has good temperature resistance in COD removal. In contrast, θ_{TN} was 1.0727 in this system, which was greater than that during the traditional activated sludge process (1.056) [9] and the traditional biological membrane method (1.043) [10], indicating that the influence of temperature on TN removal in the system was significant.

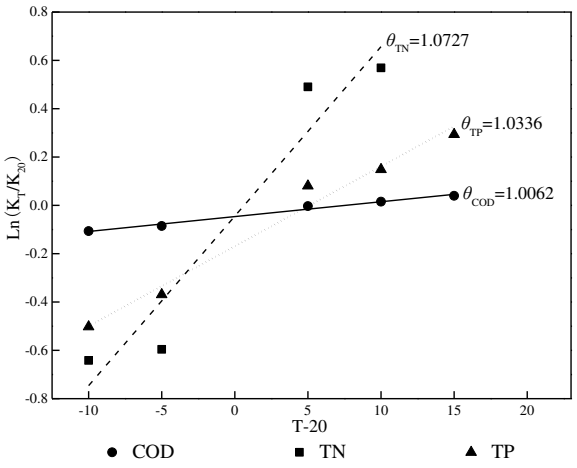

FIGURE 3
Graphical representation of Ln (K_T/K_{20}) as a function of T-20

To verify that the temperature coefficient (θ) is accurate, the measured and predicted values of the removal rate (K) at different temperatures in this study were compared by the chi-square test. No significant difference was found between measured and predicted values.

Effects of temperature on the microbial community. The analysis of the microbial community structure in the initial and final layers of different temperatures was shown in Fig. 4. The structure of the microbial community in the system was changed with temperature and a significant succession process was observed. Compared with the initial layer, some strains could not adapt to the operating conditions of the system and their domination gradually weakened and even disappeared (bands B, D, G, I, and P) in the final layer. However, some strains could be dominant at all temperatures. With an increase in temperature, the domination of psychrophilic microorganism populations (bands A, B, J, M, and N) gradually weakened or disappeared. Some mesophilic microorganism populations (bands C, H, K, L and Q) gradually increased.

As shown in Table 1, the Shannon-Wiener indices at 15°C and 20°C were 3.04 and 3.08, respectively, which were higher than those at other

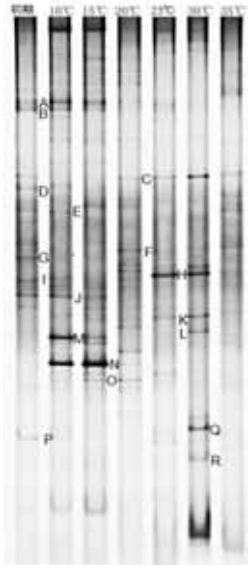

FIGURE 4
Density gradient gel electrophoresis profiles of the samples

temperatures, it indicated that the microbial diversity at 15℃ and 20℃ were higher than those at other temperature. The temperature range (15°C –20°C) was a transition zone for the microbial growth (from low-temperature to medium-temperature environment); therefore, not only psychrophilic microorganisms but also mesophilic microorganisms could thrive in this temperature range. The Shannon-Wiener indices at other temperatures were not significantly different.

The number of common bands in the DGGE profiles indicated the similarity among different samples (Fig. 4). As shown in Table 2, Dice indices among all samples were <60%, which indicated that the influence of temperature on the microbial community structure was significant. The Dice indices were relatively higher (>50%) at 10°C, 15°C, 25°C, and 30°C than those at other temperatures. The temperature ranges of 10°C –15°C and 25°C–30°C were stable growth environments for psychrophilic and mesophilic microorganisms; therefore, the effects of temperature on the microbial community were not significant in these ranges.

Eight bands (bands C, E, F, H, J, K, N, and O) were selected for the cloning and sequencing of DGGE profiles. The sequences were compared using BLASTN in the GenBank database (Table. 3). Among these, six bands belonged to Bacteroidetes (bands F, N), Proteobacteria (bands E, H), Firmicutes (band O), *Chlamydia* (band J), respectively, which were common strains in activated sludge [11]. Bands C and K were uncultured bacteria acquired from the sewage treatment system.

The Bacteroidetes species in this system, *Mucilaginibacter ginsenosidivorax* (Band F) was a facultative anaerobic bacterium. The temperature range for its growth was 4°C –32°C; therefore, the bacteria had a certain advantage in the temperature range of 20°C –25°C [12] and it could hydrolyze half-and-half lactose, maltose, sucrose and glucose but there was no effect of denitrify. *Flavobacterium oncorhynchi* (Band N) was an aerobic bacteria, which also could grow in the anoxic condition with a certain removal effect for nitrate and nitrite [13]. Studies have showed that the growth temperature of *Flavobacterium oncorhynchi* was relatively low and the bacteria would not survive at temperatures > 37°C; it was dominant at temperatures of 10°C –20°C, but gradually disappeared from the system with increasing temperature in AEB system.

TABLE 2
Dice index among different samples (%)

	Initial	**10**°C	**15**°C	**20**°C	**25**°C	**30**°C	**35**°C
Initial	100	37.2	38.2	53.4	54.9	43.3	39.4
10°C		100	53.3	34.2	32.2	22.0	16.0
15°C			100	47.0	30.3	25.5	16.0
20°C				100	46.8	33.8	25.7
25°C					100	51.2	35.7
30°C						100	33.8
35°C							100

TABLE 3
Comparison of nucleotide sequences and abundance of sequenced DGGE bands

Bands	**Closest relative**	**Accession no.**	**Identity (%)**	**Phylogenetic division**
Band C	Uncultured bacterium TB127-12	AB_196114	99%	-
Band E	*Defluviimonas denitrificans*	NR_118305	94%	Proteobacteria
Band F	*Mucilaginibacter ginsenosidivorax*	NR_109374	97%	Bacteroidetes
Band H	*Undibacterium parvum*	NR_115015	98%	Proteobacteria
Band J	*Parachlamydia acanthamoebae* UV-7	NR_074972	92%	Chlamydiae
Band K	Uncultured bacterium bf1-54	GU_257772	99%	-
Band N	*Flavobacterium oncorhynchi*	NR_117031	100%	Bacteroidetes
Band O	*Dorea formicigenerans*	NR_044645	91%	Firmicutes

The Proteobacteria species in this system, *Defluviimonas denitrificans* (Band E) was an aerobic bacterium, which grows in a wide temperature range of 10°C –40°C [14] . It existed at different temperature stages, but the dominant position was at a lower temperature as it was dominant at 10°C. Nitrate and nitrite were utilized as electron acceptors and translated into N_2 eventually, it was indicated that *Defluviimonas denitrificans* (Band E) could remove nitrogen which means it was responsible for nitrogen removal rate at 10°C. *Undibacterium parvum* (Band H) was a gram-negative and oxidase-positive bacterium, but it had no obvious effect on hydrolysis and the removal of organic matter [15] . Its optimum growth temperature range was 25°C –30°C, which agreeed with its dominance at 25°C –30°C .

The Firmicutes species in this system, *Dorea formicigenerans* (Band O) was heterotrophic bacterium which widely existed in water and soil and it could utilize cellulose, cellobiose, malt sugar, starch as the main carbon source for fermentation, resulting in the production of butyric acid, formic acid, small amounts of hydrogen and ethanol. It also had certain effect on COD removal [16] . In AEB system, it was dominant mainly from 15°C to 20°C. *Parachlamydia acanthamoebae* UV- 7 (Band J) widely existed in soil and the urban sewage treatment system [17]. it appeared in the temperature range of 10°C to 15°C in AEB system.

Uncultured bacterium TB127-12 (Band C) was isolated from a livestock-excreta treatment process and it could partially remove nitrate and ammonia with nitrification and denitrification occurring simultaneously. *Uncultured bacteriu- m TB127-12* (Band C) grew well and dominant in the temperature range of 20°C-35°C [18]. *Uncultured bacterium bf1-54* (Band K) was extracted from the MBR wastewater treatment system with the reaction temperature of 25 ± 2 °C [19] , which agreed with its dominant temperature range in the AEB system.

This study only set the temperature as control variables to determine the sewage processing characteristics and the influence on the microbial community. In the future work, it will be combined with other factors to optimize the overall performance of the AEB system, the function and dominant strains will be separated and enriched, the AEB system provide sufficient basis for engineering applications in the actual.

CONCLUSION

Temperature was the variable in this study aimed at evaluating the influence of temperature on AEB processing characteristics. PCR-DGGE and cloning sequencing technologies were utilized to study the system structure characteristics of the microbial community at different temperatures. The results were as follows:

1. In the AEB system, in the range of 10°C to 35°C, the removal rate of COD and TP increased with the rose of temperature. When the temperature rose from 15°C (low temperature) to 20°C (medium temperature) , the amplitude of the removal rates were the highest. However, the removal rate of TN showed a trend of declined after first increasing and the highest removal rate was observed at 30°C.

2. In the range of 10°C to 35°C, the temperature coefficients of COD and TP was 1.0062 and 1.0336, respectively. In the range of 10°C to 30°C, the temperature coefficient of TN was 1.0727. The influence of temperature on TN was the most obvious in the Atmosphere-Exposed Biofilm system.

3. With the change of the temperature in the AEB system, the Shannon-Wiener index and Dice index were changed, the succession in the microbial community was significant. The dominant strains were *Flavobacterium oncorhynchi* and *Parachlamydia acanthamoebae UV-7* (low temperature). *Uncultured bacterium TB127-12*, *Undibacterium parvum,* and *Uncultured bacterium bf1-54* were the significant dominant strains (medium-high temperature).

ACKNOWLEDGEMENTS

This study was supported by the National Science Fund of China (Grant No. 51269032). This study was a project of the Department of Education, Jilin Province (Reference: Jilin Education [2015] No. 39).

REFERENCES

[1] Li, J., Li, B., Zhu, G., Ren, N., Bo, L., and He, J. (2007). Hydrogen production from diluted molasses by anaerobic hydrogen producing bacteria in an anaerobic baffled reactor

(abr). International Journal of Hydrogen Energy, 32(15), 3274-3283.

[2] Chinese SEPA (2002) Water and Waste water Monitoring Methods, fourth ed. Chinese Environmental Science Publishing House, Beijing, China.

[3] Lapara, T. M., Nakatsu, C. H., Pantea, L. M. and Alleman, J. E. (2002). Stability of the bacterial communities supported by a seven-stage biological process treating pharmaceutical wastewater as revealed by pcr-dgge. Water Research, 36(3), 638-46.

[4] Helmer, C. and Kunst, S. (1998). Low temperature effects on phosphorus release and uptake by microorganisms in ebpr plants. Water Science & Technology, 37(4–5), 531-539.

[5] Zhang, T. T., Zhang, J., Yang, F., Xie, H. J., Zhen, H. U. and Yi-Ran, L. I. (2012). Effect of temperature on pollutant removal and nitrous oxide emission of wastewater nitrogen removal system. Environmental Science, 33(4), 1283-1287.

[6] Chiemchaisri, C. and Yamamoto, K. (1993). Biological nitrogen removal under low temperature in a membrane separation bioreactor. Water Science & Technology, 28(10), 325-333.

[7] Peng, Y. and Zhu, G. (2006). Biological nitrogen removal with nitrification and denitrification via nitrite pathway. Applied Microbiology & Biotechnology, 73(1), 15-26.

[8] Tchobanoglous, G. F. L. B. (1991). Wastewater engineering - treatment disposal, and reuse. third edition, revised. Dong Hwa technology, Seoul, Korea.

[9]Groeneweg, J., Sellner, B. and Tappe, W. (1994). Ammonia oxidation in nitrosomonas at nh 3, concentrations near *km* : effects of ph and temperature. Water Research, 28(12), 2561-2566.

[10]Zhu, S. and Chen, S. (2002). The impact of temperature on nitrification rate in fixed film biofilters. Aquacultural Engineering, 26(4), 221-237.

[11]Hu, M., Wang, X., Wen, X. and Xia, Y. (2012). Microbial community structures in different wastewater treatment plants as revealed by 454-pyrosequencing analysis. bioresour technol. Bioresource Technology,117(10), 72-79.

[12]Jiang, F., Dai, J., Wang, Y., Xue, X.,Xu, M., Gou, Y., Li, W., Fang, C. and Peng, F. (2012) Mucilaginibacter soli sp. nov., isolated from Arctic tundra soil.International Journal of Systematic & Evolutionary Microbiology, 62(Pt 7), 1630-1635.

[13]Zamora, L., Fernández-Garayzábala, J. F., Svensson-Stadler, L. A., Palacios, M. A., Dominguez, L., Moore, E. R. B. and Vela, A. I. (2012) Flavobacterium oncorhynchi sp. nov., a new species isolated from rainbow trout (Oncorhynchus mykiss).(oncorhynchus mykiss). Systematic & Applied Microbiology, 35(2), 86-91.

[14]Foesel, B. U., Drake, H. L. And Schramm, A. (2011). Defluviimonas denitrificans gen. nov. sp. nov. and pararhodobacter aggregans gen. nov. sp. nov. non-phototrophic rhodobacteraceae from the biofilter of a marine aquaculture. Systematic & Applied Microbiology, 34(7), 498-502.

[15]Kämpfer, P., Rosselló-Mora, R., Hermansson, M., Persson, F., Huber, B., Falsen, E. and Busse, H. J. (2007). Undibacterium pigrum gen. nov. sp. nov. isolated from drinking water. International Journal of Systematic & Evolutionary Microbiology, 57(4), 1510-1515.

[16]Taras, D., Simmering, R., Collins, M. D., Lawson, P. A. and Blaut, M. (2002). Reclassification of eubacterium formicigenerans holdeman and moore 1974 as dorea formicigenerans gen. nov. comb. nov. and description of dorea longicatena sp. nov. isolated from human faeces.International Journal of Systematic & Evolutionary Microbiology, 52(Pt 2), 423-428.

[17]Collingro A; Tischler P; Weinmaier T; Penz T; Heinz E; Brunham RC; Read TD; Bavoil PM; Sachse K; Kahane S; Friedman MG; Rattei T; Myers GS; Horn M. (2011). Unity in variety-the pan-genome of the chlamydiae. Molecular Biology & Evolution, 28(12), 3253-70.

[18]Hoshino, T., Terahara, T., Yamada, K., Okuda, H., Suzuki, I.Tsuneda, S., Hirata, A. and Inamori, Y. (2006). Long-term monitoring of the succession of a microbial community in activated sludge from a circulation flush toilet as a closed system. Fems Microbiology Ecology, 55(3), 459-70.

[19]Xia, S., Li, J., He, S., Kang, X., Wang, X., Zhang, Y. and Duan,L. (2010). The effect of organic loading on bacterial community composition of membrane biofilms in a submerged polyvinyl chloride membrane

bioreactor. Bioresource Technology, 101(17), 6601-6609.

Received: **18.12.2015**
Accepted: **14.06.2016**

CORRESPONDING AUTHOR

Ming-Ji Jin
Agricultural College of Yanbian University, Yanji Jilin 133000, China

email: jinmingji@ybu.edu.cn

© by PSP Volume 25 – No. 10/2016, pages 4235-4241 Fresenius Environmental Bulletin

FEASIBILITY AND ECONOMIC ANALYSIS FOR SUPERCRITICAL CO2 EXTRACTION OF DIESEL FROM OIL SANDS

Wang Yuzhen[1,2*], Pu Lei[3], Gao Fen[1], Yang Jianqiao[2], Fang Changqing[1], Zhao Gaoyang[1], Li Yanhui[2], Wang Shuzhong[2]

[1]Xi'an University of Technology, Shaanxi Xi'an 710048, China
[2]Key Laboratory of Thermo-Fluid Science and Engineering of MOE, Xi'an Jiaotong University, Xi'an, Shaanxi ,710049, China
[3]Research Institute of Petroleum Exploration and Development, Petro China Changqing Oilfield Company, Xi'an, Shaanxi, 710018, China

ABSTRACT

In order to analyze the technical feasibility and economy of diesel extraction from oil sands using supercritical CO_2 as solvent. Supercritical CO_2 extraction of the long-chain alkanes of C_{10}, C_{16}, C_{18} and C_{20}, which are the main compounds in diesel were studied. Influences of the operating prameters of pressure, extraction time, CO_2 flow rate, and effect of methanol as cosolvent were investigated. Aspen Plus software was also used to simulate the extraction efficiencies, and the results were consistent with the experiment results. Results indicated that the extraction efficiency of C_{10}~C_{20} could reach 95% at 35°C, 20 MPa, with a flow rate ratio of methanol to CO_2 of 0.3, and extraction time of 180 min. Technical economy of the supercritical CO_2 extraction system with a processing capacity of 20 $t \cdot d^{-1}$ were evaluated. Results indicated that when treated the oil sands with an oil content of 21wt%, the system investment was 2.4 million dollars, with a daily revenue of 3740 dollars, and the investment can be recouped within two years.

KEYWORDS:
Supercritical CO_2 extraction, diesel, oil sands, economy.

INTRODUCTION

During the crude drilling and mining process, a lot of oil sands will be generated. According to a conservative estimate, a single drilling would contaminate at least 6666 m^2 land. These contaminated lands generally contain an oil content of 20%~30% and are unlikely to be reclaimed. Without appropriate treating, the remaining oil in the lands would continue to contaminate surrounding lands, water, and air through permeation and vaporization [1]. China currently has 128 oil-gas fields and 24 large oilfields. Generally, one small to medium sized oilfield produces approximately 100 tons of oil sands per day. Since China began oil exploitation in 1935, even a small oilfield could have accumulated as much as 400,000 tons of oil sands [2]. Without being effectively processed, these sands are collected and stored in the open air, which result in tremendous environmental pollution and energy waste. Additionally, it would further reduce the farmland which already has been a scarce resource in China.

Oil sands pollution is a kind of major waste pollution widely existed in Chinese oilfields. As early as 1998, the State Environmental Protection Administration listed oil sands as a kind of hazardous waste and required that oil sands must be harmless teated. Oil sands are a valuable secondary resource. Effectively collecting and recycling oil sands can not only recover large quantities of crude oil and create economic benefits for oilfields, but also effectively protect the environment and reduce the huge disposing costs. Therefore, from economic and environmental perspectives, it is essential and urgent to recycle oil sands and make them harmless. Currently, hot alkali washing and solvent extraction are primary methods used to extract oil [3]. However, these two methods have somewhat disadvantages. For example, hot alkali washing requires large quantities of hot alkaline water to soak and wash oil sands. This method is expensive and labor-intensive, consumes large quantities of water and produces a large amount of wastewater, which causes secondary pollution. Whlie the solvent extraction usully use hydrocarbons as solvent oil, the system is very comlicated and the equipment investment is high. In addition, solvent oil has a very low flash point and is highly combustible, it poses a great fire safety hazard and has no obvious economic benefits. Therefore, it is imperative to develop an efficient, economic, and clean oil sands separation technology.

Recent years, as a clean and efficient separation technology, supercritical CO_2 extraction has received wide attention for oil extraction and separation [4,5,6]. Supercritical CO_2 is a fluid state of CO_2 where it is held at or above its critical temperature (31°C) and critical pressure (7.38 MPa). Supercritical CO_2 has properties of both liquid and

gas, such as the high diffusivity of gas and the high solubility of liquid. The low viscosity, and low surface tension, make it able to quickly penetrate into microporous substances. Therefore, supercritical CO_2 is more efficient and effective than liquid when used for extraction. Currently, supercritical CO_2 extraction technology has been widely used in the fields of food and medicine. However, it is seldom to be reported to be used to extract diesel from oil sands. This paper evaluates the feasibility and technical economy of diesel extraction from oil sands using supercritical CO_2 in order to provide a new idea for oil sands treatment.

MATERIALS AND APPARATUS

CO_2 (99% purity) was purchased from Xi'an Chenzhong Chemical Industry Co., Ltd. Alkanes of C_{10}, C_{16}, C_{18} and C_{20} (analytically pure) were purchased from Sinopharm Chemical Reagent Beijing Co., Ltd.

Supercritical CO_2 extraction equipment (HA221-40-20) were purchased from Nantong Yichuang Experiment Instruments Co., Ltd. The exraction simulation process was operated by Aspen Plus 11.1 software.

Concentration of C_{10}, C_{16}, C_{18} and C_{20} were determined using a gas chromatograph (Shanghai, GC-112) equipped with a flame ionization detector (FID) and a 30 m × 0.25 mm DB-5 elastic quartz capillary column.

FEASIBILITY ANALYSIS OF DIESEL EXTRACTION FROM OIL SANDS BY SUPERCRITICAL CO2

Solubility of the main compounds in diesel in supercritical CO2. Diesel is made up of different hydrocarbons and mainly consists of long-chain alkanes (mainly C_{10}~C_{20}), naphthenes and aromatics, with an average molecular weight of 220~240.
Its chemical and physical properties range between those of gasoline and heavy oil, with a boiling point of 200°C~350°C and a specific gravity of 0.82 $kg \cdot L^{-1}$ ~ 0.845 $kg \cdot L^{-1}$. The types and mass fractions of the compounds in diesel are shown in Table 1[7].

The solubility of the main compounds in diesel in supercritical CO_2 is shown in Figure 1[8]. According to Figure 1, the increasing pressure promotes alkanes dissolve in supercritical CO_2, and the effects are more significantly at a pressure greater than 12.5 MPa for C_{10}, C_{18} and C_{20}. At 35°C and 20 MPa, the solubility of C_{18} and C_{20} are as great as 30.08 $g \cdot (100gCO_2)^{-1}$ and 12.74 $g \cdot (100gCO_2)^{-1}$. The effect of pressure on C_{16}'s solubility is little at 10 MPa~12 MPa, while the solubility increased with the increasing pressure (higher than 12MPa). At a pressure greater than 12 MPa, the solubility of alkanes reduces as the number of carbon atoms increases under the same conditions.

A comparison of C_{18} and C_{20} at 35°C and 45°C at the same pressure shows that an increase in temperature reduces the solubility of alkanes, which mainly due to the efffect of temperature on the density of fluid and the vapor pressure (volatility) of solute, both of which constrain the dissolving capacity of supercritical fluid [8]. When the volatility and diffusivity of separated constituents improved by increased temperature are not sufficient to offset the decrease in dissolving capacity caused by the sharp decline in the density of supercritical CO_2 due to the increasing temperature, the increase in temperature will cause a decrease in the solubility of substances in supercritical CO_2.

Figure 1 also shows that the pressures for the maximum solubility of different substances differ. In practice, pressure can be regulated based on the properties of substances in order to realize the efficient extraction of soluble substances. Although the solubility of alkanes larger than C_{20} is relatively low, it can be improved by adding cosolvents during extraciton process.

TABLE 1
Types and mass fractions of the compounds in diesel.

Compounds	n-alkanes	isoparaffin	mononuclear aromatics	polycyclic aromatic hydrocarbon	oxide	substituted amides
Types	15~19	20~29	3~13	3~19	3~17	1
Mass fractions (%)	49.02~59.66	13.16~25.16	1.62~4.08	2.15~18.25	1.21~14.42	0~ 3.77

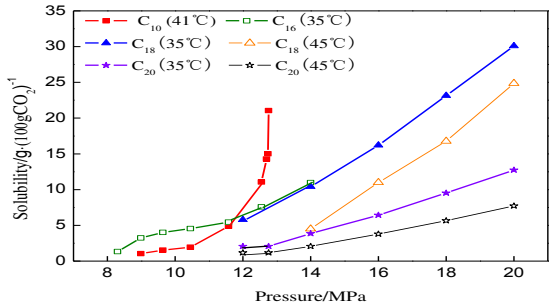

FIGURE 1
The solubility of the main compounds in diesel in supercritical CO_2.

Experiments and simulation results. The supercritical CO_2 extraction process is primarily performed at constant temperature and varying pressure, constant temperature and constant pressure, and constant pressure and varying temperature. As without temperature changes, the process at constant temperature and varying pressure is easy to operate and is commonly used. In this paper, the process at constant temperature and varying pressure was selected. The influences of operating parameters of temperature, pressure, extraction time, and CO_2 flow rate were investigated by numerical simulation and experiment. In order to reduce the energy consumption of the system, a low operating temperature of 35°C was selected. The treated capacity of C_{10}~C_{20} is 10g.

The effect of pressure on extraction efficiency. The curve in Figure 2 shows the simulation results of the effects of pressure on extraction efficiencies of C_{10}, C_{16}, C_{18}, C_{20} using supercritical CO_2 as solvent at 35°C, CO_2 flow rate of 0.4 ml·min^{-1} and extraction time of 180 min. The experiments results are shown in scatter plot in Figure 2. Results indicated that the simulation values and the experimental values were basically consistent, proving the reliability of the simulation results.

As pressure increased, the extraction efficiencies increased. And the extractioin efficiencies decreased as the number of carbon atoms increased at the same condition when pressure higher than 12MPa. At a pressure of 14 MPa, the extraction efficiency of C_{10} reached 98% while that of C_{20} was lower than 50%; when pressure increased to 20 MPa, the extraction efficiency of C_{20} was only 70%. To achieve an extraction efficiency of above 90%, extraction pressure should increase to 24 MPa, which is primarily due to the low solubility of C_{20} in supercritical CO_2 (Figure 1).

In order to increase the solubility of C_{20} in supercritical CO_2 and improve the corresponding extraction efficiency, methanol was used as a cosolvent with a mass flow rate ratio of methanol to CO_2 of 0.3. The extraction efficiency of C_{20} with and without addition of methanol at 35°C is shown in Figure 3. According to this figure, after addition of methanol, C_{20} could obtain an extraction efficiency of greater than 95% at 20 MPa. Therefore, the operating pressure of the extraction system was set as 20 MPa.

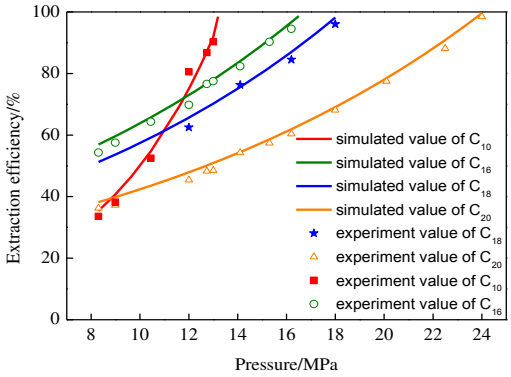

FIGURE 2
Effect of pressure on extraction efficiencies (35°C).

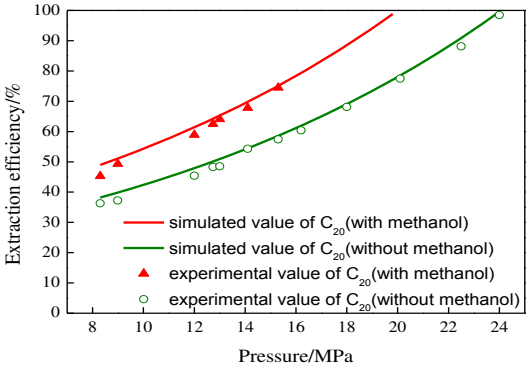

FIGURE 3
The extraction efficiency of C_{20} with and without methanol (35°C)

The effects of CO_2 flow rate and reaction time on extraction efficiency. The above results indicated that the extraction of high carbon number alkanes largely determined the overall extraction efficiency of diesel in oil sands. This section selected C_{20} as model compound of the high carbon number alkanes. The influences of extraction times and CO_2 flow rates at the extraction efficiencies of C_{20} were evaluated at 35°C, 20 MPa. The results are shown in Figure 4.

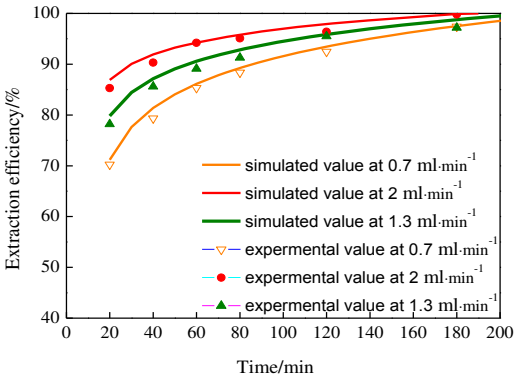

FIGURE 4
Influences of the extreaction time and CO_2 flow rates on C_{20} extraction efficiencies (35°C, 20 MPa).

According to Figure 4, the extraction efficiency gradually increased as the CO_2 flow rate increased, which primarily because the increase in the CO_2 flow rate intensified the collision between the feed and the supercritical CO_2 and helped strengthen mass transfer and improve extraction efficiency. The increasing extraction time also improved the extraction efficiency before 180min. And the positive effects was little after 180 min. The extraction efficiency of C_{20} can reach 95% at an extraction time of 180 min, indicating that it is feasible be extracted using supercritical CO_2.

ECONOMIC ANALYSIS OF DIESEL EXTRACTION FROM OIL SANDS USING SUPERCRITICAL CO2.

Process. Taking the oil sands (an initial diesel content (mass fraction) of 21%, a specific gravity of 1.6 g·(cm^{-3}) of ** oilfield as an example, a process was designed for a supercritical CO_2 extraction system with a handling capacity of 20 t·d^{-1}, and its technical economy was assessed. The process of the supercritical CO_2 extraction system is shown in Figure 5. The system operates at constant temperature and decreased pressure. The supply of a cosolvent is provided in order to further improve the extraction efficiency of high-carbon alkanes.

The operating procedure is as follows: The oil sands are sent to the extraction kettle through a conveyor firstly, and then the CO_2 in CO_2 storage tank and the cosolvent in storage tank of cosolvent enter the buffer tank through gas compressor and liquid compression pump, respectively. The mixture in the buffer tank enters the extraction kettle, and the valves at the inlet and outlet of the extraction kettle are closed. Then the heater is switched on. After a period of time after the temperature in the kettle reaches the extraction temperature, the valve at the bottom of the kettle is opened in order to discharge the sands. The valve at the exit on the top of the kettle is opened, and the gas-phase fluid enters the separator via the throttle valve. Diesel is discharged from the exit at the bottom of the separator. The gas at the top returns to the buffer tank via the purifier. Two extraction kettles are set in the system to operate alternately in order to realize continuous operation.

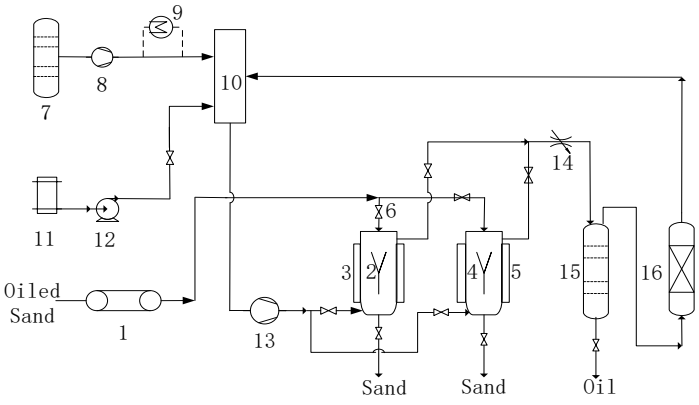

FIGURE 5
The process of the supercritical CO_2 extraction system.
1 - band conveyor, 2 - the first extraction kettle, 3 - the first heater, 4 - the second extraction kettle, 5 - the second heater, 6 - valves, 7 - CO_2 storage tank, 8 - low-pressure gas compressor, 9 - preheater, 10 - buffer tank, 11 - storage tank of cosolvent, 12 - liquid compression pump, 13 - high-pressure gas compressor, 14 – throttle valve, 15 - separator, 16 - gas purifier.

TABLE 2
Main technical parameters and production capacity of the supercritical CO_2 extraction system.

Items	Technical parameters	
Main technical parameters	particle size of the oil sludge sand	≥840 μm
	the maximum extraction pressure	35 MPa
	extraction temperature	20°C ~80°C
Production capacity/24h	volume of the extraction kettle	1200 L
	effective volume of the extraction kettle	935 L
	daily production	11 kettles
Occupied area	32m × 24 m=768 m^2	

The configuration of the extraction system is shown in Table 3. Through calculation, the complete set of devices of this system costs 2.4 million dollars.

TABLE 3
Configuration of the extraction system.

Items	Equipment	Material	quantity	Price/million dollars
Materials cost	extraction kettle	22253 duplex stainless steel	2	1.40
	separator	22253 duplex stainless steel	2	
	purifier	22253 duplex stainless steel	2	
	purification column	silica gel	2	
	preheater	22253 duplex stainless steel	1	
	heater	22253 duplex stainless steel	2	
	storage tank of CO_2	Q345R seamless steel pipe	1	
	buffer tank	31353 duplex stainless steel	1	
	storage tank of entrainer	30408 duplex stainless steel	1	
Equipment cost	belt conveyor	—	2	0.50
	liquid compression pump	—	2	
	low-pressure gas	—	2	
	high-pressure gas	—	2	
	pipes and valves	—	80	
	instrumentation and controls	—	1	
Processing	—	—	—	0.32
Installation	—	—	—	0.08
Cost of material	—	—	—	0.12
Total	—	—	—	2.42

Technical parameters and economic analysis. The main technical parameters and production capacity of the supercritical CO_2 extraction system is shown in Table 2. The design pressure of the system is 35 MPa and can be adjusted according to experimental results in practice. The design volume of the extraction kettle is 1200 L, and the effective volume of the extraction kettle is 935 L.

TABLE 4
Operating cost of the extraction system.

Items	Quantity	Price	Operation cost/$·t^{-1} oil sands
CO_2 consumption	35 kg·kettle^{-1}	125 $·t^{-1}$CO_2$	2.4
Power consumption	240 kW·h	0.2 $·(kW·h)$^{-1}$	57.6
Labor	5 person	470 $·(month·person)$^{-1}$	4
Total (excludes the diesel earning)			64

The operating cost of the extraction system is shown in Table 4. It takes the supercritical CO_2 extraction system 64 dollars to treat a ton of oil sands, and the diesel production is 4 t·d^{-1} when calculated for an extraction efficiency of 95%. If the market price of diesel is 1,256 dollars per ton, processing a ton of oil sands will directly earn 251 dollars, and a profit of 3,740 dollars can be obtained per day after subtraction of the operating cost. The investment in equipment will be recouped within two years. Existing technology for solidification and burning of oil sands can only earn 48 dollars per ton of oil sands through recovery of crude oil (a recovery rate of 10%), and a profit of 386 dollars can be obtained per day (calculated based on a handling capacity of 20 t·d^{-1}) after subtraction of the processing cost of 28.5 dollars per ton of oil sands [9], far lower than that obtained using supercritical CO_2 extraction technology. However, the oil sand can be harmless treated by solidification and burning technology, as the organic matter carried by them will be completely removed and can be discharged directly. By contrast, although supercritical CO_2 can be used to obtain an extraction efficiency of saturated alkanes C_{10}~C_{20} of 95%, the extraction efficiency of the resin and asphaltene in oil sands are only 54% and 33% [10], and the treaded oil sands still have a high content of organic matter and need to be further treated. Therefore, the expenses required for subsequent treating should also be taken into account. Taking the solidification and burning disposal cost for the treated oil sands by supercritial CO_2 into account, the operating cost of the system increases from 64 dollars per ton to 89 dollars per ton, and the net profit reduces from 3740 to 3138 dollars, also proving the economic advantages of supercritical CO_2 extraction technology.

However, it needs to be pointed out that supercritical CO_2 extraction technology is of value to diesel recovery only when used treating oil sands with a high diesel content. It will be of no value if the diesel content is lower than 8%, because the profit obtained through diesel recovery is lower than the operating cost under this condition. Therefore, although supercritical CO_2 extraction technology can obtain economic benefits when used to recover diesel from oil sands, its widespread application should be based on the characteristics of oil sands.

CONCLUSION

Diesel extraction from oil sands using supercritical CO_2 is efficient and clean. The main compounds in diesel are alkanes, naphthenes and arenes. According to the simulation and experimental results, the extraction efficiency of C_{10}~C_{20} can reach 95% at 35°C, 20 MPa, a mass flow rate ratio of methanol to CO_2 of 0.3 and extraction time of 180 min, proving the feasibility of using supercritical CO_2 to extract diesel from oil sands.

The economic analysis for a supercritical CO_2 extraction system with a treatment capacity of 20 t·d^{-1} showed that the whole investment would cost 2.4 million dollars. And a profit of 3740 dollars can be obtained per day for a diesel production of 4 t·d^{-1}, and the equipment investment can be recouped within two years. However, supercritical CO_2 extraction technology cannot completely make oil sands harmless, and the processed oil sands need to be further processed. In addition, this technology can produce economic benefits only when used to process oil sands with a diesel content of higher than 8%.

ACKNOWLEDGEMENTS

The study was supported by Postdoctoral Science Foundation of China (126540), and Shaanxi Colleges Association of Science and Technology for Young Talent Lifts (20160115).

REFERENCES

[1] Zhang, W., Mclellan, B. and Sha Y. (2010) The first domestic sludge separation equipment was born in Zhen Jiang. Zhenjiang daily 02.
[2] Li, X. (2012) The study on Northeast Asia regional energy security and energy cooperation. Ph.D. Thesis. Jilin University, Jilin, China.
[3] Lin, W., Jiang, W., Wei, F. and Zhen, G. (2013) The new progress of Oily Sludge Treatment

Technology. Guangzhou Chemical Industrial 14, 14-26.
[4] Wang, J., Wang, Y., Zhen, L., Ni, S., Fan, Z., Yao, R. and Chen, K. (2014) Kinetic study on extraction of red pepper seed oil with supercritical CO_2. Chinese Journal of Chemical Engineering 22, 44-50.
[5] Bagheri, H., Manap, M.Y.B.A. and Zeinab, S. (2014) Antioxidant activity of piper nigrum L. essential oil extracted by supercritical CO_2 extraction and hydro-distillation. Talanta 121, 220-8.
[6] Jin, J. and Tong, J. (2014) Optimization of supercritical extraction of oil from onion by supercritical CO_2. Asian Journal of Chemistry 26, 142-144.
[7] Huang, T., Wei, F., Xu, S.Y., Gu, Y.D. and Qian, S. (1998) Application of GC-MS to analysis of fraction of saturated hydroearbons and single-ring aromatics of light diesel oil from catalytic cracking. Petrochemical Technology 17, 652-659
[8] Karen, C., Frederic, L.L., Pouillot, L. and Eckert. C. A. (1996) Phase equilibria of alkanes in natural gas systems. 3. alkanes in carbon dioxide. Journal of Chemical and Engineering Data 41, 6-10.
[9] J. Liu. (2006) The study on incineration technology and integrated utilization of oil-sand in Shengli oilfield. M.S. Thesis, Ocean University, Qingdao, China.
[10] L. Lian. (2011) Study on supercritical CO2 extraction of oily sludge. M.S. Thesis, China University of Petroleum, Beijing, China.

Received: **18.12.2015**
Accepted: **25.07.2016**

CORRESPONDING AUTHOR

Wang Yuzhen
Xi'an University of Technology
Xi'an, Shaanxi, CHINA

E-mail: yzwangxjtu@163.com

© by PSP Volume 25 – No. 10/2016, pages 4242-4245 Fresenius Environmental Bulletin

ONE-POT METHOD FOR SYNTHESIS OF $CoSe_2$-ETHYLENEDIAMINE NANOFLOWERS

Xian Zhang*, Fengqiong Shi

State Key Laboratory of Environmental Chemistry and Ecotoxicology, Research Center for Eco-Environmental Sciences, Chinese Academy of Sciences, Beijing, 100085, PR China

ABSTRACT

The inorganic-organic hybrid composites $CoSe_2$-ethylenediamine ($CoSe_2(en)_{1.4}$) were successfully synthesized via a simple hydrothermal method. The structure and morphology of obtained sample were characterized by X-ray diffraction (XRD), scanning electron microscopy (SEM), and energy dispersive X-ray spectrum (EDS) and X-ray photoelectron spectrometer (XPS). The as-obtained samples were consisted of $CoSe_2(en)_{1.4}$ nanoflowers with the size of ca. 5 μm. In addition, the thermogravimetric (TG) analysis study of $CoSe_2(en)_{1.4}$ presented a certain thermodynamic stability. We believed also that it would accelerate the development of $CoSe_2$-amine in their promising applications, such as thermal and magnetic fields.

KEYWORDS:

$CoSe_2(en)_{1.4}$, hydrothermal synthesis, inorganic-organic, flower-like.

INTRODUCTION

Inorganic-organic hybrid composites have attracted considerable interest from material scientists and engineers owing to their occurring new properties and technological applications [1]. In these special composite structure, the materials usually enhance or combine the inorganic frameworks magnetic, optical, thermal, rigidity properties with the organic molecules structural flexibility and diversity [2]. Low dimensional inorganic-organic hybrid nanocrystals were described previously for their potential applications as building blocks for the production of electronic, magnetic and optical nanodevices, such as ZnS/amine [3]. Only a few studies, have been focus on the synthesis of the metal selenide, moreover, the two or three dimensional structure of inorganic-organic hybrid composites with a well–defined shape building units have been reported.

Until now, $CoSe_2$, an important pyrite-type semiconductor, were carried out by some research groups [4–10]. Additionally, some groups have successfully synthesized the $CoSe_2$ on the carbon, metal or metallic oxide, such as $CoSe_2$/C [5–7], Mn_3O_4/$CoSe_2$ [4] and Pt/$CoSe_2$ [10]. However, the related extraordinary capability of $CoSe_2$ has rarely been researched with nanoscale building units primarily due to the limited availability of high-quality materials. Herein, in this study, we synthesized a new $CoSe_2$-amine (amine: ethylenediamine (en)) material via a simple hydrothermal method.

MATERIALS AND METHODS

All reagents were analytical grade and used without further purification and the water used was deionized. $CoSe_2(en)_{1.4}$ nanoflowers were synthesized by hydrothermal reaction of 0.5 mmol $CoCl_2{\cdot}6H_2O$ and 1.0 mmol Na_2SeO_3, in a mixed solution with 3 mL deionized water, 5 mL $N_2H_4{\cdot}H_2O$ (85%), and 22 mL ethylenediamine at 180 °C for 24 h. After heating, it was removed from the oven and naturally cooled to room temperature. The prepared sample was collected by centrifugation, washed with deionized water and absolute ethanol three times respectively, and the obtained sample was dried in vacuum at 60 °C for 12 h.

The products were characterized by X-ray diffraction measurements carried out on X-ray diffractometer (XRD, Bruker D8 Advance diffractometer) with Cu-Ka radiation in the range of 10–80° at a scanning rate of 7 °min^{-1} at the same research condition without further treatment. The morphology and energy dispersive X-ray spectrum (EDS) of samples were observed by a scanning

electron microscopy (SEM, S-4800). The investigation of the surface of material was by an X-ray photoelectron spectrometer (XPS, PHI-5300). The thermogravimetric analysis of $CoSe_2(en)_{1.4}$ was measured by integrated thermal analyzer (TG, STA 449C) with 10 °C min^{-1} from room temperature to ca. 1000 °C under N_2 atmosphere.

RESULTS AND DISCUSSION

As presented in the Fig. 1(a), the wide angle reflections can be ready indexed to a cubic phase of $CoSe_2$ with lattice constants a=0.586 nm (JCPDS 9-234). Some broadening width of all reflection peaks should be related to the special structure with 2D nanosheets building units. The morphology and size of the products prepared by the procedures described in the experimental section are visualized by SEM as shown in Figs. 1(b)-(c). The low-magnification SEM image (Fig. 1(b)) reveals that the as-obtained products are composed of uniform flower-like structures with an average diameter of ca. 5 μm. The high-magnification SEM images (Fig. 1(c)) show that the flower-like structure $CoSe_2(en)_{1.4}$ are composed of lots of two dimensional structure nanosheets with thickness of ca. 100 nm and length of 1.5–2.5 μm as building units. EDS analysis shows the mean atom ratio of Co/Se is nearly 1:2. We have found that the N element in the products.

The quality and composition of the as-prepared samples are further studied by X-ray photoelectron spectroscopy analysis. The N1s features of the samples shown in Fig. 2(b), have a binding energy of 399.24 eV. The Se 3d features of $CoSe_2(en)_{1.4}$ nanoflowers shown in Fig. 2(c) have a binding energy of 56.18 eV. Fig. 2(d) presents the Co 2p XPS spectrum of the composite, which exhibits two peaks at 798.98 eV and 781.62 eV, corresponding to the Co $2p_{1/2}$ and Co $2p_{3/2}$, respectively, which are in agreement with correspond to the previous reports [11].

The TG result further supports the proposed formula. It is obvious that the product shows continuous weight loss from 25 to 1000 °C (Fig. 3). The continuous weight change of 1.93% (wt) from room temperature to 300 °C is due to the release of freely bound water and ethylenediamine (step A); step B shows a distinct weight loss of 27.86% (wt) over 400–600 °C, resulting from the release of en; the another marked weight loss in step C is due to the loss of selenium. The 27.86% (wt) loss from 400 to 600 °C is consistent with the calculated mass loss of 27.94% (wt) for the thermal decomposition reaction of $CoSe_2(en)_{1.4}$ into $CoSe_2$ under ideal state without the loss of Se.

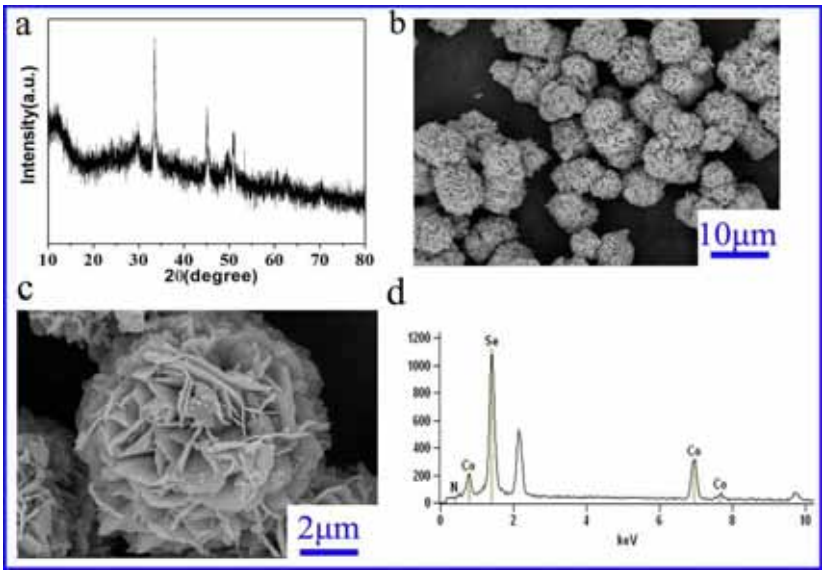

FIGURE 1
(a) XRD pattern of the typically as-synthesized $CoSe_2(en)_{1.4}$ nanoflowers; (b) Low- and (c) high-magnification SEM images of as-obtained flower-like $CoSe_2(en)_{1.4}$; (d) The EDS image of the above obtained sample.

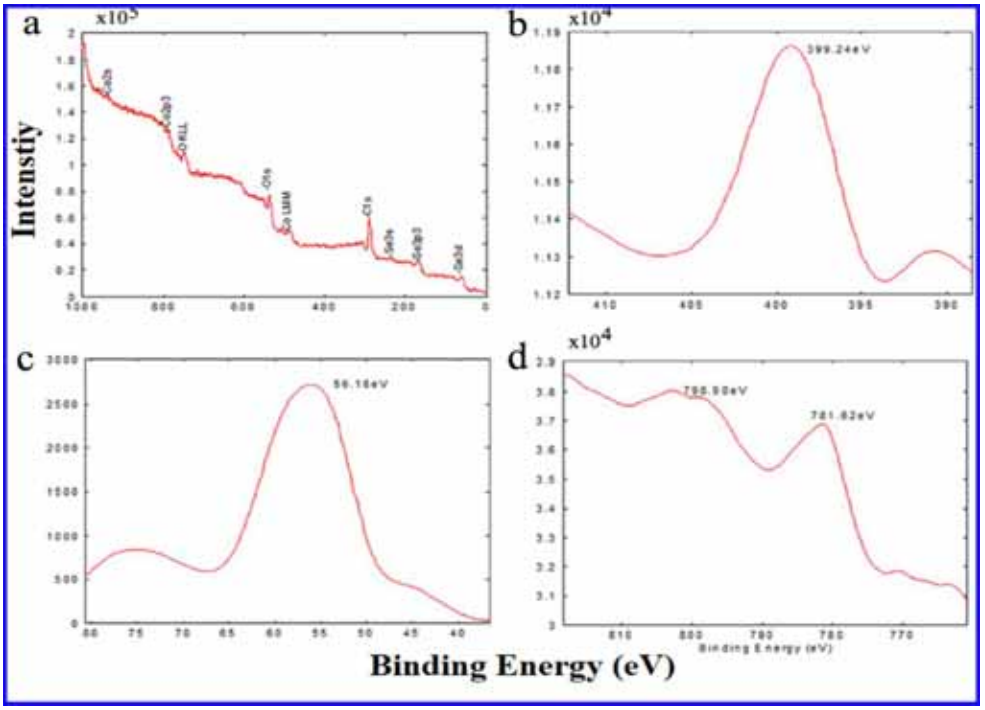

FIGURE 2
XPS pattern of the as-prepared $CoSe_2(en)_{1.4}$ sample.

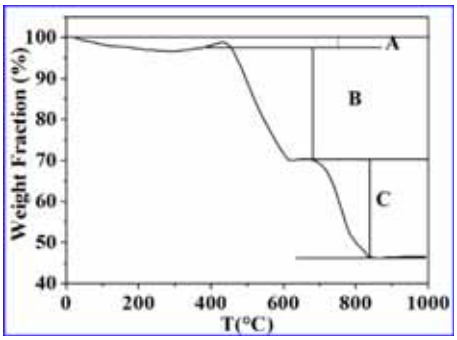

FIGURE 3
TG curve of the obtained $CoSe_2(en)_{1.4}$ nanoflowers under N_2 atmosphere.

CONCLUSION

In this study, we reported a simple and controllable hydrothermal synthetic approach of $CoSe_2(en)_{1.4}$ nanoflowers with nanosheets as building units for the first time. We have measured the obtained samples with the XRD, SEM, EDS and XPS. In addition, $CoSe_2(en)_{1.4}$ nanoflowers displayed a certain thermodynamic stability. We believe that our work will be supporting the basic theory study and practical implication for the $CoSe_2$ and its organic hybrid composites.

REFERENCE

[1] Yao, W. T. and Yu, S. H. (2008) Synthesis of semiconducting functional materials in solution: from II-VI semiconductor to inorganic-organic hybrid semiconductor nanomaterials. Advanced Functional Materials 18, 3357–3366.

[2] Huang, X. and Li, J. (2007) From single to multiple atomic layers: A unique approach to the systematic tuning of structures and properties of inorganic-organic hybrid nanostructured semiconductors. Journal of the American Chemical Society 129, 3157–3162.

[3] Yao, W. T., Yu, S. H. and Wu, Q. S. (2007) From mesostructured wurtzite ZnS-nanowire / amine nanocomposites to ZnS nanowires exhibiting quantum size effects: a mild-solution chemistry approach. Advanced Functional Materials 17, 623–631.

[4] Gao, M. R., Xu Y. F., Jiang J., Zheng Y. R. and Yu S. H. (2012) Water oxidation electrocatalyzed by an efficient Mn3O4/CoSe2 nanocomposite. Journal of the American Chemical Society 134, 2930–2933.

[5] Feng, Y., He, T. and Alonso-Vante, N. (2007) In situ free-surfactant synthesis and ORR-electrochemistry of carbon-supported

Co3S4 and CoSe2 nanoparticles. Chemistry of Materials 20, 26–28.

[6] Feng, Y., He, T. and Alonso-Vante N. (2010) Carbon-supported CoSe2 nanoparticles for oxygen reduction reaction in acid medium. Fuel Cells 10, 77–83.

[7] Kong, D., Wang, H., Lu, Z. and Cui Y. (2014) CoSe2 nanoparticles grown on carbon fiber paper: an efficient and stable electrocatalyst for hydrogen evolution reaction. Journal of the American Chemical Society 136, 4897–4900.

[8] Gao, M. R., Liu, S., Jiang, J., Cui, C. H., Yao, W.T. and Yu, S. H. (2010) In situ controllable synthesis of magnetite nanocrystals/CoSe2 hybrid nanobelts and their enhanced catalytic performance. Journal of Material Chemistry 20, 9355–9361.

[9] Gao, M. R., Yao, W. T., Yao, H. B. and Yu, S. H. (2009) Synthesis of unique ultrathin lamellar mesostructured CoSe2-amine (protonated) nanobelts in a binary solution. Journal of the American Chemical Society 131, 7486–7487.

[10] Gao, M. R., Gao, Q., Jiang, J., Cui, C. H., Yao, W.T. and Yu S. H. (2011) A methanol-tolerant Pt/CoSe2 nanobelt cathode catalyst for direct methanol fuel cells. Angewandte Chemie 123, 5007–5010.

[11] Jiang, J., Shi, W., Song, S., Hao, Q., Fan, W., Xia, X., Zhang, X., Wang, Q., liu, C. and Yan, D. (2014) Solvothermal synthesis and electrochemical performance in super-capacitors of Co3O4/C flower-like nanostructures. Journal of Power Sources 248, 1281–1289.

Received: **27.12.2015**
Accepted: **23.07.2016**

CORRESPONDING AUTHOR

Xian Zhang
State Key Laboratory of Environmental Chemistry and Ecotoxicology, Research Center for Eco-Environmental Sciences, Chinese Academy of Sciences, Beijing, 100085, PR CHINA

E-mail: zx2010413@hotmail.com

© by PSP Volume 25 – No. 10/2016, pages 4246-4252 Fresenius Environmental Bulletin

DISAPPEARANCE OF SOME FUNGICIDES IN MATURE APPLES IMMEDIATELY BEFORE SUPPLYING FRUIT TO THE CONSUMER

Bartosz Piechowicz[1*], Stanisław Sadło[1], Ewa Szpyrka[2], Kinga Stawarczyk[3], Michał Stawarczyk[1], Przemysław Grodzicki[4]

[1] Department of Ecotoxicology, Institute of Applied Biotechnology and Basic Science, University of Rzeszów, Werynia, Poland
[2] Experimental Station in Rzeszów, Institute of Plant Protection–National Research Institute, Rzeszów, Poland
[3] Department of Botany, Institute of Applied Biotechnology and Basic Science, University of Rzeszów, Werynia, Poland
[4] Department of Animal Physiology, Faculty of Biology an Environmental Protection, Nicolaus Copernicus University, Toruń, Poland

ABSTRACT

Studies on dissipation of active ingredients (AIs) of plant protection products (PPPs), after their application against diseases of fungal origin, which may develop during the period from fruit harvesting to the day of their consumption, were carried out. Just after the last spraying, the average residue levels of the tested fungicides in ripe fruits were 3.586 ±0.511 and 2.090 ±0.545 mg kg^{-1} (captan), 0.237 ±0.061 mg kg^{-1} (boscalid), 0.092 ±0.034 mg kg^{-1} (pyraclostrobin), 0.106 ±0.031 and 0.126 ±0.016 mg kg^{-1} (trifloxystrobin), 0.236 ±0.064 mg kg^{-1} (cyprodinil) and 0.294 ±0.039 mg kg^{-1} (fludioxonil), and then were decreasing by half ($t_{1/2}$) within 6−11 days after the treatment. On the other hand, the residues of those substances at the day of harvest were still significantly higher than 0.01 mg kg^{-1}, which means that the apples were not suitable for the production food for infants and young children.

KEYWORDS:
ripe apples, fungicide residues, dissipation rate, maximum residue levels, safe consumption levels

INTRODUCTION

Many studies have shown that application of plant protection products (PPPs), commonly known as pesticides, may cause a health hazard to consumers [1-4], especially to the children [5-9], whose detoxification mechanisms yet, are not fully developed [7]. Paradoxically, the abandonment of the fungicides use may lead to the infection of fruits or vegetables, and in effect, to the occurrence of mycotoxins, organic compounds much more toxic than active ingredients (AIs) of currently used PPPs [10,11]. Therefore, the usage of fungicides, especially in commercial farms, is now necessary not only from an economic point of view, but also with regard to the consumer's health.

The residue levels of any AI of PPP in fruit or vegetables, depend on many factors. The most important is its application rate, and then a time elapsing from the treatment day to the harvest (the actual disappearance of residues), and a growth of edible parts of the plant (biological dilution of residues) which took place at that time [12]. Therefore, we may expect of the relatively higher residues, when a given substance is applied immediately before the harvest. In the case of apple orchards, such situation is caused by the need of protection ripe fruit against *Venturia inaequalis*, an *Ascomycetae* fungus, that causes the apple scab, and the bitter rot. The perpetrator of these diseases is *Pezicula* spp., while the gray mold (*Botrytis cinerea*), which constitutes a serious threat to the health and quality of fruits, during the period from their harvesting to delivery to the consumer [13].

The aim of our study was to determine the residue levels of captan, boscalid, pyraclostrobin, trifloxystrobin, cyprodinil and fludioxonil, active ingredients of fungicides, which are now commonly used to protect apples against the developing diseases, during the period from fruit harvesting until the delivery to the consumer, and to establish the dissipation rate of these substances in ripe apples. Based on this, in relation to currently in force Maximum Residue Levels (MRLs), as well to Acceptable Daily Intakes (ADIs), the consumer's health hazards were estimated.

MATERIALS AND METHODS

Field trials. The field trials were carried out in the commercial orchard, implementing the principles of Integrated Pest Management (IPM). In total, six trials were performed, and as a result, dissipation trends of the following AIs were established:

- cyprodinil and fludioxonil in Gloster variety after a single application of Switch 62.5 WG (trial 1),

- captan in Gloster variety after two applications of Merpan 80 WG at an interval of seven days (trial 2),
- captan in Lobo variety after a single application of Merpan 80 WG (trial 3),
- trifloxystrobin in Lobo and Gloster varieties after a single application of Zato 50 WG (trials: 4 and 5),
- boscalid and pyraclostrobin in apples and Golden Delicious after a single application of Bellis 38 WG (trial 6).

The tested substances are AIs of some fungicides, that effectively protect the ripe apples against fungal diseases. The treatments were performed on day 8 (trials: 3−5) or 15 (trials: 1, 2, and 6) before fruit harvesting.

Sampling. The sampling was started on next day after the treatment, and then it was continued by 7 and 14 following days (only in the case of trial 1, 2, and 6). In each sampling date, and for each combination active ingredient − apple variety, four laboratory samples (each consisting of 8 ripe fruits, about 1.5 kg) were collected from eight trees selected randomly (the apples from each tree, were also selected randomly) and then the samples were transported to the laboratory where they were prepared for analysis by grinding and mixing, for the removal of analytical portions with minimal sampling error.

Extraction procedure. Analytical portions (about 100 g of homogenized laboratory sample) were blended in a Waring Commercial 8010 EG blender with 150 mL of acetone and filtered under vacuum in a Büchner's funnel [14-16]. The blender jar was flushed with 50 mL of acetone and the washings were used to wash the filter cake. 1/5 of the volume of the obtained filtrate (the equivalent of approx. 20.0 g of fruit) was used for further analysis and placed in a separatory funnel together with 100 mL of 2.5% solution of sodium sulphate(VI) (Na_2SO_4). The pesticide residues were extracted three times with 20, 10 and 10 mL of dichloromethane. The combined extracts were evaporated to dryness, dissolved in approx. 10 mL of petroleum ether and cleaned up on a florisil mini-column [17]. Pesticides were eluted with 70 mL of a mixture of ethyl ether - petroleum ether 3:7 (*v/v*), and then 70 mL of the mixture of acetone-petroleum ether 1:9 (*v/v*).

Gas chromatographic determination. The final extracts were analysed on Agilent 7890 gas chromatograph equipped with the Microcell Electron Capture Detector (μECD) and Nitrogen Phosphorus Detector (NPD), and fused silica column (HP-5ms Ultra Inert column: Length: 30 m, I.D.: 0.32 mm, Film Thickness: 0.25 μm). Temperature of the injector and detectors was 250 and 300ºC, respectively. The extracts (2 μL) were injected in splitless mode. The oven temperature was programmed as follows: 100°C – 0 min → 10°C/min → 180°C – 4 min → 3°C/min → 220°C – 15 min → 10°C/min → 260°C – 11 min; the total time of the analysis was 55.3 minutes. Nitrogen (purity 6.0, flow 4.14 mL min^{-1}) was the carrier gas and the makeup gas for the μECD (30 mL min^{-1}) and NPD (10 mL min^{-1}). For the NPD, hydrogen and air flows were kept at 3 and 60 mL min^{-1}, respectively.

Dissipation kinetics. After the treatment, ripe apples stayed on the trees yet, for a short time of Pre-Harvest Intervals (PHIs; 7 or 14 days), and due to this, the sampling was carried out only in two or three dates. Nevertheless, we decided to describe the dissipation trends of the tested substances by the exponential function,

$$R_t = R_0 e^{-k \times t},$$

where R_t represents the residue (concentration in mg kg^{-1}) of any pesticide on a *t*-day after treatment, R_0 represents the initial pesticide concentration at $t=0$, and k is the rate constant (in day^{-1}), corresponding to the first-order kinetics equation. Based on obtained equations, we determined the half-life ($t_{1/2}=ln2/k$) for each substance, as well $R_{t=7}$ and $R_{t=14}$, which represented their average residue levels after 7 and 14 days (PHIs established in Poland) and the minimum time

$$t_R = 0.01 mg \times kg^{-1},$$

that must elapse before the residues will fall below the level of 0.01 mg kg^{-1}, the standard for baby food.

The average residue levels of the tested substances just after their application (R_0; mg kg^{-1}), derived from exponential equations, were compared to MRLs, as well, were used for estimation of the safe consumption level (*SCL*; kg) of apples for toddlers (body weight = 16.7 kg), and for adult consumer (body weight = 60 kg) according to the following equation:

$$SCL = \frac{ADI \times b.w.}{R_0} \text{ [kg]}.$$

RESULTS

Residue levels of tested fungicides. The average levels (±standard deviations) of captan (3.586 ±0.511 mg kg^{-1}, and 2.090 ±0.545 mg kg^{-1}; trials 2 and 3), boscalid (0.237 ±0.061 mg kg^{-1}), pyraclostrobin (0.092 ±0.034 mg kg^{-1}), trifloxystrobin (0.126 ±0.016 mg kg^{-1}, and 0.106 ±0.031 mg kg^{-1}; trials 4 and 5), cyprodinil (0.236 ±0.064 mg kg^{-1}) and fludioxonil (0.294 ±0.039 mg kg^{-1}) residues in samples of ripe apples collected just after treatments, then a week (trials 1−6), and two weeks later /after (trials: 1, 2, and 6), were determined. Based on those experimental data, the

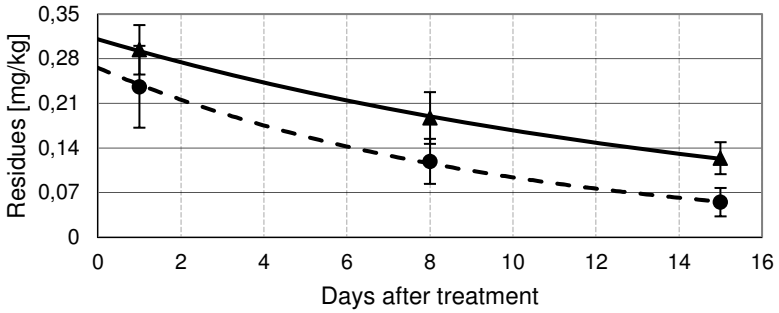

FIGURE 1
Disappearance trends of cyprodinil (●) and fludioxonil (▲) residues in apples of Gloster variety, Trial 1

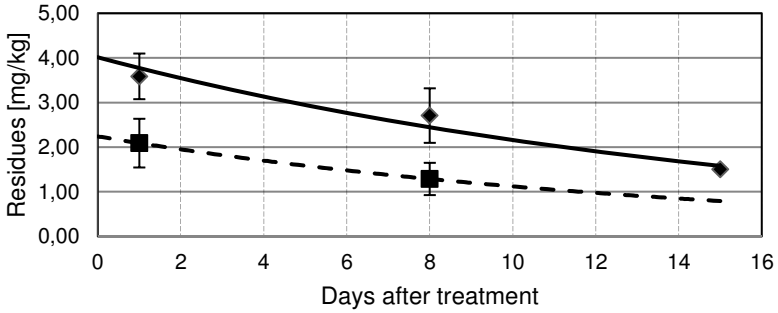

FIGURE 2
Disappearance trends of captan residues in apples of Gloster (♦ Trial 2) and Lobo (■ Trial 3) varieties.

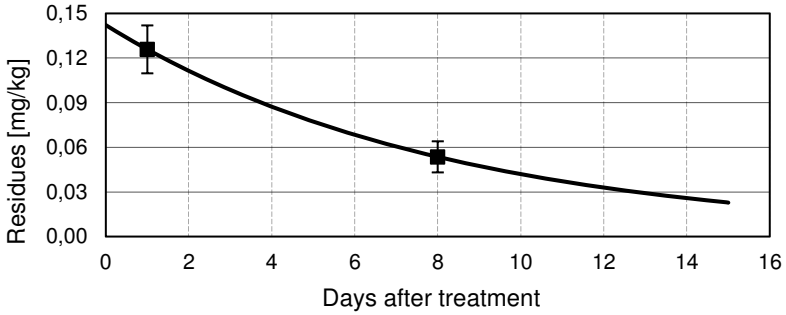

FIGURE 3
Disappearance of trifloxystrobin (■) residues in apples of Lobo variety, Trial 4

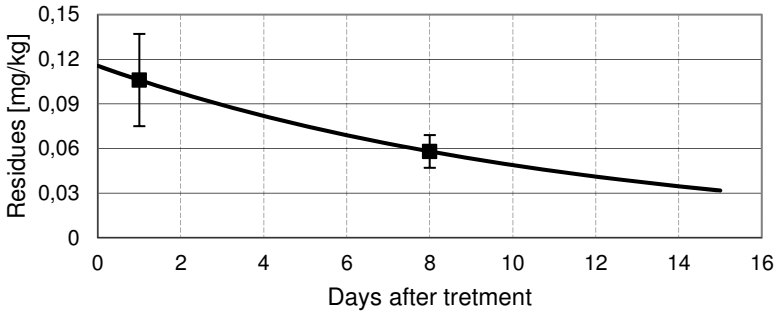

FIGURE 4
Disappearance of trifloxystobine (■) residues in apples of Gloster variety, Trial 5.

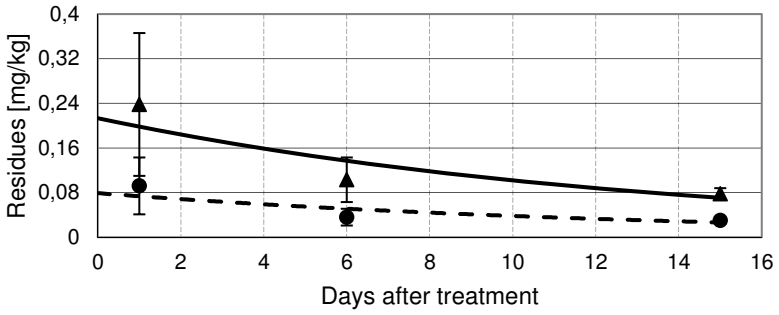

FIGURE 5
Disappearance trends of boscalid (▲) and pyraclostrobin (●) residues in apples of Golden Delicious, Trial 6.

exponential equations of dissipation trends of all substances within the last two weeks before fruit harvesting were derived (Fig. 1−5).

According to the established exponential equations (Figure 1−5), initial residues (R_0) of AIs of the tested fungicides were proportional to their application rates. As a result, the average residues of captan (application rate: 1.9 kg of AI per ha) reached the highest values, which, after a single application of Merpan 80 WG (AI: 80% captan) amounted to 2.240 mg kg^{-1} (trial 3), and after two applications of the same formulation at the one week interval, 4.016 mg kg^{-1} (trial 2). The average residues of other substances included in our field trials were at the range from 0.084 (pyraclostrobin) to 0.311 mg kg^{-1} (fludioxonil). Therefore, except for captan after two applications (4.016 mg kg^{-1}; trial 2), the average residue levels of all the tested substances present in ripe apples at the next day after treatment, ranged well below the current MRLs, and after fourteen days (R_{14}) dropped to the levels of 11% (trifloxystrobin) to 42% (captan; Test 2) of R_0.

Dissipation of captan, boscalid, pyraclostrobin, trifloxystrobin, cyprodinil and fludioxonil residues in ripe apples

Fludioxonil and captan residues (after two applications of Merpan 80 WG; trial 2) decreased most slowly, and their dissipation rate constants, k, amounted to 0.062 day^{-1} (trial 1 and 2), while the same parameter determined for other substances were in the range of 0.069 day^{-1} (captan, trial 3) to 0.122 day^{-1} (trifloxystrobin, trial 4), on average about 0.093 day^{-1}. As a result of those differences, the initial average residues of fludioxonil and captan decreased by half within 11 days, and the remaining AIs within 6−10 days (Table 1).

Based also on the parameters of the exponential decay (R_0, k; Table 1), we have calculated the approximate period of time within which the residues should drop to the level of 0.01 mg kg^{-1} (t_R = *0.01 mg/kg*), permitted in foods destined for infants and young children. The results obtained indicated that within 22−35 days the average residues of cyprodinil, trifloxystrobin, pyraclostrobin and boscalid should drop below the rigorous level of 0.01 mg kg^{-1}, mentioned above, whilst the residue of fludioxonil, but especially captan (tests 2 and 3; the highest application rates, replication of spraying), not earlier than in two months, which means that these fruits are not eligible as a food, safe for administration to infants and young children.

TABLE 1
Dissipation parameters of tested substances established for ripe apples

Common name of AI (trial number)	R_0 [mg kg^{-1}]	k [day^{-1}]	$t_{1/2}$ [day]	$t_{R=0.01}$ [day]	$P_{t=8}$ [mg kg^{-1}]	$P_{t=15}$ [mg kg^{-1}]
Cyprodinil (1)	0.266	0.104	7	32	0.128	0.062
Fludioxonil (1)	0.311	0.062	11	56	0.202	0.131
Trifloksystrobin (4)	0.142	0.122	6	22	0.061	0.026
Captan (2)	4.016	0.062	11	97	2.599	1.682
Captan (3)	2.240	0.069	10	78	1.379	0.848
Boscalid (6)	0.226	0.090	8	35	0.120	0.064
Piraclostrobin (6)	0.084	0.089	8	24	0.045	0.024
Trifloksystrobin (5)	0.116	0.086	8	28	0.063	0.035

TABLE 2
SCL and percentage of MRLs (% MRL) calculated for ripe apple containing the highest possible (initial) residue levels (R_0) of tested fungicides

Common name of AI (trial number)	R_0 [mg kg^{-1}]	ADI [mg kg^{-1} b. w.]	SCL		MRL [mg kg^{-1}]	% MRL
			Toddler [kg]	Adult [kg]		
Cyprodinil (1)	0.266	0.03	1.6	6.8	1	26.6
Fludioxonil (1)	0.311	0.37	17.3	71.4	5	6.2
Trifloksystrobin (4)	0.142	0.1	10.2	42.3	0.5	28.4
Captan (2)	4.016	0.1	0.4	1.5	3	133.9
Captan (3)	2.24	0.1	0.6	2.7	3	74.7
Boscalid (6)	0.226	0.04	2.6	10.6	2	11.3
Piraclostrobin (6)	0.084	0.03	5.2	21.4	0.3	28.0
Trifloksystrobin (5)	0.116	0.1	12.5	51.7	0.5	23.2

Protection of apple orchards versus the consumer's health hazards

In general, the initial residue levels (R_0, Table 1) of all tested substances, within the first week after the treatment, decreased significantly. From the consumer's point of view, what is most desirable effect [18]. However, the growers, performing a treatment in the apple orchard two weeks before harvesting do not know when their product will reach the consumer, therefore, they expect the effective protection of apples against diseases of fungal origin, which not only alter their organoleptic characteristics [13], but also produce toxic patulin [19,20] disqualifying the fruit. Thus, a question arises whether the fungicide deposits, still present on ripe apples 7 days (PHI) after the treatment, when the residue dropped by half of the initial value, and especially 14 days after treatment, when the average initial residues decreased by 75%, will provide effective protection of the apples against the diseases of fungal origin, during several days of their transportation to the consumer [10,19,11]. Knowing that the daily consumption of apples in different countries is varied, in order to estimate the consumer's health hazards, we decided to calculate, and compare, the Safe Consumption Levels (SCLs) for apples containing possibly the highest residue levels. As Table 2 shows, that a real threat, especially for young people, may constitute ripe apples containing relatively high captan residues, close to those residues which were found immediately after the treatment. The estimated SCLs (Table 2) of apples by toddlers on a daily basis over a lifetime without an appreciable health risk amounted to 0.4 kg (Table 2) (after two applications of Captan 80 WG) and 0.6 (after single application of the same or similar fungicides). Consumption of fresh apples which previously have contained residues such as those found in present study immediately after the treatments, after PHIs should be completely safe for the both groups of consumers. Moreover, taking into account that Acute Reference Doses (ARfDs) are two to five times greater than ADIs, we may conclude that apples, containing trifloxystrobin, cyprodinil, fludioxonil, boscalid and piraclostrobin residues should not cause any acute health problems

Pesticide residues versus MRLs. The highest residue levels were found in apples of Gala variety, and they included captan just after the applications of Captan 80 WG. In general, the average captan contents constituted 134% (after a double application) and 75% of MRL (after a single application), while the average trifloxystrobin, cyprodinil, fludioxonil, boscalid and piraclostrobin residues after a single application of Zato 50 WG, Switch 62.5 WG, and Bellis 38 WG, ranged from 6.2% of MRL (fludioxonil) to 28.4% of MRL for trifloxystrobin, respectively. Based on the above relative residue levels of the tested substances present on ripe apples next day after the treatment (R_0), as well taking into account established exponential equations of their dissipation, on day 7 (R_7), and, in particular, on day 14 (R_{14}) after treatments (see Table 1), it may be concluded that in some cases, the MRLs (Table 1) were fixed at an undue levels. It is, therefore, necessary to consider the need of lowering their levels, while maintaining the current PHI (7 and 14 days), or to shorten the PHI in such a way to give competent authorities a tool to assess plant protection program of a given grower in the light of principles of Good Plant Protection (GPP) practice. Otherwise, some MRLs currently in force will continue to meet only the formal and legal requirements.

DISCUSSION AND CONCLUSIONS

The residues of captan, boscalid, pyraclostrobin, trifloxystrobin, cyprodinil and fludioxonil in ripe apples, except of captan residues (3.586 ±0.511 mg kg^{-1}, vs MRL = 3.0 mg kg^{-1}) after double application of Merpan 80 WG, just after treatments were well below their MRLs. Based on their average values, the exponential equations of

dissipation trends of all substances within the last two weeks before fruit harvesting were derived.

Fludioxonil and captan residues (after two applications of Merpan 80 WG) decreased most slowly (respectively, k = 0.062 day^{-1}), while dissipation rate constants (k) of other substances were in the range from 0.069 to 0.122 day^{-1}, and on average amounted to about 0.093 day^{-1}.

The decrease in residue level below 0.01 mg kg^{-1}, now in force in the States of European Union, is possible in the cases of strobilurins: trifloxystrobin (within 22 and 28 days), and pyraclostrobin (within 24 days), while for cyprodinil and boscalid, not earlier then after 32 and 35 days, respectively.

Currently in force MRLs, in the cases of boscalid, pyraclostrobin, trifloxystrobin, cyprodinil and fludioxonil were set at too high levels, and as a result, they meet formal and legal requirements only.

The estimated Safe Consumption Level of apples by toddlers on a daily basis over a lifetime without an appreciable health risk amounted to 0.4 kg (after two applications of Captan 80 WG) and 0.6 (after a single application of the same or similar fungicide) thus, taking into account respective PHIs, the apples should be completely safe for the both groups of consumers.

REFERENCES

[1] Bretveld, R. W., Thomas, C. M. G., Scheepers, P. T. J., Zielhuis, G. A. and Roeleveld, N. (2006) Pesticide exposure: the hormonal function of the female reproductive system disrupted? Reproductive Biology And Endocrinology 4, 30.

[2] Lai, B. C. L., Marion, S. A., Teschke, K. and Tsui, J. K. C. (2002) Occupational and environmental risk factors for Parkinson's disease. Parkinsonism & Related Disorders 8, 297−309.

[3] Piechowicz, B., Stawarczyk, K and Stawarczyk, M. (2012) Hazard posed by using chemicals for plant. Bezpieczeństwo Pracy 3, 5−7.

[4] Zala, S. M. and Penn, D. J. (2004) Abnormal behaviours induced by chemical pollution: a review of the evidence and new challenges. Animal Behaviour 68, 649−664.

[5] Bailey, H. D., Armstrong, B. K., de Klerk, N. H., Fritschi, L., Attia, J., Scott, R. J., Smibert, E. and Milne, E. (2011) Exposure to professional pest control treatments and the risk of childhood acute lymphoblastic leukemia. International Journal of Cancer 129, 1678−1688.

[6] Piechowicz, B. (2013) Impact of the use of pesticides on children's health. Bezpieczeństwo Pracy 12, 22−24.

[7] Holland, N., Furlong, C., Bastaki, M., Richter, R., Bradman, A., Huen, K., Beckman, K. and Eskenazi, B. (2006) Paraoxonase polymorphisms, haplotypes, and enzyme activity in latino mothers and newborns. Environmental Health Perspectives 114, 985−991.

[8] Pierik, F. H., Burdorf, A., Deddens, J. A., Juttmann, R. E. and Weber, R. F. A. (2004) Maternal and paternal risk factors for cryptorchidism and hypospadias: a case–control study in newborn boys. Environmental Health Perspectives 112, 1570−1576.

[9] Wohlfahrt-Veje, C., Main, K. M., Schmidt, I. M., Boas, M., Jensen, T. K., Grandjean, P., Skakkebæk, N. E. and Andersen, H. R. (2011) Lower birth weight and increased body fat at school age in children prenatally exposed to modern pesticides: a prospective study. Environmental Health 10, 79.

[10] Asam, S. and Rychlik, M. (2013) Potential health hazards due to the occurrence of the mycotoxin tenuazonic acid in infant food. European Food Research and Technology 236, 491−497.

[11] Kuiper-Goodman, T. (1995) Mycotoxins: risk assessment and legislation. Toxicology Letters 82/83, 853−859.

[12] Kostka, G., Urbanek-Olejnik, K. and Liszewska, M. (2011) Risk assessment for cumulative exposure to pesticide residues in food. Roczniki PZH 62, 127−136.

[13] Kühn, B. F. and Thybo, A. K. (2001) Sensory quality of scab-resistant apple cultivars. Postharvest Biology And Technology 23, 41−50.

[14] Sadło, S. and Szpyrka, E. (2001) Behaviour of pyrimethanil residues on tomato plants. Journal of Plant. Protection Research 41, 302−308.

[15] Sadło, S., Szpyrka, E., Piechowicz, B. and Grodzicki, P. (2015) A case study on toxicological aspects of the pest and disease control in the production of the high-quality raspberry (*Rubus idaeus* L.). Journal of Environmental Science and Health B. 50, 8−14.

[16] Sadło, S., Szpyrka, E., Stawarczyk, M. and Piechowicz, B. (2014) Behavior of pyrimethanil, pyraclostrobin, boscalid, cypermethrin and chlorpyrifos residues on raspberry fruit and leaves of Laszka variety. Journal of Environmental Science and Health B 49, 159−168.

[17] Valverde-Garcia, A., Gonzalez-Pradas, E. and Aguilera-Del Real, A. (1993) Analysis of buprofezin residues in vegetables. Application

to the degradation study on eggplant grown in a greenhouse. Journal of Agricultural and Food Chemistry 41, 2319−2323.
[18] Czernyszewicz, E. (2011) Fruit quality as assessed by consumers. Żywność Nauka Technologia Jakość 5, 173−187.
[19] Kawauchiya, T., Takumi, R., Kudo, Y., Takamori, A., Sasagawa, T., Takahashi, K. and Kikuchi, H. (2011) Correlation between the destruction of tight junction by patulin treatment and increase of phosphorylation of ZO-1 in Caco-2 human colon cancer cells. Toxicology Letters 205, 196−202.
[20] Morales, H., Sanchis, V., Rovira, A., Ramos, A. J. and Marín, S. (2007) Patulin accumulation in apples by *Penicillium expansum* during postharvest stages. Food Control 18, 1443−1448.

Received: **25.12.2015**
Accepted: **25.07.2016**

CORRESPONDING AUTHOR

Bartosz Piechowicz
Department of Ecotoxicology,
Institute of Applied Biotechnology and Basic Science, University of Rzeszów,
Werynia 502, 36-100 Kolbuszowa, Poland

e-mail: bpiechow@poczta.onet.pl

© by PSP Volume 25 – No. 10/2016, pages 4253-4260 Fresenius Environmental Bulletin

EVALUATION OF CHOLINESTERASE FROM THE MUSCLE AND BLOOD OF *ANABAS TESTUDINEUS* AS DETECTION OF METAL IONS

Siti Aqlima Ahmad[1*], Mohd Khalizan Sabullah[2], Ain Aqilah Basirun[1], Ariff Khalid[4], Nur Adeela Yasid[1], Izzuanuddin Muhammed Iqbal[1], Nor Aripin Shamaan[4], Mohd Arif Syed[1] , Mohd Yunus Shukor[1].

[1]Department of Biochemistry, Faculty of Biotechnology and Biomolecular Sciences, Universiti Putra Malaysia, 48300 Serdang, Selangor, Malaysia.
[2]Faculty of Sciences and Natural Resources, Universiti Malaysia Sabah, Jalan UMS, 88000 Kota Kinabalu, Sabah, Malaysia.
[3]Faculty of Health Sciences, Universiti Kebangsaan Malaysia, Jalan Raja Muda Abdul Aziz, 50300 Kuala Lumpur, Malaysia.
[4]Faculty of Medicine and Health Sciences, Universiti Sains Islam Malaysia, 13th Floor, Menara B, Persiaran MPAJ, Jalan Pandan Utama, Pandan Indah, 55100 Kuala Lumpur, Malaysia.

ABSTRACT

Another alternative source of cholinesterase (ChE) that is sensitive towards metal ion has been revealed. ChE from muscle and blood of *Anabas testudineus* were extracted and purified through ammonium sulphate precipitation followed by an ion exchange chromatography with a total recovery of 47.66% and 7.92%, respectively. Kinetic study measured that BTC was the most preferable synthetic substrate to blood ChE while muscle ChE preferred PTC with the biomolecular constant of 1.07 and 0.53 mM, respectively. Optimum pH for blood and muscle ChE were determined at 8 and 9. Both ChE shared an optimum temperature of 30°C. Inhibition study showed that muscle ChE has inhibited more than 50% of metal ions namely arsenic, chromium, copper, mercury and zinc compared to blood ChE with only copper and mercury. Studies on half inhibitory effect (IC_{50}) of blood and muscle ChE were tested with series concentration of mercury calculated at 1.003 and 1.048 mg/L. This result will be used as a reference for future development of biosensor.

KEYWORDS:
Cholinesterase, Metal ions, Purification, *Anabas testudineus*

INTRODUCTION

In recent years, there has been an increase of awareness on the wide occurrences of heavy metals pollution in the environment especially towards the aquatic system. Heavy metals are able to transform into persistent metallic compound in which it can accumulate organisms' body system, disturbing the food chain and eventually threatened the human life [1]. In trace amount, metal ions actually aid to maintain the homeostasis as well as being important for cellular growth [2]. The presence of metal ions normally facilitates the formation of enzyme – substrate complex. However, some metal ions such as lead and cadmium that have the similarities with substrates will form stable conjugates with the active site or allosteric site of enzyme consequences to the alteration of the active site conformation and physical function failure [3-5].

Cholinesterase (ChE) enzyme is one of the targets of toxic effect of metal ion [6]. ChE such as acetylcholinesterase (AChE; E.C.3.1.1.7) play its role in catalysing the hydrolytic cleavage of acyl group in various esters of choline at the synaptic cleft, while butyrylcholinesterase (BChE) that is able to hydrolyse larger molecules such as butyrylcholine work as co-regulator of cholinergic neurotransmission, and involved in detoxification of several compounds [7-10]. Propionylcholinesterase (PChE) has a similar function with BChE as both enzymes shared an enzyme classification code; E.C. 3.1.1.8, and also known as pseudocholinesterase. The inhibition of ChE may cause the accumulation of acetylcholine, which results to biological complications such as diarrhoea, muscle weakness, headache associated with the development of Alzheimer disease and paralysis [11,12]. Tilton et al. (2008) demonstrated that the alteration of swimming performance and natural behaviour of zebrafish and annelid worms are related to the inhibition of ChE, respectively [13].

The utilisation of ChE extracted from aquatic organisms especially fish as a biomarker to study the effect of anticholinesterase has been developed according to the study on biological responses of organisms to pollutants especially in aquatic system [14,15]. ChE has been reported as a broad type toxicant biosensor as since it has the capability to sense the sensitive towards the present of pesticides, surfactant, drug, heavy metals even also mycotoxin [16-20]. However, other source of ChE needs to be observed to obtain the most sensitive biosensor towards various types of contaminant.

ChE from fish is even more useful as there are a lot of freshwater bodies and also due to the substantial aquaculture industry in Malaysia. The use of inhibitive ChE-based assay of heavy metals is significant due to low – cost, fast and need no tedious technique to be done. Thus, in the present study, ChE was extracted from the blood and muscle tissue of climbing perch (*Anabas testudineus*) was tested its sensitivity by exposing it to metal ions. Therefore, the objectives of this study are: 1) to extract and purify cholinesterase (ChE) from the blood and muscle of *Anabas testudineus* through salt precipitation followed by ion exchange chromatography, 2) to investigate the optimal characteristics of ChE including substrate specificity, optimum pH and temperature, and 3) to assess the *in-vitro* effects of various metal ions on the enzymatic activity of ChE.

MATERIALS AND METHODS

Preparation of crude homogenate. *A. testudineus* were bought alive from a fish dealer in Selangor, Malaysia. The size of the fishes was approximately 15 cm. The fishes were freeze–killed by immersing them into the ice cube within 30 min, decapitated and their blood and muscle were collected after that. The extraction process was carried out by separately homogenising both samples with 0.1 M Tris-HCl buffer, pH 8.0 containing 1 mM phenylmethylsulfonyl fluoride (PMSF) with a buffer ratio of 1:4 (w/v). The crude was homogenised using Ultra-Turrax T25 homogeniser. The homogenate was then centrifuged at 5000 xg with the temperature of 4°C within 20 min. The supernatant was collected and stored at -25°C for further purification process.

Ammonium sulphate precipitation. Each supernatant were separately transferred into a beaker that was placed in iced condition. The sample was slowly stirred while adding the ammonium salt was slowly. The amount of ammonium sulphate powder required to give the desired percentage of saturation was determined based on the ammonium sulphate precipitation table has been prepared by Green and Hughes (1955) [21]. The mixture was centrifuged at 10000 rpm for 15 min at 4°C. The pellet was collected and redissolved by adding a small amount of 0.1 M sodium phosphate buffer followed by dialysis to remove ammonium salt, while the supernatant was continued for the next round of precipitation. This technique was repeated at the salt concentration of 0-30, 30-40, 40-50, 50-60, 60-70 and 70-80%. The fraction with the highest ChE activity was subjected for ion exchange chromatography.

Ion exchange chromatography. DEAE-cellulose column was equilibrated with 20 mM sodium phosphate buffer, pH 7 before the loading of blood or muscle extract. For this experiment, the column volume obtained was 75 mL. 15 mL of the extract was loaded into the set up column and wisely dropped to prevent the disturbance of column. The column was then washed twice by washing buffer (20 mM phosphate buffer, pH 7) with a slow flow rate at 0.5 mL/min starting from 0 to 150 min. Washing stage is crucial to remove unbound protein molecules from the matrix of column. After the washing stage, the enzyme of interest was eluted by the gradient of elution buffer (20 mM phosphate buffer, pH 7 containing 1.0 M NaCl), which involves the steady increase of eluent solution ionic strength. The gradient of increasing the ionic strength started by replacing the washing buffer in the column from 150 to 330 min reaction. Each 1 mL fraction collected from washing and elution stage was tested for enzyme activity and protein content determination using Ellman [22] and Bradford [23] assay, respectively.

Ellman assay and protein content determination. The enzyme activity of cholinesterase enzyme was tested using developed Ellman assay method [22]. This method has been slightly modified to micro assay using 96 well microplate to assure absorbance through spectrophotometer at the wavelength of 405 nm. The assay has used synthetic substrates of acetylthiocholine iodide (ATC), butyrylthiocholine iodide (BTC) and propionylthiocholine iodide (PTC) to determine the most preferable substrate from each sample. The mixture of 200 µL of 0.1 M sodium phosphate buffer (pH 7.0), 20 µL of 0.1 mM DTNB and 10 µL ChE were pipetted into the microplate. The mixture was incubated for 15 min prior the addition of 20 µL substrates. The mixtures were incubated for 10 min after adding the substrates and the absorbance was read after that. Protein content quantification of enzyme was done using Bradford protein assay [23]. The reaction samples contain 20 µL sample and 200 µL Bradford reagent. The mixtures were then incubated for 10 minutes at room temperature. After incubation, an absorbance at 595 nm was taken using a microplate reader.

Optimal assay determination. Optimal assay determination includes the optimisation of substrate specificity, pH and temperature as well as the effect of metal ions. ChE was incubated with ATC, BTC, and PTC with the concentration ranging from 0.1 to 2.5 mM. Maximal velocity and biomolecular constant were determined using GraphPad PRISM 5.0 software. Temperature profile was carried out by separately incubating ChE at the temperature of

15, 20, 25, 30, 35, 40, 50 and 60°C. Beyond this range, the activity of ChE was considered to be denatured. For pH determination, there are several pHs from different buffers were used, namely acetate buffer, sodium phosphate buffer, and TRIS-HCl buffer. The overlapping buffer system used in this step consists of 0.1 M acetate buffer (pH 3 to 5.5), 0.1 M phosphate buffer (pH 5.5 to 8), and 0.1 M tris-HCl buffer (pH 7 to 10).

Metal ions inhibition study. Several metal ions such as zinc, plumbum, nickel, mercury, cobalt, copper, chromium, cadmium, silver, and arsenic are the compounds for metal ion effect determination. The method used in these steps is Ellman et al. (1961) [22] as well as the optimised buffer system and specific substrate concentration. The reaction mixture consists of 150 µL of Tris-HCl buffer (0.1 M, pH 9), 50 µL of metal ions, 20 µL of 0.1 mM DTNB and 10 µL ChE were pipetted into the microplate. The mixture was then incubated for 15 min prior the addition of 20 µL of substrates. After addition of the substrates, mixtures were incubated for 10 min, resulting to an absorbance reading at 405 nm. The highest inhibition was selected for half inhibitory concentration (IC_{50}) determination by incubating ChE with the metal ion concentrations ranging 0.1 to 6 mg/L. IC_{50} value was calculated using GraphPad PRISM software

RESULTS AND DISCUSSION

Purification and SDS PAGE visualisation. Ammonium sulphate was selected as the preferred salt for precipitation because it has high solubility and relatively low cost [24]. Figure 1 shows the precipitation profile of ChE at a variety of ammonium sulphate saturation levels ranging from 0 to 80%. In this study, the highest activity of muscle ChE was obtained at 30 to 40% while blood ChE showed the percentage concentration at 60-70% considering that all ChE were salted out at that percentage range. Theoretically, ammonium sulphate precipitation was the first-step purification in this experiment. It purifies protein by altering the solubility of protein [25]. The solubility of protein depends on salt concentration added into the solution. Besides, ammonium sulphate precipitation will purify the solution by removing the unwanted as well as damaged protein. Ammonium sulphate consists of two purifying steps, which are *salting in* and *salting out. Salting in* refers to a condition when there is a presence of salt at low concentration solution. It stabilises various charged groups of protein in the solution, attracts the protein and eventually increases the solubility of protein. When salt concentration increased, protein solubility will reached the maximum point and finally starts to precipitate, as there are insufficient water molecules to interact with protein. This phenomenon is known as *salting out*.

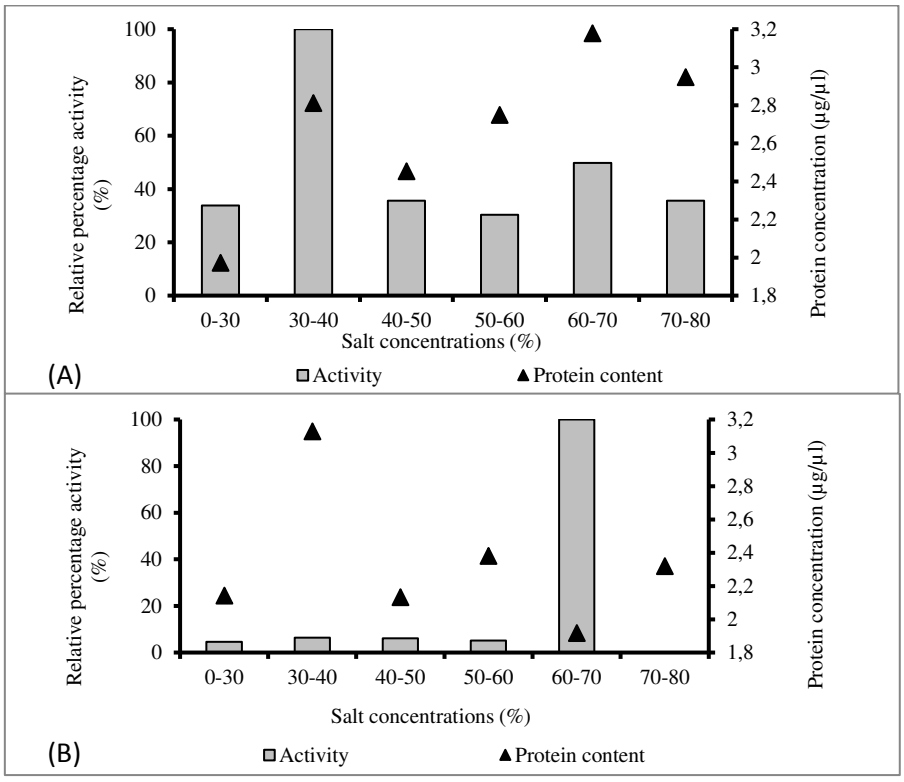

FIGURE 1
Precipitation of ChE from muscle (A) and blood (B) extract of A*nabas testudineus.*

TABLE 1
Purification table of blood and muscle ChE. U expressed as µmole.min-1mg-1

Step	Total protein (mg)	Total activity (U)	Specific Activity (U/mg)	Purification fold	Yield (%)
Blood					
Homogenisation	9.11	1884.19	206.3	1.00	100.00
60-70% Ammonium sulphate percepitation	1.90	1610.56	849.32	4.11	85.48
Ion Exchange Chromatography	0.52	897.98	1730.87	8.37	47.66
Muscle					
Homogenisation	712.26	8647.60	12.14	1	100
30-40% Ammonium sulphate percepitation	162.90	2053.60	12.607	1.038	23.75
Ion Exchange Chromatography	53.52	685.20	12.803	2.055	7.92

Protein stability in solution depends on electrostatic interactions, H-bridges and hydrophobic interactions. A classic first step to fractionate proteins by causing perturbations in the solvent with respect to ionic strength is ammonium sulphate precipitation. The major advantage of ammonium sulphate is that it causes a reversible precipitation of the protein, maintains the native form of the protein structure, and aids in concentrating the protein from dilute solution, while at the same time removes large amounts of contaminant proteins [26,27]. The fraction with high percentage relative activity was collected and used for the next step of purification using ion exchange chromatography.

Purification table shows the changes and efficiencies of different purification step (Table 1). The purification method on blood and muscle ChE has recovered 47.66 and 7.92% of total activity with 8.37 and 2.06 purification fold, respectively. ChE from blood and muscle were successfully purified as the specific activity throughout the purification step increased.

Enzyme assay parameter. Substrate specificity. The substrate specificity assay was carried out using three different substrates, which were ATC, BTC and PTC with the concentrations ranging from 0 to 2.5 mM. The result as in Table 2 shows that the purified ChE from blood and muscle has hydrolysed BTC and PTC at the highest rate with the V_{max} value of 171.9 and 6.44, respectively. Additionally, based on the calculation of catalytic efficiencies, the highest degradation of BTC and PTC by blood and muscle ChE were and 161.11 and 12.06, respectively (Table 2). According to Sole et al. (2008) positive and significant correlation was found between all these three substrates regarding different species [28]. The pattern of their study recorded the presence of three forms ChE, with AChE being the most predominant, followed by PrChE and BChE. This statement has been proved in the previous study on several fish species such as *Prionace glauca* (juvenile blue sharks) [29], *Lipophorys pholis* (shanny) [28], and another aquatic animal such as *Capitella teleta* (polychaete) [30]. The highest V_{max} value obtained using BTC as substrate for blood ChE indicates the largest amount of products formed as the result of ChE-BTC interactions. However, further study is needed to support this result due to insufficient data on PrChE as the predominant in muscle tissue.

pH Profile. In this study, Acetate, Sodium Phosphate and Tris-HCl buffer were used to create overlapping pH condition for the determination of optimum of ChE. Figure 3 shows the optimal pH for ChE from the muscle of *A. testudineus,* which was Tris-HCl buffer with pH 9. On the other hand, blood ChE showed maximum value at sodium

TABLE 2
Kinetic study on blood and muscle ChE

Substrate	V_{max} (U/mg protein)	K_m (mM)	K_{cat}
Blood			
ATC	36.43	0.2734	133.2480
BTC	171.9	1.067	161.1059
PTC	77.57	0.7547	102.7825
Muscle			
ATC	2.200	0.3158	6.966
BTC	3.599	0.850	4.234
PTC	6.439	0.5339	12.06

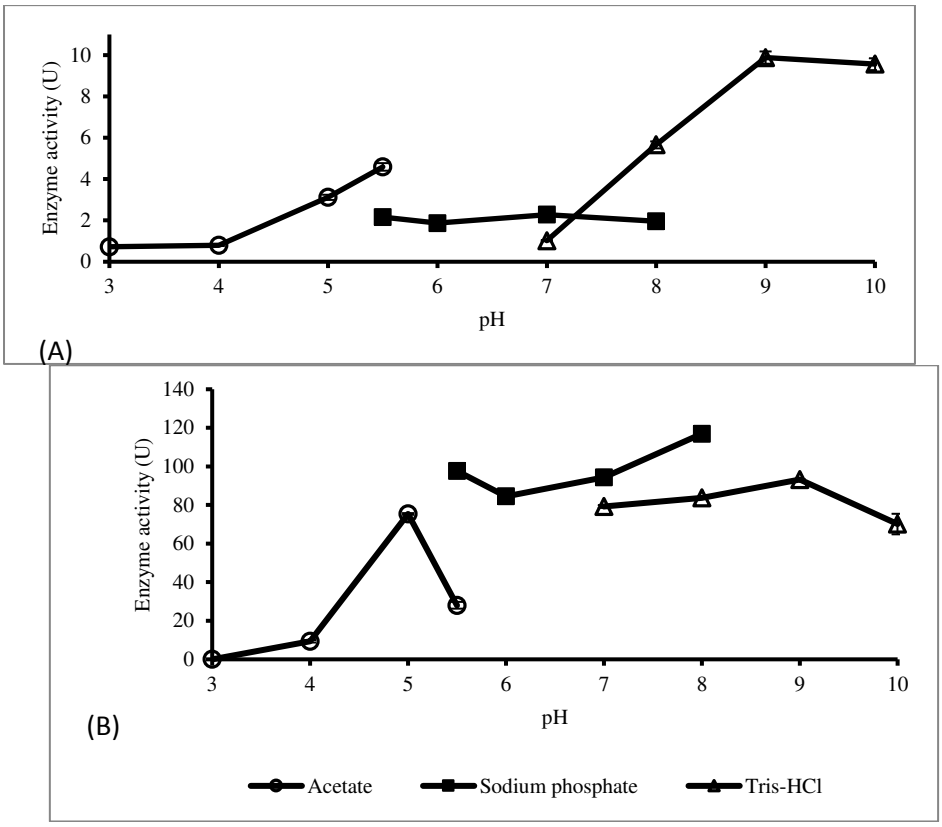

FIGURE 2
pH profile on the activity of partial purified BChE from (A) blood and (B) muscle extract of A. testudineus with the mean point of triplicate assay and Y error bars represent for standard deviation of mean

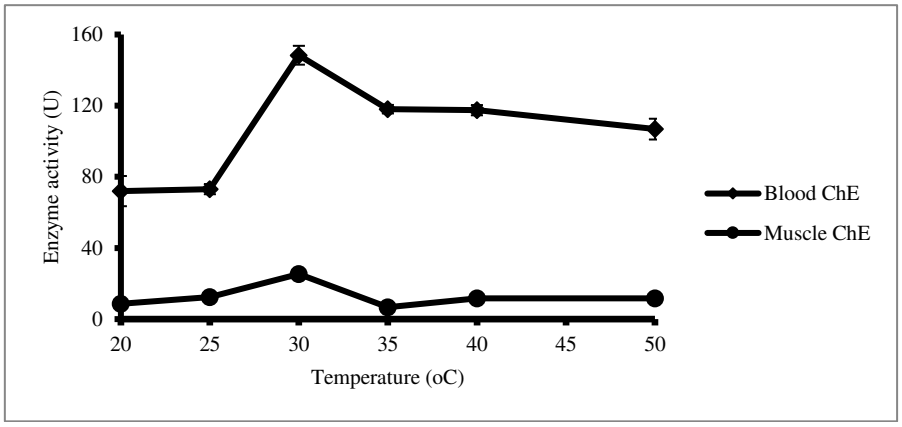

FIGURE 3
Temperature profile on the activity of partial purified BChE from blood and muscle extract of A. testudineus with the mean point of triplicate assay and Y error bars represent for standard deviation of mean.

phosphate buffer pH 8. pH has a greater influence towards the formation of enzyme–substrate complex. Result shows (Figure 2) the overlapping between enzyme activity in Sodium Phosphate buffer and Tris-HCl. This phenomenon was due to the different buffer capacities in which a measurement of the buffer efficiency in resisting changes in pH. ChE altered its conformation and lost its activity in a very high and low pH [31]. The alteration of conformation was due to the protonation of catalytic histidine when the pH was titrated from low to high [32]. The ionic state of enzyme would experience changes at the active sites, causing the decrease in the rate of enzyme-substrate collision when the enzyme is subjected to various pHs and buffers [33].

Temperature profile. The effect of temperature on the partially purified ChE extracted from blood and muscle of *A. testudineus* was carried out by incubation in different temperatures ranging from 15–50°C. Temperature is the crucial

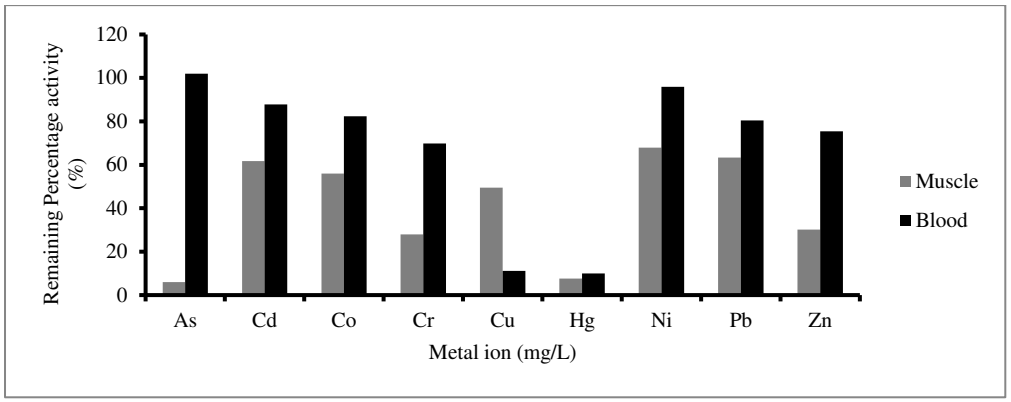

FIGURE 4
Remaining percentage activity of blood and muscle ChE after exposed with selected metal ions.

stimulation of interaction between enzyme and substrate where enzyme is a protein, and the changes of temperature would affect enzyme activity by altering the conformation of enzyme at the active site (Figure 3). Partially purified ChE activity will be truncated at low temperature as it faces limited kinetic energy for ChE to hydrolyse PTC substrate. However, the activity increases as the temperature rises until it reaches its maximum point in obtaining maximum enzyme activity [31]. In this study, muscle ChE achieved its maximum activity in the range of 25 to 40°C (no significant different between the mean points: $p > 0.05$) while blood ChE at 30°C (Figure 3). The pattern of ChE activity profile increases at temperature ranging from 20°C to 30°C probably due to the increase in the rate of collisions between enzyme and substrate per unit time. Thus, the formation of enzyme-substrate complexes are higher, leading to an increase in the amount of products produced. Conversely, at high temperature, the vibration within the molecule is great enough to disrupt the non-covalent bonds that maintain the three-decreased to 5.9%. However, blood ChE exhibited higher inhibition towards copper. Metal ions disrupted the conformation of ChE active site, particularly catalytic triad of the ChE, which consists of carboxylate groups of aspartic and glutamic acid, and the ring nitrogen atom of histidine. Other side chains that bind metal ions include tryptophan, cysteine, methionine, serine, threonine, tyrosine, and asparagine [3]. Devi and Fingerman (1995) stated that three of these metal ions produced a strong inhibition of a large number of enzymes that have functional sulfhydryl group [34]. The present study showed that zinc and chromium have inhibited ChE activity with more than 50% of the control. This is because both metal ions were included in the list of metal ions, which produced strong inhibitory effect to ChE [35-37]. Meanwhile, the reason for other metal ions that do not inhibit higher ChE activity was due to low sensitivity of ChE towards those metal ions. dimensional structure of the enzyme beyond the optimum temperature. This phenomenon will resulted in conformational changes of BChE due to thermal denaturation. It is crucial to carefully control the temperature during measurements of enzyme activity because the temperature of the reaction mixture could have a dramatic effect on the kinetic parameters of an enzyme catalysed reaction. Hence, the optimum temperature of 30°C for blood and muscle ChE was selected as the incubation temperature for the analysis on BChE activity.

Inhibition study. Nine selected metal ions were used *in vitro* to examine the inhibition capability of each metal ion towards the partially purified ChE. In figure 4, muscle ChE activity was inhibited with more than 50% by arsenic, chromium, copper, mercury and zinc compared to blood ChE that shows only two metals, namely mercury and copper. Moreover, both ChE were strongly inhibited by mercury with more than 90%. Arsenic seems like to be unaffected to muscle ChE compared to blood ChE activity, which has been Besides, according to Broderick et al. (2001) [38], metal ions could also act as cofactors where they can promote enzyme activity, which contradicts earlier findings.

Half inhibitory effect determination between mercury and ChE activity. Half maximal inhibitory concentration (IC_{50}) indicated the concentration of antagonists (metal ions) respond that inhibit half of the enzyme activity. In this study, IC_{50} of mercury was done to identify the concentration required to inhibit 50% of partially purified ChE activity extracted from *A. testudineus.* The result was obtained using GraphPad Prism, which was recorded at 1.003 and 1.048 mg/L on muscle and blood ChE, respectively (Figure 5). Frasco et al. (2007) mentioned the inhibition mechanism of mercury towards ChE activity [39]. Basically, mercury inhibits the activity of enzyme efficiently by targeting sulfhydryl group of the

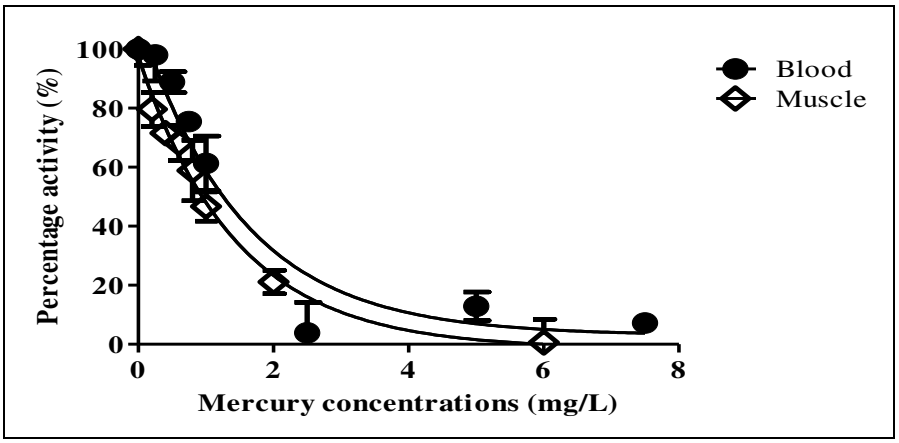

FIGURE 5
Percentage inhibition of Blood and muscle ChE by mercury with series of concentrations. IC50 was analysed by using GraphPad Prism. Error bars represent mean ± standard error (n=3).

enzyme. The disruption of sulfhydryl group will alter the conformation of protein binding side and eventually stopping the ability of enzyme to efficiently hydrolyse the substrate. This can be also applied to the ChE as ChE have free cysteine at the active site that provides sulfhydryl group [40,41]. Frasco et al. (2007) also stated that metals are also capable of forming very tight bonds with histidine and methionine side chains [39].

CONCLUSION

ChE from the muscle and blood extract of *Anabas testudineus* had been partially purified through ammonium sulphate precipitation and DEAE-Cellulose ion exchange chromatography with the determination of each optimum assay parameter done. Both ChE activities were sensitive towards several metal ion especially mercury, which exhibited higher inhibition. However, muscle ChE showed higher sensitivity in which more metal ions are inhibiting the enzyme activity and lowest mercury IC_{50} value compared to blood ChE. Future study is needed to compare other alternative sources, which is more sensitive towards broad types of toxicant.

ACKNOWLEDGEMENTS

This project was supported by fund from The Ministry of Science, Technology and Innovation (MOSTI), Malaysia, under FRGS Grant no. 02-02-13-1256FR (FRGS/2/2013/SG05/UPM/02/16) and Sciencefund (02-01-04-sf1473).

The authors declare that there is no conflict of interests regarding the publication of this article.

REFERENCES

[1] Jaishankar, M, Tseten, T, Anbalagan, N., Mathew, B.B., and Beeregowda, K.N. (2014) Toxicity, mechanism and health effects of some heavy metals. Interdisciplinary Toxicolology, 7(2), 60–72.

[2] Sabullah, M.K., Ahmad, S.A., Shukor, M.Y., Gansau, A.J., Syed, M.A., Sulaiman, M.R., and Shamaan, N.A. (2015). Heavy metal biomarker: Fish behavior, cellular alteration, enzymatic reaction and proteomics approaches. International Food Research Journal, 22(2), 435–454.

[3] Glusker, J.P., Katz, A.K. and Bock, C.W. (1999). Metal ions in biological systems. The Rigaku Journal, 16(2), 8–19.

[4] Tchounwou, P.B., Yedjou, C.G., Patlolla, A.K., and Sutton, D.J. (2012). Heavy metals toxicity and the environment. Exs, 101, 133–164.

[5] Sharma, B., Singh, S., and Siddiqi, N.J. (2014). Biomedical Implications of Heavy Metals Induced Imbalances in Redox Systems. BioMed Research International, 640754, 1–26.

[6] Muhammad, A., Odunola, O.A., Gbadegesin, M.A. Sallau, A.B., Ndidi, U.S., and Ibrahim, M.A. (2015). Inhibitory Effects of Sodium Arsenite and Acacia Honey on Acetylcholinesterase in Rats. International Journal of Alzheimer's Disease, 903, 603–610.

[7] Geula, C. and Darvesh, S. (2004). Butyrylcholinesterase, cholinergic neurotransmission and the pathology of Alzheimer's disease. Drugs Today 40(8), 711-721.

[8] Gonzalez, V., Huen, K., Venkat, S. Pratt, K., Xiang, P., Harley, K.G., Kogut, K., Trujillo, C.M., Bradman, A., Eskenzi, B. and Holland N.T. (2012). Cholinesterase and paraoxonase (PON1) enzyme activities in Mexican–American mothers and children from an

agricultural community. Journal of Exposure Science and Environmental Epidemiology, 22, 641–648.

[9] Bajda, M., Więckowska, A., Hebda, M., Guzior, N., Sotriffer, C.A. and Malawska, B. (2013). Structure-Based Search for New Inhibitors of Cholinesterases. International Journal Molecular Science, 14(3), 5608–5632.

[10] Nadorp, B. and Soreq, H. (2014). Predicted overlapping microRNA regulators of acetylcholine packaging and degradation in neuroinflammation-related disorders. Frontier Molecular Neuroscience, 7,1–9.

[11] Onor, M.L., Trevisiol, M. and Aguglia, E. (2007). Rivastigmine in the treatment of Alzheimer's disease: an update. Journal of Clinical Intervention Aging 2(1), 17–32.

[12] Leibson, T. and Lifshitz, M. (2008). Organophosphate and carbamate poisoning: Review of the current literature and summary of clinical and laboratory experience in Southern Israel". Journal of Toxicology 10, 7704–7727.

[13] Tilton, F., Tilton, S.C., Bammler, T.K., Beyer, R., Farin, F., Stapleton, P.L. and Gallgher, E.P. (2008). Transcriptional biomarkers and mechanisms of copper-induced olfactory injury in zebrafish. Environmental Science Technology, 42(24), 9404–9411.

[14] Monteiro, M., Quintaneiro, C., Morgado, F., Soares, A.M.V.M. and Guilhermino, L. (2005). Characterization of the cholinesterases present in head tissues of the estuarine fish Pomatoschistus microps: Application to biomonitoring. Ecotoxicology Environmental Safety, 62(3), 341–347.

[15] Sabullah, M.K., Sulaiman, M.R., Shukor, M.S., Yusof, M.T., Wan Johari, W.L., Shukor, M.Y. and Syahir, A. (2015). Heavy metals biomonitoring via inhibitive assay of acetylcholinesterase from Periophthalmodon schlosseri. Rendiconti Lincei. Scienze Fisiche e Naturali Journal, 26, 151–158.

[16] Kucherenko, I.S., Soldatkin, O.O., Arkhypova, V.M., Dzyadevych, S.V. and Soldatkin, A.P. (2012). Novel biosensor method for surfactant determination based on acetylcholinesterase inhibition. Measurement Science Technology, 23(6), 45–55.

[17] Soldatkin, O.O., Burdak, O.S., Sergeyeva, T.A., Arkhypova, V.M., Dzyadevych, S.V. and Soldatkin, A.P. (2013). Acetylcholinesterase-based conductometric biosensor for determination of aflatoxin B1. Sensors and Actuators B-Chem ical, 188, 999–1003.

[18] Sabullah, M.K., Ahmad, S.A., Shukor, M.Y., Shamaan, N.A., Khalid, A., Gansau, A.J., Dahalan, F.A. and Sulaiman, MR. (2015). Acetylcholinesterase from Puntius javanicus for the detection of carbamates and organophosphates. Journal of Pharmaceutical Science, 8, 348–353.

[19] Sabullah, M.K., Sulaiman, M.R., Shukor, M.Y.A., Shamaan, N.A., Khalid, K.A. and Ahmad, S.A. (2015). In vitro and in vivo effects of Puntius javanicus cholinesterase by copper. Fresenius Environmental Bulletin, 24(12), 4615–4621.

[20] Sabullah, M.K., Shukor, M.Y.A., Shamaan, N.A., Khalid, K.A., Ganzau, A.J., Sulaiman, M.R., Jirangon, H. and Ahmad, S.A. (2015). Purification and anticholinesterase sensitivity of cholinesterase extracted from liver of Puntius javanicus. International Journal of Agriculture and Biology, 17, 1025–1030

[21] Green, A.A. and Hughes, W.L. (1955). Protein solubility on the basis of solubility in aqueous solutions of salts and organic solvents. Methods Enzymology, 1, 67–90.

[22] Ellman, G.L., Courtney, D.K., Andres, V., and Featherstone, R.M. (1961). A new and rapid colorimetric determination of acetylcholinesterase activity. Biochemical Pharmacology, 7, 88–95.

[23] Bradford, M.M. (1976). A rapid and sensitive for the quantitation of microgram quantities of protein utilizing the principle of protein-dye binding. Analytical Biochemistry, 72(1), 248–254.

[24] Mirica, K.A., Lockett, M.R., Snyder, P.W., Shapiro, N.D., Mack, E.T., Nam, S. and Whitesides, G.M. (2012). Selective precipitation and purification of monovalent proteins using oligovalent ligands and ammonium sulphate. Bioconjugate Chemistry, 23(2), 293–299.

[25] Lang, G.J., Shang, J.Y., Chen, Y.X., Chui, Y.J., Wang, Q., Tang, Z.H. and Zhang, C.X. (2010) Expression on the housefly acetylcholinesterase in a bioreactor and its potential application in a detection of pesticide residues. World Journal of Microbiology and Biotechnology, 26, 1795–1801.

[26] Fong, B.A., Wu, W.Y. and Wood, D.W. (2009) Optimization of ELP-intein mediated protein purification by salt substitution. Protein Exprimental Purification, 66(2), 198–202.

[27] Baracat-Pereira, M.C., Barbosa, M.D.O., Magalhães, M.J., Carrijo, L.C., Games, P.D., Almeida, H.O., Netto, J.F.S., Pereira, M.R. and Barros, E.G.D. (2012). Separomics applied to the proteomics and peptidomics of low-abundance proteins: Choice of methods and challenges – A review. Genetic Molecular Biology, 35, 283–291.

[28] Sole, M., Loberaa, G., Aljinovica, B., Riosb, L.M., Parrab, F. and Maynouna, J.E. (2008). Cholinesterases activities and lipid peroxidation levels in muscle from shelf and slope dwelling fish from the

NWMediterranean: Its potential use in pollution monitoring. Scientific of The Total Environment, 402, 306–317.

[29] Alves, L.M., Lemos, M.F., Correia, J. and Novais, C.S. (2014). Characterization of cholinesterases present in brain and muscle tissues of juvenile blue shark (Prionace glauca). Journal of Frontier in Marine Medicine, 7, 1–17.

[30] Gomes, I.D.L, Lemos, M.F.L., Soares, A.M.V.M. and Faria, C.M. (2014). The use of cholinesterase as potential biomarker: In vitro characterization in the polychaete Capitella teleta. Marine Pollution Bulletin, 85, 179–185.

[31] Sabullah, M.K., Sulaiman, M.R., Shukor, M.Y., Syed, M.A., Shamaan, N.A., Khalid, A. and Ahmad, S.A. (2014). The assessment of cholinesterase from the liver of Puntius javanicus as detection of metal ions. The Scientific World Journal, 14, 1-9.

[32] Masson, P., Schopfer, L.M., Bartels, C.F., Frometit, M.T., Ribes, F., Nachon, F. and Lockridge, O. (2001). Substrate activation in acetylcholinesterase induced by low pH or mutation in the π-cation subsite. Biochimica et Biophysica Acta, 1594, 313–324.

[33] Sharma, R. (2012). Enzyme inhibition: mechanisms and scope. R. Sharma (Ed.), Enzyme Inhibition and Bioapplications InTech Pp.3–36. Rijeka, Croatia

[34] Devi, M. and Fingerman, M. (1995). Inhibition of acetylcholinesterase activity in the central nervous system of the red swamp crayfish, Procaambarus clarkia by mercury, cadmium, and lead. Bulletin of Environment Contamination Toxicology, 55, 746–750.

[35] Diamantino, T.C., Guilhermino, L., Almeida, E. and Soares, A.M.V.M. (2000). Toxicity of sodium molybdate and sodium dichromate to Daphnia magna Straus evaluated in acute, chronic, and acetylcholinesterase inhibition tests. Ecotoxicology Environmental Safety, 45, 253–259.

[36] Diamantino, T.C., Almeida, E, Soares, A. and Guilhermino, L. (2003). Characterization of cholinesterases from Daphnia magna straus and their inhibition by zinc. Bulletin of Environmental Contamination Toxicology, 71, 219–225.

[37] Hayat, N.M., Shamaan, N.A., Shukor, M.Y., Sabullah, M.K., Khalid, A., Dahalan, F.A., Khalil, K.A. and Ahmad, S.A. (2015). Cholinesterase-based biosensor using Lates calcarifer (Asian Seabass) brain for detection of heavy metals. Journal of Pharmaceutical Sciences, 8, 376–381.

[38] Broderick, J.B. (2001). Coenzymes and Cofactors: John Wiley & Sons, Ltd. Pp. 105–116 Chichester.

[39] Frasco, G.R., Colletier, J.P., Weik, M. Carvalho, F., Guilhermino, L., Stroja, J. and Fournier, D. (2007). Mechanism of cholinesterase inhibition by inorganic mercury. Federation of European Biochemical Societies Journal, 274, 1849–1861.

[40] Morel, N., Bon, S., Greenblatt, H.M., Belle, D.V., Wodak, S.J., Sussman, J.L., Massoulie, J. and Silman, I. (1999). Effect of mutations within the peripheral anionic site on the stability of acetylcholinesterase. The American Society for Pharmacology and Experimental Therapeutics, 55, 982–992.

[41] Zhong, F., Lisi, G.P., Collins, D.P. Dawson, J.H. and Pletneva, E.V. (2013). Redox-dependent stability, protonation, and reactivity of cysteine-bound heme proteins. Proceeding of National Academy of Sciences of USA 1, 306–315.

Received: **02.01.2016**
Accepted: **15.06.2016**

CORRESPONDING AUTHOR

Dr. Siti Aqlima Ahmad,
Department of Biochemistry, Faculty of Biotechnology and Biomolecular Sciences,
Universiti Putra Malaysia, UPM 43400 Serdang, Selangor, Malaysia

© by PSP Volume 25 – No. 10/2016, pages 4261-4268 Fresenius Environmental Bulletin

ASSESSMENT OF HIGHWAY-INDUCED POLLUTION THROUGH PLANT AND SOIL ANALYSES, IN CASE OF ORDU CITY SECTION OF BLACK SEA COASTAL HIGHWAY

Omer Atabeyoglu*, Pervin Yesil, Murat Yesil

Agricultural Faculty Landscape Architecture Department, Ordu University Ordu, Turkey

ABSTRACT

Mankind have been modifying and altering natural environment in line with his needs and desires since the day one of his presence. Such a transformation accelerated with the diversified and ever-increasing demands and turned into a threat for both the nature and human life. Environmental pollution is the leading threat. The reasons and the results of pollution are diverse and traffic has the greatest share in environmental pollution. Urban are under the threat of highway-induced pollution. Exhaust gases are the greatest source of pollution in urban. Heavy metal accumulation is evident over both leaf and soil surfaces. In this study, leaf and soil samples were collected around and different distances from Ordu City section of Black Sea Coastal Highway in two different seasons (wet and dry) and heavy metal analyses were performed on these samples. Nerium oleander plant was used as bio-receptor and heavy metal pollution levels were assessed through plant and soil analyses. Results revealed that highway with current traffic circulation and heavy vehicle intensity created heavy metal pollution in city center.

KEYWORDS:
Heavy metal, urban space, environmental pollution, highway, soil, plant.

INTRODUCTION

Rapid technological progress facilitates human life. However, such progress brings about various environmental problems. The problems behind living conditions created by urbanization, technological and industrial developments in countries with high living standards increased the negative impacts on environment [35]. Developing cities, ever-increasing needs and diversified functions also increased atmospheric pollutants. As it has been throughout the world for many years, environmental problems have become the most significant problem affecting the quality of life in Turkey. The primary environmental problems with negative impacts on living quarters can be enumerated as follows: natural destruction, weakened flora, erosion, urban sprawl, chemicals, industrial activities, soil, water and air pollution.

Vehicle-induced heavy metal pollution is one the most significant problems in the cities of modern times. Heavy metals have significant adverse effects on living ecosystems and can easily accumulate in both plant and soil materials [12, 26, 27, 6, 13, 30]. Heavy metal pollution and accumulation in soils is generally observed over the soil surface or through the upper soil layers close to surface. Heavy metals create stable forms through creating organo-mineral compounds with the organic compounds of the soils. Heavy metal accumulation and potential adverse impacts of heavy metals decrease with the depth of soil [31, 1, 30]. The pollutants creating air and soil pollution are mainly composed of fossil fuel-originated wastes like CO_2, SO_2, NO_x, CO and hydrocarbons [21, 16, 15]. The waste materials creating air pollution are either suspended in air or fixed into the soil creating damages on plant mechanisms and destructing the proper operation of the system [7]. Air pollutants may create significant damages on plant roots, stems, branches and leaves and may also result is various deficiencies [23].

According to [20], heavy metals are mostly mentioned in case of environmental problems and they are defined as “the metals with relatively high densities and noxious or toxic impacts even at low concentrations”. Heavy metals are scientifically defined as “the metals with densities over 5g/cm^3. There are more than 60 metals in this group including lead, cadmium, chrome, iron, cobalt, copper, nickel, mercury and zinc. These elements by their natures exist as either stable compounds like carbonates, silicates and sulphur bounded in silicates. According to [5], metals occur naturally and some are real pieces of global ecosystem. Copper (Cu) and zinc (Zn)-like metals are essential for the life. Zinc is essential for enzyme system of plants to regulate metabolic processes. However, a beneficial function of lead (Pb) and mercury (Hg) has not been reported, yet. According to [28],

despite their toxic effects at high concentrations, copper and zinc play a key role in photosynthetic electron transfer and they are micro nutrients essential for various enzyme activities. According to [33], the group includes about 70 metals and 20 of them are remarkable ones for ecology (Fe, Mn, Zn, Cu, V, Mo, Co, Ni, Cr, Pb, Be, Cd, Tl, Sb, Se, Sn, Ag, As, Hg, Al). Some of them are micro nutrients for plants and animals (Fe, Cu, Zn, Mn, Mo, Ni) and they have toxic impacts at concentrations over the threshold values [24].

Exhaust gas-originated heavy metals are transported to soil through air. Increasing number of vehicles also increased the amount of heavy metals released to air. Heavy metal concentration in air can reach to significantly high levels over the roads with heavy traffic load. Heavy metals can suspend in air for long durations because of small particle sizes and fly through long distances. Particles also are attached to plant surfaces close to roads and gets into the soil with precipitations [9, 10]. Herbal material and soil are the best indicators for the spread and effects of heavy metals in urban spaces. The places under intensive highway pressure and the places with intensive daily uses of urbanites are exposed to air pollution. Heavy metals accumulated over soil and plant surfaces reveal the extent of pollution in urban environments [3, 17, 15, 25, 8, 18, 34, 13, 2, 19, 29, 14].

The study was made Ordu Province in Turkey. Ordu Province is a potential candidate for heavy metal pollution because of the highway passing through the province. About 14 km section of the highway passes through the province. The most intense housing, business, commerce, education and recreation sites of the province are located along the highway route. The highway is used by heavy vehicles for transit transport and such vehicles exert a strong pressure over the province. Thus, highway-induced heavy metal pollution is a significant threat for the province.

The present study was conducted to determine the spread and size of heavy metal pollution originated from highway passing through the city center through their accumulation over the soil and plant leaves. In this way, negative effects of inner state highways on urban functions and urban life will also be presented.

MATERIAL

The research material, highway, extends along the Black Sea cost and passes through the Ordu City center. The province is located in Eastern Black Sea Region. About 14 km section of the highway passing through urban area was selected as the research material. Highway extends parallel to the sea and divides the province into two sections. Southern part of the highway is composed of city center, settlements and commerce sites with intense constructions and the northern part of the highway is composed of relatively low density and regular settlements and covers coastal sections, settlements, education and recreation sites.

METHOD

Possible highway-induced heavy metal pollution was assessed through the analyses performed on plant and soil samples. Therefore, heavy metal accumulation in plants and soils were separately determined. Experiments were carried out simultaneously for both plant and soil samples. Samples were collected in highway-oriented design. Samples were taken from the median, wayside, 50 and 100 meters from the road and a control treatment was also included in the study. Leaf and soil samples were taken from 3 different points at each distance. In this way, 15-group soil and 15-group leaf samples were collected. Leaf samples were collected from Nerium oleander plants since they have already been used and have biosensor characteristics [32, 22, 4]. Samples were collected from 1.5 m elevation and all around the plants. A total of 15 fully developed leaves were sampled from each plant. Ceramic knife and plastic gloves were used while taking leaf samples to prevent possible contaminations. Collected samples were placed into paper bags to prevent decays. Soil samples were taken from the soils just beneath the plants from where the leaf samples were taken. While taking soil samples, initially upper soil was scraped off and samples were taken from 15 cm soil depth. Collected samples were placed into polyethylene bags. Both the leaf samples and soil samples were taken and sent to laboratory in the same day. Al, Cd, Cr, Cu, Fe, Mn, Ni, Pb, S, Zn and SO_2 were performed both on leaf and soil samples in both seasons. Samples were collected in two seasons as of dry and wet season. In this way, variations through leaching were also assessed. A total of 60 samples were evaluated through the experiments. Resultant data were then subjected to statistical analyses and the variations in highway-induced pollution were assessed based on the distance and seasons. Data normality was checked with Anderson Darling test and variance homogeneity was checked with Bartlett test. Variables were subjected to two-way ANOVA and Tukey test was used to identify the significantly different means. Tukey test results were indicated with letters placed by descriptive statistics. Significance level (α) was set as 5%. All calculations were performed with Minitab 17 statistical software.

RESULTS

While Al contents of soil samples were not significantly different from each other, season*location was found to be significant with regard to leaf Al contents ($p<0.001$). Median was different from the other locations in wet season and had the highest Al content. In dry season on the other hand, wayside was different from the other locations and had the greatest Al content. Considering the leaf Al contents, locations were exhibited differences and median had the highest value in wet season and wayside had the highest value in dry season (Table 1).

Variance analyses on Cd contents of both plants and soils revealed that only the season* location interaction was significant ($p<0.01$). There were not significant differences in Cd contents of different locations in dry season, however wayside had significantly higher Cd contents than the other locations in wet season ($p<0.05$). With regard to differences between the locations in different seasons, it was observed that Cd contents were higher in dry season of all locations ($p<0.05$).

With regard to Cr contents of leaf and soil samples, only the differences in general means of the seasons were found to be significant ($p<0.001$). Higher Cr contents were observed in both leaves and soils in dry season.

Considering Cu contents, general means of the seasons for plants and season*location interaction for soils were found to be significantly different ($p<0.05$). Leaf Cu contents were higher in wet season ($p<0.05$). Soil Cd contents of the locations in wet season were not significantly different. In dry season on the other hand, control treatment was different from all locations; 50 m was different from wayside; 100 m was different from median and wayside; median was different from 100 m; and wayside was different from 50 and 100 m. In both seasons, only 100 m location exhibited differences and such differences were higher in dry season.

With regard to Fe contents, while season*location interaction was found to be significant in leaf samples, only the differences in general means of seasons were found to be significant in soil samples ($p<0.001$). While there were not any significant differences in Fe contents of the location in dry season, Fe contents of the median were about 3-4 times higher than the other locations in wet season ($p<0.05$). With regard to locations, differences were observed in Fe contents of median in wet and dry season and the values in wet season were higher ($p<0.001$). Differences were also observed in Fe contents of the seasons ($p<0.001$).

Considering the Mn contents, significant differences were observed only in general means of the seasons in both leaf and soil samples ($p<0.001$). Higher values were observed in soils of dry season and leaves of wet season ($p<0.001$).

With regard to Ni contents, the differences in leaf Ni contents of season*location interaction ($p<0.01$) and in general means of soil Ni contents were found to be significant ($p<0.05$). Significant differences were not observed in leaf Ni contents of the locations in wet season. In dry season, the greatest Ni content was observed in control location and the lowest value was seen in median location. However, only the difference between control and median was found to be significant ($p<0.05$) and the difference between control and the others and between median and the others were not found to be significant ($p>0.05$). For soil samples, interaction was not found to be significant and only the difference between the seasons was found to be significant. Ni contents of soil samples were higher in dry season ($p<0.05$).

Variance analysis on Pb contents revealed significant differences in leaf Pb contents of the seasons ($p<0.001$) and in soil Pb contents of season*location interaction ($p<0.05$). Leaf Pb contents were higher in dry season. In soil samples, significant differences were not observed between the locations in wet season. In dry season on the other hand, control was significantly different from 50 and 100 m; the location of 100 m was significantly different from control, median and wayside; median was significantly different from 100 m; and wayside was significantly different from 50 and 100 m. With regard to Pb content of the seasons, the locations of 50 and 100 m were found to be significantly different and higher values were observed in dry season.

While the differences in S contents of both the leaves and soils of the seasons were found to be significant ($p<0.001$), the differences between leaf S contents of the locations were also found to be significant ($p<0.05$). In both cases, the values were higher in dry season. For plant analyses, differences between the locations were also significant. While 100 m and wayside were found to be significantly different ($p<0.05$), the difference between the others were not found to be significant ($p>0.05$). Although the greatest values were observed in wayside, it was significantly different only from 100m and it was not significantly different from 50 m, median and control.

With regard to Zn contents, only the season*location interaction in soil samples was found to be significant ($p<0.01$). In soil samples, the values for wayside were different from the other locations in wet season and 100 m location was different from the others in dry season. These locations had the greatest values. Between two seasons, the differences in 50m, 100m and wayside were found to be significant.

Variance analysis on SO_2 contents revealed significant differences between general mean

values of the seasons ($p<0.001$). The differences between leaf SO_2 contents of the locations were also found to be significant ($p<0.05$). Significant differences were observed between leaf SO_2 contents of the seasons and the values were higher in dry season. Also in leaf analysis, 100 m and wayside locations were significantly different from each other and the wayside had the highest value. For soil samples, there were significant differences between the seasons and the values were higher in dry season.

TABLE 1
Introductory statistics for Al (mg/kg) in plants and soils and Tukey test results.

		PLANT				SOIL			
	L	Wet season	Dry season	Total	P-Value	Wet season	Dry season	Total	P-Value
		Mean±SEM	Mean±SEM			Mean±SEM	Mean±SEM		
Al	1	22.070±2.580 Ba	23.980±6.320 Ba	23,030± 3,080	S:0.647 L:0.000 S*L: 0.000***	0.603±0.025	0.603±0.025	0,387± 0,102	S:0.807 L:0.558 S*L: 0.418
	2	54.700±13.200 Ba	27.890±7.520 Ba	41,300± 9,060		0.464±0.211	0.464±0.211	0,444± 0,114	
	3	24.890±3.220 Ba	18.220±3.020 Ba	21,560± 2,480		0.498±0.059	0.498±0.059	0,967± 0,561	
	4	114.600±28.100 Aa	51.840±7.140 Bb	83,200± 19,100		0.432±0.096	0.432±0.096	0,324± 0,077	
	5	55.510±5.660 Bb	133.000±12.500 Aa	94,200± 18,400		0.911±0.548	0.911±0.548	0,621± 0,278	
	T	54,400±10,400	51,000±11,800			0,516±0,235	0,581±0,111		
Cd	1	0.007±0.00296 Bb	2.106±0.003 Aa	1,056± 0,469	S:0.000 L:0.000 S*L: 0.000***	0.024±0.008 Ba	0.042±0.018 Aa	0,033± 0,010	S:0.400 L:0.027 S*L: 0.006**
	2	0.016±0.00668 Bb	2.089±0.005 Aa	1,052± 0,464		0.019±0.002 Ba	0.133±0.090 Aa	0,076± 0,048	
	3	0.008±0.00434 Bb	2.094±0.007 Aa	1,051± 0,466		0.037±0.005 Ba	0.174±0.084 Aa	0,105± 0,049	
	4	0.012±0.00335 Bb	2.109±0.004 Aa	1,061± 0,469		0.035±0.009 Ba	0.067±0.014 Aa	0,051± 0,010	
	5	0.072±0.0135 Ab	2.098±0.011 Aa	1,085± 0,453		0.263±0.024 Aa	0.074±0.004 Aa	0,169± 0,044	
	T	0,023±0,007	2,099±0,003			0,076±0,026	0,098±0,025		
Cr	1	0.583±0.080	0.583±0.080	1,129± 0,247	S: 0.000*** L:0.773 S*L: 0.726	0.00427±0.00003	0.05733±0.00176	0,0308± 0,0119	S:0.000*** L: 0.306 S*L: 0.389
	2	0.805±0.141	1.677±0.006	1,241± 0,205		0.00493±0.00030	0.05733±0.00318	0,0311± 0,0118	
	3	0.605±0.119	1.687±0.004	1,146± 0,248		0.00467±0.00088	0.06033±0.00088	0,0325± 0,0125	
	4	0.806±0.053	0.806±0.053	1,234± 0,193		0.00327±0.00019	0.06167±0.00318	0,0325± 0,0131	
	5	0.676±0.279	1.636±0.025	1,156± 0,249		0.0062±0.00046	0.06200±0.00115	0,0341± 0,0125	
	T	0,6949±0,0641^{B}	1,6675±0,00649^{A}			0,004667±0,000311^{B}	0,05973±0,00101^{A}		
Cu	1	17.149±0.507	0.669±0.512	8,910± 3,700	S: 0.043* L:0.270; S*L: 0.270	2.849±0.367 Aa	6.190±2.310 ABCa	4,520± 1,290	S:0.236 L: 0.764 S*L: 0.025*
	2	407.000±232.000	1.166±0.885	204.000± 138.000		2.461±0.516 Aa	7.790±3.920 ABa	5,130± 2,130	
	3	18.620±1.880	1.090±0.396	9,850± 4,010		2.258±0.508 Ab	8.660±3.200 Aa	5,460± 2,040	
	4	473.000±368.000	0.825±0.472	237.000± 195.000		4.329±0.325 Aa	1.920±1.630 BCa	3,123± 0,917	
	5	31.010±2.090	0.812±0.241	15,910± 6,820		6.740±1.120 Aa	1.465±0.995 Ca	4,100± 1,360	
	T	189,400±91,800^{A}	0,912±0,212^{B}			3,727±0,507	5,210±1,270		
Fe	1	55.200±16.900 Ba	7.200±2.150 Aa	31,200± 13,200	S:0.000 L:0.000 S*L: 0.000***	2.913±0.156	21.440±7.580	12,180± 5,350	S:0.000*** L: 0.944 S*L: 0.477
	2	90.100±32.700 Ba	10.940±3.060 Aa	50,500± 23,000		3.800±1.110	19.630±3.600	11,710± 3,920	
	3	54.100±9.280 Ba	4.980±1.170 Aa	29,500± 11,800		6.330±2.670	12.810±1.830	9,570± 2,050	
	4	280.200±39.400 Aa	29.410±3.150 Ab	154,800± 58,800		3.116±0.766	20.670±5.050	11,890± 4,540	

	5	104.800±27.500 Ba	58.360±4.550 Aa	81,600± 16,200		2.927±0.725	18.360±4.210	10,650± 3,940	
	T	116,9±24,7	22,18±5,48			3,817±0,626[B]	18,580±2,00[A]		
Mn	1	24.090±3.830	1.029±0.454	12,560± 5,440	S:0.000*** L:0.330 S*L 0.962	0.244±0.072	57.800±10.600	29,000± 13,700	S:0.000*** L: 0.564 S*L: 0.507
	2	26.660±7.870	1.501±0.513	14,080± 6,640		1.093±0.421	55.000±17.900	28,100± 14,500	
	3	40.800±13.800	9.100±7.530	25,000± 10,000		1.760±1.050	32.820±2.720	17,290 ±7,070	
	4	28.050±7.120	1.885±0.461	14,970± 6,660		0.560±0.105	61.600±15.700	31,100± 15,400	
	5	30.080±3.930	1.086±0.389	15,580± 6,720		0.680±0.411	37.100±18.900	18,900± 11,800	
	T	29,940±3,450[A]	2,920±1,530[B]			0,867±0,248[B]	48,880±6,280[A]		
Ni	1	0.604±0.239 Aa	1.658±0.088 Aa	1,131± 0,262	S:0.072 L:0.266 S*L 0.006**	0.038±0.016	0.172±0.050	0,1046± 0,0382	S:0.012* L:0.954 S*L: 0.904
	2	0.605±0.0902 Aa	0.831±0.320 ABa	0,718± 0,157		0.031±0.009	0.159±0.093	0,0949± 0,0505	
	3	0.453±0.107 Aa	1.408±0.293 ABa	0,930± 0,255		0.061±0.012	0.090±0.027	0,0753± 0,0146	
	4	0.993±0.198 Aa	0.324±0.138 Ba	0,658± 0,184		0.064±0.025	0.181±0.141	0,1227± 0,0693	
	5	1.072±0.0557 Aa	0.902±0.452 ABa	0,987± 0,207		0.040±0.007	0.152±0.054	0,0963± 0,0350	
	T	0,7454±0,0871	1,025±0,166			0,04672±0,00673[B]	0,1508±0,0326[A]		
Pb	1	0.125±0.044	2.955±0.097	1,540± 0,635	S:0.000*** L:0.968 S*L:0.615	0.626±0.185 Aa	2.810±1.910 BCa	1,720± 0,990	S:0.067 L: 0.189 Season S*L: 0.022*
	2	0.227±0.022	2.862±0.187	1,544± 0,595		0.586±0.100 Ab	18.200±11.700A Ba	9,410± 6,540	
	3	0.123±0.049	2.8053±0.093	1,464± 0,602		0.933±0.062 Ab	25.700 ±12.100 Aa	13,310± 7,730	
	4	0.380±0.119	2.769±0.396	1,574± 0,565		2.136±0.762 Aa	1.790±1.560 BCa	1,964± 0,779	
	5	0.306±0.040	2.727±0.154	1,517± 0,546		11.676±0.444 Aa	0.362±0.181 Ca	6,020± 2,540	
	T	0,2321±0,0362[B]	2,8237±0,0844[A]			3,190±1,150	9,780±3,970		
S	1	273.100±63.800	681.300±90.100	477.200± 103.776[ab]	S:0.000*** L:0.025* S*L: 0.510	12.730±2.710	27.640 ±4.410	20,180 ± 4,060	S:0.000*** L: 0.470 S*L: 0.121
	2	202.900±22.800	914.000±109.000	558.200± 166.480[ab]		20.660±7.350	30.650±4.470	25,650± 4,450	
	3	94.300±18.800	568.400±68.700	331.300± 110.676[b]		10.420±8.730	26.330±5.150	18,370 ± 5,760	
	4	167.400±29.400	705.000±177.000	436.100± 144.520[ab]		18.160±3.040	20.660±4.710	19,410± 2,570	
	5	342.00±113.00	342.000±113.000	645.400± 148.766[a]		1.740±1.220	31.820±3.020	16,780± 6,880	
	T	216,000±32,400[B]	763,300±57,300[A]			12,740±2,710 [B]	27,420±1,970[A]		
Zn	1	32.280±3.760	52.133±0.278	42.210± 4.750	S:0.519 L:0.447 S*L: 0.467	3.920±1.860 Ba	3.310±2.440 Ba	3.610± 1.380	S:0.591 L: 0.247 S*L: 0.007**
	2	37.190±2.120	51.990±1.210	44.590± 3.480		1.068±0.531 Bb	19.800±14.100A Ba	10.460± 7.580	
	3	171.000±133.000	54.080±1.440	112.300 ± 65.000		3.664±0.935 Bb	22.800±11.600A a	13.240± 6.720	
	4	36.790±2.870	54.030±0.595	45.410± 4.070		4.470±1.170 Ba	2.450±1.470 Ba	3.460± 0.954	
	5	76.100±19.600	52.363±0.644	64.200± 10.30		26.330±1.100 Aa	1.205±0.495 Bb	13.770 ± 5.640	
	T	70.600±26.700	52.919±0.433			7.89±2.52	9.92±4.00		
SO 2	1	546.000±128.000	1363.000±180.000	954.500± 208.000 [ab]	S:0.000*** L:0.025* S*L:	25.451±5.410	55.280±8.820	40,370± 8,120	S:0.000*** L: 0.470
	2	405.800±45.60	1827.000±217.0	1116.500		41.300±14.700	61.290±8.950	51,300±	

	0	00	± 333.000[ab]	0.510			8,900	S*L: 0.121
3	188.600±37.600	1137.000±137.000	662.700± 221.000[b]		20.800±17.500	52.700±10.300	36,700± 11,500	
4	334.800±58.900	1409.000±354.000	872.100± 289.000[ab]		36.330±6.080	41.330±9.420	38,830± 5,140	
5	685.000±225.000	1897.000±158.000	1290.700 ± 298.000[a]		3.480±2.440	63.630±6.030	33,600± 13,800	
T	432,1±64,8 [B]	1526.5±115[A]			25,480±5,420[B]	54,840±3,940[A]		

1: Control; 2: 50m; 3: 100m; 4: Refuge; 5: Roadside; T: Total; L: Location; S: Season; SEM, standard error of mean; SD, standard deviation;

*, statically Significant ($p<0.05$); **, statically Significant ($p<0.01$); ***, Significant ($p<0.001$)

The difference between the means indicated with different upper-case letters in the same season is significant ($p<0.05$)

The difference between the means indicated with different lower-case letters in the same location is significant ($p<0.05$).

According to variance analysis, the difference between the season means indicated with different exponent upper-case letters is significant according to variance analysis ($p<0.001$). According to Tukey test, the difference between the location means indicated with different exponent lower-case letters is significant according to variance analysis ($p<0.05$).

CONCLUSION AND DISCUSSION

The Black Sea coastal highway is among the significant transportation routes of Turkey. It connects entire Black Sea provinces and provides a route for international transport. The highway is thus used by heavy vehicles intensely. Such an intense traffic of the road exerts significant pressure on environment and creates various negative impacts. Vehicle-originated exhaust gases pollute air and environment. The resultant pollution is transported to long distances via air movements. Pollution is also accumulated over soil, plant and urban surfaces. Accumulated material is then mixed into water resources through leaching. Leaf and soil samples were collected in different seasons from Nerium oleander plants in this study to put forth the spread of heavy metals.

In wet season, the highest leaf Al content was observed in median. On the other hand, the highest Al content in dry season was observed in wayside. Al was primarily observed in the closest locations to road since the location is the best suitable place for pollution. While the accumulation in soil did not exhibited differences with the distance, higher accumulation levels were observed in plant leaves close to the road. Such a case indicated that Al was transported to long distances with the winds, but suspended particles were held by plant leaves at close distance. The highest leaf Cd level in wet season was observed on wayside. Considering the season means, higher Cd levels were observed in dry season. Higher Cd accumulation levels were observed in locations close to the road. Because of leaching in wet season, concentrations were higher in dry season. Both leaf and soil Cr contents were higher in dry season. Again leaching with precipitations increased Cr accumulations in dry season. In plants, Cu levels were generally higher in wet season than in dry season. In dry season, the highest soil Cu content was observed in 100 m location and the smallest value was observed in wayside. As it was expected, the greatest Cu accumulation was observed in dry season. However, there was a reverse case with the distance. Such a case can be interpreted as rapid movement of Cu with air motions. In wet season, leaf Fe contents were about 3-4 times higher in median than in other locations. In soil samples, dry season had higher Fe contents than wet season. The plants close to road held higher amounts of Fe. Accumulations increased in dry season without any leaching. Considering the general means of the seasons, the highest soil Mn content was observed in dry season and the highest leaf Mn content was observed in wet season. In this case, Mn did not leach through soil, accumulated increasingly in soil and removed from plant surfaces. Increasing soil Mn levels can be attributed to incorporation of Mn leached from plant surfaces into soil. In dry season, the greatest Ni content was observed in control location and the lowest value was seen in median location. With regard to season-based soil Ni contents, higher values were observed in dry season. Leaf Pb contents were higher in dry season. The greatest soil Pb content in dry season was observed in 100 m and the lowest value was seen in wayside. Pb levels in 50 and 100m locations were higher in dry season than in wet season. Air movements also triggered the transport of Pb to long distances. S contents were higher in dry season than in wet season. The highest leaf S content was observed in wayside. Soil Zn level was higher in

wayside in wet season and in 100 m location in dry season. SO_2 content was higher in dry season. The highest leaf SO_2 level was observed in wayside. The greatest soil SO_2 content was observed in dry season.

While majority of heavy metals accumulated at higher levels in locations close to the road, some accumulated at higher levels in locations farther from the road. Such a variation can be related to particle transport to long distances through air motions. The section of highway passing through the city center is quite close to the sea and exposed to winds coming from the sea. The sea breezes transport the particles through inner parts of the city. In general, higher particle concentrations were observed in dry season than in wet season. A temporary decrease was observed in wet season because of metal leaching with precipitations. However, higher values were also seen in wet season in some cases. This may be because of incorporation of leached metals from the plants and other urban surfaces into soil. More amount of material leached from plant surfaces, but such a case was not observed in soil. In both wet and dry season, both the plants and soil held high amounts of particles. Such a case was inversely proportional to distance.

Analyses results and statistic assessments revealed that highway with intense traffic load and passing through the city center had significant contributions to urban pollution. Exhaust gas-induced particulate pollution was observed throughout the city regardless of the distance. Only the particle density changed with the distance. In some cases, sea breeze transported the particles to long distances. With the completion of belt highway already under construction, highway-induced pollution will significantly be reduced since the primary reason of rood-induced pollution is transit heavy vehicles. Reduced traffic intensity over the highway passing through the city center and transfer of transit heavy vehicles to belt highway will be a significant step to solve urban pollution problem.

ACKNOWLEDGEMENT

I thank Assist.Prof.Dr. Yeliz Kasko Arıcı for the statistical analysis.

REFERENCES

[1] Adiloğlu, A., S. Adiloğlu, K. Bellitürk, Ö. Karakaş, A. Sümer, Gönülsüz, E., Sarı, H. (2011). Tekirdağ Kıyı Şeridi Topraklarında Ağır Metal Kirliliği. Kıyı Bölgelerinde Çevre Kirliliği ve Kontrolü Sempozyumu, 17--- 20 Kasım, s: 351--- 365, Tekirdağ.

[2] Akgüç, N, Özyiğit, İ., İ., Yarcı C. (2008). Pyracantha coccınea Roem. (Rosaceae) as a Bıomonıtor for Cd, Pb and Zn ın Mugla Provınce (Turkey). Pak. J. Bot., 40(4): 1767-1776.

[3] Aksoy, A., Öztürk, M A. (1997). Nerium oleander L. as a bio monitor of lead and other heavy metal pollution in Mediterranean environments. Science of the Total Environment, 205 (2–3), 145–150.

[4] Aksoy, A., Çelik, A., Öztürk, M., Tulu, M. (2000). Roadside Plants as Possible Indicators of Heavy Metal Pollution in Turkey. Chemia i Inżynieria Ekologiczna, 7 (10), 991-996.

[5] Allan, R. (1997). Introduction: mining and metals in the environment. J. Geochem. Expl. 58:95-100

[6] Aslan, A., Budak, G., Karabulut, A. (2005). Theamounts Fe, Ba, Sr, K, Caand Ti in some lichens growing in Erzurum province (Turkey). Journal of Quantitative Spectroscopy & Radiative Transfer, 88 (4), 423-431.

[7] Asri, F.,Ö., Sönmez, S. (2006). The Effect of Heavy Metal Toxicity on Plant Metabolism. Derim, vol 23, issue 2.

[8] Atiq-ur-rehman, S.,Iqbal, M. Z. (2008). Level of heavymetals in the foliage of naturally growing plants collected from Koran giand Landhi industrial areas of Karachi City, Pakistan. Pak. J. Bot., 40(2): 785-789.

[9] Bingöl Ü. (1992). Ankara Cadde Ağaçlarından Aesculus hippocastanum L.'da Kurşun (Pb) Birikimi. Yüksek Lisans Tezi, 62 s, Ankara Üniversitesi, Fen Bilimleri Enstitüsü, Ankara.

[10] Bingöl Ü, Geven F and Güney K. (2008). Heavy Metal (Pb andNi) Accumulation in the Branchand Bark Tissues of Street Tree Sophora japonica L. Kastamonu Üniversitesi, Orman Fakültesi Dergisi 8 (1): 93–96.

[11] Bingöl, M., Ü., Geven, F., Güney, K., Ketenoğlu, O., Erdoğan, N. (2010). Influences of Exhaust Gases on Plants and Protecting Suggestions. Research Journal of Biological Sciences, 3 (2): 63-67.

[12] Çavuşoğlu, K., Budak, A., Arıca, Ş., Ç. (2008). Investigation Of Lead (Pb) Pollution Caused By Vehicles On The Kırıkkale-Kırşehir Road. Science and Eng. J. Of Fırat Univ., 20 (2), 223-231.

[13] Dursun, A., Aslantaş, R., Pırlak, L. (1998). The Effects of Air Pollution on Horticultural Crops. Ecology, vol:7, issue:27, 11-14.

[14] Duru, N., Türkmen, Z., Çavuşoğlu, N., Yalçın, E., Yapar, K. (2011). Investigation of the Effects of Heavy Metal Pollution in Black Sea Seaside Caused from Vehicles by Using Verbascum Sinuatum l. (Scrophulariaceae). SAÜ. Science Journal, 15. Vol, 2. Issue, p89-96.

[15] Elkoca, E. (2003). Air Pollution and Its Effects on Plants. Journal of Agricultural Fac. Atatürk Univ. 34 (4), 367-374.
[16] Eraslan, İ. (1988). Effect of Air Pollution on Urban and Forest Trees and Our Environment Regulation. Envronment'88: 4. Scientific and Technique Environment Congress, 5-9 June, Izmir.
[17] Fakayode, S. O., Olu-Owolabi, B. I. (2003). Heavy metal contamination of road side top soil in Osogbo, Nigeria: its relationship to traffic density and proximity to high ways. Environmental Geology, 44 (2), 150-157.
[18] Huseyinova, R., Kutbay, H., G., Bilgin, A., Kılıç, D., Horuz, A., Kırmanoğlu, C. (2009). Sulphur and Some Heavy Metal Contents in Foliage of Corylus avellana and Some Road side Native Plants in Ordu Province, Turkey. Ekoloji 18, 70, 10-16.
[19] Kabır, M., Iqbal, M., Z., Shafıq, M., and Farooqı, Z., R. (2008). Reduction in Germination and Seedling Growth of Thespesia populnea L., Caused by Lead and Cadmium Treatments. Pak. J. Bot., 40(6): 2419-2426.
[20] Kahvecioğlu, Ö., Kartal G., Güven A. and Timur S. (2007). Environmental Effects of Metals I. (www.metalurji.org.tr/dergi/dergi136/d136_4753.pdf, Date of Access: 07.04.2015).
[21] Medeiros, W.H., Moskowitz, P.D. (1983). Quantifying effects of oxidant air pollutants on agricultural crops. Environment International, 9 (6): 505-513.
[22] Mingorance, M. D.,Valdes, B., Oliva, S. R. (2007). Strategies of heavy metal uptake by plants growing under industrial emissions. Environment International. 33(4), 514–520.
[23] Nuhoğlu, Y. (1996). Effect of Air Pollution on Plants. Lecture Notes of Graduate, Atatürk Univ. Science Enst., Erzurum.
[24] Okcu, M., Tozlu, E., Kumlay, A.M., Pehluvan, M. (2009). The Effects of Heavy Metals on Plants. Alınteri, 17(B), 14-26.
[25] Oliva, S., R., Espinosa, A. J. F. (2007). Monitoring of heavy metals in top soils, atmospheric particles and plant leaves to identify possible contamination sources. Micro chemical Journal, 86(1) ,131–139.
[26] Osterli, V.P., McNelly, L.B. (1968). Air Pollution and Agriculture Today. California Agr. 22(9):8-9.
[27] Pasqualini, V., Robles, C., Garzino, S., Greff, S., Melau, A. B., Bonin, G. (2003). Phenolic compounds content in Pinus halepensis Mill. Needles: a bio indicator of air pollution. Chemosphere, 52, 239-248.
[28] Raven, J.A., Evans M.C.W. and Korb R.E. (1999). The role of trace metals in photosynthetic electron transport in O2-evolving organisms. Photosynth. Res. 60:111-49.
[29] Rehman, S., A., U., Iqbal, M., Z. (2008). Level of Heavy Metals in the Foliage of Naturally Growing Plants Collected from Korangi and Landhi Industrial Areas of Karachi City, Pakistan., Pak. J. Bot., 40(2): 785-789
[30] Sümer, A., Adiloğlu, S., Çetinkaya, O., Adiloğlu, A., Sungur, A., Akbulak, C. (2013). An Investigation of Some Heavy Metals (Cr, Ni, Pb) Pollution of Karamenderes Basin Soils in Çanakkale. Journal of Tekirdağ Agricultural Faculty, 10 (1).
[31] Tok, H. H. (1997). Environmental Pollution. 404s, Anatolia Press, Istanbul.
[32] Verma,, D., K., Gupta, A., P., Dhakeray, R. (2013). Bioindicators: A Comparative Study on Uptake and Accumulation of Heavy Metals in Some Plant's Leaves of M.G. Road, Agra City, India. International Journal of Environmental Pollution and Solutions, 2:37-53.
[33] Yıldız, N. (2004). Heavy Metal in Soil and Plant Ecosystem. ZT-531. Lecture Notes of Graduate. Erzurum.
[34] Yılmaz, S., Zengin, M. (2004). Monitoring environmental pollution in Erzurum by chemical analysis of Scotspine (Pinus sylvestris L.) needles. Environment International 29, 1041– 1047.
[35] Yılmaz, S., Öz, I., S. (2004). Public Sensitivity against Air Pollution Determined by Surveys in Erzurum. Akdeniz Univ. Journal of Agriculture, 17(2), 199-206.

Received: **13.01.2016**
Accepted: **20.06.2016**

CORRESPONDING AUTHOR

Omer Atabeyoglu
Agricultural Faculty Landscape Architecture Department
Ordu University
Ordu-TURKEY

E-mail: atabey6@hotmail.com

© by PSP Volume 25 – No. 10/2016, pages 4269-4276 Fresenius Environmental Bulletin

INFLUENCE OF *Capreolus capreolus* L. AND *Cervus elaphus* L. FEEDING SIMULATION ON DISEASE INCIDENCE RATE AND MAIZE YIELDING

Korbas Marek, Wegorek Paweł*, Zamojska Joanna, Danielewicz Jakub, Jajor Ewa, Dworzanska Daria, Bandyk Andrzej, Horoszkiewicz-Janka Joanna

Institute of Plant Protection – National Research Institute - ul. Władysława Węgorka 20, 60-318 Poznań

ABSTRACT

Crop damage caused by game animals has been a serious problem in Poland and other member states of the European Union for many years. This is due both to increases in numbers of the main damage-causing species (the wild boar, the red deer, and the roe deer) and to increases in the acreage of crops that constitute an attractive source of food or shelter to the animals. Maize is one of the most at-risk crops in terms of damage caused by game animals. Animal feeding directly affects yield, not only through mechanical damage to plant tissue, but also due to the increased incidence of pathogenic fungi in the damaged plants. The paper presents the results gathered during two years of field studies on the influence of mechanical damage to maize, mimicking that caused by cervid feeding, on fungal infection incidence and on yielding. A strong correlation was found between the extent of damage and the incidence of common corn smut on stalks and tassels, and of common corn rust. Damage also was found to have a weaker influence on the incidence of *Helminthosporium turcicum* and *Kabatiella zeae* infections. Furthermore, a clear correlation was shown between plant damage and yielding. Damaged plants failed to grow cobs more often than undamaged ones, and the weight of the cobs that did develop was distinctly lower than in the control group. Damage also slowed plant maturation. The results obtained indicate that game damage in maize crops is a significant economic issue that must not be overlooked by science.

KEYWORDS:
maize, roe deer, red deer, game damage, pathogenic fungi

INTRODUCTION

In recent years, Poland and other European states have experienced a growing problem of crop damage caused by some game species, mainly the red deer (*Cervus elaphus* L.), the wild boar (*Sus scrofa* L.) and the roe deer (*Capreolus capreolus* L.). This is due to numerous factors, including an increase in numbers of those species and their distribution throughout Poland. In agriculture, crop seeding structures undergo changes involving increases in acreage of species attractive to said animals as food sources and refuge areas. Therefore, adaptive changes occur in the animals' behavior. The amount of game damage has also recently been influenced by European Union policy, aiming at transforming the agricultural landscape by promoting biodiversity.

In Poland, particularly significant damage due to said game species' activity occurs in maize crops, the acreage of which has increased radically in the recent years, reaching approx. 900,000 ha (according to the Polish Central Statistical Office). The harm caused by red deer, roe deer, and wild boar feeding and dwelling in maize crops involves, apart from parts of plants being eaten, damage due to biting and tramping that may promote the development of fungal pathologies. It is estimated that approximately 10-20% of all damage is caused by the eating of whole maize plants by boars and deer, while the remaining 80-90% results from slight biting of leaves, stalks, and cobs, as well as from plant trampling. In practice, maize plants damaged by cervids seldom wither. The damage is typically repaired to some extent and vegetation continues. Most research on damage caused by game mammals in Poland and Europe focuses on boars [1], [2], [3], [4], while fewer papers document crop damage caused by cervids [5], [6], [7], [8], [9], [10],[11], [12]. In literature, no reports are to be found on the influence of cervid feeding on fungal infection spread in maize. However, because such a correlation has been found for rapeseed [13], and because an increase in fungal pathology incidence has been found for plants that were mechanically damaged in other ways [14],[15], the authors decided to experimentally verify the existence of a similar relationship for maize plants suffering mechanical damage by game mammals.

In the experiments described in the present paper, maize damage typically caused by cervids was simulated. In Poland, the largest threat is posed by the following pathogenic fungi: *Kabatiella zeae*

TABLE 1
Variants of the experiment

Variant number	Damage in stage 1, plant development stage 34	Damage in stage 2, plant development stage 59
1	control – no damage	control – no damage
2	30% damage of leaves	3 leaves of each plant cut in half
3		2 leaves of each plant cut in half
4		1 leaf of each plant cut in half
5	whole plants cut at 40 cm above ground	1 leaf of each plant cut in half
6		2 leaves of each plant cut in half
7		3 leaves of each plant cut in half

TABLE 2
Weather conditions during the experiments

Meteorological station: PSD Winna Góra

month/year	weather parameters	decades			mean/total
		I	II	III	
07-2012	mean temp. [°C]	22.35	16.67	20.71	19.91
	mean humidity [%]	80.46	81.59	72.08	78.04
	total precipitation [mm]	41.90	27.30	29.70	98.90
08-2012	mean temp. [°C]	20.04	18.34	18.85	19.08
	mean humidity [%]	75.65	76.60	76.54	76.26
	total precipitation [mm]	20.50	5.00	10.80	36.30
09-2012	mean temp. [°C]	16.31	14.47	12.74	14.51
	mean humidity [%]	81.35	82.98	77.69	80.67
	total precipitation [mm]	41.00	25.20	0.70	66.90
07-2013	mean temp. [°C]	20.08	17.80	22.10	19.99
	mean humidity [%]	78.43	84.01	73.13	78.52
	total precipitation [mm]	12.80	11.70	18.20	42.70
08-2013	mean temp. [°C]	22.14	20.98	17.09	20.07
	mean humidity [%]	81.71	63.40	69.33	71.48
	total precipitation [mm]	7.20	1.80	0.70	9.70
09-2013	mean temp. [°C]	15.73	12.84	10.46	13.01
	mean humidity [%]	71.03	90.14	83.87	81.68
	total precipitation [mm]	20.10	77.60	8.50	106.20
10-2013	mean temp. [°C]	8.9	10.20	12.5	10.53
	mean humidity [%]	76.64	89.04	71.02	78.86
	total precipitation [mm]	0.00	17.30	0.0	17.3

(brown spot), *Helminthosporium turcicum* (northern leaf blight) and *Fusarium* spp. (Fusarium wilt, Fusarium stalk rot) [16], [17]. Maize crops are also threatened by common smut of corn (*Ustilago maydis*) [18]. The incidence of *Fusarium* and *Ustilago maydis* fungi also entails a risk related to the harmful effects of the toxic metabolites produced by the fungi [19]. The increase in maize crop acreage and the agrometeorological changes in Poland result in higher risk from pests and pathogenic fungi [20]. Maize diseases, along with the major pests, may directly cause grain yield losses of 20-30% or even 40-50% [21].

The experiments performed aimed at determining the correlation between the extent of maize plant damage at development stages BBCH 34 – BBCH 59, and plant yielding and infection pathogenic by fungi.

MATERIAL AND METHODS

Two studies on the consequences of roe deer and red deer feeding depending on the extent of plant damage were performed on experimental plots at the Animal Breeding Center of the Plant Protection Institute – National Research Institute in Poznań, in the years 2012 and 2013. Each experiment variant was performed on 10 rows of maize, each 47 m in length. For the experiment, an area with no maize damage caused by roe deer and red deer was selected. In the two subsequent experimental stages within each study, such damage was simulated (in one day each time). The first simulated damage (first experimental stage) was introduced on July 4, 2012, and July 5, 2013, respectively. At those times, plants were at BBCH development stage 34. More damage (second

experimental stage) was introduced on August 10, 2012, and August 23, 2013, respectively, when BBCH plant development stage was 59.

The incidence of fungal infections was assessed on September 18, 2012, and October 3, 2013, respectively. The researchers assessed the incidence of the following diseases: common smut of corn (*Ustilago maydis*) on stalks, tassels and cobs; northern corn leaf blight (*Helminthosporium turcium*); common corn rust (*Puccinia sorghi*); and brown spot (*Kabatiella zeae*).

On September 25, 2012, and October 15, 2013, respectively, 100 cobs were collected from each row in each experimental variant. For each experimental variant, the following parameters were determined: the percentage of plants that failed to develop cobs, the weight of all green and mature cobs per 100 cobs, the percentage of green cobs, the mean weight of a single green cob, and the mean weight of a single mature cob.

The maize disease incidence was assessed in compliance with the EPPO guidelines (PP 1/272 (1)). Maize health was assessed three weeks after each damage simulation. Cob infection by the common smut fungus was assessed when the grains were milky ripe (BBCH stage 75).

A test was performed in greenhouse conditions to verify that maize could be infected using the northern corn leaf blight-causing *Helminthosporium turcicum* isolated from affected leaves.

TABLE 3

The incidence of fungal diseases in maize plants depending on the extent of damage caused by cervids in the years 2012 and 2013. Values in the table are means calculated for a single row in each experimental variant.

Experimental variant	Common smut *Ustilago maydis* [% afflicted]						Northern corn leaf blight *Helminthosporium turcicum* [% of plants afflicted]		Common corn rust *Puccinia sorghi*				Brown spot *Kabatiella zeae*	
	tassel		cob		stalk				mean % of leaf area afflicted		% of plants afflicted		% of plants afflicted	
	2012	2013	2012	2013	2012	2013	2012	2013	2012	2013	2012	2013	2012	2013
1	1	0	1	1	1	0	1	0.7	0	1	0	3	0	0
2	0	0	1	0	0	0	1	1	7	3.6	5	5	0	2
3	1	0	5	1	8	0	0	0	2	3	10	5	1	1
4	1	0	5	1	3	0	0	0	1	1.7	4	6	0	2
5	0	1	1	0	0	0	0	1	2	1.64	10	3.7	0	1
6	0	0	3	1	7	0	0	2	3	0	15	0	0	2.3
7	0	0	6	4	10	0	0	3	4	1	15	1	0	6

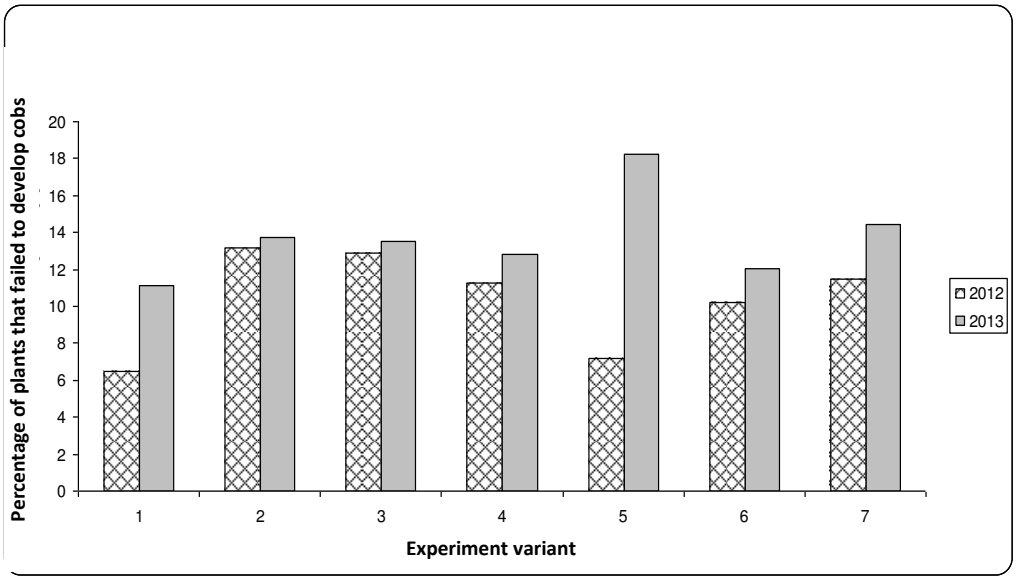

FIGURE 1

Percentage of plants that failed to grow cobs in each experimental variant. Values in the diagram are means calculated for a single row in each experimental variant.

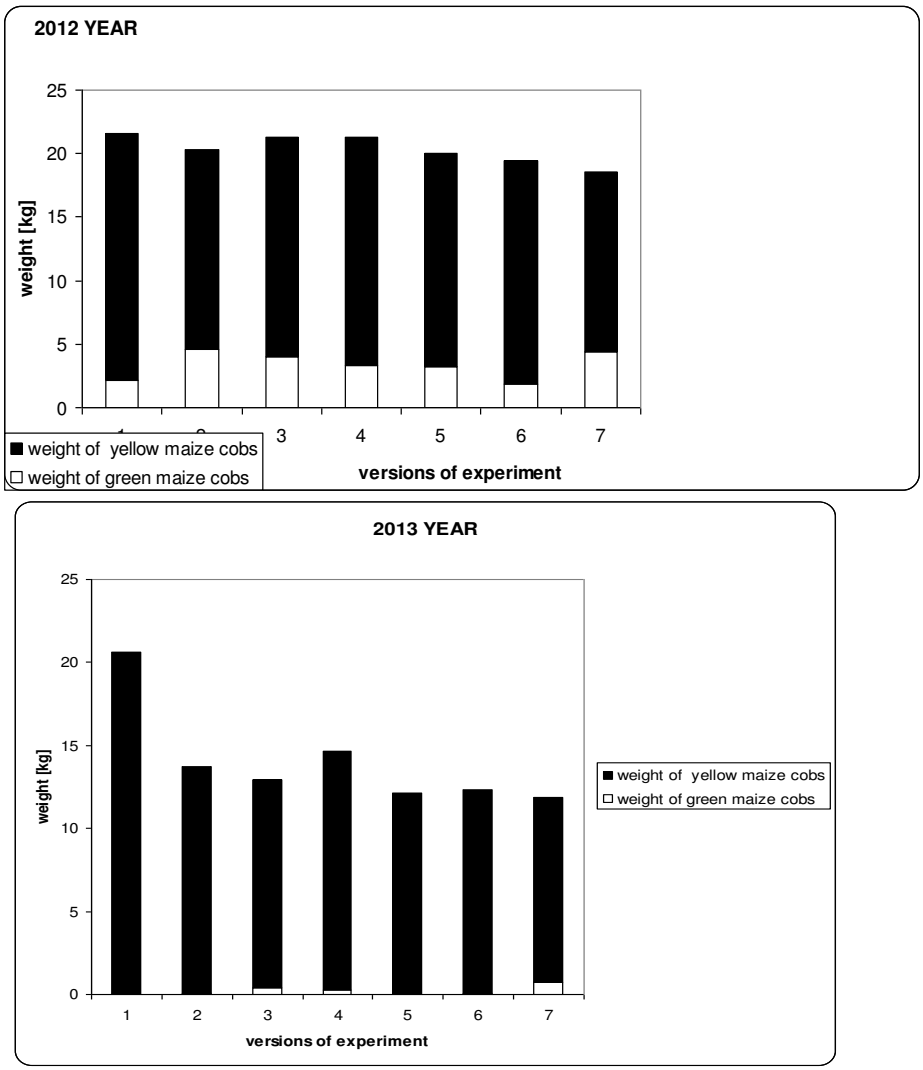

FIGURE 2
Green and mature cob weight per 100 cobs in each experimental variant. Values in the diagram are means calculated for 100 cobs from a single row in each experimental variant
a) 2012 b) 2013

For this purpose, "Kosynier" variety maize was sown in pots. At BBCH stages 11–12 (1–2 leaves unfolded), the plants were sprayed with a suspension containing *Helminthosporium turcicum* spores obtained from 4-week-old *Helminthosporium turcicum* cultures. 1 ml^3 of the suspension contained 1 x 10^5 conidial spores. After 24 days the leaves were examined for signs of infection. The test was performed in the years 2012 and 2013, in 4 series involving 25 plants each (5 pots, 5 plants each in each series).

RESULTS

Results clearly indicate that the intensity of cervid feeding on maize, and the resulting mechanical damage to the plants, influences the extent of pathogenic fungi infection (Tab. 3). In 2012, the percentage of cobs affected by common smut and common rust increased together with the degree of plant damage. In 2013, no influence of damage on tassel and stalk affliction with the common smut was found. However, there was a clear correlation between the largest damage at experimental stages 1 and 2, and cob affliction. In 2013, most damage variants also entailed increased spread of common rust. In 2012, no correlation was found between plant damage and infection with the fungi causing northern leaf blight and brown spot. In 2013, plants that have undergone more damage in the two subsequent experimental stages had higher rates of affliction with *Helminthosporium turcicum* (causing northern leaf blight). Similarly, plants that have undergone more damage in the two subsequent experimental stages also had higher

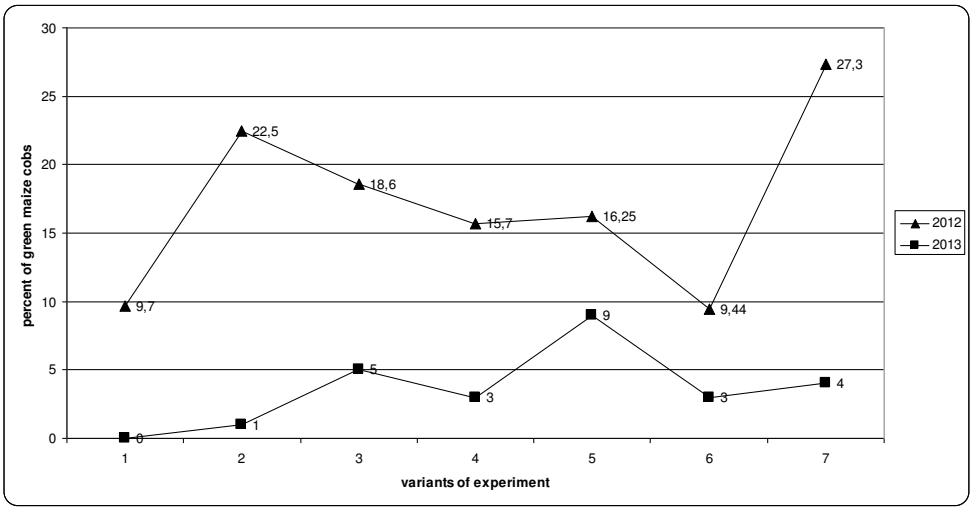

FIGURE 3
Green cob percentage in each experimental variant. Values in the diagram are means calculated for 100 cobs from a single row in each experimental variant

rates of affliction with the fungus causing brown spot.

Helminthosporium turcicum isolates obtained from the plants afflicted in the field experiments caused lesions on maize leaves studied in the pathogenicity test (on average, 95% of plants showed infection symptoms) (Tab. 4). The extent of mechanical damage also significantly influenced the number of cobs grown (Fig. 1). In all experiment variants, both in 2012 and 2013, the percentage of plants that failed to grow cobs was higher in damaged plants than in controls. All experimental variants showed similar correlations, which indicates that even slight losses in green weight interfere with maize plant maturation.

TABLE 4
Results of the *Helminthosporium turcicum* fungi pathogenicity test

Test series	Mean % of plants afflicted
I	90
II	100
II	100
IV	90
Mean	95

The extent of damage was also clearly correlated with the weight of cobs obtained and their maturity (Fig. 2a, 2b, 3). In both years, the weight per 100 cobs and the weight of mature cobs were higher in controls; the difference was more marked in 2013. (As in the case of cob percentage, all experimental variants yielded similar results). The percentage of green cobs was higher in 2012 than in 2013, and in all variants involving damage, except for variant 6, was higher than in controls. In 2013, the percentage of green cobs was much lower: from 0 in controls, through 1% (variant 2 – the smallest percentage of green cobs in variants involving damage), to 9% (variant 5 – the largest percentage of green cobs in variants involving damage).

An analysis of mean weights of green and mature cobs (Tab. 5) shows that in both study years all variants involving damage produced lower weights than control variants. This does not apply to green cob weight in 2013, as no green cobs were found in the control variant that year. However, in the 2013 variants involving damage, the mean green cob weight was significantly lower than in 2012, which indicates very poor development of the cobs. Also, in all 2013 variants, including control ones, the mean mature cob weight was lower than in 2012. Furthermore, in 2013, a steady trend was observed – in all variants involving damage, cob weight was lower than in control variants (with similar results in all damage variants).

TABLE 5
Mean weight of a single green cob and mean weight of a single mature cob in each experimental variant. Values in the table are means calculated for 100 cobs from each row in each experimental variant.

Experimental variant	Mean weight of a single green cob [g]		Mean weight of a single mature cob [g]	
	2012	2013	2012	2013
1	233	0	222	206.38
2	228	43.3	199	137.95
3	198	78.44	219	132.38
4	186	80.40	216	148.32
5	217	75.73	200	122.95
6	153	31.03	202	126.5
7	209	75.925	181	123.21

DISCUSSION

Maize (*Zea mays*) is a member of the true grasses (*Poaceae*) family. However, contrary to most species in the family, including most cereals, it does not tiller. This characteristic may have affected the experiment results. The results obtained prove that above-ground damage of maize plants in BBCH development stage 34 causes poorer yielding and a higher incidence of some fungal diseases, despite the plants' ability to compensate for the damage. The assimilatory leaves and the meristem are the most susceptible to damage by herbivores at the early phenological development stages. The decreased yielding of the damaged maize plants is likely related to a loss of assimilatory surface, which adversely affects the intensity of photosynthesis, retards plant growth, and consequently, inhibits access to light when competing with other, undamaged plants. Therefore, maize does not exhibit the same behavior as that observed in other grasses by other authors, where defoliation resulting from herbivore feeding significantly intensified photosynthesis in new tissue. A similar plant adaptation, called **compensatory growth**, constituting a physiological response to damage due to large herbivore feeding, was described by McNaughton [22], [23]. Other authors also corroborate the increase in green weight production by grasses fed on by large ungulates [24]. In the own research, **compensatory growth** was not observed in maize.

Plant damage analogous to that done by cervids is extensive, stresses maize plants and affects their morphology. Similar results as those presented herein were obtained by Obrtel and Holisowa [25], [26], [27] in the studies on maize damage caused by roe deer (*Capreolus capreolus*). The author reported a weight decrease in cobs produced by plants sustaining such damage. In other studies on simulated maize damage mimicking that caused by roe deer, the author reported impaired growth and decreased cob yielding, as well as increased incidence of common smut (*Ustilago maydis*). Mechanical damage of plant tissue by herbivores is a known contributing factor in fungal, bacterial, and viral infections. Many animals are hosts and vectors to pathogenic microbes and viruses [28], [13]. There are also cases of infection with no animal factor, where pathogens are carried by air. Plants that are slightly damaged by insects respond by releasing volatile substances that indirectly protect them from the pests [29]. One metabolite released by maize plants damaged by herbivores is methyl salicylate, mediating immune signals against pathogenic fungi, bacteria and viruses [30]. The role of secondary metabolites in maize plants' passive defense against herbivore mammals has not yet been well understood. Recently, a conceptual theory of another indirect defense mechanism against herbivores present in plants was proposed, linking physiological mechanisms with the theory of ecological changes in the environment, favorable to the attacked plant. One example of maize's indirect influence on cervid population in Poland is the sharp increase in numbers of wolves, which curb cervid populations. This results from the environmental advantage for wolves resulting from the large maize field acreages.

In summary, it can be concluded that maize plants damaged by feeding cervids survive. The animals do not typically destroy the whole plant, only biting several leaves. This damage is partially repaired by maize plants, but nonetheless results in poorer growth, maturation, and yielding. The observed infection by the studied fungi indicates that damaged plants are more susceptible to common corn rust. Observations performed in many maize fields, both in industrial and individual plantations, suggest a growing concern with the disease in Poland. Maize damage retarded its maturation, prolonging the vegetation period and consequently increasing the risk of *Puccinia sorghi* infection, which causes common corn rust. The effect is similar with regard to *Ustilago zeae*, the fungus causing the common smut. Plant tissue damage by animals is conducive to infection by *Helminthosporium turcicum*. The northern corn leaf blight is becoming an increasingly serious issue in Poland due to the growing acreage and monoculture of maize crops [31]. Nonetheless, the incidence rates varied in the two study years. This can be explained by the difference in weather conditions during the studies in 2012 and 2013 (table 2).

The results presented herein constitute a scientific basis for estimating game damage in maize crops. This is a significant issue in contemporary agricultural practice, due to the increase in acreages of crops attractive to animals, animal numbers, and damage caused by these animals. At the same time, no scientific reports are available as a basis for estimating the losses. The experiments described above are the second part in a series of studies addressing the issue (the first being those presented by Węgorek et al. for rapeseed — 2014 [13]).

REFERENCES

[1] Schley, L., Roper, T.J. (2003) Diet of wild boar Sus scrofa in Western Europe, with particular reference to consumption of agricultural crops. Mammal Review, 33,43–56.

[2] Schley, L., Dufrene, M., Krier, A., Frantz, A.C. (2008) Patterns of crop damage by wild boar (Sus scrofa) in Luxemburg over a 10-year

period. European Journal Wildlife Research, 54, 589-599.

[3] Klein, F., Baubet, E., Toigo, C., Leduc, D., Saint-Andrieux, C., Saïd, S., Fréchard, C., Vallance, M. (2007) La gestion du sanglier. Des pistes et des outils pour réduire les populations. [Wild boar management. Methods and instruments for population reduction.] Office national de la 598. European Journal Wildlife Research (2008) 54, 589–599.

[4] WWęgorek P. (2002) Cykl zasiedlania wielkoobszarowych upraw kukurydzy przez subpopulacyjne ugrupowania dzików i dynamika narastania szkód w zależności od fazy rozwoju tych upraw. [Cyclic dwelling of subpopulational groups of boars in large-area maize crops and the dynamics of damage increment depending on the developmental stage of the crops]. Progress in Plant Protection/Postępy w Ochronie Roślin, 42 (2), 730–736.

[5] Styszko, L. (2009) Szkody łowieckie w uprawach roślin energetycznych. [Game damage in energy crops]. Progress in Plant Protection/Postępy w Ochronie Roślin, 49 (1), 145-149.

[6] Styszko, L., Borzykowska, A. (2011) Wpływ szkód łowieckich powodowanych przez jeleniowate na plonowanie wierzby. [The influence of damage caused by cervids on willow yielding] . Progress in Plant Protection/Postępy w Ochronie Roślin, 51 (1), 217-222.

[7] Callender, R.F., MacKenzie, N.A. (1991) The management of wild red deer in Scotland. Rural Forum, Perth.

[8] Putman, R.J. (1986) Foraging by roe deer in agricultural areas and impact on arable crops. Journal of Applied Ecology, 23, 91-99.

[9] Marshall, F. (1970) Deer and the farmer. Deer, 2, 514-516.

[10] Salter, H.B. (1972) Deer in my corn. Deer, 2, 815.

[11] Putman, R.J., Moore, N.P. (1998) Impact of deer in lowland Britain on agriculture, forestry and conservation habitats. Mammal Review, 28, 141-164.

[12] Szemethy, L., Heltai, M., Matrai, M., Peto, Z. (1998) Home ranges and habitat selection of red deer (*Cervus elaphus*) on a lowland area. Gibier Faune Sauvage, 15, 607-615.

[13] WWęgorek, P., Korbas, M., Jajor, E., Zamojska, J., Bandyk, A., Danielewicz, J. (2014) Influence of *Capreolus capreolus* L. and *Cervus elaphus* L. feeding simulation on disease incidence rate and winter rape yielding. Fresenius Environmental Bulletin, (23) 7a, 1610 – 1617.

[14] Jajor, E., Korbas, M., Kozłowski, J., Mrówczyński, M., Pruszyński, G., Wachowiak, H., Walczak, F., Węgorek, P. (2008). *Poradnik sygnalizatora ochrony rzepaku. [Rapeseed Protection Signaller's Guide]* (F. Walczak ed.). Institute of Plant Protection – National Research Institute, Poznań, ISBN 978-83-89867-29-2.

[15] Gwiazdowski, R., Korbas, M., Jajor, E. (2008). Ochrona rzepaku przed chorobami. [Protection against rapeseed diseases]. In M. Mrówczyński & S. Pruszyński (Eds.), *Integrowana produkcja rzepaku ozimego i jarego [Integrated Production of Winter and Spring Rapeseed]* (pp. 42–55) Institute of Plant Protection – National Research Institute, Poznań, 105 pp. ISBN 978-83-89867-24-7.

[16] Korbas, M., Czubiński, T., Horoszkiewicz-Janka, J., Jajor, E., Danielewicz, J. (2015) Atlas chorób rolniczych dla praktyków. [Practical Atlas of Agricultural Diseases]. Polskie Wydawnictwo Rolnicze Sp. z o.o., Poznań, 368 pp.

[17] Tekiela, A. (2005) The occurance and economic importance of eyespot [*Aureobasidium zeae (Narita et Hiratsuka) J.N.Dingley*] and leaf spot (*Trichometasphaeria tarcica* Luttr.) of maize diseases in south-eastern Poland. Progress in Plant Protection/Postępy w Ochronie Roślin, 45(1), 484-486.

[18] Tekiela, A. (2011) Występowanie głowni guzowatej kukurydzy (Ustilago zeae Beckm.) w południowo-wschodniej Polsce. [The incidence of common corn smut (Ustilago zeae Beckm.) in South-East Poland]. Progress in Plant Protection/Postępy w Ochronie Roślin ,51 (4), 1655–1658.

[19] TTwarużek, M., Grajewski, J., Grajewska-Wanat, N. (2013) Cytotoxicity of *Ustilago maydis* isolated from maize. Nauka Przyroda Technologie, 7(1), 1-7.

[20] Bereś, P., Mrówczyński, M., Korbas, M., Paradowski, A. (2013) Integrated maize protection in Poland – current state of research and implementation. Progress in Plant Protection/Postępy w Ochronie Roślin, 53(1), 167-175.

[21] Bereś, P., Kaniuczak, Z., Tekiela, A., Mrówczyński, M., Pruszyński, G., Paradowski, A. (2007) Ochrona kukurydzy przed agrofagami w integrowanej produkcji. [Maize protection against agrophages in integrated production]. Progress in Plant Protection/Postępy w Ochronie Roślin, 47(4), 275-284.

[22] McNaughton, S.J. (1979) Grazing as an optimization process: grass-ungulate relationships in the Serengeti. American Naturalist, 113, 691-703.

[23] McNaughton, S.J. (1985) Interactive regulation of grass yield and chemical properties by defoliation, a salivary chemical and inorganic nutrition Oecologia, 65, 478–486.
[24] Knepp, R. G., Hamilton, J. G. Mohan, J. E. Zangerl, A. R. Berenbaum, M. R. DeLucia, E. H. (2005) Elevated CO_2 reduces leaf damage by insect herbivores in a forest community. New Phytologist, 167, 207-218.
[25] Obrtel, R., Holisova, V. (1983) Effects of a stimulated damage done to maize plants by roe deer *Capreolus capreolus*. Folia Zoologica, 32, 33-39.
[26] Holisova, V., Kozena, I., Obrtel, R. (1984) The summer diet of field roe deer bucks(*Capreolus capreolus*) in Southern Moravia. Folia Zoologica, 33, 193-208.
[27] Holisova, V., Obrtel, R., Kozena, I. (1986) Seasonal variation in the diet of field roe deer (*Capreolus capreolus*) in Southern Moravia. Folia Zoologica, 35, 97-115.
[28] Klepzig, K. D., Raffa, K. F., Smalley, E. B. (1991) Association of an insect-fungal complex with red pine decline in Wisconsin. Forest Science, 37, 1119-1139.
[29] Baldwin, I.T., Preston, C.A. (1999) The eco-physiological complexity of plant responses to insect herbivores. Planta, 208, 137–145.
[30] Park, S.W., Kaimoyo E., Kumar D., Mosher, S., Klessing, D.F. (2007) Methyl salicylate is a critical mobile signal for plant systemic acquired resistance. Science, 318, 113-116.
[31] Korbas, M., Jajor, E., Horoszkiewicz-Janka, J., Danielewicz, J. (2015) Atlas of Crop Diseases. Hortpress Warszawa, 202 pp.

Received: **08.01.2016**
Accepted: **23.07.2016**

CORRESPONDING AUTHOR

Wegorek Paweł
ul. Władysława Węgorka 20,
60-318 Poznań

e-mail: p.wegorek@iorpib.poznan.pl

© by PSP Volume 25 – No. 10/2016, pages 4277-4286 Fresenius Environmental Bulletin

HEAVY METALS POLLUTION AND HEALTH RISK ASSESSMENT OF ATMOSPHERIC DUST OF LESS THAN 100μm ALONG A TYPICAL INDUSTRIAL CORRIDOR, CENTRAL CHINA

Yong Zhang[1,2], Jiaquan Zhang[1*], Changlin Zhan[1], Ruizhen Yao[1], Ting Liu[1], Li Zhang[1], Wensheng Xiao[1], Yongkui Wang[1], Jingru Zheng[1], Hongxia Liu[1]

[1]School of Environment Science and Engineering, Hubei Polytechnic University, Hubei Key Laboratory of Mine Environmental Pollution Control and Remediation, Huangshi, 435003, China

[2]Key Laboratory of Aerosol Chemistry & Physics, Institute of Earth Environment, Chinese Academy of Sciences, Xi'an 710075 China,

ABSTRACT

Twenty nine of atmospheric dust samples at a height of 1.2-1.5 m were collected along a typical industrial corridor, central China during May, 2012. Total concentrations (As, Cr, Mn, Ni, Co, Cu, Zn, Pb and Fe) in less than 100 μm particles of the samples were determined by X-ray fluorescence spectrometry. The average concentration of As, Cr, Mn, Ni, Co, Cu, Zn, Pb and Fe in the samples was 283.66, 218.78, 1040.33, 75.70, 18.18, 1485.54, 10133.13, 445.28 mg/kg, and 6.67%, respectively. The higher concentrations were located at Huangshi City, and Cr, Ni, Mn, Co and Fe were all high in the study area. Geo-accumulation index indicated contamination of Cu, Zn and Pb were more serious than other elements in atmospheric dust by the industrial activities. Pearson's correlation analysis, enrichment factor analysis and PCA comprehensively indicated that the major contribution of heavy metals pollution in the study area were Pb, As, Cu and Co, which showed significant correlation between each other. Health risk assessment showed that there was no cancer risk for metals pollution, but As and Pb harming to people health with non - cancer risk, especially for children. And the major harm method for human health was through ingestion.

KEYWORDS:

industrial corridor, national highway G316, atmospheric dust, heavy metals, pollution characteristics, heath risk assessment

INTRODUCTION

With the rapid development of industrialization and urbanization in China, the problems of environmental pollution caused by heavy metals have become increasingly serious than other types of pollution. The high concentrations of these substances have serious implications for the environment, ecological systems, human health, and may become enriched through the food chain. Atmospheric dust an important environmental indicator of heavy metal contamination from atmospheric deposition, receives varying inputs of anthropogenic heavy metals from various mobile and stationary sources [1]. The source of atmospheric dust particulate is mainly from soil minerals, traffic and industrial emissions, and biomass burning [2-5]. Different size particles of atmospheric dust have different methods of transport, such as creep, saltation and suspended. The particles more than 500 μm are too large to enter the wind stream, it can be moved by creep on the surface during wind erosion, while 100-500 μm may enter the wind stream momentarily for saltation. The less than 100 μm particles in atmospheric dust is easily re-suspended into atmosphere under the pedestrian flow, traffic stream and wind for a long time and can be transported in long-distance [6,7]. Due to that dust particulate always combined with many other toxic chemicals, such as heavy metals (e.g. Cu, Zn, Pb, Cd, Ni, Cr, As, and Hg) [8-10] and organic pollutants (PAHs) [11-13], thus it will make an enormous effect on the earth environment and human health. In the past decades, many studies have been carried out on heavy metal pollution in urban areas and industrial zone, and the results showed that heavy metal may reach high concentrations in dusts [14-16]. So, the research on heavy metal contamination in less than

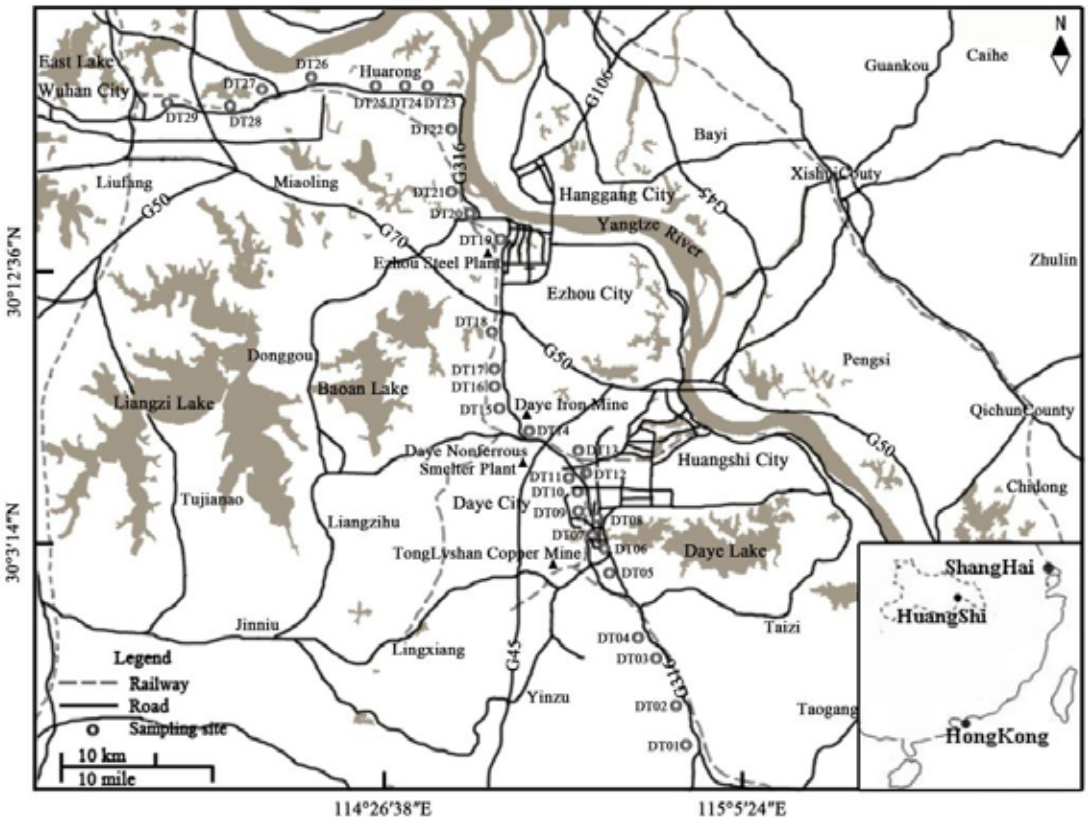

FIGURE 1

The location of sampling sites

100 μm particles of atmospheric dust is very important for urban environmental.

The studied area is mainly composed of three different scale industrial cities (Wuhan, E'zhou and Huangshi) which form a metal - working corridor in central China. The atmospheric pollution along the highway is very serious because there are many industrial and mining enterprises nearby, such as E'zhou Steels Plant, Daye Iron Mine, Daye Nonferrous Smeltery, Tonglvshan Copper Mine, and so on. This area can be called a typical industrial corridor in Hubei Province, central China. Studies of heavy metals along the industrial corridor will make it possible to evaluate the contributions of the heavy industries and transportation to the atmospheric burdens of heavy metals. Furthermore, it is equally important to evaluate the human health risks associated with exposure to heavy metals in the region for the government to alleviate heavy metals pollution of the street environment. Therefore, the objectives of the present study were to (a) investigate the concentrations and distribution of heavy metals in atmospheric dust; (b) determine the potential sources for the heavy metals; and (c) evaluate the potential cancer risks of heavy metals using the incremental lifetime cancer risk approach.

MATERIALS AND METHODS

Sampling and pretreatment. Total of 29 samples were collected at the industrial corridor during May 2012 (D01 - D14 was in Huangshi City, D15 - D25 was in E'zhou City and D26 – D29 was in Wuhan City). The location of sampling sites was shown in Fig.1. Each individual sample was composed of several dust samples and collected from the smooth and rustless surface, the sampling height was 1.2-1.5 m above the floor, thus simulating the human breathing zone. All the samples were sieved through Tyler 150 mesh sieves to obtain approximately 30 g of particles with physical diameters less than 100 μm until analysis.

Heavy metals analysis. As, Cr, Mn, Ni, Co, Cu, Zn, Pb, and Fe concentrations were determined by using a PANalytical PW4400 X-ray fluorescence (XRF) analyzer at the Institute of Earth Environment, Chinese Academy of Sciences. All powder samples were dried at low temperature (35ºC) for 72 hours. Six grams of each sample were compacted (30 tons in pressure) into a disc of ~ 3.2 cm in diameter. A calibration curve was developed using sixteen Chinese national soil reference samples (from GSS-1 to GSS-16), twelve stream sediment reference samples (from GSD-1 to

GSD-12). The reproducibility of elemental measurements were evaluated by repeat analysis using the National Standard soil reference sample GSS-8, with analytical uncertainties < 3% for major elements and < 5% for trace elements. XRF has been widely used in street dust samples analysis [14].

Geo-accumulation index. Geo-accumulation index was firstly proposed to evaluate heavy metals pollution in sediments by Muller [17]. Until now, it had been widely applied to investigate heavy metals contamination in other media such as soils, atmospheric particle and atmospheric dust [18,19]. The geo-accumulation index could be calculated by following equation:

$$I_{geo} = \log_2[C_n/(k \times B_n)]$$

Where I_{geo} is on behalf of geo-accumulation; C_n is concentration of analyzed element; B_n is concentration of reference element; k is a dimensionless constant considering the change of reference element content due to crustal movement; k is usually set up to 1.5. If $I_{geo} \leq 0$, it donates media is non-pollution; if $0 \leq I_{geo} \leq 2$; it donates media is polluted slightly; if $2 \leq I_{geo} \leq 4$; it donates media is polluted moderately; if $I_{geo} \geq 4$; it donates media is polluted seriously.

Enrichment factor. Enrichment factor (EF) analysis had been used to assess the degree of heavy metals contamination in different median for many years [20]. Otherwise, it could identify source of heavy metals according calculated value of EF. If value of EF is lower than 2, it could explain discussed element was scarcely enriched. When value of EF is between 2 and 5, it indicates analysed element was in level of moderate enrichment and its source primarily comes from nature actions such as soil weathering and volcano eruption. If value of EF is greater than 5, especially more than 10, which means the aimed element was enriched significantly and mainly controlled by anthropogenic source [21]. The equation of EF is suggested by

$$EF = (C_x/C_i)_{sample}/(C_x/C_i)_{reference}$$

Where C_x is concentration of analysed element, C_i is concertation of referenced element.

Health risk assessment. The health risk assessment method is wildly used to heavy metals in dust [22-24]. The pathways of pollutants absorbed on atmospheric dust entering human body include hand-to-mouth ingestion, dermal absorption and mouth and nose inhalation. The exposure dose via each of the three paths was computed by the follow equations [25,26]:

$$D_{ing} = C \times \frac{R_{ing} \times EF \times ED}{BW \times AT} \times 10^{-6} \quad (1)$$

$$D_{inh} = C \times \frac{R_{inh} \times EF \times ED}{BW \times AT \times PEF} \times 10^{-6} \quad (2)$$

$$D_{dermal} = C \times \frac{SL \times SA \times ABS \times EF \times ED}{BW \times AT} \times 10^{-6} \quad (3)$$

$$HQ = D/RfD \quad (4)$$

$$HI = \sum HQ_i \quad (5)$$

$$Risk = D_{inh} \times SF_{inh} \quad (6)$$

Where D_{ing} is the daily exposure dose of falling dust via hand-to-mouth ingestion; D_{inh} is the daily exposure dose of re-suspend particles via inhalation through nose and mouth; D_{demal} is the daily exposure dose of heavy metals in dust adhered to skin via dermal absorption; C is exposure-point concentration; R_{ing} is ingestion rate; R_{inh} is inhalation rate; PEF is particle emission factor; SA is exposure skin area; SL is skin adherence factor; ABS is dermal absorption factor; ED is exposure duration; EF is exposure frequency; BW is average body weight; AT is average time. HQ is hazard quotient; HI is equal to sum of HQ; RfD is reference dose of individual trace element. If the value of HQ and HI is less one, it indicates there is no significant risk of non-carcinogenic effects. If HQ or HI exceeds one, it presents there is a possibility that non-carcinogenic may occur. $Risk$ represents cancer risk; SF is slope factor of individual element. The level of cancer risk associated with exposure to individual element in atmospheric dust is the range of threshold values (10^{-6}-10^{-4}). If value of $Risk$ exceeds threshold, it means those trace elements are hazard for residents' health. Some values of that parameter as follow Table 1 [27-29] and Table 2 [30,31].

Statistical analysis. Descriptive statistics including average, maximum, minimum, standard deviation and variation coefficient were displayed after analysis. The standard deviation and variation coefficient could reflect the level of dispersion distribution of different metals and indirectly assess the activity of analyzed elements in the study area. Multivariate analysis of the dust data set was performed using Pearson's correlation analysis and principal component analysis (PCA) [32-35] with SPSS17.0 for windows.

RESULTS AND DISCUSSION

Concentrations. Concentrations of As, Cr, Mn, Ni, Co, Cu, Zn, Pb, and Fe in less than 100 μm

particles of atmospheric dust from the section of G316 were shown in Table 3. The concentrations of heavy metals in less than 100 μm particles of atmospheric dust were shown a great difference. Mean concentrations of As, Cr, Mn, Ni, Co, Cu, Zn, Pb, and Fe were 283.66, 218.78, 1040.33, 75.7, 18.18, 1485.54, 10133.13, 445.28 $mg \cdot kg^{-1}$ and 6.07%, respectively. Compared with the background values of soils in Hubei province and State Department of Environmental Conservation of China Environmental Monitoring Centre in 1990, all the elements showed higher values, especially for As, Cu, Zn, and Pb. The mean contents of these four elements (As, Cu, Zn, and Pb) were roughly 23, 48, 121, 16 times those of background value of soils in Hubei province and 25, 65, 136, 17 times those of background value of soils in China, respectively. It showed that the concentrations of heavy metals in the atmospheric dust along the section of G316 were more serious than the standard.

TABLE 1
Parameter value of daily dose model of heavy metals in atmospheric dustfall

Parameter	Unit	Values		Reference
		Child	Adult	
C	mg/kg	95%UCL	95%UCL	This study
R_{ing}	mg/d	200	100	USEPA, 2001
R_{inh}	m^3/d	7.600	20	Van den Berg, 1995
PEF	m^3/kg	1.36×109	1.36×109	USEPA, 2001
SA	cm^2	2800.000	5700	USEPA,2001
SL	mg/(cm^2/h)	0.2	0.7	USEPA,2001
ABS	Unit-less	0.001	0.001	Ferrria-Baptista & De Miguel, 2005
ED	y	6	24	USEPA, 2001
EF	d/y	180	180	Ferrria-Baptista & De Miguel, 2005
BW	kg	15	70	Ferrria-Baptista & De Miguel, 2005
AT	d	*ED*×365(for non-carcinogens) 70×365(for carcinogens)		USEPA, 2001

TABLE 2
Reference dose and slope factor of individual elements via different pathway (mg/kg·d)

Element	As	Cr	Mn	Ni	Co	Cu	Zn	Pb
RfD_{ing}	3.00E-04	3.00E-03	4.60E-02	2.00E-02	2.00E-02	4.00E-02	3.01E-01	3.50E-03
RfD_{inh}	3.01E-04	2.86E-05	1.43E-05	2.06E-02	5.71E-06	4.02E-02	3.01E-01	3.52E-03
RfD_{dermal}	1.60E-02	6.00E-05	1.84E-03	5.40E-03	1.60E-02	1.20E-02	6.00E-02	5.25E-04
SF_{inh}	15.1	42.0		0.840	9.80			

TABLE 3
Concentration of heavy metals in atmosphere dust

Elements	Unit	Minimum	Maximum	Mean	SD[a]	VC[b]	HSBV[c]	NSBV[d]
As	mg/kg	17.31	1694.62	283.66	428.57	1.51	12.3	11.2
Cr	mg/kg	53.45	1138.35	218.78	197.93	0.9	86.0	61.0
Mn	mg/kg	432.29	2380.73	1040.33	512.59	0.49	712	583
Ni	mg/kg	20.03	412.99	75.7	77.24	1.02	37.3	26.9
Co	mg/kg	10.12	40.26	18.18	6.88	0.38	15.4	12.7
Cu	mg/kg	42.98	9290.07	1485.54	2362.18	1.59	30.7	22.6
Zn	mg/kg	217.11	66754.39	10133.13	19571.01	1.93	83.6	74.2
Pb	mg/kg	79.57	1578.51	445.28	438.24	0.98	26.7	26.0
Fe	%	2.96	11.94	6.07	2.51	0.41	3.96	2.94

a SD: Standard deviation; b VC: Variation coefficient; c background value of soils in Hubei province; d background value of soils in China.

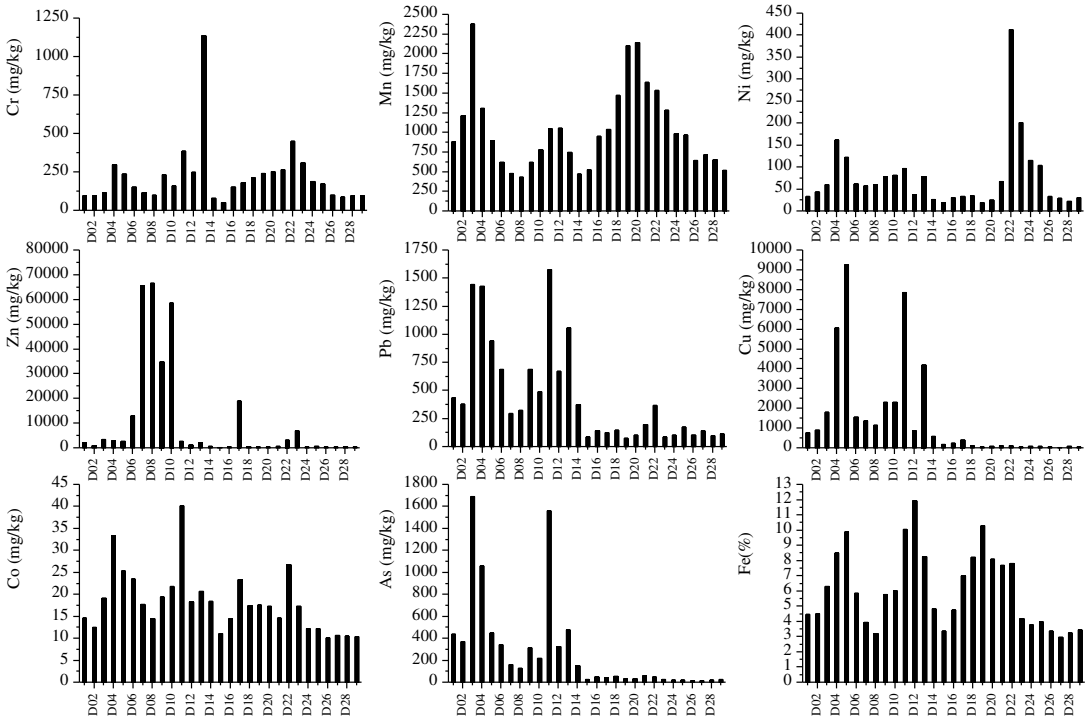

FIGURE 2
Spatial variations of heavy metals in atmospheric dust

Spatial distribution. The spatial distribution of the heavy metals in atmospheric dust was shown in Fig 2 (D01 - D14 was in Huangshi City, D15 - D25 was in E'zhou City and D26 – D29 was in Wuhan City). Generally, Pb, Cu and As concentrations in the sampling sites from D01 to D14 in Huangshi City were much higher than E'zhou City. For all sites, Pb concentration was much higher than background value of soils in Hubei province and background value of soils in China, which could be attributed to the traffic emissions induced by the large traffic flow along G316. Thus the sources of Pb, Cu, and As in these regions were mainly from industrial emissions. The distribution of Cr, Mn, Ni, Co, and Fe showed a similar trend that several peaks arisen in the section of G316, which were located in the sections of D03-D05, D11-D13, and D22-D23. On the contrary, the valley values were always found in the sites D08 and D15. For Zn, extremely high concentrations were distributed in the sections of D07-D10. The high concentrations found in the section of D01 to D14 in Huangshi City, which could be explained by the dense distribution of industrial factories around the region, such as Daye Iron Mine, Daye Nonferrous Smeltery Plant and Tonglvshan Copper Mine, which could discharge a lot of industrial dust. Furthermore, E'zhou Mills and some industrial plants including cement factory and steel plant located in the section of D22 to D23. These industrial activities possibly contributed to the contamination of atmospheric dust.

Geo-accumulation index. Geo-accumulation index of heavy metals in different sampling sites were calculated in figure 3, which indicates the I_{geo} of Cu, Zn and Pb in area of D01 to D14 were higher than other zone. It may be contributed by plenty of industrial activities around area. In other elements and sampling sites, varying degrees of heavy metals pollution in atmospheric dust were reflected. In summary, heavy metals contamination in atmospheric dust along the National Highway G316 was influenced by various industrial productions and manufactures.

Enrichment factor. In present study, Fe is chosen to use to reference element. The results of enrichment factor for elements was showed in Figure 4, The EF values of Cr, Mn, Ni and Co in most sampling sites were lower than 5. However, the elements of As, Cu, Zn and Pb present different trend with respect to Cr, Mn, Ni, and Co. In most sampling sites, the EF values of As, Cu, Zn and Pb were greater than 10. The EF value of Cr in sampling site of D13 and Ni in D22 and D23 were over 5, that because sampling site of D13 was close to Daye Iron Mine and Daye Nonferrous Smelter Plant and in the downwind of them, the site of D22 and D23 were in the range of influence of E'zhou Steel Plant and some industrial plants including

cement factory and machine processing factory. As, Cu, Zn and Pb were marked materials in industrial activities, such as metals smelting, ferrous smelting, metallurgical transportation and so on. Many industrial firms were near to G316, especially in area of D01 to D14.

Pearson's correlation analysis. Pearson's correlation coefficients of the nine elements in atmospheric dust were summarized in Table 4. All the elements were positively correlated with Fe, except for Zn. The significant relationships between Fe with other elements possibly indicate the common source from iron and steel smelting industry. As content was positively moderately correlated with Co (r=0.64, p<0.01) and Cu (r=0.65, p<0.01), particularly significantly for Pb (r=0.93, p<0.01), indicating that apart from a natural source, it may also be influenced by traffic and industrial activities. The relationship between Cu and Pb was positive and significant (r=0.81, p<0.01), which could probably be related the smelting of copper and lead ores. Nevertheless, Zn content generally presented negative relationships with other elements, except for Co and Cu, reflecting different sources of Zn.

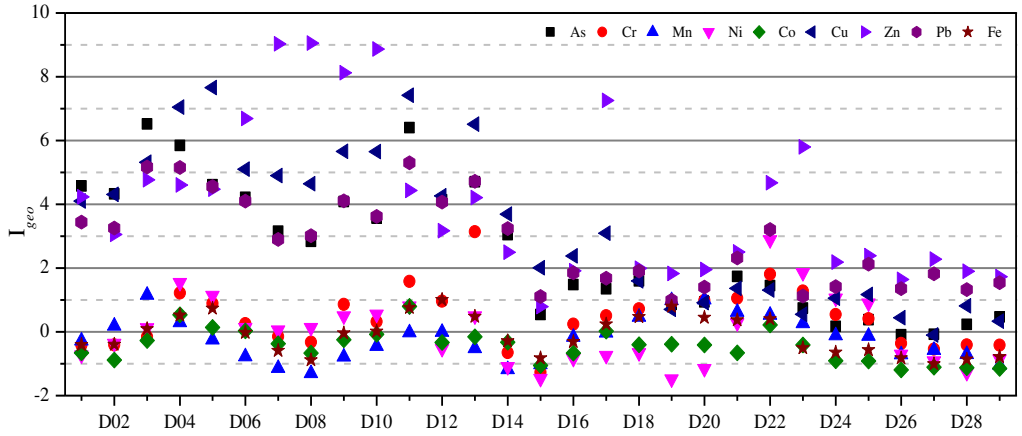

FIGURE 3
Geo-accumulation index of heavy metals in different sampling sites

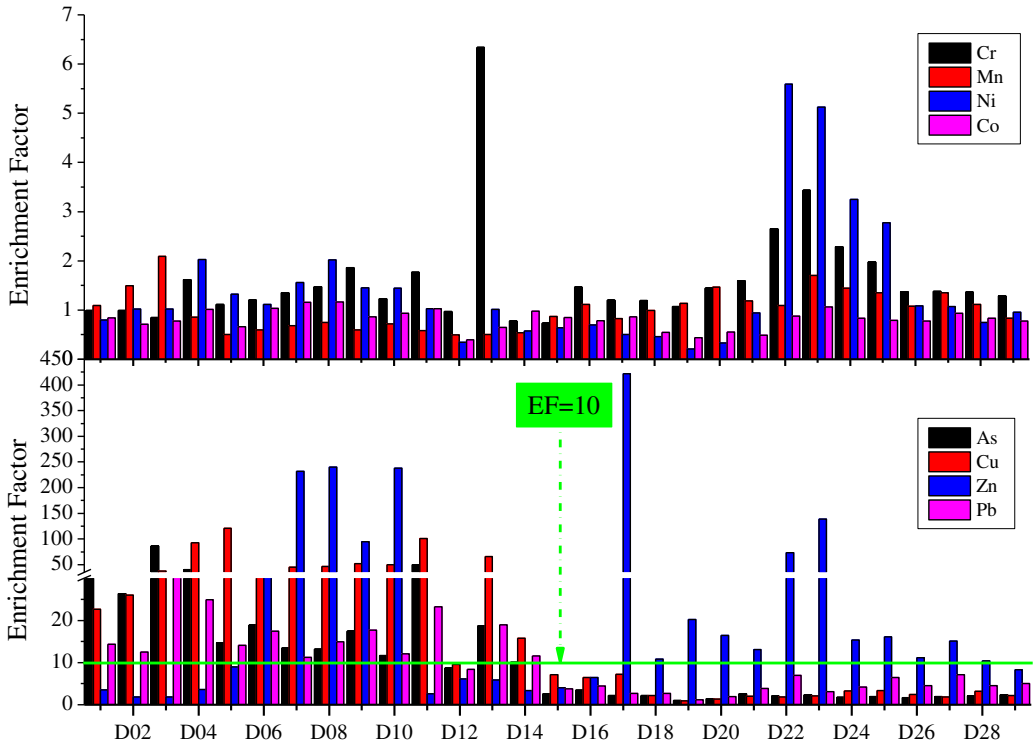

FIGURE 4
Enrichment factor of elements in different sampling sites

TABLE 4
Pearson's correlation matrix for the element concentrations

Element	As	Cr	Mn	Ni	Co	Cu	Zn	Pb	Fe
As	1.000								
Cr	0.183	1.000							
Mn	0.297	0.127	1.000						
Ni	0.077	0.352	0.184	1.000					
Co	0.642 **	0.395 *	0.190	0.439 *	1.000				
Cu	0.652 **	0.361	-0.063	0.181	0.747 **	1.000			
Zn	-0.068	-0.140	-0.360	-0.014	0.071	0.047	1.000		
Pb	0.926 **	0.388 *	0.147	0.192	0.753 **	0.806 **	-0.006	1.000	
Fe	0.374 *	0.470 *	0.514 **	0.175	0.661 **	0.499 **	-0.214	0.498 **	1.000

Note: ** P<0.01 (2-tailed); * P<0.05 (2-tailed).

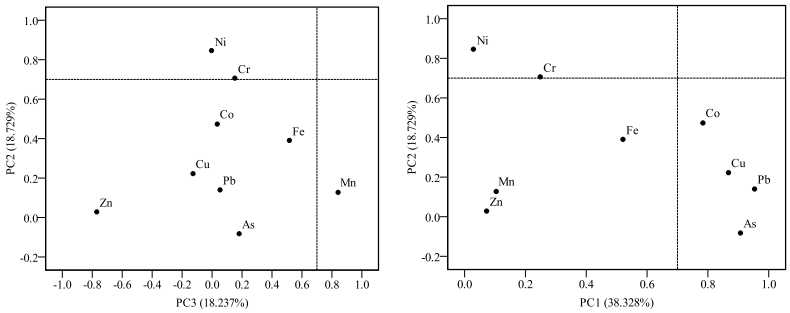

FIGURE 5
Rotated component matrix for data of atmospheric dust

Principal component analysis. PCA was applied to assist in the identification of sources of pollutants. Fig 5 displayed the factor loadings with a VARIMAX rotation. Three factors were obtained, accounting for 77.29% of the total variance. PC1 was dominated by As, Co, Cu, and Pb, accounting for 38.33% of the total variance. This principal component determines the major source of heavy metals: Pb mostly comes from traffic emissions, coal combustion, and industrial emissions such as iron smelting. While As mainly comes from coal combustion and iron smelting. Cu and Co were typical industrial contaminations. And that, As was positively well correlated with Co, Cu, and Pb, thus we could speculate that PC1 could be attributed to source of industrial smelting. PC2, dominated by Cr and Ni, was account for 18.73% of the total variance. Ni was mainly produced by combustion of fossil fuels (petroleum and coals) and emissions from metal smelting boiler [36]. Cr was regarded as the marker of coals combustion. Thus PC2 could be attributed to fossil fuel combustion, which also was affected by industrial manufacturing. PC3 was dominated by Mn, accounting for 18.24% of the total variance. The content of Mn was a little lower than those of Zn and Cu, but positively correlated with Fe. Therefore, PC3 could represent natural source, which originate mainly from soils.

Health risk assessment. The results of health risk assessment of individual trace element were showed in Table 5. For eight studied metals both child and adult, the main trend of non-cancer indexes were appeared as following order: ingestion>dermal contact>inhalation. This indicated that the ingestion was a prime pathway of heavy metals damaging human health, then the dermal contact and inhalation was lowest. The result of present study was consistent with previous researches [37,38]. For children, HQs of eight metals are almost all lower than safe threshold (=1) except for HQ_{ing} of As (=9.85) and Pb (=1.16), HI of metals for children is as order of As>Pb>Cr>Cu>Zn>Mn>Ni>Co. Summarized, elements of As and Pb potentially harmed to children health. For adults, HQs of metals were also almost all lower than safe threshold except HQ_{ing} of As (=1.06), HI of metals for adults decreased in the order of As>Cr>Pb>Zn>Mn>Ni>Cu. Of cancer risk of As, Cr, Cr, and Co both child and adult were all lower than threshold values (10^{-6}-10^{-4}). This means there no cancer risk for residents at the section of G316. As a whole, the pathway of ingestion was primary route harming to human health. The children bear attack with non-cancer risk of heavy metals more than adults, especially for As and Pb. However, there no cancer risk for both of children and adults at the section of G316.

TABLE 5
Health risk assessment of heavy metals in atmospheric dust

Element	Child					Adult				
	HQ_{ing}	HQ_{inh}	HQ_{dermal}	*HI*	*Risk*	HQ_{ing}	HQ_{inh}	HQ_{dermal}	*HI*	*Risk*
As	9.85	2.74E-04	5.17E-04	9.85	1.07E-07	1.06	1.55E-04	7.90E-04	1.06	2.41E-07
Cr	6.47E-01	1.90E-03	9.06E-02	7.40E-01	1.95E-07	6.94E-02	1.07E-03	1.38E-01	2.09E-01	4.41E-07
Mn	1.77E-01	1.59E-02	1.24E-02	2.05E-01		1.90E-02	8.97E-03	1.89E-02	4.69E-02	
Ni	3.47E-02	9.42E-07	3.60E-04	3.51E-02	1.40E-09	3.72E-03	5.31E-07	5.50E-04	4.27E-03	3.15E-09
Co	6.85E-03	6.71E-04	2.40E-05	7.55E-03	3.22E-09	7.34E-04	3.78E-04	3.66E-05	1.15E-03	7.25E-09
Cu	3.95E-01	1.10E-05	3.68E-03	3.98E-01		4.23E-02	6.19E-06	5.62E-03	4.79E-02	
Zn	3.87E-01	1.08E-05	5.43E-03	3.92E-01		4.14E-02	6.10E-06	8.30E-03	4.98E-02	
Pb	1.16	3.21E-05	2.16E-02	1.18		1.24E-01	1.81E-05	3.29E-02	1.57E-01	

CONCLUSION

The concentrations of heavy metals in atmospheric dust from the section of G316 all exceed background value of soils in Hubei province and background value of soils in China, especially for Zn, which concentration exceed 121.2 times for background value of soils in Hubei province and 136.6 times for background value of soils in China. Influenced by industrial production and manufacturing around the section of G316, heavy metals contamination were more serious at the region of D01 to D14. The results of geo-accumulation index indicated that the pollution of Cu, Zn and Pb in the area of D01-D14 were more serious than other zone. The results of health risk assessment show that As and Pb affect human health with non-cancer risk, and children was more than adults, meanwhile, there are no cancer risk for residents. The primary pathway of pollutants attached to atmospheric dust attacking human's body was through ingestion. Comprehensive analysis of Pearson's correlation, enrichment factor and principal component indicated that heavy metals from the typical industrial corridor were from industry sources, impacted by traffic sources, combustion sources and the natural emissions.

ACKNOWLEDGEMENTS

The research was supported by the Nature Science Foundation of Hubei Province, China (No. 2013CFC099), Outstanding Youth Science and Technology Innovation Team Projects of Hubei Polytechnic University (No. 13xtz07), the Talent Introduction Projects of Hubei Polytechnic University (No. 12xjz05R), and the Nature Science Foundation of China (No. 41303090)

REFERENCES

[1] Lu X, Wang L, Li LY, Lei K, Huang L, et al. (2010) Multivariate statistical analysis of heavy metals in street dust of Baoji, NW China. Journal of Hazardous Materials 173: 744-749.

[2] Gómez E, Sanfeliu T, Jordán M, Rius J, De la Fuente C (2004) Geochemical characteristics of particulate matter in the atmosphere surrounding a ceramic industrialized area. Environmental Geology 45: 536-543.

[3] Li X, Huang C (2007) Environment impact of heavy metals on urban soil in the vicinity of industrial area of Baoji city, PR China. Environmental Geology 52: 1631-1637.

[4] Banerjee AD (2003) Heavy metal levels and solid phase speciation in street dusts of Delhi, India. Environmental Pollution 123: 95-105.

[5] Begum BA, Kim E, Biswas SK, Hopke PK (2004) Investigation of sources of atmospheric aerosol at urban and semi-urban areas in Bangladesh. Atmospheric Environment 38: 3025-3038.

[6] Zhao N, Lu X, Chao S, Xu X (2015) Multivariate statistical analysis of heavy metals in less than 100 μm particles of street dust from Xining, China. Environmental earth sciences 73: 2319-2327.

[7] Han Y, Cao J, Posmentier ES, Fung K, Tian H, et al. (2008) Particulate-associated potentially harmful elements in urban road dusts in Xi'an, China. Applied Geochemistry 23: 835-845.

[8] Pekey H, Karakas D, Ayberk S, Tolun L, Bakoğlu M (2004) Ecological risk assessment using trace elements from surface sediments of Izmit Bay (Northeastern Marmara Sea) Turkey. Marine pollution bulletin 48: 946-953.

[9] Sezgin N, Ozcan HK, Demir G, Nemlioglu S, Bayat C (2004) Determination of heavy metal concentrations in street dusts in Istanbul E-5 highway. Environment international 29: 979-985.

[10] Wang X-S, Qin Y (2007) Some characteristics of the distribution of heavy metals in urban

topsoil of Xuzhou, China. Environmental geochemistry and health 29: 11-19.
[11] Mackay D, Arnot JA (2011) The application of fugacity and activity to simulating the environmental fate of organic contaminants. Journal of Chemical & Engineering Data 56: 1348-1355.
[12] Shin J-Y, Choi YY, Jeon H-S, Hwang J-H, Kim S-A, et al. (2010) Low-dose persistent organic pollutants increased telomere length in peripheral leukocytes of healthy Koreans. Mutagenesis: geq035.
[13] Lee D-H, Steffes MW, Sjodin A, Jones RS, Needham LL, et al. (2010) Low dose of some persistent organic pollutants predicts type 2 diabetes: a nested case-control study. Environmental health perspectives 118: 1235-1242.
[14] Wang G, Oldfield F, Xia D, Chen F, Liu X, et al. (2012) Magnetic properties and correlation with heavy metals in urban street dust: a case study from the city of Lanzhou, China. Atmospheric Environment 46: 289-298.
[15] Zhu Z, Li Z, Bi X, Han Z, Yu G (2013) Response of magnetic properties to heavy metal pollution in dust from three industrial cities in China. Journal of Hazardous Materials 246: 189-198.
[16] Lu X, Wu X, Wang Y, Chen H, Gao P, et al. (2014) Risk assessment of toxic metals in street dust from a medium-sized industrial city of China. Ecotoxicology and environmental safety 106: 154-163.
[17] Chabukdhara M, Nema AK (2012) Assessment of heavy metal contamination in Hindon River sediments: A chemometric and geochemical approach. Chemosphere 87: 945-953.
[18] Xiao R, Bai J, Wang Q, Gao H, Huang L, et al. (2011) Assessment of heavy metal contamination of wetland soils from a typical aquatic–terrestrial ecotone in Haihe River Basin, North China. CLEAN–Soil, Air, Water 39: 612-618.
[19] Chabukdhara M, Nema AK (2013) Heavy metals assessment in urban soil around industrial clusters in Ghaziabad, India: probabilistic health risk approach. Ecotoxicology and environmental safety 87: 57-64.
[20] Bilos C, Colombo J, Skorupka C, Presa MR (2001) Sources, distribution and variability of airborne trace metals in La Plata City area, Argentina. Environmental Pollution 111: 149-158.
[21] Choi JC, Lee M, Chun Y, Kim J, Oh S (2001) Chemical composition and source signature of spring aerosol in Seoul, Korea. Journal of geophysical research 106: 18,067-018,074.
[22] Zhang M, Wang H (2009) Concentrations and chemical forms of potentially toxic metals in road-deposited sediments from different zones of Hangzhou, China. Journal of Environmental Sciences 21: 625-631.
[23] Duzgoren-Aydin N, Wong C, Aydin A, Song Z, You M, et al. (2006) Heavy metal contamination and distribution in the urban environment of Guangzhou, SE China. Environmental geochemistry and health 28: 375-391.
[24] Healy M, Harrison P, Aslam M, Davis S, Wilson C (1982) Lead sulphide and traditional preparations: routes for ingestion, and solubility and reactions in gastric fluid. Journal of Clinical Pharmacy and Therapeutics 7: 169-173.
[25] Zheng N, Liu J, Wang Q, Liang Z (2010) Health risk assessment of heavy metal exposure to street dust in the zinc smelting district, Northeast of China. Science of the Total Environment 408: 726-733.
[26] Shi G, Chen Z, Bi C, Wang L, Teng J, et al. (2011) A comparative study of health risk of potentially toxic metals in urban and suburban road dust in the most populated city of China. Atmospheric Environment 45: 764-771.
[27] USEPA (2001) Risk assessment guidance for superfund: Volume III. Part A: Process for conducting probabilistic risk assessment. Environmental Protection Agency; Office of Emergency and Remedial Response Washington^ eDC DC.
[28] Ma J, Singhirunnusorn W (2012) Distribution and health risk assessment of heavy metals in surface dusts of maha sarakham municipality. Procedia-Social and Behavioral Sciences 50: 280-293.
[29] Ferreira-Baptista L, De Miguel E (2005) Geochemistry and risk assessment of street dust in Luanda, Angola: a tropical urban environment. Atmospheric Environment 39: 4501-4512.
[30] Barnes DG, Dourson M, Preuss P, Bellin J, Derosa C, et al. (1988) Reference dose (RfD): Description and use in health risk assessments. Regulatory toxicology and pharmacology 8: 471-486.
[31] USEPA M (1996) Soil screening guidance technical background document. Office of Solid Waste and Emergency Response, Washington, DC EPA/540 95.
[32] Chen B, Stein AF, Maldonado PG, de la Campa AMS, Gonzalez-Castanedo Y, et al. (2013) Size distribution and concentrations of heavy metals in atmospheric aerosols originating from industrial emissions as predicted by the HYSPLIT model. Atmospheric Environment

71: 234-244.
[33] Spurgeon DJ, Rowland P, Ainsworth G, Rothery P, Long S, et al. (2008) Geographical and pedological drivers of distribution and risks to soil fauna of seven metals (Cd, Cu, Cr, Ni, Pb, V and Zn) in British soils. Environmental Pollution 153: 273-283.
[34] Hall JR, Ashmore M, Fawehinmi J, Jordan C, Lofts S, et al. (2006) Developing a critical load approach for national risk assessments of atmospheric metal deposition. Environmental Toxicology and Chemistry 25: 883-890.
[35] Xia L, Gao Y (2011) Characterization of trace elements in PM 2.5 aerosols in the vicinity of highways in northeast New Jersey in the US east coast. Atmospheric Pollution Research 2.
[36] Thomaidis NS, Bakeas EB, Siskos PA (2003) Characterization of lead, cadmium, arsenic and nickel in PM 2.5 particles in the Athens atmosphere, Greece. Chemosphere 52: 959-966.
[37] Wang L, Lu X, Ren C, Li X, Chen C (2014) Contamination assessment and health risk of heavy metals in dust from Changqing industrial park of Baoji, NW China. Environmental earth sciences 71: 2095-2104.
[38] Lin Y, Fang F, Wang F, Xu M (2015) Pollution distribution and health risk assessment of heavy metals in indoor dust in Anhui rural, China. Environmental monitoring and assessment 187: 1-9.

Received: **07.01.2016**
Accepted: **15.06.2016**

CORRESPONDING AUTHOR

Jiaquan Zhang
School of Environment Science and Engineering, Hubei Polytechnic University, Hubei Key Laboratory of Mine Environmental Pollution Control and Remediation, Huangshi, 435003, China

Email: jiaquanzh@163.com

© by PSP Volume 25 – No.10/2016, pages 4287-4293 Fresenius Environmental Bulletin

OPTIMIZATION OF HYDROTHERMAL SYNTHESIS CONDITIONS OF N-DOPED TiO_2 USING RESPONSE SURFACE METHODOLOGY FOR PHOTOCATALYTIC DEGRADATION OF METHYLENE BLUE

Xiaodan Zhao[1,2], Donghui Chen[1,3], Yurong Zhang[2], Manhong Huang[2], Zhenbang Deng[2], Zhen Zhou[2,*]

[1] School of Environmental Science & Engineering, Donghua University, Shanghai, P. R. China;
[2] College of Environmental & Chemical Engineering, Shanghai University of Electric Power, Shanghai, P. R. China;
[3] Shanghai Institute of Technology, Shanghai, P. R. China.

ABSTRACT

The hydrothermal preparation process of N-doped TiO_2 was optimized to enhance photocatalytic activity under visible irradiation by the response surface methodology. The results indicated that calcination temperature was the main factor for N-doped TiO_2 preparation. The maximum methylene blue removal efficiency of 95.6% was achieved at pH 6.05, calcination time 6.87 h and calcination temperature 403 °C. Fourier transform infrared and X-ray photoelectron spectroscope spectra both confirmed that N-doped TiO_2 calcined at 400 °C had more surface-adsorbed water and hydroxyl group to enhance the photocatalytic activity. X-ray diffraction spectra indicated that anatase phase was the predominant structure in N-doped TiO_2.

KEYWORD:
N-doped TiO_2; hydrothermal synthesis; response surface methodology; photocatalytic degradation

INTRODUCTION

TiO_2 has been known as a prevailing semiconductor photocatalyst for decomposing organic contaminants in aqueous systems owing to its low cost, nontoxicity, strong oxidizing power [1, 2]. However, TiO_2 is activated only in the ultraviolet region ($\lambda \leq 387$ nm) that accounts for only about 4% of the solar energy, which restricted its application in a natural light condition [3]. Thus, there have been many researchers making great efforts to modify it to shift its photocatalytic activity to visible region [4-7]. Since Asahi et al [8] successfully demonstrated the visible-light photocatalytic reactivity of the TiO_2 semiconductor through nitrogen doping, N-TiO_2 materials had attracted considerable interest and been investigated widely. Up until now, various kinds of synthesis routes have been developed to prepare N-TiO_2 materials [9], but the synthesis conditions are still not definite for all kinds of preparation approaches, which leads to spending a lot of time and energy to set the synthesis parameters for achieving optimum results [10, 11].

The response surface methodology (RSM) can be deemed to be a collection of statistical and mathematical techniques in favor of optimizing objective functions by means of building models [12, 13]. RSM is faster for obtaining research results than the conventional and time consuming one-variable-at-a-time approach [14, 15]. In this study, an attempt had been made to apply the RSM for optimizing the synthesis parameters (i.e. pH, calcination temperature and calcination time) of the hydrothermal preparation method to obtain N-TiO_2 materials with the maximum photocatalytic activity. The desired response values predicted using the RSM were compared with experimental photocatalytic degradation efficiencies of methylene blue (MB).

EXPERIMENTAL

Preparation of photocatalysts. It is a simple method to synthesize N-TiO_2 nanoparticles through a hydrothermal precipitation process using titanium tetrachloride ($TiCl_4$) and ammonia [16], respectively. Ordinarily, certain amount of dilute aqueous solution of $TiCl_4$ (5.0 mol·L^{-1}) was carefully added into ice-deionized water with gentle stirring to avoid a drastic hydrolysis of $TiCl_4$ in water till to a white sol was obtained. The pH of the sol was adjusted by ammonia to 6~8 and then the white precipitate gradually formed. The precipitates were separated from the suspension through vacuum filtration and washed by distilled water repeatedly till pH was maintained at 7. The cleaned precipitates were dried at 105℃ and then the dried samples were calcined in an air atmosphere at a certain temperature (400, 500, 600℃) for 3~7 h to

TABLE 1
Design matrix and experimental and predicted values of response variable

Test	Factor level			MBRE(%)	
	X_1(pH)	X_2(Time, h)	X_3(Temperature, ℃)	Experimental	Predicted
1	7	7	600	78.69	77.10
2	7	7	400	86.75	86.37
3	7	3	400	80.51	82.09
4	7	3	600	79.56	79.94
5	6	5	400	95.16	93.71
6	6	5	600	88.68	88.43
7	8	5	400	89.42	89.67
8	8	5	600	82.08	83.53
9	8	3	500	87.35	85.52
10	6	3	500	85.71	85.58
11	8	7	500	81.69	81.82
12	6	7	500	88.87	90.70
13	7	5	500	83.22	80.94
14	7	5	500	80.62	80.94
15	7	5	500	78.63	80.94
16	7	5	500	81.33	80.94
17	7	5	500	80.88	80.94

N-TiO_2 powders were yielded. TiO_2 was prepared through the same procedures and conditions, except replacing ammonia with sodium hydroxide solution (NaOH) to adjust pH of the sols from the hydrolysis of $TiCl_4$.

Box-Behnken experimental design. The synthesis conditions of N-TiO_2 were optimized through the Box-Behnken design that was applied to evaluate relationships among effective parameters and effects of independent variables on the photocatalytic degradation of MB. According to the results in the preliminary experiments, the three independent variables were selected as pH (X_1: 6.0-8.0), calcination time (X_2: 3.0-7.0 h) and calcination temperature (X_3: 400-600ºC), with which 3-level Box-Behnken experimental design reduced the amount of require experiments to 17. The experimental levels of each variable were lower limit, median and upper limit of the selected range, which were designated as -1, 0, and +1, respectively [17], as given in Table 1. MB removal efficiency (MBRE) was adopted as Y, and a second-order model was applied to indicate the interaction between the dependent and independent variables. The Design Expert software 8.0 was introduced for regression analysis and model development of experimental results.

Photocatalytic degradation experiments. The photocatalytic activity of all the catalyst samples was evaluated by degrading MB solution under visible irradiation. Undoped or N-doped TiO_2 powders (dosage of 0.2 $g \cdot L^{-1}$) were dipped into MB solution (20 $mg \cdot L^{-1}$) respectively, which was put into a photochemical glass reactor positioned under 150 W xenon lamp with a cutoff filter of 400 nm in order to filter the ultraviolet light. Before the lamp was switched on to start the degradation process, the suspension had to be stirred magnetically for 30 min in the darkness to establish adsorption and desorption equilibrium between photocatalysts and MB. No oxidants or no aerated conditions were used for the photocatalytic degradation experiments. During the light irradiation, the suspension was kept being stirred by magnetic rotor as well and preserved in a constant temperature of 25℃ through a cooling-water system around the outside wall of the reactor. At a 20 min interval, aliquots of the solution were sequentially extracted by a set of disposable syringes, filtered through 0.15μm cellulose acetate membrane filters for analysis with a UV-Visible spectrophotometer. The concentration of MB was obtained according to the standard curve of concentration and absorbance. MBRE was calculated by Eq. (1):

$$\mathrm{MBRE} = \left(C_0 - C_t\right)/C_0 \times 100\% \qquad (1)$$

Where, C_0 and C_t are concentrations of MB at illumination time 0 and t, respectively.

Characterization of materials. Phase identification and crystallite sizes of these powder samples were evaluated by X-ray diffraction (XRD) on a Philips X-ray diffractometer (X'PERT PRO, Panalytical, Netherlands). The monochromatic radiation used was Cu Kα radiation (λ=0.1541 nm) in the 20-80° (2θ) range operating at 40 kV and 50 mA. The surface chemical states of TiO_2 and N-TiO_2 composites were analyzed using X-ray photoelectron spectroscope (XPS) (ESCALAB 250Xi) equipped with Al-Kα radiation (1486.71 eV) with spot dimensions of 200×750 μm and a pass

TABLE 2
The statistical results of ANOVA

Source	Sum of squares	d*f*	Mean square	*F* value	*p* value
Model	320.81	9	35.65	9.17	<0.01
X_1	39.96	1	39.96	10.28	0.01
X_2	1.03	1	1.03	0.26	0.62
X_3	65.15	1	65.15	16.76	<0.01
$X_1 \times X_2$	19.45	1	19.45	5.00	0.06
$X_1 \times X_3$	0.18	1	0.18	0.05	0.83
$X_2 \times X_3$	12.64	1	12.64	3.25	0.11
X_1^2	162.55	1	162.55	41.82	<0.01
X_2^2	6.52	1	6.52	1.68	0.24
X_3^2	11.97	1	11.97	3.08	0.12
Residual	27.21	7	3.89		
Lack of fit	16.41	3	5.47	2.03	0.25
Pure error	10.79	4	2.70		
Cor total	348.02	16			

energy of 25 eV. Survey scans were collected in the energy range of 0-1200 eV. Transmission electron microscopy (TEM) experiments were performed using an electron microscope (JEOL JEM-2100) with the accelerating voltage of 200 kV. Fourier transform infrared (FT-IR) spectroscopy was carried out on NICOLET 5700 FT-IR spectrophotometer with ATR unit.

RESULTS AND DISCUSSION

Response surface analysis. Regression model development. Table 1 reported the design matrix and the experimental and predicted values of response variable obtained from the Box-Behnken experimental results. The MBRE was ranged from 78.6% to 95.2% and the average value of tests from 13 to 17 was 80.94%, which was consistent with the predicted one. The RSM analysis was in favor of the understanding significant factors and interactive effects of independent variables on MBRE using N-TiO_2. The regression analysis results suggested that, among all of the polynomial models for the modeling of MBRE, the quadratic model (Eq. (2)) was the most appropriate.

$$Y=80.94-2.24X_1+0.36X_2-2.85X_3-2.20X_1X_2-0.22X_1X_3-1.78X_2X_3+6.21X_1^2-1.24X_2^2+1.69X_3^2 \quad (2)$$

For Eq. (2), R^2 and adjusted-R^2 values were 0.9218 and 0.8213, respectively, which indicated a high correlation between predicted values and experimental data.

ANOVA analysis. An analysis of variance (ANOVA) was further employed to evaluate the significance, inspect the correctness and fitness of the established quadratic model, and determine the interactive relationships between independent variables and dependent variable. The statistical results of ANOVA were shown in Table 2. The sum of squares was 65.15 for X_3, 39.96 for X_1 and 1.03 for X_2, respectively, which implied that calcination temperature had greater influence on MBRE than calcination time and pH. The probability values (*p*-value) were calculated to access the significance. It is well known that the variable with *p*-value less than 0.05 is significant[17]. From Table 2, X_1, X_3, X_1^2 were significant model terms at *p*-value <0.01 level. The *F*-value and *p*-value of the regression model were 9.17 and less than 0.01 respectively, demonstrating that the proposed model was significant as well. The "Adeq Precision" of 10.98 suggested an adequate signal as it is desirable that the signal-to-noise ratio measured from the "Adeq Precision" is greater than 4. Meanwhile, the *F*-value and *p*-value of "Lack of fit" were 2.03 and 0.25, respectively, which presumed the term was insignificant and the model adequately described the relationship between independent variables and MBRE.

Response surface plots were formed based on the model in order to investigate the nonlinear interactions among the independent variables on MBRE and the optimal levels. Fig. 1 revealed contour plots of the anticipated quadratic model for the MBRE.

Fig. 1a showed the interaction effect of calcination time and pH on MBRE. MBRE decreased firstly and then increased with the increasing pH, as the minimum value appeared at pH=7.1. With the enhancement of calcination time, MBRE increased firstly and then decreased. The depth of color on surface plot indicated that the influence caused by pH on the degradation efficiency of MB was greater than induced by calcination time, which was in accordance with the statistical results in Table 2. F-value in Table 2 showed that the interaction between pH and calcination time was the most significant.

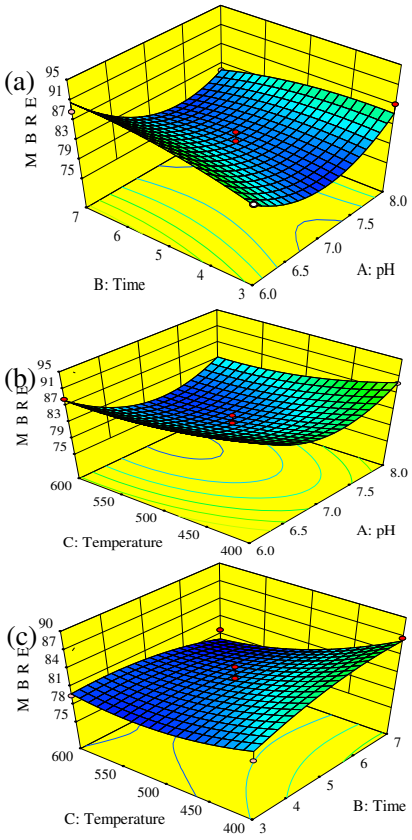

FIGURE 1

3D response surface plots for combined effects on the MBRE. (a) pH and calcination time, calcination temperature =500℃; (b) pH and calcination temperature, calcination time=5h; (c) calcination time and temperature, pH=7.0.

The interaction effect of calcination temperature and pH on MBRE was shown in Fig. 1b. Calcination temperature had the most prominent influence on the characteristics of N-TiO_2 during the synthesis process, which correlated with the photocatalytic degradation of MB. MBRE decreased evidently with the increase of calcination temperature. Calcination temperature and pH were the two significant factors on MBRE (p<0.01), but the interaction effect of them was insignificant.

With the increase of calcination time, the effect of calcination temperature was more obvious (Fig. 1c), and MBRE decreased greatly with the increasing temperature. The interaction effect of calcination time and calcination temperature on the MBRE was insignificant (p>0.05). From Fig. 1c, it was observed that the influence of calcination temperature on MBRE was more significant than calcination time.

Adequacy of the developed model. The predicted result for MBRE was achieved to be 95.6% with the optimum parameters of 6.05 for the reaction pH, 6.87 h for calcination time and 403℃ for calcination temperature. These optimum conditions for N-TiO_2 preparation were inspected experimentally to validate the model adequacy, the result of which was 95.1% of MBRE by photocatalytic degradation test. The low relative deviation (0.05%) between the experimental and predicted results confirmed the correctness of the developed model and the optimization of synthesis conditions.

Photodegradation kinetics. Fig. 2 showed the photodegradation kinetics of MB aqueous solution respectively by TiO_2 and N-TiO_2 samples under visible irradiation, which were prepared with the same reaction pH of 6.05 and calcination time of 6.87 h. TiO_2 was calcined at 400 ℃ (T400), and the N-TiO_2 samples were calcined at different temperatures, with 400, 500 and 600 ℃ designated as NT400, NT500 and NT600, respectively. It was illustrated that the photocatalytic degradation of MB followed a pseudo-first-order kinetics equation. The rate constants for NT400, NT500, NT600 and T400 were calculated as 0.638, 0.504, 0.408 and 0.160 h^{-1}, respectively, which made it clear that degradation rate of NT400 was highest due to preferable visible light photocatalytic activity. Besides, N-TiO_2 unsurprisingly demonstrated low degradation ability with 59.93% of MBRE, but the N-TiO_2 samples displayed better photocatalytic activity under visible light irradiation with 83.8-95.1% of MBRE.

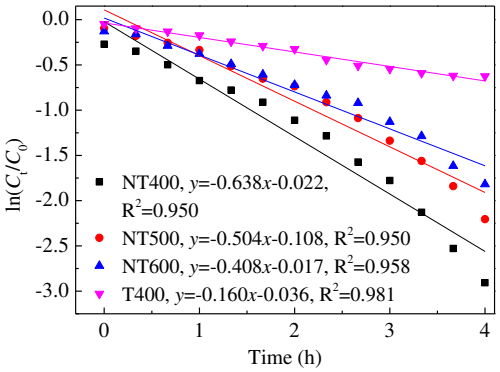

FIGURE 2

The relation between ln(C/C_0) and time (h) of MB photo-degradation reaction under visible irradiation by NT400, NT500, NT600 and T400.

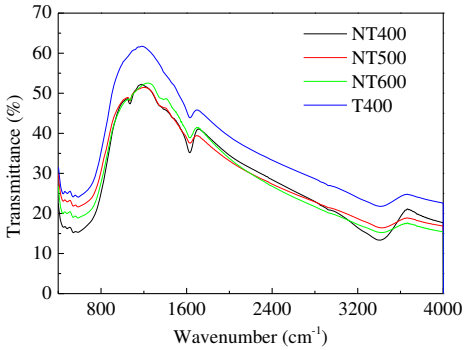

FIGURE 3

FT-IR spectra of NT400, NT500, NT600 and T400.

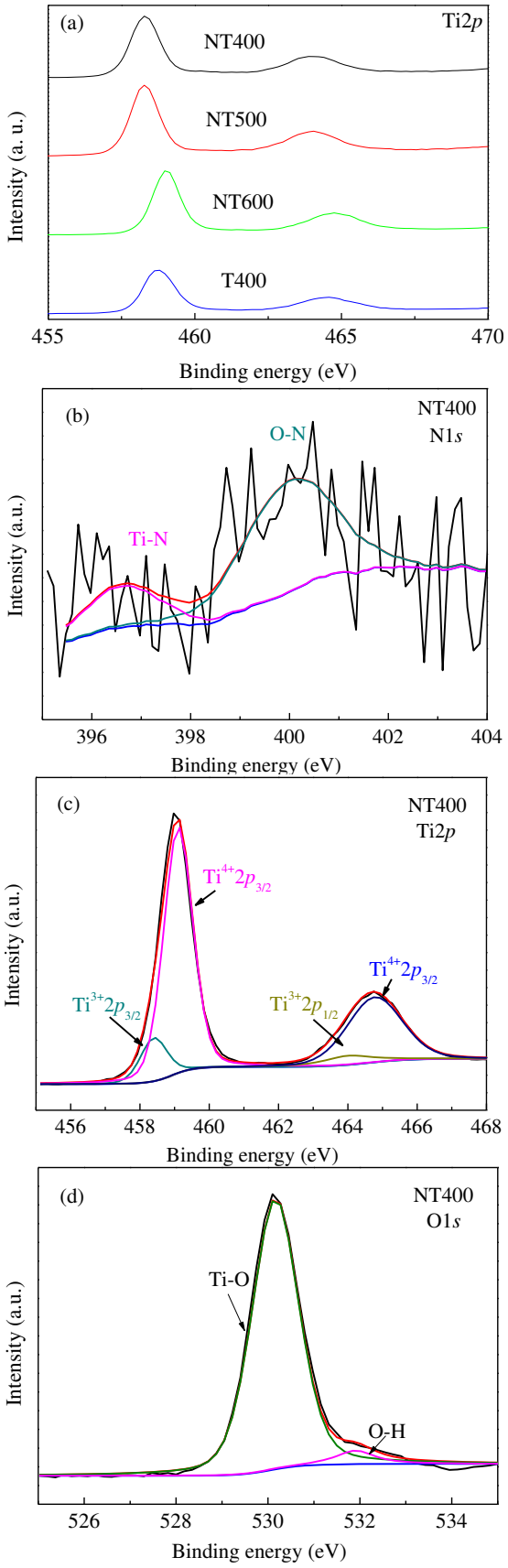

FIGURE 4
XPS spectra of pure TiO_2 and N-TiO_2.

Characterization analysis of N-TiO_2. FT-IR spectra of N-TiO_2 nanoparticles calcined at different temperatures and undoped TiO_2 were presented in Fig. 3.All these samples exhibited homologous vibrations in the IR region. The sharp peak at about 1610 cm^{-1} and the broad peak at around 3400 cm^{-1} were ascribed to the bending and stretching vibrations of hydroxyl group on the surface of the samples respectively, which may have a crucial role in the photocatalytic reaction [18, 19]. Intensities of the two absorption bands decreased with increasing calcination temperatures, indicating that more hydroxyl groups on the surface of NT400 were ready to form hydroxyl radicals in favor of the enhancement of photocatalytic activity. The fluctuant and broad band developed at around 520 cm^{-1} were due to the stretching vibrations of Ti–O bond [20] The peaks at 1370 and 1070 cm^{-1} were contributed to N–O and N–Ti stretching vibrations, respectively. The two peaks present in NT400, NT500 and NT600 indicated that some lattice oxygen was substituted by nitrogen and formed Ti–O–N or O–Ti–N bonds [18].

The XPS survey spectra were analyzed to investigate the chemical states of samples (Fig. 4). It was observed from the Ti2*p* spectra in Fig. 4(a) that all the samples demonstrated two principal peaks identified to Ti2$p_{1/2}$ and Ti2$p_{3/2}$ transitions, with binding energies at 464 and 458 eV, respectively [21]. It was noticed that the Ti signal of NT400 and NT500 were shifted to lower energies compared with the position of pure TiO_2, possibly due to the presence of Ti-N bonds and the decrease of electron cloud density around Ti^{4+} in the N-TiO_2 [22]. Nevertheless, it was observed that there was not evident Ti signal shifts for NT600 annealed at a higher temperature. As seen from Fig. 4b, two peaks were fitted in the N1s spectra of NT400. The one at 396 eV was attributed to substitutional N in Ti-N bonds that were detected through FT-IR as well, which can narrow the band gap of semiconductors to trigger the visible light response. Another one at 400 eV represented the interstitial N of Ti-O-N, samples with which performed better photocatalytic activity under visible irradiation than the substitutional N because it was more facile to excite electrons from interstitial N energy states to the conduction band [21]. Fig. 4c and 4d displayed the fitting of the Ti2*p* peaks and O1s peaks for NT400 XPS spectra, respectively. There were four peaks in the Ti2*p* spectrum, which evinced the presence of two states, Ti^{4+} and Ti^{3+}. It was reported that doping nitrogen resulted in the deficiency of oxygen, leading to reducing Ti^{4+} to Ti^{3+} [19, 23-25]. Two peaks presented in the unsymmetrical O1s XPS spectra at the binding energy of 530 and 532 eV, which were assigned as crystal lattice oxygen and chemisorbed oxygen, respectively. The crystal lattice oxygen was mainly due to the supply of Ti-O, while the

chemisorbed oxygen was believed to be provided by the hydroxyl groups from the surface chemisorbed water. The chemisorbed oxygen had the advantage in trapping electrons to prevent the recombination of electron/hole pair and forming hydroxyl radicals or atomic oxygen radical anions to react with contaminants during the photocatalysis process [26].

CONCLUSIONS

Hydrothermal synthesis conditions for N-TiO_2 were successfully optimized by RSM for photocatalytic degradation of MB under visible irradiation. Statistical analyses indicated that the influence of calcination temperature on photocatalytic activity of N-TiO_2 was more significant than calcination time and reaction pH. The response surface graphs showed that the optimum parameters of reaction pH, calcination time and calcination temperature were 6.05, 6.87 h and 403 ^oC, respectively. The photocatalytic degradation of MB using N-TiO_2 was accordance with a pseudo-first-order kinetics. FT-IR spectra indicated that N-TiO_2 calcined at 400 ^oC had more surface-adsorbed water and hydroxyl group to enhance the photocatalytic activity. XPS analysis showed that substitutional N and interstitial N beneficial to visible light photocatalytic activity were present in NT400 sample. XRD spectra and TEM results indicated that the anatase phase was the predominant structure in N-TiO_2, but the crystallite size increased with the increase of calcination temperature.

ACKNOWLEDGEMENTS

The authors acknowledge the Center of Forecasting and Analysis at Wuhan University and Postgraduate Course Construction (YKJ-2016004) of Shanghai University of Electric Power for supporting this research.

REFERENCES

[1] Fujishima, A., Rao, T.N. and Tryk, D.A. (2000) Titanium dioxide photocatalysis, J. Photochem. Photobiol., C 1: 1-21.

[2] Pelaez, M., Nolan, N.T., Pillai, S.C., Seery, M.K., Falaras, P., Kontos, A.G., Dunlop, P.S.M., Hamilton, J.W.J., Byrne, J.A., O'Shea, K., Entezari, M.H. and Dionysiou, D.D. (2012) A review on the visible light active titanium dioxide photocatalysts for environmental applications, Appl. Catal. B-Environ. 125: 331-349.

[3] Ren, W., Ai, Z., Jia, F., Zhang, L., Fan, X. and Zou, Z. (2007) Low temperature preparation and visible light photocatalytic activity of mesoporous carbon-doped crystalline TiO_2, Appl. Catal. B-Environ. 69: 138-144.

[4] Fujishima, A., Zhang, X. and Tryk, D.A. (2008) TiO_2 photocatalysis and related surface phenomena, Surf. Sci. Rep. 63: 515-582.

[5] Lee, H.U., Lee, Y.-C., Lee, S.C., Park, S.Y., Son, B., Lee, J.W., Lim, C.-H., Choi, C.-J., Choi, M.-H., Lee, S.Y., Oh, Y.-K. and Lee, J. (2014) Visible-light-responsive bicrystalline (anatase/brookite) nanoporous nitrogen-doped TiO_2 photocatalysts by plasma treatment, Chem. Eng. J. 254: 268-275.

[6] Devi, L.G. and Kavitha, R. (2013) A review on non metal ion doped titania for the photocatalytic degradation of organic pollutants under UV/solar light: Role of photogenerated charge carrier dynamics in enhancing the activity, Appl. Catal. B-Environ. 140-141: 559-587.

[7] Shahid, M., McDonagh, A., Kim, J.H. and Shon, H.K. (2014) Magnetised titanium dioxide (TiO_2) for water purification: preparation, characterisation and application, Desalin. Water Treat. 54: 979-1002.

[8] Asahi, R., Morikawa, T., Ohwaki, T., Aoki, K. and Taga, Y. (2001) Visible-light photocatalysis in nitrogen-doped titanium oxides, Science 293 269-271.

[9] Chakrabortty, D. and Gupta, S.S. (2014) Decolourisation of Metanil Yellow by visible-light photocatalysis with N-doped TiO_2 nanoparticles: influence of system parameters and kinetic study, Desalin. Water Treat. 52: 5528-5540.

[10] Collazzo, G.C., Foletto, E.L., Jahn, S.L. and Villetti, M.A. (2012) Degradation of Direct Black 38 dye under visible light and sunlight irradiation by N-doped anatase TIO_2 as photocatalyst, J. Environ. Manage. 98: 107-111.

[11] Akpan, U.G. and Hameed, B.H. (2012) Photocatalytic degradation of wastewater containing acid red 1 dye by titanium dioxide: Effect of calcination temperature, Desalin. Water Treat. 43: 84-90.

[12] Box, G.E.P. and Wilson, K.B. (1951) On the experimental attainment of optimum conditions, J. R. Stat. Soc. 13: 1-35.

[13] Jiang, W., Joens, J.A., Dionysiou, D.D. and O'Shea, K.E. (2013) Optimization of photocatalytic performance of TiO_2 coated glass microspheres using response surface methodology and the application for degradation of dimethyl phthalate, J. Photochem. Photobiol., A 262: 7-13.

[14] Mohammadi, M.M., Vossoughi, M., Feilizadeh, M., Rashtchian, D., Moradi, S. and Alemzadeh, I. (2014) Effects of electrophoretic deposition

parameters on the photocatalytic activity of TiO_2 films: Optimization by response surface methodology, Colloids Surf., A 452: 1-8.
[15] Shoaebargh, S. and Karimi, A. (2014) RSM modeling and optimization of glucose oxidase immobilization on TiO_2/polyurethane: Feasibility study of AO7 decolorization, J. Environ. Chem. Eng. 2: 1741-1747.
[16] Cheng, X., Yu, X. and Xing, Z. (2012) Characterization and mechanism analysis of N doped TiO_2 with visible light response and its enhanced visible activity, Appl. Surf. Sci. 258: 3244-3248.
[17] Zhou, Z., Qiao, W., Lin, Y., Shen, X., Hu, D., Zhang, J., Jiang, L.-M. and Wang, L. (2014) Phosphonate removal from discharged circulating cooling water using iron–carbon micro-electrolysis, Water Sci. Technol. 70: 524-532.
[18] Brahimi, R., Bessekhouad, Y. and Trari, M. (2012) Physical properties of NxTiO2 prepared by sol–gel route, Physica B 407: 3897-3904.
[19] Livraghi, S., Pelaez, M., Biedrzycki, J., Corazzari, I., Giamello, E. and Dionysiou, D.D. (2013) Influence of the chemical synthesis on the physicochemical properties of N-TiO_2 nanoparticles, Catal. Today 209: 54-59.
[20] Hu, S., Li, F. and Fan, Z. (2011) The influence of preparation method, nitrogen source, and post-treatment on the photocatalytic activity and stability of N-doped TiO_2 nanopowder, J. Hazard. Mater. 196: 248-254.
[21] Dawson, M., Soares, G.B. and Ribeiro, C. (2014) Influence of calcination parameters on the synthesis of N-doped TiO_2 by the polymeric precursors method, J. Solid State Chem. 215: 211-218.
[22] Lin, Y.-H., Chiu, T.-C., Hsueh, H.-T. and Chu, H. (2011) N-doped TiO_2 photo-catalyst for the degradation of 1,2-dichloroethane under fluorescent light, Appl. Surf. Sci. 258: 1581-1586.
[23] Jaiswal, R., Patel, N., Kothari, D.C. and Miotello, A. (2012) Improved visible light photocatalytic activity of TiO_2 co-doped with Vanadium and Nitrogen, Appl. Catal. B-Environ. 126: 47-54.
[24] Monteiro, R.A.R., Miranda, S.M., Vilar, V.J.P., Pastrana-Martínez, L.M., Tavares, P.B., Boaventura, R.A.R., Faria, J.L., Pinto, E. and Silva, A.M.T. (2015) N-modified TiO_2 photocatalytic activity towards diphenhydramine degradation and *Escherichia coli* inactivation in aqueous solutions, Appl. Catal. B-Environ. 162: 66-74.
[25] Kuo, Y.-L., Su, T.-L., Kung, F.-C. and Wu, T.-J. (2011) A study of parameter setting and characterization of visible-light driven nitrogen-modified commercial TiO_2 photocatalysts, J. Hazard. Mater. 190: 938-944.
[26] Asiri, A.M., Al-Amoudi, M.S., Bazaid, S.A., Adam, A.A., Alamry, K.A. and Anandan, S. (2014) Enhanced visible light photodegradation of water pollutants over N-, S-doped titanium dioxide and n-titanium dioxide in the presence of inorganic anions, J. Saudi Chem. Soc. 18: 155-163.

Received: **15.01.2016**
Accepted: **08.08.2016**

CORRESPONDING AUTHOR

Zhen Zhou
College of Environmental & Chemical Engineering, Shanghai University of Electric Power 2588#, Changyang Road, Yangpu District, Shanghai 200090, P. R. CHINA

e-mail: zhouzhen@shiep.edu.cn

© by PSP Volume 25 – No. 10/2016, pages 4294-4298 Fresenius Environmental Bulletin

DETERMINING THE IMPACT OF EXCESSIVE BORON ON SOME GROWTH CHARACTERS AND SOME NUTRIENTS AT THE EARLY GROWTH STAGE OF SUNFLOWER (*Helianthus annuus* L.)

Sibel Day*

Department of Field Crops, Faculty of Agriculture, University of Ankara, 06110, Ankara, Turkey.

ABSTRACT

The effect of excess boron (B) on growth and nutrient content in sunflower (*Helianthus annuus* L.) were investigated due to the evaulate the capacity of cv. Sirena for phytomining. Study was carried out in a green house conditions to assess the impact of increasing levels of boron (B) on cv. Sirena. The soil was treated with 0, 4, 8, 16, 32, 64 and 128 mg kg^{-1} B as H_3BO_3. Results indicated that plant growth was depressed with the increasing level of B. The highest B uptake was obtained from 64 mg kg^{-1} B level with 695.2 mg kg^{-1}. Increasing B also enhanced calcium (Ca) and phosphorus (P) contents in sunflower shoots but led to decrease in sodium (Na) and potassium (K) uptake. Results also revealed that the sunflower cv. Sirena did not germinate at the highest boron level (128 mg kg^{-1}). The results of this study indicate that cv. Sirena could be cultivated in soils containing B up to 8 mg kg^{-1}.

KEYWORDS: Boric acid, toxicity, sunflower, phytoremediation

INTRODUCTION

Sunflower one of the most important oil crop in Turkey is commonly cultivated in Central Anatolia where has low precipitation during the summer. B toxicity is a severe environmental constraint on crop cultivation in some areas of Turkey and in Central Anatolia [11]. Apart from that it has an importance in developing technologies and more than 50 % of B reserves of the world located in Turkey [19]. Especially in the areas around the B reserves, mining and industrialization facilities threatens agricultural soils. Toxic levels of B reduce crop yields and limit crop production [23].

B is essential for plants and B toxicity and deficiency level for plants is relatively close to each other than the other micro elements [4]. On the other hand B could regulate or inhibite the other plant nutrients depending on the supply [3]. Also it was concluded that excessive amount of B may affect the uptake and utilization of other elements [7]. It was earlier stated that application of increased level of B has different impact on the element concentration of plant species and antagonistic or synergetic interaction with other elements depend on plant species and varieties [24]. B uptake system of sunflower plants is influenced by B supply. At high B supply the uptake of B could be explained as passive diffusion, Whereas at low B supply passive and active uptake system works together to accumulate B in the symplasm [21].

Plants so called hyperaccumulators uptake high levels of an element from the soil [15] and these kind of plants mostly used for phytoremediation. Hyperaccumulation studies of B in Turkey mostly includes species that are growing around B rich areas [19].

Aim of this study was to evaulate whether it is possible to cultivate cv. sirena for phytoremediation or not by screening during the early growth stage.

MATERIALS AND METHODS

Experimental design and management. The experiment was conducted with oil type sunflower cultivar 'Sirena' in greenhouse, in Ankara, Turkey. The soil used in the experiment was clay loam (27 % sand, 43 % clay, 30 % silt), non-saline (Ec, 0.11 dS m^{-1}), alkaline (pH, 7.6), low in organic matter (1.18 %), moderately calcareous ($CaCO_3$, 7.35 %). The soil contained 0.15 % total N, 13 mg kg^{-1} available P, 180 mg kg^{-1} K and 0.18 mg kg^{-1} B. Analysis of the soil characteristics were determined according to the methods by Page et al. [20].

The experiment was conducted in a completely randomized factorial design with 7 B levels (0, 4, 8, 16, 32, 64 and 128 mg kg^{-1}) and each treatment was replicated four times. Pots lined with polyethylene bags were filled with 2 kg sifted soil. The source of B applied to soil in pots was H_3BO_3. It was dissolved in water and levels of B applied as a solution. Basal doses of N (nitrogen), P (phosphorus) and K (potassium) were applied as ammonium nitrate (NH_4NO_3), potassium dihydrogen phosphate (KH_2PO_4), and potassium

sulfate (K_2SO_4). The soil was left to air-dry after application then thoroughly mixed to ensure uniform distribution of B and other nutrients. Four seeds were sown per pot. After germination, these were thinned to one plant in each pot. Plants were grown for 60 days in nondrained plastic pots containing 2 kg of airdried soil and then harvested. The water content of the soil was maintained at 70 % of field capacity irrigating with B free water during the experiment.

Plant height was measured before harvest. Plants were harvested 8 weeks after sowing. Fresh weights of the shoots were recorded soon after harvest to avoid loss in weight due to evapotranspiration. Thereafter, they were dried in oven at 70 ºC for three days to take dry weight. All shoots were seperately ground and kept for boron (B), sodium (Na), potassium (K), calcium (Ca), phosphorus (P) determination. To measure mineral nutrients, samples were ashed in a muffle furnace at 500 °C for 6 h and the ash dissolved in 0.1 M hydrocloric acid. Eventually the nutrient ions were determined by Inductively Coupled Plasma-Optical Emission Spectrometry (ICP-OES, Perkin Elmer Optima 2100 DV, Waltham, MA).

Statistical analysis. The experimental data were analysed using statistical analysis by MSTAT-C and Duncan's Multiple Range Test was used for post-hoc test.

RESULTS AND DISCUSSIONS

No results were obtained at 128 mg kg^{-1} B level for any parameter, therefore, these values are not given for respective parameters in each table.

Visual observations. Emergence was visible 10 days after sowing in all levels except for 128 mg kg^{-1} B. Emergence in 128 mg kg^{-1} B level was observed 20 days after sowing. The seedlings in 128 mg kg^{-1} B level did not survive any longer and died at the V-2 growth stage.

The symptoms first appeared at the margins of mature leaves as brownish necrotic spots at an early growth stage and became more visible with growing.

Plant height. Plant height response to B levels varied. Plant height increased with 4 mg kg^{-1} B level and after that decrease was observed.
The maximum and minimum plant height values were obtained from 4 mg kg^{-1} and 64 mg kg^{-1} B levels respectively (Table 1). Decreased growth in plants evaluated by Oztürk et al. [19] with excess B can cause inhibiton of cell access to mitosis and cell multiplication. Plant height reduction due to high B levels was also reported in cotton [1].

Fresh weight. B levels had significant impact on fresh weight ($P < 0.01$). Shoot fresh weight increased with 4 mg kg^{-1} B level. However reduction in fresh weight occurred very significant with further increase in B. The minimum fresh weight was recorded in 64 mg kg^{-1} B level (Table 1). As in most ionic stresses, excess B level generates ROS that causes membrane damage and eventually leads to cell death [14]. Reduction in fresh weight of shoots could be attributed to decreased cell multiplication and death of cells due to the ROS caused by excess B.

Dry weight. Response of dry weight varied with different levels of B. Dry weight of shoots increased with 4 mg kg^{-1} B level and it decreased with further levels. Especially at 64 mg kg^{-1} B level the minimum dry weight was obtained (Table 1). Decreased fresh weight with increased B levels also led to decrease in dry weight of sunflower shoots. Reduction due to toxic B levels was also reported in tomato and cucumber [2].

Uptake of some nutrients. B uptake of shoots significantly increased with high B levels ($P < 0.01$). Maximum B uptake was observed in the 64 mg kg^{-1} B level and the minimum B uptake was observed in the 0 mg kg^{-1} level (Table 2). The similar increases in B uptake were also observed in wheat [16] and tomato [6]. Boric acid is highly permeable to the lipid blayers and the movement is depend on the concentration [23]. Also when level of B in soil solution is at toxic level, B transportation throughout the plant in transpiration stream, leads to B accumulation in leaf margins and tips.

Na uptake of shoots decreased with B doses but differences among treatments were statistically non significant (Table 2). Negative correlation (r = -0.913*) between B and Na was also recorded (Table3). Excess B

TABLE 1
Effects of B application on some growth parameters of sunflower cultivar (Sirena)

Growth parameters	Boron concentrations (mg kg^{-1})					
	0	4	8	16	32	64
Plant height (cm)	58.00 abc	63.75 a	61.00 ab	49.75 bcd	47.75 cd	41.75 d
Shoot fresh weight (g)	25.90 ab	29.42 a	21.24 bc	15.83 cd	15.31 cd	11.62 d
Shoot dry weight (g)	3.39 b	3.75 a	2.89 c	2.24 d	2.04 d	1.7 e

All values in a row designated with different letters are significantly different using Duncan's Multiple Range Test ($P < 0.01$)

level in soil did not effect the Na uptake of sunflower shoots. The maximum Na uptake in shoots were obtained from 0 mg kg^{-1} B level and the minimum was obtained from 32 mg kg^{-1} B level. These reduction in Na uptake of shoots with increasing level of B showed similarity to the findings of Grieve et al. [13] in broccoli.

The soil used in the experiment is rich in available K content and we also added basal doses of K to all pots however there is gradually decrease in K uptake of shoots with increasing levels of B compared to 0 mg kg^{-1} application (Table 2). Significant correlation was also observed (r = -0.979) and in this case it is possible to say excess B causes inhibition of K uptake from the soil (Table 3). It is assumed that the reduction in K uptake might be due to the antagonism. Results on K uptake are in contrast with the findings of Alpaslan and Gunes [2].

Higher level of B concentration in soil led to significantly increase in Ca uptake of shoots ($P <$ 00.1). Particularly in 32 and 64 mg kg^{-1} B application the Ca uptake of shoots increased compared to other treatments (Table 2). The Ca uptake of shoots with the increasing level of B were scored between 6.93 and 10.02 g kg^{-1}. Minimum Ca uptake was observed in 0 mg kg^{-1} B level and maximum Ca uptake was observed in 32 mg kg^{-1} B level. Reduction in K uptake was observed and there is a competition between these two elements due to the physiological properties of these ions [10]. Ca correlations with B and K were significant. Positive correlation with B (r = 0.916*) and negative correlation with K (r = -0.918**) were recorded (Table 3). It is assumed that depressed K uptake due to the excess B (especially at 32 and 64 mg kg^{-1} B levels) in sunflower shoots could be the reason of increase in Ca uptake. Ca is an important plant nutrient taking place in cell wall metabolism like B [8] and they have similarites such as low mobility, high extra-cytoplasmic concentration and growth alterations during deficiency [5].

Our results demonstrate that increase in P uptake of sunflower shoots was significant with the boron application ($P <$ 0.05). The scores were between 1.95 and 2.93 g kg^{-1}. The minimum and the maximum scores were determined at 0 and 32 mg kg^{-1} B treatment (Table 2). The increase in P could be attributed to Ca increase in shoots and the signifcant correlation (r = 0.858*) was recorded between P and Ca (Table 3). Increase in P uptake with B supply was also recorded in tobacco [17] and in pepper & tomato [9].

Boron interaction based on synergism or antagonism could be affected by different growth media, plant species or varieties, analysed plant part, plant age and environmental conditions [24].

CONCLUSIONS

In conclusion it is possible to say that cv. Sirena could be cultivated for phytomining in soils containing B up to 8 mg kg^{-1}. It could be also possible to cultivate it in the further B levels (ranging from 8 mg kg^{-1} to 64 mg kg^{-1}) till the R1 growth stage and harvest the plants to use as manure in soils that have low B content.

TABLE 2
Effects of B application on nutrient uptake of sunflower cultivar (Sirena)

Mineral Concentrations	Boron concentration (mg kg^{-1})					
	0	4	8	16	32	64
B (mg kg^{-1}) **	57.19 b	108.03 b	121.55 b	228.80 b	622.05 a	695.18 a
Na (mg kg^{-1})	705.00	630.00	655.00	585.00	520.00	535.00
K (g kg^{-1}) **	76.62 a	73.63 a	74.01 a	73.62 a	66.02 b	66.18 b
Ca (g kg^{-1}) **	6.93 c	7.01 c	8.19 bc	8.22 bc	10.02 a	9.40 ab
P (g kg^{-1}) *	1.95 b	2.28 b	2.51 ab	2.35 ab	2.93 a	2.43 ab

**All values in a row designated with different letters are significantly different using Duncan's Multiple Range Test ($P < 0.01$).

*All values in a row designated with different letters are significantly different using Duncan's Multiple Range Test ($P < 0.05$).

TABLE 3
Correlation coefficients (r) between some elements observed in shoots of cv. Sirena

	B	Na	K	Ca	P
B	1	-	-	-	-
Na	-0,913*	1	-	-	-
K	-0,979**	0,930**	1	-	-
Ca	0,916*	-0,890*	-0,918**	1	-
P	0,665	-0,773	-0,764	0,858*	1

*. Correlation is significant at the 0.05 level. **. Correlation is significant at the 0.01 level.

REFERENCES

[1] Ahmed, N., Muhammad, A., Ahmad, F. (2008) Boron toxicity in irrigated cotton (*Gossypium hirsutum* L.). Pak. J. Bot. 40, 2443-2452.

[2] Alpaslan, M., Gunes, A. (2001) Interactive effects of boron and salinity stres on the growth, membrane permeability and mineral composition of tomato and cucumber plants. Plant and Soil, 236, 123-128.

[3] Alvarez-Tinaut, M.C., Leal, A., Agui, I., Recalde-Martinez, L. (1979) Physiological effects of B-Mn interaction in tomato plants. II. The uptake and translocation of macroelements. Analse de Edafologia y Agrobiologia 38(5/6), 991-1012.

[4] Blamey, F.P.C., Zollinger, R.K., Schneiter, A.A. (1997) Sunflower production and culture. In Schneiter A.A. (ed) Sunflower technology and production. American Society of Agronomy, Madison, Wis. pp. 595-670.

[5] Bonilla, I., El-Hamdaoui, A., Bolaños, L. (2004) Boron and calcium increase *Pisum sativum* seed germination and seedling development under salt stress. Plant and Soil, 267, 97-107.

[6] Cervilla, L. M., Blasco, B.A., Rios J. J., Romero, L., Ruiz, J.M. (2007) Oxidative stress and antioxidants in tomato (*Solanum lycopersicum*) plants subjected to boron toxicity. Ann. Bot. 100, 747–756.

[7] Corey, R.B., Schulte, E.E. (1973) Factors affecting the availability of nutrients to plants. In: Soil Testing and Plant Analysis. Walsh, L.M. and J.D. Beaton (Eds) Soil Sci. Soc. Am. Inc. Madison,Wisconsin,USA. pp: 23-24.

[8] Dela-Fuente, R.K., Tang, P.M., Guzman, C.C. (1986) Plant growth substances, 1985. Proceedings of the 12th international conference on plant growth substances, Berlin, In: Plant-Environment Interactions. Wilkinsin, R.E. (Ed). 1994. Marcel Deckker, Inc. 270, Madison Avenue, Newyork, USA., pp: 227.

[9] Eraslan, F., Inal, A., David, J.P., Gunes, A. (2007) Boron toxicity alters nitrate reductase activity, proline accumulation, membrane permeability and mineral constituents of tomato and pepper plants. Sci Hort. 30(60), 981-994.

[10] Fageria FD. (2001) Nutrient interactions in crop plants. Journal of Plant Nutrition, 24, 1269-1290, DOI: 10.1081/PLN-100106981

[11] Gezgin, S., Dursun, N., Hamurcu, M., Harmankaya, M., Önder, M., Sade, B., Topal, A., Soylu, S., Akgün, N., Yorgancılar, M., Ceyhan, E., Çiftçi, N., Acar, B., Gültekin, I., Işık, Y., Şeker, C., Babaoğlu, M. (2002) Boron content of cultivated soils in Central-Southern Anatolia and its relationship with soil properties and irrigation water quality. Boron in plant and animal nutrition.1(1), 391-400.

[12] Goldbach, H.E. (1984) Influence of boron nutrition on net uptake and efflux of ^{32}P and ^{14}C-glucose in *Helianthus annuus* roots and cell cultures of *Daucus carota*. J. Plant Physiol. 118, 431-438.

[13] Grieve, C., Poss, M.J.A., Grattan, S.R., Suarez, D.L., Smith, T.E. (2010) The combined effects of salinity and excess boron on mineral ion relations in broccoli. Scientia Horti. 125, 179-187.

[14] Karabal, E., Yucel, M., Oktem, H.A. (2003) Antioxidant responses of tolerant and sensitive barley cultivars to boron toxicity. Plant Sci 164, 925–933.

[15] Karenlampi, S., Schat, H., Vangronsveld, J., Verkleij, J.A.C., Van der Lelie, D., Mergeay, M., Tervahauta, A.I. (2000) Genetic engineering in the improvement of plants for phytoremediation of metal polluted soils. Environ Poll 107, 225–231

[16] Korzeniowska, J. (2008) Response of ten winter wheat cultivars to boron foilar application in a temperate climate (South-West Poland). Agronomy Research 6(2), 471-476.

[17] Lopez-Lefebre, L. R., Rivero, R.M., Garcia, P.C., Sanchez, E., Ruiz, J.M., Romero L. (2002) Boron effect on mineral nutrients of tobacco. J. Plant Nutr. 5, 509-522.

[18] Nable, R.O., Bañuelos, G.S., Paull, J.G. (1997) Boron toxicity. Plant and Soil, 193, 181-198.

[19] Oztürk, M., Sakcali, S., Gucel, S., Tombuloglu H. (2010) Boron and plants, pp. 275-311. In: Ashraf M., Ozturk M., Ahmad M.S.A. (eds). Plant adaptation and phytoremediation. Springer; Dordrecht, Heidelberg, London, New York.

[20] Page, A.L., Miller, R.H., Keeney, D.R. (1982) Methods of Soil Analysis. Part 2 - Chemical and Microbiological Properties, 2nd Edition. Agronomy Society of America. Madison, WI.

[21] Pfeffer, H., Dannel, F., Römheld, V. (1999) Are there two mechanism for boron uptake in sunflower. J. Plant Physiology 155, 34-40.

[22] Robertson, G.A., Loghman, B.C. (1974) Reversible effects of boron on the absorbtion and incorporation of phosphate in *Vicia faba* L. New Phytol. 73, 291-98.

[23] Tanaka, M., Fujiwara, T. (2008) Physiological roles and transport mechanisms of boron: perspectives from plants. Pflugers Arch Eur J Physiol 456, 671–677

[24] Tariq, M., Mott, C.J.B. (2007) Effect of Boron on the behaviour of nutrients in soil-plant systems-A review. Asian Journal of Plant Sciences 6(1), 195-202.

Received: **15.01.2016**
Accepted: **20.07.2016**

CORRESPONDING AUTHOR

Sibel Day
Department of Field Crops, Faculty of Agriculture, University of Ankara, 06110, Ankara, Turkey.

Email: day@ankara.edu.tr

© by PSP Volume 25 – No. 10/2016, pages 4299-4308 Fresenius Environmental Bulletin

PHOTOCATALYTIC DEGRADATION OF DICLOFENAC AND IBUPROFEN FROM SIMULATED WASTEWATER USING SiO2-TiO2-(Ru, N) BY ARTIFICIAL LIGHT

Waed R Alahmad[1] , Mahmoud A Alawi[2,*]

[1]Faculty of Science, Deapartment of Chemistry, Hail University, Kingdom of Saudi Arabia
[2] Faculty of Sciences, Department of Chemistry, University of Jordan, Amman 11942, Jordan

ABSTRACT

The degradation of Diclofenac and Ibuprofen in simulated wastewater using synthesized catalysis , parent catalyst SiO_2/TiO_2 , and doping with N and Ru, under UV light. The % removal ranged between 63%-75% for Diclofenac, 43%-90% for ibuprofen using several amounts of catalyst weight (0.2, 0.4, 0.6, 0.8, 1 g /100mL). The degradation fits with pseudo-first order Langmuir–Hinshelwood kinetic model.

KEYWORDS:
photodegradation, wastewater, Diclofenac, Ibuprofen, kinetics

INTRODUCTION

Growth in the global population, the diminishing supply of clean water, heightened environmental concerns, and the strong link between water quality and human health require the identification and employment of effective sustainable water treatment to meet the urgent global need for clean water [1].

Advanced oxidation processes (AOPs) have shown tremendous promise in water purification and treatment, including for the destruction of naturally occurring toxins, contaminants of emerging concern, pesticides, and other deleterious contaminants.

The chances and potential fields of application of photocatalytic systems with artificial UV-sources include new water treatment plants or plants where conventional methods need to be replaced and the treatment of water contaminated with trace organic contaminants such as estrogens, the treatment of industrial wastewater contaminated with high loads of organic compounds as well as small scale systems, for example, for the disinfection of swimming pools [2-5].

Heterogeneous photocatalysis has been used to decompose natural organic matter, volatile organic compounds in water, air and soil and there are applications in consumer goods, food and medicine [5].

The two most significant applications of photocatalysis have been in solar water splitting and the purification of air and water containing low concentrations of pollutants [1].

The photocatalytic process gradually breaks down the contaminant molecules, no residue of the original material remains and therefore no sludge requiring disposal to landfill is produced. Additionally, because the contaminant is attracted strongly to the surface of the catalyst, the process will continue to work at very low concentrations. Taken together, these advantages mean that the process results in considerable savings in water production cost and keeping the environment clean [2-3].

Among the various semiconductors, TiO_2 are the most widely used in environmental application because of its low cost, non-toxicity, and high oxidizing power.

Photocatalyst doping has spanned several decades [6-9]. Technically, doping is the introduction of foreign elements into the parent photocatalyst without giving rise to a new crystallographic forms, phases or structures and the aims are to enhance the net separation of photo-generated charges and thereby efficiently harness the wide visible-light component of about 43% in the solar spectrum as opposed to the narrow ultraviolet component of 5% [5].

Diclofenac (DCF) is a non-steroidal anti-inflammatory drug (NAID) most prevalently used as analgesic, anti-arthritic and anti-rheumatic and about 15% is excreted unchanged after human consumption. Though it has been confirmed that diclofenac is rapidly degraded by direct photolysis under normal environmental conditions, it is still one of the most frequently detected pharmaceutical in the water environment [10]. The DCF is found to be present in aquatic environment [11-13]. DCF is known to undergo solar radiation induced photochemical decomposition in surface waters [14].

Ibuprofen (IBU) is one of the most widely-used pain reliever in the world. This weakly acidic

(NAID) have been detected in natural water system at concentrations down to the ppb (nM) level [12, 13, and 15]. In spite of the high biodegradation of IBU, the rest of ecological risk remains high, due to the main byproducts generated during the biological oxidation. The byproducts hydroxyl-IBP and carboxy-IBP have shown quite similar toxicological consequences in aquatic environment [15]. IBU does not absorb light at wavelength longer than 285 nm and has been reported to resist direct photodegradation because its absorption spectrum does not overlap with the solar radiation spectrum [15].

Photocatalytic destruction of pollutants in aqueous solutions are facilitated mainly by a series of hydroxylation reactions initiated by hydroxyl radicals (˙OH). Upon UV light illumination, electron-hole pairs are formed on semiconductor photocatalyst. Holes are positive charges, which when in contact with water molecules, produce ˙OH and H^+ ions. Electrons react with dissolved oxygen to form superoxide ions ($O_2^{-\cdot}$), which react with water molecules to produce hydroxide ions (OH^-) and peroxide radicals (˙OOH). Peroxide radicals combine with H^+ ions to form ˙OH and OH^-, and holes oxidize OH^- to ˙OH. Thus, all species eventually facilitate the formation of ˙OH, and these radicals attack the pollutants present in the aqueous solution [5].

The kinetics of the photocatalytic degradation of aqueous pollutants is still a subject of debate [16–18]. Several recent reports claim that it follows the Langmuir-Hinshelwood model (L-H model) of kinetics [10, 14-19]. Therefore reporting L-H model of kinetics in photocatalytic degradation without proper experimental evidences is dubious.

Langmuir–Hinshelwood (L-H) model represents the mechanism required for the contaminant adsorbs on the catalyst surface as a prerequisite for efficient oxidation.

The adsorption–desorption process is characterized by the transfer of the reactants in the aqueous phase to the surface; adsorption of the reactants; reaction in the adsorbed phase; desorption of the products; and removal.

Although the L-H model seems to describe adequately the macroscopic kinetics when dealing with very dilute aqueous solutions of photodegradable contaminants, some of the inherent assumption of the model may not be valid at the microscopic level, which includes its failure to account for simultaneous adsorption (or desorption) L-H model equation is represented in equation 1:

$$r = k\theta = -dC / dt = k(KC/1+KC) \quad (1)$$

where r is the rate of mineralization, k is the reaction rate constant, C is the concentration, K is the adsorption coefficient and θ is the fractional site coverage for the reactant as KC<<1, the equation became as in 2 or 3:

$$C(t) = C_0 e^{-krt} \quad (2)$$

$$\text{Ln } C = \text{Ln } C_0 - krt \quad (3)$$

Where: k_r is the rate constant for the first-order photocatalytic reaction [20, 21].

In this work, we prepared a TiO_2 supporting with SiO_2 by incipient wetness impregnation method, then doping with Nitrogen (N) and Ruthenium (Ru) which were used in a kinetic degradation study of Diclofenac and Ibuprofen in a simulated wastewater sample using HPLC/UV.

EXPERIMENTAL

Materials. Cabosil M-5 silica oxide was purchased from Sigma-Aldrich, titanium isopropoxide (Ti(i-OC3H7)4, 97% purity) was purchased from Aldrich. Absolute Ethanol, Ru(III) acetylacetonate, Urea, Ethyl acetate , Methanol, Acetonitrile, Diclofenac (DCF), Ibuprofen (IBU) , Nifidipen and Methelyene Blue were purchased from Sigma-Aldrich.

Preparation of SiO_2 /TiO_2 Catalyst. The investigated modified titanium-silica systems were prepared by incipient wetness impregnation method. Silica with titanium precursor was followed by a re-impregnation procedure with a metal precursor [22]. The silica support used for this study was Cabosil M-5 silica oxide. This material was treated with water in order to condense its volume for easier handling. The wet SiO_2 was dried at 110ºC in order to remove the physical adsorbed water before impregnation. TiO_2/SiO_2 supported oxide catalyst was prepared by the incipient wetness impregnation of SiO_2 with an ethanol solution of titanium isopropoxide. After impregnation at room temperature, the sample was kept overnight. The removal of the solvent was carried out by conventional drying, first at room temperature for 24 h, and after that at 110 oC for 2 h. Removal of residual organics and thermal stabilization of the materials was carried out by calcination for 5 h at 400ºC in air atmosphere.

Preparation of Ru Supported Catalysts. The impregnation was carried out using ethanol solutions of 2 weight % of transition metal salt (Ru(III) acetylacetonate) [0.02g Ru: 1g SiO_2/TiO_2] for 24 h at room temperature stirring. The removal of the solvent was carried out by conventional drying, first at room temperature for 24 h then at 110ºC for 2 h. Removal of residual organics and thermal stabilization of the materials was carried out by calcination for 5 h at 400ºC. The resulted photocatalyst was denoted as SiO_2 /TiO_2 /Ru.

Preparation of N Supported Catalysts. The impregnation was carried out using ethanol solutions, 1g urea in 20 ml (1M) HCl added to 1 g SiO_2 /TiO_2 for 24 h at 80ºC stirring. The removal of the solvent was carried out by conventional drying, first at room temperature for 24 h, then at 110ºC for 2 h. Removal of residual organics and thermal stabilization of the materials was carried out by calcination for 5 h at 400ºC. The resulted photocatalyst denoted as SiO_2 /TiO_2 /N.

Validation of the analytical procedure. The range of linearity for the studied pharmaceuticals was calculated and calibrated with the internal standard. A 6-point calibration curve was established at the concentrations of 5, 10, 20, 30, 40 and 50 mg/L, using UV detection and the internal standard (nifidipen). The average of four injections of each concentration was used to establish the linear curves and correlation coefficients. Table 1 summarizes the calibration results: retention times (t_R), limits of detection (LOD), limits of quantification (LOQ), the linear equations, the correlation coefficients (R^2), as well as the recovery of three quality control concentrations 10, 20, 30 mg/L with their standard deviations (S.D.).

Extraction. The extraction recoveries of the pharmaceuticals were estimated by spiking each analyte in deionized water at the concentrations of 10, 20 and 30 mg/L. The internal standard (I.S.) nifidipen was added to the samples after extraction. To determine the extraction recoveries, concentrations of the spiked samples were compared to the unextracted solutions (calibration curve).

For standard curve, calibration and quality control 100 ml deionized water were spiked with the desired drug concentration. An SPE cartridge was conditioned using 6 ml of methanol (2ml ×3 times) and 6 ml of distilled water (2 × 3) at a slow flow-rate. 5ml of the spiked sample was transferred to the SPE cartridges through at slow flow-rate.

The loaded cartridges were rinsed with 3 ml deionized water; then eluted with 10 mL (35% ethyl acetate: 52% ethanol: 13% methanol) (2.5ml ×4 times). The combined aliquots were evaporated to dryness using a gentle stream of nitrogen. The residues were dissolved in 0.25 ml mobile phase, sonicated to insure complete dissolution and 20µL were injected onto the HPLC column.

HPLC procedure. The HPLC system consisted of a Shimadzu delivery pump (LC-20AD), equipped with an auto-sampler model (SIL-20 AHT), degasser model (DGU-20 AS) and a diod array detector model (SPD-M20A). The mobile phase was acetonitrile/water (1/1) with 0.1% TFA pumped at a flow rate of 1 mL/ min. The run time was 15 min. The UV detector was operated at 225 nm for the detection of I.S., Diclofenac (DCF) and Ibuprofen (IBU).

Photocatalytic Removal of Methylene Blue. Methylene blue (MB dye) used as a model contaminant. The degradation of 100 mL aqueous MB solutions of 10 mg/L concentration using 0.2% amount of each catalysts: SiO_2/TiO_2, $SiO_2/TiO_2/N$ and $SiO_2/TiO_2/Ru$. The sample was illuminated using an UVA lamp (315-400 nm) for 180 min. at a 10 cm distance with magnetic stirring.

Also MB removal behavior from aqueous suspension was investigated in continuous adsorption equilibrium experiments in the dark (to exclude photo-degradation). The MB solution in each sample was stirred magnetically at a moderate speed and then allowed to sediment. At various time intervals of 30 min., an aliquot of the solution was taken and the remaining dye was measured using a UV-VIS Double Beam Spectrophotometer Model UVD-2950 at an incident wavelength of 665 nm.

The initial and equilibrium dye concentrations are determined using a calibration curve based on the absorbance at λ_{max} = 665 nm versus dye concentration in standard dye solutions. To construct a calibration curve, the MB concentrations of 0.5, 1.0, 3.0, 5.0, 7.0, 10.0, 15.0 and 20.0 mg/ L were prepared in volumetric flasks and the absorbance of each of the standard MB solutions was measured at the maximum absorption wavelength of 665 nm [23].

Photocatalytic activity of DCF and IBU. For each catalyst (SiO_2 /TiO_2) , (SiO_2 /TiO_2 /Ru) and (SiO_2 /TiO_2 /N) the amounts of (0.0g/ 0.2g/ 0.4g/ 0.6g/ 0.8g/ 1.0g) each in 100 ml water spiked with 30 ppm concentration of DCF and IBU as a mixture was used. The illumination time under the UVA lamp (315-400 nm) was for 60 min. Each 15 minute 5 mL sample was taken and extracted as above. The lamp was at 10cm distance from the beaker (magnetically stirring). The sample was filtrated fast and then extracted to avoid any further degradation.

RESULTS AND DISCUSSION

Validation of the analytical procedure. Table 1 summarizes the method's Validation parameters including: recoveries, the correlation coefficient (R^2), the linear equation, limits of quantification (LOQ), limits of detection (LOD) and retention times (t_R), and the recovery of three quality control concentrations namely: 10, 20 and 30 mg/L with their standard deviations (S).

TABLE 1
Method's Validation parameters (% Recoveries, R^2, Linear equations, LOQ, LOD and t_R,) for DIC and IBU

%Recovery (X_{av} ± S) for 30 mg/L	%Recovery (X_{av} ± S) for 20 mg/L	%Recovery (X_{av} ± S) for 10 mg/L	R^2	Linear Equation	LOQ µg /L	LOD µg /L	t_R (min.)	Drug
96%±4.0	92%±8.0	107%±7.0	0.973	Y=0.015x+0.307	0.3	0.1	4.58	DCF
91%±9.0	94%±6.0	111%±11.0	0.987	Y=0.016x+0.145	0.3	0.1	5.13	IBU

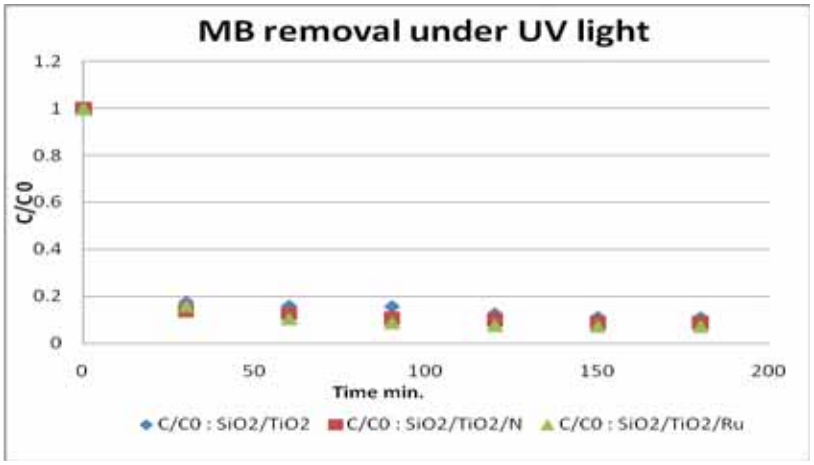

FIGURE 1
Removal of MB under UV light, C/C0 vs. Time (min.)

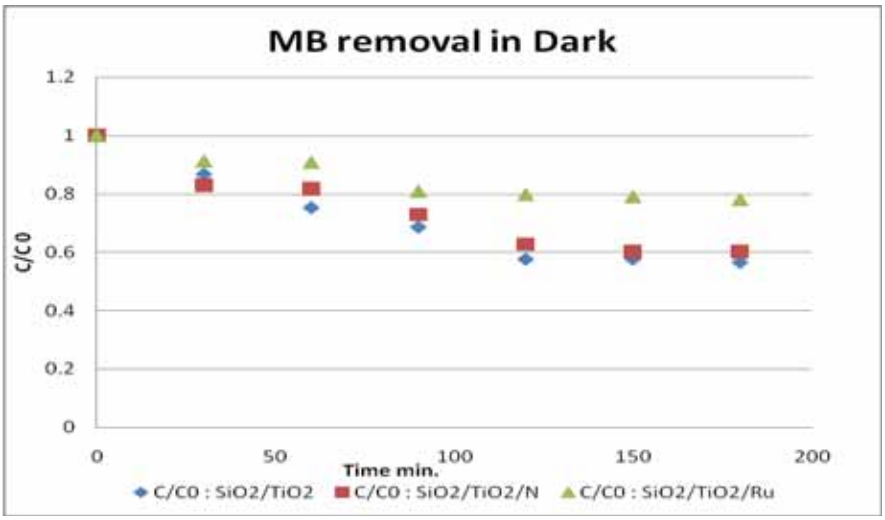

FIGURE 2
Removal of MB in Dark, C/C0 vs. Time (min.)

Photocatalytic Removal of Methylene Blue. Methylene blue (MB dye) used as a model contaminant, the calibration curve of MB concentrations of 0.5, 1.0, 3.0, 5.0, 7.0, 10.0, 15.0 and 20.0 mg/ L standard measured at the maximum absorption wavelength of 665 nm. the concentration of MB calculated from the regression equation: y = 0.114x + 0.074 with R^2 = 0.992.

Figures 1 and 2 show the degradation of MB under light and in Dark respectively. This Indicate that the MB degradation by the direct photolysis only, is unimportant. Therefore, the reduction of MB concentration is primarily caused by the photocatalytic reaction.

Photocatalytic removal of DCF and IBU. For each catalyst (SiO_2 /TiO_2), (SiO_2 /TiO_2 /Ru) and (SiO_2 /TiO_2 /N), the following weights of the catalysts (0.2g/ 0.4g/ 0.6g/ 0.8g/ 1.0g) were used under artificial light

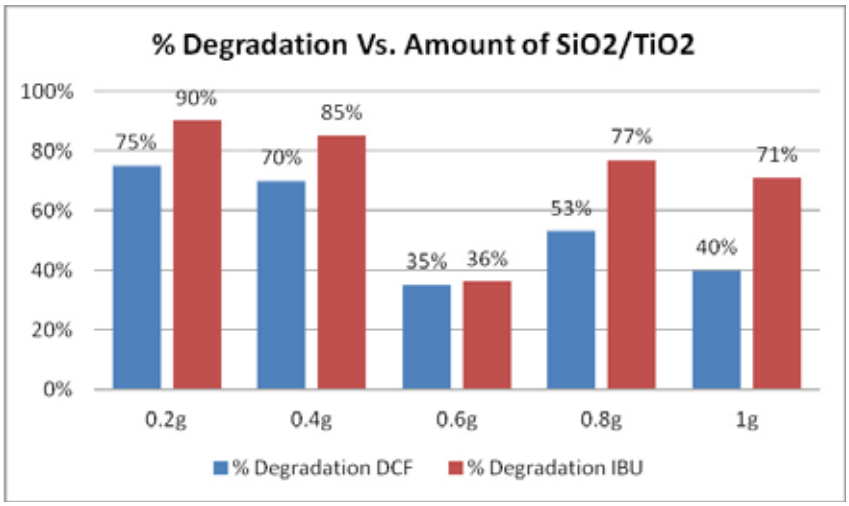

FIGURE 3
% Degradation for DFC and IBU vs. Amount of catalyst SiO2/TiO2

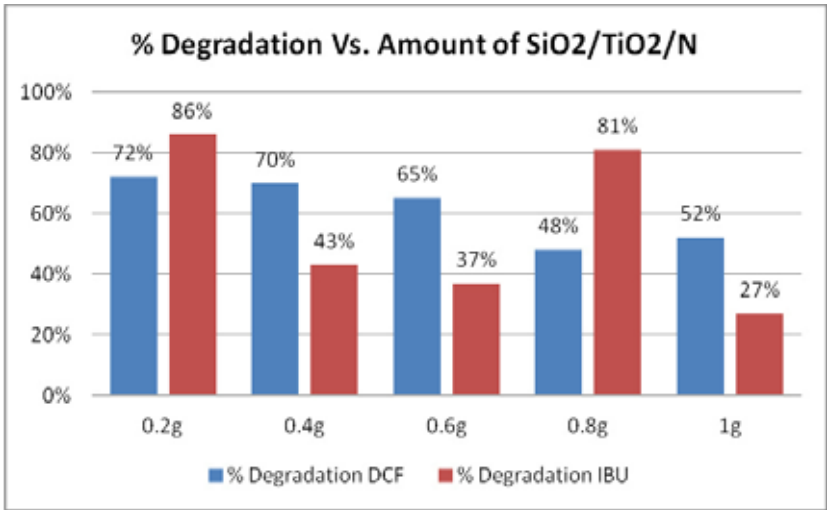

FIGURE 4
% Degradation DFC and IBU vs. Amount of catalyst SiO2/TiO2/N

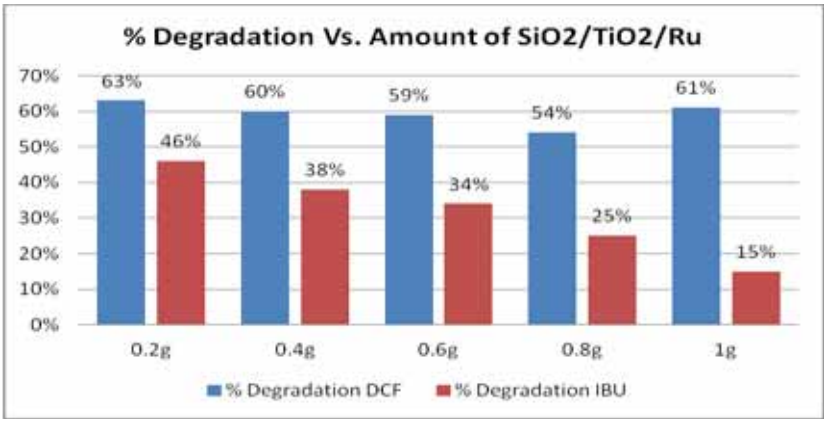

FIGURE 5
% Degradation for DFC and IBU vs. Amount of catalyst SiO2/TiO2/Ru

TABLE 2
Maximum % degradation of DCF and IBU using different amounts of catalysts, 0.2 g/100 mL

Catalyst	Amount of catalyst/ max. % degradation DCF	Amount of catalyst/ max. % degradation IBU
SiO_2/TiO_2	0.2g /75%	0.2g /90%
$SiO_2/TiO_2/N$	0.2g /72%	0.2g /86%
$SiO_2/TiO_2/Ru$	0.2g /63%	0.2g /46%

Kinetic study. Figures 6 and 7 show the kinetic results of DCF and IBU degradation respectively, using different photo catalysts. In this study, photocatalytic degradation kinetics of the photo catalyst follow pseudo-first order kinetic as illustrated in equations 2 and 3 [20, 21]. This is obvious with the straight line relationship on the linearized plot of $-Ln(C/C_0)$ vs. time. The calculated R^2 values exhibited the tendency of the reaction which fits best with the pseudo-first order reaction. The rate constant (k) can be calculated using the given slope of the plot.

According to the L-H model, at low pollutant concentrations and below the catalyst saturation level the adsorption of the reactant only account.

The photocatalytic degradation rate of pollutant should increase with an increase in the catalyst loading because of the additional available active sites for adsorption, defecting in this concern is due to three reasons mainly ascribed: at higher catalyst loading, (i) deactivation of activated catalyst could occur upon collision with ground state catalyst, (ii) there is a higher possibility of agglomeration and sedimentation, and (iii) there is decreased light penetration through the reaction medium [5,30].

UV light flux is an important influence on the degradation kinetics of pollutant in aqueous medium [30].

Figures 6 and 7 represent the $-LnC/C_0$ vs. Time in min. where the C_0 is the initial concentration of the drug. The % degradation was highest at 0.2g/100ml (0.2 %) as mentioned before.

Table 3 gives the k value (adsorption rate constant) for the highest % removal of both DCF and IBU 0.2%. The k value for DCF using SiO_2/TiO_2 is the highest value of 0.0254 min^{-1}. The k value for IBU is the highest value of 0.0288 min^{-1} using $SiO_2/TiO_2/N$.

The real meanings of the parameters (k) in the L–H model have not been clarified. Thus, kinetics is related to these factors, that is, initial organic content, light intensity and some parameters, related to the adsorption of catalyst, and these factors should be included into the kinetic model.

illumination for 60 min. Figures 3-5 illustrate the maximum percent degradation found for DCF and IBU. The degradation results were found when using 0.2g/100 mL for all used three catalysts as shown in table 2.

Doping TiO_2 with metals and non-metals creates new energy levels between the VB and CB of TiO_2, which in turn reduces its band gap and helps the doped catalyst to absorb in the visible region [4, 5]. The visible light photocatalytic activity was mainly attributed to the associated red shift that originated from the creation of local bands between the VB and CB of TiO_2 [24, 25].

Photodegradation of samples exposed to the UV-light should be more degradable than those subjected to the direct sunlight or visible light. This is because, the emission spectra of UV-light mainly focuses on the ultraviolet band having the advantageous of short-wave emission and high energy to initiate photodegradation of compounds. However, the spectrum of sunlight ranged from ultraviolet to near infrared and with the main flux concentrated on the visible light band [26].

The highest degradation was found at 0.2g/100mL for the three catalysts, as the loading increase above the optimal limit, the degradation percentage decreased due to the opacity of the suspension and light scattering which was found in other literature [26, 27].

The % removal of DCF was ranged from 63%-75%, while for IBU ranged from 90%-46%. IBU resist direct photodegradation comparing to DCF. The rate of Photodegradation for IBU increased with increasing concentration of the aromatic ketone (4-isobutylacetophenone) the major degradation product [28], where the addition of just 8 µM of the aromatic ketone increased the rate of photodegradation by almost a factor of 10 [28]. The gray color of $SiO_2/TiO_2/Ru$ may decrease the light penetration as it gave the lowest % degradation for both DCF and IBU, While the color for SiO_2/TiO_2 and $SiO_2/TiO_2/N$ is white color and both gave close % removal.

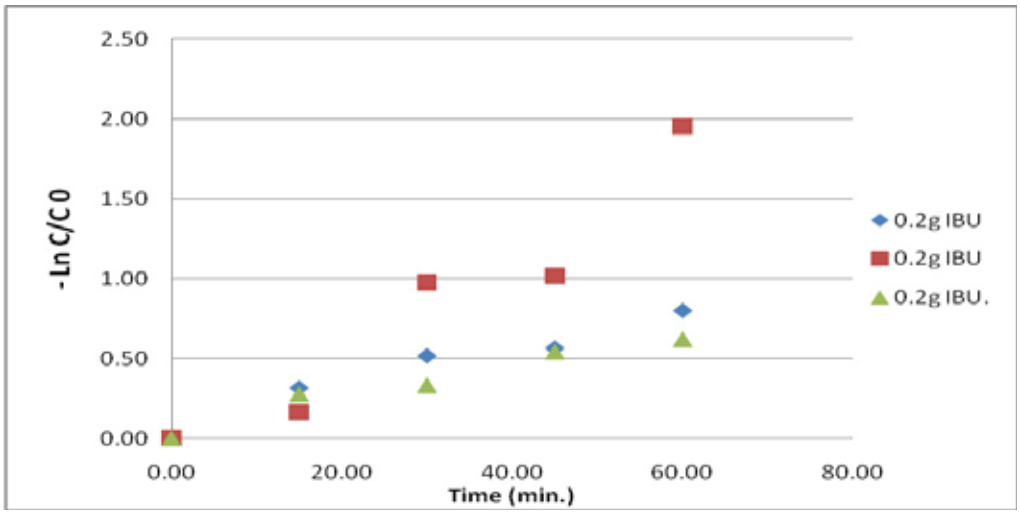

FIGURE 6
Kinetic plot for IBU Degradation for a catalyst dosage of 0.2g /100ml (0.2%) under artificial light sources.

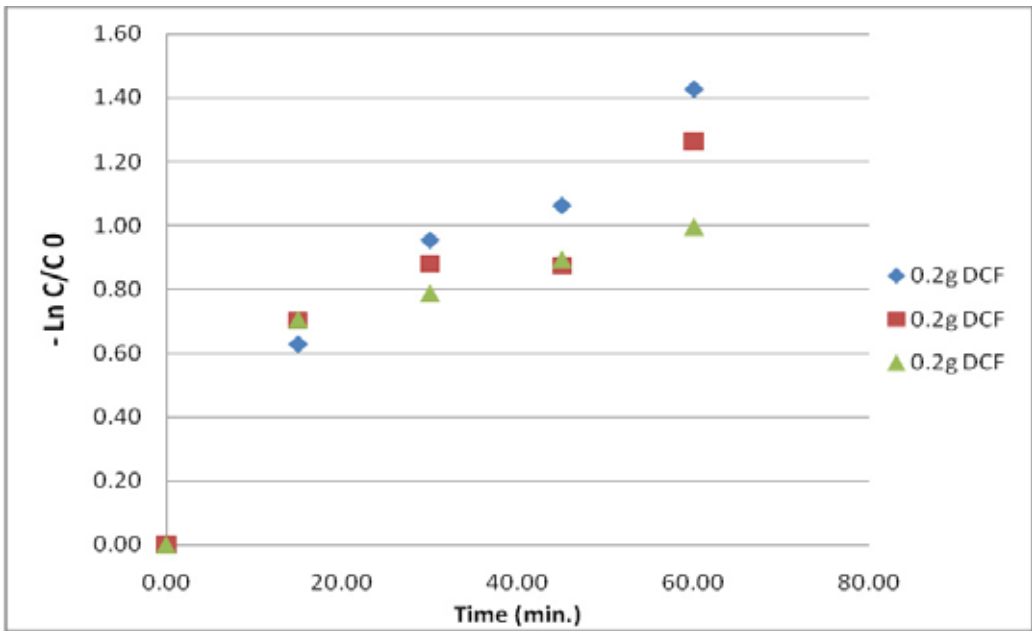

FIGURE 7
Kinetic plot for DCF Degradation for a catalyst dosage of 0.2g /100 ml (0.2%) under artificial light sources.

TABLE 3
Results of kinetic disappearance of the studied drugs

k (min^{-1}) DCF	R^2	k (min^{-1}) IBU	R^2	Catalyst
0.0254	0.9569	0.0139	0.9275	SiO_2/TiO_2
0.0228	0.9409	0.0288	0.9122	$SiO_2/TiO_2/N$
0.0185	0.8783	0.0112	0.9338	$SiO_2/TiO_2/Ru$

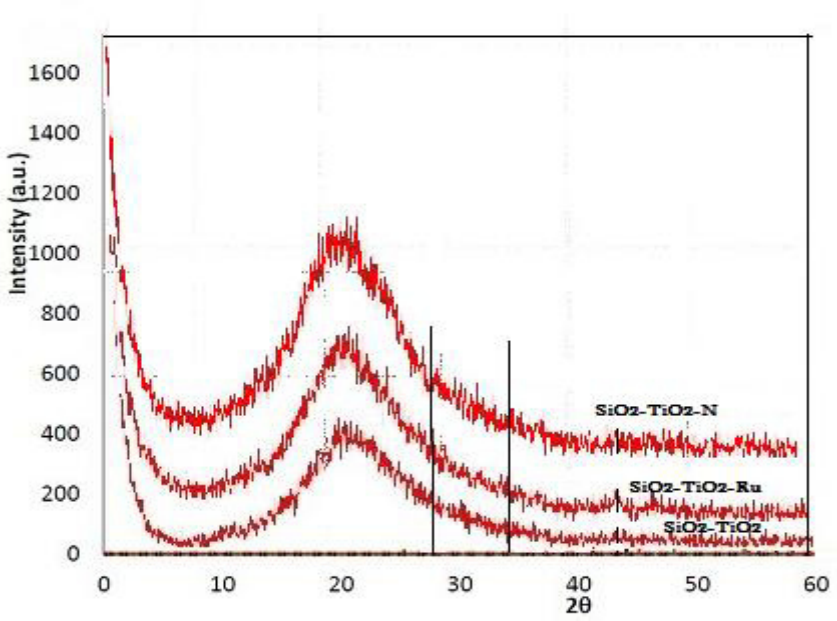

FIGURE 8
X-Ray diffraction of the supports and the catalysts.

The order of the degradation reaction determined by three different adsorption situations: (i) weak adsorption (ii) medium adsorption and (iii) strong adsorption. In the case of weak adsorption of the pollutant on catalyst, pseudo-first-order expression is applied as shown in Equations 2 and 3 [5].

PHOTOCATALYTIC CHARACTERIZATION (XRD CHARACTERIZATION)

The XRD patterns of the prepared catalysts are shown in Figure 8. These pattern show that these catalysts are amorphous, due to the structure of fumed SiO_2 ,which is compatible with the results of Ekou *et al.*, (2011), while Ru was observed by small peaks at 28º, 35 º and 54 º that because of the 2% w/w [30, 31].

The results show no significant peaks could be detected for TiO_2. This could be related to the low titanium loading (25 wt. %), indicating that the grafting of titanium results in the formation of small TiO_2 particles [32, 33]. Some investigators reported that XRD cannot detect the presence of TiO_2 crystallites below 30% loading, suggesting that the TiO_2 crystalline particles on SiO2 are very small and below the detection sensitivity of the XRD technique (< 40 Å) [30- 33].

CONCLUSION

Photocatalytic degradation of Diclofenac and Ibuprofen in aqueous solution was investigated using synthetic doped (SiO_2/TiO_2), (SiO_2/TiO_2/N) and (SiO_2/TiO_2/Ru)

Catalysts under artificial UV light source, results show good degradation. The % removal for DCF was (63% - 75%) and for IBU (90%- 46%) from simulated wastewater samples. This technique could be applied in homes, hospitals, which may also improve the quality of the water released from wastewater treatment plants by assisting traditional treatment methods to target more substances and thereby obtain a higher efficiency of the whole process.

Kinetic study illustrated that photocatalytic degradation of Diclofenac and Ibuprofen fit well-to the pseudo-first order model.

The kinetics of photocatalytic degradation was found to depend on catalyst loading which ranged from 0.2g/100mL -1g/100mL for the parent catalyst SiO_2/TiO_2 and the doped with N and Ru.

REFERENCES

[1] Ibhadon, A.O. and Fitzpatrick, P. (2013) Heterogeneous Photo-catalysis: Recent Advances and Applications, Catalysts, 3, 189-218.

[2] Ibhadon, A.O. (2008) Multifunctional TiO_2 Catalysis and Applications. In Proceedings of Green Chemistry and Engineering International Conference, Washington, DC, USA, 24–26 June.

[3] Fujishima, A., Zhang, X. and Tryk, D.A. (2008) TiO_2 photocatalysis and related surface phenomena. Surf. Sci. Rep. 63, 515–582.

[4] Ochiaia, T. and Fujishima,A. (2012) Photo electrochemical properties of TiO_2 photocatalyst and its applications for environmental purification. Journal of Photochemistry and Photobiology C: Photochemistry Reviews 13, 247– 262

[5] Lazar,M.A., Varghese, S. and Nair,S.(2012) Photocatalytic Water Treatment by Titanium Dioxide, Catalysts 2, 572-601.

[6] Hongjun, J., Xiaoheng, L., Xin, W. and Xiaxi, Y. (2011) Self-assembly and photocatalytic property of amorphous cubic-like TiO_2-ZnO hybrid film. Rare Metals 30, 225- 228.

[7] Liang, W., Li, J., and Jin, Y.(2012), Photo-catalytic degradation of gaseous formaldehyde by TiO_2/UV, Ag/TiO_2/UV and Ce/TiO_2/UV, Building and environment. 51, 345-350.

[8] Tada, S., Kikuchi R., Wada, K., Osada, K., Akiyama K., Satokawa, S., Kawashima Y. (2014) Long-term durability of Ni/TiO_2 and Ru-Ni/TiO_2 catalysts for selective CO methanation. Journal of Power Sources. 264, 59-66.

[9] Yanga, L., Peng L., Xi L., Song L. (2012) The photo-catalytic activities of neodymium and fluorine doped TiO_2 nanoparticles 38(6), 4791–4796.

[10] Basavaraju, M., and Mahamood, R. (2012) Degradation Kinetics of Diclofenac in water by Fenton's Oxidation. Journal of Sustainable Energy & Environment 3, 173-176

[11] Zhang, Y., Geibe,n SU., Gal, C. (2008) Carbamazepine and diclofenac: remova in wastewater treatment plants and occurrence in water bodies, Chemosphere 73/8, 1151-1161.

[12] Jux, U., Baginski, RM., Arnoldm HG., Kronkem M. and Seng, PN. (2002) Detection of pharmaceutical contaminations of river, pond, and tap water from Cologne (Germany) and surroundings, Int J Hyg Environ Health 205, 393-398.

[13] Alahmad, W.R., and Alawi, M.A. (2010) HPLC/ UV/ Fluorescence Detection of Several Pharmaceuticals in Sewage Treatment Plant Wastewaters of Jordan. Fresenius Environmental Bulletin 19 (5)..

[14] Epold,I., Dulova,N., Trapido,M.(2012) Degradation of diclofenac in aqueous solution by homogeneous and heterogeneous photolysis. Journal of Environmental Engineering & Ecological Science 1323, 1-3,

[15] Me´ndez-Arriaga,F., Esplugas,S., Gime´nez, J. (2009) Degradation of the emerging contaminant ibuprofen in water by photo-Fenton. Water Research, 44 (2), 589 –595

[16] Wang, C., Zhang, X., Liu, H., Li, X., Li, W., Xu, H. (2009) Reaction kinetics of photocatalytic degradation of sulfosalicylic acid using TiO_2 microspheres. J. Hazard. Mater. 163, 1101–1106.

[17] Montoya, J.F., Velasquez, J.A., Salvador, P. (2009) The direct-indirect kinetic model in photocatalysis: A reanalysis of phenol and formic acid degradation rate dependence on photon flow and concentration in TiO_2 aqueous dispersions. Appl. Catal. B 88, 50–58.

[18] Tasseroul, L., Pirard, S.L., Lambert, S.D., Paez, C.A., Poelman, D., Pirard, J.-P., Heinrichs, B. (2012) Kinetic study of *p*-nitrophenol photodegradation with modified TiO_2 xerogels. Chem. Eng. J. 191, 441–450.

[19] Meng-xiong, Z., You-ji, L., Ming-yuan, M., Wei, C., Lei-yong, L. (2013) Photocatalytic activity and kinetics for acid yellow degradation over surface composites of TiO_2-coated activated carbon under different photocatalytic conditions. Trans. Nonferrous Met. Soc. China 23,1019−1027

[20] Alahmad, W.R., Alawi, M.A. (2010) Kinetic Study of Photocatalytic Degradation of Several Pharmaceuticals Assisted by SiO_2/ TiO_2 Catalyst in Solar Bath System.Jordan Journal of Pharmaceutical Sciences 3 (2), 126-136.

[21] Lourdes, P.M., Dalida and Kristine Marie S. Amer , Chia-Chi, S., , Ming-Chun, L. (2014) Photocatalytic degradation of acetaminophen in modified TiO_2 under visible irradiation, Environ Sci Pollut Res 21,1208–1216.

[22] Neat,S., Paˆrvulescu,V.I., Epure,G., Nicoleta, P., Vasile S.¸ Ricchiardi, G., Bordiga, S., Zecchina,A. (2009) M/TiO_2/SiO_2 (M = Fe, Mn, and V) catalysts in photo-decomposition of sulfur mustard. Applied Catalysis B: Environmental 91, 546–553.

[23] Thomas, R.T., Nair, V., Sandhyarani, N.(2013). TiO_2 nanoparticle assisted solid phase photocatalytic degradation of polythene film: A mechanistic investigation. Colloids and Surfaces A Physicochem. Eng. Aspects 422, 1–9.

[24] Priya, V.S. and Philip,L. (2015) Photocatalytic Degradation of Aqueous VOCs Using N Doped TiO2: Comparison of Photocatalytic Degradation under Visible and Sunlight Irradiation. International Journal of Environmental Science and Development, 6(4), 286-291.

[25] Lin, Y., Ferronato, C., Deng, N., Wu, F., Chovelon, J.-M.(2009) Photocatalytic degradation of methylparaben by TiO_2: Multivariable experimental design and mechanism. Appl. Catal., 88, 32–41.

[26] Hemmateenejad, B., Katayoun, J., Saeidi-Boroujeni,M. (2008) Spectrophotometric monitoring of nimesulide photodegradation by a combined hard – soft multivariate curve

resolution alternative least square method. J. Pharmaceut. Biomed. Anal. 47, 625.
[27] Baran, W.E., Adamek, W., Makowski, A., (2008) The influence of selected parammeters on the photocatalytic degradation of azo-dyes in the presence of TiO_2 aqueous suspension. J. Chem Eng 145, 242.
[28] Cory,W., DeSantis, A., and Ulmer,C. (2011) Photo-degradation of Naproxen and Ibuprofen and the Formation of Ecotoxic Photoproducts in Natural Water sample, Conference Proceedings for NOM, the 4th IWA Specialty Conference on Natural Organic Matter, July 27-30 2011, Costa Mesa CA.
[29] Tolosa, N.C., Lu, M.C., Mendoza, H.D., Rollon, A.P. (2011) The effect of the composition of tri-elemental doping (K, Al, S) on the photocatalytic performance of synthesized TiO_2 nanoparticles in oxidizing 2-chlorophenol over visible light illumination. Appl Cataly A Gen 401:233–238.
[30] Ma, L. and He, D. (2009) Hydrogenolysis of Glycerol to Propanediols Over Highly Active Ru–Re Bimetallic. Catalysts Topics in Catalysis 52, 834.
[31] Lanza, R., Järås, S.G., and Canu, P. (2007) Partial oxidation of methane oversupported ruthenium catalysts. Applied Catalysis A: General 325(1), 57 -67.
[32] Ekou, T., Ekou, L., Vicente, A., Lafaye, G., Pronier,S., Especel C., Marécot, P., (2011) Citral hydrogenation over Rh and Pt catalysts supported on TiO_2: Influence of the preparation and activation protocols of the catalysts. Journal of Molecular Catalysis A Chemical 337(1-2), 82 -88.
[33] Ekou, T., Especel, C., Royer, S. (2011) Catalytic performances of large pore Ti-SBA_{15} supported Pt nanocomposites for the citral hydrogenation reaction, Catalysis Today, 173, 44-46.

Received: **07.01.2016**
Accepted: **03.08.2016**

CORRESPONDING AUTHOR

Mahmoud A. Alawi
Faculty of Sciences, Department of Chemistry, University of Jordan, Amman 11942, Jordan

Email: alawima@ju.edu.jo

© by PSP Volume 25 – No. 10/2016, pages 4309-4318 Fresenius Environmental Bulletin

DYNAMIC CHARACTERIZATION OF PARTICLE-BOUND AND DISSOLVED NUTRIENTS IN ROOF RUNOFF

Fa-hui Nie, Qing Yu*, Rong-rong Liu, Zhan-meng Liu, Biao Wang

School of Civil Engineering and Architecture, East China Jiao Tong University, Nanchang 330013, China

ABSTRACT

Typical rainfall runoff events were monitored from a concrete roof by a traffic artery in Shanghai from May 2014 to July 2014 to characterize the particle-bound and dissolved nutrients in roof runoff. Water quality parameters such as total nitrogen(TN), dissolved nitrogen(DN), total phosphorus (TP), dissolved phosphorus(DP), total suspended solids(TSS) and particle size distribution (PSD) and the variations of the pollutants concentration were analyzed. Results indicated that event mean concentrations (EMC) of TN range between 4.61 and 8.53 mg/L compared to 0.11 ～ 0.21 mg/L for TP. DN accounts for 76.7% ～ 96.0% of TN and particle-bound phosphorus(PP) 60.0% ～ 78.9% of TP. Regression analysis between TSS and TP & PP of samples in the early 10 min of runoff results in a high R^2, however, the relationship in the entire runoff is not as close as the 10 min. First flush of TP is stronger than that of TN and the discharge load of dissolved nutrients is more stable than particle nutrients. In addition, more nitrogen absorbed by small particles to a certain degree weakens the first flush of TN.

KEYWORDS:
Rainfall runoff, water quality parameters, pollutants concentration, dynamic characterization.

INTRODUCTION

Roof runoff is one of the important sources of urban non-point pollution[1-3]. In the 1990s, Forster began to study systematically the pollution characteristics of roof runoff [4]and the early research focused on first flush, the water quality of roof runoff and its influencing factors. And then, taking account of local situation, researchers from many countries investigated various aspects of roof runoff. In New Zealand, researchers examined the safety of using roof-collected rainwater as potable water [5]. And much work had been done to discuss the potential hazard of the supplement of groundwater with roof runoff in Sweden [6, 7]. In China, the effects of roof material, temperature, rainfall intensity and air pollution on the runoff characteristics in Beijing were investigated and a utilization scheme was proposed [8]. And there were also some researchers to examine the dynamic behavior of the pollutants washed from asphalt roof and the effect of antecedent dry period on the quality of roof rainwater [9, 10].

However, the above researches all took the particle-bound pollutants and the dissolved pollutants as single body to be studied, but didn't consider the difference between two kinds of existence status. As a matter of fact, because the production mechanism of particle pollutants and dissolved pollutants is different, the characteristics of particle-bound pollutants differ greatly from those of dissolved pollutants. In addition, the distribution of pollutants in solid phase and liquid phase is important for its transportation and removal in the receiving water [11, 12]. Then, it is meaningful theoretically and practically to investigate the existence status of pollutants in roof runoff.

METHODS AND DATA

Sampling Methods and Analysis Procedure. The examined concrete roof was on a building of 5 storeys by Miyun Road, which was a main artery in Shanghai with daily traffic flow of about 21000. The catchments area and the slope of the roof is about 120m^2 and 2%, respectively. The samples were taken from the outlet of roof siphon drainage system connecting

to inspection well. When runoff was generated, samples were collected at the outlet of each site with an interval of 5 min in the first 30 min followed by 10 min intervals until runoff ceased. Time of sampling and runoff volume were recorded simultaneously. Flow rate was monitored with a velocity-area flowmeter (NIVUS PCMPro). In addition, Rainfall intensity data was recorded by an automated gauge in the nearby sampling place. Rainfall patterns of sampling events were summarized in Table 1.

After being collected, all samples were brought back to the laboratory of work station for analysis. particle size distribution (PSD) was analyzed with a laser particle sizer(Ankersmid, eyetech-laser). Suspended solids(SS) were measured according to Standard Methods of APHA [13]. US EPA approved methods were used for all the other water quality analysis. All the samples were filtrated with 0.45 μm millipore filter. The filtrate was used for measuring constituents of dissolved nitrogen (DN) and dissolved phosphorus(DP). All the filtered and unfiltered water samples were digested with K2S2O7 solution simultaneously for determination of total nitrogen and total phosphorus concentrations [14].

Rainfall Data. The detailed characteristics of 6 typical rainfall events are shown in Table 1.

RESULTS AND DISCUSSION

The quality of roof runoff. Usually an event mean concentration(EMC) is used to evaluate the effects of stormwater runoff on receiving water [9] and its value is computed as the total pollutant mass divided by the total runoff volume. The related statistical values are shown in Table 2.

TABLE 1
The major characteristics of 6 rainfall events.

No	Rainfall event	Rainfall/mm	Duration/min	Rainfall intensity /mm·min^{-1}	Antecedent dry weather period/d	The last rainfall/mm
1	2014-05-09	18.9	86	0.219	2.28	3.8
2	2014-05-26	39.8	97	0.410	4.44	5.6
3	2014-06-07	46.1	71	0.649	3.13	10.9
4	2014-06-22	8.66	23	0.377	8.14	16.1
5	2014-06-27	31.8	108	0.294	10.35	12.4
6	2014-07-05	22.7	52	0.437	1.11	36.7

TABLE 2
The existence status of roof runoff nutrients.

No.	EMC Rainfall event	TN/ mg·L^{-1}	DN/ mg·L^{-1}	DN/ TN(%)	TP/ mg·L^{-1}	PP/ mg·L^{-1}	PP/ TP(%)	TSS/ mg·L^{-1}
1	2014-05-09	5.18	4.79	92.5	0.18	0.11	61.1	78.1
2	2014-05-26	4.67	3.58	76.7	0.19	0.15	78.9	148.6
3	2014-06-07	4.61	3.92	85.0	0.15	0.09	60.0	36.8
4	2014-06-22	7.86	6.71	85.4	0.16	0.12	75.0	152.6
5	2014-06-27	5.49	4.47	81.4	0.21	0.15	71.4	146.9
6	2014-07-05	8.53	8.19	96.0	0.11	0.06	54.5	31.9
	average	6.06	5.28	86.20	0.17	0.11	66.82	99.20
	Variation coefficient	0.256	0.311	0.075	0.192	0.292	0.132	0.524

As indicated in Table 2, both EMC and its average of TN exceed class V according to the Environmental quality standards for surface water (GB 3838-2002), while EMC and its average of TP are lower than III class. The variation of EMC of both TN and TP is similar (0.256 and 0.192, respectively). DN is the main form of TN, accounting for 81.4%, while 76.7% of TP is in the particle-bound form. The average of TN in 6 roof runoff was 6.06 mg/L and the background value of TN in natural rainwater approximated to the average TN(4.74 mg/L) of natural rainfall in Shanghai from 1998 to 2003 [15], then it could be estimated that natural rainfall contributes to 78.2% of TN in 6 roof runoffs, that is to say, natural rainfall is the most important source of TN in roof runoff.

Dynamic behavior of particle size distribution (PSD). Particles is one of the most important pollutants, which has attracted much attention in the non-point pollution study [16]. In addition, as the absorbed pollutant concentration varied throughout the particle size [17], examining the variation of PSD in the runoff process can help understand the dynamic behavior of pollutant concentration. In this work, all samples from 2 rainfall events were analyzed for PSD.

As shown in Figure 1, one of the main characteristics of runoff process in 2014-06-27 was tow flow peaks. After the runoff was generated, the number ratio of small particles gradually increased until 12:42. But the number ratio of large particles rose compared with the sample in 12:42 and approximated to that of 12:37, which was because the flow increase enhanced washing on roof and more large particles were produced. Then along with the runoff, the number ratio of small particles increased again.

Compared with the runoff in 2014-06-27, runoff process in 2014-07-05 only had one flow peak. Under this flow condition, the number ratio of small particles increased slowly from 16:43 to 16:53, which was similar to that of the initial runoff in 2014-06-27. The affected by the flow peak, the number ratio of large particles increased slightly and approximated to that of 16:53 soon. In the final phase(17:08～17;33), the particle size distribution was kept almost still.

Dynamic behavior of nutrients in roof runoff. Taking 2 runoff process (2014-05-09 and 2014-06-07) as example, the variation of nutrients' concentration was shown in Figure 2.

As shown in Figure 2 and 3, the variation of TSS have a very close relationship with flow rate. Both the flow process and TSS concentration process in 2014-05-09 only have one peak and those in 2014-06-07 represents fluctuation. In both two runoff processes, the dynamic behavior of TP was similar to TSS, but the TN-TSS relationship in the course of runoff was not obvious.

As discussed, the PSD of samples varied throughout the runoff process. It was easy to know that PP/TSS and PN/TSS were greatly influenced by the nutrient concentration on particles of various sizes. The variation of PP/TSS and PN/TSS of the runoff in 2014-06-07 was not regular. But PN/TSS in the late phase in 2014-05-09 represented a stable rise. The flow process in 2014-05-09 was similar to that of 2014-07-05, it was expected that the number ratio of small particles would increase gradually or keep stable. Then it could be inferred that if nitrogen concentration on particles of any size was permanent, nitrogen on unit mass particle was more on small particles than large particles. In the same period, PP/TSS was nearly stable, which meant that the variation of PSD in the late phase of runoff had no great effect on PP concentration on particles.

However, PP/TSS represented more variation in the entire runoff process. The core relation between TSS and TP & PP of all samples in the early 10 minutes and the entire course of roof runoff was analyzed. As shown in Figure. 4, in the early 10 minutes, TSS and TP & PP represented a high degree of correlation(R2 was 0.9194 and 0.9475, respectively), while the correlation of them in the entire runoff was weaker(R2 was 0.8069 and 0.8278, respectively), which indicated the fluctuation of phosphorus mass per unit mass particle in the entire runoff is more than that in the early 10 minutes.

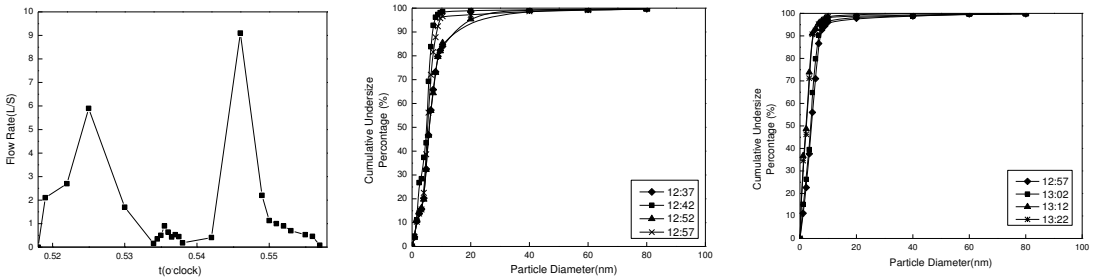

(a) 2014-06-27

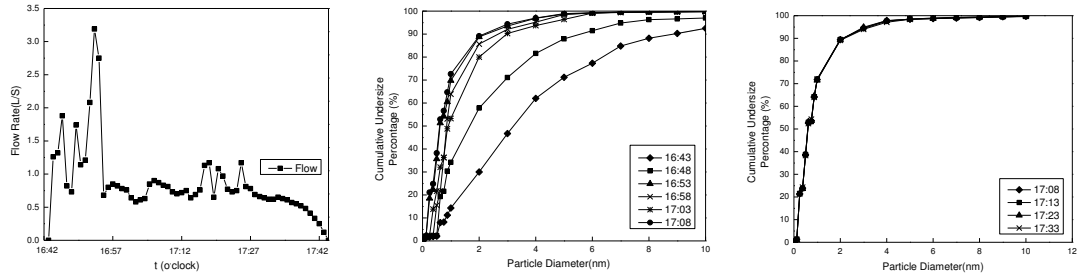

(b) 2014-07-05

FIGURE 1
Dynamic behavior of particle size distribution.

First flush. First flush has been utilized to indicate a disproportionately high delivery of either concentration or mass of a constituent during the initial portions of a rainfall runoff event and accordingly it can be classified into concentration-based first flush(CBFF) and mass-base first flush(MBFF) [18]. In this study, M(V) curve was used to characterize the MBFF [19, 20]. The horizontal coordinate is the ratio of v(t) (flow volume up to time t) to V(total volume of flow over entire event duration) and the vertical coordinate is the ratio of m(t) (mass transported up to time t) to M(total mass of constituent over entire event duration). When m(t)/M exceeds v(t)/T, it can be considered that first flush exists. The more m(t)/M exceeds v(t)/V, the more obvious first flush is.

As indicated in Figure. 6, TN only represented an obvious first flush in the runoff 2014-06-27, but in other 3 runoff events the discharge of TN load was much even. Compared with TN, TP showed an obvious first flush in all runoff events with the exception of event in 2014-06-07 and its first flush was much similar to that of TSS. Because the main component of TN and TP was DN and PP, respectively, it could be concluded that the discharge load of dissolved matter was evener than that of particle matter, which was primarily attributed to their production mechanism: particles mainly came from roof washing, which was influenced greatly by the flow rate, while the dissolved matter resulted from the dissolution of pollutants in runoff or natural rainwater, which was affected weakly by the flow rate or rainfall. In addition, first flush of TN was to a certain degree weakened by more nitrogen attached on large particles in comparison with small particles in the late runoff phase would increase according to the analysis of 2.2 and 2.3. Because of high PN concentration on small particles, the decrease of TN concentration had slow down and the strength of first flush of TN was weakened. It can also be expected that the existence of first flush of TN in 2014-06-07 and 2014-06-27 related somewhat to the flow fluctuation and the corresponding variation of PSD.

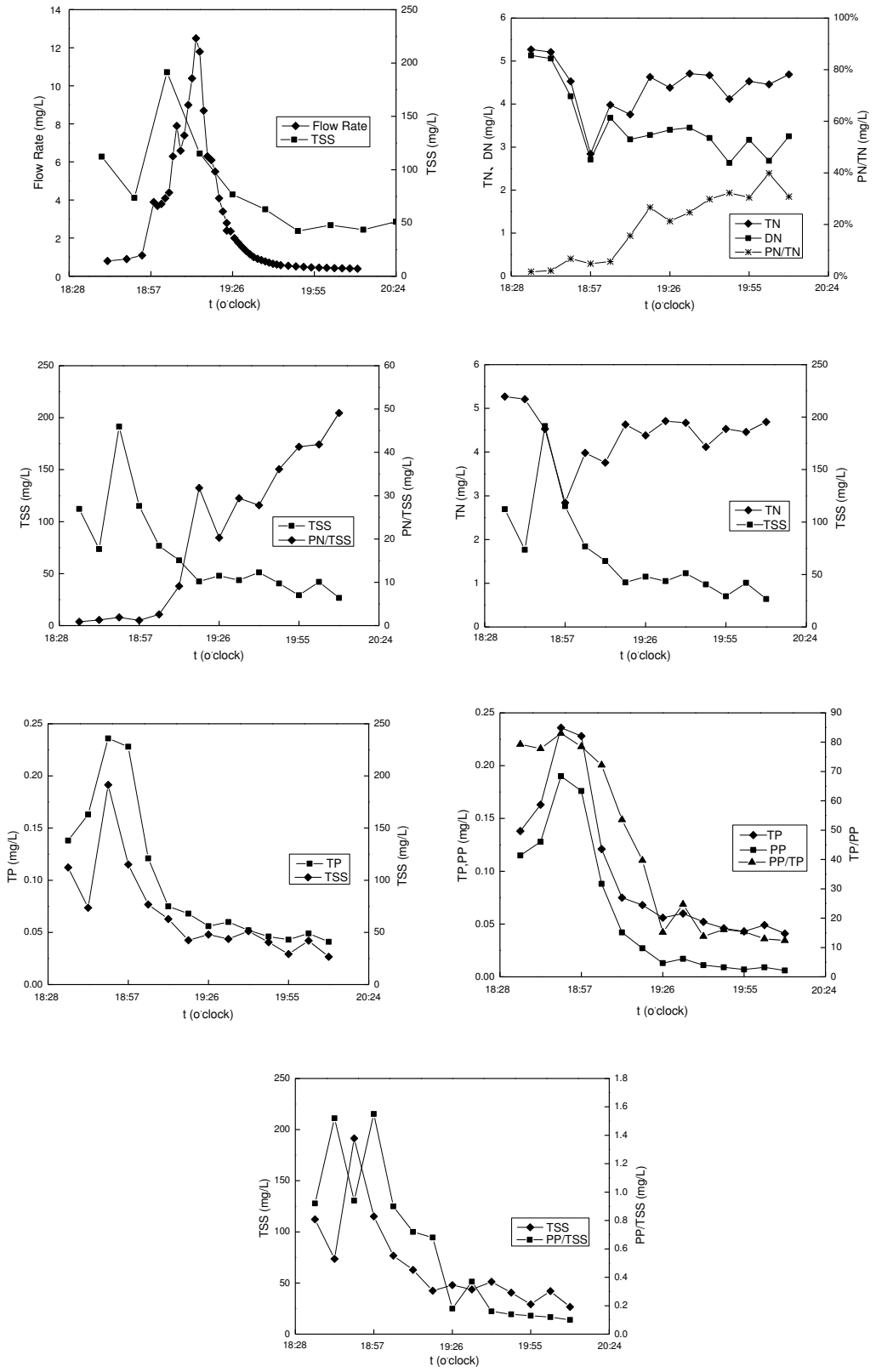

FIGURE 2
Dynamic behavior of nutrients of roof runoff (2014-05-09).

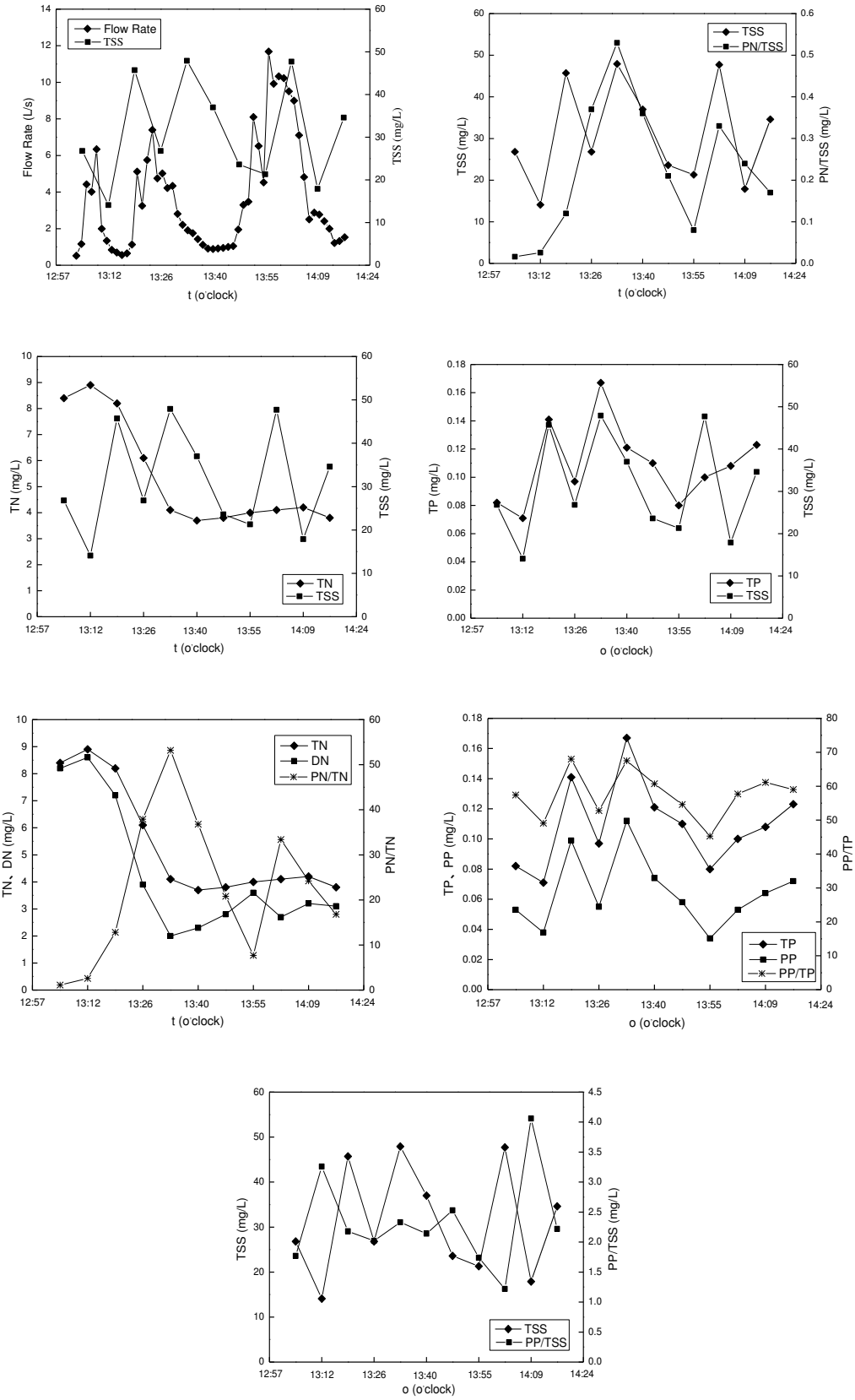

FIGURE 3
Dynamic behavior of nutrients of roof runoff (2014-06-07).

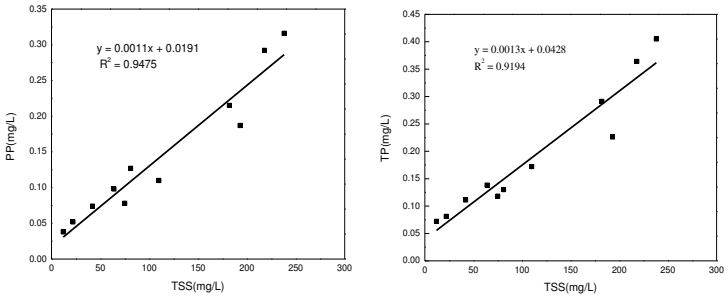

FIGURE 4
Correlation between TSS and TP & PP in the early 10 minutes of roof runoff.

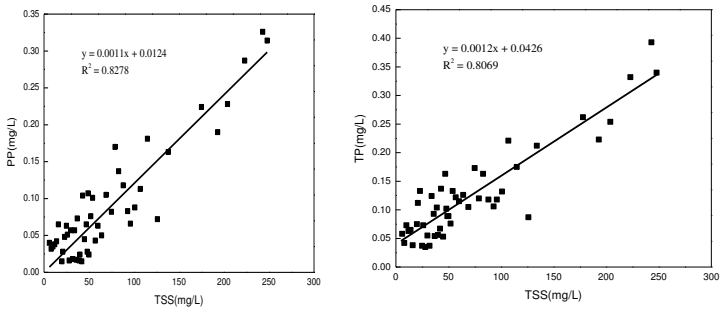

FIGURE 5
Correlation between TSS and TP & PP in the entire roof runoff.

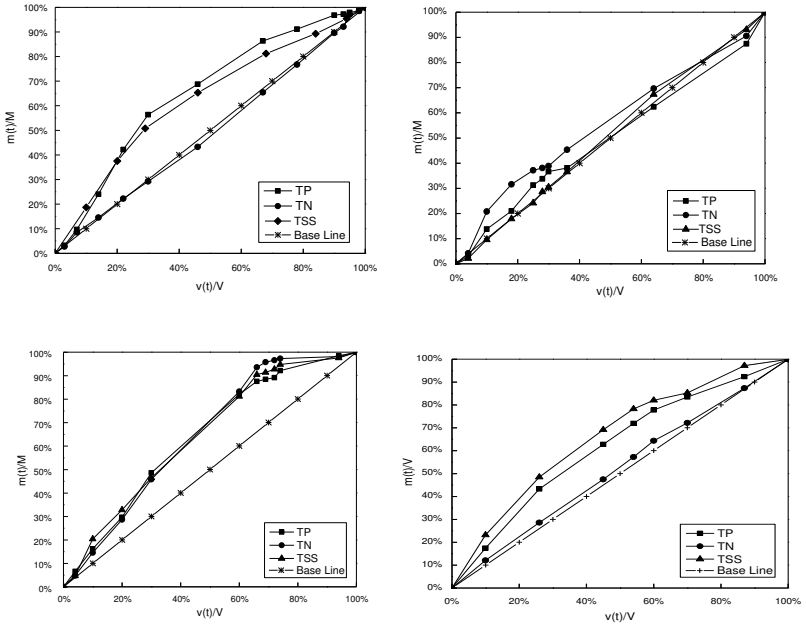

FIGURE 6
First flush analysis of 4 roo f runoff events.

CONCLUSION

The dynamic behavior of PSD has a very close relationship with the flow process. TSS concentration varies with the change of flow rate. The dynamic behavior of TP is similar to TSS, but the TN-TSS relationship in the course of runoff is not obvious. In the late runoff phase, the PSD has a great influence on the PN/TSS but little effect on PP/TSS. The variation of PP/TSS of the entire runoff process is greater than that of the early 10 minutes.

TP represents first flush more frequently than TN. In addition, the variation of PSD and more nitrogen attached on small particles to a certain degree weaken first flush of TN.

ACKNOWLEDGEMENTS

The authors gratefully acknowledge the economic support to Natural Science-Foundation of China(Project No.: 51168031) and Science and Technology Support Project of Jiangxi, China (Project No.: 20151BBF60031).

REFERENCES

[1] Daub J., Förster J., Herrmann R., Robien A.and Striebel T. (2014)Chemodynamics of trace pollutants during snowmelt on roof and street surfaces. Research, 30(1), 73-85.

[2] Hou P., Ren Y., Zhang Q., Lu F., Ouyang Z.and Wang X. (2012)Nitrogen and phosphorous in atmospheric deposition and roof runoff. Polish Journal of Environmental Studies, 21(6), 1621-1627.

[3] Teemusk A.and Mander Ü. (2011)The Influence of Green Roofs on Runoff Water Quality: A Case Study from Estonia. Water Resources Management, 25(14), 3699-3713.

[4] Förster J. (1999)Variability of roof runoff quality. Water Science & Technology, volume 39(5), 137-144(138).

[5] Simmons G., Hope V., Lewis G., Whitmore J.and Gao W. (2001)Contamination of potable roof-collected rainwater in Auckland, New Zealand. Water Research, 35(6), 1518-1524.

[6] Barrett M.E., Malina J.F., Charbeneau R.J.and Ward G.H. (1998)Characterization of Highway Runoff in Austin, Texas, Area. Journal of Environmental Engineering, 124(2), 131-137.

[7] Bucheli T.D., Müller S.R., Andreas Voegelin A.and Schwarzenbach R.P. (1998)Bituminous Roof Sealing Membranes as Major Sources of the Herbicide (R,S)-Mecoprop in Roof Runoff Waters: Potential Contamination of Groundwater and Surface Waters. Environmental Science & Technology, 32(22), 3465-3471.

[8] Hou L.and Zhang X. (2014)Comparing urban runoff quality of a felt roof and an asphalt road in Beijing. Hydrology Research, 45(2), 282-291.

[9] Debusk K.M.and Hunt W.F. (2014)Water Quality Benefits of Harvesting Rooftop Runoff. World Environmental and Water Resources Congress, 592-602.

[10] Zhang Q., Wang X., Hou P., Wan W., Li R. and Ren Y.. (2014)Quality and seasonal variation of rainwater harvested from concrete, asphalt, ceramic tile and green roofs in Chongqing, China. Journal of Environmental Management, 132C(132C), 178-187.

[11] Bielmyer G.K., Arnold W.R., Tomasso J.R., Isely J.J.and Klaine S.J. (2011)Effects of roof and rainwater characteristics on copper concentrations in roof runoff. Environmental Monitoring & Assessment, 184(5), 2797-2804.

[12] Characklis G.W., Dilts M.J., Iii O.D.S., Likirdopulos C.A., Krometis L.A.H.and Sobsey M.D. (2005)Microbial partitioning to settleable particles in stormwater. Water Research, 39(9), 1773-1782.

[13] APHA(American Public Health Association). (1992) American Water Works Association, and Water Environment Federation. Standard methods for the examination of water and wastewater[M]. Washington, DC: Am Public Health Assoc.

[14] Ebina J., Tsutsui T.and Shirai T. (1983)Simultaneous determination of total nitrogen and total phosphorus in water using peroxodisulfate oxidation. Water Research, 17(12), 1721-1726.

[15] Zhang X. (2006)Atmospheric nitrogen wet deposition and its effects on wetland water environment of Shanghai area. The journal of applied ecology / Zhongguo sheng tai xue xue hui, Zhongguo ke xue yuan Shenyang ying yong sheng tai yan jiu suo

zhu ban, 17(6), 1099-1102.
[16] Wang L.Y., Qin H.P., Tan X.L., Kang-Mao H.E.and Tang Q.L. (2013)Study on Water Quality of Roof-Runoff Affected by Atmospheric Wet Deposition in Shenzhen. Environmental Science & Technology,
[17] Li-Qing L.I., Shu-Cong L., Zhu R.X., Liu Z.Q.and Shan B.Q. (2012)Nitrogen and Phosphorus Composition in Urban Runoff from the New Development Area in Beijing. Huan jing ke xue, 33(33), 3760-3767.
[18] Sansalone J.J.and Cristina C.M. (2004)First Flush Concepts for Suspended and Dissolved Solids in Small Impervious Watersheds. Journal of Environmental Engineering, 130(11), 1301-1314.
[19] Athanasiadis K., Horn H.and Helmreich B. (2010)A field study on the first flush effect of copper roof runoff. Corrosion Science, 52(1), 21-29.
[20] Sansalone J.J.and Buchberger S.G. (1997)Partitioning and First Flush of Metals in Urban Roadway Storm Water. Journal of Environmental Engineering, 123(2), 134-143.

Received: **19.01.2016**
Accepted: **19.07.2016**

CORRESPONDING AUTHOR

Qing Yu
School of Civil Engineering and Architecture
East China Jiao Tong University
Nanchang , 330013 P.R.CHINA

Email: yuqing171984@163.com

© by PSP Volume 25 – No. 10/2016, pages 4318-4323 Fresenius Environmental Bulletin

POTENTIAL OF DIFFERENT EUROPEAN WHITE ELM (ULMUS LAEVIS PALL.) GENOTYPES FOR PHYTOEXTRACTION OF HEAVY METALS

Jovana Devetakovic[1,*], Dragica Stankovic[1], Vladan Ivetic[1], Mirjana Sijacic-Nikolic[1], Zoran Maksimovic[2]

[1]Faculty of Forestry, University of Belgrade, Kneza Višeslava St. No.1, Belgrade, Serbia
[2]SE "Srbijašume", Bul.Mihajla Pupina St. No.113, Belgrade, Serbia

ABSTRACT

This research present the content of lead and nickel in the soil and plants from the area of Protected natural resource "Veliko ratno ostrvo". The concentration of heavy metals Pb and Ni was investigated in the vegetative parts European white elm - *Ulmus laevis* Pall..

The research objective of this paper is focused on the evaluation of the potential of different European white elm genotypes to the uptake of heavy metals and their accumulation in the leaves of plants, also as determine potential ability of European white elm for phytoextraction.

The concentration of heavy metals in leaves of European white elm shows a statistically significant difference between the trees, and different genotypes, having as good batteries are specifically allocated tree 19, 21 and 35.

KEYWORDS:
Veliko ratno ostrvo, lead, nickel, protected natural area, contamination.

INTRODUCTION

Veliko ratno ostrvo is an island at the confluence of the Sava and Danube near Belgrade, and due to their beauty, location and ecological importance represents a protected natural area. Total area of protected natural area is 211 ha 36 a 78 m^2 and consists from two islands, Veliko and Malo ratno ostrvo. Vegetation and forests on the island belong floodplain forests and wetland vegetation type. The island represent very important habitat for some bird species and favorit resort of many people [1].

European white elm (*Ulmus laevis* Pall.) as a common species of European riparian forest exist here, but natural population of this species is reduce, also as across Europe [2]. The main reason for extinction this species is draining wetland habitats for growing poplar and needs of agricultural production, while other species which belong Ulmus genus are endangered by DED [3].

Some of the main features of this species, such as rapid growth, ornamental value, tolerance to compaction and soil salinity, resistance to air pollution and greater resistance to DED, classified as a species suitable for use in urban areas [3,4]. Previously mentioned is just one of the motives for this type of research. Consequently, the aim of this study was focused on the genetic evaluation of the potential of different European white elm genotypes to the uptake of heavy metals and their accumulation in the leaves of plants, and to determine potential ability of European white elm for phytoextraction.

MATERIAL AND METHODS

Natural population of European white elm at Veliko ratno ostvo island include 89 different genotypes which are distributed across island. Selection of genotypes was carefully chosen and sample of 13 European white elm trees was taken for analysis.

Soil samples for analysis of heavy metal content is collected on 5 sites at Veliko ratno ostrvo island and every sample consist soil sample from 3 different depth of soil (0-10 cm; 10-20 cm; 20-40 cm) (Figure 1).

Leaves and soil sample are collected on September 2014th. Samples are dried on air temperature and after that prepared for laboratory analysis.

FIGURE 1
Distribution of selected trees and sites at Veliko ratno ostrvo island

TABLE 1
Concentration of haevy metals Pb and Ni in soil at Veliko ratno ostrvo island

SOIL LAYER	Pb	Ni
	SITE 1	
0-10 cm	43.29	24.48
10-20cm	44.08	25.28
20-40cm	43.32	25.01
AVERAGE	**43.56**	**24.92**
	SITE 2	
0-10cm	85.26	37.08
10-20cm	88.36	39.04
20-40cm	70.96	34.60
AVERAGE	**81.53**	**36.91**
	SITE 3	
0-10cm	71.37	35.72
10-20 cm	44.32	33.92
20-40cm	39.06	32.55
AVERAGE	**51.58**	**34.06**
	SITE 4	
0-10 cm	83.19	36.09
10-20 cm	32.92	28.95
20-40 cm	30.31	33.51
AVERAGE	**48.81**	**32.85**
	SITE 5	
0-10 cm	77.67	38.47
10-20 cm	76.52	29.22
20-40 cm	65.80	26.86
AVERAGE	**73.33**	**31.52**
TOTAL AVERAGE	**59.76**	**32.05**

TABLE 2
Analysis of variance between 13 European white elm genotypes

ANOVA One-Way p < .05000								
	SS	**Df**	**MS**	**SS**	**df**	**MS**	**F**	**p**
Pb	3.06271	12	0.255226	1.483646	26	0.057063	4.47268	0.000678
Ni	48.96920	12	4.080767	1.202378	26	0.046245	88.24176	0.000000

The milled soil (3g) was digested with aqua regia under reflux for 2 hours with water-cooled condensers on a digestion block using the standard procedure [5]. The digest was cooled, filtered and diluted with 0.5 M HNO3. The available Pb and Ni contents of soils were determined by extraction in the DTPA (a mixture of 0.005 mol l-1 DTPA, 0.01 mol l-1 CaCl2, 0.1 mol l-1 triethanolamine (TEA) with the pH adjusted to 7.3 and with a 1 mol l-1 HCl solution).

The leaves are milled into powder. The Pb and Ni contents were determined using the same procedure as the one described for determining aqua regia-extractable trace elements in soil samples.

Analyses were performed in the laboratories of the Faculty of Forestry, University of Belgrade. The contents of Pb and Ni were determined by flame atomic absorption spectrophotometer.

The obtained values were processed using STATISTICA 7.0, and descriptiv statistic, analysis of variance, post-hoc Tukey HSD test and cluster analysis were done. The results are presented in tables and charts.

RESULTS

The content of heavy metals in the soil is in the range of 43.56 mg kg^{-1} at the site 1 to 81.53 mg kg^{-1} at the site 2 for lead and of 24.92 mg kg^{-1} at the site 1 to 36.91 mg kg^{-1} at the site 2 for nickel (Table 1). Soil at Veliko ratno ostrvo island is selective, because it different absorbs elements, so that the first layers generally contain the highest concentrations of heavy metals.

The content of lead and nickel in the soil of all five examined localities, i.e. in the area Veliko ratno ostrvo island, does not exceed the legally permitted quantities (Critical values: Pb = 100 ppm, Ni = 50 ppm) [6], what indicating that soil at the area do not contaminated with the heavy metals.

Concentrations of heavy metals in leaves are significantly different between all 13 European white elm tested genotypes (Tables 2 and 3).

Based on these facts, it can be concluded that the greatest potential for phytoextraction of lead shows genotype 35 at site 3 and for phytoextraction of nickel genotypes 19 and 21 at the site 2. The lowest potential for phytoextraction of both tested elements (lead and nickel), was recorded in leaves of the tree 29 on the site 1 (Table 3).

TABLE 3
Average values (results of Tukey HSD post hoc test), standard deviation (variance) and minima and maxima values at tested genotypes

GENOTYPE		**Pb**			**Ni**		
		MEANS	STD.DEV.(VARIANCE)	MIN-MAX	MEANS	STD.DEV.(VARIANCE)	MIN-MAX
1.	**13**	$1,24^{bc}$	0,20(0,04)	1,03-1,44	$1,45^{b}$	0,31(0,10)	1,12-1,74
2.	**14**	$0,95^{abc}$	0,22(0,05)	0,70-1,11	$1,40^{ab}$	0,11(0,01)	1,32-1,53
3.	**18**	$1,18^{bc}$	0,18(0,03)	0,99-1,35	$2,83^{ef}$	0,21(0,04)	2,61-3,02
4.	**19**	$1,28^{bc}$	0,04(0,00)	1,23-1,32	$4,52^{g}$	0,18(0,03)	4,37-4,72
5.	**21**	$0,87^{abc}$	0,22(0,05)	0,69-1,12	$4,92^{g}$	0,19(0,04)	4,72-5,10
6.	**29**	$0,45^{a}$	0,27(0,07)	0,24-0,75	$0,77^{a}$	0,19(0,04)	0,58-0,96
7.	**31**	$0,69^{ab}$	0,24(0,06)	0,49-0,95	$2,15^{cd}$	0,17(0,03)	1,96-2,30
8.	**32**	$1,40^{bc}$	0,29(0,09)	1,16-1,73	$2,03^{bc}$	0,11(0,01)	1,93-2,14
9.	**33**	$1,14^{abc}$	0,21(0,04)	0,90-1,27	$2,45^{cde}$	0,13(0,02)	2,30-2,56
10.	**34**	$1,12^{abc}$	0,12(0,01)	0,99-1,22	$2,29^{cde}$	0,30(0,09)	2,00-2,60
11.	**35**	$1,54^{c}$	0,25(0,06)	1,26-1,74	$3,18^{f}$	0,20(0,04)	3,00-3,40
12.	**36**	$1,04^{abc}$	0,46(0,021)	0,76-1,58	$2,73^{def}$	0,37(0,14)	2,39-3,13
13.	**37**	$0,97^{abc}$	0,13(0,02)	0,82-1,07	$2,91^{ef}$	0,10(0,01)	2,85-3,03
AVERAGE		1,07	0,35 (0,12)	0,24-1,74	2,59	1,15(0,05)	0,58-5,10
Average ECCE[7]**			**0,1-5**			**0.4-4**	

*Tukey HSD post hoc test

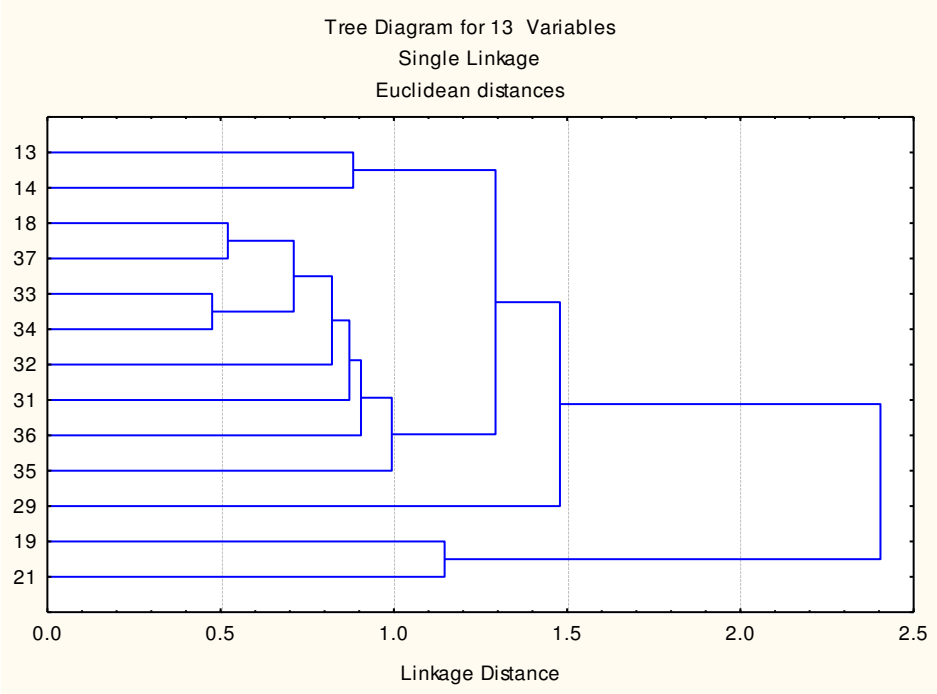

FIGURE 1
The dendrogram of cluster analysis for 13 different European white elm genotypes based on the content of heavy metals (Ni and Pb) in leaves

Content of Pb and Ni in leaves of different European white elm genotypes primarily affects of genotype. The contents of Pb and Ni in leaves of different genotypes is consequence of the genotype, which can be explained by differences between trees which are on same site. The presence of significantly higher concentrations of nickel in leaves taken from the site 2, indicating existence of chemical contamination of soil with this pollutant. These findings confirmed by the data of average values on all layers of soil on the site 2 that are larger than the other sites. Average nickel concentrations in soils are 36,91 mg kg^{-1}, but do not in excess of critical values (Table 1).

For a clearer overview of relations and the accumulation of heavy metals in all tested genotypes, cluster analysis was performed. The aim of cluster analysis is formation of groups where similar objects will be in a same group. Similarity is operationalized usually as a kind of distance. In these studies cluster analysis for 13 different genotypes of Ulmus laevis is made on the basis of the content of heavy metals (Ni and Pb) in leaves (Figure 1). Genotypes were grouped into groups (clusters) on the basis of statistical closeness potential in phytoextraction of analyzed heavy metals. Genotypes 29 and genotypes 19 and 21, which constitute a special group, are grouped at the highest distance, than other trees which are grouped at the separate group. Specificity of genotypes 29 and 19 and 21, which recorded large potential in the phytoextraction of heavy metals, is also reflected in their grouping, a relatively large distance to each other, and with all other analyzed genotypes.

DISCUSSION

Plants, also as soil, pollute often a combination of different pollutants do not just only one [8, 9]. The elements that participate in plant tissue do not have the same significance. Some are necessary because without them plants can not normally complete their life cycle, the other can have a stimulating effect, while a group of elements, especially heavy metals, at higher concentrations have very toxic effect to plants [10, 11].

All of the heavy metals are toxic in large quantities and it should be emphasized. Knowledge about accumulation and toxic effects of heavy metals in all environmental media is extremely important, because on that way they enter in the food chain [12, 13].

Previous studies, which research the potential of different woody species genotypes for heavy metals phytoextraction showed that tolerance to a greater extent correlated with the genotype, ie. hybrids than with the species as a taxonomic category. Accumulation degree of heavy metals in plant tissue is determined by numerous of biotic and abiotic factors, but the genotypic specificity is one of the dominant factors [14, 15, 16].

Numerous toxic effects of heavy metals endanger the survival of species that live in polluted

environment. Accumulation of heavy metals as well as those with predominantly toxic effects for plants in the soil, may be due to natural lithogenic and pedogenic processes [17], or anthropogenic factors which result in environmental pollution [18].

Accumulation and concentration of heavy metals in plant tissues indicate an important role of some plant species as indicators for pollution degree of environment [19, 20, 21].

Adaptation or resistance of plants involves the submission of effect on the plant. Therefore, certain plant species including Ulmus species, have not only a certain resistance to low or high temperatures, to the mineral nutrition, and even to a particular anion and cation, accumulation of pollutants, including diseases etc. However, an adaptation is complex and on the degree of submission have effect biological characteristics of the plants, but on the other hand a number of factors of the environment, during the life of the plant, but and in a certain moment of evaluating resistance [22].

According Pählosson-Balsberg [23] lead concentration in plant tissue of forest trees, which do not cause damage effects is Pb <15 mg g^{-1}, and a decrease in physiological activity and growth in the case where lead concentrations greater than 20-70 mg g^{-1}.

Nickel is considered as necessary element for woody plants [24], on the other hand, a high concentration of nickel are toxic for plants [25].

Increased quantities of this element can be the result of natural or anthropogenic factors. Kabat-Pendias and Pendias [26] found a value of 0.19 - 9 mg kg^{-1} of dry matter in the aboveground parts of herbaceous plants on contaminated soil, while the content of lead on contaminated soils was 63-232 mg kg^{-1}. The same authors state that the natural concentration of lead in plants is in range 5 -10 mg kg^{-1}.

The average concentration Ni is 40 mg kg^{-1} soil, although the concentration varies greatly depending on the type of soil [27].

Limit values of Pb in soil which may be tolerated are from 50 to 100 mg kg-1, but the negative effects of the increase of lead content in the soil observed at a concentration of 50 to 250 mg kg^{-1} [28].

In the area of the specific effects of microelements on physiological and biochemical processes and now has unexplained facts about their necessity and biological function, and in future it will be continue and probably very topical issues for research Limit values of Pb in soil can be tolerated are from 50 to 100 mg kg^{-1}, but the negative effects of the increase of lead content in the soil observed at a concentration of 50 to 250 mg kg^{-1} [22].

CONCLUSION

One can say that the area of Veliko ratno ostrvo island is ecologically preserved, which is in accordance with the declaration for the protected area. Clearly, it should be noted that the concentration of heavy metals in the soil at protected natural resource Veliko ratno ostrvo do not show a danger to the emergence of visible damage to plants, for now. It is confirmed by the analysis of plant materials, but also is necessary to constantly monitoring the situation of pollution in this area, in order to timely detect the negative effects and take appropriate protection measures.

This research can be a good basis for future research which would include European white elm. It will be necessary to test different genotypes on the contaminated soils and their response to different pollutants. In this case protected natural area Veliko ratno ostrvo do not contaminated but differences between genotypes are statistical significance and exist .

REFERENCES

[1] Special base of forest managment (2008-2017) for GJ "Veliko ratno ostrvo".Faculty of Forestry-University of Belgrade, Belgrade, 1-85 (in Serbian).

[2] Mackenthun, G.H. (2000): The role of Ulmus laevis in German floodplain landscapes. Invest Agrar: Sist Recur For, 13 (1), 55-63.

[3] Collin, E. (2003): EUFORGEN Technical Guidelines for genetic conservation and use for European white elm (Ulmus laevis). International Plant Genetic Resources Institute, Rome, Italy. 6 pages

[4] Kadović, R., Knežević, M. (2002): Heavy metals in forest ecosystems of Serbia. Faculty of Forestry-University of Belgrade,Belgrade, 278 (in Serbian)

[5] International Organization for Standardization ISO 11466:1005 Soil quality 1995 In: Extraction of Trace Elements Soluble in Aqua Regia, BSI, London.

[6] Official Gazette of Republic of Serbia, No.23 / 1993. (in Serbian).

[7] Element Concentration Cadaster in Ecosystems - ECCE, (1994): Progres Report, presented at the 25th general Assembly of International Union of Biological Sciences, Paris.

[8] Stanković, D., Šijačić-Nikolić M., IVETIĆ V., Karić D., Veselinović M. (2014): Iron (Fe) content in vegetation cover of the natural protected area Kosmaj (Serbia). Fresen. Environ. Bull. 24 (2): 1-6

[9] Stanković, D., Jokanović, D., Veselinović, M., Letić, Lj., Jović, Đ., Karić, D. (2015): Zinc concentration in woody and herbaceous plants

at Kosmaj area, Fresen. Environ. Bull., Freising-Germany (in press, accepted).
[10] Stanković, D., Krstić, B., Nikolić, N. (2008): Effect of trafic on the soil contamination with polyciclyc aromatic hydrocarbons (PAHs) Journal of Biotechnology & Biotechnological Equipment 22, 2, 736-741.
[11] Stanković, D., Šijačić-Nikolić, M., Krstić B., Vilotić D. (2009): Heavy metals in the leaves of tree species Paulownia elongata S.Y.Hu in the region of the city of Belgrade. Biotechnology&BiotechnologicalEquipment.Diagnosis,Volume 23, Number 3., 1330-1336.
[12] Krstić, B., Stanković, D., Nikolić, N. (2008): Effect of traffic on the concentration of PAHs in NP „FRUŠKA GORA" . Journal of Biotechnology & Biotechnological Equipment. Sofia, Bulgaria, 736-741.
[13] Stankovic, D, Krstic, B., Igic, R., Trivan, G., Petrovic, N., Jovic Dj. (2011): Concentration of pollutants in the air, soil and plants in the area of National Park "Fruska gora" – Serbia. Fresen. Environ. Bull., Psp.Germany, 20(1), 44-50.
[14] Kraljević-Balalić, M., Mladenovo, N., Balalić, I., Zorić, M. (2009): Variability of leaf cadmium content in tetraploid and hexaploid wheat. Genetika, 41 (1), 1-10.
[15] Borišev, M. (2010): Potential of willow (Salix spp.) clones for heavy metal phytoextraction. Faculty of Science-University of Novi Sad, PhD thesis, 1-187.
[16] Sijacic-Nikolic, M., Stankovic, D., Krstic, B., Vilotic, D., Ivetic, V. (2012): The Potential of Different Lime Tree (Tilia spp) Genotypes for Phytoextraction of Heavy Metals. GENETIKA-BELGRADE, 44 (3), 537-548.
[17] Woolhouse, H.W. (1983): Toxicity and tolerance in the response of plants to metals. IN: Encyclopedia of Planr Phisiol., New Series, Vol. 12 C, Springer-Verlag, New York, Heidelberg, Berlin, 246-289.
[18] Piperski, J., Radišić, A. (2003): Kvalitet ambijentalnog vazduha: Zakonska regulativa EU i Republike Srbije. Eko konferencija 2003, 24-27 septembra, Novi Sad 251-255.
[19] Ten Houten, J. G. (1983): Biological indicators of air pollution. Environmental monitoring and assessment 3 (3-4), 257-261.
[20] Prasad, M. N. V., Freitas H. M. (2003): Metal hyperaccumulation in plants – biodiversity prospecting for phytoremediation technology. Electronic Journal of Biotechnology, 6 (3), 286-290.
[21] Stanković, D., Medarević, M., Krstić, B., Bjelanović, I., Šljukić, B., Karić, D., Janić, M. (2013): Concentration of heavy metals and stand state of Sesille oak (Quercus petraea (Matt.) Liebl.) on Avala mountain (SERBIA). Carpathian Journal of Earth and Environmental Sciences, 8 (3), 59-66.
[22] Krstić, B. Oljača, R., Stanković, D., 2011: Physiology of woody plants. University of Banja Luka, Faculty of Forestry (Fiziologija drvenastih biljaka. Univerzitet u Banjoj Luci, Šumarski fakultet), Banja Luka, p. 352. (in Serbian)
[23] Pählosson-Balsberg, A.M. (1989): Toxycity of heavy metals (Zn, Cu, Cd, Pb) to vascular plants. A literature review, Water, Air and Soil Poll. 47, Kluwer Academic Publishers, Amsterdam, 287-319
[24] Brown, P.M., Welch, R.M., Cary, E.E., Checkai, R.T (1987): Beneficial effects of nickel on plant growth. J. Plant Nutr.10, 2125-2135.
[25] Yang, X., Baligar, V.C., Martens, D.C., Clark, R.B (1996): Plant tolerance to nickel toxicity Influx, transport, and accumulation of nickel in four specie. J. Plant. Nutr., 19 (1), 73-85.
[26] Kabata-Pendias A., Pendias X.(1989): Agricultural trace elements in soils and plants. M/: Mir, 439.
[27] Brooks, R. R. (1987): Serpentine and its vegetation: a multidisciplinary approach. Dioscorides Press, Portland, Oregon, USA.
[28] Vrbek, B., Pilaš, I. (2004): Heavy metals (Pb, Cu and Zn) in the soil of a peduncled oak and common hornbeam forest (Carpino betuli-Quercetum roboris, Anić 1956/emed. Rauš 1969) in north-west Croatia. Radovi, Croatian Forest Research Institute, 39 (2): 169-184 (in Croatian).

Received: **21.12.2015**
Accepted: **21.07.2016**

CORRESPONDING AUTHOR

Jovana Devetakovic
University of Belgrade
Faculty of Forestry
Kneza Višeslava St. No. 1
11000 Belgrade
SERBIA

E-mail: jovana.devetakovic@sfb.bg.ac.rs

© by PSP Volume 25 – No. 10/2016, pages 4324-4326 Fresenius Environmental Bulletin

THE EFFECTS OF COPPER ($CuCl_2$) ON MITOTIC CELL DIVISION OF LEBANON CEDAR (*Cedrus libani*)

Ayse Ak Can[1], Gulcin Isik[2*], Ersin Yucel[2]

[1] Erzincan University, Faculty of Engineering, Department of Biomedical Engineering, Erzincan/TURKEY
[2] Anadolu University, Faculty of Science, Biology Department, 26470 Eskisehir/TURKEY

ABSTRACT

Copper is an essential micronutrient for all living microorganisms. Although it is toxic, copper is a cofactor of many enzymes and play an important role in electron transport. It alters membrane permeability, chromatin structure, enzyme activities photosynthesis and respiratory processes. Recently copper is released into the environment by anthropogenic activities, such as from pesticides, fungicides and industrial wastes. In this study, the effects of copper ($CuCl_2$), one of the significant environmental pollutants, on mitotic divisions of *Cedrus libani* was investigated. Different concentrations (0,5, 1, 2 mM Cu^{+2}) of copper were applied. Due to the increase of the copper concentrations, cell division was decreased; several mitotic anomalies such as fragmented nucleus, micronucleus, breaking chromosomes and chromosome bridges were increased.

KEYWORDS:
Cedrus libani, copper, mitotic cell division

INTRODUCTION

Cedrus libani is a micro thermic and ancient woody element of the Anatolian flora [4]. It's known that *Cedrus libani* has ethnobotanical importance in Anatolia. This plant was used for gastrointestinal diseases, pyrosis, reflux, ulcer and boiled as decoction when raw [8]. The resins are chewed or infused; and its pix is used as cinder and lixivium [8]. Resins and cambium parts are often used in Anatolia [9]. Baydoun et al. [3] also reported that *Cedrus libani* is used for fever, infant insomnia and agitation, wounds, sciatica, lumbago, rheumatism and skin injuries by using its fruit, bark and cones. Senol et al. [11] reported that the needle-Ace extract of *Cedrus libani* was the most effective in inhibiting BChE (butyryl cholinesterase) and the shoot EtOAc extract had the highest metal chelation capacity.

Woody species can be very sensitive to moderate concentrations of heavy metals. These elements may reduce biomass accumulation in tree seedlings. Inhibition of root growth, decrease of the availability of essential elements and modification of root morphology and architecture compromise root capacity to explore soils. The excess or deficiency of essential metals may also inhibit protein and enzyme function, and thus impair photosynthetic electron transport at the reaction centers. Heavy metals may indirectly affect seedling performance by reducing plant ability to access and transport soil resources; particularly water [5].

Copper is naturally found in rocks, water and air. Among the most important reasons for Cu pollution are home tools, metal manipulation, timber industry and ashes. Copper is known to be an essential oligo-nutrient for plants growth, but it can also be a toxic element, whose toxic effects can be observed even at tissue contents slightly higher than its optimal physiological levels. At elevated concentrations, copper becomes toxic to plant and alters membrane permeability, chromatin structure, enzyme activities photosynthesis and respiratory processes and may induce senescence [7].

Copper concentrations in soil generally contains between 2 and 250 ppm and healthy plant tissues range from 20 to 30 μg g^{-1} dry weight (dw). In particular, free copper ions can catalyze the formation of highly toxic reactive oxygen species (ROS) such as hydroxyl radicals (OH•) from superoxide anions (O_2•−) or hydrogen peroxide (H_2O_2) via the Haber–Weiss reaction. However, in excess, copper can interfere with numerous physiological processes such as enzyme activity, DNA alterations, protein oxidation, and membrane integrity, all of which could lead to growth inhibition of the plant [2].

MATERIALS AND METHODS

Cedrus libani seeds were used in this study. The experiments were carried out in plant growth chambers (MLR-350 Model Sanyo, Japan). For the duration of the experiments, a constant temperature (+25°C) and photo-period of 8 hours light, 16 hours darkness was maintained.

Different concentrations (0,5, 1, 2 mM Cu^{+2}) of copper were applied. 0,5, 1, 2 mM Cu^{+2} chloride

were prepared with distilled water. Planted petri dishes were filled with 9 ml of copper solution containing different copper concentrations. Control groups were filled with only distilled water. They were covered and kept in the plant growth cabinet for 5 days.

The root tips of germinated seeds were cut and were fixed in acetic acid-alcohol (1:3) for 24 h and were transferred in 70 % alcohol and stored in the fridge. For mitotic preparation, root tips were removed from alcohol and washed with tap water and hydrolyzed with 5 N HCl, at 60 °C for 15 min. Then they were dyed with Feulgen reactive for 1 h. After that the root tips were kept in tap water for 15 min. Finally, the last parts of root tips which were dyed very densely were cut and their crushed preparats in 45 % acetic acid were made. Specimens were observed with a light microscope and photographs taken.

The results are expressed as means ± standard error. The data were compared with ANOVA test using a significant level of $p<0.05$.

RESULTS AND DISCUSSION

Mitotic index was decreased with increase of copper concentration. Abnormalities in root tips exposed to copper and control groups were observed. Table 1 shows mitotic index in treated and control groups. The number of cells in mitosis is shown in Table 2.

Observed chromosomal abnormalities were shown in Figure 1 (A, B, C, D) by arrows.

TABLE 1
Mitotic index in groups of *Cedrus libani*

Groups	Number of Dividing Cells	Mitotic Index (dividing cells/ total cells x 100)
Control	9,11	4
0,5 mM $CuCl_2$	8,58	2,95
1 mM $CuCl_2$	10,11	4,19
2 mM $CuCl_2$	6,36	2,48

TABLE 2
Number of cells in prophase, metaphase, anaphase and telophase in groups of *Cedrus libani*

Groups	Control	0,5mM $CuCl_2$	1 mM $CuCl_2$	2 mM $CuCl_2$
Prophase	1,72	1,54	1,36	1,44
Metaphase	2,61	2,17	2,17	1,67
Anaphase	4,11	2,69	3,78	2,14
Telophase	2,67	2,11	2,78	1,25

In this study, cytogenetic effects of copper chloride on root tip cells of *Cedrus libani* seed were investigated.

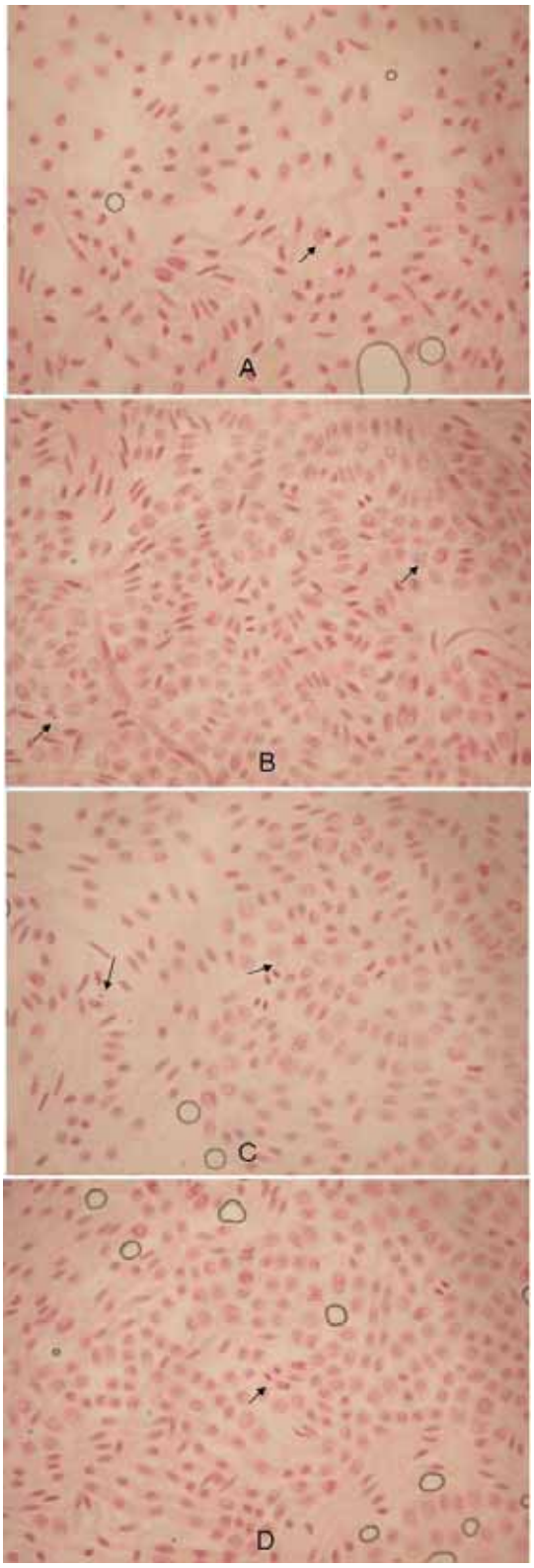

FIGURE 1
Several mitotic anomalies such as fragmented nucleus (A), micronucleus (B), breaking chromosomes (C) and chromosome bridges (D)

It was found that cell division was inhibited by copper chloride. It caused chromosomal changes and normal cell division was affected. Mitotic index was decreased by increasing copper concentration. Several mitotic anomalies such as micronucleus, breaking chromosomes, fragmented nucleus and chromosome bridges were increased by copper concentrations.

To parallel with our findings, another study of ours which is about effects of lead in Black pine, lead concentrations significantly increase mitotic cell division whereas they decrease mitotic index and also cause various mitotic abnormalities [12].

It was reported that Pb/Cu affected the mechanisms controlling the organization of microtubule cytoskeleton, and induces the following aberrations in interphase and mitotic cells [6].

Atay and Ozkoc [1] reported that high concentrations of Cu and Zn may damage *Pseudokirchneriella subcapitata*, the EC50 values indicating that Cu was much more toxic than Zn both with and without sediment.

At elevated concentrations of >20–30 μg g^{-1} dw, copper becomes toxic to plants and alters membrane permeability, chromatin structure, protein synthesis, enzyme activities, photosynthesis and respiratory processes and may induce senescence [10].

In conclusion, the result of this study showed that copper concentrations significantly increase mitotic cell division whereas they decrease mitotic index and also cause various mitotic abnormalities. Our findings about copper are parallel with other investigations in many plant species. These data show that copper damages development of plants and also leads to loss of crop.

REFERENCES

[1] Biltekin, D., Popescu, S.M., Suc, J.P., Quézel, P., Jiménez-Moreno, G., Yavuz, N. and Cagatay, N.M. (2015) Anatolia: A long-time plant refuge area documented by pollen records over the last 23 million years. Review of Palaeobotany and Palynology, 215: 1–22.

[2] Sargin, S.A., (2015) Ethnobotanical survey of medicinal plants in Bozyazi district of Mersin, Turkey. Journal of Ethnopharmacology, 173: 105–126.

[3] Sargin, S.A., Selvi, S. and Buyukcengiz, M., (2015) Ethnomedicinal plants of Aydincik District of Mersin, Turkey. Journal of Ethnopharmacology, 174: 200–216.

[4] Baydoun, S., Lamis, C., Helena, D. and Nelly, A., (2015) Ethnopharmacological survey of medicinal plants used in traditional medicine by the communities of Mount Hermon, Lebanon. Journal of Ethnopharmacology, 173: 139–156.

[5] Senol, F.S., Orhan, I.E. and Ustun, O. (2015) In vitro cholinesterase inhibitory and antioxidant effect of selected coniferous tree species. Asian Pacific Journal of Tropical Medicine, 8 (4): 269-275.

[6] Fuentes, D., Disante, K.B., Valdecantos, A., Cortina, J. and Vallejo, V.R., (2007) Response of *Pinus halepensis* Mill. seedlings to biosolids enriched with Cu, Ni and Zn in three Mediterranean forest soils. Environmental Pollution, 145, 316-323.

[7] Monferran, M.V., Sanchez Agudo, J.A., Pignata, M.L. and Wunderlin, D.A. (2009) Copper-induced response of physiological parameters and antioxidant enzymes in the aquatic macrophyte *Potamogeton pusillus*. Environmental Pollution, 157 (8): 2570–2576.

[8] Babar Ali, M., Hahn, E.J. and Paek, K.Y., (2006) Copper-induced changes in the growth, oxidative metabolism, and saponin production in suspension culture roots of *Panax ginseng* in bioreactors. Plant Cell Rep, 25: 1122–1132.

[9] Yucel, E., Hatipoglu, A. and Guner, S.T., (2008) The Effects of the lead ($PbCl_2$) on mitotic cell division of Anatolian Black Pine (*Pinus nigra* ssp. *pallasiana*). Biological Diversity and Conservation, 1 (1): 1-14.

[10] Liu, D., Xue, P., Meng, Q., Zou, J.,Gu, J. and Jiang, W. (2009) Pb/Cu effects on the organization of microtubule cytoskeleton in interphase and mitotic cells of *Allium sativum* L. Plant Cell Rep, 28: 695–702.

[11] Atay, S. and Ozkoc, H. B., (2010) Effect of Sediment on the Bioavailability and Toxicity of Copper and Zinc to a Green Alga. Fresenius Environmental Bulletin, 19 (12a): 3018-3027.

[12] Srivastava, S., Mishra, S., Tripathi, R.D., Dwivedi, S. and Gupta, D.K., (2006) Copper-induced oxidative stress and responses of antioxidants and phytochelatins in *Hydrilla verticillata* (L.f.) Royle. Aquatic Toxicology, 80, 405–415.

Received: **19.01.2016**
Accepted: **18.08.2016**

CORRESPONDING AUTHOR

Gulcin Isik
Anadolu University, Faculty of Science, Biology Department, 26470 Eskisehir / TURKEY

e-mail: glcnylmz@gmail.com

© by PSP Volume 25 – No.10/2016, pages 4327-4333 Fresenius Environmental Bulletin

COMPOSITE BENTONITE MODIFICATED BY 3-AMINOPROPYLTRIETHOXYSILANE AND SODIUM SILICATE AND ITS EFFECTIVENESS TO CADMIUM REMOVAL

Xingjie Hao, Xiaping Zhu*, Li Zhou, Lin Wu

College of Materials and Chemistry & Chemical Engineering, Mineral Resources Chemistry Key Laboratory of Sichuan Higher Education Institutions, Chengdu University of Technology, Chengdu 610059, China

ABSTRACT

The modification of bentonite (Bt) was performed using the 3-aminopropyltriethoxysilane (γ-APS) and sodium silicate (Na_2SiO_3) as main and auxiliary modifier, respectively. The composite modified bentonite (M-Bt) was characterized by Fourier transform infrared (FTIR) spectroscopy, X-ray diffraction (XRD) and thermo gravimetric analysis (TGA). The results showed that the γ-APS was successfully intercalated in the interlayer space of Bt and suggested a parallel-bilayer arrangement. The Na_2SiO_3 not only reduced the electropositive of the end surface of Bt, but also improved the suspension property of bentonite. The preparation conditions were optimized by the adsorption test of Cd^{2+} in water. The optimum ratio of Bt to γ-APS dosage was 1:1(g/mL); the dosage of Na_2SiO_3 was 10% of Bt quality; the ratio of liquid-solid was 40:1(mL/g); the pH was at 10; and the reaction lasted 3 hours at room temperature. The saturated adsorption amount of the M-Bt to Cd^{2+} reached to 35.7mg/g, which was significantly improved compared with those without modification (1.38mg/g).

KEYWORDS:
Bentonite, 3-aminopropyltriethoxysilane, sodium silicate, cadmium, adsorption.

INTRODUCTION

During the industrialization process, the harm of heavy metal pollution was gradually revealed, causing serious atmosphere, water and soil pollution, and threatening human health. Therefore, the management of heavy metal pollution was imminent. As a representative clay mineral, bentonite (Bt) was a sheet like clay. The main composition was mineral montmorillonite, a kind of 2:1 type of alumino silicate [1]. Because of the larger specific surface area, high swelling capacity, high cation exchange capacity, low-cost and environment friendly, Bt had been shown to be very good adsorbent for water treatment and it became a kind of basic repair material for heavy metal pollution. However, the strong hydrophilicity and weak bonding ability on the surface of natural Bt made the force between the Bt and heavy metal weak, and the reaction was easily affected by many environmental factors. To improve the adsorption capacity to heavy metals, it was necessary to add certain additives or polymers to functionalization the natural Bt

Different methods were used to modify bentonite [2]. Activation and adding modifier were the commonly modified ways. Activation was attained by means of acidification, calcination, salt activation and other methods. According to adding different kinds of modifiers, it could be divided into pillared modified and organically modified. Hydrated hydroxyl-polymeric metal cation [3-5] such as polymeric cationic hydroxyl aluminum was a common pillared modifier. The organic modifier included ammonium salt [6-8], polymerization performance modifier [9-10] and the silane coupling agent [12-13]. The various types of ammonium salts not only expanded the layer spacing, but enhanced the adsorption capacity. The quaternary ammonium cationic surfactant was most widely used. Organic silanes were grafted on the surface of bentonite to improve the thermal stability by reaction with active hydroxyl groups. The modifier helped make the surface properties and interlayer structure of bentonite change. The organic matter content increased and the layer spacing enlarged which increased the hydrophobic properties, and further improved the adsorption capacity.

The main purpose of this work was to use organic silane modified bentonite, however, previous research had focused on the single reagent modified, and less attention was paid to the multiple. Therefore, in this work, we studied the composite modification of Bt with 3-aminopropyltriethoxysilane (γ-APS) and sodium silicate (Na_2SiO_3). The optimum preparation conditions were discussed based on adsorption to Cd^{2+} on modified bentonite, and the structure of the modified bentonite was characterized by X-ray diffraction (XRD), thermo gravimetric analysis (TGA) and Fourier transform infrared spectroscopy (FTIR).

MATERIALS AND METHODS

Apparatus and reagents. The Bt used in this work was come from Sihui, Guangdong, China. Montmorillonite (Ca-Mt) content was more than 80 %, chemical components of Bt were showed in table 1. The γ-APS with a purity of 98 % was provided by Aladdin, $CdCl_2 \cdot 2.5H_2O$, KNO_3, HCl, and NaOH were of analytical grade. All the glassware was treated in 10% nitric acid prior to use, and the experimental water was distilled water.

AA7000W atomic absorption spectrometer (Beijing Sanxiong science and technology company), Tensor-27 Fourier transform infrared spectrometer (Bruker, Germany), DX-2700 X-ray diffractometer (Dandong fangyuan instrument company), STA409PCLuxx Simultaneous thermal gravimetric analyzer (Netzsch, Germany).

Bentonite modified method. 2.00 g Bt suspended in distilled water, 2.00 mL γ-APS was dissolved in the 8 mL ethanol, then the γ-APS solution and 0.20 g Na_2SiO_3 were added into the suspension under stirring. Adjusted the value of pH to 10, the modification lasted for 3 h at room temperature. The composite modified bentonite (M-Bt) was washed several times with distilled water until the filtrate became neutral, then dried at 40 ℃, milled through 100 mesh sieve and kept in a desiccator at room temperature.

Adsorption experiment methods. 0.1250 g M-Bt was put in 50mL conical flasks, a certain amount of distilled water was added, adjusted the pH to 6, 1 M KNO_3 was added to adjusting the ionic strength, and a certain concentration of Cd^{2+} was added. The mixture was oscillated for 60 min at room temperature, transferred into centrifuge tubes and centrifuged for 30 min at 3000 rpm. The concentration of Cd^{2+} in supernatant was determined by flame atomic absorption spectrometer [14].

Characterization. Infrared spectra were performed on Tensor-27 Fourier transform infrared spectrometer in the range of 400-4000 cm^{-1} using KBr pressed-disk technique.

The XRD pattern was obtained using a DX-2700 diffractometer with CuKα, radiation at 40 kV and 30 mA. Scan was recorded between 3°and 50° (2θ) with a step size of 0.06°.

Thermogravimetric analysis was obtained using STA409PCLuxx Simultaneous thermal gravimetric analyzer. This was done in the temperature range from 30 to 900 ℃ at a scanning rate of 10 ℃/min under a high-purity flowing nitrogen atmosphere (50 cm^3/min).

RESULTS AND DISCUSSION

Design of the composite modification. As shown in Fig 1, bentonite was modified using Na_2SiO_3 and γ-APS. The addition of sodium silicate, not only reduced the electropositive of the end surface of Bt, but also improved the suspension property of Bt, which made good contact between bentonite and modifier. The γ-APS was successfully inserted into the Bt layer, and the adsorption rate of M-Bt was significantly improved. Fig 2 showed that this composite modification process was successful and feasible. Therefore, we discussed the condition of modification in detail.

TABLE 1
Chemical components of bentonite.

Item	Na_2O (%)	MgO (%)	Al_2O_3 (%)	SiO_2 (%)	K_2O (%)	CaO (%)	Fe_2O_3 (%)	MnO (%)
Value	0.22	3.79	16.48	56.54	0.63	2.95	5.08	0.17

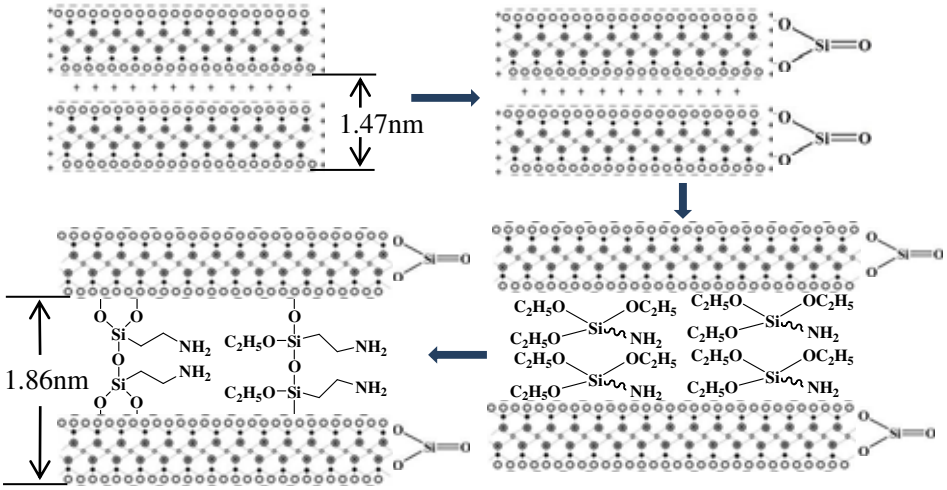

FIGURE 1
Design of the composite modification

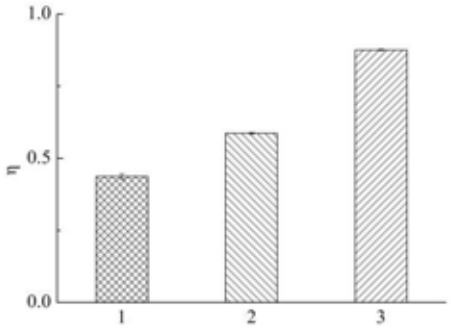

FIGURE 2
1: Original bentonite. 2: Bentonite modified by γ-APS. 3: Composite modified by Na_2SiO_3 and γ-APS. (Initial Cd^{2+}: 10 mg/L)

Modified conditions. Effect of sodium silicate. The crystal layer plane of Bt is with negatively charged owing to the isomorphous substitution in the lattice. However, the end surface is positively charged due to the break of the silicon oxygen tetrahedron and alumina octahedral, and the end surface accounts for around 10% of the total surface area of Bt, which may reduce the adsorption to cation. If the Bt end surface turns into negative charge, the aggregate of interlayer and end surface disperses, the absorption capacity will be improved. Silica sol is an anionic polymers, negatively charged, there are a large number of Si-OH bond. The Al-OH bond exists on the break of the interlayer edge of Bt, and it reacts easily with Si-OH, so the silica sol negatively charged can be linked on the crystal end surface of Bt, reduces the end electropositive, and improves the adsorption ability to cation [15-17]. In the other hand, the Na_2SiO_3, as a dispersing agent, is beneficial to improve the suspension property of bentonite, which makes good contact with bentonite and modifier.

Therefore, this study chose Na_2SiO_3 as auxiliary modifier.

This study further explored the dosage of Na_2SiO_3 on the adsorption property of M-Bt (Fig 3). When the initial concentration of Cd^{2+} was 10μg/mL, the adsorption rate of M-Bt modified by single γ-APS was 0.58. With the addition of Na_2SiO_3, the dispersity of bentonite increased and the electropositive of the end surface gradually reduced, which improved the effect of modification and the adsorptive performance. When the amount of Na_2SiO_3 was 10 % (relative to the quality of Bt), the adsorption rate reached highest. However, excessive Na_2SiO_3 would gather on the end surface of Bt and hinder γ-APS into interlayer. Therefore, the optimal amount of Na_2SiO_3 was 10%.

Effect of γ-APS dosage. As main modification agent, the γ-APS entered the layers of Bt, which could cause the silylation reaction with interlayer hydroxyl groups. The complexation reaction between amino of silane molecules chain and heavy metal increased the adsorption capacity of heavy metal. With the increase of γ-APS (Fig 4), the amount of γ-APS grafted onto Bt interlayer increased, and the adsorption rate also increased. When the mass-volume ratio of Bt to γ-APS increased, the adsorption rate increased continuously. Taking into the cost and efficiency, the mass-volume ratio of Bt to γ-APS was 1:1 (g/mL).

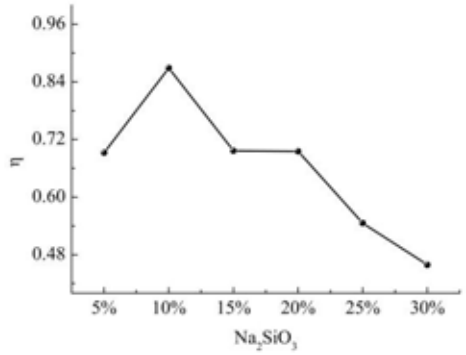

FIGURE 3
Effect of Na_2SiO_3 dosage. Initial Cd^{2+}: 10 mg/L, Na_2SiO_3: 0 5 10 15 20 25 30(%), γ-APS: 2 mL, liquid-solid ratio: 30:1, Time: 5 h, Temp: room temperature, pH: without adjusting pH

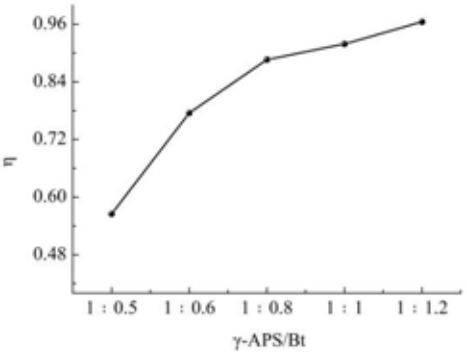

FIGURE 4
Effect of γ-APS dosage. Initial Cd^{2+}: 10 mg/L, Na_2SiO_3: 10 %, γ-APS: 1, 1.2, 1.6, 2, 2.4 mL, liquid-solid ratio: 30:1, Time: 5 h, Temp: room temperature, pH: without adjusting pH

Effect of the liquid-solid ratio. With the liquid-solid ratio increased(Fig 5), the adsorption rate of M-Bt to Cd^{2+} increased gradually, when the ratio was 40:1, the adsorption rate reached to the maximum, and continued to raise the liquid-solid ratio , the adsorption rate decreased gradually. The liquid-solid ratio actually reflected the concentration of Bt slurry, when the ratio was too low, the mobility of Bt would become poor and caused less contact between the modified agent and Bt. On the contrary, the concentration of Bt was too low to react with

modified agent when the liquid-solid ratio increased further. So the best liquid-solid ratio of 40:1 was selected.

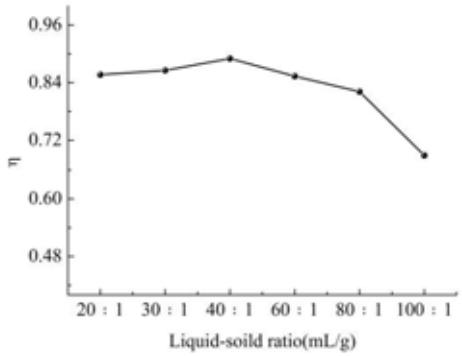

FIGURE 5
Effect of liquid-solid ratio. Initial Cd^{2+}: 10 mg/L, Na_2SiO_3: 10 %, γ-APS: 2 mL, liquid-solid ratio: 20:1, 30:1, 40:1, 60:1, 80:1, 100:1, Time: 5 h, Temp: room temperature, pH: without adjusting pH

Effect of modified pH, Temperature and Time. The experimental results showed that, the Cd^{2+} adsorption on M-Bt firstly increased and then decreased with the increase of pH (Fig 6A). The optimal pH was 10 to 12. Elevated modification temperature was not conducive to the adsorption of Cd^{2+} on M-Bt (Fig 6B), room temperature was the best. As the growth of the modification time (Fig 6C), the adsorption rate of Cd^{2+} on M-Bt increased slightly. When the time prolonged, the adsorption rate decreased, the best modification time was 3-5 h.

The characterization of the composite modified bentonite. Fourier transforms infrared spectroscopy (FTIR). Infrared spectroscopy was very sensitive to the clay mineral structure, and the changes could be observed in all frequency ranges. The peak at 3621 cm^{-1} corresponded to the -OH stretching vibration of structural hydroxyl groups. The peaks at 3438 cm^{-1} and 1633 cm^{-1} owned to the -OH stretching and deformation vibration of water, respectively. The peak at 1035 cm^{-1} attributed to the stretching vibration of Si-O bond [18-19]. After modification, the structure of the material had not been destroyed, and basic skeleton still preserved.

In Fig 7, a new peak at 2937 cm^{-1} was due to antisymmetric stretching of $-CH_2$ group of γ-APS. Similarly, the band at 1506 cm^{-1} corresponded to the bending vibration of $-NH_2$, which indicated the existence of γ-APS in M-Bt [19].

X-ray diffraction (XRD). As shown in Fig 8, the XRD pattern clearly showed an increase of the basal spacing from 1.47 nm of Bt to 1.86 nm of M-Bt, indicating that the γ-APS was intercalated or grafted in the interlayer region [19].

The height of the interlayer space could be estimated with the basal spacing and the thickness (0.96nm) of the sheet of phyllosilicate, calculated by Eq (1).

Interlayer spacing height (Å) = Distance (d_{001}) – 0.96 nm. (1)

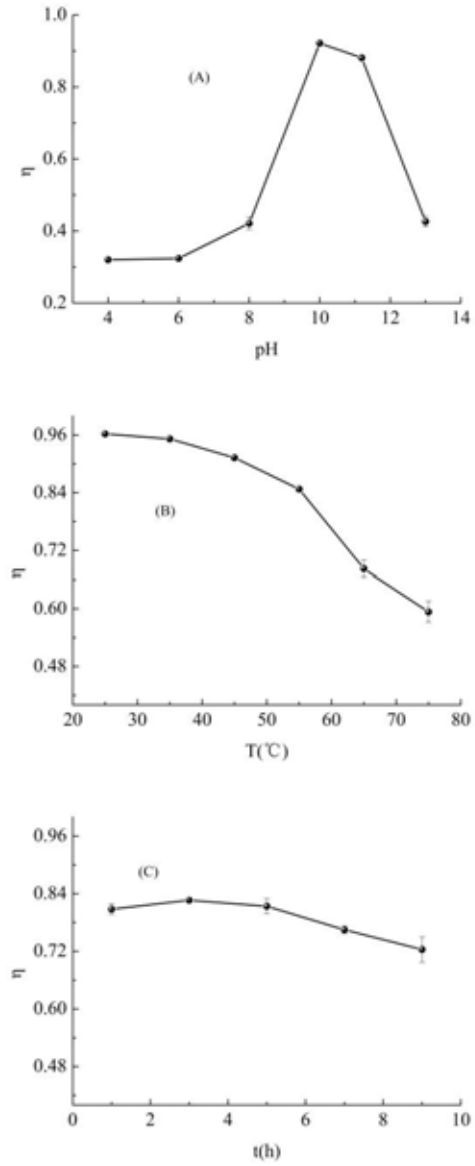

FIGURE 6
Effect of modified pH, temperature and time. Initial Cd^{2+}: 10 mg/L, Na_2SiO_3: 10 %, γ-APS: 2 mL, liquid-solid ratio: 40:1, (A, pH: 4, 6, 8, 10, 11.3, 13), (B, Temperature: 25, 35, 45, 55, 65, 75 ℃), (C, Time: 1, 3, 5, 7, 9 h)

After hydrolysis, the configuration of γ-APS was different from the original one and the height of the aminopropyl group was ca. 0.4 nm, which similar to the alkyl chain. Accordingly, the gallery heights of 0.90 nm indicated the parallel-bilayer arrangement of γ-APS was in the galleries of M-Bt [20].

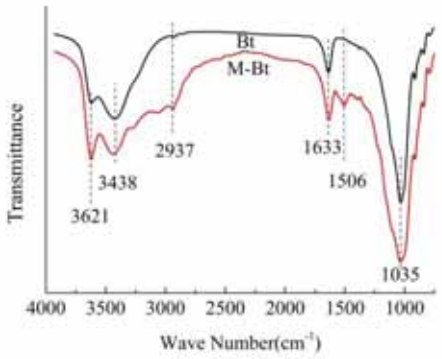

FIGURE 7
FTIR spectra(500-4000cm^{-1}) of Bt and M-Bt

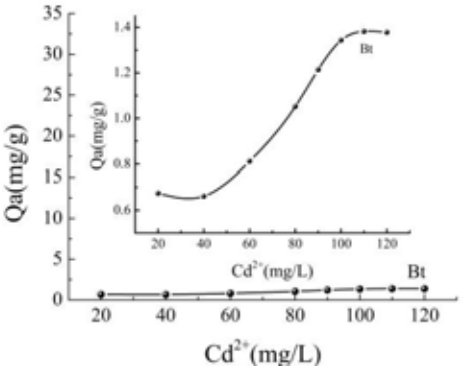

FIGURE 10
Saturated adsorption capacity of Bt

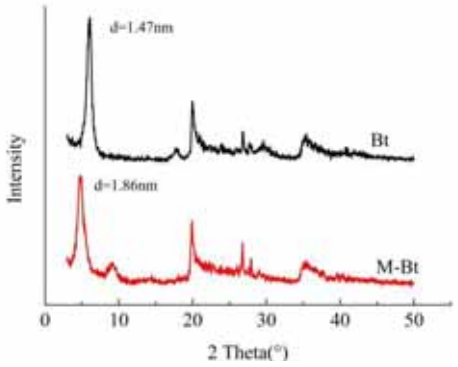

FIGURE 8
XRD patterns of Bt and M-Bt

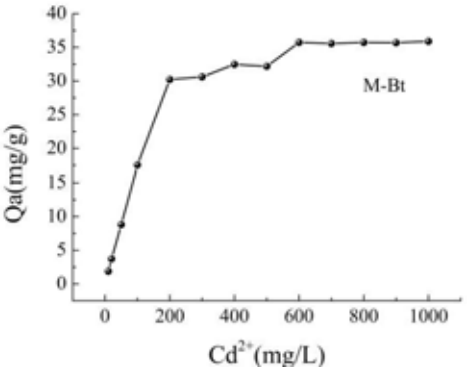

FIGURE 11
Saturated adsorption capacity of M-Bt

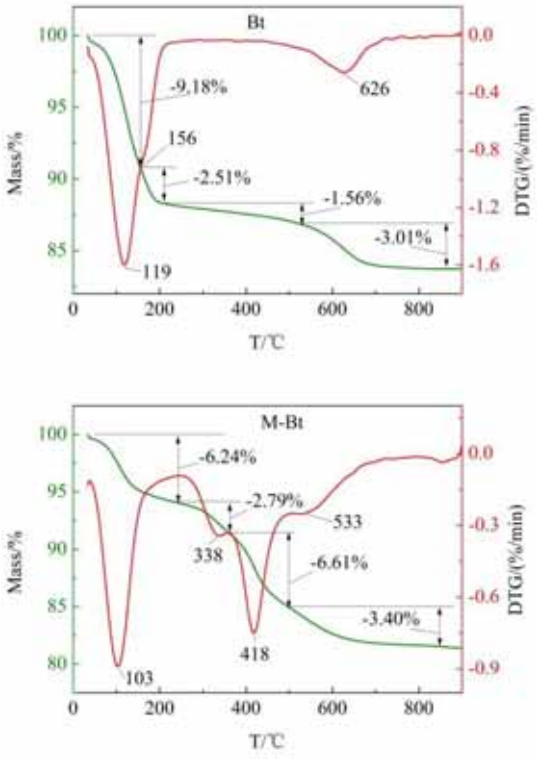

FIGURE 9
TGA and DTG curves of Bt and M-Bt

Thermogravimetric analysis (TGA). The thermograms of TG and derivative thermograms (DTG) for the Bt and M-Bt were shown in Fig 8. The M-Bt showed greater weight loss than the Bt.

DTG curves of the Bt showed two thermal events: the first event occurring at a temperature of 119 ℃ was attributed to the loss of physically adsorbed water, and the second event occurring at a temperature of 626 ℃ was corresponded to the dehydroxylation of aluminosilicate. There was a slight weight loss (ca. 1.5 %) in the range of 200-500 ℃, possibly corresponded to the loss of the bonded H_2O within the gallery [19, 21].

The peak at 103 ℃was corresponded to loss of the physically adsorbed water. Depigmentation temperature was lower than the Bt, which indicated that the hydrophilicity of the surface of M-Bt decreased. The peak at 338 ℃ was ascribed to desorption of γ-APS linked with hydroxyl group by hydrogen bonds on the edge of M-Bt. Meanwhile, the temperature was higher than the literature [10], which may be caused by the addition of Na_2SiO_3. The peak at 418 ℃ represented desorption of the intercalated γ-APS, and the weight loss at 533 ℃was corresponded to the γ-APS chemically bonded with the layers of M-Bt.

The application of the composite modified bentonite. Fig 10 and 11 illustrated that, with the increase of Cd^{2+} concentration, adsorption capacity of Bt and M-Bt increased gradually, and finally reached a plateau, the saturated adsorption capacity of the Bt was only 1.38 mg/g, and that of the M-Bt reached to 35.7 mg/g, the adsorption capacity had been significantly improved. The γ-APS was successfully grafted to the surface or inserted into the interlayer of Bt, then the adsorption of Cd^{2+} mainly relied on the complexation of amino in addition to electrostatic adsorption and cation exchange.

CONCLUSION

The M-Bt was prepared successfully by using γ-APS and Na_2SiO_3. The addition of Na_2SiO_3 not only reduced the end surface electropositive but also made the bentonite completely dispersed in the modification process. The γ-APS inserted or grafted to the layers of bentonite and suggested a parallel-bilayer arrangement. So the adsorption ability of heavy metals on the M-Bt was further improved, the saturated adsorption capacity reached to 35.7mg/g which was much higher than that of Bt. The complexation was mainly adsorption process after modified except for physical adsorption and ion exchange. It is hoped that this composite modified bentonite could be used as a kind of promising environmental remediation agent for the treatment of heavy metal pollution in water body.

ACKNOWLEDGEMENTS

Authors wish to acknowledge financial support from nonprofit special research projects of Ministry of Land and Resources of the People's Republic of China (No. 201111016).

The authors have declared no conflict of interest.

REFERENCES

[1] Alexandre, M. and Dubois, P. (2000). Polymer-layered silicate nanocomposites: preparation, properties and uses of a new class of materials. Materials Science and Engineering, 28, 1-63.

[2] Bergaya, F. and Lagaly, G. (2001). Surface modification of clay minerals. Applied clay science, 19, 1-3.

[3] Hutson, N. D., Gualdoni, D. J. and Yang, R. T. (1998). Synthesis and characterization of the microporosity of ion-exchanged Al2O3-pillared clays. Chemistry of materials, 10, 3707-3715.

[4] Roulia, M. (2005). Synthesis and characterization of novel chromium pillared clays. Materials chemistry and physics, 91, 281-288.

[5] Thomas, S. M., Bertrand, J. A., Occelli, M. L., Stencel, J. M. and Gould, S. A. C. (1999). Synthesis and characterization of expanded smectites containing trinuclear Co complexes. Chemistry of materials, 11, 1153-1164.

[6] Xiang, N. N., Zhu, X. P., Tian, Y. F., Tan, J., Liu, W. H., Zhao, Q. X. and Li, H. P. (2013) Preparation, characterization and adsorption ability to Cu^{2+}, Ni^{2+}, Cd^{2+} of amine-modified bentonite. Non-Metallic Mines, 36, 79-82.

[7] Yilmaz, N. and Yapar, S. (2004). Adsorption properties of tetradecyl-and hexadecyl trimethylammonium bentonites. Applied Clay Science, 27, 223-228.

[8] Yapar, S., Özbudak, V., Dias, A. and Lopes, A. (2005). Effect of adsorbent concentration to the adsorption of phenol on hexadecyl trimethyl ammonium-bentonite. Journal of hazardous materials, 121, 135-139.

[9] Carrado, K. A. (2000). Synthetic organo-and polymer–clays: preparation, characterization, and materials applications. Applied Clay Science, 17, 1-23.

[10] Inyang, H. I. and Bae, S. (2005). Polyacrylamide sorption opportunity on interlayer and external pore surfaces of contaminant barrier clays. Chemosphere, 58, 19-31.

[11] Shen, Z., Cheng, Y. B. and Simon, G. P. (2005). Sequential and simultaneous melt intercalation of poly (ethylene oxide) and poly (methyl methacrylate) into layered silicates. Macromolecules, 38, 1744-1751.

[12] He, H. P., Duchet, J., Galy, J. and Gerard, J. F. (2005). Grafting of swelling clay materials with 3-aminopropyltriethoxysilane. Journal of colloid and interface science, 288, 171-176.

[13] Bertuoli, P. T., Piazza, D., Scienza, L. C. and Zattera, A. J. (2014). Preparation and characterization of montmorillonite modified with 3-aminopropyltriethoxysilane. Applied Clay Science, 87, 46-51.

[14] Zhu, X. P., Hao, X. J, Xiang, N. N., Tan, J., Liu, W. H. and Zhao, Q. X. (2014). Characteristic of Montmorillonite and its Adsorptive Behavior to Cadmium Fresenius Environment Bulletin, 23, 3434-3441.

[15] Cao, S. Q. and Wei, Q. J. (2004). The preparation and properties of bentonite cross-linked by silicon and aluminum. Journal of Xinyang Agricultural College, 14, 32-33.

[16] Fan, X., Shi, D. l., Zhang, J. and Ma, F. S. (2001). A study of the mechanism of modified bentonite edges with silica-alumina gel. Advance Science and Technology, 7, 19-21.

[17] Ma, F. S., Qin, Y. N. and Liang, Z. C. (1996). Study on adsorbability of bentonite by silicic

sol treatment. Journal of Tianjin University, 29, 792-793.
[18] Madejová, J. (2003). FTIR techniques in clay mineral studies. Vibrational spectroscopy, 31, 1-10.
[19] Shanmugharaj, A. M., Rhee, K. Y. and Ryu, S. H. (2006). Influence of dispersing medium on grafting of aminopropyltriethoxysilane in swelling clay materials. Journal of colloid and interface science, 298, 854-859.
[20] Shen, W., He, H., Zhu, J., Yuan, P. and Frost, R. L. (2007). Grafting of montmorillonite with different functional silanes via two different reaction systems. Journal of colloid and interface science, 313, 268-273.
[21] Paul, B., Martens, W. N. and Frost, R. L. (2011) Organosilane grafted acid-activated beidellite clay for the removal of non-ionic alachlor and anionic imazaquin. Applied Surface Science, 257, 5552–5558.

Received: **07.01.2016**
Accepted: **20.08.2016**

CORRESPONDING AUTHOR

Xiaping Zhu
College of Materials and Chemistry &
Chemical Engineering Mineral Resources Chemistry Key Laboratory of Sichuan Higher Education Institutions Chengdu University of Technology
Chengdu 610059 P.R. CHINA

E-mail: zhuxiaping@cdut.edu.cn

© by PSP Volume 25 – No. 10/2016, pages 4334-4344 Fresenius Environmental Bulletin

SIMULTANEOUS PROCESSES OF MINOCYCLINE DEGRADATION AND ELECTRICITY GENERATION IN AN AIR-CATHODE SINGLE CHAMBER MICROBIAL FUEL CELL

Xiang Hu[1,2*], Lingjuan Luo[1,2], Zhirong Sun[3]

[1] College of Chemical Engineering, Beijing University of Chemical Technology, Beijing 100029, China
[2] Research Centre for Environmental Pollution Control and Resource Reuse Engineering of Beijing City, Beijing 100029, China
[3]College of Environmental & Energy Engineering, Beijing University of Technology, Beijing 100124, China

ABSTRACT

A single-chamber and membrane-less microbial fuel cell (MFC) with an air cathode is successfully used to degrade minocycline and produce electricity synchronously using glucose-minocycline sodium mixtures as fuel. Results show that, compared with traditional anaerobic reactors, the removal of minocycline in the MFC increased by 67%. Compared with the dextrose broth, the critical amount of minocycline that is conducive to producing electricity in the MFC was 2 mg/L. Experimental results also showed that when the inlet minocycline concentration was 2 mg/L, the HRT was 24 h, the pH was 7.0 and the phosphate buffered saline concentration was 100 mmol/L, the MFC had the highest removal of minocycline and the best electricity-generating performance. The removal of minocycline was 84.3% and the removal of COD was 88.9%. Furthermore, the MFC had a stable voltage of 538 mV, an internal resistance of 160.3 Ω and a maximum power density of 371.1 mW/m^2.

KEY WORDS:
MFC; Minocycline; degradation; electricity generation

INTRODUCTION

Our energy choices have direct implications on our health, environment and our climate. Presently, we are extremely dependent on coal and other fossil fuels for most of our electricity needs. Hence, it is necessary to find a better and cleaner way to meet our energy needs. Microbial fuel cells (MFC) are a promising technology for energy recovery using microorganisms. An MFC is a device that transforms chemical energy into electricity via electrochemical reactions [1-5]. The substrates can be glucose, sucrose, etc. It can also use wastewater as a substrate to remove contaminants within itself and produce electricity simultaneously, thus decreasing the operational costs of wastewater treatment. Over the past decade, microbial fuel cell has been a subject of intensive research. However, most studies were based on various biodegradable organic matter as substrates, for example, glucose, acetate, sucrose, domestic wastewater, brewery wastewater and starch processing wastewater [6-12]. There are only a few reports on biorefractory compounds as fuel, for instance, phenol, furfural, pyridine and p-nitrophenol [13-15]. These papers indicated that some toxic and bio-refractory organics may be removed in MFC and may have an active role in electricity generation [16, 17].

The occurrence of antibiotics as contaminants in wastewater and in the aquatic environment has attracted increased attention. Every year, there is a large amount of antibiotics used in medicines for humans and animals to prevent diseases as well as promote growth and agriculture. However, not all antibiotics can be consumed by humans and animals; a high percentage of antibiotics are excreted unchanged via urine and faeces into the sewage. Nowadays, antibiotics are being detected in the rivers in many countries. The main way of entry of antibiotics into the environment is through a sewage treatment plant. Many studies show that antibiotics in sewage treatment plants cannot be removed completely [18-20]. Nowadays, there are two main processes to treat wastewater with antibiotics in sewage treatment plants, i.e. biological and physical–chemical methods. Each has its own characteristics. As antibiotics are refractory organics, biological processes are economical but ineffective. The physical–chemical process can achieve high efficiency and is stable

with a high quality effluent, but the process cost is high [21-23]. This suggests that we need to find a better method. In this study, we focus on minocycline, a kind of tetracycline antibiotics. Tetracycline antibiotics are probably the most important class of antibiotics in human and veterinary medicines because of their broad activity spectrum and good oral absorption. Large amounts of tetracycline antibiotics are produced every year. Hence, many researchers have been seeking suitable methods to treat tetracycline antibiotics wastewater.

To our knowledge, minocycline as a substrate in an MFC has not been reported previously. The aims of this study are as follows: (i) to investigate the degradation feasibility of minocycline in an MFC, (ii) to examine the influence of minocycline on MFC power generation and substrate degradation, (iii) to evaluate the differences in minocycline degradation between MFC and traditional anaerobic reactors and (iv) to optimize the operational conditions of MFC. The experimental results could help in understanding the MFC as well as some practical aspects of its potential application.

MATERIALS AND METHODS

Air-cathode MFC configuration. An air-cathode, single-chambered MFC was constructed using an organic glass (PMMA) vessel. The reactor reaction chamber is a cylinder with a diameter of 4.5 cm and length 5 cm. The total volume of the reactor is 79.5 mL. Water inlets and outlet port were set up on the upper portion of the reactor. A port with an inner diameter of 8 mm was used for sampling and installing the reference electrode. The anode was made of carbon cloth (5 × 5 cm) loaded with carbon nanotubes. Prior to use, carbon nanotubes were purified using 5.0 mol/L nitric acid. Then, 40 mg of the purified carbon nanotubes were placed into a plastic vial and mixed with 20 μL PTFE (75%) and 400 μL deionized water. Using a small paintbrush, the carbon nanotubes were pasted evenly to coat the fabric surface and dried for 24 h. The air-cathode was also made of carbon cloth (5 × 5 cm), which was manufactured by pressing a carbon-based layer, a diffusion layer and a catalyst layer. The projected surface area of the cathode and anode was 15.9 cm^2. The air-cathode and anode were on both ends. The two electrodes were 5 cm apart [8, 24-28]. Sealing was assured by a blind plate, flange and silica gel pad to maintain an anaerobic microenvironment. The two electrodes were connected using copper wires through a rheostat (0.1–9999 Ω).

Culture and operation. Experimental strains were taken from an anaerobic wastewater treatment plant in Beijing. The anaerobic sludge was domesticated and cultivated in a glucose nutrient solution under anaerobic conditions. They were used as inoculums in the anode chamber of the MFC for electricity generation. The MFC was fed with artificial wastewater, and its main components contain a self-made glucose solution, phosphate buffer solution (PBS) and solutions of trace elements and vitamins that is required by the microorganisms for growth. The glucose solution was 1000 mg/L. The phosphate buffer contained: KCl, NaH_2PO_4 and Na_2HPO_4; the solution of trace elements contained: $MgSO_4 \cdot 7H_2O$, $FeSO_4 \cdot 7H_2O$, $ZnSO_4 \cdot 7H_2O$, $CaCl_2$, $MnSO_4 \cdot H_2O$ and NH_4Cl. The vitamin solutions contained Vitamin B_1, B_2, B_3, B_6 and PABA. The proportions of the main components were determined by the microorganism growth and the experiment.

In this study, four reactors were operated containing three MFCs and a traditional anaerobic reactor. The nutrient solution was exposed to a nitrogen broth for 2 min to remove the oxygen and maintain an anaerobic environment. Experiments were conducted in a constant temperature (35 ± 1 °C).

Analyses and calculations. Insulated copper wires were used to connect the microbial fuel cell with an external resistor (1000 Ω, unless stated otherwise) into the circuit. The circuit was connected to a computer by a Personal Daq/56 automatic data acquisition device; the voltage data was recorded once every 60 s. Current was calculated according to Ohm's law as $I = U / R$, where U is the voltage and R is the resistance. Current density was calculated as $I_A = I / A$, where I is the current and A is the effective surface area of the anode. Power (P) was calculated as $P = IU$. Power density was calculated as $PA = P / A$. A polarization curve was obtained by varying the external resistance over a range of 1–9000 Ω and recording the voltage. The power density curve was obtained when the MFC voltage is stable, changing the external circuit resistance to 2000, 1500, 1000, 700, 500, 300, 200 and 100 Ω.

Experimental Design. The experiment was divided into two phases. In the first phase, three MFCs and a traditional anaerobic reactor were fed with a nutrient solution of 1000 mg/L glucose and 100 mmol/L phosphate buffer. pH of the solution was 7.0. After stable voltage outputs were achieved, minocycline-glucose mixtures were used to replace the solutions in the MFC. The minocycline-glucose mixtures comprised 1 mg/L minocycline sodium + 1000 mg/L glucose and 100 mmol/L phosphate buffer. pH of the solution was 7.0.

For both phases, this study adopted the single factor experiment to investigate the key factors of minocycline degradation and synchronous electricity production, and optimized the operating conditions on tetracycline degradation and synchronous electricity production. The factors were minocycline concentration, hydraulic retention time, pH and concentration of PBS.

RESULTS AND DISCUSSION

Degradation of minocycline in the MFC and conventional anaerobic reactor. Application of MFC in the field of wastewater treatment requires that minocycline can be utilized and degraded. In order to investigate the substrate degradation capability in the MFC and the differences from conventional anaerobic reactor (MFC reactor with an open circuit and everything else was the same), experiments were conducted to investigate the degradation of minocycline sodium and the chemical oxygen demand (COD).

COD removal. At first, the MFC and the conventional anaerobic reactor were fed with artificial wastewater. After stable voltage outputs were achieved, the minocycline-glucose mixtures included 1 mg/L minocycline sodium + 1000 mg/L glucose and 100 mmol/L phosphate buffer. Solutions with a pH of 7.0 were used to replace the solutions in the MFC and the conventional anaerobic reactor. After stable voltage outputs were achieved, we measured the COD removal of the two reactors when the HRT was 24 h. The COD removal efficiency of a conventional anaerobic reactor was approximately 75%, whereas it was more than 90% for MFCs.

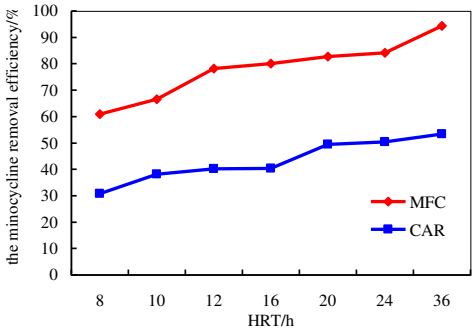

Minocycline degradation. After stable voltage outputs were achieved, we measured the minocycline removal of the two reactors when the HRT was 8, 10, 12, 16, 20 and 24 h.

FIGURE 1
Minocycline removal efficiency of MFC and conventional anaerobic reactor (CAR)

As represented in Fig. 1, the removal efficiencies of minocycline in MFC were higher than those of the anaerobic reactor at any given time during the 36 h experiment. For the substrates of 1000 mg/L glucose + 1 mg/L minocycline sodium, the minocycline sodium removal efficiencies in the MFC were 80% in 24 h and were 90% in 36 h, while in the conventional anaerobic reactor, minocycline sodium removal efficiencies were 50% and 53% in 24 h and 36 h, respectively. These results revealed the following: (i) it was feasible to treat wastewater containing minocycline sodium in MFC; (ii) the removal efficiencies of minocycline sodium and COD in MFC were higher than those in the conventional anaerobic reactor. The result was similar to the result summed up by Wen, et al. [17] that the presence of penicillin enhanced the degradation efficiency of substrates.

Electricity production from minocycline sodium-glucose mixtures in the MFC. The circuit was connected to a computer by a Personal Daq/56 automatic data acquisition device; the voltage data recorded once every 60 s. The external resistor was 1000 Ω. During the start-up phase, the MFC was fed with a glucose solution (1000 mg/L). When stable voltage outputs were achieved, we recorded the voltage in 12 h. Then we changed the glucose solution to the mixture (1000 mg/L glucose + 1 mg/L minocycline sodium). Other experimental procedures were the same.

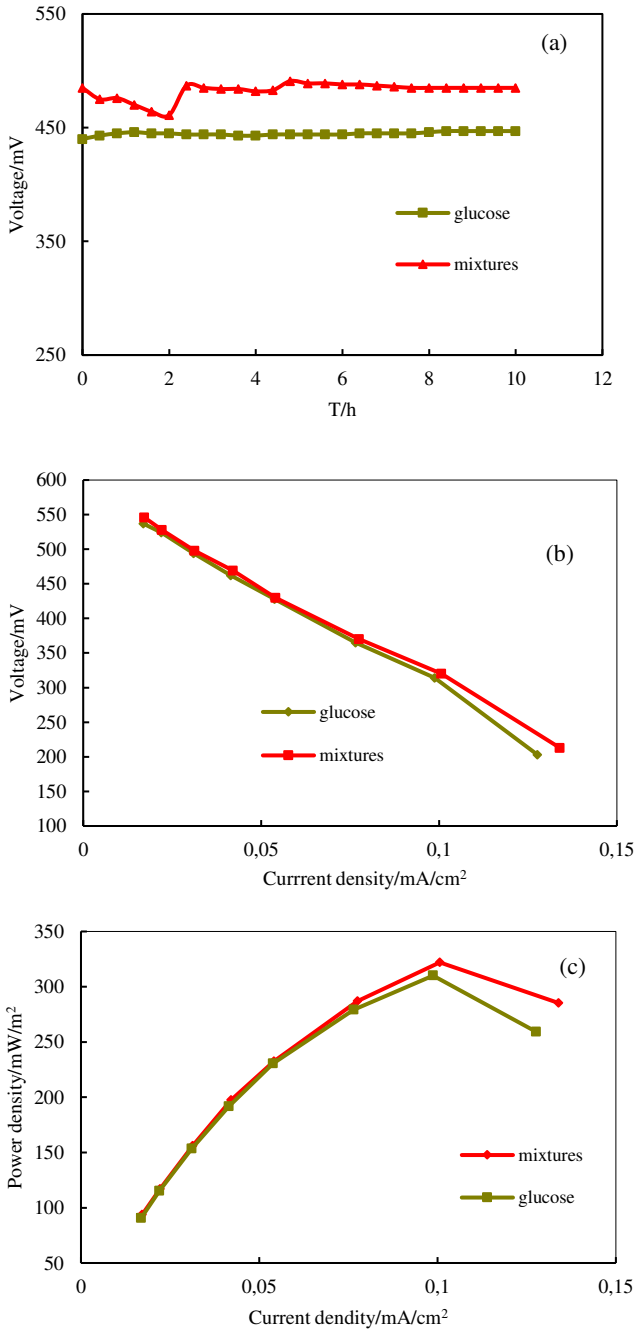

FIGURE 2
Power Generation (A), Polarization Curve (B), And Power Density Curve (C) From Different Nutrient.

As shown in Fig. 2a, when the nutrient was glucose, the stable voltage output of MFC was 450 ± 5 mV. When the nutrient was the mixture (1000 mg/L glucose + 1 mg/L minocycline sodium), the stable voltage output of MFC was 485 ± 5 mV. Voltages decreased when the mixture was added into the MFC. The decrease in the voltage indicates that minocycline sodium might reduce the electrochemical activity of bacteria on the anode.

As shown in Fig. 2b, irrespective of using mixture or glucose as the nutrient, current density increases and the voltage decreases. We can obtain the resistance of the MFC from the voltage and current. When the nutrient was glucose and after stable voltage outputs were achieved, the resistance of the MFC was 183.7 Ω. However, when the nutrient was the mixture (1000 mg/L glucose + 1 mg/L minocycline sodium) and after stable voltage

outputs were achieved, the resistance of the MFC was 174.3 Ω.

As shown in Fig. 2c, when the nutrient was glucose and after stable voltage outputs were achieved, the maximum power density of the MFC was 310.1 mW/m^2. When the nutrient was the mixture (1000 mg/L glucose + 1 mg/L minocycline sodium) and after stable voltage outputs were achieved, the maximum power density of the MFC was 322.0 mW/m^2. This further indicated that some amount of minocycline is beneficial in producing electricity.

These results revealed that MFC using co-substrates might show different electricity generation characteristics, enhance the energy output and decrease the internal resistance compared with using pure organic matter. Similar to the phenol and pyridine results of Luo et al. [7] and Zhang et al. [14], co-substrates can enhance the energy output.

Effect of different HRT. HRT is an important parameter affecting the minocycline degradation and electricity production in the MFC. The MFC reactor is an anaerobic microenvironment. Microorganisms are anaerobic and their growth cycles are long. If the HRT is shorter, then the degradation effect is not ideal; if the HRT is too long, the construction investment will increase. As is shown in Fig. 3, while the HRT is longer, the minocycline removal efficiency increases. When the HRT is longer than 16 h, the minocycline removal efficiency is more than 80%. Based on our experience, we believe that an HRT of 24 h is ideal. As shown in Fig. 3, after stable voltage outputs were achieved, HRT has no effect on voltage.

Effect of different minocycline sodium concentrations. Some amount of minocycline-glucose is conducive to producing electricity for MFC. Antibiotics have an antiseptic effect, so a high concentration of minocycline could inhibit the growth of microorganisms and affect the MFC electricity generation. In these experiments, we want to achieve a suitable inlet concentration of minocycline such that the minocycline removal efficiency is high and the MFC has good electricity production.

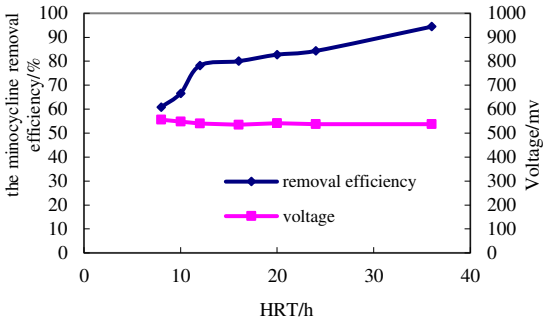

FIGURE 3
Minocycline Removal Efficiency And Power Generation Of MFC Under Different HRT.

After stable voltage outputs were achieved, we measured the COD removal efficiency in 24 h under different minocycline sodium concentrations. When the inlet concentration of minocycline was 2 mg/L, the COD removal efficiency was the best, up to 88.9%. When the inlet concentration of minocycline was 1 mg/L, the COD removal efficiency is 85%. For the inlet concentrations of minocycline 3, 4 and 5 mg/L, the COD removal efficiencies remained the same, i.e. 81%. As shown in Fig. 4a, when the inlet concentration of minocycline was 2 mg/L, the minocycline removal efficiency was obviously the best, up to 94.4% within 36 h. When the inlet concentrations of minocycline were 4 and 5 mg/L, the minocycline removal efficiency decreased to 83.9% and 79.4%, respectively, in 36 h. These results indicated that when the inlet concentration of minocycline is too high, it could inhibit microbial life activities.

As shown in Fig. 4b, when the inlet concentrations of minocycline were 3 and 4 mg/L, the stable voltage outputs of the MFC were the highest, up to 552 and 553 mV, respectively. When the inlet concentrations of minocycline were 2 and 5 mg/L, the stable voltage outputs of the MFC were almost similar, 538 and 540 mV, respectively. When the inlet concentration of minocycline was 1 mg/L, the stable voltage output of the MFC was the lowest, 485 mV.

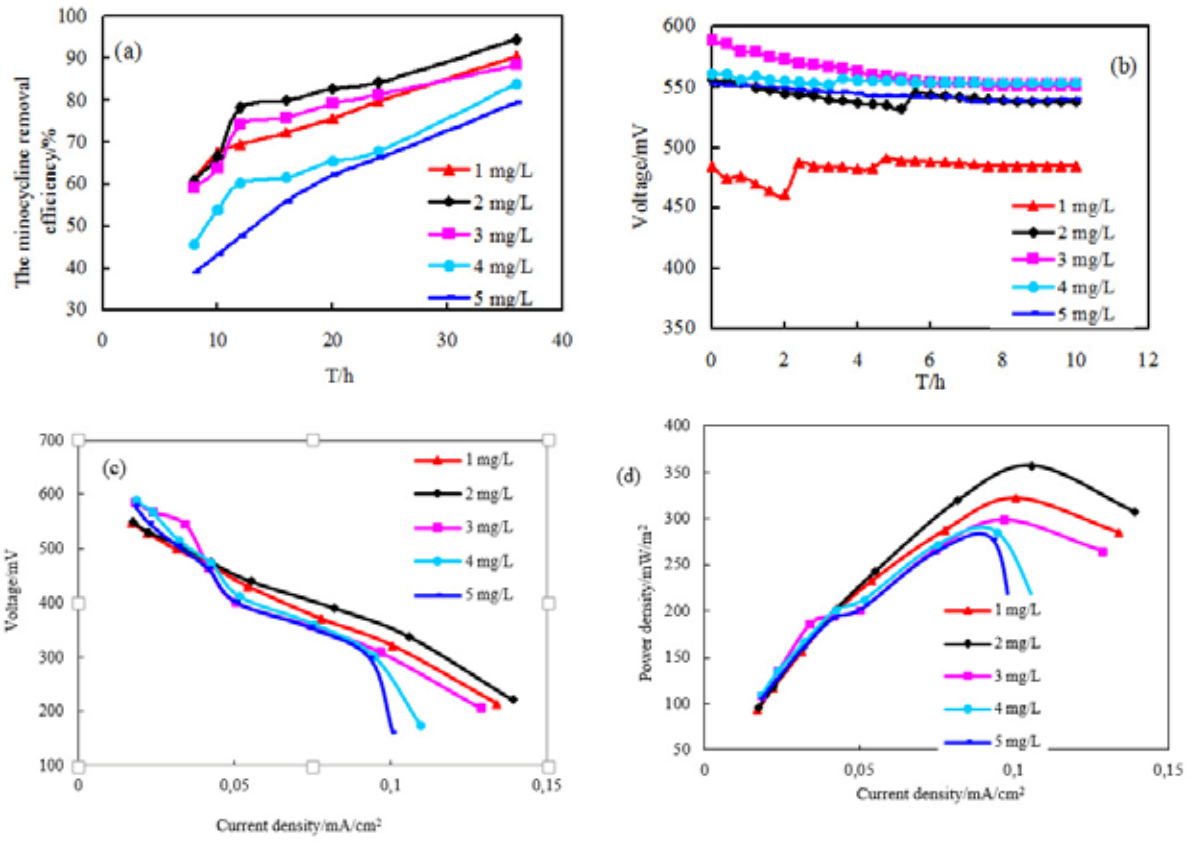

FIGURE 4
Minocycline Removal Efficiency (A), Power Generation (B), Polarization Curve (C), And Power Density Curve (D) Under Different Minocycline Sodium Concentrations.

As shown in Figs. 4c and 4b, when the inlet concentration of minocycline was 2 mg/L and after stable voltage outputs were achieved, the resistance of the MFC was the lowest, 160.3 Ω, and the maximum power density of the MFC was the highest, 357.1 mW/m^2. When the inlet concentration of minocycline was 5 mg/L and after stable voltage outputs were achieved, the resistance of the MFC was the highest, 270.2 Ω, and the maximum power density of MFC was the lowest, 277.4 mW/m^2. When the inlet concentrations of minocycline were 1, 3 and 4 mg/L, and after stable voltage outputs were achieved, the resistances of the MFC were 174.3, 215.6 and 260.4 Ω, respectively. Their maximum power densities for inlet concentrations of 1, 3 and 4 mg/L were 322.0, 298.3 and 284.9 mW/m^2, respectively. These results could explain the high stable output voltages of MFC and low minocycline degradation rates when inlet concentrations of minocycline were 3 mg/L, 4 mg/L and 5 mg/L.

Within a certain concentration range, co-substrates can increase current density, improve the electron transfer capability and decrease internal resistance. Considering the effect of minocycline on cell walls and membranes, we supposed that the minocycline might increase the permeability of electro gens membranes and increase the enzyme release and activity, which would make the diffusion of the redox species easier and the action of the redox enzymes faster [29], leading to the increased direct electron transfer from the cell to the outer membrane and consequently improve the performance of the MFC. Minocycline is a broad-spectrum antibacterial agent and a high concentration has sterilizing effects. Hence, when the inlet concentrations of minocycline were 3, 4 and 5 mg/L, the degradation rates of minocycline were not high.

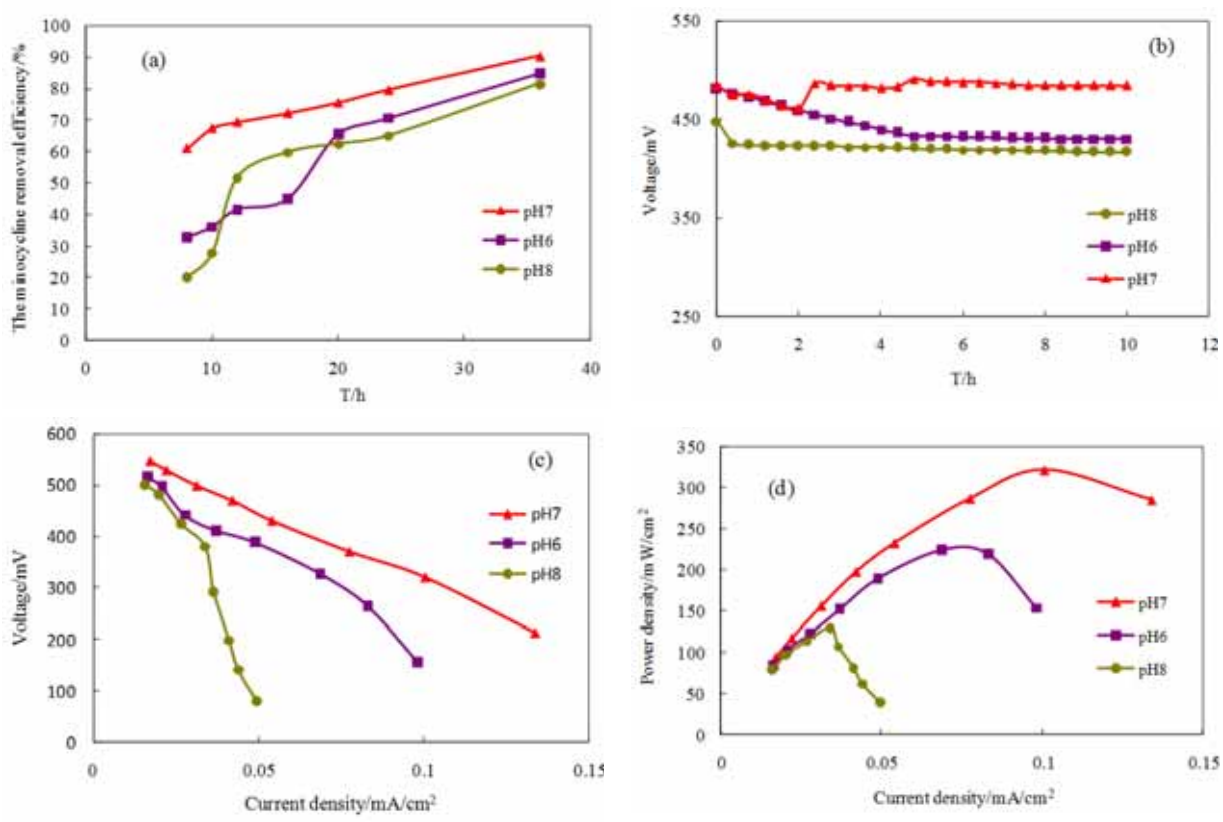

FIGURE 5
Minocycline Removal Efficiency (A), Power Generation (B), Polarization Curve (C), And Power Density Curve (D) Under Different pH.

Effect of pH. pH is one of the important factors that affect the growth of microbial activity, so it is also significant for minocycline degradation and electricity production in the MFC. The nutrient and water that goes in and out in this experiment is normally close to neutral pH. In general, bacterial growth is best in neutral conditions. Here, we use hydrochloric acid and sodium hydroxide to adjust the pH. We found that when the pH is 7, the COD removal efficiency and the minocycline removal efficiency were optimum; the minocycline removal efficiency was 90.5% in 36 h. When the pH is 6, the minocycline removal efficiency was 85.0% in 36 h, and when the pH is 8, the minocycline removal efficiency was 81.7% in 36 h (Fig. 5a).

As shown in Figs. 5b, 5c and 5d, when the pH is 7 and after stable voltage outputs were achieved, the stable voltage output of MFC was the highest, up to 485 mV, the resistance was the lowest, 173.4 Ω and the maximum power density was the highest, 322.0 mW/m^2. When the pH was 6 and 8 and after stable voltage outputs were achieved, the stable voltage outputs of the MFC were 430 and 417 mV, the resistances were 248.6 and 821.1 Ω and the maximum power densities were 224.2 and 129.1 mW/m^2, respectively. To sum up, under neutral conditions, microbial growth was the best; in acidic or alkaline conditions, the growth of the microorganisms was more or less subdued, and compared to the alkaline environment, microorganisms adapted better to the acidic environment.

The increased pH in the cathode compartment can significantly decrease current generation. According to the Nernst equation, the potential of the oxygen reduction reaction should increase with a decrease in the pH value. Decreasing the operational pH would be beneficial for the oxygen reduction and consequently for the current output from MFCs [30]. In addition, generally, bacteria require neutral pH for their optimal growth, and they respond to the changes in internal and external pH by adjusting their activity [31].

Effect of different phosphate buffer sodium concentrations. The best pH for this experiment is 7. However, this will result in the H^+ concentration not reaching the electrolyte levels in an acid or alkali chemical fuel cell, causing the internal resistance to increase. Increasing the concentration of the phosphate buffer sodium (PBS) can increase the

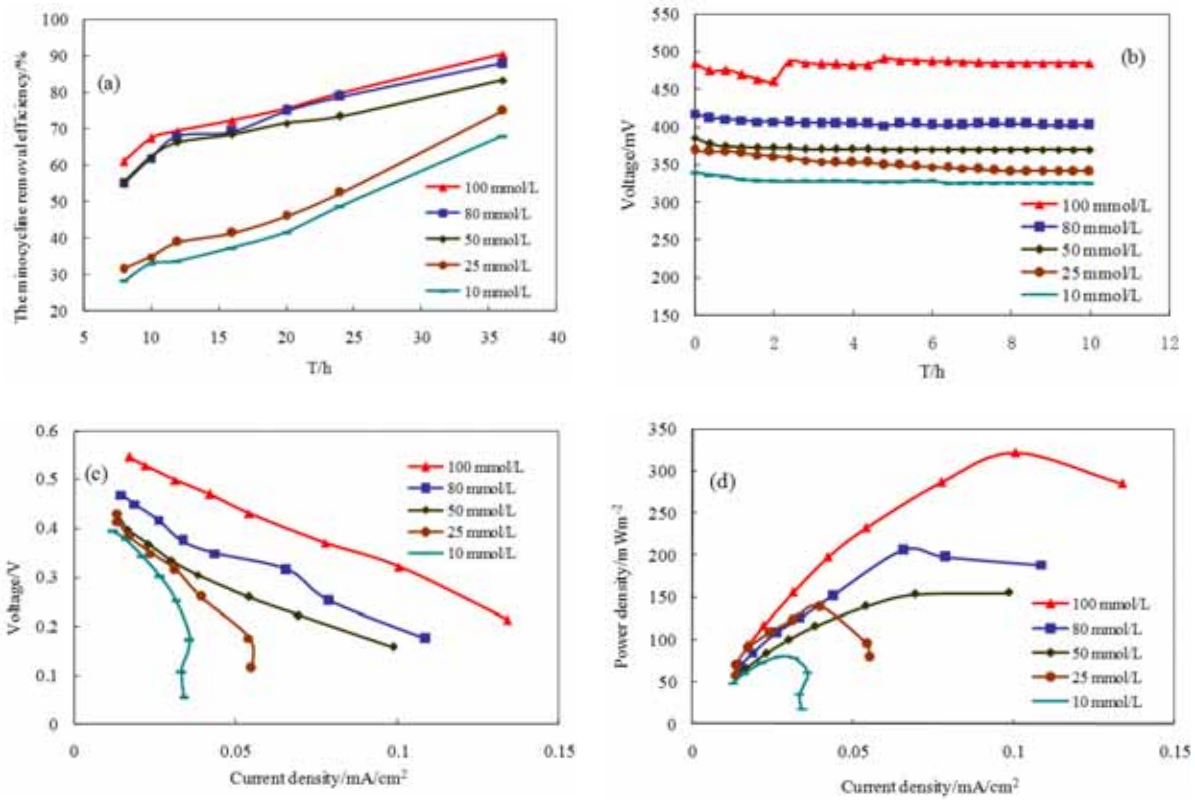

FIGURE 6
Minocycline Removal Efficiency (A), Power Generation (B), Polarization Curve(C), And Power Density Curve (D) Under Different PBS Concentrations.

ionic strength, thereby increasing the electrical conductivity and reducing the internal resistance. In the industrial wastewater, salt concentration is not high. Therefore, in this study, we investigated the effect of different concentrations of PBS on minocycline degradation and electricity production, as shown in Fig. 6a. We found that as the concentration of PBS declines, the COD removal efficiency and the minocycline removal efficiency also fell. When the PBS concentration was 100 mol/L, the COD removal efficiency and the minocycline removal efficiency were optimum; the COD removal efficiency was 82.1% in 24 h, and the minocycline removal efficiency was 90.5% in 36 h. When the PBS concentration was 10 mmol/L, the COD removal efficiency and the minocycline removal efficiency were the worst, the COD removal efficiency was 72.1% in 24 h, and the minocycline removal efficiency was 67.9% in 36 h.

As shown in Figs. 6b, 6c and 6d, when the PBS concentration was 100 mmol/L and after stable voltage outputs were achieved, the stable voltage output of the MFC was the highest, up to 485 mV, the resistance was the lowest, 173.4 Ω and the maximum power density was the highest, 322.0 mW/m^2. When the concentrations of PBS were 80, 50, 25 and 10 mmol/L, and after stable voltage outputs were achieved, the stable voltage outputs of the MFC were 403, 370, 341 and 325 mV; the resistances of the MFC were 190.1, 192.6, 344.4 and 793.0; and the maximum power densities of the MFC were 206.7 mW/m^2, 155.0 mW/m^2, 139.5 mW/m^2 and 80.3 mW/m^2, respectively. To sum up, under neutral conditions, microbial growth was best. In acidic or alkaline conditions, the growth of microorganisms was more or less subdued, and compared to the alkaline environment, microorganisms adapt better to the acidic environment.

Above all, the concentration of PBS has a very important role in an MFC system. The addition of PBS can increase the conductivity of the solution, reduce the internal resistance of an MFC system and achieve higher output voltage and power density. However, in theory, the MFC system relies mainly on the microbial oxidation of organic substrates liberating electrons, to achieve the goal of electricity production. In addition, microorganisms have a certain tolerance to salinity. Beyond the tolerance range, microbial metabolism

will be suppressed and may even result in bacterial dehydration and death. This experiment is based on actual live wastewater where the concentration of PBS is not high. Therefore, we focused on the exploration of low PBS concentration, and we did not consider the condition of high PBS concentration.

The PBS chemical composition and its interaction with electrodes, bacteria and membrane affects the MFC performance. In addition, the buffer helps to reduce changes in pH in the bulk solution and in the biofilm, and therefore it maintains the pH in the range suitable for the growth of microorganisms. Moreover, it has been shown that increasing phosphate concentration within certain ranges increases power output. However, addition of high concentration of PBS is expensive, especially for wastewater treatment, and phosphates can contribute to the eutrophication of water bodies if the effluents are discharged without the removal of these compounds. In addition, the lack of cost effective phosphate recovery techniques makes it impractical for wastewater treatment [32, 33].

CONCLUSIONS

Electricity was successfully generated using minocycline sodium-glucose mixtures as the fuel in the air-cathode single chamber MFC. Compared with conventional anaerobic reactors, the removal efficiencies of minocycline and COD are significantly improved. Interestingly, the critical amount of minocycline, which is conducive to producing electricity, is 2 mg/L. When the concentration of minocycline is 2 mg/L, the removal efficiencies of minocycline and COD are 94.4% and 88.9%, respectively, the resistance was 160.3 Ω and the maximum power density was 357.1 mW/m^2. This study shows the potential of biodegradation of wastewater containing low concentration of antibiotic by using the MFC.

ACKNOWLEDGEMENTS

This research was funded by the National Natural Science Foundation of China with Grant No. 51278022.

REFERENCES

[1] Zhao H.R., Guo S., Fu L.W. (2014) Review on the costs and benefits of renewable energy power subsidy in China. Renew Sustain Energy Rev. 37:538-549.

[2] Ishugah T.F., Li Y, Wang R.Z., Kiplagat J.K. (2014) Advances in wind energy resource exploitation in urban environment: A review. Renew Sustain Energy Rev. 37: 613-626.

[3] Huang C., Su J., Zhao X., Sui J., Ru P., Zhang, H., Wang X. (2012) Government funded renewable energy innovation in China. Energy Policy. 51: 121-127.

[4] Zhao Z.Y., Zuo J., Fan L.L., Zillante G. (2011) Impacts of renewable energy regulations on the structure of power generation in China–a critical analysis. Renew Energy. 36(1): 24-30.

[5] Liu L.Q., Liu C.X., Wang J.S. (2013) Deliberating on renewable and sustainable energy policies in China. Renew Sustain Energy Rev. 17: 191-198.

[6] Lu N., Zhou S.G, Zhuang L., Zhan J.T, Ni J.R. (2009) Electricity generation from starch processing wastewater using microbial fuel cell technology. Biochem. Eng. J. 43(3): 246-251.

[7] Luo H., Liu G., Zhang R., Jin S. (2009) Phenol degradation in microbial fuel cells. Chem. Eng. J. 147(2-3): 259-264.

[8] Logan B., Cheng S., Watson V., Estadt G. (2007) Graphite fiber brush anodes for increased power production in air-cathode microbial fuel cells. Environ. Sci. Technol. 41(9): 3341-3346.

[9] Catal T., Li K, Bermek H., Liu H. (2008) Electricity production from twelve monosaccharides using microbial fuel cells. J. Power Sources. 175(1): 196-200.

[10] Behera M., Ghangrekar M.M. (2009) Performance of microbial fuel cell in response to change in sludge loading rate at different anodic feed pH. Bioresour. Technol. 100(21): 5114-5121.

[11] Wang X., Feng Y., Ren N., Wang H., Lee H., Li N., Zhao Q. (2009) Accelerated startup of two-chambered microbial fuel cells: effect of positive poised potential. Electrochem. Acta 54(3): 1109-1114.

[12] Wen Q., Wu Y., Zhao L., Sun Q., Kong F. (2010) Electricity generation and brewery wastewater treatment from sequential anode-cathode microbial fuel cell. J. Zhejiang Univ. Sci. B. 11(2): 87-93.

[13] Luo Y., Liu G., Zhang R., Zhang C. (2010) Power generation from furfural using the microbial fuel cell. J. Power Sources. 195(1): 190-194.

[14] Zhang C., Li M., Liu G., Luo H., Zhang R. (2009) Pyridine degradation in the microbial fuel cells. J. Hazard. Mater. 172(1): 465-471.

[15] Zhu X.P., Ni J.R. (2009) Simultaneous processes of electricity generation and pnitrophenol degradation in a microbial fuel cell. Electrochem. Commun. 11(2): 274-277.

[16] Wen Q., Kong F., Zheng H., Yin J., Cao D., Ren Y., Wang G. (2011) Simultaneous processes of electricity generation and ceftriaxone sodium degradation in an air-cathode single chamber microbial fuel cell. J. Power Sources. 196(5): 2567-2572.

[17] Wen Q., Kong F., Zheng H., Cao D., Ren Y., Yin J. (2011) Electricity generation from synthetic penicillin wastewater in an air-cathode single chamber microbial fuel cell. Chem. Eng. J. 168(2): 572-576.

[18] Qiang Z., Macauley J.J., Mormile M.R., Surampalli R., Adams C.D. (2006) Treatment of Antibiotics and Antibiotic Resistant Bacteria in Swine Wastewater with Free Chlorine. J. Agric. Food Chem. 54(21) 8144-8154.

[19] Tong C.L., Zhuo X.J., Guo Y. (2011) Occurrence and Risk Assessment of Four Typical Fluoroquinolone Antibiotics in Raw and Treated Sewage and in Receiving Waters in Hangzhou, China. J. Agric. Food Chem. 59(13): 7303-7309.

[20] Abramzon N., Joaquin, J.C., Bray J. (2006) Biofilm Destruction by RF High Pressure Cold Plasma Jet. IEEE Trans. Plasma Science. 34(4): 1304-1308.

[21] Anderl J.N., Franklin M.J., Stewart P.S. (2000) Role of antibiotic penetration limitation in Klebsiella pneumoniae biofilm resistance to ampicillin and ciprooxacin. Antimicrob Agents Chemother. 44(7): 1818-1824.

[22] Cokgor E.U., Alaton, I.A., Karahan, O., Dogruel, S., Orhon, D. (2005) Biological treatability of raw and ozonated penicillin formulation effluent. J. Hazard. Mater. 116(1-2): 159-166.

[23] Wen Q., Wu Y., Cao D., Zhao L., Sun Q. (2009) Electricity generation and modeling of microbial fuel cell from continuous beer brewery wastewater. Bioresour. Technol. 100(18): 4171-4175.

[24] Yin H., Hu X. (2013) Comparison of power generation performance of different types of anodes in microbial fuel cells. Chin. J. Environ. Eng. 7(2): 608-612.

[25] Oliveirab V.B., Simões M., Melob L.F., Pinto A.M.F.R. (2013) Overview on the developments of microbial fuel cells. Biochem. Eng. J. 73:53-64.

[26] Yan H., Saito T., Regan J.M. (2012) Nitrogen removal in a single-chamber microbial fuel cell with nitrifying biofilm enriched at the air cathode. Water Res. 46(7): 2215-2224.

[27] Liu H, Logan B.E. (2004) Electricity generation using an air-cathode single chamber microbial fuel cell in the presence and absence of a proton exchange membrane. Environ. Sci. Technol. 38(14): 4040-4046.

[28] Cheng S., Logan B.E. (2011) Increasing power generation for scaling up single-chamber air cathode microbial fuel cells. Bioresour Technol. 102(6): 4468-4473.

[29] Ramanavicius A., Ramanaviciene A. (2009) Hemoproteins in design of biofuel cells. Fuel cells. 9(1): 25-36.

[30] Nimje V.R., Chen C.Y., Chen C.C., Tsai J.Y., Chen H.R., Huang Y.M., Jean J.S., Chang Y.F., Shih R.C. (2011) Microbial fuel cell of Enterobacter cloacae: effect of anodic pH microenvironment on current, power density, internal resistance and electrochemical losses. Int. J. Hydrogen Energy. 36(17): 11093-11101.

[31] Raghavulu S.V, Mohan S.V., Reddy M.V., Mohanakrishna G., Sarma P.N. (2009) Behaviour of single chambered mediator less microbial fuel cell (MFC) at acidophilic, neutral and alkaline microenvironments during chemical wastewater treatment. Int. J. Hydrogen Energy. 34(17): 7547-7554.

[32] Jadhav G.S., Ghangrekar M.M. (2009) Performance of microbial fuel cell subjected to variation in pH, temperature, external load and substrate concentration. Bioresour. Technol. 100(2): 717-723.

[33] Erable L., Etcheverry A. (2009) Increased power from a two-chamber microbial fuel cell with a low-pH air-cathode compartment. Electrochem. Commun. 11(3): 619-622.

Received: 24.01.2016
Accepted: 19.07.2016

CORRESPONDING AUTHOR

Xiang Hu.
College of Chemical Engineering, Beijing University of Chemical Technology, Beijing 100029, China

E-mail: huxiang@mail.buct.edu.cn

© by PSP Volume 25 – No.10/2016, pages 4345-4350 Fresenius Environmental Bulletin

DECREASING MULTIPLE FRUIT IN PEACH (*PRUNUS PERSICAE* L.) USING SHADE NET AND KAOLIN

Burhanettin Imrak*

[1]Department of Horticulture Faculty of Agriculture, Cukurova University, Adana, Turkey

ABSTRACT

The study was carried out at the experimental area of Pozanti Agricultural Research and Application Center in Adana at 2012 and 2013. Ten years old Françoise peach trees grafted on GF-677 rootstock were used as experimental material. The aim of the present study was to reduce multiple pistil formation usually occurred in early ripening peach cultivars grown in subtropical regions. The high temperatures during flower differentiation are influenced the occurrence of multiple pistil in peaches. Black colored net which had the feature to shade 55%, white colored net with the feature to shade 30%, kaolin and their combinations were applied for the control of high temperatures. The combination of kaolin and black shading system with 55% of light transmission application decreased the temperatures 7.05^{0}C in the flower buds. As a result, the combination of kaolin and black shading system was found to be the best application on decreasing multiple pistil formation for about 68.75% and followed by white net with kaolin application with 62.50% reduction rate compared with control. The results showed that, black shade net with kaolin treatment significantly ($P < 0.05$) reduced the multiple fruit formation percentages and positive effects were observed on the leaf gas exchange parameters (photosynthetic rate (PN), stomatal conductivity (gS), leaf transpiration rate (E), leaf water use efficiency (WUE), SPAD, quantum yield (PSII) compared with the control plants.

KEYWORDS:
Peach, Multiple Fruit, Shade Net, Kaolin, Gas Exchange

INTRODUCTION

Turkey is one of the important producer with the 545.902 tons of peach and nectarine after China (12.000.000 ton), İtaly (1.331.621 ton), Spain (747.200 ton), USA (1.058.830 tons) and Greece (760.200 ton) in the world [1]. In an evaluation report about global warming, it is stated that up to 2100 the average temperature in our world would increase 1.4-5.8^{o}C [2]. It caused negative effects on some plant and fruit characteristics such as loss of vigor, decrease of fruit bearing ability, lower of fruit quality [3]. The high temperature causes the photosynthetic activity reduction and fruit deformation (multiple pistils) in areas where the temperature reaches to 42^{o}C [4]. Moreover, stoma are closes, CO_2 fixation is decreases and it damages to cell activities and photosynthetic membranes [4]. In recent years, light photo-selective net is used for reducing solar radiation and temperature [5,6]. Photo-selective nets have a positive effects on photosynthesis rate by affecting to the spectral quality and quantity of light which is taken by plants [7,8,9]. Moreover, [10] indicated that black colored covers are more effective to reduce the temperature and for coloration white and red colored covers has better results. Increase in daily average temperatures up to 35-45^{o}C cause's yield loses and by increasing double fruit formation so the fruit quality is decreased [11,12,13]. Multiple fruit formation occurs under water stress and increase with the high temperatures at flower bud differentiation period [14]. This period is especially occurred in June, July and August [15,16]. Recently, kaolin are studied and used with many crops to reduce heat stress and sunburn damage [17].

The aim of this study was to reduce the multiple fruit formation by lowering the high temperatures during the bud differentiation period by using net (cover) system with different colors and transmission. Also kaolin applications and combinations with netting.

MATERIALS AND METHODS

Plants, treatments and growth conditions. This study was carried out at Cukurova University Pozantı Agricultural Research Center experimental field at Adana (37^o 03 11'54"N.35^o 21'53.13"E) and at a level of 110m altitude. The plant materials were used ten years old Françoise peach variety which one of the highest double fruiting cultivars grafted on the GF-677 rootstock. In order to reduce the temperature, two different net, kaolin and combined usages were applied. Kaolin is a white colored organic substance and with aluminosilicates composition [18]. Net and kaolin treatments started

in May after harvesting time and terminated in September. The trees were irrigated with drip irrigation and a standard program was applied for plant nutrition. The trial was established with 4m x 2m and Goble pruning system was applied. Françoise is low chilling requirements (200- 300 hours) peach variety and it has high ratio of double fruit formation. The treatment were as follows, black net (55% shade), white net (35% shade), kaolin (6%, 3%, 3%), and combinations. Kaolin was applied three times with three weeks interval. In the first application 6% (6kg/100 lt) ratio of kaolin was sprayed to the leaves and buds with water and 3 weeks later 3% kaolin (3kg/100 lt) was applied [19,20,21].

Chilling accumulation, temperature and gas exchange measurements. For the calculations two different methods were used as chill unit (effective temperatures between 2.5°C and 9.1°C) and standard method (<+7.2°C (45°F)) [22,23,24,25,26]. The leaf and bud temperatures were measured simultaneously with laser thermometer on ten buds and ten leaves chosen randomly all around the trees. The measurements were done between 9:30am and 12:00am when the air was clear. Finally all the fruits over the trees were counted as single or multiple fruits in all treatments.

Transpiration rate (E) ($mmolm^{-2}s^{-1}$), stomatal conductance (gS) ($mmol\ m^{-2}s^{-1}$), net photosynthetic rate (PN) ($\mu mol\ [CO_2]\ m^{-2}s^{-1}$), The instantaneous photosynthetic leaf water use efficiency (WUE) was calculated as WUE = PN/E, according to researchers [27,28,29]. All gas exchange measurements were taken on attached the youngest and completely developed four peach leaves in each replication. The leaf temperature range was between 26 and 28°C and the relative humidity was 65% during the experimental period. PPFD was 250–300 $\mu mol\ m^{-2}s^{-1}$. All gas exchange measurements rate was measured by portable photosynthesis measurements set LCA-4 (ADC, Bio Scientific Ltd., England).

Photosystem II measurement, QY = FV'/FM'; FV'= The changing chlorophyll radiation value on the leaf which's adapted to light; FM'= The maximum chlorophyll radiation value on the leaf which's adapted to light were determined by Fluor Pen TM (Photon System Instruments Ltd, Czech Republic). However leaf chlorophyll concentration was fixed with SPAD-502 meter. The measurements were performed on the young leaves which completed its development in each replication [28,29,30]. The measurements were taken between 9:30am and 12:00am when the air was clear. All photosynthetic measurements were made in four different periods including 15th May- June- July- August and these four values were used in statistical analysis [28].

Statistical analysis. Experiments were carried out as a complete randomized design. Each treatment consisted of three replicates and each replicate included three plants. Data were subjected to ANOVA using SAS 9.0 software. Means comparison were performed by using the LSD test at a significance level of α=0.05.

RESULTS

Chilling accumulation. The chilling accumulation of the region were calculated in two different methods in 2012-2013 period (Table 1). The calculation was started in September but no cold accumulation was seen in September or October concerning two different methods. According to the standard method there was no cold accumulation in November (<7.2°C), but it was calculated as 19 units according to the chill unit method. The cold accumulation continued rising in December and January. According to the standard method cold accumulation was calculated as 497 hours, for cold unit method it was calculated as 375 units. 2012-2013 winter period was warmer than 2011-2012 winter period (Table 1).

TABLE 1
Chilling accumulation in 2012-2013 winter season.

Months	2012 - 2013 Season	
	Standard Method <7.2°C	Chill Unit Method (CU)
November	0	19
December	119	107
January	216	123
February	76	66
March	86	42
Total	497	357

Temperature measurement at plant and multiple fruit formation ratio (%). The temperature was determined that buds were warmer than the leaves in general. The applications reduced the temperature on the flower buds between 7.05°C and 3.5°C on the leaves (Table 2). The temperature could be reduced maximum 16.25% in general (Table 2). The multiple fruit formation rate and the data obtained from the temperature measurements showed parallel results. The maximum double fruit rate obtained from control trees (80%), while the minimum rate detected in black net + kaolin application with the 25% rate. This is followed by white net + kaolin application (30%), only kaolin (34%), black net (57%) and white cover (69%) in sequence (Figure 1A).

TABLE 2
The average temperature reducing effects of treatments on buds and leaves (°C)

Treatments	Bud Temperature (^{0}C)	Leaf Temperature (^{0}C)	Temperature Reducing Effect		
			Bud	Leaf	General
Control	34.21 ± 0.01^a	30.16 ± 0.02^a	-	-	-
White Net (%30)	33.15 ± 0.01^b	30.02 ± 0.01^a	3.09	0.46	1.77
Black Net (%55)	32.10 ± 0.01^c	29.77 ± 0.01^b	6.16	1.29	3.77
Kaolin	30.20 ± 0.02^d	26.75 ± 0.01^c	11.72	11.30	11.51
White Net + Kaolin	27.26 ± 0.01^e	26.68 ± 0.01^{cd}	20.31	11.53	15.92
Black Net + Kaolin	27.16 ± 0.01^f	26.57 ± 0.01^d	20.60	11.90	16.25
$D_{\%5}$	*0.02*	*0.15*	-	-	-

TABLE 3
Effects of treatments on leaf photosynthetic activity

Treatment	P_N	g_S	E	WUE	SPAD (µmol m^{-2})	PSII (Fv'/Fm')
B. Net +Kaolin	14.45 ± 1.04^a	177.75 ± 12.24^a	3.23 ± 0.27^a	4.49 ±0.01^{ab}	42.60 ± 4.31^a	0.74 ± 0.02^a
W. Net+ Kaolin	14.44 ± 1.26^a	168.41 ± 8.22^a	3.21 ± 0.19^a	5.31 ± 0.01^a	41.78 ± 4.52^a	0.73 ± 0.01^a
Kaolin	13.80 ± 1.03^{ab}	165.50 ± 9.44^{ab}	2.97 ± 0.30^{ab}	4.30 ± 0.01^b	41.01 ± 5.24^{ab}	0.71 ± 0.01^b
Black Net	12.60 ± 1.22^{bc}	154.00 ± 9.12^{bc}	2.95 ± 0.21^{ab}	4.29 ± 0.01^b	39.83 ± 2.42^{ab}	0.70 ± 0.01^{bc}
White Net	12.04 ± 1.43^{cd}	145.83 ± 17.22^{cd}	2.81 ± 0.15^b	4.09 ± 0.01^b	39.08 ± 0.55^b	0.70 ± 0.01^{bc}
Control	11.00 ± 0.87^d	138.75 ± 8.52^d	2.38 ± 0.35^c	4.70 ± 0.01^{ab}	38.50 ± 0.89^{bc}	0.69 ± 0.01^c
D%5	*1.36*	*13.25*	*0.37*	*0.91*	*1.52*	*0.015*

B: Black, W: white, P_N: net photosynthetic rate (µmol CO_2 m^{-2} s^{-1}), g_S: stomatal conductivity (mmol m^{-2} s^{-1}), E: transpiration rate (mmol H_2O m^{-2} s^{-1}), WUE: leaf water usage efficiency (µmol (CO_2) mmol (H_2O)$^{-1}$)

Gas exchange measurements: In the trial, the effects of the applications on the leaf net photosynthetic rate (PN) (µmol [CO_2] $m^{-2}s^{-1}$) were determined as maximum with black net + kaolin and white net + kaolin application respectively (14.45-14.44) and the minimum value was 11.09 (µmol CO_2 m^{-2} s^{-1}) in control (Table 3). Leaf stomatal conductivity (gs) (mmol $m^{-2}s^{-1}$) determined that the maximum value to effect were in the applications with black net + kaolin and white net + kaolin (175.78- 168.4 µmol CO_2 m^{-2} s^{-1}) the lowest value was measured 138.75 (µmol CO_2 m^{-2} s^{-1}) in control (Table 3). In the present study, leaf stomatal transpiration ratio (E) (mmol H_2O m^{-2} s^{-1}), since the effects of the applications were studied in the trial. It's determined that the maximum value was 2.38 (mmol H_2O m^{-2} s^{-1}) in control (Table 3).

In terms of PSII maximum value is detected in black net + kaolin and white net + kaolin application (0.74-0.73). And the minimum value is recorded (0.69) in control trees (Table 3). Although there were no big differences in water usage activity (µmol (CO_2) mmol (H_2O)$^{-1}$) the maximum value was determined as 5.31µmol (CO_2) mmol (H_2O)$^{-1}$in white net + kaolin application. The minimum value was determined 4.09µmol (CO_2) mmol (H_2O)$^{-1}$ in white cover application. The other values were taken place among these.

The leaf chlorophyll quantity was examined that it's found important at the level 5%. The values showed differences between 42.60 and 38.50 (µmol m^{-2}) (Table3). The lowest values were recorded in control plants and white net respectively 38.50-39.08 (µmol m^{-2}). The maximum leaf chlorophyll quantity were determined as maximum with black net + kaolin and white net + kaolin application respectively 42.60, 41.78 (µmol m^{-2}) (Table 3).

Consequently no differences were seen in the phenological phases of the types took place in the trial. The treatments in the research applied after the harvesting time, so there is no negative impact on fruit quality criteria including, fruit discoloration, delaying harvesting date and kaolin spot on fruit.

DISCUSSION AND CONCLUSIONS

Double fruit formation is a problem in many warm climatic regions [12]. Researchers [14,31] indicated that multiple pistil formation occurs with the water stress and high temperatures during the differentiation period. This period is especially comes seasonably to July and August [15,31]. The shade net system formed over fruit trees reduces the double fruit formations [32,33]. However, varieties

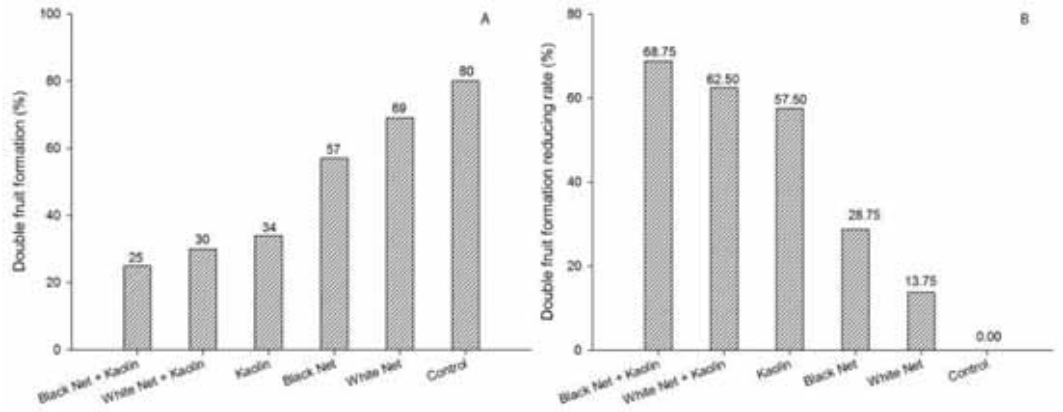

FIGURE 1
The effect of the treatments on multiple fruit in comparison with control (%). Double fruit formation (A), reducing rate (B)

is another important factor [34,35]. Chilling accumulation in 2012-2013 periods was calculated totally 497 hours as standard method and 357 units according to chill unit method. The results were in harmony with the study of researchers [25]. Researchers [32] carried out experiments on the effects of artificial shading on "Satohnishiki" cherry variety. The shade net reduced the light at about 53% and 78% ratio and the temperature between 1.8ºC and 3.2ºC according to the controls. The authors [36] stated that the differentiation period is changing according to the region and type occurs in June or July. Moreover, [35] indicated that on peach trees at the previous year in late July, the temperatures over 30ºC and 35ºC had a direct effect on double fruit formation. The temperature reducing effect of the net and kaolin applications were in harmony with findings obtained from the studies that were done by many researchers [16,19,20,32,33]. Our results showed that the black net + kaolin application which was the most effective method of reducing the temperature (7.05ºC) and decreased the double fruit formation with 68.75%. This was followed with white cover and kaolin (62.5%), kaolin (57.5%), black cover (28.75%) and white cover (13.75%) (Figure 1B). According to the results, the chlorophyll speed (µmol CO_2 $m^{-2}s^{-1}$), stomatal conductance (mmol $m^{-2}s^{-1}$), respiration (mmol H_2O $m^{-2}s^{-1}$), leaf water usage activity (µmol (CO_2) mmol $(H2O)^{-1}$) chlorophyll radiation productivity over PSII and SPAD (µmol m^{-2}) applications had no negative effects on these parameters on the contrary they gave the best results (Table 3). The results were found in accordance with some researchers [7,8]. The authors carried out an experiment on Royal Gala to prevent sunburn. At the end of the research they [21] were stated that all applications reduced the temperatures but the best result was taken from the black net. Also indicated that the similar results with the present study. Moreover, they [20,21] reported that using green shading nets together with kaolin was the most efficient treatment in order to reduce temperature resulting the decrease in multiple pistil formation. In a research [37] to prevent water stress in production of rose 5% kaolin sprayed to the rose shoot and leaves. It was stated that this application decreased the temperature about 2-5ºC according to control and in addition it had no effect on photosynthesis and leaf chlorophyll amount. Our results were found accordance with this research [37] results.

As a result, the applications in the research, to reducing double fruit especially in warm climatic conditions, the best results were seen in the black net + kaolin and white net + kaolin applications, they were followed by black net, kaolin and white net applications in comparison with control. Additionally, it was determined that all applications have positive effects on the growth, photosynthesis and chlorophyll content by reducing the temperature. Because the treatments in the research applied after the harvesting time, there is no negative impact on fruit quality criteria such as, fruit discoloration, delaying harvesting date and kaolin spot on fruit. Moreover, the cover application does not cause an extra cost on account of usage by producers to prevent hail damages.

REFERENCES

[1] FAOSTAT (2012). Food and agricultural commodities production.
[2] IPCC (2007). Climate change 2007. The physical science basis. In: Contribution of Working Group I to the Fourth Assessment Report of the Intergovernmental Panel on Climate Change. Cambridge University Press, Cambridge, UK and New York, USA, 996.
[3] Jangra, M.S., Sharma, J.P. (2013). Climate resilient apple production in Kullu Valley of Himachal Pradesh. International Journal of Farm Sciences 3:91-98.

[4] Guo, Y.P., Zhou, H.F., Zhang, L.C. (2006). Photosynthetic characteristics and protective mechanisms against photo-oxidation during high temperature stress in two citrus species. Scientia Horticulture 108,260–267.

[5] Zoran, S., Ilic-Lidija, M. (2012). The influence of photo-selective shade nets on quality of tomatoes grown under plastic tunnels and field conditions. Scientia Horticulture 139, 90-95.

[6] Lobos, G.A., Retamales, J.B., Hancocb, J.F., Flore, J.A., Romero-Bravo, S., del Pozo, A. (2013). Productivity and fruit quality of Vaccinium Corymbosum Cv. Elliott under photo-selective shading nets. Scientia Horticulture 153,143-149.

[7] Shahak, Y., Gussakovsky, E.E., Cohen, Y., Lurie, S., Stern, R., Kfir, S., Naor, A., Atzmon, I., Doron, I. and Greenblat-Avron, Y. (2008). Colour nets: A new approach for light manipulation in fruit trees. Acta Horticulture 636, 609-616.

[8] Justen, V.L., Fritz, V.A., Cohen, J.D. (2012). Seasonal variation in Glucosinolate accumulation in turnips grown under photo selective nettings. Horticulture Environment and Biotechnology 53(2), 108-115.

[9] [9] Stamps, R.H. (2009). Use of colored shade netting in horticulture. Horticulture Science 44,239–241.

[10] Bastías, R.M., Manfrini, L. and Grappadelli, L.C. (2012). Exploring the potential use of photo-selective nets for fruit growth regulation in apple. Chilean Journal of Agricultural Research 72(2), 224-231

[11] Adir, N., Zer, H., Shochat, S., Ohad, I. (2003). Photo inhibition, a historical perspective. Photosynthesis Resources 76, 343-370.

[12] Kudela, V. and Krejzar, V. (2005). Occurrence of fruit doubles in the 2004 season associated with heat and drought stress in previous year. Plant Protection Science 41(1), 27-32.

[13] Lopez, G. and Dejong, T.M. (2007). Spring temperatures have a major effect on early stages of peach fruit growth. Journal of Horticultural Science and Biotechnology 82(4), 507–512.

[14] Naor, A., Stern, R., Peres, M., Greenblat, Y., Gal, Y. and Flaishman, M.A. (2005). Timing and severity of postharvest water stress affect following-year productivity and fruit quality of field-grown 'Snow Queen' nectarine. Journal American Society Horticulture Science 130, 806-812.

[15] Naor, A. (2006). Irrigation scheduling of peach – deficit irrigation at different phenological stages and water stress assessment. Acta Horticulture 713, 339-350.

[16] İmrak, B., Küden A.B., Küden, A., Sarıer, A. and Tütüncü, M. (2014). Studies on shading system in sweet cherries prevent from double fruit formation under subtropical conditions. Acta Horticulture 1059, 171-176.

[17] Maletsika, P. A., Nanos, G.D., Stavroulakis, G.G. (2015). Kaolin effect on fresh and canned clingstone peach fruit quality and inorganic element composition. Acta Horticulture doi 10.17660/ActaHortic.2015.1084.45

[18] Gleen, D.M., Proda, E., Erez, A., Puterka, G.J. and Gundrum, P. (2003). Particle film affect carbon assimilation and yield in 'Empire' apple. Journal American Society Horticultural Science 128(3), 356-362.

[19] Gleen, D.M., E. Proda, A. Erez, J. Mcferson, and Puterka, G.J. (2002). A reflective, processed-kaolin particle film affects fruit temperature, radiation reflection and solar injury in apple. Journal American Society Horticultural Science 127(2)188-193.

[20] Yazıcı, K. and Kaynak, L. (2007). Bahçe bitkilerinde kaolin kullanım durumu ve etki mekanizması. Türkiye V. Ulusal Bahçe Bitkileri Kongresi, Erzurum, 872-876.

[21] Gindaba, J., Wand, S.J.E. (2007). Do fruit sunburn control measures affect leaf photosynthetic rate and stomatal conductance in "Royal Gala" apple. Environmental and Experimental Botany 59, 160-165.

[22] Richardson, E.A., Seeley, S.D. and Walker, D.R. (1974). A model for estimating the completion of rest of 'Redhaven' and 'Elberta' peach trees. Horticulture Science 9,331–332.

[23] Rose, G.A. and Cameron, R.W. (2009). Chill unit models for Blackcurrant (*Ribes Nigrum* L.) Cultivars 'Ben Gairn', 'Ben Hope' and 'Ben Tirran'. Scientia Horticulture 122,654-657.

[24] İmrak, B. (2010). Performances of Some sweet Cherry Cultivars (*Prunus Avium* L.) Under the Subtropical Climatıc Conditions and Researches to the Solution of Multiple Pistil. Cukurova University, ADANA, 193.

[25] Rai R, Joshi S, Roy S, Singh O, Samir M, et al. (2015) Implications of changing climate on productivity of temperate fruit crops with special reference to apple. Journal of Horticulture 2(2), 135-141. doi:10.4172/2376-0354.1000135

[26] Luedling, E., Zhang, M., Gale, M. and Charles, L. (2009). Validation of winter chill models using historic records of walnut phenology. Agricultural and Forest Meteorology 149, 1854–1864.

[27] Ribeiro, R.V., Machado, E.C., Santos, M.G., Oliveira, R.F. (2009). Photosynthesis and water relations of well watered orange plants

as affected by winter and summer conditions. Photosynthetica 47, 215‑222.
[28] Hardıng, S.A., Jarvıe, M.M., Lındroth, R.L. and Tsaı, C.J. (2009). A comparative analysis of phenyl popanoid metabolism, utilization and carbon partitioning in fast and slow growing populus hybrid clones. Journal of Experimental Botany 60(12), 3443-3452.
[29] Jifon, J.L., Syvertsen, J.P., Whaley, E. (2005). Growth environment and leaf anatomy affect nondestructive estimates of chlorophyll and nitrogen in citrus leaves. Journal of American Society Horticulture Science 130, 152–158.
[30] Binayak, C., Singh, P. N., Singh, A. K. and Srivastava, P. C. (2014). Evaluation of different iron sources for iron chlorosis recovery in low-chill peach cultivars. Journal of Plant Nutrition, 37:2, 224-231, DOI: 10.1080/01904167.2013.859693
[31] Engin, H., and Ünal, A. (2007). Examination of flower bud initiation and differentiation in sweet cherry and peach by scanning electron microscope. Turkish Journal of Agriculture and Forestry 31, 373-379.
[32] Beppu, K. and Kataoka, I. (2000). Artificial shading reduces the occurrence of double pistil in 'Satohishiki' sweet cherry. Scientia Horticulture 83, 241-247.
[33] Briassoulis, D., Mistriotis, A. and Eleftherakis, D. (2007). Mechanical behavior and properties of agricultural nets testing methods for agricultural nets. Polymer Testing. 26, 882-832.
[34] Ogašanovic, D., Ognjanov, V., Mitrovic, M., Radulovic, M, Plazinic, R., Leposavic, A., Lukic, M. and Radièevic, S. (2005). Nove sorte podloge vocaka. Vocarstvo 39, 213-232.
[35] Engin, H. and Ünal, A. (2004). The effects of water deficits on fruit doubling peach cultivars. Ege Üniversitesi Ziraat Fakültesi Dergisi 41(2), 29-36.
[36] Chılders, N.F. (1961). Modern fruit science. Printed by Somerset Press, Inc., Somerville, New Jersey, 128-132.
[37] Yuly, M., Sotelo, C., Hermann, R., Alexandra, G., Augusto, R. and Victor, R. (2011). Effect of kaolin film particle applications (surround wp®) and water deficit on physiological characteristics in rose cut plants (*rose spp* l.). American Journal of Plant Sciences 11(2), 354-358. Doi:10.4236/Ajps.2011.

Received: **28.01.2016**
Accepted: **16.08.2016**

CORRESPONDING AUTHOR

Burhanettin Imrak
Faculty of Agriculture,
Department of Horticulture,
University of Cukurova,
01130, Sarıcam, Adana, Turkey

e-mail: bimrak@cu.edu.tr

© by PSP Volume 25 – No. 10/2016, pages 4351-4361 Fresenius Environmental Bulletin

INTEGRATED HEALTH RISK ASSESSMENT NEAR A SMELTER BASED ON SOIL CD(II) POLLUTION

Wen-bin Li[1], Zhao-fu Meng[1, 2*], Hua-yun Chen[3], Ze Liu[1], Lu Yu[1], Shao-e Xu[4], Wei Liu[1]

[1]Department of Natural Resource and Environment, Northwest A&F University, Yangling, Shaanxi, 712100, China
[2]Key Laboratory of Plant Nutrition and Agri-Environment in Northwest China, Ministry of Agriculture, Yangling 712100, China
[3]Department of Agricultural, Northwest A&F University, Yangling, Shaanxi, 712100, China
[4]Department of Biological and Agriculture Engineering, University of Arkansas, Fayetteville 72707, US

ABSTRACT

In this study, we established a systematic health risk evaluation model by using the assessment of Cd(II) risks in different sources (soil, dust, and crop). A metallic smelter was selected in this paper. Cd(II) contents in different soil areas (116 soil samples) were determined, and the Cd(II) contents in dust and crop were calculated based on soil content. The acceptability of the health risks of Cd(II) in soil, dust, and crop in different R regions (annular regions were created based on 500 m interval) were analyzed to determine the overall acceptable limit of Cd(II) content. Results showed that: 1) The average Cd(II) contents of the surface soil ranged from 0.20 mg kg^{-1} to 0.55 mg kg^{-1}, and the highest Cd(II) content (1.81 mg kg^{-1}) was found in the NW direction. 2) The total carcinogenic risk of Cd(II) in R1 was 1.59×10^{-6}, which was beyond the safe level of 1×10^{-6}. The total non-carcinogenic risk for children was greater than that for adult, risk values were all lower than the limit level of 1. 3) The risk contribution of carcinogenic through ingestion (> 90%) was the largest among the other pathways, while the non-carcinogenic risk was over than 99%. Carcinogenic and non-carcinogenic risks were mainly originated from Cd(II) pollutants in soil and plant, respectively. 4) In the R1-NW area, mandatory management should be performed (> safety level). The R1-SW and R2-NW/WSW areas only need an early warning for carcinogenic risk, as well as the R1-NW area for non-carcinogenic risk(> 80% safety level). However, carcinogenic risk should be given particular attention in the R1-SSW/ESE/SE/W, R2-NNE, R3, SE, R5-SSW, and R7-ESE areas (> 60% safety level). The acceptable Cd(II) contents were 1.14 and 2.40 mg kg^{-1} for the carcinogenic and non-carcinogenic risks, respectively.

KEYWORDS:
Smelter, Cd(II) pollution, health risk assessment, safety level.

INTRODUCTION

Metal smelting is considered as a pillar industry in China and an important source of heavy metals pollution [1, 2]. Its processes significantly affect the surrounding environments by accumulating and transferring heavy metals in soil, plant, and air [3, 4], thereby posing a potential risk for human health [5]. However, heavy metals contamination is usually unnoticeable compared with other forms of pollution [6, 7]. Therefore, a risk assessment of heavy metals pollution is an urgent measure to alert nearby residents of smelter regarding their safety [8].

The accumulation of heavy metals in the human body can lead to kidney, bone and pulmonary damage. Heavy metals can enter human body through different potential sources, such as soil [9], dust [10], and crop [11], as well as through various absorption pathways, such as direct ingestion, dermal contact, inhalation, and oral intake [12-16]. Methods have been proposed by USEPA (United States Environmental Protection Agency) for the assessment of heavy metals pollution [17-19]. However, the selection of heavy metal ions content in calculation models are diverse, and maximum content is often used to reflect all potential risks [20, 21]. Moreover, the commonly used parameter, i.e., total heavy metal ions concentration [22], is sufficient for exposure and health risk assessment and toxic effect determination [23, 24]. Various indices may produce inconsistent results even at the same sampling site because of limited performance for evaluation [25-27]. Currently available assessment approaches tend to focus more on a single pollution source, such as soil dust, ash soil, and agricultural products [9, 11, 12, 28], and risk analysis with probability of dust production from contaminated soil [29]. Several studies also showed that agricultural soil contaminated by heavy metal ions can result in high levels of heavy metal ions in crops [30-32].

Current methods in risk management application are convenient but not very efficient considering the risk of sedimentation from atmospheric particle pollution and the transfer of

pollution from soil to plant. To attain complete assessment of the risk of soil pollution and potential pollution caused by soil, the risk caused by atmospheric sedimentation and pollution transfer to plants should be considered. A comprehensive evaluation method with the use of soil, dust, and plant must also be established to obtain reasonable remediation limit of soil. The evaluation methods recommended by US Environment Protection Agency (USEPA), as well as by domestic scholars should be considered. We chose Cd(II) as representative heavy metal ions. Cd(II) contents in soil, calculated Cd(II) contents in dust and crop were used to scientifically assess the health risk in contaminated site. Distribution characteristics of Cd(II) in R1-R8 were analyzed. Contribution rates of non-carcinogenic and carcinogenic risk in different pollution pathways and exposure routes were discussed. Existing risk areas, risk pre-warning areas, risk attention areas were partitioned particularly and the acceptable limit of Cd(II) content under different critical levels were proposed.

MATERIALS AND METHODS

Background of the contaminated site. The study area is located in Northeastern China and surrounded by a smelter (Fig. 1), which covers a rectangular area of about (500 × 1300) m^2, and the long axis is located at the NW-SE direction. The elevation ranges from 629.4 m to 632.9 m, with a higher terrain in the South than in the North. A railway is close to the factory on the NE direction, and a river in the NW direction is 500–700 m away from the factory. A reservoir also lies in the South part of the area. The main crop planted at the surrounding fields is wheat. The prevailing wind directions are NW-SE and WNW-ESE.

Collection and determination of the soil sample. The total soil survey area was about 44 km^2 (from the factory boundary outward with 0–4 km range). Centered on the contaminated site and annular regions were created based on 500 m interval. Then each annular region was divided into 16 sectors based on the direction (Fig. 1). Four samples in each sector were collected with uniform sample size of 20 cm × 20 cm × 20 cm. The location of the sampling sites is shown in Fig. 1. Soil samples of about 1 kg were collected and homogenized to make a model sample from each section of the site. Grass, stones and other particles were removed from the soil, and then the soil was oven dried, sieved through a 0.25 mm sieve, and stored in the sampling bags.

The Cd(II) concentrations in the supernatant were determined using a Hitachi Z-5000 atomic absorption spectrometer. Background absorption was corrected using the Zeeman effect.

Establishment of assessment method. The subjects for risk assessment involve pollution in soil, as well as in dust and crop (wheat), which was caused by soil pollution.

Risk assessment model for soil. The basic equations for calculating carcinogenic and non-carcinogenic risks from ingestion, inhalation, and dermal contact through soil were as follows [33, 34]

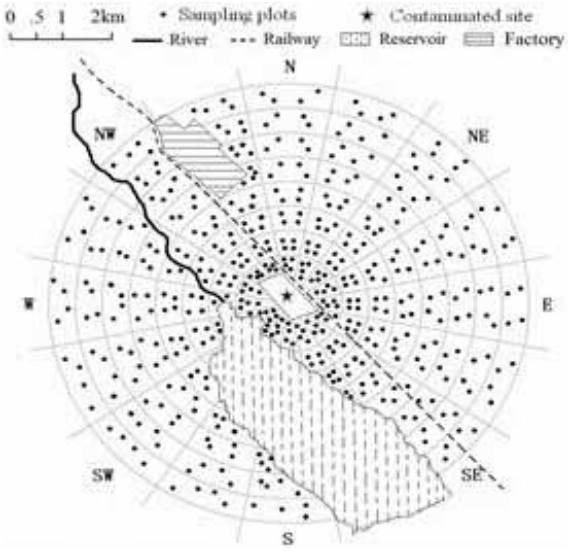

FIGURE 1
Study area and sampling points.

1) Carcinogenic risk

$$HR = CDI \times SF$$

Where HR is the probability of an individual to develop cancer over a lifetime (unitless), CDI is chronic daily intake or dose (mg/kg/day), and SF is the slope factor expressed in (mg/kg/day) $^{-1}$. CDI for carcinogenic risk of the three pathways:

$$CDI = \frac{C_S \times EF}{AT} \times \left(\frac{CR_{ad} \times ED_{ad}}{BW_{ad}} + \frac{CR_{ch} \times ED_{ch}}{BW_{ch}} \right)$$

C_s is the Cd(II) concentrations in soil and dust (mg kg^{-1}). CR = IR_{Ing} and CR = IR_{Inh} denote the ingestion and inhalation pathways, respectively, whereas CR = SA × SL × ABS refers to the dermal contact pathway.

2) Non-carcinogenic hazard quotient

$$HQ = CDI / RFD$$

Where CDI refers to the chronic daily intake of the toxicant, (mg/kg/day), RFD is the chronic reference dose of the toxicant (mg/kg/day), and HQ is the cumulative non-carcinogenic hazard for multiple exposure pathways (unitless).

CDI (soil and dust ingestion) for non-carcinogenic risk:

$$CDI_{Ing} = \frac{C_S \times EF \times ED \times IR_{Ing}}{AT \times BW}$$

CDI (inhalation of particles emitted from soil and dust) for non-carcinogenic risk:

$$CDI_{Inh} = \frac{C_S \times ED \times EF \times IR_{Inh}}{AT \times BW \times PEF}$$

CDI (dermal contact with soil and dust) for non-carcinogenic risk:

$$CDI_{Der} = \frac{C_S \times EF \times ED \times SA \times SL \times ABS}{AT \times BW}$$

Risk assessment model for dust. The form of heavy metal in dust was similar with that in soil and accumulated by sinking into the soil, thereby increasing the contaminants. Therefore, the carcinogenic and non-carcinogenic risks of ingestion, inhalation, and dermal contact through dust pathway can be calculated using the model for soil. The Cd(II) content in dust could be calculated using the following equation:

$$W_n = BK^n + RK\frac{1-K^n}{1-K}$$

Where W_n is soil heavy metal ions content after n years (mg kg^{-1}), B is the initial content of heavy metal ions in soil (mg kg^{-1}), R is the average corrected soil content by sedimentary dust into the soil every year (mg kg^{-1}), K is the residual rate of heavy metal in soil (unitless), and n is the age of pollution (years).

Risk assessment model for crop (wheat). The Cd(II) content in wheat grain (edible part) was calculated using bioconcentration factors (BCFs), and the relationship between Cd(II) in soil and grain can be obtained through the following equation:

$$BCF = C_{Crop} / C_{Soil}$$

Where BCF is the bioconcentration factor (unitless), C_{Crop} is Cd(II) content in wheat grain (mg kg^{-1} of dry weight), and C_{Soil} is Cd(II) content in soil (mg kg^{-1}). Based on the studies of Liu [35] and Zhang [36] regarding bioconcentration in this area, 0.0210 was chosen as the BCF of the wheat grain.

The health risk of Cd(II) ingestion was assessed using the target hazard quotients (THQ) [37]:

$$THQ = \frac{C_f \times EF \times ED \times F_{IR}}{RFD \times BW \times AT}$$

Where C_f is Cd(II) content in food (mg kg^{-1}), and F_{IR} is the food ingestion rate of food (kg d^{-1}); The ingestion rate for adult and child was 0.428 and 0.325 kg day^{-1}, respectively [38]. The other parameters were similar with the ones mentioned in in Table 1.

Selection of parameters. Maximum Cd(II) concentrations were used to calculate the potential carcinogenic and non-carcinogenic risks for children and adults in the study area. The parameters for international exposure dose and risk assessment model were established basically for Europeans and Americans; therefore, with the differences in race, daily habits, and so on, parameters need to be modified according to specific conditions [39]. The exposure parameters of the population in China surveyed by some domestic scholars and related institutions [40, 41] were combined with other foreign literature for reference dose, carcinogenic slope factor, and other parameters [33, 42]. The parameters for calculating the values of the exposed model are shown in Table 1.

TABLE 1
Exposure factors for dose models.

Parameters	Adult	Child	References
SF (slope factor)	Ingestion=Dermal (0.38); Inhalation (6.3)		(Li 2012) [43]
RFD (chronic reference dose)	Ingestion=Inhalation(1×10^{-3}); Dermal (1×10^{-5})		(Li 2012) [43]
EF (exposure frequency)	350 days year^{-1}	320 days year^{-1}	(Li 2012) [43]
ED (exposure duration)	24 year	6 year	(USEPA 2001) [44]
AT (averaging time)	Carcinogens (365 days/year/71.4 years); Non-carcinogens (365 days/year/ED child or adult)		(USEPA 1989) [45]
IR_{Ing} (ingestion rate)	150 mg day^{-1}	250 mg day^{-1}	(Li 2012) [43]
IR_{Inh} (inhalation rate)	12.8 m^3 day^{-1}	7.63 m^3 day^{-1}	(Li 2012) [43]
BW (body weight)	58.6 kg	15 kg	(Li 2012) [43]
PEF (particulate emission factor)	region-specific 1.36×10^9 (unitless)		(USEPA 2002) [33]
SA (exposure skin area)	2145 cm^2	1150 cm^2	(USEPA 2001) [44]
SL (skin adherence factor)	0.07mg/(cm^2·day)	0.2 mg/(cm^2·day)	(USDOE 2001) [46]
ABS (dermal absorption factor)	0.001 (unitless)		(Ferreira-Baptism and De-Miguel 2005) [20]

RESULTS AND DISCUSSION

Concentration distribution of Cd(II) under different areas. The Cd(II) contents under different distances from the pollution source are presented in Fig. 2. The average Cd(II) contents of the surface soil ranged from 0.20 mg kg^{-1} to 0.55 mg kg^{-1}, which gradually decreased from R1 to R4. A stable Cd(II) content was observed when the distance from the pollution source went beyond 2 km, which might be caused by dust settlement in the atmosphere around the smelter. Moreover, the polluted range and extent of damage were related to factors such as the soot particle size, chimney height, wind power, wind speed, and terrain [5, 9]. At the distance of 3.5 km, a modest increase was observed because another pollution source was nearby. The highest Cd(II) content was found in the NW direction (1.81 mg kg^{-1}), within the distance of 500 m and 3.02 times higher than the national standard II (0.6 mg kg^{-1}). The highest Cd(II) content in each R region was found at NW (R1 and R2), SE (R3), WNW (R4), SSW (R5), S (R6), ESE (R7), and ENE (R8). This result was consistent with the prevailing winds (NW-SE and WNW-ESE) in the region.

Cd(II) risk in soil, dust, and crop under different areas. The carcinogenic risk is considered low when it is less than 10^{-6} and high when it is more than 10^{-6}. Meanwhile, 1 is the critical level of non-carcinogenic risk.

Carcinogenic risk. Table 2 shows that the carcinogenic risk of Cd(II) in soil gradually reduced with the increase in the distance from the factory. The risk in R1 was 1.41×10^{-6}, which was beyond the safe level of 1×10^{-6}. Carcinogenic risk already exists in this area. The carcinogenic risk in dust for R1–R4 (2 km outside the factory boundary) areas was uniformly distributed with high Cd(II) content in soil on an average, hence the low carcinogenic risk. The carcinogenic risk in crop for the whole

area was not significant. For the total carcinogenic risk, the R1 area exceeded the safety level, indicating a dire need of risk management. The carcinogenic risk in the R2 area reached 88% of the critical value, indicating a need for an early warning. Finally, R3–R5 and R7 areas reached 60% of the critical value, which means some attention must be paid to risk prevention.

Non-carcinogenic risk. The non-carcinogenic risk in soil and dust were smaller in the whole area, and the risk for children was greater than for adults. The crop risk value for children in R1 reached 0.721, which was close to the limit level (1), whereas the risks in the other R regions were lower. Therefore, R1 should be given more attention for its high total HQ value (HQ = 0.754).

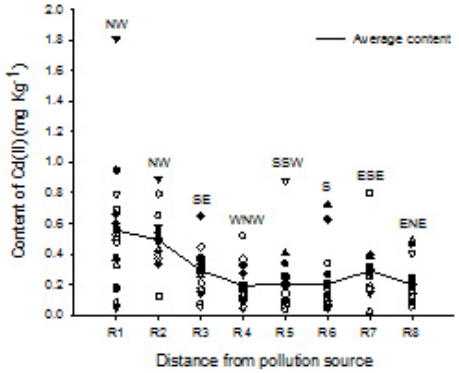

FIGURE 2
Cd(II) contents under different distances from the pollution source (R1-R8: annular regions were created based on 500 m interval within a 4 km radius, the same below).

TABLE 2
Carcinogenic risk of Cd(II) in soil, dust, and crop under different areas.

Pollution sources	Pathways	Assessment areas							
		R1	R2	R3	R4	R5	R6	R7	R8
Soil	Ingestion	1.41×10^{-6}	6.97×10^{-7}	5.04×10^{-7}	4.02×10^{-7}	6.87×10^{-7}	5.65×10^{-7}	6.23×10^{-7}	3.81×10^{-7}
	Inhalation	1.23×10^{-9}	6.07×10^{-10}	4.39×10^{-10}	3.50×10^{-10}	5.98×10^{-10}	4.92×10^{-10}	5.43×10^{-10}	3.32×10^{-10}
	Dermal contact	1.34×10^{-9}	6.63×10^{-10}	4.80×10^{-10}	3.83×10^{-10}	6.54×10^{-10}	5.38×10^{-10}	5.94×10^{-10}	3.63×10^{-10}
Dust	Ingestion	1.79×10^{-7}	1.79×10^{-7}	1.79×10^{-7}	1.79×10^{-7}	-	-	-	-
	Inhalation	1.56×10^{-10}	1.56×10^{-10}	1.56×10^{-10}	1.56×10^{-10}	-	-	-	-
	Dermal contact	1.71×10^{-10}	1.71×10^{-10}	1.71×10^{-10}	1.71×10^{-10}	-	-	-	-
Crop	Ingestion	$< 10^{-10}$	$< 10^{-10}$	$< 10^{-10}$	$< 10^{-10}$	$< 10^{-10}$	$< 10^{-10}$	$< 10^{-10}$	$< 10^{-10}$
Total		1.59×10^{-6}	0.88×10^{-6}	0.68×10^{-6}	0.58×10^{-6}	0.69×10^{-6}	0.57×10^{-6}	0.62×10^{-6}	0.38×10^{-6}

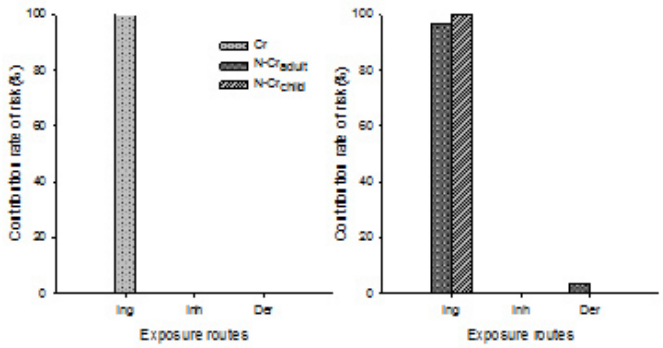

FIGURE 3
Contribution rates of non-carcinogenic and carcinogenic risk in children and adults under different exposure routes. Ing, Inh and Der are ingestion, dermal contact and inhalation, respectively.

TABLE 3
Non-carcinogenic risk of Cd(II) in soil, dust, and crop under different areas.

Groups	Pollution sources	Pathways	Assessment areas							
			R1	R2	R3	R4	R5	R6	R7	R8
Child	Soil	Ingestion	2.64×10^{-2}	1.30×10^{-2}	9.45×10^{-3}	7.53×10^{-3}	1.29×10^{-2}	1.06×10^{-2}	1.17×10^{-2}	7.14×10^{-3}
		Inhalation	5.93×10^{-7}	2.93×10^{-7}	2.12×10^{-7}	1.69×10^{-7}	2.89×10^{-7}	2.38×10^{-7}	2.62×10^{-7}	1.60×10^{-7}
		Dermal contact	2.43×10^{-3}	1.20×10^{-3}	8.69×10^{-4}	6.92×10^{-4}	1.18×10^{-3}	9.74×10^{-4}	1.07×10^{-3}	6.57×10^{-4}
	Dust	Ingestion	3.36×10^{-3}	3.36×10^{-3}	3.36×10^{-3}	3.36×10^{-3}	-	-	-	-
		Inhalation	7.54×10^{-8}	7.54×10^{-8}	7.54×10^{-8}	7.54×10^{-8}	-	-	-	-
		Dermal contact	3.09×10^{-4}	3.09×10^{-4}	3.09×10^{-4}	3.09×10^{-4}	-	-	-	-
	Crop	Ingestion	7.21×10^{-1}	3.56×10^{-1}	2.58×10^{-1}	2.05×10^{-1}	3.51×10^{-1}	2.89×10^{-1}	3.19×10^{-1}	1.95×10^{-1}
	Total		0.754	0.374	0.272	0.217	0.365	0.301	0.332	0.203
Adult	Soil	Ingestion	4.44×10^{-3}	2.19×10^{-3}	1.59×10^{-3}	1.26×10^{-3}	2.16×10^{-3}	1.78×10^{-3}	1.96×10^{-3}	1.20×10^{-3}
		Inhalation	2.79×10^{-7}	1.38×10^{-7}	9.96×10^{-8}	7.93×10^{-8}	1.36×10^{-7}	1.12×10^{-7}	1.23×10^{-7}	7.53×10^{-8}
		Dermal contact	4.45×10^{-4}	2.19×10^{-4}	1.59×10^{-4}	1.27×10^{-4}	2.16×10^{-4}	1.78×10^{-4}	1.96×10^{-4}	1.20×10^{-4}
	Dust	Ingestion	5.65×10^{-4}	5.65×10^{-4}	5.65×10^{-4}	5.65×10^{-4}	-	-	-	-
		Inhalation	3.54×10^{-8}	3.54×10^{-8}	3.54×10^{-8}	3.54×10^{-8}	-	-	-	-
		Dermal contact	5.65×10^{-4}	5.65×10^{-4}	5.65×10^{-4}	5.65×10^{-4}	-	-	-	-
	Crop	Ingestion	2.66×10^{-1}	1.31×10^{-1}	9.51×10^{-2}	7.57×10^{-2}	1.29×10^{-1}	1.07×10^{-1}	1.18×10^{-1}	7.19×10^{-2}
	Total		0.272	0.135	0.098	0.078	0.131	0.109	0.120	0.073

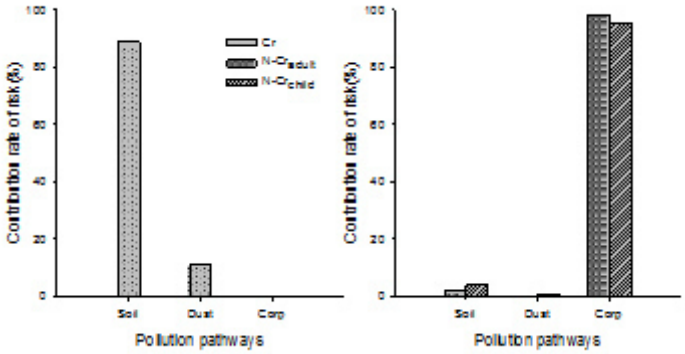

FIGURE 4
Contribution rates of non-carcinogenic and carcinogenic risk in children and adults under different pollution pathways.

Contribution rate of risk for Cd(II). The contribution rates of non-carcinogenic and carcinogenic risks in children and adults under different exposure routes are shown in Fig. 3. The values for the pathways in this study decreased in the order of ingestion > dermal contact > inhalation. The contribution of ingestion was the highest with more than 95%, and even 99% for children. This result indicated that ingestion is the primary pathway of heavy metal harm to human health.

Dermal contact and inhalation were the lowest, which was consistent with the previous study [32]. As shown in Fig. 4, pollution mainly originated from Cd(II) in soil for the carcinogenic risk, with more than 95% contribution, whereas pollution originated from metal pollutants in plants for the non-carcinogenic risk. For the heavy metals pollution area, residents can take appropriate measures to reduce harm to their bodies according to the results.

Division of different pollution levels. Based on the above risk assessment standard, the maximum Cd(II) content in R1–R8 areas was adopted, but this can only evaluate the risk in maximum direction. The risks on other directions (outside maximum direction) cannot be ruled out. Therefore, the maximum Cd(II) content cannot fully reflect the existing risk area of the contaminated site.

Through the above evaluation results, those areas with risk beyond the safety level should take urgent measures, whereas those under more than 80% level should be given an early warning, and those under 60% level should pay some attention to risk prevention. The risks of all directions in R1–R8 areas were calculated from high to low, so as to fully reflect the specific contaminated areas in the study site (Table 4). The carcinogenic risk in the R1-NW area was larger than 10^{-6}, hence the necessity for mandatory management. An early warning on Cd(II) pollutants should be provided for the R1-SW and R2-NW/WSW areas, whereas R1-SSW/ESE/SE/W, R2-NNE, R3, SE, R5-SSW, and R7-ESE areas should pay some attention to risk reduction. In terms of non-carcinogenic risk for children, R1-NW area should be given an early warning. However, no non-carcinogenic risk was observed in adults. By comparing the main directions of the wind, which were WNW, NW, SE, ESE, in the field throughout the year, health risks and hidden dangers were found to exist in radioactive-polluted areas close to the main directions of the wind.

Acceptable limit of Cd(II) content under different critical levels (safe levels). The carcinogenic risk of Cd(II) mainly originated from the contaminated soil through ingestion. For the non-carcinogenic risk, pollution was derived from plants and through ingestion; however, the calculated acceptable threshold was within the acceptable limits of Cd(II) content (Table 5 for the soil pollution remediation limit and detailed parameters). When the Cd(II) content went beyond 1.14 mg kg^{-1}, the carcinogenic risk was over the safety level, which was close to the third-class standard (1.0 mg kg^{-1}) of the soil environmental quality standard in China (Table 6). A total Cd(II) content of 2.40 mg kg^{-1} showed that carcinogenic and non-carcinogenic (child) risks was found. A value of over 6.67 mg kg^{-1} indicated that carcinogenic and non-carcinogenicrisks were present in child and adult.

TABLE 4
Risk values and their directions in different areas. NO_1 to NO_6 means the risk order from high to low.

Risks	Orders	Distribution	Assessment areas							
			R1	R2	R3	R4	R5	R6	R7	R8
HR ($\times10^{-6}$)	NO_1	Value	Oca.59	0.88	0.68	-	0.69	-	0.69	-
		Direction	NW	NW	SE		SSW		ESE	
	NO_2	Value	0.92	0.80						
		Direction	SW	WSW						
	NO_3	Value	0.79	0.69						
		Direction	SSW	NNE						
	NO_4	Value	0.72							
		Direction	ESE							
	NO_5	Value	0.69							
		Direction	SE							
	NO_6	Value	0.65							
		Direction	W							
HQ (Child)	NO_1	Value	0.75							
		Direction	NW							

TABLE 5
Cd(II) contents under different critical levels.

Risks	Cd(II) content under different critical levels (mg Kg^{-1})			
	Three pollution pathways (soil, dust and crop)			Only soil pathway
	Safe level	80% safe level	60% safe level	Safe level
Carcinogenic	1.14	0.91	0.68	1.28
Non-carcinogenic (child)	2.40	1.92	1.44	62.41
Non-carcinogenic (adult)	6.67	5.34	4.00	624.14

TABLE 6
Standards for soil Cd(II) limitation in China. GB15618-1995 is soil environmental quality standard, and HJ 332-2006 is farmland environmental quality evaluation standards for edible agricultural products.

Standards	Indexs	Cd(II) content (mg Kg^{-1})
GB 15618-1996	Primary	0.20
	Secondary (pH>7.5)	0.60
	Third class	1.00
HJ 332-2006 (pH>7.5)	Dry-cultivation and water-cultivation, fruit trees, etc	0.60
	Vegetables	0.40

Furthermore, if the Cd(II) content went beyond 0.91 mg kg^{-1}, the carcinogenic risk would reach 80% of the safety level, in which an early warning is needed, whereas with the Cd(II) content of 0.68 mg kg^{-1}, some attention to carcinogenic risk should be given, the content approach the secondary (pH > 7.5) standard (0.6 mg kg^{-1}) of soil environmental quality standard (GB 15618-1996) and the dry-cultivation, water cultivation, fruit trees, etc standard (0.6 mg kg^{-1}) of farmland environmental quality evaluation standards for edible agricultural products (HJ 332-2006 pH > 7.5) in China.

Considering only the health risks in soil, the remediation limit for soil pollution with carcinogenic risk increased to 1.28, and 62.41 (child) and 624.14 (adult) with non-carcinogenic risk. This result may increase the acceptable range of risk, although some potential threats for human health might still exist. Under normal circumstances, the heavy metals pollution in soil are always multiple and simultaneous, and studies of the total pollution risk assessment are common both locally and abroad. Therefore, considering the potential risk for all existing heavy metals contamination is significantly important in controlling the risks of pollution and protecting human health [24, 28].

CONCLUSION

The average Cd(II) contents of the soil surface ranged from 0.20 mg kg^{-1} to 0.55 mg kg^{-1}, which gradually decreased with the increase in distance from R1 to R4. A stable Cd(II) content was observed when the distance from the pollution source was beyond 2 km. In terms of existing carcinogenic risk of Cd(II), the carcinogenic risk in R1-NW area was higher than 10^{-6}, which mainly originated from contaminated soil and through ingestion. For the non-carcinogenic risk, pollution was derived from plants and through ingestion. The acceptable limit of Cd(II) content was 1.14 mg kg^{-1}. Areas with Cd(II) content of more than 0.68 mg kg^{-1} must be given particular attention.

ACKNOWLEDGEMENTS

The authors wish to acknowledge with thanks the financial assistance from the National Natural Science Foundation of the P. R. of China (No. 41271244), Social Development Project (No. 2013K0105) in Shaanxi province.

REFERENCES

[1] Deng, C. B., Li, L. H., Wang, S. F., Li, N., Zhang, C. L., & Li, Z. Y. (2009). Pollution characteristics of heavy metal in paddy soil near a typical Pb-Zn mining area. *Journal of Agro-Environment Science, 28*(11), 2297-2301.

[2] Tserenpil, S., & Liu, C. Q. (2011). Study of antimony(Ⅲ)binding to soil humic acid from an antimony smelting site. *Microchemical Journal, 98*, 15-25.

[3] Li, Y., Wang, Y. B., Gou, X., Su, Y. B., & Wang G. (2006). Risk assessment of heavy metals in soils and vegetables around non-ferrous metals mining and smelting sites, Baiyin, China. *Journal of Environmental Science, 18*(6), 1124-1134.

[4] Wu, C. F., Wu, J. P., Luo, Y. M., Zhang, H. B., Teng. Y., Song. J., & Wu, L. H. (2009). Identification and uncertainty analysis of scope of heavy metal pollution in the vicinity of secondary copper smelteries. *Acta Pedologica Sinica, 46*(6), 1006-1012.

[5] Bi, X. Y., Feng, X. B., Yang, Y. G., & Li, G. H. (2006). Environmental contamination of heavy metals from zinc smelting areas in Hezhang County, western Guizhou, China. *Environment International, 32*, 883-890.

[6] Wang, Q. R., Dong, Y., Cui, Y., & Liu, X. (2001). Instances of soil and crop heavy metal contamination in China. *Soil and Sediment Contamination, 10*, 497-510.

[7] Acosta, J. A., Faz, A., Martinez-Martinez, S., Zornoza, R., Carmona, D. M., & Kabas, S. (2011). Multivariate statistical and GIS-based approach to evaluate heavy metals behaviour in mine sites for future reclamation. *Journal of Geochemical Exploration, 109*, 8-17.

[8] Yadav, R. K., Goyal, B., Sharma, R. K., Dubey, S. K., & Minhas, P. S. (2002). Post-irrigation impact of domestic sewage effluent on composition of soils, crops and ground water-a case study. *Environment International, 28*(6), 481-486.

[9] Hu, Y., Liu, X., Bai, J., Shih, K., Zeng, E.Y., & Cheng, H. (2013). Assessing heavy metal pollution in the surface soils of a region that had undergone three decades of intense industrialization and urbanization. *Environmental Science and Pollution Research, 20*(9), 6150-6159.

[10] Li, H. M., Qian, X., Hu, W., Wang, Y., & Gao, H. (2013). Chemical speciation and human health risk of trace metals in urban street dusts from a metropolitan city, Nanjing, SE China. *Science of the Total Environment, 456*, 212-221.

[11] Bermudez, G. M. A., Jasan, R., Plá, R., & Pignata, M.L. (2011). Heavy metal and trace element concentrations in wheat grains: assessment of potential non-carcinogenic health hazard through their consumption. *Journal of Hazardous Materials, 193*, 264-271.

[12] Muhammad, S., Shah, M. T., & Khan, S. (2010). Arsenic health risk assessment in drinking water and source apportionment using multivariate statistical techniques in Kohistan region, northern Pakistan. *Food and Chemical Toxicology, 48*(10), 2855-2864.

[13] Park, R. M., Bena, J. F., Stayner, L. T., Smith, R. J., Gibb, H. J., & Lees, P. S. (2004). Hexavalent chromium and lung cancer in the chromate industry: a quantitative risk assessment. *Risk Analysis*, *24*(5) , 1099-1108.

[14] Al-Saleh, I., Shinwari, N., El-Doush, I., Biuedo, G., Al-Amodi, M., & Khogali, F. (2004). Comparison of mercury levels in various tissues of albino and pigmented mice treated with two different brands of mercury skin-lightening creams. *Biometals, 17*(2), 167-175.

[15] Komárek, M., Chrastný, V., & Mihaljevič, M. (2008). Lead isotopes in environmental sciences: a review. *Environment International, 34*, 562-577.

[16] Lu, Y., Yin, W., Huang, L. B., Zhang, G. L., & Zhao, Y. G. (2011). Assessment of bioaccessibility and exposure risk of arsenic and lead in urban soils of Guangzhou City, China. *Environmental Geochemistry and Health, 33*(2), 93-102.

[17] Wang, X., Sato, T., Xing, B., & Tao, S. (2005). Health risks of heavy metals to the general public in Tianjin, China via consumption of vegetables and fish. *Science of the Total Environment, 350*, 28-37.

[18] Sridhara, C. N., Kamala, C. T., & Raj, D. S. S. (2008). Assessing risk of heavy metals from consuming food grown on sewage irrigated soils and food chain transfer. *Ecotoxicology Environment Safety, 69*(3), 513-524.

[19] Yang, Q. W., Xu, X., Liu, S. J., He, J. F., & Long, F. Y. (2011). Concentration and potential health risk of heavy metals in market vegetables in Chongqing, China. *Ecotoxicology Environment Safety, 74*(6), 1664-1669.

[20] Ferreira-Baptism, L., & De-Miguel, E. (2005) Geochemistry and risk assessment of street dust in Luanda, Angola : A tropical urban environment. *Atmospheric Environment, 39*(25), 4501-4512.

[21] De-Miguel, E., Iribarren, I., Chacón, E., Ordoñez, A., & Charlesworth, S. (2007) Risk-based evaluation of the exposure of children to trace elements in playgrounds in Madrid(Spain). *Chemosphere, 66*(3), 505-513.

[22] Praveena, S. M., Aris, A. Z., & Radojevic, M. (2010). Heavy metals dyanamics and source in intertidal mangrove sediment of Sabah, Borneo Island. *Environment Asia, 3*, 72-81.

[23] Szakova, J., & Sysalova, J. (2006). Mobility assessment and validation of toxic elements in tunnel dust samples-subway and road using sequential chemical extraction and ICP-OES/GF AAS measurements. *Environmental Research, 101*(3), 287-293.

[24] Zhao, X., Dong, D., Hua, X., & Dong, S. (2009). Investigation of the transport and fate of Pb, Cd, Cr(VI) and As(V) in soil zones derived from moderately contaminated farmland in Northeast, China. *Journal of Hazardous Materials, 170*, 570-577.

[25] Yang, Z., Wang, Y., Shen, Z., Niu, J., & Tang, Z. (2009). Distribution and speciation of heavy metals in sediments from the mainstream, tributaries, and lakes of the

Yangtze River catchment of Wuhan, China. *Journal of Hazardous Materials, 166*(2-3), 1186-1194.

[26] Yu, G., Liu, Y., Yu, S., Wu, S., Leung, A., Luo, X., Xu, B., Li, H., & Wong, M. (2011). Inconsistency and comprehensiveness of risk assessments for heavy metals in urban surface sediments. *Chemosphere, 85*(6), 1080-1087.

[27] Qiao, Y., Yang, Y., Gu, J., & Zhao, J. (2013). Distribution and geochemical speciation of heavy metals in sediments from coastal area suffered rapid urbanization, a case study of Shantou Bay, China. *Marine Pollution Bulletin, 68*(1-2), 140-146.

[28] Zhu, Y., Zhao, Y., Sun, K., Chen, Z., Qiao, J., & Ji, Y. (2011). Heavy metals in wheat grain and soil: assessment of the potential health risk for inhabitants in a sewage-irrigated area of Beijing, China. *Fresen. Environ. Bull., 20*, 1109-1116.

[29] Spurgeon, D. J., Rowland, P., Ainsworth, G., Rothery, P., Long, S., & Black, H. I. J. (2008). Geographical and pedological drivers of distribution and risks to soil fauna of seven metals (Cd, Cu, Cr, Ni, Pb, V and Zn) in British soils. *Environmental Pollution, 153*(2), 273-283.

[30] Pandey, J., & Pandey, U. (2008). Accumulation of heavy metals in dietary vegetables and cultivated soil horizon in organic farming system in relation to atmospheric deposition in a seasonally dry tropical region of India. *Environmental Monitoring and Assessment, 148*(1), 61-74.

[31] Bermudez, G. M. A., Jasan, R., Plá, R., & Pignata, M. L. (2012). Heavy metals and trace elements in atmospheric fall-out: their relationship with topsoil and wheat element composition. *Journal of Hazardous Materials, 213-214*, 447-456.

[32] Sharma, R. K., Agrawal, M., & Marshall, F. M. (2008). Heavy metal (Cu, Zn, Cd and Pb) contamination of vegetables in urban India: a case study in Varanasi. *Environmental Pollution, 154*(2), 254-263.

[33] USEPA. (2002). Supplemental guidance for developing soil screening levels for superfund sites OSWER 9355 (pp.4-24).

[34] RAIS. (2007). The risk assessment information system. http://rais.ornl.gov/.

[35] Liu, W. X., Zhao, Q. Y., & Qin, L. (2004). Pollution and accumulation of heavy metals in the soils and wheat. *Henan Science*, 22(6): 870-872.

[36] Zhang, S. J., Xiao, L., Sun, K., Zhang, Y. H., Guan, S. P., & Cheng, D. G. (2009). Study on Characteristic of Heavy Metals Contaminated Farm land Soil around a Smelter. *Research of Agricultural Modernization, 30*(2), 243-247.

[37] USEPA. (2000). Supplementary guidance for conducting health risk assessment of chemical mixtures, Risk Assessment Forum Technical Panel. [EPA/630/R-00/002].

[38] Guan, S. P., Zhao, X. G., & Liang, N. (2008). On safety threshold of agricultural water resources based on food security in Shaanxi Province. *Agricultural Research in the Arid Areas, 26*(6), 241-244.

[39] Li, R. Z., Zhou, A. J., Tong, F., Wu, Y. D., Zhang, P., & Yu, J. (2011). Distribution of Metals in Urban Dusts of Hefei and Health Risk Assessment. *Environmental Science, 32*(9), 2661-2668.

[40] Wang, Z., Liu, S. Q., Chen, X. M., & Lin, C. Y. (2008) Estimates of the exposed dermal surface area of Chinese in view of human health risk assessment. *Journal of Safety and Environment, 8*(4), 152-156.

[41] Ministry of Health of the People's Republic of China. (2007). China Health Statistical Yearbook. Beijing: Beijing union medical university press, 207-208.

[42] Lim, H. S., Lee. J. S., Chon, H. T., & Sager, M. (2008). Heavy metal contamination and health risk assessment in the vicinity of the abandoned Songeheon Au-Ag mine in Koma. *Journal of Geochemical Exploration, 96*(2/3), 223-230.

[43] Li R. Z., Pan C R., Chen J., Jiang Y M., & Ding G Z. (2012). Heavy metal contamination and health risk assessment for urban top soil and dust in Tongling City. *China Environmental Science, 32,* 2261-2270.

[44] USEPA. (2001). Risk Assessment Guidance for Superfund: Volume III–Part A, Process for Conducting Probabilistic Risk Assessment. US Environmental Protection Agency, Ishington, D.C. EPA 540-R-02-002.

[45] USEPA. (1989). Risk assessment guidance for superfund, Vol. 1: Human Health Evaluation Manual. EPA/540/1-89/002. Ishington. D.C: Office of Soild Iste and Emergency Response.

[46] USDOE. (2011). The Risk Assessment Information System (RAIS). U.S. Department of Energy's Oak Ridge Operations Office (ORO).

Received: **28.01.2015**
Accepted: **20.07.2016**

CORRESPONDING AUTHOR

Zhaofu Meng
Department of Natural Resource and Environment
Northwest A&F University
Key Laboratory of Plant Nutrition and Agri-Environment in Northwest China
Ministry of Agriculture
Yangling 712100 - CHINA

Email: zfmeng@hotmail.com

© by PSP Volume 25 – No. 10/2016, pages 4362-4373 Fresenius Environmental Bulletin

HABITAT PREFERENCES OF AQUATIC OLIGOCHAETA (ANNELIDA) SPECIES IN THE LAKE DISTRICT (TURKEY)

Seray YILDIZ*

Ege University, Faculty of Fisheries, Department of Hydrobiology, 35100 Bornova-İzmir-Turkey

ABSTRACT

In order to determine habitat preferences of aquatic Oligochaeta in the Lake District area of Turkey, quantitative sampling and measurements of some of the selected physicochemical variables were done seasonally from June 1999 to November 2000. Total of 45 Oligochaeta species were collected from 75 different habitats. Canonical Correspondence Analysis (CCA) explained 81% of the correlation among species and environmental variables with about % 32.5 of variance. Influential variables on the species distribution from most to least affective follow as water depth, Secchi depth, pH, dissolved oxygen, elevation, temperature, $CaCO_3^=$, electrical conductivity and salinity. Species were clustered into six groups with Unweighted Pair Group Mean Averages (UPGMA) analyses based on species occurrence. Overall, results suggest that each Oligochaeta species has species-specific habitat preferences although some of them overlap in their requirements.

KEYWORDS:
Aquatic Oligochaeta, Habitat Preferences, CCA, Lake District, Turkey

INTRODUCTION

The ecological requirements of aquatic Oligochaeta (Annelida) and their relationship to abiotic factors in inland waters of Turkey have received little attention up to date. While many taxonomic studies on oligochaetes have been published, a few ecological studies based on these organisms have been conducted [1-10]. The Lake District region, covering about 36,672 km^2 of area, is located in the western part of Mediterranean including three cities as Antalya, Isparta and Burdur. The topography of the area is composed of narrow and long mountain ranges surrounding depression areas where lakes are formed. The altitude is relatively high, but decreasing slightly in depression areas like Burdur and Eğirdir [11]. The area is known one of the richest areas with hundreds of natural and man-made lakes. Although its importance cannot be ignored for many reasons, there have been a few limnology-based studies on the area. For example, one of the earlier studies done by Sözen and Yiğit [12] reported the benthic fauna and some limnological properties of the Lake Akşehir. Species of Tubificidae family of Oligochaetae were reported and these species were left at the level of genus. Kazanci et al. [13] reported members of Lumbriculidae family in Eğirdir, Bafa and Eber Lakes and Büyük Menderes Delta but they did not perform detailed species description on Oligochaeta. Zeybek et al. [10] investigated that the effects of environmental variables on distribution of aquatic Oligochaeta and Chironomidae at Kovada Channel and the linked lakes (Lakes Eğirdir and Kovada). The other studies were mostly researched based on taxonomical features of aquatic Oligochaeta of The Lake District [5, 14-19]. The current study is different from the others; it covers the whole water bodies of the area and researched habitat preferences of aquatic Oligochaeta species in the Lake District.

Thus, the aims of this study include (1) understanding the range of species distribution in the area, (2) to show species habitat preferences, and (3) to deduce the relationships between individual species and environmental variables.

MATERIALS AND METHODS

Sampling procedure and environmental variables. Samples of macrozoobenthos were collected from 75 localities including 21 lakes, 12 dams, 30 underground water sources, 7 streams, 3 canals, one pond and one cave within two years from June 1999 to November 2000 in the Lake District (Figure 1).

A standard Hand dip-net was used for shore samplings in streams and standing waters but Ekman-Birge grab (15x15 cm) was used in open water of lakes, ponds and dams. Depth, water temperature, dissolved oxygen values; pH, salinity, electrical conductivity and alkalinity as well as altitude and coordinates were determined at the most stations. Alkalinity and $CaCO_3^=$ analysis were conducted in the laboratory.

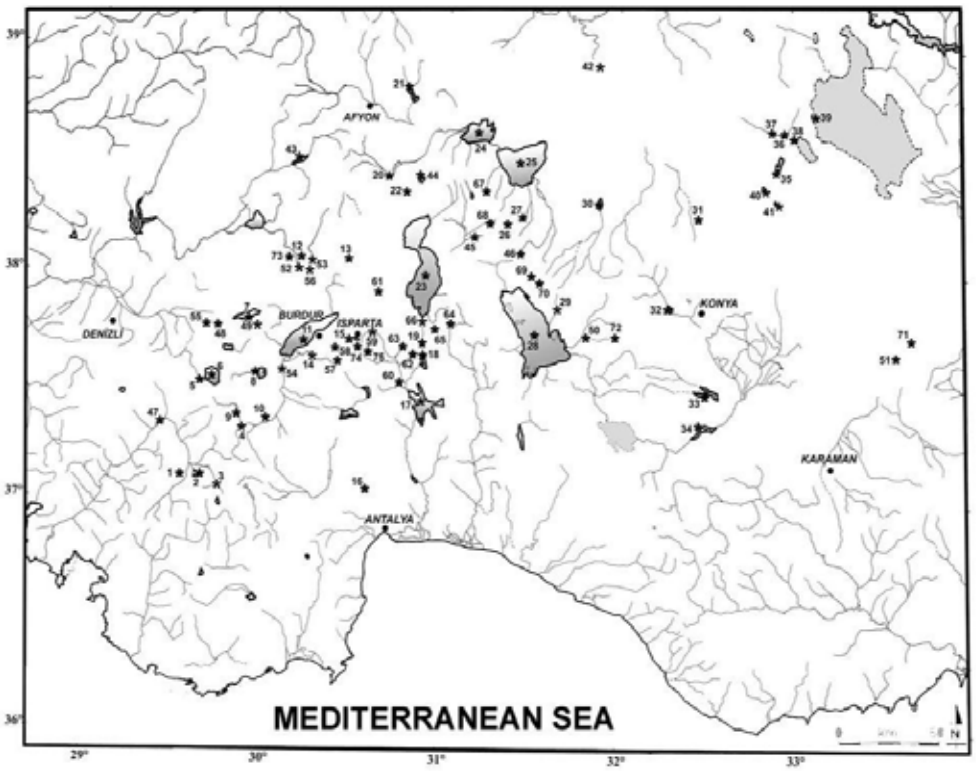

FIGURE 1
Map of Lake District in Turkey (Station numbers and codes of stations are given in Appendix).

The material was fixed on sites with 4% formaldehyde and brought to the laboratory where it was filtered by a sieve (500 µm mesh size). After sorting the material, Oligochaete specimens were preserved in 70% alcohol and prepared for identification as temporary mounts using Amman's Lactophenol solution.

Species identification was done based on some of the systematic keys such as Brinkhurst [20], Brinkhurst and Jamieson [21], Brinkhurst and Wetzel [22], Kathman and Brinkhurst [23], Nielsen and Christensen [24], Sperber [25, 26] and Timm [27].

Data Analysis. Faunistic and environmental data were analyzed by Canonical Correspondence Analysis (CCA) after testing the data with Detrended Correspondance Analysis (DCA). During the CCA progress in CANOCO program [28] we preferred 63 stations at which species occurred at least four times. This method permits the construction of theoretical variables (ordination axes) that best fit the species data according to a unimodal method of ordination [29]. In order to eliminate or reduce the effect of skewness of the data, we log-transformed [ln (x+1)] the environmental variables except pH. The statistical significance of the relationship between all species and all variables was tested by Monte Carlo permutation test using 199 permutations. Rare species were downweighted and taxa encountered in only one sample were excluded to reduce multicolinearity [30,31]. A Nonparametric Spearman Rank correlation analysis was performed to show the relationships between species and environmental variables. A clustering analysis of unweighted pair group mean averages (UPGMA) was used to identify different taxonomic assemblages among the species in each sampling site. UPGMA analysis, was conducted using the Multi-Variate Statistical Package (MVSP) program version 3.1 [32] and Spearman CorrelationAnalysis was applied by using SPSS 17.0.

RESULTS AND DISCUSSION

Qualitative analysis. During the sampling periods in 1999 and 2000, 4100 individuals belonging to 24 genera and 45 species (2 species from Lumbriculidae, 1 species from Haplotaxidae, 3 species from Enchytraeidae, 23 species from Tubificinae, 14 species from Naidinae, 1species from Lumbricidae and 1 species from Glossoscolecidae) were collected. The abbreviation for each taxon used in analyses is given in Table 1. *Tubifex tubifex, Limnodrilus hoffmeisteri, Limnodrilus udekemianus, Potamothrix hammoniensis* (Tubificinae) and *Dero digitata*

TABLE 1
Abbreviations and list of 45 Oligochaete species collected from the Lake District area during this study.

Species	Abbreviation
Lumbriculus variegatus (Müller, 1774)	*Lumb.var*
Tatriella slovenica Hrabe, 1936	*Tat.slov*
Haplotaxis gordioides (Hartmann, 1821)	*Hapl.gor*
Henlea nasuta (Eisen, 1878)	*Hen.nasu*
Henlea ventriculosa (Udekem, 1854)	*Hen.vent.*
Mesenchytraeus armatus Levinsen, 1884	*Mes.arma*
Tubifex tubifex (Müller,1774)	*Tub.tub.*
T. tubifex f. bergi (Müller,1774)	*T.tub.f.*
T. ignotus (Stolc, 1886)	*Tub.igno*
T.nerthus Michaelsen, 1908	*Tub.nert*
T. montanus Kowalewski,1919	*Tub.mont*
Limnodrilus hoffmeisteri Claparede,1862	*Lim.hoff*
L. hoffmeisteri f. parvus Southern, 1909	*L.hoff.f*
L. udekemianus Claparede,1862	*Lim.udek*
L. profundicola (Verrill, 1871)	*Lim.prof*
Psammoryctides albicola (Michaelsen, 1901)	*Psam.alb*
P.deserticola (Grimm,1877)	*Psam.des*
Potamothrix heuscheri (Bretscher, 1900)	*Pot.heus*
P. hammoniensis (Michaelsen,1901)	*Pot.ham.*
P. bavaricus (Öschmann, 1913)	*Pot.bav.*
P. bedoti (Piguet, 1913)	*Pot.bed.*
Ilyodrilus templetoni (Southern,1909)	*Ily.temp*
Ilyodrilus frantzi Brinkhurst, 1965	*Ily.fran*
Haber speciosus (Hrabe,1931)	*Hab.spec*
Quistadrilus multisetosus (Smith, 1900)	*Quis.mul*
Spirosperma ferox (Eisen,1879)	*Spir.fer*
S. nikolskyi Lastockin and Sokolskaya, 1953	*Spir.nik*
Aulodrilus pluriseta (Piguet, 1906)	*Aul.plu*
A. pigueti Kowalewski, 1914	*Aul.pig*
Paranais frici Hrabe, 1941	*Para.fri*
Ophidonais serpentina (Müller, 1773)	*Oph.serp*
Nais communis Piguet, 1906	*Nais com*
N. variabilis Piguet, 1906	*Nais var*
N. pardalis Piguet, 1906	*Nais par*
N. elinguis Müller,1773	*Nais eli*
N. barbata Müller,1773	*Nais bar*
N. pseudobtusa Piguet, 1906	*Nais pse*
Stylaria lacustris (Linnaeus, 1767)	*Sty.lac.*
S. fossularis Leidy, 1852	*Sty.foss*
Dero digitata (Müller,1773)	*Dero dig*
D. obtusa d'Udekem,1855	*Dero obt*
Pristinella acuminata Liang,1958	*Pris.acu*
P. osborni (Walton, 1906)	*Pris.osb*
Eiseniella tetraedra (Savigny,1826)	*Eis.tetr*
Criodrilus lacuum Hoffmeister,1845	*Cri.lac.*

(Naidinae) were found as the dominant species. The similar results were found by Zeybek et al. [10]). The author reported that *T. tubifex, L. hoffmeisteri* in Lake Eğirdir and Channel Kovada, and *T. tubifex* in Lake Kovada were determined as a dominant species. Also, *T. tubifex, L. hoffmeisteri, P. hammoniensis, Ophidonais serpentina* were determined as a dominant species in Lake Eğirdir [5]. *P. hammoniensis, T. tubifex, L. hoffmeisteri* and *Nais communis* was the dominant in Lake Kovada [19]. The findings support each other. According to Siraj et al. [33], the abundance of some pollution indicator species, -for example *Limnodrilus* sp, *T. tubifex*-, is depictive of transition in trophic status of the wetland from meso- to eutrophy [33].

Statistical Analysis.UPGMA analysis of the 19 Oligochaeta species yielded 6 major groups (Figure 2).

While the five clustering group of UPGMA dendogram covered three Oligochaeta species (such as groups I, III, IV, V and VI), only the group II included two Oligochaeta species. These can be arranged in the following way: the first group (group I); *Stylaria lacustris,* α-oligohaline freshwater species [34]*, D. digitata,* β-oligohaline freshwater species [34] and *Ilyodrilus frantzi*, to survive in fairly eutrophic waters as well as under oligotrophic conditions [35], the second group (group II); *Lumbriculus variegatus,* has very wide ecological valence [36] and *Criodrilus lacuum*, common in pools [37], the third one (group III); *T. tubifex,* a cosmopolitan species [38], *P. hammoniensis,* a freshwater euryhalin form [39] and *Potamothrix bedoti*, a freshwater form [27], the fourth group (group IV); *P. bavaricus,* a euryhalin salt form [39], *I. templetoni, T. tubifex f. bergi*, the fifth group (group V); *L. udekemianus, L. hoffmeisteri f. parvus* and *L. hoffmeisteri,* which are cosmopolitan species [40], and lastly the sixth group (group VI); *Spirosperma nikolskyi,* a oligotrophic species [41]*, Psammoryctides deserticola*, a euryhalin salt form [39], and *Ophidonais serpentina*, β-oligohaline freshwater species [34]. Two species, *Eiseniella tetraedra* and *L. profundicola*, which indicates oligotrophy [42] were not clustered with others.

According to the UPGMA analysis, percent habitat similarities of each sampling station were the highest between stations A53 (spring) and A312 (spring). Stations A725 (dam lake), A129 (lake) and A125 (channel) were also found to be similar to each others. In contrast, Station A27 (lake) was found to be the most different one from all the other stations for the oligochaete fauna (Figure 3).

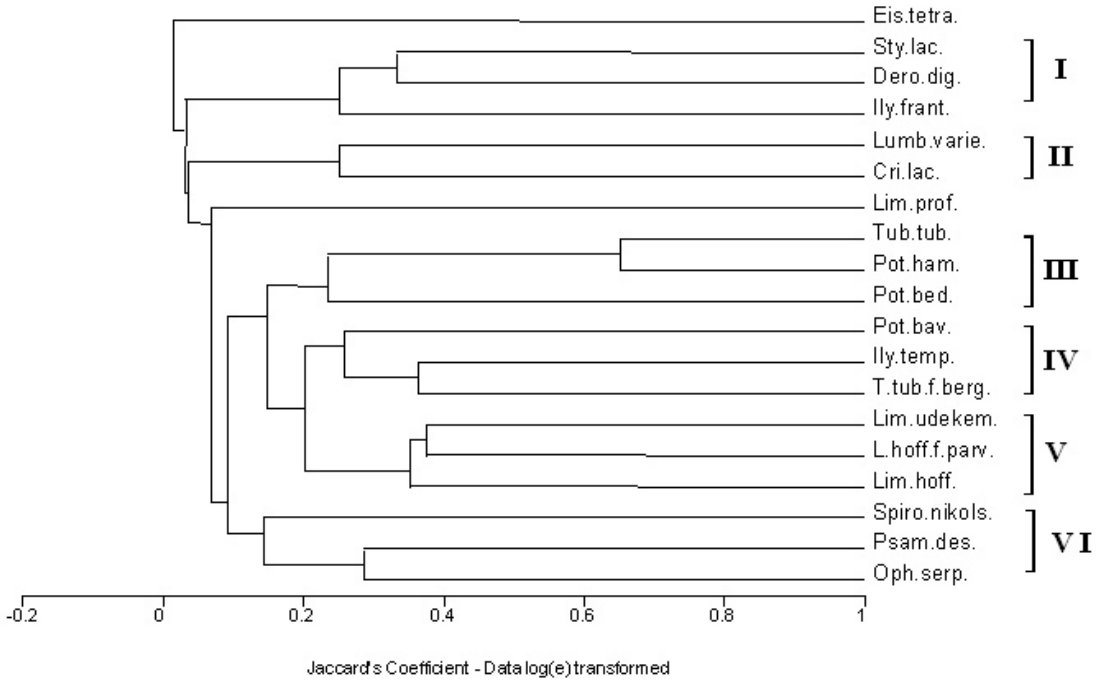

FIGURE 2
UPGMA dendogram illustrating relationship among 19 oligochaeta species from 33 stations.

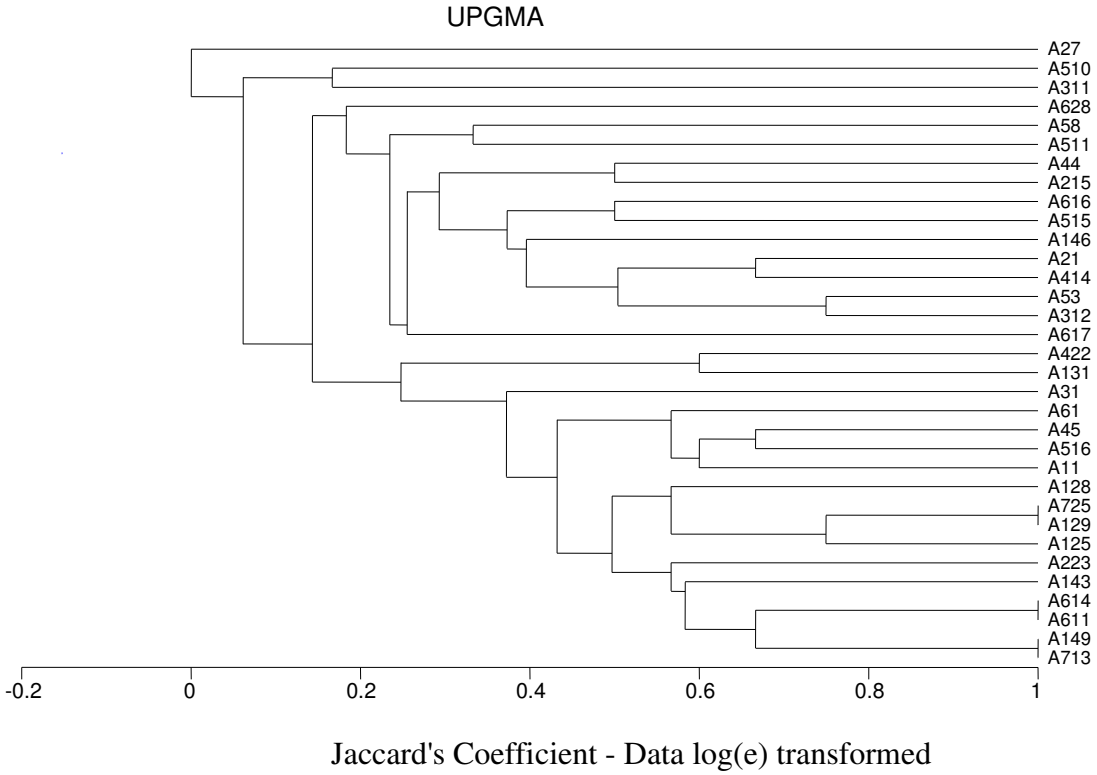

FIGURE 3
UPGMA dendogram illustrating relationship among 33 stations studied (Codes of stations are given in Appendix).

TABLE 2
Correlations between aquatic Oligochaeta species and environmental parameters. *. p<0.05; **: p<0.01.

Species	Temp.	pH	DO	$CaCO_3^=$	Alt.
Lim.hoff	0.185	0.056	-0.046	-0.128	**.347***
L.hoff.f	0.073	**-.283****	-0.065	-0.199	0.134
Lim.udek	0.158	-0.178	-0.189	-0.131	**.306***
Ily.temp	0.18	-0.086	**-.243***	-0.261	0.288
Oph.serp	-0.132	**-.228***	-0.068	0.178	-0.204
Dero dig	0.09	0.054	-0.005	**-.293***	-0.1
T.tub.f.	-0.034	**-.322****	0.071	0.066	-0.028
Spir.fer	**-.209***	**-.261***	0.159	0.168	-0.247
Aul.plu	0.002	**-.334****	-0.041	0.067	-0.172
Nais com	-0.033	**-.320****	0	0.024	0
Pot.ham.	-0.16	**-.317****	0.028	-0.08	0.119
Psam.des	-0.096	**-.214***	-0.026	0.003	0

Correlations of Oligochaeta species with physical and chemical parameters of water and with habitat code in the study area are presented in Table 2.

Spearman Rank Correlation analyses illustrated a significant negative correlation between pH and eight species for *L. hoffmeisteri f. parvus, T. tubifex f. bergi, A. pluriseta, Nais communis, P. hammoniensis, O. serpentina, S. ferox*, and *P. deserticola*. The only species *S. ferox* showed a negative correlation with temperature in a moderate extent (P<0.05). Also abundance of *I. templetoni* was negatively correlated with dissolved oxygen in moderate extent (P<0.05) and *D. digitata* was negatively correlated with $CaCO_3^=$ (P<0.05). Among the analysis, only the altitude was positively correlated with two Oligochaeta species, *L. hoffmeisteri and L. udekemianus* (P<0.05).

Canonical correspondence analysis (CCA) concerned 9 environmental variables with one nominal variable (habitat type) and 19-selected taxa that showed wide distribution in 237 samples (Figure 4). Accordingly, CCA was able to explain 81% of the species environment relationship with about 32.5 variance (Table 3).

The following environmental factors were found to have significant effect on species distribution: pH, depth, Secchi depth, dissolved oxygen, $CaCO_3^=$, altitude, salinity, temperature and electricity conductivity (P <0.01). The distribution of species along with the first axis reflects their requirements regarding dissolved oxygen, electricity conductivity and pH. A positive correlation for temperature was shown by the second axis, while positive correlations for temperature and $CaCO_3^=$ were shown by the third axis. The distribution of species along the second and third axis can be explained by the pH, depth and secchi depth.

Many authors emphasize the overall importance of interspecific competition between the species involved and their environment. The distribution of species can rarely be exactly correlated with the variation of chemical or physical factors one by one, which hardly comprises. In the light of recent experience that aquatic oligochaetes may interact very strongly with each other for different resources, there is naturally a great risk that the occurrence of one species or the other in a particular situation is mostly attributable to the simultaneous occurrence of other species and thus not necessarily to abiotic factors alone [43].

Most oligochaete species found in the Lake District occurred within a wide range of environmental conditions, demonstrating a large temporal and spatial variability. Habitat preferences of various species were evaluated using CANOCO. As can be seen from Fig. 4, pH, depth, Secchi depth, dissolved oxygen, $CaCO_3^=$,

TABLE 3
Main results of Canonical Correspondence Analysis (CCA).

Axes	1	2	3	4	Total inertia
Eigenvalues:	0.343	0.180	0.166	0.129	6.408
Species-environment correlations:	0.811	0.575	0.607	0.476	
Cumulative percentage variance					
of species data :	5.4	8.2	10.7	12.8	
of species-environment relation:	32.5	49.5	65.2	77.4	
Sum of all eigenvalues					6.408
Sum of all canonical eigenvalues					1.056

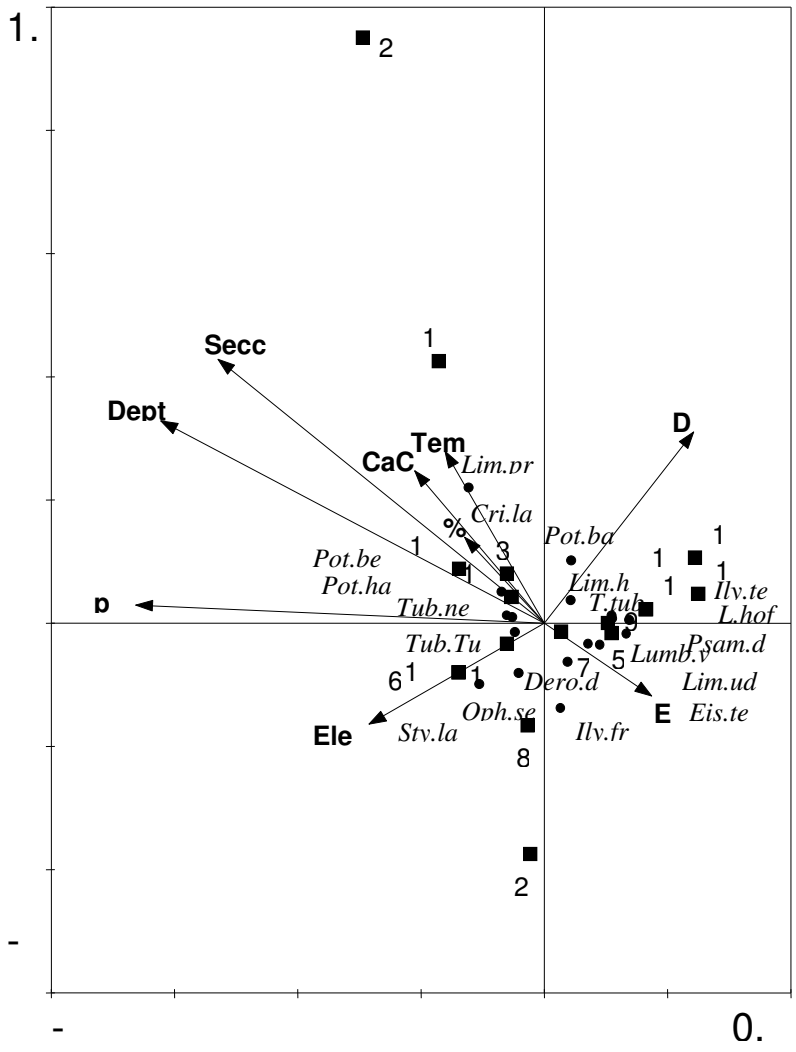

FIGURE 4
Canonical correspondence analysis (CCA), ordination plot of species (for abbreviations see Table 1) and main environmental variables on the first two axes. (Habitat Codes: 1- mud; 3- sand + macrophyte vegetation; 5- stone + gravel; 6- reedbed; 7- detritus; 8- macrophyte; 9- sand + stone; 10- mud + sand + macrophyte; 11- mud + stone; 12- detritus + macrophyte; 13- detritus + gravel; 14- detritus + stone; 15- detritus + stone + macrophyte; 17- sand + gravel; 19- sand + stone + gravel + macrophyte; 20- mud + sand; 22- sand + stone + macrophyte). Abbreviations: DO, dissolved oxygen; Temp, temperature; Elev, elevation; Secchi, Secchi depth.

altitude, salinity, temperature and conductivity are the primary factors influencing the distribution of oligochaeta in the Lake District.

The distributions of *L. profundicola*, *P. hammoniensis*, *P. bedoti*, *T. nerthus* and *C. lacuum* are positively correlated with pH, depth, secchi depth, dissolved oxygen, $CaCO_3^=$, altitude, salinity, temperature and negatively correlated with electricity conductivity (Figure 4). Zeybek et al. [10] detected the relationships between environmental parameters and aquatic oligochaeta in the Lakes Eğirdir and Kovada. The researchers reported that distribution of species is mostly related to NO_3-N, ΣP and BOD, and the most important variable effecting the distribution is NO_3-N. *Potamothrix hammoniensis* and *Tubifex tubifex* are in a positive correlation with DO and pH. Similar results were found in Lake Uluabat [8].

Among 24 taxa of benthic macroinverebrates in Lake Uluabat, Insecta and Oligochaeta were the most abundant groups, dominated by species characteristic to nutrient rich waters, including *Pristina aequiseta, N. communis, T. tubifex, L. hoffmeisteri, P. hammoniensis* and *Tanypus punctipennis*. Most of the variance (63.5%) in relations between species and environmental variables as explained by the first two axes of a canonical correspondence analysis (CCA) and placed most Oligochaeta and Chironomidae near the vectors of high nutrients and chlorophyll-a concentrations, while the sensitive Crustacea and some Oligochaeta (Lumbricidae) species on sectors

of the plot with the smallest weight of those variables [8].

Major changes in the structure of oligochaete assemblages related to water mineralization, substrate type and current velocity were documented by Martínez-Ansemil and Collado [44], who studied Oligochaeta inhabiting largely unpolluted watercourses in Galicia (Spain) and Northern Portugal. Dumnicka and Pasternak [45], in their studies of oligochaeta in the River Nida, Poland, concluded that bottom type and current speed as well as hardness or Ca^{2+} and Mg^{2+} content determine the composition of oligochaete communities. Dumnicka and Pasternak [45], also showed that certain oligochaete species were not habitat selective. In our study, *L. udekemianus, I. frantzi* and *E. tetraedra* showed similarity to this conclusion. Many of the early workers on the bottom fauna have stressed the importance of the abiotic factors such as the quality of the sediment, e.g. its texture, its organic contents etc. Alsterberg [46], Berg et al. [47] and Palmer [48] have found the oxygen factor to be of decisive importance for the composition of species [43]. Schenková et al. [37], who studied the relationship between oligochaete species, habitat diversity and environmental variables of the Morava and Odra River Basins, Czech Republic, found that chemical oxygen demand (COD), water hardness, NO_3^--N, Ca^{2+}, Mg^{2+}, altitude, and substrate type were to be the primary factors influencing the distribution of aquatic Oligochaeta. In our study, only the altitude and substrate type are similar to these results. Again, Schenková and Helešic [49] were carried out a study to determine the aquatic habitat preferences in the Rokytná River (Thaya River Basin) in the Czech Republic. In this study, they found that biochemical oxygen demand (BOD), temperature, streamline as habitat type, nitrate (NO_3^-), current velocity at 40 %, summer sampling and conductivity were significant of the distribution of oligochaeta. Kökmen et al. [7] and Arslan et al. [6] found that vegetation was the most important factor for distribution of the oligochaete species. In our study, only the habitat codes 10 (mud + sand + macrophyte), 20 (mud + sand) and 22 (sand + stone + macrophyte) were found ineffective from the other habitat types, which is important for distribution of oligochaetes. Yıldız et al. [9] investigated distribution of aquatic oligochaetes of high-elevation lakes in the Eastern Black Sea Range of Turkey and they determined four most important environmental variables (elevation, water depth, dissolved oxygen, and temperature) affecting species. Timm [36] and Verdonschot [50] found that, the two naidids, *S. lacustris* and *O. serpentina*, are known to dwell between vegetation in standing or slowly flowing waters [51]. Our conclusions are similar to those of Verdonschot [51], who studied the influence of different substrates in lowland rivers. In our study, CCA analysis showed that, the distributions of *S.lacustris* and *O. serpentina* are positively correlated with number 8 (macrophyte) habitat codes, which indicates the vegetation. Verdonschot [50], in his studies of aquatic oligochaeta in ditches, found that *P. hammoniensis* showed a positive linear correlation with depth and pH. *P. hammoniensis* (Tubificidae) were related to dissolved oxygen concentrations and water temperatures [42]. We found similar results in our study.

Battegazzore and Renoldi [52] found that *L. profundicola* and *T. tubifex* was negatively correlated with oxygen and conductivity and *T. tubifex* is usually recognized as the member of macroinvertebrates typical of nutrient rich lakes [42]. Our results showed a similar trend with this finding.

Some earthworm species were obviously able to withstand long durations of continual submergence [53]. *Eiseniella* is the only water-dwelling genus of family Lumbricidae and it is distributed by man to both temperate zones [54]. The limicolous species *E. tetraedra* is probably native to the western Palearctic but is also known with widespread distribution in mainly temperate regions in both hemispheres of the world [55]. Semi aquatic *E. tetraedra* was the typical species for flooded meadows community positively influenced by moisture and organic matter content [56]. A nominal subspecies of the peregrine species, *E. tetraedra tetraedra*, is known in the Aegean, Marmara, and central and northern Anatolian regions [57]. Armend´ariz and C´esar [58] found *E. tetraedra* is in stations with silt or silt-sand sediments tolerating eutrophic conditions, although its faunal characteristics were highly variable. Martinez- Ansemil and Collado [44] found this species was negatively correlated with depth in CCA diagram. Our findings are similar to this conclusion.

The most common species is *T. tubifex* in this study, a cosmopolitan species that is not commonly encountered, is locally abundant in habitats of marginal water quality pristine alpine and subalpine lakes [38], the bottoms of large, unproductive, oligotrophic lakes, grossly polluted and organically enriched sites with low oxygen tensions, and aquatic habitats supporting few other species [59]. In areas with heavy organic pollution, *T. tubifex* is usually associated with *L. hoffmeisteri*, where the two species are often the dominant oligochaetes or even the dominant or exclusive benthic invertebrates [59]. Brinkhurst [60], also suggested that *T. tubifex* may prefer situations in which other species find it difficult to survive - either because there is too little active decomposition, or too much. *L. hoffmeisteri*, a cosmopolitan species, is perhaps the most commonly collected freshwater oligochaete throughout the worldwide. It occurs in

a wide variety of surface water habitats, reaching very high abundance in organically enriched areas - often with *T. tubifex* [61]. *L. udekemianus*, a cosmopolitan species, is often found in organically polluted waters as well as oligotrophic habitats [38]. This species is often together with *L. hoffmeisteri* but less numerous [36].

Probs [62] and Särkkä [63] noticed that while *L. hoffmeisteri* diminishes its density with depth, *T. tubifex* increases its density in deeper waters [64]. In our study, *T. tubifex,* which was seen as a dominant species, was encountered in depth of 45.5 meters and it was one of the species found at the deepest points.

The Lumbriculidae is a thermophobe family of the northern temperate zone [54] and was represented by two species in this study (*Tatriella slovenica* and *L. variegatus*). *L. variegatus* has very wide ecological valence; it occurs in the littoral zones of lakes, in running waters, springs, ponds and pools, also in bog waters and ephemeral pools which are unsuitable for the majority of Oligochaeta [36].

The primary home of the Glossoscolecidae, partly dry-land megadrile family, is also supposed to be the northern temperate zone where only few species of the general. *Criodrilus* is in among them [54]. In our study this two semi-aquatic (*L. variegatus* and *C. lacuum*) oligochaeta species were involved in the same group of UPGMA (group II) as suitable for their ecological characteristics.

According to the UPGMA analysis, stations A53 and A312 were the most similar stations. These are springs. Stations A725 (dam lake), A129 (lake) and A125 (channel) were also found to be similar to each other's. In contrast, Station A27 (Lake Karataş) was found to be the most different one from all the other stations for the oligochaete fauna. It is a shallow, stream-fed freshwater lake situated in the northeast Tefenni plain, surrounded by arable land. Fringing vegetation is restricted to the western shore. The abundant vegetation of west part of Lake Karataş can explain the existence of Naididae species, which are typical organisms of the littoral region characterized by abundant free-floating vegetation, such as *N. communis, N. variabilis, N. pardalis, N. elinguis* and *O. serpentina*. This lake is different from the others that keeping all these Naidid species together in it.

CONCLUSIONS

The results of this study suggest that there is still a need for much intensive investigation about aquatic Oligochaeta and their habitat preferences. Future study of the Lake District can reveal more about the behaviour and ecology of oligochaete species.

ACKNOWLEDGEMENTS

This project has been supported by The Fund of Scientific Research of Ege University (Project: 1999/SUF/001) and The Scientific and Technical Research Council of Turkey (TUBITAK Project: 199/Y/071). The author thanks to Prof. Dr. Okan Külköylüoğlu (Abant Izzet Baysal University) for the statistical analysis and reviewing the manuscript. The author also are grateful to retired Prof. Dr. Süleyman BALIK, and Prof. Dr. Hasan M. SARI for various helps.

APPENDIX

1. Yaprakli Dam	(A719)
2. Gölhisar Lake	(A61)
3. Kızıllar Çavdır Dam	(A716)
4. Kırkpınar Springs	(A65)
5. Salda Creek	(A614)
6. Salda Lake	(A611)
7. Acıgöl Lake (Denizli)	(A43)
8. Yarışlı Lake	(A215)
9. Karamanlı Dam	(A713)
10. Karataş Lake	(A27)
11. Burdur Lake	(A315)
12. The Sources of the B. Menderes River (İncirli Springs.-Dinar- Afyon)	(A44)
13. Uluborlu Dam	(A71)
14. İnsuyu Cave	(A157)
15. Gölcük Lake (Isparta)	(A11)
16. Kırkgöz Springs (Antalya)	(A616, A617)
17. Karacaören-I Dam (Çandır-Isparta)	(A131)
18. Kovada Lake (Isparta)	(A128, A129)
19. Kovada Channel (Isparta)	(A125)
20. Selevir Dam (Afyon)	(A722)
21. Seyitler-Gebiciler Dam	(A725)

22. Karamık Bataklığı Springs (Dinar-Afyon)	(A311)
23. Eğirdir Lake	(A45)
24. Eber Lake	(A621)
25. Akşehir Lake	(A618)
26. Sultan Mountains Çeşme Basin (Afyon)	(A48)
27. The Creek created by snow waters of Akşehir on The Sultan Mountains	(A49)
28. Beyşehir Lake	(A143, A146, A149,
29. The Srping on road-fork between Beyşehir-İmrenler (Beyşehir-Konya)	(A628)
30. Çavuşçu Lake	(A223)
31. Başhüyük Pond	(A410)
32. Altınapa Dam	(A78)
33. May Dam	(A77)
34. Apa Dam	(A74)
35. Bolluk Lake	(A411)
36. Pınarbaşı Springs (Cihanbeyli–Konya)	(A415)
37. İnsuyu Channel (Cihanbeyli–Konya)	(A414)
38. Tersakan Lake (Konya)	(A412)
39. Tuz Lake	(A413)
40. Köpek Lake (Kulu-Konya)	(A416)
41. Düden Lake (Kulu-Konya)	(A417)
42. Bademli Dam (Burdur)	(A710)
43. Örenler–Akharım Dam (Afyon)	(A728)
44. Karamık Marshy Area	(A220)
45. The Creek on the intersection among Yalvaç-Isparta-Akşehir	(A118)
46. The Waetrin canal on entrance of the County Göksöğüt	(A119)
47. Dalaman River-Çamköy	(A21)
48. Gemiş County-Pınar-Çardak (Denizli)	(A31)
49. Aşağı Akpınar Place- II. Spring- Çardak (Denizli)	(A32)
50. The Creek between Beyşehir-Konya (Konya)	(A33)
51. Meke Saltpan (Karapınar-Konya)	(A34)
52. B.Menderes Eldere-Pınarbaşı Springs-Dinar (Afyon)	(A53)
53. B.Menderes Su Çıkan Dinar İçi Springs-Dinar (Afyon)	(A314)
54. The Creek Karaçal (Burdur)	(A319)
55. Çaltı (Kurugöl) Lake–Çardak (Afyon)	(A41)
56. B. Menderes Düden Springs-Dinar (Afyon)	(A52)
57. Taşkapı-Çatak-Beldibi (Burdur)	(A54)
58. Gökçebağ Dam-Pınargözü Springs (Gelincik-Isparta)	(A55)
59. Pınarbaşı Springs-Sav (Isparta)	(A57)
60.Gökböget Springs-The Village Aşağı Gökdere -(Eğirdir-Isparta)	(A58)
61. Kısık Spring-Atabey (Isparta)	(A59)
62. Kocapınar Spring. - The Village Yukarı Gökdere	(A510)
63. Su Gözü Spring-The Village Çukur (Eğirdir-Isparta)	(A511)
64. Zindan River- Front of Zindan Cave (Aksu-Isparta)	(A512)
65. Akdoğan Spring (Akdoğan-Isparta)	(A513)
66. Pınar Pazarı (Eğirdir-Isparta)	(A517)
67. Hisarardı Spring (Yalvaç-Isparta)	(A514)
68. Su Gözü Spring–Bağkonak (Yalvaç-Isparta)	(A518)
69. Fele Spring–The Village Fele (Yalvaç-Isparta)	(A515)
70. Başpınar–Köprüköy (Şarkikaraağaç-Isparta)	(A516)
71. Acıgöl Lake (Karapınar-Konya)	(A36)
72. The Starting point of Gölyaka–spring (Beyşehir-Konya)	(A156)
73. Kocapınar Spring–Karakuyu Pond (Dinar-Afyon)	(A312)
74. Milas Spring (Yakaören-Isparta)	(A522)
75. Starting point of Milas Spring – The way Gölcük (Isparta)	(A523)

REFERENCES

[1] Kazancı, N. and Girgin, S. (1998). Distribution of Oligochaeta species as bioindicators of organic pollution in Ankara Stream and their use in biomonitoring. Turkish Journal of Zoology 22, 83-87.

[2] Çamur-Elipek, B. (2003). The Dynamics of benthic macroinvertebrates in a mesotrophic lake: Terkos (Turkey). Ekologija 38 (1-2), 31-40.

[3] Balık, S., Ustaoğlu, M. R., Özbek, M., Taşdemir, A., Yıldız, S., Topkara, E.T. (2005). A preliminary study on the macrobenthic invertebrate fauna of Kuş Lake (Bandırma). Ege University Journal of Fisheries and Aquatic Sciences 22 (3-4), 347-349.

[4] Balık, S., Ustaoğlu, M. R., Özbek, M., Yıldız, S., Taşdemir, A., İlhan, A. (2006). Determination of pollution at lower basin of Küçük Menderes River (Selçuk, İzmir) by using macro benthic invertebrates. Ege University Journal of Fisheries and Aquatic Sciences 23 (1-2), 61-65.

[5] Arslan, N. (2006). Littoral Fauna of Oligochaeta (Annelida) of Lake Eğirdir (Isparta). Ege University Journal of Fisheries and Aquatic Sciences 23 (3-4), 315-319.

[6] Arslan, N., İlhan, S., Şahin, Y., Filik, C., Yılmaz, V., Öntürk, T. (2007). Diversity of Invertebrate Fauna in Littoral of Shallow Musaözü Dam Lake in Comparison with Environmental Parameters. Journal of Applied Biological Sciences 1 (3), 67-75.

[7] Kökmen, S., Arslan, N., Filik, C., Yilmaz, V. (2007). Zoobenthos of Lake Uluabat, a Ramsar Site in Turkey, and Their Relationship with Environmental Variables. Clean. Soil, air, water 35, 266-274.

[8] Çelik, K., Akbulut, N., Akbulut, A., Özatlı, D. (2010). Macro Zoobenthos of Lake Uluabat, Turkey, related to some physical and chemical parameters. Pan-American Journal of Aquatic Sciences 5(4), 520-529.

[9] Yıldız, S., Özbek, M., Ustaoğlu, M.R., Somek, H. (2012). Distribution of aquatic oligochaetes (Annelida, Clitellata) of high-elevation lakes in the Eastern Black Sea Range of Turkey. Turkish Journal of Zoology 36 (1), 59-74.

[10] Zeybek, M., Kalyoncu, H. and Ertan, Ö.O. (2013). The Effects of Environmental Variables on Distribution of Aquatic Oligochaeta and Chironomidae at Kovada Channel and The Linked Lakes (Isparta/Turkey). Fresenius Environmental Bulletin 22 (11), 3160-3169.

[11] Yıldırım, M.Z. and Kebapçı, Ü. (2004). Slugs (Gastropoda: Pulmonata) of the Lakes Region (Göller Bölgesi) in Turkey. Turkish Journal of Zoology 28, 155-160.

[12] Sözen, M. and Yiğit, S. (1999). The Benthic Fauna and some Limnological Aspects of Lake Akflehir (Konya). Turkish Journal of Zoology 23, 829-847.

[13] Kazancı, N., Girgin, S., Dügel, M., Oğuzkurt, D., Mutlu, B., Dere, S., Barlas, M., Özçelik, M. (1999). Köyceğiz, Beyşehir, Eğirdir, Akşehir, Eber, Çorak, Kovada, Yarışlı, Bafa, Salda, Karataş, Çavuşcu Gölleri, Küçük ve Büyük Menderes Deltası, Güllük Sazlığı, Karamuk Bataklığı'nın Limnolojisi, Çevre Kalitesi ve Biyolojik Çeşitliliği. Türkiye İç Suları Araştırmaları Dizisi: IV, 371 s.

[14] Bildiren, A. (1991). Eğirdir Gölü Köprü Avlağı Bentik Faunası Üzerinde Bir Araştırma. Akdeniz Üniversitesi Fen Bilimleri Enstitüsü, Yüksek Lisans Tezi, 109s, Isparta.

[15] Turhan, F.L. (1992). Eğridir Gölü Oligochaeta faunası üzerine sistematik araştırmalar. Hacettepe Üniversitesi Fen Bilimleri Enstitüsü, Yüksek Lisans Tezi, 64 s, Isparta.

[16] Karaşahin, S. (1998). Kovada Gölü ve Kanalı Bentik Faunası Üzerine Bir Araştırma. Süleyman Demirel Üniversitesi, Fen Bilimleri Enstitüsü, Yüksek Lisans Tezi, 123 s., Isparta.

[17] Aksoylar, M.Y. and Ertan, Ö.O. (2002). Hydrobiological Characteristics of Lake Eğirdir. Eğirdir, Isparta, Turkey: DPT Project No:97K122330.

[18] Yıldız, S. and Balık, S. (2005). The Oligochaeta (Annelida) Fauna of the Inland Waters in the Lake District (Turkey). Ege University Journal of Fisheries and Aquatic Sciences 22 (1-2), 165-172.

[19] Arslan, N., Şahin, Y. (2006). A Preliminary Study on the Identification of The Littoral Oligochaete (Annelida) and Chironomidae (Diptera) Fauna of Lake Kovada A National Park in Turkey. Turkish Journal of Zoology 30, 67-72.

[20] Brinkhurst, R. O. (1971). A Guide for the Identification of British Aquatic Oligochaeta, Freshwater Biological Association Scientific Publication 22: 55 pp.

[21] Brinkhurst, R.O. and Jamieson, B.G.M. (1971). Aquatic Oligochaeta of the World. Edinburg: University of Toronto Press.

[22] Brinkhurst, R. O., M. J. Wetzel. (1984). Aquatic Oligochaeta of the World: Supplement a Catalogue of New Freshwater Species, Descriptions and Revisions, No: 44, Canadian Technical Report of Hydrography and Ocean Sciences, Canada, 101 pp.

[23] Kathman, R.D. and Brinkhurst, R.O. (1998). Guide to The Freshwater Oligochaetes of North America. Tennessee, USA: Aquatic Resources Center.

[24] Nielsen, C.O., B. Christensen. (1959). The Enchytraeidae Critical Revision and Taxonomy of European Species, (Studies on Enchytreidae VII). Naturhıstorısk Museum-Aarhus, 160 pp.

[25] Sperber, C. (1948). A Taxonomical Study of the Naididae. Zoology, Bidrag, Uppsala Bd, 28, 1-296.

[26] Sperber, C. (19509. A Guide for the Determination of European Naididae, Zoology, Bidrag, Uppsala Bd, 29, 45-78.

[27] Timm, T. (1999). A Guide to the Estonian Annelida. Naturalist's Handbooks 1. Tartu-Tallinn: Estonian Academy Publishers.

[28] Ter Braak, C. J. F. (1989). CANOCO – an extension of DECORANA to analyze species environment relationships. Hydrobiologia 184, 169-170.
[29] Ter Braak, C. J. F. (19879. The analysis of vegetation-environment relationships by canonical correspondence analysis. Vegetatio 69, 69-77.
[30] Ter Braak, C. J. F., Barendregt, L. G. (1986). Weighted averaging of species indicator values: its efficiency in environmental calibration. Mathematical Biosciences 78, 57-72.
[31] Ter Braak, C. J. F. (1995). Ordination. In: Jongman, R.H.G., Ter Braak, C.J.F., Van tongeren, O.F.R. (Eds.), Data Analysis in Community and Landscape Ecology. Cambridge University Press, Cambridge, pp. 91-173.
[32] Kovach, W. (1998). MultiVariate Statistical Package. Ver. 3. 01. Wales: Kovach Computing Services, Pentraeth.
[33] Siraj, S., Yousuf, A.R., Bhat, F.A., Parveen, M. (2010). The ecology of macrozoobenthos in Shallabugh wetland of Kashmir Himalaya, India. Journal of Ecology and The Natural Environment 2 (5), 84-91
[34] Laakso, M. (1969). Oligochaeta from brackishwater near Tvärminne, south-west Finland. Annales Zoologici Fennici 6, 98-111.
[35] Spencer, D.R., Denton, R.L. (2003). Aquatic Oligochaeta (Annelida : Lumbriculidae, Haplotaxidae, Naididae, Tubificidae) of Utah. Western North american Naturalist 63 (3), 343-352.
[36] Timm, T. (1970). On the Fauna of Estonian Oligochaeta. Institute of Zoology and Botany of the Academy Of Sciences of the Estonian S.S.R., Tartu.
[37] Schenková, J., Komárek, O., Zahrádková, S. (2001). Oligochaeta of the Morava and Odra River basins (Czech Republic): species distribution and community composition. Hydrobiologia 463, 235-240.
[38] Klemm, D.J. (1985). A Guide to the Freshwater Annelida (Polychaeta, Naidid and Tubificid Oligochaeta and Hirudinea) of North America. Dubuque, Iowa: Kendall/Hunt Publishing Company.
[39] Grigelis, A. (1980). Ecological Studies of Aquatic Oligochaetes in the USSR, In R. O. Brinkhurst & D.G. Cook Eds, Aquatic Oligochaeta Biology, Plenum press, New York, 225-240.
[40] Howmiller, R.P. (1974). Some Naididae and tubificidae From Central America. Hydrobiologia 44, 1-12.
[41] Chapman, P.M., Farrell, M.A., Brinkhurst,R.O. (1982). Relative tolerances of selected Aquatic Oligochaetes to Individual pollutants and environmental factors. Aquatic Toxicology 2, 47-67.
[42] Milbrink, G., Timm, T., Lundberg, S. (2002). Indicative Profundal Oligochaete assemblages in selected small Swedish lakes. Hydrobiologia 468, 53-61.
[43] Milbrink, G. (1980). Oligochaeta communities in pollution biology: the European situation with special reference to lakes in Scandinavia. (In: R.O. Brinkhurst and D.G. Cook (Eds.), Proceedings of the Aquatic Oligochaete Biology (pp. 433-455). New York: Plenum Press.
[44] Martínez-Ansemil, E., Collado, R. (1996). Distribution patterns of aquatic oligochaetes inhabiting watercourses in the Northwestern Iberian Peninsula. Hydrobiologia 334, 73-83.
[45] Dumnicka, E., Pasternak, K. (1978). The influence of physico-chemical properties of water and bottom sediments in the River Nida on the distribution and numbers of Oligochaeta. Acta Hydrobiol. 20, 215-232.
[46] Alsterberg, G. (1922). Die respiratorischen Mechanismen der Tubificiden, Lunds Univ. Arsskr. N. F. Avd., 18, 1-175.
[47] Berg, K., Jonason, P. M., Ockelman, K.W. (1962). The respiration of some animals from the profundal zone of a lake. Hydrobiologia 19, 1-39.
[48] Palmer, M.F. (1968). Aspects of the respiratory physiology of *Tubifex tubifex* in relation to its ecology. J. Zool. Lond. 154, 463-473.
[49] Schenková, J., Helešic, J. (2006). Habitat preferences of aquatic Oligochaeta (Annelida) in the Rokytná River, Czech Republic-a small highland stream. Hydrobiologia 564, 117-126.
[50] Verdonschot, P.F.M. (1987). Aquatic Oligochaetes in ditches. In R.O. Brinkhurst and R. J. Diaz (eds) Aquatic Oligochaeta. Hydrobiologia 155, 283-292.
[51] Verdonschot, P.F.M. (2001). Hydrology and substrates: determinants of oligochaete distribution in lowland streams (The Netherlands). Hydrobiologia 463, 249-262. In: P. Rodriguez & P.F.M. Verdonschot (eds), Aquatic Oligochaete Biology VIII. 2001 Kluwer Academic Publishers. Printed in the Netherlands.
[52] Battegazzore, M., Renoldi, M. (1995). Integrated Chemical And Biological Evaluation of the Quality of the River Lambro (Italy). Water, Air And Soil Pollution 83, 375-390.
[53] Ausden, M., Sutherland, W.J., James, R. (2001). The effects of flooding lowland wet grassland on soil macroinvertebrate prey of breeding wading birds. Journal of Applied Ecology 38, 320–338.
[54] Timm, T. (1980). Distribution of Aquatic Oligochaetes. In R. O. Brinkhurst & D.G.

Cook Eds, Aquatic oligochaeta Biology, plenum press, New York, 55-77.
[55] Blakemore, R. J., Ito, M.T., Kaneko, N. (2006). Alien earthworms in the Asia/Pacific region with a checklist of species and the first records of Eukerria saltensis (Oligochaeta: Ocnerodrilidae) and Eiseniella tetraedra (Lumbricidae) from Japan, and Pontoscolex corethrurus (Glossoscolecidae) from Okinawa. In Koike, F., Clout, M.N., Kawamichi, M., De Poorter, M. and Iwatsuki, K. (eds), Assessment and Control of Biological Invasion Risks. Shoukadoh Book Sellers, Kyoto, Japan and IUCN, Gland, Switzerland, 173-181.
[56] Ivask, M., Truu, J., Kuu, A., Truu, M., Leito, A. (2007). Earthworm communities of flooded grasslands in Matsalu, Estonia. European Journal of Soil Biology. 43, 71-76.
[57] Mısırlıoğlu, M. (2008). Some Earthworm Records from Anatolia (Oligochaeta, Lumbricidae. Turkish Journal of Zoology 32, 469-471.
[58] Armend´ariz, L. C., C´esar, I. I. (2001). The distribution and ecology of littoral Oligochaeta and Aphanoneura (Annelida) of the Natural and Historical Reserve of Isla Mart´ın Garc´ıa, R´ıo de la Plata River, Argentina. In: P. Rodriguez & P.F.M. Verdonschot (eds), Aquatic Oligochaete Biology VIII. Hydrobiologia 463, 207–216.
[59] Brinkhurst, R.O. (1996). On the role of tubificid oligochaetes in relation to fish disease with special reference to the Myxozoa: Annual Review of Fish Diseases 6, 29-40.
[60] Brinkhurst, R.O. (1970). Distribution and abundance of tubificid (Oligochaeta) species in Toronto Harbour, Lake Ontario. Journal of the Fisheries Research Board of Canada 27, 1961-1969.
[61] Brinkhurst, R.O. 1975. Oligochaeta, *in* Parrish, F.K., ed., Keys to the water quality indicative organisms of the southeastern United States: Cincinnati, OH, U.S. Environmental Protection Agency, Office of Research and Development, Environmental Monitoring and Support Laboratory, pp 69-85.
[62] Probst, L., 1987. Sublittoral and Profundal Oligochaeta Fauna of the Lake Constance (Bodensee-Obersee). Hydrobiologia 1552, 77-282.
[63] Särkkä, J. (1987). The occurrence of oligochaetes in lake chains receiving pulpl mill waste and their relation to eutrophication on the trophic scale. Hydrobiologia 155, 259-266.
[64] Peralta, L., Escobar, E., Alcocer, J., Lugo, A. (2002). Oligochaetes from six tropical crater lakes in Central Mexico: species composition, density and biomass. Hydrobiologia 467 (1-3): 109-116.

Received: **26.01.2016**
Accepted: **18.08.2016**

CORRESPONDING AUTHOR

Seray YILDIZ
Ege University, Faculty of Fisheries, Department of Hydrobiology, 35100 Bornova-İzmir-Turkey

E-mail: seray.yildiz@ege.edu.tr

© by PSP Volume 25 – No. 10/2016, pages 4374-4380 Fresenius Environmental Bulletin

EVALUATION OF THE EFFECTS ON SOIL CARBON MINERALIZATION OF DELTAMETHRIN AND LAMBDA-CYHALOTHRIN USED TO CONTROL OF SOME INSECTS IN OLIVE ORCHARDS

Husniye Aka Sagliker*, Ilay Cevik

University of Osmaniye Korkut Ata, Faculty of Science and Letters,
Department of Biology, 80000 Osmaniye, Turkey

ABSTRACT

Deltamethrin and lambda-cyhalotrin are insecticides widely used in Turkish olive trees (*Olea europaea* L., Oleaceae). An experiment was conducted to determine effects of deltamethrin and lambda-cyhalotrin on soil microorganisms and their microbial activities by carbon mineralization. Both insecticides (25 g of active ingredient l^{-1} for deltamethrin and 50 g of active ingredient l^{-1} for lambda-cyhalotrin) were applied to the soils of olive trees growing on Adana (Karataş) and Osmaniye (Fakıuşağı) under Mediterranean climate conditions at different doses (the recommended dose: RD, 2 and 4 folds of RD) and then incubated under the same laboratory conditions (28 °C at 80% of field capacity).for 45 days by the CO_2 respiration method. Cumulative C(CO_2) respired of Adana control soil was significantly lower than both 4×RD of deltamethrin and RD of lambda-cyhalotrin in same soil (P = 0.000 ve P = 0.002, respectively). C mineralization ratio of soil added 4×RD of deltamethrin in Adana was significantly higher from all the other treatments ($P < 0.05$). Deltamethrin was more biodegradable insecticide than lambda-cyhalothrin for soil microorganisms in Adana olive soil. It might be explained that deltamethrin has shorter half life and different chemical content than lambda-cyhalothrin. In our study, the impact of insecticides on carbon mineralization was dependent upon type of insecticide, insecticide dose and incubation time.

KEYWORDS:
Carbon, Deltamethrin, Lambda-cyhalothrin, Insecticide, Mineralization, Olive

INTRODUCTION

Olive tree (*Olea europaea* L.), a valuable and characteristic plant species best adapted to the semiarid Mediterranean environment, has experienced an increase in cultivation in recent decades [1,2]. Some insects can damage to olive tree and losses up to 75% of the potential crop yield [3]. Farmers apply at the end of the May (2–3 times/year) quantities of lambda-cyhalotrin chemical name is Petra which range from 1.0 to 1.5 kg ha^{-1} totally for *Prays oleae, Ceratitis capitata* [4,5]. *Dacus oleae, Phloeotribus scarabaeoides* and *Prays oleae* are major pests for olive tree [2,6] and deltamethrin chemical name is Decis use for these insects in the entire Mediterranean zone [7,8].

Deltamethrin and lambda-cyhalotrin insecticides have also a widespread use in olive trees of Turkey [9]. Some farmers have applied these both insecticides on their own olive trees at 2, 4 or 6 folds of the recommended field dose (RD) for achieving more and better products in Turkey [10]. These practices might cause undesirable side effects on the other non-target soil microorganisms in the olive tree soils in the time [11-14]. Soil respiration is affected by many conditions such as temperature, moisture, soil properties, quality and quantity of organic matter [15,16]. The presences of deltamethrin and lambda-cyhalotrin in soil may create some modifications in the microbial populations and activities of soils [13,17].

Microorganisms and their activities [CO_2 and mineral nitrogen (NH_4–N and NO_3–N) evolutions resulting from the degradation of organic materials] in the soil are a ideal way for monitors of soil pollution [17-19]. Microbial parameters (biomass, activity and diversity of soil microbial communities) are worthwhile indicators of the impact of disturbances (like pesticide application) on soil quality [20,21]. Inorganic or organic pollutants like insecticide or herbicide are studied by C mineralization, N mineralization, CO_2 production and enzyme activities in the soil [10,13,22].

In our study, RD (recommended dose) and 2 and 4 folds of RD of both deltamethrin (25 g/l) and lambda-cyhalotrin (50 g/l) insecticides were separately applied to olive (*Olea europaea* L., Oleaceae) soil samples in two districts (Adana and Osmaniye) of the Eastern Mediterranean region, Turkey, under the same laboratory conditions (28°C

and 80% of field capacity) in order to (i) determine their effects on soil carbon mineralization and (ii) observe comparatively effects on soil microorganisms of two insecticides. Pesticides responses of C mineralization rates have been extensively investigated in numerous fields and laboratory experiments [23-25].

MATERIALS AND METHODS

Study sites and preparation of soil samples. The two different sites selected are characterized by semiarid Mediterranean climate conditions. One of the sites was at Karataş, 48 km south west of Adana city (mean annual precipitation of 663 mm and mean annual temperature of 18.7 °C) and the other was at Fakıuşağı in Osmaniye (mean annual precipitation of 808 mm and mean annual temperature of 18.2 °C) (Figure 1). The precipitation and temperature data of Adana and Osmaniye are approximately based on 50 years for Adana and 27 years for Osmaniye.

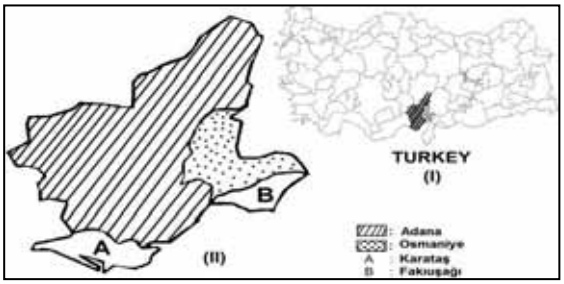

FIGURE 1
(I) Location of Adana and Osmaniye Cities in Map of Turkey. (II) Location of Adana (A: Karataş) and Osmaniye (B: Fakıuşağı) in Maps of Adana and Osmaniye Cities

In May 2014, 5 upper soil samples from the upper 0-20 cm of olive tree soil were taken from each of 5 corners of both sites. The 5 samples were mixed, homogenized, and then considered as a composite and representative sample. After removing recognizable plant debris, these composite samples were air-dried and sieved through a 2-mm mesh sieve.

Soil analysis and measurements of the aerobic mineralization. The soil texture was determined with a Bouyoucos hydrometer [26], field capacity (%) with a vacuum pump at 1/3 atmospheric pressure [27], and pH with a WTW Inolab 720 pH-meter in 1:2.5 soil-water suspension [28]. $CaCO_3$ content (%) was measured with a Scheibler calcimeter [29], organic carbon content (%) by the Anne method [30], and organic nitrogen content (%) by the Kjeldahl method [30].

Lambda-cyhalotrin (chemical formula: $C_{25}H_{19}ClF_3NO_3$; molecular weight: 449.9 g/mol; trading name: Petra 5 EC; production firm: Agrobest; 50 g active ingredient l^{-1}) and deltamethrin (chemical formula: $C_{22}H_{19}Br_2NO_3$; molecular weight: 505.2 g/mol, trading name: Decis EC 2.5; production firm: Bayer; 25 g active ingredient l^{-1}) insecticides were added to olive soils at RD (recommended field dose; 15 ml/100 l, 50 g active ingredient l^{-1} for lambda-cyhalotrin; 20 ml/100 l, 25 g active ingredient l^{-1} for deltamethrin), 2×RD, and 4×RD according to their own prospectuses for olive trees. The amounts of C and N (mg kg^{-1}) added to the soils by lambda-cyhalotrin were 6.34 and 2.96 for RD, 12.7 and 5.92 for 2×RD, and 25.4 and 11.8 for 4×RD, respectively. The amounts of C and N (mg kg^{-1}) added to the soils by deltamethrin were also 52.3 and 2.77 for RD, 104.6 and 5.54 for 2×RD, and 156.9 and 11.1 for 4×RD, respectively. Soil microbial activity in both of the soils without insecticide was used as a control.

Soil samples were placed in 750 ml incubation vessels for carbon mineralization and the insecticide dissolved in distilled water was added. The final moisture contents of both soils were adjusted to 80% of their own field capacity before incubation at 28°C over 45 days [31]. Free CO_2 derived from activities of microorganisms was absorbed in 40 ml of saturated $Ba(OH)_2$ solution in beakers, placed in the center of the soils in closed incubation vessels, and then transferred to an incubator. The amount of CO_2 produced was measured once every 3 days by titration with oxalic acid [32]. Empty vessels were used as blanks. The rate (%) of carbon mineralization was counted by dividing the cumulative amount of $C(CO_2)$ produced in 45 days into total organic carbon.

Statistical analysis. Repeated measures (general linear model) analysis was performed to determine the differences in carbon mineralization over incubation time between 2 sites (Adana and Osmaniye), 2 insecticides (deltamethrin and lambda-cyhalotrin), 3 different doses [(RD, 2×RD, and 4×RD), 33]. Three replicates were used for each combined soil for statistical comparisons. Data were analyzed by a series of analyses of variance. Results were shown as mean ± standard error (S.E.) in the tables and the figures. The values of $P \leq 0.05$ were accepted as statistically significant. SPSS 11.5 was used in statistical analyses.

RESULTS

Adana (Karataş) and Osmaniye (Fakıuşağı) olive soils used in the incubation had the same textured (sandy loam, Table 1). There was a

TABLE 1
Some physical and chemical characteristics of Adana and Osmaniye soils used in incubation treatments

Characteristics	Sites		Significance between sites
	Adana	Osmaniye	
Sand [2–0.02 mm (%)]	72.5 ± 1.70	71.6 ± 2.70	0.762
Silt [0.02–0.002 mm (%)]	13.2 ± 2.30	10.6 ± 1.97	0.429
Clay [<0.002 mm (%)]	14.3 ± 1.95	17.8 ± 1.33	0.174
Texture type	Sandy loam	Sandy loam	-
Field capacity (%)	27.1 ± 0.42	19.5 ± 1.10	0.000
pH	7.64 ± 0.03	7.80 ± 0.03	0.005
$CaCO_3$ (%)	37.6 ± 3.40	51.0 ± 3.33	0.022
C (%)	1.42 ± 0.20	1.60 ± 0.14	0.500
N (%)	0.13 ± 0.01	0.14 ± 0.02	0.543
C/N ratio	10.9 ± 1.30	11.3 ± 0.99	0.830

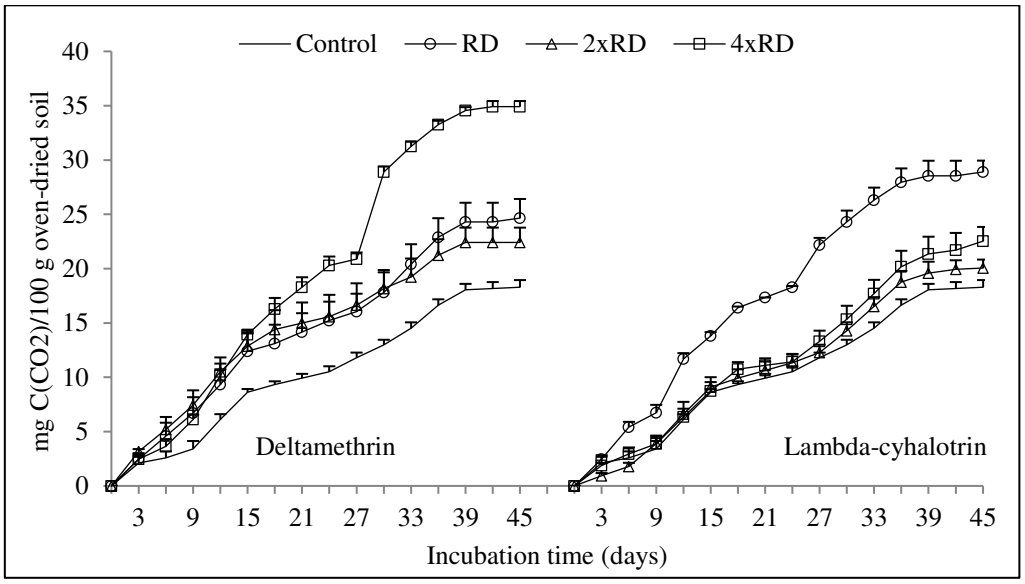

FIGURE 2
Cumulative carbon mineralized (mean ± SE; n = 3) at the RD, 2 and 4 folds of RD of deltamethrin and lambda-cyhalotrin during incubation period (28°C, 45 days) in Adana olive soil

difference between two soils from the point of view of field capacity (P = 0.000). pH and $CaCO_3$ concept (%) of two soils were significantly different from the each other (P = 0.005 and P = 0.022, respectively). C, N contents (%) and C/N ratio were statistically similar values (P ≥ 0.05).

Control soil of Adana was significantly lower within incubation time than both 4×RD of deltamethrin and RD of lambda-cyhalotrin in Adana soil from the poin of view of cumulative $C(CO_2)$ respired (P = 0.000 ve P = 0.002, respectively, Figure 2). 4×RD of deltamethrin was statistically higher than own RD and 2×RD (P = 0.003 and P = 0.000, respectively). 4×RD of deltamethrin also showed higher activity than 2×RD and 4×RD of lambda-cyhalotrin (P = 0.000 for both of them). RD of lambda-cyhalotrin in Adana soil was found statistically higher than 2×RD of the same insecticide (P = 0.015, Figure 2).

At the end of the incubation period, C mineralization of Osmaniye control soil was not significantly different from the other three doses for both deltamethrin and lambda-cyhalotrin (P > 0.05, Figure 3).

C mineralization ratio of Adana soil added 4×RD of deltamethrin was significantly found higher from all the other treatments with across doses except for both Osmaniye soil added 4×RD of deltamethrin and Adana soil added RD of lambda-cyhalotrin (P < 0.05, Figure 4). Adana soil added RD of lambda-cyhalotrin was also statistically higher than both Adana control soil and Adana soil added 2×RD of lambda-cyhalotrin (P = 0.005 ve P = 0.034, respectively).

It was shown that there were significantly interactions among incubation time, incubation time and sites, incubation time and doses, incubation time, sites and doses (P < 0.001, Table 2).

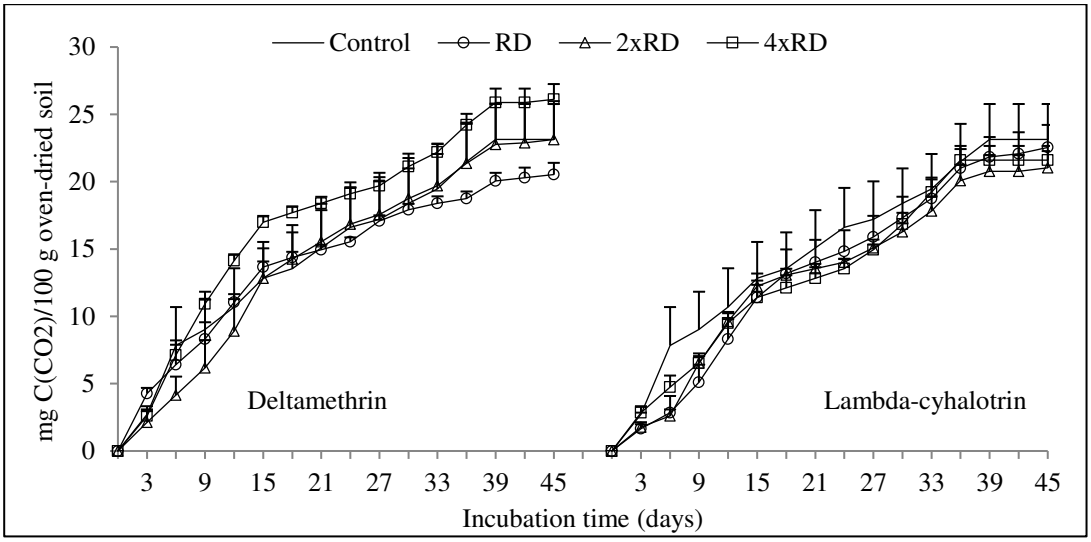

FIGURE 3
Cumulative carbon mineralized (mean ± SE; n = 3) at the RD, 2 and 4 folds of RD of deltamethrin and lambda-cyhalotrin during incubation period (28°C, 45 days) in Osmaniye olive soil

TABLE 2
Results of ANOVA (General Linear Model) for repeated measures of C mineralized. Effects of incubation time, soil and dose

	Type III Sum of Squares	df	Mean Square	*F*	Sig.
Incubation time	27923.167	1	27923.167	5137.571	< 0.000
Incubation time × soil	255.859	1	255.859	47.075	< 0.000
Incubation time × dose	712.298	6	118.716	21.843	< 0.000
Incubation time × soil × dose	490.977	6	81.829	15.056	< 0.000
Error (time)	152.183	28	5.435		

DISCUSSION

At the end of the incubation period, it was the first striking result that carbon mineralization of Adana soils added specially 4×RD of deltamethrin and RD of lambda-cyhalotrin was significanly higher than its own control soil ($P < 0.05$). Carbon mineralization values of Osmaniye soils was close to each other and not significantly different from the other doses ($P > 0.05$). It was observed that microorganisms living into Osmaniye olive soil did not positively or negatively affect from RD, 2×RD and 4×RD of the deltamethrin and lambda-cyhalotrin additions. Similar situation was not current for microorganisms living in Adana olive soil. 4×RD of deltamethrin in Adana was detected as a new additional organic matter by soil microorganisms. This situation and it's microbial activities were disclosed in the Figure 2. Similar result was also shown in Adana soils added RD of lambda-cyhalotrin. RD of lambda-cyhalotrin insecticide was also used as a organic matter source by soil microorganisms. This result is shown similarities with findings of some other studies [13,22]. In a different study, the bacteria isolates utilized deltamethrin as a sole source of carbon and energy. While it is generally assumed that soil microorganisms play a major role in the degradation of pyrethroids, they have isolated a bacterial species from a soil capable of utilizing deltamethrin as a sole source of carbon [25].

It was the second valuable result obtained from the study that soil microorganisms preferred deltamethrin from Adana olive soil added the two insecticides to use as a organic matter source or carbon source from the point of view of their exhibited microbial activities. Deltamethrin is more suitable and biodegradable insecticide than lambda-cyhalothrin in Adana olive soil. Lambda-cyhalothrin is moderately resistant in the soil with half-lives ranging from 4 to 12 weeks [35] while a half-life of deltamethrin is the range of 1-8 weeks in mineral soils [36,37]. Lambda-cyhalothrin being compound less bioavailable causes strong sorption to soil and sediment particles [38].

It was the third important result of the study that cumulative $C(CO_2)$ values among the control,

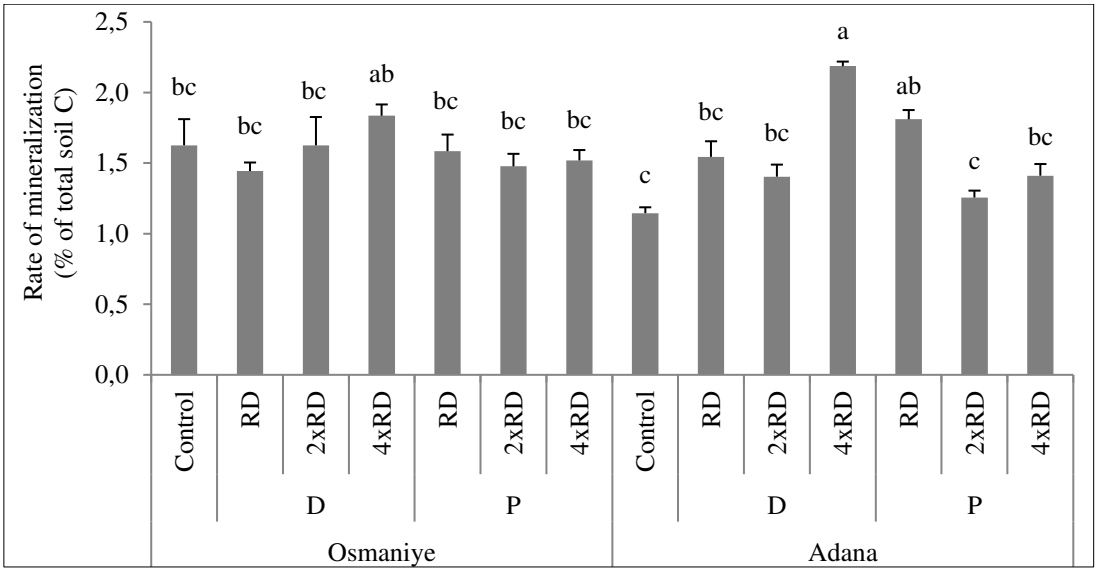

FIGURE 4

Rate of mineralization (Rm) of organic carbon (mean ± SE; n = 3) at the RD, 2 and 4 folds of RD of deltamethrin (D) and lambda-cyhalotrin (L) at the end of incubation period (28°C, 45 days) in Adana and Osmaniye olive soils. a, b and c letters show significant differences among two sites, three dose levels and two insecticides (P ≤ 0.05)

RD, 2 and 4 folds of RD of two insecticides during 45 days in Osmaniye soil did not statistically change. This result was also valid for carbon mineralization ratios of Osmaniye. It might be said that in this case that soil microorganisms did not significantly affect from the all doses of both deltamethrin and lambda-cyhalotrin additions in Osmaniye olive soil and not use to as a organic matter source or soil organic carbon to these both insecticides. The reason of this result might be explained with strong sorption on Osmaniye soil and the resulting slow degradation of especially lambda-cyhalothrin. It might also cause long-term effects on beneficial soil microorganisms. The high carbonaceous of soils cause adsorption and dilution of pesticides that may result in decreased bioactivity and increased persistance of the additive [23]. This result is not clarified with soil C and N contents or texture types of Adana and Osmaniye soils. Because both of soils had similar C, N values and texture type. But soil organic matter quality and microorganism potential of two soils might be different from the each other. Significant differences between $CaCO_3$ contents and pH levels of Adana and Osmaniye soils might be created different effect on the soil microorganisms. pH level and $CaCO_3$ content of Osmaniye soil was higher than Adana soil (7.8 and 51% for Osmaniye soil, 7.64 and 37.6 for Adana soil, respectively). Activities of soil microorganisms with existence of two different insecticides in both soils might also be affected and changed from these differences between two soils. Soil characteristics may cause different activities of the microbiological parameter studies in some pesticide (like deltamethrin, dimethoato, endosulfan, methyl parathion and etc.) applications [39]. The nature and concentration of pesticides are among the main factors affecting the existence and extent of non-target effects [40].

ACKNOWLEDGMENTS

The authors thank Research and Application Center of Osmaniye Korkut Ata University for financial support (Project number: OKÜBAP-2013-PT3-014).

REFERENCES

[1] Gimenez, C., Fereres, E., Ruz, C. and Orgaz, F. (1997) Water relations and gas exchange of olive trees: diurnal and seasonal patterns of leaf water potential, photosynthesis and stomatal conductance. Acta Hort. 449, 411–415.

[2] Rodríguez, E., Peña, A., Sánchez Raya, A.J. and Campos, M. (2003) Evaluation of the effect on arthropod populations by using deltamethrin to control *Phloeotribus scarabaeoides* Bern. (Coleoptera: Scolytidae) in olive orchards. Chemosphere 52, 127–134.

[3] González, R. and Campos, M. (1994) A preliminary study of the effect of attacks by *Phloeotribus scarabaeoides* (Bern.) (Col., Scolytidae) on the productivity of the olive tree (*Olea europaea* L.). Bull. Soc. Entomol. Suisse 67, 67–75.

[4] Vontas, J., Hernández-Crespo, P., Margaritopoulos, J.T., Ortego, F., Feng, H.T., Mathiopoulos, K.D. and Hsu, J.C. (2011) Insecticide resistance in Tephritid flies. Pesticide Biochemistry and Physiology 100, 199–205.
[5] Michos, M.C., Mamolos, A.P., Menexes, G.C., Tsatsarelis, C.A., Tsirakoglou, V.M. and Kalburtji, K.L. (2012) Energy inputs, outputs and greenhouse gas emissions in organic, integrated and conventional peach orchards. Ecol. Indicators 13, 22–28.
[6] Ruano, F., Campos, M., Sánchez-Ray, J. and Peña, A. (2008) Deltamethrin application on colonized olive logs: Effect on the emergence of the olive bark beetle Phloeotribus scarabaeoides Bernard 1788 (Coleoptera: Scolytidae) and its associated parasitoids. Crop Prot. 27, 614–621.
[7] Civantos, M. (1999) Control de Plagas del Olivar. COI, Madrid.
[8] Amvrazi, E.G. and Albanis, T.A. (2008) Multiclass Pesticide Determination in Olives and Their Processing Factors in Olive Oil: Comparison of Different Olive Oil Extraction Systems. J. Agric. Food Chem. 56, 5700–5709.
[9] Tarım ve Köy İşleri Bakanlığı (2010) Zeytin Hastalık ve Zararlıları ile Mücadele. Koruma ve Kontrol Genel Müdürlüğü Yayınları, Ankara.
[10] Aka Sağlıker, H. (2009) Effects to soil carbon mineralization of the different doses of trifluralin at the different temperature conditions. Eur. J. Soil Biol. 45, 473-477.
[11] Datta, S., Shah, P.S. and Das, R.C. (2002) Soil sediment and hardness of wayer reduce the acute toxicity of deltamethrin to scale carp. Pestic. Res. J. 14, 327-336.
[12] Ferreira E.P.B., Dusi, A.N., Costa, J.R., Xavier, G.R. and Rumjanek, N.G. (2009) Assessing insecticide and fungicide effects on the culturable soil bacterial community by analyses of variance of their DGGE fingerprinting data. Eur. J. Soil Biol. 45, 466–472.
[13] Muñoz-Leoz, B., Garbisu, C. , Charcosset, J.Y., Sánchez-Pérez, J.M., Antigüedad, I. and Ruiz-Romera, E. (2013) Non-target effects of three formulated pesticides on microbially-mediated processes in a clay-loam soil. Sci. Total Environ. 449, 345–354.
[14] Bozdoğan, A.M. and Yarpuz Bozdoğan, N., 2015. Determination of potential risks of pesticide applications in peanut cultivation on human health and environment. Fresen. Environ. Bull. 24, 683 – 689.
[15] Kirschbaum, M. U. F. (2000) Will changes in soil organic carbon act as a positive or negative feedback on global warming? Biogeochemistry 27, 753–760.
[16] Raich, J. and Tüfekçioğlu, A. (2000) Vegetation and soil respiration: correlation and controls. Biogeochemistry 48, 71–90.
[17] Vig, K., Singh, D.K., Agarwal H.C., Dhawan A.K. and Dureja P. (2008) Soil microorganisms in cotton fields sequentially treated with insecticide. Ecotox. Environ. Safe. 69, 263–276.
[18] Brooks, P.C. (1995) The use of microbial parameters in monitoring soil pollution by heavy metals. Biol. Fertil. Soils 19, 269–279.
[19] Aka, H. and Darıcı, C. (2005) Carbon and nitrogen mineralization in carob soils with Kermes oak and Aleppo pine leaf litter. Eur. J. Soil Biol. 41, 31-38.
[20] Epelde, L., Mijangos, I., Becerril, J.M. and Garbisu, C. (2009) Soil microbial community as bioindicator of the recovery of soil functioning derived from metal phytoextraction with sorghum. Soil Biol. Biochem. 41, 1788–1794.
[21] Garbisu, C., Alkorta. I. and Epelde, L. (2011) Assessment of soil quality using microbial properties and attributes of ecological relevance. Appl. Soil Ecol. 49, 1–4.
[22] Aka Sağlıker, H., N. Kızıldağ, Ş. Cenkseven, C. Darıcı, B. Koçak, N. Yarpuz Bozdoğan and Dağlıoğlu, N. (2014) Effects of imazamox on soil carbon and nitrogen mineralization under two different humidity conditions. Ekoloji, 91, 22-28.
[23] Zhang, L.Z., Khan,S.U. Akhtar, M.H. and Ivarson, K.C. (1984) Persistence, Degradation, and Distribution of Deltamethrin in an Organic Soil under Laboratory Conditions. J. Agr. Food Chem. 32, 1207-1211.
[24] Hill, B.D. and Schaalje, G.B. (1985) A Two-Compartment Model for the Dissipation of Deltamethrin on Soil. J. Agric. Food Chem. 1085, 33, 1001-1006.
[25] Khan, S.U., Behki, R.M., Tapping, R.I. and Humayoun Akhtar, M. (1988) Deltamethrin Residues in an Organic Soil under Laboratory Conditions and Its Degradation by a Bacterial Strain[1]. J. Agr. Food Chem. 36, 636-638.
[26] Bouyoucos, G. S. (1951) A recalibration of the hydrometer for making mechanical analysis of soil. Agron. J. 43, 434-438.
[27] Demiralay, I. (1993) Toprak Fiziksel Analizleri, Atatürk Üniversitesi Ziraat Fakültesi Yayınları, Erzurum, Türkiye.
[28] Jackson, M. L. (1958) Soil Chemical Analysis. Prentice-Hall, Inc, New Jersey.
[29] Allison, L. E. and Moodie, C. D. (1965) Carbonate. American Soc. Agron. 9, 1379-1396.
[30] Duchaufour, P. (1970) Precis de pedologie. Masson et C[1e], Paris.
[31] Schaefer, R. (1967) Characteres et evolution des activites microbiennes dans une chaine de

sols hydromorphes mesotrophiques de la plaine d'Alsace. Rev. Ecol. Bio. Sol. 4, 567–592.
[32] Benlot, C. (1977) Recherches sur les activites biochimiques dans les successions de sols derives de cendres volcaniques sous climat tropical humide (Zaire- Indonesie), ENS Lab. De zoologie, Paris.
[33] Kleinbaum, D. G., Kupper, L. L., Muller, K. E. and Nizam, A. (1998) Applied regression analysis and other multivariable methods, Duxbury Press, California.
[34] Schaefer, R. (1967) Characteres et evolution des activites microbiennes dans une chaine de sols hydromorphes mesotrophiques de la plaine d'Alsace. Rev Ecol Biol Sol 4, 567–592.
[35] Tomlin, C. (1994) The Pesticide Manual Incorporating the Agrochemicals Handbook. BCPC & The Royal Society of Chemistry, NY.
[36] Chapman, R.A., Tu, C.M., Harris, C.R. and Cole, C. (1981) Persistence of Five Pyrethroid Insecticides in Sterile and Natural, Mineral and Organic Soil. Bull. Environ. Contam. Toxicol. 26, 513-516.
[37] Hill, B.D. (1983) Persistence of Deltamethrin in a Lethbridge Sandy Clay Loam. J. Environ. Sci. Health, Part B 18, 691-696.
[38] Matsumura, F. (1985) Toxicology of Insecticides. Plenum Press, New York.
[39] Andréa, M.M., Peres, T.B., Luchini, L.C.and Pettinelli, A.Jr. (2000) Impact of long-term pesticide applications on some soil biological parameters. J. Environ. Sci. Health, B 35, 297-307.
[40] Chen, S.K., Edwards, C.A. and Subler, S. (2001) Effects of the fungicides benomyl, captan and chlorothalonil on soil microbial activity and nitrogen dynamics in laboratory incubations. Soil Biol Biochem. 33, 1971–1980.

Received: **02.02.2016**
Accepted: **18.08.2016**

CORRESPONDING AUTHOR

Husniye Aka Sagliker

University of Osmaniye Korkut Ata,
Faculty of Science and Letters,
Department of Biology, 80000
Osmaniye, TURKEY

e-mail: hasagliker@osmaniye.edu.tr

© by PSP Volume 25 – No. 10/2016, pages 4381-4386 Fresenius Environmental Bulletin

EFFECTS OF FERTILIZER INPUT ON HEAVY METAL IN DIFFERENT SOILS

Yukui Rui*, Shutong Liu, Shengliang Li, Liming Liu

College of Resources and Environmental Sciences, China Agricultural University, Beijing, China

ABSTRACT

Food production is becoming critical to national security to effectively protect and increase the income of farmers. Increasing inputs of fertilizer and pesticides provides the fastest way to improve yield, but many studies have shown this will directly or indirectly result in an increase in the heavy metal content. This study used field sampling and laboratory analysis methods to study the major corn producing areas of Lishu County, Jilin Province, China. The effects of inputs of chemical fertilizer, mixed chemical and organic fertilizer, mixed chemical and straw fertilizer were analyzed with four kinds of agricultural soils. The accumulation of six heavy metals, Cr, Ni, Cu, As, Cd, and Pb, was analyzed. Results showed that Cd accumulation in soil is associated with the application of organic fertilizer, and As accumulation is associated with chemical fertilizer. Cd's cumulant in black and sandy soil is much lower than in the other two soils. As accumulation is likely in all four soils, especially under high fertilization rates; all four soils were prone to accumulate As. Nevertheless, Cr, Ni, Cu, and Pb did not accumulate significantly in the four soils analyzed here, and maintaining these inputs in the short term will not cause soil pollution.

KEYWORDS:

Heavy metal, different input mode, different soil, soil pollution.

INTRODUCTION

Soil serves as a precious natural resource required for human survival and development, and is also an important part of the environment; nevertheless, soil pollution caused by heavy metal element accumulation is becoming increasingly serious as a result of intensified industrial development and related urban pollution as well as an increase in the number of species planted in agricultural fields and high intensity land use [1]. Soil pollution seriously affects soil quality and health, and soil heavy metal content has been an important index used to evaluate soil quality, soil health and the soil environment. Soil pollution was both somewhat cryptic and irreversible in the short term because microbes have difficulty degrading heavy metals. The metals would be absorbed by microbes and plants where they accumulate and migrate, to be ultimately transformed into part of the human food chain. Eventually, the metals would be absorbed into the bodies of humans and animals, harming their health. In terms of ecological benefits, on the one hand, heavy metals in soil lead to serious soil degradation and have a profound impact on soil quality and soil health [2]. Furthermore, high concentrations of heavy metals in soil can easily be transferred into the atmosphere and water, and under the action of wind and water cause serious pollution of the atmosphere and surface water, leading to environmental risk, such as groundwater pollution [3].

To increase grain yield and income, improving farming yield is the most effective way to solve food production [4]. Increasing the agricultural input of fertilizer and pesticide is the fastest way to improve the yield. However, a large number of studies have shown that increased inputs of fertilizer and pesticide will directly or indirectly increase the risk of the heavy metal accumulation in soil [5]. Xu et al. [6] studied three different soils with different fertilizers over 17 years of fertilization, and found that the long-term application of organic fertilizer leads to significant accumulation of Cu and Cd in black and red soil. Hugo et al. [7] studied the input of agrochemical, the fertilizers were identified as the primary source of heavy metals. Mehrdad et al. [8] found that long-term application of phosphate fertilizers on vegetable production fields, the high concentrations of elemental As, Cd, Cr, Cu, Pb, and Zn were found

in potatoes. About the organic fertilizer, Florencio et al. [9] studied the influence of composting on the organic matter content, humus fractions and bioavailability of heavy metals in the sludge. However, studies that compare the accumulation of heavy metals and soil quality in natural farmland under different levels of fertilizer and pesticide application over a long time period are rare.

Lishu County was selected as the research object in this study because the county promotes efficient maize yield in the entire county. To achieve the goal of producing corn "one ton each" (one ton of corn per hm^2), the county recommends farmland fertilizer inputs of about 650–1250 $kg \cdot hm^{-2}$—significantly higher than the national average of 375 $kg \cdot hm^{-2}$ [10]; farmers in the county also apply 15–50 $t \cdot hm^{-2}$ of organic manure from chicken farms, according to a survey of 60–70% of farms. And Lishu County has rich black, sandy, alluvial, and other soils.

Therefore, this allows the exploration of different long-term fertilizers and soils on the accumulation of heavy metals including: 1) chemical fertilizer, mixed chemical and organic fertilizer, mixed chemical and straw fertilizer returned to soil as fertilizer, and 2) different types of farmland soil conditions, allowing us to determine the conditions needed for high quality food production in different soils and an appropriate fertilizer input method.

EXPERIMENTAL SCHEME

Experimental design. Four typical types of Lishu County farmland soil were analyzed in this experiment: black, sandy, alluvial, and brown soil. Three inputs methods were also reviewed: chemical fertilizer, mixed chemical and organic fertilizer, mixed chemical and straw fertilizer.

In the studied areas, chemical fertilizer had been used for more than 10 years with an average application rate of more than 750 $kg \cdot hm^{-2}$; organic fertilizer had been used for more than 10 years with an average of more than 15 $t \cdot hm^{-2}$; straw had been used for more than 5 years with an application rate of 7.5 $t \cdot hm^{-2}$. The heavy metals analyzed here were Cr, Ni, Cu, As, Cd and Pb.

Sample collection and processing. The collection of soil samples was completed based on the method of *The Farmland Soil Environment Quality Monitor Technology Specifications* (NY/T395-2000), sampling depth of 0–20 cm. 51 samples were collected from each type of soil, for a total of 204 samples. A grid layout method was used for soil sample collection; three sampling points were established within each 1 km^2 area. At each sample point 3–5 soil collections were made using a stainless steel auger to collect 0–20 cm mixed topsoil samples. Samples were sieved through a 20 nylon mesh sieve, and mixed until homogeneous.

Determination of heavy metal elements. The heavy metal content of corn samples was determined by inductively coupled mass spectrometry; for the process and parameters, refer to *The Influence of Nitrogen Fertilization on Heavy Metal in Maize Seed* [11]. The qualitative and quantitative analysis of soil samples was done using the XRF method for corn samples; for the process and parameters refer to *26 Kinds of Secondary Elements and Trace Elements in Soil with the XRF Method* [12]. Soil fluid samples were used to determine the content of Cr, Ni, Cu, As, Cd, and Pb with the ICP-MS method (The Thermoelectric ICP-MS X7, West Chester, Pennsylvania, United States). The process used parallel double samples, a blank and a reagent correction experiment for quality control.

The statistical analysis and the schematic diagrams and charts for the experimental data were prepared using SPSS, Origin, WPS and AutoCAD software.

ANALYSIS OF THE RESULTS

The accumulation content of heavy metals in the black soil under different fertilizer. Fig. 1 shows statistical results of the analysis of heavy metal content in black soil with different fertilizer inputs. Based on Fig. 1, no significant differences in the content of Cr, Cu, As, and Pb were observed based on the three kinds types of fertilizer input. The accumulation of Ni under a mixture of chemical and organic fertilizer was significantly higher than under the mixture of chemical and straw fertilizer. The accumulation of Cd increased more significantly with the application of both chemical fertilizer and a mixture of chemical and organic fertilizer, than with the mixed chemical and straw fertilizer.

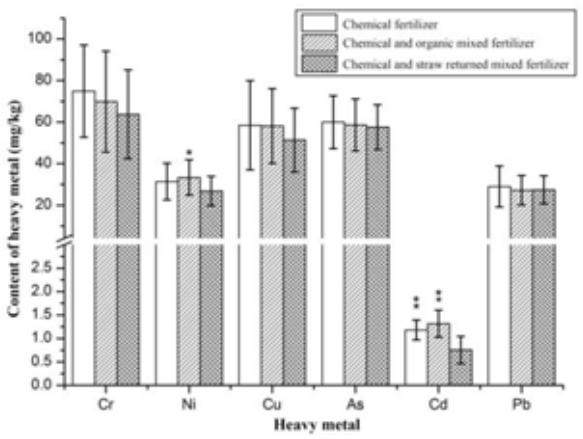

FIGURE 1
Heavy metal content of black soil with different fertilizer input.

Note: "*"and "**" indicate distinct differences ($P < 0.05$) or significant distinct differences ($P < 0.01$) for content of each metal, the same as the following figures.

The accumulation of Cr under the chemical fertilizers was 7.2% and 17.5% higher, respectively, than under the other two fertilizer treatments used here. The Ni content was 6.2% and 24.3% higher, respectively, in soils with the mixture of chemical and organic fertilizer than in the other two fertilizer treatments; under the mixed chemical and organic fertilizer treatment, the accumulation of Ni was significant ($P < 0.05$) when compared with the mixed chemical and straw fertilizer treatment. Almost no change was observed in the Cu content under the chemical fertilizer and mixed chemical and organic fertilizer treatments where the Cu content was 13.8% and 13.1% higher, respectively, than in the mixed chemical and straw fertilizer treatment, although the difference was not significant. The accumulations of As and Pb were almost the same under the three types of fertilizer input. Under the three types of fertilizer input, Cd content varied most obviously; the average Cd content under the use of either chemical fertilizer or a mixture of chemical and organic fertilizer was higher than the third-level for soil under the national soil environment quality standard (1 $mg \cdot kg^{-1}$); therefore, Cd pollution was present and extremely significant ($P < 0.01$) when compared with the mixture of chemical and straw fertilizer. Among these three fertilizer treatments, Cd accumulation was highest with the mixture of chemical and organic fertilizer; 16 of 17 test samples exceeded the threshold (1 $mg \cdot kg^{-1}$), and Cd accumulation was two and 12 times higher, respectively, than the chemical fertilizer treatment and the mixture of chemical and straw fertilizer treatment, with all three treatments being over the limit by 82.4%, 94.1% and 23.5%, respectively.

The accumulation content of heavy metals in the sandy soil under different fertilizer. No significant difference in the accumulation of Cr, Ni, Cu, As and Cd was observed in sandy soil under three kinds of fertilizer input (Fig. 2). The accumulation of Pb in areas with mixed chemical and organic fertilizer was significantly different from areas with mixed chemical and straw fertilizer.

In the sandy soil with mixed chemical and organic fertilizer, the accumulation of Ni and Cd was lower than areas with the other two kinds of fertilizer; the remaining elements had higher accumulation rates with this fertilizer than with the other two kinds of fertilizer and Pb accumulation was significantly higher. With chemical fertilizer, the average accumulation amount for Cr was 68.68 $mg \cdot kg^{-1}$; this was 8.66% and 3.87% lower than the other two fertilizer treatments, mixed chemical and organic fertilizer and mixed chemical and straw fertilizer, respectively. The average Ni accumulation was 32.86 $mg \cdot kg^{-1}$, 6.6% and 0.65% higher than the other two treatments, respectively. The average Cu accumulation was 53.88 $mg \cdot kg^{-1}$, 10.61% and 1.71% lower than the other two treatments, respectively. With the mixed chemical and organic fertilizer treatment, the average As accumulation was 57.98 $mg \cdot kg^{-1}$, 8.66% and 4.61% higher than chemical fertilizer and mixed chemical and straw fertilizer treatments, respectively. The average Cd accumulation was 1.30 $mg \cdot kg^{-1}$, which was 0.12 $mg \cdot kg^{-1}$ and –0.23 $mg \cdot kg^{-1}$ higher than the other two treatments, respectively. Under all three fertilizers, the Cd accumulation was always higher than the third-level soil quality standard (1 $mg \cdot kg^{-1}$), indicating the presence of Cd pollution. The amount of Pb was significantly higher when the mixed chemical and straw fertilizer treatment was compared with the mixed chemical and organic fertilizer treatment.

The accumulation content of heavy metals in the alluvial soil under different fertilizer. Fig. 3 shows the statistical results of the alluvial soil under different fertilizer treatments. The accumulation of Cr, Ni, As and Pb was not significantly different in the three fertilizer treatments. Under the mixed chemical and organic

fertilizer treatment, the accumulation of Cu and Cd was significant and highly significant ($p < 0.01$) higher, respectively, than that under the chemical fertilizer treatment.

During this experiment, under the mixture of chemical and organic fertilizer and the mixture of chemical and straw fertilizer, the accumulation of Ni, As, Pb and Cd occurred with different amplitudes of increase. The increase in Cr content was: mixed chemical and organic fertilizer > mixed chemical and straw fertilizer > chemical fertilizer; when compared with the mixed chemical and organic fertilizer and mixed chemical and straw fertilizer, the accumulation of Cr was lower by 13.3% and 11.4% when compared with the chemical fertilizer treatment. The accumulation of Cr was basically unchanged in the mixed chemical and organic fertilizer and mixed chemical and straw fertilizer treatments. The accumulation of Ni was respectively 8% and 5% higher than chemical fertilizer and mixed chemical and straw fertilizer when compared with the mixed chemical and organic fertilizer treatment. The Cu content among the three treatments was: mixed chemical and organic fertilizer > mixed chemical and straw fertilizer > chemical fertilizer. Regarding the chemical fertilizer and mixed chemical and straw fertilizer treatments, the Cu accumulation was 27.2% and 10% higher, respectively, when compared with the mixed chemical and organic fertilizer; that is, the accumulation of Cu obviously tended to increase under the mixed chemical and organic fertilizer treatment. The accumulations of As and Pb were basically the same in all three fertilizer treatments. The accumulation of Cd was most obvious, with the order of: mixed chemical and organic fertilizer > mixed chemical and straw fertilizer > chemical fertilizer. Under the mixed chemical and organic fertilizer and mixed chemical and straw fertilizer treatments, the accumulation of Cd was 50.8% and 20.8% higher, respectively, than that under the chemical fertilizer treatment. Under these two fertilizer treatments, the average Cd accumulation was higher than the third-level soil quality standard (1 $mg \cdot kg^{-1}$), indicating the presence of Cd pollution. The chemical fertilizer treatment also highly significantly exceeded ($P < 0.01$) the second-level soil quality standard (0.6 $mg \cdot kg^{-1}$).

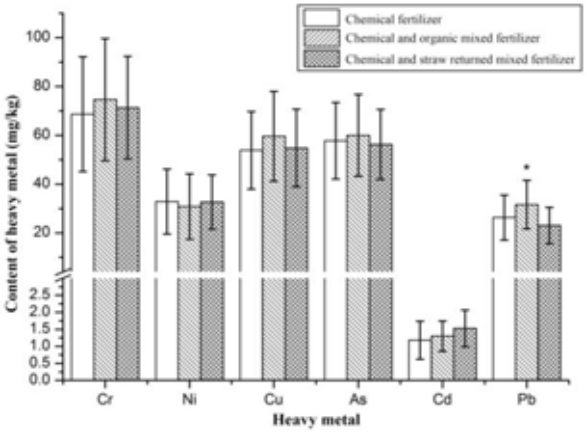

FIGURE 2
Heavy metal content of sandy soil with different fertilizer input.

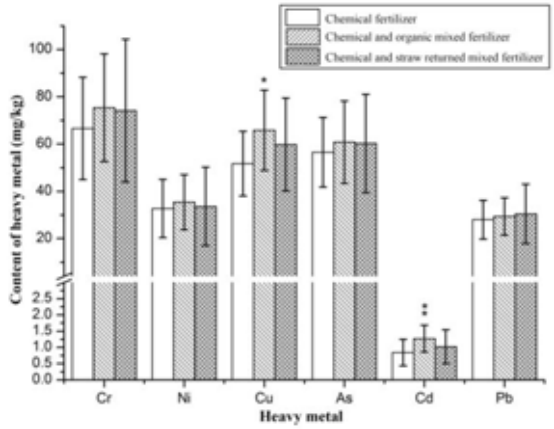

FIGURE 3
Heavy metal content of alluvial soil with different fertilizer input.

The accumulation content of heavy metals in the brown soil under different fertilizer. The accumulation of Cr, Ni, As and Pb was not significantly different in the brown soil for all three fertilizer treatment (Fig. 4). Under the mixed chemical and organic fertilizer treatment, the accumulation of Cu and Cd was significantly higher than in the chemical fertilizer treatment.

In the three fertilizer treatments, the order of the size of the accumulation of Cr was: mixed chemical and straw fertilizer > chemical fertilizer > mixed chemical and organic fertilizers, although the differences between the three fertilizer treatments were small. Under the chemical fertilizer treatment, the Ni accumulation was, respectively, 18.3% and

12.2% higher than the other two fertilizer treatments. For all three fertilizer treatments, the Cu accumulation in the mixed chemical and organic fertilizer treatment was significantly higher than that in the chemical fertilizer treatment, and was,respectively, 22.4% and 19.9% higher than the other two fertilizer treatments. The As and Pb accumulations were not obviously different among the three fertilizer treatments.

The order of the size of As was: chemical fertilizer > mixed chemical and organic fertilizers >mixture of chemical and straw fertilizer, and the order of Pb was the same as that of As. The Cd accumulation was most obvious in the three fertilizer treatments when compared with other heavy metals, and exceeded the third-level soil quality standard (1 $mg \cdot kg^{-1}$), indicating Cd pollution. The accumulation of Cd with the mixed chemical and organic fertilizer and chemical fertilizer treatments was significant. Among the 17 tested samples in each of the three fertilizer treatments, the Cd content was higher than 1 $mg \cdot kg^{-1}$ or 11, 16 and 13, respectively, or 64.7%, 94.1% and 76.5% over the limit, respectively.

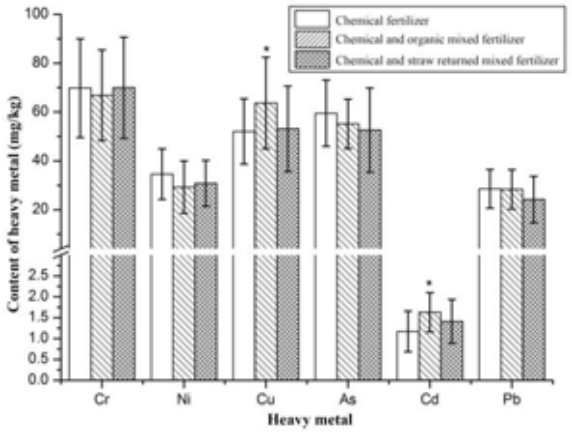

FIGURE 4
Heavy metal content of brown soil with different fertilizer input.

CONCLUSION

1) Long-term fertilizers input have caused Cr, Ni, Cu, As, Cd and Pb to accumulate in the soils. Compared with background data from the 1990s, Cd and As content have the largest increases in the four soils, and appear to exceed the minimum level that indicates pollution to some extent. The content of Cr, Ni, Cu and Pb in some soils also significantly increased.

2) When mixed chemical and organic fertilizers were used, the accumulation of Cd was significant or extremely significant different from areas with other fertilizers; this suggests the accumulation of Cd was related to the use of organic fertilizer. The accumulation of As was not significantly different with all three types of fertilizer, but the amount of As found was partly above the third-level soil quality standard, reaching the point where it could be considered a pollutant; the accumulation of As was related to the use of chemical fertilizers.

3) Based on the above analysis, we can conclude that the accumulation of As was related to the use of chemical fertilizer, and the Cd accumulation was closely related to the content of heavy metal in organic fertilizer. The effect of soil types on the accumulation of heavy metal in soil was less than the effect of fertilizer.

ACKNOWLEDGEMENTS

This was supported by the National Natural Science Foundation of China (No. 41371471).

REFERENCES

[1] Song Chun-ran, He Jin-lin, Tan Hong, et al.2005. Primary Appraisal for Heavy Metals Pollution in Farm Soils of Guizhou Province[J]. Guizhou Agricultural Sciences, 33(2):13-16.

[2] Bai Ling-yu, Zeng Xi-bai, Li Lian-fang, et al. 2010. Effects of Land Use on Heavy Metal Accumulation in Soils and Source Analysis [J]. Scientia Agricultura Sinica, 43(1):96-104.

[3] Sui HongJian, Wu Xuan, Cui Yanshan. 2006. Modeling heavy metal movement in soil: review and further study directions [J]. Transactions of the CSAAE, 22(6):197-200.

[4] Ma Wen-qi, Zhang Fu-suo, Zhang Wei-feng. 2005. Fertilizer Production and Consumption and the Resources, Environment, Food Security and Sustainable Development in China[J]. RESOURCES SCIENCE, 27(3): 33-40.

[5] Li Shuang-yi, Liu He, Wang Jing-kuan. 2010. Effects of Long-term Located Fertilization on Heavy Metals and Their Availability in Brown Earth[J]. Journal of Agro-Environment Science, 29(6): 1125-1129.

[6] Xu Ming-gang, Wu Haigwen, Liu Jing. 2010. Evolution of Heavy Metal Contents of Three soils Under Long-term Fertilizations [J]. Journal of Agro-Environment Science, 29(12): 2319-2324.

[7] Hugo José Oliveira Zoffoli, Nelson Moura Brasil Amaral-Sobrinho, Everaldo Zonta, Marcus Vinícius Luisi,Gracioso Marcon, Alfredo Tolón-Becerra. Inputs of heavy metals due to agrochemical use in tobacco fields in Brazil's Southern Region [J]. Environmental Monitoring and Assessment, 2013, 185(3):2423-2437.

[8] Mehrdad Cheraghi, Bahareh Lorestani, Hajar Merrikhpour, Nasim Rouniasi. Heavy metal risk assessment for potatoes grown in overused phosphate-fertilized soils [J]. Environmental Monitoring and Assessment, 2013, 185(2): 1825-1831.

[9] Florencio Ingelmo, Maria José Molina, Maria Desamparados Soriano, Antonio Gallardo, Leonor Lapeña. Influence of organic matter transformations on the bioavailability of heavy metals in a sludge based compost[J]. Journal of Environmental Management,2012, 95(S): S104-S109.

[10] Xing Wei-qin, Ran Yong-liang, Liang Shuang, et al. 2010. The research progress of the effect of fertilizer to heavy metals in soil[J]. Journal of Henan Agricultural Sciences, 5: 129-133.

[11] Rui Y. K., F. S Zhang.,J. B Shen. 2009. Effects of nitrogen fertilization on heavy metal content of corn grains. International Journal of Experimental Botany, 78: 101-104.

[12] Yuan Hui, Zhang Li-hua, Jin LI-yun. 2001.Determination of 26 major, minor and trace elements in soil by X-ray fluorescence spectrometric method[J]. Journal of Nuclear and Radiochemistry, 23(3): 134-139.

Received: **06.02.2016**
Accepted: **23.07.2016**

CORRESPONDING AUTHOR

Yukui Rui
College of Resources and Environmental Sciences
China Agricultural University
Yuanmingyuan Xilu No.2
Haidian District, Beijing, CHINA

E-mail: ruiyukui@163.com

© by PSP Volume 25 – No. 10/2016, pages 4387-4392 Fresenius Environmental Bulletin

HYDROCHEMISTRY OF GROUNDWATER FROM THE LOOSE LAYER AQUIFER: QUALITY AND CONTROLLING FACTOR ANALYSIS

Xianghong Liu [1, 2, *], Jingcun Yu [1], Linhua Sun [2], Herong Gui [2]

1. School of Resources and Geosciences, China University of Mining and Technology, Jiangsu 221116, P.R.China
2. School of Resources and Civil Engineering, Suzhou University, Anhui 234000, P.R.China

ABSTRACT

Groundwater in the loose layer aquifer system is important for the water supply and safety of mining in the coal mines. In this study, a total of fifty-two groundwater samples from the Zhuxianzhuang coalmine in northern Anhui Province, China have been collected, and their major ion concentrations have been measured for evaluating the quality of the water and identifying the main mechanisms controlling the chemical variations. The results suggest that the groundwater from the loose layer aquifer system have pH values in the permissible range of World Health Organization (WHO), whereas they should be treated before drinking according to their high contents of total dissolved solids (TDS). The groundwater samples were classified to be Na–SO_4 and Na-Cl types, which related to the hydrological condition of the water. The Water Quality Index (WQI) values of the groundwater were 79 to 188 (mean = 149), suggesting that these groundwater samples are poor for drinking when considering about only their major ion concentrations. However, they can be used for irrigation according to their sodium absorption ratio (SAR) and residual sodium carbonate (RSC) values. Moreover, Gibbs diagrams, relationships between major ions and factor analysis suggest that water rock interaction and evaporation (related to discharging) are the main mechanisms controlling groundwater chemistry.

KEYWORDS:
Groundwater; quality assessment; water rock interaction; loose layer aquifer; coal mine

INTRODUCTION

Coal mining has greatly contributed to the development of the economy and society of China, because more than 50% of the primary energy was contributed by coal during the recent years. However, water shortage in China is serious, especially in coal mining areas. Previous studies revealed that more than 71% of the coal mining areas in China were lacking of water and 40% of them were serious [1]. And therefore, the groundwater in the coal mining area has attracted large number of studies, which focused on the quality evaluation and controlling factor analysis [2, 3].

Previous studies revealed that there are four main aquifer systems related to the safety of coal mining in the northern Anhui Province, China: the loose layer, the coal bearing sandstone, the Taiyuan Formation limestone and the Ordovician limestone aquifer systems [4]. Among these four aquifer systems, the groundwater in the loose layer and the Taiyuan Formation limestone aquifer systems are the most important ones for water supply, because the groundwater in the loose layer aquifer system is buried shallow (< 300 m), which can be pumped easily, whereas the groundwater in the Taiyuan Formation limestone aquifer system is relatively clean with large amount.

Water pollution is a global problem [5-8]. It has been suggested that water pollution is the leading worldwide cause of deaths and diseases and, it accounts for the deaths of more than 14,000 people daily [9]. And therefore, water quality is a major concern by the government and scientists, and the most common standards used to assess water quality relate to health of ecosystems, safety of human contact and drinking water, such as the water quality standards of WHO [10], have been released.

The quality of the groundwater from the Taiyuan Formation limestone aquifer system has long been concerned by previous studies [2, 3]. However, similar work related to the groundwater in the loose layer aquifer system has not been reported yet. In this study, a total of fifty-two groundwater samples from the Zhuxianzhuang coalmine in northern Anhui Province, China have been collected, and their major ion concentrations have been measured for evaluating the quality of the water (including drinking and irrigation) and identifying the main mechanisms controlling the chemical variations of the water. The study can provide information for the usage of the water.

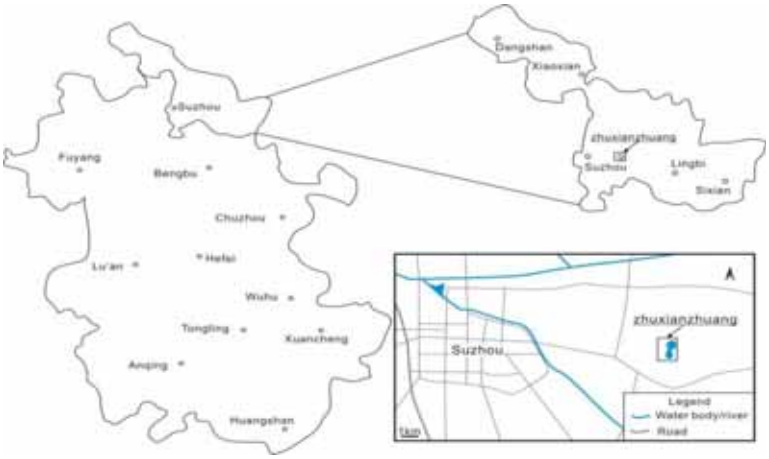

FIGURE 1
Location of the Zhuxianzhuang coalmine

MATERIALS AND METHODS

Hydro- and geological background. The Zhuxianzhuang coal mine is located 13 km east of the Suzhou City, northern Anhui Province, China (Fig. 1) between latitude 33º33′31.4″-33º39′37.6″ and longitude 117º05′37.6″-117º09′23″. The length of the coal mine is 9 km from south to north, and the width is 1.5–5.8 km from east to west, and the total area is 21.6 km^2. The depth of coal mining is between -250 m and -700 m.

The mine is located in the Huaibei plain with elevation between 23 and 27 m. Tuohe River is the only one flow through the region, but most of the water supplies for drinking, irrigation and industry are taken from underground. The climate of the area is mild and belongs to marine - continental climate with an annual average temperature of 14.3 °C. The average annual rainfall is 941 mm, and most of them concentrated in July.

The coalmine is covered by the loose layer sediments, including the Tertiary and Quaternary, the thicknesses of them are 250-260 m in the north and 246-250 m in the south of the coalmine. Multi-layer composite structure is observed in the loose layer, including four aquifers and three water-resisting layers from shallow to deep. The first aquifer is a semi confined aquifer near the surface with thickness between 15 and 30 m, whereas the second, third and fourth ones are confined aquifers, their thicknesses are 10-60, 20-80 and 0-57 m. The fourth aquifer is rich in water and directly contacted with the coal bearing strata. Moreover, because of the stable distribution of the water-resisting layers, there is no hydraulic connection between these four aquifers. The main rock types in the loose layer aquifer system include clay, sandy clay and calcareous clay.

Sampling and analytical methods. A total of fifty-two water samples have been collected from the loose layer aquifer system in the Zhuxianzhuang coalmine. Water pH and TDS were measured in the field with a portable pH- and TDS- meter. Water samples were filtered through 0.45 μm pore size membranes and collected into 2 L polyethylene bottles that had been cleaned in the laboratory. Then, the samples were sent to the laboratory for analysis of major ions. Concentrations of eight kinds of major ions (Na^+, K^+, Ca^{2+}, Mg^{2+}, Cl^-, SO_4^{2-} and HCO_3^-) have been analyzed. The analytical methods are as follows: Na^+, K^+, Ca^{2+}, Mg^{2+}, Cl^- and SO_4^{2-} were analyzed by ion chromatography, whereas HCO_3^- was analyzed by acid–base titration in the Engineering and Technological Research Center of Coal Exploration, Anhui Province, China. Because of the low concentrations of K^+, the Na^+ and K^+ are merged to be (Na^++K^+) in the following discussion.

RESULTS AND DISCUSSION

Major ion concentrations. The analytical results of the major ion concentrations are listed in Table 1 As can be seen from the table, pH values of the groundwater samples range from 7.1 to 8.2 with mean= 7.7, indicating that they are generally neutral to slightly alkaline. In comparison with WHO [10], all of the samples were in the permissible range (6.5-8.5). TDS contents of the groundwater samples vary from 913 to 3066 mg/l (Table 1) with a mean of 1614 mg/l, and only one sample has TDS lower than the guideline value of WHO (<1000 mg/l) [10], indicating that these groundwater samples are generally moderately saline or brackish (1000-10000 mg/l) [11]. The groundwater samples have Na^++K^+ from 89 to 424 mg/l, Ca^{2+} from 37 to 235 mg/l, Mg^{2+} from 10 to185 mg/l, Cl^- from 72 to 379 mg/l, SO_4^{2-} from 227 to 734 mg/l and HCO_3^- from 123 to 545 mg/l.

TABLE 1
Major ion concentrations of groundwater samples (mg/l)

	Na^++K^+	Ca^{2+}	Mg^{2+}	Cl^-	SO_4^{2-}	HCO_3^-	TDS	pH
N of Cases	52	52	52	52	52	52	52	52
Minimum	89	37	10	72	227	123	913	7.1
Maximum	424	235	185	379	734	545	3066	8.2
Mean	283	131	85	308	511	394	1614	7.7
Coefficient of variation	0.249	0.411	0.372	0.195	0.214	0.177	0.219	0.032
p-value	>0.15	>0.15	<0.01	<0.01	<0.01	0.035	<0.01	0.13

In comparison with the permissible limits of WHO [10], 6, 44, 48, 8, 2 and 1 samples can meet the demands of Na^+, Ca^{2+}, Mg^{2+}, Cl^-, SO_4^{2-} and HCO_3^- concentrations for drinking.

It can also be obtained from the table that the groundwater samples have low to moderate coefficients of variations (0.249, 0.411, 0.372, 0.195, 0.214, 0.177, 0.219 and 0.032 for Na^++K^+, Ca^{2+}, Mg^{2+}, Cl^-, SO_4^{2-}, HCO_3^-, TDS and pH, respectively), indicating that the sources of the major ions in the loose layer aquifer system are relatively stable. Similar conclusion can also be achieved by the p-values of Anderson-Darling tests, as Na^++K^+, Ca^{2+} and pH have normal distributions (> 0.05), whereas Mg^{2+}, Cl^-, SO_4^{2-}, HCO_3^- and TDS might have multi sources because of their low p-values (< 0.05).

Hydro-chemical types. Classification of hydro-chemical types for groundwater is important because of the dominant anion species of water change systematically from HCO_3^-, $SO_4^{2-}$to Cl^- as groundwater flows from the recharge zone to the discharge zone [12]. Classification of water in this study is based on the concentrations of major ions by using Piper diagram. The result in Fig. 2 indicates that most of the groundwater samples are classified to be Na–SO_4 type (39 samples) and Na-Cl type (6 samples), suggesting that the Zhuxianzhuang coalmine is not located in the recharge zone, but discharging is important for the chemical variations of these groundwater samples.

Quality evaluation for drinking. The water quality index (WQI) was calculated for evaluating the quality for drinking based on several key parameters of water chemistry, which has long been used for groundwater and surface water [13, 14]. To calculate the WQI, the weight has been assigned for the physico-chemical parameters according to the parameters relative importance in the overall quality of water for drinking purposes. The assigned weight ranges from 1 to 5. The maximum weight of 5 has been assigned for TDS, Cl^- and SO_4^{2-}, 4 for Na^+, 3 for Ca^{2+} and Mg^{2+} [15]. The relative weight is computed from the following equation:

$$\mathrm{Wi} = \mathrm{wi}/\sum_{i=1}^{n} wi \quad (1)$$

Where Wi is the relative weight, wi is the weight of each parameter, n is the number of parameters.

$$Qi=100\times Ci/Si \quad (2)$$

Where Qi is the quality rating, Ci is the concentration of each chemical parameter (mg/l), and Si is the World Health Organization standard (Na^+ 200 mg/l, Ca^{2+} 300 mg/l, Mg^{2+} 30 mg/l, Cl^- 250 mg/l, SO_4^{2-} 250 mg/l, TDS 1500 mg/l) [10].

$$\mathrm{WQI}=\sum_{i=1}^{n} Wi \times Qi \quad (3)$$

Based on the calculation results, the quality of the water for drinking can be classified to be five classes (excellent < 50, good 50-100, poor 100-200, very poor 200-300 and unsuitable >300). The groundwater samples from the Zhuxianzhuang coalmine in this study have WQI range from 79 to 188 (mean = 149), and only two samples have WQI values lower than 100, suggesting that these groundwater are poor for drinking when considering about only their major ion concentrations, which is similar to the results obtained from the comparison of major ion concentrations with WHO standards [10]. It is also noticed that the mean contributions of TDS, Cl^-, SO_4^{2-}, Na^+, Ca^{2+} and Mg^{2+} for the WQI are 15%, 17%, 27%, 15%, 4% and 23%. Therefore, before the application of these groundwater, SO_4^{2-} and Mg^{2+} should be firstly considered, and then the Cl^-, TDS and Na^+.

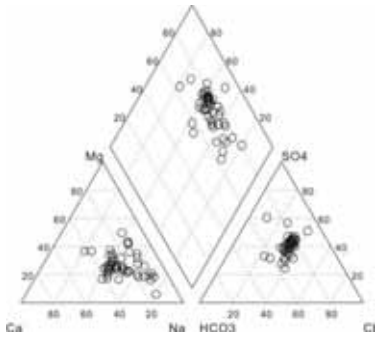

FIGURE 2
Piper diagram

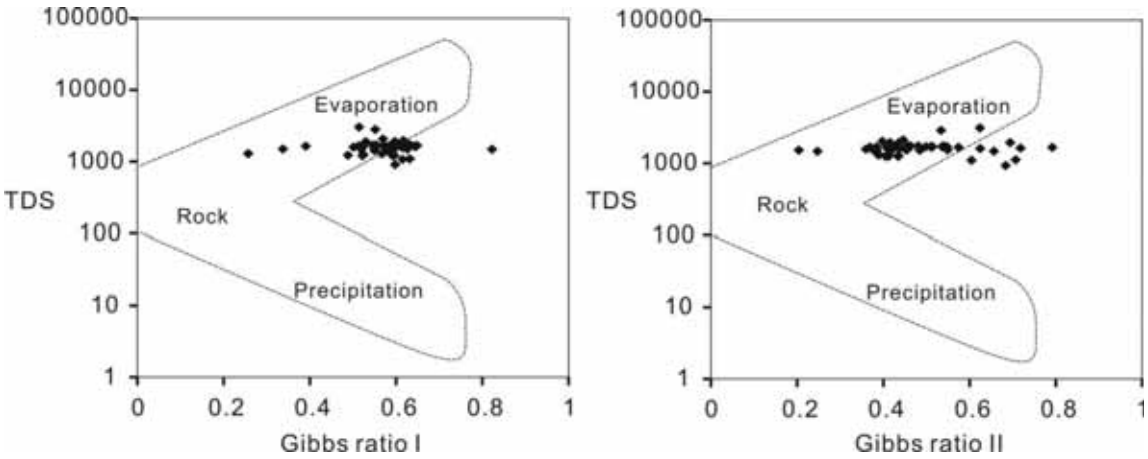

FIGURE 3
Gibbs diagrams

Quality evaluation for irrigation. There are several parameters have been applied for quality evaluation of irrigation, including sodium absorption ratio (SAR), percentage sodium (% Na) and permeability index (PI), residual sodium carbonate (RSC), Kelly's ratio and magnesium ratio. In this study, the most popular applied parameters (SAR and RSC) have been chosen for quality evaluation of irrigation.

The index used is the SAR ($2\times Na^+/(Ca^{2+} + Mg^{2+})$, in meq/l) expresses the relative activity of sodium ions in the exchange reactions with the soil. This ratio measures the relative concentration of sodium to calcium and magnesium. Excess sodium concentration can reduce the soil permeability and soil structure [16]. Irrigation using water with high SAR may require amendments to prevent long-term damage to the soil [17]. The calculated values of SAR in this study ranges from 0.51 to 7.67 (mean = 2.10), and all of the samples were within permissible limit (< 10).

RSC ($(CO_3^{2-} + HCO_3^-)-(Ca^{2+}+ Mg^{2+})$, in meq/l) exists in irrigation water when the carbonate (CO_3) plus bicarbonate (HCO_3) content exceeds the calcium (Ca^{2+}) plus magnesium (Mg^{2+}) content. An excess value of RSC in water leads to an increase in the adsorption of sodium in soil [18], and then loss of soil structure and decrease in soil permeability [19]. RSC value < 1.25 meq/l indicates good water quality. If the value of RSC is between 1.25 and 2.5 meq/l, the water is slightly suitable while a value >2.5 meq/l the water is considered as unsuitable for irrigation. RSC values in this study range from -12.8 to 2.52 meq/l (mean = -7.08 meq/l) and suggesting that all of the water samples can be used for irrigation purpose.

Mechanism controlling water chemistry. Gibbs [20] proposed a diagram to understand the relationship of the chemical components of water from their respective aquifer lithology. Various factors controlling groundwater chemistry are analyzed by the diagram, including precipitation, evaporation and rock dominance. The Gibbs ratios are calculated by: Gibbs ratio I= $(Cl^-/Cl^-+HCO_3^-)$ and Gibbs ratio II= $(Na^+ + K^+)/(Na^+ + K^+ + Ca^{2+})$ (in meq/l). In the present study, Gibbs ratio I values range from 0.26 to 0.82 (mean = 0.57) and Gibbs ratio II values range from 0.20 to 0.79 (mean = 0.48). From Fig. 3, it is clear that all of the samples fell in the area between rock and evaporation dominance, indicating that water rock interaction and discharge related evaporation are the main mechanism controlling groundwater chemistry.

Moreover, it can be obtained from Fig. 4 that the water samples in this study have Ca^{2+}/Na^+ and Mg^{2+}/Na^+ ratios range from 0.13 to 2.13 (mean = 0.60) and 0.08 to 1.81 (mean = 0.62), respectively, suggest that the weathering of silicate minerals and dissolution of evaporate are important in the aquifer system. It is also supported by the plots of Ca^{2+}/Na^+ versus HCO_3^-/Na^+ (Fig. 4).

For getting more information about the source of major ions in the water, factor analysis has been applied to the data, which have long been used for identifying the source of pollutants in environmental studies [21, 22]. With eigenvalue higher than one after varimax rotation, two factors have been obtained (Table 2). As can be seen from the table, the first factor has high positive loadings of Mg^{2+}, Ca^{2+} and SO_4^{2-}, which accounts for 37.7 % of the total variance, and the second factor has high positive loadings of Na^+, Cl^- and HCO_3^-, which accounts for 26.1 % of the total variance. According to the discussions above, as well as the relationships between major ions during dissolution or weathering of minerals, the first factors can be explained to be dissolution of sulfate minerals (e.g. gypsum, $CaSO_4$) and the second factor can be explained to be weathering of silicate minerals (which can generate Na^+ and HCO_3^-) and dissolution of chloride minerals (e.g. halite, NaCl).

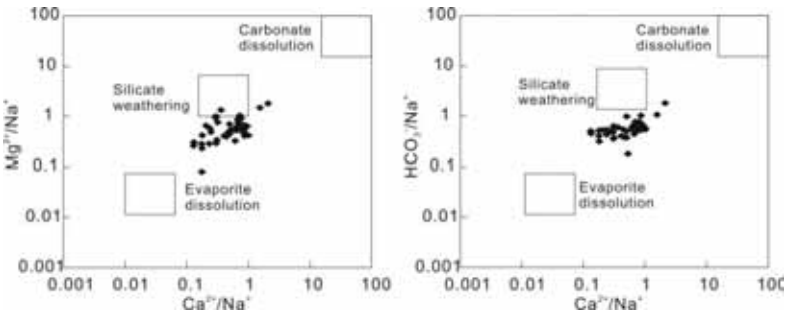

FIGURE 4
Na^+ normalized Ca^{2+}, Mg^{2+} and HCO_3^- plots

TABLE 2
Results of factor analysis

	Factor 1	Factor 2
Na^++K^+	0.059	0.886
Mg^{2+}	0.846	0.029
Ca^{2+}	0.698	-0.277
Cl^-	-0.397	0.631
SO_4^{2-}	0.945	-0.069
HCO_3^-	-0.064	0.548
Eigen value	2.26	1.566
Variance explained (%)	37.7	26.1

CONCLUSIONS

Based on the major ion concentrations of groundwater samples from the loose layer aquifer in the Zhuxianzhuang coal mine, northern Anhui Province, China, the following conclusions have been obtained:

(1) The groundwater from the loose layer aquifer system have pH values in the permissible range of WHO, whereas they should be treated before drinking according to their high TDS contents;

(2) The groundwater samples were classified to be Na–SO_4 and Na-Cl types, indicating that the discharge is important for the chemical variations of them.

(3) The WQIs for the groundwater from the Zhuxianzhuang coalmine in this study suggest that they are poor for drinking when considering about only their major ion concentrations.

(4) SAR and RSC values of the groundwater imply that they can be used for irrigation purpose.

(5) Gibbs diagrams and relationships between major ions, as well as factor analysis suggest that water rock interaction and discharge related evaporation are the main mechanism controlling groundwater chemistry.

ACKNOWLEDGEMENTS

This work was financially supported by National Natural Science Foundation of China (41302274) and the Foundation of Scholarship Leaders in Suzhou University (2014XJXS05).

REFERENCES

[1] Gui, H. R., Yao, E. Q., Song, X. M., Yuan, Z. H. and Zhang, G. (2011) Research on recycling technology of coalmine water. China University of Mining and Technology Press, Xuzhou.

[2] Sun, L. and Gui, H. (2013) Groundwater quality and evolution in a deep limestone aquifer, northern Anhui Province, China: evidence from hydrochemistry. Fresen. Environ. Bull., 22(4): 1126-1131.

[3] Sun, L., Gui, H. and Lin, M. (2013) Major ion chemistry of groundwater from limestone aquifer in Taoyuan coal mine, northern Anhui Province, China. Fresen. Environ. Bull., 22(2): 537-543.

[4] Gui, H. R. and Chen, L. W. (2007) Hydrogeochemistric evolution and discrimination of groundwater in mining district. Geological Publishing House, Beijing.

[5] Bao, L. J., Maruya, K. A., Snyder, S. A. and Zeng, E. Y. (2012) China's water pollution by persistent organic pollutants. Environmental Pollution, 163: 100-108.
[6] Demir, M., Goktug, T. H. and Bulut, Y. (2014) Human-induced water pollution and management. Fresen. Environ. Bull., 23(2): 478-488.
[7] Kurniawan, T. A., Sillanpää, M. E. T. and Sillanpää, M. (2012) Nanoadsorbents for remediation of aquatic environment: local and practical solutions for global water pollution problems. Critical Reviews in Environmental Science and Technology, 42(12): 1233-1295.
[8] Williams, R., Keller, V., Voss, A., Barlund, I., Malve, Olli., Riihimaki, J., Tattari, S. and Alcamo, J. (2012) Assessment of current water pollution loads in Europe: estimation of gridded loads for use in global water quality models. Hydrological Processes, 26(16): 2395-2410.
[9] Nwachcuku, N. and Gerba, C. P. (2004) Emerging water borne pathogens: can we kill them all? Current Opinion Biotechnology, 15(3):175-180.
[10] WHO. (2008) Guidelines for drinking water quality. World Health Organization, Geneva.
[11] Davis, S. N. and De Wiest, R. J. M. (1966) Hydrogeology. Wiley, New York.
[12] Toth, J. (1999) Ground-water as a geologic agent: an overview of the cause, processes and manifestations. Hydrogeology Journal, 7: 1-14.
[13] Ramakrishnaiah, C. R., Sadashivaiah, C. and Ranganna, G. (2009) Assessment of water quality index for the groundwater in Tumkur Taluk, Karnataka State, India. E-Journal of Chemistry, 6 (2): 523-530.
[14] Vasanthavigar, M., Srinivasamoorthy, K., Vijayaragavan, K., RajivGanthi, R., Chidambaram, S., Anandhan, P., Manivannan, R. and Vasudevan, S. (2010) Application of water quality for groundwater quality assessment: Thirumanimuttar Sub basin, Tamil Nadu, India. Environmental Monitering and Assessment, 171 (1-4): 595–609.
[15] Varol, S. and Davraz, A. (2015) Evaluation of the groundwater quality with WQI (Water Quality Index) and multivariate analysis: a case study of the Tefenni plain (Burdur/Turkey). Environmental Earth Sciences, 73 (4): 1725-1744.
[16] Todd, D. K. (1995) Groundwater Hydrology. Wiley and Sons Inc, New York.
[17] Michael, A. M., Kherpar, S. D. and Sondhi, S. D. (2008) Water wells and pumps. McGraw-Hill, New Delhi.
[18] Eaton, F. M. (1950) Significance of carbonate in irrigation waters. Soil Science, 67(3): 128–133.
[19] Ragunath, H. M. (1987) Groundwater. Wiley Eastern, New Delhi.
[20] Gibbs, R. J. (1970) Mechanisms controlling world water chemistry. Science, 17: 1088–1090.
[21] Wang, M., Markert, B., Chen, W., Peng, C., and Ouyang, Z. (2012) Identification of heavy metal pollutants using multivariate analysis and effects of land uses on their accumulation in urban soils in Beijing, China. Environmental Monitoring and Assessment, 184(10): 5889-5897.
[22] Huang, H. and Lu, J. (2014) Identification of river water pollution characteristics based on projection pursuit and factor analysis. Environmental Earth Sciences, 72(9): 3409-3417.

Received: **08.02.2016**
Accepted: **20.07.2016**

CORRESPONDING AUTHOR

Xianghong Liu
School of Resources and Geosciences,
China University of Mining and Technology, Jiangsu 221116, P.R.China

e-mail: liuxh2016@sina.com

© by PSP Volume 25 – No. 10/2016, pages 4393-4400 Fresenius Environmental Bulletin

PHENOTYPIC, SEROTYPIC AND GENETIC CHARACTERIZATION AND ANTIMICROBIAL SUSCEPTIBILITY DETERMINATION OF *Vibrio anguillarum*, ISOLATED FROM CULTURED SEA BASS (*Dicentrarchus labrax* L., 1758) IN THE SOUTHEAST BLACK SEA, TURKEY

Fikri Balta*

Recep Tayyip Erdoğan University, Faculty of Fisheries Science, 53100 Rize, Turkey

SUMMARY

In this study, identification of *Vibrio* isolates from infected sea bass (*Dicentrarchus labrax* L., 1758) in the Black Sea was performed by using conventional methods, and API 20E test kits. All isolates were confirmed by PCR assays specific to the 16S rRNA gene of bacterium. Lam agglutination test was carried out on all vibrio isolates by using raised rabbit serum against *Vibrio anguillarum* O1. According to the result of agglutination, biochemical and PCR tests isolated bacteria determined as *V. anguillarum*. API 20E profile for *V. anguillarum* isolates was usually determined as 3207526. The sequenced *Vibrio* isolates were found to be similar to *V. anguillarum* strain at the rate of 98-100% in GenBank under different accession numbers. In addition, in the treatment for vibriosis, it was intended to detect the most effective agents. Results of the testing susceptibility to antibiotics showed that *V. anguillarum* isolates were resistant to 100% ampicillin, 63.6% erythromycin, 59.1% sulfamethoxazole, 54.6% streptomycin, 45.5% sulfamethoxazole-trimethoprim, and 40.9% oxytetracycline, but all strains except two *V. anguillarum* were found susceptible to 9.1% other antibiotics (oxolinic acid, enrofloxacin and florfenicol). According to the results of the susceptibility test, florfenicol and enrofloxacin were suggested as the most effective chemotherapeutics for vibriosis treatment.

KEYWORDS:
Dicentrarchus labrax, *vibrio anguillarum,* slide agglutination, API 20E, PCR.

INTRODUCTION

Vibriosis causes some of the most important diseases of marine fish and it is characterized by hemorrhagic septicemia. The disease also affects farmed bivalve mollusks and crustaceans [1]. All marine fish are probably susceptible to at least one species. *Vibrio anguillarum* is the most common pathogenic *Vibrio* strain in fish. *V. anguillarum* is a Gram-negative, facultative rod-shaped bacterium [2]. The results of 5S rRNA phylogenetic data of *V. anguillarum* were reclassified as *Listonella*, *Listonella anguillarum* [3]. *V. anguillarum* (=*L. anguillarum*) is a bacterium recently classified under the family Vibrionaceae, the Proteobacteria group, and the Gamma subdivision [2]. However, the name change has not been widely accepted, consequently, the organism is still regarded as *V. anguillarum* [2]. There are a total of 23 O-serotypes of *V. anguillarum* isolates, but only serotype O1, O2, are considered to be the most virulent serotypes and serotype O3 is, to a less extent, associated with significant fish mortalities in farmed and wild fish throughout the world [2, 4]. However, it is still not clear that which of the virulent serotypes has the highest pathogenic potential for fish [5]. Many workers have been used the API 20E system for the identification of fish-pathogenic bacteria [4, 6, 7]. *V. anguillarum* can grow in water with concentrations of NaCl in the range of 0.5%-7%. The optimum concentration is about 1%. When the pathogen is exposed to the sterilized aged lake water, it loses its culture ability without losing respiratory activity [8].

In this study, identification of vibrio species from infected farmed sea bass (*Dicentrarchus labrax* L., 1758) in the Black Sea was performed using API 20E test kits. All identified strains were subsequently confirmed by PCR using the gram negative bacteria specific 16S rRNA universal primers. In addition, for the treatment of vibriosis, it was intended to detect the most effective antimicrobials.

MATERIAL AND METHODS

Fish sampling. Specimens of the sea bass (*Dicentrarchus labrax*) were collected from the 5 different fish farms where disease outbreaks prevail (a fish farm in Persembe in the Ordu Province, three fish farms in Arsin, Darıca and Yomra in the Trabzon Province, a fish farm in Ardesen in the Rize Province) in the Southeast Black Sea, Turkey, between 2004 and 2014. All data of isolates are given in Table 1.

Isolation and identification of bacteria isolates. In the study, twenty two *V. anguillarum* strains isolated from diseased fish were used for material. These strains were isolated from live sea bass showing symptoms of vibriosis sent to the laboratory from different sea farms. Samples from kidney and spleen of infected sea bass showed that typical disease symptoms were streaked with the help of a loop onto the surface of tryptic soya agar (TSA, Merck) with 1.5% sodium chloride (salt). The plates were incubated in the cooled incubator at 20±2°C for 24 and 48 hours to obtain visible bacterial growth. Colonies were purified by spreading on thiosulphate citrate bile salts sucrose agar (TCBS, Merck). Pure yellow colonies on TCBS agar was transferred to TSA supplemented with 1.5 % salt. All strains were stored in TSB added 1.5 % salt with 20% glycerol at -80ºC until used [9].

Phenotypic characterization of bacterial isolates. Cryopreserved stocks of bacteria isolates were revived and cultured in 2 ml TSB at 20°C. All isolates were grown on tryptic soya agar for conventional biochemical tests. Biochemical characterization of all strains was carried out by the following tests: Motility test, Gram staining, catalase, oxidase activity, OF test, growth test on 5% sheep blood agar and resistance to O/129 vibriostatic agent (10 and 150µg; Oxoid). Tolerance to salt was determined by the addition of salt to 1% pepton medium with percentage of 0% and 7% and cultures were examined for growth after 7 days at 25°C. All isolates were inoculated in API 20E kits by adjusting to a turbidity matching a 0.5 McFarland standard in 1.5% sterile saline water. The API 20E kits were incubated at 25°C for 96 h [7, 10, 11].

Serologic characterization. Slide agglutination test was carried out on all isolates by using raised rabbit serum against *V. anguillarum* O1 (ATTC43305) according to Toranzo et al. [12]. Pure colonies derived from the strains were inoculated on TSA added with 1.5 % salt and incubated at 25±1°C for 48 h. They were checked by a slide agglutination test using rabbit anti-*V. anguillarum* serotype O1 serum. A dense suspension of *V. anguillarum* colonies was made in 5 µl of isotonic saline to separate glass slides. Then, 10µl of O1 antiserum was added to one of the suspensions and observed for agglutination. A negative control slide was checked for the absence of auto-agglutination [12, 13, 14].

16S rRNA sequence analysis. To prepare DNA templates for PCR assays, the strains were inoculated into 2 ml TSB containing 2% salt for 18 h at 25±1°C with shaking incubator and transferred to 1 ml centrifuge tubes, and then centrifuged at 12000×g for 3 minutes (min). After decanting the supernatant, the pellet was re-suspended in 500µl of sterile deionized water. Bacterial cells were lysed by boiling for 13 min in thermo shaker incubator and centrifuged at 13000×g for 10 min after cooling for 5 min. After the debris was removed by centrifugation and supernatants were stored in a deep freezer at -20°C, a 1-µl of supernatant was used as template for all PCRs. In the PCR program a first denaturation step at 94°C for 3 min was included, followed by 34 amplification cycles consisting of 94°C for 30 seconds (s), annealing of primers at 47°C for 40 s, and 72°C for 1 min. A final extension step of 5 min at 72°C was also included in the PCR program. The PCR products were then electrophoresed on 1% agarose gel containing 0.5 µg/ml ethidium bromide and visualized with UV light [13, 15, 16]. To identify bacteria that caused vibriosis of sea bass, the universal primers (27 F 5' *AGA GTT TGA TCC TGG CTC AG*-3', 1492 R 5' *GTT TAC CTT GTT ACG ACT T*-3') specific for 16S rRNA gene of eubacteria were used [9]. These primers were then used to yield a 1465-bp 16 S rRNA gene product by PCR. These reactions were performed in a thermal cycler. The 1465-bp PCR product was purified with a NucleoSpin PCR purification kit and PCR products were sent to Macrogen for sequencing. The results of the sequence information were used for homology searches by the BLAST (http://www.ncbi.nlm.nih.gov).

Antimicrobial sensitivity. Antimicrobial susceptibility tests of the *V. anguillarum* isolates were determined by the standard disk diffusion method on Müller-Hilton agar (Merck) plates, by using the nine antibiotics. The plates were incubated at 25°C for 20 h. The following antibiotic disks (Oxoid) were used: oxytetracycline, oxolinic acid, sulfamethoxazole, ampicillin, florfenicol, streptomycin, enrofloxacin, erythromycin and sulfamethoxazole-trimethoprim. The antibiotic disks were placed on the Müller-Hilton agar by using a disc dispenser. Reference strain *Escherichia coli* ATCC 25922 was used as quality a control in the antimicrobial susceptibility tests in Table 2 [13].

RESULTS AND DISCUSSION

During the infection period, water temperature was measured between 18.5 °C and 27.8 °C from June to October peaking in August, besides pH and salinity were found as 7.74 and 17 ppt, respectively. Mortality rates varied from 20-30% in different cages. This disease caused significant economical loses in cultured sea bass in the eastern Black Sea Region. Clinical symptoms of infected fish were erratic swimming, bilateral exophthalmia and hemorrhage in eyes, swelling in the abdomen, common reddish necrotic lesion, ulcer in the body surface, and erythema at the base of the fins, around the vent, and within the mouth. Some clinical symptoms of the infected sea bass are shown ulserative skin lesions and loose scales, exophthalmos in eye, hemorrhaging and erythema at base of fins, focal hemorrhaging and petechial on skin, gills and operculum (Fig. 1).

Internal organs showed typical findings such as enlarged spleen, pale gills, liver and kidney. The gut and rectum were distended and filled with clear yellow viscous fluid. A total of 22 *V. anguillarum* were isolated from the 200 fish samples (Table 1).

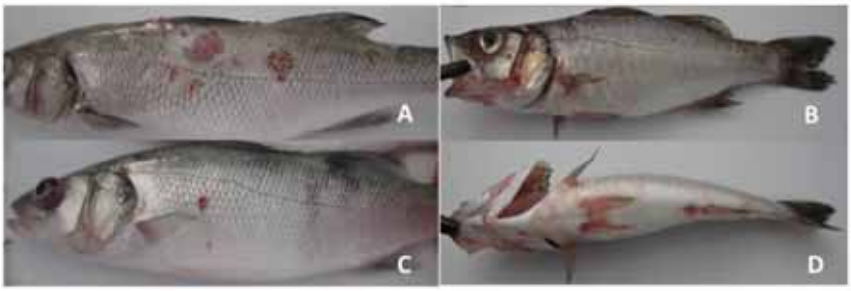

FIGURE 1
Ulserative skin lesions and loose scales (A), focal hemorrhaging and petechial on skin, gills and operculum (B), exophthalmos in eye (C), hemorrhaging and erythema at base of fins (D).

TABLE 1
Epidemiological properties of *V. anguillarum* serotype O1 strains isolated from sea bass.

İsolate no	Farmed place	Isolated organs	Isolation dates	GenBank accession no	Similarity ratio (%)
R327	Ordu / Perşembe	Kidney	20.06.2004	CP006699	98
R352	Ordu /Perşembe	Spleen	06.07.2005	KJ028214	99
R353	Trabzon / Yomra	Kidney	01.10.2006	DQ068933	99
R354	Trabzon / Yomra	Spleen	10.09.2007	DQ068933	100
R655	Trabzon/ Yomra	Kidney	28.05.2008	CP002284	100
R698	Trabzon/ Darıca	Kidney	25.07.2009	LK021130	99
R935	Rize/Ardeşen	Kidney	04.07.2010	KF150786	99
R936	Rize/Ardeşen	Spleen	25.07.2010	CP006699	99
R952	Rize/Ardeşen	Kidney	14.06.2011	LK021130	99
R953	Rize/Ardeşen	Spleen	18.08.2011	KF150786	98
R954	Rize/Ardeşen	Kidney	07.07.2012	CP006699	99
R971	Trabzon/Yomra	Kidney	03.06.2013	LK021130	99
R972	Trabzon/Arsin	Spleen	27.06.2013	LK021130	99
R973	Trabzon/Yomra	Kidney	03.06.2013	CP006699	100
R974	Trabzon/Darıca	Spleen	15.07.2013	KF150786	99
R975	Trabzon/Darıca	Kidney	09.08.2013	CP006699	99
R976	Ordu/Perşembe	Kidney	05.07.2014	LK021130	100
R977	Trabzon/Arsin	Kidney	12.07.2014	KF150786	100
R978	Ordu/Perşembe	Kidney	17.07.2014	CP006699	99
R979	Trabzon/Yomra	Kidney	20.07.2014	LK021130	99
R980	Trabzon/Yomra	Spleen	27.08.2014	KF150786	99
R981	Trabzon/Arsin	Kidney	31.08.2014	CP006699	99

TABLE 2
The comparison with the results of other researchers of the morphologic, biochemical and API 20E test results belong to *Vibrio anguillarum*.

Morphologic and Biochemical Properties	Isolates No																											
	R327	R352	R353	R354	R655	R698	R935	R936	R952	R953	R954	R971	R972	R973	R974	R975	R976	R977	R978	R979	R980	R981	Ref.-1	Ref.-2	Ref.-3	Ref.-4	Ref.-5	Ref.-6	Ref.-7
Gram stain	-	-	-	-	-	-	-	-	-	-	-	-	-	-	-	-	-	-	-	-	-	-	-	-	-	-	-	-	-
Motility by flagella	+	+	+	+	+	+	+	+	+	+	+	+	+	+	+	+	+	+	+	+	+	+	+	+	+	+	+	+	+
Catalase production	+	+	+	+	+	+	+	+	+	+	+	+	+	+	+	+	+	+	+	+	+	+	+	+	+	+	+	+	+
Oxidase production	+	+	+	+	+	+	+	+	+	+	+	+	+	+	+	+	+	+	+	+	+	+	+	+	+	+	+	+	+
Growth in % 0 NaCl	-	-	-	-	-	-	-	-	-	-	-	-	-	-	-	-	-	-	-	-	-	-	N	N	N	-	V	N	-
Growth in % 7 NaCl	+	+	+	+	+	+	+	+	+	+	+	+	+	+	+	+	+	+	+	+	+	+	N	N	N	-	V	+	-
Effect to O/129 150µg	+	+	+	+	+	+	+	+	+	+	+	+	+	+	+	+	+	+	+	+	+	+	N	N	N	+	+	+	+
Effect to O/129 10µg	+	+	+	+	+	+	+	+	+	+	+	+	+	+	+	+	+	+	+	+	+	+	N	N	N	+	+	+	+
Acid from O/F	+	+	+	+	+	+	+	+	+	+	+	+	+	+	+	+	+	+	+	+	+	+	N	N	N	+	+	+	+
Hemolysis on BA	β	β	β	β	β	β	β	β	β	β	β	β	β	β	β	β	β	β	β	β	β	β	N	N	N	N	N	N	N
ONPG	+	+	+	+	+	+	+	+	+	+	+	+	+	+	+	+	+	+	+	+	+	+	+	+	+	+	V	V	+
ADH	+	+	+	+	+	+	+	+	+	+	+	+	+	+	+	+	+	+	+	+	+	+	V	+	V	+	+	+	+
LDH	-	-	-	-	-	-	-	-	-	-	-	-	-	-	-	-	-	-	-	-	-	-	-	-	-	-	-	-	-
ODC	-	-	-	-	-	-	-	-	-	-	-	-	-	-	-	-	-	-	-	-	-	-	-	-	-	-	-	-	-
CIT	+	+	+	+	+	+	+	+	+	+	+	+	+	+	+	+	+	+	+	+	+	+	+	V	+	+	V	V	+
H_2S	-	-	-	-	-	-	-	-	-	-	-	-	-	-	-	-	-	-	-	-	-	-	-	-	-	-	-	-	-
URE	-	-	-	-	-	-	-	-	-	-	-	-	-	-	-	-	-	-	-	-	-	-	-	-	-	-	-	-	-
TDA	-	-	-	-	-	-	-	-	-	-	-	-	-	-	-	-	-	-	-	-	-	-	-	-	-	-	-	-	-
IND	+	+	+	+	+	+	+	+	+	+	+	+	+	+	+	+	+	+	+	+	+	+	V	V	V	+	V	V	-
VP	+	+	+	+	+	+	+	+	+	+	+	+	+	+	+	+	+	+	+	+	+	+	+	V	V	+	+	+	+
GEL	+	+	+	+	+	+	+	+	+	+	+	+	+	+	+	+	+	+	+	+	+	+	+	V	+	+	+	+	+
GLU	+	+	+	+	+	+	+	+	+	+	+	+	+	+	+	+	+	+	+	+	+	+	+	+	+	+	+	+	+
MAN	+	+	+	+	+	+	+	+	+	+	+	+	+	+	+	+	+	+	+	+	+	+	+	+	+	+	+	+	+
INO	+	+	+	+	+	+	+	+	+	+	+	+	+	+	+	+	+	+	+	+	+	+	-	-	-	-	V	V	+
SOR	+	+	+	+	+	+	+	+	+	+	+	+	+	+	+	+	+	+	+	+	+	+	+	-	V	+	+	+	+
RHA	-	-	-	-	-	-	-	-	-	-	-	-	-	-	-	-	-	-	-	-	-	-	-	-	-	-	-	-	-
SAC	+	+	+	+	+	+	+	+	+	+	+	+	+	+	+	+	+	+	+	+	+	+	+	V	V	+	+	+	+
MEL	-	-	-	-	-	-	-	-	-	-	-	-	-	-	-	-	-	-	-	-	-	-	-	-	-	-	-	-	-
AMY	-	-	-	-	-	-	-	-	-	-	-	-	-	-	-	-	-	-	-	-	-	-	+	+	V	+	V	V	-
ARA	+	+	+	+	+	+	+	+	+	+	+	+	+	+	+	+	+	+	+	+	+	+	V	V	V	+	V	V	+

Ref.: References, Ref.-1: Kent, (1982); Ref.-2: Maugeri et al., (1983); Ref.-3: Grisez et al., (1991); Ref.-4: Austin and Austin, 1999; Ref.-5: Tanrıkul et al., 2005; Ref.-6: Demircan and Candan, 2006; Ref.-7: Tanrıkul, 2007. +: Positive, -: Negative, V; Variable, N: not stated.

Bacterial strains were founded to be moving, gram-negative, positive of catalase and oxidase testes and fermentative of OF test. The API 20E gave positive results for β-galactosidase, arginine dihydrolase, citrate utilization, indol production, voges-proskuaer reaction and gelatin, but negative results for lysine, ornithine decarboxylase, hydrogen sulphide production, urease production and tryptophan deaminase. Carbohydrate utilization tests showed positive reactions for the acid production from sugar and the others except rhamnose, mellibiose and amygdaline. All the isolates showed results of phenotypic, biochemical and API 20E tests and they were compared with the results of other researchers' API 20E test results regarding to *V. anguillarum* isolates (Table 2).

All the tested *V. anguillarum* isolates were sensitive to the vibriostatic agent, O/129 (10µg and 150µg). All of the *V. anguillarum* isolates were growth in 1% pepton medium containing 7% sodium chloride but not growing 0% salt. All of the *V. anguillarum* isolates showed β-hemolysis onto 5% sheep blood agar plates after 24 h at 25°C. Colony characteristics on the TSA containing 2 % salt have been described as round, cream-colored, entire, raised and shiny colonies. According to the result of agglutination and biochemical tests, isolated bacteria were determined as *V. anguillarum*. API 20E profile for *V. anguillarum* isolates was usually determined as 3207526.

On a lam agglutination tests with anti *V. anguillarum* O1 serum showed that all isolates were serotype O1. All strains identified as *V. anguillarum* with biochemical and agglutination methods were subsequently confirmed by PCR using the universal primers 16S rRNA gene. According to results of the molecular diagnosis, the *Vibrio* strains isolated from sea bass were determined to be similar to *V. anguillarum* at 98-100% compared in GenBank under different accession numbers (Table 1).

In the study, antimicrobial susceptibility test breakpoints were carried out by using nine different antimicrobial agents. The method is in accordance with Clinical Laboratory Standards Institute (CLSI, 2014). The results were interpreted as described in the Clinical Laboratory Standards Institute guidelines for the family Enterobacteriaceae and Gram negative bacteria in human and veterinary medicine, including those used in aquaculture [18].

All of strains were resistant to three or more of nine antimicrobial drugs (Table 3). The highest incidence of resistance was to ampicillin (100%) followed by erythromycin (63.6%), sulfamethoxazole (59.1%), streptomycin (54.6%), sulfamethoxazole-trimethoprim (45.5%), oxytetracycline (40.9%), but all isolates were less resistant to oxolinic acid (9.1%), enrofloxacin (9.1%) and florfenicol (9.1%) (Fig. 2).

Vibriosis, due to *V. anguillarum,* is one of the most important bacterial diseases of fish throughout the world. The *Vibrionaceae* is an important and ubiquitous group of bacteria in marine and estuarine environments and these bacteria are associated with fish and other poikilothermic animals [2, 19, 20]. Among the 40 different vibrio species recorded from wild and cultured fish, nine species i.e., *Vibrio alginolyticus*, *Vibrio anguillarum*, *V. ordalii*, *V. damsela*, *V. pelagius*, *Vibrio harveyi*, *V. splendidus*, *V. salmonicida*, *V. vulnificus* were reported as pathogens infecting the marine fish [6, 21, 22]. *V. anguillarum* was isolated from different marine species by Toranzo and Barja [1].

In this study, all of the vibrio isolates were motile, oxidase and catalase positive, Gram-negative that reduced nitrate to nitrite, grew in TCBS agar medium and was sensitive to the vibriostatic agent O/129 as reported by West and Colwell, 1984 [23]. The diseased fish were noted to have petechiae at the base of the fins and on the skin. Internally, our findings are similar to those of other studies [2, 7, 24, 25]. Colony morphology on the TSA containing 2 % salt has been similarly reported by other researchers [20, 24, 26]. Tanrikul et al. (2005) reported that API 20E strips were used for the identification of *V. anguillarum* O1 which was isolated from cultured sea bass (*D. labrax* L., 1758) in Turkey [27].

TABLE 3
Antimicrobial susceptibility test breakpoints used in the study and sensitivity profile of *V. anguillarum* isolates according to antibiogram test results.

Antimicrobial agents and disc concentration	Diameter of zone of inhibition (mm)			Antimicrobial sensitivity (%)		
	R	IM	S	R	IM	S
T (30 µg)	≤ 14	15-18	≥ 19	9 (40.9%)	6 (27.3%)	7 (31.8%)
OA (2 µg)	≤ 10	11-12	≥ 13	2 (9.1%)	0	20 (90.9%)
SMZ (100 µg)	≤ 12	13-16	≥ 17	13 (59.1%)	3 (13.6%)	6 (27.3%)
AM (10 µg)	≤ 13	14-16	≥ 17	22 (100%)	0	0
FFC (30 µg)	≤ 14	15-18	≥ 19	2 (9.1%)	0	20 (90.9%)
S (10 µg)	≤ 11	12-14	≥ 15	12 (54.6%)	7 (31.8%)	3 (13.6%)
ENR (5 µg)	≤ 16	17-20	≥ 21	2 (9.1%)	0	20 (90.9%)
E (15 µg)	≤ 11	14-22	≥ 23	14 (63.6%)	6 (27.3%)	2 (9.1%)
SXT (25 µg)	≤ 10	11-15	≥ 16	10 (45.5%)	4 (18.1%)	8 (36. 4%)

AM: Ampicillin, E: Erythromycin, ENR: Enrofloxacin, FFC: Florfenicol, OA: Oxolinic acid,
T: Oxytetracycline, S: Streptomycin, SMZ: Sulfamethoxazole, STX: Sulfamethoxazole-Trimethoprim.
R: Resistance**,** IM: Intermediate, S: Sensitive.

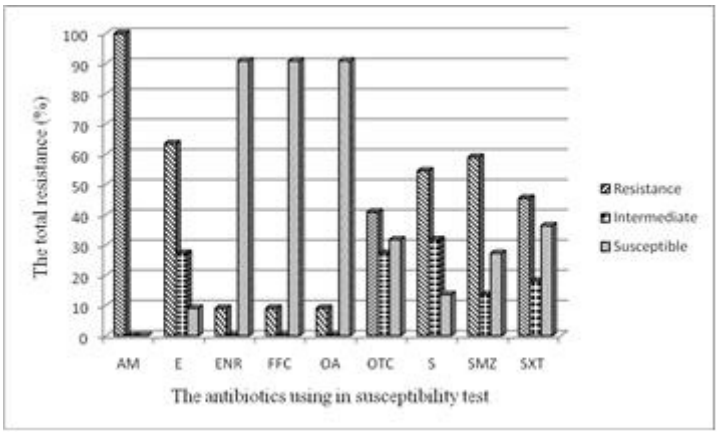

FIGURE 2
Antibiotic susceptibility profiles of *V. anguillarum* isolates.

Phenotypic characteristics of *V. anguillarum* isolates were found significantly similar in comparison with other reference study results showed in Table 2. In addition, according to the API 20E test results, the identified *V. anguillarum* isolates were found to be the similar strain as those identified in other studies [6, 17, 27, 28].

The decisive diagnosis was accomplished by PCR analysis, using universal primers specific to 16S rRNA gene of eubacteria. PCR amplified only 16S rRNA gene of isolates which was subsequently confirmed by sequencing of PCR product. Pure culture of *V. anguillarum* was isolated and confirmed by biochemical tests, lam agglutination test and sequencing of 16S rRNA gene of bacteria.

In order to cope with vibriosis, prophylactic or therapeutic antibiotics are used in fish farms. Antimicrobial compounds including oxytetracycline, sulfamethoxazole-trimethoprim, sulfamethoxazole, oxolinic acid, florfenicol and enrofloxacin have been proved to be useful in the bacterial fish diseases management [6]. However, the extensive use of antibiotics results in an increase in drug-resistance of bacteria in aquatic environments. The microbial biodiversity consisting of beneficial microbes will be affected partially by the normal micro flora of the fish. Prior to using an antibiotic, it is essential to perform susceptibility tests so as to reduce the indiscriminate use of antibiotics. Oxytetracycline and sulfamethoxazole-trimethoprim are used to control vibriosis outbreaks in the sampling marine cultured fish farms.

Although resistance frequency of oxytetracycline and sulfamethoxazole-trimethoprim are higher than oxolinic acid, enrofloxacin and florfenicol; oxytetracycline and sulfamethoxazole-trimethoprim are commonly used to treat bacterial infections of fish in the sampling region because it is cheaper than the others. This treatment protocol is really effective to control the vibriosis outbreaks according to the feedback of the fish farms in the region. Sulfamethoxazole is the most commonly used antibiotics in fish farms in Turkey. Therefore, 100% of the bacteria are resistant to sulfamethoxazole [29].

In this study, the results of susceptibility tests indicated that all the *V. anguillarum* isolates were susceptible to broad spectrum antibiotics like florfenicol, enrofloxacin, oxolinic acid, oxytetracycline by flowed sulfonamides. Several vibrio isolates have acquired resistance to the most commonly employed antibiotics (e.g., oxytetracycline and sulfamethoxazole-trimethoprim and sulfamethoxazole) in sea bass rearing. Antimicrobial test results were found similar resistances to ampicillin, streptomycin and sulfamethoxazole-trimethoprim [30]. It was reported that the resistances of bacteria against the antibiotics were gradually raised by applying oxytetracycline [17]. Consequently, random application of these antimicrobials has led to the generation of resistant strains of vibrios. Vaccination has been successfully used by intra peritoneal injection to control *V. anguillarum* infections in fish**.**

CONCLUSIONS

Consequently, random application of the antimicrobial agents has led to a generation resistant against antibiotics in *Vibrio anguillarum* strains. A judicious exploitation of antibiotics for treatment of diseases in fish farms should be followed to struggle these drugs resistance in pathogenic gram negative bacteria. In this study, infected sea bass were treated with florphenicol (30 mg Kg/day 10 days orally) and mortalities were completely controlled at the end of teatment period. It is thought to be a need on vaccine studies to protect from vibriosis (*V. anguillarum*) that cause

serious economic losses from sea bass farms in Black sea region, in the future years.

ACKNOWLEDGEMENTS

This study was funded by the Recep Tayyip Erdoğan University Research Project Fund (Project No. 2015.103.02.1)

REFERENCES

[1] Toranzo, A.E. and Barja, J.L. (1990) A review of the taxonomy and seroepizootiology of *Vibrio anguillarum*, with special reference to aquaculture in the northwest of Spain. Dis. Aquat. Org., 9, 73-82.

[2] Austin B. and Austin D.A. (1999) Vibrionaceae representatives: characteristics of the disease. In: Austin B, Austin DA (ed) Bacterial fish pathogens: diseases of farmed and wild fish. Springer Praxis Publ, London, pp. 29-30.

[3] MacDonell M.T., Swartz, D.G. Ortiz-Conde, B.A., Last, G.A. and Colwell, R.R. (1986) Ribosomal RNA phlogenies for the vibrio-enteric group of eubacteria. Microbiologycal Sciences, 3, 172-179.

[4] Pedersen, K., Grisez, L., van Houdt, R., Tiainen, T., Ollevier, F. and Larsen, J.L. (1999) Extended serotyping scheme for *V. anguillarum* with the definition and characterization of seven provisional O-serogroups. Curr Microbiology, 38, 183-189.

[5] Toranzo, A.E. and Barja, J.L. (1993) Virulence factors of bacteria pathogenic for cold water fish. Annu. Rev. Fish Dis., 3, 5-36.

[6] Austin, B. and Austin, D.A. (2007) Bacterial Fish Pathogens: Disease of Farmed and Wild Fish. 4th edn., Springer-Praxis Publishing, Chichester, UK, P. 552.

[7] Grisez, L., Ceusters, R. and Ollevier, F. (1991) The use of API 20E for the identification of *Vibrio anguilla*rum and *V. ordalii*. Journal of Fish Diseases, 14, 359-365.

[8] Eguchi, M., Fujiwara, E. and Miyamoto, N. (2000) Survival of *Vibrio anguillarum* in freshwater environments: adaptation or debilitation? Journal of Infection and Chemotherapy, 6, 126-129.

[9] Sharma, S.R. K., Rathore, G., Verma, D.K., Sadhu, N. and Philipose, K.K. 2013. *Vibrio alginolyticus* infection in Asian seabass (*Lates calcarifer*, Bloch) reared in open sea floating cages in India. Aquaculture Research, 44, 86-92.

[10] Kent, ML. (1982) Characteristics and identification of *Pasteurella* and *Vibrio* species pathogenic to fish using API 20 E (Analytab Products) multitube test strips. Canadian Journal of Fisheries and Aquatic Science, 39, 1725-1729.

[11] Maugeri, T.L., Crisafi, E., Genovese, L. and Scoglio, M.E. (1983) Identification of *Vibrio anguillarum* with the API 20 E system. Microbiologica, 1, 73-79.

[12] Toranzo, A.E., Santos, Y. and Barja, J.L. (1997) Immunization with bacterial antigens: Vibrio infections. Dev. Biol. Stand., 90, 93-105.

[13] Balta, F., Sandalli, C., Kayis, S. and Ozgumus, O.B. (2010) Molecular analysis of antimicrobial resistance in *Yersinia ruckeri* strains isolated from rainbow trout (*Oncorhynchus mykiss*) grown in commercial fish farms in Turkey. Bulletin of the European Association of Fish Pathologists, 30, 211-219.

[14] Santos, Y., Pazos, F., Bandin, I. and Toranzo A.E. (1995) Analysis of Antigens Present in the Extracellular Products and Cell Surface of *Vibrio anguillarum* Serotypes O1, O2, and O3. Applied and Environmental Microbiology, 61(7), 2493-2498.

[15] Drancourt, M., Bollet, C., Calioz, A., Martelin, R., Gayral, J. and Raoutt, D. (2000) 16s Ribosomal DNA sequence Analysis of a large collection of Environmental and clinical Un identifiable Bacterial isolates. Journal of Clinical Microbiology, 38, 3623-3630.

[16] Weisburg, W.G., Barns, S.M., Pelletier, D.A. and Lane, D.J. (1991) 16S ribosomal DNA amplification for phylogenetic study. Journal of Bacteriology, 173, 697-703.

[17] Tanrıkul, T.T. (2007) Vibriosis as an epizootic disease of rainbow trout (*Onchorhynchus mykiss*) in Turkey. Pakistan Journal Biological Sciences 10(10), 1733-1737.

[18] CLSI., (2008) Performance Standards for Antimicrobial Disk and Dilution Susceptibility Tests for Bacteria Isolated from Animals; Approved Standar-Third Edition. CLSI document M31-A3. Wayne, PA: Clinical and Laboratory Standards Institute.

[19] Anderson, I.G., Shamsudin, M.N. and Nash, G. (1989) Preliminary study on the aerobic heterotrophic bacterial flora in giant freshwater prawn *M. rosenbergii* hatcheries in Malaysia. Aquaculture, 81, 213-223.

[20] Austin B. Austin D.A. (1993) Vibrionaceae representatives. In: Bacterial Fish Pathogens, 2nd Edition (ed. Austin B, Austin DA). EIlis Horwood Ltd., Chichester, UK, pp. 265-307.

[21] Farto, R., Pérez, M.J., Fernández-Briera, A. and Nieto, T.P. (2002) Purification and partial characterisation of a fish lethal extracellular protease from *V. pelagius.* Veterinary Microbiology, 89(2-3), 181-194.

[22] Toranzo, A.E., Magarinos, B. and Romalde, J.L. (2005) A review of the main bacterial fish diseases in mariculture systems. Aquaculture, 246, 37-61.
[23] West, P.A. and Colwell, R.R. (1984) Identification and Classification of Vibrionaceae - An Overview. Ch. 20. In Vibrios in the Environment, R. Colwell (Ed.), John Wiley & Sons, New York, NY. pp. 285-363.
[24] Actis, L.A., Tolmasky, M.E. and Crosa, J.H. (1999) Vibriosis. In: Woo P.T.K., Bruno D.W., Eds. Fish Diseases and Disorders, Volume 3: Viral, Bacterial and Fungal Infections. CAB International, Oxfordshire, UK, pp. 523-557.
[25] Demircan, D. and Candan, A. (2006) Identification of *Vibrio anguillarum* by PCR (rpoN gene) associated with vibriosis in marine fish in Turkey. Turk. J. Vet. Anim. Sci., 30, 305-310.
[26] Inglis, V., Roberts R.J., and Bromage, N.R. (1993) Vibriosis. In: Bacterial Diseases of Fish. Blackwell Scientific Publications, Oxford, UK, pp. 109-121.
[27] Tanrıkul, T.T., Çağırgan, H., and Tokşen, E. (2005) Levrek'lerden (*D. labrax* L., 1758) İzole Edilen Vibrio Türlerinin API 20E Yöntemiyle İdentifikasyonu. E.U. Su Ürünleri Dergisi, 21(3-4): 243– 247.
[28] Tanrikul, T.T. and Gultepe, N. (2011) Mix Infections in Rainbow Trout (*O. mykiss,* Walbaum): *L. garvieae* and *V. anguillarum* O1. Journal of Animal and Veterinary Advances, 10(8), 1019-1023.
[29] Kayis, S., Capkin, E., Balta, F. and Altinok, I. (2009) Bacteria in rainbow trout (*Oncorhynchus mykiss*) in the southern Black Sea region of Turkey-A Survey. Israeli Journal of Aquaculture-Bamidgeh, 61, 339-344.
[30] Santos. Y., Pazos, F. and Toranzo, A.E. (1996) Biochemical and serological analysis of *Vibrio anguillarum* related organisms. Diseases of Aquatic Organisms, 26: 67-73.

Received: **09.05.2016**
Accepted: **10.08.2016**

CORRESPONDING AUTHOR

Fikri Balta
Recep Tayyip Erdoğan University
Faculty of Fisheries Science
53100 Rize - TURKEY

E-mail**:** fikri.balta@erdogan.edu.tr

© by PSP Volume – No. 10/ 2016, p. 4401-4408 Fresenius Environmental Bulletin

RESPONSES OF CO_2 AND N_2O EMISSIONS TO CARBON AND PHOSPHORUS ADDITIONS IN TWO CONTRASTING ALPINE MEADOW SOILS ON THE QINGHAI-TIBETAN PLATEAU

Dongxue Wang[1,2], Yongheng Gao[2], Ping Wang[1]*, Xiaoyang Zeng[3]

[1]College of Resources and Environment, Gansu Agricultural University, Lanzhou 730070, China
[2]Institute of Mountain Hazards and Environment, Chinese Academy of Sciences, Chengdu 610041, China
[3]Department of Landscape Architecture, Sichuan College of Architectural Technology, Deyang 610081, China

ABSTRACT

A 45-day incubation experiment in laboratory was conducted to examine the effects of the carbon (C) and phosphorus (P) additions on carbon dioxide (CO_2) and nitrous oxide (N_2O) emissions from two alpine meadow soils sampled on the Qinghai-Tibetan Plateau: one with acid pH and high organic carbon content (HM), and the other one with alkaline pH and low organic carbon content (CM). The concentrations of DOC, NO_3^--N, NH_4^+-N and DTN in soils were measured at the end of the incubation. Addition of C significantly increased soil CO_2 and N_2O emissions in both alpine meadow soils. No significant effect of P addition on CO_2 and N_2O emission was detected in both soils. Data analysis revealed a significant positive correlation between the cumulative CO_2 emissions and the soil DOC concentration, and a significant negative correlation between the cumulative N_2O emissions and soil NO_3^--N concentration. These results suggest that soil CO_2 and N_2O emission is directly linked to the availability of soil C, while P is not the limiting factor for soil microbial activity in alpine meadow soils.

KEYWORDS:
alpine meadow, greenhouse gases, glucose, phosphorus, soil DOC.

INTRODUCTION

Global warming and climate change are the rising concerns in the 21st century. It is predicted that the mean global temperature would increase 1.8 to 4.0 °C over the next 100 years [1]. Soil represents one of the major global sources of carbon dioxide (CO_2) and nitrous oxide (N_2O) [1, 2]. These two important greenhouse gases are directly linked to climate change, which may vary with nutrients supply [3, 4]. In recent decades, anthropogenic activities have increased nutrients inputs to terrestrial ecosystems, primarily due to the application of fertilizer [5]. Furthermore, global warming could promote microbial activity and decomposition of organic materials [6], causing more nutrients to be mineralized and released into the soil [7]. The increasingly released nutrients are likely to have effect on soil CO_2 and N_2O emissions. Therefore, as global warming continues, there is a strong need to understand the links between nutrients inputs and soil CO_2 and N_2O emissions.

Recent studies mostly focused on the changes of CO_2 and N_2O emissions in response to nitrogen (N) addition [8-12], very few studies have examined the ecological effects of carbon (C) and phosphorus (P) additions on terrestrial ecosystems [13, 14]. Studies on the effects of C and P additions on CO_2 and N_2O emissions were mostly limited to forest soils [15-17], agricultural soils [18, 19] and plantation soils [20]. These studies show that C addition generally stimulates CO_2 and N_2O emissions [19]. There are uncertain conclusions about the effect of P addition on the CO_2 and N_2O emissions. For example, Amador and Jones [21] reported the positive effect of P addition on CO_2 emission from peat soils. In contrast, Aerts and Toet [22] found that P addition exerted no effect on CO_2 emission from peatland soils. So far, the effect of simultaneous C and P additions still remains poorly understood and has not been assessed in the alpine meadow of the Qinghai-Tibetan Plateau.

The Qinghai-Tibet Plateau is located in the central part of the troposphere in the mid-latitude

westerlies. It is regarded as Earth's third pole and the highest unique territorial unit in the world. Thus, its ecosystems and natural environment are inherently fragile and instable, making them especially vulnerable to global warming [23-25]. Moreover, the high altitude ecosystems store the greatest fraction of carbon in soils [1]. A slight change in these large C pools may have a substantial influence on global C cycling. Therefore, as the trend of global warming remains irreversible, increased soil-nutrient availability may cause changes in this ecosystem and affect greenhouse gas exchange. However, relatively little attention has been paid to the question of how increased nutrient availability affect the emissions of both CO_2 and N_2O from alpine meadow soils on the Qinghai-Tibetan Plateau. The objective of this study is to experimentally examine the effects of C and P additions on the emissions of CO_2 and N_2O from two contrasting alpine meadow soils on the Qinghai-Tibetan Plateau, China.

MATERIALS AND METHODS

Site description and soil samplings. The two study sites were located at Hongyuan County (33°03′N, 102°36′E, site HM) and the Fenghuoshan region (34°43′N, 92°53′E, site CM), Qinghai-Tibet Plateau, China, separately (Fig. 1). The first site in Hongyuan County is 3462m above sea level, with a continental harsh climate. The mean annual temperature is 1.1 °C and the mean annual precipitation is 752 mm, with about 86% received from May through September. The second site in the Fenghuoshan region has an altitude of around 4600 - 4800 m. The climate is cold and dry. The mean annual temperature is -5.3 °C and the mean annual precipitation is 269.7 mm, with about 80% received from May through September. Detailed descriptions of these two sites were given by Li et al. [23] and Gao et al. [24].

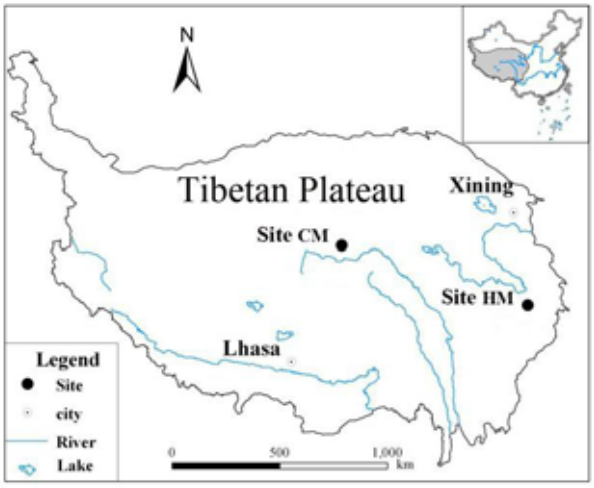

FIGURE 1
Location of the study sites.

Soil samples were collected from four random sampling plots at each stand in early August 2012. Within each plot, the plants were cut and removed using scissors, and then one composite sample of a depth of 15 cm was taken by an auger (7 cm diameter). Roots and other impurities were removed from the soil samples by hand. Then the samples were air-dried, grounded to pass through a 2-mm sieve, and stored at 4 °C before use. Selected physical and chemical properties of the two soil samples are presented in Table 1.

Soil incubation. Incubation experiments were conducted in the laboratory as described by Lang et al. [26]. For each soil sample, a total of 12 conical flasks of 250 mL volume were prepared; 30 g of oven-dried soil was placed in each. Deionized water was added evenly over the soil surface with a pipette to bring the moisture content to 40% water-holding capacity (WHC). The flasks were pre-incubated at 10 °C in the dark for 7 days. After the pre-incubation, carbon (glucose) and phosphorus (NaH_2PO_4) solutions were applied to the pre-incubated soils. The abbreviations of

TABLE 1
Selected physicochemical properties of the two alpine meadow soils.

Study sites	pH (2.5:1)	Organic C (g. kg^{-1})	Total N (g. kg^{-1})	Total P (g. kg^{-1})	C/N	Sand (%)	Silt (%)	Clay (%)
HM	5.97±0.05	49.93±1.37	4.92±0.08	1.18±0.05	10.14±0.24	53.35±0.54	28.73±0.79	17.92±0.34
CM	8.76±0.06	16.62±0.27	1.38±0.06	0.44±0.03	12.04±0.29	70.39±1.34	18.75±1.27	10.86±0.26

C, carbon; N, nitrogen; P, phosphorus.values are means±standard errors (n = 3).

each treatment and the amounts of added compounds were: CK, untreated soil; C, glucose added at 2000 mg C kg soil^{-1}; P, NaH_2PO_4 added at 40 mg P kg soil^{-1}; CP, combined addition of C and P (glucose added at 2000 mg C kg soil^{-1} and NaH_2PO_4 added at 40 mg P kg soil^{-1}). Then the final soil moisture content was adjusted to 60% WHC. At last all the flasks were incubated at 10 °C in the dark for 45 days. The moisture content of incubated soil was maintained by the addition of deionized water every 2 or 3 days to compensate for water loss through evaporation.

Gas and Soil sampling and analysis. After 7 days soil pre-incubation, the headspace air in each flask was sampled at day 1, 3, 6, 10, 15, 20, 25, 30, 35, 40 and 45 of the incubation. Prior to sampling, each flask was sealed air tight and allowed to accumulate gas for 2 h. The headspace gas was drawn at 0 and 2 h after sealing using a 10 mL syringe equipped with a three-way stopcock that was connected to the septum in the middle of the lid [27]. Gas samples were analyzed using a gas chromatograph (Agilent 7890A, USA) equipped with two detectors for CO_2 and N_2O, respectively. The analysis followed the method described by Wang et al. [28].

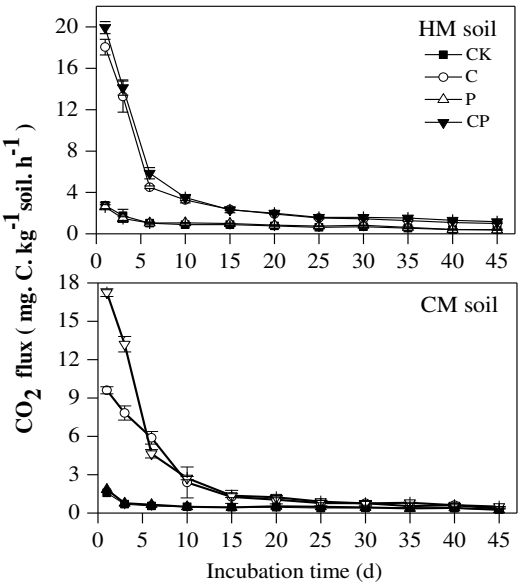

FIGURE *2*

Soil CO_2 flux over the 45 days of incubation in the HM soil and CM soil. The presented values are the means and vertical bars indicate the standard errors (n=3).

The soil samples were collected at the end of 45 days incubation. Soil DOC, NO_3^--N and NH_4^+-N concentrations were analyzed using a continuous flow autoanalyzer (AutoAnalyzer III, Bran + Luebbe GmbH, Germany). Total N concentration was determined with the continuous flow autoanalyzer after the samples were digested with a mixture of $K_2S_2O_8$ and NaOH as catalyst.

Statistical analyses. All data were reported as the means and standard errors of the three replicates. One-way ANOVA and Duncan's multiple range test (DMRT) with a significance level of 0.05 were applied to determine the differences between nutrient addition treatments in terms of selected soil properties on a given day of incubation. Relationships between cumulative CO_2 and N_2O emissions and soil properties were examined using Pearson's correlation.

RESULTS

CO_2 emission. For the HM soil, the addition of glucose resulted in a large increase in the CO_2 flux during the first day of the incubation (Fig. 2). For the C treatment, the highest CO_2 flux was observed at Day 1, and then sharply decreased over the following 15 days to approximately constant values. Similar trend was also observed in the CP treatment. For the entire experimental period, the cumulative CO_2 emission increased over time (Fig. 3). At the end of the 45-day incubation, the cumulative emissions of CO_2 were 1.05, 4.88, 1.08, 5.39 g.kg^{-1} for CK, C, P and CP treatment, respectively. The C and CP treatments significantly increased the cumulative emission of CO_2 than the CK treatment, but P treatment did not significantly increase cumulative CO_2 emission. In general, soil CO_2 emission was higher in HM soil than that in CM soil regardless of nutrient addition.

N_2O emission. The largest fluxes of N_2O occurred at Day 1 after glucose addition in the HM and CM soils, respectively (Fig. 4). Afterwards, N_2O flux decreased rapidly over the following 3 days to approximately constant values in the HM soil. For the CM soil, secondary peaks appeared at Day 20. Similar trend was also observed in the CP treatment. But the P treatment did not increase the N_2O flux in the both soils. There was a significant difference between the C treatment and the CP

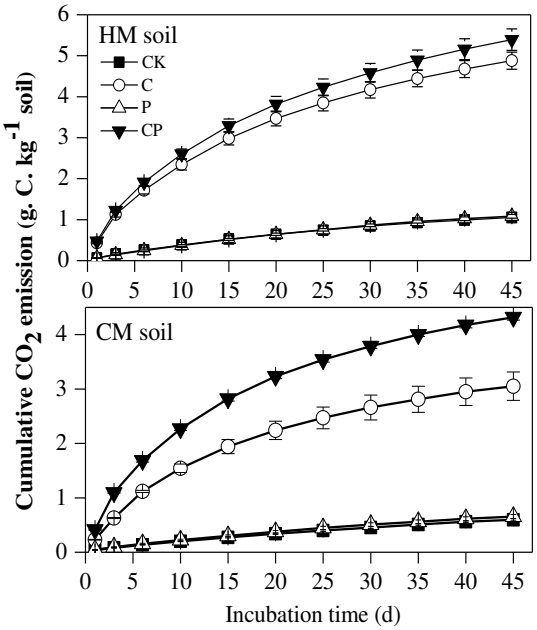

FIGURE 3

The cumulative CO_2 emission over the 45 days of incubation in the HM soil and CM soil. The presented values are the means and vertical bars indicate the standard errors (n=3).

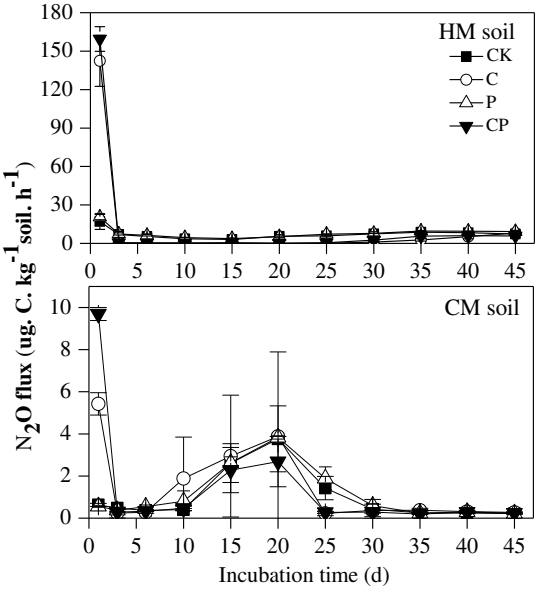

FIGURE 4

Soil N_2O flux over the 45 days of incubation in the HM soil and CM soil. The presented values are the means and vertical bars indicate the standard errors (n=3).

treatment in the CM soil.

As for N_2O emissions, the C and CP treatments were significantly higher than the CK treatment at the end of the 45-day incubation in the both soils (Fig. 5). However the P treatment did not significantly increase cumulative N_2O emission. Generally, the cumulative N_2O emission was higher in the HM soil than in the CM soil under the same treatment.

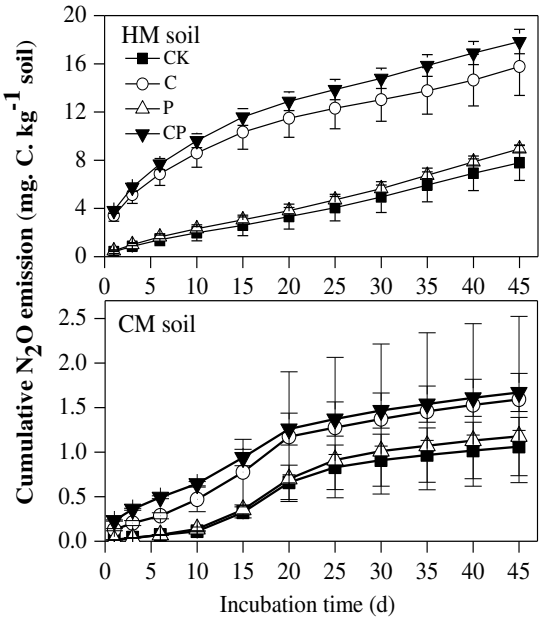

FIGURE 5

The cumulative N_2O emission over the 45 days of incubation in the HM soil and CM soil. The presented values are the means and vertical bars indicate the standard errors (n=3).

Soil properties. For the HM soil, the C treatment and CP treatment significantly ($P<0.05$) increased soil DOC concentration, while the P treatment did not have significant impact on soil DOC concentration (Fig. 6). Similar phenomenon was also observed in the CM soil (Fig. 6).

TABLE 2
Relationship between cumulative CO_2, N_2O emission and measured soil properties of two soils at the end of 45-day incubation.

Study sites		DOC	NO_3^--N	NH_4^+-N	DON	DTN
HM	CO_2	0.921**	-0.968**	-0.802**	-0.849**	-0.953**
	N_2O	0.867**	-0.884**	-0.706*	-0.757**	-0.873**
CM	CO_2	0.972**	-0.973**	0.316ns	-0.894**	-0.974**
	N_2O	0.356ns	-0.145ns	-0.305ns	-0.288ns	-0.179ns

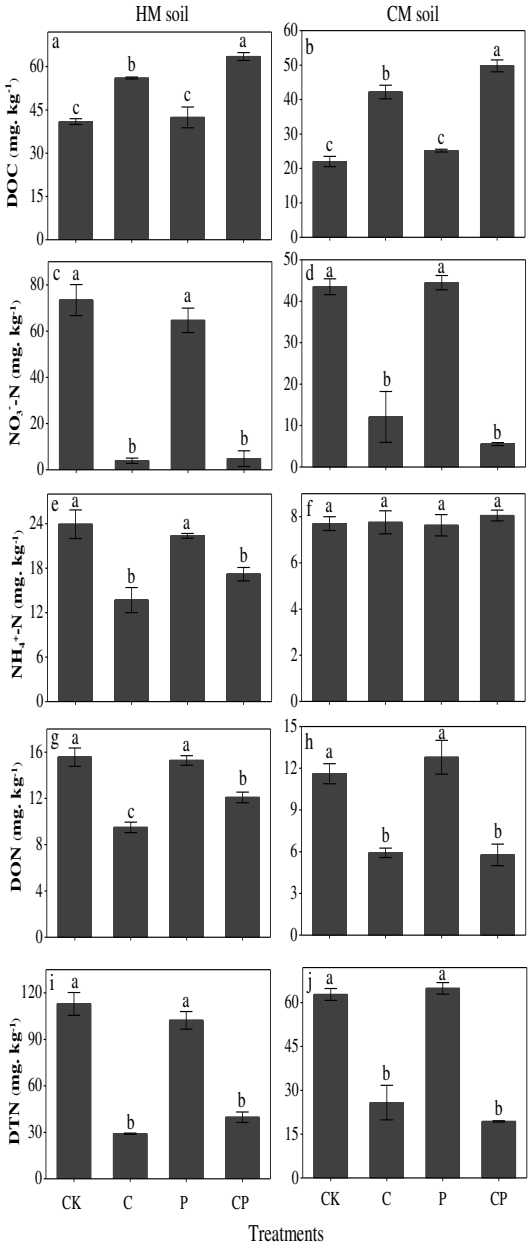

FIGURE 6
Effect of different treatments on soil chemical properties in the HM soil and CM soil at the end of 45-day incubation. The presented values are the means and vertical bars indicate the standard errors (n=3). Different lowercase letters are significantly different at P < 0.05 using Duncan's multiple range test.

The C treatment and the CP treatment markedly ($P<0.05$) affected soil NO_3^--N, NH_4^+-N, DON and DTN concentrations, while no significant effect of the P treatment on soil NO_3^--N, NH_4^+-N, DON or DTN concentrations was detected (Fig. 6). For the CM soil, the effect of the each treatment on soil NO_3^--N, DON and DTN concentrations were similar to what was observed in the HM soil, except that the effects of the C treatment and the CP treatment on NH_4^+-N concentration were not statistically significant (Fig. 6).

Relationship between gas emission and soil variables. The cumulative CO_2 emission showed significant positive correlation with soil DOC concentration, but negatively correlated with NO_3^--N, DON and DTN concentrations in both soils (Table 2). The cumulative N_2O emission had a significant negative correlation with NO_3^--N, DON and DTN concentrations in the HM soil (Table 2).

DISCUSSION

Treatments effect on the CO_2 and N_2O emissions. Our results showed that glucose addition initially had a positive effect on the CO_2 flux (Fig. 2), which is similar to the findings of previous studies [10, 20]. The P treatment did not increase CO_2 flux, while the CP treatment significantly increased CO_2 flux during the investigation period. This result is in line with previous studies [20]. The cumulative CO_2 emission was higher in the HM soil than in the CM soil across all treatments (Fig. 3), which might be due to the differences in soil chemical and physical properties, especially organic carbon content and soil pH (Table 1). In addition, for the P addition, conflicting effects on CO_2 emission were reported before. Cleveland et al. [15] found a positive effect of P addition on CO_2 emission in forest soils, while decreased soil CO_2 emission after P addition was reported in other soils

[29, 30]. Besides, no effect of P addition on CO_2 emission was observed in peatlands [22]. These studies suggest that our understanding of the effects of P addition on CO_2 emission is still incomplete.

For N_2O fluxes, the maximum peaks appeared on Day 1 in both soils (Fig. 4), which is similar with what were observed in other studies [31]. The cumulative N_2O emission in the C treatment was significantly higher than the control for both soils (Fig. 5). This phenomenon could be the result of elevated denitrificaiton activities stimulated by the addition of organic C as energy source [32], given that denitrification is the dominant process responsible for N_2O emission from the soil, especially in soils with water contents of 60% water-filled pore space (WFPS) or higher [33-35]. This finding is also in agreement with previous studies [36]. Meanwhile, the cumulative N_2O emission was significantly increased in the CP treatment after 45 days incubation (Fig. 5). This may be also due to the variability in effects of organic C on denitrificaiton activities [32]. Nevertheless, the cumulative N_2O emission was not significantly increased in the P treatment for both soils (Fig. 3c and d), indicating that P may not the limiting factor for N_2O emission in alpine meadow soils. Furthermore, the cumulative N_2O emission was higher in the HM soil than in the CM soil across all treatments (Fig. 5), suggesting that soil chemical and physical properties, such as organic carbon content and pH may be related to N_2O emission variation (Table 1).

Treatments effect on soil properties. Our results showed that the C treatment and the CP treatment resulted in an increase of soil DOC concentration after 45-day incubation in both soils (Fig. 6). Meanwhile, a positive relationship between emissions of CO_2 and soil DOC concentration was found in both soils (Table 2), suggesting that soil DOC concentration might be an important source for the emission of CO_2 from alpine meadow soils [30]. Similar results were also observed in a former study [26]. On the other hand, P addition did not significantly affect soil DOC concentration or total N content (Fig. 4), which confirms what was observed in semi-arid, sandy grassland [37]. At the end of incubation, soil NO_3^--N concentrations in the C treatment and CP treatment were significantly lower, while cumulative CO_2 and N_2O emissions were significantly higher than those in the CK treatment. Similar results were found by Wang et al. [19]. A possible explanation is that glucose addition promoted the denitrification activities, which consumed more organic C to fulfill higher energy demand [38].

CONCLUSIONS

This study demonstrated that the addition of C to the two alpine meadow soils can significantly increase the emissions of CO_2 and N_2O. Moreover, the C treatment also increased soil DOC concentration. Conversely, these treatments resulted in lower soil NO_3^--N concentration compared with the CK treatment. However, no significant effect of the P treatment on CO_2 and N_2O emissions, soil DOC concentration or soil NO_3^--N concentration was detected, indicating that P is not the limiting factor for soil microbial activity in alpine meadow soils.

ACKNOWLEDGEMENTS

This research was supported by the National Basic Research Program (973) of China (2012CB417101), and the National Science Foundation (40801089). The authors gratefully acknowledge the assistance of Zhang C.B. and Liu G. during the field work.

REFERENCES

[1] Intergovernmental Panel on Climate Change, 2007. Chapter 8: agriculture. In: Metz, B., Davidson, O., Bosch, P., Dave, R., Meyer, L. (Eds.), Climate change 2007. Contribution of working group III to the fourth assessment report of the Intergovernmental Panel on climate change. Cambridge University Press, Cambridge and New York, pp. 498-540.

[2] Akbolat D., Şenyiğit U., 2012. Short-term effect of different irrigation water levels on soil carbon dioxide (CO_2) emission. Fresen. Environ. Bull. 21, 3869-3873.

[3] Luo, Y.Q., Zhou, X.H. (2006). Soil respiration and the environment. Academic Elsevier, San Diego, USA. 239 pp.

[4] Raich, J.W., Schlesinger, W.H. (1992). The global carbon dioxide flux in soil respiration and its relationship to vegetation and climate. Tellus B 44, 81-99.

[5] Cleveland, C.C., Townsend, A.R., Schmidt, S.K. (2002). Phosphorus limitation of microbial processes in moist tropical forests: evidence from short-term laboratory incubation and field studies. Ecosystems 5, 680-691.

[6] Nadelhoffer, K.L., Shaver, G.R., Giblin, A .E., Rastetter, E.B. (1997). Potential impact of climate change on nutrient cycling, decomposition, and productivity in arctic ecosystems. In: Oechel, W.C., Callaghan, T., Gilmanov, T., Holten, J.I., Maxwell, B., Molau, U., Sveinbjörnsson, B. (Eds.), Global Change and Arctic Terrestrial Ecosystems. Springer-Verlag, New York, pp. 349-364.

[7] Schmidt, I.K., Jonasson, S., Michelsen, A. (1999). Mineralization and microbial immobilization of N and P in arctic soils in relation to season, temperature and nutrient amendment. Applied Soil Ecology 11, 147-160.

[8] Li, Y.C., Song, C.C., Hou, C.C., Sun, X.X., Wang, X.W. (2012). Effect of nitrogen availability on residue decomposition and N_2O emission in wetland ecosystems of northeast china. Fresen. Environ. Bull. 21, 1127-1132.

[9] Matson, P., Lohse, K.A., Hall, S.J. (2002). The globalization of nitrogen deposition consequences for terrestrial ecosystems. Ambio 31, 113-119.

[10] Song, M.H., Jiang, J., Xu, X.L., Shi, P.L. (2011). Correlation between CO_2 efflux and net nitrogen mineralization and its response to external C or N supply in an alpine meadow soil. Pedosphere 21, 666–675.

[11] Gao, Y.H., Chen, H., Zeng, X.H. (2014). Effects of nitrogen and sulfur deposition on CH_4 and N_2O fluxes in high-altitude peatland soil under different water tables in the Tibetan Plateau. Soil Science and Plant Nutrition, 60, 404–410.

[12] Gao, Y.H., Ma, G., Zeng, X.Y., Xu, S.Q., Wang, D.X. (2015). Responses of microbial respiration to nitrogen addition in two alpine soils in the Qinghai-Tibetan Plateau. Journal of Environmental Biology 35, 261-265.

[13] Bennett, L.T., Adams, M.A. (2001). Response of a perennial grassland to nitrogen and phosphorus additions in sub-tropical, semi-arid Australia. Journal of Arid Environment 48, 289-308.

[14] Gao, Y.H., Chen, H., Schumann, M., Wu, Y.Y., Zeng, X.Y. (2015) Short-term responses of nitrous oxide fluxes to nitrogen and phosphorus addition in a peatland on the Tibetan Plateau. Environmental Engineering and Management Journal 14, 121-127.

[15] Cleveland, C.C., Townsend, A.R., Schmidt, S.K. (2002). Phosphorus limitation of microbial processes in moist tropical forests: evidence from short-term laboratory incubation and field studies. Ecosystems 5, 680-691.

[16] Groffman, P.M. (1999). Carbon additions increase nitrogen availability in northern hardwood forest soils. Biology and Fertility of Soils 29, 430-433.

[17] Ouyang, X.J., Zhou, G.Y., Huang, Z.L., Zhou, C.Y., Li, J., Shi, J.H., Zhang, D.Q. (2008). Effect of N and P addition on soil organic C potential mineralization in forest soils in South China. Journal of Environmental Sciences 20, 1082–1089.

[18] Martın, L.S., Vallejo, A., Dick, J., Skiba, U.M. (2008). The influence of soluble carbon and fertilizer nitrogen on nitric oxide and nitrous oxide emissions from two contrasting agricultural soils. Soil Biology & Biochemistry 40, 142-151.

[19] Wang, L.F., Cai, Z.C., Yang, L.F., Meng, L. (2005). Effects of disturbance and glucose addition on nitrous oxide and carbon dioxide emissions from a paddy soil. Soil & Tillage Research 82, 185-194.

[20] Mori, T.K., Ohta, S.C., Ishizuka, S.H., Konda, R., Wicaksono, A., Heriyanto, J., Hardjono, A. (2010). Effects of phosphorus addition on N_2O and NO emissions from soils of an Acacia mangium plantation. Soil Science and Plant Nutrition 56, 782-788.

[21] Amador, J. A., Jones, R.D. (1993). Nutrient limitations on microbial respiration in peat soils with different phosphorus content. Soil Biology & Biochemistry 25, 793-801.

[22] Aerts, R., Toet, S. (1997). Nutritional controls on carbon dioxide and methane from carex-dominated peat soils. Soil Biology & Biochemistry 29, 1683-1690.

[23] Li, N., Wang, G.X., Yang, Y., Gao, Y.H., Liu, G.S. (2011). Plant production, and carbon and nitrogen source pools, are strongly intensified by experimental warming in alpine ecosystems in the Qinghai-Tibet Plateau. Soil Biology & Biochemistry 43, 942-953.

[24] Gao, Y.H., Luo, P., Wu, N., Chen, H., Wang, G.X. (2008). Impacts of grazing intensity on nitrogen pools and nitrogen cycle in an alpine meadow on the eastern Tibetan Plateau.

Applied Ecology and Environmental Research 6, 67-77.

[25] Gao, Y.H., Zeng, X.Y., Xie, Q.Y., Ma, X.X. (2015). Release of carbon and nitrogen from alpine soils during thawing periods in the eastern Qinghai-Tibet Plateau. Water, Air, and Soil Pollution 226, 209.

[26] Lang, M., Cai, Z.C., Chan, S.X. (2010). Effects of land use type and incubation temperature on greenhouse gas emissions from Chinese and Canadian soils. Journal of Soils and Sediments 11, 15-24.

[27] Min, K., Kang, H., Lee, D. (2011). Effects of ammonium and nitrate additions on carbon mineralization in wetland soils. Soil Biology & Biochemistry 43, 2461- 2469.

[28] Wang, J.Y., Pan, X.J., Liu, Y.L., Zhang, X.L., Xiong, Z.Q. (2012). Effects of biochar amendment in two soils on greenhouse gas emissions and crop production. Plant and Soil 360, 287- 298.

[29] Illeris, L., Michelsen, A., Jonasson, S. (2003). Soil plus root respiration and microbial biomass following water, nitrogen, and phosphorus application at a high arctic semi desert. Biogeochemistry 65, 15-29.

[30] Song, C.C., Liu, D.Y., Song, Y.Y., Yang, G.S., Wan, Z.M., Li, Y.C., Xu, X.F. (2011). Effect of exogenous phosphorus addition on soil respiration in Calamagrostis Angustifolia freshwater marshes of Northeast China. Atmospheric Environment 45, 1402-1406.

[31] Martın, L.S., Vallejo, A., Dick, J., Skiba, U.M. (2008). The influence of soluble carbon and fertilizer nitrogen on nitric oxide and nitrous oxide emissions from two contrasting agricultural soils. Soil Biology & Biochemistry 40, 142-151.

[32] Nobre, A.D., Keller, M., Crill, P.M., Harriss, R.C. (2001). Short-term nitrous oxide profile dynamics and emissions response to water, nitrogen and carbon additions in two tropical soils. Biology and Fertilizer of Soils 34, 363-373.

[33] Aulakh, M.S., Rennie, D.A., Paul, E.A. (1984). Gaseous nitrogen losses from soil under zero tillage as compared with conventional tilled system. Journal of Environmental Quality 13, 130-136.

[34] Mathieu, O., Henault, C., Levesque, J., Baujard, E., Milloux, M.J., Andreux, F. (2006). Quantifying the contribution of nitrification and denitrification to the nitrous oxide flux using 15N tracers. Environmental Pollution 144, 933-940.

[35] Wolf, I., Russow, R. (2000). Different pathways of formation of N_2O, N_2 and NO in black earth soil. Soil Biology & Biochemistry 32, 229-239.

[36] Jahangir, M.M.R., Khalil, M.I., Johnston, P., Cardenas, L.M., Hatch, D.J., Butler, M., Barrette, M., flaherty, V. O., Richards, K.G. (2011). Denitrification potential in subsoils: A mechanism to reduce nitrate leaching to groundwater. Agriculture, Ecosystems and Environment 147, 13-23.

[37] Li, L.J., Zeng, D.H., Fan, Z.P., Mao, R. (2010). Soil microbial properties under N and P additions in a semi-arid, sandy grassland. Biology and Fertilizer of Soils 46, 653-658.

[38] Wrage, N., Velthof, G.L., Beusichem, M.L., Oenema, O. (2001). Role of nitrifier denitrification in the production of nitrous oxide. Soil Biology & Biochemistry 33, 1723-1732.

Received: **20.07.2015**
Accepted: **03.04.2016**

CORRESPONDING AUTHOR

Ping Wang,
College of Resources and Environment, Gansu Agricultural University, Lanzhou 730070, China

Email: ecologist@126.com

© by PSP Volume 25 – No. 10/2016, pages 4409-4438 Fresenius Environmental Bulletin

RADON IN THE INDOOR ENVIRONMENT

-A REVIEW-

Sabah Ahmed Abdul-Wahab[1,2,*], Emmanuel Ikhile[2], Lena Ahmadi[2], Ali Elkamel[2], Kaan Yetilmezsoy[3]

[1]Department of Mechanical and Industrial Engineering, College of Engineering, Sultan Qaboos University, P.O. Box 33, Al-Khod, Postal Code 123, Muscat, Sultanate of Oman
[2]Department of Chemical Engineering, University of Waterloo, Waterloo, Ontario, Canada
[3]Department of Environmental Engineering, Faculty of Civil Engineering, Yildiz Technical University, 34220, Davutpasa, Esenler, Istanbul, Turkey

ABSTRACT

Radon being radioactive gas has adverse impacts on human health. In recent decades, radon gas has been listed as a human carcinogen sincethe massive effect of radon gas associated with lung cancer is widely recognized.Moreover, the health effects of indoor air pollution, with radon being one of the major contributors is aseriousconcern. The radon gas exposure limits are mainly obtained by various epidemiological and toxicological studies. Accordingly, different surveys conducted in particular parts of the world. Considering the harmful effects of radon gas on human life, quantitative researches are carried onto emphasize the importance of monitoring indoor radon gas levels. One of the main goal is to accommodate more accurate estimation for protection from the risks of long-term exposures to radon gas in the indoor environment. In this paper, the recent status of radon gas and its contributions to indoor air pollution aresummarized. Results of the comprehensive review demonstrate that, however treat of radon gas exposure as an air pollutant is being raised overtime, the knowledge and awareness of the impacts of these exposures in different situations still need more investigations. In case of encountering radon gas problems, specialists should be consulted toutilize appropriate radon testing and mitigation techniques. Studies are still being conducted to clarify certain discrepancies with the aim of providing consistent results and informationon the impacts of radon gas on environment and human health.

KEYWORDS:
Radon gas exposures; Indoor pollution; Health effects; Air pollutant; Testing

INTRODUCTION

History. Acknowledgement of a specific scientist for the discovery of radon is not straightforward because of several complications. Who essentially discover the radon gas, or publish the finished work, and what was involved in the discovery are not clear. Other issues that may arise are improper documentation of events or lack of evidence for assigning credibility [1].

Although, a number of publications propose Ernest Rutherford, a professor at McGill University, Canada, is the original founder of radon gas by discovering an isotope of radon (^{220}Rn) having a half-life of 55.6 s; [2] a report to International Union of Pure and Applied Chemistry (IUPAC) is stated radon was originally first discovered in 1900 by a chemist from Germany named Frederick Ernst Dorn. The handbook of chemistry and physics supports the both former and latter scientists as the discoverers of radon gas.

Before 1900, other scientists who were also involved in the discovery of radon were M. and Mme. Curie [1,3]. In 1899, they observed when air came in contact with radium compounds, it turns radioactive. The Curries attempt to hold credit for the discovery of radon.

Radon is an inert radioactive gas that is tasteless, colorless and odorless [4]. It was essentially explored because of the radioactive disintegration/decay of two of the oldest most naturally occurring radioactive elements, uranium and thorium. Other radon isotopes were also identifiedthrough fusion evaporation, light particle reactions, projectile fission or fragmentation and spallation [5].

Radon has a variety of isotopes, 39 in number with mass numbers ranging from 193-231. It was reported that about 48 more isotopes could be in existence but haven't been found yet. Among all possible isotopes, the most stable is^{222}Rn, which was detected to be a member of the uranium series, due to the radioactive disintegration of uranium, in 1900 by Dorn [5]. The ^{222}Rn is a distinguished gas having a half-life of approximately 3.8 days [6]. All the above mentioned discoveries accomplished within the late 1800s and in the most part of the

19th century.

Radon became officially accepted as a new element in the year 1912 by the International commission of Atomic Weights. The IUPAC as well as the International Committee for Chemical Elements officially ratified the name "radon" short form "Rn" for the most stable isotope ^{222}Rn.

Radon and Indoor Pollution. Radon gas has adverse effects on human health because of being radioactive. The harmful effects of radon on human life has concerned people since long time ago. In 1950's, radon gas and its progeny were first established as the major role players in the cause of lung cancer of underground uranium miners. Another interesting historical health effect of radon occurred in the 16th century.Lunge cancer affected the miners in Saxony and Bohemia, because of high radon levels in the mines. The early occurrence has persuaded researchers to investigate the public health effects of radon and its exposures in indoor environment as a priority in recent decades [7].

Consequently the massive effect of radon gas on lung cancer is widely recognized. In 1988, radon gas was listed as a human carcinogen by the International Agency for Research on Cancer. Twenty-one years later in 2009, the World Health organization (WHO) established radon as the second leading cause of lung cancer. In recent times, the impactof radon gas on public health is considered more seriouse issue than 1950's. With to the aim of reducing risk of radon gas penetration on the public health, the indoor air quality is now being effectively controlled by laws passed by various governments all around the world. The laws have a multidisciplinary approach and involve public health professionals, occupational medicine practitioners and local building engineers [7,8].

An estimate of 21,000 deaths is recorded annually in the US residents from lung cancer caused by radon gas exposures Radon gas is more probable to be a cause of lung cancer in smokers compared to non-smokers [9]. In addition, data analysis of thirteen case studies around Europe exhibited a strong proof of the connection between residential radon exposures and lung cancer. Many studies confirm radon gas in homes currently account for nine percent of deaths and two percent of all cancer deaths in the whole of Europe [10].

Remarkable developments has been revealed onthe effects of radon gas on human body organs. Starting from the 1990s, studies propose radon inhalation can deliver slight amount ofirradiation to the bone marrow and increasing risks of leukemia and lymphoma. In addition, radon-infested drinking water might have a negative effect on stomach and cause stomach cancer.Human stomach is the critical organ for ingested radon by having ten times more dosage than other organs [10].

Health Canada estimates sixteen percent of lung cancer deaths result from radon gas exposures. It also reiterates the increased risk of lung cancer to smokers who are subjected to elevated radon exposures. One in three smokers and one in twenty non-smokers subjected to high radon exposures arelikely to be infected by lung. Risks of developing lung cancer as a result of radon gas exposures also depends on the period of exposure and radon concentration in ambient air [11].

Radon gas level in ambient air are usually higher during the fall and winter seasons when there is less air circulation and ventilation [12]. This leads to a dramatic increase in radon gas amount during these seasons. Radon testing can be used to determine the radon gas level in residential buildings. Radon gas levels vary over time, therfore, it is recommended that radon testing be carried out over a long period of time (about three-six months) during the fall/winter seasons.Thisstatesa more reliablerepresentative and accurate result of radon exposures than short period testing [12]. The test should be performed in the lowest levels being occupied in a presented residential dwelling [13]. A household could have the testing kit sent to them to perform the testing themselves or by calling radon-testing professionals.Even in recent times, a number of people are still unaware of the potential dangers of radon exposures.. Many housedolds do not consider testing their homes for radon levels due to an optimistic bias, as they do not believe their homes have a problem [14]. Therefore, it is essential toconductcontinuous awareness programs to educate people on the dangers of radon exposures. Case studies are also anexcellentmethodto assess the health effects of radon exposures, however it is complicated to yield consistent results from case studies.

The negative children health effects of indoor air pollution, with radon being one of the major contributors is also agreat concern. Most kids from birth about the age of eightareplaying indoors most of the time. On average, children spend approximately fifteenhours while infants spend about 20 hours indoors at home aday. Hence, children are more vulnerable to air pollution in the indoor environment than adults. The emission levels of air pollutants in the indoor environment are higher at levels closer to the ground, which is where most infants and kids are often found. Moreover, children have higher respiratory rates, meaning they consume more oxygen, thatcontributes to a higher risk of intake of air pollutantssuch as radon. Their respiratory systems are not completely developed until the age of six and this could lead to severe damage of their respiratory tracts.

In 2010, a population based controlled study was conducted inHong Kong, China.Women and various factors including environmental exposures,

smoking and occupationwere put into consideration. Unlike men, most Chinese women were not smokers and stayed indoors for more hours. Hence the most effective cause of lung cancer in these women was exposures to indoor air pollutants such as radon. The study indicates most house maids who stayed indoors more often were more likely affected by indoor air pollutants such as radongas. Hereditary factors were also considered but were not found to be of much negative impacts compared to indoor exposures [15].

Radon's presence in the air is usually due to radioactive decay of uranium and other radioactive elements present in soil and rock [16]. Different cement mixtures (which also contain soil) used in constructing buildings can be another source of radon emanation. The main isotope contained in these cement mixtures is ^{222}Rn. Radon gas being gaseous can easily transfusethrough the pores in the soil and get into residentials from the foundation of the buildings. Many studies have been conducted to determine the types of cement mixtures that pose the least and greatest risk to radon release and exposures, for the purposes of picking the safest type of cement mixtures for construction of residential buildings. Results present Supplementary Cementitious Materials (SCM) such as fly ash can curb indoor radon exposuresresulting from concrete, producing a 3.4% reduction in the concrete emanation fraction of radon [17].

Furthermore, most concrete constituents contain uranium (^{238}U). Regardless of the economic and environmental savings, the use of fly ash as a replacement for cement or an additive to cement mixtures has raised concerns, as uranium levels in the cement mixtures are increased as a result offly ash addition, leading to an increase in radon levels in the indoor environment. Studies investigatedexhalation rates of radon from concretes containing fly ash.It was discovered that using 15 wt% and 35 wt% fly ash decreased exhalation rates of radon relative to similar concrete samples having no fly ash. Thisconfirms the facts that specific amount of fly ash helps to curb radon gas exposures [18].

Primarily, radon exposure mostly affects the uranium miners and workersin the nuclear power stations. A debate about the high and low levels of radon exposure persists and Epidemiological studies are still being carried out.a number of nuclear power workplaces have been suspended by the studies development regarding hazardous side effects of the atomic bombs usage.Radon gas exposures in detonation of atomic bombspose significant threat to people who are involveddirectly and indirectly on the receiving end of nuclear stations [19].

Additionally, there is the potential existence of uranium and radon in ground water. Currently, bedrock wells mostly serve as sources of drinking water where construction of water networks are difficult due to inadequate funds and wide distances. Theconcentration of these pollutants typically are 200 times higher than the threshold specified by WHO of about 15 μg/L. In addition to the already established health effects of leukemia, stomach and urinary tract cancers, adverse renal and bone effects might be identified [20]. Because of the abovementioned issues,studying the radon gas exposure as a result of radiation in the indoor air pollution would be deeply important.

In this paper, the recent status of radon gas and its contributions to indoor pollution are summarized. The review is on the basis of literature search conducted using the available scientific papers in reputablejournals, producing over 24,000 hits between the years of the late 1990s till 2014. Keywords are "radon", "radon indoor", "radon" "health effects", "radon" "history", "radon" "air pollutant", etc. Other trusted web sources, e.g. Health Canada, credible scientific papers available on the Internet were also used for the purpose of this research and can be viewed in the citations.

General description. Physical and Chemical Properties. Radon is odorless, colorless and tasteless. It is a noble, naturally occurring, monoatomicgas [21]. It is radioactive in nature and emanates from the uranium concentrations of about 1-4 ppm in soil and rock [22]. It possesses several isotopes, due to its radioactivity, as the number of neutrons change quite rapidly. Besides, the molecular weight of each isotope is changed continuously. The majority of these isotopes have considerably short half-lives thatlast only few seconds, and make them remarkablyunstable. Furthermore, radon gas has the highest density, about nine times of the air density, among indoor pollutants. Radon is not commercially produced anywhere in the world;itis producedfrom radioactive decay of uranium and its parent isotopes. Table 1 indicates the uranium radioactive decay series chain, listing the radionuclides and their respective half-lives. ^{222}Rn, the most common and most stable isotope of radon is the seventh member of the series directly obtained from radium (^{226}Ra) [22,23]. Radon is a chemically unreactive inert gas, hence it does notreact with other elements or compounds. However at temperatures between 18°C and 25°C, radon gas is partially solublein water and several other organic solvents for instance carbon di-sulphide, di-ethyl ether, benzene, hexane, cyclohexane, chlorophorm and Toluene [24].

The partial dissolution of radon gas in water explains the presence of radon in underground water. Risks of radon exposures are no longer only prompted bydecay of uranium in rocks and soil but also the partial dissolution of radon gas in water close to the soil due to the diffusion of radon gas in

soil pores. A number of people living in residential rural areas consumewell water as a result of absence of water pipeline networks.

TABLE 1
Uranium radioactive decay series [22].

Radio-nucleotides	Half lives
^{238}U	4.5 Billion Years
^{238}Th	24 Days
^{234m}Pa	1.2 Minutes
^{234}U	250,000 Years
^{230}Th	80,000 Years
^{226}Ra	1,600 Years
^{222}Rn	3.82 Days
^{218}Po	3.05 Minutes
^{214}Pb	26.8 Minutes
^{214}Bi	19.7 Minutes
^{214}Po	16 Milliseconds
^{216}Pb	22 Years
^{210}Bi	5 Days
^{210}Po	138 Days
^{206}Pb	Stable

Unfortunately, well water is one of the sources of radon gas exposures to human beings. The potential sources of radon and its movement are displayedin Figure 1 [25].

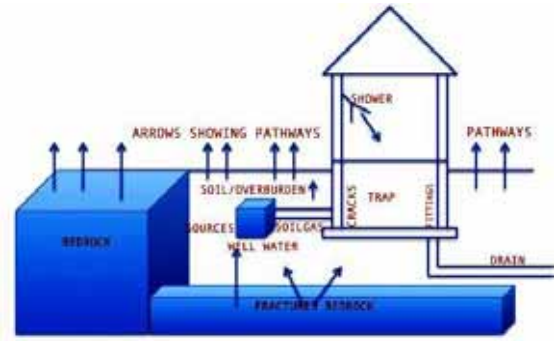

FIGURE 1
Illustration of the sources and movement of radon [25].

Radon gas belongs to the 18th group and 6th period in the periodic table with an atomic radius of 1.34 Å (Å: Angstroms). Radon gas possesses a total number of 86 electrons and 86 protons. The number of neutrons in a radon atom is not measurable clearlyas the number of neutrons continuously variesin each isotope. However, focusing on the most stable isotope, ^{222}Rn, the difference between themass number and the number of electrons yields the number of neutrons, which is 136.

Radon gasoxidation numbers are 0 and +2 [26].Although not many research on radon's chemical activity has been carried out, it has been discoveredthat radon can be oxidized to RnF_2 (radon di-fluoride) by fluorine. The Lewis structure of radon is indicatedin Figure 2. The electronic configuration is $1s^22s^22p^63s^23p^64s^23d^{10}4p^65s^24d^{10}5p^66s^24f^{14}5d^{10}6p^6$. A short form used to represent the electronic configuration is in the form of [Xe] $4f^{14}5d^{10}6s^26p^6$. The symbol of Xenon is emplyed to represent the initial part of the electronic configuration.

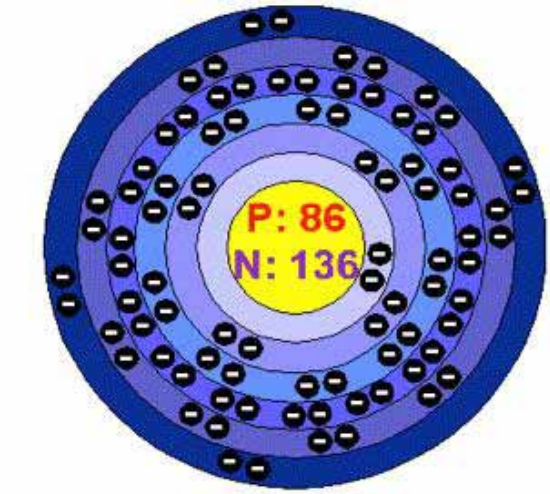

FIGURE 2
Lewis structure for radon.

The molecular weight and density of radon are222 g/mole and 9.73 g/L correspondingly [26]. Radon melts at 202°K and boils at 211.4°K [27], its triple point temperature and pressure are 202°K and 66.7 kPa respectively. The critical temperature and pressure are 377°K and 6282 KPa [28]. The structure is a face centered cubic crystal [29] with an atomic packing factor of 0.74. Some physical properties of radon such as the Henry's law constant vary with temperature. The Henry's law constant for radon at 20°C, which is quite close to room temperature, is 2.641 ± 0.179 [30].

A number of radon gas thermodynamic properties have been measured experimentally and by employing certain correlations and equations. The molar heat of vaporization and sublimation are determined to be 15.7 kJ/mole and 17.2 kJ/mole respectively. The molar heat of fusion that is obtained from the previous results are 1.4 kJ/mole [30]. The specific heat capacityand the first ionization energy of radongas at 20°C are 0.094 J/g.mole and 1036.5 kJ/mole correspondingly. The Chemical Abstracts Service (CAS) number of radon gas is is 10043-92-2. The viscosity of radon at ambient conditions is $1.8e^{-5}$ $kg.m^{-1}s^{-1}$, however the viscosity of gases generally varies with changing the temperature. Radongas diffusivity coefficient is$10e^{-6}$ m^2s^{-1}. All chemical and physical properties of radon gas are indicated in Table 2 [31].

Toxicology. Couple of epidemiological researches have been conducted on radon gas in various geographical locations of the world. Most of these case studies have yielded results that are intertwined and/or slightly connected.

TABLE 2
Physical and chemical properties of radon (^{222}Rn) [26,27,28,29,30,31].

Properties	Numerical values
Atomic radius	1.34 Å
Oxidation numbers	0 and +2
No of electrons/protons	86
Molecular weight	222 g/mole
Density	9.73 g/L
Melting point	202 °K
Boiling point	211.4 °K
Triple point temperature	202 °K
Triple point pressure	66.7 Kpa
Critical temperature	377 °K
Critical pressure	6282 Kpa
Crystal structure	Face centered cubic
Atomic packing factor	0.74
Henry's law constant at 20 °C	2.641 +/- 0.179
Heat of vaporization	15.7 KJ/mole
Heat of sublimation	17.2 KJ/mole
Heat of fusion	1.4 KJ/mole
Specific heat capacity at 20 °C	0.094 J/g.mole
First ionization energy	1036.5 KJ/mole
CAS number	10043-92-2
Viscosity at room temperature	$1.8e^{-5}$ kg.m^{-1}s^{-1}
Diffusivity coefficient	$10e^{-6}$ m^{2}s^{-1}

Because of Radon's ability to diffuse through the soil and rock particles, it is presence in residential homes especially in case of cracks and poor foundation structures [32]. The level of exposures obviously differs from zone to zone. Some geographical zones are rich in rocks and other organic matter in the earth's crust containing high amounts of uranium, that is the principal source of radon. Plus, topography of land and presence of natural minerals play a significant role in the levels of exposures.

The most common primary sources of radon gas exposures are uranium mines, underground water and well water.Ingestion or intake of radon gas into the body are predominant around these sources.One of the issue with indoor radon gas exposures is that indoor gases cannot be diluted by air the same level of outdoor radon exposures which are spreading into the atmosphere.Radon exposures frequently are known as second leading cause of Lung cancer.As previously stated, sixteen percent of lung cancer in Canada are as a result of radon exposures in residential buildings [32]. The human respiratory system becomes the major target for damage by radon gas exposures because of inhalation of the gases.

Radon as a radioactive gas rapidly decays, andemits other tiny radioactive particles. The inhalation of these radioactive particles damages the cells that create lung linings. Moreover, long-term exposures can cause accumulated damage leading to lung cancer. Other rare effects of radon gas exposures are stomach cancer and leukemia.These are consequent damage of radon ingestion included inwater.The stomachisthe prime target of drinking waterdamage.Through digestion and absorption into the blood stream suppression in the normal blood cells production may occur [32].

Therefore conducting radon gas tests to determine the exposures in various homes is essential. Prescribed radon tests by the Canadian Lung Association stipulates testing be carried out in winter months, when ventilation is the leastamong other months in a year[32]. Performing radon tests on a long-term basis for at least three months is remarkable important. The long-term radon tests are more accurate as it compensates fluctuations in the radon exposures as time changes. In addition, Radon gas tests shouldbe carried out in the lowest levels of buildings, because the highest amount of radoncan be detected considering the down-to-up movement of radon gas from the soil. For safety, the maximum radon level byHealth Canada should be 200 Bq/m^3. Levels higher than 200 Bq/m^3 are harmful and specific mitigation technique like repairing buildings' foundations and floor cracks should promptly be executed to decreasethe radon gas level [32].

Applications of Radon Gas. The applications of radon gas has not been fully investigated, therefore it is not commercially significantly available. In the 1980's, radon gas was indicated that could be used as a natural tracer in oil reservoirs. The ^{222}Rn isotope was observedto be a suitable natural tracer in thermodynamic researches,

transport features and geological studies ofthermal oil reservoirs. Later inthe year 1993, spotting the contamination in oil pores was inhanced by employing radon gas which was practical as a partition tracer. Also an investigation has been continued to determine quantity of oil volumes in porous spaces of oil reservoirs. When the distribution coefficients of radon in oil and water are identified, new technologies involving the application of radon gas could be developed with regards to the oil mining industries [33].

Regrettablypeople consciously expose themselves to radon gas for therapeutic purposes. For example, many patients claim radon aids in pain relief. Radon gas can serve as another option to usual biomedical treatments that help in pain relief and treat other symptoms of arthritis and other inflammatory diseases. Due to the fact that the radon alternative is long lasting, patients of arthritis and several other inflammatory diseases can go without using their normal medications for months. Also, using radon gas is significantly effective and reasonably economical compared to the normal medicals. Even if health agencies still do not clarifyradon exposures side effects for any reason, patients who suffer from chronic illnesses consider it as a practical alternative for treatment [34].

Using radon in therapy leads tothe intake of radon gas either by inhalation or consumption of water containing dissolved radon. Majority of the radon ingested is eventually released by exhalation but a portion of radon stays in the body in form of radioactive radon progeny which is physiologically active as they persistently radioactively decay. The radon application is mainly popular in patients of United States. However, in the United States, the therapy involving radon destined only by inhalation. Patients visitfour old mines around two small towns named Basin and Boulder in Montana, USA. Radon therapy in Europe is obtainable in different formsincluding baths containing radon, gas inhalation inmines and ofsteams [34].

Furthermore, Radon (^{222}Rn) could be a prime tracer in the study of atmospheric processes and for validation of models of chemical transport. The main challenges of the recent application are the uncertainties in the distribution and magnitude of radon flux density over the earth crust. These uncertainties lead to overestimation or underestimation of the radon flux densities in several areas, andit may be effect the confidence in results. Radionucleotides are present in the soil estimatethe radon flux densities with satisfyingconfidence, enhancing the implementation of radon as a tracer for atmospheric studies [35].

Moreover, geologists have developed significant improvementtothe application of radon gas. Radon gas concentrations are usually high over faults,therefore, radon gasis useful to detect underground faults and monitor temperature changes and gradients within the earth's crust. Accordingly, prediction of earthquakes is indeterminate by specifying the radon gas levels in certain cases. During the early stages of earthquakes, vibrations occur through therocks containing radon. These vibrations prompt the release of radon fromthe rocks into groundwater. As a result of high water pressure, the groundwatermoves through micro-cracks caused by the vibration. This water makes the radon break down remarkable rapid. The water released from the rocks later return as the vibrations subside. Newly saturated water then escapes through the micro-cracks to the earth surface, resulting in high levels of radon on the surface. Because of all above mentioned facts, high radon levels might indicate disturbances in the earth's crust and possible signs of earthquakes [36].

Sources of radon gas. Outdoors Sources. Soil Gas. The principal outdoor source of radon gas is soil gas. Almost all soils contain uranium. Uranium, being radioactive, rapidly decays and forms radon gas as one of its progeny. Certainigneous rocks are also present in soil and variousparts of the earth's crust. These rocks maycontain uranium as well. As radioactive decay continues to occur in the soil, soil gas becomes richer in radon gas. Besides, gas diffuses through layers of soil and moves up to the air above the ground. Radon gas in the air then get into homes through holes and cracks in the foundations and floors of buildings. In addition, radon gas could be trapped in these buildings as a result of inadequateventilation [37].

Water. Water fluidconstitute outdoor sources of radon. Radon gas couldpossibly containhigh concentration of radon gas in hot springs, lakes, rivers and certain streams. Even non-natural water sourcessuch as wells couldcontain high concentrations. Radon's presence in water sources is as a result of the radioactive disintegration of uranium and radium deposits. Radon gas gets dissolved ingroundwater by moving through rock and soil that containtheradioactive materials. As depth increases in the earth's crust, radon concentrations in groundwater become higher. Due to geothermal changes, groundwater travels upward through cracks and faults, reaches the earth surface and arrivesto hot springs finally. Cracks in the walls of wells could also be a pathfor radon gas to penetrateinto well water [38].

Uranium Mines. Uranium mines might overlap with soil as the uranium mines are located underground. The uranium mines is a prime outdoor source of radon exposure because of exceedingly high uranium levels present through the mining processes. High concentrations of

uranium in relatedmines undergoes radioactive decay andproduce radon leading to radon exposures to the atmosphere. Literally, uranium mines were the first identified sources of radon exposures.Since then, the release of radon gas and its progeny from the milling has been recognized as a potent radiological health hazard [39].

Indoor Sources. Building and Construction Materials. Reasonable portion of construction materials are soil and rockswhich containes radon. Common building materials like sandstones, bricks, concrete, marble and granite are principally involved in building construction. These materials areconsidered as the secondary sources of indoor radon exposures in residential and non-residential buildings. Recently, the uranium (and radon) content in building materials, plays a significant role in the selection of building materials needed for construction. Measurements are taken to reduce the uranium content in building materials and control indoor radon exposures [40].

Domestic Gas. Utilized gas for heating and cooking purposes maycontain high radon concentrations. The radon involvedin these gases is released upon combustion. Under normal conditions, this source of radon gas exposure is practicallyuncommon and insignificant. Radon exposures of heating and cooling gases could be effectively regulated at distribution and transmission points. Precisely, the concentration of radon in natural gas is about 1000 Bq/m^3. The natural gas sourcescontain several gases from various fields and wells, therefore radon gas concentrations might vary depending on the portions supplied by individual gas sources [41].

Sampling And Analysis Of Radon Gas. Sampling and analysis of radon gas applies both to indoor and outdoor sources. Several methods are implemented forthese processes. A numberof Indoor Radon Concentration (IRC) measurementsare taken in dwellings in different parts of the world,then these data are stored in a database pending to be analyzed. Various instruments are used to measure indoor radon concentrations, of which electret and alpha particles detector are inclusive. These instruments couldbe sent to homeowners who then expose them to indoor air for a minimum period of three months. Extra pieces of information are also generatedfor data analysis. Information may include level of floor of a building that measurement was taken in, types of foundation, habitation of measurement area, etc. [42].

Practical sampling and analysis of radon gas is principally needed for outdoor sources testing. These outdoor sources basically producea platform. Several case studies are being carried out overtimeRadon levels were investigated in ground water in La Garrotxa, Spain,2013[43]. Samples were taken from 42 private wells and eleven springs. For consistency the sample measurements are taken a number of times at specifictimes of a year. These samples are crosschecked to confirm measurements that are from the same source implementsimilar results.Then new measurement wastaken one month after the latest sampling. In the process of sampling, taking springs' samples directly from the sources and wells' samples from a minimum depth of onemeter below the surface is significantlyessential. The type of detector used in this case study was the RAD 7 portable monitor withan accessory RAD H_2O. The detector has an electrodepositing chamber and a semiconductor to differentiate the two major isotopes ^{222}Rn and ^{220}Rn contained in the samples [43].

For monitoring of radiological and chemical content in ground waters, a case study was studied in the Dikili geothermal waters in turkey [44]. Different method was developedfor the sampling and analysis. The method applied in this case is entitledthe collector chamber method. Theabove-mentioned method capitalizes on the fundamental theory that radioactive daughter elements emit alpha and beta particles. Thus the method is conducted on the basis of alpha particle measurements emanated by the radon progeny. The most effective operating conditions for the collector chamber method are 4.5 cm diameter copper plate, approximately 2.5 m^3 volume collector chamber and an applied electric potential of 600 Volts [44].

Water samples obtained from earthly sources are stored in 100 ml bubbler bottles. Radon leakage is prevented by keeping the bottles airtight.Radon gas is removed from the bottles via a carrier gas which is ripe air. In the Lab, the bottle inlets are connected to the outlet of the gas regulators containing ripe air while the bottle outlets are connected to the gas collector chamber inlet. A suitable vacuum pressure of about 0.6 mb is set in the system to facilitate movement of the gas [45].

Then, the gas is carried from the bubbler bottles into the collector chamber. When the vacuum pressure reads 0 mb the valve of the collector chamber is closed. The closed valve is then connected to an electrostatic field having an electric potential of 600 V (Direct Current) for a period of four hours. Next, radon and its progeny are gathered on the collector plate.The alpha particles are produced in the form of positive ions becausethey carry electrons from their parent atoms. The decay of alpha particles emanated by the radon progeny is measured by the alpha scintillation counter system. A counting time of 20 min is allowed for each sample [45].

In the recent method of radon analysis, radon activities need to be determined. Hence, a particular formula used to calculate the radon activity

concentrations. This formula is indicated as

$$CRn = \frac{(C-B)/t}{cf} \times e^{\lambda t1} \quad (1)$$

where C_{Rn} represents radon activity concentration in Bq/L (Bq/L: Becquerel per liter), *C*is the total counts per time interval (t), *B* is the back ground counting, λ is the decay constant of radon in s-1, *cf* is the coefficient of calibration in (cpm/pCi/L: count per minute per picocuries per liter), *t* the counting time, and *t1* is the interval between sampling and measurement given as one day. When the radon activities are calculated they are interpreted into concentrations [46]. The gas collector chamber is presentedin Figure 3.

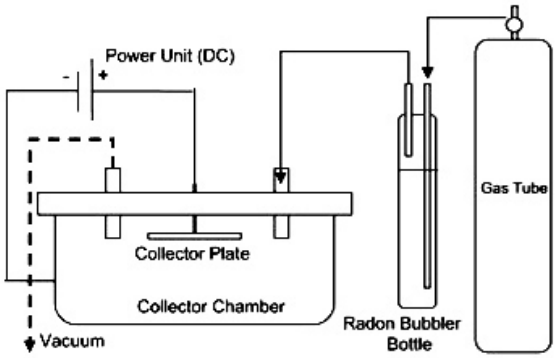

FIGURE 3
Simplified sketch of the gas collector chamber apparatus [45].

Another case study involved in measurement and analysis of radon gas was on air and hot springs in mineral water in Thailand. Air radon concentrations were measured at several points in hot spring areas for an interval of 30 minutes. The effective radon concentrations were calculated using the following equation:

$$C_{Rn} = (EERC) \times (EFRC) \times (t) \times (DCFRn) \quad (2)$$

where *EERC* represents equilibrium equivalent radon concentration in Bq/m^3, *EERC* represents the equilibrium factor for radon given to be 0.4, *t* is the period spent in indoor radon exposure (h) and *DCFRn* is the radon dose conversion factor indicatedto be 9 nSv/h/Bq/m^3 (nanosievert per hour per Becquerel per cubic meter) [47].

For hot springs, samples werecollected in glass bottles. In the process of sampling, the glass bottles are dipped in hot springs, filled and covered while still immersed in water. The samples are taken to the lab and analyzed within the next two days to restrain radon leakage from them. For the mineral plants, samples were collected directly from the production plants since these serve as the original representatives. The dissolved radon gas concentrations in six different brands of bottled mineral waters were considered. The diagrammatic representation of the set up for the measurement of dissolved radon from the bottles is illustrated in Figure 4 [48].

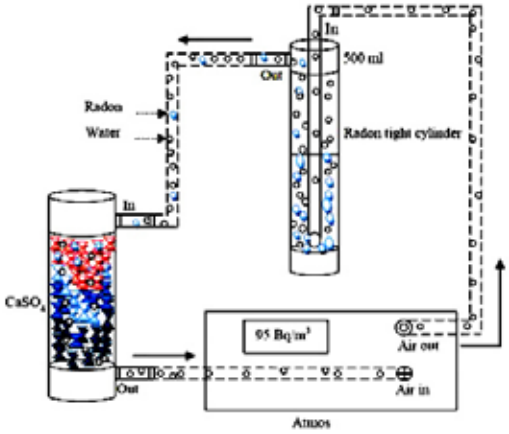

FIGURE 4
Dissolved radon measurement system [49].

The process entails bubbling of water samples by air. The air contained radon passes through silica on its way to the inlet. Then, exhaled radon air is transited to the radon gas pulse ionization chamber for alpha spectrometric measurements. Approximately 86% of the radon gas is transferred to air. This method facilitates the measurement of ^{222}Rn movement from water to air without interrupting samples. Concentration of radon in water is obtained from radon concentration in void air using the following equation:

$$Ca = \frac{\alpha 1}{\alpha 1 + \alpha 2} \frac{Vw \times Cw}{Va} \left[e^{-\lambda t} - e^{-(\alpha 1 + \alpha 2 + \lambda)t} \right] \quad (3)$$

Ca is the concentration of radonin the air, λ is the decay constant, *t* is the measuring time, V is the volume with the subscripts *w* and *a* being water and air respectively. $\alpha 1$ and $\alpha 2$ are the transfer factors of movement of radon gas from air to water and back to air correspondingly [48]. $\alpha 1$ and $\alpha 2$ are determined experimentally and specifiedto be 0.0845 and 0.00813 min^{-1} respectively [49].

To conclude, wide range of indoor radon gas analysis exists. There are no particular preferenceinradon indoor air analysis. Carrying out various case studies in different parts of the world is the most common technique. Several devices operate on variousprinciples and facilitate to measure and analyze radon gas from both indoor and outdoor sources. In addition, measuring devices are applicablefor private use and radon level monitoring. These methodsare straightforward, economical and robustdevices. Besides, exposimeters are convenient to be ordered online for indoor radon measurements [50]. Applying the right procedures, indoor radon concentrations couldbe obtained.

Indoor radon gas guidelines. National Reference Levels. Various occupational health and safety authorities all around the world have stipulated peculiar radon gas levels. These radon exposure limits are mainly obtained by various epidemiological and toxicological studies and surveys conducted in various parts of the world. The studies could involve humans or animals subjected to radon exposures or the assessment of potential health hazards of radon exposures. Due to the nature of radon gas as an indoor pollutant, i.e being radioactive, taking radon indoor concentrations in remarkablyshort duration of time is not ordinary.National radon gas reference levels are mostly based on annual or semi-annual averaging periods. The detection of indoor radon gas concentrations in long periods determines a better estimate of indoor radon exposures [51].

The reference level depicts the highest accepted annual average concentration of radon in residential dwellings. National reference radon levels are an important part of national radon gas programmes and are usually established by the responsible agency in respective countries. Monitoring of radon gas levels in residential dwellings is supported by the stipulated radon exposure limits with respect to a particular part of the world. If radon measurements are higher than the exposure limits, it is highly recommended that suitable technique be generatedto decrease the radon levels. In certain countries like Switzerland, Czech republic and Sweden, it is mandatory to lower indoor radon concentrations, with immediate effect, in case of radon gas penetrations above the exposure limits [52].

A national reference level does not presentspecifications or boundaries between safety and danger for radon exposures. However, it explicitly defines a health risk level of indoor radon gas. Retain radon gas level below the indicatedexposure limit is highly dependent on the occupants of a particular residential dwelling. Residents often start applying indoor radon concentration reduction measures when the indoor radon levels are quite close to the threshold exposure limit. A World Health Organization (WHO) survey of 36 countries has discovered approximately all countries setthe indoor radon exposure limit between 200 Bq/m^3 and 400 Bq/m^3. Indoor radon levels are typicallymaintainedas low as practically achievable [52].

The decision making process involved in setting national radon gas levels includes the process of optimization and consideration of the dominant socio-economic circumstances consideringspecific part of the world. Moreover, certain factors are considered including radon gas distribution, the amount of homes subjected to high radon exposures, the mean indoor radon air level and the prevalence of smoking. For mitigated dwellings and newly built dwellings, low radon gas concentrations couldefficientlybe achieved at lower costs compared to long existing dwellings. Hence, for mitigated and new built dwellings, radon gas concentrations should regularlybe maintained below the national reference level [52].

It is remarkably important to note that the national reference levels are only utilized as a means to decreasethe negative health effects due to radon exposures. Depending on the population of various countries that are exposed to indoor gas radon, it is the responsibility of a national radon programme to implement adequate building regulations and codes as an approach to generally reduce the mean indoor radon concentration in a particular country [52].

Radon Reference Levels in Dwellings. The guidelines for indoor radon gas concentration, just like any other pollutant, differs in different locations all over the world. Different agencies in various parts of the world are responsible for setting these guidelines. Therefore permitted radon gas levels are not the same in different locations even if the concentrations are within a close range. Following paragraphes mention reference levels of radon in different countries based on the reliable litreture review..

For the purpose of collecting information about national reference indoor radon levels, the International Commission on Radiological Protection (ICRP) and the Council of the European Union sent questionnaires to 57 countries in December of the year 1997. Initially only 42 countries statedanswers to the questionnaires. In early 1998, countries that didn't responded to the questionnaires were contacted again. In the fall of 1998, accurate responses were gathered from all 57 countries. The complete list of these countries is presented in Table 3. The questionnaires sent served the purpose of determining the radon gas reference levels for existing and planned residences, radioactive elements in building materials, drinking water and directives of radon planning. [53].

Among the fifteen EU member states that responded to the questionnaires, ten of them have a specific reference level and specifiedaction to curb radon exposures regards to their existing dwellings. Five countries had no specific reference levels. Sweden is the only country that implements an enforced radon level of 400 Bq/m^3. Seven out of seventeen non-EU European countries whofilled the questionnaires had enforced reference levels.

TABLE 3
Countries who responded to the questionnaire [53].

EU member states	Non-EU European countries	Non-European countries
Austria	Albania	Canada
Belgium	Belarus	USA
Denmark	Croatia	Mexico
Finland	Czech Republic	
France	Estonia	Zimbabwe
Germany	Hungary	
Greece	Latvia	Isreal
Ireland	Lithuania	Syria
Italy	Norway	
Luxembourg	Poland	Japan
The Netherlands	Romania	Hong Kong
Portugal	The Russian Federation	
Spain	Slovak Republic	Australia
Sweden	Slovenia	New Zeland
United Kingdom	Switzerland	
	Turkey	
	Federal Republic of Yugoslavia	

Five of these seven countries had advisory reference radon levels. The advisory reference levels are usually not enforced unlike the normal reference levels, which are built into the environmental law of a particular country. The remaining five countries had no radon gas reference levels. A numberof the countries such as Hungary planned to introduce reference levels. All the countries involved apply the same reference levels for dwellings and other types of residences, government buildings, and co-operative of rental. The only exception was Luxembourg, which had only a reference radon gas level for private homes [53].

The general practical range ofradon gas reference levels is between 150 and 1000 Bq/m^3. For European countries, EU member states including Austria, Sweden, Greece and Denmark, and non-EU European countries of Belarus, Lithuania, Estonia, Norway, Poland, Russia, Yugoslavia, and Slovak Republic consider 400 Bq/m^{3}as radon reference level for already existing dwellings.The United Kingdom (UK) and Ireland have an advisory reference level of 200 Bq/m^3 while Luxembourg has an advisory level of 150 Bq/m^3 for already existing dwellings [53].

Certain countries implement two reference levels. An upper reference level which specifies that costly strong mitigation measures be taken with immediate effect against radon and a lower reference level applicable for buildings where radon levels can effortlessly be lowered by reasonably priced mitigation measures. Countries that utilize two reference levels include Germany having an upper and lower reference levels of 1000 Bq/m^3 and of 250 Bq/m^3, Switzerland having an enforced level of 1000 Bq/m^3 with an advisory level of 400 Bq/m^3 for new and existing buildings and Sweden having an enforced upper and lower reference levels of 400 Bq/m^3 and 200 Bq/m^3(recommended) for new and existing buildings [53].

Slovak Republic and Czech Republic adopt reference levels in form of concentrations of radon gas progeny for both new and existing buildings. The upper reference level enforced by the Slovak republic is 200 EEC Bq/m^3 (Equilibrium Equivalent Concentration Becquerel per cubic meter) for existing residences. Czech Republic utilizes four advisory levels. The purpose of considering four levels (indicated below) is tocategorizesuitable mitigation technique

- ”200-300 EEC Bq/m3 simple mitigation, e.g. improved ventilation;
- 300-600 EEC Bq/m3 expensive mitigation;
- 600-2000 EEC Bq/m3 sophisticated mitigation measures;
- >2000 EEC Bq/m3 people stay isolated” [53].

To conclude, many countries consider lower reference levels for newconstruction compared to existing buildings. For instance, amongst the EU member states, two countries(U.K and Sweden) have imposed radon reference levels of 200 Bq/m^{3}onnew buildings. Generally, eight of these countries possess advisory levels while five countries have no specified reference levels at all. Between the non-EU European countries, nine of them have enforced reference levels; three possess advisory levels while the remaining five countries possess no reference level at all. Latvia has a 300 Bq/m^3 enforced reference level, and Switzerland has a 1000 Bq/m^3 enforced reference level and a400 Bq/m^3 advisory reference level [53]. Besides, Canada, Syria, Israel, Australia and the U.S.A, have advisory radon reference levels. Theyare generally

applicable to all residences irrespective of the form of ownership be it co-operative, rental, private or Government owned. In U.S.A, the radon gas reference level, 150 Bq/m^3, is simillar for already existing and new buildings.In Syria, Australia and Israel reference level is 200 Bq/m^3, whilein Canada is 800 Bq/m^3.In Japan, the council for radon gas penetration is presently working on providingrecommendations onradon reference levels ondwellings [53]. As mentioned previuosly, majority of the countries apply a 200 Bq/m^3 reference level.

Reference Levels For Radon Gas in Work Places. A total of fourteen countries have defined specific reference levels for radon gas in workplaces environment located above the ground. These reference levels are in the range of 200 – 3000 Bq/m^3. For Belgium, the reference level for radon gas in above ground work places is is 800 kBq/m^{3}h/year (kiloBecquerel per cubic meter-hour per year). All countries except Switzerland have specified reference levels above 1000 Bq/m^3 in workplace environment. In addition, defined radon gas level agrees with the recommendations stated in ICRP 65 [54] and Radiation 88 [55]. Radiation Protection 88 [55] has recommended the radon reference level in the member states of the EU should maintainin the range of 500–1000 Bq/m^3. Therefore, any worker would not receive an effective dose of radon higher than 6 mSv, the designated dose for a 'category A' worker [54–56]. Member states have the freedom of setting a reference level lower than the specified range.

Ireland, Germany and France all possess two reference levels in workplaces. In Germany, the reference levels are applicable to buildings like offices. The lower reference level, 200 Bq/m^3 is set for new buildings while the higher reference level, 400 Bq/m^3 is set for existing buildings. Recently, 100 Bq/m^{3}reference level for new and existing buildings is considered in some cases. In France, reference levels specified are only applicable to workplaces with notable public occupancy such as retired homes, schools, hospitals, prisons etc. Simple mitigation measures have to be applied when Indoor Radon Concentrations (IRC) are higher than 400 Bq/m^3. Serious mitigation measures are accomodated when the indoor radon concentration is above 1000 Bq/m^3. For Ireland, a 200 Bq/m^3 advisory reference level is issued for schools habitual institutions such as nursing homes and prisons. Most reference levels for workplaces are enforceable in most countries. It is mandatory for applying measures when indoor radon gas levels isabove the specified limit [56]. Underground work places are considered separately. A total of fifteen countries have defined specific radon reference levels for underground work places. Most of these reference levels are expressed in terms of radon concentrations. Sweden, Germany and Belgium have specifiedtheir reference level in terms of radon gas exposure. Similar to the above ground workplaces, the reference levels set by individual countries is in the range of 400–1000 Bq/m^3. In Poland, underground workers are not allowed to receive doses of radon higher than 20 mSv in an annual period. In Romania, an underground workersannually could only be subjected to radon exposures for four working level months. Countries have set reference levels by national regulatory authorities in terms of radon exposure, the exposure limits range from 800 to 2500 kBq/m^3, which is the same as 400 to 1250 Bq/m^3. Based on the German radiation protection regulation, a dose of 6 mSv annually is equal to 2000 kBq/m^{3}h/year. 2000 kBq/m^{3}h/year is applicable to workers in caves, mines, water works and spas. In addition, the permissible limit of effective dose of radon exposure for German workers underground is set at 20 mSv per year, equivalent to a 6000 kBq/m^{3}h/year radon exposure [56]. To conclude, Table 4 displays countries and their respective radon reference levels for underground and above ground work places.

Reference Levels for Radon Gas in Drinking Water. The dangers of radon gas exposures because of its presence in drinking water have been considered in the past few years. Currently, the doses infants might receive from decay radon products and water containing radon have been analysedseriously [57–59]. In late 1988, the EU article 31 Group of EU Experts on Radiation Protection, at the direction of the EU Committee on Water Intended for Human Consumption, assessed the dangers associated with radioactive substances contained in water, and as a result The EU radiation protection experts agreed to set the reference level of radon on drinkingwater. The reference level was in form of an effective dose proposed by the WHO in 1993 and was specifiedto be 0.1 mSv annually. The dangers caused by radon and its progeny in drinling water is considered to be deeplylimited by EU experts and the WHO.

The council of the European union studied the proposal given by the Article 31 group and concluded the reference numberfor total effective dosage of radioactive elements contained in drinking water consumed by humansshouldbe 0.10 mSv annually. The dosage leaves out the doses from potassium-40, radon and itsdaughtersas well as tritium. The reference dosage of 0.10 mSv was applicable to water supplies servicing more than 50 people [60]. The council gave instructions to the Article 31 Group to hand in proposals for reference parameters and for overseeing programmes within a year from 5/12/1988. Besides, the EU council instructed the Article 31 Group of experts to perform more investigations on the risks of

TABLE 4
Radon reference levels in underground and above ground workplaces [56].

Countries	Radon reference levels in above ground workplaces	Radon reference levels in Underground Workplaces
Austria	N/A	N/A
Belgium	800 kBq/m^3.h/yr.	800 kBq/m^3.h/yr.
Czech Republic	1000 Bq/m^3	1000 Bq/m^3
Denmark	400 Bq/m^3	400 Bq/m^3
Finland	400 Bq/m^3	400 Bq/m^3
France	400 Bq/m^3 (lower limit) 1000 Bq/m^3 (upper limit)	N/A
Germany	200 Bq/m^3 (New buildings) 400 Bq/m^3 (existing buildings)	2000 kBq/m^3.h/yr.
Greece	400 Bq/m^3	400 Bq/m^3
Hungary	1000 Bq/m^3	1000 Bq/m^3
Ireland	200 Bq/m^3 (lower limit) 400 Bq/m^3 (upper limit)	400 Bq/m^3
Italy	500 Bq/m^3	500 Bq/m^3
Netherlands	N/A	N/A
Poland	N/A	20 mSv/yr.
Portugal	N/A	N/A
Romania	N/A	4 working level months of exposure
Slovenia	1000 Bq/m^3	1000 Bq/m^3
Spain	N/A	N/A
Sweden	400 Bq/m^3	3000 kBq/m^3.h/yr.
Switzerland	3000 Bq/m^3	3000 Bq/m^3
UK	400 Bq/m^3	400 Bq/m^3

exposure to radon and its progeny in drinking water and indicate recommended reference levels of dosage and exposures.

In 1988, a multidisciplinary committee was appointed by the National Research Council responding to the request of the Environmental Protection Agency (EPA) in the U.S.A. The appointment goal was to facilitate the purpose of coordinating a study and providing a report on the dangers of radon exposures in drinking water. The report was presented at the end of 1998 [61]. The committee recommendation was that the value of the Alternative Maximum Contaminant Level (AMCL) for the mean radon ambient concentration in drinking water should be fixed at 150 Bq/l. Moreover, water supplies with radon levels higher than 150 Bq/lshould be subjected to mitigation measures to decrease the radon level to at least the level of the AMCL.

Among all the countries of the world, only seven ones, Finland, Romania, Czech Republic, Norway, Sweden, Russia and the Slovak Republic, had reference levels for radon in drinking water bythe end of 1998. About seven other countries were plannning to introduce radon reference levels at the time. .These countries have their supply source of water from underground wells instilled into soil and bedrock, therefore they have the most important reason for implementing reference levels.Soil and crystalline bedrock contain uranium of remarkableamounts.The radioactive decay of uranium transports radon gas. In above mentionedcountries, thousands of wells with radon levels over 1000 Bq/l are located. Other wells with radon levels over 20,000 Bq/l have also been discovered. A typical example is Sweden having about 200,000 wells fordrinking water supplies which45% of them include radon levels of over 100 Bq/l and 10,000 ones consists of radon levels greater than 1000 Bq/l.

The Czech republic has two reference levels for public water, an enforced reference level of 300 Bq/l and an advisory reference level of 50 Bq/l. For the case of private homes, two advisory reference levels exist, 1000 Bq/l and 200 Bq/l depending in various remediation measures. Finland considersa 300 Bq/m^{3}imposed reference level for public waters while Norway specifies one advisory reference level of 500 Bq/l. Regardless of the type of ownership, Russia has one enforced level of 120 Bq/l for all drinking waters. The Slovak republic has two reference levels for all drinking water despite of ownership; A 1000 Bq/l enforced reference level and an advisory reference level of 50 Bq/l. Sweden employs two limits; radon levels

TABLE 5
Radon reference levels for drinking water [53].

Applicable Countries	Radon level
Czech Republic	50 Bq/L (advisory level) 300 Bq/L (enforced level)
Finland	300 Bq/L
Norway	500 Bq/L
Romania	200 Bq/L
Russia	120 Bq/L
Slovak Republic	50 Bq/L
Sweden	100 Bq/L
UK	100 Bq/L
USA	150 Bq/L

greater than 100 Bq/l is supposed for consumption with reservations while radon levels greater than 1000 Bq/l is harmful for human intake. The limits in Sweden are mandatory for public waters and advisory for private homeowners. List of countries and their respective reference levels for radon ofdrinking water are presented in Table 5.

Radon Gas Emission Data. Large number of studies considering radon gas emission have been conducted in different parts of the world. Radon emission data are obtained from various radon-emanating sources depending on various researchers interests. The most common sources of radon emission data are from studies accomplished on soil gas and underground water because of containing uranium. Emission data encourages interestedenvironmental protection agencies to regulate exposures to radon gas due to its health risks. In addition, gathered dataspecifies an insight to how often remediation measures should be applied to reduce the health effects of radon exposures.

Emission Modeling of Radon Gas in Indoor Air. Modeling of radon gas concentrations in the air is significantlycommon aspect of radon emission modeling.There are several factors that determine the contributions of radon contained in water to indoor air radon exposure, including radon concentration in water supplies, amount of water used, manner in which water is used and features of the dwelling in question. The presence of radon in water can result from radioactive decay of radium. Radium penetratesinto water in contacts with radium-containing soil or bedrock or dissolved radium in household plumbing. As mentioned previously, the specific application of water persuade the release of radon as well, which influences theradon concentration in the air. Household heating and cooling watercould cause higher release of radon into the air. Moreover, the mode of ventilation and volume or space occupied by the home would impact the level of radon content in the air.

The National Academy of Sciences (NAS) published two reviews regarding the public dangers of radon contained in drinking water [62]. The most current report presents a summary of the findings from the investigation on the movement of radon from water to air. In the report, the the following equation is discussed for modelling an estimation of the mean incremental concentration that radon in water contributes to the air:

$$Ca = \frac{Cw\,We}{V\lambda} \quad (4)$$

where, Ca is the mean incremental increase of radon in the air in units of (Bq/m^3), Cw is the concentration of radon in water entering the dwelling of interest (Bq/m^3), W is the water use rate per resident (m^3/person/hr), e is the use-weighted meanefficiency of radon transfer to air, a dimensionless quantity, V is the volume per resident (m^3/person) and λ is the exchange rate of air of the dwelling (hr^{-1}).Besides, ventilation is assumed to lower radon levels much quicker than the physical decay of radon in the air (0.0076 hr^{-1})[62,63].

The transfer efficiency, in water applications, volume and air exchange parameters couldbe substituted by a single overall transfer parameter (f). The simplified model is:

$$Ca = f\,Cw \quad (5)$$

where $f = \frac{We}{V\lambda}$, a dimensionless transfer factor. The value of (f) is determined from experiment or estimated using mathematical methods. To determine the value of f, the radon concentration in the air and water in a dwelling is measured by one of the following procedures. The first procedure entails the continuous measurement of radon in the air for several days, and calculation of the difference in the mean concentrations between time periods at home when water is being used and when water is not. The difference in these concentrations would represent the contribution of water-sourced

radon in the indoor air. The other approach involves continually measuring indoor radon in the air and identifying periods involving peaks concentrations. The peak periods, which are correspond to the periods in which water is being used, are attributed to waterborne radon liberated to the air. a number of challengesare associated with the study designs. One of the main challenge is inaccuracy of radon measurements due to uncertainty. The uncertainty is because of collecting radon measurements over short periods. Measurements over longer periods (at least 6 months)yields more accurate results of radon measurements in the airthat could be generalized.

In addition tothe experimental approach, mathematical models assist in understanding the contribution of radon transferred from the water to the air. Significantly, the distribution factor can be estimated by preparing a model to dictate the relationship between water usage (*W*), volume (*V*), exchange (λ) and transfer efficiency (*e*). Mean values of these parameters could be applied. A study carried out by Nazaroff et al.. 1987 indicatesusing different values of λ, *W*, *v* and *e* to determine an estimate of fwith similar results; (*f*) is usually determinedto be close to 1.0×10^{-4}. Likewise, the report presentedby NAS, committee recommended 1.0×10^{-4} as the best estimate of *f* [64]. In case of inaccuracies or uncertainties, a range in which the value of *f* wouldmost likely adjustwas demonstrated by the committee to be 0.8 to 1.2×10^{-4} [64].

In a work published by A.N Sheikh et al., a comprehensive study was conducted to monitor and model indoor radon gas levels in a multi-storey building in Mumbai, India [65]. Radon (^{222} Rn) indoor concentrations were measured and compiled for a period of 12 months, considering all the seasons. The time-integrated passive detector technique was employed for monitoring of radon gas. The equipment used was the Kodak-115 type Solid State Nuclear Track Detector (SSNTD) films of size 2.5×2.5 cm. The measured concentrations indicated a trend existed in the relationship between height and indoor radon levels. Measurements were in the range of 41 Bq/m^3 (on the lowest floor) to 15 Bq/m^3 (on the highest floor). Using confidentdosage conversion factors obtained from UNSCEAR (United Nations Scientific Committee on the Effects of Atomic Radiation) 1993 [66] the intake dose of radon gas by breathing was determined to be 1.03 mSv/year at the lowest floor and 0.38 mSv/year at the highest one. Furthermore, the computed values of indoor radon concentrations were compared with the measured mounts for each floor of the building. The results were similar under certain limitations of several parameters.

The indoor radon gas concentration in above mentionedparticular high-rise building is dependent on a number offactors. These factors include the volume of air in the indoor environment of interest, the rate of generation of the radionuclide (^{222}Rn), the rate of disappearance of the radionuclide and the rate of air exchange or ventilation [67].The Solid State Nuclear Track Detector (SSNTD) technique [68] was utilizedto monitor radon. A 12 μm thick Kodak LR 115 Type II strippable film 2.5 by 2.5 cm in size was placed beneath an aluminum cup of 6.5 cm diameter and 5 cm height. The cup was sealed with a semi-permeable membrane, which permits only radon gas flow. The indoor radon gas measurements were conducted on the ground floor, 1st, 3rd, 5th, 8th, 10th, 13th, 16th and 19th floors. The building was made of concrete roofs and floors, with cement and brick sidewalls.

Moreover, a dosimeter with an SSNTD film was placed in the same locations in every corner apartment of the building. In the process of exposure, the alpha particles emanating from radon gas leave tracks in SSNTD films. These films were left exposed for duration of 90 days at a height of 1.5 m in each room. Then, the dosimeters as well as the SSNTD films were analysed in the laboratory.The films were treated using 2.5 N NaOH under controlled temperature conditions (60°C) for 60 min. A spark counter counted the treated films. The amounts of tracks were counted a number of times for verification after which an average value was calculated. Afterward, the recorded tracks were converted into radon concentrations using a calibration factor determined experimentally. The procedure above mentioned experiment is presented in details by Subba Ramu et al.., 1988 [69].

The general mass balance equation applies to the modelling of indoor radon gas concentrations is:

$$Accumulation = Input - Output - Reaction \quad (6)$$

The first assumption is forming homogeneous mixture of radon gas and room air. Anotherrealistic assumption is that radon is not envolved in chemical reaction. In addition, it is assumed that radon does not disappear by any means other than radioactive decay and ventilation. Other sources of radon are also assumed to be negligible. A linear differential equation could be used to represent the concentration of radon gas as a function of time $C_i(t)$ in a single room with specified volume V [70,71]:

$$\frac{dCi(t)}{dt} = J\frac{S}{V} + Co\lambda v - Ci\,(\lambda + \lambda v) \quad (7)$$

where $C_i(t)$ is the radon gas concentration at time *t* (Bq m^{-3}) in the room, *J* is the exhalation rate of radon from concrete (Bq m^{-2} s^{-1}), *S* is the surface area (m^2), *V* is the volume of the room (m^3), C_o is the radon gas concentration in the outside air (Bq m^{-3}), λ_v is the ventilation rate (s^{-1}) and λ *is* the decay constant of radon (2.1×10^{-6} s^{-1}). Equation analysis indicates the concentration of radon is dependent on

the source of emanationincluding building materials and outdoor radon levels, radon flux, volume and rate of ventilation. All these parameters areeither determined from experiment or obtained from other trusted results ofsimilar case studies.

Several other models are established to investigate trend of indoor radon gas concentrations in various situations. One of these models was a useful model demonstratedby W. Jacobi [72]. The model isremarkablyuseful for the prediction of radon levels in the air of uranium mines. Porstendorfer et al.. developed the model later to revealinfluences of the different physical parameters on indoor radon gas concentrations [73]. Plus, Kuntson critically revised the model in 1988 [74]. He confirmed that both unattached fractions and equilibrium could be predicted. In the case of mixing of indoor air, the radon concentration can be modeled by the following equation:

$$C_i = E/V + C_o \quad (8)$$

where C_i and C_o are the respective radon concentrations indoor and outdoor, E is the total volume-specific rate ofentry of the radon sources (building materials and soil) which gives the supply of radon in area per unit of time and air volume. The rate of ventilation in dwellings is in the range of 0.1 - 1.5 h^{-1}.

Emission Modeling of Radon Gas in Outdoor Air. A environmental boundary layer model is employed for estimation and modeling of outdoor radon gas levels. Vinod Kumar et al.. proposed the model in a published work in 1999 [75]. For application purposes, one of the main assumptions is that radon flux generated from the earth's surface is entirely horizontally uniform. Therefore, all the sources of the radon flux are uniform. To investigate the atmospheric distribution of radon gas, a one-dimensional Planetary Boundary Layer (PBL) model is implemented. In addition, Turbulence is considered in the vertical directions. The one-dimensional PBL is a meteorological model applied in outdoor radon concentration modelling. The fundamental equations of the planetary model are presented by Holt and Raman (1988) [76].

These equations are derived by compromising conservation of thermodynamics equations, water vapor and momentum. The turbulence is facilitated in the equation by employing supplementary equations of kinetic energy (E) resulting from turbulence and energy dissipated (ε) [77]. The viscosity of flow is obtained by implementing the Prandtl Kolmogorov hypothesis relating E, ϵ and turbulent Prandtl number (ratio of conductivity to flowviscosity; assumed to be 1.4 for unstable cases and 1.0 for stable atmospheric conditions) [78]. To determine the soil temperature, the force restore techniqueisapplied [79,80]. Long and short wave flux divergence at specific vertical layers were evaluated by radioactive flux computations. Logarithmic and linear vertical grid structures were used for vertical resolution of the boundary layer up to a height of 2 km. For the surface layer, Monin–Obukhov similarity theory ispresentedfor turbulence flux calculations [81].

The equation governs the time dependent vertical dispersion of outdoor radon is presented below:

$$\frac{dn}{dt} = \frac{\partial[Kd(z,t)\partial n/\partial z]}{\partial z} - \lambda n \quad (9)$$

where n represents the concentration as the number of atoms of radon, λ is the decay constant, K_d is the eddy diffusivity coefficient assumed to be equal to eddy conductivity generated in the one-dimensional meteorological model used for indoor modelling [82]. Boundary conditions were also determined for the differential equation, which served as the model. The emission of radon from soil helped form the lower boundary condition. The radon flux at the surface is indicated below:

$$-Kd(z,t)\frac{\partial n}{\partial z(lowest\ grid)} = Em \quad (10)$$

Em is the rate of emanation, and is assumed to be 10^4 atom m^{-2} sec^{-1}. Besides, the emission rate is assumed not vary with temperature on a daily basis. The disappearance of radon gas ispresumed to be due to radioactive disintegration and formation of radon products' decay. The upper boundary conditions aregiven to be the same as the gradient boundary conditions as presented below:

$$\frac{\partial n}{\partial z} = 0 \quad (11)$$

To conclude, modelling of radon gas concentrations is still a major aspect of radon gas studies as an indoor pollutant. A number of researchesare being conducted to improve the accuracy ofpredicting the characteristic of radon gas emissions from different sources. The most consistent and accurate results currentlyareestablishedin the modelling of indoor and outdoor radon emissions as mentioned in the above mentioned case studies.

Radon Gas Concentrations Indoors. Evaluation of Data. Indoor radon gas levelsofresidential and other occupational dwellings are measured and analyzed through several studies.These studies are differrentdepending on the types of residence, geographical location, weather, altitude etc.based on their influence of obtained individual data. Two approaches mainly employed in these case studies: (i) obtaining numerous samples from a huge number of homes selected at

random to supply an estimate of the exposure to the higherpopulated area or (ii) monitoring a small-scale number of residential dwellings to determine trend ofthe indoor radon concentration overtime, and toforecast the concentrations over a long-term [83].

Generally, the concentration of indoor pollutants including radon gas are identifiedto be distributed log-normally.In addition, the geometric mean, instead of the arithmetic mean is discovered to be considered during analysis and statistical evaluation. 50-Pisa propermedian to considered.. In most of the cases, the range of results (minimum-maximum) is also determined. Comparisons of studies are constantly revealed. However, more information concerning the process of individual case studies is required to effectively and efficiently compare two or more case studies. As previously mentioned, each data is based oneach case study and influencing factors (types of residence selected, geographical location, weather, altitude, sampling types and procedures etc.) [83].

Radon Gas in Conventional Houses. A wide range of reseacheshas been conducted concerning radon in homes all around the world.Particularly, acomprehensive study carried out the Cross-Canada Survey of Radon Concentrations in Homes by Health Canada. The duration of survey was two years and involvde compiling long-term (at least three months) indoor radon level measurements across Canada. The final result of the survey wasa platformproviding a better understanding and information of indoor radon concentrations, as well as protecting Canadians from the risks of long-term exposures to radon in the indoor environment [84].

The study involved about 18,000 participants contactedby telephone. In the first year of the study, nearly 9000 homes were selected randomlyacross Canada including specific territories. A long-term test for radon was conducted in the fall of 2009 and winter of 2010. To obtain accurate estimates, the sampling process involved diverse sources (Canada wide), rather than just a few large cities.Another advantage of providingsamples from a wide geographical distribution, is specifyinggeneral estimation of indoor radon gas concentrations countrywide [84].

All the participants from the first year of the survey were informed of the radon gas levels in their households. Information on radon gas remediation and mitigation techniques were suppliedto the households with high radon levels. The result also indicatedmost of the placescontain radon gas levels below the prescribed guideline ofradon level in Canada, which is 200 Bq/m^3. This conclusion reinforce the importance of monitoring indoor radon gas levels inside thehousesall across Canada. Although, the obtained results after the first year of the study confirmshigh levels of radon gas in aboutseven percent of Canadian residences. [84].

In general the results indicated wide range of distribution in the indoor radon concentration around houses in Canada. Moreover, certain areas containedmore extensive high radon levelthan others. For instance, Manitoba contained 24.8% higher radon levels than the guideline in Canada. New Brunswick, Saskatchewan and Yukon included 21.7%, 16.4% and 15.9% higherradon levels than the prescribed guideline of 200 Bq/m3 in Canada respectively. Radon gas levels in territories, Nunavut (zero pecent), Northwest Territories (3.9%), and Prince Edward Island (4.5%) were the lowestin the country [84].

These results changedin the second year of study. The results from Nunavut depict radon gas level less than the guideline level. Sixteen percent of all Health Regions sampled experienced same changes. The percentages do not mean that high levels of radon is not present in certainhousesin Nunavut and/or other health regions. Data only estimate an approximationof the number of Canadian houseswith radon levels higher than the Canadian radon guideline. For a resident, the most confident method to determineif a household containhigh radon levels is to carry out a test irrespective of his/her place[84].

One of the main motivationof previous study was to create awareness about the dangers of radon gas exposures especially in the indoor environment. Health Canada is working united with a couple of organizations to raise consciousness regarding risks of radon gas exposures. The Canadian Lung Association, Canadian Cancer Society and the Canadian Medical Association are all in co-operation with health Canada in this regard. In addition,Health Canada has presenteda number of resources, includingbrochures, factsheets and guides to help the Canadian gain knowledge about risks of radon and how to utilize protective measures against radon exposures [84].

Radon Gas in New and Renovated Houses. In the past few years, the recognition of radon gas as a potent indoor air pollutant and one of the major causes of devastatinghealth effects has encreased requiring certain proactive measures to curb radon's negativeeffects. To mitigate the effects of high indoor radon gas levels inside houses, new measures are suppliedtodecrease the future impactsof radon gas in new residences. Homebuyers interested in purchasing new housesneed to be informedof new measures that facilitate dealing with indoor radon gas levels. The most recent version of the National Building Code of Canada encapsulates several measures concerning reduction of radon in new houses. Besides, the provinces assume these building codes in respective provincial building codes which are

executed and isa requirement in every province [85].

Requirements respectingradon gas control of new housesstill vary across Canada. Requirements for radon control are non-existent in certain areas. Several homebuilders adopt these new measures voluntarily especially in locations identifiedwith high radon gas levels. Despite the fact some parts of the country are more likely exposed to radon gas than others, the gas occurs just almostanywhere. Radon gas is continually releases from soil and rock and penetratesin the air at significantlylow concentrations,however accumulated gas would concern residents as Long exposures of radon gas are harmful to human health [85].

In relatively radon-free areas, individual housescould contain higher radon gas than desired radon levels. Other than ordinary radon gas exposure factors, particular influencing factors might determine indoor radon gas levels, such asthe dynamics of the construction of a home and the lifestyle of those dwelling in a home. Neighbors who are living directly next to each other might have significantlydistinct radon gas levels in their houses. Over the years, radon has been distinguished as a prime cause of lung cancer particularly in smokers.Therefore, in the year 2007, Health Canada recommendedreducing the acceptable limit ofradon gas in buildingsas well as making it consistent with conventional radon limits ofinternational standards. New guidelines were also suppliedfor dealing with radon levels for new and existing houses. As mentioned in previus sections, currently the reference level is 200 Bq/m^3 for new Canadian houses[85].

In the process of building a new home, several approaches couldbe utilized to decreasethe negative effects of radon gas exposures. A numberof these approaches include installing an air barrier underneath the foundation slab and an airtight cover for the sump pit to restrain radon entry. All The above mentioned strategies are the preventive measures assumed by homebuilders in recent times. These measures are also embedded in the Canadian National Building Code. For homebuyers, the most excellent measure is communicating with new homebuildersin order to gain knowledge of building code requirements and radon control measures. There is no identifiedmethodto accurately predict in advance if a housewouldcontainhigh radon gas level, even after implementing radon preventive measures [85].

Therefore, it is essential for homebuyers to test radon gas level immediately oftheir new house. Several methods for radon testing are available including “do it yourself kit”, which is relatively more economical compared to performing byradon-testing professionals. Regularly, radon-tests confirm the most reliable results when they are conducted over a long period of time (at least 6 months). Active depressurization systems are presentedto reduce radon gas levels and prevent radon gas issuesin the future [85].

The United States Environmental Protection Agency (USEPA) confirms the positive effects of radon-resistant techniques in new buildings. Radon-resistant systems are passive techniques which when installed properly reduce radon gas levels. Besides, installation is straightforward andnot expensive. Moreover, installing these systems at the time of construction savesmoney on initial construction expensesinstead of fixing radon gas issuesin the future. Keeping the radon gas level below 4 pci/L (picocuries per liter) would also be achievable. In addition, Radon-resistant measures in new houses might reduce moisture levels and other indoor pollutants [86].

Influence of Climatic Parameters on Radon Gas Levels. Climate couldbe thought of as a more permanent weather condition of any specified geographical location. Climatic conditions usually last for an extended period of time (decades) compared to weather conditions, which last for several months depending on the season. The main outcomes of weather conditions that affect air pollutants are the atmospheric conditions namedair parameters including temperature, pressure and relative humidity. For a better comprehension of the impactsof the above-mentioned air parameters on the efficiency or radon gas detection, several studies have been conducted. V. Roca at al worked on the effect of air parameters on the detection efficiency of a radon monitor based on solid silicon detectors and radon daughter electrostatic collection. The study also involved a system capable of multiparameter acquisition which was employedto monitor radon, pressure, relative humidity and temperature [87].

Recently, solid silicon detector based radon monitors and radon daughter electrostatic collection have been adoptedin variousradon gas studies. A number of these studies include emanation power, rate of exhalation, radon daughter distribution etc. Employing radon monitors with solid silicon detector where the air conditions are controlled lead tosignificantreliability, high accuracy and high efficiency. The efficiency of radon daughter detection depend on the intensity of the electrostatic field as well as cell geometry. The accumulation of radon daughters on the surface of the detector also highly influences the efficiency of detection. These accumulation rely on the gas density and probability of recombination of polonium ions thatvarieswithtemperature, pressure and relative humidity changes [88,89].

Workingunder completely controlled air conditions is impracticable most of the time.Therefore making the monitor response a function of the air parameters, which represent the

air conditions, is essential. Efficiency reduction in radon gas daughter detection is almost exclusively attributed to the recombination of polonium ions with OH^- ions whose concentration depends on the relative humidity of the air. At a fixed value of relative humidity, which means fixed concentration of $[OH^-]$ in the cell air, the number of recombination every second is a fraction of the ion number. This is indicatedin the equation below:

$$\frac{dNt}{dt} = VnNt \quad (12)$$

where *Vn* represents the fraction of recombined ions while *Nt* is number of ions at time *t.* Integrating the above equation state the law ofthe process recombination which is quite similar to govering a radioactive decay. The equation is mentioned below:

$$Nt = Noe^{-(t-t0)Vn} \quad (13)$$

Vn represents the recombination velocity, which depends on the relative humidity. In a model proposed by Kopkel [90] the recombination velocity was a function of the OH^- ions concentration as indicates below:

$$Vn = 1.14\sqrt{[H2O} \ for \ [H2O] < 1800 \ Ppm \ (U < 10\%) \quad (14)$$

$$Vn = 47.9 \ for \ [H2O] \geq 1800 \ Ppm \ (U \geq 10\%) \quad (15)$$

Vn has units of S^{-1}, U represents the relative humidity and $[H_2O]$ is the concentration of water vapor in parts per million (ppm). Hence at a temperature of 27 °C, $[H_2O]$ of 1800 ppm, and a pressure of 0.1 MPa (Mega Pascals) the relative humidity wouldbe ten percent. As the relative humidity ranges from one to ten percent the recombination velocity *Vn* would vary from 1.14 to 47.6 s^{-1} respectively. Therefore, recombination time could be compared to the ion collection time which is about 1 Ms. This is accountable for the efficiency reductionwhen the relative humidity increases. Investigating the variation in efficiency as air parameters change was the major goal of the study. The experiments were conducted using the "RaMonA" multiparametric acquisition system, which is capable of carrying out simultaneous alpha particle spectrometry of radon daughters and monitoring other climatic parameters [91].

The climatic parameters and reference air atmosphere for controlled radon gas were obtained from measurements at the Metrology Institute for Ionizing Radiation in Italy [92]. Previously, the effects of temperature were studied in a university in Naples, where measurements were applied at fixed temperatures. Further, the outcomeswere cross-referenced with obtained results applyinga ready-made code. The ready-mode code was written on the basis of accurate description of the polonium ions movement in electrostatic cells. The experimental set up includes a "RaMonA" radon monitor supplyingpressure, relative humidity and temperature sensors, a second electrostatic cell, set of climatic sensors, a rotary pump (for air circulation and regulate internal air pressure), valves and filters (to facilitate inlet and outlet of air and radon enriched air).All items of experimental set up wereconnected in series. The start up radon gas was kept in a 33 cm^3 glass container. The radon gas is flowingin a closed circuit byan oil-free membrane pump [92].

To take measurements at different relative humilities, dry radon-free air was first spreadedthrough the circuit for certaintime. A bubbler filled with deionized water was employed. Varying relative humidities within the range of ten to ninety percentwas achieved in the equalcondition. Radon gas was first flewinto the system at relative humidity of ten percent. Applyingradon monitors included manyconstraints. The application of the monitorwaslimited atnormal pressure conditions i.e. (0.0990–0.101 MPa), however the pressure fluctuations at these conditions did not impactthe ion collection. Measurements were carried out at pressure values within the range of 0.02–0.10 Mpa. Changing the pressure was achieved by pumping out air from the circuit or pumping dry radon-free air into the circuit. Pumping was carried out until steady state condition. Pumping was turned off while data were taken.

In addition, the temperature that effected on collection efficiency were studied. For purposes of varying temperature, the electrostatic cell was placed in a temperature control chamber. The chamber possed Peltier cellsto maintain temperature within 0.1°C. The study was conducted at ambientenvironmental temperatures (15°C to 35°C) with a 5°C interval change in every successive variation. The first hour was considered for reaching steady state conditions. Then, five alpha spectra with a counting time of 600 s was readfrom the silicon detector under steady state conditions. Identifying accurate volume of the circuit was important, because volumeis a key variable in calculating the radon concentration. Besides, the concept of isothermal transformation of an ideal gas was employed in measuring the internal volume of the circuit. A vessel filled with argon at specifiedpressure, with identified volume was connected to the circuit.The pressure drop was measured. Then, the relative increase in volume was obtained. After three successive measurements the internal volume of the circuit was determined to be 5.46 ± 0.08 dm^3.

The results of the study indicates the detection

efficiency of radon daughters is fairly constant at relative humidities higher than fifty percent. For relative humidities lower than fifty percent, the detection efficiency does notpresentany systematic change.The efficiency fluctuates without any regular repeating pattern. For temperature modifications, the detection efficiency decreases to rise the temperature. In the temperature range of 15 to35 °C, the efficiency dropped by 2.2% for every degree Celsius. The detection efficiency drop was because of increasing ion mobility as a result of having higher thermal energy at higher temperature.Besides, the detection efficiency decreases with an increase in the air pressure. The efficiency is almost halved as the pressure is increasedfrom 0.02 to 0.09 Mpa. The reason ision mobility drop when less gas molecules are available in the air.

Environmental atmospheric conditions could be extended based on the relative humidity, temperature and air pressure. To conclude, radon detection is more probable at lower temperatures and pressures. In addition, at high relative humidities, radon detection is not effective. Therefore, most radon tests are conducted in the cold months of the year to guarantee acceptable results.

Exposures And Risk Assessment. Calculation of the Daily Intake. Shain C.D et al. conducted survey of surface water in specific areas around a phosphate plant in North Carolina [93]. Outcomesof this study revealed most of the wells contained lower than 500 Pci/L of ^{222}Rn; however the maximum concentration of radon obtained was 19,000 Pci/L. Reports indicated that a constant drinking of water containing radon in concentrations between 3000 and 7000 Pci/L would yield an equivalent dose of 0.5 Rem/yr (Roentgen equivalent in man per year), which isequivalent to about 1.4×10^{-3} Rem/yr. Besides, a constant intake of water from wells containing radon in concentration of 9000 pCi/l would yield a dose of 2 Rem/yr equivalent to 5.5×100^{-3} Rem/yr [93].

For exposures in general, recognizingcomplexity of individual exposures idicators and exposure pathways is remarkably significant. Fully investigation of the relationship between exposure effects in conjunction with chemical or natural carcinogens and lifestyle factors is challenging [94–96]. Therefore, determining effective dosages is practically not straighforward.The determination corresponds to a large population regardless of the geographical location and other influencing factors. Based on standard risk assessment methods [97–99] and certain assumptions daily intake in micrograms per kilogram of body weight can be calculated for an exposure pathway of either indoor or outdoor air, dust or drinking water. The following equation is employed to calculate daily intake:

$$DI = \frac{(Cp \times EFP)(Ir)(Tl)}{BW} \quad (16)$$

DI represents the daily intake; *Cp* is the concentration in pathway (outdoor air, indoor air, dust, soil, drinking water), *EFP* is the exposure frequency for a specific pathway, *IR* is the daily intake rate either by ingestion or inhalation, *TL* is the percentage of time each day spent indoor or outdoor and *BW* is the body weight at a specifiedlife stage.

Calculating the daily intake from beverages is possible with a specific technique, however as beverage intake are not considered as a radon gas source. The exposure frequency, *EFP* facilitates in the modification of estimations of the exposure frequency occurrence. An *EFP* value of oneis appliedin the case of a carcinogen, which is exposed to all the members of a population applying to outdoor exposures. An EFP of one hundred percent is applicable when a specifiedscenario involves intake amounts containing detectable levels,i.e.. people consuming well water contaminated with benzene. Using an EFP less than 100%, for instance 0.35 indicates that exposure occurs in 35% of the intake amount [100].

Further more after estimation of the average daily intake for a particular life stage, an approximation of exposure intake over a seventy year lifetimecouldbe calculatedby the below equation:

$$LSWdi = S(LSi \times Ti) \quad (17)$$

LSWdi is the life-stage weighted daily intake, *LSi* is the daily intake for a given life-stage *i*, *Ti* is the percentage of time spent in life-stage *i*, which is expressed as life stage time/total lifetime. With considering specified estimated lifetime, average daily intake in mg/kg of bodyweight and cancer effectiveness factors, estimating the associated Lifetime Excess Cancer Risk (LECR) is possible by the following equation:

$$LECR = Average\ daily\ intake \times cancer\ potency\ factor \quad (18)$$

It is important to note that even though this approach applies to most carcinogens, in the case of radon, the lifetime excess cancer risk is calculated using the total lifetime dose and not the average daily intake. The basic assumptions made to execute these estimated calculations are indicated in Table 6 [100,101].

Certain limited dose have also been recommended concerning safety of radon

TABLE 6
Basic assumptions for calculation of daily intake [100].

Characteristic	Units	Adults	Teenagers	Children	Young children	Infants
Age	Years	20 - 70	12 - 19	5 - 11	0.5 - 4	0 - 0.5
Body weight	Kilograms	70	57	27	13	6
Breathing	m^3/day	23	21	12	5	2
Drinking water	L/day	1.5	13	0.9	0.8	0.75
Dust ingestion	g/day	0.02	0.02	0.035	0.05	0.035
Time outdoor	% of 24 hrs.	6.25	6.25	8.2	8.2	8.2
Time indoor	% of 24 hrs.	93.75	93.75	91.8	91.8	91.8

exposures. The Canadian Nuclear Safety Commission (CNSC) has listed regulatory dose limits for Nuclear Energy Workers as well as public. For a nuclear energy worker, including pregnant energy workers, an effective dose for a one-year dosimetry period is 50 mSv (mSv: millisievert), which translates to 0.137 mSv daily and for a five-year dosimetry period, 100 mSv, which translates to 0.274 mSv daily. For people who are not nuclear energy workers, an effective dose for a calendar year is 1 mSv, which translates to 0.003 mSv daily. Several measures are utilized to ensure the above listed limits are satisfied. A typical measure is development of Radiation protection programs, which address potential harmful radon exposures [102].

Radon Gas as a Human Carcinogen. A carcinogen is simply any substance that has the ability to induce biological activities that lead to cancer in human cells, tissues or organs. The International Agency for Research on Cancer (IARC) has named a total of 109 environmental factors that couldcause increacing of humans' cancer risks. These include chemicals, exposures, mixtures, physical factors such as solar radiation, biological factors and lifestyle [103,104]. Up to 29% of cancers are due to environmental exposures of the air pollutants. The contributions of low amounts of radon gas exposures incarcinogens in the environment to cancer burdens have been underrated. New mitigating standards and measures are being considered in this regard. These measures are targeted at limiting exposures of environmental and occupational carcinogens as well as implementing diet and lifestyle measures against carcinogens [105,106].

Radon gas as an air pollutant is attributed to lung cancer, considerinit an established human carcinogen. Relationships have been discovered between lung cancer and occupational exposures, including radon gas amongst other substances. A number of studies suggest the risks of carcinogenic diseases depends on the dynamics of environmental exposures and individual immunity and vulnerability [107]. Therefore, the ultimate risk factors are the specific occupation and the particular substance being exposed. These exposures have less contribution to lung cancer thansmoking cigarette. Although studies have also indicatedthat these exposures cause an higher risk of lung cancer in smokers compared to non-smokers.

International Agency for Research on Cancer (IARC) categorizes carcinogens into four groups based on the levels of carcinogenic potential. The levels of carcinogenic potential are determined by the amount of available evidence that prove a specifiedcarcinogen is carcinogenic to a certain extent.

1- Group one carcinogens are the major substances entitled carcinogenic to humans with significantly sufficient proof.

2- Group two carcinogens are probably carcinogenic to humans with limited evidence of carcinogenicity to humans but sufficient proof in animals.

3- Group three carcinogens are possibly carcinogenic to humans but carcinogenic to experimental animals with limited evidence.

4- Group four carcinogens are probably not carcinogenic to humans but have been proven to be carcinogenic in animals[108, 109].

Radon gas being radioactive has the ability to disintegrate forming radon progeny or daughters. The radioactive decays by emitting alpha particles, thatadhere to aerosols, air-borne particles and dust [110]. These radioactive particles present in the air are inhaled and deposited in the bronchus or in certain parts of the respiratory tract. Besides, the particles have the ability to cause damage to the surrounding tissue and DNA in the respiratory tract leading to lung cancer or other respiratory diseases [111]. Radon gas levels in the outdoor surrounding is quite low, usually between fiveand fifteenBq/m3. Indoor radon levels are usually higher due to limitedspace and lowair circulation. Closed environments could contain significantly high radon gas levels over time. A numberof examples of these closed environments include caves, mines and plants utilizedfor water treatment.

Typical workplaces with radon exposures include underground vanadium and uranium mines,

oil refineries, hot springs and spas, wineries and natural caves [112]. Up to fourteen percent of lung cancers are attributed to radon present in the air [113]. The possibility of tumor formation depends on the duration and the intensity of exposure. Effects ofexposure might remainin the environment fortwenty-five years. The most importantimpactsof radon exposure were discovered in uranium miners. The effects were still noticableeven after twenty-fiveyears from the exposures time. Besides, in certain cases the effecting period is longer than twenty-five year [114,115]. Additionally, several studies conducted in various parts of the world concludedeven low radon exposures in indoor environment such as homes could cause health risks leading to lung cancers on certain people [116].

In 1997, an analysis representedthat radon gas exposure of up to fourpicocuries of radon per liter of air (pCi/L) in housesis capable of high risk oftumors development [117]. Recently, radon gas exposures in dwellings (mostly domestic buildings) are the second most feasible reason of lung cancers in smokers. In addition, radon penetration is the possible cause of lung cancers in non-smokers or never smokers. An increase of radon level by a value of 100 Bq/m^3 causes an increament in the risk of lung cancer by sixteen percent.

To conclude, the trend ofradon exposure doses and harmful effect on human life is linear, therefore risks of lung cancer might increase considerably with increasing of radon exposures. Research is still being carried out to confirm the higherrisks of lung cancers due to radon exposures, as existing data have not been able to fully verify the influence of radon on risks of lung cancer yet. Consiquesntly, a conclusion regarding the all negative effects of radon gas exposures on smokers and non-smokers coulod notbe validated. [118,119].

Radon Gas and Sick Building Syndrome. Sick Building Syndrome (SBS) has been investigated in recent years. SBS is connected to materials employedin building construction mostly for domestic houses. A number of these materials were once deemed to be reliablein terms of durability, insulation, strength and serviceability. Years later after these materials have been widely used; new developments in researches concerned possibility of harm to the health. A typical example is asbestos exposure. Asbestos is a particularly exceptionalbuilding material that implementinsulation, soundproofingwith a significant tensile strength. Never the less, discoveries have listed asbestos as one of the building materials capable of causing cancer. The term SBS is used to explicateparticularlynonspecific and boundless complaints of the occupants of dwellings. These complaints areremarkably general and usually involve acute health discomforts sue to time spent in a dwelling or construction [120].

Brightman and Moss described SBS as a health effect symptom that its etiology is not obviuos and should notbe attributed to any specific exposure in the building environment [121,122]. Another definition idicatesthe most common symptoms of SBS as nose, throat and eye irritation; itching and dry skin, undefined hypersensitivity, sensation of dry mucous membranes, headache, fatigue, cough, sneezing, nausea and dizziness. In general the studyrecommended, SBS does not involve just one specific symptom.SBS is associated with indoor air quality and in 1984 the World Well being Organization Committee reportedthat about thirty percent of both new and renovated buildings around the world are involvedwith indoor air quality problems. The conditions are uncertain for some buildings as well as being challenging for other buildings.

There is also the possibility of occupants in dwellings, reporting personal symptoms, which might not immediately be appeared asa SBS case. In these cases, the key to find a connection with SBS is an increase and consistent incidence of illness with most symptoms of SBS through the weeks. In Most cases, SBS symptoms are relieved as soon as the occupants leave the particular zone or area of residence. However there are other lingering impactsof some toxins, thatmight not be eliminated completely even after leaving the polluted residence.These might be long-term health effects on certain individuals.

Radon gas is not connected to SBS generally. The causes of radon gas exposures are defined clearly. Radons penetrations' effects onhuman health with noticable symptoms are also investigated properly.It is unidentified if there are any connections between radon and SBS. Considering nose irritation as an established symptom of SBS, radon gas ingestedin the body would bemainly harmful to the respiratory system. Radon gas is not recognized to cause any irritations to the respiratory system however that is the only relationship that might exist.

Sick building syndrome could be improved. Treating the recurring symptoms is the most important goal. Measures should be taken to improve the quality of air inside dwellings. A numberof these measures include detoxification, circulation, and ventilation. Othernatural techniquescouldbe employed in cleaning the air. The natural negative ionization and ultra violent waves from the sun facilitate in cleaning the air. Therefore, opening the curtain blinds to have the sunraysin the houses could be useful. In addition, opening the windows and doors helps ozone and adverse ions eliminate toxins from the air. Certain plants like Peace lilies, Golden Pothos, and Dracaenas also aid to remove toxins from the air.

Reduction Of Indoor Radon Gas Pollution. The only techniqueto adequately determine the risks of radon gas exposurein dwellings is by carrying out radon tests to determine radon levels. The occupancy pattern of any individual resident in any given houseor dwelling directly influences the hours radon gas exposure. Other factors such asindividual vulnerability and uptake could notbe estimated.Several economical interventions couldbe implemented,including encouraging occupants of dwellings to reduce the amount of time spent in the basement and lower floors, and try to spend time outdoors as much as possible [123,124]. For people who livein a rental places, a second levelunit is recommended to be rented if available. A basement or first levelshouldbe rented as long as the landlord can generateproper documentation of safe radon gas levels.

Five major strategies are presented to reduce radon exposures in dwellings. Two of these strategies help to reduce particle emissions in the houses; another two ones help to filter particles in the residences,andthe last one is based on proper air circulation in the target area.

***First strategy*:** Advising tobacco smokers to enroll in a termination program or to smoke outside the building.

***Second strategy*:**Advising families to reduce their dependence on wood heat or to consume EPA-certified wood stove [125,126,127].

***Third strategy*:** Reducingthe amounts of fine particles in the air. These particles could be radioactive, dust or other forms of particulates.Certaindesign of air cleaners have the ability to reduce radioactive particles in the air by 72-89% [128]. These air cleaners are equipped with high-grade carbon plus filter thatsignificantly reduce the particles in the air [129]. Besides,air to air heat exchangers reduce indoor radon gas exposures [130]. For tenants, mechanical filtration by portable air cleaning devices is particularly a properoption as can be employedwithout landlord or property managers permission . Several studies indicate that mechanical filtration of indoor air could be installed in the house. Wang et al. reported a 45% reduction in radioactive particles in the air by using a surgical mask placed over a household fan [131]. Hinds et al. presented a portable fan to decrease64% ofRadon Decay Products(RDP) and a ceiling fan to reduce54% of RDP [132]. Extra advantages of mechanical filtration of indoor airinclude reducing allergens, dust and other particles in the airwhich is capable of causing asthma.

***Fourth strategy*:** Employing electronic filters. Hinds et al. demonstrated electronic filters as a usefulmedium for radon gas reduction [132]. Theyreported 72% reduction ofRDP by means of an electronic filter. Mechanism of electronic filters enables them to convey surface charges. Kladder studied replacement of a one-inch electronic filter without duct modifications [133]. The study indicated,even if electronic filters were typically designedto reduce allergen antigens, they also could reduce RDP to below the EPA action level. Afterward, the measurements confirmed that RDP wasstill reduced significantlyalthough the radon gas level was still above 4 pCi/L. Thethreats of radon gas inhalation are remarkebly strongbyinhaling particles in the air because ofconveying radioactive substances into the body.

***Fifth strategy*:**Encouraging families to ventilate theirplaces by keeping doors and windows open. Outdoor radon gas concentration is quite negligible compared to the indoor ones. Radon gas trapped inside the house couldbe released into the outdoor environment by air circulation. Opening doors and windows yieldsalmost same results as air cleaning. Drawbacks of the fifth strategy are not being a long-term or permanent mitigation measure, and being dependent on weather conditions.

Employing exhaust fans, air exchangers, oscillating fans are another techniquespotentially improve indoor air quality, but not decrease the amount of radon gas in the houses. [134]. Besides, radon gas harmful doses leading to adverse health effects is because of inhalation of RDP and not the radon gas itself. Hence, reduction of RDP would not reduce the radon gas levels but would reduce the inhalation of RDP. Fans and air circulators drive radioactive particles against interior walls or towards the filter media helping the process of removingradon from the air. The main purpose is removing RDP from the breathing zones The only concern of employing the later technique is encreasing the household energy expences.In addition, direct measurement of RDP levels should be carried out to evaluate the performance of the conducting these methods over time.Therefore, RDP level is more serious than radon gas level. Federal statutes specify a working levels of 0.02 as the cleanup standard for RDP [135,136].

Mitigation of radon gas in buildings extends to the homebuilders. Certain measures are now being implement in the building of new homes. Most of these measures are installing certain radon-resistant features in building structures particularly the concrete slabs and foundations. The United States Environmental Protection Agency has made some recommended approaches to be incorporated in new buildings. A gas semi-permeable layer is placed underneath the slab or flooring system of houses to enable free movement of soil gas underneath the house. Afour-inch layer of clean gravel is the material of this process.

Gas permeable layers are utilized only in houses with a basement and slab-on-grade foundation. It isn't utilizedin houses having a crawlspace foundation. Then, plastic sheeting is placed on top of the gas permeable layer and under

the slab to restrain soil gas from entering the house. In the case of having crawlspaces, plastic sheeting is places on top the crawlspace floor. Sealing and caulking theopen areaunderthe concrete foundation reduce soil gas enteringto the home. Next, three or four inch gas tight pipe or PVC (polyvinylchloride) pipe is installed to run from the gas permeable layer to the roof of the house and vent radon and several other soil gases to the top of the house, and finally into the atmosphere [137].

Even after builting a new house with employing all above mentioned technique, certain devices could be installed to help reducing radon gas levels of the rooms. These devices include indoor and outdoor radon mitigation systems. The indoor radon mitigation system is similar to the system installed in new buildings. The only difference is the methodthe pipe run. A number ofpipes operate to the sides of the house instead of the roof. An exterior radon mitigation system consists of a ventilator at the outside of the building. The ventilator is mostly located behind the home out of the view of the street to avoid visual and noise concerns. The indoor and outdoor systems are equally efficient for reducing radon gas levels in houses. The outdoor mitigation system is more cost effective approach thanthe indoor one[138].

Other Emissions Related To Radon Gas. Radon is primarily sourced from soil and rock. Uranium is largely present in soil and rock underneath the top layer of the earth. Radon occurs as a result of uranium radioactive decay. Radon gas is capable of transfusing through rock and soil pores and enter buildings through cracks in concrete slabs, falls and walls. In thebuildings' basements vacuum can be formed by the soil causing a pressure difference and cosequently inducing radon entry into the house [139].

The other emissions related to radon are not fully developed. They include underground water, well water, hot springs, spas, uranium mines and caves. Radon gas includedinthe well waterwhich is being used during baths or other household activities couldcause radon gas penetrationinto the indoor air. Although radon gas emissions from water is considered slighter than radon emissions from soil [139]. Besides, radon gas is contained in certain building materials including concrete bricks and cement. Most of these materials are made from soil and other materials that potentially contain some radioactive elements, which can radioactively decay and emit radon progeny.

Discoveries in the southern part of Brazil indicatemany springs have certain radioactivity, principally due to the presence of radon [140,141]. Radon gas from soil and rock escapes into the surrounding fluid phase of groundwater and air. It depends on the quantity of uranium, radium and thoron, and the surface area of the solids in the springs [142]. Decent studies have been accommodated on the potential health effects of natural water consumption includingradio nucleotides. Most countries now adhere to the guidelinesprovided by the WHO [143].

The emissions of radon gas are moderately specific and significantlyrelated because of radon'snature. More emissions of radon gas would penetrate if it was produced commercially; consequently radon gas emissions are remarkablylimited and typically occur due to nature.

Summary And Outlook. Wide variety of indoor air pollutants are emmited in the world, however radon gas is recognized to be one of the most prominent because of its environmental impacts and harmful health effects Most studies on radon gas levels and indoor pollution propose the possibility of unidentified effects of radon gas on thehuman health and environment. Based on litreture, the concerns inradon gas exposures as an indoor air pollutant will not be fully satisfiedin the near future.

Radon gas is quite peculiar; it is emanated from soil and rock as a result of radioactive decay, and is significantly active in the environment. Studiesconfirm propagates of several radon isotopes and progeny, that could be harmful to human health as well. The most stable isotope of radon with the longest half-life, ^{222}Rn, hasexceedingly beenwell-considered. Consequently^{222}Rn is remarkablyimportant regardingindoor pollution investigations. Radon gas is capable of diffusing through rock and soil, which enables it to penetrateinto housesand other dwellings. Besides, Radon might enterbuildings through the piping system and open door/window or cracks offoundations and floors in the lower levels of buildings. Radon gas levels in the housesare not only determined by the amount of radon that is able to penetrateinto the area, but also by the lifestyle of the occupants and their attitudes towards the indoor air quality of their home.

Radon gas is a carcinogen. It is the second leading cause of Lung cancer in smokers and the prime cause of lung cancer in non-smokers. Several studies carried out on radon gasto demonstrate a potential danger of stomach cancer and other lethal health effects to the respiratory system. Radon enter the body typically by inhalation. In addition, radon gas could be penetrate to the body ingestion organs by drinkingunderground water containing radon in high levels.

The fundamental research of radon gas as a prime indoor pollutant has grown within the past years. Several measures are now being employedto decreaseits harmful effects. Most countries implement a national reference level for radon.

Radon reference levelserves as a guideline and indoor radon level should not exceeded limited value. Amount of radon gas in the outdoor environment is not amajor concern, because of the large size of the environment as well as the constant air movement and availability. The radon gas that radiates from soil and rock into the outdoor air couldare diluted by the excess amount of air present in the atmosphere. Therefore,considerably low radon concentration is contained outdoors. But, same condition is not presented for the indoor environment cases. Indoor air availability is regularly restricted particularly in cases of poor air circulation and ventilation. The boundaries of the indoor environment limit air circulation from outside and making radon gas dilution impracticable.

National radon reference levels named "building codes" are being considered in constructing new houses by law for a number of places around the world. These building codes forcesutilizingof preventive measures during construction. Generally, preventive measures involve the installation of several systems during construction to reduce radon gas exposures into the buildings. Consequently, containing lower level of indoor radon gas leads tolower level of risks of radon exposures' health effects in the houses. Besides, studies encourage reducing indoor radon gas penetrations for the purpose of improvement of air quality.

Radon gas mostly enter the body through the inhalation of Radon Decay Products, RDP. RDP present asradionuclide isotops in the air. Mechanical air cleaning is a technique to reduce presented RDP in the air. Air filters, oscillating fans and other mechanical devices couldbe employed for indoor air cleaning. By employing these techniques, RDP could be drivenfrom the breathing areas to the walls in the houses. A number of natural methodsare also possible, includingradon absorbing plants, that absorb radon gas from the indoor environment.

Generally, Radon testing is excessively essential for regulating indoor radon levels. Employing these techniques are the most reliable available means of improving safety aspects of mitigating radon gas exposures. Studies have indicatedhouses might still containhigh radon gas levels even if preventive measures are applied. A number of houses have long-lasting radon issueseven after adopting mitigation measures. In addition, radon gas tests help resident to determine if radon level is below or above the recommended limit. One of the challenges of employing radon tests is long processing time. A reliableradon test should last for at least sixmonths, because of the fluctuations of radon gas contained in the air. For assurance, a longer duration of time would reveal the excellent estimation radon level in the indoor environment. Conducting tests in certain areas inside the houses are more essential than other parts. In the lowest level of the house (typically basements)more radon gas exposures are expected to occur. In addition, radon gas levels vary through theseasons due to the changes in atmospheric conditions and air parameters. Therefore, the most suitable periods to conduct radon gas tests are in the fall and winter seasons because of being more detectable by the radon gas measures of at lower temperatures.

ACKNOWLEDGEMENTS

The authors would like to acknowledge University of Waterloo Library for provisions of the resources including online journals and articles needed for conducting the research of this paper. The content of the paper contain statements made by the authors only.

The authors have declared no conflict of interest.

REFERENCES

[1] James, L. M., and Virginia, R. M. (2003). Ernest Rutherford, the "true discoverer" of radon. Bull. Hist. Chem., 28(2), 76-78.

[2] Thornton, B. F., and Burdette, S. C. (2013). Recalling radon's recognition. Nature Chemistry, 5(9), 804.

[3] Mc Laughlin, J. (2013). Radon: Past, present and future. Romanian Reports of Physics, 58(Supplement.), S5-S13.

[4] Yamada, Y. (2003). Radon exposure and its health effects. Journal of health science, 49(6) 417-422.

[5] George, A. C. (2008). World history of radon research and measurement from the early 1900's to today. Paper presented at the AIP Conference Proceedings, 1034 20-33.

[6] Fry, C., and Thoennessen, M. (2013). Discovery of the astatine, radon, francium, and radium isotopes. Atomic Data and Nuclear Data Tables, 99(5), 497-519.

[7] Laughlin, J. M. (2012). An historical overview of radon and its progeny: Applications and health effects. Radiation Protection Dosimetry, 152(1-3), 2-8.

[8] Iloeje, U. H., and Redlich, C. A. (2000). Indoor air pollution: An update for the clinician. Clinical Pulmonary Medicine, 7(3), 128-133.

[9] Groves-Kirkby, C. J., Timson, K., Shield, G., Denman, A. R., Rogers, S., Campbell, J., . . . Ekberg, M. (2014). Influences motivating smokers in a radon-affected area to quit

smoking. Perspectives in Public Health,134(1), 44-56.
[10] Weitzman, M., Baten, A., Rosenthal, D. G., Hoshino, R., Tohn, E., and Jacobs, D. E. (2013). Housing and child health. Current Problems in Pediatric and Adolescent Health Care, 43(8), 187-224.
[11] Health Canada. What are the Health Effects of Radon?. Available from: http://www.hc-sc.gc.ca/ewh-semt/radiation/radon/effects-effets-eng.php (accessed on 1/31/2014).
[12] Health Canada. How to test for radon? Available from: http://www.hc-sc.gc.ca/ewh-semt/radiation/radon/testing-analyse-eng.php (accessed on 1/31/2014).
[13] Health Canada. Radon: Is It in your Home? Available from: http://www.hc-sc.gc.ca/ewh-semt/pubs/radiation/radon_brochure/index-eng.php#a8 (accessed on 1/31/2014).
[14] Clifford, S., Hevey, D., and Menezes, G. (2012). An investigation into the knowledge and attitudes towards radon testing among residents in a high radon area. Journal of Radiological Protection, 32(4), N141-N147.
[15] Chiu, Y., Wang, X., Qiu, H., and Yu, I. T. (2010). Risk factors for lung cancer: A case-control study in Hong Kong women. Cancer Causes and Control, 21(5), 777-785.
[16] Bissett, R. J., and McLaughlin, J. R. (2010). Radon. Chronic Diseases in Canada, 29 Suppl 1, 38-50.
[17] Taylor-Lange, S. C., Juenger, M. C. G., and Siegel, J. A. (2014). Radon emanation fractions from concretes containing fly ash and metakaolin. Science of the Total Environment, 466-467, 1060-1065.
[18] Taylor-Lange, S. C., Stewart, J. G., Juenger, M. C. G., and Siegel, J. A. (2012). The contribution of fly ash toward indoor radon pollution from concrete. Building and Environment, 56, 276-282.
[19] Sutcliffe, J. (2010). Radiation a new paradigm...societal impacts. Mutation Research - Fundamental and Molecular Mechanisms of Mutagenesis, 687(1-2), 67-72.
[20] Prat, O., Vercouter, T., Ansoborlo, E., Fichet, P., Perret, P., Kurttio, P., and Salonen, L. (2009). Uranium speciation in drinking water from drilled wells in southern finland and its potential links to health effects. Environmental Science and Technology, 43(10), 3941-3946.
[21] Huxol, S., Brennwald, M. S., Henneberger, R., and Kipfer, R. (2013). 220Rn/222Rn isotope pair as a natural proxy for soil gas transport. Environmental Science and Technology, 47(24), 14044-14050.
[22] Jon, E. S. Radon Gas: A Geological Hazard in Arizona. Available from: http://www.azgs.az.gov/HomeOwners-OCR/radongasinarizona.pdf (accessed 2/3/2014).
[23] Air Chek, Inc. Radon Fact Sheet. Available from: http://www.radon.com/radon/radon_facts.html (accessed 2/3/2014).
[24] Kal'muk, S. D., Makitra, R. G., and Pal'chikova, E. Y. (2007). Solubility and distribution of radon in organic solvents. Russian Journal of General Chemistry, 77(4), 503-508.
[25] Patricia A. Shapley. Radon and other noble gases. University of Illinois at Urbana-Champaign, Available from: http://butane.chem.uiuc.edu/pshapley/GenChem1/L6/web-L6.pdf (accessed 2/3/2014).
[26] Gary, J. S. Radon (Rn), Available from: http://www.britannica.com/EBchecked/topic/489337/radon-Rn (accessed 2/3/2014).
[27] Anne, M. H. Radon Chemical and Physical Properties. Available from: http://chemistry.about.com/od/elementfacts/a/radon.htm (accessed 2/3/2014).
[28] Ferreira, A. G. M., and Lobo, L. Q. (2007). On the vapor pressure of radon. Journal of Chemical Thermodynamics, 39(10), 1404-1406.
[29] Michael, P. Radon Crystal Structure, Available from:http://www.pilgaard.info/Elements/Radon/Crystallography.htm (accessed 2/3/2014).
[30] Lee, K. Y., Yoon, Y. Y., and Ko, K. S. (2010). Determination of the emanation coefficient and the henry's law constant for the groundwater radon. Journal of Radioanalytical and Nuclear Chemistry, 286(2), 381-385.
[31] Keramatollah, A., kbari1, J.Simulation of Radon Mitigation in Residential Building with Ventilation. Available from: http://www.scansims.org/sims2008/22.pdf (accessed on 2/3/2014).
[32] Canadian Lung Association. Pollution and Air Quality. Available from: http://www.lung.ca/protect-protegez/pollution-pollution/indoor-interieur/radon-radon_e.php (accessed on 2/3/2014).
[33] Pinto, A. M. F., Barreto, A. A., Moreira, R. M., and Tambourgi, E. B. (2013). Extended application of radon as a natural tracer in oil reservoirs
[34] Erickson, B. E. (2004). The therapeutic use of radon: A biomedical treatment in europe: An "alternative" remedy in the united states. Paper presented at the Abstracts of the Pacific Basin Nuclear Conference, 177.
[35] Manohar, S. N., Meijer, H. A. J., and Herber, M. A. (2013). Radon flux maps for the

Netherlands and Europe using terrestrial gamma radiation derived from soil radionuclides. Atmospheric Environment, 81, 399-412.

[36] Joshuah, W. The Uses for Radon, Available from: http://www.ehow.com/info_8073940_uses-radon.html (accessed on 2/3/2014).

[37] United States Environmental Protection Agency. A Citizen's Guide to Radon. Available from: http://www.epa.gov/radon/pubs/citguide.html #howdoes (accessed on 2/3/2014).

[38] Sola, P., Srisuksawad, K., Loaharojanaphand, S., O-Manee, A., Permnamtip, V., Issarapan, P., and Thummagarun, L. (2013). Radon concentration in air, hot spring water, and bottled mineral water in one hot spring area in thailand. Journal of Radioanalytical and Nuclear Chemistry, 297(2), 183-187.

[39] Mudd, G. M. (2008). Radon releases from australian uranium mining and milling projects: Assessing the UNSCEAR approach. Journal of Environmental Radioactivity, 99(2), 288-315.

[40] Kumar, A., and Chauhan, R. P. (2013). Back diffusion correction for radon exhalation rates of common building materials using active measurements. Materials and Structures/Materiaux Et Constructions, 1-10.

[41] http://www.inive.org/medias/ECA/ECA_Report15.pdf

[42] Kropat, G., Bochud, F., Jaboyedoff, M., Laedermann, J., Murith, C., Palacios, M., and Baechler, S. (2014). Major influencing factors of indoor radon concentrations in switzerland. Journal of Environmental Radioactivity, 129, 7-22.

[43] Moreno, V., Bach, J., Baixeras, C., and Font, L. (2014). Radon levels in groundwaters and natural radioactivity in soils of the volcanic region of la garrotxa, spain. Journal of Environmental Radioactivity, 128, 1-8.

[44] Kumru, M. N., and Oznur, O. (1994). Investigations of some parameters of the collector chamber method for the determination of radium-226. Applied Radiation and Isotopes, 45(11), 1113-1114.

[45] Tabar, E., Kumru, M. N., Saç, M. M., Icedil, hedef, M., Bolca, M., and Özen, F. (2013). Radiological and chemical monitoring of dikili geothermal waters, western turkey. Radiation Physics and Chemistry, 91, 89-97.

[46] Kumru, M. N. (1992). Determination of radium-226 in environmental samples by the collector chamber method. Applied Radiation and Isotopes, 43(8), 1031-1034.

[47] UNSCEAR (2000) Sources and effects of ionization radiation, report of the United Nation Scientific Committee on the effects of atomic radiation to the General Assembly, with scientific annexes. United Nations, New York.

[48] Sola, P., Srisuksawad, K., Loaharojanaphand, S., O-Manee, A., Permnamtip, V., Issarapan, P., and Thummagarun, L. (2013). Radon concentration in air, hot spring water, and bottled mineral water in one hot spring area in thailand. Journal of Radioanalytical and Nuclear Chemistry, 297(2), 183-187.

[49] Salih, I., Pettersson, H., and Lund, E. (2000). Determination of 222Rn and 226Ra in water using a large volume ionisation chamber. Journal of Environmental Radioactivity, 48(2), 235-245.

[50] Radon Analytics. Measuring Devices for radon. Available from http://www.radon-analytics.com/ (accessed 2/16/2014).

[51] Yarmoshenko, I., Onishchenko, A., and Zhukovsky, M. (2013). Establishing a regional reference indoor radon level on the basis of radon survey data. Journal of Radiological Protection, 33(2), 329-338.

[52] WHO (2009). World Health Organization Handbook on Indoor Radon. A public Health Perspective. Available from:http://goo.gl/0CFXAx (Accessed 3/11/2014)

[53] Gustav, A. Radon Legislation and National Guidelines. Available from: http://www.elradon.com/web/wp-content/uploads/2011/08/Radon-Legislation-and-National-Guidelines.pdf (Accessed 3/15/2014).

[54] ICRP (International Commission on Radiological Protection) Statement on Radon. Available from: http://www.icrp.org/docs/ICRP_Statement_on_Radon_AND_Lung_cancer_risk_from_radon_and_progeny(for_consultation).pdf (Accessed 3/11/2014).

[55] EC (European Commission). European guidelines on radiation protection in dental radiology. Available from: http://ec.europa.eu/energy/nuclear/radiation_protection/doc/publication/136.pdf (Accessed 3/11/2014)

[56] Hugh S., David, F. (2005). An Evaluation of Radon Reference Levels and Radon Measurement Techniques and Protocols in European Countries. Available from: http://www.rpii.ie/RPII/files/b5/b5991662-b082-4fc4-a90e-29e74c6bd6d7.pdf (Accessed 3/11/2014).

[57] UNSCEAR, 1993: United Nations Scientific Committee on the Effects of Atomic Radiation. Report to the General Assembly, with scientific annexes. New York. Untied

Nations 54. ISBN 92-1-142200-0.

[58] Swedjemark, G. A. (1997). Exposure to natural radiation. In Proceedings New Risk Frontiers, 10th Anniversary. The Society for Risk Analysis - Europe, Stockholm 1977, pp. 7-16.

[59] Kendall, G. M., Fell, T. P., Phipps, A. W.(1988). A model for evaluating doses from radon in drinking water. NRPB Radiological Protection Bulletin. 1988:97.

[60] EU (European Commission). (2000).Radiation Protection 122:Practical use of the concepts of Clearance and Exemption (Part 1): Guidance on general clearance levels for practices: Recommendations of the group of Experts established under the terms of Article 31 of the Euratom Treaty, Available from: http://ec.europa.eu/energy/nuclear/radiation_protection/doc/publication/122_part1.pdf (Accessed 3/11/2014).

[61] National Research Council, 1998: Risk Assessment of Radon in Drinking Water. Committee on the Risk Assessment of Exposure to Radon in Drinking water. Board on Radiation Effects Research. Commission on Life Sciences. National Research Council. National Academy Press. Washington, DC, 1998.

[62] BC Centre for Disease Control. Radon in Household Well Water: Contributions to Indoor Air Radon Concentrations. Available from: http://ncceh.ca/sites/default/files/BCCDC-Radon_Well_Water_Dec_2011.pdf (Accessed 3/21/2104).

[63] National Research Council; Committee on Risk Assessment of Exposure to Radon in Drinking Water. Risk assessment of radon in drinking water. Washington, DC: National Academies Press; 1999. Available from: http://www.nap.edu/openbook.php?record_id=6287.

[64] Nazaroff, W. W., Doyle, S. M., Nero, A. V., Sextro, R. G. Potable water as a source of airborne 222Rn in U.S. dwellings: a review and assessment. Health Phys. 1987 Mar;52(3):281-95.

[65] Shaikh, A. N., Ramachandran, T. V., and Vinod Kumar, A. (2003). Monitoring and modelling of indoor radon concentrations in a multi-storey building at mumbai, India. Journal of Environmental Radioactivity, 67(1), 15-26.

[66] UNSCEAR, 1993. United Nations Scientific Committee on the Effect of Atomic Radiation. Sources and biological effects of ionizing radiation. United Nations, New York.

[67] Jones, A. P. (1999). Indoor air quality and health. Atmospheric Environment, 33(28), 4535-4564.

[68] Subba Ramu, M. C., Shaikh, A. N., Muraleedharan, T. S., Ramachandran T. V. Measurement of indoor radon in dwellings using nuclear track etch detectors. Bulletin of Radiation Protection, 10 (1987), pp. 49–52.

[69] Subba Ramu, M. C., Muraleedharan, T. S., and Ramachandran, T. V. (1988). Calibration of a solid state nuclear track detector for the measurement of indoor levels of radon and its daughters. Science of the Total Environment, 73(3 0715), 245-255.

[70] UNSCEAR, 1982. United Nations Scientific Committee on the Effect of Atomic Radiation, Sources and biological effects of ionizing radiation. United Nations, New York.

[71] Man, C. K., and Yeung, H. S. (1999). Modeling and measuring the indoor radon concentrations in high-rise buildings in Hong Kong. Applied Radiation and Isotopes, 50(6), 1131-1135.

[72] Jacobi, W. (1972). Activity and potential alpha-energy of 222 radon-and 220 radon-daughters in different air atmospheres. Health Physics, 22(5), 441-450.

[73] Porstendörfer, J. (1994). Properties and behaviour of radon and thoron and their decay products in the air. Journal of Aerosol Science, 25(2), 219-263.

[74] Kuntson, E. O.Modelling indoor radon concentrations of radon decay products. W.W. Nazaroff, A.V. Nero (Eds.), Radon and its decay products in indoor air, John Wiley, New York (1988), pp. 161–202.

[75] Vinod Kumar, A., Sitaraman, V., Oza, R. B., and Krishnamoorthy, T. M. (1999). Application of a numerical model for the planetary boundary layer to the vertical distribution of radon and its daughter products. Atmospheric Environment, 33(28), 4717-4726.

[76] Holt, T., and Raman, S. (1988). A review and comparative evaluation of multilevel boundary layer parameterizations for first-order and turbulent kinetic energy closure schemes. Reviews of Geophysics, 26(4), 761-780.

[77] Duynkerke, P. G. (1988). Application of the E - ε turbulence closure model to the neutral and stable atmospheric boundary layer. Journal of the Atmospheric Sciences, 45(5), 865-880.

[78] Huang, C. and Raman, S. (1991). Numerical simulation of January 28 cold air outbreak during GALE part I: The model and sensitivity tests of turbulence closures. Boundary-Layer Meteorology, 55(4), 381-407.

[79] Bhumralkar, C. M.Numerical experiments on the computation of surface temperature in atmospheric general circulation model. Journal of Applied Meteorology, 14 (1975), pp. 1246–1258.

[80] Deardorf, J. W. Efficient prediction of ground surface temperature and moisture with inclusion of a layer of vegetation. Journal of Geophysics Research, 83 (1978), pp. 1889–1903.

[81] Louis, J. (1979). A parametric model of vertical eddy fluxes in the atmosphere. Boundary-Layer Meteorology, 17(2), 187-202.

[82] Stull, R. B. (1988).An introduction to boundary layer meteorology. Academic Publishers, Kluwer, The Netherlands.

[83] Salthamer, T., Mentese, S., Marutzky, R. (2008). Formaldehyde in the indoor environment. Chem. Rev. 2010, 110, 2536-2572.

[84] Health Canada. Cross-Canada Survey of Radon Concentrations in Homes Year 1 Interim Report. Available from:http://www.chba.ca/uploads/Policy%20Archive/2010/Health%20Canada%20Radon%20Survey%2015%20Dec%202010.pdf (accessed 3/3/2014).

[85] Canadian Home Builders' Association. Radon and New Home Construction. Available from: http://www.chba.ca/buying/why-new/radon-and-new-home-construction.aspx (accessed 3/3/2014).

[86] USEPA (United States Environmental Protection Agency).What are radon-resistant features?. Available from:http://www.epa.gov/radon/pubs/hmbyguid.html#4 (accessed 3/3/2014).

[87] Roca, V., De Felice, P., Esposito, A. M., Pugliese, M., Sabbarese, C., and Vaupotich, J. (2004). The influence of environmental parameters in electrostatic cell radon monitor response. Applied Radiation and Isotopes, 61(2-3), 243-247.

[88] Hopke, P. K. (1989). Use of electrostatic collection of 218Po for measuring rn. Health Physics, 57(1), 39-42.

[89] De Martino, S., Sabbarese, C., and Monetti, G. (1998). Radon emanation and exhalation rates from soils measured with an electrostatic collector. Applied Radiation and Isotopes, 49(4), 407-413.

[90] Nazaroff, W.W., Nero, A.V. (1988). Radon and its Decay Products in Indoor Air. Wiley, New York.

[91] Pugliese, M., Baiano, G., Boiano, A., D'Onofrio, A., Roca, V., Sabbarese, C., Vollaro,P. A compact multiparameter acquisition system for radon concentration studies. Appl. Radiat. Isot. 53 (2000), p. 2

[92] De Felice, P., and Myteberi, X. (1996). The 222Rn reference measurement system developed at ENEA. Nuclear Instruments and Methods in Physics Research, Section A: Accelerators, Spectrometers, Detectors and Associated Equipment, 369(2-3), 445-451.

[93] Shain, C. D., Watson Jr., J. E., and Fong, S. (1979). An evaluation of 226Ra and 222Rn concentrations in ground and surface water near a phosphate mining and manufacturing facility. Health Physics, 37(6), 779-783.

[94] Clapp, R. W., Jacobs, M. M., Loechler, E. L. Environmental and occupational causes of cancer: new evidence 2005–2007. Rev Environ Health 2008, 23:1–38.

[95] Kriebel, D. Cancer prevention through a precautionary approach to environmental chemicals. (2011). Rev Environ Health 2011, 24:271–278.

[96] Merlo, D. F, Filiberti, R., Kobernus, M., Bartonova, A., Gamulin, M., Ferencic, Z.,

Dusinska, M., Fucic, A. Cancer risk and the complexity of the interactions between environmental and host factors: HENVINET interactive diagrams as simple tools for exploring and understanding the scientific evidence. Environ Health 2012, 11:S9.

[97] Health Canada Environmental Health Assessment Services Safe Environments Programme: Federal Contaminated Site Risk Assessment in Canada Part I: Guidance on Human Health Preliminary Quantitative Risk Assessment (PQRA). Ottawa: Government of Canada; 2004.

[98] Health Canada Great Lakes Health Effects Program: Investigating Human Exposure to Contaminants in the Environment: A Handbook for Exposure Calculations. Ottawa: Government of Canada; 1995.

[99] Health Canada Environmental Health Assessment Services Safe Environments Programme: Federal Contaminated Site Risk Assessment in Canada Part II: Health Canada Toxicological Reference Value (TRVs). Ottawa: Government of Canada; 2004.

[100] Setton, E., Hystad, P., Poplawski, K., Cheasley, R., Cervantes-Larios, A., Keller, C. P., and Demers, P. A. (2013). Risk-based indicators of Canadians' exposures to environmental carcinogens. Environmental Health: A Global Access Science Source, 12(1).

[101] Radionuclide Carcinogenicity Slope Factors: HEAST User Guide. Available from: http://www.epa.gov/rpdweb00/heast/index.html .2-8-2012 (accessed 3/26/2014).

[102] http://www.nwmo.ca/uploads/DGR%20PDF/Licensing/Radon-Assessment.pdf

[103] IARC Monographs on the Evaluation of Carcinogen Risks to Humans. Available from:http://monographs.iarc.fr/index.php (acc essed on 3/25/2014).
[104] IARC (International Agency for Research on Cancer). Monographs on the Evaluation of Carcinogenic Risks to Humans - Classifications. Available from:http://monographs.iarc.fr/ENG/Classific ation/index.php (accessed on 3/25/2014).
[105] Sethi, T. K., El-Ghamry, M. N., and Kloecker, G. H. (2012). Radon and lung cancer. Clinical Advances in Hematology and Oncology, 10(3), 157-164.
[106] Clapp, R. W., Jacobs, M. M., and Loechler, E. L. (2008). Environmental and occupational causes of cancer: New evidence 2005-2007. Reviews on Environmental Health, 23(1), 1-37.
[107] Alberg, A. J, Ford, J. G, Samet, J. M. (2007). Epidemiology of lung cancer. ACCP evidence-based clinical practice guidelines. Chest 2007; 132: 29S-55S.
[108] International Agency for Research on Cancer. Barriers to early breast cancer diagnosis in the South African setting. Available from: http://www.iarc.fr/ (accessed on 3/25/2014).
[109] Fernández, R., Rubinos, G., Exposito, A. R., and Martinez, C. (2012). Lung cancer of occupational origin. Current Respiratory Medicine Reviews, 8(6), 412-417.
[110] Porstendorfer, J. Properties and behaviour of radon and thoron and their decay products in the air. J Aerosol Science 1994; 25: 219 - 63.
[111] WHO (2010). Guidelines for indoor air quality. Selected pollutants. Radon. ISBN 978 92 890 02134. Page 347-375.
[112] Perez de las Casas M., Fernandez Infante, B. (2005). Occupational lung cancer. An Sist Sanit Navar 2005; 28 (Suppl 1): 101-6.
[113] Lubin, J. H., Boice J. D., Edling, C. (1995). Lung Cancer in radon exposed miners and estimation of risks from indoor exposure. J Natl Cancer Inst 1995; 85: 817-27
[114] Schubauer-Berigan, M. K, Daniels, R. D, Pinkerton, L. E. Radon exposure and mortality among white and American Indian uranium miners: an update of the Colorado Plateau cohort. Am J Epidemol 2009; 169: 718-30.
[115] Brüske- Honhlfeld I, Rosario AS, et al.. Lung cancer risk among former uranium miners of the WISMUT Company in Germany. Health Phys 2006; 90: 208-16.
[116] NTP (National Toxicology Program). (2011). NTP 12th Report on Carcinogens. US Department of Health and Human Services.
[117] WHO (World Health Organization). Zeeb H, Shannoun F, editores Handbook on indoor radón: a public health perspective. Geneve, Switzerland: WHO Library cataloguing-in-Publicationa Data; 2009.
[118] Couraud, S., Zalcman, G., Milleron, B., Morin, F., and Souquet, P. (2012). Lung cancer in never smokers - A review. European Journal of Cancer, 48(9), 1299-1311.
[119] Oh, S. S., Koh, S. B., and Yong, S. J. (2012). Radon and environmental diseases. Journal of the Korean Medical Association, 55(3), 223-229.
[120] Colin, L. Radon truth: Exploring the facts about radon.Available from:http://radontruth.com/sick-building-syndrome/ (Accessed 4/7/2014)
[121] Godish, T. (1995). Sick Buildings: Definition, Diagnosis and Mitigation. Lewis Publishers: Boca Raton, FL.
[122] Brightman, H. S., Moss, N., Samet, J. M., Spengler, J. D., McCarthy, J. F., Eds. Indoor Air Quality Handbook. (2001) McGraw Hill: New York.
[123] Barnes, G., Fisher, B., Postma, J., Harnish, K., Butterfield, P., and Hill, W. (2010). Incorporating environmental health into nursing practice: A case study on indoor air quality. Pediatric Nursing, 36(1), 33-39, 52; quiz 40.
[124] Hancock, T. (2002). Indicators of environmental health in the urban setting. Canadian Journal of Public Health, 93(S1), S45–S51.
[125] Lichtenstein, E., Boles, S. M., Lee, M. E., Hampson, S. E., Glasgow, R. E., and Fellows, J. (2008). Using radon risk to motivate smoking reduction II: Radonmized evaluation of brief telephone counseling and a targeted video. Health Education Research, 23(2), 191–201.
[126] Mendez, D., Warner, K. E., and Courant, P. N. (1998). Effects of radon mitigation vs smoking cessation in reducing radon-related risk of lung cancer. American Journal of Public Health, 88(5), 811–812.
[127] Noonan, C. W., Ward, T. J., Navidi, W., Sheppard, L., Bergauff, M., and Palmer, C. (2011). Assessing the impact of a wood stove replacement program on air quality and children's health. Research Report/Health Effects Institute, 162, 3–37; discussion 39-47.
[128] Hinds, W. C., Rudnick, S. N., Maher, E. F., and First, M. W. (1983). Control of indoor radon decay products by air treatment devices. Journal of Air Pollution Control Association, 33(2), 134–136.
[129] Yasuoka, Y., Ishikawa, T., Tokonami, S., Takahashi, H., Sorimachi, A., and Shinogi, M. (2009). Radon mitigation using an air cleaner. Journal of Radioanalytical and Nuclear Chemistry, 279(3), 885–891.

[130] Hellevang, K., and Pedersen, C. (2009). Air-to-air heat exchangers for healthier energy-efficient homes. Fargo: North Dakota State University Extension Service.
[131] Wang, J., Meisenber, O., Chen, Y., Karg, E., and Tschiersch, J. (2011). Mitigation of radon and thoron decay products by filtration. Science of the Total Environment, 409, 3613–3619.
[132] Hinds, W. C., Rudnick, S. N., Maher, E. F., and First, M. W. (1983). Control of indoor radon decay products by air treatment devices. Journal of Air Pollution Control Association, 33(2), 134–136.
[133] Kladder, D. L. (2011). Colorado vintage companies case report and technical document 16–03. Colorado Springs, CO: Case Report and technical document. Progeny Group Limited.
[134] EPA (2009). Residential air cleaners: A summary of available information. (EPA 402-F-09002). Available from: http://www.epa.gov/iaq/pubs/airclean.html (Accessed 3/25/2014).
[135] Code of Federal Regulations. (2012). Title 40 Protection of the Environment Guidance for implementation, 40 CFR, Chapter 1, Sub chapter F, Subpart B, Section 192.12 Pub. L. No. 92-314.
[136] Larsson, L. S. (2014). Risk-reduction strategies to expand radon care planning with vulnerable groups. Public Health Nursing.
[137] USEPA (united Stated Environmental Protection Agency. Home Buyer's and Seller's guide to radon. Available from: http://www.epa.gov/radon/pubs/hmbyguid.html#4.(Accessed 4/11/2014).
[138] RHMM (Radon home measurement and mitigation) Inc. Respecting your Family's need for a Healthy Indoor Environment. Available from: http://www.radon-mitigation.org/services-mitigation.htm (Accessed 4/11/2014).
[139] RTCA (Radon Testing Cooperation of America). Sources of Radon in the Home.Available from: http://www.rtca.com/radon_sources.asp (Accessed 4/11/2014).
[140] Bonotto, D. M. (2014). 222Rn, 220Rn and other dissolved gases in mineral waters of southeast Brazil. Journal of Environmental Radioactivity, 132, 21-30.
[141] DFPM (Division for Supporting the Mineral Production). (1966).The Mining Code, the Mineral Waters Code and How Applying Research in a Mineral Deposit, eighth ed.DFPM, Rio de Janeiro.
[142] Flügge, S., and Zimens, K. E. (1939). The determination of major grain and diffusion constant of the emaniervermogen (the theory of emanier method). Z.Phys.Chem, 179-220.
[143] WHO (World Health Organization) Guidelines for Drinking Water Quality, fourth ed. (2011). WHO Press, Geneva (2011).

Received: **31.01.2016**
Accepted: **07.07.2016**

CORRESPONDING AUTHOR

Sabah A. Abdul-Wahab
Department of Mechanical and Industrial Engineering, College of Engineering, Sultan Qaboos University, P.O. Box 33, Al-Khod, Postal Code 123, Muscat SULTANATE OF OMAN

e-mail: sabah1@squ.edu.om

© by PSP Volume 25 – No. 10/2016, pages 4439-4446 Fresenius Environmental Bulletin

ISOLATION AND IDENTIFICATION OF *GLOMUS INTRARADICES* IN SALT-ALKALI GRASSLAND AND ITS EFFECTS ON SALT TOLERANCE OF *TRIFOLIUM REPENS*

Chunxue Yang[1], Fei Chen[1], Lili Li[1], Cong Li[2], Dafu Yu[3], Jixiang Lin[2*]

1. College of Landscape Architecture, Northeast Forestry University, Harbin, 150040, China.
2. Laboratory of Saline-Alkali Vegetation Ecology Restoration in Oil Field, Ministry of Education, Alkali Soil Natural Environmental Science Center, Northeast Forestry University, Harbin, 150040, China.
3. Key Laboratory of Vegetation Ecology of Ministry of Education, Institute of Grassland Science, Northeast Normal University, Changchun, 130024, China

ABSTRACT

The arbuscular mycorrhizal fungi (*Glomus intraradices*) in Songnen salt-alkali grassland was isolated and identified by morphology and molecular biological methods, then inoculated with *Trifolium repens* to research its effect on the salt-alkali tolerance of *Trifolium repens*. The results showed that net photosynthetic rate (Pn) and transpiration rate (Tr) of the *T. repens* inoculated by *G. intraradices* were significantly enhanced. Under salt-alkali stress, stomatal conductance (Gs) of the mycorrhizal plant was obviously higher than that of the non mycorrhizal plant. Intercellular CO_2 concentration (Ci) was significantly lower than that of the non mycorrhizal plant. In addition, the chlorophyll content of mycorrhizal plant leaves augmented. The activity of the two protective enzymes SOD and CAT increased in mycorrhizal plants, and the soluble protein content was also increased. These results showed that inoculation with *G. intraradices* can make *T. repens* leaves maintain higher defense enzyme activity and photosynthetic capacity. The results can help to understand the effects of *G. intraradices* on the salt tolerance of plant and provide important theoretical basis on its application on the restoration of salt-alkali grassland.

KEYWORDS:
Arbuscular mycorrhizal; *Glomus intraradices*; Salt-alkali stress; *Trifolium repens*

INTRODUCTION

Arbuscular mycorrhizal fungi (AMF) is widely distributed in various terrestrial ecosystems. It plays a vital role in improving the soil evolution, maintaining soil health and enhancing the grain yield[1]. Many previous studies have indicated that arbuscular mycorrhizal fungi could not only change the structure of salt-alkali soil, but also enhance the adaptability of plants in salt-alkali soil and promote their growth and development[2,3]. Nowadays, researches about the application of arbuscular mycorrhizal fungi on the ecological restoration of salt-alkali soil has been paid much attention all over the world [4].

Salt affected lands are estimated at about 955 million hm^2 worldwide, which occupied 7% of the world's total arable land. [5] Salt-alkali soil inhibits the growth of crops, and how to develop scientific measures to restore and improve the utilization of salt-alkali land is becoming more and more important.

Identification methods of AM fungi consist of morphological identification and molecular biology identification. At present, the morphological way is mainly based on the morphological characteristics of spores, including their shape, size, wall characteristics and structure, etc[6]. In recent years, with the development of molecular biological technology, the specific sequences of some genes play an increasing large role in the process of AM fungi identification. *Inula japonica* (*Asteraceae*), a herbal flower widely distributed in China[7] can grow in the salt-alkali soil even if the pH reached above 9[8,9], and form symbiont with arbuscular mycorrhizal fungi in the songnen grassland with the colonization rate of 85.75%[8]. In this research, *Glomus intraradices* was isolated from the rhizosphere of *Inula japonica* in Songnen salt-alkali grassland and identified by the morphological method combined with the molecular biological method, then inoculated with *Trifolium repens*. The results of the study can not only help to understand the morphological as well as the molecular biological features of *G. intraradices*, and its effects of salt tolerance of the plant , but also

provide an important theoretical basis for its application in the restoration of salt-alkali grassland.

MATERIALS AND METHODS

Experimental materials. Soil samples in *Inula japonica* rhizosphere were collected at Zhaodong city of Songnen grassland on July, 2014. Four sample points from north, south, east and west were determined, and then 5 strains of *Inula japonica* from each sample point were randomly selected. After 5 cm thick surface soil were removed, profile of 10 ~ 20 cm depth was dug and the rhizosphere soil of about 1 kg were collected. Impurities in the soil sample were then removed after natural air dry at shady place, and the bugged and numbered soil samples were saved for later use.

Isolation and morphological analysis of spores. Spores of AM fungi were isolated from the sample soil by the wet sieving and decanting method[10]. Petri dish with the sieved out culture was placed under the double entity microscope, and the size, color, wall layers and the thickness of spores were observed and photographed by light microscope and then the spores were stained with Meler's agent. Species of the spores were primarily identified according to the species described and pictures provided on the Manual for the Identification of VA Mycorrhizal Fungi, the international AM international website (INVAM), and the published books and literatures[11,13].

Molecular identification of fungal spores. Single spore was picked out and washed with distilled water for five times. After being put in a 0.2 ml PCR tube, it was crushed by pipette gun and then added with 1μL sterilized water. The mixture above was directly treated as the Nested-PCR template with the primers as follows [13]:

ITS1 5′-TCCGTAGGTGAACCTGCGG-3′

NDL22 5′-TGGTCCGTGTTTCAAGACG-3′

LR1 5′-GCATATCAATAAGCGGAGGA-3′

Partial 28 S rDNA gene fragments were amplified using nested PCR, the first PCR was performed using universal eukaryotic primers ITS1-NDL22, with 4μl 10×PCR Buffer, 1.6μl 2.5mM dNTPs, 0.5μl of each 20μM primer, 1μl 20μm DNA template added with ddH_2O to the total volume of 20 ml. The amplification program was as follows: 5 min initial denaturation at 94 ℃, followed by 30 cycles of 1 sec denaturation at 94℃, 30 sec primer annealing at 60 ℃ and 1 min extension at 72℃, followed by a final extension period at 72℃ for 10 min. The second PCR was the same with the first one except that the primers was LR1-NDL22 and the annealing temperature 60℃. 3μl products of the second PCR was taken and detected by 1% agarose gel electrophoresis.

Determination and analysis of DNA sequence. The total volume of 50 μl was run on a 1.0% agarose gel to cut out and purify object bands using the Qiaquick Gel Extraction Kit (TaKaRa), the purified products were linked to pMD-18T (TaKaRa) and transformed into 5α competent Escherichia coli cells (Trans), then single colony were picked out for monoclonal verification. The monoclonal was cultured by LB solid medium for enlargement, after which 1ml positive clones were sequenced. The most similar sequences for AM fungal spores were obtained from the GenBank through BLAST at the National Center for Biotechnology Information (NCBI) and used for molecular identification of AM fungal spores. MEGA5.1 was used for alignment of DNA sequence and phylogenetic tree was constructed using neighbor-joining methods.

Design on salt-alkali stress and inoculation experiment. According to the composition and content of saline soil in Songnen alkaline grassland and the salt-alkali ion concentration ratio[14], four salt-alkali concentration gradient were formulated respectively with the distilled water as control (Table 1). Two inoculation treatments were used in the same salt-alkali concentration by Mixed Inoculation Method[15]: 30g *G. intraradices* was inoculated on each flowerpot as the first treatment(GI); the second treatment was that each flowerpot was inoculated with 30g sterilization inoculant. Each treatment was repeated 3 times. The total was 30 pots. *G. intraradices* inoculant were purchased from Key Laboratory of Oasis Crop Disease Control and Prevention in Shihezi University. The spore density of inoculant was 18 inds·g^{-1}.

Seed germination experiment. Seed of *T. repens* were purchased from the Heilongjiang Provincial Academy of Agricultural Sciences. The seed were surface sterilized with 0.3%$KMnO_4$ for 30 min, and then sowed in every flowerpot (15 cm × 15 cm). After the mixture of river sand: vermiculite: garden soil (1 : 1 : 3) was sterilized by the autoclave at 120℃, 30 grains of seed were sowed in each pot. They were kept under Biotron

TABLE 1
Preparation and concentration of compound saline solution

Treatment concentration	$MgCl_2$/ $g \cdot L^{-1}$	KCl/ $g \cdot L^{-1}$	NaCl/ $g \cdot L^{-1}$	$CaCl_2$/ $g \cdot L^{-1}$	Na_2SO_4/ $g \cdot L^{-1}$	$NaHCO_3$/ $g \cdot L^{-1}$	pH
Control sample (NO.0)	--	--	--	--	--	--	7.00
Concentration 1 (NO.1)	0.0988	0.0861	0.1387	0.1110	0.1683	1.2510	9.02
Concentration 2 (NO.2)	0.1796	0.1721	0.2773	0.2220	0.3365	2.5200	9.38
Concentration 3 (NO.3)	0.3592	0.3442	0.5546	0.4440	0.6730	5.0400	9.72
Concentration 4 (NO.4)	0.5928	0.5163	0.8319	0.6660	1.0095	7.5600	10.04

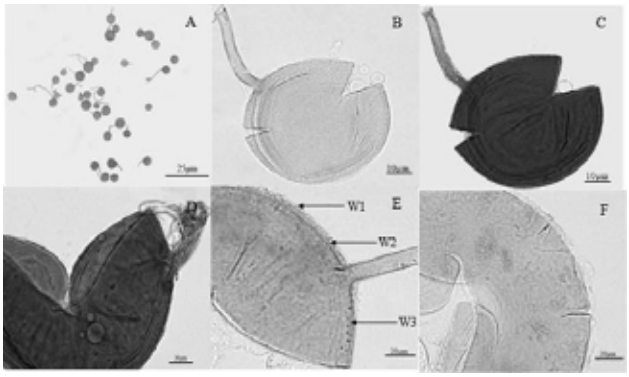

FIGURE 1
Morphological characteristic of spores
Note: A: Spores under the double entity microscope; B: Holistic morphology characteristic of spores; C, D: In Melzer's reagent; E: subtending hypha and the shape of the base of attachment hypha; F: The state of W1 about to fall off

Dark Room Type (5000 lx Light intensity; light cycle for 4 h; 25/20℃day/night; 60-70% relative humidity). All plants were watered with distilled water every two days and 50ml 1/5MS nutrient solution twice every week. After *G. intraradices* infection was tested in the first treatment plants by microscopic examination, plants were treated with complex salt-alkali stress and watered with 200ml saline solution or distilled water every two days.

Methods of physiological index determination. Mycorrhizal infection was tested 60 days after the growth of *T. Repens* seedlings. The leaves photosynthetic indexes including net photosynthetic rate (Pn), stomatal conductance (Gs), intercellular CO_2 concentration (Ci), and transpiration rate (Tr) were measured by a portable photosynthetic apparatus LI-6400 with the light intensity of 1000lx. Chlorophyll content was measured by 95% ethanol extraction method; soluble protein content by coomassie brilliant blue G-250 staining method; activity of superoxide dismutase (SOD) by nitroblue tetrazolium (NBT) method; and catalase (CAT) activity by permanganate titration.

Data analysis. All parameters were analyzed by one-way ANOVA using the statistical Software SPSS 13.0 (SPSS Inc, Chicago, IL, USA). The means and standard errors (SE) were reported. The level of statistical significance was $P<0.05$.

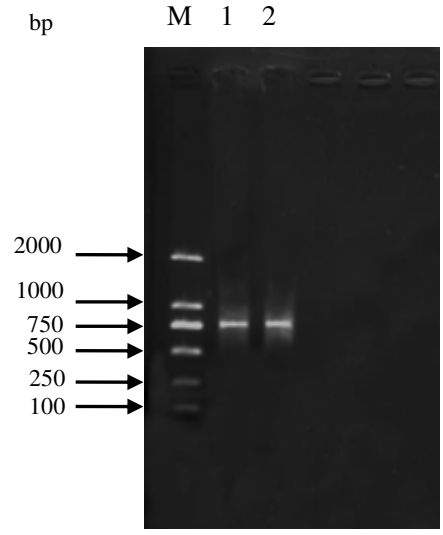

FIGURE 2
Electrophoresis map of Nested-PCR amplified products of *G. intraradices*
Note: M means 2K Marker; 1 and 2 both mean amplified products

RESULTS

Morphological characteristic of AM fungal spores. A large amount of AM fungal spores were

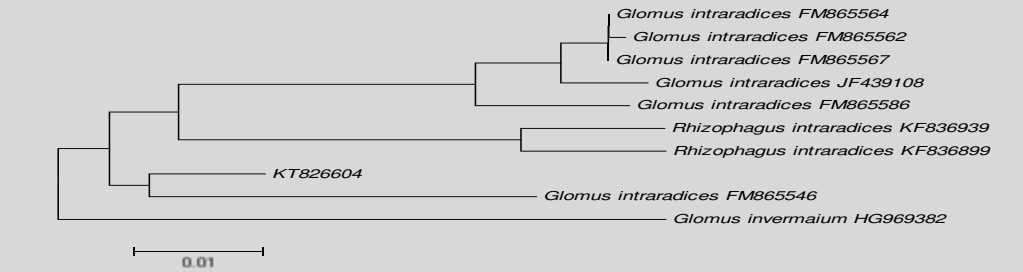

FIGURE 3
KT826604 Phylogenetic tree

isolated from *Inula japonica* rhizosphere in Songnen salt-alkali grassland, among which the one with highest appearance frequency is *Glomus intraradices* according to morphological identification. The morphology of spores is shown in figure 1. The shape of spores is globose or subglobose, the color from pale cream (0-0-10-0) to yellow brown (0-10-40-0) with yellow oil droplets inside. The diameter of spores is 60-170 µm. Some spores are connected together by hyphae, the length and width of which is 120-340 µm and 10-20 µm respectively (Fig 1 A). Spore wall includes three layers (W1, W2 and W3). W1 is colorless, transparent and membranous, sometimes with impurities. This layer always becomes red in Melzer's reagent (Fig 1 C and D) and exfoliates easily with age (Fig 1 F).W2 layer, hyaline and adherent to the W1 layer, always degrades and decomposes naturally with the maturation of spores (Fig 1 B). W3 consists of pale yellow-brown sublayers which are easily separated under external pressure. So it presents the characteristics of many layers of wall overlay together (Fig 1 D and E). Radical texture often appeared when the spores are squeezed by external forces (Fig 1 E and F). Each spore has a single subtending hypha which always has branches. The subtending hypha wall has three layers and the connection point where hyphae attached to spores is frequently thickened with the trumpet shape (Fig 1 D and E).

Nested-PCR amplification of *G. Intraradices*. Nested-PCR amplification was carried on using DNA extracted from single spore of *G. intraradices* as template. The DNA copy number obtained by the first amplification was too low to be detected by gel electrophoresis. After the second Nested-PCR amplification, good specific amplification of *G. intraradices* 25S rDNA fragment was obtained with the fragment size of about 750bp (Fig. 2).

Molecular biological detection of *G. Intraradices*. The DNA fragments amplified by Nested-PCR were sequenced. Results showed that the effective sequence length was 779bp with the GenBank receipt number KT826604. The phylogenetic tree showed that KT826604 and *G. intraradices* (FM865546.1) gathered into a cluster (Fig. 3). As a result, KT826604 was identified as *G. intraradices* by comprehensive methods of both morphological characteristics and DNA sequence analysis.

The physiological response of *T. repens* inoculated by *G. intraradices* to salt- alkali stress. The experimental results showed that under different concentrations of mixed salt alkali stress, the net photosynthetic rate (Pn), stomatal conductance (Gs), intercellular CO2 concentration (Ci), and transpiration rate (Tr) of *T. repens* leaves those of the non-mycorrhizal plants. With the increasent of salt-alkali stress, the net photosynthetic rate (Pn) of both mycorrhizal and non-mycorrhizal plants showed a trend of first increasing and then decreasing. The net photosynthetic rates of both of them reached the maximum at salt content of 0.394% (NO.2), but the net photosynthetic rate of mycorrhizal plants was significantly higher than that of non-mycorrhizal plants (Fig. 4I). The stomatal conductance (Gs) increased first and then decreased with the increasement of salt-alkali concentration stress. For the mycorrhizal plants, the stomatal conductance (Gs) was always higher than that of the non-mycorrhizal plants (Fig. 4II) and reached the maximum at salt content of 0.788% (NO.3), while the intercellular CO2 concentration (Ci) of the mycorrhizal plants was always lower than that of the non-mycorrhizal plants, and the maximum value of difference (Fig. 4 III) appeared in the soil salinity of 1.182% (NO.4); under different saline alkali stress, the transpiration rate (Tr) of the mycorrhizal plants was significantly higher than

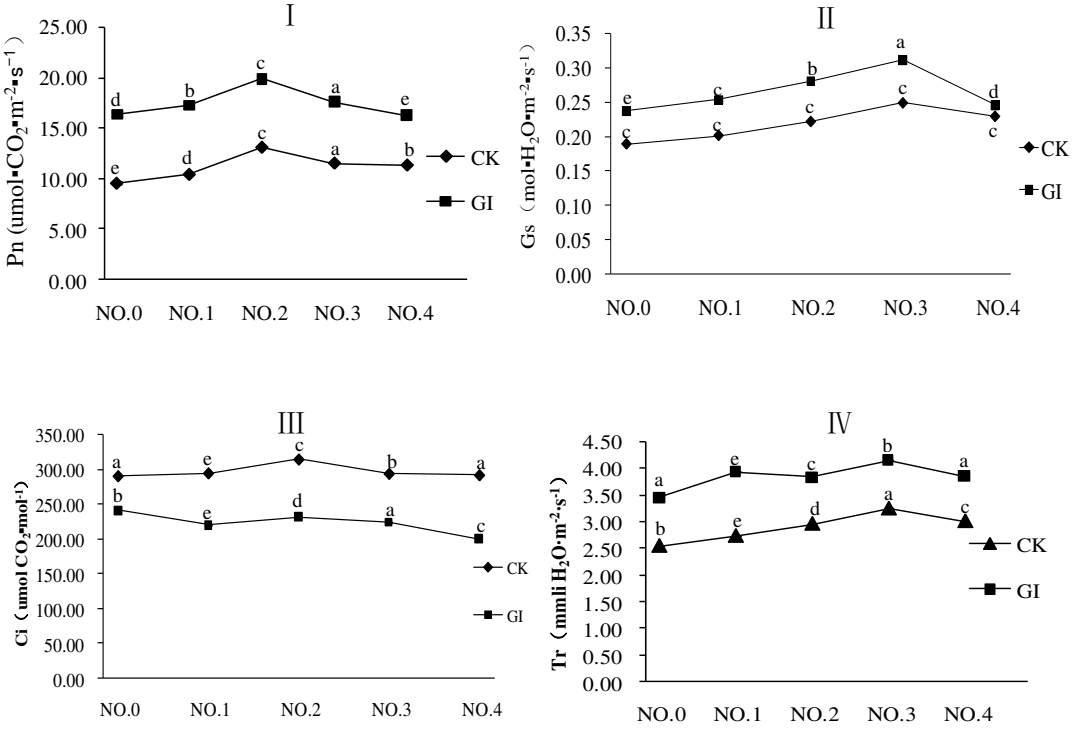

FIGURE 4

Net photosynthetic rate (Pn), Stomatal conductance (Gs), Intercellular CO_2 concentration (Ci) and Transpiration rate (Tr) under saline alkali stress at different concentrations

Note：Different small English letters in the figure indicate significant difference at 0.05 level

that of the non-mycorrhizal plants, and the maximum value of difference appeared (Fig. 4 IV) when the soil salt content was 0.197% (NO.2)

Meanwhile the results showed that the soluble protein content, chlorophyll content, the activities of two defense enzyme SOD and CAT in the physiological and biochemical metabolism of *T. repens* of mycorrhizal plants were significantly higher than those in non mycorrhizal plants. With the increasement of salt-alkali concentration, the content of soluble protein showed rising trend. Under different concentration of salt-alkali stress, the soluble protein content in leaves of *T. repens* inoculated with GI was higher than that of non-mycorrhizal plants all along. When the soil salt content was 1.182% (No.4), soluble protein content difference between the mycorrhizal plants and non-mycorrhizal plants was maximum (Fig. 5 Ⅰ). Under different concentration of salt-alkali stress, the chlorophyll content in leaves was different. Under NO.0, NO.1, NO.3 and NO.4 of the four treatment conditions, the chlorophyll content of mycorrhizal plants were higher than non-mycorrhizal plants, and under the NO.2 treatment, chlorophyll content of mycorrhizal plants reached the minimum value, and was lower than that of the non-mycorrhizal plants (Fig. 5 Ⅱ). As the salt-alkali concentration increased, the SOD activity of leaves of mycorrhizal plants and non-mycorrhizal plants increased first, then decreased, and then increased, and SOD activity of mycorrhizal plants was always higher than that of non-mycorrhizal plants (Fig. 5 Ⅲ). On the other hand, the CAT activity of mycorrhizal plants was also higher than that of non-mycorrhizal plants under different salt-alkali concentrations, and the difference was greatest when the soil salinity was 0.788% (NO.3) (Fig. 5 Ⅳ).

DISCUSSION

Morphological identification method is the most widely applied way on AM fungal species identification, while the results are often influenced by the environmental conditions and the spore development stages etc. In this study, *G. intraradices* isolated from rhizosphere of *I. japonica* in Songnen salt-alkali grassland soil was identified by morphological combined with molecular biological method.

Many studies have indicated that inoculation of AM fungi can improve the salt tolerance of plants[16]. Under salt stress conditions, *Funneliformis mosseae* inoculation could significantly promote the growth of *Lagerstroemia indica*, increased its root growth, reduced its leaf

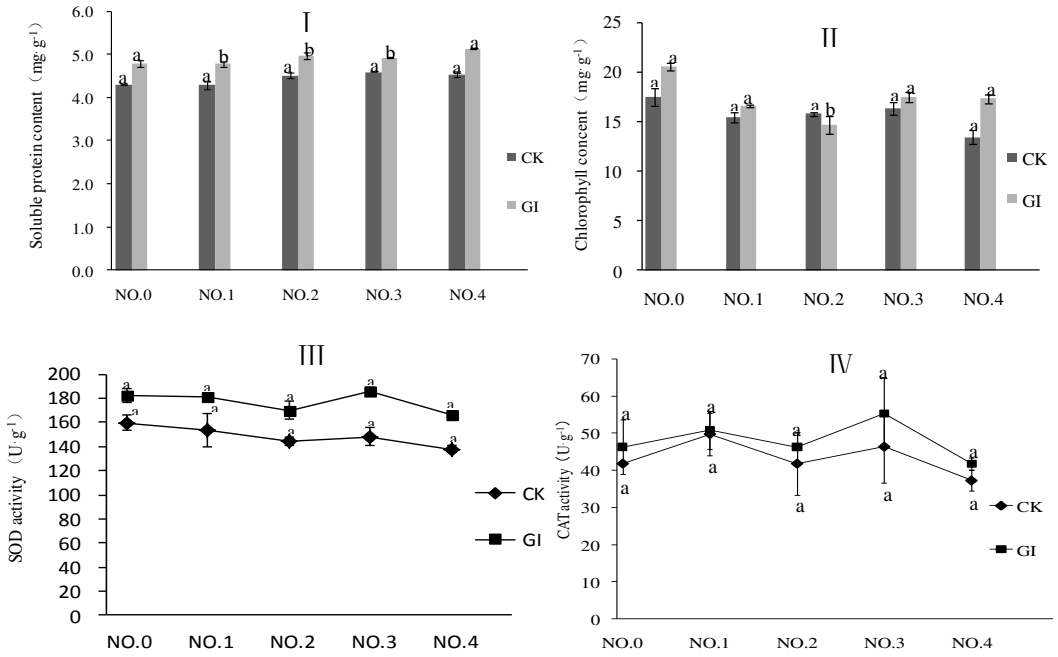

FIGURE 5

Soluble protein content, Content of chlorophyll, SOD activity and CAT activity in leaves of *G. intraradices*-colonized and non-AMF *T. repens* under saline alkali stress.

Note：Different small English letters in the figure indicate significant difference at 0.05 level

MDA content and membrane permeability and also mitigated the toxicity of Na^+ and Cl^-, thus improved the salt tolerance of *L. Indica*[17]. The inoculation with *G. macrocarpum* can increase both the growth and chlorophyll content of seedlings of *Sesbania grandiflora* and *S. aegyptiaca*, which promote the reduction in Na^+ uptake together with a concomitant increasement in P, N and Mg absorption, then alleviate the effects of salt stress on plant[18]. It is confirmed in this study, that inoculation with *G. intraradices* can alleviate the effects of salt-alkali stress on *T. repens*, which indicate that the potential application value of *G. intraradices* in improving the salt tolerance of *T. repens*.

The decrease of photosynthesis is one of the important reasons depressing the plant growth. The result showed that when the soil salinity was lower than 0.788%, the intercellular CO_2 concentration showed a downward trend, while the net photosynthetic rate, stomatal conductance and transpiration rate showed a gradually rising trend. When the soil salinity reached 1.182%, they showed a significant downward trend. These indicated that *T. repens* had a certain ability of salt tolerance, that low concentration of salt-alkali ions can promote its growth. While inoculating with GI could significantly increased the photosynthetic capacity of the *T. repens*. This is consistent with the results of Feng *et al*[19]. In addition, the physiological metabolism of plant is a reliable indicator that estimates the ability of plant salt tolerance. The increasement of chlorophyll content was closely related to the raise of photosynthetic capacity of plants. Bhoopander *et al*.[18], found that inoculating AM fungi can increase the content of soluble protein and chlorophyll content in the host plant. Our experiment also proved that when the soil salt content reached 1.182%, the soluble protein content and the chlorophyll content of mycorrhizal plants were significantly higher than those of non mycorrhizal plants. The increasement of the soluble protein content in mycorrhizal plants might illustrate that the infection of *G. intraradices* decreased the degradation of RNA in plants, enhanced the ability of non enzymatic defense system, and also enhanced water retaining capacity of host cells. Moreover, the SOD and CAT activity in the leaves of mycorrhizal plants was higher than that of non mycorrhizal plants under salt stress, which might indicate that the inoculation improved the enzyme catalyzed reaction system, and reduced the accumulation of reactive oxygen species due to salt-alkali stress.

In summary, *G. intraradices* isolated and identified from rhizosphere of *I. japonica* in Songnen salt-alkali grassland can form a good symbiotic relationship with *T. repens*, significantly improve the photosynthetic growth and the activity of two leaf defense enzymes SOD and CAT, then increase the content of chlorophyll and soluble protein in the leaves of plants. When salt content

reach 1.182%, *T. repens* inoculated with *G. intraradices* can still grow well, which proved that *G. intraradices* inoculation can significantly increase the salt tolerance of *T. repens*. This study can provide a reference for exploring the advantages of AM fungi and furthermore use these AM fungi resources in the restoration and reestablishment of Songnen salt-alkali grassland.

ACKNOWLEDGEMENTS

The research was supported by the Fundamental Research Funds for the Central Universities (2572015CA22), the Heilongjiang Postdoctoral Grant (LBH-Z11250), and the National Natural Science Foundation of China (31502013).

REFERENCES

[1] Yang H. X., Li S. M., Guo S. X. (2014). Effects of arbuscular mycorrhizalfFungi on salinity tolerance of lagerstroemia indica. Plant Physiology Journal, 50(9), 1379-1386.

[2] Leifheit E. F., Verbruggen E., Rillig M. C. (2015). Arbuscular mycorrhizal fungi reduce decomposition of woody plant litter while increasing soil aggregation. Soil Biology & Biochemistry, 81, 323-328.

[3] Kevin Garcia and Sabine D. Z. immermann (2014). The role of mycorrhizal associations in plant potassium nutrition. Plant science, 7(17), 337-345.

[4] Yuan W. F., Xu D. C. (2011). Functions and application of arbuscular mycorrhiza in the plant restoration. Guangxi Agricultural Sciences, (7), 161-163.

[5] Liu M, Liang Z W, Ma H Y, et al. Responses of rice(oryza saliva) growth and yield to phosphogypsum amendment in saline-sodic soils of North-East China. Food Agriculture and Environment. 2010, 8(2), 827-833.

[6] Yang C. X., and Li L. L. (2014). Research progress in arbuscular mycorrhizal fungi identification method application. Guizhou Agricultural Sciences, 42(7), 93-97.

[7] Donggen Piao, Taein Kim, Zhang H. Y. et,al (2016). DNA Topoisomerase Inhibitory Activity of Constituents from the Flowers of Inula japonica. Chem. Pharm. Bull.64, 276-281

[8] Yue Y. N., Yang C. X. (2014). Relationship between soil properties and the colonization of arbuscular mycorrhizae in Songnen Saline-alkaline Grassland. Pratacultural science. 31(8), 1437-1444.

[9] Huang H. L. (2011). Comparison of osmoregulation and ion balance strategies of eight species of alkali-resistant halophytes during adaption to salt-alkalinized habitat. Master Degree Thesis of Northeast Normal University.

[10] Liu R. J., Chen Y. L. (2007). Mycorrhizology. Bei Jing:Science Press, 1-404.

[11] Jaikoo Lee, Sang-Hyeon Park, and Ahn-Heum Eom. (2006). Molecular identification of arbuscular mycorrhizal fungal spores collected in Korea. Mycobiology, 34(1), 7-13.

[12] Wang Y. S., Zhang S. B. and Zhang M. Q. (2012). Resources of the mycorrhizal fungi and germplasm resource in China. Beijing: China Agriculture Press.

[13] Yang C. X., Chen F., Yue Y. N. *et al* (2015). Diversity of arbuscular mycorrhizal fungi in the rhizosphere of twenty six species of plants in Songnen plain. Pratacultural science, 32(12): 2008-2020.

[14] Li S. J., Zhan Y. G., Yang C. P. *et al.* (2010). Effects on growth and physiological indices of introduced species of *Fraxinus velutina* under mixed salt stress. Journal of Northeast Forestry University, 38(1), 15-17.

[15] Wu Q. S. (2010). Research and application of the mycorrhizal fungi in horticultural plants. Bei Jing: Science Press, 1-139.

[16] Liu S. L., Guo X. L., Feng G. et al. (2016).Indigenous arbuscular mycorrhizal fungi can alleviate salt stress and promote growth of cotton and maize in saline fields[J]. Plant and Soil, 398(1), 195-206.

[17] Yang H. X., Guo S. X., Liu R. J. (2015).Characteristics of arbuscular mycorrhizal fungal diversity and functions in saline-alkaliland. Chinese Journal of Applied Ecology, 26(1), 311-320.

[18] Bhoopander G., Mukerji K. G. (2004). Mycorrhizal inoculant alleviates salt stress in *Sesbania aegyptiaca* and *Sesbania grandiflora* under field conditions:evidence for reduced sodium and improved magnesium uptake. Mycorrhiza, 14(5), 307-312.

[19] Feng G., Zhang F. S., Li X. L. *et al* (2002). Improved tolerance of maize plants to salt stress by arbuscular mycorrhiza is related to

higher accumulation of soluble sugars in roots. Mycorrhiza, 12(4), 185-190.

Received: **03.04.2016**
Accepted: **07.08.2016**

CORRESPONDING AUTHOR

Jixiang Lin
Laboratory of Saline-Alkali Vegetation Ecology Restoration in Oil Field, Ministry of Education, Alkali Soil Natural Environmental Science Center, Northeast Forestry University, Harbin, 150040, China.

email: linjixiang@nefu.edu.cn

AUTHOR INDEX

A

Aasim, M. 3907
Abdul-Wahab, S.A. 4409
Abudi, Z. 4130
Ahmad, S. 4253
Ahmadi, L. 4409
Ahmadianfar, I. 4111
Akbolat, D. 4026
Aksu, Y. 4163
Alahmad, W. 4299
Alawi, M. 4299
Ale, A. 4052
Alkan, M. 4171
Andrzej, B. 4269
Atabeyoglu, O. 4261
Avsar, C. 4103

B

Bacchetta, C. 4052
Badr, E. 4118
Bai, D. 3993
Balta, F. 4393
Baraj, B. 3941
Baraj, E. 3941
Bartoszek, L. 3859
Basirun, A. 4253
Baysal, A. 4045
Berber, I. 4103
Besli, E.S. 4141
Bilici, S. 4045
Bitrak, B. 4026

C

Cai, G. 4217
Cai, Z. 3867
Caglar, M. 4157
Cakmak, D. 3907
Can, A. 4324
Canpolat, O. 4157
Cao, X. 3886
Cazenave, J. 4052
Celo, V. 3941
Cevik, I. 4374
Changqing, F. 4235
Chao-Heng, T. 3875
Chen, D. 3867, 4287
Chen, F. 4439
Chen, H. 4351
Chen, S. 4130
Cheng, K. 4088
Cicek, T. 4045
Civek, S. 4103

D

Daria, D. 4269
Day, S. 4294
Dehaghi, S. 3962
Deng, Z. 4287
Devetakovic, J. 4318
Dobaradaran, S. 3955
Dogan, M. 4171
Dong, G. 3847

E

Ekinci, K. 4026
Elkamel, A. 4409
Erdal, I. 4026
Ewa, J. 4269

F

Fang, Z. 3867
Farat, R. 3923
Fen, G. 4235
Feng, Y. 4067
Fu, L. 3895

G

Gajewski, P. 4184
Gao, J. 3895
Gao, P. 4067
Gao, Y. 4401
Gaoyang, Z. 4235
Gaweł, E. 4184
Geravandi, S. 3955
Glina, B. 4184
Gorecki, K. 3923
Goudarzi, G. 3955
Grodzicki, P. 4246
Grzelak, M. 4184
Gu, L. 4004
Gui, H. 4387
Gunduz, Z. 4171
Guo, L. 3981

H

Hao, F. 3847
Hua, Z. 4004

Hashemzadeh, B. 3955
Heydari, M. 4111
Hu, X. 4334
Hu, Z. 4130
Huang, J. 4197
Huang, M. 4287
Huang, Q. 3867

I

Idani, S. 3955
Ikhile, E. 4409
Ilnicki, P. 3923
Imrak, B. 4345
Iqbal, I. 4253
Isik, G. 4324
Iskender, N. 4163
Ivetic, V. 4318

J

Jakub, D. 4269
Jiang, M. 3915
Jianqiao, Y. 4235
Jiao, S. 4036
Jichao, S. 4093
Jin, M. 4227
Joanna, H. 4269
Joanna, Z. 4269

K

Kaczmarek, Z. 4184
Kang, S. 3875
Karaoglu, C. 3907
Khaefi, M. 3955
Khalid, A. 4253
Koenig, M. 4224
Kucuk, F. 4013
Kula, I. 4078
Kumbul, B. 4026

L

Lei, P. 4235
Lei, T. 3837
Lewandowski, P. 3923
Li, C. 4036, 4439
Li, D. 3895
Li, H. 3971
Li, J. 3948
Li, L. 4439
Li, S. 4381
Li, W. 3867, 3993, 4351
Liang, S. 3948
Liao, J. 3981
Liao, M. 4088
Lin, J. 4217, 4439
Ling, L. 4197
Liu, H. 3886, 4277
Liu, L. 3971, 4381
Liu, R. 4309
Liu, S. 3948, 4217, 4381
Liu, T. 4277
Liu, W. 4067, 4088, 4351
Liu, X. 4004, 4387
Liu, Z. 4309, 4351
Lou, H. 3847
Lu, B. 4067
Lu, D. 3948
Lu, J. 3895
Lu, Y. 3993
Luo, J. 4052
Luo, L. 4334
Luo, Y. 3987

M

Maksimovic, Z. 4318
Marek, K. 4269
Mei, S. 4004
Meng, Z. 3993, 4351
Mocek – Płociniak, A. 4184
Mohammadi, M.J. 3955

N

Naeem, A. 4118
Nan, L. 4067
Nguyen, N. 3875
Nie, D. 4227
Nie, F. 4309
Nikolic, M. 4318
Noack, M. 4224
Noack, U. 4224
Nowakowski, T. 4224
Nozari, M. 3962

O

Owczarzak, W. 4184
Ozcan, S. 3907
Ozmen, S. 4209

P
Parlak, K. 4192
Parmaksiz, I. 3907
Pawel, W. 4269
Peng, R. 3987
Peng, S. 3837
Piechowicz, B. 4246
Puppala, A. 4217

Q
Qian, L. 4093
Qian, Q. 3886
Qin, Z. 3948

R
Rajaa, N. 4130
Ren, N. 4067
Rui, Y. 4381

S
Sabullah, M. 4253
Sadło, S. 4246
Sadeghian, M.S. 4111
Sagliker, H. 4374
Salarijazi, M. 4111
Sancak, C. 3907
Senturk, B. 4202
Sevindik, T. 4013
Shahriar, A. 3955
Shamaan, N. 4253
Shehu, A. 3941
Shen, F. 3886
Shen, J. 3981
Shen, K. 4148
Shen, Q. 3981
Shi, F. 4242
Shih, Y. 3875
Shukor, M. 4253
Shuzhong, W. 4235
Sivritepe, H.O. 4202
Stankovic, D. 4318
Stawarczyk, K. 4246
Stawarczyk, M. 4246
Sun, L. 4387
Sun, Q. 4197
Sun, Y. 4052
Sun, Z. 4334
Swierk, D. 4184
Syed, M. 4253
Szpyrka, E. 4246

T
Terzi, E. 4141
Tomaszek, J. 3859
Tong, J. 3886
Totoni, R. 3941
Tseng, C. 3875
Tu, Q. 4004

U
Ugurlu, M. 4078
Unlu, E. 4045
Uysal, E. 4045

V
Vaizogullar, A. 4078
Verep, B. 4141

W
Wang, A. 3875
Wang, B. 4309
Wang, D. 4401
Wang, G. 3915
Wang, M. 3915, 4197
Wang, P. 4401
Wang, Q. 3886
Wang, X. 3837
Wang, Y. 4277
Wang, Z. 3847
Wu, L. 3847, 4327
Wu, Q. 3993

X
Xiang, W. 4148
Xiao, B. 4130
Xiao, W. 4277
Xu, H. 3971
Xu, M. 3867, 4227
Xu, Q. 3895
Xu, S. 3993, 4351
Xu, Y. 4052

Y
Yang, C. 4439
Yildiz, S. 4362

Yang, L. 4148
Yang, S. 3847
Yang, Y. 3847
Yanhui, L. 4235
Yao, R. 4277
Yari, A.R. 3955
Yasid, N. 4253
Yegin, Z. 4103
Yesil, M. 4261
Yesil, P. 4261
Yetilmezsoy, K. 4409
Yin, D. 4052
Youesfi, F. 3955
Yu, D. 4439
Yu, J 4387
Yu, L. 4351
Yu, P. 3987
Yu, Q. 4309
Yuan, J. 3971
Yucel, E. 4324
Yuzhen, W. 4235

Z

Zeng, X. 4401
Zhan, C. 4277
Zhang, H. 4036, 4197
Zhang, J. 3837, 4277
Zhang, L. 4277
Zhang, X. 4242
Zhang, Y. 4148, 4197, 4277, 4287
Zhang, Z. 4067
Zhao, C. 3847, 3948
Zhao, X. 4287
Zhao, Y. 4088
Zhao, Z. 4036
Zheng, J. 4277
Zhou, C. 4148
Zhou, J. 3886, 4197
Zhou, L. 4327
Zhou, R. 3837
Zhou, Z. 4287
Zhu, X. 4327
Zou, H. 4217

SUBJECT INDEX

A

AAS 3941
Aazotica 3981
Acarlar 4013
Acartia tonsa 4224
activated carbon 4060
acute toxicity 3941, 4141, 4224
adsorption 4060, 4327
adsorption isotherm 3993
aged refuse 4036
Ahvaz 3955
Air pollutant 4409
Albanian oilfield brines 3941
Al-Hassa 4118
alpine meadow 4401
aminopropyltriethoxysilane 4327
Anabas testudineus 4253
Anaerobic co-digestion 4130
anaerobic oxidation of CH4 4036
Anaerobic sequencing 4197
API 20E 4393
approaching anodes (AAs) 3867
Aquatic Oligochaeta 4362
Arbuscular mycorrhizal 4439
asorbate peroxidase 4192
atmosphere-exposed biofilm 4227
atmospheric dust 4277

B

Bacillus spp 4103
bacterial flora 4163
Batch reactor 4197
Bensulfuron-methyl 3981
Bentonite 4327
biodegradability 3941
biological control 4163
Black Sea Region of Turkey 4209
Boric acid 4294
bottom sediments 3859
bulblets 3907

C

cadmium 4327
Calamagrostis angustifolia 3915
Canned fish 4157
Carbon 4374
catalase 4192
CCA 4362
Cd(II) pollution 4351
Cedrus libani 4324
Cell morphology 3981
Cerium 4148
chemical oxygen demand 3987
Cholinesterase 4253
clinical symptoms 3886
CO2 monitor module 3875
Coal combustion 3895
coal mine 3886, 4387
coal miner 3886
COD fractionation 3941
coking wastewater 3987
Combined exposure 4067
Composting 4026
contamination 4318
copper 4324
CoSe2(en)14 4242
cover soil 4036
Crown imperial 3907
cumulative abnormal rate of 3886
cumulative total dust exposures 3886
Cyprinion kais 4045

D

dam reservoirs 3859
Decay ratio 4088
degradation 3971, 4334
Deltamethrin 4374
dendrogram 4103
diatom 4013
diatom indices 4013
Dicentrarchus labrax 4393
Diclofenac 4299
Dichlorophenole 4224
diesel 4235
different input mode 4381
different soil 4381
Differential evolution (DE) 4004
directional permeability 4093
Discriminant analysis 4045
dissipation rate 4246
dominant strains 4227
dust exposure year 3886
dynamic characterization 4309

E

ECH2O-5TE probe 4209
ecological quality 4013
economy 4235
electricity generation 4334
EM-A preparation 4184
environmental parameters 4013
environmental pollution 4261
Estrogen 4067

electro-Fenton 3987
Electrokinetic remediation 3867

F
Fenton treatment 3987
fish 4052
Flood Discharge 4111
floodplain forest 4013
flower-like 4242

G
game damage 4269
Gas Exchange 4345
geophytes 3907
Glomus intraradices 4439
glucose 4401

H
Habitat Preferences 4362
Haihe River 3837
Hao, X. 4327
hazelnut tree 4209
Health effects 4409
Health risk 3837
health risk assessment 4277, 4351
Heat-sensitive substances 4088
Heavy metal 4261, 4381
heavy metals 3837, 4052, 4157,
Ibuprofen 4299
Indoor pollution 4409
industrial corridor 4277
Influenza A virus 4088
inorganic-organic 4242
Insecticide 4374

K
Kaolin 4345
Kaolinite/PDMS paste 4171

L
Lake District 4362
Lake Van 4103
Lambda-cyhalothrin 4374
Land use change 3847
lead 4318

M
maize 4269
Marine Copepod 4224
matrix interferences 3941
maximum residue levels 4246
mechanism 3867
Mercury 3895
meristic 4045
Metal ions 4253
Metals 4141
Methyl Orange 3962
eutrophication 3923

food safety 4157
forced vital capacity 3886
freshwater marsh 3915
fungicide residues 4246

Graphene-like BN 3971
greenhouse gases 4401
Ground Level Ozone 3955
groundwater 4118, 4387

hematology 4052
Herschel-Bulkley model 4171
Heterocyst 3981
heterogeneity 4103
High carbon-nitrogen waste water 4197
High Pressure Capillary Reheometer 4171
highway 4261
Hospital admissions 3955
hydrophobic bond 3993
hydrothermal synthesis 4242, 4287

Interaction 4148
Interval partial leastsquares 4197
Ion exchange 3993
iron 3941
isolation 4163

Kinetic study 4130
kinetics 4299

lipid peroxidation 4192
liquefaction 4217
load 3923
loose layer aquifer 4387

Microbial community structure 4227
micropropagation 3907
Micro-sponge 4078
mid-high latitude agricultural region 3847
Mineralization 4374
Minocycline 4334
mitotic cell division 4324
MoO3 3971
morphometric 4045
Multiple Fruit 4345

methylene blue 4078
MFC 4334

N
N2O emissions 4036
Nano Photocatalyst 3962
national highway G316 4277
N-doped TiO2 4287
Near infrared spectroscopy 4197
nickel 4318
multiple regression analysis 3859
municipal open market wastes 4026
nitrate and fluoride 4118
nitrogen 3923
Nitrogen addition 3915
Nitrogen dioxide 3955
NO 4148
non-Newtonian 4171

O
OFMSW 4130
oil sands 4235
Oligonychus ununguis 4163
Olive 4374
Oncorhynchus mykiss 4141
Optimization 4004
organic agriculture 4209
oxidative stress 4052

P
Parameter identification 4004
Particle materials 4088
Particle matter 3955
particle size distribution 3941
pathogenic bacteria 4163
pathogenic fungi 4269
PCR 4393
PCR-DGGE 4227
Peach 4345
Permeability coefficient 4093
Persian lily 3907
pest 4163
Pharmaceutical wastewater 3941
phosphorus 3923, 4401
phosphorus content 3859
Photoactivity 3971
photocatalytic degradation 4078, 4287
photodegradation 4299
phytoremediation 4294
piezocone penetration test 4217
plant 4261
Poland 3923
pollutants concentration 4309
Pollution 4118
pollution characteristics 4277
polymeric resin 4060
Potable water quality 4118
priming 4202
Proline 4192
protected natural area 4318
Purification 4253

Q
quality assessment 4387

R
Radon gas exposures 4409
Rainbow trout 4141
Rainfall runoff 4309
random field 4093
random field model 4217
RAPD-PCR 4103
red deer 4269
Removal 3895
response surface methodology 4287
Rice straw 4130
ripe apples 4246
River network 4004
rock layer angle 4093
roe deer 4269
rose oil processing wastes 4026

S
safe consumption levels 4246
safety level 4351
salinity 4202
Salt-alkali stress 4439
secondary aggregation 4184
sediment components 3859
seed bank 3915
seed germination 3915
Seed viability 4202
seedling biomass 3915
Smelter 4351
sodium silicate 4327
soil 4261
soil ammonium nitrogen 3847
soil DOC 4401
soil pollution 4381
soil remediation 3867
Sol-Gel 3962
sulfanilic acid 4060
Sulfur dioxide 3955
sunflower 4294

seedling emergence and 4202
Selective catalytic reduction 4148
SF VIS 3941
Shade Net 4345
slide agglutination 4393

T
Temperature 4227
Temperature coefficient 4227
Testing 4409
the first second of time vital 3886
Tidal Flood 4111
Tidal Limit 4111
Tigris River 4045
TiO2/CeO2 4078
TiO2/Sb 3962
TiO2-SnO2 4148

U
Ultraviolet radiation 4088

V
Vanadium 4148
Vanselow selectivity 3993
Vegetative cells 3981
Veliko ratno ostrvo 4318

W
Warta River 3923
wastewater 4299
Water Level 4111
Water Source 3837
water pollution 4141

Y
Yeast estrogen screen assay 4067

Z
Zn contamination 3867

Supercritical CO2 extraction 4235
superficial characteristics 3993
superoxide dismutase 4192
Synergic effect 4067

total soil nitrogen 3847
Toxic unit 4067
toxicity 4294
transaminases 4052
Transformation 3895
trend 3923
Trifolium repens 4439
Turkey 4362
TWAS 4130

urban space 4261

vibrio anguillarum 4393
Vibro-compaction 4217
Volatile fatty acids 4197

Warta River 3923
wastewater 4299
Water Level 4111
Water Source 3837
water pollution 4141
Water quality model 4004
water quality parameters 4309
water resistance 4184
water rock interaction 4387
water treatment 4078

FEB – GUIDE FOR AUTHORS

General

FEB accepts original papers, review articles, short communications, research abstracts from the entire sphere of environmental-chemistry,-biology,-microbiology,- technology, -biotechnology and-management, furthermore, about residue analysis/ and ecotoxicology of contaminants.

Acceptance or no acceptance of a contribution will be decided, as in the case of other scientific journals, by a board of reviewers. Papers are processed with the understanding that they have not been published before (except in form of an abstract or as a part of a published lecture, review or thesis);that they are not under consideration for publication elsewhere; that their publication has been approved by all co-authors, if any, as well as-tacitly or explicitly- by the responsible authorities at the institute where the work has been carried out and that, if accepted, it will not be published elsewhere in the same form, in either the same or another language, without the consent of the copyright holders.

Language

Papers must be written in English. Spelling may either follow American (Webster) or British (Oxford) usage but must be consistent. Authors who are less familiar with the English language should seek assistance from proficient colleagues in order to produce manuscripts that are grammatically and linguistically correct.

Size of manuscript

Review articles should not exceed 30 typewritten pages. In addition up to 5 figures may be included.

Original papers must not exceed 14 typewritten pages. In addition up to 5 figures may be included.

Short-Communications should be limited to 4 typewritten pages plus not more than 1 illustration.

Short descriptions of the authors, presentation of their groups and their research activities (with photo) should together not exceed I typewritten page. Short research abstracts should report in a few brief sentences (one-fourth to one page) particularly significant findings. Short articles by relative newcomers to the chemical innovation arena highlight the key elements of their Master and PhD-works in about I page.

Book Reviews are normally written in-house, but suggestions for books to review are welcome.

Preparation of manuscript

Dear authors,

FEB is available both as printed journal and as online journal on the web. You can now e-mail your manuscripts with an attached file. Save both time and money. To avoid any problems handling your text please follow the instructions given below:

When preparing your manuscripts have the formula K/SS (Keep It Simple and Stupid) in mind. Most word processing programs such as MS-Word offer a lot of features. Some of them can do serious harm to our layout. So please do not insert hyperlinks and/or automatic cross-references, tables of contents, references, footnotes, etc.

1. Please use the standard format features of your word processor (such as standard.dot for MS Word).
2. Please do not insert automatisms or secret link-ups between your text and your figures or tables. These features will drive our graphic department sometimes mad.
3. Please only use two fonts for text or tables "Times New Roman" and for graphical presentations "Arial".
4. Stylesheets, text, tables and graphics in shade of grey
5. Turn on the automatic language detection in English (American or British)
6. Please - check your files for viruses before you send them to us!!

Manuscripts should send to:parlar@wzw.tum.de
or:parlar@prt-parlar.de

Thank you very much!

STRUCTURE OF THE MANUSCRIPT

Title page: The first page of the manuscript should contain the following items in the sequence given: A concise title of the paper (no abbreviations). The names of all authors with at least one first name spelled out for every author. The names of Universities with Faculty, City and Country of all authors.

Abstracts: The second page of the manuscript should start with an abstract that summarizes briefly the contents of the paper (except short communications). Its length should not exceed 150-200 words. The abstract should be as informative as possible. An extended repetition of the paper's title is not considered to be an abstract.

Keywords: Below the Summary up to 6 key words have to be provided which will assist indexers in cross-indexing your article.

Introduction: This should define the problem and, if possible, the frame of existing knowledge. Please ensure that people not working in that particular field will be able to understand the intention. The word length of the introduction should be 150 to 300 words.

Materials and methods:
Please be as precise as possible to enable other scientists to repeat the work.

Results: Only material pertinent to the subject must be included. Data must not be repeated in figures and tables.

Acknowledgements: Acknowledgements of financial support, advice or other kind of assistance should be given at the end of the text under the heading "Acknowledgements". The names of funding organisations should be written in full.

References: Responsibility for the accuracy of references rests with the authors. References are to be limited in number to those absolutely necessary. References should appear in numerical order in brackets and in order of their citation in the text. They should be grouped at the end of the paper in numerical order of appearance. Abbreviated titles of periodicals are to be used according to Chemical or Biological Abstracts, but names of lesser known journals should be typed in full. References should be styled and punctuated according to the following examples:

ORIGINALPAPERS:
l. Author, N.N. and Author, N.N. (Year) Full title of the article. Journal and Volume, first and last page.
BOOK OR PROCEEDING:
2. Author, N.N. and Author, N.N. (Year) Title of the contribution.
In: Title of the book or proceeding. Volume (Edition
of klitor-s, ed-s) Publisher, City, first and last page

DOCTORALTHESIS:
3. Author, N.N. (Year) Title of the thesis, University and
Faculty, City

UNPUBLISHED WORK:
Papers that are unpublished but have been submitted to a journal may be cited with the journal's name followed by "in press". However, this practice is acceptable only if the author has at least received galley proofs of his paper. In all other cases reference must be made to “unpublished work" or "personal communication".

Discussion and Conclusion: This part should interpret the results in reference to the problem outlined in the introduction and of related observations by the author/s or others. Implications for further studies or application may be discussed. A conclusion should be added if results and discussion are combined.

Corresponding author: The name of the corresponding author with complete postal address

Precondition for publishing:
A minimum number of 25 reprints must be ordered and prepaid.
1 - 4 pp.: 200,- EURO + postage/handling
5 - 8 pp.: 250,- EURO + postage/ handling
More than 8pp: 1.50 EURO/page x number of reprints +postage/ handling.
The prices are based upon the number of pages in our journal layout (not on the page numbers of the submitted manuscript).
Postage/ Handling: The current freight rate is Germany 10 €, Europe 18,00 €, International 30 €.
VAT: In certain circumstances (if no VAT registration number exists) we may be obliged to charge 7% VAT on sales to other EU member countries.MESAEP and SECOTOX members get a further discountof 20% (postage/ handling full).